BULLETIN OF THE EARTHQUAKE RESEARCH INSTITUTE,
TOKYO UNIVERSITY. Vol. XXIX, Part 1. March, 1951.

東京大學

地震研究所彙報

第29號　第1册

昭和26年3月

目　次

論文及報告

頁
1. 表面波の研究 I　ラブ波の速度 (英文) …… 佐藤泰夫 1
2. レーリー波を發生しない震源 (英文) …… 佐藤泰夫 13
3. 層のある媒質を傳はる表面波の研究 (2) (英文) …… 佐藤泰夫 21
4. M_2波 (妹澤波) について (英文) …… 金井清 39
5. 分散性表面波の群速度について (英文) …… 金井清 49
6. 地球内の電磁感應およびその地球内部の電氣的性質との關係 第3報 (英文) …… 力武常次 61
7. 本邦太平洋沿岸各地に於ける津浪の危險度 (英文) …… 高橋龍太郎 71
8. 東北日本における爆破地震動の觀測 (英文) …… 東大地震研究所
東大地球物理學教室
中央氣象台地震課
地質調査所第4部 97
9. 地下における地震動の觀測結果　第1報 (英文) …… 金井清
田中貞二 107
10. 地震動の尾部について (其の6) (英文) …… 表俊一郎 115
11. 今市地震 (1949) に伴う地殼の垂直變動について (英文) …… 井上英二 143
12. 小型磁氣感應儀 (英文) …… 力武常次 147
13. 三原山火口附近における放送電波の廻折 (英文) …… 力武常次 153
14. 伊豆大島における地磁氣伏角分布と三原山噴火に伴うその變化 (英文) …… 力武常次 161
15. 名古屋市における地盤と震害の關係 (英文) …… 表俊一郎
宮村攝三 183
16. 火薬の爆發によつて起される地動について (英文) …… 池上良平 197
17. 非木造建物の震害と地盤の性質との關係　第2報 (英文) …… 金井清
吉澤靜代 209
18. 木造家屋の震害について (邦文) …… 金井清 215

(The titles in occidental languages are given on the back cover.)

本彙報ハ年4回 (但シ第1號ヨリ第6號マデハ不定期ニ，第7號ハ3冊トシテ發行セリ)，彙報別冊ハ不定期ニ發行ス．

本彙報掲載ノ論文及ビ報告ノ內容ニ關シテハ著者ノミニ其責任アルモノトス．

本彙報ニ關スル照會通信ハ東京大學地震研究所長ヘ宛テラレタシ．

The Bulletin is published quarterly. (Vols. I–VI were published at irregular intervals and Vol. VII consisted of three parts.)

Supplementary Volume is published at irregular interval.

The authors of the papers alone are responsible for the statements and opinions contained in their respective papers.

All communications relating to this Bulletin should be addressed to the Director of the Earthquake Research Institute, Tokyo University.

1. *Study on Surface Waves I.*
Velocity of Love-Waves.

By Yasuo SATÔ,

Earthquake Research Institute.

(Read Dec. 19, 1950.—Received Dec. 20, 1950.)

1. Introduction.

The world in which we live is limited. However great it may seem to us, it always has its own limits. Of course the theory of elastic waves was at first studied under the assumption of isotropic, homogeneous, perfect and infinite elastic body. And this is very natural from the point of view of practical treatment, such a theory being most simple, fundamental and useful. And yet our elastic body is neither perfect nor infinite. Our globe is a spherical body with finite dimension, and the elastic waves generated must necessarily receive the effect of boundary surfaces. Then, how is the effect of boundaries? What will happen when waves come to these surfaces? Such doubts naturally lead us to the investigation of boundary waves or surface waves. First, G. Green[1] treated this problem, and fifty years later, C. G. Knott[2] took up the same problem from the standpoint of a seismologist. And after that, many prominent authors[3] have studied the same kind of problems; that is the reflection and refraction of plane waves at the contact serface of two semi-infinite elastic bodies, or at the free surface of them.

On 1885 Lord Rayleigh[4] published a famous paper which opened a new age in our study of surface waves. Since then the theory of surface waves upon elastic solids became one of the main battle-ground of seismologists, and a number of authors were engaged in the investigations how to comprehend and explain the nature of these waves.

---

[1] G. GREEN, *Cambridge Phil. Soc. Trans.*, **7** (1839). The author has not yet read this paper.

[2] C.G. KNOTT, "Earthquake and Earthquake Sounds; As Illustration of General Theory of Elastic Vibrations." *Trans. Seism. Soc. Japan,* **12** (1888), 115.

[3] e.g. B. GUTENBERG, Über Erdbebenwellen IV, *Göttingen Nachrichten,* (1912), 321. G.W. WALKER, "Surface Reflection of Earthquake Waves." *Phil. Trans.*, **218** (1919), 373. H. JEFFREYS, "The Refection of Elastic Waves." *M.N.R.A.S. Geo. Sup.*, **1** (1926), 321. T. MATUZAWA, *Zisin*, **4** (1938), 7, (in Japanese). H. KAWASUMI and T. SUZUKI, *Zisin*, **4** (1932), 277 (in Japanese).

[4] Lord RAYLEIGH, "On Waves Propagated along the Plane Surface of an Elastic Body." *Proc. Math. Soc. London,* **17** (1885) or *Scientific Papers*, **2**, p. 441.

In the following study we shall develop several calculations in the said part of elastic waves.

2. Love-waves.

When we study the property of elastic waves, we usually take up the velocity of propagation first of all. For, it is one of the most fundamental quantities which show the nature of waves, and also has a strong point that scarcely suffers fatal change by observation instruments and by the nature of soil or rock on which the station is situated. Consequently, when we intend to discriminate a special phase in seismograms, the arrival time or in other words the velocity of propagation always affords the best key for our purpose.

Since the celebrated paper of Lord Rayleigh was published,[5] various cases were investigated in which some boundary waves can exist, and the velocity in question is given as an eigen-value or some eigen-values of equation which is introduced, in our problems, as boundary conditions.

Of these investigations, the most important and interesting one is the so-called Love-waves discovered by A.E.H. Love in 1911.[6] In view of the observational facts, the existence of such waves is today doubted by nobody, and yet the study of Love-waves is far behind that of Rayleigh-weves. This is partly because the theory of Love-waves is mathematically simple and has hardly attracted the interest of mathematicians. However, there still remain a number of problems to be clarified and moreover it is one of the fundamental type of surface waves, whose importance the writer wishes to assert.

3. One explanation of the characteristic equation of Love-waves.

Throughout this study, we will only treat the two-dimensional problems. The mathematical analysis is so complicated that we must make every possible effort to simplify the problem, and fortunately the nature of phenomena in three dimensional space may be fully understood through this simplified treatment.

---

[5] *Ibid.*

[6] A.E.H. LOVE, *Some Problems of Geodynamics* (1911).

We take x-axis along the lower boundary plane of the stratum and z-axis vertically upwards. Further, we employ the following notations ;

	Within stratum	Within substratum medium
Density	ρ	ρ'
Lamé's constants	$\lambda,\ \mu$	$\lambda',\ \mu'$
Velocity of S waves	V_s	V_s'
and	$b = 1/V_s$	$b' = 1/V_s'$
	$k = bp$	$k' = b'p$
	$\beta = \sqrt{(f^2 - k^2)} = i\tilde{\beta}$	$\beta' = \sqrt{(f^2 - k'^2)}$

in which p means circular frequency and $f = 2\pi/(\text{wave-length})$. These notations will be always used hence.

Displacement v in the upper layer is expressed by using the above notations ;

$$v = A\{\exp(i\tilde{\beta}z) + \exp(-i\tilde{\beta}z)\}\exp(ifx + ipt) \dots\dots\dots (3.1)$$

From the boundary conditions necessary for the existence of SH waves in the above medium (continuity of displacement and stress at the boundary surface and vanishing of stress at the free surface), we get the following characteristic equation

$$(\mu\beta + \mu'\beta')\exp(\beta H) - (\mu\beta - \mu'\beta')\exp(-\beta H) = 0 \dots\dots\dots (3.2)$$

which is the well-known velocity equation of Love-waves.

Slightly modifying the form of equation, we get

$$\exp\{-i2\Theta + i2\tilde{\beta}H\} = 1$$

or

$$-2\Theta + 2\tilde{\beta}H = 2n\pi \dots\dots\dots\dots\dots\dots (3.3)$$

where

$$\exp\{i2\Theta\} = -(\chi\beta' - i\tilde{\beta})/(\chi\beta' + i\tilde{\beta})$$

$$\Theta = \arctan(\chi\beta'/\tilde{\beta})$$

It is well known that Love-waves can only exist when $V_s < V_s'$, and the phase velocity V satisfies the relation $V_s < V < V_s'$; therefore $\tilde{\beta}$ and β' are both real and $\varkappa\beta' - i\tilde{\beta}$ and $\varkappa\beta' + i\tilde{\beta}$ are conjugate complex to each other, so that $|\exp\{i\Theta\}| = 1$ and Θ takes real value.

This last eqation may be interpreted as follows. (See Fig. 1.)

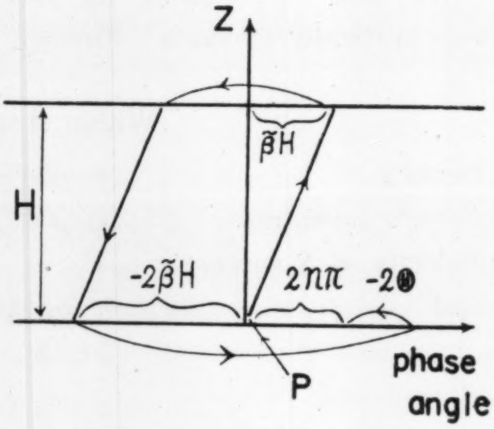

Fig. 1.

Consider a wave which is just passing a point P lying on the lower boundary of the layer. (For example we may notice the first term in the parentheses { } of (3.1).) This wave suffers the variation of phase by the angle $\tilde{\beta}H$ before reaching the upper surface of the layer. When it is reflected at the free surface the phase angle becomes reverse and takes the value $-\tilde{\beta}H$, (cf. the second term of (3.1)) and when it reaches the lower boundary again, the phase angle becomes $-2\tilde{\beta}H$. However, when it is reflected by the boundary surface, the phase angle again undergoes a change in sign and becomes $2\tilde{\beta}H$, and furthermore the jump of phase (by the angle Θ) occurs and the final value becomes $2\tilde{\beta}H-\Theta$. The second expression of (3·3) requires that this (change of) phase angle is the multiple of 2π. And it may be regarded that when the waves satisfying the said condition are superposed and predominate, they constitute Love-waves. This interpretation reminds us of the Lummer-Gehrcke plate in spectroscopy. The Lummer-plate is an apparatus using the interference of wave-trains such as A, B, C... in Fig. 3, and Love-waves are, as is clear from the above explanation, also a kind of interference phenomena between the wave-trains such as A, B, C... in Fig. 2.⁷⁾ Of course this sort of interpretation is not always applicable to every velocity equation of surface waves, therefore the above nature is not the essential property of characteristic equation obtained from boundary conditions. For, the interpretation of that of Rayleigh-waves is quite different from above, and also the Rayleigh-waves in stratified medium are not interpreted in the same way.

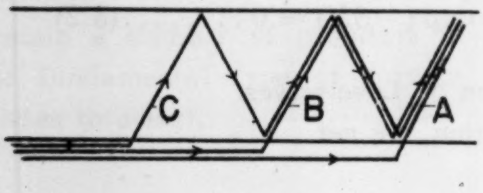

Fig. 2

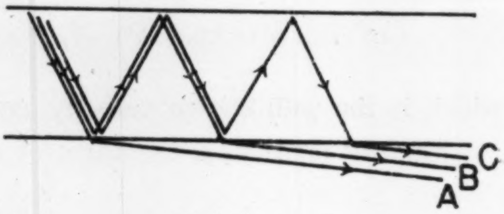

Fig. 3

---

7) Y. SATÔ, *Kagaku* **19** (1949), 311, (in Japanese).

Table I.

Value of ρ'/ρ corresponding to every pair of χ and $\mathrm{Sin}^2\,\theta_0$.

$\chi = \mu'/\mu$

$\mathrm{Sin}^2\,\theta_0 = \left(\frac{\mu}{\rho}\right) \Big/ \left(\frac{\mu'}{\rho'}\right) = V_s^2/V_s'^2$

$\mathrm{Sin}\,\theta_0$ = ratio of the velocity of S waves in the upper layer to that of the lower medium.

θ_0 = minimum value of the angle between wave surface of Love-waves **and free surface.**

	$\mathrm{Sin}^2\,\theta_0$	1/100	1/20	1/10	1/5	1/3	1/2	2/3	5/6	10/11
$\chi = \mu'/\mu$	$\mathrm{Sin}\,\theta_0$	.1	.22361	.31623	.44721	.57735	.70711	.81650	.91287	.95346
	$\mathrm{Cosec}\,\theta_0$	10	4.4721	3.1623	2.2361	1.73205	1.41421	1.22474	1.09545	1.04881
	θ_0	5°44′20″	12°55′15″	18°26′06″	26°33′54″	35°15′52″	45°0′0″	54°44′10″	65°54′20″	72°27′06″
0.9					.18	.30	.45	.60	.75	.81818
1.0				.10	.20	.33333	.50	.66667	.83333	.90909
1.1				.11	.22	.36667	.55	.73333	.91667	1.0
1.2				.12	.24	.40	.60	.80	1.00	1.09091
1.5				.15	.30	.50	.75	1.0	1.25	1.36364
2			.10	.20	.40	.66667	1.00	1.33333	1.66667	1.81818
3			.15	.30	.60	1.00	1.50	2.00	2.50	2.72727
5			.25	.50	1.00	1.66667	2.50	3.33333	4.16667	4.54545
10		.10	.50	1.00	2.00	3.33333	5.00	6.66667	8.33333	9.09091
20		.20	1.00	2.00	4.00	6.66667	10.00			
100		1.00	5.00	10.00						

Table II.

Minimum group velocity of Love-waves $\mathfrak{V}_{\min}$ (unit; $V_s = \sqrt{(\mu/\rho)}$) and the corresponding values of phase velocity $\mathfrak{v}$, period τ (unit; H/V_s) and wave-length λ (unit; H) [Branch L_0].

χ \ $\sin^2\theta_0$		1/100	1/20	1/10	1/5	1/3	1/2	2/3	5/6	10/11
0.9	$\mathfrak{V}_{\min}$				.9674	.9738	.9812	.9880	.9942	.9969
	$\mathfrak{v}$				1.113	1.089	1.058	1.036	1.017	1.008
	τ				2.7207	2.4371	1.9519	1.5448	1.0570	.7397
	λ				3.028	2.654	2.065	1.600	1.075	.746
1.0	$\mathfrak{V}_{\min}$			.9567	.9628	.9703	.9788	.9864	.9936	.9965
	$\mathfrak{v}$			1.149	1.120	1.095	1.063	1.039	1.018	1.009
	τ			3.0171	2.7167	2.4355	1.9857	1.5830	1.0896	.7543
	λ			3.467	3.043	2.667	2.111	1.645	1.109	.761
1.1	$\mathfrak{V}_{\min}$			.9514	.9584	.9669	.9763	.9848	.9928	.9961
	$\mathfrak{v}$			1.158	1.129	1.101	1.068	1.042	1.020	1.010
	τ			3.0122	2.7397	2.4424	2.0123	1.5977	1.1214	.7745
	λ			3.488	3.093	2.689	2.149	1.665	1.144	.782
1.2	$\mathfrak{V}_{\min}$			.9462	.9540	.9634	.9739	.9835	.9920	.9956
	$\mathfrak{v}$			1.175	1.140	1.109	1.072	1.045	1.022	1.011
	τ			3.1004	2.7846	2.4861	2.0321	1.6177	1.1439	.7897
	λ			3.643	3.174	2.757	2.178	1.690	1.169	.798
1.5	$\mathfrak{V}_{\min}$			.9309	.9413	.9536	.9671	.9791	.9901	.9947
	$\mathfrak{v}$			1.211	1.170	1.127	1.085	1.051	1.024	1.012
	τ			3.1795	2.8962	2.5394	2.1000	1.6579	1.1542	.8145
	λ			3.850	3.389	2.862	2.279	1.742	1.182	.824
2	$\mathfrak{V}_{\min}$		.8998	.9079	.9219	.9386	.9569	.9726	.9869	.9930
	$\mathfrak{v}$		1.292	1.260	1.209	1.156	1.102	1.060	1.028	1.015
	τ		3.4101	3.2558	2.9737	2.6264	2.1753	1.7035	1.1853	.8725
	λ		4.406	4.102	3.595	3.036	2.397	1.806	1.218	.886
3	$\mathfrak{V}_{\min}$		.8562	.8686	.8897	.9140	.9399	.9622	.9821	.9904
	$\mathfrak{v}$		1.400	1.346	1.272	1.198	1.129	1.076	1.034	1.019
	τ		3.5455	3.3619	3.0786	2.7113	2.2673	1.7866	1.2137	.9188
	λ		4.964	4.525	3.916	3.248	2.560	1.922	1.255	.936
5	$\mathfrak{V}_{\min}$		.7918	.8110	.8431	.8787	.9158	.9474	.9752	.9866
	$\mathfrak{v}$		1.562	1.480	1.363	1.255	1.164	1.096	1.042	1.023
	τ		3.6568	3.4863	3.1826	2.8056	2.3587	1.8771	1.2830	.9541
	λ		5.712	5.160	4.338	3.521	2.746	2.057	1.337	.976
10	$\mathfrak{V}_{\min}$	.6686	.6969	.7268	.7759	.8283	.8816	.9264	.9652	.9816
	$\mathfrak{v}$	1.976	1.831	1.673	1.492	1.333	1.209	1.117	1.053	1.027
	τ	3.8752	3.7484	3.5626	3.2754	2.8982	2.4514	1.9335	1.3590	.9852
	λ	7.657	6.863	5.960	4.887	3.863	2.964	2.160	1.431	1.012
20	$\mathfrak{V}_{\min}$	.5634	.6049	.6465	.7119	.7804	.8490			
	$\mathfrak{v}$	2.421	2.103	1.877	1.610	1.407	1.249			
	τ	3.9254	3.7690	3.6107	3.3266	2.9736	2.5238			
	λ	9.503	7.926	6.777	5.356	4.184	3.152			
100	$\mathfrak{V}_{\min}$	.3660	.4370	.5022						
	$\mathfrak{v}$	3.742	2.816	2.323						
	τ	3.9523	3.8217	3.6828						
	λ	14.790	10.762	8.555						

Table III.

Minimum group velocity of Love-waves $\mathfrak{V}_{\min}$ (unit; $V_s=\sqrt{(\mu/\rho)}$) and the corresponding values of phase velocity $\mathfrak{v}$, period τ (unit; H/V_s) and wave-length λ (unit; H) [Branch L_1].

Sin$^2\theta_0$ χ		1/100	1/20	1/10	1/5	1/3	1/2	2/3	5/6	10/11
0.9	$\mathfrak{V}_{\min}$				.7670	.8364	.8948	.9378	.9718	.9852
	$\mathfrak{v}$				1.748	1.445	1.254	1.138	1.059	1.030
	τ				1.4661	1.2646	1.0398	.8119	.5542	.3993
	λ				2.563	1.827	1.304	.924	.587	.411
1.0	$\mathfrak{V}_{\min}$			.6970	.7768	.8422	.8978	.9391	.9722	.9854
	$\mathfrak{v}$			2.203	1.710	1.424	1.244	1.133	1.058	1.028
	τ			1.6032	1.4247	1.2245	1.0064	.7840	.5399	.3791
	λ			3.532	2.436	1.744	1.252	.888	.571	.390
1.1	$\mathfrak{V}_{\min}$			.7096	.7842	.8458	.8992	.9394	.9722	.9854
	$\mathfrak{v}$			2.144	1.666	1.407	1.233	1.128	1.055	1.027
	τ			1.5680	1.3783	1.1889	.9714	.7603	.5185	.3675
	λ			3.362	2.296	1.673	1.198	.858	.547	.377
1.2	$\mathfrak{V}_{\min}$			.7194	.7890	.8480	.8999	.9397	.9723	.9853
	$\mathfrak{v}$			2.069	1.639	1.390	1.225	1.126	1.054	1.027
	τ			1.5254	1.3444	1.1548	.9444	.7451	.5092	.3602
	λ			3.156	2.203	1.605	1.157	.839	.537	.370
1.5	$\mathfrak{V}_{\min}$			.7341	.7941	.8485	.8986	.9379	.9713	.9848
	$\mathfrak{v}$			1.919	1.572	1.365	1.215	1.123	1.053	1.028
	τ			1.4223	1.2550	1.0900	.8962	.7147	.4853	.3569
	λ			2.729	1.973	1.488	1.089	.803	.511	.367
2	$\mathfrak{V}_{\min}$		.6953	.7333	.7880	.8413	.8924	.9336	.9691	.9837
	$\mathfrak{v}$		2.089	1.807	1.537	1.348	1.211	1.123	1.053	1.028
	τ		1.4113	1.3181	1.1820	1.0302	.8573	.6910	.4697	.3487
	λ		2.948	2.382	1.817	1.389	1.038	.776	.495	.358
3	$\mathfrak{V}_{\min}$		.6735	.7101	.7660	.8228	.8790	.9250	.9650	.9814
	$\mathfrak{v}$		2.006	1.784	1.540	1.365	1.219	1.125	1.055	1.028
	τ		1.3166	1.2462	1.1325	1.0022	.8395	.6699	.4640	.3387
	λ		2.641	2.223	1.744	1.368	1.023	.754	.490	.348
5	$\mathfrak{V}_{\min}$		.6246	.6654	.7288	.7939	.8587	.9123	.9588	.9781
	$\mathfrak{v}$		2.103	1.856	1.592	1.393	1.239	1.135	1.060	1.031
	τ		1.2807	1.2186	1.1182	.9943	.8400	.6694	.4672	.3443
	λ		2.693	2.262	1.780	1.385	1.041	.760	.495	.355
10	$\mathfrak{V}_{\min}$	.4894	.5500	.5994	.6756	.7534	.8306	.8950	.9507	.9738
	$\mathfrak{v}$	2.803	2.323	2.018	1.689	1.450	1.271	1.146	1.066	1.034
	τ	1.3202	1.2682	1.2160	1.1233	1.0060	.8547	.6846	.4762	.3496
	λ	3.701	2.946	2.454	1.897	1.459	1.086	.785	.508	.361
20	$\mathfrak{V}_{\min}$	.4175	.4806	.5396	.6277	.7171	.8055			
	$\mathfrak{v}$	3.326	2.613	2.195	1.784	1.509	1.300			
	τ	1.3182	1.2705	1.2220	1.1334	1.0235	.8710			
	λ	4.384	3.320	2.682	2.022	1.544	1.132			
100	$\mathfrak{V}_{\min}$	.2750	.3640	.4393						
	$\mathfrak{v}$	4.810	3.236	2.549						
	τ	1.3193	1.2802	1.2368						
	λ	6.346	4.143	3.153						

However, a similar explanation will be seen in the investigation of bodily waves.

4. Velocity of Love-waves.

Using new notations

$$f = k\sin\theta, \quad k' = k\sin\theta_0, \quad kH = \omega \qquad \text{..........(4.1)}$$

we have from (3.2)

$$\omega_n = \sec\theta[\mathrm{Tan}^{-1}\{\chi\sec\theta\sqrt{(\sin^2\theta - \sin^2\theta_0)}\} + n\pi] \qquad \text{......(4.2)}$$

Tan^{-1} means the principal value of inverse tangent function and the suffix n implies the number of node in the layer.

Displacement in the surface layer is expressed as

$$\begin{aligned} v \propto & \exp\{ik(x\sin\theta + z\cos\theta - V_s t)\} \\ & + \exp\{ik(x\sin\theta - z\cos\theta - V_s t)\} \qquad \text{..............(4.3)} \end{aligned}$$

therefore θ is the angle between the direction of wave path and z-axis. By means of this variable, the velocity is expressed as cosec θ, and the period of waves as $2\pi/\omega$.

Now, we will show the results of calculations; here two parameters $\chi\,(=\mu'/\mu)$ and $\sin\theta_0\,(=k'/k = V_s/V_s')$ are used.

On considering the physical constants of elastic substances which commonly exist around us, we notice that the values of elastic constants vary very widely. On the contrary it is very seldom that the ratio of density of two substances arbitrarily chosen amounts to as large as ten. While the value of $\sin^2\theta_0$ is always smaller than unity, consequently the possible range of values of two parameters is naturally determined.

Under the condition $1/10 \leq \rho'/\rho \leq 10$ we chose 76 pairs of χ and $\sin^2\theta_0$ which is shown in Tab. I, and calculated the value of cosec θ ($= \mathfrak{v} =$ velocity of Love-waves whose unit is V_s) and ω_0 and ω_1 (=circular frequency, time unit is H/V_s) with every degree of θ from θ_0 to 90°. The reason why we did not calculate the branch $\omega_2, \omega_3 \ldots$ and so on, will be found in the later part of our study.

4.1 Minimum value of group velocity.

The importance of the minimum value of group velocity has been already noticed by several authors; for example, K. Sezawa and K. Kanai's

M_2 waves[8] correspond to the minimum group velocity of certain branch of layered Rayleigh-waves, and recently an interesting investigation was published by a number of authors in America.[9] We will here show, using the above numerical data, the minimum group velocity and the corresponding phase velocity and period of every branch of Love-waves. (Tabs. II~III and Figs. 4~7.)

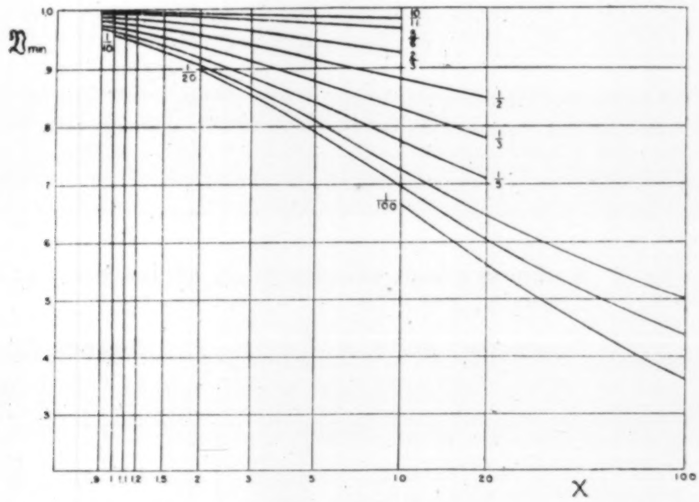

Fig. 4 Minimum group velocity $\mathfrak{V}_{\min}$ of Love-waves.
Abscissa ; $\chi = \mu'/\mu$

Parameter ; $\text{Sin}^2\theta_0 = \left(\frac{\mu}{\rho}\right) \Big/ \left(\frac{\mu'}{\rho'}\right)$ (Branch L_0)

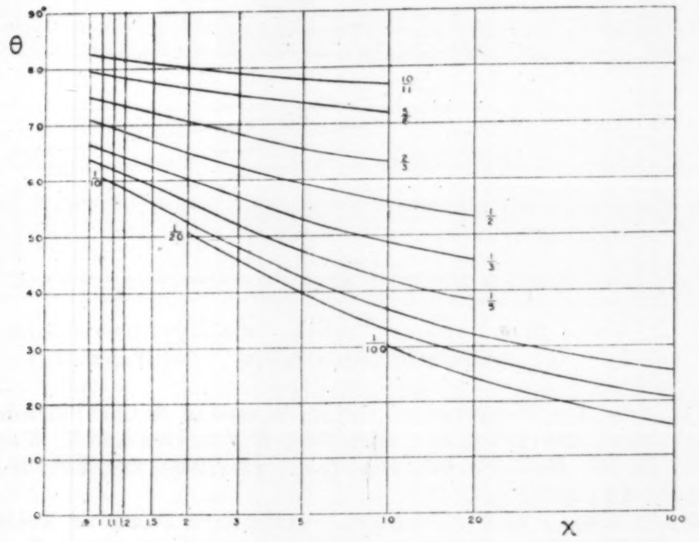

Fig. 5 Value of θ (=cosec^{-1} (phase velocity)) corresponding to minimum group velocity. (Branch L_0)

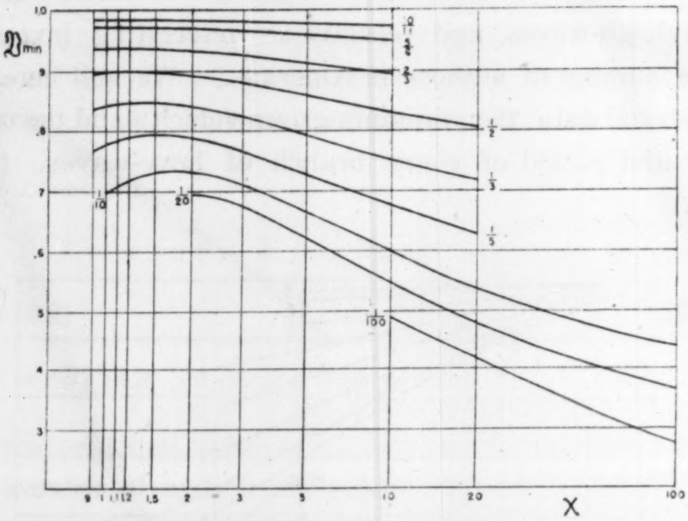

Flg. 6 Minimum group velocity $\mathfrak{B}_{\min}$ of Love-waves.
Abscissa ; $\chi = \mu'/\mu$
Parameter ; $\text{Sin}^2\,\theta_0 = \left(\dfrac{\mu}{\rho}\right) \Big/ \left(\dfrac{\mu'}{\rho'}\right)$ (Barnch L_1)

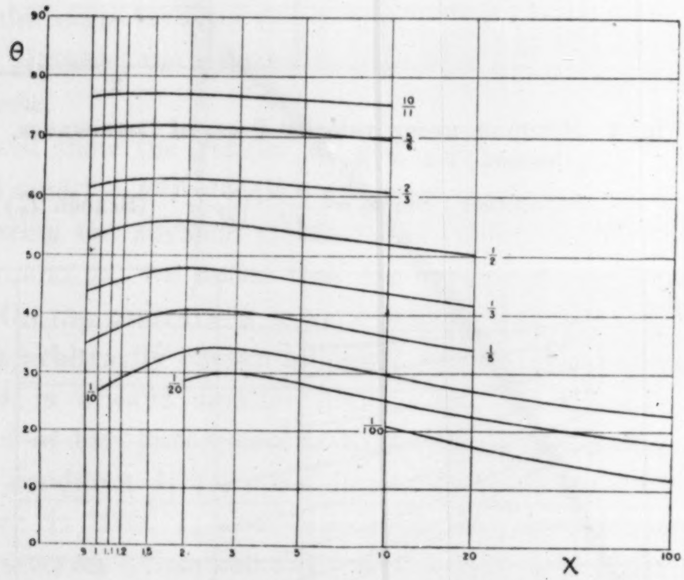

Fig. 7 Value of θ (=cosec^{-1} (phase velocity)) corresponding to minimum group velocity. (Branch L_1)

---

8) K. KANAI, "On the Existence of the M_2 Waves in Actual Seismic Disturbance", *Bull Earthq. Res. Inst.*, **26** (1948), 57. Also See. K. SEZAWA and K. KANAI, *Proc. Imp. Acad.*, **11** (1935), 13, 96; *Bull. Earthq. Res. Inst.*, **13** (1935), 237, 471; K. SEZAWA, *Bull. Earthq. Res. Inst.*, **16** (1938), 1.

9) F. PRESS, M. EWING and I. TOLSTOY, "The Airy Phase of Shallow Fucus Submarine Earthquakes." *Bull. Seism. Soc. Amer.*, **40** (1950), 111. C. ECKART, "The Approximate Solution of One-Dimensional Wave Equations." *Rev. Mod. Phys.*, **20** (1948), 399.

Further for convenience of calculations concerning Love-waves, we will show various forms of characteristic equation.

One of the most fundamental forms is

$$(\mu'\beta' + i\mu\tilde{\beta}) \exp (i\tilde{\beta}H) + (\mu'\beta' - i\mu\tilde{\beta}) \exp (-i\tilde{\beta}H) = 0 \quad \ldots\ldots (4.4)$$

Considering that $\tilde{\beta}$ and β' are real, with slight transformation we get the three following forms;

$$\begin{aligned} &\exp (i2\tilde{\beta}H) = -(\chi\beta' - i\tilde{\beta})/(\chi\beta' + i\tilde{\beta}), \ \chi = \mu'/\mu \\ &\tan \tilde{\beta}H = \chi\beta'/\tilde{\beta} \quad \ldots\ldots\ldots\ldots\ldots\ldots\ldots\ldots (4.5) \\ &-\boldsymbol{\theta} + \tilde{\beta}H = n\pi, \ \boldsymbol{\theta} = \mathrm{Tan}^{-1}(\chi\beta'/\tilde{\beta}) \end{aligned}$$

For numerical calculations, non-dimensional notations are desirable; therefore putting

$$fH = \xi, \ kH = \omega, \ V/V_s = \mathfrak{v} = \operatorname{cosec} \theta$$

we have

$$\begin{aligned} &\tan (\xi\sqrt{(\mathfrak{v}^2 - 1)}) = \chi\sqrt{(1 - \mathfrak{v}^2 \sin^2\theta_0)}/\sqrt{(\mathfrak{v}^2 - 1)} \\ &\qquad\qquad \sin^2\theta_0 = k'^2/k^2 = V_s^2/V_s'^2 \quad \ldots\ldots (4.6) \\ &\omega_n = \sec \boldsymbol{\theta}[\mathrm{Tan}^{-1}\{\chi \sec \theta\sqrt{(\sin^2\theta - \sin^2\theta_0)}\} + n\pi] \end{aligned}$$

We used this last form of equation for our calculation.

---

1. 表面波の研究 I

ラブ波の速度

地震研究所　佐藤泰夫

半無限彈性體，又はそれに表面層がある場合の表面波の研究は，從來多くの大家によつて研究されてゐるが，なほ十分とはいへない．

ここでは先づラブ波について考へ，その速度方程式を變形して調べてみることにより，分光器として使はれる Lummer-Gehrcke 板の作用と極めて似てゐる事を示した．

次に上層と下部の速度の比 Sin $\theta_0 = V_s/V_s'$ 及び剛性率の比 $\chi = \mu'/\mu$ を色々に與へて，實在しうるやうな組合せ 76 通りについて，ラブ波の基本分枝 L_0 と節を一つもつ分枝 L_1 の位相速度を求め，さらにこれからラブ波の極小群速変を出した，この速度に相當する時よりも後に到着した波は，ラブ波としては解釋されない．

2. *Seismic Focus without Rayleigh-Waves.*

By Yasuo Satô,

Earthquake Research Institute.

(Read Sept. 20, 1949.—Received Dec. 20, 1950.)

1. Introduction.

It is clearly verified, practically and theoretically that when some force acts upon or within a semi-infinite elastic body, certain waves with special velocity are propagated along the plane surface. Today, these waves are called Rayleigh-waves and nobody doubts their existence. However the mechanism of the generation of these waves are not yet fully understood. Although great efforts are being made[1] to make clear this problem, we do not know how the energy of Rayleigh-waves is supplied and how the waves with velocity different from either P or S can grow and be maintained. And it seems to us that if a certain origin without Rayleigh-waves should exist, and further, if it should lack some property which is inherent in an origin which radiates Rayleigh-waves, then this property must be closely connected with the generation of them. However, can such a seismic origin exist? Can it have or lack such a special property? We will treat these problems in the following articles.

2. Solutions satisfying boundary conditions.

At first we will assume a seismic origin of a dilatational type. We take a scalar potential

$$\Phi = A_n^m \cdot (hR)^{-\frac{1}{2}} H_{n+\frac{1}{2}}^{(2)}(hR) \bar{P}_n^m(\cos\theta) \exp\{\pm im\varphi\} \exp\{ipt\} \quad \ldots\ldots (2.1)$$

in which R, θ, φ are spherical coordinates

and $h = ap = p/V_P = p/\{(\lambda+2\mu)/\rho\}^{\frac{1}{2}}$, ($\rho$, λ, μ are density and Lamé's constants)

---

[1] e.g. H. Jeffreys, "The Formation of Love Waves", *Beitr. z. Geophys.*, **30** (1931), 336, K. Sezawa and K. Kanai, "The Action of Soil Loyers and of the Ocean as Dynamic Dampers to Seismic Surface Waves, and Notes on a Few Previous Papers," *Bull. Earthq. Res. Inst.*, **18** (1940), 150~168. T. Hirono, "Mathematical Theory of Shallow Earthquake," *Geophys. Mag.*, **21** (1949), 1.

$$\bar{P}_n^m(\zeta) = (1-\zeta^2)^{m/2}\left(\frac{d}{d\zeta}\right)^m P_n(\zeta)$$

$H_\nu^{(\ )}(\zeta)$ means Hankel's function.

If this focus is situated at $z = -d$ (xy-plane coincides with the free surface and z-axis is taken vertically upwards), then the above expression takes the following form[2] (omitting time factor exp {ipt})

$$\begin{aligned}\Phi &= A_n^m \mu_n^m h^{-2} \exp\{\pm im\varphi\}\int_0^\infty J_m(rs)\, P_n^m\{(h^2-s^2)^{\frac{1}{2}}/h\}\exp\{-i(h^2-s^2)^{\frac{1}{2}}(d+z)\} \\ &\qquad \cdot \{h/(h^2-s^2)^{\frac{1}{2}}\}sds \\ r^2 &= x^2+y^2 \\ \mu_n^m &= \pi^{-\frac{1}{2}}2^{\frac{1}{2}}\, i^{n-2m} \qquad \dots\dots\dots\dots\dots(2.2) \\ P_n^m(\zeta) &= (\zeta^2-1)^{m/2}\left(\frac{d}{d\zeta}\right)^m P_n(\zeta)\end{aligned}$$

and $J_m(\ )$ means Bessel function.

As already known by the past study of the generation of Rayleigh-waves, the displacement vector ϑ in the above case is obtained by the next formula[3]

$$\vartheta = \operatorname{grad}(\Phi+\Phi^1) + \operatorname{rot}\operatorname{rot}(0,0,\Pi^1) \quad \dots\dots\dots\dots(2.3)$$

or

$$\vartheta_x = \frac{\partial}{\partial x}(\Phi+\Phi^1) + \frac{\partial^2}{\partial x\partial z}\Pi^1$$

$$\vartheta_z = \frac{\partial}{\partial z}(\Phi+\Phi^1) - \left(\frac{\partial^2}{\partial x^2}+\frac{\partial^2}{\partial y^2}\right)\Pi^1 \quad \dots\dots\dots\dots(2.4)$$

and stress components are

$$\left\{\begin{aligned}\widehat{xz} &= \mu\left\{2\frac{\partial^2}{\partial x\partial z}(\Phi+\Phi^1) + \left(\frac{\partial^3}{\partial x\partial z^2} - \frac{\partial^3}{\partial x^3} - \frac{\partial^3}{\partial x\partial y^2}\right)\Pi^1\right\} \\ \widehat{zz} &= \lambda\Gamma^2(\Phi+\Phi^1) + 2\mu\frac{\partial^2}{\partial z^2}(\Phi+\Phi^1) - 2\mu\left\{\frac{\partial^3}{\partial x^2\partial z} + \frac{\partial^3}{\partial x^2\partial z}\right\}\Pi^1 \dots(2.5)\end{aligned}\right.$$

where Φ^1 is interpreted as reflected P-waves, and Π^1 as reflected S waves. The expressions of Φ^1 ane Π^1 take the following forms ;

---

2) Y. Satô, "Transformation of Wave-functions related to the Transformation of Coordinates Systems." *Bull. Earthq. Res. Inst.*, **28** (1949), 1.

3) e.g. S. Syôno, "On the Propagation of Tremors over the Plane Surface of a Semi-Infinite Perfect Elastic Solid." (1) *Geophys. Mag.*, **12** (1938), 67.

$$\left\{\begin{aligned} \Phi^1 &= A_n^m \mu_n^m h^{-2} \exp\{\pm im\varphi\} \int_0^\infty S\cdot J_m(rs)\, P_n^m\{(h^2-s^2)^{\frac{1}{2}}/h\} \\ &\qquad \cdot \exp\{-i(h^2-s^2)^{\frac{1}{2}}(d-z)\}\cdot\{h/(h^2-s^2)^{\frac{1}{2}}\}sds \\ \Pi^1 &= A_n^m \mu_n^m h^{-2} \exp\{\pm im\varphi\} \int_0^\infty T\cdot J_m(rs)\, P_n^m\{(h^2-s^2)^{\frac{1}{2}}/h\} \\ &\qquad \cdot \exp\{-i(h^2-s^2)^{\frac{1}{2}}d + i(k^2-s^2)^{\frac{1}{2}}z\}\cdot\{h/(h^2-s^2)^{\frac{1}{2}}\}sds \end{aligned}\right. \qquad \ldots.(2.6)$$

The explicit expression of S and T must be determined by the boundary conditions which are known as

$$\widehat{xz} = \widehat{yz} = \widehat{zz} = 0 \quad \text{at} \quad z = 0 \quad \ldots\ldots\ldots\ldots\ldots\ldots\ldots\ldots(2.7)$$

Therefore

$$\left\{\begin{aligned} &\lambda\nabla^2(\Phi+\Phi^1) + 2\mu\frac{\partial^2}{\partial z^2}(\Phi+\Phi^1) - 2\mu\Big(\frac{\partial^3}{\partial x^2\partial z} + \frac{\partial^3}{\partial y^2\partial z}\Big)\Pi^1 = 0 \\ &2\frac{\partial}{\partial z}(\Phi+\Phi^1) + \Big(\frac{\partial^2}{\partial z^2} - \frac{\partial^2}{\partial x^2} - \frac{\partial^2}{\partial y^2}\Big)\Pi^1 = 0 \end{aligned}\right. \quad \ldots\ldots\ldots\ldots(2.8)$$

Since Φ and Φ^1 satisfy the differential equation of the form $\nabla^2\Phi = -h^2\Phi$ and Π^1 satisfies $\nabla^2\Pi^1 = -k^2\Pi^1$ $(k^2 = b^2p^2 = p^2/V_s^2 = p^2.(\mu/\rho))$, (2.8) is somewhat simplified by the aid of this relation and the following two expressions must hold at the boundary surface.

$$\left\{\begin{aligned} &\int_0^\infty\Big[\Big\{-(\gamma^2-2)h^2 + 2\frac{\partial^2}{\partial z^2}\Big\}\cdot\exp\{-i(h^2-s^2)^{\frac{1}{2}}z\} \\ &\qquad + \Big\{-(\gamma^2-2)h^2 + 2\frac{\partial^2}{\partial z^2}\Big\}\cdot S\exp\{i(h^2-s^2)^{\frac{1}{2}}z\} \\ &\qquad + \Big\{2k^2\frac{\partial}{\partial z} + 2\frac{\partial^3}{\partial z^3}\Big\}\cdot T\exp\Big\{i(k^2-s^2)^{\frac{1}{2}}z\Big\}\Big] \\ &\qquad \cdot J_m(rs)\,P_n^m\{(h^2-s^2)^{\frac{1}{2}}/h\}\cdot\exp\{-i(h^2-s^2)^{\frac{1}{2}}d\}\cdot\{h/(h^2-s^2)^{\frac{1}{2}}\}sds \\ &\int_0^\infty\Big[2\frac{\partial}{\partial z}\exp\{-i(h^2-s^2)^{\frac{1}{2}}z\} + 2\frac{\partial}{\partial z}S\exp\{i(h^2-s^2)^{\frac{1}{2}}z\} + \Big\{2\frac{\partial^2}{\partial z^2} + k^2\Big\}T\Big] \\ &\qquad \cdot J_m(rs)\,P_n^m\{(h^2-s^2)^{\frac{1}{2}}/h\}\cdot\exp\{-i(h^2-s^2)^{\frac{1}{2}}d\}\cdot\{h/(h^2-s^2)^{\frac{1}{2}}\}sds \end{aligned}\right.$$

$$\ldots\ldots\ldots\ldots\ldots\ldots\ldots(2.9)$$

where $\gamma^2 = (\lambda + 2\mu)/\mu$

Since these two integral expressions must hold without regard to r, we may equate the two parentheses [ ] to zero ; therefore we have

$$\begin{cases} \{-\gamma^2h^2 + 2s^2\}S + i2(k^2 - s^2)^{\frac{1}{2}}s^2T = -\{-\gamma^2h^2 + 2s^2\} \\ i2(h^2 - s^2)^{\frac{1}{2}}S + (2s^2 - k^2)T = i2(h^2 - s^2) \end{cases} \qquad \ldots\ldots\ldots\ldots\ldots(2.10)$$

Solving these equations

$$S = H/D, \qquad T = J/D \quad ,$$

where

$$\begin{aligned} D &= (2s^2 - k^2)^2 + 4s^2\tilde{\alpha}\tilde{\beta} \quad , \qquad \tilde{\alpha} = (h^2 - s^2)^{\frac{1}{2}} \\ H &= -(2s^2 - k^2)^2 + 4s^2\tilde{\alpha}\tilde{\beta} \quad , \qquad \tilde{\beta} = (k^2 - s^2)^{\frac{1}{2}} \ldots\ldots(2.11) \\ J &= i4(2s^2 - k^2)\tilde{\alpha} \end{aligned}$$

We intoroduce (2.11) into (2.2) and (2.6), and get

$$\begin{cases} \Phi = A_n^m\mu_n^m h^{-2}\cdot\exp\{\pm im\varphi\}\int_0^\infty J_m(rs)\,P_n^m\{\tilde{\alpha}/h\}\exp\{-i\tilde{\alpha}(d+z)\}(h/\tilde{\alpha})sds \\ \Phi' = A_n^m\mu_n^m h^{-2}\cdot\exp\{\pm im\varphi\}\int_0^\infty \frac{H}{D}J_m(rs)\,P_n^m\{\tilde{\alpha}/h\}\exp\{-i\tilde{\alpha}(d-z)\}(h/\tilde{\alpha})sds \\ \Psi' = A_n^m\mu_n^m h^{-2}\cdot\exp\{\pm im\varphi\}\int_0^\infty \frac{J}{D}J_m(rs)P_n^m\{\tilde{\alpha}/h\}\exp\{-i\tilde{\alpha}d+i\tilde{\beta}z\}(h/\tilde{\alpha})sds \end{cases}$$

$$\ldots\ldots\ldots\ldots(2.12)$$

3. Displacement components of Rayleigh-waves.

The vertical distribution of the amplitude of Rayleigh-waves is uniquely determined by Poisson's ratio of the elastic medium ; so that, if the surface amplitude of both components of displacement vanish, not even a single train of Rayleigh-wave can exist in this medium.

Introducing (2.12) into (2.4) we have at once

$$\vartheta_x = A_n^m\mu_n^m h^{-2}\frac{\partial}{\partial x}\exp\{\pm im\varphi\}\int_0^\infty J_m(rs)\,P_n^m\{\tilde{\alpha}/h\}\exp\{-i\tilde{\alpha}d\}$$

$$\cdot\left\{\exp(-i\tilde{\alpha}z) + \frac{H}{D}\exp(i\tilde{\alpha}z) + \frac{J}{D}i\tilde{\beta}\exp(i\tilde{\beta}z)\right\}(h/\tilde{\alpha})sds \quad ..(3.1)$$

At the free surface $z = 0$ the above expression can be written as

$$\vartheta_x = A_n^m\mu_n^m h^{-2}\cdot 4hk^2\cdot\frac{\partial}{\partial x}\exp\{\pm im\varphi\}\int_0^\infty J_m(rs)P_n^m\{\tilde{\alpha}/h\}\exp\{-i\tilde{\alpha}d\}\frac{1}{D}\tilde{\beta}sds$$

$$\ldots\ldots(3.2)$$

and ϑ_y is obtained from (3.2) by substituting y for x. Similarly

$$\vartheta_z = A_n^m \mu_n^m h^{-2} \cdot i2hk^2 \cdot \exp\{\pm im\varphi\} \int_0^\infty J_m(rs) P_n^m\{\tilde{\alpha}/h\} \exp\{-i\tilde{\alpha}d\} \frac{1}{D}(2s^2 - k^2) s ds \qquad \ldots\ldots\ldots(3.3)$$

Since

$$J_m(rs) = \frac{1}{2}\{H_m^{(1)}(rs) + H_m^{(2)}(rs)\}, \quad H_m^{(2)}(-rs) = (-)^{m+1} H_m^{(1)}(rs) \qquad \ldots(3.4)$$

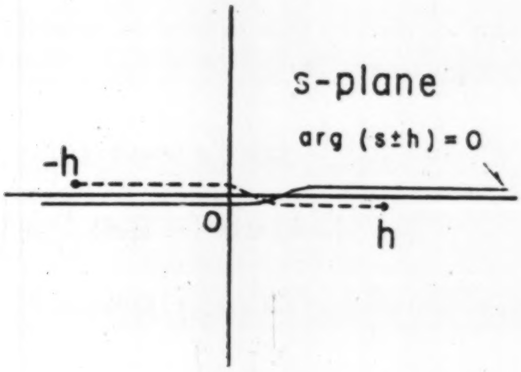

Fig. 1

and the sign of $\tilde{\alpha} = \sqrt{(h^2 - s^2)}$ should be taken as is shown in Fig. 1, the above two integrations are transformed into the next form

$$\vartheta_x = A_n^m \mu_n^m \cdot 2h^{-1} k^2 \frac{\partial}{\partial x} \exp\{\pm im\varphi\} \int_{-\infty}^\infty H_m^{(1)}(rs)\, P_n^m\{\tilde{\alpha}/h\} \exp\{-i\tilde{\alpha}d\} \frac{1}{D} \tilde{\beta} s ds \qquad \ldots\ldots\ldots(3.5)$$

and

$$\vartheta_z = A_n^m \mu_n^m \cdot ih^{-1} k^2 \exp\{\pm im\varphi\} \int_{-\infty}^\infty H_m^{(1)}(rs) P_n^m\{\tilde{\alpha}/h\} \exp\{-i\tilde{\alpha}d\} \frac{1}{D}(2s^2 - k^2) s ds$$

From these integral representations, displacement components of Rayleigh-waves are, multiplying $2\pi i$ to the residue of the integrand,

$$\left\{\begin{aligned} \vartheta_x[R] &= 2\pi i A_n^m \mu_n^m \cdot 2h^{-1} k^2 \Big[\frac{\partial}{\partial x} \exp\{\pm im\varphi\} \cdot H_m^{(1)}(rs) \\ &\qquad \cdot P_n^m\{\tilde{\alpha}/h\} \exp\{-i\tilde{\alpha}d\} \frac{1}{D} \tilde{\beta} s\Big]_{s=K} \\ \vartheta_z[R] &= 2\pi i \cdot A_n^m \mu_n^m \cdot ih^{-1} k^2 \Big[\exp\{\pm im\varphi\} \cdot H_m^{(1)}(rs) \\ &\qquad \cdot P_n^m\{\tilde{\alpha}/h\} \exp\{-i\tilde{\alpha}d\} \cdot \frac{1}{D}(2s^2 - k^2) s\Big]_{s=K} \end{aligned}\right. \qquad \ldots\ldots\ldots(3.6)$$

where K is the root of $D = 0$.

4. Superposition of two seismic origins.

Now we will consider another seismic origin which is specified by a scalar potential Φ' situated at the same point with the former one.

$$\Phi' = A^m_{n'}\mu^m_{n'}\exp\{\pm im\varphi\}\int_0^\infty J_m(rs)P^m_{n'}\{a/h\}\cdot\exp\{-i\tilde{\alpha}(z+d)\}(h/\tilde{\alpha})sds \quad ..(4.1)$$

Displacement vector ϑ' due to this origin is readily gained from (3.5) and the phase of Rayleigh-waves is

$$\left\{\begin{aligned} \vartheta'_x[R] &= 2\pi i\cdot A^m_{n'}\mu^m_{n'}\cdot 2h^{-1}k^2\Big[\frac{\partial}{\partial x}\exp\{\pm im\varphi\}\cdot H^{(1)}_m(rs) \\ &\qquad \cdot P^m_{n'}\{\tilde{\alpha}/h\}\exp\{-i\tilde{\alpha}d\}\frac{1}{D}\tilde{\beta}s\Big]_{s=K} \quad ......(4.2) \\ \vartheta'_z[R] &= 2\pi i\cdot A^m_{n'}\mu^m_{n}\cdot ih^{-1}k^2\Big[\exp\{\pm im\varphi\}\cdot H^{(1)}_m(rs) \\ &\qquad \cdot P^m_{n'}\{\tilde{\alpha}/h\}\exp\{-i\tilde{\alpha}d\}\frac{1}{D}(2s^2-k^2)s\Big]_{s=K} \end{aligned}\right.$$

Comparing the two pairs of expressions (3.6) and (4.2), we easily notice that $\vartheta_r[R]$, $\vartheta_z[R]$ and $\vartheta_x'[R]$, $\vartheta_z'[R]$ are quite similar in form; the only difference between them are the factors $A^m_n\mu^m_nP^m_n\{\tilde{\alpha}/h\}_{s=K}$ and $A^m_{n'}\mu^m_{n'}P^m_{n'}\{\tilde{\alpha}/h\}_{s=K}$. Therefore, if the two origins are superposed, and besides, if the relation

$$\Big[A^m_n\mu^m_nP^m_n\{\tilde{\alpha}/h\}+A^m_{n'}\mu^m_{n'}P^m_{n'}\{\tilde{\alpha}/h\}\Big]_{s=K}=0 \quad ....(4.3)$$

holds, then the Rayleigh-waves generated from these origins, which are situated at the same point $x=y=0$ and $z=-d$, will cancel each other and no Rayleigh-waves will be observed.

As is clear from the expressions (3.5) or (4.1), above relation holds without regard to epicentral distance r, azimuthal angle φ and focal depth d. Moreover, the condition (4.3) contains no function concerning time, hence Rayleigh-waves can never be generated from the seismic origin of the above type, even if the time factor may take an arbitrary functional form.

5. Numerieal calculations.

In this article we will perform the numerical calculations assuming $\lambda=\mu$.

When $\lambda=\mu$

$$K^2/h^2 = 3(3+\sqrt{3})/4 = 3.54904$$

$$[\tilde{\alpha}/h]_{s=K} = -i\,1.59656 \quad \ldots\ldots\ldots\ldots\ldots\ldots\ldots\ldots(5.1)$$

therefore we have from (4.3)

$$\frac{A_{n'}^m}{A_n^m} = -\frac{\mu_n^m}{\mu_{n'}^m}\left[\frac{P_n^m\{\tilde{\alpha}/h\}}{P_{n'}^m\{\tilde{\alpha}/h\}}\right]_{s=K} = -i^{n-n'}\frac{P_n^{(m)}\{-i\,1.59656\}}{P_{n'}^{(m)}\{-i\,1.59656\}} \quad \ldots\ldots(5.2)$$

where $\qquad P_n^{(m)}(\zeta) = (d/d\zeta)^m P_n(\zeta)$

Results of calculations are as follows;

$$\begin{array}{lll}
A_1^0/A_0^0 = -0.62637, & & \\
A_2^0/A_0^0 = -0.23129, & A_2^0/A_1^0 = -0.39627, & \\
A_3^0/A_0^0 = -0.07956, & A_3^0/A_1^0 = -0.12702, & A_3^0/A_2^0 = -0.34398 \\
 & A_2^1/A_1^1 = -0.20878, & \\
 & A_3^1/A_1^1 = -0.04850, & A_3^1/A_2^1 = -0.23257 \\
 & & A_3^2/A_2^2 = -0.12527 \\
 & & \ldots\ldots\ldots\ldots\ldots\ldots(5.3)
\end{array}$$

6. Conclusions.

By the calculations so far obtained, we have seen that seismic origin which radiates no Rayleigh-waves can exist. If two origins which are of the type (2.1) and (4.1) and which satisfy one of the relations shown in (5.3), are superposed, we will observe no Rayleigh-waves. Thus we have made clear the first problem in § 1, however, we cannot reply in the affirmative to the second problem. Even if we examine the nature of the origin specified by (5.3), we can scarcely discover the property which we had expected at the beginning of this study.

When we look at seismograms we often notice that while one seismogram shows a remarkably large surface wave phase, another seismogram on the contrary shows hardly any evidence of the same phase. Hitherto these phenomena were attributed solely to the depth of foci, and not to the mechanism of them. But, as we have seen in this paper we should also pay attention to the latter cause.

Next, consider a seismic origin of a dilatational type

$$A_n^{m\prime}\cdot(hR)^{-\frac{1}{2}}H_{n+\frac{1}{2}}^{(2)}(hR)\,\bar{P}_n^m(\cos\theta')\exp\{\pm im\varphi'\}\exp\{ipt\}$$

$$+\ A_{n'}^{m\prime}\cdot(hR)^{-\frac{1}{2}}H_{n'+\frac{1}{2}}^{(2)}(hR)\,\bar{P}_{n'}^m(\cos\theta')\exp\{\pm im\varphi'\}\exp\{ipt\},\ \ldots(6.1)$$

where the spherical coordinates R, θ', φ' refer to the same origin with above, but to the different axes x', y', z', and $A_n^{m\prime}$ and $A_{n'}^{m\prime}$ satisfy the relation (5.2). If the axes x', y', z' coincide with the former axes x, y, z, the focus (6.1) naturally radiate no Rayleigh-waves. Now, if z' axis does not coincide with z, what will happen in this case?

For brevity we will take a simple example; putting $m = 0, n = 0, n' = 1$ into (6.1) we have

$$\Big[A_0^{0\prime}\cdot(hR)^{-\frac{1}{2}}H_{\frac{1}{2}}^{(2)}(hR) + A_1^{0\prime}\cdot(hR)^{-\frac{1}{2}}H_{\frac{3}{2}}^{(2)}(hR)\,P_1(\cos\theta')\Big]\exp\{ipt\}\ldots\ldots(6.2)$$

Referring to (x, y, z)-system, (6.2) can be transformed into the following form

$$\Big[A_0^{0\prime}\cdot(hR)^{-\frac{1}{2}}H_{\frac{1}{2}}^{(2)}(hR) + A_1^{0\prime}\cdot(hR)^{-\frac{1}{2}}H_{\frac{3}{2}}^{(2)}(hR)\Big\{\mathfrak{A}_1^0 P_1(\cos\theta) + (\mathfrak{A}_1^1\cos\varphi + \mathfrak{B}_1^1\sin\varphi)\,\bar{P}_1^1(\cos\theta)\Big\}\Big]\exp\{ipt\}\ldots\ldots(6.3)$$

A glance at the last line will show that this focus generates Rayleigh-waves. Hence the said property is not inherent in the mechanism of the focus itself, but consists in the relation between the free surface and the focus.

---

2. レーリー波を發生しない震源

地震研究所　　佐　藤　泰　夫

半無限体内にある震源で，レーリー波を發生しないやうなものが存在し得ることを証明した．簡單な例をあげれば，(自由表面に垂直に軸をとり，これを基準にして θ をはかれば)

$$\Phi = (hR)^{-\frac{1}{2}}\Big[H_{\frac{1}{2}}^{(2)}(hR) - 0.23129\ H_{\frac{5}{2}}^{(2)}(hR)\,P_2(\cos\theta)\Big]f(t)$$

で表はされる震源などはその一つである．ここに $f(t)$ は t の勝手な函數である．

しかしこの震源が，何か明かにわかる特殊の性質をもつてゐるか，といへば，答は否定的である．又たとへ上と同じ力の加はり方をしても，z 軸が自由表面に垂直でない場合にはレーリー波は必ず發生する．

3. *Mathematical Study of the Propagation of Waves upon Stratified Medium.* (2)

By Yasuo SATÔ,

Earthquake Research Institute.

(Read Dec. 16, 1947.—Received Dec. 20, 1950.)

In the previous paper,[1] we have shown the way of getting asymptotic expansions of the integral of the form $\int_a^b \substack{\cos \\ \sin} \xi x \, F(\xi) \, d\xi$, and the main results obtained are as follows;

When $F(\xi)$ is differentiable at the closed domain $[a, b]$

$$\begin{aligned}\int_a^b F(\xi) \substack{\cos \\ \sin} \xi x d\xi = {} & x^{-1}\Big[\pm F(b) \substack{\sin \\ \cos} bx \mp F(a) \substack{\sin \\ \cos} ax\Big] \\ & + x^{-2}\Big[F'(b) \substack{\cos \\ \sin} bx - F'(a) \substack{\cos \\ \sin} ax\Big] \\ & + x^{-3}\Big[\mp F''(b) \substack{\sin \\ \cos} bx \pm F''(a) \substack{\sin \\ \cos} ax\Big] \qquad ..(2.1),\ (2.2) \\ & + x^{-4}\Big[-F'''(b) \substack{\cos \\ \sin} bx + F'''(a) \substack{\cos \\ \sin} ax\Big] + \dots\end{aligned}$$

When $F(\xi)$ contains $\sqrt{\xi^2 - a^2}$

$$\begin{aligned}\int_a^b F(\xi) \substack{\cos \\ \sin} \xi x \, d\xi = {} & x^{-\frac{1}{2}} F_{-1}(a) \sqrt{\pi} \cdot \substack{\cos \\ \sin} (ax + \pi/4) \\ & + x^{-1}\Big[\pm F(b) \substack{\sin \\ \cos} bx \mp F_0(a) \substack{\sin \\ \cos} ax\Big] \qquad ..(3.5),\ (3.6) \\ & \mp x^{-\frac{3}{2}} F_1(a) \frac{1}{2} \sqrt{\pi} \cdot \substack{\sin \\ \cos} (ax + \pi/4) + x^{-2}[\cdots\cdot] + \dots\end{aligned}$$

in which $F_{-1}(a)$, $F_1(a)$... are defined by the following expression

$$F(\xi) = F_{-1}(a) \ (\xi - a)^{-\frac{1}{2}} + F_0(a) + F_1(a) \cdot (\xi - a)^{\frac{1}{2}} + F_2(a) \cdot (\xi - a) + \dots..$$

When $F(\xi)$ contains $\sqrt{\xi^2 - b^2}$.

$$\begin{aligned}\int_a^b F(\xi) \substack{\cos \\ \sin} \xi x d\xi = {} & \mp i x^{-\frac{1}{2}} F_{-1}(b) \sqrt{\pi} \cdot \substack{\sin \\ \cos} (bx + \pi/4) \\ & + x^{-1}\Big[\pm F_0(b) \substack{\sin \\ \cos} bx \mp F(a) \substack{\sin \\ \cos} ax\Big] \qquad ..(3.7),\ (3.8) \\ & - i x^{-\frac{3}{2}} F_1(b) \frac{1}{2} \sqrt{\pi} \cdot \substack{\cos \\ \sin} (bx + \pi/4) + x^{-2}[\cdots\cdot] + \dots\end{aligned}$$

in which $F_{-1}(b)$, $F_1(b)$... are defined by a similar expression with the above case.

---

1) Y. SATÔ, *Bull. Earthq. Res. Inst.*, **26** (1948), 1.

When $F(\xi)$ contains $\sqrt{\xi^2-c^2}$, where $a<c<b$.

$$\int_a^b F(\xi)\begin{matrix}\cos\\ \sin\end{matrix}\xi x\,d\xi = x^{-\frac{1}{2}}F_{-1}(c)\sqrt{\pi}\cdot\exp\{-i(cx\pm\pi/4)\}$$

$$+\,x^{-1}[F(b)\begin{matrix}\sin\\ \cos\end{matrix}bx - F(a)\begin{matrix}\sin\\ \cos\end{matrix}ax] \qquad \ldots\ldots(4.1)$$

$$\mp x^{-\frac{3}{2}}F_1(c)\frac{1}{2}\sqrt{\pi}\cdot\exp\{-i(cx\mp\pi/4)\}+x^{-2}[\cdots\cdot]+\cdots$$

and for convenience of practical use, we have described a small lemma;

When $F(\xi)$ is expressed as

$$F(\xi) = A_{-1}(\xi)\cdot(\xi^2-c^2)^{-\frac{1}{2}} + A_0(\xi) + A_1(\xi)(\xi^2-c^2)^{\frac{1}{2}} + \cdots\cdot \qquad \ldots(5.1)$$

where $A_{-1}(\xi)$, $A_0(\xi)\ldots$ are functions that are identically zero, or not zero and differentiable at $\xi=c$, then $F(\xi)$ may be developed in the following scheme

$$F(\xi) = A_{-1}(c)\cdot(2c)^{-\frac{1}{2}}(\xi-c)^{-\frac{1}{2}} + A_0(c)$$

$$+\{-A_{-1}(c)/4c + A_1'(c) + A_1(c)\cdot 2c\}\,(2c)^{-\frac{1}{2}}(\xi-c)^{\frac{1}{2}} + \cdots \qquad (5.2)$$

§ 6. Examples.

In the first report we could not give applied examples of our formulae owing to limited space. Now we will show it in this report.

As the first example we will adopt

$$I(x) = I_c(x) + iI_s(x) = \frac{2}{\pi}\int_1^\infty \frac{1}{\sqrt{(\xi^2-1)}}\exp(i\xi x)d\xi\,{}^{2)} \qquad \ldots.(6.1)$$

As we can easily see, the branch points of the integrand is ± 1, and the lower and upper limits of the integral are 1 and ∞, therefore this is an example of formula (3.5) and (3.6). Using the same notations $F(\xi)$, $A_{-1}(\xi)$ etc. with the previous paper,

$$a = 1 \text{ (branch point)},\quad b=\infty,$$

$$F(\xi) = \frac{2}{\pi}(\xi^2-1)^{-\frac{1}{2}} \qquad \ldots.(6.2)$$

$$A_{-1}(\xi) = \frac{2}{\pi},\quad A_n(\xi) = 0 \quad (n \geqq 0)$$

Therefore from (5.2)

$$F(\xi) = \frac{2}{\pi}\cdot 2^{-\frac{1}{2}}(\xi-1)^{-\frac{1}{2}} + \left\{-\frac{2}{\pi}\cdot\frac{1}{4}\right\} 2^{-\frac{1}{2}}(\xi-1)^{\frac{1}{2}} + \cdots \qquad \ldots .(6.3)$$

Placing the above expression into (3.6), we have

$$\begin{aligned} I_s(x) \equiv J_0(x) &= x^{-\frac{1}{2}}\cdot\frac{2^{\frac{1}{2}}}{\pi}\sqrt{\pi}\cdot\sin\left(x+\frac{\pi}{4}\right) - x^{-1}[\ 0\ ] \\ &\quad + x^{-\frac{3}{2}}\frac{2^{-\frac{3}{2}}}{\pi}\cdot\frac{1}{2}\sqrt{\pi}\cdot\cos\left(x+\frac{\pi}{4}\right) + \cdots \\ &= \sqrt{\left(\frac{2}{\pi x}\right)}\left[\cos\left(x-\frac{\pi}{4}\right) + \frac{1}{8x}\sin\left(x-\frac{\pi}{4}\right) + \cdots\right] \qquad \ldots .(6.4) \end{aligned}$$

Similarly from (3.5)

$$I_c(x) \equiv Y_0(x) = \sqrt{\left(\frac{2}{\pi x}\right)}\cdot\left[\cos\left(x+\frac{\pi}{4}\right) + \frac{1}{8x}\sin\left(x+\frac{\pi}{4}\right) + \cdots\right] \ldots (6.5)$$

This is the well-known asymptotic expansion of Bessel functions $J_0(x)$[3] and $Y_0(x)$[4].

Now, we will show another example.

According to H. Lamb[5] horizontal displacement u_0 of a point situated on the surface of a semi-infinite elastic solid when a concentrated force is applied vertically to the origin is expressed by

$$u_0 = -\frac{iQ}{2\pi\mu}\int_{-\infty}^{\infty}\frac{\xi(2\xi^2-k^2-2\alpha\beta)}{F(\xi)}\exp(i\xi x)d\xi \qquad \ldots\ldots (6.6)$$

in which

$$F(\xi) = (2\xi^2-k^2)^2 - 4\xi^2\alpha\beta$$

$\alpha = \sqrt{(\xi^2-h^2)}$, $\beta = \sqrt{(\xi^2-k^2)}$ and Q is a constant.

Since $F(\xi)$, α and β are even functions

$$u_0 = \frac{Q}{\pi\mu}\int_0^{\infty} G(\xi)\sin\xi x d\xi \qquad \ldots\ldots (6.7)$$

where $G(\xi) = \xi(2\xi^2-k^2-2\alpha\beta)/F(\xi)$

---

2) **Watson**, *Theory of Bessel Fun tions*, p. 180, expression (14) and (15).

3) *Ibid.*, p. 194.

4) *Ibid.*, p. 199.

5) H. **Lamb**, *Phil. Trans.* A **203** (1904), 1. Expression (52).

$G(\xi)$ has more than one branch point, that is $\xi^2 = h^2$ and $\xi^2 = k^2$, and we must somewhat modify the previously obtained formula (4.1). However, the procedure is easy and we have not to state it precisely in this paper.

From (6.7)

$$\begin{aligned} &G_{-1}(h) = 0 \\ &G_0(h) = G(h) = h/(2h^2 - k^2) \\ &G_1(h) = [(\xi - h)^{-\frac{1}{2}}\{G(\xi) - G_0(h)\}]_{\xi=h} \qquad \ldots.(6.8) \\ &\qquad = i2^{\frac{3}{2}} h^{\frac{3}{2}} k^2 (k^2 - h^2)^{\frac{1}{2}} (2h^2 - k^2)^{-3} \end{aligned}$$

and

$$\begin{aligned} &G_{-1}(k) = 0 \\ &G_0(k) = G(k) = 1/k^2 \\ &G_1(k) = [(\xi - k)^{-\frac{1}{2}}\{G(\xi) - G_0(k)\}]_{\xi=k} \qquad \ldots.(6.9) \\ &\qquad = 2^{\frac{3}{2}} (k^2 - h^2)^{\frac{1}{2}} / k^{\frac{5}{2}} \end{aligned}$$

The asymptotic expansion of u_0 is, using the latter formula of (4.1) and adding the effect at two branch points, h and k, as follows;

$$\begin{aligned} u_0 = &\frac{Q}{\pi\mu} x^{-\frac{3}{2}} \cdot i \frac{2^{\frac{3}{2}} h^{\frac{3}{2}} k^2 \sqrt{k^2 - h^2}}{(2h^2 - k^2)^3} \cdot \frac{1}{2}\sqrt{\pi} \cdot \exp\{-i(hx + \pi/4)\} \\ &+ \frac{Q}{\pi\mu} x^{-\frac{3}{2}} \cdot 2^{\frac{3}{2}} \frac{\sqrt{k^2 - h^2}}{k^{5/2}} \cdot \frac{1}{2}\sqrt{\pi} \cdot \exp\{-i(kx + \pi/4)\} + \cdots\cdot \qquad (6.10) \end{aligned}$$

This is the very expression which H. Lamb had obtained in his famous paper.[6] Of course the vertical component v_0 may be also obtained in a similar manner.

PART II. GENERATION AND PROPAGATION OF WAVES UPON STRATIFIED MEDIUM.

§ 7. Fundamental equations.

Equations of the motion of elastic body in two dimensional space referring to cartesian coordinates are

---

[6] H. LAMB, *Phil. Trans.* A **203** (1904), 1. Expression (90).

$$\left\{\begin{aligned} \rho\frac{\partial^2 u}{\partial t^2} &= (\lambda+\mu)\frac{\partial\Delta}{\partial x}+\mu\Gamma^2 u \\ \rho\frac{\partial^2 w}{\partial t^2} &= (\lambda+\mu)\frac{\partial\Delta}{\partial z}+\mu\Gamma^2 w \end{aligned}\right. \qquad \ldots.(7.1)$$

where ρ.... density ; λ, μ.... Lamé's constants
u, w.... displacement component in x and z direction

$$\Delta=\frac{\partial u}{\partial x}+\frac{\partial w}{\partial z}, \quad \Gamma^2=\frac{\partial^2}{\partial x^2}+\frac{\partial^2}{\partial z^2}$$

Using displacement potentials Φ and Ψ,

$$\left\{\begin{aligned} u &= \partial\Phi/\partial x+\partial\Psi/\partial z \\ w &= \partial\Phi/\partial z-\partial\Psi/\partial z \end{aligned}\right. \qquad \ldots.(7.2)$$

Introducing (7.2) into (7.1) we have

$$\left\{\begin{aligned} \partial^2\Phi/\partial t^2 &= V_p^2\Gamma^2\Phi \\ \partial^2\Psi/\partial t^2 &= V_s^2\Gamma^2\Psi \end{aligned}\right. \quad \text{where} \quad \begin{aligned} V_p^2 &= (\lambda+2\mu)/\rho \\ V_s^2 &= \mu/\rho \end{aligned} \qquad \ldots.(7.3)$$

When we may assume that Φ and Ψ are proportional to $\exp(ipt)$ we get from the above equations

$$\left\{\begin{aligned} (\Gamma^2+h^2)\,\Phi &= 0 \\ (\Gamma^2+k^2)\,\Psi &= 0 \end{aligned}\right. \quad \text{where} \quad \begin{aligned} h &\equiv ap\equiv p/V_p \\ k &\equiv bp\equiv p/V_s \end{aligned} \qquad \ldots.(7.4)$$

And the solutions of this equation are written in the following form

$$\left\{\begin{aligned} \Phi &= \exp(\pm\alpha z+ifx+ipt) \\ \Psi &= \exp(\pm\beta z+ifx+ipt) \end{aligned}\right. \quad \text{where} \quad \begin{aligned} \alpha &= \sqrt{(f^2-h^2)} \\ \beta &= \sqrt{(f^2-k^2)} \end{aligned} \qquad \ldots.(7.5)$$

Displacement components u and w are expressed by the linear combination of the terms obtained by the introduction of (7.5) into (7.2).

On the other hand stress components are expressed in the following form

$$\left\{\begin{aligned} \widehat{xx}/\mu &= (\lambda/\mu)\Delta+2\partial u/\partial x = -k^2\Phi-2\partial^2\Phi/\partial z^2+2\partial^2\Psi/\partial x\partial z \\ \widehat{xz}/\mu &= \partial w/\partial x+\partial u/\partial z = 2\partial^2\Phi/\partial z\partial x-k^2\Psi-2\partial^2\Psi/\partial x^2 \\ \widehat{zz}/\mu &= (\lambda/\mu)\Delta+2\partial w/\partial z = -k^2\Phi-2\partial^2\Phi/\partial x^2-2\partial^2\Psi/\partial x\partial z \end{aligned}\right. \qquad \ldots.(7.6)$$

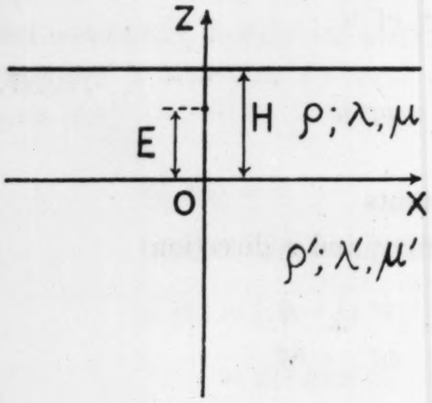

Fig. 1.

§ 8. Simple source in the above layer and boundary conditions.

We wish to determine the component displacements u and w due to a point source of compressional waves at $x=0$, $z=E$ (cf. Fig. 1).

Following H. Nakano's[7] procedure we assume simple harmonic origin

$$\begin{cases} \Phi_0 = QH_0^{(2)}(hr)\exp(ipt) = Q\dfrac{i}{\pi}\exp\{\mp\alpha(z-E)+ifx+ipt\}df, \quad z \gtrless E \\ \Psi_0 = 0 \end{cases} \qquad \ldots.(8.1)$$

where subscription refers to the said origin and the integral sign $\int_{-\infty}^{\infty}$ is abridged for simplicity. The corresponding stress components are (omitting the time factor $\exp(ipt)$)

$$\begin{cases} \widehat{zz}_0/\mu = Q\dfrac{i}{\pi}(2f^2-k^2)\exp\{\mp\alpha(z-E)+ifx\}df \\ \widehat{xz}_0/\mu = Q(\pm)\dfrac{1}{\pi}2f\exp\{\mp\alpha(z-E)+ifx\}df \end{cases} \qquad \ldots.(8.2)$$

Displacements due to this origin are

$$\begin{cases} u_0 = Q(-)\dfrac{1}{\pi}\dfrac{f}{\alpha}\exp\{\mp\alpha(z-E)+ifx\}df \\ w_0 = Q(\mp)i\dfrac{1}{\pi}\exp\{\mp\alpha(z-E)+ifx\}df \end{cases} \qquad \ldots.(8.3)$$

Therefore,

horizontal displacement at $z=0$ is $u_0 = Q(-)\dfrac{1}{\pi}\dfrac{f}{\alpha}\exp\{-\alpha E+ifx\}df$

vertical displacement at $z=0$ is $w_0 = Qi\dfrac{1}{\pi}\exp\{-\alpha E+ifx\}df$

tangential stress at $z=0$ is $\widehat{xz}_0 = Q(-)\mu\dfrac{1}{\pi}2f\exp\{-\alpha E+ifx\}df$

---

[7] H. NAKANO, *Jap. Journ. Astro. Geophys.*, **2** (1925), 1.

normal stress at $z = 0$ is $\widehat{zz}_0 = Q\mu \cdot i\frac{1}{\pi}\frac{2f^2 - k^2}{\alpha}\exp\{-\alpha E + ifx\}df$

tangential stress at $z = H$ is $\widehat{xz}_0 = Q\mu \cdot \frac{1}{\pi}2f\exp\{-\alpha(H - E) + ifx\}df$

normal stress at $z = H$ is $\widehat{zz}_0 = Q\mu \cdot i\frac{1}{\pi}\frac{2f^2 - k^2}{\alpha}\exp\{-\alpha(H - E) + ifx\}df$

$$\ldots\ldots(8.4)$$

Conditions required at the boundary surfaces are the continuity of displacement and stress components at $z = 0$, and the vanishing of stress at the free suface $z = H$. Therefore we must combine displacements such as derived from potentials in (7.5) and satisfy the boundary conditions. For this purpose we assume

$$\begin{cases} \Phi' = \mathbf{A}\exp\{\alpha' z + ifx\} \\ \Psi' = \mathbf{B}\exp\{\beta' z + ifx\} \end{cases} \qquad \ldots\ldots(8.5)$$

where $\alpha' = \sqrt{(f^2 - h'^2)}$, $h' = a'p = p/V_{p'} = p/\{(\lambda' + 2\mu')/\rho'\}^{\frac{1}{2}}$

$\beta' = \sqrt{(f^2 - k'^2)}$, $k' = b'p = p/V_{s'} = p/\{\mu'/\rho'\}^{\frac{1}{2}}$

in the semi-infinite part; and in the upper stratum

$$\begin{cases} \Phi = \{\mathbf{C}\cosh\alpha z + \mathbf{D}\sinh\alpha z\}\exp(ifx) \\ \Psi = \{\mathbf{E}\cosh\beta z + \mathbf{F}\sinh\beta z\}\exp(ifx) \end{cases} \qquad \ldots\ldots(8.6)$$

Six equations which must hold at boundary surfaces are

$$\begin{cases} \mathbf{A}if + \mathbf{B}\beta' + \mathbf{C}(-if) + \mathbf{F}(-\beta) = Q(-)\frac{1}{\pi}\frac{f}{\alpha}\exp(-\alpha E)df \\ \mathbf{A}\alpha' + \mathbf{B}(-if) + \mathbf{D}(-\alpha) + \mathbf{E}(if) = Qi\frac{1}{\pi}\exp(-\alpha E)df \\ \mathbf{A}i2\chi f\alpha' + \mathbf{B}\chi(2f^2-k^2) + \mathbf{D}(-i2f\alpha) + \mathbf{E}[-(2f^2-k^2)] = Q(-)\frac{1}{\pi}2f\exp(-\alpha E)df \\ \mathbf{A}\chi(2f^2-k^2) + \mathbf{B}(-i2f\beta') + \mathbf{C}[-(2f^2-k^2)] + \mathbf{F}(i2f\beta) = Qi\frac{1}{\pi}\frac{2f^2-k^2}{\alpha}\exp(-\alpha E)df \\ \mathbf{C}[-i2f\alpha\mathfrak{S}] + \mathbf{D}[-i2f\alpha\mathfrak{C}] + \mathbf{E}[-(2f^2-k^2)\mathfrak{C}'] + \mathbf{F}[(2f^2-k^2)\mathfrak{S}'] = Q\frac{1}{\pi}2f\exp(-\alpha E')df \\ \mathbf{C}[-(2f^2-k^2)\mathfrak{C}] + \mathbf{D}[-(2f^2-k^2)\mathfrak{S}] + \mathbf{E}[i2f\beta\mathfrak{S}'] + \mathbf{F}[i2f\beta\mathfrak{S}'] = Qi\frac{1}{\pi}\frac{2f^2-k^2}{\alpha}\exp(-\alpha E')df \end{cases}$$

$$\ldots(8.7)$$

in which $\chi = \mu' / \mu, \qquad E' = H - E$

$$\mathfrak{C} = \cosh \alpha H, \quad \mathfrak{S} = \sinh \alpha H$$

$$\mathfrak{C}' = \cosh \beta H, \quad \mathfrak{S}' = \sinh \beta H.$$

§ 9. Formal solution.

From the equations (8.7) we can determine **A, B....F** formally; that is....

$$\mathbf{A} = Q\frac{df}{\pi} A/M, \qquad \mathbf{C} = Q\frac{df}{\pi} C/M$$

$$\mathbf{B} = Q\frac{df}{\pi} B/M, \qquad \mathbf{D} = Q\frac{df}{\pi} D/M$$

$$\mathbf{E} = Q\frac{df}{\pi} E/M$$

$$\mathbf{F} = Q\frac{df}{\pi} F/M$$

where

$$M = \begin{vmatrix} if & \beta' & -if & 0 & 0 & -\beta \\ \alpha' & -if & 0 & -\alpha & if & 0 \\ i2\chi f\alpha' & \chi(2f^2-k^2) & 0 & -i2f\alpha & -(2f^2-k^2) & 0 \\ \chi(2f^2-k'^2) & -i2\chi f\beta & -(2f^2-k^2) & 0 & 0 & i2f\beta \\ 0 & 0 & -i2f\alpha\mathfrak{S} & -i2f\alpha\mathfrak{C} & -(2f^2-k^2)\mathfrak{C}' & -(2f^2-k^2)\mathfrak{S}' \\ 0 & 0 & -(f^2-k^2)\mathfrak{C} & -(2f^2-k^2)\mathfrak{S} & i2f\beta\mathfrak{S}' & i2f\beta\mathfrak{C}' \end{vmatrix}$$

and $A, B, C \dots F$ is obtained by replacing the 1st, 2nd, 3rd . . . 6th column of M by $-\frac{f}{\alpha}\exp(-\alpha E)$, $i\exp(-\alpha E)$, $-2f\exp(-\alpha E)$, $i\frac{2f^2-k^2}{\alpha}\exp(-\alpha E)$, $2f\exp(-\alpha E')$ and $i\frac{2f^2-k^2}{\alpha}\exp(-\alpha E')$ respectively.

Expanding the determinants M and C, D, E, F, we have (A and B are not necessary for the calculation of surface displacements)

$$M = k^4 L_1 N_5 - k^2 \alpha L_2 N_6 \qquad C = -i\frac{1}{\alpha} k^4 \mathfrak{E} L_1 N_5 + ik^2 \mathfrak{E} L_2 N_6 \qquad D = k^4 L_1 P_4 + ik^4 \frac{1}{\alpha} \mathfrak{E} L_1 N_3 + ik^2 \mathfrak{E} L_2 N_6$$

$$\begin{array}{lll}
-k^2\alpha L_3N_3 & -k^2\alpha L_3P_4-ik^2\mathfrak{C}L_3N_5 & +ik^2\mathfrak{C}L_3N_3\\
+k^2\beta L_4N_4 & -ik^2\dfrac{\beta}{\alpha}\mathfrak{C}L_4N_4 & +k^2\beta L_4P_3+ik^2\dfrac{\beta}{\alpha}\mathfrak{C}L_4N_2\\
-k^2\beta L_5N_1 & -k^2\beta L_5P_2 & +k^2\beta L_5P_1\\
+\alpha\beta L_6N_2, & +\alpha\beta L_6P_3+i\beta\mathfrak{C}L_6N_4, & -i\beta\mathfrak{C}L_6N_2,
\end{array}$$

$$\begin{array}{ll}
E=-k^2\alpha L_2P_4-ik^2\mathfrak{C}L_2\{N_3+N_5\} & F=-k^4L_1P_2-ik^4\dfrac{1}{\alpha}\mathfrak{C}L_1N_1\\
\quad -k^2\beta L_4P_2-ik^2\dfrac{\beta}{\alpha}\mathfrak{C}L_4N_1 & \quad +k^2\alpha L_2P_3+ik^2\mathfrak{C}L_2\{N_2+N_4\}\\
\quad -\alpha\beta L_6P_1+i\beta\mathfrak{C}L_6N_1, & \quad +k^2\alpha L_3P_1-ik^2\mathfrak{C}L_3N_1
\end{array} \qquad \ldots\ldots(9.3)$$

where

$$L_1=\begin{vmatrix} ifU_1 & \beta'U\\ \alpha'U & -ifU_1\end{vmatrix}=f^2U_1^2-\alpha'\beta'U \qquad U=1+2\chi'/\mathfrak{v}^2$$

$$L_2=\begin{vmatrix} ifU_1 & \beta'U\\ i2\chi'f\alpha' & f''\end{vmatrix}=if(U_1f''-2\chi'\alpha'\beta'U), \qquad U_1=U-\chi\sigma^2,\quad \chi=\mu'/\mu$$

$$L_3=\begin{vmatrix} ifU_1 & \beta'U\\ f'' & -i2\chi'f\beta'\end{vmatrix}=\chi\sigma^2k^2\beta' \qquad \chi'=\chi-1$$

$$L_4=\begin{vmatrix} \alpha'U & -ifU_1\\ i2\chi'f\alpha' & f''\end{vmatrix}=-\chi\sigma^2k^2\alpha', \qquad f'=2f^2-k^2,\quad f''=2\chi'f^2-\chi k'^2$$

$$L_5=\begin{vmatrix} \alpha'U & -ifU_1\\ f'' & -i2\chi'f\beta'\end{vmatrix}=L_2, \qquad \gamma^2=(\lambda+2\mu)/\mu$$

$$L_6=\begin{vmatrix} i2\chi'f\alpha' & f''\\ f'' & -i2\chi'f\beta'\end{vmatrix}=4\chi'^2f^2\alpha'\beta'-f''^2, \qquad \sigma^2=\left(\frac{\mu}{\rho}\right)\Big/\left(\frac{\mu'}{\rho'}\right),$$

$$N_1=\begin{vmatrix} -i2f\alpha\mathfrak{S} & -i2f\alpha\mathfrak{C}\\ -(2f^2-k^2)\mathfrak{C} & -(2f^2-k^2)\mathfrak{S}\end{vmatrix}=-i2ff'\alpha \qquad \mathfrak{v}=\left(\frac{p}{f}\right)\Big/V.$$

$$N_2=\begin{vmatrix} -i2f\alpha\mathfrak{S} & -(2f^2-k^2)\mathfrak{C}'\\ -(2f^2-k^2)\mathfrak{C} & i2f\beta\mathfrak{S}'\end{vmatrix}=4f^2\alpha\beta\mathfrak{S}\mathfrak{S}'-f'^2\mathfrak{C}\mathfrak{C}'$$

$$N_3 = \begin{vmatrix} -i2f\alpha\mathfrak{S} & -(2f^2-k^2)\mathfrak{S}' \\ -(2f^2-k^2)\mathfrak{C} & i2f\beta\mathfrak{C}' \end{vmatrix} = 4f^2\alpha\beta\mathfrak{S}\mathfrak{C}' - f'^2\mathfrak{C}\mathfrak{S}'$$

$$N_4 = \begin{vmatrix} -i2f\alpha\mathfrak{C} & -(2f^2-k^2)\mathfrak{C}' \\ -(2f^2-k^2)\mathfrak{S} & i2f\beta\mathfrak{S}' \end{vmatrix} = 4f^2\alpha\beta\mathfrak{C}\mathfrak{S}' - f^{2\prime}\mathfrak{S}\mathfrak{C}'$$

$$N_5 = \begin{vmatrix} -i2f\alpha\mathfrak{C} & -(2f^2-k^2)\mathfrak{S}' \\ -(2f^2-k^2)\mathfrak{S} & i2f\beta\mathfrak{C}' \end{vmatrix} = 4f^2\alpha\beta\mathfrak{S}\mathfrak{S}' - f'^2\mathfrak{S}\mathfrak{S}'$$

$$N_6 = \begin{vmatrix} -(2f^2-k^2)\mathfrak{C} & -(2f^2-k^2)\mathfrak{S}' \\ i2f\beta\mathfrak{S}' & i2f\beta\mathfrak{C}' \end{vmatrix} = -i2f\beta f', \qquad \begin{matrix} \mathfrak{E} = \exp(-\alpha E) \\ \mathfrak{E}' = \exp(-\alpha E') \end{matrix}$$

$$P_1 = \begin{vmatrix} 2f\mathfrak{E}' & -i2f\alpha\mathfrak{S} \\ i\frac{1}{\alpha}f'\mathfrak{E}' & -f'\mathfrak{C} \end{vmatrix} = -2ff'\mathfrak{E}^{-1}, \qquad P_3 = \begin{vmatrix} 2f\mathfrak{E}' & -f'\mathfrak{C}' \\ i\frac{f'}{\alpha}\mathfrak{E}' & i2f\beta\mathfrak{S}' \end{vmatrix}$$

$$P_2 = \begin{vmatrix} 2f\mathfrak{E}' & -i2f\alpha\mathfrak{C} \\ i\frac{1}{\alpha}j'\mathfrak{E}' & -f'\mathfrak{S} \end{vmatrix} = P_1, \qquad P_4 = \begin{vmatrix} 2f\mathfrak{E}' & -f'\mathfrak{S}' \\ i\frac{f'}{\alpha}\mathfrak{E}' & i2f\beta\mathfrak{C}' \end{vmatrix}$$

§ 10. Horizontal and vertical displacements.

With these preparations we can calculate the expression of u and w, by introducing (8.6)—**C**, **D**, **E** and **F** contained in this expression are obtained in § 9—into (7.2), we have

and
$$\begin{cases} u = [if\{\mathbf{C}\cosh\alpha z + \mathbf{D}\sinh\alpha z\} + \beta\{\mathbf{E}\sinh\beta z + \mathbf{F}\cosh\beta z\}]\exp(ifx) \\ w = [\alpha\{\mathbf{C}\sinh\alpha z + \mathbf{D}\cosh\alpha z\} - if\{\mathbf{E}\cosh\beta z + \mathbf{F}\sinh\beta z\}]\exp(ifx) \end{cases} \qquad \ldots\ldots(10.1)$$

of which the values at the free surface are

$$\begin{cases} u = [if\{\mathbf{C}\mathfrak{C} + \mathbf{D}\mathfrak{S}\} + \beta\{\mathbf{E}\mathfrak{S} + \mathbf{F}\mathfrak{C}\}]\exp(ifx) \\ w = [\alpha\{\mathbf{C}\mathfrak{S} + \mathbf{D}\mathfrak{C}\} - if\{\mathbf{E}\mathfrak{C} + \mathbf{F}\mathfrak{S}\}]\exp(ifx) \end{cases} \qquad \ldots\ldots(10.2)$$

or, using (9·1)

$$\begin{cases} u = Q\dfrac{1}{\pi}\dfrac{1}{M}[i\{C\mathfrak{C} + D\mathfrak{S}\} + \beta\{E\mathfrak{S} + F\mathfrak{C}\}]\exp(ifx)df \\ w = Q\dfrac{1}{\pi}\dfrac{1}{M}[\alpha\{C\mathfrak{S} + D\mathfrak{C}\} - if\{E\mathfrak{C} + F\mathfrak{S}\}]\exp(ifx)df \end{cases} \qquad \ldots\ldots(10.3)$$

in which $\int_{-\infty}^{\infty}$ is omitted for brevity.

Since the integrand of u is, excluding $\exp(ifx)$, an odd function of f, and that of w is even, (10.3) may be transformed as

$$\begin{cases} u = Q\dfrac{1}{\pi}\cdot i2\displaystyle\int_0^\infty \dfrac{1}{M}\left[if\{C\mathfrak{C}+D\mathfrak{S}\}+\beta\{E\mathfrak{S}+F\mathfrak{C}\}\right]\sin(fx)df \\ w = Q\dfrac{1}{\pi}\cdot 2\displaystyle\int_0^\infty \dfrac{1}{M}\left[\alpha\{C\mathfrak{S}+D\mathfrak{C}\}-if\{E\mathfrak{C}+F\mathfrak{S}\}\right]\cos(fx)df \end{cases} \qquad \ldots(10.4)$$

This is exactly the same form of integration that we learned in the first part, therefore, in order to obtain the asymptotic expansion of the integral we have only to calculate the coefficients of the expressions at branch points and upper and lower limits of the integral. We will consider them in order.

For convenience of description we will simply write

$$\begin{cases} u = Q\dfrac{1}{\pi}i2\displaystyle\int_0^\infty U(f)\sin(fx)df \\ w = Q\dfrac{1}{\pi}\ 2\displaystyle\int_0^\infty W(f)\cos(fx)df \end{cases} \qquad \ldots\ldots(10.5)$$

At first, we will take up the effect of the lower limit of the integral. Terms concerning this point are, using the formulae in § 2 ((2.1) and (2.2)), written down as

$$\begin{aligned} &u\,; && x^{-1}U(0)\cos(0x) - x^{-2}U'(0)\sin(0x) + \cdots\cdots \\ &w\,; && -x^{-1}W(0)\sin(0x) - x^{-2}W'(0)\cos(0x) + \cdots\cdots \end{aligned} \qquad \ldots\ldots(10.6)$$

Since $U(f)$ is an odd and $W(f)$ an even function of f, the above terms all vanish, and no effect of lower limits remains.

Similarly the effect of upper limit vanishes in our case. Therefore, it is sufficient for us to consider the effects near the branch points, which are $f = h, k, h'$ and k'. From the experience of our past study, these branch points correspond with the various phases of seismic waves; that is to say, $f = k$ and h correspond with S and P waves in the upper layer, and $f = k'$ and h' with S and P waves in the substratum medium, which in this paper, is denoted by S, P and S', P' respectively.

Thus our present task is reduced to the problem of how to expand the two functions $U(f)$ and $W(f)$ to the form of (5.1) at the points $f = h, k, h,$

and k'. We express the expansion of any function $F(f)$ at the point $f = k$ as

$${}_{S}F(f) = {}_{S}F_{-1}\cdot\beta^{-1} + {}_{S}F_0 + {}_{S}F_1\cdot\beta + {}_{S}F_2\cdot\beta^2 + \cdots\cdot$$

Similarly

$$\begin{aligned} {}_{P}F(f) &= {}_{P}F_{-1}\cdot\alpha^{-1} + {}_{P}F_0 + {}_{P}F_1\cdot\alpha + {}_{P}F_2\cdot\alpha^2 + \cdots\cdot \\ {}_{S'}F(f) &= {}_{S'}F_{-1}\cdot\beta'^{-1} + {}_{S'}F_0 + {}_{S'}F_1\cdot\beta' + {}_{S'}F_2\cdot\beta'^2 + \cdots\cdot \qquad (10.7) \\ {}_{P'}F(f) &= {}_{P'}F_{-1}\cdot\alpha'^{-1} + {}_{P'}F_0 + {}_{P'}F_1\cdot\alpha' + {}_{P'}F_2\cdot\alpha'^2 + \cdots\cdot \end{aligned}$$

in which $\beta = \sqrt{(f^2 - k^2)}, \qquad \alpha = \sqrt{(f^2 - h^2)}$

$$\beta' = \sqrt{(f^2 - k'^2)}, \qquad \alpha' = \sqrt{(f^2 - h'^2)}$$

and the suffixes S, P, S' and P' mean the expansion with respect to β, α, β' and α' respectively. (This notation will be often used in future.)

However the coefficients ${}_{S}F_0, {}_{S}F_2, \ldots, {}_{P}F_0, \ldots$ are not always involved in the final expression (cf. (5.2)), therefore we need not always calculate these quantities for our present purpose. It is sufficient for us to obtain only ${}_{S}U_{-1}, {}_{S}U_1, {}_{P}U_{-1}$ etc. for getting the asymptotic values of displacement components.

Applying the similar way of description with (10.7) to the functions. M, C, D, E and F, we have

$$\begin{cases} {}_{P}U(f) = if\cdot\dfrac{{}_{P}C_0}{{}_{P}M_1}\cdot\alpha^{-1} + \cdots\cdot \\ {}_{P}W(f) = \{{}_{P}C_0\cdot H + {}_{P}D_1 - if\cdot{}_{P}E_2 - if\cdot{}_{P}F_2\}\dfrac{1}{{}_{P}M_1}\cdot\alpha + \cdots\cdot \end{cases}$$

$$\begin{cases} {}_{S}U(f) = \{if\cdot{}_{S}C_2\mathfrak{C} + if\cdot{}_{S}D_2\mathfrak{S} + {}_{S}F_1\}\dfrac{1}{{}_{S}M_1}\beta + \cdots\cdot \\ {}_{S}W(f) = \{\alpha\cdot{}_{S}C_2\mathfrak{S} + \alpha\cdot{}_{S}D_2\mathfrak{C} - if\cdot{}_{S}E_2 - if\cdot{}_{S}F_2\}\dfrac{1}{{}_{S}M_1}\beta + \cdots\cdot \end{cases}$$

$$\begin{cases} {}_{P'}U(f) = \Big[\{if\cdot{}_{P'}C_1\cdot\mathfrak{C} + if\cdot{}_{P'}D_1\cdot\mathfrak{S} + \beta\cdot{}_{P'}E_1\mathfrak{S}' + \beta\cdot{}_{P'}F_1\mathfrak{C}'\} \\ \qquad -\dfrac{{}_{P'}M_1}{{}_{P'}M_0}\{if\cdot{}_{P'}C_0\cdot\mathfrak{C} + if\cdot{}_{P'}D_0\cdot\mathfrak{S} + \beta\cdot{}_{P'}E_0\cdot\mathfrak{S}' + \beta\cdot{}_{P'}F_0\cdot\mathfrak{C}'\}\Big]\dfrac{1}{{}_{P'}M_0}\cdot\alpha' + \cdots \\ {}_{P'}W(f) = \Big[\{\alpha\cdot{}_{P'}C_1\cdot\mathfrak{S} + \alpha\cdot{}_{P'}D_1\cdot\mathfrak{C} - if\cdot{}_{P'}E_1\cdot\mathfrak{C}' - if\cdot{}_{P'}F_1\mathfrak{S}'\} \\ \qquad -\dfrac{{}_{P'}M_1}{{}_{P'}M_0}\{\alpha\cdot{}_{P'}C_0\cdot\mathfrak{S} + \alpha\cdot{}_{P'}D_0\cdot\mathfrak{C} - if\cdot{}_{P'}E_0'\mathfrak{C} - if\cdot{}_{P'}F_0\mathfrak{S}'\}\Big]\dfrac{1}{{}_{P'}M_0}\cdot\alpha' + \cdots \end{cases}$$

$$\left\{\begin{aligned}
{}_{s'}U(f) &= \Big[\{if\cdot{}_{s'}C_1\cdot\mathfrak{C}+if\cdot{}_{s'}D_1\cdot\mathfrak{S}+\beta\cdot{}_{s'}E_1\mathfrak{S}'+\beta\cdot{}_{s'}F_1\cdot\mathfrak{C}'\}\\
&\quad -\frac{{}_{s'}M_1}{{}_{s'}M_0}\{if\cdot{}_{s'}C_0\cdot\mathfrak{C}+if\cdot{}_{s'}D_0\cdot\mathfrak{S}+\beta\cdot{}_{s'}E_0\cdot\mathfrak{S}'+\beta\cdot{}_{s'}F_0\cdot\mathfrak{C}'\}\Big]\frac{1}{{}_{s'}M_0}\cdot\beta'+\cdots\\
{}_{s'}W(f) &= \Big[\{\alpha\cdot{}_{s'}C_1\cdot\mathfrak{S}+\alpha\cdot{}_{s'}D_1\cdot\mathfrak{C}-if\cdot{}_{s'}E_1\cdot\mathfrak{C}'-if\cdot{}_{s'}F_1\cdot\mathfrak{S}'\}\\
&\quad -\frac{{}_{s'}M_1}{{}_{s'}M_0}\{\alpha\cdot{}_{s'}C_0\cdot\mathfrak{S}+\alpha\cdot{}_{s'}D_0\mathfrak{C}-if\cdot{}_{s'}E_0\cdot\mathfrak{C}'-if\cdot{}_{s'}F_0\mathfrak{S}'\}\Big]\frac{1}{{}_{s'}M_0}\cdot\beta'+\cdots
\end{aligned}\right.$$

$$\ldots\ldots(10.8)$$

§ 10.1 Preparation for the above calculations.

We have thus obtained the expansions of $U(f)$ and $W(f)$. We have to proceed and get the coefficients ${}_{P}M_0$, ${}_{P}M_1$, ${}_{S}C_2$.... which are involved in the expression (10.8). For this purpose, we will prepare some formulae which will help us in the following calculations.

$M(f)$, $C(f)$, $D(f)$.... contain N_k ($k = 1, 2, \ldots. 6$) and P_k ($k = 1, 2, 3, 4$), and this N_k and P_k contain α and β, therefore we will at first express these quantities as power series with respect to α and β.

Power series with respect to α;

$$\left\{\begin{aligned}
N_1 &= -i2ff'\alpha\\
N_2 &= \{-f'^2\mathfrak{C}' + (4f^2\beta H\mathfrak{S}' - \tfrac{1}{2}f'^2H^2\mathfrak{C}')\alpha^2 + 0(\alpha^4)\}\\
N_3 &= \{-f'^2\mathfrak{S}' + (4f^2\beta H\mathfrak{C}' - \tfrac{1}{2}f'^2H^2\mathfrak{S}')\alpha^2 + 0(\alpha^4)\}\\
N_4 &= \{(4f^2\beta\mathfrak{S}' - f'^2H\mathfrak{C}')\alpha + 0(\alpha^3)\}\\
N_5 &= \{(4f^2\beta\mathfrak{C}' - f'^2H\mathfrak{S}')\alpha + 0(\alpha^3)\}\\
N_6 &= -i2ff'\beta
\end{aligned}\right. \quad \ldots.(10.9)$$

$$\left\{\begin{aligned}
P_1 &= -2ff'(1 + \alpha H + 0(\alpha^2))\\
P_2 &= P_1\\
P_3 &= \left(i\frac{1}{\alpha}f'^2\mathfrak{C}' + i4f^2\beta\mathfrak{S}'\right)\\
P_4 &= \left(i\frac{1}{\alpha}f'^2\mathfrak{S}' + i4f^2\beta\mathfrak{C}'\right)
\end{aligned}\right.$$

Power series with respect to β;

$$\begin{cases} N_1 = -i2ff'\alpha \\ N_2 = \{-f'^2\mathfrak{C} + (4f^2\alpha H\mathfrak{S} - \frac{1}{2}f'^2H^2\mathfrak{C})\beta^2 + 0(\beta^4)\} \\ N_3 = \{(4f^2\alpha\mathfrak{S} - f'^2H\mathfrak{C})\beta + 0(\beta^3)\} \\ N_4 = \{-f'^2\mathfrak{S} + (4f^2\alpha H\mathfrak{C} - \frac{1}{2}f'^2H^2\mathfrak{S})\beta^2 + 0(\beta^4)\} \\ N_5 = \{(4f^2\alpha\mathfrak{C} - f'^2H\mathfrak{S})\beta + 0(\beta^3)\} \\ N_6 = -i2ff'\beta \end{cases}$$

$$\begin{cases} P_1 = -2ff'\mathfrak{C}^{-1} \\ P_2 = P_1 \\ P_3 = \left\{i\frac{1}{\alpha}f'^2 + (i4f^2H + i\frac{1}{\alpha}f'^2\frac{1}{2}H^2)\beta^2 + 0(\beta^4)\right\} \\ P_4 = \left\{\left(i\frac{1}{4}f^2 + i\frac{1}{\alpha}f'^2H\right)\beta + 0(\beta^3)\right\} \end{cases} \quad \ldots\ldots(10.10)$$

Introducing (10.9) and (10.10) into (9.2) and (9.3), we have expansions of $\boldsymbol{M}, \boldsymbol{C}, \boldsymbol{D}, \boldsymbol{E}$ and $\boldsymbol{F}$ as the power series of α, β, α' and β'.

§ 10-2 Expression by the non-dimensional quantities.

In the preceding articles we have obtained the expressions of ${}_PU(f)$, ${}_PW(f)$, ${}_SU(f)$ and so on; however, these are not the most convenient form for our present purpose. Because, for numerical calculations, non-dimensional quantities are always preferable. Therefore, we will rewrite the above expression by means of such quantities.

We will employ the following notations which are all dimensionless.

$$\begin{aligned} &\xi \equiv fH, \\ &\alpha_1 \equiv \alpha/f, \qquad \alpha_2 \equiv \alpha'/f, \\ &\beta_1 \equiv \beta/f, \qquad \beta_2 \equiv \beta'/f. \end{aligned} \quad \ldots\ldots(10.11)$$

(Since α, β, α' and β' are even-functions of f, $\alpha_1, \beta_1, \alpha_2$ and β_2 must be assumed as odd-functions of ξ, although they do not contain ξ.)

Further, by putting the sign $\sim$ to any function F, which is a simultaneous polynomial of the n-th degree of f, we mean

$$\tilde{F}(\xi) \equiv F(f)\,/f^{n}. \qquad \ldots.(10.12)$$

Now we will come back to the first equation of (10.7). Employing the above notations

$$\begin{aligned} {}_sF(f) &= f^{n}\cdot {}_s\tilde{F}(\xi) \\ &= f^{n}\cdot\{{}_s\tilde{F}_{-1}\cdot\beta_1^{-1} + {}_s\tilde{F}_0 + {}_s\tilde{F}_1\cdot\beta_1 + {}_s\tilde{F}_2\cdot\beta_1^2 + \cdots\} \\ &= {}_s\tilde{F}_{-1}\cdot\beta^{-1}f^{n+1} + {}_s\tilde{F}_0\cdot f^{n} + {}_s\tilde{F}_1\cdot\beta f^{n-1} + {}_s\tilde{F}_2\cdot\beta^2 f^{n-2} + \cdots. \end{aligned}$$

On the other hand, the same function is written in the first equation of (10.7)

$${}_sF(f) = {}_sF_{-1}\cdot\beta^{-1} + {}_sF_0 + {}_sF_1\cdot\beta + {}_sF_2\cdot\beta^2 + \cdots.$$

Therefore

$$\begin{aligned} {}_sF_{-1} &= {}_s\tilde{F}_{-1}\cdot f^{n+1} \\ \text{or} \qquad {}_sF_k &= {}_s\tilde{F}_k\cdot f^{n-k} \end{aligned} \qquad \ldots.(10.13)$$

Similar reasoning of course holds in the expansions of ${}_PF(f)$, ${}_{S'}F(f)$ and ${}_{P'}F(f)$.

Since M is the 10-th degree and C, D, E and F the 9-th degree of f,

$$\begin{aligned} {}_sM_k &= {}_s\tilde{M}_k\cdot f^{10-k} \\ {}_sC_k &= {}_s\tilde{C}_k\cdot f^{9-k}, \quad {}_sD_k = {}_s\tilde{D}_k\cdot f^{9-k} \text{ etc.} \end{aligned} \qquad \ldots..(10.14)$$

Introducing the above relations into (10.8) we have

$$\left|\begin{aligned} {}_PU(f)\,df &= i\frac{{}_P\tilde{C}_0}{{}_P\tilde{M}_1}\,\xi\,\frac{d\xi}{\sqrt{(\xi^2-\omega^2/\gamma^2)}} \\ {}_PW(f)df &= \{\xi\cdot{}_P\tilde{C}_0 + {}_P\tilde{D}_1 - i_P\tilde{E}_2 - i_P\tilde{F}_2\}\frac{1}{{}_P\tilde{M}_1}\frac{1}{\xi}\sqrt{(\xi - \omega^2/\gamma^2)}\cdot d\xi \end{aligned}\right. \qquad \ldots..(10.15)$$

Now, we will simply express the above expressions as

$${}_PU(f)df = {}_PU\cdot\frac{1}{\alpha_1}d\xi, \quad {}_PW(f) = {}_PW\cdot\alpha_1 d\xi;$$

and similarly

$$\begin{aligned} {}_sU(f)df &= {}_sU\cdot\beta_1\,d\xi, & {}_sW(f) &= {}_sW\cdot\beta_1\,d\xi, \\ {}_{P'}U(f)df &= {}_{P'}U\cdot\alpha_2\,d\xi, & {}_{P'}W(f) &= {}_{P'}W\cdot\alpha_2\,d\xi, \\ {}_{S'}U(f)df &= {}_{S'}U\cdot\beta_2\,d\xi, & {}_{S'}W(f) &= {}_{S'}W\cdot\beta_2\,d\xi. \end{aligned} \qquad \ldots..(10.16)$$

New notations ${}_{P}U$, ${}_{S}W$ etc. will be easily found by comparing the above three sets of expressions (10.8), (10.15) and (10.16).

As is explained in § 10, four phases of waves P, S and P', S' appear corresponding to the four pairs of expressions in (10.16). We will express them as $u[P]$, $w[P]$ and so on hereafter. Of course another important phase exists; that is the Rayleigh-waves (we express them by R), which results from the poles of the integrands $U(f)$ and $W(f)$. Hence we may write as

$$\left\{\begin{aligned} u &= u[P] + u[S] + u[P'] + u[S'] + u[R] \\ w &= w[P] + w[S] + w[P'] + w[S'] + w[R] \end{aligned}\right. \qquad \ldots\ldots(10.17)$$

and the component waves $u[P]$, $w[P]$ .... are easily obtained by referring to (4.1), (5.1) (10.5) (10.15) and (10.16).

$$\left\{\begin{aligned} u[P] &= \tilde{Q}\frac{i2}{\pi}\left[x^{-\frac{1}{2}}\cdot{}_{P}U\cdot(2\omega/\gamma)^{-\frac{1}{2}}\sqrt{\pi}\cdot\exp\{-i(hx-\pi/4)\}\right] \\ w[P] &= \tilde{Q}\frac{2}{\pi}\left[-x^{-\frac{3}{2}}\cdot{}_{P}W\cdot(2\omega/\gamma)^{-\frac{1}{2}}\frac{1}{2}\sqrt{\pi}\cdot\exp\{-i(hx-\pi/4)\}\right] \end{aligned}\right.$$

$$\left\{\begin{aligned} u[S] &= \tilde{Q}\frac{i2}{\pi}\left[x^{-\frac{3}{2}}\cdot{}_{S}U\cdot(2\omega)^{\frac{1}{2}}\cdot\frac{1}{2}\sqrt{\pi}\cdot\exp\{-i(kx+\pi/4)\}\right] \\ w[S] &= \tilde{Q}\frac{2}{\pi}\left[-x^{-\frac{3}{2}}\cdot{}_{S}W\cdot(2\omega)^{\frac{1}{2}}\cdot\frac{1}{2}\sqrt{\pi}\cdot\exp\{-i(kx-\pi/4)\}\right] \end{aligned}\right.$$

$$\left\{\begin{aligned} u[P'] &= \tilde{Q}\frac{i2}{\pi}\left[x^{-\frac{3}{2}}\cdot{}_{P'}U\cdot(2\omega\sigma/\gamma)^{\frac{1}{2}}\cdot\frac{1}{2}\sqrt{\pi}\cdot\exp\{-i(h'x+\pi/4)\}\right] \\ w[P'] &= \tilde{Q}\frac{2}{\pi}\left[-x^{-\frac{3}{2}}\cdot{}_{P'}W\cdot(2\omega\sigma/\gamma)^{\frac{1}{2}}\cdot\frac{1}{2}\sqrt{\pi}\cdot\exp\{-i(h'x-\pi/4)\right] \end{aligned}\right.$$

$$\left\{\begin{aligned} u[S'] &= \tilde{Q}\frac{i2}{\pi}\left[x^{-\frac{3}{2}}\cdot{}_{S'}U\cdot(2\omega\sigma)^{\frac{1}{2}}\cdot\frac{1}{2}\sqrt{\pi}\cdot\exp\{-i(k'x+\pi/4)\}\right] \\ w[S'] &= \tilde{Q}\frac{2}{\pi}\left[-x^{-\frac{3}{2}}\cdot{}_{S'}W\cdot(2\omega\sigma)^{\frac{1}{2}}\cdot\frac{1}{2}\sqrt{\pi}\cdot\exp\{i(k'x-\pi/4)\}\right] \end{aligned}\right.$$

$$\ldots\ldots(10.18)$$

in which $\tilde{Q} = Q/H$

Of these expressions $u[S]$ and $w[S]$ always vanish, which fact is anticipated from the nature of waves and their paths, and may be verified by slight calculations.

$u[R]$ and $w[R]$ can be calculated in a similar manner from (10.3)

$$\left\{\begin{aligned} u[R] &= 2\pi i\cdot\sum_n Q\frac{1}{\pi}\frac{1}{M'(f)}\left[if\{C\mathfrak{C}+D\mathfrak{S}\}+\beta\{E\mathfrak{S}+F\mathfrak{C}\}\right]_{f=K_n} \\ w[R] &= 2\pi i\cdot\sum_n Q\frac{1}{\pi}\frac{1}{M'(f)}\left[\alpha\{C\mathfrak{S}+D\mathfrak{C}\}-if\{E\mathfrak{C}+F\mathfrak{S}\}\right]_{f=K_n} \end{aligned}\right. \qquad \ldots(10.19)$$

where K_n implies the n-th root of $M(f)=0$ and the notation $\sum$ implies the summation with respect to every branch of dispersion curve of Rayleigh-waves.

Since $M(f)=f^{10}\widetilde{M}(\xi)$ and $M(K_n)=0$,

$$\left[\frac{d}{df}M(f)\right]_{f=K_n}=f^{9}\left\{10\,\widetilde{M}(\xi)+\xi\frac{d}{d\xi}\widetilde{M}(\xi)\right\}=K_n^{9}\left[\xi\frac{d}{d\xi}\widetilde{M}(\xi)\right]_{\xi=\Xi_n}. \qquad \ldots\ldots(10.20)$$

in which $\Xi_n=K_nH$

Therefore (10.19) may be written in the following form:

$$\left\{\begin{aligned} u[R] &= 2\tilde{Q}\sum\left\{1\Big/\frac{d}{d\xi}\widetilde{M}(\xi)\right\}\cdot\left[-\{\tilde{C}\mathfrak{C}+\tilde{D}\mathfrak{S}\}+i\beta_1\{\tilde{E}\mathfrak{S}+\tilde{F}\mathfrak{C}\}\right]_{\xi=\Xi_n} \\ w[R] &= 2\tilde{Q}\sum\left\{1\Big/\frac{d}{d\xi}\widetilde{M}(\xi)\right\}\cdot\left[i\alpha_1\{\tilde{C}\mathfrak{S}+\tilde{D}\mathfrak{C}\}+\{\tilde{E}\mathfrak{C}+\tilde{F}\mathfrak{S}\}\right]_{\xi=\Xi_n} \end{aligned}\right. \qquad \ldots\ldots(10.21)$$

Now, in our study, we will take only two branches $\xi=\Xi_0$ and Ξ_1; that is to say the ordinary Rayleigh-waves and M_2-waves.[8]

In the next article we will show the numerical calculations of the above expressions corresponding to several values of p, or period, assuming some appropriate values for the physical constants and the structure of media.

---

[8] K. Sezawa and K. Kanai, *Proc. Imp. Acad.*, **11** (1935), 13, 96; *Bull. Earthq. Res. Inst.*, **13** (1935), 237, 471. **18** (1940), 1.
K. Sezawa, *Bull. Earthq. Res. Inst.*, **16** (1938), 1.
K. Kanai, *Bull. Earthq. Res. Inst.*, **26** (1948), 57.

Errata of 1st Paper.

Page	Line			
2	4	$\int_{ax}^{bx} F\left(\frac{z}{x}\right)\frac{1}{x}dx$	Read	$\int_{ax}^{bx} F\left(\frac{z}{x}\right)\cos z\cdot\frac{1}{x}dz$
,,	6	$F''(b)$	,,	$-F''(b)$
,,	,,	$[F'''(b)$,, $-F'''(a)$,, $]$	,,	$[-F'''(b)$,, $+F'''(a)$,, $]$
,,	9	(1.2)	,,	(2.2)
,,	14	$F_{-1}(a)\frac{1}{2}(\xi-a)^{\frac{1}{2}}$	,,	$F_{-1}(a)(\xi-a)^{-\frac{1}{2}}$
3	10	$x^{-\frac{1}{2}}$	,,	$x^{-\frac{3}{2}}$
4	21	(4c)(+	,,	(4c)+
,,	28	$\alpha=\sqrt{\xi^2-k^2}$	,,	$\alpha=\sqrt{\xi^2-h^2}$

---

3. 層のある媒質を傳はる表面波の研究 (2)

地震研究所　佐藤泰夫

第一報において我々は $\int_a^b F(\xi)\begin{matrix}\cos\\\sin\end{matrix}\xi x\,d\xi$ の形の定積分を x の漸近級數に展開する一つの方法を示したのであつた。その結果は本文に再錄してある (2.1), (2.2); (3.5), (3.6; (3.7), (3.8); (4.1) である。

この方法は，新しいやり方であるので，一二の例題を扱ふはづであつたが，前にはそのよゆうがなかつたので，本報告においてまずそれを行つた。

以上が第一部であり，第二部として，半無限彈性体の上に一樣な表面層がのつてゐる場合，その層内に震源があつた時に，十分遠くはなれた所ではどのやうな波が傳はつてくるか，といふ問題を理論的にといた。途中の計算はやゝ複雜であるが，上に求めた積分の計算法によつて，比較的簡便に結果の式をもとめる事ができる。

實際の場合に適合するやうな數値を入れての計算は次の報告で發表する豫定である。

4. *On the M_2-waves (Sezawa-waves).*

By Kiyoshi KANAI,

Earthquake Research Institute.

(Read Dec. 17, 1946; July 18, 1950.—Received Dec. 20, 1950.)

1. Introduction.

Many years ago we found[1] that there are generally two kinds of different wave types of the dispersive Rayleigh-waves transmitted along the surface of a stratified body. But, our previous studies being restricted mainly to the fundamental nature of these waves, no detailed condition of the range of possible existence of these waves has yet been determined, owing to the extremely complicated forms of the mathematical solutions. In the present investigations, we shall extend our studies to the condition of the range of possible existence of dispersive Rayleigh-waves. Next, as we are now in a position to confirm the existence of M_2-waves in actual seismic waves, we shall deal with the general natures of the M_2-waves to a greater extent.

2. The dispersion curves of the M_2-waves.

The equation of dispersion curves of the Rayleigh-waves transmitted through a stratified body originally obtained by us is

$$\begin{aligned}
&\frac{4r's'}{f^2}\Big(2-\frac{k'^2}{f^2}\Big)\eta-\frac{r's'}{f^2}\Big\{4\vartheta+\Big(2-\frac{k'^2}{f^2}\Big)^2\zeta\Big\}\cosh r'H\cosh s'H\\
&\quad+\frac{r'}{f}\varphi\Big\{\frac{s}{f}\Big(2-\frac{k'^2}{f^2}\Big)^2-4\frac{rs'^2}{f^3}\Big\}\cosh r'H\sinh s'H\\
&\quad+\frac{s'}{f}\varphi\Big\{\frac{r}{f}\Big(2-\frac{k'^2}{f^2}\Big)^2-\frac{4sr'^2}{f^3}\Big\}\sinh r'H\cosh s'H\\
&\quad+\Big\{\Big(2-\frac{k'^2}{f^2}\Big)^2\vartheta+\frac{4r'^2s'^2}{f^4}\zeta\Big\}\sinh r'H\sinh s'H=0, \quad \ldots .(1)
\end{aligned}$$

---

[1] K. SEZAWA and K. KANAI, "Discontinuity in the Dispersion Curves of Rayleigh Waves", *Bull. Earthq. Res. Inst.*, **13** (1935), 238.
K. SEZAWA and K. KANAI, "The M_2-Seismic Waves", *Bull. Earthq. Res. Inst.*, **13** (1935), 471.

where

$$\left.\begin{aligned}
&\varphi = \frac{\mu' k^2 k'^2}{\mu f^4}, \quad \zeta = \frac{4rs}{f^2}\left(\frac{\mu'}{\mu}-1\right)^2 - \alpha^2, \quad \eta = \frac{2rs}{f^2}\left(\frac{\mu'}{\mu}-1\right)\beta - \alpha\gamma, \\
&\vartheta = \frac{rs}{f^2}\beta^2 - \gamma^2, \quad \alpha = \frac{2\mu'}{\mu} - \left(2-\frac{k^2}{f^2}\right), \quad \beta = \frac{\mu'}{\mu}\left(2-\frac{k'^2}{f^2}\right) - 2, \\
&\gamma = \frac{\mu'}{\mu}\left(2-\frac{k'^2}{f^2}\right) - \left(2-\frac{k^2}{f^2}\right), \\
&r^2 = f^2-h^2, \quad s^2 = f^2-k^2, \quad r'^2 = f^2-h'^2, \quad s'^2 = f^2-k'^2, \\
&h^2 = \rho p^2/(\lambda+2\mu), \quad k^2 = \rho p^2/\mu, \quad h'^2 = \rho' p^2/(\lambda'+2\mu'), \quad k'^2 = \rho' p^2/\mu',
\end{aligned}\right\} \quad (2)$$

in which H is the thickness of the stratum, $2\pi/f$ the wave length, ρ', λ', μ'; ρ, λ, μ the densities and elastic constants of the stratum and the subjacent medium respectively.

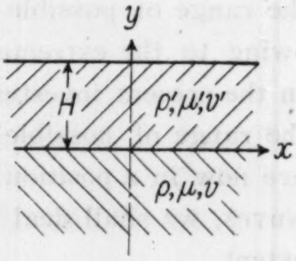

Fig. 1.

In our previous studies, the dispersion curves corresponding to the M_2-waves of very small wave length and the vicinity of critical condition were left untouched, owing to the extremely complex numerical calculations.

We shall now examine more closely the cases in which the ratios of the rigidity of the subjacent medium to that of the stratum are 2, 5, 20, ∞, the densities of both media being the same and Poisson's condition of elastic

Table I. $\mu/\mu'=5$, $\rho/\rho'=\lambda/\mu=\lambda'/\mu'=1$.

$p/f.\sqrt{\rho'/\mu'}$		1.0	1.2247	1.414	1.4491	1.5497
L/H	M_2	0	0.9079	—	1.358	1.782
	M	—	2.904	3.85	4.050	4.812

Table II. $\mu/\mu'=20$, $\rho/\rho'=\lambda/\mu=\lambda'/\mu'=1$.

$p/f.\sqrt{\rho'/\mu'}$		1.0	1.0954	1.500	1.6432
L/H	M_2	0	0.5981	1.387	1.929
	M	—	1.818	3.484	3.9077

Table III. $\mu/\mu'=\infty$, $\rho/\rho'=\lambda/\mu=\lambda'/\mu'=1$.

$p/f.\sqrt{\rho'/\mu'}$		1.0	1.0954	1.4142	1.6432	1.8974
L/H	M_2	0	0.609	1.20	1.861	—
	M	—	2.098	3.120	3.730	4.37

constants being satisfied, and also the case in which the rigidity ratio is $\mu/\mu'=1.65$ and the density ratio $\rho/\rho'=1.14$. The results are given in Tables I, II, III (other values taken from previous papers[2]) and plotted in Figs. 2~6.

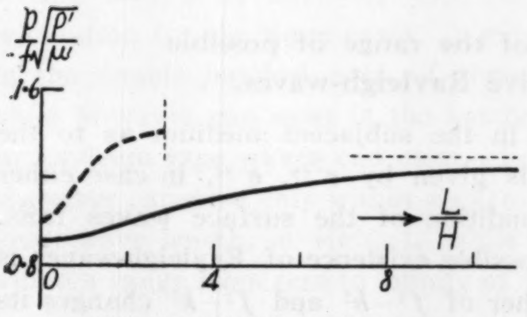

Fig. 2. The dispersion curves of a case in which $\lambda/\mu=\lambda'/\mu'=1$, $\rho/\rho'=1$, $\mu/\mu'=2$.

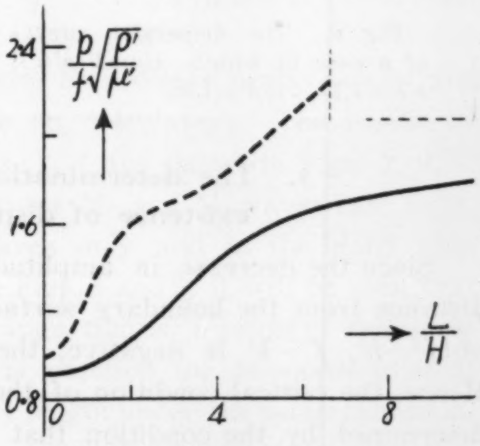

Fig. 3. The dispersion curves of a case in which $\lambda/\mu=\lambda'/\mu'=1$, $\rho/\rho'=1$, $\mu/\mu'=5$.

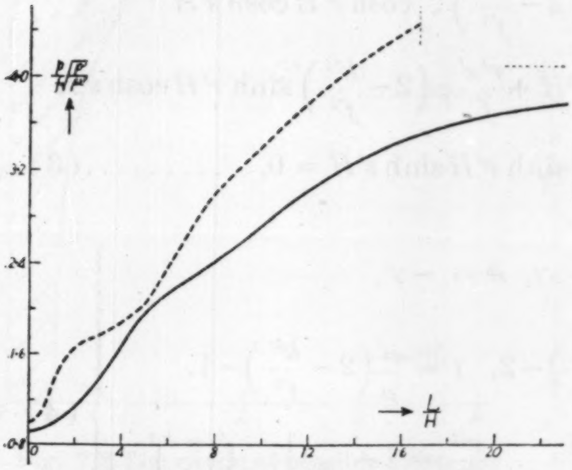

Fig. 4. The dispersion curves of a case in which $\lambda/\mu=\lambda'/\mu'=1$, $\rho/\rho'=1$, $\mu/\mu'=20$.

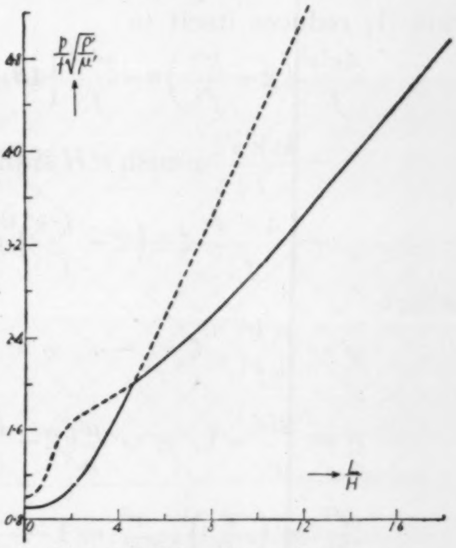

Fig. 5. The dispersion curves of a case in which $\lambda/\mu=\lambda'/\mu'=1$, $\rho/\rho'=1$, $\mu/\mu'=\infty$.

---

[2] *Bull. Earthq. Res. Inst.*, **3** (1927), 1; **13** (1935), 238; 239; 472.

It will be seen from these figures that M_2-waves exist within a narrow range, that is, a range of relatively small wave length, while M-waves exist in throughout whole range of wave length. The velocity of transmission of the M_2-waves at critical condition reaches to the velocity of transverse waves of subjacent medium and those at $L/H \to 0$ tends to the velocity of the Stoneley-waves in case the Stoneley-wave can exist and to the transverse waves of stratum in case it cannot.

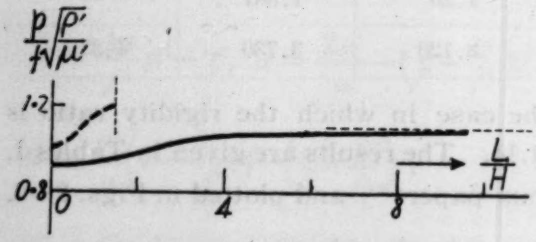

Fig. 6. The dispersion curves of a case in which $\lambda/\mu=\lambda'/\mu'=1$, $\rho/\rho'=1.14$, $\mu/\mu'=1.65$.

3. The determination of the range of possible existence of dispersive Rayleigh-waves.

Since the decrease in amplitudes in the subjacent medium as to the distance from the boundary surface is given by e^{-ry}, e^{-sy}, in case either of f^2-h^2, f^2-k^2 is negative, the condition of the surface waves fails. Hence, the critical condition of the possible existence of Rayleigh-waves is determined by the condition that either of f^2-h^2 and f^2-k^2 changes its sign from positive to negative. From the nature of things $h^2<k^2$, the condition under consideration is given by $f^2=k^2$. Then, the velocity equation (1) reduces itself to

$$\begin{aligned}&\frac{4r's'}{f^2}\left(2-\frac{k'^2}{f^2}\right)\eta-\frac{r'\;'}{f^2}\left\{4\vartheta+\left(2-\frac{k'^2}{f^2}\right)^2\zeta\right\}\cosh r'H\cosh s'H\\&-\frac{4rr's'^2}{f^4}\varphi\cosh r'H\sinh s'H+\frac{r's'}{f^2}\varphi\left(2-\frac{k'^2}{f^2}\right)^2\sinh r'H\cosh s'H\\&+\left\{\frac{4r'^2s'^2}{f^4}\zeta+\left(2-\frac{k'^2}{f^2}\right)^2\vartheta\right\}\sinh r'H\sinh s'H=0,\qquad\dots\dots\dots(3)\end{aligned}$$

where

$$\left.\begin{aligned}&\varphi=\frac{\mu'k'^2}{\mu f^2},\ \zeta=-\alpha^2,\ \eta=-\alpha\gamma,\ \vartheta=-\gamma^2,\\&\alpha=\frac{2\mu'}{\mu}-1,\ \beta=\frac{\mu'}{\mu}\left(2-\frac{k'^2}{f^2}\right)-2,\ \gamma=\frac{\mu'}{\mu}\left(2-\frac{k'^2}{f^2}\right)-1,\\&\frac{k'^2}{f^2}=\left(\frac{v}{v'}\right)^2,\ \frac{r^2}{f^2}=1-\frac{1}{\lambda/\mu+2},\ \frac{r'^2}{f^2}=1-\frac{1}{\lambda'/\mu'+2}\left(\frac{v}{v'}\right)^2,\\&\frac{s'^2}{f^2}=1-\left(\frac{v}{v'}\right)^2.\end{aligned}\right\}\ (4)$$

In special case $(v/v')^2=1$, equations (3) and (4) become

$$\frac{4r'}{f}\eta-\frac{r'}{f}(4\vartheta+\zeta)\cosh r'H+\frac{r}{f}\varphi\sinh r'H+(fH)\vartheta\sinh r'H=0, \quad (5)$$

where

$$\left.\begin{aligned} &\varphi=\frac{\mu'}{\mu},\ \ \zeta=-\left(\frac{2\mu'}{\mu}-1\right)^2,\ \ \eta=-\left(\frac{2\mu'}{\mu}-1\right)\left(\frac{\mu'}{\mu}-1\right),\\ &\vartheta=-\left(\frac{\mu'}{\mu}-1\right)^2,\ \ \frac{r^2}{f^2}=1-\frac{1}{\lambda/\mu+2},\ \ \frac{r'^2}{f^2}=1-\frac{1}{\lambda'/\mu'+2}. \end{aligned}\right\}\dots\dots(6)$$

Using equations (3)~(6), the special cases for Poisson's ratio ($\sigma=1/4$ and $\sigma'=1/4$, that is to say, $\lambda/\mu=\lambda'/\mu'=1$) are on calculation. The results of calculation for the three cases, $(v/v')^2=1/2$, 2, 1 are shown in Figs. 7, 8, 9. In the double hatched area of these figures M- and M_2-waves can exist, while M-waves can exist in the hatched area only and in the blank area no Rayleigh type waves can exist. From Figs. 8 and 9, it will be seen that M_2-waves can exist only within a narrow range, that is, a range of relatively small wave length, in $v/v'\geq 1$, while it is possible for M-waves to exist within a range from zero to infinity of wave length under the same condition.

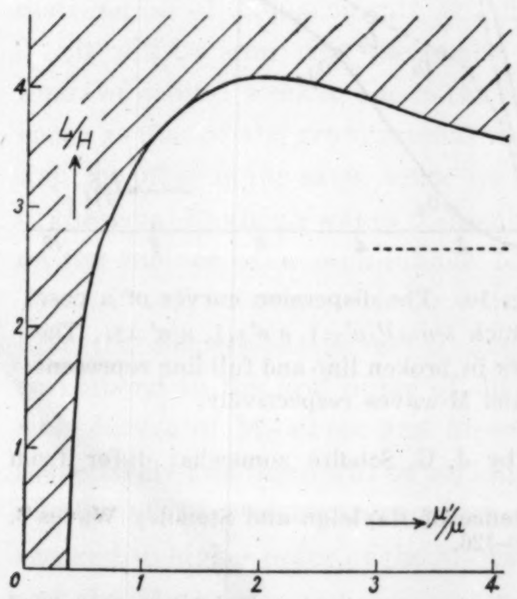

Fig. 7. The range of possible existence of M_2- and M-waves for the case $(v/v')^2=1/2$. In the hatched area M-waves only can exist; in the blank area no surface waves can exist.

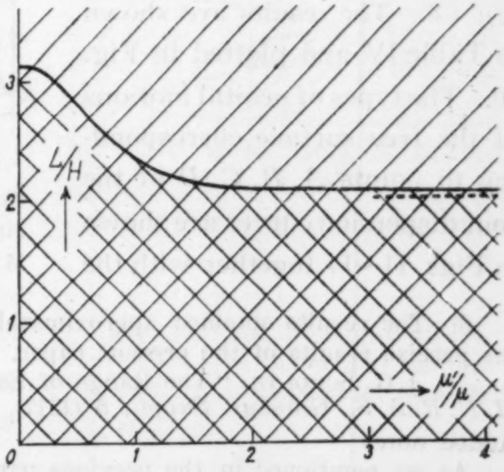

Fig. 8. The range of possible existence of M_2- and M-waves for the case $(v/v')^2=2$. In the double hatched area M_2- and M-waves can exist; in the hatched area M-waves only can exist.

On the other hand, Fig. 7 shows that, under the condition of $v/v' < 1$, no M_2-waves can exist in any wave length, while M-waves exist in relatively large wave length unless the condition of possible existence of the Stoneley-waves be satisfied, that is to say, $\mu'/\mu > 0.39$, and exist for any wave length within the range $\mu'/\mu \leq 0.39$ where Stoneley-waves can exist, under the condition of $v/v' < 1$.[3]

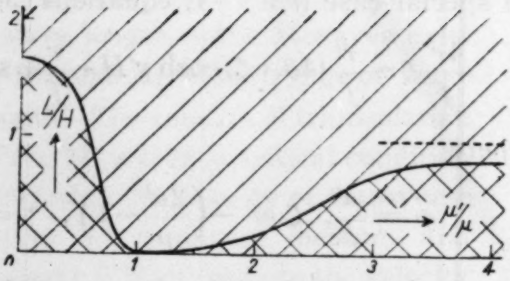

Fig. 9. The range of possible existence of M_2- and M-waves for the case $(v/v')^2=1$. In the double hatched area M_2- and M-waves can exist; in the hatched area M-waves only can exist.

4. Dispersion curves of higher order of M- and M_2-waves.

In order to make the nature of M_2-waves clear, we determined the dispersion curves of M- and M_2-waves of higher order in the bodies whose densities and elastic constants are specified by $\lambda/\mu=\lambda'/\mu'=1$, $\rho/\rho'=1$, $\mu/\mu'=8$. The results are shown in Table IV and plotted in Fig. 10. The types of orbital motions of the free surface corresponding to points *A*, *B*, *C*, *D* of the four dispersion curves are shown in Figs. 11~14 together with the

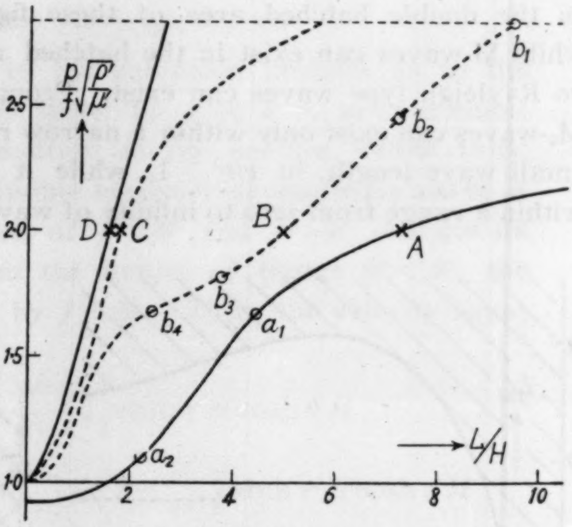

Fig. 10. The dispersion curves of a case in which $\lambda/\mu=\lambda'/\mu'=1$, $\rho/\rho'=1$, $\mu/\mu'=8$. The curves in broken line and full line represent M_2- and M-waves respectively.

---

[3] The results obtained approximately by J. G. Scholte somewhat differ from the precise results of the present paper.
J. G. SCHOLTE, "The Range of Existence of Rayleigh and Stoneley Waves", *M. N. R. A. S., Geophys. Suppl.*, **5** (1947), 120–126.

Added note:

As we mentioned in the previous paper,[4] our numerical calculations concerned with Stoneley waves were carried out by means of the equations which were led by introducing $f^2=k^2$ or $f^2=k'^2$ into (4). The form of the equations used but not written in the paper is reduced to that[5] of (1) and (2) of Scholte's paper.

[4] K. SEZAWA and K. KANAI, "The Range of Possible Existence of Stoneley waves, and Some Related Problems", *Bull. Earthq. Res. Inst.*, **17** (1939), 3.

[5] *loc. cit.*, 3), 120.

Table IV. $\mu/\mu'=8,\ \rho/\rho'=\lambda/\mu=\lambda'/\mu'=1.$

$p/f.\sqrt{\rho'/\mu'}$		1.0	1.1	1.32	1.44	1.56	1.68	1.8166	2.000	2.4495
L/H	M_2	0	0.62832	1.0665	1.2913	1.617	2.436	3.763	4.942	7.154
	M	—	2.2258	3.0998	3.5508	—	4.434	5.427	7.270	24.05

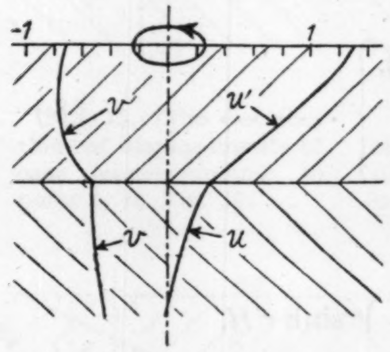

Fig. 11. The distributions of displacements and orbital motion of case corresponding to point A in Fig. 10.

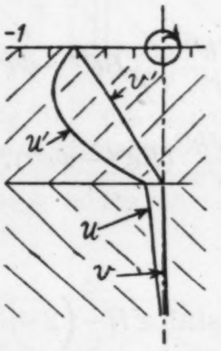

Fig. 12. The distributions of displacements and orbital motion of case corresponding to point B in Fig. 10.

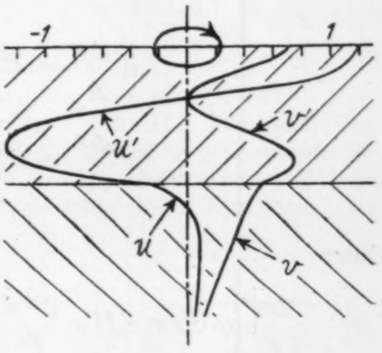

Fig. 13. The distributions of displacements and orbital motion of case corresponding to point C in Fig. 10.

distribution of displacements at different depths.

It will be seen that there are two kinds of orbital motion, one in the same sense as that of the gravitational waves and the other in the same sense as that of the usual Rayleigh-waves transmitted on the surface of a semi-infinite body. Then, it will be reasonable to consider that the dispersion curves C and D correspond to the first order of dispersion curves of M_2-waves and M-waves respectively and there will be an infinite number of dispersion curves which correspond to higher order of the M_2-waves and the M-waves.

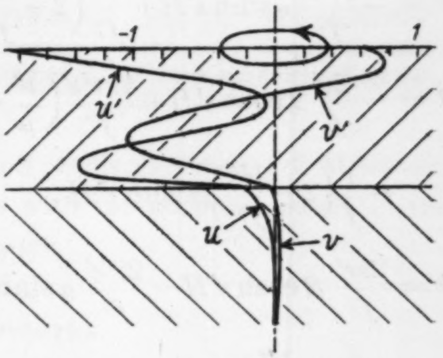

Fig. 14. The distributions of displacements and orbital motion of case corresponding to point D in Fig. 10.

5. Distribution of displacements at different depths.

We also studied closely the distribution of displacements at different depths. Horizontal and vertical components of displacement within the stratum and in the subjacent medium is reduced to

$$\left.\begin{aligned} u'\frac{\Phi f}{A} &= \frac{s'}{f}\left(C\cosh r'y + D\sinh r'y + \frac{s'}{f}E\sinh s'y + F\cosh s'y\right), \\ v'\frac{\Phi f}{A} &= i\left(\frac{r's'}{f^2}C\sinh r'y + \frac{r's'}{f^2}D\cosh r'y + \frac{s'}{f}E\cosh s'y + F\sinh s'y\right), \end{aligned}\right\} \tag{7}$$

$$\left.\begin{aligned} u\frac{\Phi f}{A} &= \frac{\mu' s' k'^2}{\mu f^3}\left(\frac{s}{f}Be^{sy} - \Phi e^{ry}\right), \\ v\frac{\Phi f}{A} &= \frac{i u' s' k'^2}{\mu f^3}(Be^{sy} - \Phi e^{ry}), \end{aligned}\right\} \quad \dots\dots\dots\dots\dots\dots (8)$$

where

$$\left.\begin{aligned} C &= -\frac{2sr'}{f^2}\varphi\cosh s'H + \frac{2r's'}{f^2}\zeta\sinh s'H - \left(2-\frac{k'^2}{f^2}\right)\eta\sinh r'H, \\ D &= -2\vartheta\cosh s'H - \frac{2rs'}{f^2}\varphi\sinh s'H + \left(2-\frac{k'^2}{f^2}\right)\eta\cosh r'H, \\ E &= \frac{2r'}{f}\eta\cosh s'H - \frac{r'}{f}\left(2-\frac{k'^2}{f^2}\right)\zeta\cosh r'H + \frac{r}{f}\left(2-\frac{k'^2}{f^2}\right)\varphi\sinh r'H, \\ F &= -\frac{2r's'}{f^2}\eta\sinh s'H + \frac{sr'}{f^2}\left(2-\frac{k'^2}{f^2}\right)\varphi\cosh r'H + \left(2-\frac{k'^2}{f^2}\right)\vartheta\sinh r'H, \\ B &= -\frac{2r'}{f}\gamma\cosh s'H + \frac{4rr's'}{f^3}\left(\frac{\mu'}{\mu}-1\right)\sinh s'H + \frac{r'}{f}\left(2-\frac{k'^2}{f^2}\right)\alpha\cosh r'H \\ &\quad - \frac{r}{f}\left(2-\frac{k'^2}{f^2}\right)\beta\sinh r'H, \\ \Phi &= \frac{2sr'}{f^2}\beta\cosh s'H - \frac{2r's'}{f^2}\alpha\sinh s'H - \frac{2sr'}{f^2}\left(2-\frac{k'^2}{f^2}\right)\left(\frac{\mu'}{\mu}-1\right)\cosh r'H \\ &\quad + \left(2-\frac{k'^2}{f^2}\right)\gamma\sinh r'H. \end{aligned}\right\} \tag{9}$$

The results of calculations of the cases corresponding to points b_1, b_2, b_3, b_4, a_1, a_2 indicated in Fig. 10, are shown in Figs. 15~20. These figures show that the distribution of displacements of waves corresponding to M_2-waves is somewhat different from that of M-waves. It appears that there is the maximum of horizontal displacements having no horizontal nodal plane in the stratum for M_2-waves excepting relatively small wave length, while it

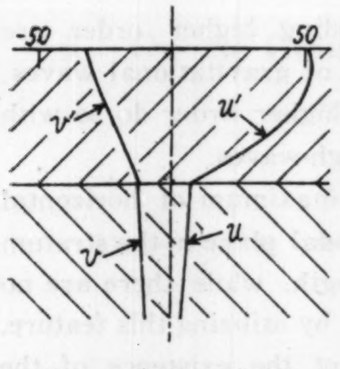

Fig. 15. The distributions of displacements of case corresponding to point b_1 in Fig. 10.

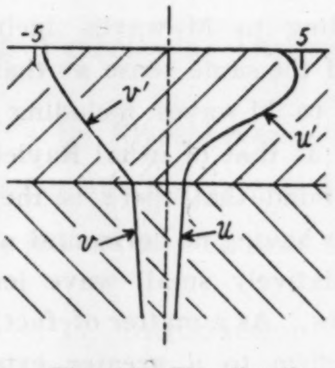

Fig. 16. The distributions of displacements of case corresponding to point b_2 in Fig. 10.

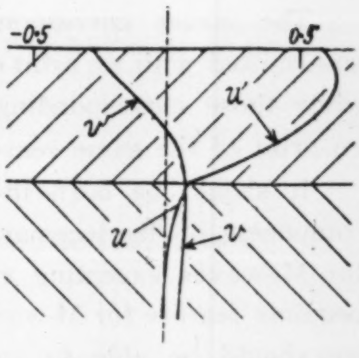

Fig. 17. The distributions of displacements of case corresponding to point b_3 in Fig. 10.

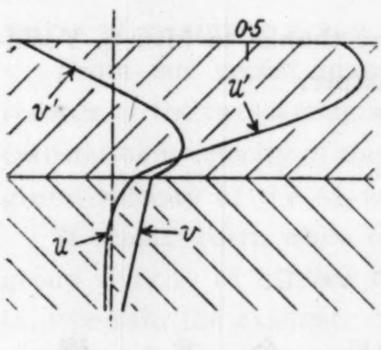

Fig. 18. The distributions of displacements of case corresponding to point b_4 in Fig. 10.

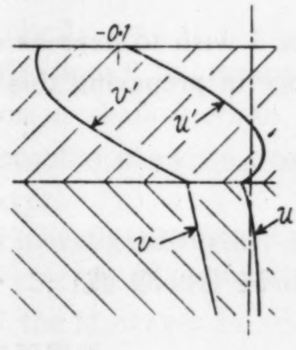

Fig. 19. The distributions of displacements of case corresponding to point a_1 in Fig. 10.

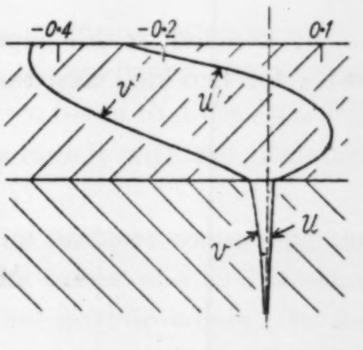

Fig. 20. The distributions of displacements of case corresponding to point a_2 in Fig. 10.

seems no particular feature in the distribution of displacements of M-waves. It would be useful to identify the M_2-waves with the peculiar waves in the seismic records at different depths of the earth.

6. Concluding remarks.

From mathematical investigations it is ascertained that the two kinds of dispersive Rayleigh-waves, which we have previously found, fairly differ in their nature. It has been ascertained fairly that M_2-waves can exist in a narrow range, that is the range of relatively small wave length, in $v/v' \geq 1$, and impossible to exist in any wave length in $v/v' < 1$. While, M-waves exist in any wave length in $v/v' \geq 1$, and in the range $v/v' < 1$ for $\mu'/\mu \leq 0.39$, and are possible to exist for relatively large wave length in the range $\mu'/\mu > 0.39$ under the condition of $v/v' < 1$.

The waves corresponding to M_2-waves including higher order are transmitted with an orbit of the same sense as that of gravitational waves, while those corresponding to M-waves including higher order do so with an orbit of the same sense as that of usual Rayleigh-waves.

It should be born in mind that there is the maximum of horizontal component of displacements having no horizontal nodal plane in the stratum for M_2-waves excepting relatively small wave length, while there are no peculiar feature for M-waves. As a matter of fact, by utilizing this feature, we should be able to confirm to a greater extent the existence of the M_2-waves in actual seismic disturbance.

These results were found from complex numerical calculations, and not immediately from the mathematical expressions.

In concluding this paper I wish to express my thanks to Miss S. Yoshizawa for her kind assistance in preparing this paper.

---

4. M_2 波 (妹澤波) について

地震研究所　金井　清

一つの表面層がある場合の２種類の表面波，即ち分散性レーレー波及び M_2 波，の性質を數理的にしらべた。$\lambda/\mu=\lambda'/\mu'=1$ の場合，v, v' を夫々下層，表面層の横波の速度とすると，M_2 波は $v/v'\geqq 1$ の場合には比較的に短波長の範圍に存在し得るが，$v/v'<1$ の場合には實在し得ない。M 波の方は $v/v'\geqq 1$ の場合には，あらゆる波長にわたつて存在し得，$v/v'<1$ の場合には $\mu'/\mu\leqq 0.39$ の範圍ではあらゆる波長にわたつて存在し得るが，$\mu'/\mu>0.39$ の範圍では比較的に長波長のところにのみ存在することができる。

M_2 波と M 波について，地表面よりの深さと振幅との關係をしらべたところ，M_2 波の水平成分の分布に限つて，多くの場合表面層中に極大ができることがわかつた。この性質は地表面における波點の運動軌跡が普通のレーレー波と逆である性質と相まつて，實際の地震記象を解析して M_2 波の實在性を確める上に相當に役立つことであろう。

尙，M_2 波は，M 波の中の表面層中に節のできる，いわゆる，M 波の高次の波とは異ることを確めておいた。

5. *On the Group Velocity of Dispersive Surface Waves.*

By Kiyoshi Kanai,

Earthquake Research Institute.

(Read Sept. 18, 1945; Mar. 19, May 21, 1946.—Received Dec. 20, 1950.)

1. Introduction.

The problem concerning group velocity of seismic waves already was paid attentions to by Nagaoka,[1] Gutenberg[2] about a quarter of a century ago. Several years ago Stoneley[3] showed that, as to be expected from the approximate theory of waves, the Love-waves and the dispersive Rayleigh-waves of minimum group velocity tend to predominate in seismograms.

From our recent investigations[4] by means of analysing the seismic records of the two earthquakes of shallow origin, we found that the apparent transmission velocity of the peculiar phases agrees closely with the minimum group velocity of the M_2-waves.

It seems worth while to investigate further the problem concerning the group velocity of dispersive surface waves because we are now in a position to ascertain the existence of the M_2-waves in actual seismic waves. In the present paper we shall deal with the problem of group velocity of Love-waves, dispersive Rayleigh-waves and M_2-waves mathematically.

2. Group velocity of the Love-waves.

In the case of a one-stratified body, the velocity[5] of Love-waves is expressed by

$$\tan\left(\frac{2\pi}{\lambda}\sqrt{c^2-1}\right)=\frac{\mu}{\mu'}\sqrt{\frac{1-\frac{\rho\mu'}{\rho'\mu}c^2}{c^2-1}}\,, \qquad \ldots\ldots\ldots\ldots\ldots\ldots\ldots(1)$$

---

[1] H. Nagaoka, "Group Velocity in Distant Earthquakes", *Proc. Phys.-Math. Soc., Japan*, **3** (1906), 44.

[2] B. Gutenberg, "Über Gruppengeschivindigkeit bei Erdbebenwellen", *Phys. Z. S.*, **27** (1926), 114.

[3] R. Stoneley, "Surface-waves associated with 20° Discontinuity", *M.N.R.A.S., Geophys. Suppl.*, **4** (1937), 39.

[4] K. Kanai, "On the Existence of the M_2-waves in Actual Seismic Disturbances", *Bull. Earthq. Res. Inst.*, **26** (1948), 57.

[5] A. E. H. Love, "Some Problem of Geodynamics", (Cambridge, 1911), 162.

where $\lambda = L/H$, $c^2 = \rho' p^2/\mu' f^2$, $2\pi/f = L =$ wave length, $2\pi/p = T =$ period, $H =$ thickness of the stratum, ρ, ρ'; μ, μ'; v, v' densities, rigidities and velocities of transverse waves of the subjacent medium and the stratum respectively.

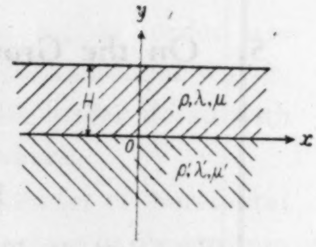

Fig. 1.

The equation of group velocity of waves is written in the form

$$U = c - \lambda \frac{\partial c}{\partial \lambda}, \quad \dots\dots\dots\dots\dots\dots\dots\dots (2)$$

where U is the ratio of the group velocity of waves to the velocity of transverse waves of the stratum (v'). From (1) and (2), we get

$$U = c - \frac{2(c^2-1)}{c\Phi}, \quad \dots\dots\dots\dots\dots\dots\dots\dots (3)$$

where

$$\Phi = \frac{4\pi}{\lambda}\sqrt{c^2-1}\left(1 - \frac{\rho\mu'}{\rho'\mu}c^2\right) + \left(1 - \frac{\rho\mu'}{\rho'\mu}\right)\sin\frac{4\pi}{\lambda}\sqrt{c^2-1}. \quad \dots (4)$$

By means of equations (1) and (3), we determined the dispersion curves of Love-waves and calculated the group velocity of those with the following ratios of densities and rigidities.

$$\text{(i)} \quad \frac{\rho}{\rho'} = 1; \quad \frac{\mu}{\mu'}\left\{ = \left(\frac{v}{v'}\right)^2 \right\} = \frac{5}{4},\ 2,\ \frac{10}{3},\ 6,\ 10,\ 25,$$

$$\text{(ii)} \quad \frac{\rho}{\rho'} = 1.1; \quad \frac{\mu}{\mu'} = 2.2,\ 4.4,\ 11,\ 27.5 \left\{\text{i.e.} \left(\frac{v}{v'}\right)^2 = 2,\ 4,\ 10,\ 25\right\},$$

$$\text{(iii)} \quad \frac{\rho}{\rho'} = 2; \quad \frac{\mu}{\mu'} = 4,\ 10,\ 25,\ 50 \left\{\text{i.e.} \left(\frac{v}{v'}\right)^2 = 2,\ 5,\ 12.5,\ 25\right\}.$$

The results of calculations of the fourteen cases given above are plotted in Figs. 2~15. In these figures, phase velocities and group velocities are indicated respectively by full lines and broken ones.

Next, we determined graphically the conditions of the minimum group velocities by means of Figs. 2~15. The relations of the minimum group velocity and phase velocity as well as the period of waves corresponding with the minimum group velocity to the velocity ratio of the two mediums, under the condition in which the density ratio of the two mediums is kept

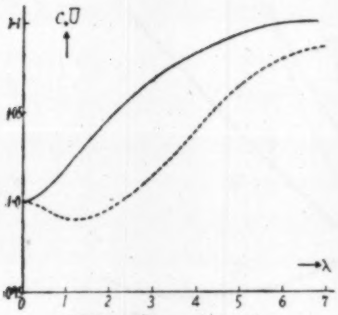

Fig. 2. $\rho/\rho'=1$, $\mu/\mu'=1.25$.

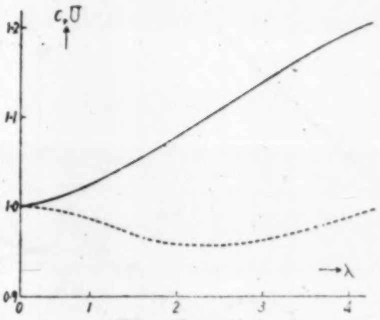

Fig. 3. $\rho/\rho'=1$, $\mu/\mu'=2$.

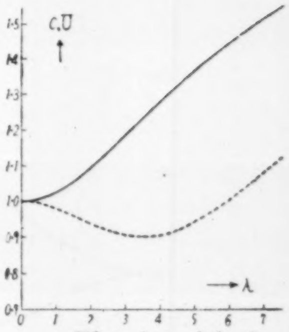

Fig. 4. $\rho/\rho'=1$, $\mu/\mu'=10/3$.

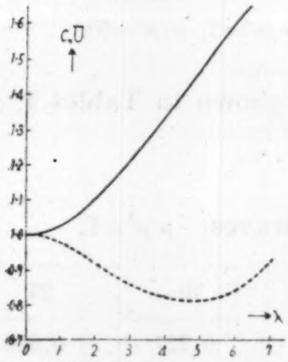

Fig. 5. $\rho/\rho'=1$, $\mu/\mu'=6$.

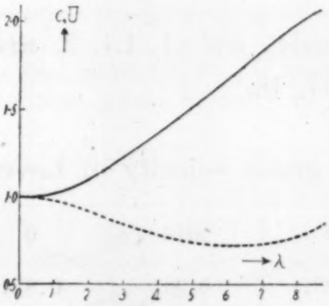

Fig. 6. $\rho/\rho'=1$, $\mu/\mu'=10$.

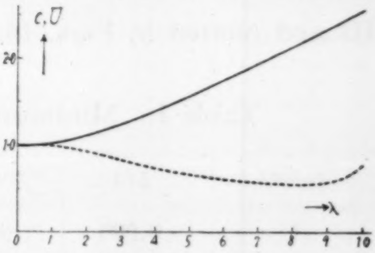

Fig. 7. $\rho/\rho'=1$, $\mu/\mu'=25$

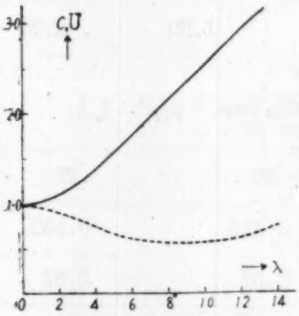

Fig. 8. $\rho/\rho'=1.1$, $\mu/\mu'=2.2$.

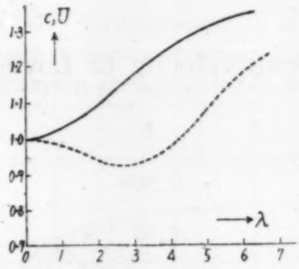

Fig. 9. $\rho/\rho'=1.1$, $\mu/\mu'=4.4$.

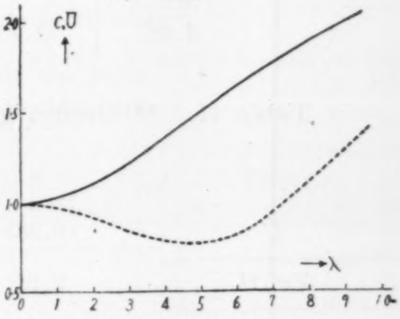

Fig. 10. $\rho/\rho'=1.1$, $\mu/\mu'=11$.

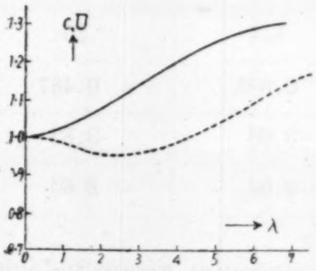

Fig. 11. $\rho/\rho'=1.1$, $\mu/\mu'=27.5$.

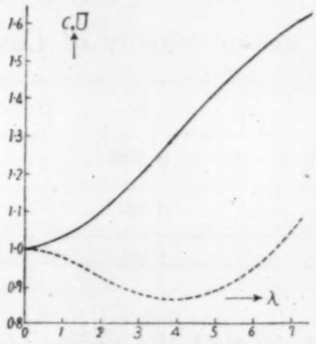

Fig. 12. $\rho/\rho'=2$, $\mu/\mu'=4$.

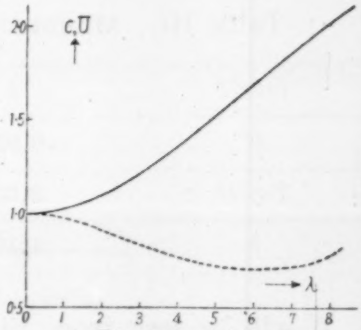

Fig. 13. $\rho/\rho'=2$, $\mu/\mu'=10$.

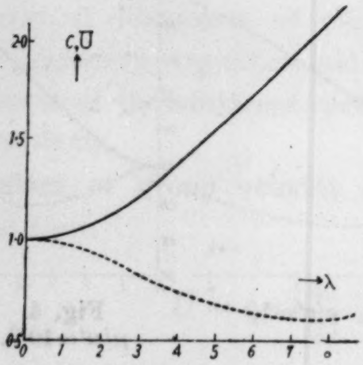

Fig. 14. $\rho/\rho'=2,\ \mu/\mu'=25.$

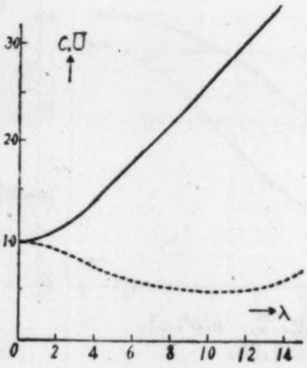

Fig. 15. $\rho/\rho'=2,\ \mu/\mu'=50.$

constant in three cases, namely, $\rho/\rho'=1$, 1.1, 2, are shown in Tables I, II, III and plotted in Figs. 16, 17, 18.

Table I. Minimum group velocity of Love-waves. $\rho/\rho'=1$.

$(v/v')^2$	5/4	2	10/3	6	10	25
U	0.990	0.957	0.901	0.814	0.727	0.566
Tv'/H	1.20	2.18	2.84	3.31	3.61	3.79
c	1.025	1.10	1.23	1.435	1.69	2.24

Table II. Minimum group velocity of Love-waves. $\rho/\rho'=1.1$.

$(v/v')^2$	2	4	10	25
U	0.953	0.868	0.715	0.552
Tv'/H	2.22	2.95	3.57	3.82
c	1.11	1.30	1.70	2.35

Table III. Minimum group velocity of Love-waves. $\rho/\rho'=2$.

$(v/v')^2$	2	5	5/4	25
U	0.927	0.776	0.605	0.487
Tv'/H	2.33	3.30	3.69	3.83
c	1.15	1.50	2.04	2.60

It will be seen from Fig. 16 that the value of minimum group velocity of Love-waves decreases with the increase in the velocity ratio of the

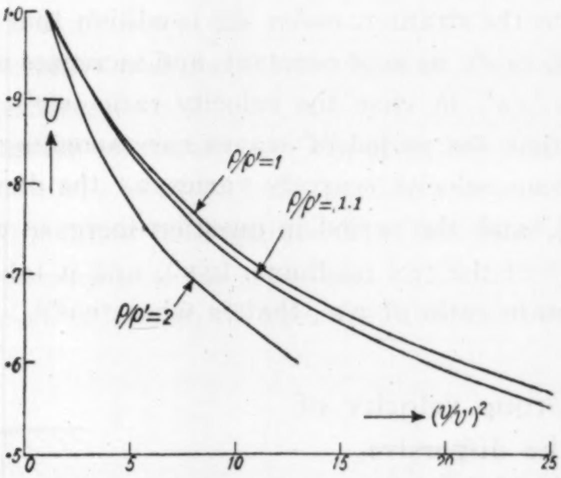

Fig. 16. Love-waves. *U* is in the ratio of minimum group velocity to *v'*.

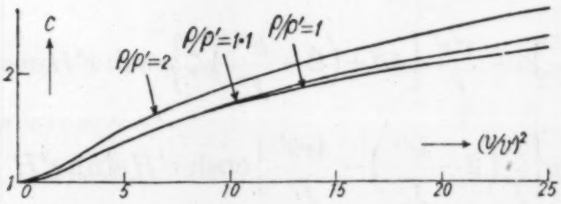

Fig. 17. Love-waves. *c* is in the ratio of phase velocity correspond to the case in minimum group velocity to *v'*.

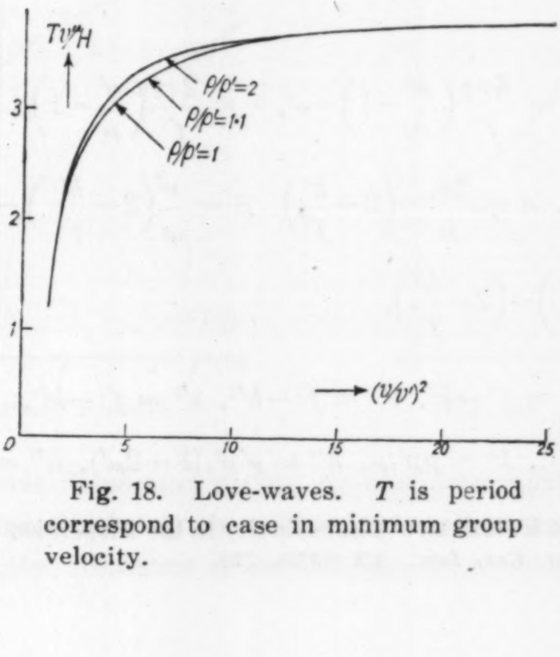

Fig. 18. Love-waves. *T* is period correspond to case in minimum group velocity.

subjacent medium to the stratum, under the condition that the density ratio of the two mediums, (ρ/ρ'), as kept constant, and increases with the decrease in the density ratio (ρ/ρ') in case the velocity ratio (v/v') is kept constant.

Fig. 17 shows that the period of waves corresponding to the condition in the minimum group velocity scarcely varies as the density ratio of the two mediums, (ρ/ρ'), and the period in question increase with the increase in the velocity ratio of the two mediums, (v/v'), and it takes an asymptotic value beyond a certain ratio of v/v', that is when $(v/v')^2 > 10$.

3. Group velocity of the dispersive Rayleigh-waves.

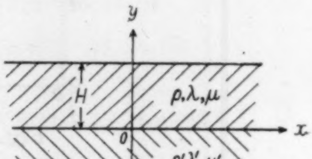

Fig. 19.

It was already found that the velocity equation of dispersive Rayleigh-waves transmitted through a stratified body is expressed by[6]

$$\begin{aligned}
&\frac{4r's'}{f^2}\left(2-\frac{k'^2}{f^2}\right)\eta-\frac{r's'}{f^2}\left\{4\vartheta+\left(2-\frac{k'^2}{f^2}\right)^2\zeta\right\}\cosh r'H\cosh s'H\\
&\quad+\frac{r'}{f}\varphi\left\{\frac{s}{f}\left(2-\frac{k'^2}{f^2}\right)^2-\frac{4rs'^2}{f^3}\right\}\cosh r'H\sinh s'H\\
&\quad+\frac{s'}{f}\varphi\left\{\frac{r}{f}\left(2-\frac{k'^2}{f'^2}\right)^2-\frac{4sr'^2}{f^3}\right\}\sinh r'H\cosh s'H\\
&\quad+\left\{\left(2-\frac{k'^2}{f^2}\right)^2\vartheta+\frac{4r'^2s'^2}{f^4}\zeta\right\}\sinh r'H\sinh s'H=0\,, \qquad \ldots\ldots(5)
\end{aligned}$$

where

$$\left.\begin{aligned}
&\varphi=\frac{\mu'k^2k'^2}{\mu f^4},\ \zeta=\frac{4rs}{f^2}\left(\frac{\mu'}{\mu}-1\right)^2-\alpha^2,\ \eta=\frac{2rs}{f^2}\left(\frac{\mu'}{\mu}-1\right)\beta-\alpha\gamma,\\
&\vartheta=\frac{rs}{f^2}\beta^2-\gamma^2,\ \alpha=\frac{2\mu'}{\mu}-\left(2-\frac{k^2}{f^2}\right),\ \beta=\frac{\mu'}{\mu}\left(2-\frac{k'^2}{f^2}\right)-2,\\
&\gamma=\frac{\mu'}{\mu}\left(2-\frac{k'^2}{f^2}\right)-\left(2-\frac{k^2}{f^2}\right),\\
&r^2=f^2-h^2,\ s^2=f^2-k^2,\ r'^2=f^2-h'^2,\ s'^2=f^2-k'^2,\\
&h^2=\rho p^2/(\lambda+2\mu),\ k^2=\rho p^2/\mu,\ h'^2=\rho'p^2/(\lambda'+2\mu'),\ k'^2=\rho'p^2/\mu',
\end{aligned}\right\}(6)$$

---

[6] K. SEZAWA and K. KANAI, "Discontinuity in the Dispersion Curves of Rayleigh Waves", *Bull. Earthq. Res. Inst.*, **13** (1935), 238.

in which H is the thickness of the stratum, $2\pi/f$ the wave length, and ρ, λ, μ; ρ', λ', μ' the densities and elastic constants of the subjacent medium and the stratum respectively.

Dispersion curves of cases $\mu/\mu'=3$, 5, 8, 20 ($\lambda=\mu$, $\lambda'=\mu'$, $\rho/\rho'=1$) and $\mu/\mu'=1.65$ ($\lambda=\mu$, $\lambda'=\mu'$, $\rho/\rho'=1.14$) calculated by means of the above equation are shown by full lines in Figs. 20~24. The third and the fifth cases correspond approximately to the superficial condition of the Kwanto district in Japan and the stratification of Eurasian Continent respectively.

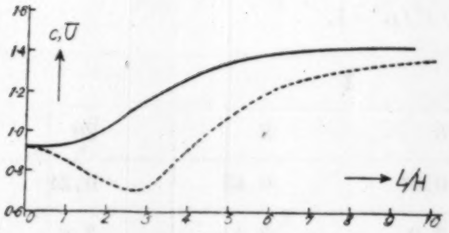

Fig. 20. $\rho/\rho'=1$, $\mu/\mu'=3$.

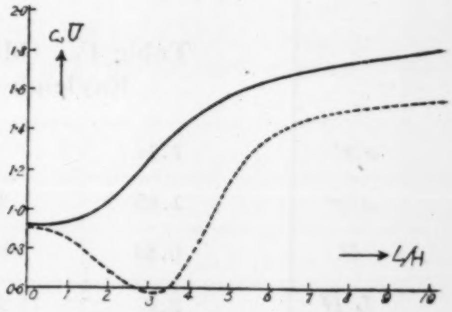

Fig. 21. $\rho/\rho'=1$, $\mu/\mu'=5$.

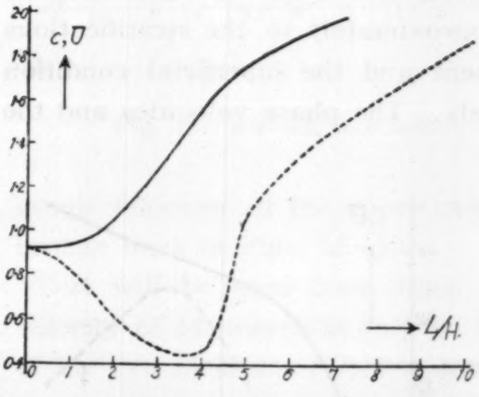

Fig. 22. $\rho/\rho'=1$, $\mu/\mu'=8$.

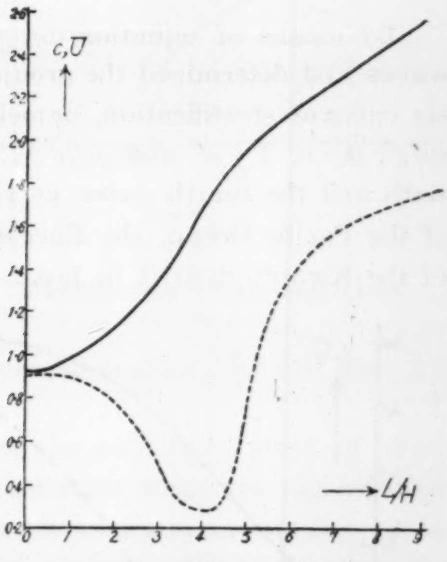

Fig. 23. $\rho/\rho'=1$, $\mu/\mu'=20$.

Using the above dispersion curves, we next determined the group velocity graphically, the results being shown by broken lines in Figs. 20~24. The relations among the minimum group velocity, the wave length corresponding

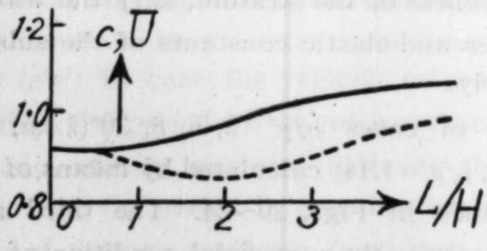

Fig. 24. $\rho/\rho'=1.14$, $\mu/\mu'=1.65$.

to the minimum group velocity and the rigidity ratio of the two mediums are shown in Table IV.

Table IV. Minimum group velocity of Rayleigh-waves, $\lambda/\mu=\lambda'/\mu'=1$.

ρ/ρ'	1.14	1			
μ/μ'	1.65	3	5	8	20
U	0.84	0.71	0.61	0.45	0.24
L/H	2.0	2.5	3.0	3.4	3.8

4. Group velocity of the M_2-waves.

By means of equation (5), we calculated the dispersion curves of M_2-waves and determined the group velocity of them graphically. We selected six cases of stratification, namely $\mu/\mu'=2, 3, 5, 8, 20$ under the conditions of $\rho=\rho'$, $\lambda=\mu$, $\lambda'=\mu'$ and $\mu/\mu'=1.65$, $\rho/\rho'=1.14$, $\lambda/\mu=\lambda'/\mu'=1$. The first, the sixth and the fourth cases correspond approximately to the stratifications of the Pacific Ocean, the Eurasian Continent and the superficial condition of the Kwanto district in Japan respectively. The phase velocities and the

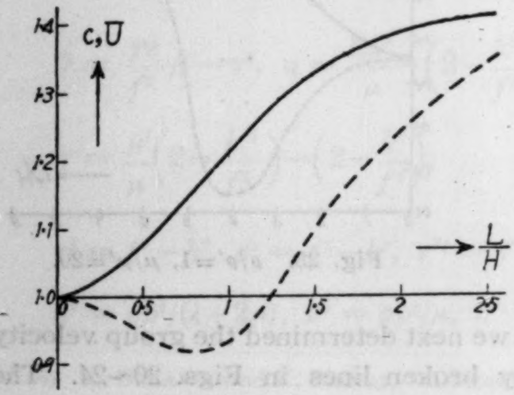

Fig. 25. $\rho/\rho'=1$, $\mu/\mu'=2$.

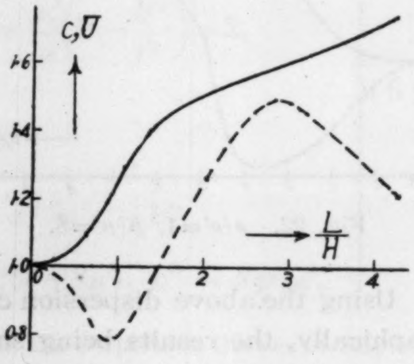

Fig. 26. $\rho/\rho'=1$, $\mu/\mu'=3$.

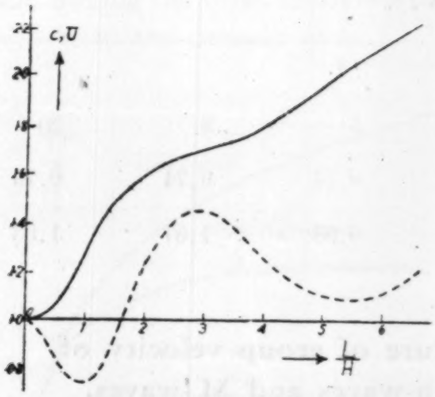

Fig. 27. $\rho/\rho'=1$, $\mu/\mu'=5$.

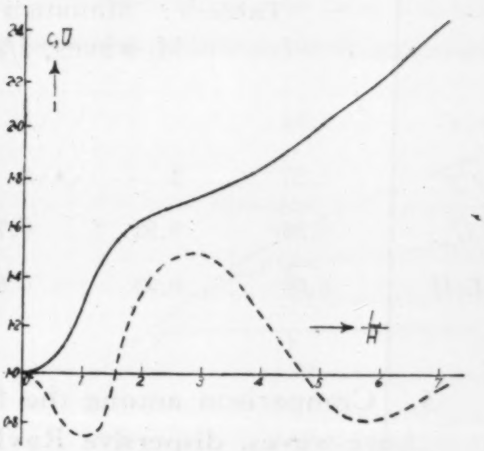

Fig. 28. $\rho/\rho'=1$, $\mu/\mu'=8$.

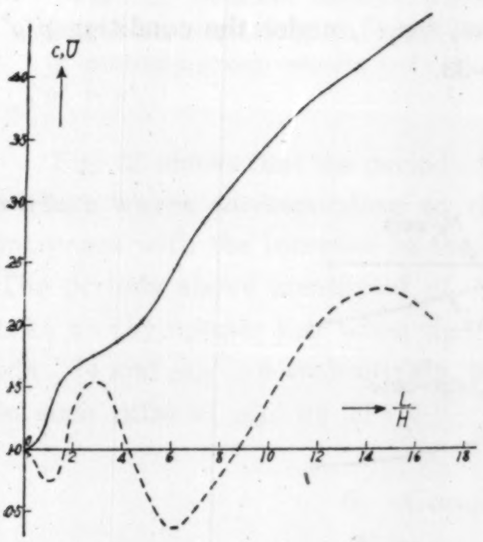

Fig. 29. $\rho/\rho'=1$, $\mu/\mu'=20$.

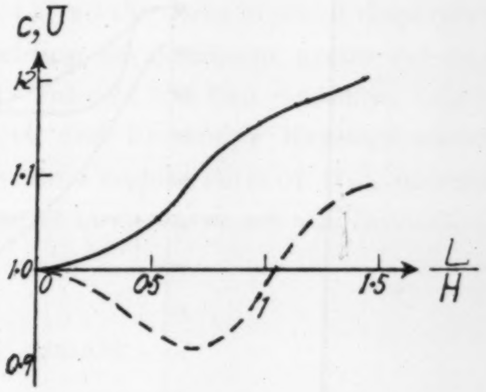

Fig. 30. $\rho/\rho'=1.14$, $\mu/\mu'=1.65$.

group velocities of the above cases are shown respectively by full lines and broken lines in Figs. 25~30.

It will be seen from Figs. 25~30 that the stationary state of group velocity of M_2-waves is only in the minimum state when the rigidity ratio of the two mediums (μ/μ') is small, such a phenomenon is similiar to the feature of the group velocity of Love-waves as well as Rayleigh-waves, but the number of the state mentioned above increases with increase in the rigidity ratio of two mediums, (μ/μ'). The relations among the first minimum group velocity, wave length corresponding to the minimum group velocity and rigidity ratio of the two mediums are shown in Table V.

Table V. Minimum group velocity of
M_2-waves, $\lambda/\mu=\lambda'/\mu'=1$.

ρ/ρ'	1.14	1				
μ/μ'	1.65	2	3	5	8	20
U	0.93	0.92	0.79	0.74	0.74	0.75
L/H	0.66	0.83	0.96	0.98	1.07	1.03

5. Comparison among the feature of group velocity of Love-waves, dispersive Rayleigh-waves and M_2-waves.

The relations among the minimum group velocity, wave length as well as phase velocity corresponding to the condition in the minimum group velocity and rigidity ratio of two mediums, (μ/μ'), under the condition $\rho/\rho'=1$, $\lambda/\mu=\lambda'/\mu'=1$, are shown in Figs. 31~33.

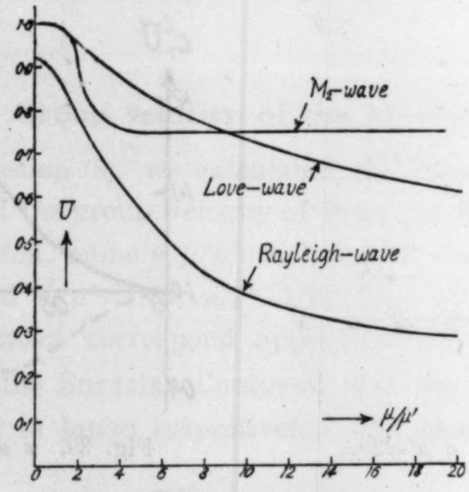

Fig. 31. Relation between the minimum group velocity and ratio of μ/μ'.

From Fig. 31 we found that the value of minimum group velocity of the three kinds of dispersive surface waves tends to decrease with the increase in the rigidity ratio of two mediums, (μ/μ'). The values mentioned above of dispersive Rayleigh-waves are the smallest among the three kinds of waves and decrease rapidly with the increase in the ratio μ/μ', and those of Love-waves decrease somewhat gradually with the increase in the ratio μ/μ', while those of M_2-waves, in case they are beyond a certain ratio of

μ/μ', namely $\mu/\mu' > 4$, tend to be an asymptotic line, and take the largest value among the three kinds of waves beyond a certain ratio of μ/μ', namely $\mu/\mu' > 8$, in the present case.

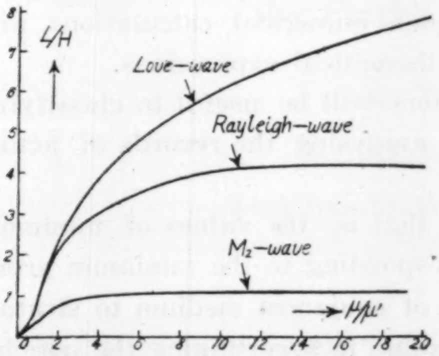

Fig. 32. Relation between wave length corresponding to condition in minimum group velocity and ratio of μ/μ'.

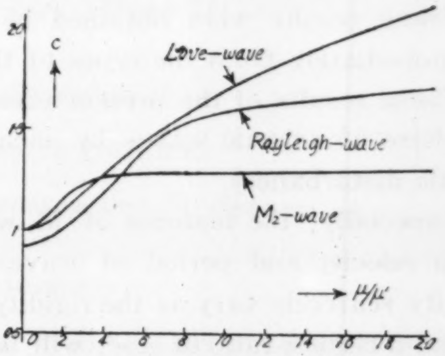

Fig. 33. Relation between phase velocity corresponding to condition in minimum group velocity and ratio of μ/μ'.

Fig. 32 shows that the period of waves of all the three kinds of dispersive surface waves corresponding to the condition in minimum group velocity increases with the increase in the rigidity ratio of the two mediums, (μ/μ'). The periods above mentioned of M_2-waves and dispersive Rayleigh-waves take an asymptotic line when they go beyond a certain ratio of μ/μ', namely $\mu/\mu' > 4$ and $\mu/\mu' > 8$ respectively, but those of Love-waves are still increasing in such ratio of μ/μ' as 20.

6. Concluding remarks.

From the results of the mathematical investigations concerned with the nature of group velocity of Love-waves, dispersive Rayleigh-waves and M_2-waves, we found that there is a little difference between the values of minimum group velocity of M_2-waves and Love-waves, when the rigidity ratio of subjacent medium to stratum is small, namely μ/μ' is more than several times smaller, while that of Rayleigh-waves is smaller than or at least half of the other two.

Concerning the period of waves corresponding to the minimum group velocity, Love-waves rank first, next dispersive Rayleigh-waves, then come M_2-waves, and the difference among them are considerably large.

On the other hand, when μ/μ' is more than several times smaller, the values of minimum group velocity of the three kinds of dispersive surface waves differ little, and the periods of waves corresponding to the condition in the minimum group velocity of Love-waves and Rayleigh-waves differ little but that of M_2-waves is smaller than that is about one third of the other two.

These results were obtained by complex numerical calculations, and not immediately from the types of the mathematical expressions.

These results of the present investigations will be useful in classifying the phase of seismic waves by means of analysing the records of actual seismic disturbances.

Especially, the features of M_2-waves, that is, the values of minimum group velocity and period of waves corresponding to the minimum group velocity scarecely vary as the rigidity ratio of subjacent medium to stratum beyond a certain ratio of μ/μ', will be utilizable in ascertaining the possible existence of M_2-waves in actual seismic disturbances.

In conclusion I wish to express my thanks to Mrs. S. Izumi who has assisted me in preparing this paper.

---

5. 分散性表面波の群速度について

地震研究所　金井　清

ラブ波，分散性レーレー波並びに M_2 波の群速度の性質を數理的に研究した。2層の密度が等しい場合に，下層の剛性が表面層の剛性に比べて大きいとき，即ち μ/μ' が數倍以上のとき，には M_2 波とラブ波の極小群速度の値は餘り變らないが，レーレー波のそれは 1/2 或はそれ以上小さい。極小群速度にあたるところの波の周期はラブ波のものが最も大きく，レーレー波，M_2 波の順に小さく，各々の間の差違は相當に大きい。

μ/μ' が數倍以下のときには，3種類の波の極小群速度の値は大して變らない。極小群速度にあたるところの波の周期は，ラブ波とレーレー波とはその差違が小さいが，M_2 波の値は兩者の 1/3 近くも小さい。

これらの數理的研究結果は地震記象を解析して，表面波の各位相をきめる際に，相當に役立つであろう。又，特に M_2 波の極小群速度の値と，そのときの波の周期の値とが，μ/μ' が或程度大きくなると，μ/μ' に關してほとんど變らなく一定の値をとる性質は，地震記象の上で M_2 波の實在性を確める上に非常に便利な筈である。

6. *Electromagnetic Induction within the Earth and Its Relation to the Electrical State of the Earth's Interior. Part III.*

By Tsuneji RIKITAKE,

Earthquake Research Institute.

(Read June 20, 1950.—Received Dec. 20, 1950.)

1. Introduction.

In the previous papers,[1] the writer studied electromagnetic induction by various variations in the earth's magnetic field, the slowest of them being the main phase of magnetic storm (D_{st}) with a duration-time of a few days. In order to study the electric and magnetic properties in the deeper part of the earth's interior, however, it was considered necessary to investigate some variations, the periods of which are longer than the ones treated in the previous papers.

Taking into consideration the fact that geomagnetic condition has the 27-day recurrence-tendency, it may be possible to find out an apparent geomagnetic variation of about 27-day period with suitable means. In this paper, the 27-day period variation will be analyzed in regard to the electrical state of the earth's interior.

2. Magnetic data and the analysis.

In order to avoid irregularities, the daily means of the magnetic field are superposed with 27-day interval throughout nearly half a year. The reports during the years 1924 and 1925 from several magnetic observatories are used, the names of the observatories being given in Table I together with their geomagnetic latitudes and longitudes.

The mean variations in the horizontal and vertical components superposed throughout the period I (from Jan. 1 to July 7, 1924), II (from July 8 to Dec. 16, 1924), III (from Dec. 17, 1924 to June 23, 1925) and IV (from June 24 to Dec. 29, 1925) are respectively shown in Figs. 1, 2, 3, and 4. As the variations in the declination are usually very small, we may approximately consider the variations in the horizontal component to be those in the

---

[1] T. RIKITAKE, *Bull. Earthq. Res. Inst.* **28** (1950), 45, 219 and 263.

Table I. List of the magnetic observatories.

Observatory	Geomagn. latitude	Geomagn. longitude
Sitka	60.°0	275.°4
Val-Joyeux	51.3	84.5
Cheltenham	50.1	350.5
Tucson	40.4	312.2
Vieques	29.6	3.9
Kakioka	26.0	206.0
Honolulu	21.1	266.5
Alibag	9.5	143.6
Rio de Janeiro	−12.5	24.3

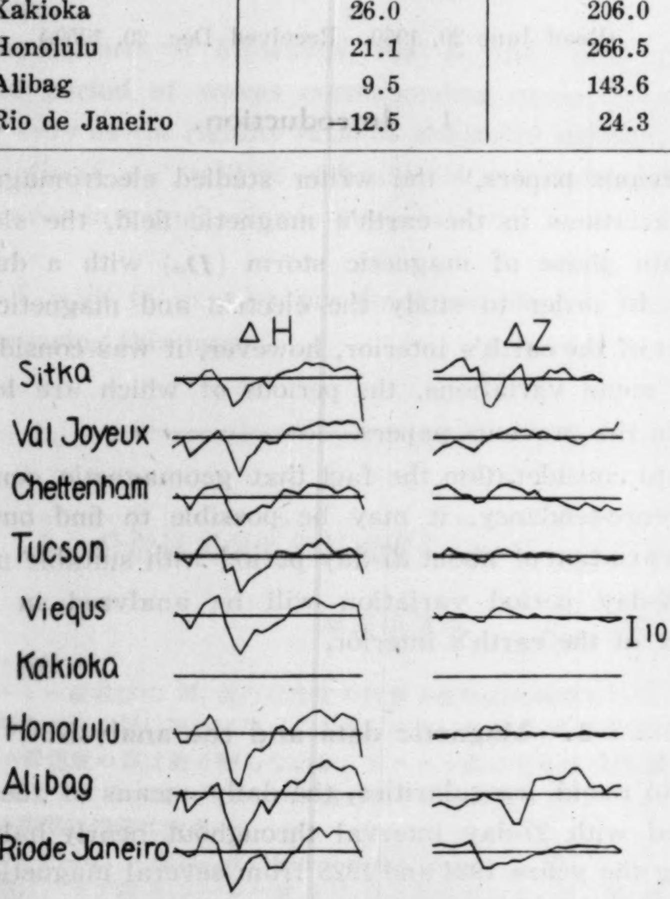

Fig. 1. Mean variation in the components of the earth's magnetic field during the period I. The left and right ends of the curves correspond respectively to 0 and 27 day.

geomagnetic north component. The variations at Kakioka during the periods I and II are omitted because the observations on many days were missing. Meanwhile, the reports in the year 1925 from Tucson and Vieques were not available.

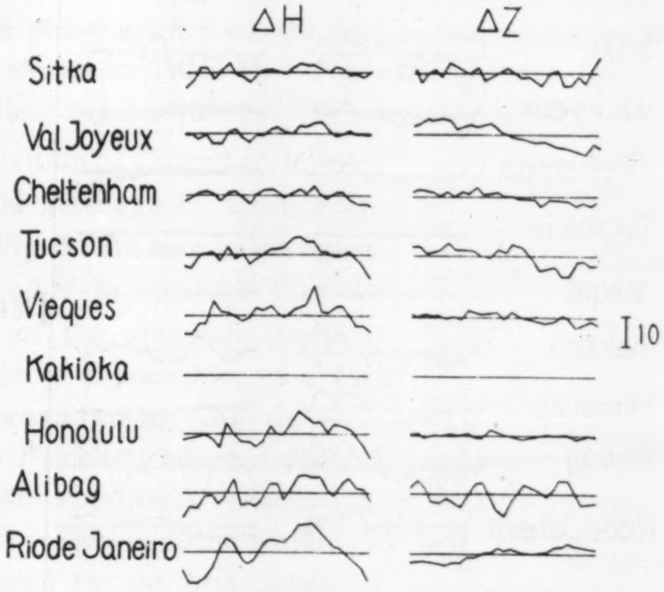

Fig. 2. Mean variation in the components of the earth's magnetic field during the period II.

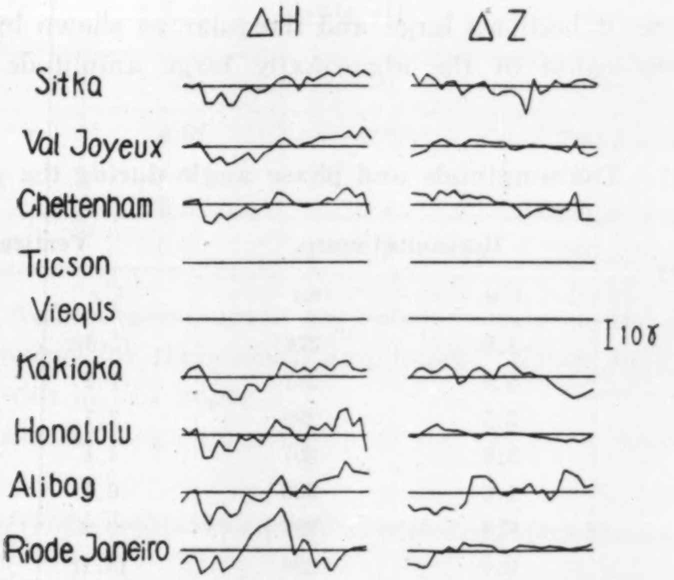

Fig. 3. Mean variation in the components of the earth's magnetic field during the period III.

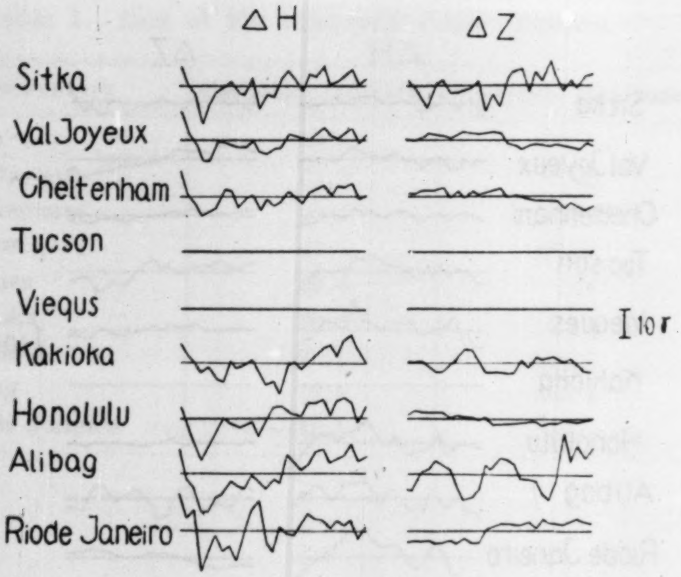

Fig. 4. Mean variation in the components of the earth's magnetic field during the period IV.

As seen in the figures, the geomagnetic north component appears to be small at high latitude. It increases equatorwards, however, attaining its maximum near the equator. On the other hand, the vertical one is becoming smaller near the equator, where a reversal of sign seems to occur. Near the auroral zone, it becomes large and irregular as shown by the curve at Sitka, while the cause of the abnormally large amplitude at Alibag is unknown.

Table II. The amplitude and phase angle during the period I.

Observatory	Horizontal comp.		Vertical comp.	
	C_H	α_H	C_Z	α_Z
Sitka	3.8γ	276°	(1.6)γ	(342)°
Val-Joyeux	5.4	287	1.5	210
Cheltenham	3.5	298	2.7	112
Tucson	3.6	307	1.1	102
Vieques	4.6	306	0.9	110
Honolulu	6.9	297	0.8	137
Alibag	9.0	296	(5.1)	(273)
Rio de Janeiro	5.8	321	−3.6	151
Mean		299		137

The variations thus obtained are subjected to Fourier analysis, the amplitude and phase angle[2] of the first harmonic during the period I, for example, are shown in Table II. The values of the vertical component at Sitka and Alibag are omitted for the next calculation.

The distribution of C_H and C_Z bearing reference to the geomagnetic latitude are illustrated in Fig. 5. As seen in the figure, it will be possible to consider that the greatest part of the magnetic potential of the variation is expressible, to a fair degree of approximation, with the term including only $P_1(\cos\theta)$, where θ denotes the geomagnetic colatitude. Assuming, then, that the distribution of the amplitude can be expressed by the first spherical harmonic such as

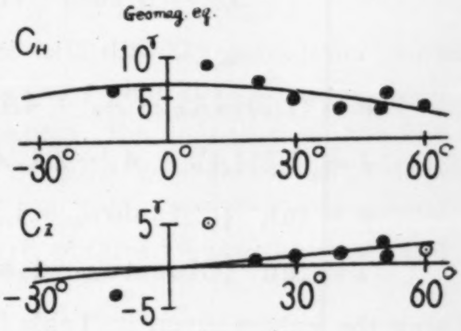

Fig. 5. The distribution of C_H and C_Z referred to the geomagnetic latitude.

$$C_H = A_H \sin\theta, \quad C_Z = A_Z \cos\theta\,, \quad \dots\dots\dots\dots\dots\dots (1)$$

the coefficients are determined by means of the least square method as given in Table III, while the phase angles are obtained by using arithmetical means as stated above.

Table III.

Period	A_H	A_Z	α_H	α_Z
I	6.8γ	2.7γ	299°	137°
II	4.0	3.2	226	106
III	5.5	3.4	275	122
IV	5.5	3.2	298	93

As to the higher harmonics of the Fourier analyses, the coefficients are almost meaningless for their small amplitudes. Hence, only the first term will be dealt with in this paper.

Now, we take the magnetic potential of the variation which is expressed by

$$W = a\{(r/a)e\cos(t-\epsilon) + (a/r)^2\, i\cos(t-\iota)\}P_1(\cos\theta)\dots\dots\dots\dots (2)$$

where a denotes the radius of the earth. e and i denote respectively the amplitude of the coefficient of the potential of external and internal origins, while ϵ and ι denote that of the phase angle. The geomagnetic north component and vertical component at $r=a$ are derived from (2) as follows:

---

[2] The first harmonic is expressed by $C\cos(t-\alpha)$.

$$\left.\begin{aligned} \varDelta H &= -\{e\cos(t-\epsilon)+i\cos(t-\iota)\}\sin\theta, \\ \varDelta Z &= \{e\cos(t-\epsilon)-2i\cos(t-\iota)\}\cos\theta . \end{aligned}\right\} \qquad \ldots\ldots\ldots\ldots(3)$$

Hence, comparing (3) with (1), we get

$$\left.\begin{aligned} e &= (1/3)\{4A_H^2+A_Z^2+4A_HA_Z\cos(\alpha_H-\alpha_Z)\}^{1/2}, \\ i &= (1/3)\{A_H^2+A_Z^2-2A_HA_Z\cos(\alpha_H-\alpha_Z)\}^{1/2}, \\ \epsilon &= \tan^{-1}\{(2A_H\sin\alpha_H+A_Z\sin\alpha_Z)/(2A_H\cos\alpha_H+A_Z\cos\alpha_Z)\}, \\ \iota &= \tan^{-1}\{(A_H\sin\alpha_H-A_Z\sin\alpha_Z)/(A_H\cos\alpha_H-A_Z\cos\alpha_Z)\}. \end{aligned}\right\} \qquad (4)$$

Using the values given in Table III, e, i, ϵ, and ι are calculated in regard to every period as shown in Table IV where the amplitude ratio and phase difference are also given.

Table IV.

Period	I	II	III	IV
e	5.4γ	3.4γ	4.8γ	4.7γ
i	1.5	1.2	1.0	1.0
ϵ	122°	62°	101°	112°
ι	107	−3	64	146
e/i	3.7	2.8	4.8	4.7
$\iota-\epsilon$	15°	65°	37°	−34°

The most probabe values of e/i and $\epsilon-\iota$ are respectively obtained to be 4.0 ± 0.4 and $22^\circ\pm16^\circ$.

As the amplitude ratio and phase difference for each period are somewhat scattered, a more complete analysis with abundant data will be needed for a more accurate research. However, it may be of some interest to investigate tentatively the process of the 27-day period variation by the present analysis.

3. The relation to the electrical state of the earth's interior.

In Part II of this paper, the writer determined approximately the distribution of the electrical conductivity from the studies of various geomagnetic variations, the distribution being determined to be

$$\sigma = \sigma' \quad \text{for} \quad 1 > \rho > q,$$

$$\sigma = \sigma_0 \rho^{-l} \quad \text{for} \quad q > \rho,$$

σ', σ_0, q and l being 10^{-15} *emu*, 1.0×10^{-12} *emu*, 0.94 and 11 respectively, where ρ denotes the radial distance divided by the earth's radius.

In the first place, electromagnetic induction by 27-day period variation within the earth having the electrical conductivity cited above will be dealt with. As often studied in the previous papers, the influence of the low conducting layer is negligible for variation of such long period as 27-day. In that case, the amplitude ratio and phase difference of the magnetic potential of external and internal origins are obtained from the *mod.* and *arg.* of $I(i\omega)$. $I(i\omega)$ is given by

$$I(i\omega) = \frac{n}{n+1} q^{2n+1} \frac{K_{\nu-1}(z_1)}{K_{\nu+1}(z_1)}, \ldots\ldots\ldots\ldots\ldots\ldots\ldots (5)$$

where

$$z_1 = x\sqrt{i}\,,\ x = \frac{4a\sqrt{\pi\sigma_0\omega}}{|l-2|}\,,\ \nu = \frac{2n+1}{|l-2|} \ \text{and}\ \omega = \frac{2\pi}{T}.$$

K_ν is the modified Bessel function, while n and T denote respectively the degree of the spherical harmonic and the period of the variation. As x amounts to 1.09 in the present case, an expansion in ascending power of $x/2$ is available for the calculation as given in the following:

$$K_\nu(x\sqrt{i}) = (1/2)\pi \operatorname{cosec} \nu\pi\{(\Phi_{-\nu}+i\Psi_{-\nu})e^{-i\nu\pi/4}-(\Phi_\nu+i\Psi_\nu)e^{i\nu\pi/4}\}\ldots (6)$$

where

$$\Phi_\nu = \sum_{r=0}^{\infty} \frac{(-1)^r (x/2)^{\nu+4r}}{(2r)!\,\Gamma(\nu+2r+1)}, \quad \Psi_\nu = \sum_{r=0}^{\infty} \frac{(-1)^r (x/2)^{\nu+4r+2}}{(2r+1)!\,\Gamma(\nu+2r+2)}. \quad (7)$$

Thus the amplitude ratio and phase difference for the 27-day period variation are obtained as

$$3.52 \quad \text{and} \quad 14.^\circ 2$$

which agree with the values obtained from the analysis within the errors of determination.

Hence, it may be said that the conductivity-distribution obtained in the previous papers is approximately compatible with longer period variation such as 27-day period one.

4. The distribution of the induced currents.

In order to study how deep the induced currents penetrate into the earth, the distribution of the induced currents is calculated in the same way as in the previous studies.

According to B. N. Lahiri and A. T. Price,[3] the current intensity is proportional to v which is given by

$$v = \rho^{-l-1/2} K_\nu(\rho^{-l/2+1} x\sqrt{i})/K_\nu(x\sqrt{i}) . \quad \ldots\ldots\ldots\ldots (8)$$

mod. v is easily calculated with the aid of (6) and (7) for various values of ρ. Thus the distribution of current intensity is obtained as shown in Fig. 6 in arbitrary unit. Strictly speaking, the phase of the induced currents differs from each other at different depths, but its difference is neglected here as well as in Part II. As the period of the variation is larger than any other variation hitherto treated, the induced currents flow in appreciably deeper part, the maximum occuring at as deep as about 1500 *km*. The contribution of the current at any depth to the magnetic field at the earth's surface is also calculated as shown in Fig. 7. As done in Part I, we define the "effective radius" of the electrical conductivity by $\int \rho\varphi(\rho)\, d\rho / \int \varphi(\rho)\, d\rho$ where $\varphi(\rho)$ denotes the contribution of the current. In the present case, the "effective depth" is calculated to be 1200 *km*. Hence, we may consider that the electrical state at a depth of about 1200 *km* is the most effective for the 27-day period variation.

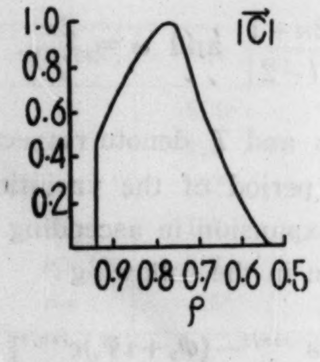

Fig. 6. The distribution of the induced currents in the earth.

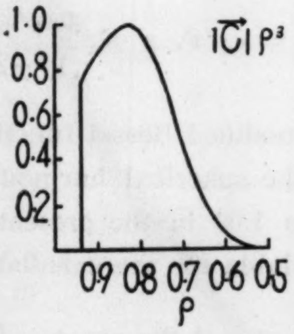

Fig. 7. The contribution of the currents to the magnetic field at the earth's surface.

---

[3] B. N. LAHIRI and A. T. PRICE, *Trans. Roy. Soc. London* A **237** (1939), 509.

5. Summary and conclusion.

In addition to the electromagnetic induction by various variations which were already studied in the previous papers, the 27-day period variation, the period of which is larger than any other variation treated before, is studied here in regard to the electrical state of the earth's interior. Though the results of the analysis for various epochs are somewhat scattered, the relation between the external and internal parts is fairly consistent with the conductivity-distribution which was determined in the former studies. From the investigation of the induced currents, it is concluded that the electrical state at a depth of about 1200 *km* is the most effective for the 27-day period variation. Taking into consideration, then, the increase in the electrical conductivity in greater depth and the accompanying screening effect for current penetration, it will be of great difficulty to investigate the electrical properties at further depth even in case of much longer period variation.

In conclusion, the writer wishes to express his hearty thanks to Dr. T. Nagata for his helpful discussions. To Miss Y. Hishiyama who always assisted the writer throughout the numerical work the writer's hearty thanks are also due.

---

6. 地球内の電磁感應およびその地球内部の電氣的性質との關係 第3報

地震研究所　力武常次

第 1, 2 報で解析した各種の地磁氣變化のほかに，地球磁場の 27 日週期變化を取扱つた。8 箇所の觀測所の資料を 27 日毎に半年間かさねあわせたものについて解析したところ，内外磁場の振幅比および位相差としてそれぞれ 4.0 ± 0.4, $22^\circ \pm 16^\circ$ という結果を得た。これは前報における地球内部の電氣的性質を考慮するとき，よく調和する。この結果より 27 日という長週期變化によつても，深さ 1500 *km* 程度以上の地球内部の電氣的性質をしらべることは困難なことが推察される。

5. Summary and conclusion.

In addition to the electromagnetic induction by various variations which were already studied in the previous papers, the 27-day period variation, the period of which is larger than any other variation treated before, is studied here in regard to the electrical state of the earth's interior. Though the results of the analysis for various epochs are somewhat scattered, the relation between the external and internal parts is fairly consistent with the conductivity-distribution which was determined in the former studies. From the investigation of the induced currents, it is concluded that the electrical state at a depth of about 1300 km is the most effective for the 27-day period variation. Taking into consideration, then, the increase in the electrical conductivity in greater depth and the accompanying screening effect for current penetration, it will be of great difficulty to investigate the electrical properties at further depth even in case of much longer period variation.

In conclusion, the writer wishes to express his hearty thanks to Dr. T. Nagata for his helpful discussions. To Miss Y. Hishiyama who always assisted the writer throughout the numerical work the writer's hearty thanks are also due.

[illegible]

[illegible]

7. *An Estimate of Future Tsunami Damage Along the Pacific Coast of Japan.*

By Ryutaro TAKAHASI,

Earthquake Research Institute.

(Read Oct. 24, 1942 & Nov. 9, 1949.—Received Dec. 20, 1950.)

Abstract.

Assuming that tsunami activity recorded during historic times is still continuing at present and will continue also in the future, the writer has estimated the degree of danger of tsunami for each village on the Pacific coast of Japan which may be expected in the future. Results are given in Fig. 2 and in Table III.

1. To minimize damage from tsunamis, various types of structures have been devised such as breakwaters, embankments, artificial bars, coastal forests, cushion zones, etc. The most economical and effective type of structure depends, however, on the topography, mainly submarine, of the place under consideration and also on the intensity of the tsunami at that place. In this respect, it is desirable to determine the maximum height of tsunami which may be expected in the future for each village on the Pacific coast.

2. Tsunamis or seismic sea waves occur more frequently in Japan than in any other country in the world. There is no coast line in Japan which has not experienced past tsunamis. According to "Earthquake Records for Japan" (Nippon Jishin Shiryo), about 75 tsunamis have occurred in the sea adjacent to Japan, the oldest one occurring in 684 A.D. and the latest in 1946 at the time of the Nankai Earthquake. Smaller tsunamis which caused no damage and accordingly were not included in the record must be innumerable. Among the tsunamis recorded, there is one that caused the loss of 27,000 lives. In Table I, the dates of historical tsunamis are listed together with the name of the region which suffered damage, the position of the tsunami center and the magnitude *M*. The origins of these tsunamis are plotted in Fig. 1. Numerals beside the circles are the serial numbers in Table I. Radius of the circle indicates the magnitude of the tsunamis.

Table I. List of Tsunamis.

No.	Date	Damaged Region	Magnitude *M*	Origin
1	684 Nov. 29	Tosa, Tokaido & Seikaido	3	32.5 N, 134.0 E
2	799 Sept. 18	Hitachi		Distant origin
3	850 Nov. 17	Dewa	1	39.0 N, 139.5 E
4	869 July 13	Sanriku	4	38.5 N, 143.8 E
5	887 Aug. 2	Echigo	1	37.5 N, 138.1 E
6	887 Aug. 26	Nankaido	3	33 N, 135.3 E
7	922	Kii & Kumano	1	33.8 N, 136.7 E
8	1096 Dec. 17	Tokaido	2	34.2 N, 137.3 E
9	1241 May 22	Kamakura	1	35.3 N, 137.3 E
10	1257 Oct. 9	S. Kwanto	1	35.2 N, 140.9 E
11	1360 Nov. 22	Kii, Settsu	2	33.4 N, 135.2 E
12	1361 Aug. 3	Kii, Tosa & Settsu	3	33 N, 135 E
13	1403	Kii	1	33.7 N, 136.5 E
14	1408 Jan. 21	Kii	2~1	33.8 N, 136.9 E
15	1420 Sept. 6	Hitachi	1	Distant origin
16	1433 Nov. 7	Sagami	1	34.9 N, 139.5 E
17	1495 Sept. 12	Sagami	2	35.5 N, 139.2 E
18	1498 Sept. 20	Tokaido	3	34.1 N, 138.2 E
19	1510 Sept. 21	Settsu	0	34.6 N, 135.7 E
20	1520 April 4	Kii	1	33.6 N, 136.3 E
21	1562 June 15	Higo	1	Distant origin
22	1585 June 21	Rikuzen	0	Distant origin
23	1596 Sept. 4	Bungo	2	33.3 N, 131.7 E
24	1605 Feb. 3	Tokaido & Nankaido	3	A 34.3 N, 140.4 E B 33 N, 134.9 E
25	1611 Dec. 2	Sanriku & Hokkaido	4	37.7 N, 144.3 E
26	1614 Nov. 26	Echigo	1	37.5 N, 138 E
27	1616 Sept. 9	Sendai	1	38.1 N, 142 E
28	1633 Mar. 1	Sagami & Suruga	1	35.6 N, 139.2 E
29	1640	Hokkaido	1	Eruption of Komagatake

(to be continued.)

Table I. List of Tsunamis. (continued.)

No.	Date	Damaged Region	Magnitude M	Origin
30	1650 Oct. 31	Echizen	1	
31	1662	Hiuga & Osumi	2	31.7 N, 132 E
32	1676	Hitachi	0	Distant origin?
33	1677 April 13	Rikuchu	2	38.7 N, 144 E
34	1677 Nov. 4	Iwaki, Hitachi & Owari	2	36.6 N, 141.5 E
35	1687 Oct. 22	Rikuzen	0	Distant origin?
36	1696 Feb. 25	Rikuzen	1	Distant origin?
37	1703 Dec. 31	Kwanto	3	34.7 N, 139.8 E
38	1707 Oct. 28	Tokaido, Nankaido & Seikaido	4	33.2 N, 135.9 E
39	1711 Dec. 20	Sanuki	1	34.3 N, 134 E
40	1731 Oct. 7	Rikuzen	1	37.9 N, 140.6 E
41	1741 Aug. 28	Hokkaido & Sado	3	41.5 N, 139.4 E
42	1751	Rikuchu	1	
43	1762 Oct. 31	Sado	1	38.1 N, 138.7 E
44	1763 Jan. 29	Mutsu, Hachinohe	2	40.8 N, 142 E
45	1763 Mar. 15	Mutsu, Hachinohe	1	
46	1768 July 22	Ryukyu Kerama Is.	1	
47	1771 April 24	Ryukyu Ishigaki Is.	3	
48	1780	Etorohu, Chishima	1	
49	1782 Aug. 23	Sagami	0	35.1 N, 139.7 E
50	1791 May 13	Ryukyu	1	Distant origin?
51	1792 May 21	Shimabara	2	32.8 N, 130.3 E Land-slide of Unzendake
52	1792 June 13	Shiriheshi	1	43.6 N, 140.3 E
53	1793 Feb. 8	W. Tsugaru	1	40.7 N, 140 E
54	1793 Feb. 17	Rikuzen, Rikuchu	2	38.3 N, 142.4 E
55	1804 July 10	Uzen, Ugo	1	39 N, 140 E
56	1810 Sept. 25	Oga Penn.	0	39.9 N, 139.9 E
57	1833 Dec. 7	Sado, Uzen	2	38.7 N, 139.2 E
58	1834 Feb. 9	Ezo (Ishikari)	1	43.3 N, 141.4 E

(to be continued.)

Table I. List of Tsunamis. (continued.)

No.	Date	Damaged Region	Magnitude M	Origin
59	1835 July 20	Rikuzen	2	37.9 N, 141.9 E
60	1836 Sept. 5	Rikuzen	1	
61	1843 April 25	Kushiro & Nemuro	2	41.8 N, 144.8 E
62	1854 Dec. 23	Tokaido, Nankaido	3	34.1 N, 137.8 E
63	1854 Dec. 24	Ise, Tosa, Kii & Kyushu	3	33.2 N, 135.6 E
64	1856 Aug. 23	Toshima	2	43 N, 141.1 E
65	1865	Ryukyu	1	
66	1867	Formosa (Kiirun)	2	
67	1868 (Aug. 16?)	Ryukyu, Rikuzen	0	Distant origin (Equador)
68	1872 Mar. 14	Iwami	1	34.8 N, 132 E
69	1883 Aug. 27	Sagami, Satsuma	0	Distant origin (Eruption of Krakatoa)
70	1894 Mar. 22	Nemuro, Kushiro	2	(42 N, 145.1 E)
71	1896 June 15	Sanriku	4	39.4 N, 144.4 E
72	1897 Aug. 5	Sanriku	1	38.2 N, 143.7 E
73	1912 June 8	Sanriku	0	
74	1915 Nov. 1	Sanriku	1	
75	1917 May 6	Formosa	1	
76	1918 Sept. 8	Etorohu	2~3	
77	1922 Nov. 12		0	Chili Tsunami
78	1923 Sept. 1	Kwanto	2	35 N, 139.8 E
79	1933 Mar. 3	Sanriku	3	39.1 N, 144.2 E
80	1939 May 1	Oga Penn.	0	40 N, 139.8 E
81	1940 Aug. 2	Shakotan Penn.	1	44.1 N, 139.2 E
82	1944 Dec. 7	Tokaido	3	34 N, 137.1 E
83	1945 Jan. 13	Mikawa	1	34.8 N, 137.2 E
84	1946 Dec. 21	Nankaido	3	33 N, 134.8 E

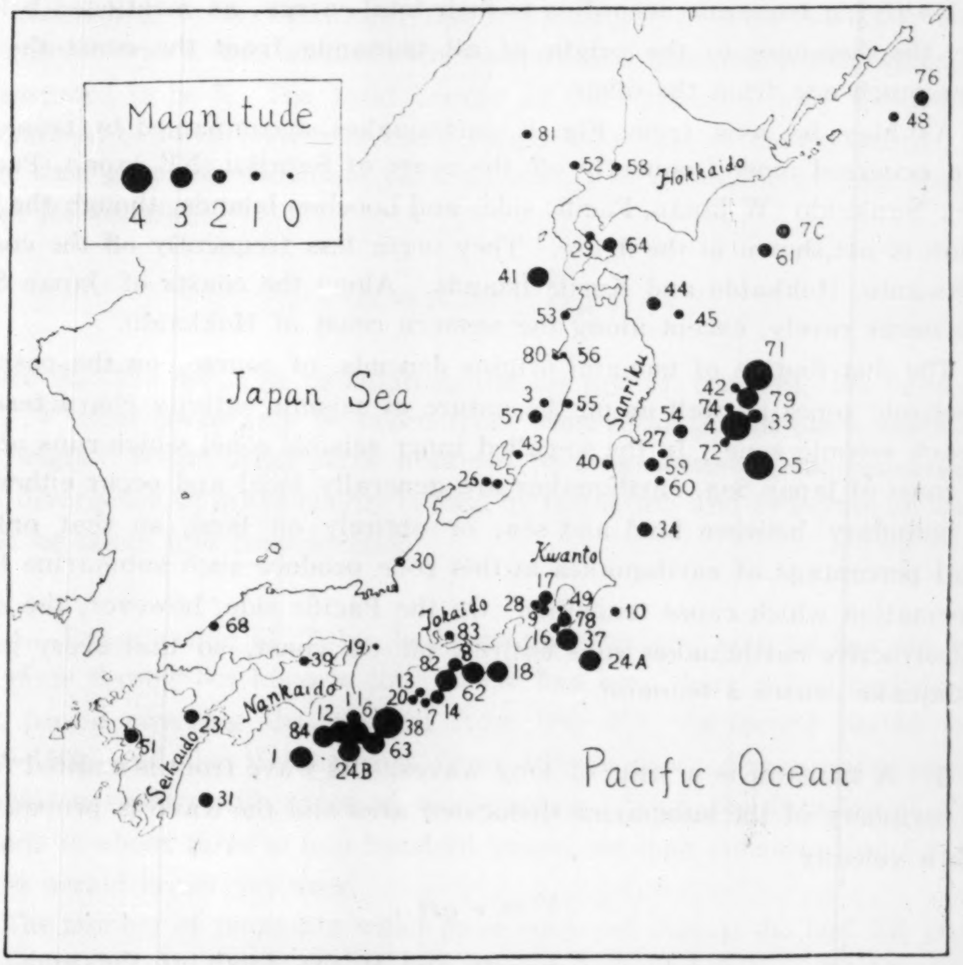
Magnitude
4 3 2 1 0
76
48
81
52
58
Hokkaido
7C
61
29
64
41
44
45
53
80
56
Sanriku
71
42
79
74
33
4
3
55
57
54
Japan Sea
43
27
72
25
40
59
60
26
34
30
Kwanto
17
28
49
9
78
10
Tokaido
83
16
37
24A
39
19
68
82
8
18
13
62
Nankaido
20
7
14
11
6
12
38
84
63
1
24B
23
51
Sekaido
31
Pacific Ocean

Fig. 1. Distribution of tsunami centers.

The position of the origin of each tsunami was determined from the distribution of damage caused not only by the tsunami but also by earthquake motions. In this connection, the list of earthquakes in historic times prepared by H. Kawasumi[1] has been of great help. As to the magnitude of tsunamis, they have been classified into five classes, according to the maximum wave height observed at the coast, as A. Imamura[2] formerly did. The severest or the fifth class tsunamis are those with a maximum wave height of 30 m or more, and the fourth class ones with a wave height of 15 m. In this classification, the maximum wave height is reduced by one-half with decreasing magnitude of unity. This classification amounts in the end to classifying tsunamis according to their total energy, as mentioned below, since the distances to the origin of all tsunamis from the coast do not differ much one from the other.

---

[1] H. KAWASUMI, On Some Measure of Earthquake Danger. The IXth I.U.G.G. Congress Rep.

[2] A. IMAMURA, *The Science of the Sea*, Vol. II, p. 2.

As may be seen from Fig. 1, earthquakes accompanied by tsunamis have occurred most frequently off the coast of Sanriku (NE Japan, Pacific side), Nankaido (W Japan, Pacific side) and Loochoo Islands, though the last region is not shown in the figure. They occur less frequently off the coasts of Kwanto, Hokkaido and Kurile Islands. Along the coasts of Japan Sea, they occur rarely, except along the western coast of Hokkaido.

The distribution of tsunami origins depends, of course, on the position of seismic zones as well as on the nature of seismic activity characteristic to each seismic zone. In the so-called inner seismic zone, which runs along the coast of Japan Sea, earthquakes are generally local and occur either on the boundary between land and sea, or entirely on land, so that only a small percentage of earthquakes in this zone produce such submarine land deformation which cause tsunamis. On the Pacific side, however, the zone of destructive earthquakes runs entirely off the coast, so that every great earthquake causes a tsunami.

3. A tsunami is a train of long waves. Its wave front is emitted from the periphery of the submarine dislocated area and the wave is propagated with a velocity

$$V = \sqrt{gH} ,$$

where g is the acceleration of gravity and H the depth of the sea. The total energy emitted from the origin is given by

$$E = \pi \rho g V R \sum A^2 T ,$$

where ρ is the density of sea water, R the distance from the origin, A the amplitude and T the half-period of tsunami waves. The summation must be made with respect to all half-periods. In the case of 1933 tsunami, the wave height A at the 200 m depth line off the bay of Ohunato has been estimated to be 3 m by Stokes' law since the wave height at a cape, where the sea depth is 20 m, was observed to be 5 m. Average half-period was 7.5 min. and the number of main half waves 5. The total energy thus calculated, is 16×10^{22} erg, and is about 1/1000 of the total energy of seismic waves as given by H. Kawasumi[3] and others.

---

[3] H. KAWASUMI, *1948 New Zealand Pan Pacific Congress Rep.*; B. GUTENBERG, *Seismicity of the Earth.*

According to A. Imamura, the wave height of 1611 tsunami, whose magnitude was 4, was about twice those of 1933 tsunami, whose magnitude is assumed to be 3. The total energy of 1611 tsunami may therefore be considered to have been four times larger than that of 1933 tsunami. We may then generally calculate the total energy of a tsunami of magnitude M from the relation

$$E = E_0\, 10^{0.6M}\, \mathrm{erg}\ ,$$

where $E_0 = 25 \times 10^{20}$. In calculating the energy of tsunami, the values of A, T, V must preferably be taken from observation at the place nearest to the origin. When using data obtained at long distances, the convergence and divergence of wave energy caused by refraction and reflection of waves must be taken into consideration.

4. Examination of Table I shows that tsunami activity has not been the same throughout historic time; there has been three active periods, the first period covering the interval from 680~950, the second period from 1200~1500, and the third period from 1600 to date. These active periods coincide naturally with those of earthquakes. Since the duration of these periods is about three to four hundred years, we may consider that the last active period is not yet over.

The number of tsunamis which have occurred during the last 350 years, classified according to their magnitude and region of occurrence, is shown in Table II.

Table II.

Region / Magnitude	From Loochoo Is. to Kwanto	From Sanriku to Kurile Is.	W. Kyushu and Japan Sea	Total
4	1	2	0	3
3	7	2	1	10
2	3	7	2	12
1	5	9	9	23
0	1	1	2	4
Total	17	21	14	52

The energy of these tsunamis becomes as follows (unit: 10^{20} erg):

Table III.

Region	From Loochoo Is. to Kwanto	From Sanriku to Kurile Is.	W. Kyushu and Japan Sea	Total
During 350 years	19330	19730	3350	42400
Per 100 years	5520	5640	960	12110
Per 1 tsunami	1139	940	240	810

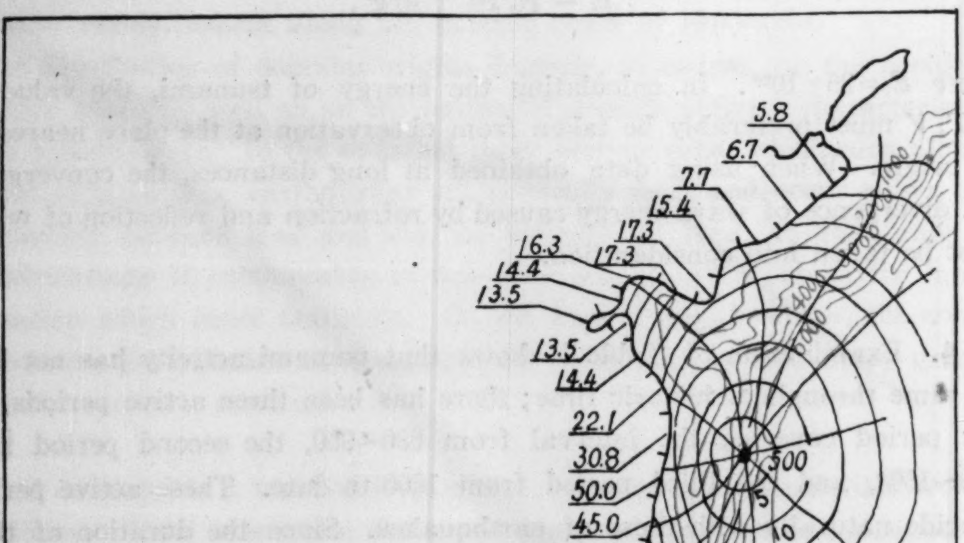
5.8
6.7
7.7
15.4
17.3
16.3
17.3
14.4
13.5
13.5
14.4
22.1
30.8
50.0
45.0
24.0
3.8
8.7
2.5
0.4
0.4
0.2
200 M. ISOBATH
500
5
10
15
20
25
30
40
50
60
70
80
90
min
100
150
200 min
1000
2000
3000
4000
6000

Fig. 2. An example of the refraction diagram.

It may not be absurd, then, to expect, that energy of tsunami to be liberated from each region will be at the same rate as those calculated above during the coming several decades. We may assume further that the energy will be emitted from each part of the seismic zone in proportion to the tsunami activity of that part in the past.

5. When a quantity of energy $\phi(Q)\,dS$ is emitted uniformly in all directions from an area dS around a place Q, the quantity of energy that reaches the unit length (83 km) of 200 m depth line off P will be given by $\phi(Q)D(P,Q)dS$. $D(P,Q)$ represents the distribution function and its numerical value can be obtained graphically from refraction diagrams drawn according to Huygens' principle and the velocity formula. The 200 m depth line is adopted here instead of the beach line for reasons given below.

Fig. 2 is an example of the refraction diagram. In the figure, $\phi(Q)\,dS$ is taken as 500. Numerals on the 200 m depth line represent values of $\phi(Q)\,D(P,Q)\,dS$ for this case.

If we denote the energy which will be emitted from Q during the coming 100 years by $\phi(Q)$, the total energy which will reach the 200 m depth line off P becomes

$$\int_Q \phi(Q)\,D(P,Q)\,dS\,.$$

Integration must cover all sources.

In the actual calculation of the values of the above integral, assuming for $\phi(Q)$ the values given in Table III, the energy sources were concentrated, for the sake of simplicity, into several points in the manner indicated in Table IV to obtain the final values shown in Fig. 3. In this figure, the thick lines indicate the 200 m isobathymetric lines, and numerals show the values of the integral in units of 10^{20} ergs. Values are not given for the coast of Japan Sea, as it was not possible to estimate the values of $\phi(Q)$ with any degree of certainty due to scarcity of distribution of tsunami origins. Danger of tsunami occurring is great at the coast which is near to the section with large values.

This is correct, however, only with respect to average or general tendency for a locality and its neighbourhood; it is, of course, a different problem to estimate in what proportion the energy which reaches a section of 200 m depth line will be distributed among the villages on the coast adjacent to that section. It depends mainly on the submarine topography

Table IV. $\int \phi(Q)\,D(P,Q)\,dS$ (in units of 10^{20} ergs.)

Concentrated tsunami origins					No. of sections of 200 m isobathymetric line																	
No.	Locality	N. Lat.	E. Long.	$\phi(Q)$	1	2	3	4	5	6	7	8	9	10	11	12	13	14	15	16	17	18
1	Off Iterup Is.	44.2	148.5	500	24.2	11.4	4.0	3.2	0.6	0.6	0.6	0.2	0.2	0.2	0.2	1.2	1.4	1.4	0.8	0.4	0.4	0.4
2	Off Shikotan Is.	43.3	147.1	500	51.6	41.6	21.0	22.5	3.8	0.5	1.0	1.0	0.2	0.2	0.2	2.0	4.0	4.0	4.0	4.0	4.0	3.2
3	Off Kushiro	42.3	145.5	700	56.0	67.6	63.0	56.0	31.5	9.1	4.4	2.3	2.3	2.3	2.3	11.2	11.2	9.1	9.1	6.8	4.0	1.9
4	Off Erimo C.	41.5	144.5	800	17.8	31.0	53.5	71.6	89.0	20.2	13.2	8.9	4.4	4.3	13.2	28.8	26.8	24.5	24.5	4.3	3.2	0.9
5	Off Aomori	40.6	144.2	500	4.3	9.8	20.6	26.1	26.1	13.0	9.8	5.5	5.5	8.7	15.2	37.0	37.0	28.2	21.8	9.8	4.3	2.0
6	Off Kamaishi	39.6	143.8	1000	11.6	13.4	15.4	30.8	34.6	34.6	32.6	28.8	27.0	27.0	28.8	44.2	61.6	100.0	90.0	48.0	17.4	7.6
7	Off Kinkasan	38.3	143.0	1000	15.5	15.5	4.0	3.0	5.0	3.8	6.0	6.0	2.0	8.5	15.5	48.8	83.0	83.0	90.3	83.0	39.0	24.5
8	Off Fukushima	37.1	142.4	500	2.0	1.2	1.4	1.4	2.0	0.8	0.8	1.6	2.2	3.2	3.2	12.0	19.2	32.8	52.0	46.2	30.8	21.2
9	Off Hitachi	36.0	141.8	200	0.4	0.2	0.2	0.2	0.2						4.0	1.0	2.6	8.0	13.0	16.0	20.0	22.0
10	Off Boso Penn.	35.2	141.1	500	1.0	0.5	0.0	0.0	0.0							1.5	2.5	16.0	16.0	31.5	31.5	47.0
11	Off Boso Penn.	34.3	140.2	1000	0.5	0.5	0.2	0.2	0.0						0.2	0.5	1.5	6.5	17.3	21.7	28.4	50.0
12	Off Ise Bay	34.0	137.3	1000													0.2	0.2	0.3	0.3	0.3	0.4
13	Off Kii	32.8	134.7	1500													0.2	0.4	0.9	1.9	3.4	4.1
14	Loochoo Is.	29.8	130.2	1500															0.2	0.3	0.3	0.3
Sum					185	193	183	215	193	83	68	54	44	54	79	188	251	314	340	274	187	186

(to be continued.)

Table IV. $\int \phi(Q) D(P, Q) dS$ (in units of 10^{20} ergs.) (continued.)

Concentrated tsunami origins					No. of sections of 200 m isobathymetric line																
No.	Locality	N. Lat.	E. Long.	$\phi(Q)$	19	20	21	22	23	24	25	26	27	28	29	30	31	32	33	34	35
1	Off Iterup Is.	44.2	148.5	500	0.4	0.4	0.2	0.2	0.2	0.2											
2	Off Shikotan Is.	43.3	147.1	500	3.2	3.2	0.8	0.2	0.2	0.2	0.2										
3	Off Kushiro	42.3	145.5	700	0.9	0.7	0.5														
4	Off Erimo C.	41.5	144.5	800	0.9	0.9	0.5														
5	Off Aomori	40.6	144.2	500	0.6	0.2	0.2														
6	Off Kamaishi	39.6	143.8	1000	5.0	0.8	0.8	0.4													
7	Off Kinkasan	38.3	143.0	1000	9.8	3.8	1.5	0.8	0.8	1.0	1.0	0.5	0.5	0.5	0.2						
8	Off Fukushima	37.1	142.4	500	16.0	10.0	2.0	1.6	1.4	0.8	0.8	0.4	0.2	0.2	0.2						
9	Off Hitachi	36.0	141.8	200	12.0	4.0	4.0	1.0	0.6	0.2	0.2	0.2	0.2	0.2	0.2						
10	Off Boso Penn.	35.2	141.1	500	62.5	15.0	10.0	5.0	2.5	2.5	1.5	0.5	0.5	0.5							
11	Off Boso Penn.	34.3	140.2	1000	113.2	47.8	41.3	10.8	4.3	15.2	21.6	17.2	6.5	8.7	6.5	2.7	0.7	0.8	1.3	0.5	0.2
12	Off Ise Bay	34.0	137.3	1000	0.6	0.8	1.0	6.0	0.0	69.0	367.0	118.0	9.0	1.0							
13	Off Kii	32.8	134.7	1500	2.6	2.6	2.6	2.6	4.5	25.0	75.0	94.3	229.0	244.0	151.0	75.0	75.0	19.9	19.3	7.5	2.1
14	Loochoo Is.	29.8	139.2	1500	0.3	0.3	0.2	0.3	0.5	1.4	2.7	4.2	5.8	6.7	7.5	29.2	19.2	63.4	91.6	183.0	127.0
Sum					228	91	66	29	15	116	470	215	252	262	166	107	95	84	112	191	129

between the 200 m depth line and the shore, on the shape and direction of a bay, and on the position of any village in the bay.

The 200 m depth line generally corresponds to the brink of continental shelves, the slope of the sea bottom suddenly becoming steep from here towards the sea. Consequently the wave front of tsunamis becomes almost parallel to isobathymetric lines at or near the depth of 200 m, regardless of the position of tsunami centers, since the velocity of propagation of long waves is proportional to the square root of the sea depth. It is only natural that the ratios of energy distributed among different but nearby villages are always similar and almost independent of the position of tsunami sources.

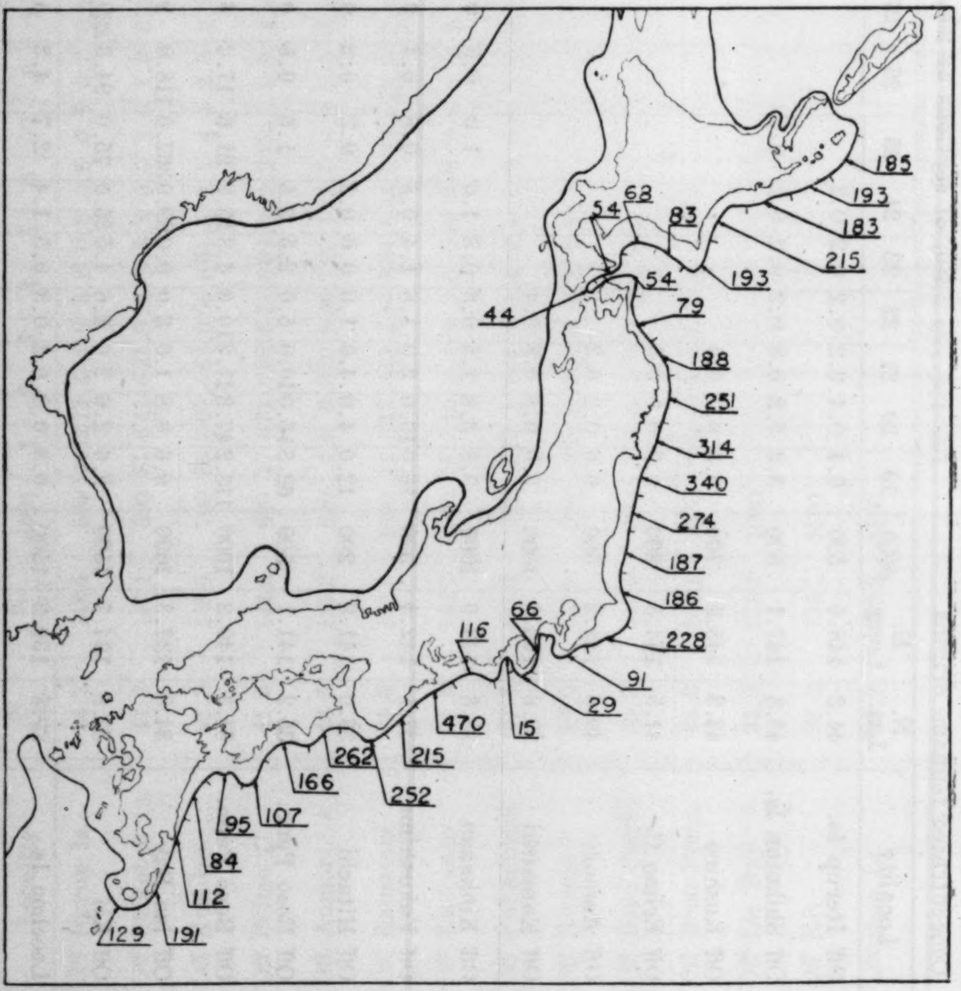
185
193
183
215
68
54
83
193
54
44
79
188
251
314
340
274
187
186
66
116
228
91
29
470
15
215
262
252
166
107
95
84
112
129
191

Fig. 3. Estimated amount of energy (in units of 10^{20} ergs) that will reach each section (83 km long) of 200 meter isobath within the next 100 years.

If we denote this ratio of distribution by $T(P)$, an estimate of the energy at any particular village P becomes

$$T(P) \int \phi(Q)\, D(P, Q,) dS \,.$$

6. As observed at the sea shore, a tunami may appear sometimes merely as a gradual rise and fall of the sea surface (calm case), sometimes as a progressive, rolling or breaking water wall (moderate to severe case) or sometimes as a water jet with a great velocity rushing toward the shore (extremely severe case). These features depend on the wave height of tsunamis and these different features may sometimes be observed at different portions of one and the same bay.

Even when the sea surface rises gradually, the water gains remarkable velocity when it reaches land, especially when the land is broad and flat. In many cases, this velocity exceeds 1 m/sec. Damage to houses is caused directly or indirectly by the hydrodynamical pressure due to this water flow. This pressure is proportional to the square of the velocity so that, in final, damage may be regarded to be proportional to the square of the water height or to the energy, since the periods of tsunami waves are almost the same everywhere and at any time. This conception may be allowed when we consider that the area invaded by the tsunami at any village is in most cases proportional to the square of the wave height at the village.

We may, therefore, consider the sum of the energy of all tsunamis that may attack P within the next century as the index $K(P)$ of the danger of tsunami at the place P. We then obtain

$$K(P) = T(P) \int \phi(P)\, D(P, Q) dS \,.$$

As mentioned above, $T(P)$ is a coefficient which depends on the topography, on land and under water, of the point P. It is very difficult or troublesome, if not impossible, to determine $T(P)$ theoretically. The value of $T(P)$ is most simply obtained from the relation

$$T(P) = A^2/E \cdot D(P, Q) \,,$$

if the total energy E of a tsunami, the position Q of the tsunami center, and the wave height A of the tsunami observed at P are known.

The values of $T(P)$ have been calculated in this way for all villages on the Pacific coast of Japan from the data on 1933 tsunami ($E = 1600 \times 10^{20}$ erg),

Table V. Wave heights of tsunamis and $T(P)$.

Locality	1896 Tsunami	1933 Tsunami	1944 Tsunami	1946 Tsunami	$2\,T(P)$
	m	m	m	m	
Same	3.3	2.9			0.230
Yagi	10.6	3.5			0.340
Ogonai	12.1	3.0			0.250
Kuki	12.1	3.3			0.300
Tamagawa	18.2	4.2			0.490
Horiuchi	12.1	8.0			1.750
Ootanabe	15.2	7.4			1.500
Raga	22.7	8.4			1.950
Omoto	12.1	4.4			0.540
Taro	14.6	10.0			2.000
Chikei	17.0	12.1			2.900
Aneyoshi	18.8	21.0			8.850
Omoe	10.9	8.8			1.550
Otobe	9.1	10.9			2.400
Aramaki	12.1	7.2			1.025
Miyako Bay:					
Shirahama	8.5	1.0			0.020
Kuwagasaki	9.1	4.0			0.320
Sokei	6.0	4.0			0.320
Takahama	3.0	2.0			0.080
Kanahama	3.9	2.0			0.080
Yamada Bay:					
Oosawa	3.9	2.0–2.5			0.950
Yamada	5.5	3.0–4.0			0.320
Origasa	3.3	1.9			0.070
Funakoshi Bay:					
Koyadori	15.2	6.6 (12.0)			1.250
Tanohama	9.1	5.1			0.500
Funakoshi	15.2	5.0			0.500
Kirikiri	10.6	5.5			0.600
Namiita	10.6	5.2			0.550
Oozuchi Bay:					
Ando	4.2	3.4			0.230
Oozuchi	2.7	3.3			0.215
Hakozaki	5.8	4.3			0.370
Nehama	5.5	4.0			0.320
Ryooishi	11.2	10.0			2.000

(to be continued.)

Table V. Wave heights of tsunamis and $T(P)$. (continued.)

Locality	1896 Tsunami	1933 Tsunami	1944 Tsunami	1946 Tsunami	$2T(P)$
	m	m	m	m	
Kamaishi Bay:					
Kamaishi	4.5–8.2	3.7			0.275
Ureishi	4.2	3.9			0.300
Hirata	5.2	3.7			0.275
Hongo	14.0	12.0			2.850
Koshirohama	16.4	8.6			1.500
Arakawa	10.6	5.8			0.675
Yoshihama	24.2(?)	13.6–16.3			4.559
Okirai Bay:					
Imaurahama	9.7	9.9			1.225
Okirai	10.3	11.1			1.550
Koishihama	10.3	8.3			0.850
Shirahama	21.8	22.1–28.7			8.150
Ryori	10.6	8.6–9.7			1.050
Oofunato Bay:					
Nagahama-takonoura	—	4.1			0.210
Akazaki	3.6	2.4			0.070
Oofunato	3.3	3.4			0.145
Shimo-funato	5.5	4.1			0.210
Suezaki-hosoura	6.7	4.1–6.2			0.325
Hirota Bay:					
Tadaide	10.6	9.0			1.000
Atsumari	2.7	19.5			4.750
Oonohara	7.9	9.8			1.075
Takata Bay:					
Tomarihama	7.6	6.4–8.5			0.700
Mikkaichi	2.4	3.0			0.115
Osabe	3.3	6.0			0.450
Tadakoshi	8.5	8.6			0.925
Ishihama	8.5	6.0–9.5			0.750
Kesennuma Bay:					
Tsurugaura	4.2	4.5			0.250
Shukuhama	4.2	3.0			0.115
Ooshima-nagasaki	6.7	6.3			0.500
Ooshima-urahama	2.1	2.0			0.050
Koizumi Bay:					
Ooya	5.2	4.5–5.5			0.305

(to be continued.)

Table V. Wave heights of tsunamis and $T(P)$. (continued.)

Lacality	1896 Tsunami	1933 Tsunami	1944 Tsunami	1946 Tsunami	$2\,T(P)$
	m	m	m	m	
Koizumi Bay:					
Hikadohama	5.2	4.0			0.200
Oosawa	8.2	5.7			0.490
Nijuichihama	6.0	5.9			0.435
Kurauchihama	6.0	4.4			0.240
Minatohama	6.7	3.5			0.150
Tanoura	4.9	5.1			0.325
Shizukawa Bay:					
Irimae	3.3	3.6			0.160
Hosoura	3.6	2.5			0.075
Shimizuhama	3.3	2.2			0.060
Hiraiso	4.0	3.0			0.115
Shizukawa	2.1	1.5			0.030
Hayashihama	1.8	3.2			0.130
Oritate	2.7	2.7			0.090
Mitobe	2.4	2.1			0.055
Tsunomiya	4.0	3.6			0.160
Takihama	4.0	2.4			0.070
Fujihama	5.2	5.3			0.350
Nagashimizu	4.9	4.6			0.265
Kotaki	6.0	9.7			1.175
Oppa Bay:					
Oozashi	5.2	3.8			0.180
Kozashi	4.6	4.6			0.265
Aikawa	4.6	5.5			0.375
Oomuro	4.0	3.7			0.170
Naburihama	3.3	3.3			0.135
Okachi Bay:					
Myojinhama	2.4	2.0			0.050
Okachi	3.0	3.9			0.190
Funato	2.7	3.5			0.150
Karakuwa	1.8	2.1			0.055
Wakehama	2.1	1.8			0.040
Namiita	2.4	2.1			0.055
Sashihama	2.7	2.1			0.055
Omaehama	3.0	2.2			0.060
Oura	2.4	2.7			0.090

(to be continued.)

Table V. Wave heights of tsunamis and $T(P)$. (continued.)

Locality	1896 Tsunami	1933 Tsunami	1944 Tsunami	1946 Tsunami	$2\,T(P)$
	m	m	m	m	
Onagawa Bay:					
Takenoura	6.1	2.0			0.050
Ishihama	2.4	2.6			0.085
Onagawa	2.7	2.2–2.8			0.080
Nonohama	3.0	2.4			0.070
Iikonohama	2.7	2.0			0.050
Sameura Bay:					
Yoriiso	2.7	2.4			0.080
Maetsuna	2.4	2.0			0.055
Samenoura	3.0	5.0			0.350
Yakawa	3.3	5.2			0.375
Ojika Penn.:					
Tomarihama	6.0	3.7			0.190
Yamadori	4.2	3.0–3.6			0.150
Ayukawa	2.1	2.3–3.2			0.110
Kobuchi	2.4	2.9			0.115
Ooharahama	1.8	2.3			0.075
Koamikura	2.1	3.0			0.125
Oginohama	2.1	2.9			0.115
Momoura	1.2	1.2			0.020
Ishinomaki	0.6	1.0			0.015
Tsu			1		0.009
Kawana			0.5		0.003
Matsuzaka			1.0		0.009
Oominato			2		0.040
Kagamiura			2.5		0.049
Nagaoka			2.0		0.031
Matoya			3		0.070
Nakiri			3.5	1.0	0.044
Funakoshi-sotoura			3.5	1.2	0.044
Funakoshi-uchiura				1.8	0.590
Katada			3	2.2	0.034
Fuseda			2.2	1.0	0.010
Wagu			5	1.0	0.009
Koshiga				1.5	0.418
Ago Bay:					
Ugata			2		0.032

(to be continued.)

Table V. Wave heights of tsunamis and $T(P)$. (continued.)

Locality	1896 Tsunami	1933 Tsunami	1944 Tsunami	1946 Tsunami	$2\,T(P)$
	m	m	m	m	
Ago Bay:					
Goza			2.5	1.6	0.051
Hamashima				1.0	0.203
Hiyamaji				0.9	0.184
Shioya				1.0	0.203
Nanbari			3.5	2.0	0.099
Gokasho Bay:					
Syukudaso				1.0	0.203
Gokashoura			3	1.6	0.073
Shimotsuura				1.6	0.518
Hazamaura				1.6	0.518
Konza			3.4		0.094
Nakajima			3.5		0.099
Yoshizu			6		0.410
Shimazu			6		0.410
Nagashima			4		0.233
Nishiki			6		0.437
Kaino			4.6		0.309
Katsuragi			4		0.233
Owashi Bay:					
Sugari			5	1.1	0.364
Yaguchi			7.5	2.3	0.816
Ikuma				1.9	0.341
Hikimoto			3	0.8	0.131
Owashi			5.0	2.0	0.364
Kuki			7	1.1	0.715
Hayata				1.1	0.715
Gata Bay:					
Mikiura			3.9	2.1	0.249
Nagara				2.3	0.500
Mikisato			3.9	2.6	0.249
Furue				2.4	0.544
Kada			7.1	3.6	0.823
Minamiwanai			5.5	2.8	0.735
Kajiga			4.9	2.1	0.394
Arasaka			7.1	3.5	0.824
Arashika			8.4	3.0	1.150

(to be continued.)

Table V. Wave heights of tsunamis and $T(P)$. (continued.)

Locality	1896 Tsunami	1933 Tsunami	1944 Tsunami	1946 Tsunami	$2T(P)$
	m	m	m	m	
Ootomari			5.2	2.0	0.377
Kodomari			5.5	2.1	0.415
Kinomoto			3.0	4.0	1.510
Atawa				2.0	0.285
Udono				1.5	0.161
Shingu			3	3.5	0.580
Ukui			3		0.316
Ookarachi			3		0.316
Nachi			4.5	3	0.710
Katsuura			2.4	2	0.202
Taiji			4.5		0.710
Shimosato			2.5		0.377
Uragami			6.2	3	1.351
Koza			3.5	3.6	0.736
Nishimukai			1.9		0.217
Tahara			2.5		0.731
Ooshima			2		0.241
Hashigui				4.6	0.567
Kushimoto			2	4.2	0.282
Fukuro				6.2	0.702
Arita				5.4	0.534
Tanami				4.1	0.306
Eda				4.8	0.419
Esumi			2.5		0.876
Susami				4.2	0.501
Hiki			1	3.0	0.256
Asaragi			4	4.0	0.686
Fukurotani				5.8	1.445
Shirahama				3.7	0.585
Tanabe Bay:					
Tanabe			1	2.7	0.315
Mikonohama				3.2	0.438
Mōri				4.7	0.950
Atonoura				4.4	0.828
Uchinoura				4.4	0.828
Ikeda				3.0	0.386
Hosono				3.1	0.411

(to be continued.)

Table V. Wave heights of tsunamis and $T(P)$. (continued.)

Locality	1896 Tsunami	1933 Tsunami	1944 Tsunami	1946 Tsunami	$2\,T(P)$
	m	m	m	m	
Tanabe Bay:					
Kogaura				3.2	0.439
Amishirazu				2.9	0.360
Nabemachi-yamauchi				2.1	0.189
Nabemachi				1.2	0.062
Matsubara				2.5	0.268
Shioya				2.8	0.336
Kiripe				1.7	0.073
Inami				4.9	0.604
Hachimanhashi Joryu				2.7	0.183
Gobo			0.5	3.0	0.465
Hii Bay:					
Mio				3.8	0.761
Ao				2.9	0.433
Ubuu				3.0	0.464
Koura				3.3	0.559
Yura Bay:					
Yura				4.0	0.824
Fukei				3.8	0.740
Itotani				3.5	0.630
Jin				1.3	0.090
Ato				3.9	0.778
Ooi				3.3	0.561
Kashiwa				3.0	0.464
Ogui				2.5	0.321
Katakui				2.5	0.321
Yuasa Bay:					
Yuasa				3.2	0.665
Hiro				4.9	1.134
Minojima-tatsugahama				1.5	0.158
,, takata				1.9	0.185
,, sunohara				1.8	0.167
,, yaki				1.1	0.062
Shimotsu Bay:					
Shimotsu			0.5	3.0	0.458

(to be continued.)

Table V. Wave heights of tsunamis and $T(P)$. (continued.)

Locality	1896 Tsunami	1933 Tsunami	1944 Tsunami	1946 Tsunami	$2\,T(P)$
	m	m	m	m	
Shimotsu Bay:					
Kata				2.5	0.322
Oosakiura				2.3	0.272
Tosaka				2.5	0.322
Shioura				2.5	0.322
Kuroe Bay:					
Kotoura				2.4	0.296
Nadaka				4.1	0.865
Torii				4.1	0.865
Shimizu				3.6	0.667
Suwasaki				4.2	0.905
Wakanoura Bay:					
Dejima				2.7	0.375
Wakanoura				1.9	0.186
Kata				1.6	0.132
Oosaka-chikuko				0.6	0.019
Hamadera				1.0	0.053
Kishiwada				1.0	0.053
Sano				0.3	0.005
Tannowa				0.3	0.005
Sumoto				0.9	0.042
Fukura				1.8	0.322
Yura				0.9	0.042
Nada				1.5	0.116
Nujima				1.5	0.116
Ama				1.5	0.116
Minato				0.3	0.005
Shitsuki				1.0	0.053
Naya				0.3	0.005
Sano				0.3	0.005
Tokushima				2.0	0.128
Muya				0.6	0.012
Komatsujima				2.0	0.128
Tachibanaura:					
Ookata				2.0	0.128
Tomosaki				1.9	0.119
Tachibana				3.3	0.348

(to be continued.)

Table V. Wave heights of tsunamis and $T(P)$. (continued.)

Locality	1896 Tsunami	1933 Tsunami	1944 Tsunami	1946 Tsunami	$2\,T(P)$
	m	m	m	m	
Tachibanaura :					
Kugui				3.6	0.415
Akaishi				2.5	0.200
Yuki Bay :					
Yuki				4.0	0.286
Tai				2.0	0.071
Kiki				4.2	0.314
Hiwasa Bay :					
Ebisu				3.6	0.232
Tai				1.5	0.032
Inoue				4.4	0.345
Mugi				4.5	0.334
Asakawa Bay :					
Awaura				4.0	0.264
Asakawa				4.7	0.364
Sawase				2.9	0.139
Dewashima				3.2	0.168
Tomooku				1.6	0.048
Nasa				3.7	0.294
Hamazaki				2.0	0.086
Shishikui				4.5	0.434
Tsubakidomari Bay :					
Tsubakidomari				1.9	0.115
Kobukikawara				2.2	0.155
Tsubaki				3.0	0.288
Hiramatsu				2.8	0.247
Shirigui				1.4	0.063
Kannoura				3.9	0.325
Nene				5.0	0.535
Shiina				3.0	0.105
Muroto				2	0.086
Ioki				3	0.386
Aki				3	0.376
Tei				2.9	0.361
Urato Bay :					
Kōchi				0.5	0.017
Tanezaki				1.4	0.135

(to be continued.)

Table V. Wave heights of tsunamis and $T(P)$. (continued.)

Locality	1896 Tsunami	1933 Tsunami	1944 Tsunami	1946 Tsunami	$2\,T(P)$
	m	m	m	m	
Urato Bay:					
Urato				1.5	0.155
Mimase				1.3	0.117
Usa Bay:					
Hashida				3.9	1.050
Usa				3.7	0.945
Fukushima				1.2	0.099
Yokonami				1.3	0.116
Susaki Bay:					
Koura				4.6	2.120
Miyanotani				5.2	2.695
Nomi				4.2	1.760
Oonogo				2.7	0.840
Susaki				3.3	1.087
Anwa				4.7	2.210
Kure Bay:					
Kure				3.9	1.518
Kamata				2.8	0.820
Kaminokae				2.7	0.730
Saga				4.7	0.950
Kamikawaguchi				4.5	0.870
Shimota				3.5	0.358
Nuno				2.0	0.117
Shimonokae				3.2	0.298
Iburi				2.7	0.213
Shimizu				0.8	0.119
Komame				3.0	0.676
Urajiri				1.2	0.185
Sukumo				1.2	0.185
Morosaki				0.5	0.003
Nishiura				0.5	0.003
Fukue				0.5	0.003
Maisaka				0.8	0.024
Onmaezaki				2.0	0.421
Uchiura				1.0	0.088

1944 tsunami ($E = 880 \times 10^{20}$ erg) and 1946 tsunami ($E = 720 \times 10^{20}$ erg). They are tabulated in Table V.

According to the results of calculation, $T(P)$ is constant for each of these tsunamis. From $T(P)$ and the values shown in Fig. 2, we can estimate, in a statistical sense, the maximum wave height, the velocity of the overflowing water, and many other quantities regarding future tsunamis at each place on the coast.

The author believes that this estimation on the probable future tsunamis will be useful in planning various means to guard against future tsunamis.

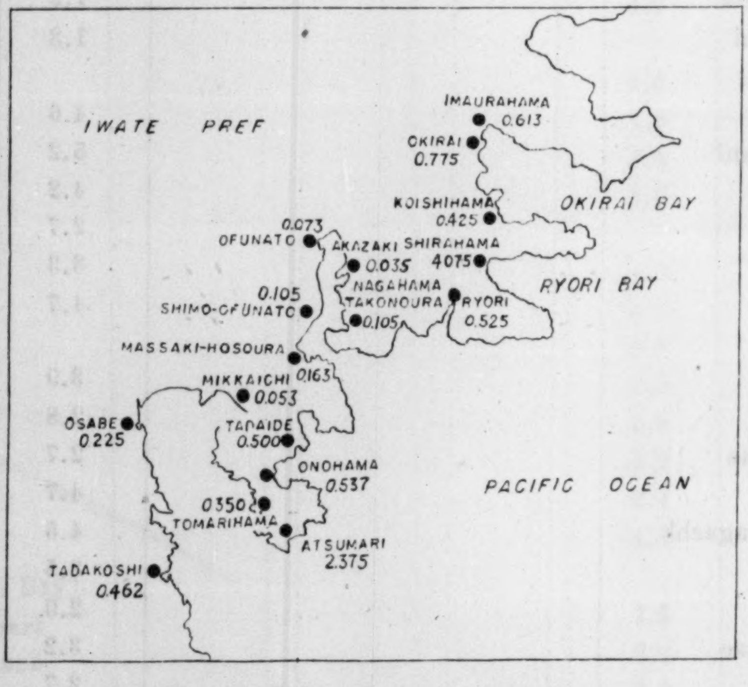
IWATE PREF
IMAURAHAMA 0.613
OKIRAI 0.775
KOISHIHAMA 0.425
OKIRAI BAY
0.073 OFUNATO
AKAZAKI 0.035
SHIRAHAMA 4075
NAGAHAMA
RYORI BAY
0.105 SHIMO-OFUNATO
TAKONOURA 0.105
RYORI 0.525
MASSAKI-HOSOURA 0.163
MIKKAICHI 0.053
OSABE 0.225
TADAIDE 0.500
ONOHAMA 0.537
PACIFIC OCEAN
0350
TOMARIHAMA
ATSUMARI 2.375
TADAKOSHI 0.462

Fig. 4. $T(P)$ and the topography.

As an example, a part of the Pacific coast (Iwate Prefecture) with a typical ria topography where damage from tsunamis is always large is shown in Fig. 4. Numerals in the figure are $T(P)$ values for the place. We can readily see in the figure how the $T(P)$ values are related to the shape of the bay. The tsunami is very violent at places where $T(P)$ values exceed 0.5.

In conclusion, the author expresses his sincere appreciation to Mr. Tokutaro Hatori, who undertook the troublesome task of arranging the observed data on the Tonankai 1944 tsunami and the 1946 tsunami and also calculated the values of $T(P)$.

7. 本邦太平洋沿岸各地に於ける津浪の危險度

地震研究所　**高橋龍太郎**

過去における地震活動の趨勢が，こゝ暫くは續くものと假定すると，太平洋沿岸の 200 m 等深線の內，P 地點の沖合に當る區分 (長さ 83 km) に，今後100年間に到達する津浪のエネルギーは

$$\int_Q \phi(Q)\, D(P, Q)\, dQ \quad \ldots\ldots\ldots\ldots\ldots\ldots\ldots\ldots(1)$$

で與へられる。此處に $\phi(Q)$ は Q 點から今後 100 年間に放出されるであらう津浪のエネルギー，$D(P, Q)$ は Q 點から出た津浪エネルギーが 200 m 等深線の P 點沖合の區分に分配される割合で，P, Q の相互位置と海深分布とから決る函數である。積分は全浪源地帶に就いて行ふ。

一方に於て，P 部落における津浪の危險度の目安として，其處で豫想される各回の津浪の波高の自乘の，100 年間に亘る總和を採ることゝすれば，此れは其の部落における延浸水面積，延被害額等に比例するものとなるであらうし，又其の部落に襲來する津浪エネルギーの總和にも比例する筈である。從つて前記 (1) 式の値と，此の危險度の目安としての波高の自乘の和との比を $T(P)$ とすれば，$T(P)$ は 200 m 等深線と部落間の海底，海岸の地形にのみよつて定まる函數で，浪源の位置や津浪の大きさには關係しない筈である。其れは 200 m 等深線といふのは大凡陸棚の緣に當つてゐて，津浪の前線は浪源の位置にかかわらず，大體この等深線に平行になるからである。

從つて (1) 式の値は津浪の地域的危險度を，$T(P)$ の値は各地の地形，位置等による，局地的危險度の相對値を示すものと見うる。(1) 式の値に $T(P)$ を乘じたものは P 地點の綜的合危險度を示すものとなる。

本文第 3 圖に於いては浪源の分布を十數ヶ所に凝集して圖式計算した (1) 式の値を示した。又第 5 表には 1933 年の三陸津浪 (總エネルギー $E=1600\times10^{20}$ エルグ), 1944 年の東南海地震津浪 ($E=880\times10^{20}$ エルグ) 及び 1946 年の南海地震津浪 ($E=720\times10^{20}$ エルグ) の際の各地の波高 A から

$$T(P) = A^2/E{\cdot}D(P, Q) \quad \ldots\ldots\ldots\ldots\ldots\ldots\ldots\ldots(2)$$

なる關係によつて計算した $T(P)$ の値が示してある。

第 4 圖に一例を示した樣に，$T(P)$ の値の大きい所は地形が津浪に對して不利な所である。

7. 本邦に於ける各地に於ける[illegible]

[illegible]

[illegible]

$$[illegible] \qquad \cdots\cdots\cdots\cdots\cdots(1)$$

[illegible]

$$[illegible] \qquad \cdots\cdots\cdots\cdots\cdots(2)$$

[illegible]

8. *Explosion-Seismic Observations in North-eastern Japan.*

By The Research Group for Explosion Seismology, Tokyo.*

Earthquake Research Institute, Tokyo University,
Geophysical Institute, Faculty of Science, Tokyo University,
Seismological Section, Central Meteorological Observatory,
Section of Geophysical Exploration, Geological Survey.

(Read Nov. 21 and Dec. 19, 1950.—Received Dec. 20, 1950.)

1. Introduction.

Our knowledge about the internal structure of the earth has been considerably enriched through the constant endeavour to revise the time-distance curves of seismic waves. But notwithstanding many brilliant achievements, the accuracy of time observations at routine stations has now reached the limit and we can expect no further development in this field without recourse to the statistical method. On the other hand, recent progress in the seismic exploration method gives promise of bringing the dead-lock in question to an end, and the highlight in recent seismology has been, in consequence, focused on this point. However, the thickness of the crust with which we have first to deal is about 50 km, so that the time-distance curve as far as 200 km or more must be determind with a higher accuracy. The explosives necessary for such explosion-seismic study amount to so much that we had such opportunities only on rare occasions. In Japan we have only one record of a blast of 20 tons by the navy on a south sea island. Unfortunately, we had no means to make observations at the surrounding ocean at the time.

2. Project of observation of Isibuti explosion.

In order to get 200,000 m^3 of rocks for the construction of the rock-fill dam, Isibuti, Wakayanagi-mura, Iwate Pref., about 20 km to the west of Mizusawa, a simultaneous explosion of 57 tons carlit had been planned to be detonated on 25th October 1950.

---

* Members of the group, who participated in the project are as follows (in alphabetic order):

AKIMA, T., KAWASUMI. H., OMOTE, S., MIYAMURA, S., SATO, Y., TAZIMA, K., TUZIURA, M., and YAMAZAKI, Y. (E. R. I.)

ASADA, T., DEN, N., MATUMOTO, T., SIMA, E., SUZUKI, Z., and TAZIME, K. (Geophys. Inst.)

AIHARA, K., ISIKAWA, M., INOUYE, W., OGAWA, T., and SUYEHIRO, S. (C. M. O.)

ITIKAWA, K., HURUYA, S., and KANEKO, T. (Geol. Surv.)

It was the first time in Japan that such a large amount of explosive was set off at one time and the explosion was a golden opportunity to seismologists. Unfortunately, it was only ten days before the explosion when we were informed of it. We at once established a project of cooperative observation though restricted in time, instruments, personnel and budget.

Amplitudes of the ground at different epicentral distances were estimated by taking into consideration the data of previous explosion seismic observations and the observing stations, instruments and personnel were distributed as are shown in Fig. 1 and Table I. As are seen in the figure, the observing stations were set up along the Tohoku railway line for transportation facilities and at the same time near the branch offices of the Tohoku Electric Supply Co., where telephone communications from the explosion point are available through private lines. No station was set up on the alluvial layers. Then, eight temporary stations were set up at about 20 km intervals starting from the Isibuti station which was 1.8 km from the explosion point as are shown in Fig. 1.

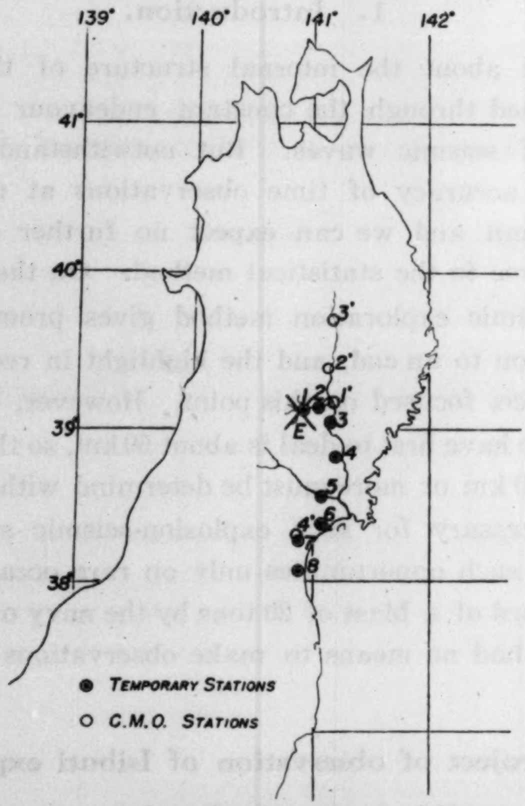

Fig. 1. Seismic observation stations for the Isibuti explosion.

Table I. Isibuti explosion seismic observation.

(1950-X-25, 12 h 06 m 07 s. $\varphi=39°\,06'\,21''$ N, $\lambda=140°\,51'\,37''$ E, $h=323$ m.)

No.	Station	Coordinates	Elevation	Distance from shot	Observers	Time signal	Paper speed	Seismographs (Component)
1	Isibuti	39° 06′ 51″ N 140° 54′ 43″ E	m 300	km 1.80	Suyehiro, Aihara, Isikawa, Ogawa (C.M.O.)	JJY	mm/sec 10	Ishimoto accel. (H), $T=0.^{s}1$, $V=100$. Hagiwara displ. (H), $T=4.^{s}4$, $V=17$.
2	Wakayanagi	39° 07′ 49″ N 141° 03′ 56″ E	100	15.06	Tazima (E.R.I.)	Chronometer	2	Ishimoto accel. (HR, HQ, V) $T=0.^{s}1$, $V=100$.
3	Maesawa	39° 02′ 46″ N 141° 07′ 38″ E	30	21.21	Miyamura, Tuziura (E.R.I.)	JJY	4	Ishimoto accel. (HR, HQ, V) $T=0.^{s}08$, $V=200$.
4	Hanaizumi	38° 50′ 07″ N 141° 10′ 17″ E	45	38.42	Omote, Yamazaki, Oosawa (E.R.I.)	JJY	2	Ishimoto tromometers ($H2$), $T=1.^{s}0$, $V=230$. Ishimoto accel. (V), $T=0.^{s}1$, $V=100$.
5	Kogota	38° 33′ 18″ N 141° 03′ 32″ E	10	62.81	Akima (E.R.I.)	Chronometer	40	Hagiwara tromometer (V), $T=0.^{s}05$, $V=40000$.
6	Matusima	38° 23′ 11″ N 141° 04′ 33″ E	10	81.37	Tazime, Den (Geophys. Inst.)	JJY	3	Mov. coil transducers $T=0.^{s}1$, $G=10^{8}$ ($H2$, V) Galva. YEW-D.
7	Sendai	38° 13′ 17″ N 140° 51′ 41″ E	67	98.24	Asada, Suzuki, Sima (Geophys. Inst.)	JJY	6	Mov. coil transducers $T=0.^{s}1$ ($V3$), $T=1.^{s}0$ ($H2$). $G=10^{8}$. Galva. YEW D.
8	Watari	38° 01′ 52″ N 140° 51′ 18″ E	15	121.91	Kaneko, Huruya, Itikawa (Geol. Surv.)	JJY	7	Mov. coil transducers $T=0.^{s}1$ ($H2$, $V2$), $G=10^{8}$. Galva. YEW D.

In order to determine the time of commencement accurately at each station, at six of the eight stations second-marks from the standard clock of the Tokyo Astronomical Observatory were placed on seismograms directly by the radio time signal, JJY (4 Mc). Others used chronometers checked by the NHK time signal at every hour. The firing time was fixed at 12 h 06 m 07 s, 25th October 1950 so as to be fit for the broadcast of the JJY time signal.

The speed of recording paper or film was 2 mm/sec at Wakayanagi and Hanaizumi, 3 mm/sec at Matusima, 4 mm/sec at Maesawa and more than 5 mm/sec at the other stations.

3. Explosion.

How the explosive was charged and detonated are described as follows. As shown in Figs. 2 and 3, seven large explosive chambers and eight small ones were dug at the height of 20 m above the adjacent river floor into the north-northeastern slope of the Saruiwa Rock, a massive igneous rock

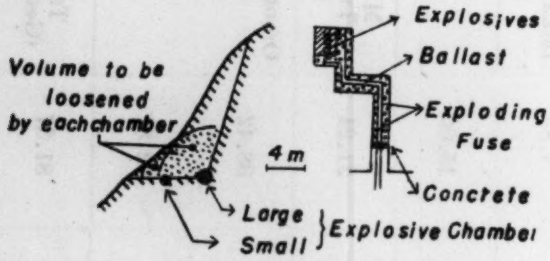
Volume to be loosened by each chamber
4 m
Large
Small
Explosive Chambei
Explosives
Ballast
Exploding Fuse
Concrete

Fig. 2. Explosive chambers.

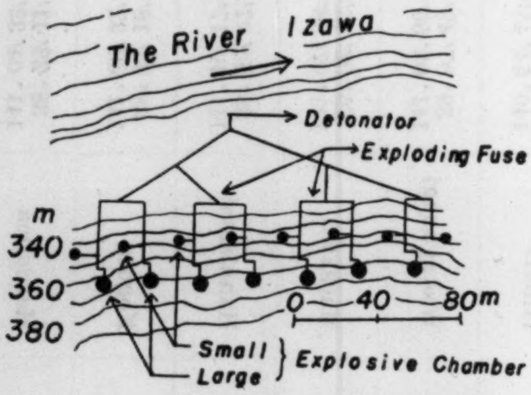
The River
Izawa
Detonator
Exploding Fuse
m
340
360
380
0
40
80m
Small
Large
Explosive Chamber

Fig. 3. Explosive chambers and the net of exploding fuse.

block. The explosive amounting to 57 tons was charged in these fifteen large and small chambers. At a distance of 300 m from the chambers, an electric detonater was placed, and an ignition switch was set at 400 m from the detonator. The detonator and each explosive chamber was connected with a fuse, each fuse having the same length so as to set off all the explosive at one time.

As scheduled beforehand, the electric switch was closed at 12h 06m 07s, 25th October 1950.1) A series of photographs in the Plates (Figs. 4~5) will show us vividly the process of explosion. From the viewpoint of civil engineering, the blast was quite successful and nearly 300,000 m^3 of rocks were loosened. However, contrary to our expectations, sounds and vibrations were not strong. Seismic intensity was II at the epicentral distance of about 2 km, and beyond 15 km no vibration was felt. But, shocks were felt by some persons at Kurosawaziri, 30 km northeast from the explosion. Closer inquiries of the shock at various places is now under way by mail.

4. Results of observations.

Favoured by clear telephone communications from the explosion point to each station, exact ignition as scheduled, and perfect receiving of the radio time signal it was possible to register the ground oscillations excellently at all stations except Kogota. Table II shows the time of commencement

Table II. Arrival times of the Isibuti explosion tremors observed at eight temporary stations of the group.

No.	Station	Arrival times (12 h 06 m.)			
		P_2	P_1	S_1	S_2
		sec.	sec.	sec.	sec.
1	Isibuti { Accel.	—	8.31	8.52	—
	Displ.	—	8.31	8.61	9.27
2	Wakayanagi	—	10.80	12.46	(13.69)
3	Maesawa	—	12.04	—	—
4	Hanaizumi	14.47	15.25	19.0	20.0
5	Kogota	—	—	—	—
6	Matusima	21.43	—	—	—
7	Sendai	24.5	—	35.9	37.2
8	Watari	28.0	—	—	—

---

1) According to a witness, the switch-in seemed to have been somewhat later than the predetermined time.

at each station checked quite independently by each observer. Seismograms at several stations are shown in Figs. 6 and 7. Fig. 8 indicates travel-time

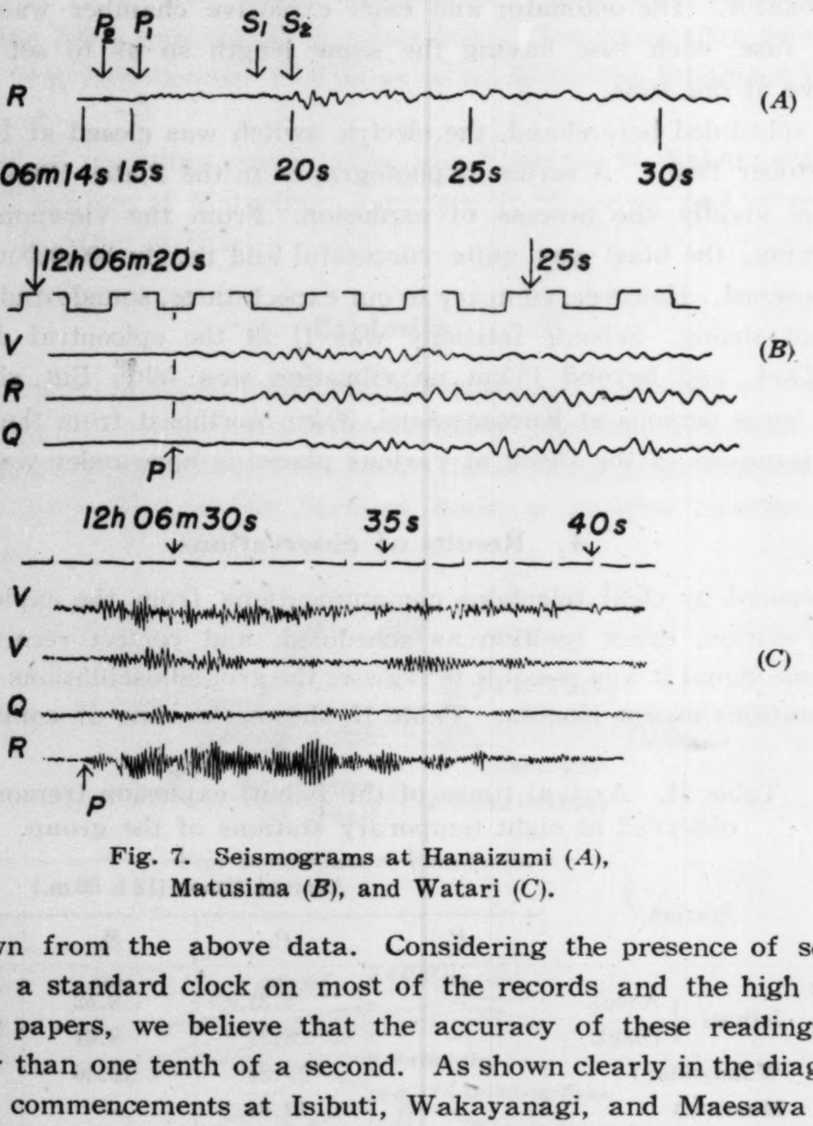

Fig. 7. Seismograms at Hanaizumi (*A*), Matusima (*B*), and Watari (*C*).

curves drawn from the above data. Considering the presence of second marks from a standard clock on most of the records and the high speed of recording papers, we believe that the accuracy of these readings are much higher than one tenth of a second. As shown clearly in the diagram, the times of commencements at Isibuti, Wakayanagi, and Maesawa seem to lie exactly in a straight line, and those of Matusima, Sendai and Watari also seem to lie in another line. A weak initial phase at Hanaizumi lies just on the former line and the following stronger onset lies on the latter line. These phases are named P_1 and P_2 respectively. Least square solutions of these lines give the velocities 5.26 ± 0.007 km/sec and 6.12 ± 0.017 km/sec and intercept times 7.97 ± 0.032 sec and 8.23 ± 0.24 sec after 12h 06m for P_1, and P_2 respectively.

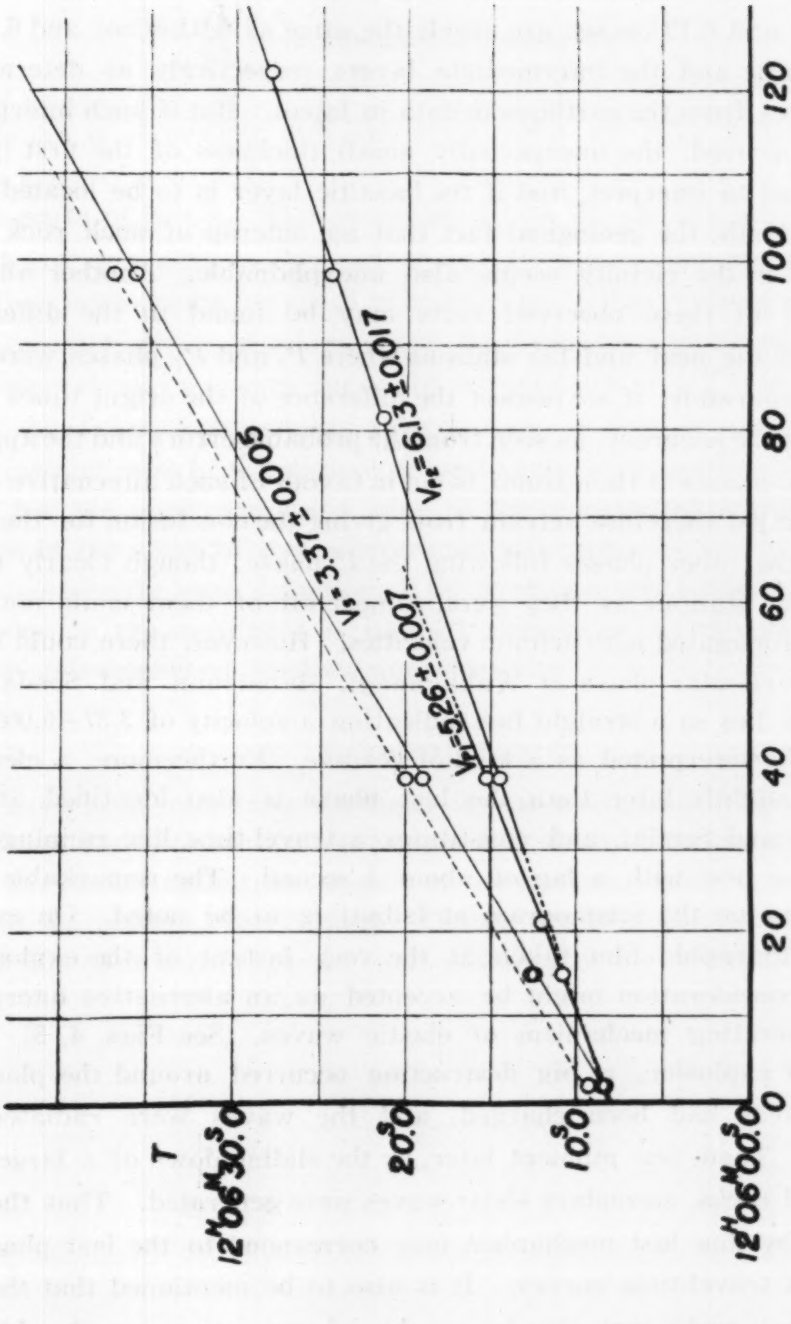

Fig. 8. Travel-time curves from the Isibuti explosion data.

The two lines intersect with each other at an epicentral distance of 9.5±9.74 km, and if we assume the existence of a uniform and horizontal layer, we have 1.3±1.27 km for the thickness. The velocities above mentioned, 5.26 km/sec and 6.13 km/sec are nearly the same as 5.0 km/sec and 6.1 km/sec in the granitic and the intermediate layers respectively as determined by T. Matuzawa from the earthquake data in Japan. But if such interpretation is to be approved, the unexpectedly small thickness of the first (granitic) layer is hard to interpret, and if the basaltic layer is to be located at such a shallow depth, the geological fact that no outcrop of such rock has yet been found in the vicinity seems also unexplainable. Another alternative explanation of these observed facts may be found in the difference in azimuths of the near and far stations where P_1 and P_2 phases were clearly observed separately, if we neglect the difference of the origin times of these waves. But the accuracy, as seen from the probable errors and the appearence of these two phases at Hanaizumi, is not in favour of such alternative explanation. We must therefore refrain from giving the conclusion for the present.

As to the other phases following the P phase, though clearly observed at respective stations as they were, almost all of them could not be seen as waves propagated with definite velocities. However, there could be found only one particular phase at Wakayanagi, Hanaizumi and Sendai, which respectively lies in a straight line indicating a velocity of 3.37±0.005 km/sec. This may be interpreted as a kind of S-wave. Furthermore, a clear phase appearing slightly later than the last phase is also identified at Isibuti, Hanaizumi and Sendai, and constitutes a travel-time line running parallel to the above line with a lag of about 1 second. The remarkable impetus of this phase on the seismogram at Isibuti is to be noted. On examining the cinematographic film taken at the very instant of the explosion, the following consideration might be accepted as an alternative interpretation of the generating mechanism of elastic waves. (See Figs. 4, 5) First, at the time of explosion, a big destruction occurred around the place where the explosives had been charged, and the waves were radiated in all directions. Then, one moment later, by tbe sliding down of a large amount of loosened rocks, secondary shear waves were generated. Thus the S-wave generated by this last mechanism may correspond to the last phase in the diagram of travel-time curves. It is also to be mentioned that the impact of the falling rocks may also be capable of generating considerable waves, since the potential energy released will amount to as large as 8×10^{17} ergs by the fall of 10 m. This amount is comparable with the energy from the explosives which is estimated at 2.4×10^{18} ergs. Therefore this may also serve as an alternative explanation of the generation of the later phases.

5. Concluding remarks.

Now we may conclude from the above statement that the crustal structure in NE Japan is somewhat different from what we have expected on the previous knowledge as deduced from the observations of natural earthquakes in other parts of Japan. The velocities of the P_1 and P_2 phases we have obtained are very near to those of $\overline{P}$ and P^* waves, but the thickness of the surface layer seems too small to be ascribed to that of the granitic layer.

The wonderfully good alignment of the travel-time plot is of course due to the observational accuracy due to the second mark of JJY from a standard clock of the Tokyo Astronomical Observatory, as directly recorded on the seismograms at most of the stations as well as the high speed of the recording papers, but we must ascribe it also to the unexpected smallness of the difference in the effect of the underground structure.

The apparently poor definition of the S phases and surface waves may also be due to the smallness of natural periods of seismometers and the recording galvanometers used through necessity.

6. Acknowledgment.

We have been very much obliged to the construction agencies of the Isibuti Dam, the Tohoku Electric Supply Co., the JJY Broadcasting Station and the provincial authorities at each of our station, which have been much helpful in the present observations. Thanks are also due to Prof. T. Matuzawa for his kind encouragement and guidance in the course of our study.

8. 東北日本における爆破地震動の觀測

爆破地震動研究グループ
東大地震研究所　東大地球物理學教室
中央氣象台地震課　地質調査所第4部

1950年10月25日岩手縣膽澤郡若柳村石淵(水澤町の西約20km)に，東北地方建設局と西松組とにより建設中の石塊堰堤の築堤用石塊採取のためおこなわれたカーリット57トンの一齊爆破に際し，われわれは爆破點よりの距離1.8kmから121kmにわたる間に8ヶ所の臨時觀測點をもうけて，この爆破による震動の觀測をおこなつた。觀測計畫の概要は第I表のとおりで，爆破點および各觀測點の位置は第1圖にしめした。爆破の方法は第2,3圖のごとき計畫にしたがい，導爆索の長さを一定にして，一齊に爆破するようにした。第4,5圖の一連の寫眞はよくその爆破狀況をしめしている。若干の地點における震動記象の複寫を第6圖，第7圖にかゝげる。初動および二三の位相の發震時は第II表にあり，これらの走時曲線は第7圖にしめす。震源にちかい4點にあらわれる，速度5.26±0.007km/secのP_1波と，とおい4點にみられる，速度6.13±0.017km/secのP_2波の兩直線は，震源より約10kmあたりでまぢわり，速度5.26km/secのうすい層が，速度6.13km/secの地殼のうえにのつていることをしめす。しかし兩直線の交點の震源距離と5.26km/secの層のあつさとは，計算によれば夫々9.5±9.74km，1.3±1.27kmとなるので，精度がわるく，したがつて，このような表面の層の存在もまだきわめて確實とはいえない。あるいわ，爆破點にちかい點は大体その東方に，遠い點は南方にあたるので，方向による傳播速度のちがいを考えることもできるかもしれない。これらの點に關しては，いまの材料の精度ではこれ以上決定的なことはいえないので，なお今後の觀測を期待して準備している。

S波にあたる位相は觀測されなかつたところがおゝいので，はつきりしたことはいえないが，一應3.37±0.005km/secの速度がえられた。これをS_1とするとき，さらに，これに約1秒おくれて位相S_2が，第8圖に破線でしめしたごとく，觀測され，石淵の變位計などでは非常にはつきりしたものである。爆破によりおこつた崩壞のはじまるときに生じたねぢり波ではないかと考えられる。

本觀測ははじめての經驗であつて，しかも非常に時間的余裕がすくなく，準備不充分でおこなつたのであつたが，さいわいにして，かなりの成果をおさめることができた。多大の便宜を與えられた東北地方建設局，西松組，東北配電株式會社，電波廳標準電波發射所および各觀測點の所在官民各位に對して深く感謝する。なお，今回の研究に對し，つねに激勵と指導とをあたえられた松澤教授にも感謝したい。

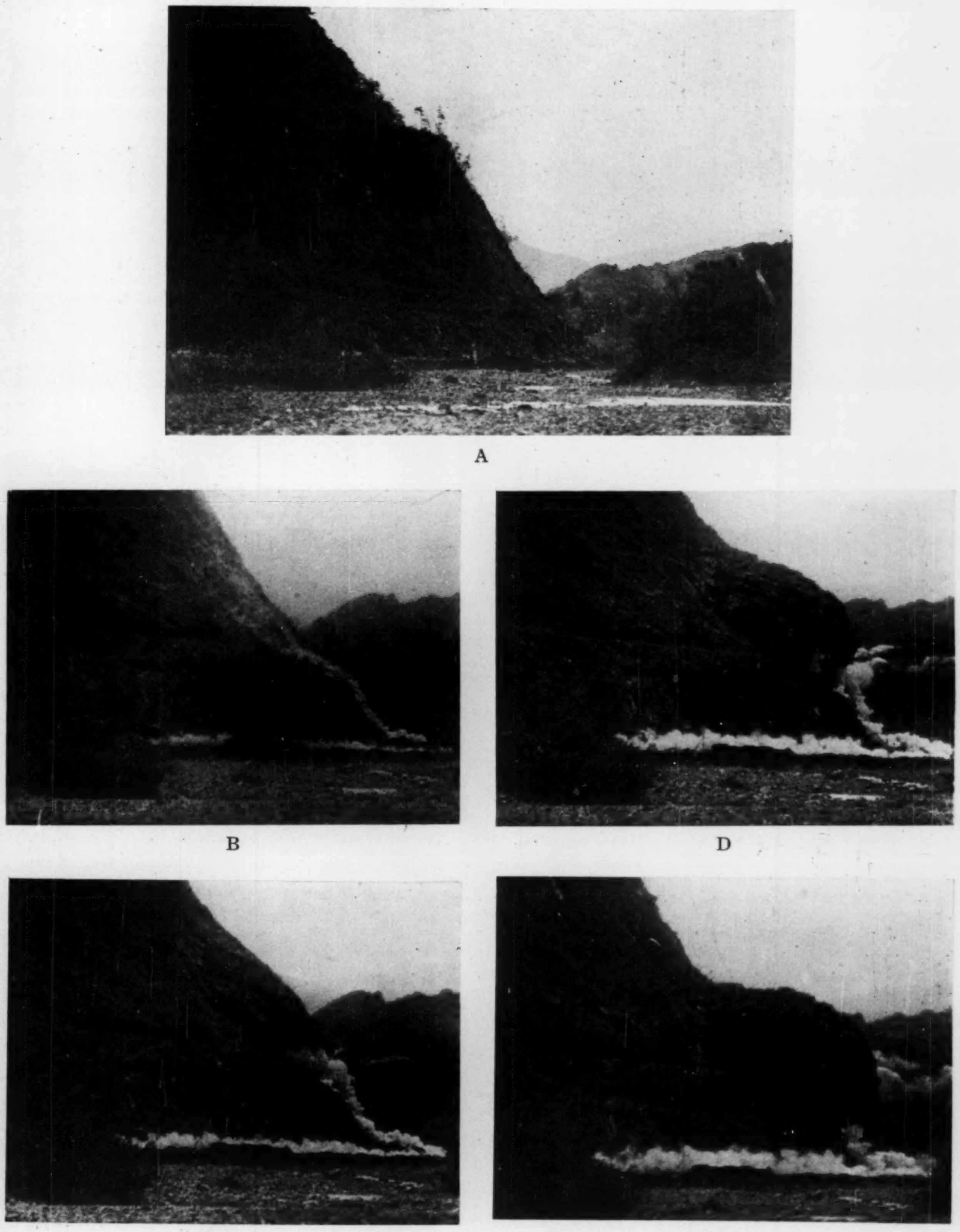

Fig. 4. Isibuti Explosion (I) A: Before the explosion. (By courtesy of the Press Asahi) B→E: Process of the explosion (From the Yomiuri News Reel). Cut interval between B and C, C and D, D and E, and E and F (Fig. 5) are 15, 15, 15, and 30 cuts respectively. Film speed was about 0.04 sec. per cut.

（震研彙報 第二十九號 圖版 爆破地震動研究グループ）

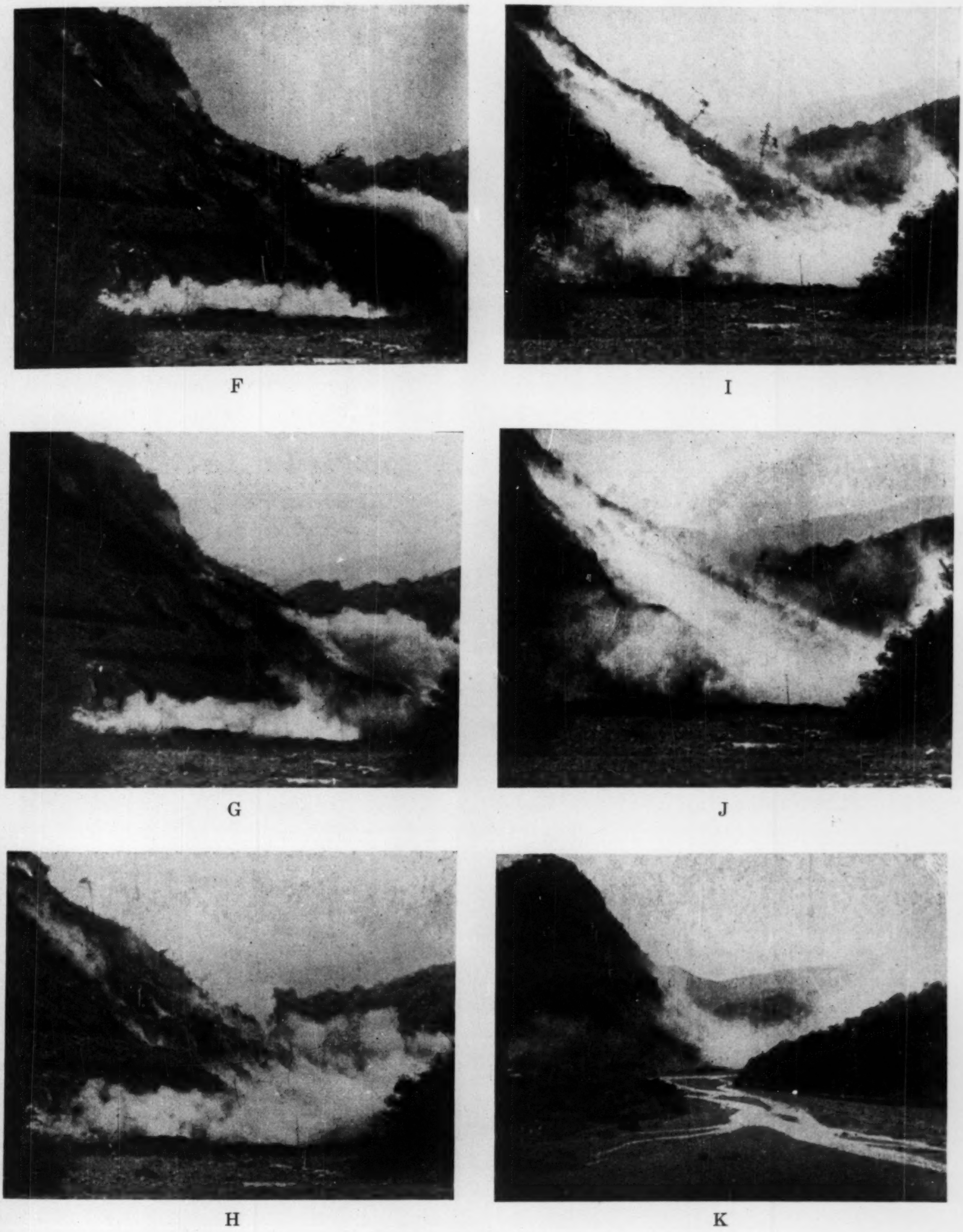

Fig. 5. Isibuti Explosion (II) F→J: Process of the explosion (From the Yomiuri News Reel). K: After the explosion (From the Yomiuri News Reel). Cut interval between E (Fig. 4) and F, F and G, G and H, H and I, and I and J are 30, 10, 95, 115, and 85 cuts respectively. Film speed was 0.04 sec. per cut.

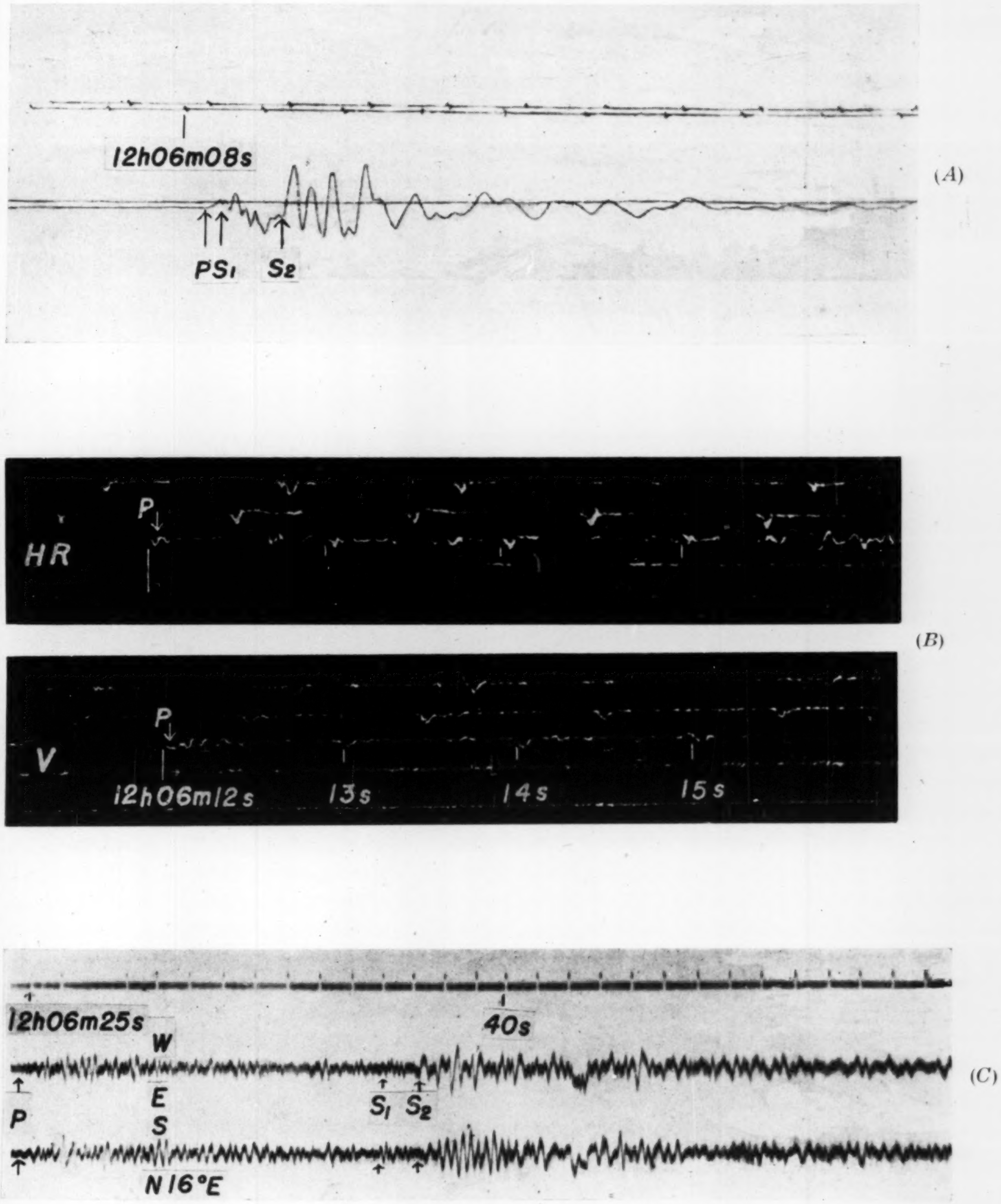

Fig. 6. Seismograms at Isibuti (*A*), Maesawa (*B*), and Sendai (*C*).

9. *Observations of the Earthquake-motion at the Different Depths of the Earth. I.*

By Kiyoshi KANAI and Teiji TANAKA,

Earthquake Research Institute.

(Read Jan. 17 and Oct. 17, 1950.—Received Dec. 20, 1950.)

1. Introduction.

The problem concerned with the earthquake-motions underground has already been paid attention to by many authors.[1] These researches, being based on observations made in comparatively shallow places in the ground, show mainly the nature of superficial layer of the earth.

In order to throw light on the important question of the nature of seismic waves, we have begun the observation of earthquake-motion by means of setting seismographs on ground surface as well as under-

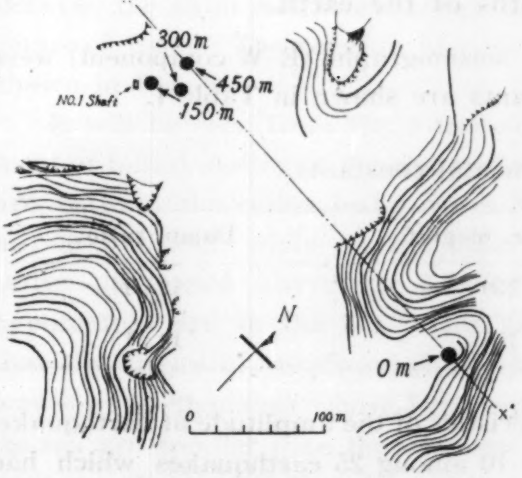
300m
450m
150m
NO.1 Shaft
N
0m
x'
0
100m

Fig. 1a. Geographical positions of seismograph stations at Hitachi mine.

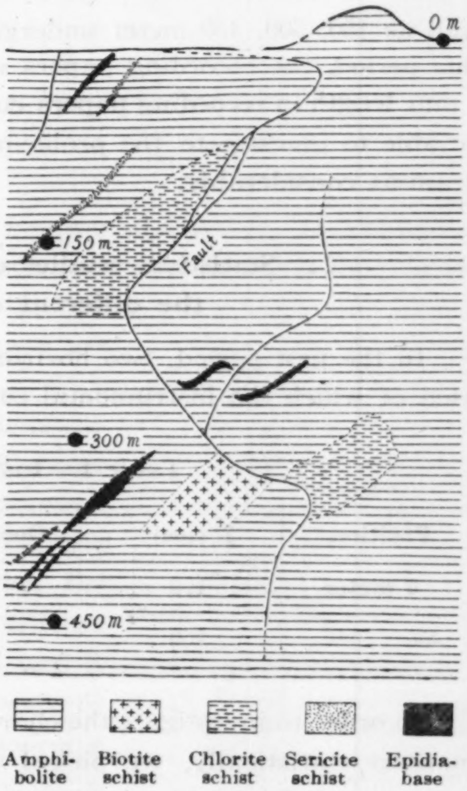
0m
150m
Fault
300m
450m
Amphibolite
Biotite schist
Chlorite schist
Sericite schist
Epidiabase

Fig. 1b. Geological formations about seismograph stations at Hitachi mine.

---

[1] F. OMORI, *Publ. Earthq. Inv. Com.*, **10** and **11** (1902),
N. NASU, *Bull. Earthq. Res. Inst.*, **9** (1931), 454,
U. INOUE, *Bull. Earthq. Res. Inst.*, **12** (1934), 712,
T. SAITA and M. SUZUKI, *Bull. Earthq. Res. Inst.*, **12** (1934), 517.

ground, at Hitachi mine in Ibaragi prefecture. Fig. 1 shows the geographical positions of seismograph stations together with the geological formations of that area.

In the first period during eleven months from Dec. 1, 1948 to Oct. 31, 1949, we made observation of earthquakes every day without intermission by means of seismographs set on the ground surface as well as at 450 meter underground, and observed 45 earthquakes. In this period, as the recording papers were changed once a week, that is to say 1 mm length in recording papers corresponded to 3 sec., we would not investigate the wave form. Therefore we shall deal with the seismogramms observed in this period statistically.

In the second period during the one month from April 7 to May 6, 1950, we carried out an observation of the earthquakes every day without intermission by means of setting the seismographs on the ground surface as well as 150, 300, 450 meter underground, and observed 14 earthquakes. In this period, the recording papers were changed once a day, that is to say, 1 mm length in recording papers corresponded to 0.5 sec., therefore we shall be able to investigate the problem concerning the wave forms of seismogramms considerably.

2. Statistical studies of the earthquake-motions at the different depths of the earth.

In the first period, two horizontal seismographs (E–W component) were used of which the instrumental constants are shown in Table I.

Table I. Instrumental constants.

Position	*T* (sec)	Geometr. magnif.	Damp. ratio
0 meter	1.0	150	13 : 1
450 〃	1.0	150	13 : 1

In order to investigate the characteristics of the amplitude of earthquake-motions statistically, we picked out 10 among 25 earthquakes which had been recorded in the period of about six months from Dec. 1, 1948 to June 3, 1949. The results of the present research are shown in Table II.

Columns 7 and 8 in Table II show that the ratio of the displacement of initial motion in *P* phase and *S* phase at 0 meter to those at 450 meter take values within the range of 1~2, but we can scarcely find out the relation

Table II. The results of observation.

No.	Date (1949)	Displacements of initial wave						Epic.	Depth of Hypoc. (km)	Intens. at Mito
		P (μ)		*S* (μ)		0 m/450 m				
		0 m	450 m	0 m	450 m	*P*	*S*			
1	II 11	—	—	2.3	2.0	—	1.2	140.0E 36.1N	Very shallow	II
2	IV 3	0.7	0.7	5.4	4.0	1.0	1.3	139.9 36.4	shallow	II
3	V 4	—	—	1.0	0.9	—	1.1	139.9 36.1	50	II
4	〃 6	—	—	2.3	1.4	—	1.8	141.8 37.5	60	II
5	〃 12	4.1	3.4	—	—	1.2	—	140.8 36.5	shallow	III
6	〃 16	—	—	5.0	4.0	—	1.3	140.6 36.3	〃	I
7	〃 22	—	—	1.4	0.8	—	1.8	142.0 38.4	〃	II
8	〃 25	1.4	0.7	14.8	8.1	2.0	1.8	141.9 37.3	〃	II
9	VI 2	4.0	2.7	28.4	16.9	1.5	1.7	141.2 36.7	30	II
10	〃 2	4.0	2.7	24.3	12.8	1.5	1.9	141.3 36.4	20	II

between the ratio mentioned above and epicentral distance, magnitude of earthquake, depth of hipocentre. And then, we tried to point out the relation between the ratio mentioned above and the epicentre of them. The relation just mentioned are shown in Fig. 2.

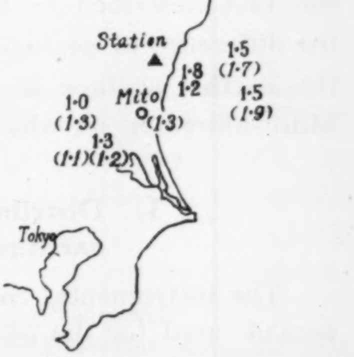

Fig. 2. The ratio of the displacement of initial motion in *S* phase (bracket) and *P* phase at 0 meter to the ones at 450 meter.

It will be seen from Fig. 2 that the displacement of initial motion at 0 meter and at 450 meter are with in the ratios 1∼1.5 when hypocentres are on the land, while on the other hand, the ratios mentioned above are 1.5∼2.0 when the hypocentres are in the sea. This fact tells us that the angles of incidence of *P* waves and *S* waves of earthquakes whose hypocentre were in the sea are smaller than those whose hypocentre were on the land,[2] that is to say, at least in the area of the present observing station, the characteristics of the path of seismic waves would differ according as the hypocentres were on the land or in the sea. Now, we will make the reason of it clear in another occasion as the number of earthquakes observed are yet insufficient.

---

[2] T. MATUZAWA, *Zishin* (*Earthquakes*), **4** (1932), 7.

Next, we shall compare the number of earthquakes observed at Hitachi mine by means of microseismograph (magnification = 150, period = 1 sec.) with those observed at Mito meteorological station, situated about 30 km to the south of Hitachi mine, by means of Wiechert seismograph (magnification = 80, period = 4 sec.). All of the felt-earthquakes at Mito station has been recorded at Hitachi station, but there are many earthquakes un-recorded at Hitachi station among the no-feeling-earthquakes recorded at Mito station. And then, we tried to point out the relation between the earthquakes recorded as well as those not recorded at Hitachi station among no-feeling-earthquakes recorded at Mito station and epicentre of them. The relation just mentioned are shown in Fig. 3. In Fig. 3, marks × and ● represent the recorded and un-recorded earthquakes respectively. The figures beside the marks in Fig. 3 indicate the depth of hypocentre. No figure beside ● and × represent that the depth of hypocentres were unknown and shallow respectively. Fig. 3 shows that the hypocentre whose motions at Hitachi mine were relatively large are shallow in general. It seems to be difficult to explain the fact described in Fig. 3 only through the difference of geological formation near the earth's surface in Hitachi (rock) and Mito (alluvium) on which seismographs operated.

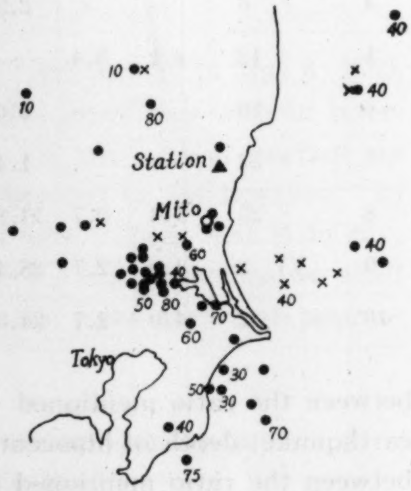

Fig. 3. Marks × and ● represent epicentre of earthquake recorded at Mito together with Hitachi and that recorded at Mito only respectively. The number beside the marks indicate the depth of hypocentre.

3. Distribution of horizontal displacements of earthquake-motions at different depths.

The instrumental constants of the horizontal seismographs (E-W component) used for the present investigations are as follows:

Table III. Instrumental constants.

Position	T (sec)	Geometr. magnif.	Damp. ratio
0 meter	0.92	150	13 : 1
150 ″	0.84	210	″
300 ″	0.83	200	″
450 ″	0.94	150	″

The seismograms of 5 earthquakes, whose records are relatively large and clear among the 15 earthquakes observed during the period of a month from April 7 to May 6, 1950, are shown in Figs. 4~8. Figs. 4, 5, 6 and Figs. 7, 8 are the records of the early parts of the main shocks and of the parts considered satisfactorily to be surface waves respectively.

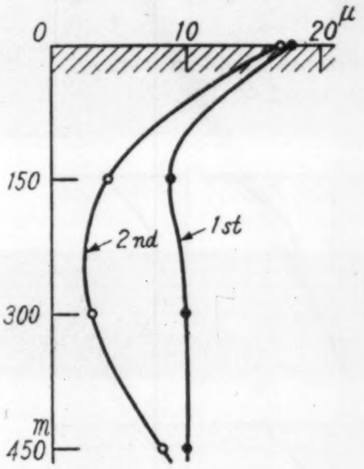

Fig. 9. The distributions of horizontal displacements at different depths of cases corresponding to Fig. 4.

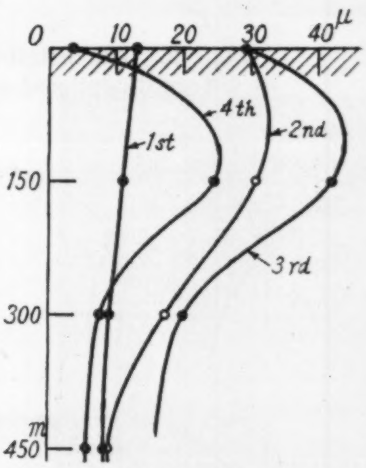

Fig. 10. The distributions of horizontal displacements at different depths of cases corresponding to Fig. 5.

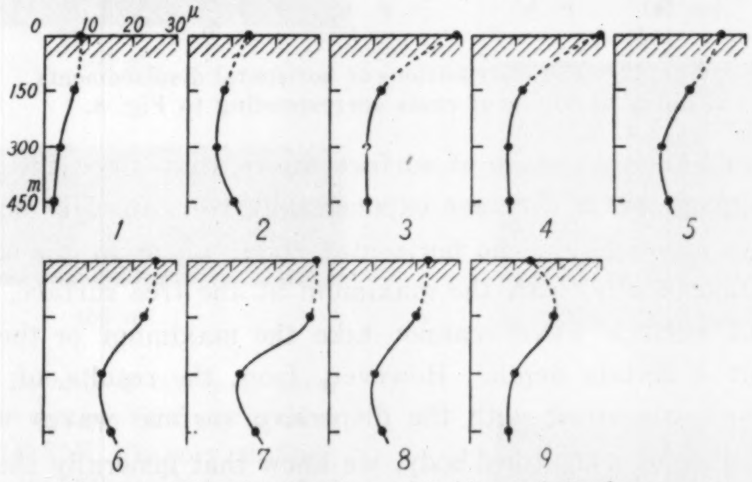

Fig. 11. The distributions of horizontal displacements at different depths of cases corresponding to Fig. 6.

The distribution of displacement at different depths which has been taken out following the order of waves of the records are shown in Figs. 9 ~13. From Figs. 9~13 we found that there are maximum or minimum displacement of waves in a certain depth, excepting the initial parts of the main shocks.

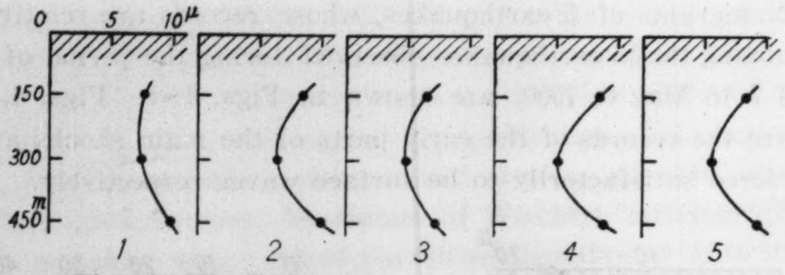

Fig. 12. The distributions of horizontal displacements at different depths of cases corresponding to Fig. 7.

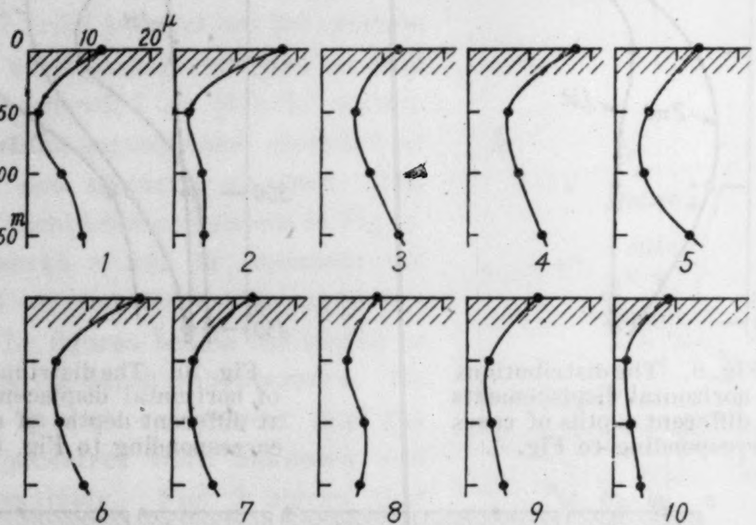

Fig. 13. The distributions of horizontal displacements at different depths of cases corresponding to Fig. 8.

It is a well-known feature of surface waves that since the amplitudes of usual Rayleigh-waves decrease exponentially from the free surface, and those of Love-waves having no horizontal nodal plane in the stratum are distributed sinusoidally, with the maximum at the free surface, then these two kinds of surface waves cannot take the maximum or the minimum amplitude at a certain depth. However, from the results of the recent investigations[3] concerned with the dispersive surface waves transmitted along the surface of a stratified body, we knew that generally the M_2-waves having no horizontal nodal plane in the stratum take a maximum amplitude of horizontal component of displacement at a certain depth.

Thus, from the above consideration, it is possible to assume that the waves having a peculiar feature in distribution of displacement are the M_2-waves.

---

[3] K. KANAI, "On the M_2-waves (Sezawa-waves)", *Bull. Earthq. Res. Inst.*, **29** (1951), 45.

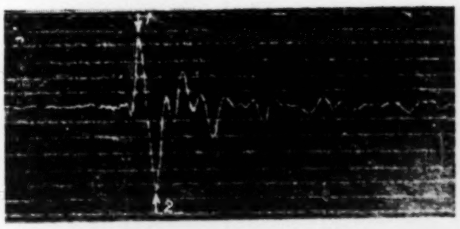

0 m

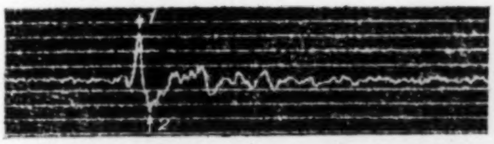

150 m

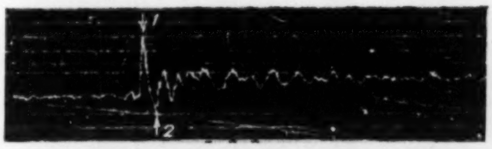

300 m

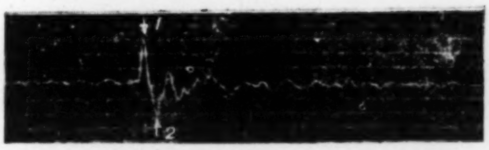

450 m

Fig. 4. Records of the early parts of the main shocks of the earthquake, 36.5° N; 140.8° E, D=very shallow, $\Delta \fallingdotseq 21$ km, 1950 IV 20. Original × 3.5.

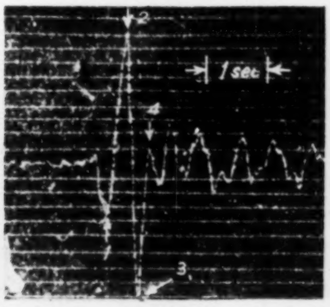

0 m

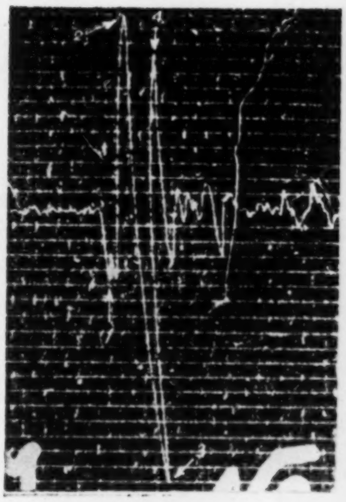

150 m

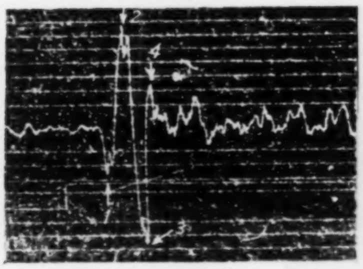

300 m

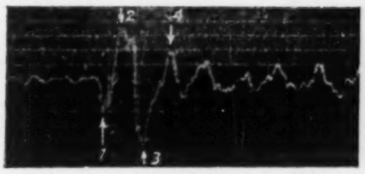

450 m

Fig. 5. Records of the early parts of the main shocks of the earthquake, 36.2° N; 140.1° E, D=50 km, $\Delta \fallingdotseq 63$km, 1950 V 11, Original × 3.5.

（震研彙報 第二十九號 圖版 金井・田中）

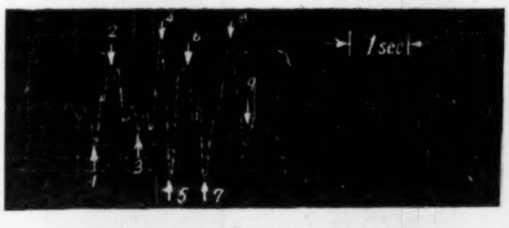

0 m

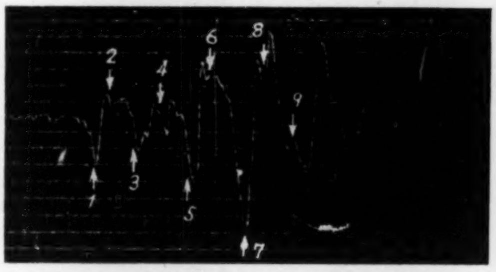

150 m

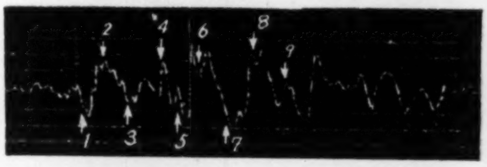

300 m

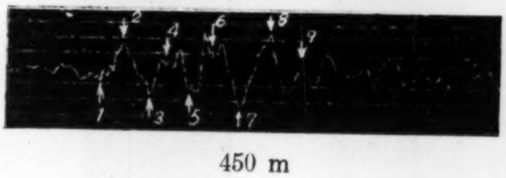

450 m

Fig. 6. Records of the early parts of the main shocks of the earthquake, 36.2° N; 141.2° E, $D=40$ km, $\Delta \fallingdotseq 70$ km, 1950 IV 14. Original × 3.5.

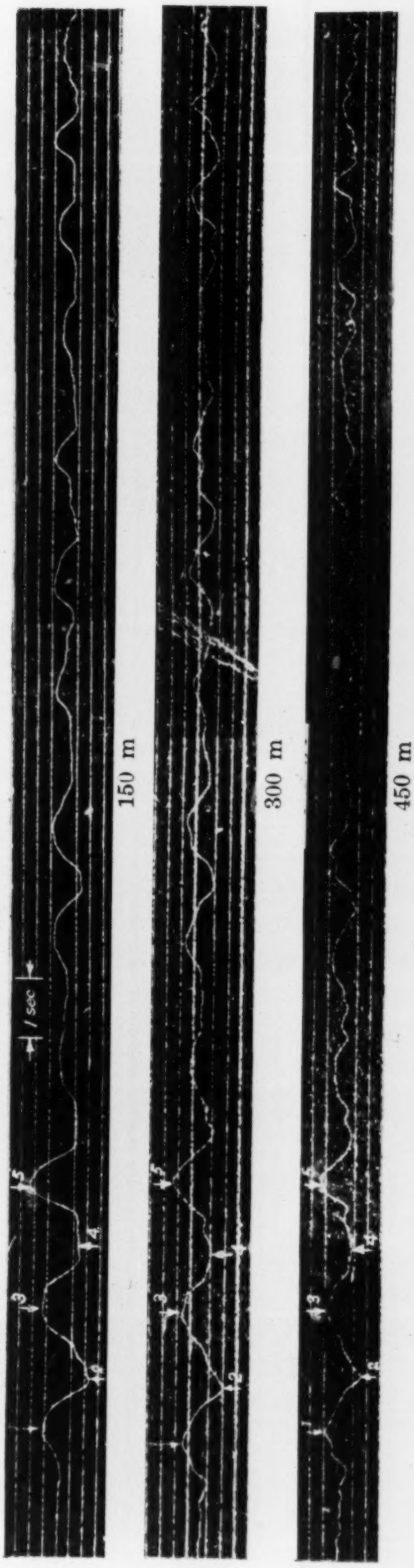

Fig. 7. Records of the parts considered satisfactorily to be surface waves of the earthquake, 33.8° N; 135.8° E, $D=40$ km, $\Delta \fallingdotseq 530$ km, 1950 IV 26. Original × 3.5.

（震研彙報 第二十九號 圖版 金井・田中）

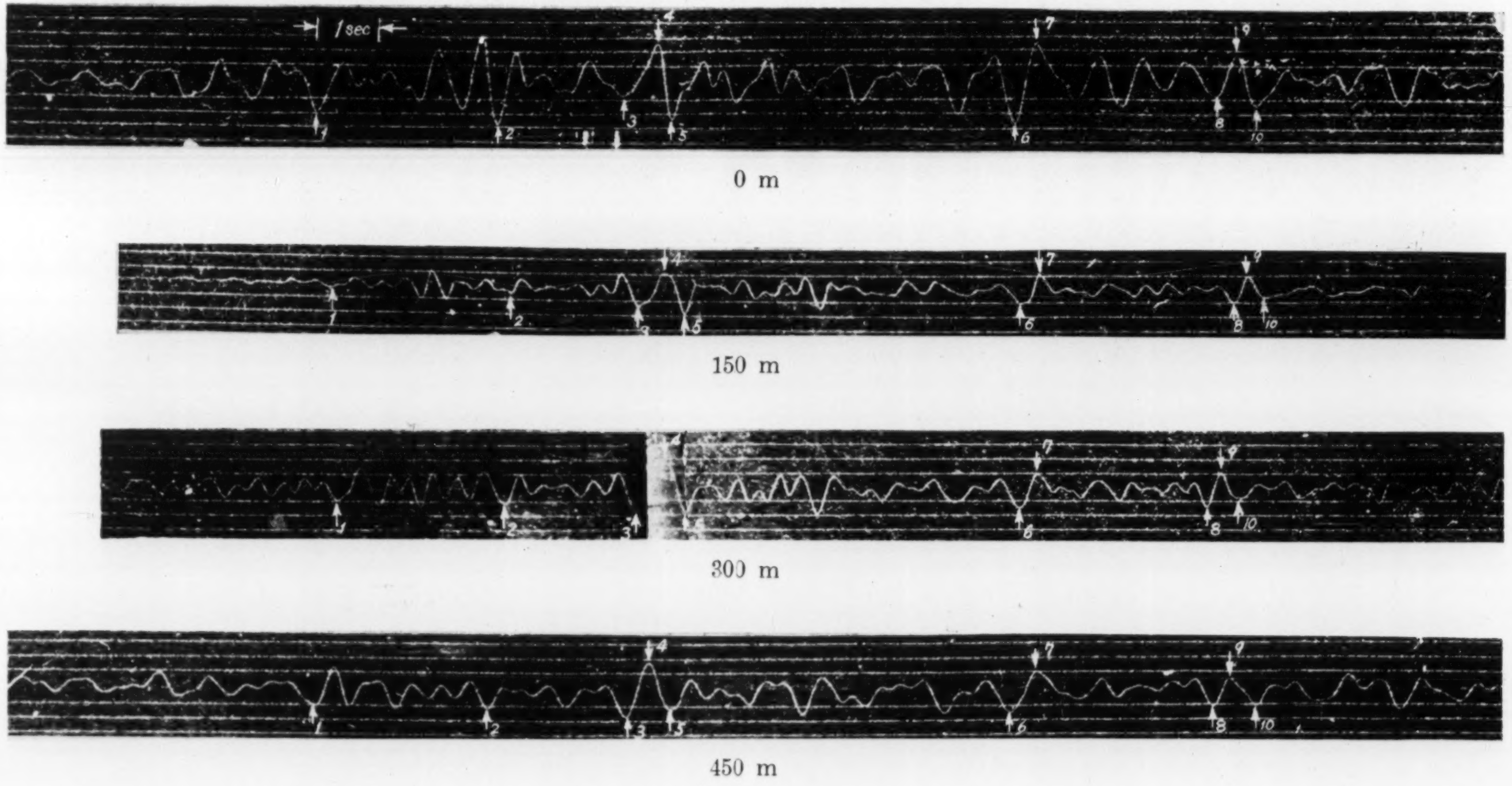

0 m

150 m

300 m

450 m

Fig. 8. Records of the parts considered satisfactorily to be surface waves of the earthquake, 37.6° N ; 142.5° E, D=very shallow, $\Delta \doteqdot 200$ km, 1950 **V** 18. Original × 3.5.

4. Concluding remarks.

From the results of the observation of earthquake-motions at different depths of Hitachi mine, we found some noteworthy facts.

One of the results of observations tells us that the angles of incidence of *P* waves and *S* waves of earthquakes whose hypocentres were under the sea are smaller than those whose hypocentres were on the land, whatever the epicentral distance, magnitude of earthquakes and depth of hypocentres may be.

It should be borne in mind that the distribution of horizontal component of seismic waves as to the depth in the earth is not so simple as considered formerly, and the component takes the maximum or the minimum amplitude of waves at a certain depth in the earth in general. From the results of the recent investigations, it is quite possible to assume that the wave having a maximum horizontal amplitude at a certain depth will be the M_2-waves.

In conclusion, we wish to express our sincerest thanks to Professor S. Nishio and the Motoyama-office of Hitachi mine with whose kind aid the present series of investigation were brought forth successfully. We also wish to express our thanks to Messrs. T. Suzuki, K. Osada and Miss S. Yoshizawa for the valuable assistance they offered in these investigations.

---

9. 地下における地震動の觀測結果 第1報

地震研究所 金井 清
地震研究所 田中貞二

茨城縣日立鑛山の地表面並びに地下 150, 300, 450 m の 4 個所で地震動の觀測を行つているが，記象を整理した結果，現在までにわかつた事項について第 1 報とする。

先づ，*P* 波，*S* 波の第 1 動について 0 m と地下 450 m との比をとると，震央距離，地震の大さ，震源の深さに無關係に，震源が海にある場合の方が陸にある場合よりも，この比が大きく，從つて，地震波の入射角は震源が海にある場合には，陸にある場合よりも小さい性質のあることがわかつた。

日立鑛山における地震動は約 30 km 南方にあたる水戸市における地震動に比べて非常に小さく，この原因は地盤の差違だけでは説明が困難のようである。

次に，主要動の水平成分の地表面よりの深さについての分布をしらべたところ，ごく最初の部分を除くと，この分布は從來考えられていたような單純なものではなく，或深さのところに水平成分の極大や極小がある場合が多いことが見出された。

最近の研究によると，M_2 波の水平成分は，多くの場合，表面層の或深さのところに極大ができるから，この M_2 波の性質を考慮に入れると觀測結果に現われた地震動の水平成分の地下分布に一應の説明をつけることができる。

10. *On the Coda Waves of Earthquake Motions.* (*Part 6*)

By Syun'itiro OMOTE,

Earthquake Research Institute.

(Read Dec. 18, 1945.—Received Dec. 10, 1950.)

CHAPTER 7. ON THE FREE OSCILLATION PERIODS OF THE EARTH'S SURFACE LAYERS REVEALED IN THE OSCILLATION PERIODS OF CODA WAVES.

§ 28. Waves that have the Periods of T_2 and T_3.

In the preceding Chapters 1 to 6[1], analyses have been carried out on the periods of waves in the coda oscillations of earthquake motions. Especially, from the analysis by Takahasi-Husimi's method explained in the previous chapter, it became clear that three sorts of waves of different periods, denoted T_1, T_2 and T_3, are to be found in the coda oscillations. Of these, T_1 becomes longer and longer as the epicentral distance increases, while T_2 and T_3 remain constant, their approximate values being $T_2 = 20$ sec., $T_3 = 16$ sec., irrespective of the difference of epicentral distances. These constant periods have not only resulted from the analysis by Takahasi-Husimi's method, but also have been obtained by other methods of analysis. Here we will compare the values of T_2 and T_3 periods arrived at in the respective chapters by different methods of analysis. In Table I-a and I-b they are tabulated in their corresponding portions. In this table we find first that T_3 period obtained by Takahasi-Husimi's method agrees quite well with the mean period T_m of the second coda waves observed in Chapters 4~5, and secondly we notice in the T_m column of the same table that, in the portions where the existence of T_2 period has been demonstrated by periodgram analyses and analyses by Takahasi-Husimi's method, there certainly exists the period of 20 sec., though its existence is not so easily perceptible.

The mean value of predominant periods with respect to the entire duration of coda waves of each earthquake is given in Table II. From this Table the values of T_2 and T_3 are found to be $T_2 = 20.0 \pm 0.2$ sec., and $T_3 = 16.0 \pm 0.1$ sec. As these periods have constant values for all the earthquakes irrespective of their different epicentral distances, it is to be suspected that they may represent the periods of the free oscillations of the earth's surface layers.

---

[1] S. OMOTE, *Bull. Earthq. Res. Inst.*, **21** (1943), 458; **22** (1944), 140; **23** (1945), 47; **28** (1950), 49; **28** (1950), 285.

§ 29. Free Oscillations of the Surface Layers.

Many papers have been written on the free oscillations of the earth's surface layers. F. Omori[2] found the proper periods of the free oscillations to be 0.26, 0.60, 1.25 and 2.6 sec. at the Tokyo University in Hongo, Tokyo, and 0.30, 0.69, 1.34 and 1.88 sec. at the Central Meteorological Observatory in Kanda. After that K. Suyehiro[3], using the wave analyser which he constructed, found that waves of the period of 0.3 sec. predominated at Hongo. Then M. Ishimoto[4], who followed with a detailed study, decided that the predominant period at Hongo was 0.3 sec. and that at Marunouti was

Table I.—a. Periods of coda oscillations in respective portions obtained by different methods.

T_2

Earthq. No.	Portion	T_2	T_m			T_A
	min. min.	sec.	sec.	sec.	sec.	sec.
34	40 ~ 42	19.8	12.7	14.5	14.5	
36	40 ~ 41	18.8	12.3	14.4		
〃	41 ~ 42	21.7	14.4	16.9		
〃	42 ~ 43	19.4	16.9	17.7		21
〃	50 ~ 51	21.7	16.8	14.5		20
〃	62 ~ 64	21.2	17.5	15.7	22.0	
37	50 ~ 52	20.8	13.7	16.3	13.5	
〃	53 ~ 55	19.7	15.6	14.3	14.8	20
49	72 ~ 73	19.2	17.1	17.1		
〃	73 ~ 74	19.7	17.1	17.8		
51	56 ~ 58	19.8	20.8	17.9	18.7	
〃	58 ~ 59	19.0	18.7	18.5		
〃	70 ~ 72	19.0	18.8	16.9	17.9	18
〃	80 ~ 82	20.0	19.9	17.2	15.8	
52	80 ~ 81	19.6	16.6	16.6		
〃	81 ~ 83	20.8	16.6	16.0	17.3	
〃	67 ~ 63	19.1	18.3	18.4		18
〃	80 ~ 81	20.9	18.4	15.9		19
〃	82 ~ 83	20.1	17.4	16.1		

---

2) F. OMORI, *Publ. Earthq. Invest. Comm.*, **11** (1902), 1.
3) K. SUYEHIRO, *Bull. Earthq. Res. Inst.*, **1** (1926), 59; **7** (1929), 467.
4) M. ISHIMOTO, *Bull. Earthq. Res. Inst.*, **12** (1934), 234.

about 0.6 sec. According to the study by T. Hagiwara⁵⁾ and the present writer the predominant period at Hongo has been found to be 0.2 sec.

In all the studies that have been made until today, the scope has been restricted to the observation of oscillations of short periods, or in other words, the observation of accelerations, as the primary object of the study was in correlating the period of earthquake motions to the destructive force of earthquake motions. Consequently the seismometers used for the above observations were those of relatively short-period types. F. Omori used those of the periods of 5~6 sec. M. Ishimoto and others used two accelerometers of 0.1 sec. and 1.0 sec. each. From the seismograms obtained by these

Table I.—b. Periods of coda oscillations in respective portions obtained by different methods.

T_3

Earthq. No.	Portion	T_3	T_m			T_A
	min. min.	sec.	sec.	sec.	see.	sec.
20	14 ~ 16	18.5	7.4	7.0	6.9	
37	69 ~ 71	16.3	16.4	13.7	14.5	[illegible]
〃	72 ~ 73	16.7	13.8	16.0		
〃	102 ~ 104	15.9	16.1	16.2	15.8	17
49	99 ~ 101	16.7	16.8	19.2	19.0	
〃	101 ~ 103	16.4	19.0	16.1	18.3	
51	122 ~ 124	16.6	19.0	16.1	18.3	16
〃	150 ~ 151	16.5	16.1	16.6		
〃	151 ~ 153	16.6	16.6	16.5	16.5	
52	107 ~ 108	16.3	15.8	16.4		
〃	108 ~ 110	16.6	16.4	15.7	15.4	
〃	120 ~ 121	16.1	17.4	16.2		
〃	121 ~ 122	16.8	16.2	15.9		
〃	122 ~ 123	16.4	15.9	17.0		
52	138 ~ 139	16.3	16.2	16.3		16
〃	139 ~ 140	16.4	16.3	15.5		
〃	140 ~ 141	16.3	15.5	15.6		
〃	115 ~ 117	16.4	14.7	18.2	15.4	
〃	117 ~ 119	16.3	15.4	15.1	15.2	
〃	130 ~ 131	16.3	16.3	18.0	16.2	
〃	131 ~ 132	16.5	16.5	16.2		
〃	132 ~ 133	16.2	16.2		16.1	
〃	133 ~ 134	16.4	16.4	16.1	17.2	

---

5) T. HAGIWARA and S. OMOTE, *Bull. Earthq. Res. Inst.*, **16** (1938), 632; **17** (1939), 118.

short-period seismometers, it is very difficult, if not impossible, to find out long period waves such as were described in the preceding chapter, and it would be quite natural that the long-period oscillations with periods of 16 sec. and 20 sec. had long been overlooked and escaped unnoticed.

The question whether free oscillations are made possible by the existence of surface layers was studied by K. Sezawa6)7)8) and others some twenty years ago from the point of view of the dispersion of seismic disturbance due to its multiple reflections in these strata. Nevertheless, no satisfactory mechanism has yet been thought of to explain how the free oscillation of the surface layer is generated.

Table II.

T ; Periods determined by means of Takahasi-Husimi's method.
T_M; Periods determined from the curve of successive one minute mean of the periods of coda oscillations.

Earthq. No.	T		T_M
	T_2	T_3	
20	—	18.5	—
54	—	16.4	—
34	19.8	—	—
36	20.8	—	—
37	20.3	16.3	—
49	19.5	16.5	16.9
51	19.5	16.6	16.5
52	20.1	16.4	16.6

§ 30. Free Oscillation Periods of the Surface Layers Calculated by the Rayleigh-Ritz's Method. I. (In Case of Two Layers.)

Thanks to the detailed studies made by T. Matuzawa9)10)11)12) and others we have a sufficiently clear knowledge on the structure of the earth's surface layers in the Tokyo district, Japan. Now the question at issue is, when there takes place in a surface layer a stationary oscillation that has the

---

6) K. SEZAWA, *Bull. Earthq. Res. Inst.*, **8** (1930), 1.

7) K. SEZAWA and G. NISHIMURA, *Bull. Earthq. Res. Inst.*, **8** (1930), 321.

8) K. SEZAWA and K. KANAI, *Bull. Earthq. Res. Inst.*, **10** (1932), 1.

9) T. MATUZAWA, K. HASEGAWA and S. HAENO, *Bull. Earthq. Res. Inst.*, **4** (1928), 85.

10) T. MATUZAWA, *ibid.* **5** (1928), 499; **6** (1929), 177.

11) T. MATUZAWA and T. FUKUTOMI, *ibid.* **10** (1932), 499.

12) T. MATUZAWA, K. YAMADA and T. SUZUKI, *ibid.* **7** (1929), 24.

node point at its lower boundary and the loop at the free surface of the earth's crust, what period is to be expected of such an oscillation?

Table III.
Arrangement of surface layers after T. Matuzawa.

Velocity / Surface layer	V_P	V_S
km km	km/sec	km/sec
0 ~ 4	1.94	1.14
4 ~ 20	5.0	3.15
20 ~ 50	6.1	3.7
50 ~	7.5	4.5

The result of the studies by T. Matuzawa are reproduced in Table III, and Z. Kinosita[13] assumed one more thin layer in the upper most part of Matuzawa's first layer, the thickness d'' of that uppermost layer being $d''=360^{\mathrm{m}}$, provided that $V_P=450$ m/s, and $V_S=240$ m/s. Then according to these studies we will assume that there are three layers in the earth's surface and that a stationary oscillation due to the distortional type of waves has been generated in them.

In the first place, assuming that a stationary wave takes place in the upper layer of Matuzawa, in which the thin layer explained by Kinosita is supposed to be lying in the upper part, we calculated the period of the stationary wave in these two layers by the Rayleigh-Ritz's method.

As seen in Fig. 1, we denote these layers as the first and the second layers according to the order of their vertical arrangement, draw the axis of x upward from the lower boundary of the second layer, and let u', ρ', λ' and μ' represent the displacement, density and Lamé's elastic constants of the lower medium. The similar displacement, density, and the elastic constants of the surface layer of the thickness d'' are to be represented by u'', ρ'', λ'' and μ''. The x-ordinates of the free surface and the lower boundary of the first layer will be taken as H'' and H'. Then, though the mode of the stationary wave that takes place in such layers may not be known precisely, there is the advantage that in calculating the period of such a wave by the Rayleigh-Ritz's method that period will be affected only slightly by the difference of the assumed mode.

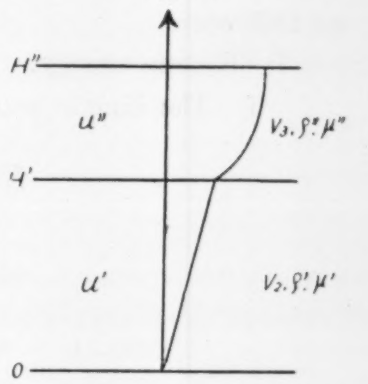

Fig. 1.

Then we will put

$$u'' = A\cos\frac{2\pi}{H''}x+B\,, \qquad \ldots\ldots\ldots\ldots\ldots\ldots (30\cdot1)$$

$$u' = kx \qquad \ldots\ldots\ldots\ldots\ldots\ldots\ldots\ldots\ldots (30\cdot2)$$

---

[13] Z. Kinosita, *Bull. Earthq. Res. Inst.*, **15** (1937), 965.

As the oscillation in question has a node at the lower boundary of the second layer and a loop at the free surface, the boundary conditions will be given by

$$\left.\begin{aligned} x = 0 \quad ; \quad & u' = 0 \\ x = H' \quad ; \quad & u' = u'', \quad \mu'\frac{\partial u'}{\partial x} = \mu''\frac{\partial u''}{\partial x} \\ x = H'' \; ; \quad & \mu''\frac{\partial u''}{\partial x} = 0 \,. \end{aligned}\right\} \qquad \text{.......}(30{\cdot}3)$$

From these conditions, the wave forms in the respective layers will be expressed by

$$u' = kx \sin pt \,, \qquad \text{.................................}(30{\cdot}4)$$

$$u'' = \left\{\frac{H'}{H''} + \frac{\lambda}{2\pi}\left(\cos\frac{2\pi H'}{H''} - \cos\frac{2\pi x}{H''}\right)\right\}kH'' \sin pt \,, \qquad \text{...}(30{\cdot}5)$$

where

$$\lambda = \frac{\mu'}{\mu''}\,\frac{1}{\sin\dfrac{2\pi H'}{H''}} \,.$$

The kinetic and the potential energies of such a wave will be calculated as follows.

1) Kinetic energy.

i) The kinetic energy L' in the second layer will be

$$\begin{aligned} L' &= \int_0^{H'} \frac{1}{2}\rho'\left(\frac{\partial u'}{\partial t}\right)^2 dx \\ &= \frac{1}{2}\rho' \int_0^{H'} k^2 x^2 p^2 \cos^2 pt \, dx \\ &= \frac{1}{6}\rho' k^2 H'^3 p^2 \cos^2 pt \,. \qquad \text{.............}(30{\cdot}6) \end{aligned}$$

ii) The kinetic energy L'' in the first layer will be

$$L'' = \int_{H'}^{H''} \frac{1}{2}\rho''\left(\frac{\partial u''}{\partial t}\right)^2 dx$$

$$= \frac{1}{2}\rho'' k^2 H''^2 p^2 \cos^2 pt \left\{\frac{\lambda^2}{4\pi^2}\int_{H''}^{H'} \cos^2\frac{2\pi x}{H''} dx - \frac{\lambda}{\pi}\left(\frac{H'}{H''} + \frac{\lambda}{2\pi}\cos\frac{2\pi H'}{H''}\right)\int_{H''}^{H'} \cos\frac{2\pi x}{H''} dx\right.$$

$$\left. + \left(\frac{H'}{H''} + \frac{\lambda}{2\pi}\cos\frac{2\pi H'}{H''}\right)^2 \int_{H''}^{H'} dx\right\}$$

$$=\frac{1}{2}\rho''k^2H''^2p^2\cos^2 pt\left[\left\{\frac{\lambda^2}{8\pi^2}+\left(\frac{H'}{H''}+\frac{\lambda}{2\pi}\cos\frac{2\pi H'}{H''}\right)^2\right\}(H''-H')\right.$$
$$\left.+\frac{\lambda}{2\pi^2}\left\{H'+\frac{H''\lambda}{2\pi}\left(\cos\frac{2\pi H'}{H''}-\frac{1}{8}\right)\right\}\sin\frac{2\pi H'}{H''}\right]. \quad\text{.................}(30{\cdot}7)$$

The total kinetic energy L_0 of the entire vibrating system will be given from (30·6) and (30·7) by,

$$L_0 = L'+L''$$
$$=\frac{1}{2}k^2p^2H''^3\cos^2 pt\left[\frac{1}{3}\rho'\delta^3+\rho''\left\{\frac{\lambda^2}{8\pi^2}+\left(\delta+\frac{\lambda}{2\pi}\cos 2\pi\delta\right)^2\right\}(1-\delta)\right.$$
$$\left.+\frac{\rho''\lambda}{2\pi^2}\left\{\delta+\frac{\lambda}{2\pi}\left(\cos 2\pi\delta-\frac{1}{8}\right)\right\}\sin 2\pi\delta\right], \quad\text{.................}(30{\cdot}8)$$

in this δ is put $\delta = H'/H''$.

2) Potential energy.

i) The potential energy V' in the second layer will be

$$V' = \int_0^{H'}\frac{1}{2}\mu'\left(\frac{\partial u'}{\partial x}\right)^2 dx$$
$$=\frac{1}{2}\mu'k^2\sin^2 pt\int_0^{H'}dx$$
$$=\frac{1}{2}\mu'k^2H'\sin^2 pt\,. \quad\text{.............}(30{\cdot}9)$$

ii) The potential energy V'' in the first layer will be

$$V'' = \int_{H'}^{H''}\frac{1}{2}\mu''\left(\frac{\partial u''}{\partial x}\right)^2 dx$$
$$=\frac{1}{2}\mu''\lambda^2k^2\sin^2 pt\int_{H'}^{H''}\sin^2\frac{2\pi}{H''}x\cdot dx$$
$$=\frac{1}{4}\mu''\lambda^2k^2\sin^2 pt\left\{(H''-H')+\frac{H'}{4\pi}\sin\frac{4\pi H'}{H''}\right\}. \quad (30{\cdot}10)$$

The total potential energy V_0 of the entire vibrating system will be given from (30·9) and (30·10) by,

$$V_0 = V'+V''$$
$$=\frac{1}{2}k^2H''\sin^2 pt\left\{\delta\mu'+\frac{1}{2}\mu''\lambda^2\left(1-\delta+\frac{1}{4\pi}\sin 4\pi\delta\right)\right\}\text{....}(30{\cdot}11)$$

where

$$\delta = \frac{H'}{H''},\quad \lambda = \frac{\mu'}{\mu''}\Big/\sin 2\pi\delta\,.$$

If we equate the maximum values of the kinetic and potential energies, the frequency equation will be obtained.

$$(L_0)_{\max} = (V_0)_{\max}$$

i.e.

$$\begin{aligned} p^2 H'' \Big[\frac{1}{3} \rho' \delta &+ \rho'' \Big\{ \frac{\lambda^2}{8\pi^2} + \Big(\delta + \frac{\lambda}{2\pi} \cos 2\pi\delta \Big)^2 \Big\} (1-\delta) \\ &+ \rho'' \frac{\lambda}{2\pi^2} \Big\{ \delta + \frac{\lambda}{2\pi} \Big(\cos 2\pi\delta - \frac{1}{8} \Big) \Big\} \sin 2\pi\delta \Big] \\ &= \delta\mu' + \frac{1}{2} \mu'' \lambda^2 \Big(1 - \delta + \frac{1}{4\pi} \sin 4\pi\delta \Big) . \qquad \text{........} (30\cdot12) \end{aligned}$$

The period T_1 will be obtained

$$\begin{aligned} T_1 &= \frac{2\pi}{p} \\ &= \frac{2\pi H''}{V_2} \sqrt{\frac{R_1}{S_1}} , \qquad \text{................} (30\cdot13) \end{aligned}$$

where

$$\begin{aligned} R_1 = \frac{1}{3}\delta &+ \frac{\rho''}{\rho'} \Big\{ \frac{\lambda^2}{8\pi^2} + \Big(\delta + \frac{\lambda}{2\pi} \cos 2\pi\delta \Big)^2 \Big\} (1-\delta) \\ &+ \frac{\lambda}{2\pi^2} \frac{\rho''}{\rho'} \Big\{ \delta + \frac{\lambda}{2\pi} \Big(\cos 2\pi\delta - \frac{1}{8} \Big) \Big\} \sin 2\pi\delta , \end{aligned}$$

$$S_1 = \delta + \frac{1}{2} \frac{\mu''}{\mu'} \lambda^2 \Big(1 - \delta + \frac{1}{4\pi} \sin 4\pi\delta \Big) ,$$

$$\lambda = \frac{H'}{H''} \frac{1}{\sin 2\pi\delta} ,$$

$$\delta = \frac{H'}{H''} .$$

Table IV.

Physical constants of surface layers.

Surface layer	V_S	μ	ρ
	km/sec.	C.G.S.	gr/cm³
1st layer	0.24	8.9×10^8	1.59
2nd layer	1.14	2.26×10^{10}	2.2

Next we will assume that the lower boundary of the second layer is at the depth of 4 km as calculated by T. Matuzawa, and that the numerical constants determining the physical qualities of these first and second layers are such as will be seen in Table IV, after T. Matuzawa and Z. Kinosita.

Then the period of the stationary wave calculated from the equation (30·13) will be shown in Fig. 2 for different values of the ratios of the thicknesses of the first and second layers. In this figure, the parameter is the depth of the lower boundary of the second layer. It will be seen from this figure

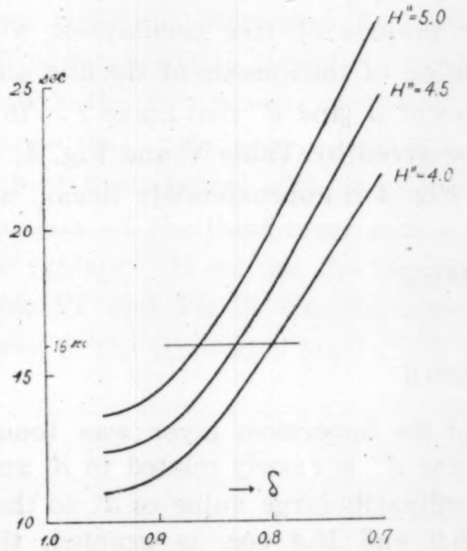

Fig. 2. Free oscillation periods of surface layers (in case of two layers). $\delta = H'/H''$.

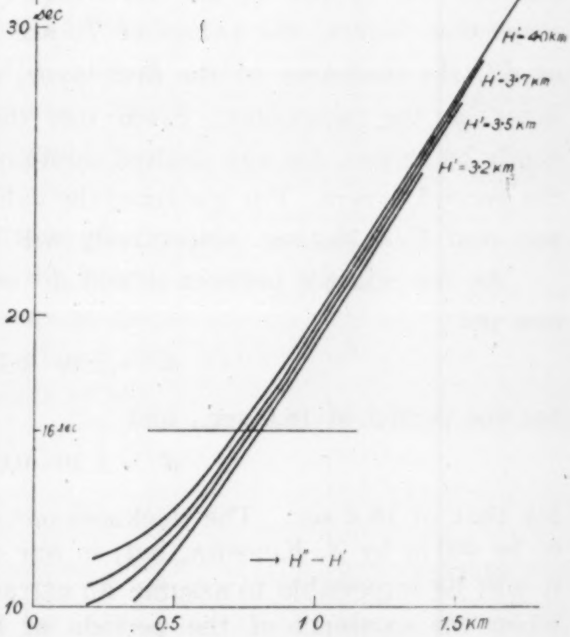

Fig. 3. Free oscillation period of surface layer (in case of two layers). Abscissa is the thickness of the upper layer; the parameter of the family of curves is the thickness of the lower layer.

Table V.

Thickness of surface layer within which the free oscillations of the period of 16.0 sec. and 16.4 sec. can take place.

d'	d'' (T = 16.0 sec.)	d'' (T = 16.4 sec.)
km	km	km
4.0	0.730	0.762
3.7	0.761	0.792
3.5	0.778	0.806
3.2	0.803	0.829

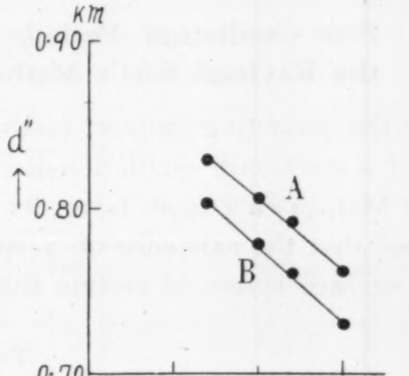

Fig. 4. Relation between d' and d'' when the free oscillation period T is T=16.4 sec. (A), and T=16.0 sec. (B).

that the value of T_l will be 16 sec. when $H''=4.5$ km and $\delta = 8.3$, or when $H'' = 5.0$ km and $\delta = 8.6$. For the purpose of making clear the relation between the period of the stationary waves and the thicknesses of the respective layers, the values of T_l are given in Fig. 3 for different values of d'', the thickness of the first layer, with d', the thickness of the second layer, as the parameter. From this the periods of free oscillations will easily be known for any desired combination of thicknesses of the first and the second layers. For instance, the values of d' and d'' that make $T_l=16.0$ sec. and $T_l = 16.4$ sec. respectively will be given by Table V and Fig. 4.

As the relation between d' and d'' in Fig. 4 is approximately linear, we can put

$$d'' = 1.10-0.0909\,d'$$

for the period of 16.0 sec., and

$$d'' = 1.10-0.0929\,d'$$

for that of 16.4 sec. The thickness d'' of the uppermost layer was found to be 400 m by Z. Kinosita, but, in our case d'' is closely related to d' and it will be impossible to assume an extraordinarily large value of d', so that when the existence of the periods of 16.0 and 16.4 sec. is granted, the thicknesses of the first and the second layers will be estimated as,

$$d' = 3.4 \text{ km}, \quad d'' = 0.79 \text{ km} \quad \text{for} \quad T_l = 16.0 \text{ sec.}$$

$$d' = 3.5 \text{ km}, \quad d'' = 0.80 \text{ km} \quad \text{for} \quad T_l = 16.4 \text{ sec.}$$

§ 31. Free Oscillation Periods of the Surface Layers Calculated by the Rayleigh-Ritz's Method. II. (In Case of Three Layers.)

In the preceding chapter, on the basis of rough calculations, we expected that, if a stationary oscillation due to transversal waves was to be generated within Matuzawa's upper layer, its period would be 16 sec. Now we have had a proof that the existence of a stationary oscillation of 16 sec. is possible when surface layers of certain thicknesses are arranged as assumed above.

Table VI.
Notation of the surface layers.

Surface layer	Displacement	Velocity	Rigidity	Density	Thickness
1	u''	V_3	μ''	ρ''	$d''=H''-H'$
2	u'	V_2	μ'	ρ'	$d'=H'-H$
3	u	V_1	μ	ρ	$d=H$

In the second place let us consider the waves of 20 sec. Already in Chapter 6 we saw that a stationary wave of 20 sec. period was to be expected in layers that have the lower boundary at the depth of about 20 km, and that this corresponded to the depth of the second layer which T. Matuzawa had assumed. We will now proceed to consider a third layer lying beneath the two layers mentioned above, and assume that a stationary oscillation takes place in these three layers with its node at the lower boundary of the third layer and a loop at the free surface. If we use the notation shown in Table VI and Fig. 5, the displacements of the waves in the respective layers will be given by

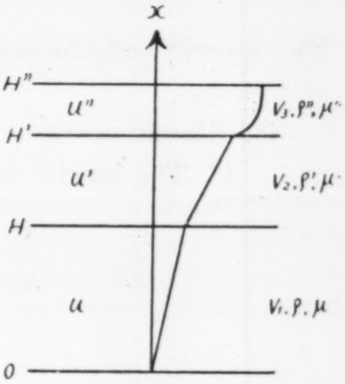

Fig. 5.

$$\left.\begin{aligned} u'' &= A\cos\frac{2\pi}{H''}x+B\,,\\ u' &= Cx+D\,,\\ u &= kx\,, \end{aligned}\right\}\quad\ldots\ldots\ldots\ldots\ldots(31\cdot 1)$$

where A, B, C, D and k are arbitrary constants to be determined from the following boundary conditions,

$$\left.\begin{aligned} &x=0\,; && u=0 && \\ &x=H\,; && u=u', && \mu\frac{\partial u}{\partial x}=\mu'\frac{\partial u'}{\partial x}\\ &x=H'\,; && u'=u'', && \mu'\frac{\partial u'}{\partial x}=\mu''\frac{\partial u''}{\partial x}\\ &x=H''\,; && && \mu''\frac{\partial u''}{\partial x}=0\,. \end{aligned}\right\}\ldots\ldots(31\cdot 2)$$

From these conditions the wave forms in the respective layers will be expressed by

$$\left.\begin{aligned} u &= kx\sin pt\,,\\ u' &= \left\{\frac{\mu}{\mu'}x+H\left(1-\frac{\mu}{\mu'}\right)\right\}k\sin pt\,,\\ u'' &= \left\{\frac{\mu}{\mu'}H'+\left(1-\frac{\mu}{\mu'}\right)H+\frac{H''}{2\pi}\alpha\cos\frac{2\pi H'}{H''}-\frac{H''}{2\pi}\alpha\cos\frac{2\pi}{H''}x\right\}k\sin pt\,, \end{aligned}\right\}(31\cdot 3)$$

where

$$a=\frac{\mu}{\mu''}\frac{1}{\sin\dfrac{2\pi H'}{H''}}\,.$$

The kinetic and the potential energies of such a wave will be calculated as follows.

1) Kinetic energy.

i) The kinetic energy L in the third layer will be

$$\begin{aligned}L&=\int_0^H\frac{1}{2}\rho\left(\frac{\partial u}{\partial t}\right)^2dx\\&=\frac{1}{6}\rho k^2p^2H^3\cos^2 pt\,.\ \ldots\ldots\ldots\ldots\ldots(31\cdot 4a)\end{aligned}$$

ii) The kinetic energy L' in the second layer will be

$$\begin{aligned}L'&=\int_H^{H'}\frac{1}{2}\rho'\left(\frac{\partial u'}{\partial t}\right)^2dx\\&=\frac{1}{2}\rho'k^2p^2\cos^2 pt\left\{\frac{1}{3}\frac{\mu^2}{\mu'^2}(H'^3-H^3)+\frac{\mu}{\mu'}\left(1-\frac{\mu}{\mu'}\right)H(H'^2-H^2)\right.\\&\left.+\left(1-\frac{\mu}{\mu'}\right)^2H^2(H'-H)\right\}.\ \ldots\ldots\ldots\ldots\ldots\ldots\ldots\ldots(31\cdot 4b)\end{aligned}$$

iii) The kinetic energy L'' in the first layer will be

$$\begin{aligned}L''&=\int_{H'}^{H''}\frac{1}{2}\rho''\left(\frac{\partial u''}{\partial t}\right)^2dx\\&=\frac{1}{4\pi^2}\rho''k^2p^2H''^2\cos^2 pt\left\{\left(\frac{a}{4}+\frac{2\pi^2}{H''^2}M^2\right)(H''-H')\right.\\&\left.-\frac{1}{16\pi}\alpha^2H''\sin\frac{4\pi H'}{H''}+\alpha M\sin\frac{2\pi H'}{H''}\right\},\ \ldots\ldots\ldots(31\cdot 4c)\end{aligned}$$

where

$$M=\frac{\mu}{\mu'}H'+\left(1-\frac{\mu}{\mu'}\right)H+\frac{H''}{2\pi}\alpha\cos\frac{2\pi H'}{H''}\,.$$

The total kinetic energy L_0 of the entire vibrating system will be given by,

$$\begin{aligned}L_0&=L+L'+L''\\&=\frac{1}{2}k^2p^2H''^3\cos^2 pt\left[\frac{1}{3}\rho\frac{H^3}{H''^3}+\rho'\left\{\frac{1}{3}\frac{\mu^2}{\mu'^2}\left(\frac{H'^3}{H''^3}-\frac{H^3}{H''^3}\right)\right.\right.\\&+\frac{\mu}{\mu'}\left(1-\frac{\mu}{\mu'}\right)\frac{H}{H''}\left(\frac{H'^2}{H''^2}-\frac{H^2}{H''^2}\right)+\left.\left(1-\frac{\mu}{\mu'}\right)^2\frac{H^2}{H''^2}\left(\frac{H'}{H''}-\frac{H}{H''}\right)\right\}\\&+\left.\frac{1}{2\pi^2}\rho''\left\{\left(\frac{\alpha^2}{4}+2\pi^2N^2\right)\left(1-\frac{H'}{H''}\right)-\frac{1}{16\pi}\alpha^2\sin\frac{4\pi H'}{H''}+\alpha N\sin\frac{2\pi H'}{H''}\right\}\right]\ (31\cdot 5)\end{aligned}$$

where $$N=\frac{1}{H''}M\,.$$

2) Potential energy.

i) The potential energy V in the third layer will be

$$V=\int_0^H\frac{1}{2}\mu\left(\frac{\partial u}{\partial x}\right)^2dx$$

$$=\frac{1}{2}\mu k^2H\cdot\sin^2pt\,.\quad\ldots\ldots\ldots\ldots\ldots\ldots(31\cdot6a)$$

ii) The potential energy V' in the second layer will be

$$V'=\int_H^{H'}\frac{1}{2}\mu'\left(\frac{\partial u'}{\partial x}\right)^2dx$$

$$=\frac{1}{2}\frac{\mu^2}{\mu'}k^2(H'-H)\sin^2pt\,.\quad\ldots\ldots\ldots\ldots(31\cdot6b)$$

iii) The potential energy V'' in the first layer will be

$$V''=\int_{H'}^{H''}\frac{1}{2}\mu''\left(\frac{\partial u''}{\partial x}\right)^2dx$$

$$=\frac{1}{4}\mu''\alpha^2k^2\sin^2pt\left\{(H''-H')+\frac{H''}{4\pi}\sin\frac{4\pi H'}{H''}\right\}.\quad\ldots\ldots(31\cdot6c)$$

The total potential energy V_0 of the entire vibrating system will be given by,

$$V_0=V+V'+V''$$

$$=\frac{1}{2}k^2\sin^2pt\left\{\mu H+\frac{\mu^2}{\mu'}(H'-H)+\frac{1}{2}\frac{\mu^2}{\mu''}\frac{H''-H'}{\sin^2\dfrac{2\pi H'}{H''}}\right.$$

$$\left.+\frac{1}{4\pi}\frac{\mu^2}{\mu''}H''\cot\frac{2\pi H'}{H''}\right\}.\quad\ldots\ldots\ldots\ldots\ldots\ldots\ldots\ldots\ldots(31\cdot7)$$

If we equate the maximum values of the kinetic and potential energies in (31·5) and (31·7), we get a frequency equation,

$$(L_0)\max=(V_0)\max$$

i.e.

$$p^2H''^2\left[\frac{1}{3}\rho\delta^3+\rho'\left\{\frac{1}{3}\frac{\mu^2}{\mu'^2}(\zeta^3-\delta^3)+\frac{\mu}{\mu'}\left(1-\frac{\mu}{\mu'}\right)\delta(\zeta^2-\delta^2)+\left(1-\frac{\mu}{\mu'}\right)^2\delta^2(\zeta-\delta)\right\}\right.$$

$$\left.+\frac{1}{2\pi^2}\rho''\left\{\left(\frac{\alpha^2}{4}+2\pi^2N^2\right)(1-\zeta)-\frac{1}{16\pi}\Big|\alpha^2\sin 4\pi\zeta+\alpha N\sin 2\pi\zeta\right\}\right]$$

$$=\mu\delta+\frac{\mu^2}{\mu'}(\zeta-\delta)+\frac{1}{2}\frac{\mu^2}{\mu''}(1-\zeta)\frac{1}{\sin^2 2\pi\zeta}+\frac{1}{4\pi}\frac{\mu^2}{\mu''}\cot 2\pi\zeta\,.\quad\ldots(31\cdot8)$$

where
$$\delta = \frac{H}{H''}, \qquad \zeta = \frac{H'}{H''}.$$

The period T_{II} will be given by

$$T_{\text{II}} = 2\pi/p$$
$$= \frac{2\pi H''}{V_1}\sqrt{\frac{R_{\text{II}}}{S_{\text{II}}}}, \qquad \text{..................}(31\cdot9)$$

where

$$R_{\text{II}} = \frac{1}{3}\delta^3 + \frac{\rho'}{\rho}\left\{\frac{1}{3}\frac{\mu^2}{\mu'^2}(\zeta^3-\delta^3) + \frac{\mu}{\mu'}\left(1-\frac{\mu}{\mu'}\right)\delta(\zeta^2-\delta^2) + \left(1-\frac{\mu}{\mu'}\right)^2\delta^2(\zeta-\delta)\right\}$$
$$+\frac{1}{2\pi^2}\frac{\rho''}{\rho}\left\{\left(\frac{a^2}{4}+2\pi^2N^2\right)(1-\zeta) - \frac{1}{16\pi}a^2\sin 4\pi\zeta + aN\sin 2\pi\zeta\right\}$$

$$S_{\text{II}} = \delta + \frac{\mu}{\mu'}(\zeta-\delta) + \frac{1}{2}\frac{\mu}{\mu''}(1-\zeta)\frac{1}{\sin^2 2\pi\zeta} + \frac{1}{4\pi}\frac{\mu}{\mu''}\cot 2\pi\zeta$$

$$a = \frac{\mu}{\mu''}\frac{1}{\sin 2\pi\zeta}$$

$$N = \frac{\mu}{\mu'}\zeta + \left(1-\frac{\mu}{\mu'}\right)\delta + \frac{a}{2\pi}\cos 2\pi\zeta$$

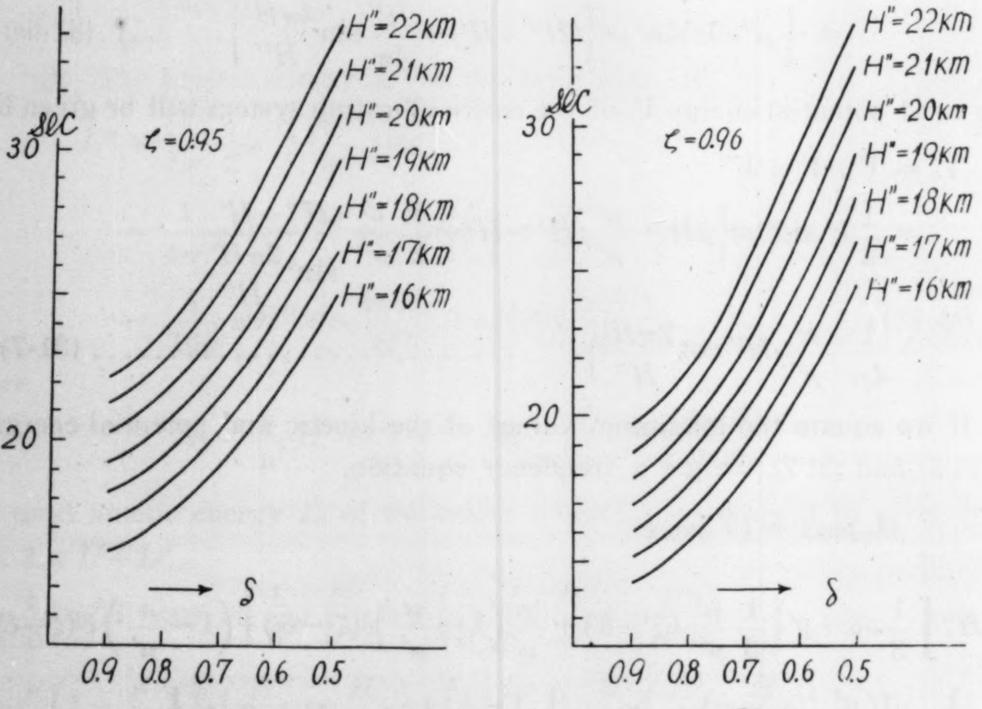

(A) (B)

Fig. 6. Free oscillation period of surface layer (in case of three layers). Abscissa δ is H/H'', parameter H'' is the total thickness of all layers. (A) $\zeta=0.95$; (B), $\zeta=0.96$; (C) $\zeta=0.97$

$$\delta = \frac{H}{H''}, \quad \zeta = \frac{H'}{H''},$$

The numerical values of the physical constants of the first and the second layers are already given in Table IV, and that of the third layer will be given by $V_3 = 3.7$ km/sec., $\mu = 26.8 \times 10^{10}$ *C.G.S.*, and $\rho = 2.7$ gr/cm³. By means of these values, the period T_{II} of the stationary waves will be calculated from the equation (31·9), and the results will be shown in Fig. 6, the parameter of the figure being the depth of the lower boundary of the third layer. It is necessary from the study in the previous paragraph that the thickness of the uppermost layer should be about 0.7 km, whence it follows that the value of ζ (which is equals to H'/H'') must be about 0.95~0.98 with respect to the assumed value of H'' (about 20 km). Fig. 6, (A), (B) and (C) are prepared for three different values of ζ, $\zeta = 0.95$, 0.96 and 0.97, respectively.

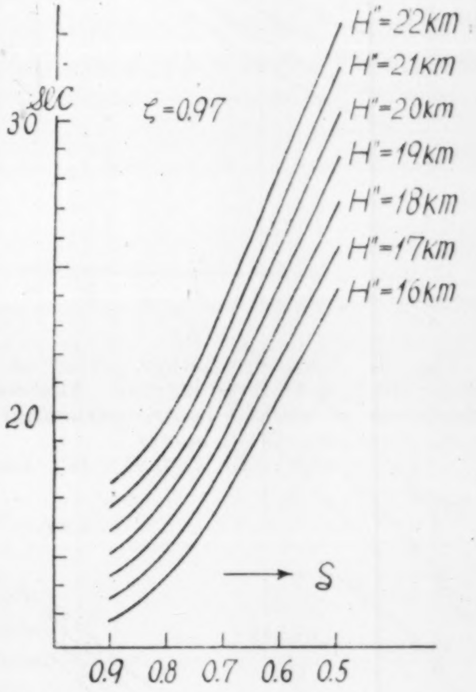

(C)
Fig. 6.

For the purpose of showing more clearly the relation between the period of the stationary wave and the thicknesses of the respective layers, Fig. 7 has been prepared with the thickness of the second layer as abscissa. On the basis of this figure the combinations of the thicknesses of the respective layers that allow the period of the stationary waves to be 20 sec. will be supposed to be as shown in Table VII, where d'' and d' are the thicknesses of the first and second layers and d that of the third layer. The relations between d'' and d' are shown by curves A, B and C in Fig. 8 for the different values of ζ. The values of free oscillations in Table V that have been obtained in the case of the period of 16 sec. are also shown in the same Figure by a broken line D. Now, if we assume that there are three layers existing near the surface, and that a stationary oscillation of 16 sec. is taking place in the first and second layers and an oscillation of 20 sec. in the first, second and third layers, it will follow that the thicknesses of d', d'' and d that have been obtained independently in Table V and Table VII have to be such as will not contradict each other. If we adopt the values of d' and d'' at the point where the two curves B and D cross each other in Fig. 8, the above conditions will at least be fulfilled.

These values are

$$d' = 2.95 \text{ km}, \quad d'' = 0.83 \text{ km},$$

and, ζ being equal to 0.97 for curve B, d will be found to be

$$d = 17.1 \text{ km}.$$

By these steps we have been able to find out the thicknesses of the respective layers, but the value of the thickness of the first layer here obtained is somewhat greater than the value determined by Kinosita. But the depth to the lower boundary of the second layer is 3.7 km which agrees quite well with Matuzawa's value of 4 km, and the thickness of the third layer which we find to be 17.1 km is also in good accord with the thickness 16 km of Matuzawa's second layer.

Thus we have been able to ascertain that, when the two constant periods found in the coda oscillations of earthquake motions are assumed to represent the free oscillation periods of the surface layers, the calculated values of the thickness of the respective surface layers show a good accord with the corresponding values obtained

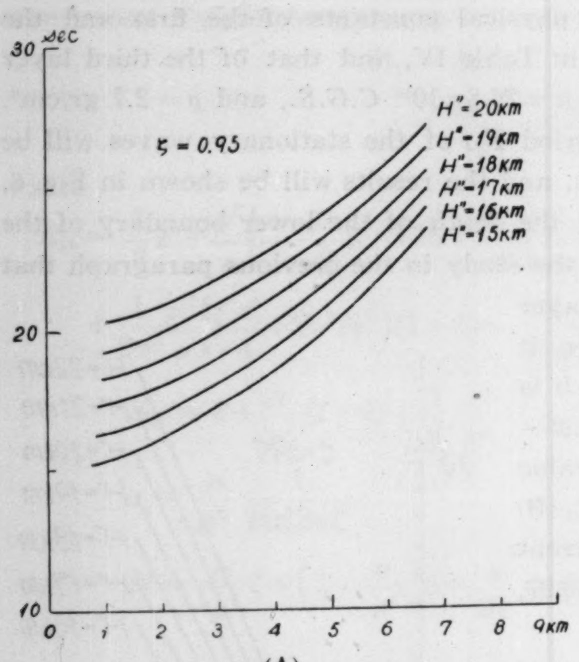

(A)

Fig. 7. Free oscillation period of surface layer (in case of three layers). Abscissa is the thickness of middle layer, parameter is the total thickness of all layers.
(A), ζ=0.95; (B), ζ=0.96; (C), ζ=0.97

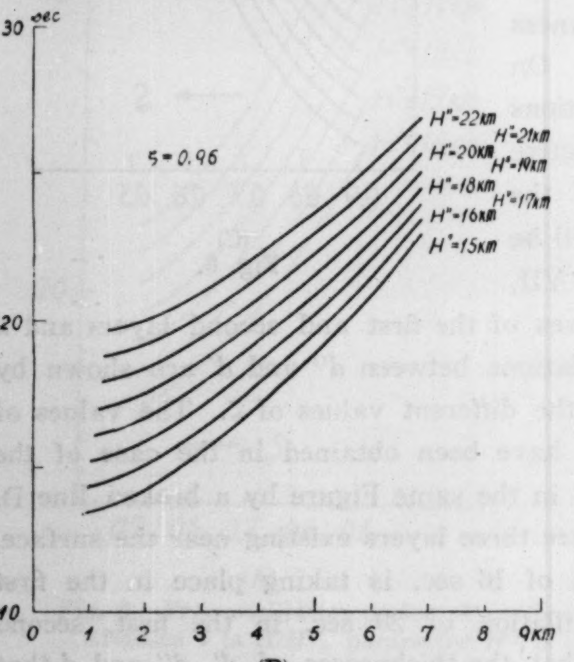

(B)

Fig. 7.

Table VII.

Thickness of surface layers within which the free oscillation of the period of 20 seconds can take place.

H''	$\zeta = 0.95$		$\zeta = 0.96$		$\zeta = 0.97$	
	d'	d''	d'	d''	d'	d''
km	km	km	km	km	km	km
22	—	—	1.95	0.88	3.88	0.66
21	—	—	2.80	0.84	4.29	0.63
20	—	—	3.54	0.80	4.63	0.60
19	2.12	0.95	4.19	0.76	4.94	0.57
18	3.08	0.90	4.55	0.72	5.24	0.54
17	3.82	0.85	4.95	0.68	5.49	0.51
16	4.42	0.80	5.27	0.64	5.68	0.48
15	4.89	0.75	5.54	0.60	5.88	0.45

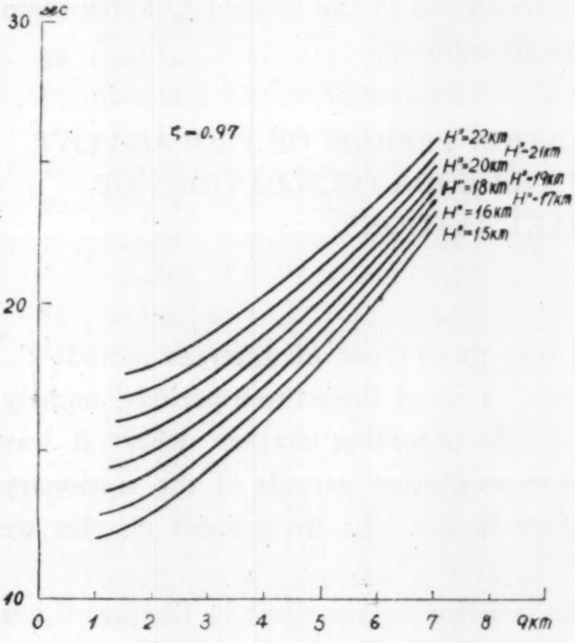

(C)
Fig. 7.

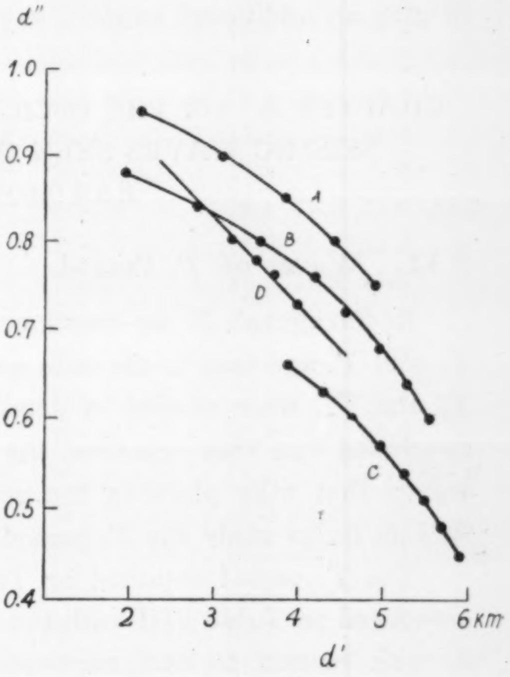

Fig. 8. Relation between d' and d'', when the free oscillation period T of surface layers (in case of three layers) is 20 seconds. The parameter of the curves A, B and C is ζ, curve D represent the relation between d' and d'' when the free oscillation of 16 seconds period takes place in the two surface layers.

from the seismometerical point of view.

In the preceding chapters we have pointed out that waves with the period of 20 sec. are seen in the first coda and those with the period of 16 sec. in the second coda, but closer examination shows, with respect to some earthquakes, that waves of 16 sec. are also seen existing in the first coda oscillations, and that this occurs only when the T_1 period of such coda oscillations is about 14~15 sec., namely very near to the period of 16 sec. On the other hand, when the coda periods are about 18~19 sec., free oscillation of the period of 20 sec. are seen to exist. Generally speaking it appears that, in accordance with the period of the external forces, that type of free oscillation whose period is nearer the period of the said forces is generated.

Now we come to the conclusion that the stationary oscillations in the surface layers whose thicknesses are 3.9 km and 21 km have periods of 16 and 20 sec. respectively. In the preceding chapter we assumed that the two sorts of periods, $T_2=20$ sec. and $T_3=16$ sec., that appear in the coda oscillations of earthquake motions may represent the free oscillation periods of the surface layers, as they display such constant values regardless of the differences in their epicentral distances.

The results of the calculations carried out in the present Chapter seem to give an additional support to this assumption.

CHAPTER 8. ON THE OSCILLATION PERIODS OF PROPAGATIVE SEISMIC WAVES SEEN IN THE CODA OSCILLATIONS OF EARTHQUAKE MOTIONS.

§ 32. Waves of T_1 Period.

In Paragraph 27 we mentioned that three types of different periods T_1, T_2 and T_3 are seen in the coda waves. Two of these three periods, namely T_2 and T_3, were studied in detail in the preceding chapter, where it was concluded that they represent the free oscillation periods of the stationary waves that take place in the surface layers. In the present chapter we will go on to study the T_1 period.

The T_1 period obtained by Takahasi-Husimi's method in Chapter 6 are compared in Table VIII with the mean periods T_m obtained in Chapters 1~4, with respect to each corresponding portion. The predominant periods T_A obtained by the method of periodgram analysis are also tabulated in the third column of the same Table.

It will be noticed in the Table that T_1 and T_m of distant earthquakes whose epicentral distances are greater than 10,000 km, have different values from time to time, a fact ascribable to the effect of the waves of T_2 period that coexisted with those of T_1 period. On the contrary, T_m of near earthquakes that has relatively small values is not much affected by T_2, so that

T_1 and T_m of the corresponding portions of near earthquakes are seen to agree quite well. This tendency will be noticed still more clearly in Table IX, in which the predominant period T_M of the respective earthquakes—which is the mean of T_m with regard to each earthquake—and the mean of T_1 of the corresponding earthquakes are compared. In particular the mean value of T_1 period and the mean value of T_m are seen to have the same values in earthquakes whose epicentral distances are smaller than 10,000 km. T_A also agrees very well with T_1 and T_M.

Table VIII.

T_1; Period determined by means of Takahasi-Husimi's method.
T_m; Means of the periods of respective one minute of the coda oscillations.
T_A; Period determined by periodgram analysis.

Earthq. No.	Portion	T_1	T_m			T_A	Earthq. No.	Portion	T_1	T_m			T_A
	min min	sec	sec	sec	sec	sec		min min	sec	sec	sec	sec	sec
16	10~12	7.0	6.3	6.2	6.4	6.5	49	90~92	17.3	17.0	17.6	16.3	
〃	12~14	7.3	6.4	6.3	6.6		〃	92~94	17.5	16.3	19.3	15.2	
〃	16~17	7.1	6.8	6.6			〃	101~103	17.0	19.0	16.1	18.3	
19	14~15	6.4	6.5	7.6			51	56~58	17.6	18.8	18.0	17.4	
20	15~17	6.8	7.0	6.9	8.0		〃	58~60	17.8	17.4	17.4	17.8	
〃	11~13	6.9	7.4	6.6	7.2	7.0	〃	71~73	17.3	16.1	17.3	15.6	18.0
〃	14~16	5.9	6.3	6.9	7.1		〃	77~79	17.5	17.5	16.5	16.5	
34	40~42	13.1	12.7	14.5	14.5		〃	79~81	17.4	16.5	16.2	16.9	
36	43~44	15.9	17.7	15.7			〃	59~61	17.8	18.5	19.2	17.2	
〃	50~51	15.1	16.8	14.5			〃	70~72	17.8	18.8	16.9	17.9	
〃	51~52	15.2	14.5	13.6		14.0	〃	72~74	17.6	17.9	17·9	18.0	
〃	60~62	15.6	17.5	15.8	17.5		〃	82~84	17.4	15.8	17.5	16.4	
〃	71~73	15.3	18.9	13.5	17.0		52	66~68	18.3	17.9	18.4	19.8	18.0
37	71~72	14.9	14.5	13.8			〃	68~70	18.3	19.8	17.5	17.3	
〃	82~84	14.9	15.4	12.4	16.9	14.0	〃	81~82	18.7	16.6	16.0	17.3	19.0
〃	93~95	15.9	14.6	17.4	19.6		〃	83~85	18.0	17.3	19.1	26.2	
〃	100~102	15.6	19.8	15.4	16.1		〃	105~107	18.2	15.8	18.1	15.8	
〃	102~104	15.5	16.1	16.2	15.8	17.0	〃	62~63	18.3	18.2	21.9		
49	69~70	17.1	17.1	16.7			〃	63~64	18.2	21.9	19.9		
〃	71~72	17.9	17.3	17.1			〃	66~67	18.3	16.9	18.3		
〃	82~84	17.9	16.7	15.8	16.3	16.0	〃	83~84	18.0	16.1	18.0		
〃	84~85	16.6	16.3	17.8									

In Chapters 1~4, where we calculated the predominant period from the mean periods of the successive one-minute means, there had been left some doubts as to whether this predominant period calculated in such a way represented a period really existing in the coda oscillations. Now, from Table IX we are convinced that the predominant period T_M determined from the mean period represents a period really existing in the coda oscillations of the respective earthquakes. As we have already noted, in this study of coda oscillations, these analyses by Takahasi-Husimi's method and periodgram analysis were carried out with only eight earthquakes

Table IX.

Comparison of T_1, T_M and T_A.

T_1; Predominant period by means of Takahasi-Husimi's method.
T_M; Predominant period determined from the curve of period of successive one minute means of the coda oscillations.
T_A; Predominant period determined by periodgram analysis.

Earthq. No.	T_1	T_M	T_A
	sec.	sec.	sec.
16	7.1	6.5	6.5
19	6.4	6.8	—
20	6.5	7.2	7
51	10.7	—	10
34	13.1	13.4	—
36	15.4	15.9	14
37	15.4	15.3	15
49	17.3	17.5	16
51	17.6	18.1	18
52	18.3	17.7	18

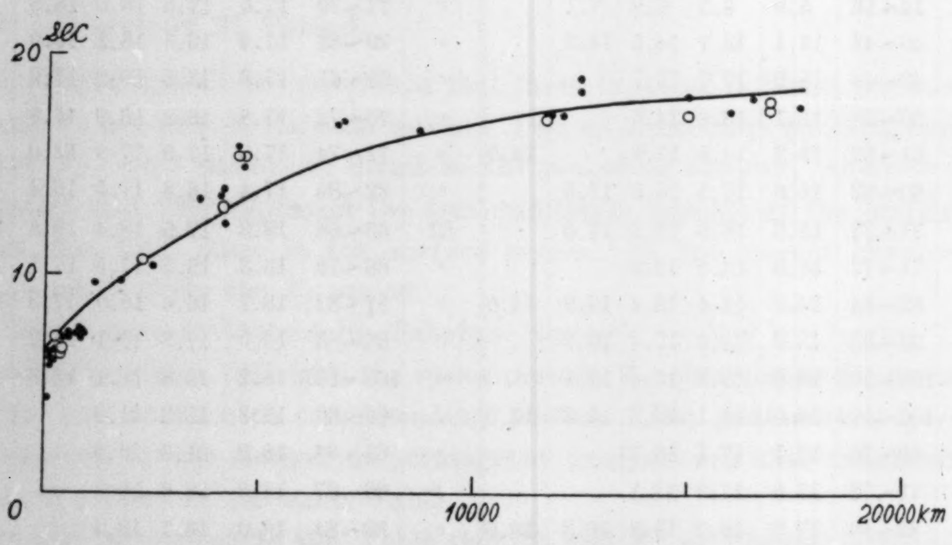

Fig. 9. Relation between T_1 period and epicentral distances.

selected out of 54 which were studied by the mean period method in Chapters 1~4. The results here obtained, however, lead us to the conjecture that the predominant coda periods of the remaining 46 earthquakes to which neither Takahasi-Husimi's method of analysis nor periodgram analysis has been applied will represent periods really existing in their coda oscillations, and further that these predominant periods are ones that belong to the T_1 group.

If it be allowed to make such a conjucture, we have now come to know the T_1 period of the coda oscillations of 54 earthquakes whose epicentral distances range from 30 km to almost 18,000 km. The relation between the period T_1 and the epicentral distance Δ of the respective earthquakes will be found from Table IV in Chapter 1, Table IV in Chapter 3, Table VI in Chapter 4 and Table VII in Chapter 6, the result being given in Fig. 9, in which it will be clearly observed that as the epicentral distance increases T_1 also increases.

§ 33. The Relation Between T_1 Period and the Epicentral Distance.

On the basis of seismometerical observations it has been pointed out by many investigators that the period of seismic waves grows larger as they are propagated to long distances. An exhaustive study of this problem, however, is only possible after observations of earthquake motions have been carried out on a worldwide scale. Owing to this difficulty, coupled by numerous others, no sufficient data on this problem have yet been collected until now. In that sense, the curve in Fig. 9 will be one of the important data concerning the propagation of seismic waves. Now, using these data and consulting the method introduced by B. Gutenberg, the present writer wants to evolve a way of interpretation cencerning the phenomenon of the period of waves increasing with the epicentral distance.

Assuming that, by the effect of the friction within the earth's crust, the period of seismic waves becomes longer and longer with the increase of epicentral distance, B. Gutenberg[14], using the equation obtained by K. Sezawa[15], put

$$\frac{\partial^2 \theta}{\partial t^2} = \frac{\lambda + 2\mu}{\rho} \Gamma^2 \theta + \frac{\lambda' + 2\mu'}{\rho} \frac{\partial \Gamma^2 \theta}{\partial t} \quad \text{.............} (33 \cdot 1)$$

$$\frac{\partial^2 \omega}{\partial t^2} = \frac{\mu}{\rho} \Gamma^2 \omega + \frac{\mu'}{\rho} \frac{\partial \Gamma^2 \omega}{\partial t} \quad \text{......................} (33 \cdot 2)$$

---

[14] B. GUTENBERG, Hand. d. Geophys., IV (1932), 16.

[15] K. SEZAWA, *Bull. Earthq. Res. Inst.*, **2** (1927), 13.

where Θ and ω give the dilatation and rotation of the body, λ and μ are Lamé's constants, and λ' and μ' the voluminal and equivoluminal viscosities. Then, for instance, the displacement near the origin will be given by $t = 0$, $u = \frac{B}{b}e^{-x^2/b^2}$; and the value of u at any time and place, by

$$u = \frac{B}{2\sqrt{4Wt+b^2}}\left[e^{-\frac{x+Vt}{4Wt+b^2}} + e^{-\frac{x-Vt}{4Wt+b^2}}\right] \ldots\ldots\ldots\ldots (33\cdot3)$$

This shows that the wave form becomes longer and longer with the increase of the epicentral distance. In this, V is the velocity of the wave, W is a term representing the effect of viscosity and is given by $W = (\lambda'+2\mu')/2\rho$. Now, with regard to the waves determined by equation (33·3), we will define the wave-length (which we will denote by L) as twice the length of the distance between the two points, a point where u is equal to half the amplitude of a maximum, and another where u is equal to half the amplitude of the next minimum.

Now, L will be given by,

$$L = (2{\cdot}86\, b^2 + 11.2\ Wt)^{1/2} = (L_0 + 11.2\ Wt)^{1/2} \ \ldots\ldots (33\cdot4)$$

Taking the period of the wave as T, the epicentral distance as Δ, we get, since $L = VT$ and $t = \Delta/V$, an equation that combines T with Δ,

$$T = \left(T_0^2 + \alpha\frac{\Delta}{V^3}\right)^{1/2} \ldots\ldots\ldots\ldots\ldots\ldots\ldots\ldots (33\cdot5)$$

This shows that the period increases hyperbolically with the epicentral distance. Since this relation seems to be perceptible in Fig. 9, we calculated the values of T_0 and α by means of the least square method, using the observed values of T_1 and Δ. In carrying out this calculation two times of weight has been put upon T_1 period obtained by Takahasi-Husimi's method, as T_1 was considered more trustworthy than the T_M period obtained

Table X.

Values of T_0, α and η.

T_0	V	α	η (C.G.S.)
sec.	km/sec.	cm^2/sec.	
7.6	3.2	0.6×10^{10}	0.3×10^{10}
	3.5	0.8×10^{10}	0.4×10^{10}
	4.0	1.2×10^{10}	0.5×10^{10}

Table XI.

Propagative velocity of the wave of T_1 period.

Earthq. No.	Epicentral distance	Commencement of T_1 wave	V
	km	about min	km/sec.
36	4,470	21	3.5
37	4,550	22	3.4
49	11,600	58	3.3
51	14,900	56	4.4
52	16,800	66	4.2
53	17,500	80	3.6

by the mean period method. The values of α and T_0 thus calculated are given in Table X. In computing the velocity V used in the above calculation, the commencement time of waves with the T_1 period has been considered the time of arrival of these waves. The values of V are tabulated in Table XI, and referring to this Table η was calculated in Table X for the values of V, $V = 3.2$, 3.5 and 4.0 km/sec.

§ 34. The Coefficient η of the Internal Friction of the Earth's Crust.

Now, after Gutenberg[16] λ' and μ' are connected to η as $\mu' = \eta$, $\lambda' = -\frac{2}{3}\mu'$ and in Table X are given the values of α, and from (33·4) and (33·5) it is to be derived the relation $\alpha \doteqdot 10\,W$, so that the order of magnitude of the values of η will be given[17] by

$$\eta \doteqdot \frac{1}{2}\alpha.$$

From this the values of η will be calculated, the result being as shown in the last column of Table X. The values of η here obtained by the present writer is somewhat smaller than the values obtained by B. Gutenberg.

From these considerations it may be safe to conclude that the coda waves of earthquake motions having their oscillation period equal to T_1 are waves of a propagative type, and that their nature is such that as they are propagated further and further their periods become longer and longer owing to the effect of the inner friction of the earth's crust. The coefficient of the inner friction calculated from the rate of elongation of the period will be $\eta = 0.4 \times 10^{10}$ C.G.S.

---

[16] B. GUTENBERG, Hand. d. Geophys., II (1931), 533.

[17] H. TAKEUCHI, Read at the meeting of *Earthq. Res. Inst.*, on July, 1, 1944.

Summary and Conclusion.

The analysis of the coda oscillations of earthquake motions has been carried out in Chapters 1 to 8 with respect to 54 earthquakes observed at Hongo, Tokyo, whose epicentral distances ranged from 33 km to almost 18,000 km.

Some examples of seismograms used for the analysis of the coda oscillations will be seen in Fig. 10.

In the first place, (1) frequency distribution diagrams of all the periods of coda waves found in every successive one minute were prepared. The peaks of such diagrams were not sharp enough to enable one to determine the predominant periods of coda oscillations.

In the second place (2) the mean period of every one minute has been calculated. The mean period of each successive one minute was, so far as a single earthquake was concerned, fairly uniform throughout the whole duration of the coda oscillations, and this mean period agreed well with the predominant period determined from the frequency diagrams of the same earthquake. In the case of extremely distant earthquakes the coda oscillations were found to continue even after the large surface waves propagated along the major arc of the earth's surface had died away. This part of the coda waves has been named "the second coda waves", and in contrast to it the coda waves that precede the large waves propagated along the earth's surface have been called "the first coda waves." The predominant periods of the second coda waves were seen to be constantly 16 sec. with all the earthquakes. These were described in Chapters 1~4.

Then (3) in Chapter 5, with a view to establishing more definitely the periodicity of coda oscillations, a method of periodgram analysis has been resorted to with eight selected earthquakes having different epicentral distances. The periodgrams of the second coda waves showed a single very high peak at about $T_A = 16$ sec. Those of the first coda waves showed two high peaks, one of which always appeared at a period that agreed well with the predominant period of the same earthquake determined by the method described in (1) and (2), while the other peak was seen at the period of about 20 sec.

Lastly (4) in Chapter 6, for the purpose of making clear the oscillation period of coda waves as accurately as possible, an expanded Takahasi-Husimi's method of analysis has been applied for the study of the period of coda oscillations of ten selected earthquakes. We obtained an oscillation curve for each portion of the respective earthquakes—a composite curve made up of two sine curves of a damping nature. After elaborate calculations we decomposed each sine curve and thus were able to find out separately the period of each of these two constituent curves.

From the studies described in (3) and (4), it has become clear that three types of waves of different periods T_1, T_2 and T_3 are existent in the first coda waves of earthquake motions. T_1 agreed well with the predominant period decided by (1) and (2), while T_2 and T_3 were constant, being 20 sec. and 16 sec. respectively. Moreover, it was remarkable to notice that T_1, when it was larger than 19 sec., was accompanied by T_2, and when much smaller than 19 sec., by T_3. In the second coda waves, however, we found only one period, i.e. T_3 ($T_3=16$ sec.), and this agreed well with the result obtained in (1) and (2).

These studies made it clear that three types of waves of different periods exist in the coda oscillations of earthquake motions. T_1 increases with the epicentral distance, while T_2 and T_3 have constant values with all the earthquakes irrespective of their difference in the epicentral distances. In Chapter 8 it was concluded that T_1 represents a period of waves propagated from the origin, and that the length of the period of those waves increases with the epicentral distances Δ, the relation between T_1 and Δ being given by $T_1 = \left(T_0^2 + \alpha \frac{\Delta}{V^3}\right)^{1/2}$, where α is a constant connected with the coefficient η of the internal friction of the earth's crust. From the observed values of T_1 and Δ we get $\eta = 0.4 \times 10^{10}$ C.G.S.

Unlike T_1, the periods of T_2 and T_3 were considered to represent the periods proper to the vibrating systems upon which the observations of earthquake motions have been made. As for the vibrating systems it will be most reasonable to think of the earth's surface layers, and it was assumed that these periods T_2 and T_3 might represent the free oscillation periods of the standing shear waves that take place in the surface layers. For the purpose of corroborating this assumption, in Chapter 7, the periods of the standing waves that take place in surface layers have been calculated by Rayleigh-Ritz's method. On the basis of the most reasonable numerical constants for the physical properties of the surface layers, it was calculated that, in order that the period of the standing shear waves taking place in the first and second layers might be equal to 16.0 sec. and that in all the three layers equal to 20 sec., the thicknesses of the three layers must of necessity be 0.83 km, 3.95 km and 17.1 km respectively. These figures agree very well with the result obtained from seismological investigations. From these facts it may be reasonably concluded that two predominant periods

T_2 and T_3 that appear in the coda oscillations of earthquake motions represent the free oscillation periods of the earth's surface layers.

Acknowledgment.

In concluding this article the present writer wishes to express his cordial thanks to Prof. H. Tsuya, the director of our Institute, for his constant encouragement. His hearty thanks are also due to Prof. T. Hagiwara for his kind guidance and apt suggestions throughout the course of this study, to Prof. C. Tsuboi for his valuable advices and encouragement, and to Prof. H. Kawasumi for his enlightening criticisms. He also heartily appreciates the collaboration of Miss K. Kobayashi, Miss M. Makino and Miss C. Kawakami, members of the Komoro Branch of the Institute, who assisted untiringly him in preparing this paper. A part of the expense of this study was defrayed out of the Scientific Research Fund from the Department of Education.

---

10. 地震動の尾部について（其の6）

地震研究所　表俊一郎

第7章　第1～6章の解析により地震動の尾部の震動の中には震央距離に拘はらず16秒及び20秒の一定の週期をもつ振動があらはれることが認められた．東京附近の地殼上層の地層の配列及それらの層の物理的性質は松澤教授其の他多くの研究者の研究の結果可なり明瞭に知られてゐるので，それらの層の中に各層の下端を節として地表面を腹とするような定常振動が生じたと考へた場合そのような定常振動の振動週期を計算してみた．この場合振動の mode は必ずしも明らかではないが振動週期だけを問題とする限りでは Rayleigh-Ritz の方法により週期の算出を行うかぎりでは，假定した mode が多少誤つていても週期の値にはあまり差異を示さないといふ利點があるのでこの方法を用ひて週期を計算した．地層配列のモデルとしては松澤教授の見出された深さ4kmの層の上に木下學士が求めた400mの薄い層があるとして，之等の中に16秒の定常振動が生じると假定し，次に之等の層の下にあつさ16kmの松澤教授の層があるとしてそれら三層の中に20秒の週期をもつ定常振動が生じると假定した．

第8章　第1～6章の週期解析の結果地震動の尾部の振動週期の中には震央距離と共に次第に長くなるものがあることが見出された．Gutenberg の考へ方に從つて震源から出發した地震波は地殼の粘性の影響により週期がのびると考へれば震央距離 Δ の所で観測される週期 T は略々

$$T = \left\{T_0^2 + \alpha\frac{\Delta}{V^3}\right\}^{1/2}$$

の關係をみたしてゐる．玆に T_0 は震源での波の週期，V は地震波の傳播速度，α は $W=(\lambda'+2\mu')/2\rho$

[S. OMOTE.]

Fig. 1.

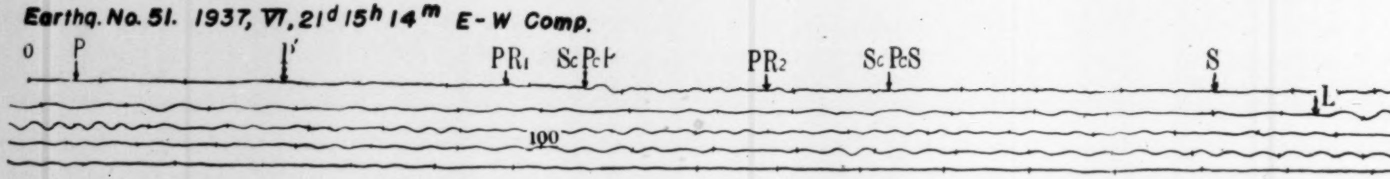

Fig. 2.

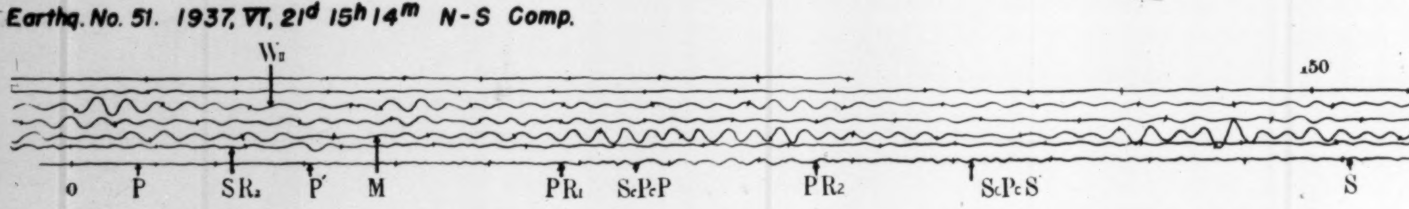

Fig. 3.

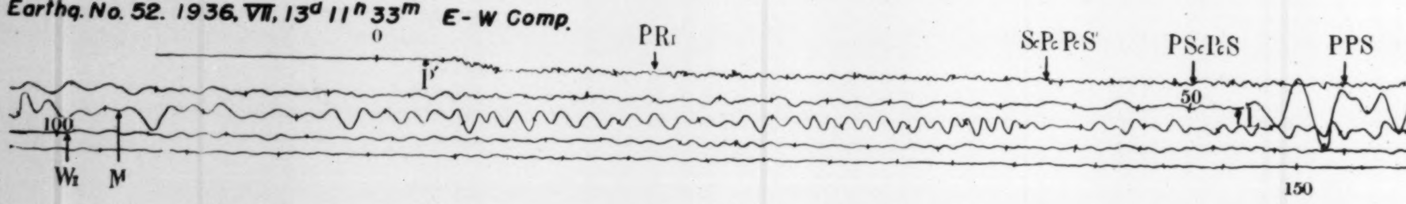

Fig. 4.

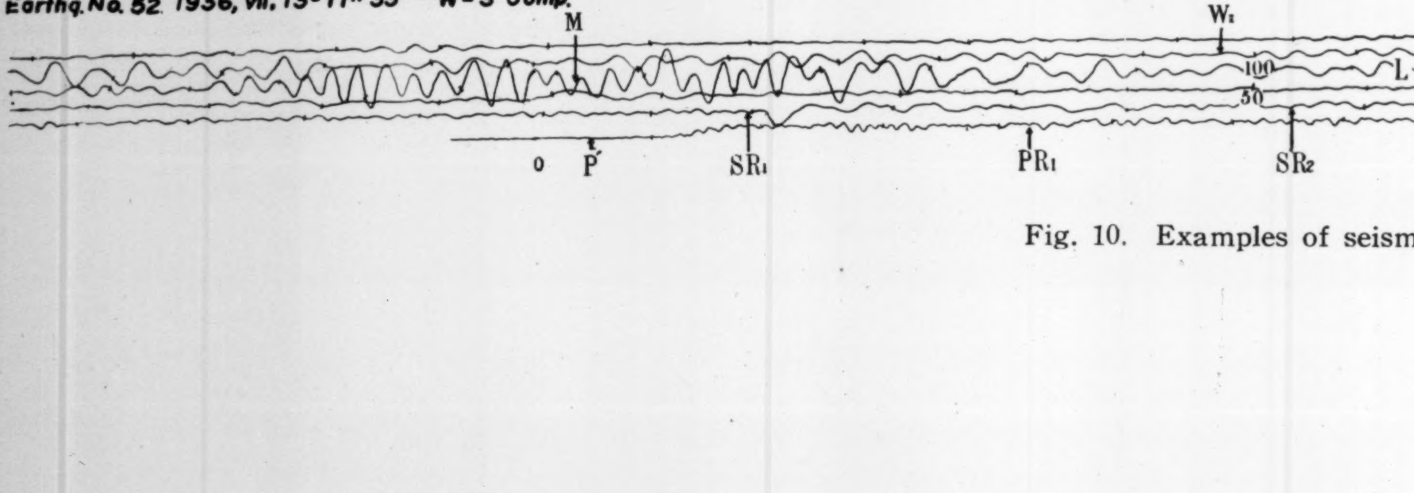

Fig. 10. Examples of seism

（震研彙報　第二十九號　圖版　表）

[Bull. Earthq. Res. Inst., Vol. XXIX, Pl. VII.]

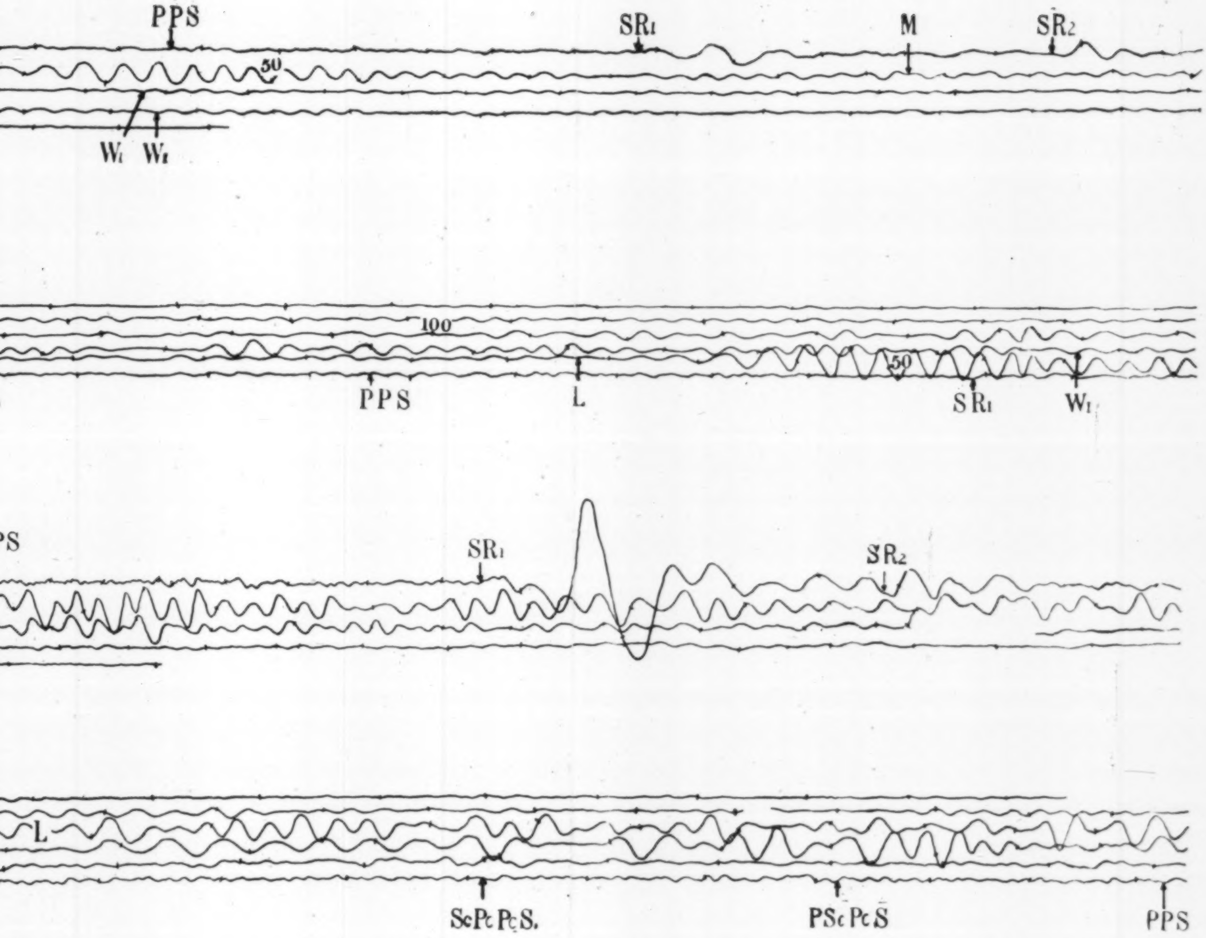

eismograms.

(λ', μ' は粘性, ρ 密度) であらはされる粘性の項 W と $\alpha \fallingdotseq 10W$ の關係をもつ値である. これより T_0 及 α を求めれば $T_0 = 7.6$ sec., $\alpha \fallingdotseq 1 \times 10^{10}$ cm^2/sec. となる. 之より地殼の內部摩擦係數を求めれば $\eta \fallingdotseq 0.4 \times 10^{10}$ C.G.S. となる.

結語　以上第 1 章より第 8 章にわたつて震央距離 33 km の近地地震から殆ど 18000 km に及ぶ遠地地震に至るまで 54 個の地震について東京本鄉に於て觀測された記錄にもとづいて尾部の振動週期の解析を行つた.

(1) 尾部の振動について 1 分每に週期頻度圖をつくつて卓越週期を求めようとしたがその peak はあまり明瞭ではなかつた (第 1〜4 章).

(2) 次に各分每の平均週期を求めた. 1 つの地震については各分每の平均週期はほぼ一定の値を示し, 各地震每に尾部の卓越週期を求めることが出來た. 震央距離の極めて大きい地震については地球の劣弧のみならず優弧に沿ふ表面波が到着した後までも尾部の振動がつづくことが認められこの部分を "第2尾部" となづけた. 之 對してそれより前の部分を "第1尾部" となづけた. 第2尾部の振動週期はいづれの地震についても 16 秒であることが見出された. (第1〜4章)

(3) 第 5 章に於ては periodgram analysis を行つた. その結果第 2 尾部では常に 16 秒の週期が見られたのに對し第 1 尾部では 2 つの peak が見られるものが多く, この 2 つの peak の中 1 つは夫々の地震について平均週期で見出された週期とほぼ一致する値を示し他は 16 秒又は 20 秒の週期を示すものであつた.

(4) 第 6 章に於ては高橋-伏見の方法により地震動の尾部の各部分の振動週期の解析を行ひ振動曲線をもとめた. 之等の振動曲線のあるものは單純な正弦曲線であつたが他のものは 2 つの正弦曲線が重ね合せられてゐるものであつた.

以上第 1〜6 章の解析の結果は互によく一致した値を與へ地震動の尾部には 3 種類の振動週期をもつ波があることが明らかとなり其等の週期を T_1, T_2, T_3 と區別した. T_1 は震央距離と共に次第に長くなる週期であり, 之に反して T_3 及び T_2 はいづれの地震についても一定の値をもち $T_2 = 20$ 秒, $T_3 = 16$ 秒となつた.

第 8 章に於て T_1 は震源から傳播してきた波の週期をあらはすものであることが結論せられ震央距離に對して週期の增加する割合から地殼の內部摩擦係數を計算した結果その値は $\eta = 0.4 \times 10^{10}$ C.G.S. と求められた.

第 7 章に於ては T_2 及び T_3 が一定の値をもつといふ點より考へ之が地殼表層の中に生ずる自由振動週期を現はすと假定して, そのような定常振動に對し適當なモードを假定し Rayleigh-Ritz の方法より週期を計算し, その第 1, 2 の層の中の定常振動に對しては丁度 16 秒, 第 1, 2, 3 層の中の定常振動に對しては丁度 20 秒となるためには第 1 層の厚さ 0.83 km. 第 2 層の厚さ 3.95 km 及び第 3 層の厚さ 17.1 km と求めることが出來た. これらの値は松澤教授及び木下學士等によつて既に求められてゐる値と極めてよく一致し驗震學的に求められてゐる地層配列と矛盾しない値が得られたこととなる.

11. *On the Vertical Displacements Accompanying Imaichi Earthquake in 1949.*

By Eiji INOUE,*

Geographical Survey Institute.

(Read Nov. 21, 1950.—Received Dec. 20, 1950.)

1. Introduction.

For the purpose of detecting the vertical displacements of the earth's crust accompanying the Imaichi Earthquake on Dec. 26 1949, the preliminary precise levelling was carried out by Geographical Survey Institute in June 1950. In this paper, the results of the survey are reported.

2. Routes of the Precise Levelling.

The main route of levelling is from Utsunomiya to Nikko via Imaichi and the branch route is from Imaichi to Fujiwara. The main and branch routes on which the precise levellings were carried out are shown in Fig. 1.

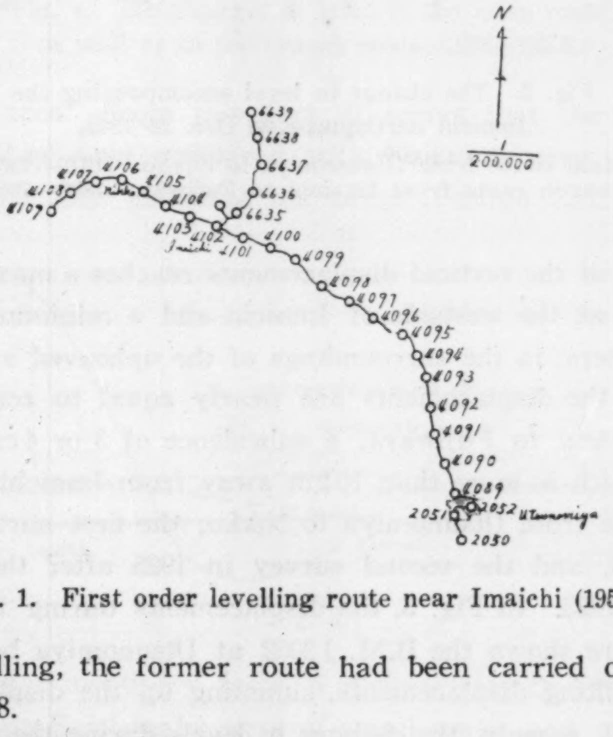
N
1/200.000
6639
6638
6637
6636
6635
4107
4106
4108
4105
Nikko
4107
4104
4103
4102
Imaichi
4101
4100
4099
4098
4097
4096
4095
4094
4093
4092
4091
4090
4089
2051
2052
Utsunomiya
2050

Fig. 1. First order levelling route near Imaichi (1950).

In the past levelling, the former route had been carried out in 1925 and the latter in 1898.

---

* Communicated by T. Hagiwara.

3. Results.

The vertical displacement of the respective bench mark is shown in Fig. 2. The curves represent the changes in levels during the period 1925-1950 and 1898-1950, the B.M. B-4 at Utsunomiya being assumed as fixed.

In Fig. 2, the area of the remarkable displacements is situated in the range within 10 km radius from Imaichi. In the outside of the area, the displacements are less than 1 cm.

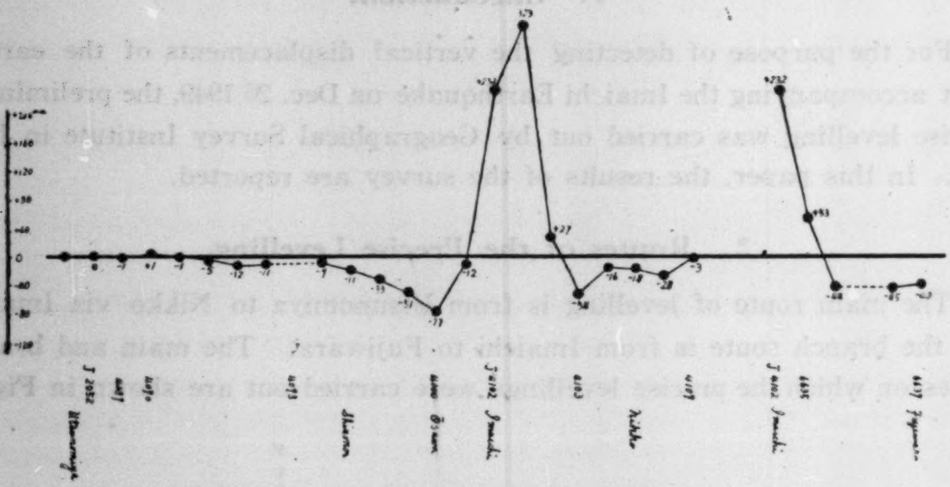

Fig. 2. The change in level accompanying the Imaichi earthquake on Dec. 26 1949.
{Main route from Utsunomiya to Nikko (1925–1950)}
{Branch route from Imaichi to Fujiwara (1898–1950)}

The amount of the vertical displacements reaches a maximum (upheaval of about 34 cm) at the westside of Imaichi and a minimum (subsidence of several centimeters) in the surroundings of the upheaved area, and outside of these areas, the displacements are nearly equal to zero. But, on the route from Imaichi to Fujiwara, a subsidence of 3 or 4 cm still remained at Fujiwara which is more than 10 km away from Imaichi.

On the route from Utsunomiya to Nikko, the first survey was carried out in 1897-1898, and the second survey in 1925 after the Great Kwanto Earthquake in 1923. In Fig. 3, the displacements during the time interval 1898 and 1925 are shown the B.M. J 2052 at Utsunomiya being assumed as fixed. The resulting displacements, summing up the displacements shown in Figs. 2 and 3, namely, the changes in levels during the period 1898-1950, are shown in Fig. 4, in which the amount of subsidence at Fujiwara is

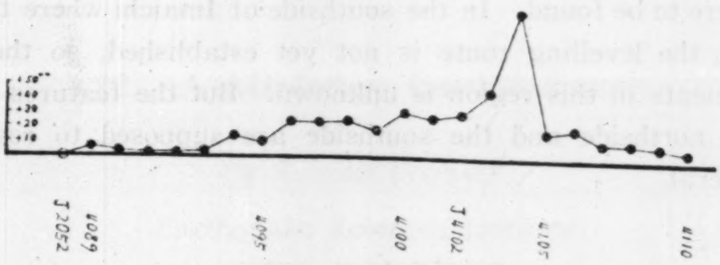

Fig. 3. The change in level in the main route (1898—1925).

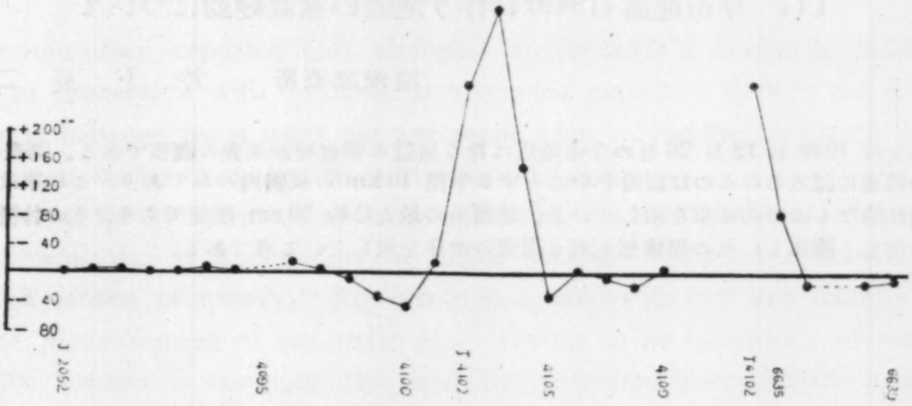

Fig. 4. The changes in level in the main route as well as in the branch route (1898—1950).

nearly equal to zero. From this fact, it seems that the area of Imaichi was upheaved 3 or 4 cm compared with Fujiwara area during the time interval 1898 and 1925 including the Great Kwanto Earthquake in 1923. (see Fig. 5)

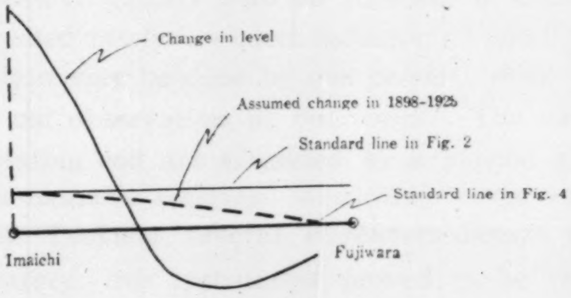
Change in level
Assumed change in 1898-1925
Standard line in Fig. 2
Standard line in Fig. 4
Imaichi
Fujiwara

Fig. 5.

From the above mentioned facts, it is considered that the displacements accompanying this Earthquake were of small scale, and only upheaval in the epicentral area near Imaichi and the subsidence in its northside surroundings were to be found. In the southside of Imaichi where the epicenter was situated, the levelling route is not yet established, so the feature of the displacements in this region is unknown. But the features of displacements in the northside and the southside are supposed to resemble each other in general.

---

11. 今市地震 (1949) に伴う地殼の垂直變動について

地理調査所　　井　上　英　二

本文は 1949 年 12 月 26 日の今市地震に伴う地殼の垂直變動調査の概報である。調査の結果，變動の顯著に認められるのは震源を中心とする半徑 10 km の範圍内のみであり，この事はこの地震が局部的なものである事を示している。變動量の最大は約 30 cm 程度であり，その特徵は震源附近が著しく隆起し，その周緣部が或る程度の沈降を示している事である。

12. *A Miniature Earth-inductor.*

By Tsuneji Rikitake,

Earthquake Research Institute.

(Read July 18, 1950.—Received Dec. 20, 1950.)

1. Introduction.

It was often reported that changes in the earth's magnetic field took place in connection with volcanic and seismic activities though the decisive relations between them were not yet made clear. Further research should be made in order to make the said relations clear.

Among the components of magnetic field, the measurement of changes in magnetic dip is the easiest to make because accurate observation of azimuth is not necessary. Dip circle and earth-inductor are usually used for the measurement of magnetic dip. Owing to its simplicity of mechanism, the former is conveniently used for field-measurement, the accuracy of measurement being about 3 *minutes* of arc in its best condition. The time needed for observation at a station amounts to 15~20 *minutes*. On the other hand, the inductor of the Nippon-Suirobu (Japaneses Hydrographic Department) Magnetometer, which is the most frequently used in Japan, has an accuracy of about 0.1 *minutes* of arc. However the transportation of the latter is not easy and it requires as much as three persons to carry out observation by it.

In order to observe quickly with an accuracy of about 1 *minute* of arc, the writer constructed newly an earth-inductor of small type. Transportation and observation may be done by one person, while it requires only 5 *minutes* to carry out observation at one point. The electromotive forces induced in the rotating coil are amplified by a special amplifier and then detected by a non-magnetic receiver. According to the result of observation carried out at Mt. Tsukuba, several *kilometers* distant from the Kakioka Magnetic Observatory, this instrument proved to be capable of use for field-observation.

2. Design and construction.

The method for measuring dip-angle is the same as that of the usual earth-inductor in principle. As schematically shown in Fig. 1, the gun-metal axis of the rotating coil is supported by the bearings imbedded in an ebonite ring which is able to rotate around a horizontal axis. The ends of the axis of the rotating coil are made so sharp that the coil will rotate by inertia for a time when the observer once makes the coil rotate with his fingers. The coil which is wound on an ebonite bobbin consists of two parts as shown in the figure, the inner and outer diameter amounting to 1.0 *cm* and 3.8 *cm* respectively, while the length of both parts is 2.0 *cm*. Enamelled copper wire of 0.07 *mm* in diameter is wound 60,000 *turns*, the ends of the wire being attatched to the axis so as to be able to pick up the electromotive forces induced in the coil through the bearings. If necessary, a high permeable rod is plunged in the aperture drilled through the centre of the bobbin to increase the sensibility. Since the coil rotates for a few *minutes* with an angular velocity of about 10 *c.p.s.* or more, the determination of dip-angle, where no electromotive force is induced, is placidly made with the microscrew attatched to the shaft of the ebonite ring. At one end of the said shaft, a vertical circle graduated at every half a *degree* is mounted. With the aid of the verniers, the angle is read up to one *minute* of arc.

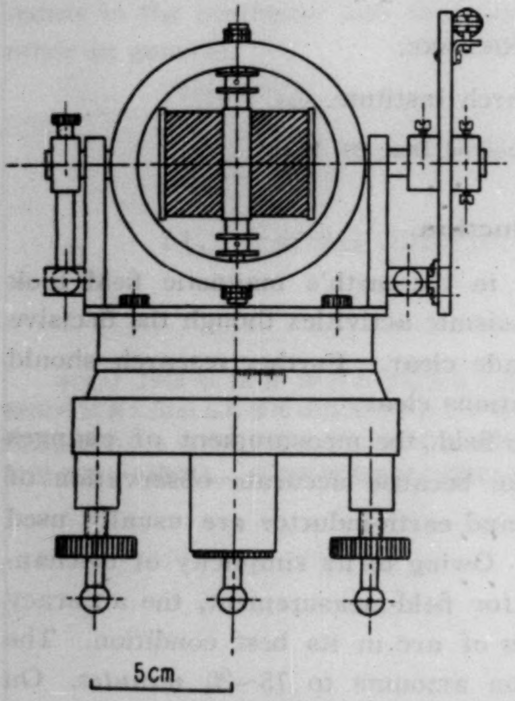

Fig. 1. Schematic view of the new earth-inductor.

The electromotive forces picked up through the bearings is introduced into a direct-current amplifier of a special kind. The voltage is converted into an alternating one of 1,000 *c.p.s.* having a rectangular wave-form by intermittent contact of the osmium point of the so-called "CI vibrator" which is excited with a circuit containing a small carbon-microphone, an electromagnet, and a 4.5 *volts* battery. The electric current needed for excitation of the vibration of the vibrator amounts to only 60 *m*A. Thus, the 1,000 *c.p.s.* alternating current voltage of which the amplitude is the same with that of the applied direct or low frequency current is implied in an ordinary audio-amplifier in which two miniature-tubes 1*T*4 are used. As 1*T*4's filament current amounts to only 50 *mA* at 1.5 *volts* it is adequate for field-measurement. The electric supply for plate and screen-grid of 1*T*4 is given from a small layer-built battery to lessen the weight. According to the result of the experiment, the gain of the amplifier is about 40 *db* when we use 67.5 *volts* battery. The out-put of the amplifier is connected with a high-impedance crystal receiver made of rochelle salt which does not disturb the magnetic field as in the case of a magnetic receiver when the observer comes very near the rotating coil. The observer hears a sound of 1,000 *c.p.s.* modulated with the frequency of the rotation of the coil, the modulation-factor being almost 100 ***per cent.*** When the axis of the coil agrees with the direction of the magnetic field, he hears no signal except a slight noise which is probably originated at the contact point of the vibrator. *A*s man's sense of hearing is most sensitive in the neighbourhood of 1,000 *c.p.s.*, the above-mentioned method of amplification is very advantageous. The circuit-diagram of the amplifier is shown in Fig. 2.

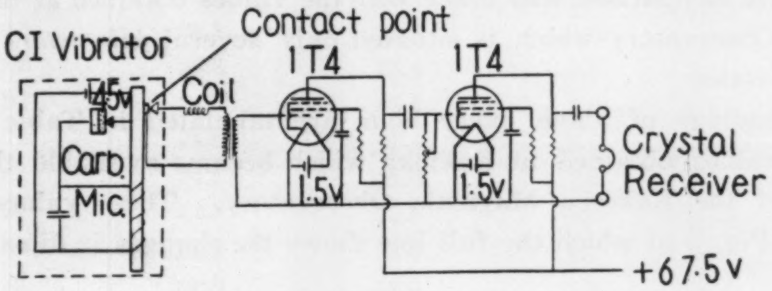

Fig. 2. Circuit diagram of the amplifier.

3. Method of observation.

In the first place, the axis of the rotating coil is roughly brought into magnetic meridian with the aid of a magnetic needle. After making the coil rotate, the observer who is hearing the signal slowly rotates the shaft of the ebonite ring so as to reduce the signal to the minimum. Then the azimuth is adjusted so as to make the signal smaller. Simultaneously, the observer further searches for the direction at which the signal vanishes by means of the microscrew attatched to the shaft. The dip-angle thus determined is read off with the aid of two verniers. Then the direction of rotation of the coil is reversed. After a process similar to that described above, we get further two readings of the dip-angle.

In the next place, the whole system is reversed in the horizontal plane, where the above-mentioned treatment is also made. In the total eight readings of the dip-angle are obtained, the averaged value being adopted as that of a station. With these treatments, we can eliminate the eccentricity of the vertical circle, the error in level and the error in the direction of the axis of the rotating coil. The whole process may be easily finished within a time of 5 *minutes*. It is of importance to economize time in the field-observations over a considerable area, hence the present instrument is more convenient than the usual dip circle though the two instruments do not differ much in accuracy.

4. Observation at Mt. Tsukuba.

In order to determine the instrumental error and accuracy, a sreies of observation were made at Mt. Tsukuba on June 6 and 7, 1950. The instrument was set in the site of Branch Station of the Earthquake Research Institute. A comparison was made with the values obtained at the Kakioka Magnetic Observatory which is situated only several ***kilometers*** distant in the NE direction.

The readings of about every hour are tabulated in Table I together with the values obtained at Kakioka which became available through the courtesy of the Kakioka Magnetic Observatory. These values are also plotted in Fig. 3 in which the full line shows the changes in dip at Kakioka.

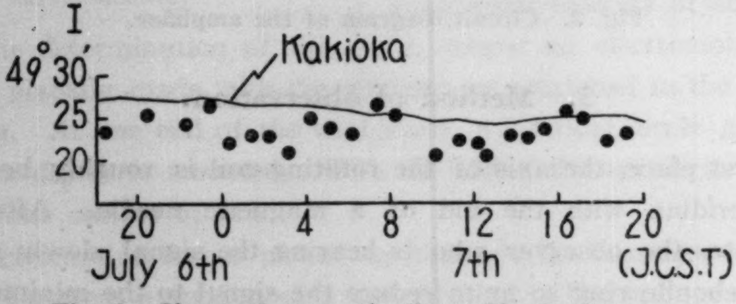

Fig. 2. Observed magnetic dip at Mt. Tsukuba and that at Kakioka Magnetic Observatory (full line).

Though the values observed by the present instrument seem somewhat scattered, the instrumental error is determined to be 2′.2 ± 0.′3. Taking into consideration, however, that the northward increase of dip-angle amounts to about 0.6 ***minutes*** of arc per ***km***, the instrumental error of the instrument is thought to be less, being probably within one ***minute*** of arc. On the other hand, the probable error of a single observation is calculated to be about ±1′.

Table I. The comparison between magnetic dip-angles observed by the present instrument at Mt. Tsukuba and that of Kakioka.

Date	Kakioka	Tsukuba	$\triangle$	$\triangle-\triangle_m$
6th				
18*h* 18*m*	49°27′.2	49°23′.4	3′.8	1′.6
20 26	27.2	25.4	1.8	-0.4
22 15	27.1	24.3	2.8	0.6
23 19	27.5	26.4	1.1	-1.1
7th				
00 14	26.8	22.1	4.7	2.5
01 20	26.5	23.0	3.5	1.3
02 15	26.5	22.8	3.7	1.5
03 10	26.5	21.0	5.5	3.3
04 10	26.4	24.9	1.5	-0.7
05 05	26.1	23.8	2.3	0.1
06 05	25.7	23.1	2.6	0.4
07 13	25.3	26.6	-1.3	-3.5
08 09	25.3	25.4	-0.1	-2.3
10 04	24.5	20.5	4.0	1.8
11 12	24.6	22.4	2.2	0.0
12 05	24.4	22.0	2.4	0.2
12 25	24.3	20.5	3.8	1.6
13 40	24.5	23.0	1.5	-0.7
14 30	24.5	22.6	1.9	-0.3
15 10	24.8	23.6	1.2	-1.0
16 15	25.0	25.6	-0.6	-2.8
17 05	25.1	24.8	0.3	-1.9
18 15	25.0	22.2	3.0	-0.8
19 10	25.0	23.0	2.0	-0.2

Mean $\triangle_m = 2.2$

5. Summary and conclusion.

The characteristics of the present earth-inductor are as follows;

a) Only one person is needed for transportation and observation.

b) The error of measurement is about ±1′, which is a little better than the usual dip circle.

c) A direct-current amplifier of a special kind and a crystal-receiver are used for detection.

After all, the instrument is thoght to be adequate for field-observation.

The writer hopes that the instrument may be used for measuring magnetic changes associated with volcanic and seismic activities. It will be also advantageous to use the instrument for magnetic prospecting.

6. Acknowledgment.

In constructing the instrument, Professor T. Hagiwara and Dr. T. Nagata offered the writer many useful suggestions. The writer wishes to express his cordial appreciations to them. The principal part of the instrument was constructed through the aid of Mr. K. Akashi of the Akashi Manufacturing Co. (Akashi Seisaku-sho), while Mr. K. Iwama of the Tokyo Tele. Com. Eng. Co. (Tokyo Tsushin-kogyo Kabushiki-kaisha) offered the "CI vibrator" which was the most important part of the amplifier. The writer's sincere thanks are also due to them.

In the course of actual observation, the writer was encouraged by Professor H. Tsuya, the director of this Institute, and Professor T. Minakami to whom the writer's hearty thanks are also due. The writer also wishes to express his sincere thanks to Mr. M. Hirayama of the Kakioka Magnetic Observatory who placed magnetic data at the writer's disposal. Mr. S. Saito and Miss Y. Hishiyama constantly assisted the writer in the course of construction and observation. The writer's cordial thanks are also due to them.

---

12. 小型磁氣感應儀

地震研究所　力武常次

野外において，地磁氣伏角を迅速に測定するために小型磁氣感應儀を製作した．輕量小型化のために，廻轉コイルに誘起する電壓を1,000サイクルの振動子の接點で機械的に斷續して交流とし，ミニアチアー管1T4を2本つかつた増幅器を通して，クリスタル受話器できくようにした．このために測定は1人の觀測者によつてなされ，1箇所5～10分で充分である．讀取は副尺によつて1′までとし，筑波山における比較觀測の結果約±1′の精度であることがわかつた．

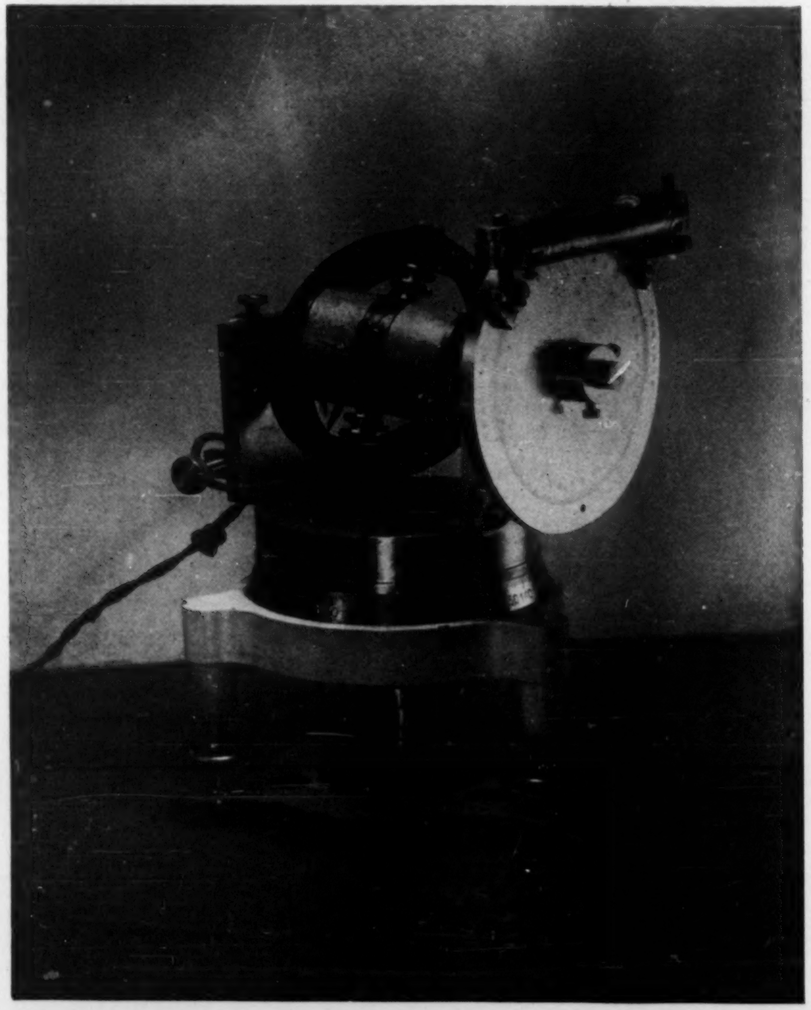

Photo. 1. The main part of the instrument.

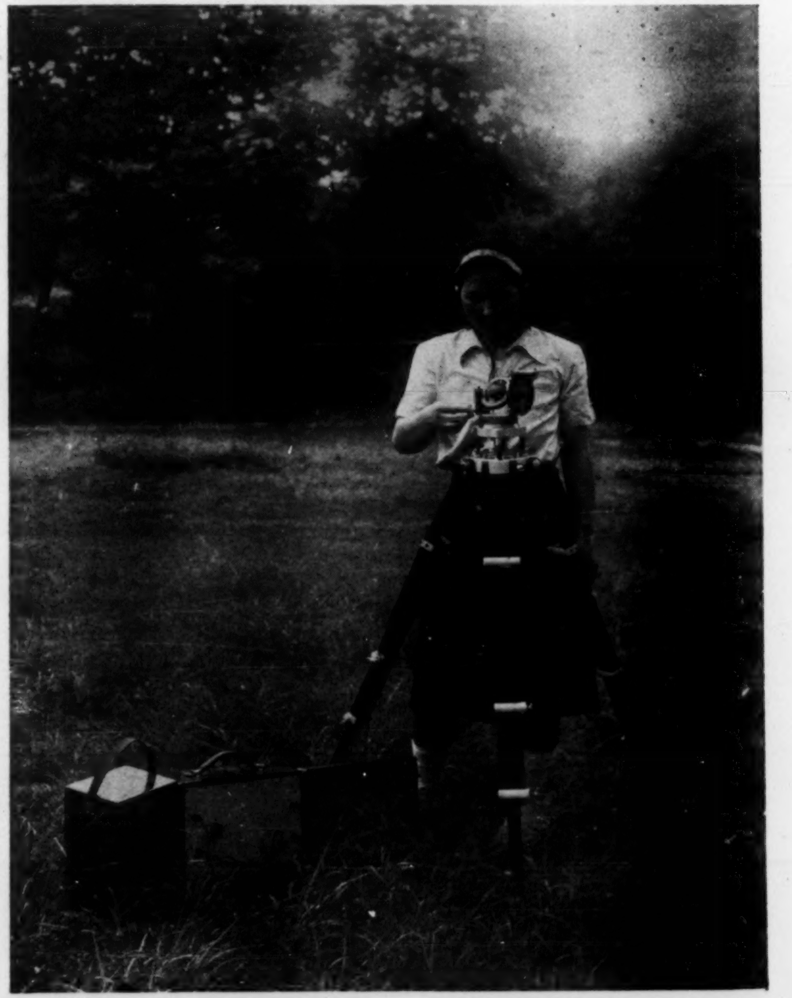

Photo. 2. The measurement with the instrument.

13. *Diffraction of Electromagnetic Waves around the Crater of Volcano Mihara.*

By Tsuneji RIKITAKE,

Earthquake Research Institute.

(Read Nov. 21, 1950.—Received Dec. 20, 1950.)

1. Introduction.

Geophysical investigations of various sorts were carried out in connexion with the recent eruption of Volcano Mihara, Ooshima (Oo-sima) Island. One of the investigations carried out was the magnetic dip survey executed by the writer throughout the island in July and September, 1950. At the second survey, the writer's party prepared a portable radio-receiver in order to catch the weather forecasting. As a loop antenna was used for the receiver, the direction of the polarization of the broadcasting radio-wave could be determined readily. Some studies concerning the diffraction of the radio-wave around the crater were made with this receiver for the purpose of inferring the electric properties of the high temperature lava filling in the crater.

According to the measurement of the electrical conductivity of igneous rocks at high temperature[1], [2], it was already found out that the conductivity increases with the increase in temperature amounting to the order of $10^{-11} \sim 10^{-10}$ ***emu*** at about 1,000° *C* though it is as low as 10^{-16} ***emu*** at the ordinary temperature. At the time of the eruption of Volcano Sakura-jima of 1946, T. Nagata[3] and others actually proved that the electrical conductivity in the moving lava-flow is considerably high.

The present measurement was carried out during the days Sept. 24 and 25. Though the eruption stopped in the night of Sept. 23, the temperature of the lava was so high that the lava-flows which overflowed the central cone were still moving down the slope. Hence, the lava filling in the crater is thought to be electrically conducting and, consequently, radio waves from JOAK Broadcasting Station may be diffracted by the lava mass which has a dimension comparable with the wave length.

---

[1] T. NAGATA, *Bull. Earthq. Res. Inst.*, **15** (1937), 663.

[2] H. P. COSTER, *M. N. R. A. S. Geophys. Suppl.*, **5** (1949), 193.

[3] T. NAGATA, S. SAKUMA and N. FUKUSHIMA, *Bull. Earthq. Res. Inst.*, **24** (1946), 161.

2. Measurement.

JOAK broadcasting wave of 590 *kc* sent from Kawaguchi about 100 *km* distant in the NNE direction were received. The loop antenna fixed to the receiver was mounted on a tripod. Rotating the horizontal circle, the direction of minimum signal was determined with a crystal receiver. As the receiver was a super-heterodyne one, the out-put signal voltage was sufficiently intense for the determination. According to the experiment, the direction was determined within an error of 1 *degree*. At the same time, the directions of several marks such as triangulation point were read on the horizontal circle with the aid of a simple finder attatched to the receiver. With these directions, the position of the measuring points and the azimuth of the polarization were determined. Thus the ultimate accuracy of the determination of the polarization-azimuth may amount to 2 or 3 *degrees*.

The measurement was made at 15 points in the caldera where tree or humid soil were not found. As the dry rocks are almost non-conducting, the anomalous distribution of the polarization of the radio wave, if it exists, may be attributed to the diffraction around the lava mass. The direction of maximum signal are shown in Fig. 1 together with the topography and the position of the measuring points. The direction from which the broadcasting waves are coming is also shown with an arrow. As seen in the figure, the direction of maximum intensity differed appreciably from place to place though their general direction agreed with the arrow, the largest deviation amounting to as

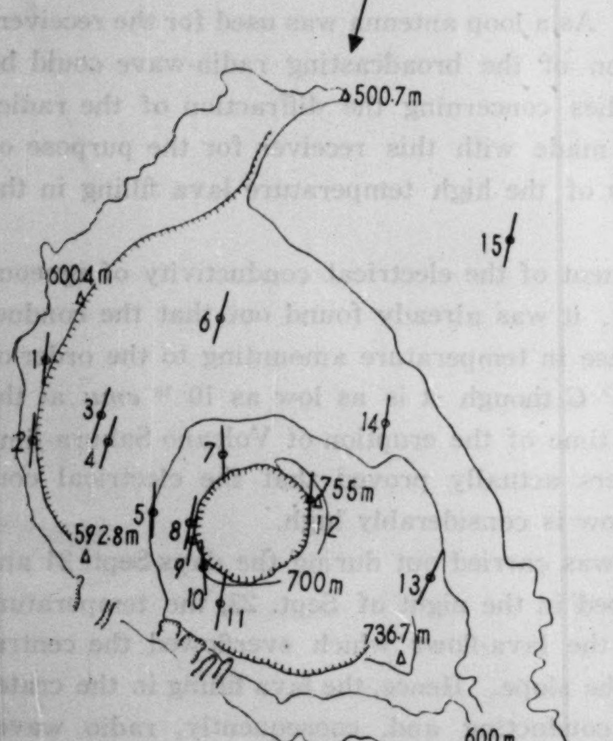

Fig. 1 The directions of maximum signal around the crater of Volcano Mihara. The arrow shows the direction from which JOAK broadcasting waves are coming.

much as 18 *degrees* as shown in Table I.

3. Interpretation of the results.

Although it is difficult to form a detailed estimate of the diffraction of the radio waves owing to the complicated shape of the lava mass, we may, to a rough degree of approximation, regard the lava mass as a conducting cylinder having a diameter of about 800 *m*. As the wave length of the incident wave amounts to 508 *m*, which is comparable with the dimension of the diffracting body, it is conceivable that the pattern of the diffracted waves will become much complicated.

According to the theory of the propagation of electric ground wave[4], the vector of the electric field slightly inclines to the direction of propagation. Neglecting the slight inclination just mentioned, we shall take here a plane wave as the incident wave such as expressed by

$$E_z = e^{i(k_1 x - \omega t)} \quad (k_1 = \omega/c)\,, \quad \dots\dots\dots\dots\dots\dots\dots\dots (1)$$

where ω and c denote respectively the angular frequency and the light-velocity. The horizontal components E_x and E_y are assumed to be zero. According to the theory[5] of diffraction around an infinite cylinder with perfect conductivity, the electric field outside the conductor is given by

$$E_z = e^{ik_1 x} - \sum_{-\infty}^{\infty} i^n J_n(k_1 a) \frac{H_n^{(1)}(k_1 r)}{H_n^{(1)}(k_1 a)} e^{in\phi}. \quad \dots\dots\dots\dots (2)$$

In this expression, the time-factor is neglected. *a* denotes the radius of the cylinder, while *r* and ϕ are the cylindrical coordinate of which the origin is taken at the centre of the cylinder. On differentiating with respect to *r* and ϕ, the real part of the accompanying magnetic field-components are obtained as follows;

$$\left.\begin{aligned} H_\phi = -\Big[& \cos k_1 x \cdot \cos\phi - \frac{J_0(k_1 a)}{|H_0^{(1)}(k_1 a)|} \{J_0(k_1 a)\, Y_0'(k_1 r) - Y_0(k_1 a) J_0'(k_1 r)\} \\ & + 2\sum_{n=1}^{\infty} (-1)^n \frac{J_{2n-1}(k_1 a)}{|H_{2n-1}^{(1)}(k_1 a)|} \{J_{2n-1}(k_1 a) J_{2n-1}'(k_1 r) + Y_{2n-1}(k_1 a)\, Y_{2n-1}'(k_1 r)\} \cos(2n-1)\phi \\ & - 2\sum_{n=1}^{\infty} (-1)^n \frac{J_{2n}(k_1 a)}{|H_{2n}^{(1)}(k_1 a)|} \{J_{2n}(k_1 a)\, Y_{2n}'(k_1 r) - Y_{2n}(k_1 a) J_{2n}'(k_1 r)\} \cos 2n\phi \Big] \cos \omega t \end{aligned}\right|$$

---

[4] J. ZENNECK, *Ann. d. Phys.*, **23** (1907), 846.

[5] P. FRANK, *Die Differential- und Integralgleichungen der Mechanik und Physik*, II, (1927), p. 494.

$$\left.\begin{aligned}
&-\Big[\sin k_1x\cdot\cos\phi+\frac{J_0(k_1a)}{|H_0^{(1)}(k_1a)|}\{J_0(k_1a)J_0'(k_1r)+Y_0(k_1a)Y_0'(k_1r)\}\\
&+2\sum_{n=1}^{\infty}(-1)^n\frac{J_{2n-1}(k_1a)}{|H_{2n-1}^{(1)}(k_1a)|}\{J_{2n-1}(k_1a)Y_{2n-1}'(k_1r)-Y_{2n-1}(k_1a)J_{2n-1}'(k_1r)\}\cos(2n-1)\phi\\
&+2\sum_{n=1}^{\infty}(-1)^n\frac{J_{2n}(k_1a)}{|H_{2n}^{(1)}(k_1a)|}\{J_{2n}(k_1a)J_{2n}'(k_1r)+Y_{2n}(k_1a)Y_{2n}'(k_1r)\}\cos 2n\phi\Big]\sin\omega t\,,\\
&H_r=\Big[\cos k_1x\cdot\sin\phi+\frac{2}{k_1r}\sum_{n=1}^{\infty}(-1)^n(2n-1)\frac{J_{2n-1}(k_1a)}{|H_{2n-1}^{(1)}(k_1a)|}\{J_{2n-1}(k_1a)J_{2n-1}(k_1r)\\
&\quad+Y_{2n-1}(k_1a)Y_{2n-1}(k_1r)\}\sin(2n-1)\phi\\
&-\frac{2}{k_1r}\sum_{n=1}^{\infty}(-1)^n(2n)\frac{J_{2n}(k_1a)}{|H_{2n}^{(1)}(k_1a)|}\{J_{2n}(k_1a)Y_{2n}(k_1r)-Y_{2n}(k_1a)J_{2n}(k_1r)\}\sin 2n\phi\Big]\cos\omega t\\
&\quad+\Big[\sin k_1x\cdot\sin\phi+\frac{2}{k_1r}\sum_{n=1}^{\infty}(-1)^n(2n-1)\frac{J_{2n-1}(k_1a)}{|H_{2n-1}^{(1)}(k_1a)|}\{J_{2n-1}(k_1a)Y_{2n-1}(k_1r)\\
&\quad-Y_{2n-1}(k_1a)J_{2n-1}(k_1r)\}\sin(2n-1)\phi\\
&\quad+\frac{2}{k_1r}\sum_{n=1}^{\infty}(-1)^n(2n)\frac{J_{2n}(k_1a)}{|H_{2n}^{(0)}(k_1a)|}\{J_{2n}(k_1a)J_{2n}(k_1r)\\
&\quad+Y_{2n}(k_1a)Y_{2n}(k_1r)\}\sin 2n\phi\Big]\sin\omega t\,.
\end{aligned}\right\}\qquad\ldots\ldots(3)$$

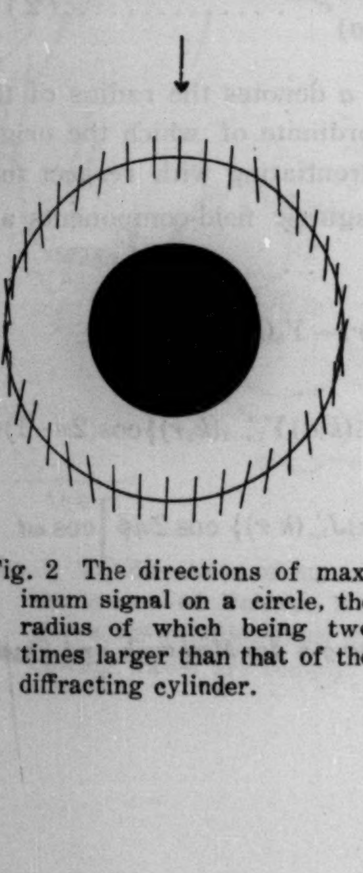

Fig. 2 The directions of maximum signal on a circle, the radius of which being two times larger than that of the diffracting cylinder.

With these expressions, the direction of the maximum intensity measured by the loop antenna is calculated for any point. For instance, the calculated directions on a circle whose radius is equal to $2a$ are illustrated in Fig. 2. As already expected, the complicated distribution of the direction is shown remarkably in the figure, the effect of the diffraction being so considerable that maximum deviation of the direction exceeds 11 *degrees*.

On the other hand, the said direction for the respective measuring points are calculated, their deviation from the incident direction are given in Table I together with the observed deviations. The calculated directions fairly agree with the observed ones except the points on the central cone, these points being situated within several *meters* from the margin of the high temperature lava mass. Thus the simple approximation for the diffracting body will be inadequate for these points.

Table I

The measured and calculated deviation of the direction of maximum intensity from the incident direction of the broadcasting radio wave. Westward deviation is taken to be plus.

Station	Distance from the centre of the crater	Measured deviation	Calculated deviation	Difference
No. 1	1840*m*	6°	6°	0°
No. 2	1640	9	6	3
No. 3	1280	–5	–3	–2
No. 4	1140	–3	–2	–1
No. 5	680	8	12	–4
No. 6	1460	–1	–1	0
No. 7*	500	12	1	(11)
No. 8*	420	3	–19	(22)
No. 9*	420	5	–22	(27)
No. 10*	420	18	–14	(32)
No. 11	580	2	0	2
No. 12*	480	11	–11	(22)
No. 13	1300	–13	–10	–3
No. 14	1180	5	3	2
No. 15	2760	–1	0	–1

(* These points are very near to the boundary of the lava, the distances being almost several *meters*.)

Taking into account the accuracy of measurement, it may be said that the general tendency of the anomalous deviation of the direction of maximum intensity is roughly explained as the diffraction of the electric waves around the conducting cylinder having the same area as that occupied by the lava mass.

4. Discussion.

In the previous section, the effect of the lava mass was assumed to be the same with that of a cylinder of infinite conductivity. On this point some discussions will be attempted here. When a plane wave is reflected by a semi-infinite conductor, the reflecting power is approximately given by

$$R = \frac{\sqrt{i\sigma}-\sqrt{\omega}}{\sqrt{i\sigma}+\sqrt{\omega}},$$

for relatively high conductor, where σ denotes the conductivity. The polarization of the electric vector is assumed to be parallel to the boundary. The reflecting power for various conductivity is calculated for the waves of 590 *kc* as shown in Fig. 3. As clearly shown in the figure, the conductor having higher conductivity than 10^{-12} *emu* may be considered to be equivalent to the perfect conductor in the calculation. Hence, the treatment in the former sections will be allowed, provided the conductivity of the lava at 590 *kc* does not differ materially from that for direct current as obtained by Nagata and Coster, the conductivity obtained by them being as high as 10^{-10} *emu* at the temperature of about 1,000° *C*.

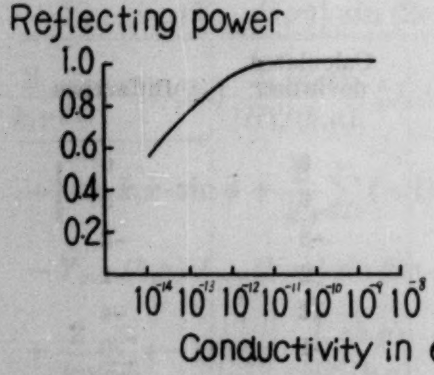

Fig. 3 The relation between the reflecting power for 590 *kc* wave and the electrical conductivity.

5. Conclusion.

As a result of the polarization measurement of the broadcasting radio waves in the vicinity of the crater of Volcano Mihara, some anomalous distribution of the polarization was found out. The distribution is roughly explained as the diffraction-effect around the high temperature lava mass filling in the crater. However, the detailed determination of the conductivity is impossible by the present simple measurement. Systematic measurements with electric waves having various frequencies will be needed for the more accurate determination of the electric properties of the lava.

In conclusion, the writer wishes to express his sincere thanks to Mr. S. Saito who constantly assisted the writer in the course of the measurement.

13. 三原山火口附近における放送電波の廻折

地震研究所　力　武　常　次

ループアンテナ使用の携帯用ラジオ受信機により，三原山外輪山内の十數箇所においてJOAK放送電波 (590 kc) の到來方向を測定して，最大 18° に達する偏倚を見出した。この異常は舊火口に充滿している高溫熔岩が高電導度を有するための廻折現象として理解される。

14. *The Distribution of Magnetic Dip in Ooshima (Oo-sima) Island and its Change that Accompanied the Eruption of Volcano Mihara, 1950.*

By Tsuneji RIKITAKE,
Earthquake Research Institute.

(Read Nov. 21, 1950.—Received Dec. 20, 1950.)

1. Introduction.

After the minor eruption on Aug. 19, 1940, Volcano Mihara in Ooshima (Oo-sima) Island had been quiet for about ten years when a new activity took place in the morning of July 16, 1950. The eruption became greater day by day and the old crater pit was filled with new lava and ejecta. At the beginning of September the lava overflowed the central cone and flowed down the slope to the caldera. The activity continued up to Sept. 23, while the total amount of the lava which welled up during the period was estimated[1] to be about 3×10^7 *metric tons.*

Magnetic dip surveys over Ooshima Island were carried out by the writer in July and September, 1950, for the purpose of finding out the changes in geomagnetism expected to accompany such severe eruption.

We have hitherto coducted several geomagnetic investigations with respect to Ooshima Island. The earliest one was by S. Nakamura[2] who made a magnetic dip survey in the north-western part of the island with a dip-circle in the year 1928. However, the topography changed so greatly during the war that it was of great difficulty to find the old measuring stations. Hence, the writer gave up the attempt to compare the result of the present survey with that of Nakamura's. In 1936, R. Takahasi and T. Nagata[3] made a magnetic survey with a magnetometer of the Japanese Hydrographic Department pattern. They measured three components of the earth's magnetic field at 12 stations which were distributed almost equidistantly along the coast of Ooshima. And at three stations within the somma only the dip was measured. At several stations, the writer could identify the places on which the measurement was made with the aid of the pegs, photographs and sketch-maps prepared by Takahasi and Nagata. After making allowances for the influence of general magnetic disturbance or secular change, some increases in magnetic dip was found out during the period 1936–1950, the increase generally amounting to several *minutes* of arc.

---

[1] R. TAKAHASI, and D. SHIMOZURU, Read at the Oct. Meeting of the Earthquake Research Institue, 1950.

[2] S. NAKAMURA, *Zisin*, **6** (1934), 637.

[3] R. TAKAHASI and T. NAGATA, *Bull. Earthq. Res. Inst.*, **15** (1937), 441.

Soon after the beginning of the eruption, the writer made a survey throughout the island with a newly constructed earth-inductor. During the surveying period July 25–30, bombs and lapillis were being ejected from a crater which newly opened at the south-western corner of the old pit, while the bottom of the pit was being upheaved gradually. The number of stations amounted to as much as 36 in the survey. With these results, magnetic anomaly due to Volcano Mihara was studied, the mean intensity of magnetization being determined to be about 0.03 *emu*. The anomaly nearer the somma was so large that the maximum dip-angle amounted to as much as 56°.

The second survey was carried out during the period Sept. 22–26, while the eruption suddenly stopped in the night of Sept. 23. At that time, the lava had already overflowed the central cone and a new cinder cone was formed in the old crater. Comparing the results of the second survey with those of the first, we found that marked geomagnetic changes occurred during the period, the maximum change in dip being as much as 30 *minutes* of arc. At almost all stations, the magnetic dip-angle decreased, the decrease becoming larger as the station approached the crater.

Generally speaking, we have had hitherto a good many number of investigations concerning the relation between local geomagnetic changes and volcanic activities. Especially, at the time of Miyake-sima eruption, 1940, R. Takahasi[4], T. Minakami[5], T. Nagata[6] and Y. Kato[7] made geomagnetic studies with various instruments, confirming the existence of local magnetic changes. Since Ooshima Island like Miyake-sima Island is composed of basaltic rocks, we may well expect some anomalous changes in the earth's magnetic field to occur at the time of eruption.

2. The instrument.

An earth-inductor of small type which was newly designed and constructed by the writer[8] was used for the survey. The instrument was so constructed as to be handy for transportation in the field and only 5–10 *minutes* are needed to carry out measurement at one station. The observation may be carried out by a single person. Some scenes of observation are, for example, shown in Photos. 1 and 2. The electromotive forces induced in the rotating coil are amplified with a special amplifier and are detected with a crystal receiver. According to the results of calibration, the accuracy of measurement amounts to 1 or 2 *minutes* of arc.

---

[4] R. TAKAHASI and K. HIRANO, *Bull. Earthq. Res. Inst.*, **19** (1941), 82 and 373.
[5] T. MINAKAMI, *Bull. Earthq. Res. Inst.*, **19** (1941), 356.
[6] T. NAGATA, *Bull. Earthq. Res. Inst.*, **19** (1941), 335.
[7] Y. KATO, *Proc. Imp. Acad. Japan*, **16** (1940), 440.
[8] T. RIKITAKE, *Bull. Earthq. Res. Inst.*, **29** (1951), 147.

Photo. 1.
Station No. 5. The Bench Mark on the central cone.

Photo. 2.
Station No. 24. Nomashi Village.

3. The results of the survey.

The results of the first and second surveys are shown in Table I together with the latitude, longitude and height above sea level of the stations. As some stations on the central cone were buried by the new lava, it was impossible to repeat the observation. Sketch-maps of the measuring points were illustrated in Figs. 1 for convenience of future measurement.

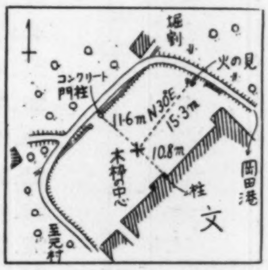

Fig. 1-1 Station No. 1
The fifth middle school.

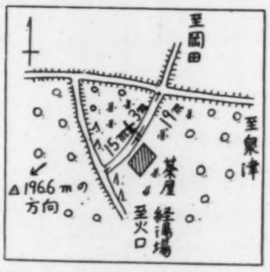

Fig. 1-2 Station No. 2
Sangome, Okada road.

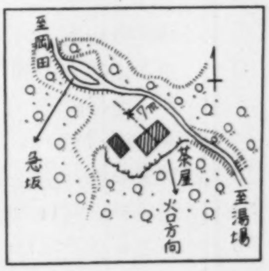

Fig. 1-3 Station No. 3
Rokugome, Okada road.

Table I. The

Nos. of station	Locality		Latitude	Longitude
1	大島第五中學校	The fifth middle school	34°46'.9 N	139°23'.8 E
2	岡田登山道三合目	Sangome, Okada road	46.5	23.8
3	同　六合目	Rokugome, Okada road	45.5	23.9
4	同　十合目	First somma	44.6	23.8
5	內輪山水準點	Central cone	43.7	23.9
6	內輪山上	Central cone	43.2	23.9
7	內輪山最高點	Central cone	43.5	24.2
8	內輪山上	Central cone	43.7	24.1
9	沙漠	Sabaku	43.9	23.2
10	自動車道路	High way	44.7	23.1
11	沙漠岡田口	Sabaku	43.9	23.8
12	公園口鳥居	Torii, Ooshima park	43.8	24.6
13	大島公園口	Ooshima park	44.2	25.0
14	動物園	Zoo	45.2	26.5
14′	ヒユツテ	Lodge	45.2	26.5
15	笠松展望台附近	Kasamatsu	46.3	25.7
16	泉津小學校	Senzu primary school	46.6	25.3
17	泉津小學校跡	Old Senzu primary school	46.7	25.1
18	泉津登山道附近	Senzu road	46.3	24.6
19	大島測候所	Ooshima meteorol. station	45.8	22.6
20	六踏園	Rokutoen	46.8	21.4
21	泉濱南端	Izumihama	45.8	21.4
22	元村小學校	Motomura primary school	44.8	21.9
23	元村小學校跡	Old Motomura primary school	45.0	21.6
24	野增村綠地	Nomashi village	43.8	21.5
25	千波崎附近	Senbazaki	41.9	22.2
26	間伏海岸	Mabushi	41.3	23.3
27	差木地小學校	Sashikiji primary school	40.9	25.0
28	波浮港小學校	Habuko primary school	41.2	26.5
29	波浮登山道	Habu road	41.7	25.6
30	白石山東方鞍部	First somma	43.2	24.6
31	沙漠中神社前	Shrine	43.4	23.4
32	沙漠野增口	Sabaku	43.8	23.2
33	野增口峠	First somma	43.8	22.9
34	椿茶屋元村口六合目	Tsubaki-chaya	44.3	22.7
35	三原茶屋元村口一合目	Mihara-chaya	44.5	22.2
36	內輪山上	Central cone	43.2	23.9

results of the surveys.

Height above sea level	Survey I			Survey II		
	Date		Dip	Date		Dip
80*m*	1950	04*h*51*m*	48° 43′.5	1950	13*h*41*m*	48° 42′.9
185	VII 25th	05 54	49 36 .5	IX 23rd	14 23	49 33 .2
370		07 05	48 30 .3		15 12	48 22 .1
560		09 35	51 33 .3		17 09	51 18 .6
660		10 49	56 26 .6	IX 25th	11 08	56 07 .0
700		12 35	53 39 .9		— —	— —
755		13 15	53 57 .0	IX 24th	16 56	53 34 .2
700		13 58	53 23 .1		— —	— —
530		14 50	48 34 .6	IX 24th	08 48	48 14 .2
440		15 50	53 00 .0	IX 23rd	17 46	52 40 .1
570	VII 26th	07 55	46 48 .9	IX 24th	15 24	46 35 .1
540		08 50	50 02 .4		13 22	49 50 .3
460		09 30	49 18 .6		— —	— —
100		13 30	48 34 .6	IX 23rd	09 10	48 24 .4
110		10 50	50 28 .1		09 36	50 18 .4
40		14 36	51 15 .5		10 28	51 07 .9
40		15 15	48 36 .9		11 00	48 37 .1
40		15 55	46 42 .5		11 36	46 42 .8
220		17 34	46 46 .4		— —	— —
180	VII 27th	10 27	48 13 .8	IX 22nd	18 15	48 10 .3
15		14 05	49 51 .8		16 49	49 46 .5
20		16 05	48 48 .4		15 47	48 44 .9
50	VII 28th	08 44	47 51 .7	IX 25th	16 45	47 42 .3
50		09 27	50 03 .3		17 16	50 00 .3
20		10 43	47 40 .3	IX 26th	08 50	47 28 .6
20		13 57	47 36 .3		12 10	47 30 .3
20		15 44	47 02 .3		13 43	46 59 .5
40		17 00	47 56 .8		15 12	47 57 .3
55	VII 29th	08 16	48 26 .5		18 12	48 22 .5
220		10 13	50 30 .4		17 17	50 30 .0
640		12 01	53 09 .9	IX 24th	12 05	52 49 .0
610		13 29	51 09 .3		10 26	50 42 .1
530	VII 30th	14 00	49 43 .5		10 03	49 26 .8
560		14 33	51 44 .4		09 16	51 27 .2
350		15 38	50 57 .5	IX 25th	14 57	50 43 .6
100		16 23	46 53 .8		15 21	46 43 .6
700		— —	— —		12 55	54 35 .8

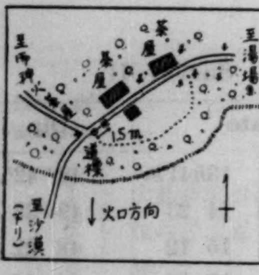
至御神火茶屋
茶屋
茶屋
至湯場
1.5m
道標
至沙漠(下り)
↓火口方向

Fig. 1-4 Station No. 4
First somma.

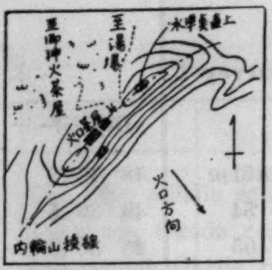
至御神火茶屋
至湯場
水準点上
火口茶屋
火口方向
内輪山稜線

Fig. 1-5 Station No. 5
Central cone.

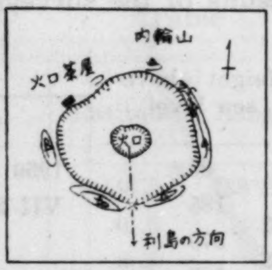
内輪山
火口茶屋
火口
↓利島の方向

Fig. 1-6 Station No. 6
Central cone.

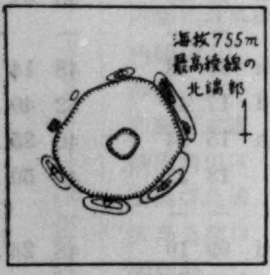
海抜755m
最高稜線の
北端部

Fig. 1-7 Station No. 7
Central cone.

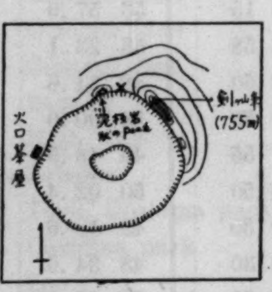
火口茶屋
剣ヶ峰
(755m)

Fig. 1-8 Station No. 8
Central cone.

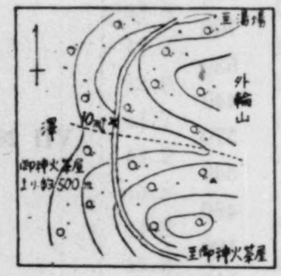
至湯場
外輪山
沢
10m
御神火茶屋
より約500m
至御神火茶屋

Fig. 1-9 Station No. 10
High way.

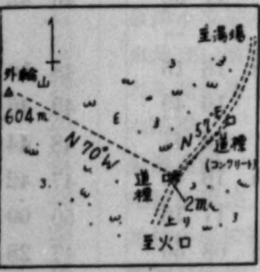
至湯場
外輪山
604m
N70°W
N57°E
道標
(コンクリート)
道標
2m
上り
至火口

Fig. 1-10 Station No. 11
Sabaku.

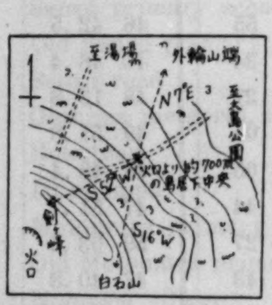
至湯場
外輪山端
N7°E
至大島公園
火口より約700mの鳥居下中央
S52°W
S16°W
剣ヶ峰
火口
白石山

Fig. 1-11 Station No. 12
Torii, Ooshima park.

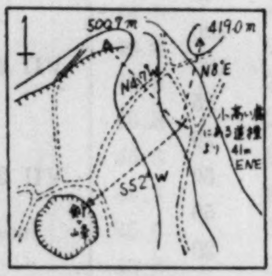
500.7m
419.0m
N47°W
N8°E
小高い所にある道標より41m ENE
S52°W
剣ヶ峰

Fig. 1-12 Station No. 13
Ooshima park.

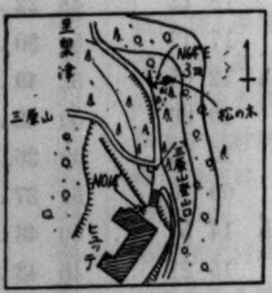
至泉津
N64°E
3m
松の木
三原山
N01°
三原山登山口
ヒュッテ

Fig. 1-13 Station
No. 14 Zoo.

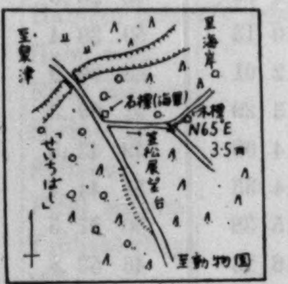
至泉津
至海岸
石標(海軍)
木標
N65°E
3.5m
至松屋茶台
せいちばし
至動物園

Fig. 1-14 Station
No. 15 Kasamatsu.

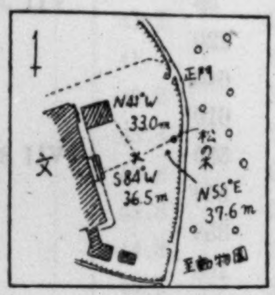
正門
N41°W
33.0m
松の木
文
S84°W
36.5m
N55°E
37.6m
至動物園

Fig. 1-15 Station No. 16
Senzu primary school.

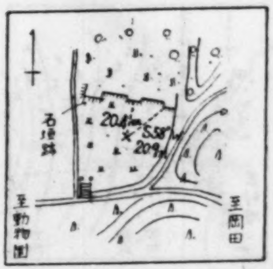
石垣跡
20.4m
S58°W
20.9m
至動物園
至岡田

Fig. 1-16 Station No. 17 Old Senzu primary school.

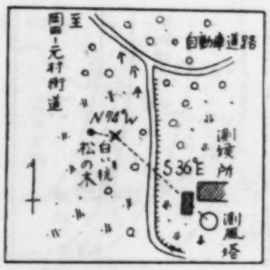
至
元村街道
自動車道路
N98°W
松の木
S36°E
測候所
測風塔

Fig. 1-17 Station No. 19 Ooshima meteorol. station.

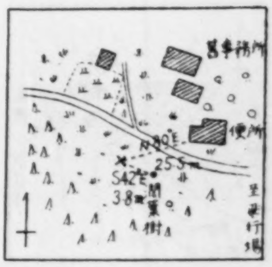
事務所
便所
N30°E
25.5m
S42°E
3.8m
至
行場

Fig. 1-18 Station No. 20 Rokutoen.

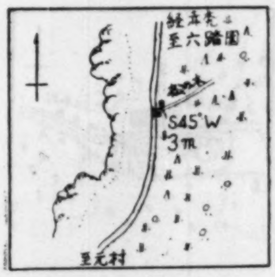
至六踏園
S45°W
3m
至元村

Fig. 1-19 Station No. 21 Izumihama.

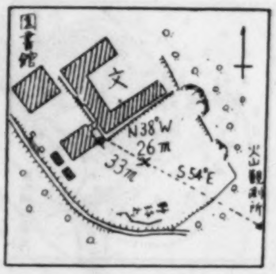
図書館
文
N38°W
26m
33m
S54°E
火山観測所

Fig. 1-20 Station No. 22 Motomura primary school.

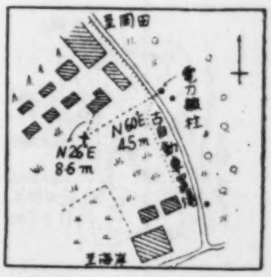
至岡田
電力
N60°E
45m
N26°E
8.6m
至海岸

Fig. 1-21 Station No. 23 Old Motomura primary school.

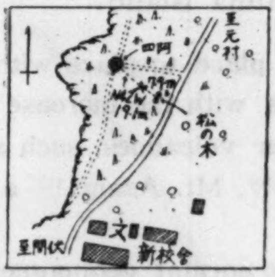
至元村
四阿
7.9m
N42°W
19.1m
松の木
文
至間伏
新校舎

Fig. 1-22 Station No. 24 Nomashi village.

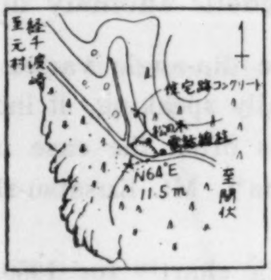
至元村
経千波崎
住宅跡コンクリート
松の木
電柱
N64°E
11.5m
至間伏

Fig. 1-23 Station No. 25 Senbazaki.

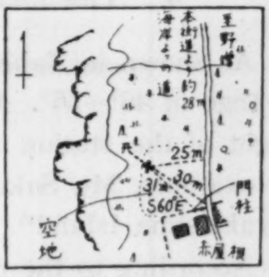
海岸より
本街道より
の道
至野増
約28m
25m
30m
31m
S60°E
門柱
空地
赤屋根

Fig. 1-24 Station No. 26 Mabushi.

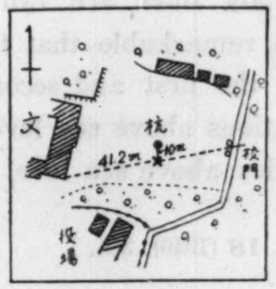
文
杭
10m
41.2m
校門
役場

Fig. 1-25 Station No. 27 Sashikiji primary school.

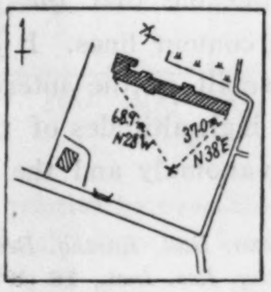
文
68.9m
N28°W
37.0m
N38°E

Fig. 1-26 Station No. 28 Habuko primary school.

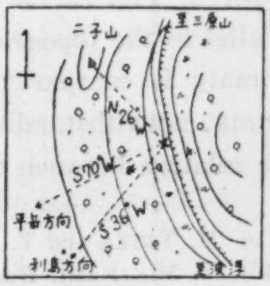
二子山
至三原山
N26°W
S70°W
S36°W
平畠方向
利島方向
至波浮

Fig. 1-27 Station No. 29 Habu road.

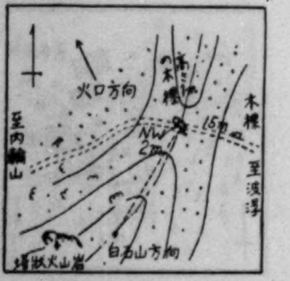
火口方向
至内輪山
NW
2m
15m
木標
至波浮
白石山方向
縄状火山岩

Fig. 1-28 Station No. 30 First somma.

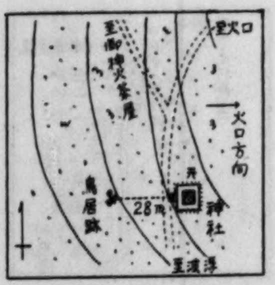
至火口
至御神火茶屋
火口方向
鳥居跡
28m
神社
至波浮

Fig. 1-29 Station No. 31 Shrine.

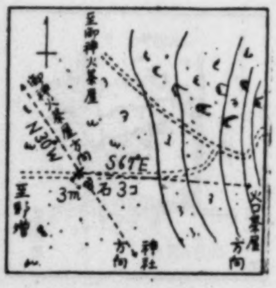
至御神火茶屋
御神火茶屋方向
N30°W
S67E
3m
石3コ
至野増
神社方向
火口茶屋方向

Fig. 1-30 Station No. 32 Sabaku.

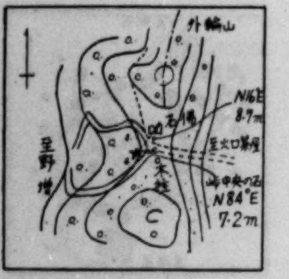
外輪山
N16E
8.7m
至火口茶屋
至野増
N84°E
7.2m

Fig. 1-31 Station No. 33 First somma.

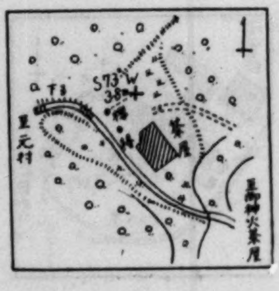
S73°W
3.8m
至元村
茶屋
至御神火茶屋

Fig. 1-32 Station No. 34 Tsubaki-chaya.

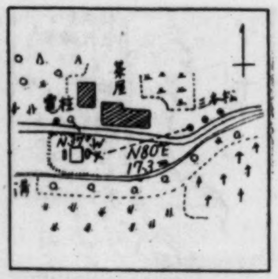
茶屋
電柱
N37°W
N80E
17.3m

Fig. 1-33 Station No. 35 Mihara-chaya.

4. The local magnetic anomaly in Ooshima Island.

As shown in Table I, the dip-angle varies from place to place within a range of 46° – 56°. Generally speaking, it increases with the increase in height of the station as was often the case in other volcanoes, such as, for example, Mt. Sakura-jima[9], Mt. Kusatsu-shirane[10], Mt. Asama[11] and Miyake-sima Island[7].

According to the magnetic chart[12] for 1950.0, the normal geomagnetic dip θ_n amounts to 47° 50′ in the vicinity of Ooshima Island. The anomly in dip-angle $\Delta\theta = \theta - \theta_n$ was calculated. The distribution of the anomaly is shown in Fig. 2. It is noticeable that the isanomaly lines are fairly parallel to the topographical contour lines. It is also remarkable that the anomaly is comparatively small in the interior of the first and second somma, notwithstanding the high altitudes of the stations above sea level. The relation between the dip-anomaly and the altitudes above sea level is

---

9) H. TSUYA and T. MINAKAMI, *Bull. Earthq. Res. Inst.*, **18** (1940), 335.
10) T. MINAKAMI, *Bull. Earthq. Res. Inst.*, **16** (1938), 117.
11) T. MINAKAMI, *Bull. Earthq. Res. Inst.*, **16** (1938), 100; **18** (1940), 178.
12) Published by the Geographical Survey Institute.

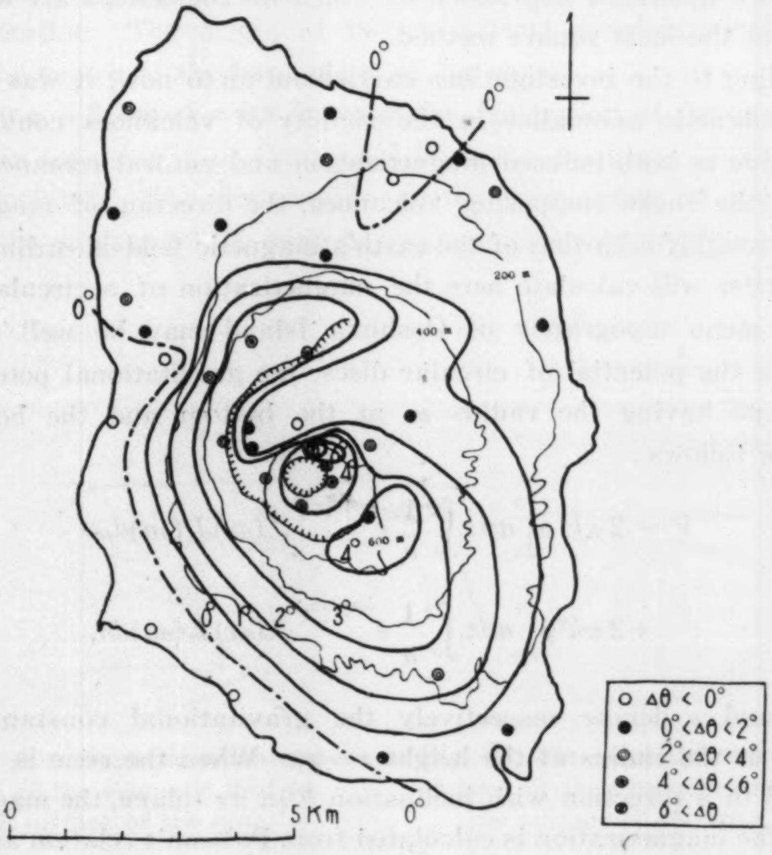
0°
0°
0
200 m
400
600 m
4
3
2
1
0
5 Km
0°
○ Δθ < 0°
● 0°<Δθ<2°
2°<Δθ<4°
4°<Δθ<6°
6°<Δθ

Fig. 2 The distribution of dip-anomaly in Ooshima Island.

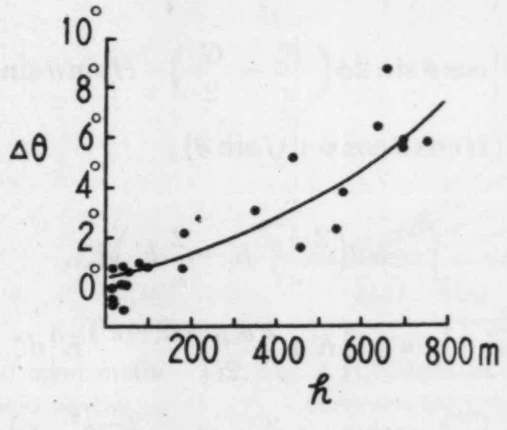

Fig. 3 The relation between dip-anomaly and height above sea level.

graphically shown in Fig. 3. The general tendency to increase as the height increases is expressed by the curve in the figure, the curve being obtained as a quadratic expression of which the coefficients are determined by means of the least square method.

According to the investigations carried out up to now, it was confirmed that the magnetic anomalies in the vicinity of volcanoes could be interpreted as due to both induced magnetization and natural remanent magnetization of the rocks composing volcanoes, the direction of magnetization coinciding roughly with that of the earth's magnetic field in ordinary cases.

The writer will calculate here the magnetization of a circular cone by which the mean topography of Ooshima Island may be well expressed. Superposing the potential of circular discs, the gravitational potential of a circular cone having the radius a_0 at the bottom and the height h is obtained as follows;

$$\begin{aligned} V &= 2\pi k^2 \rho \int_z^h a\,dz_1 \int_0^\infty \frac{1}{\alpha} e^{-\alpha(z_1-z)} J_0(\alpha r) J_1(\alpha a)\,d\alpha \\ &\quad + 2\pi k^2 \rho \int_0^z a\,dz_1 \int_0^\infty \frac{1}{\alpha} e^{-\alpha(z-z_1)} J_0(\alpha r) J_1(\alpha a)\,d\alpha, \end{aligned} \tag{1}$$

where k^2 and ρ denote respectively the gravitational constant and the density. a is the radius at the height $z = z_1$. When the cone is uniformly magnetized in a direction with inclination θ in xz -plane, the magnetic field caused by the magnetization is calculated from Poisson's relation as follows;

$$\left.\begin{aligned} \varDelta X &= J\Big\{\cos\theta\Big(\frac{F}{r}\cos 2\phi - G\cos^2\phi\Big) - H\sin\theta\cos\phi\Big\}, \\ \varDelta Y &= J\Big\{\cos\theta\sin 2\phi\Big(\frac{F}{r} - \frac{G}{2}\Big) - H\sin\theta\sin\phi\Big\}, \\ \varDelta Z &= J\{H\cos\theta\cos\phi + G\sin\theta\}, \end{aligned}\right\} \quad (2)$$

where

$$\left.\begin{aligned} F &= 2a_0\rho^{-\frac{1}{2}} \int_0^{h/a_0} \alpha^{1/2}\Big(\frac{2-\kappa^2}{\kappa}K - \frac{2}{\kappa}E\Big)d\zeta_1, \\ G &= \rho^{-\frac{1}{2}} \int_0^{h/a_0} \kappa^2 \alpha^{-1/2}\Big\{K + \frac{\kappa^2\alpha/\rho - (2-\kappa^2)}{2(1-\kappa^2)}E\Big\}d\zeta_1, \\ H &= \rho^{-\frac{3}{2}} \int_0^{h/a_0} \kappa\alpha^{-1/2}(\zeta-\zeta_1)\Big\{-K + \frac{2-\kappa^2}{2(1-\kappa^2)}E\Big\}d\zeta_1, \\ \kappa^2 &= 4\alpha\rho/\{(\alpha+\rho)^2 + (\zeta-\zeta_1)^2\}, \\ a/a_0 &= \alpha, \quad r/a_0 = \rho, \quad z_1/a_0 = \zeta_1, \quad z/a_0 = \zeta. \end{aligned}\right\} \quad \ldots\ldots(3)$$

K and E denote complete elliptic integrals, while J denotes the intensity of magnetization. The origin of the cylindrical coordinate r, ϕ, and z is taken at the centre of the base plane of the cone.

Taking $a_0 = 5\ km$, $h = 0.8\ km$ and the inclination of the cone to be 9° as the mean topography of Ooshima Island, the integrals in (3) are numerically calculated. The distribution of the components of the magnetic field over the surface of the cone is obtained as shown in Figs. 4 in which

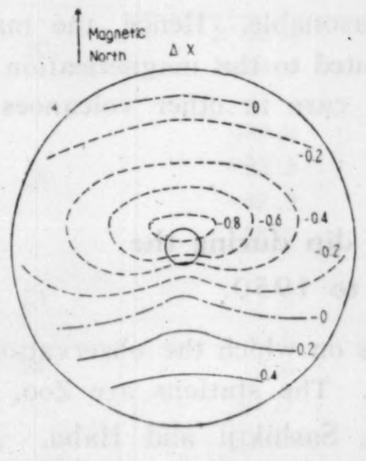

Fig. 4a The magnetic north component of the magnetic field on the surface of the cone.

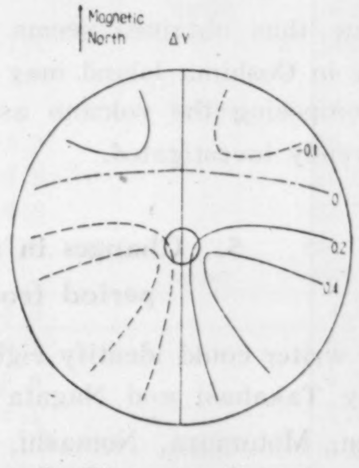

Fig. 4b The magnetic west component of the magnetic field on the surface of the cone.

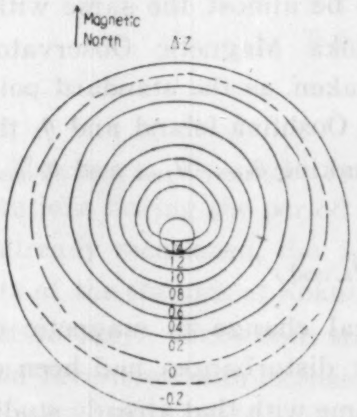

Fig. 4c The vertical component of the magnetic field on the surface of the cone.

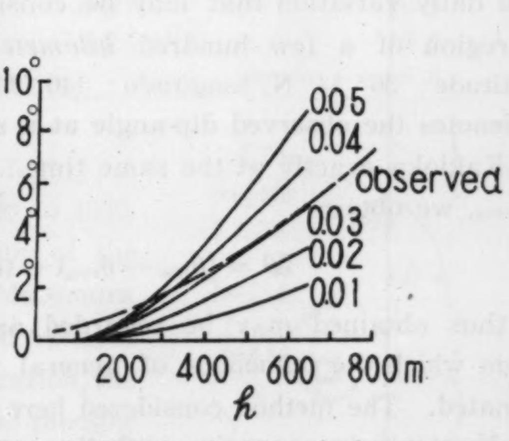

Fig. 5 Changes in the calculated and observed dip-anomaly with the height above sea level.

the intensity of magnetization is taken to be unity and θ is assumed to be 48°. As seen in the figures, the magnetic anomaly shows a particular form, the mode of distribution being approximately the same with those observed at various volcanoes. From the calculated ΔX and ΔZ, the anomaly in magnetic dip is also estimated, where the normal value for the horizontal intesity is assumed to be 0.306 *Gauss* from the chart. The increase in the dip-anomaly averaged through the whole azimuth is obtained for each respective magnetization as shown in Fig. 5. Comparing the calculated anomaly with the observed one, we may presume that the mean intensity of magnetization amounts to about 0.03 *emu*. Taking into account the magnetic properties of the rocks composing Vocano Mihara[13], the value thus obtained seems to be reasonable. Hence, the magnetic anomaly in Ooshima Island may be attributed to the magnetization of the rocks composing the volcano as was the case in other volcanoes which were already investigated.

5. Changes in magnetic dip during the period from 1936 to 1950.

The writer could identify eight stations on which the observation were made by Takahasi and Nagata[3] in 1936. The stations are Zoo, Senzu, Rokutoen, Motomura, Nomashi, Mabushi, Sashikiji and Habu. Among these stations, Rokutoen and Motomura underwent great changes in their circumstances, thus making it rather difficult to identify the stations.

In order to eliminate general secular changes, magnetic disturbance and daily variation that may be considered to be almost the same within a region of a few hundred *kilometers*, Kakioka Magnetic Observatory (latitude: 36° 14′ N, longitude: 140° 11′ E) is taken as the standard point. θ denotes the observed dip-angle at a station in Ooshima Island and θ_k that at Kakioka exactly at the same time. Then, making $\theta_{1950}-\theta_{1936}$ and $\theta_{k,1950}-\theta_{k,1936}$, we obtain

$$\delta\theta = (\theta_{1950} - \theta_{1936}) - (\theta_{k,\,1950} - \theta_{k,\,1936})\,.$$

$\delta\theta$ thus obtained may be regarded as the local change in magnetic dip from which the influences of general magnetic disturbances had been eliminated. The method considered here is the same with that already studied by Nagata[14] in connexion with the comparison of the results of magnetic surveys before and after the Niisima Earthquake, 1936.

In Table II, $\theta_{1950}-\theta_{1936}$, $\theta_{k,1950}-\theta_{k,1936}$ and $\delta\theta$ are given for the respective stations. The distribution of $\delta\theta$ is also shown in Fig. 6. Except Rokutoen

---

[13] T. NAGATA, *Bull. Earthq. Res. Inst.*, **21** (1943), 1.

[14] T. NAGATA, *Bull. Earthq. Res. Inst.*, **15** (1937), 497.

Table II. Changes in magnetic dip during the period from 1936 to 1950.

No. of station	$\theta_{1950}-\theta_{1936}$	$\theta_{k,1950}-\theta_{k,1936}$	$\delta\theta$
14	-2′.6	-6′.8	4′.2
17	3 .1	-6 .2	9 .8
	1 .9	-6 .9	8 .8
	1 .9	-5 .8	7 .7
			mean 8 .8
20	2° 05 .4	-7 .1	2° 12 .5
	2 04 .4	-7 .9	2 12 .3
			mean 2 12 .4
23	-32 .9	-6 .8	-26 .1
	-33 .5	-6 .9	-26 .1
	-32 .0	-6 .3	-25 .7
	-33 .0	-7 .3	-24 .7
			mean -26 .0
24	-4 .3	-8 .6	4 .3
26	-3 .0	-9 .7	6 .7
	-2 .9	-9 .6	6 .7
	-1 .7	-9 .1	7 .4
			mean 6 .9
27	-2 .0	-7 .5	5 .5
	-2 .8	-7 .4	4 .6
			mean 5 .1
28	1 .5	-8 .1	9 .6
	2 .1	-8 .0	10 .1
	0 .9	-8 .3	9 .2
			mean 9 .6

and Motomura, dip-angle increased slightly at all stations during the period from 1936 to 1950. As already mentioned, the identification of the points of the stations at Rokutoen and Motomura is not so easy. Since both stations are situated on old lava-flows with intense magnetization, the gradient in the earth's magnetic field is thought to be appreciable there. Hence, the chages in dip-angle at these stations are not reliable. After all, it may be said that local changes in magnetic dip of the order of several *minutes* of arc had occurred during the period though the detailed distribution of them is not clear.

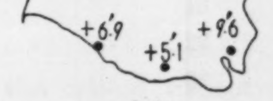

Fig. 6 The distribution of changes in magnetic dip during the period 1936-1950.

Table III. Changes in magnetic dip during the period from July to September, 1950.

Nos. of station	$\theta_{II} - \theta_{I}$	$\theta_{k,II} - \theta_{k,I}$	$\delta\theta$
1	-0′.6	0′.3	-0′.9
2	-3.3	0.8	-4.1
3	-8.2	0.7	-8.9
4	-14.7	0.8	-15.5
5	-19.6	-1.0	-18.6
6	—	—	—
7	-22.8	-2.7	-20.1
8	—	—	—
9	-20.4	-1.8	-18.6
10	-19.9	-2.6	-17.3
11	-13.8	-0.6	-13.2
12	-12.1	-0.2	-11.9
13	—	—	—
14	-10.2	-0.2	-10.0
14′	-9.7	-0.2	-9.5
15	-7.6	0.0	-7.6
16	0.2	0.2	0.0
17	0.3	0.1	0.2
18	—	—	—
19	-3.1	2.4	-5.5
20	-5.3	1.6	-6.9
21	-3.5	1.3	-4.8
22	-9.1	1.9	-11.3
23	-3.0	2.9	-5.9
24	-11.7	2.1	-13.8
25	-6.0	1.2	-7.2
26	-2.8	1.3	-4.1
27	0.5	1.4	-0.9
28	-4.0	1.8	-5.8
29	-0.4	1.7	-2.1
30	-20.9	4.0	-24.9
31	-27.2	3.1	-30.3
32	-16.7	2.6	-19.3
33	-17.2	2.5	-19.7
34	-13.9	1.6	-15.5
35	-10.2	1.8	-12.0
36	—	—	—

6. Changes in magnetic dip that accompanied the eruption, 1950.

The survey I was carried out at the early period of the present activity of Volcano Mihara, while the survey II was made just at the final stage. After correcting general magnetic disturbances as in the previous section, changes in magnetic dip during the period I–II are obtained as shown in Table III. Their distribution is also shown in Fig. 7. As seen in the figure, we find remarkable decrease in dip-angle all over the island except the northern extremity of the island. The amount of decrease becomes larger as the stations approach the central area of the island, the largest decrease amounting to as much as 30 *minutes* of arc at the station No. 31.

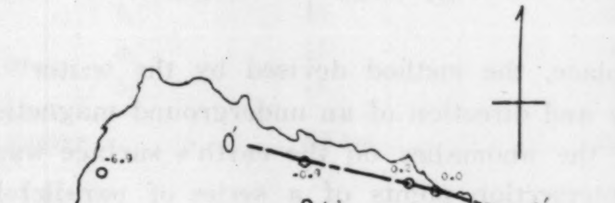
0′
-6.9
-0.9
0.2
0.0
-4.1
0′
-5′
-7.0
-4.8
-5.5
-6.9
-5′
-10.0
-9.5
-5.9
-11.3
-12.0
-17.3
-15.5
-15.5
-10′
-15′
-18.6
-13.2
-10′
-10′
-13.8
-19.7
-19.3
-18.6
-11.9
-20.1
-20
-25
-24.7
-5′
-7.2
-2.1
-5
-4.1
-5.8
-0.9
0
5Km

Fig. 7 The distribution of changes in magnetic dip associated with the eruption.

7. Discussions on the local anomalous changes in geomagenetism that accompanied the eruption.

In the case of Miyake-sima eruption of 1940, Takahasi and Hirano[4] concluded that the changes in the vertical intensity of the earth's magnetic field during the early period of the eruption may be explained by assuming that a spherical region with a radius of 3 *km* just under the centre of the island lost its magnetic property. As the mode of the changes obtained here seems very similar to that of the Miyake-sima eruption, the writer analyzed the distribution of geomagnetic changes from a similar standpoint as follows.

In the first place, the method devised by the writer[15] by which the position, intensity and direction of an underground magnetic dipole can be determined from the anomalies on the earth's surface was applied. The values of $\delta\theta$ at intersection points of a series of parallel lines which are drawn on the map at 1.5 *km* interval are read off. Using these values, the partial derivatives f_{00}, $\partial f_{00}/\partial x$, $\partial f_{00}/\partial y, \ldots,$ $\partial^3 f_{00}/\partial x \partial y^2$, $\partial^3 f_{00}/\partial y^3$ are calculated by means of least square, where f is given by

$$f(\delta\theta) = \{\tan(\theta_n + \delta_0) - \tan\theta_n\}/\tan\theta_n \quad \ldots\ldots\ldots\ldots (4)$$

and where θ_n denotes the normal dip. Thus the coefficients of spherical harmonic expansion of magnetic potential on a sphere of radius a are obtained by solving certain simultaneous equations. Then adjusting a so as to minimize the square sum of the second degree coefficients, the depth of the magnetic centre is determined to be 5.5 *km*, while the position is also obtained as shown on the map of Fig. 8 with a circle.

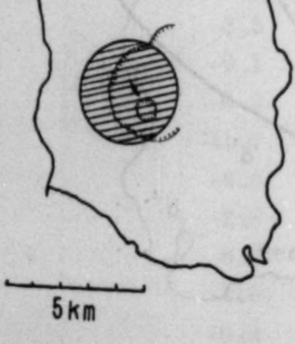

Fig. 8 The direction and position of the magnetic dipole by which the changes in geomagnetism are approximately explained. Hatched area shows the horizontal cross-section of the demagnetized region, where the original intensity of magnetization was assumed to be 0.03 *emu*, the eccentricity being introduced by the second degree term in the spherical harmonic expansion of the magnetic potential.

The obtained quantities are tabulated in Table IV. In order to compare the changes with those of the Miyake-sima erup-

---

[15] T. RIKITAKE, *Journ. Geomagn. Geoelectr.*, **2** (1950), 20 and 25.

Table IV.

The coefficients of spherical harmonic expansions and various quantities related to the determined magnetic dipoles.

		Ooshima	Miyake-sima
Coefficients	a_1^0	$-337\ \gamma$	$-300\ \gamma$
	a_1^1	130	140
	b_1^1	117	125
	a_2^0	128	107
	a_2^1	45	-47
	b_2^1	-40	-42
	a_2^2	11	-6
	b_2^2	-8	-3
Depth of centre		5.5 *km*	2.9 *km*
Azimuth of north seeking end		S42°E	S42°E
Dip of dipole		$-63°$	$-58°$
Magnetic moment		6.3×10^{14} *emu*	8.6×10^{13} *emu*

tion, a similar analysis is made with respect to Takahasi-Hirano's data, the results being also shown in Table IV.

The coefficients are given by the next expansion of magnetic potential on a sphere of radius a' which is the same with the depth of the dipole,

$$W = a' \sum_n \sum_m P_n^m (a_n^m \cos m\phi + b_n^m \sin m\phi), \ \ldots\ldots\ldots\ldots (5)$$

where the direction $\phi = 0$ is taken to the north.

Taking into account the direction of the magnetic dipole thus determined, the greatest part of the changes in geomagnetism obtained here is explained as the loss of magnetization in a roughly spherical region of which the centre is situated at a depth of about 5 *km*, the said depth as shown in Table IV, having been determined to be nearly 3 *km* in the case of the Miyake-sima eruption.

In the next place, some discussions on the intensity of magnetization and the shape of the mass by which the anomalous change may be caused will be made. As fully studied by Nagata[13] in the study of uniformity of natural remanent magnetization of rocks, the magnetic potential due to the magnetization of a mass of complex arbitrary form may be deduced from the gravitational potential as obtained by replacing the mass distribution by certain surface distribution, provided the shape does not deviate markedly from the sphere.

Let the surface of the mass be expressed by

$$l(\theta, \phi) = \sum_{n=0}^{\infty}\sum_{m=0}^{n} P_n^m (p_n^m \cos m\phi + q_n^m \sin m\phi), \quad \ldots\ldots\ldots\ldots (6)$$

where l denotes the distance of the surface from the apparent centre. When we take a as the radius of the mean sphere, the difference $l-a=d$ becomes

$$d(l, \phi) = \sum_{n=1}^{\infty}\sum_{m=0}^{n} P_n^m (p_n^m \cos m\phi + q_n^m \sin m\phi). \quad \ldots\ldots\ldots\ldots (7)$$

Since d/a is assumed to be small, the contribution of the mass distribution to the gravitational potential is almost the same with that of surface mass σ which is distributed on the sphere of radius a, where

$$\sigma(\theta, \phi) = a\rho/3 + \rho d(\theta, \phi), \quad \ldots\ldots\ldots\ldots\ldots\ldots (8)$$

and where ρ denotes the density.

The gravitational potential in the external space due to such surface distribution is readily given by

$$V = -\sum_{n=0}^{\infty}\sum_{m=0}^{n} (a/r)^{n+1} P_n^m (u_n^m \cos m\phi + v_n^m \sin m\phi), \quad \ldots\ldots (9)$$

where, by use of (7), (8) and (9), the coefficients are determined from potential-theory as follows;

$$u_0^0 = \frac{4\pi k^2 \rho a}{3}, \quad u_n^m = \frac{4\pi k^2 \rho n}{2n+1} p_n^m, \quad v_n^m = \frac{4\pi k^2 \rho n}{2n+1} q_n^m. \quad \ldots\ldots (10)$$

On the other hand, the magnetic potential due to uniform magnetization of the said mass is obtained from the well-known Poisson's relation. When the direction of the magnetization is taken in xz -plane with an angle ω from the vertical axis, the magnetic potential is given by

$$W = \frac{J}{k^2\rho}\Big\{\sin\omega\Big(\sin\theta\cos\phi\frac{\partial}{\partial r} + \frac{1}{r}\cos\theta\cos\phi\frac{\partial}{\partial\theta} - \frac{\sin\phi}{r\sin\theta}\frac{\partial}{\partial\phi}\Big)$$

$$+\cos\omega\Big(\cos\theta\frac{\partial}{\partial r} - \frac{\sin\theta}{r}\frac{\partial}{\partial\theta}\Big)\Big\}V. \quad \ldots\ldots\ldots\ldots\ldots\ldots (11)$$

From (11), W is calculated up to degree 2 as follows;

$$W=\frac{J}{k^2\rho}\Big[(a/r)^2(u_0{}^0\cos\omega P_1{}^0+u_0{}^0\sin\omega P_1{}^1\cos\phi)$$

$$+(a/r)^3\{(2u_1{}^0\cos\omega-u_1{}^1\sin\omega)P_2{}^0$$

$$+\sqrt{3}(u'_1\cos\omega+u_1{}^0\sin\omega\cos\phi+v_1{}^1\cos\omega\sin\phi)P_2{}^1$$

$$+\sqrt{3}(u_1{}^1\sin\omega\cos 2\phi+v_1{}^1\sin\omega\sin 2\phi)P_2{}^2\}\Big]. \qquad \ldots\ldots\ldots\ldots(12)$$

Equating the corresponding terms in (5) and (12) at $r = a'$, we get certain simultaneous equations from which $u_0{}^0$, $u_1{}^0$, $u_1{}^1$ and $v_1{}^1$ are solved. It must be noticed here that the direction of the magnetization is taken in xz -plane, hence the coefficients given in Table IV should be transformed to a suitable coordinate in the actual application of the above-mentioned method. After applying the method to the geomagnetic changes in Ooshima Island, we obtain

$$u_0{}^0=0.00380\frac{k^2\rho a'}{J}\left(\frac{a'}{a}\right)^2, \qquad u_1{}^0=-0.00063\frac{k^2\rho a'}{J}\left(\frac{a'}{a}\right)^3,$$

$$u_1{}^1=-0.00037\frac{k^2\rho a'}{J}\left(\frac{a'}{a}\right)^3, \qquad v_1{}^1=0.00040\frac{k^2\rho a'}{J}\left(\frac{a'}{a}\right)^3. \qquad (13)$$

Taking into account the relation (10), we have

$$J=0.00380\times\frac{3}{4\pi}(a'/a)^3,\ p_1{}^0=-0.165\,a,\ p_1{}^1=-0.097\,a,\ q_1{}^1=0.104\,a. \qquad \ldots\ldots(14)$$

If we adopt 0.03 *emu* as the intensity of magnetzation as obtained in section 4, the radius of the mean sphere a amounts to 1.7 *km*. For the lowest possible value 0.01 *emu* of the mean intensity of magnetization for volcanoes of basaltic rocks, we also obtain $a=2.5$ *km*. Hence the changes in magnetic dip in Ooshima Island seems to be caused mainly by the demagnetization of a roughly spherical region of which the centre is situated at a depth of about 5 *km* and the mean radius about 2 *km*.

The unevenness of the surface can be further estimated from (14). The horizontal cross-section at the centre thus obtained is shown in Fig. 8. Although the unevenness of higher order is neglected, it will be recognised that the shape of the mass does not materially differ from the sphere.

As clarified in the foregoing pages, the changes in the earth's magnetic field that accompanied the eruption of Volcano Mihara are explained as the apparent magnetization of an underground spherical region, the centre of the mean sphere being situated at a depth of several *kilometers* just beneath the centre of the island. The deviation of the shape of the region from the sphere seems to be comparatively small as shown, for example, in Fig. 8. Since the direction of magnetization is roughly opposite to that of the earth's magnetic field, we may presume that the said region lost its magnetic property owing to the rise in temperature associated with the eruption. Taking a probable value as the intensity of magnetization, the radius of the region is estimated to be about a few *kilometers*. Thus it may be presumed that the temperature in a roughly spherical region having a radius of a few *kilometers* becomes higher than the Curie-point of rocks in connexion with the volcanic activity.

8. Summary and conclusion.

Comparing the results of the first and second surveys over Ooshima Island, marked changes in the earth's magnetic field were found out during the period from beginning to end of the eruption of Volcano Mihara, 1950. The magnetic dip-angle decreased all over the island. The largest value of the decrease amounted to as much as 30 *minutes* of arc. Applying the method devised by the writer for finding out the position, intensity and direction of an underground magnetic dipole directly from the distribution on the earth's surface, it was found that the changes obtained here may be almost explained as due to a dipole situated just beneath the centre of the island at a depth of 5.5 *km*, the direction being approximately opposite to the earth's magnetic field. Taking into account the intensity of magnetization of rocks composing the volcano, the generation of the dipole may be attributed to the demagnetization of a roughly spherical region having a radius of a few *kilometers*, while the demagnetization seems to be due to the rise in temperature in the said region associated with the eruption. It is of interest that the general mode of the change closely resembles that observed in the case of Volcano Miyake-sima where the rocks composing the volcano is also basalt.

Comparison with the survey carried out in 1936 was also made. However, no marked changes were to be found. The writer also studied the local anomaly in magnetic dip from which the mean intensity of magnetization was estimated to be about 0.03 *emu*.

In the course of the study, the writer was encouraged by his senior colleagues. The writer wishes to express his hearty thanks to Professor H. Tsuya, Professor R. Takahasi, Professor T. Hagiwara, Professor T.

Minakami, and Dr. T. Nagata for their helpful advices. To Dr. S. Imamiti and Mr. M. Hirayama of the Kakioka Magnetic Observatory who placed magnetic data at the writer's disposal, the writer's cordial thanks are also due. The writer also wishes to express his appreciations to Mr. K. Kasahara, Mr. S. Saito, and Miss Y. Hishiyama who assisted the writer in the field-measurement. The study was done with the financial aid of the research grant from the Deparment of Education, and the writer wishes to express his cordial thanks for the grant received.

---

14. 伊豆大島における地磁氣伏角分布と三原山噴火に伴うその變化

地震研究所　力武常次

1950年7月の三原山噴火に際して，地震研究所製小型磁氣感應儀を用いて，2回にわたり地磁氣伏角測定を實施した．伏角の分布は，從來多くの火山についてしらべられたように著しい異常を示して，最小 46°，最大 56° にわたつている．この異常より山体の平均帶磁の强さとして 0.03 *emu* がえられた．1936年の高橋，永田兩博士の測量と比較して，いちじるしい變化は見出されなかつたが，島全体にわたり伏角が數分程度增加していることになつた．

噴火の初期と末期の比較から，最大 30′ に達するいちじるしい伏角の減少が見出された．この變化は 1940年三宅島噴火の際の地磁氣變化によく似ていて，解析の結果，島の中心部の地下 5.5 *km* のところに中心をもつ，半徑約 2 *km* の近似的に球形の部分が，その帶磁を失つたと考えれば解釋出來ることになつた．すなわち，上記の部分が火山活動に伴つてキューリ點以上の高温になつたとすればよいことになる．

15. *Relations between the Earthquake Damage and the Structure of Ground in Nagoya City.*

By Syun'itiro Omote and Setumi Miyamura,

Earthquake Research Institute.

(Read Nov. 21, 1950.—Received Dec. 20, 1950.)

1. Introduction.

Certain relations are likely to exist between the geologic structures of the ground at a place and the earthquake damage produced on it. The authors have investigated this problem, with special reference to the city of Nagoya which is one of the typical places in which the relations are manifested. The subsurface geologic structures in Nagoya are known by seismic prospectings which covered the large part of the city, and, on the other hand, the details of the distribution of earthquake damages wrought by the Tokaido Earthquake of Dec. 7, 1944 have been made fairly clear through the efforts of the municipal authorities. Consequently sufficient data are now available for the purpose of the present study.

2. Topography of Nagoya City.

The general topography of the city will been seen in Fig. 1. Generally speaking, the hilly grounds, which cover the eastern and northern parts of the city, gradually slope down towards south-west. The south-west part of the city consists mainly of paddy fields, which have expanded out year after year by reclamation. The history of expansion of these low-lands may be traced in Fig. 5, compliled by Mr. Ota as the result of his long investigations of it. (cf. §4.)

3. The distribution of earthquake damage.

Nagoya was attacked by a violent shock on Dec. 7, 1944 and a lot of houses were destroyed. Most of the original records by the municipal and governmental authorities which contained data as to the detailed statistics of the houses destroyed were unfortunately burnt down during the world War II fires. Fortunately some of the original records have escaped the fire, while others were prepared again by the said authorities. Consequently,

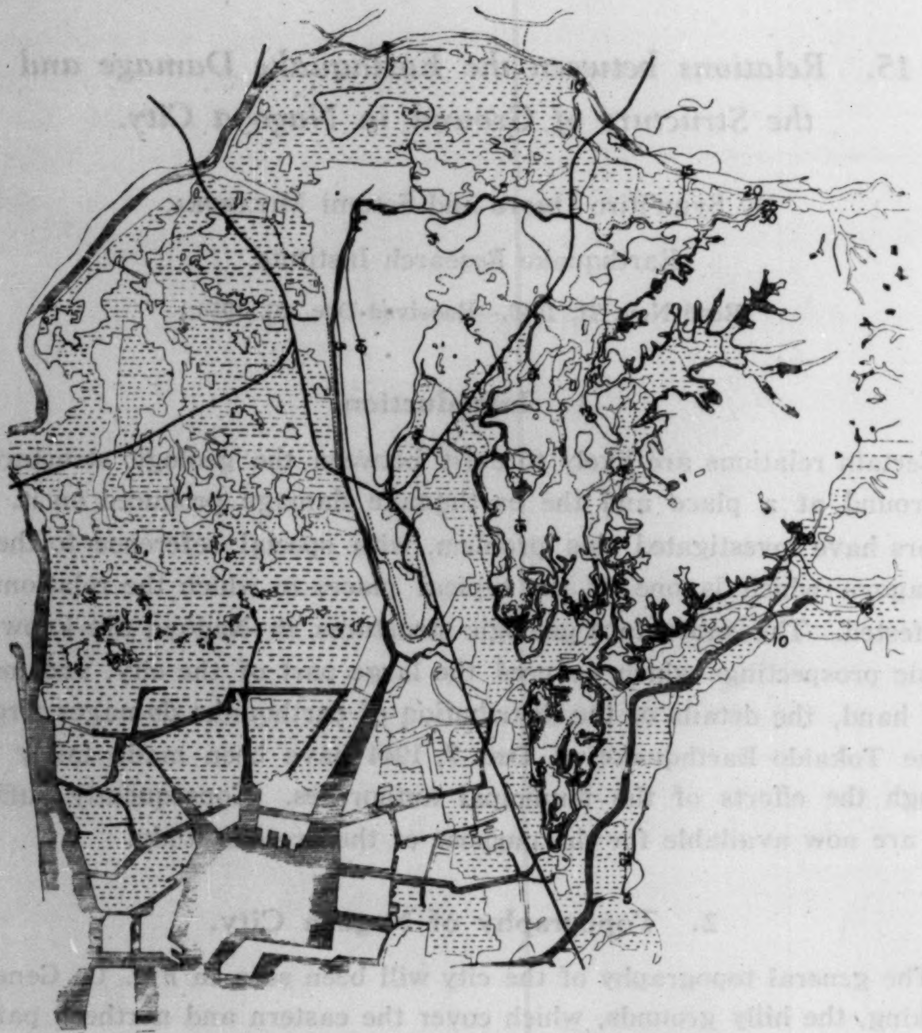

Fig. 1. General topography of Nagoya City.

N.B. ▨ : Paddy field.before 1900 A.D.

the distribution of destroyed houses has been made pretty clear throughout the whole city. A) The city is divided into 14 administrative divisions (*ku*), for each of which the damage rate *k* was calculated. *k* is defined as the ratio of (the number of the totally destroyed houses plus 1/2 of that of the partly destroyed houses) to (the total number of houses), both within the unit division under question respectively. Fig. 2 shows the distribution of the value of *k* thus calculated for the "*ku*" division. B) Each *ku* is divided into several subdivisions called "*ren-ku*", and the damage rate *k* for each "*ren-ku*" has been calculated, the result being shown in Fig. 3. In these figures, we see clearly that large damage rates are confined in some particular divisions. C) For the purpose of examining the distribution of the damage rate in the city in more datail, we further investigated the distribution in still smaller divisions "*tyo*" into which each "*ren-ku*" is divided. The damge rate with respect to each *tyo* is shown in Fig. 4. In the figure we see that the value of the damage rate for each *tyo* is by no means the same as that for *ren-ku* to which it belongs; some being very small while others very large.

4. The structure of ground within the city.

The subsurface geologic structure of Nagoya City was made clear by means of various methods. The geology of Nagoya is in general as follows:

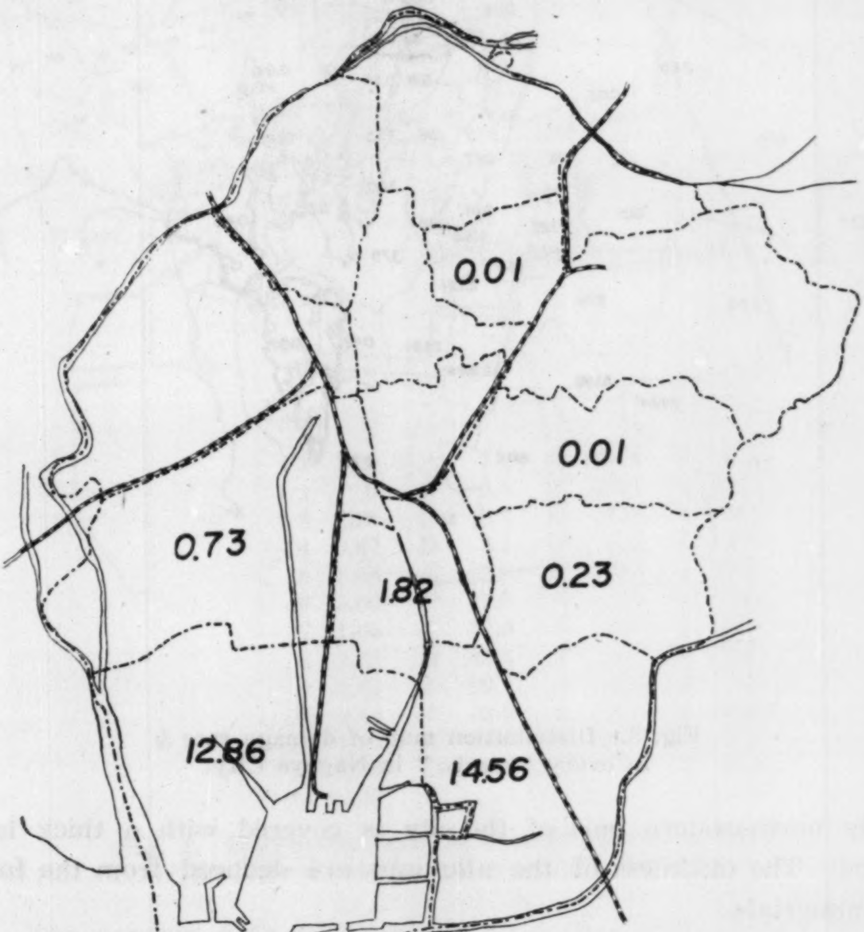

Fig. 2. Distribution map of damage rate *k* in every "*ku*" in Nagoya City.

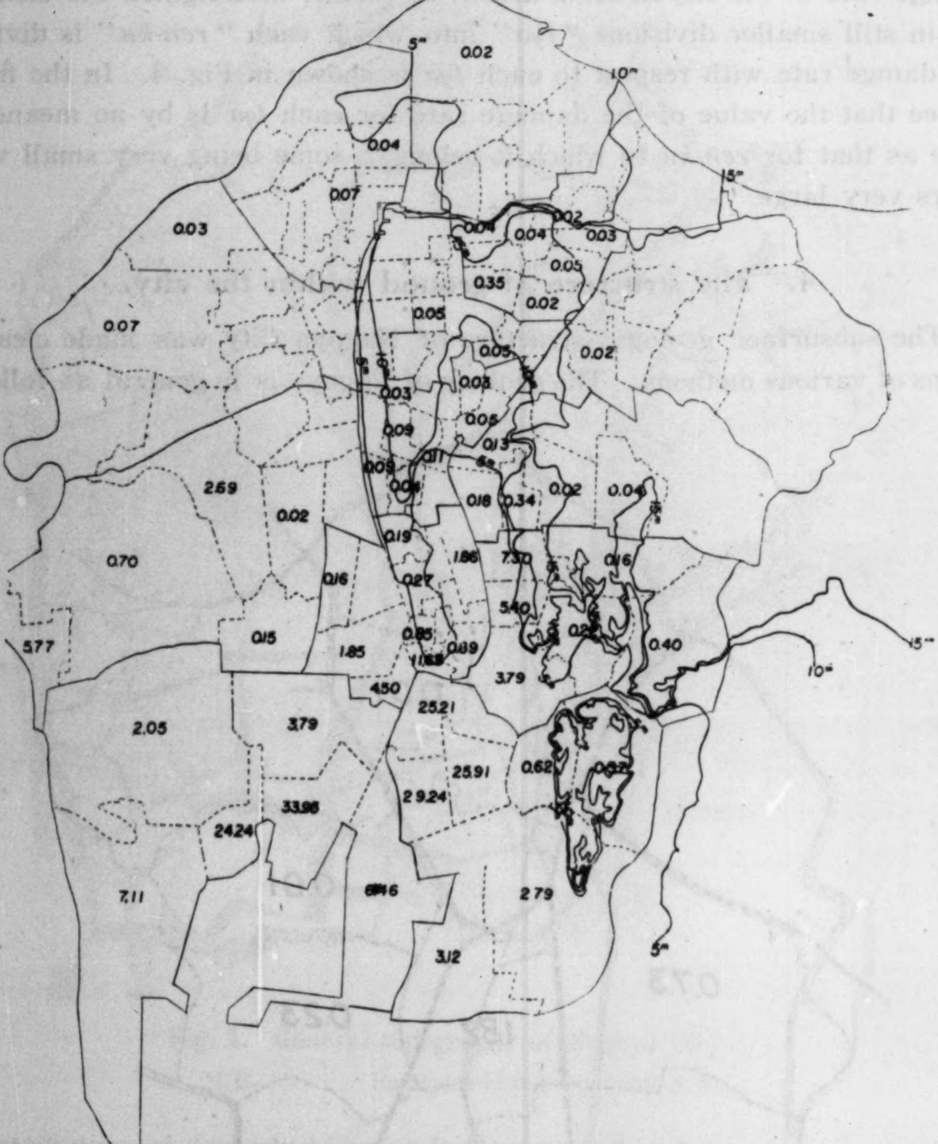
5"
0.02
10"
0.04
15"
0.07
0.03
0.04
0.04
0.02
0.03
0.05
0.35
0.02
0.07
0.05
0.05
0.02
0.03
0.03
0.09
0.05
0.13
0.11
0.09
0.08
2.59
0.18
0.34
0.02
0.04
0.02
0.19
1.86
7.30
0.16
0.70
0.16
0.27
5.40
0.22
5.77
0.15
1.85
0.85
0.89
11.83
0.40
15"
10"
3.79
4.50
25.21
2.05
3.79
25.91
0.62
29.24
33.96
24.24
68.46
2.79
7.11
5"
3.12

Fig. 3. Distribution map of damage rate k in every "*ren-ku*" in Nagoya City.

the hilly north-eastern part of the city is covered with a thick layer of alluvium. The thickness of the alluvium are deduced from the following source-materials:

i) The boring data. The columnar structures of the core borings carried out at 13 points in the city were available, but, to our great regrect, the description of the core samples was too inadequate to be useful to determine the boundary of geological formations.

Besides, since these borings were carried out to a depth of only 25 meters the base of the alluvium was not arrived at in the southwest part of the city. Thus these data could not be used for our present purpose.

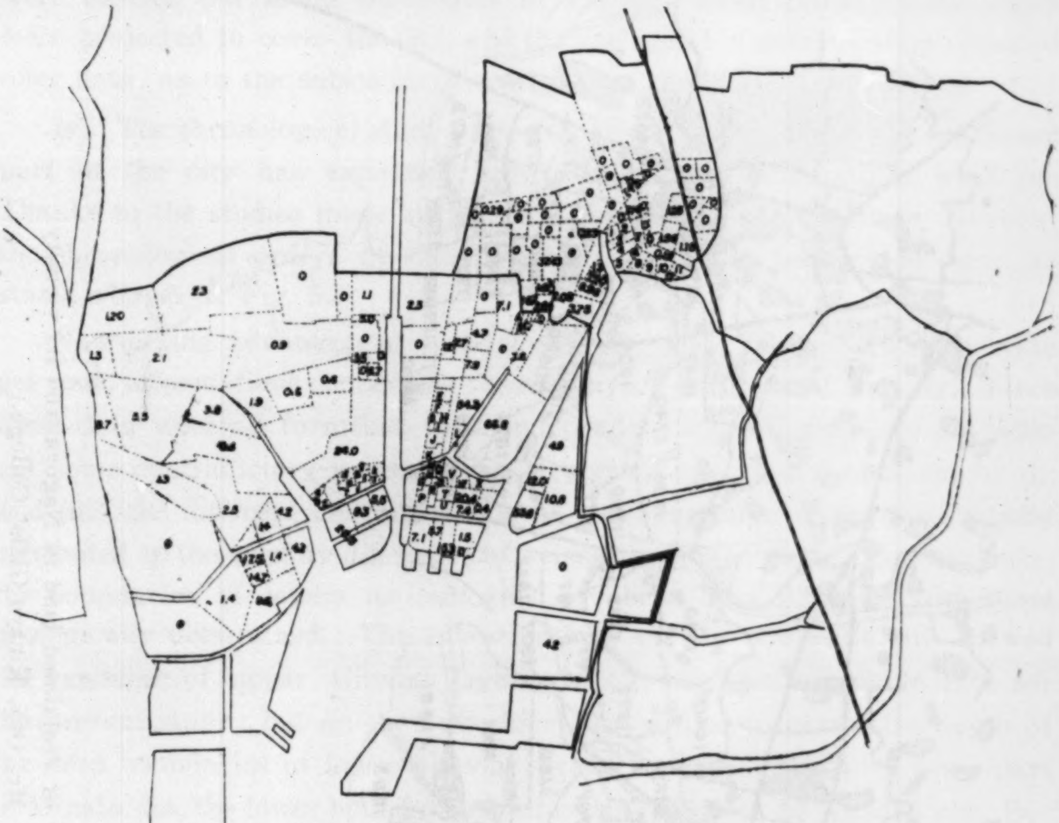

1	1.12	*A*	7.1	*M*	51.8	*a*	35.1
2	0	*B*	3.5	*N*	13.9	*b*	10.1
3	2.25	*C*	0.3	*O*	11.5	*c*	42.1
4	0.67	*D*	3.1	*P*	9.5	*d*	6.2
5	1.68	*E*	69.5	*Q*	5.5	*e*	42.0
6	5.00	*F*	47.0	*R*	4.5	*f*	1.8
7	1.00	*G*	77.8	*S*	3.5	*g*	42.8
8	1.25	*H*	48.5	*T*	2.2	*h*	17.5
9	1.60	*I*	29.7	*U*	6.0	*i*	7.2
10	9.14	*J*	39.8	*V*	2.1	*j*	15.0
11	1.90	*K*	61.5	*W*	19.5	*k*	47.6
12	1.68	*L*	87.3	*X*	7.0	*l*	11.8
13	13.23						

Fig. 4. Distribution map of damage rate k in every "*tyo*" in Minato-*ku* and a part of Atuta-*ku*.

ii) The seismic data obtained by Prof. K. Sassa, Kyoto University. Seismic prospectings were carried out soon after the end of the World War II throughout the whole city by Prof. Sassa, Kyoto University. The results obtained afforded very useful materials concerning the subsurface structure of the city.

the base of the alluvium was not arrived at in the southwest part of the city. Thus these data could not be used for our present purpose.

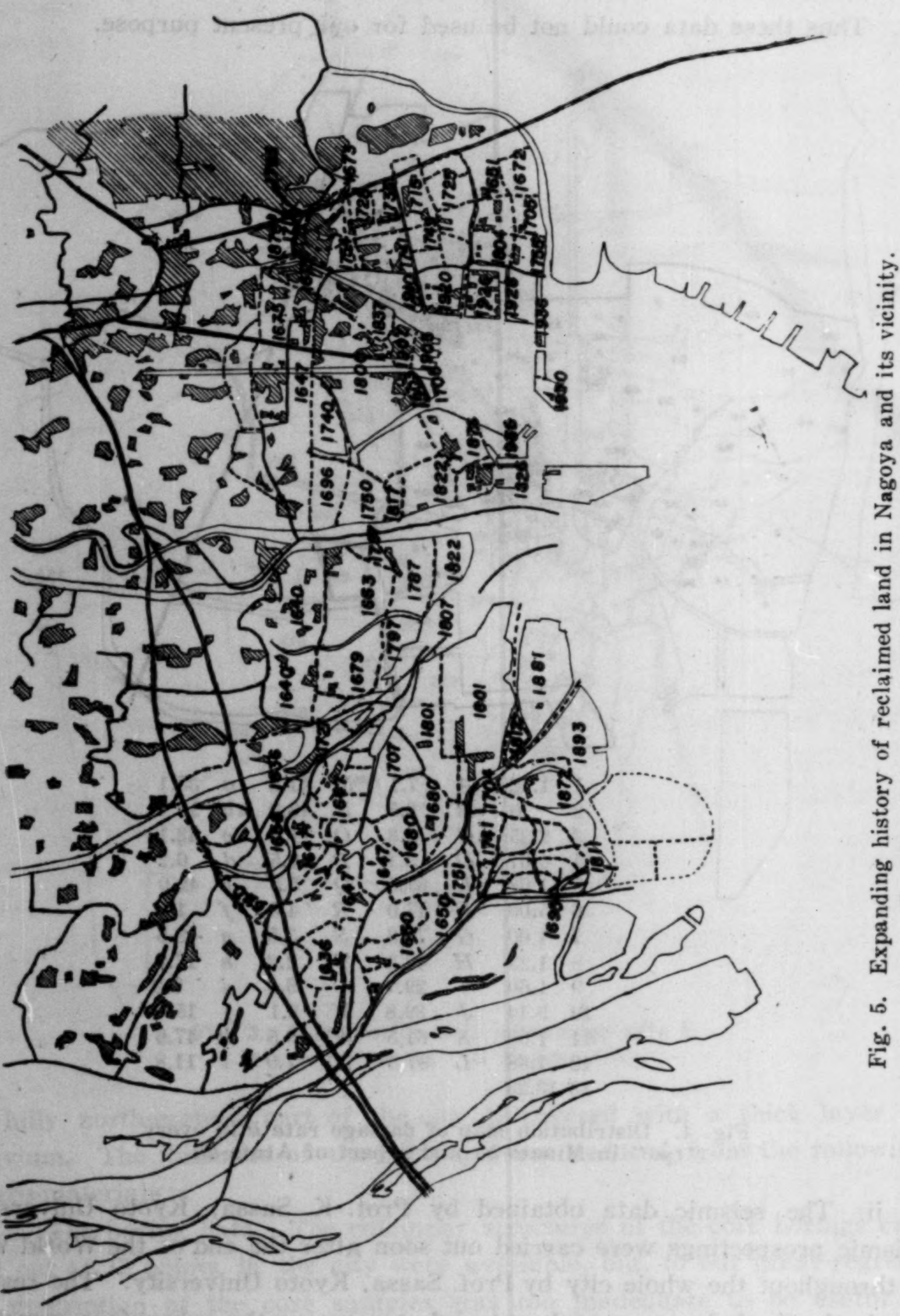
1673
1725
1672
1708
1804
1795
1928
1938
1820
1657
1809
1690
1647
1673
1740
1696
1750
1817
1822
1926
1928
1640
1683
1787
1822
1807
1797
1679
1640
1801
1801
1881
1893
1872
1707
1680
1650
1751
1761
1911
1896
1650
1659
1647
1636

Fig. 5. Expanding history of reclaimed land in Nagoya and its vicinity. (Compiled by Mr. Ota, Kinzyo Girls' College.)

iii. The seismic data obtained by Prof. K. Sassa, Kyoto University. Seismic prospectings were carried out soon after the end of the World War II throughout the whole city by Prof. Sassa, Kyoto University. The results obtained afforded very useful materials concerning the subsurface structure of the city.

iii) The seismic data by the Nippon Geophysical Prospecting Co. along the routes of the projected high speed railway lines. Seismic prospectings were carried out along the routes of the high speed railway lines which were projected to cover the city, and the geological structures thus revealed offer data, as to the subsurface structures of the city.

iv) The chronological study of reclamations. The area of the southwest part of the city has expanded gradually as the reclamations went on. Thanks to the studies made by Mr. Ota, the Kinzyo Girls' College, Nagoya, the chronological orders of these reclamations have been made clear, as stated above. (s. Fig. 5.)

Now taking advantage of these source materials the authors intended to get some informations concerning the subsurface structure of the city. Since these data were all furnished from independent sources, they are not without some contradictory points. In interpreting the results obtained by (ii) and (iii), the different characteristics of the respective strata were wholly attributed to the velocity difference of seismic waves in them. Consequently, the boundaries of layers as indicated by these data disagree with those geologically determined. The investigations of the materials (iii) showed the existence of upper alluvial layers, which furnished valuable data for the present study; but on the other hand they failed to reveal the depth of the deep boundaries of lower alluvial strata, and accordingly in some part in Minato -*ku*, the lower boundary of alluvium could not be decided clearly.

Looking at these data obtained from (ii) and (iii), we have become aware that the alluvium here is divided into two layers, the upper and the lower. The upper one has a thickness of a few meters or so and the velocity of seismic waves within it is about 200~500 m/s, while the lower one has much larger thickness and shows much higher value of the wave velocity. The upper one is considered to be made of reclaimed mud or sediments of very new ages and we shall call this "the upper alluvium". The lower layer has the velocity value of 1500 m/s, corresponding to the moderate value for the so-called alluvium and we shall call this "the lower alluvium".

The thickness of the upper alluvium. Consulting the geological sections derived from (ii) and (iii), the thickness of the upper alluvium differs very much at various places. Though the seismic prospectings covered the whole city with a fairly dense network, it could by no means be said that the data prepared are plenty enough for the contour map for the thickness of the upper alluvium to be drawn. Taking these points into account we prepared in Fig. 6 a map which shows the thickness of the upper alluvium.

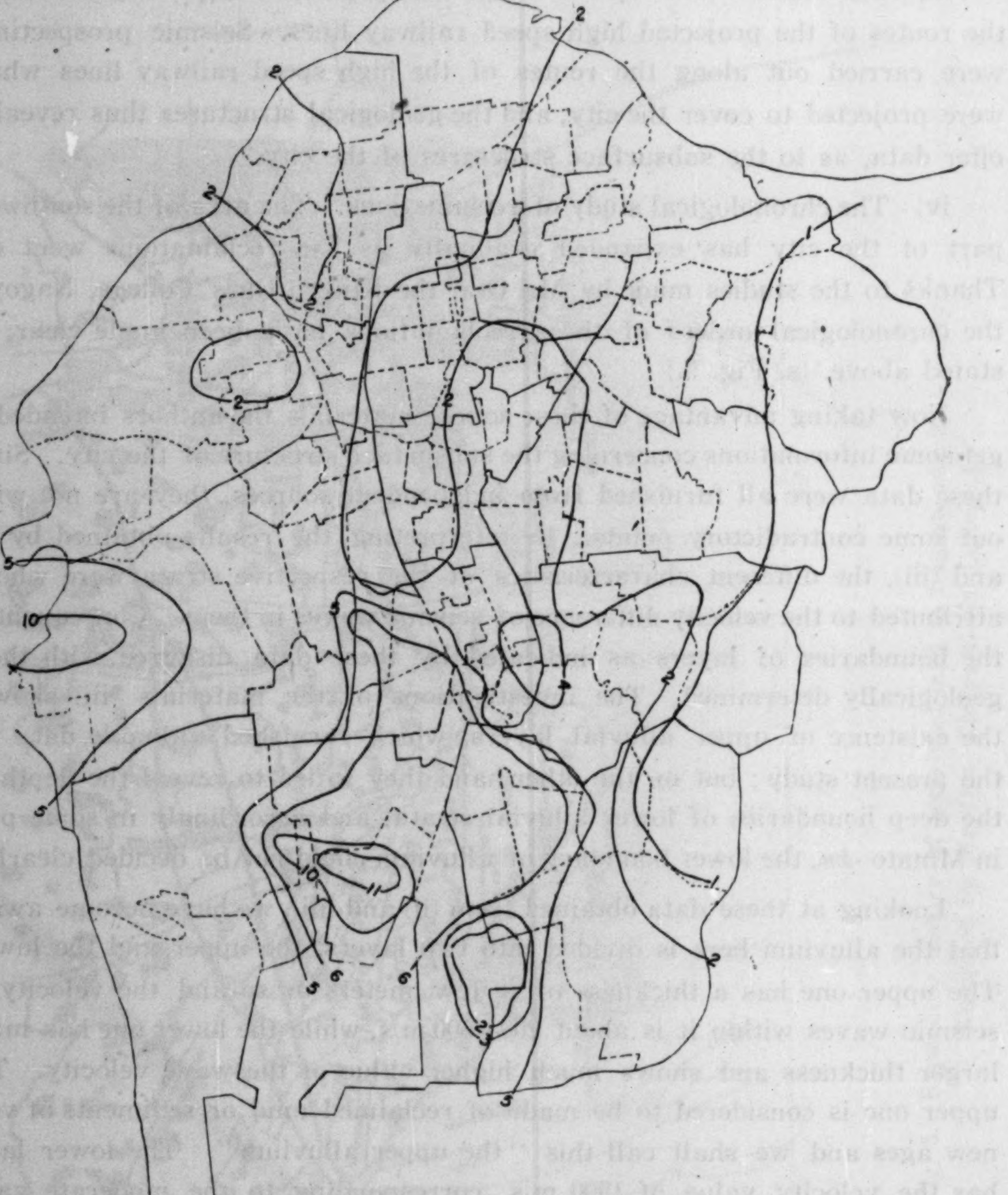

Fig. 6. Thickness of "the upper alluvium" in Nagoya City.

At first, the contour lines for every one meter were aimed at, but in some places this was not possible.

The thickness of the lower alluvium. Next, the thickness of the lower alluvium must be examined, because they have probably some close relationship to the earthquake damage. As was already stated, it was very difficult to correlate the layer succession, obtained by seismic prospectings, to that, defined from the geological point of view. As a rule, in the plain area of the southwest part of the city, the layer, in which the propagation velocity of P wave is higher than 2 km/sec. is as deep as 30~50 meters, while in the hilly regions the same velocity can be found even in the uppermost layer. From these reasons, the velocity of 2.0 km/sec. was attri-

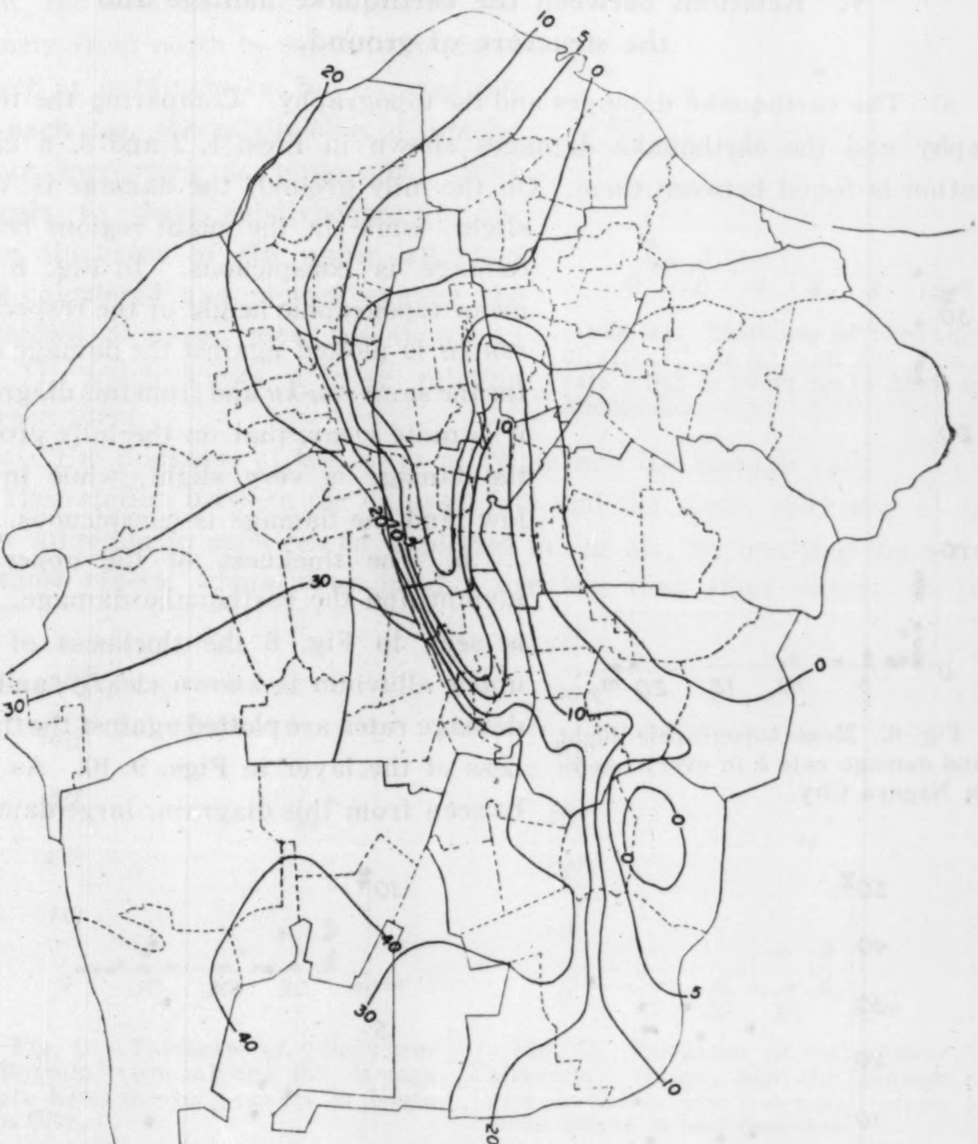

Fig. 7. Thickness of "the lower alluvium" in Nagoya City.

buted to the geological layer of the lower alluvium. The thickness of the lower alluvium within the whole city is shown in Fig. 7, by a family of contour lines.

From the above three figures (Figs. 5, 6 and 7) the general picture of the subsurface structure of the whole city may be obtained.

5. Relations between the earthquake damage and the structure of ground.

a) The earthquake damages and the topography. Comparing the topography and the earthquake damages shown in Figs. 1, 2 and 3, a close relation is found between them. On the hilly ground, the damage is very slight, while in the plain regions heavy damage is conspicuous. In Fig. 8 the mean topographic height of the respective *ren-ku* is plotted against the damage rate for the same *ren-ku* and from this diagram, it is quite clear, that on the hilly ground the damage is very slight, while in the low land the damage is conspicuous.

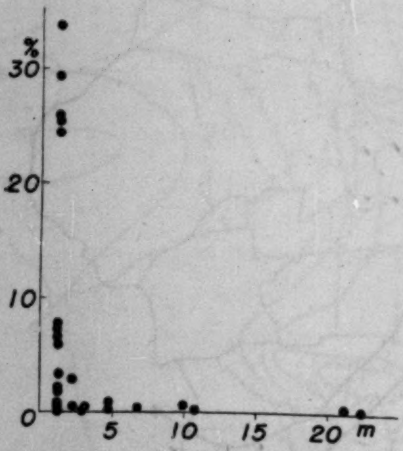

Fig. 8. Mean topographic hight and damage rate *k* in every *ren-ku* in Nagoya City.

b) The thickness of the upper alluvium and the earthquake damage. As is seen in Fig. 6 the thickness of the upper alluvium is known clearly, and the damage rates are plotted against the thickness of the layer in Figs. 9, 10. As will be seen from this diagram, large damage

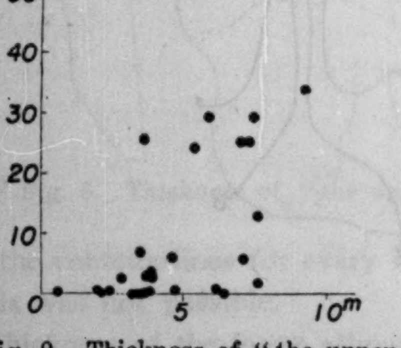

Fig. 9. Thickness of "the upper alluvium" (in m) and the damage rate *k* (%) in every *ren-ku* in Nagoya city.

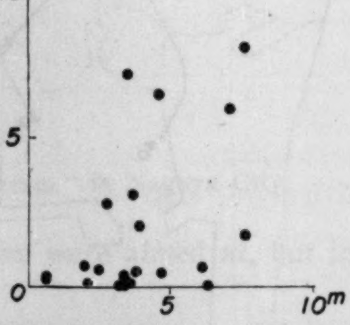

Fig. 10. Thickness of "the upper alluvium" (in m) and the damage rate *k* (%) in every *ren-ku*, whose *k* is smaller than 10%.

rates are seen only in the areas where the thickness of the upper alluvium are also large. But it must not be overlooked here that these simple relations are seen only when the unit area is taken as large as "*ren-ku*". This simple relation does not so clearly holds, if the unit area is taken smaller. As was already seen in Fig. 7, the thickness of the alluvium revealed from the seismic data, increases uniformely from north to south in Atuta-*ku* as well as in Minato-*ku*, but damage rate for each *tyo*, the subdivision of *ren-ku*, is not increasing so uniformly. With regards to these subdivisions *tyo*, the mean thickness of the upper alluvium were calculated and plotted against the respective damage rates, as shown in Fig. 11, which shows a close relation between them.

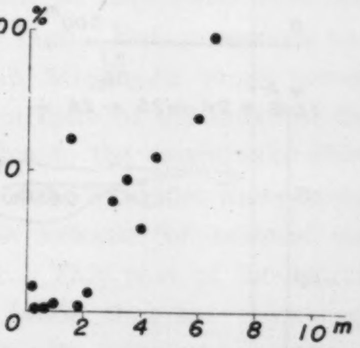

Fig. 11. Thickness of "the upper alluvium" (in m) and the damege rate *k* (%) in every *tyo* in Atuta and Minato-*ku*.

c) The thickness of the lower alluvium and the damage rate.

The relation between the damage rate and the mean thickness of the lower alluvium in each *ren-ku* is plotted in Fig. 12. By omitting the points for those *ren-ku*, whose mean heights are less than three meters, we immediately obtain Fig. 13, which shows a close linear relation between the damage rate and the thickness of the lower alluvium. In Fig. 14 the subsurface structures obtained from seismic prospecting data are compared with the earthquake damage in every *tyo* in Atuta-*ku* and in Minato-*ku*.

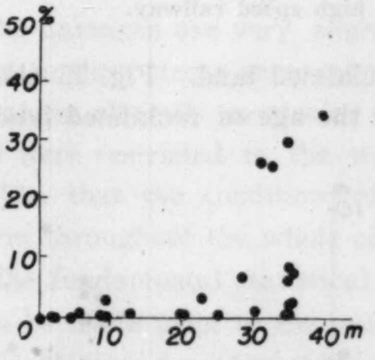

Fig. 12. Thickness of "the lower alluvium" (im m) and the damage rate *k* (%) in every *ren-ku* in Nagoya City.

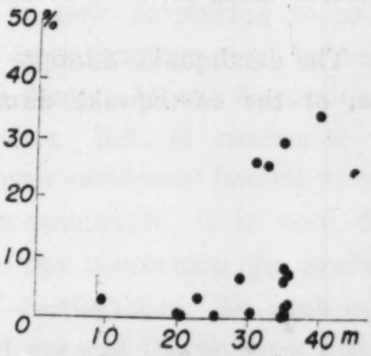

Fig. 13. Thickness of "the lower alluvium" (in m), and the damage rate *k* (%) in every *ren-ku*, whose mean height is less than 3 m.

In spite of the uniform increase of the thickness of the lower alluvium, the increase of damage is by no means parallel with it. The damage there may have probably rather closer relation to the thickness of the upper alluvium as already described in the preceding section b).

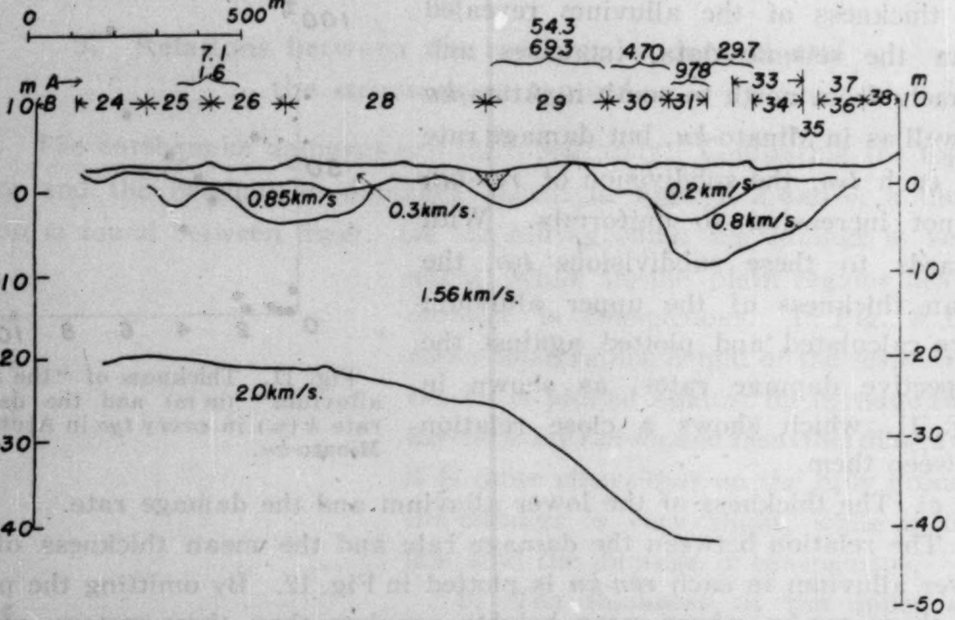
0
500m
7.1
1.6
54.3
69.3
4.70
978
29.7
33
37
m A→
10 8
24
25
26
28
29
30
31
34
36
38
35
m
10
0
-10
-20
-30
-40
-50
0.85km/s
0.3km/s.
0.2km/s
0.8km/s.
1.56km/s.
2.0km/s.

Fig. 14. Subsurface structure of ground, as indicated by seismic wave velocity (km/sec), and the damage rate *k* (%) in every *tyo* in Atuta- and Minato-*ku* along the route of the projected high speed railway.

d) The earthquake damage in the reclaimed land. Fig. 15 shows the relation of the earthquake damage and the age of reclaimed land in the

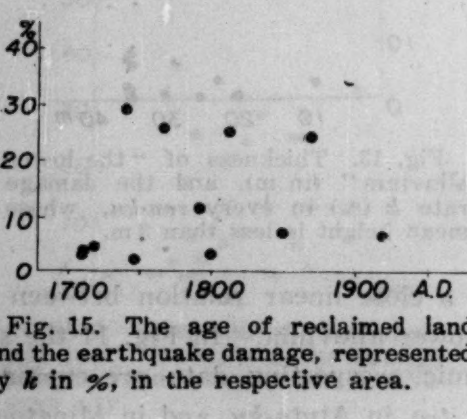

Fig. 15. The age of reclaimed land and the earthquake damage, represented by *k* in *%*, in the respective area.

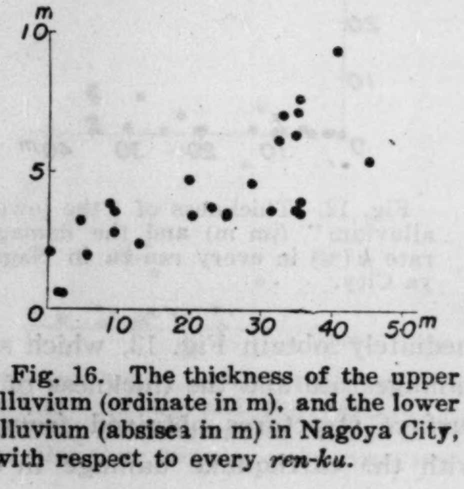

Fig. 16. The thickness of the upper alluvium (ordinate in m), and the lower alluvium (absisca in m) in Nagoya City, with respect to every *ren-ku*.

southern part of the city, and it can be said that there is at any rate a general tendency of a proportionality between them.

6. Concluding remarks.

From above considerations it may be said, at any rate, that where the alluvium is thick, the damage rate is also high. But, according to the investigations carried out in Atuta-*ku* and in Minato-*ku* more minutely with regards to each *tyo*, it was noticed that in spite of the uniform thickness of the lower alluvium, the damage rate due to the earthquake showed a very irregular distribution. The upper part of the alluvium was composed of soft muddy layer with a low propagation velocity of seismic wave. The thickness of this layer was very irregular. This part of the alluvium was called as "the upper alluvium" and we found that the thickness of the upper alluvium also play an important rôle upon the earthquake damage.

With all these considerations, however, it is still difficult to say to what extent the respective thickness of the upper and the lower alluvium affects to the damage rate. In Nagoya City the respective thickness of these layers is so closely related mutually as shown in Fig. 16, so that it will be almost impossible to know the separate influence of these two layers uppon the damage rate, provided only the data here reproduced were used.

In the northwestern part of the city, the lower alluvium is fairly thick, and the damages are very slight. This is very perplexing to us. With respect to these areas some more detailed investigations must be performed for making clear the particular conditions there. All the discussions above stated were restricted to the wooden houses. But, of course, it is quite probable, that the conditions of the wooden residental houses may not be uniform throughout the whole city and, consequently, it is very desirable that the fundamental statistical investigations concerning the conditions of houses be made prior to the occurence of earthquakes. No such investigations in Nagoya have been hitherto carried out and the uniform distribution of the conditions of the wooden houses had to be assumed. These assumptions, of course, are quite rough, so the detailed discussions can not be promoted further from these materials here given.

Though many questions are still left for furture investigations, we are convinced ourselves that the conclusions derived in this paper will furnish some new light to the relations between the earthquake damage and the structure of ground in Nagoya City.

7. Acknowledgments.

In conclusion the authors wish to express their hearty thanks to Dr. T. Tamaki, the Chief of the Architectural Section of the Provincial Office of Aiti, for his kind encouragements. Strong support of the Architectural Research Institute, Ministry of Construction, given to the present study is greatly acknowledged, too. Thanks are also due to Mr. Ota, Kinzyo Girls' College, Dr. K. Sassa, Kyoto University, and Dr. T. Watanabe, Nippon Geophysical Prospecting Co., for their kindness permitting us to use their valuable data.

The helpful cooperations of the provincial and municipal authorities of Nagoya in providing the necessary source materials must be here also gratefully acknowledged. Parts of the expense for the present study were defrayed from the fund of the Education Ministry, "Siken-Kenkyu-hi", and the grant from the Provincial Office of Aiti Prefecture.

15. 名古屋市における地盤と震害の關係

地震研究所 {表 俊一郎
宮村 攝三

名古屋市における地形，地下構造，埋立地の古さ等地盤の性質をしめす資料をあつめ，昭和19年12月7日の東海道地震による同市内の震害分布を調査し，これらの間の關係について考察した。

おもな結論として，一般に沖積層のあつさと震害の間に比例關係が見出されたが，こまかく區劃をわけ，町別位についてみると，かならずしもきれいに行かない。こゝに表土層の影響があらわれる。兩者はそれ自体第16圖にみるような關係をもつため，これらの影響を分離することはむつかしい。

16. *On Ground Vibrations Caused by Explosions.*

By Ryôhei IKEGAMI,

Earthquake Research Institute.

(Read Oct. 17, 1950. – Received Dec. 20, 1950.)

1. Introduction.

The seismic waves caused by the detonation of explosives such as dynamite or powder have been utilized for prospecting underground materials, and each phase of the waves has been elucidated. In America, however, a wave new to seismology was found for the first time by L. Don Leet[1] and again by B.F. Howell.[2] Concerning this new wave Leet stated as follows: "It causes a particle in its path to move in a longitudinal-vertical plane, clearly independent of motion on the transverse component at the same time. The unique and significant thing about the motion is that it is the opposite of the Rayleigh wave and the particle at the top of its inclined elliptical orbit moves forward as for a wave on water. For that reason it has been called a Hydrodynamic wave and tentatively labelled H."

It is worth while to ascertain whether this wave can be found in Japan or not.

We recently carried out an experimental investigation of the ground vibrations at Minami-Sunamachi, Kôtôku, Tôkyô, and we have the records obtained on that occasion by us now. The two seismometers used in the present investigation were Kishinouye's horizontal tromometers,[3] and we adjusted their periods of free vibrations to 5 seconds, their magnifications to 480, and the damping to critical. As these seismometers were originally intended for the study of microseisms, the speed of recording bromide-paper is 19 millimeters per second and too slow to distinguish the such quick oscillations as P- or S-wave, and further, these instruments do not carry the equipments to superimpose a mark of shot time on the record. Consequently we can not measure the travel time of the wave directly. Therefore these records are somewhat inconvenient for the purpose of studying a new wave.

---

[1] L. DON LEET, *American Scientist, Spring Issue*, **34** (1946), 198.

[2] B.F. HOWELL, *Bull. Seism. Soc. Amr.*, **39** (1949), 285.

[3] F. KISHIOUYE. *Bull. Earthq. Res. Inst.*, **20** (1942), 215.

On the other hand these seismometers have long periods in comparison with those of the ground motion. Therefore we can expect records quite distinct from those recorded by the conventional geophone with short period.

The one seismometer was set to respond to motions toward and away from a shot point and the other perpendicular to this, and the distances from the shot point to the seismometers were varied 40, 48, 70 and 80 meters.

A shot hole with a depth of 3 meters was drilled and shots of 45 grams (1 unit) or 67.5 grams (1.5 units) of 60% dynamite were made at the bottom of the hole.

Time-marks were electrically sent out every second from a chronometer and recorded on the records.

We could obtain five records at 48 and 80 meters distant from the shot point, respectively, but we could obtain only one record at 40 and 70 meters, respectively. Therefore we mainly depend on the records obtained at 48 and 80 meters.

2. Wave Form.

Fig. 1 shows the records observed at the distances of 48 and 80 meters, respectively, and in each distance the two records represent the motions of longitudinal and transverse components. These records are shown as an example at the respective distances and the other records at the same distance have completely similar wave forms. The records observed at the distances of 40 and 70 meters have also similar wave forms, though the records are not shown in the figure.

We will not touch on the parts of P- and S-waves, because both the amplitudes and the periods of these parts are too small and short to be measured clearly. The waves arriving after these parts have large amplitudes and long periods, and at various distances the phases are so similar in longitudinal component that they correspond to one another. The amplitudes of transverse component are remarkably small in comparison with those of loegitudinal component, and each phase hardly corresponds to each other at various distances. This fact suggests that the earth motions of this part predominate in longitudinal component and that these waves have the Rayleigh wave type.

This time we have analysed the waves using longitudinal component.

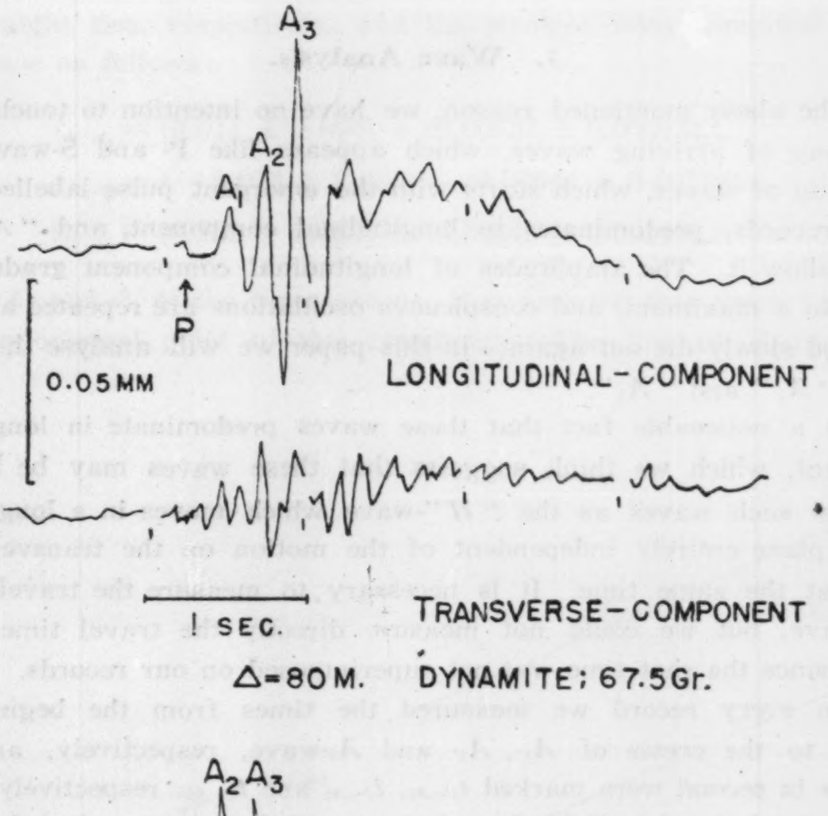

Fig. 1. Records of ground motion at distances of 80 and 48 meters.

3. Wave Analysis.

By the above mentioned reason, we have no intention to touch on the first group of arriving waves, which appears like P- and S-wave. The next group of waves, which starts with the emergent pulse labelled "A_1" on the records, predominates in longitudinal component, and "A_2" and "A_3" follow it. The amplitudes of longitudinal component gradually increases to a maximum, and conspicuous oscillations are repeated about ten times and slowly die out again. In this paper we will analyse the waves, "A_1", "A_2" and "A_3".

It is a noticeable fact that these waves predominate in longitudinal component, which we think suggests that these waves may be Rayleigh waves or such waves as the "H"-wave which moves in a longitudinal-vertical plane entirely independent of the motion on the transverse component at the same time. It is necessary to measure the travel time of each wave, but we could not measure directly the travel time on our records since the shot time was not superimposed on our records. Accordingly on every record we measured the times from the beginning of P-phase to the crests of A_1-, A_2- and A_3-wave, respectively, and these intervals in second were marked t_{P-A_1}, t_{P-A_2} ane t_{P-A_3}, respectively. These velues are tabulated in Table I, and the travel time curves plotted by these values are shown in Fig. 2. In Fig. 2 the points of each group seem to lie

Table I.

Distance	t_{P-A_1}	t_{P-A_2}	t_{P-A_3}
meters	sec.	sec.	sec.
40	0.134	0.225	0.462
48	—	0.288	0.524
	0.179	0.314	0.596
	0.172	0.290	0.524
	0.173	0.293	0.527
	0.177	0.295	0.550
70	0.268	0.466	0.705
80	0.268	0.490	0.725
	0.273	0.505	0.759
	0.274	0.489	0.728
	0.275	0.491	0.722
	0.299	0.500	0.774

in a straight line, respectively, and the straight lines computed by least square are as follows;

$$t_{P-A_1} = (0.011 \pm 0.050) + (0.00337 \pm 0.00073)\Delta,$$
$$t_{P-A_2} = (-0.014 \pm 0.080) + (0.00644 \pm 0.00124)\Delta,$$
$$t_{P-A_3} = (0.229 \pm 0.069) + (0.00646 \pm 0.00118)\Delta.$$

On A_1 and A_2 of the three phases, it is asserted that every line passes near the original point of this coordinate. The line of A_3-phase runs parallel with that of A_2-phase. To judge from this figure, A_1 and A_2 seem to be separate kinds of waves with different velocities, and A_3 to be the same kind of wave as A_2.

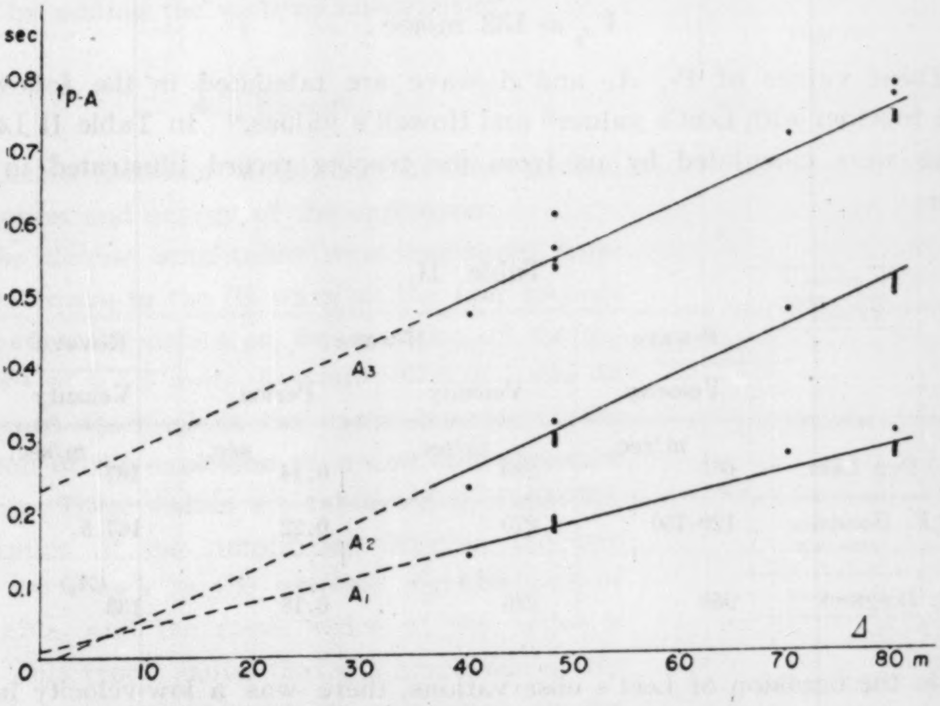

Fig. 2. Travel time curves of A_1-, A_2-, A_3-wave.

For the purpose of computing the velocities of A_1 and A_2, we assume that

$$t_{P-A_1} = 0.00337\,\Delta,$$
$$t_{P-A_2} = 0.00644\,\Delta,$$

and put these expressions into the equation

$$t_{P-A_n}=\left(\frac{1}{V_{A_n}}-\frac{1}{V_P}\right)\Delta,$$

where V_{A_n} is the velocity of the *n*th wave and V_P the velocity of P-wave.

S. Omote⁽⁴⁾ prospected at the same place by geophones and made clear that the velocity of P-wave was 950 meters per second at the surface layer with a thickness of about 10 meters.

Assuming this as the value of P-wave velocity, V_{A_1} and V_{A_2} are computed as follows;

$$V_{A_1}=226 \text{ m/sec},$$

$$V_{A_2}=133 \text{ m/sec}.$$

These values of P-, A_1- and A_2-wave are tabulated in the following table together with Leet's values⁽⁵⁾ and Howell's values.⁽⁶⁾ In Table II Leet's values were calculated by us from the tracing record illustrated in his paper.

Table II.

	P-wave	H-wave		R-wave
	Velocity	Velocity	Period	Velocity
	m/sec.	m/sec.	sec.	m/sec.
L. Don Leet	665	290	0.14	187
B.F. Howell	120–750	270	0.22	167.5
R. Ikegami	950	(A_1) 226	0.18	(A_2) 133

On the occasion of Leet's observations, there was a low-velocity layer (p=665 m/sec), with a thickness of about 16.7 meters, and the charge was set off at a depth of about 3 meters. In case of Howell's, there was a "weathered" or "low-velocity" layer with a thickness between 1.2 and 8.4 meters, its P-wave velocity between 120 and 735 meters per second, and the charges were set off at depths ranging from 6.7 to 12.5 meters. In our case, the thickness of a low-velocity layer was about 11.5 meters, according to the result of drilling, (see Fig. 3), and the charges were set off at a depth of 3 meters.

---

4) S. OMOTE, Read at *Monthly Meeting of the Earthq. Res. Inst. on September*, 1950.

5) L. DON LEET, *loc. cit.*, p. 210.

6) B.F. HOWELL, *loc. cit.*, p. 300.

Comparing these three cases, in every case there were low-velocity layers, and charges were always set off in or near that layer. These may be the conditions necessary for generating "H"-wave, and thereby we think that "A_1"-wave is "H"-wave and that "A_2"- and "A_3"-wave are Rayleigh waves.

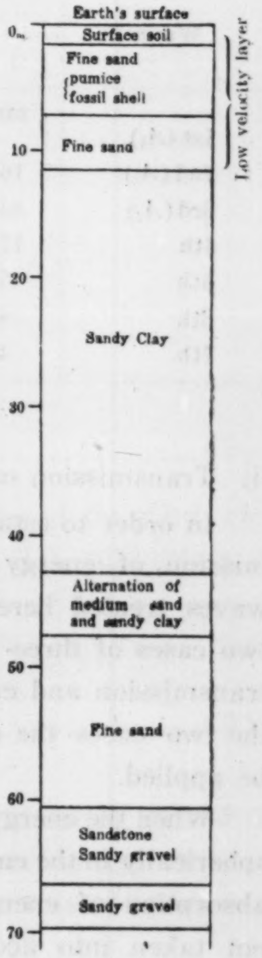
Earth's surface
0m
Surface soil
Fine sand
pumice
fossil shell
Fine sand
Low velocity layer
10
20
Sandy Clay
30
40
Alternation of medium sand and sandy clay
50
Fine sand
60
Sandstone
Sandy gravel
Sandy gravel
70

Fig. 3.

Driller's log at the site of the experiments. (By the courtesy of Chiyoda Natural-gas Co. Ltd.)

The fundamental weakness of our records is that they are wanting in vertical component and that the orbits of the earth particle were not examined. In future we will investigate this problem again by adding the vertical seismometer.

4. Energy.

i) Relation between amplitude of the ground motion and energy of the explosives.

The double amplitudes were measured from the first wave to the 7th wave on the four records observed at 80 meters on the occasion of the explosions of a 1.5 units dynamite (67.5 gr.) and on the record observed at the same distance on the occasion of the explosion of a one unit dynamite (45 gr.). These values are tabulated in Table III. The ratios of the amplitudes between the two cases are shown in the extreme right column of this table, and the mean value of the ratios is 1.33. This result shows that the amplitude of the ground motion is almost in proportion to the square root of the charge (viz. energy transmitted from the focus), and is equal to the results obtained in the past from other data.

For the purpose of calculation of the energy, the amplitudes of the third waves, (A_3), observed on the occasion of the explosion of one unit dynamite at the distance of 48 meters are shown in Table IV.

Table III.

$\varDelta$ = 80 m.

Wave	Dynamite 67.5 gr.					Dynamite 45 gr.	Amplitude ratio
	1	2	3	4	mean		
	mm.	mm.	mm.	mm.	mm.	mm.	
1st (A_1)	—	8.1	9.8	7.5	8.50	6.8	1.25
2nd (A_2)	16.4	14.4	16.9	18.1	16.45	12.3	1.33
3rd (A_3)	42.2	38.9	42.2	44.4	41.90	—	—
4th	17.7	16.7	20.1	13.1	16.80	13.9	1.20
5th	5.9	5.5	7.6	6.0	6.30	4.7	1.34
6th	8.2	7.7	—	7.6	7.80	4.9	1.59
7th	4.0	4.3	5.8	3.3	4.40	3.5	1.25
							mean 1.33

Table IV.

$\varDelta$=48 m. (Dynamite 1 unit)

Record No.	Amplitude of the 3rd wave (A_3)
	mm.
1	54.0
2	50.7
3	40.4
4	52.2
5	32.7
	mean 46.0

ii) Transmission of energy.

In order to establish a way of transmission of energy transferred by the waves treated here, we considered the two cases of three- and two-dimensional transmission and examined to which of the two cases the observed values may be applied.

When the energy is transmitted semispherically in the earth, provided that the absorption of energy into the earth is not taken into account, the energy E_1 and E_2 crossing unit surface at right angle to the direction of propagation at distances $\varDelta_1$ and $\varDelta_2$ are $E_1 = E/2\pi\varDelta_1^2$ and $E_2 = E/2\pi\varDelta_2^2$, respectively, where E is the total energy spread out from the focus. (See Fig. 4 (a)). Therefore

$$E_1/E_2 = (\varDelta_2/\varDelta_1)^2 .$$

Taking $\varDelta_1 = 48$ meters and $\varDelta_2 = 80$ meters,

$$E_1/E_2 = 2.77. \quad \ldots\ldots\ldots\ldots\ldots\ldots\ldots\ldots (1)$$

When the energy is transmitted two-dimensionally maintaining a constant depth L, E_1 and E_2 are $E/2\pi\varDelta_1 L$ and $E/2\pi\varDelta_2 L$, respectively. (See Fig. 4 (b)).

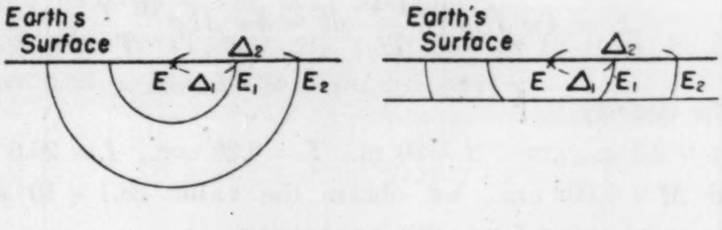

(a) (b)

Fig. 4.

Therefore

$$E_1/E_2 = \Delta_2/\Delta_1 .$$

Taking $\Delta_1 = 48$ meters and $\Delta_2 = 80$ meters,

$$E_1/E_2 = 1.66. \ldots\ldots\ldots\ldots\ldots\ldots\ldots (2)$$

On the other hand, let M_1 and M_2 be the amplitudes of the third wave at Δ_1 and Δ_3, respectively, and $M_1 = 46.0$ and $M_2 = 41.9$ millimeters on Table IV and Table III.

Considering the difference of charges,

$$E_1/E_2 = \frac{1.5(46.0)^2}{(41.9)^2} = 1.80. \ldots\ldots\ldots\ldots (3)$$

Provided that we compare the values of (3) with those of (1) and (2), we see that the energy of waves treated by us were spread out two-dimensionally. This indorses the fact that the waves treated by us were a kind of surface waves.

Jeffreys[7] showed that the energy in a Rayleigh wave is the same as if there were no vertical motion, and that the horizontal motion has the same amplitude at the surface as down to a depth of 1.12 wave-length. In the subsequent calculation we will use the wave-length as the value of L in the expression in (iii).

iii) Energy of the ground motions.

Let V be the velocity, T the period and M the amplitude of the ground motion at the distance of Δ, and let us suppose that the energy spreads out two-dimensionally from the focus. Then the energy is computed by the following expression.

---

[7] H. JEFFREYS, *Geophys. Suvp. Roy. Astro. Soc.*, **1** (1923), 24.

$$E = 4\pi^2 \Delta L\rho \int \frac{M^2 V}{T^2}\, dt = 4\pi^3 \Delta L\rho \frac{M^2 V}{T},$$

where ρ is the density.

Taking $\rho = 2.5$ gr./cm³., $\Delta = 80$ m., $T = 0.20$ sec., $L = 26.6$ m., $V = 133$ m./sec., and $M = 0.008$ cm., we obtain the value 28.1×10^9 ergs. as the energy in the third wave from this expression.

Using this value of the third wave, we computed the energy of each wave from the first wave to the tenth wave. These values are shown in Table V, and the total energy was about 4.0×10^{10} ergs. In the present case the total energy computed here is only the energy of surface waves, and the energy of the other parts of the wave train is not taken into account, since it is presumed that the energy of the other parts is weak.

Table V.

Wave	Traced amplitude	Energy
	mm.	ergs.
1st	8.50	1.1×10^9
2nd	16.45	4.3
3rd	41.90	28.1
4th	16.80	4.5
5th	6.3	0.6
6th	7.8	0.9
7th	4.4	0.3
8th	4.7	0.3
9th	3.8	0.2
10th	2.4	0.1

Total energy
40.4×10^9
$\doteqdot 4.0 \times 10^{10}$ ergs.

The charge consisted of 1.5 units (67.5 gr.) of 60% nitroglycelin, and the total energy of it is about 2.6×10^{12} ergs. Therefore the ratio between the total energy of the ground motion and the total energy spread out from the charge is

$$\frac{4.0 \times 10^{10}}{2.6 \times 10^{12}} = 1.5 \times 10^{-2}.$$

Namely, we see that 1.5×10^{-2} parts of the total energy spread out from the charge were spent as the energy of the wave-motions and the

other parts were spent as sound, heat and others.

In closing, I wish to express my appreciation to Prof. F. Kishinouye for his guidance and to Mr. Y. Sato for his advice.

---

16. 火藥の爆發によつて起される地動について

地震研究所　池上良平

東京都江東區南砂町に於て，ダイナマイトの爆發によつて起される地動を岸上式微動計で観測した。その記象を用ひて解析を行つた處，最近 L. Don Leet1) によつて最初に發見された H-波 (Hydrodynamic-wave) と同種類の波と思はれるものが存在する事が判つた。

更に地動の振幅は藥量 (エネルギー) の略々平方根に比例する事，エネルギーの傳播は我々の取扱つた波については二次元的である事，ダイナマイトが放出する全エネルギーの內約 1.5/100 が地動となつて傳播する事等が判つた。

rather parts were spent as sound, heat and others.

In closing, I wish to express my appreciation to Prof. F. Kishinouye for his guidance and to Mr. Y. Sato for his advice.

[illegible]

[illegible]

[illegible]

17. *Relation between the Earthquake Damage of Non-wooden Buildings and the Nature of the Ground. II.*

By Kiyoshi Kanai and Shizuyo Yoshizawa,

Earthquake Research Institute.

(Read March 20, 1950.—Received Dec. 20, 1950.)

In the previous investigations,[1] it has been cleared up considerably that the softer the ground is, the less the damage done to ferro-concrete buildings and brick ones by earthquakes is. On the other hand, it has been shown that the first floor was the most severely destroyed on the firm ground, while on the soft ground the second as well as the third floors suffered most damage at the time of the great earthquake. The results obtained statistically were explained by the results of the theoretical studies based upon the idea that at the time of earthquake the vibration energy of buildings dissipates to the ground again as elastic waves starting from the foundation.

In the present paper the relations among the damage of buildings due to earthquakes and the ratio of the height of building (l) to the radius (ε') of the circle to which the sectional area of the building is transformed assumedly and the nature of the ground together with the relation between the damage ratio of every story of buildings and the nature of the ground are described based upon the same data as in the previous paper regarding the damage done to ferro-concrete buildings and brick ones in the former Tokyo city at the time of the Kwanto earthquake of 1923.

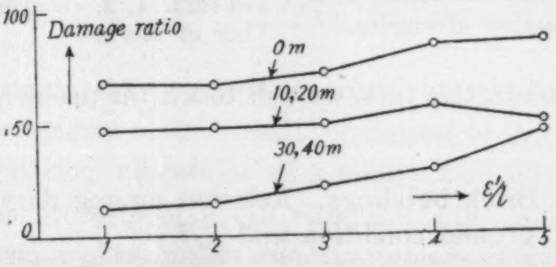

Fig. 1. The relation among the damage ratio, ground condition and ε'/l for the case of brick buildings in the former Tokyo city at the time of the Kwanto earthquake of 1923. $0_m \cdots 40_m$ represent the thickness of alluvium.

The results obtained are shown in Tables I-IV and plotted in Figs. 1-4. It is seen from Figs. 1 and 2 that the damage to buildings caused by earthquake becomes greater as the ratio of ε'/l as to every condition of the ground increases. Figs. 3 and 4 show that the damage as regard each story of buildings decrease with the increase in the thickness of alluvium.

---

[1] K. Kanai, "Relation between the Earthquake Damage of Non-woodon Buildings and the Nature of the Ground", *Bull. Earthq. Res. Inst.*, **27** (1949), 97.

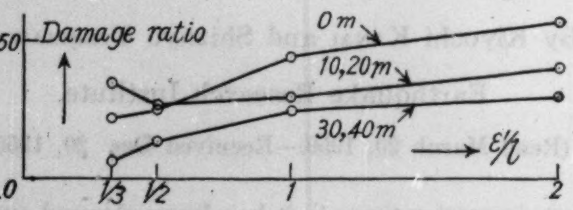

Fig. 2. The relation among the damage ratio, ground condition and ε'/l for the case of ferro-concrete buildings in the former Tokyo city at the time of the Kwanto earthquake of 1923. $0_m \cdots 40_m$ represent the thickness of alluvium.

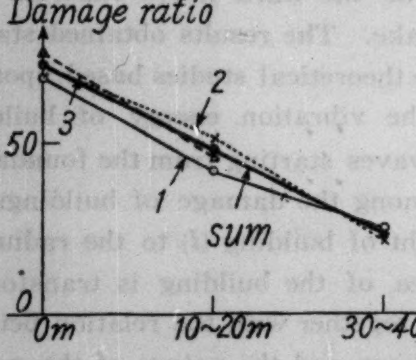

Fig. 3. The relation between the damage ratio and thickness of alluvium for the case of brick buildings in the former Tokyo city at the time of the Kwanto earthquake of 1923. 1, 2, 3 represent the number of stories.

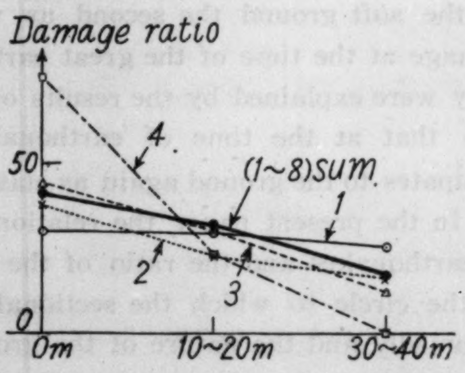

Fig. 4. The relation between the damage ratio and the thickness of alluvium for the case of ferro-concrete buildings in the former Tokyo city at the time of the Kwanto earthquake of 1923. 1, 2, ···· represent the number of stories.

In order to explain this fact, we will touch the problem by mathematical calculations.

Table I. Brick buildings. Relation among damage ratio, ground condition and ε'/l.

Ground conditions	Damage ratio (%)				
	$\varepsilon'/l=1$	2	3	4	5
Thickness of alluvium, 30～40 meter	12	14	21	28	45
Thickness of alluvium, 10～20 meter	47	48	49	57	50
Diluvium or tertialy	68	67	72	84	86

Table II. Ferro-concrete buildings. Relation among damage ratio, ground condition and ε'/l.

Ground conditions	Damage ratio (%)			
	$\varepsilon'l=1/3$	1/2	1	2
Thickness of alluvium, 30∼40 meter	6	13	25	30
Thickness of alluvium, 10∼20 meter	35	27	30	40
Diluvium or tertiary	22	25	44	57

Table III. Brick buildings. Relation between damage ratio as to every stories and ground condition.

Ground conditions	Damage ratio (%)			
	1 storey	2 stories	3 stories	total
Thickness of alluvium, 30∼40 meter	25	21	—	23
Thickness of alluvium, 10∼20 meter	42	51	46	48
Diluvium or tertiary	69	73	76	73

Table IV. Ferro-concrete buildings. Relation between damage ratio as to every stories and ground condition.

Ground conditions	Damage ratio (%)				
	1 storey	2 stories	3 ,,	4 ,,	(1∼8) total
Thickness of alluvium, 30∼40 meter	25	16	12	0	17
Thickness of alluvium, 10∼20 meter	29	22	30	23	32
Diluvium or tertiary	30	38	44	75	41

As was shown in the previous paper,[2] the motion of a tall building with rigid floors subjected to horizontal oscillation of the ground is analogous to the case of shearing vibrations of a simple structure, so we shall deal with the vibration problem of a tall structure with rigid floors subjected to incident transverse waves, under the dissipation of vibrational energy in the form of elastic waves transmitted into the ground.

Let the incident transverse waves with their displacements orientated vertically be

$$u_0=\cos(pt+kx)\ \ldots\ldots\ldots\ldots\ldots\ldots(1)$$

---

[2] K. Sezawa and K. Kanai, "Some New Problems of Free Vibrations of Structure", *Bull. Earthq. Res. Inst.*, **12** (1934), 819.

The final solutions of the stress in a structure are expressed by[3)]

$$S = 4\pi\varepsilon^2 Gk'\sqrt{\frac{\Gamma_1^2+\Gamma_2^2}{P^2+Q^2}}\sin k'(x+l)\cos\left(pt+\tan^{-1}\frac{\Gamma_2}{\Gamma_1}-\tan^{-1}\frac{Q}{P}\right), \quad (2)$$

where

$$\left.\begin{aligned}
P &= 2\Gamma_1\cos k'l+\frac{3G\varepsilon}{\mu l}\Lambda_1 k'l\sin k'l,\\
Q &= 2\Gamma_2\cos k'l+\frac{3G\varepsilon}{\mu l}\Lambda_2 k'l\sin k'l,\\
\Gamma_1 &= 3\left(\frac{\lambda}{\mu}+2\right)+\nu(k'l)^2\left(\frac{\lambda}{\mu}-3\sqrt{\frac{\lambda}{\mu}+2}\right),\\
\Gamma_2 &= \sqrt{\nu}\,(k'l)\left\{3\left(\frac{\lambda}{\mu}+2+\sqrt{\frac{\lambda}{\mu}+2}\right)+\nu(k'l)^2\left(\sqrt{\frac{\lambda}{\mu}+2}-2\right)\right\},\\
\Lambda_1 &= \left(\frac{2\lambda}{\mu}+5\right)-\nu(k'l)^2,\\
\Lambda_2 &= \sqrt{\nu}\,(k'l)\left(2\sqrt{\frac{\lambda}{\mu}+2}+1\right),\\
\nu &= \frac{\rho G\varepsilon^2}{\rho'\mu l^2},\quad k'^2=\frac{\rho'^2p^2}{G},
\end{aligned}\right\}\quad\ldots\ldots \quad (3)$$

in which ρ, λ, μ; ρ' $(=m/al_1)$, $G(=12.4\,Ej^2/l_1^2)$ are the density and the elastic constants of the earth, and the effective density and the effective rigidity of the structure, where E, j, l_1, l, a and ε are Young's modulus, radius of gyration of section, length of the column between two adjacent floors, height of the structure, sectional area of the column and radius of the column respectively.

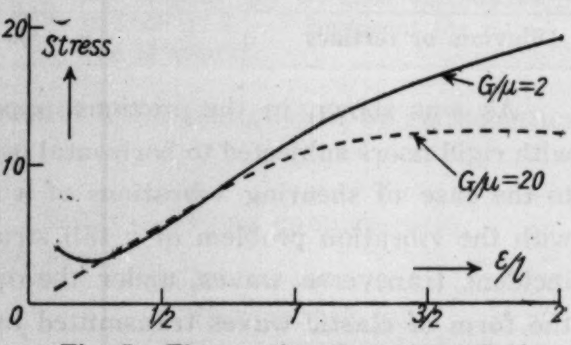

Fig. 5. The results of mathematical calculations of the relation between stress and ratio of ε/l.

---

3) K. SEZAWA and K. KANAI, "Improved Theory of Energy Dissipation in Seismic Vibrations of a Structure", *Bull. Earthq. Res. Inst.*, **14** (1936), 168.

Using equation (2) we calculated the stress and the height where the stress reaches a maximum in column at resonance condition under the conditions $\rho = \rho'$, $\lambda = \mu$. The results are plotted in Figs. 5, 6 and 7.

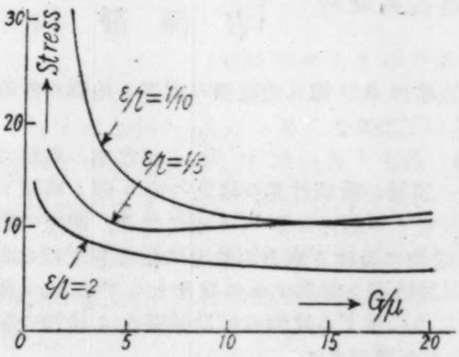

Fig. 6. The results of mathematical calculations of the relation between stress and ratio of G/μ.

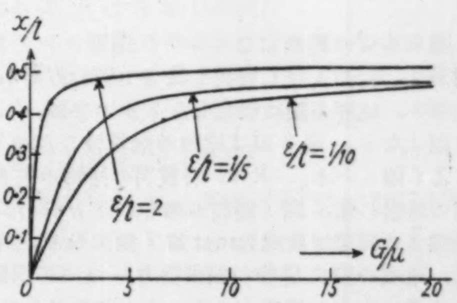

Fig. 7. The results of mathematical calculations of the relation between height where stress take maximum and ratio of G/μ.

Comparing the curves in Fig. 2 obtained statistically and the curves in Fig. 5 calculated mathematically, it will be seen that, the relation between the earthquake damage to buildings, on the ground where the thickness of alluvium are 0 meter and 10~20 meter and the ratio ε'/l fairly resembles the relation between the stress in columns under the two conditions, say $G/\mu=2{,}20$, and the ratio of ε'/l. And the features of the relation between the damage ratio as well as the places where the buildings suffered most by earthquake and the ground condition, as plotted in Figs. 3, 4 and shown in Table I, II, III, of the previous paper[4] are explained somewhat quantitatively by the results of mathematical calculations plotted in Figs. 6, 7.

The results above-mentioned tell us again that the results of theoretical studies, based upon the idea that at the time of earthquake the vibration energy of buildings dissipates to the ground again as the elastic waves which start from the foundation, are applicable to the earthquake-proof problem of structure.

---

[4] *loc. cit.*, 1).

17. 非木造建物の震害と地盤の性質との關係 第2報

地震研究所 {金井 清
吉澤 靜代

關東地震の舊東京市における鐵筋コンクリート造建物及び煉瓦造建物の震害と地盤の性質との關係を，前回と同じ資料を使つて別の方面からしらべてみた。

即ち，建坪を圓に假定したときの半經 ε' と建物の高さ l との比 (ε'/l) と被害率の關係は第1,2圖になる。第2圖は建物の振動勢力の地下逸散の問題の數値計算の結果の第5圖と模樣が非常によく似ている。次に，層數別の建物の被害率と地盤との關係は第3,4圖になり，前記の數値計算の結果の第6圖と性質が等しいことがわかる。建物における應力が最大になるところの高さと地盤との關係は數理的には第7圖になり，實際の震害狀態を說明するに足りそうである。要するに，地震の際に建物の振動勢力が地中に逸散するために生ずる建物の振動減衰性は建物の耐震性に非常に大きな影響があることが相當具体的にわかつた譯である。

18. 木造家屋の震害について

地震研究所　金井　清

（昭和22年9月16日發表～昭和25年12月20日受理）

日本における過去の多くの地震の記錄は，家屋の被害が沖積平野で大きく台地や山地で小さい事實を示している．その原因としては，沖積平野と台地山地とでは地震動の周期が異り沖積平野における地震動の周期が木造家屋の周期に近い事，沖積平野における地震動の振幅が台地山地上のそれよりも大きい事，沖積平野では地震動の繼續時間が長い事などの考え方があるが，今日までのところ，まだ滿足な解釋はついていない。

明治以來の震害調査記事を調べたところ，地震による木造家屋の破壞狀態は地盤の性質によつて相當に異ることが明かに見られた。次に，これらの調査記事の中から，地盤の性質と家屋破壞の狀態がよくわかるものを拔き出して列べてみる。（活孤內は筆者の解釋）

（1） 庄内地震（1894 X 22)。震豫調報，3 (1895)，79～134；7 (1895)，4～30。

最上川上流の細砂に富む低濕地で西海岸は砂地であるため基礎の不同沈下多し。幹部構造の弱點よりも，むしろ地形の粗悪のための損害多く，地形の不完全は庇にまで影響を及ぼす。坑打した土藏は被害なし。全潰/半潰＝2581/5891＝0.44，全潰/死者＝2581/591＝4.4。

（2） 陸羽地震（1896 VIII 31)．震豫調報，11 (1897)，50～104；77 (1913)，78～87。

被害地は半分位岩層上にあり。巡回地では土藏の無害なるもの殆んどなく，尋常建物被害少く，方向性あり。激震地 7ケ村については　全潰/半潰＝4.5，全体としては全潰/半潰＝4277/2051＝2.1，全潰/死者＝4277/205＝21。

（3） 姉川地震（1909 VIII 14)。震豫調報，69 (1910)．1～27; 70(1910)，1～84。

泥砂層，砂層，水田埋立地。薄土台による被害多し。（孤立柱とえらぶところなし）倒潰の原因は不良なる地形。激震地の民家構造は優良なるも，强弱をとわず損傷，沓石が斜に地中に沈下せるものあり，柱が沓石から落ちたための被害多し。下部結束不良のため不平均墜落衝動等の第二の出來事で損傷す。

全潰/半潰＝893/2164＝0.41，全潰/戶數＝0.13，全潰/死者＝4277/205＝21，（死者の少いことは特に調査者の注意をひいたらしく，發震時の關係等で說明が試みられている）

（4） 櫻島地震（1914 I 12)。震豫調報，80 (1915)，1～33。

鹿兒島の山の手で屋根瓦の破損多し。

（5） 秋田仙北地震（1914 III 15)。震豫調報，82(1915)，1～42。

被害激震地は球そうな砂よりなる。40% 以上の潰家を生じた區域の全潰/半潰＝

2.4，全体としては全潰/半潰＝640/575＝1.1，全潰/死者＝640/94＝6.8。（1896 年陸羽地震と比較すると全潰の割合が少く死者の割合が多いところに，兩地震の激震地の地盤の相違による影響があらわれている）。

（6） 東京地震（1922 IV 26）。震豫調報，99（1925），22～44。

東京では木造建物傾斜 3，一部破損 2，梁墜落 1，屋根瓦破損 46，土造塗家土藏の屋根瓦崩落多し。横濱山下町では木造 1 階建 21 棟，2 階建 33 棟に被害なし，煉瓦造石造等 2 階建；23/187＝12%，1 階建；13/82＝16% の被害。東京横濱共に被害は軟弱地盤上に多し（山下町の例でもわかるように剛構造程被害多く，又，屋根瓦の被害の多いことは，この時の地震動の周期が短かかつたことを示す1)）。

（7） 島原地震（1922 XII 8 。震豫調報 99（1925），1～11。

傾斜多きため建物敷地の地盤軟硬不同。脚部堅固ならざるため傾斜又は倒潰。屋根瓦の損傷極めて少し，全潰/死者＝131/27＝4.9.

（8） 關東地震（1923 IX 1）。震豫調報，100 丙（上）（1926），1～54。

軟弱地盤區域に於ては基礎の不同沈下又は移動を起し，局部的の損害を與えること多し，（軟地では全潰に比べて半潰が多く，硬地では逆に全潰が比較的に多いことが第 I 表からよくわかる）。

（9） 但馬地震（1925 V 23）。震豫調報，101（1927），1～62。

豐岡町等の地盤特に軟弱なところでは半潰多く，不同沈下多し，（被害原因を家屋の新舊等で説明し苦心が拂はれている）城崎町港村等の第三紀層上等では家屋の方向によつて損傷の差違極めて多く，津居山瀬戸では 90% は倒潰方向一致する。半潰極めて少く，全潰か安全。

（10） 丹後地震（1927 III 7）。震研彙報，3（1927），133～162。

激震地は洪積層，第三紀層，殘存家屋と全潰家屋の被害の程度に甚だしい相違あり。通常は屋根はそのまゝの形を維持するが今度の激震地では屋根自身も甚だしく破壞。（一般に被害甚大な地域は沖積層上であるため，この地震の被害狀態が特に調査者の注意をひいた）府中村では不同沈下があり，全潰/半潰の比は小。

（11） 北伊豆地震（1930 XI 26）。早稻田大學建築學報，9（1932）。

狩野川流域半潰多し。地盤のよい江間村韮山村では特に屋根瓦の落下多し。

（12） 北關東地震（1931 IX 21）。早稻田大學建築學報，9（1932）。

利根川荒川中間の沖積層被害大。建築物被害は局部的多し，被害の狀況より上下動が相當に大きかつた。不同沈下あり。地盤に龜裂が入ると上部構造の良否に拘らず大なる損害を受ける。全潰/半潰＝60/119＝0.50，全潰/死者＝60/11＝5.5。

（13） 靜岡地震（1935 VII 11）。震研彙報，13（1935），951～998。

高松，大谷は全潰/半潰＝0.64，0.56，曲金，國吉田等厚い軟弱地盤では全潰/半潰＝0.04，0.02…… で，その割合少し。靜岡驛北部，毎度山丘陵の北縁部落では瓦の墜落多し。

（14） 男鹿地震（1939 V 1）。震研彙報，17（1939），627～637。

---

1) 金井　清，地震研究所彙報，25（1947），64.

（第3圖でわかるように全潰の割合は沖積層上では小さく，山地では大きい）

(15)　長野地震 (1941 VII 15)。震研彙報，19 (1941)，647～660。

震央から遠い山地で，震央附近の沖積地上よりも全潰の割合多し。（第4圖參照）

(16)　鳥取地震 (1943 III 4)。震研彙報，21 (1944)，435～457。

被害地は砂層。家の柱のどれかが沈下しないものなし。全潰極めて少し。

(1943 IX 10 の鳥取地震以後のものは，特に詳しい調査記錄があるから，記事を拔き出して列べることを省く)。

以上の調査記事の拔書からして，良い地盤，淺い軟弱地盤，山地等と書いてある地盤上における家屋の破壞狀態としては，全潰多し，瓦破壞多し，土藏石造煉瓦造の破壞多し，倒潰の方向性顯著，破壞までに相當の時間がかゝつた等の説明が多く見られる。これに對して，砂地，低濕地，複雜な地盤，盛土，埋立地（特に水田埋立地），氾濫の多い河川流域等と記してある地盤上における家屋の破壞狀態としては，半潰多し，不同沈下，上下動强し，良構造に被害あり，地形悪し，その他無理に被害の説明をした記事が目立つている。

前者の家屋破壞原因は大体振動學的に説明がつくが，後者の原因を振動學的に説明するのはかなり困難である。尙，軟弱地盤で上下動强しとあるのは地震動の上下動と言うよりも，むしろ家がドシンと動いたという意味で，恐らく不同沈下等の影響に

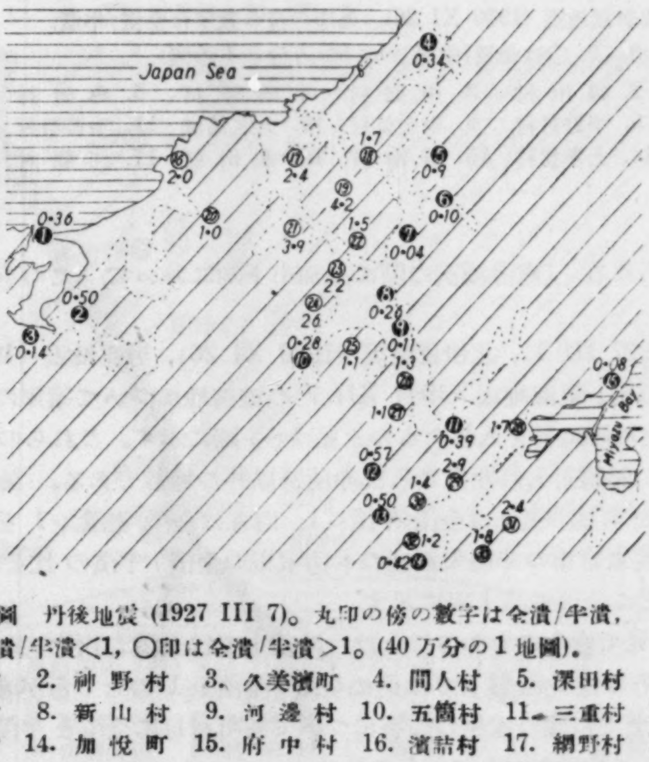
Japan Sea
Miyazu Bay
0·34
1·7
2·4
2·0
0·9
4·2
0·10
0·36
1·0
3·9
1·5
0·04
22
0·50
0·26
26
0·14
0·28
1·1
0·11
1·3
0·08
1·1
1·7
0·39
0·57
2·9
1·4
0·50
2·4
1·2
1·8
0·42

第1圖　丹後地震 (1927 III 7)。丸印の傍の數字は全潰/半潰，●印は全潰/半潰<1，○印は全潰/半潰>1。(40万分の1地圖)。

1. 湊村　2. 神野村　3. 久美濱町　4. 間人村　5. 深田村　6. 溝谷村
7. 吉野村　8. 新山村　9. 河邊村　10. 五箇村　11. 三重村　12. 常吉村
14. 岩屋村　14. 加悦町　15. 府中村　16. 濱詰村　17. 網野村　18. 島取村
19. 島津村　20. 木津村　21. 鄉村　22. 丹波村　23. 峰山町　24. 吉原村
25. 長善村　26. 口大野村　27. 奥大野村　28. 岩瀧町　29. 山田村　30. 市場村
31. 石川村　32. 三河内村　33. 桑飼村

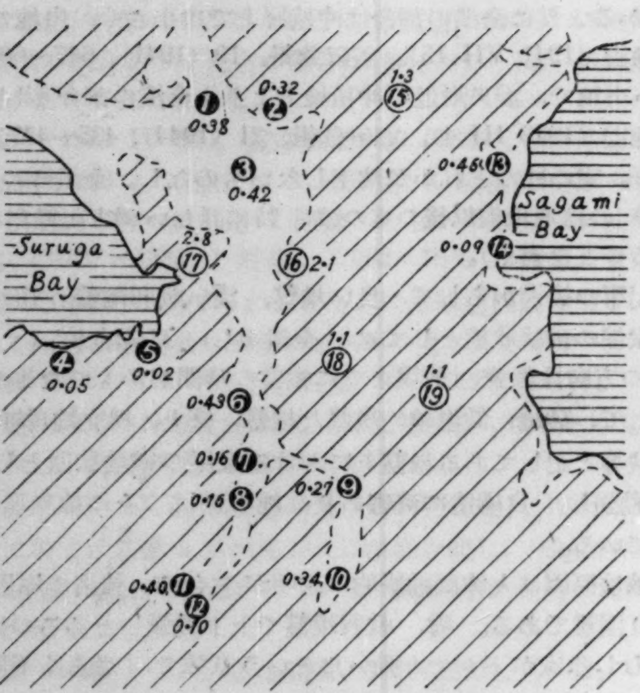
0·32
②
1·3
⑮
❶
0·38
③
0·42
0·46⑬
Sagami
Bay
2·8
⑰
Suruga
Bay
⑯2·1
0·09⑭
1·1
⑱
1·1
⑲
④
0·05
⑤
0·02
0·43⑥
0·16⑦
0·16⑧
0·27⑨
0·40⑪
⑫
0·10
0·34⑩

第2圖 北伊豆地震 (1930 XI 26)。丸印の傍の數字は全潰/半潰,
●印は全潰/半潰<1, ○は全潰/半潰>1。(40 万分の 1 地圖)。
1. 三島町 2. 錦田村 3. 中鄕村 4. 西浦村 5. 內浦村 6. 田中村
7. 修善寺町 8. 下狩野村 9. 中大見村 10. 上大見村 11. 中狩野村 12. 上狩野村
13. 熱海町 14. 上多賀村 15. 函南村 16. 韮山村 17. 江間村 18. 北狩野村
19. 下大見村。

よるものと考えられる。(南海地震の際に高知市下知において, この有様をよく見きわめた人があつた)

丹後地震 (1927 III 7), 北伊豆地震 (1930 XI 26), 男鹿地震 (1939 V 1), 長野地震 (1941 VII 15), 東海地震 (1944 XII 7)の被害地について家屋の全潰と半潰の比をとり, その數を地圖に書き入れたものを第1～5圖に示す。これらの圖中で, 無地のところは冲積層, 斜線を入れたところは冲積層以外の地盤である。又, 丸の傍の數字は全潰/半潰の比を示し, 黑丸は全潰/半潰<1, 白丸は全潰/半潰>1 を示す。關東地震 (1923 IX I) の舊東京市の非燒失區域の木造家屋の全潰/半潰の比を冲積層上と洪積層, 第三紀層上とに分けて第I表に示す。

第1～5圖を見て直ちにわかることは, 冲積上では全潰/半潰の比が 1 より小さいところが多く, その他の地盤上では逆に全潰/半潰>1 のところが多いことである。1891 から 1947 までの間の家屋の震害について各町村毎に全潰と半潰の比をとつて集計したものも, この性質を明かに示した²⁾。

---

2) 金井 清, 地震研究所彙報, 25 (1947), 63.

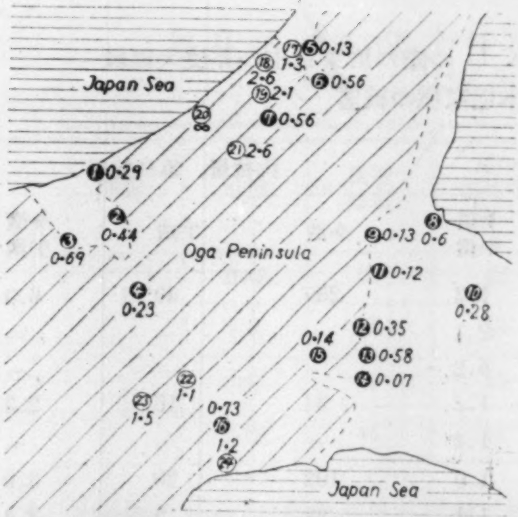
Japan Sea
Oga Peninsula
Japan Sea
⑰ ⑤ 0·13
⑱ 1·3
2·6
⑲ 2·1
⑥ 0·56
⑦ 0·56
⑳ ∞
㉑ 2·6
① 0·29
② 0·44
③ 0·69
④ 0·23
⑧ 0·6
⑨ 0·13
⑪ 0·12
⑯ 0·28
⑫ 0·35
0·14 ⑮
⑬ 0·58
⑭ 0·07
㉒ 1·1
㉓ 1·5
0·73 ⑩
1·2 ㉔

第3圖　男鹿地震 (1939 V 1)。丸印の傍の數字は全潰/半潰，●印は全潰/半潰<1，○印は全潰/半潰>1。(20 万分の 1 地圖)。

1. 濱間口　2. 中間口　3. 山田　4. 瀧川
5. 橋木　6. 中石　7. 箱井　8. 福川
9. 百川　10. 渡部　11. 櫸澤　12. 浦田
13. 飯森　14. 大倉　15. 岩倉　16. 比詰
17. 高屋　18. 地谷　19. 石神　20. 安田
21. 琴川　22. 田中　23. 馬生目　24. 羽立。

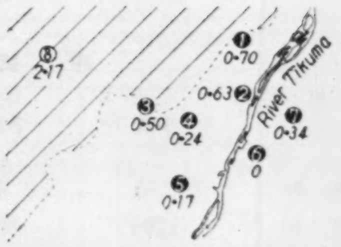
River Tikuma
⑧ 2·17
① 0·70
0·63 ②
③ 0·50
④ 0·24
⑦ 0·34
⑥ 0
⑤ 0·17

第4圖　長野地震 (1941 VII 15)。丸印の傍の數字は全潰/半潰，●印は全潰/半潰<1，○印は全潰/半潰>1。(40万分の1地圖)。

1. 神鄉村　2. 長沼村　3. 若槻村
4. 古里村　5. 朝陽村　6. 日野村
7. 豊洲村　8. 淺川村。

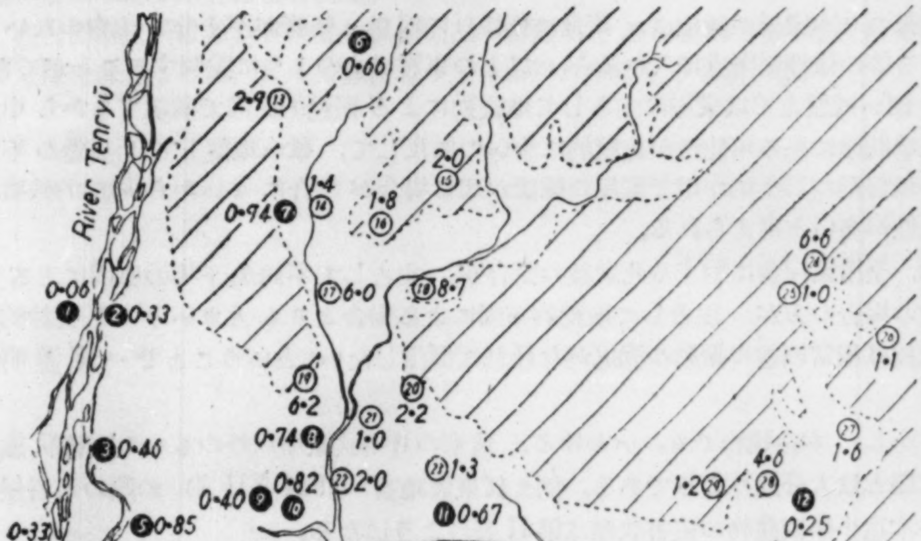
River Tenryū
River Ota
Enshū Sea
⑥ 0·66
2·9 ⑬
2·0 ⑮
1·4 ⑭
1·8 ⑯
0·74 ⑦
⑰ 6·0
⑱ 8·7
6·6 ㉔
㉕ 1·0
㉖ 1·1
0·06 ①
② 0·33
⑲ 6·2
⑳ 2·2
㉑ 1·0
0·74 ⑧
③ 0·46
㉒ 2·0
㉓ 1·3
0·82
0·40 ⑨ ⑩
⑪ 0·67
㉗ 1·6
4·6 ㉘
1·2 ㉙
⑫ 0·25
0·33 ④
⑤ 0·85

第5圖　東海地震 1944 XII 7)。丸印の傍の數字は全潰/半潰，●印は全潰/半潰<1，○印は全潰/半潰>1。(30万分の1地圖)。

1. 中ノ町村　2. 池田村　3. 十東村　4. 河輪村　5. 袖浦村　6. 岡田村
7. 向笠村　8. 南御厨村　9. 於保村　10. 福田町　11. 幸浦村　12. 千濱村
13. 三川村　14. 今井村　15. 久努村　16. 久努西村　17. 田原村　18. 袋井町
19. 御厨村　20. 上淺羽村　21. 西淺羽村　22. 豐濱村　23. 東淺羽村　24. 加茂村
25. 中內田村　26. 橫地村　27. 平田村　28. 中　村　29. 大坂村。

第 I 表 關東地震 (1923 IX 1) の際の舊東京市の非燒失區域における木造家屋の被害

舊區名	冲積層			洪積層，第三紀層		
	全潰	半潰	全潰/半潰	全潰	半潰	全潰/半潰
麹町	61	46	1.3	259	43	6.0
神田	1204	561	2.1	—	—	—
日本橋	28	175	0.2	—	—	—
京橋	47	38	1.2	34	15	2.3
赤坂	172	122	1.4	—	—	—
下谷	480	463	1.0	102	26	3.9
淺草	1967	1821	1.1	22	9	2.4
本所	4426	4712	0.9	—	—	—
深川	2064	1689	1.2	—	—	—
牛込	66	132	0.5	—	—	—
本郷	36	50	0.7	14	3	4.7
計	10551	9809	1.1	431	96	4.5

舊來の日本家屋の構造は，接合は枘仕口に頼り，基礎が不十分で土台のないものさえある等の條件を考慮に入れると，以上の事實は次のように説明することができる。即ち，硬い地盤上では家屋は主として地震動による振動的原因で破壞するから中途半端な破壞狀態に止る可能性が比較的に少いのに反して，軟い地盤上では基礎の不同沈下等の地震動の二次的作用で家屋の破壞が起る場合が割合に多いから局部的破壞に終る可能性が多いと考えられる。

尙，全潰家屋數に對する死者數の割合が，主として不同沈下等の原因による家屋の倒潰の場合の方が，主として振動的原因による場合よりも大きいという統計的結果は，家屋は相當回數の振動の繰返がなければ倒潰しない3)ということで一應説明がつく。

しかし，木造建物でも，いわゆる，舊來の日本式家屋以外のものの震害狀態は以上の狀態とは大分違うようである。例えば東海地震 (1944 XII 7) の際の名古屋市における木造小學校建物の被害狀態は第II表のようになる。

この種の木造建物では，2 階建の柱や壁の損傷は山手と下町とが殆ど等しく，1 階建では山手の損傷の方が下町のそれの 2 倍位大きいことが第II表から統計的に言え，前述の木造家屋の被害とは全く逆の傾向をとり，むしろ非木造建物の震害狀態4)に近い。

---

3) 金井 清，昭和24年 9月20日，地震研究所談話會發表

4) 金井 清，地震研究所彙報，27 (1949), 97；29 (1951), 219.

第 II 表 東海地震 (1944 XII 7) の際の名古屋市
における木造小學校建物の被害

階數	地盤	調査總數	瓦の損害率 (%)	柱，壁の損害率 (%)		
				1 階最大	2 階最大	計
2	山手	99	42	19	28	48
	下町	63	49	3	46	49
1	山手	44	35	—	55	—
	下町	41	32	—	27	

又，2階建において柱壁の最大の損害を受けた場所が山手では 2階と 1階で大した差違がないが，下町では 2階で最大の損害を受けた建物數が斷然多い狀態も非木造建物の震害狀態[5]に似ている。

次に，第 II 表から瓦の損傷は 2階建の方が 1階建よりも幾分大きいが，山手と下町ではほとんど差違がないことがわかる。建物の瓦は加速度で損傷すると考えてよさそうだから，[6] この場合には建物に影響を與えるような地震動の加速度は山手と下町で大差がなかつたものと推察される。

名古屋市における調査は愛知縣建築部の御援助と名古屋市內各小學校の御助力によつて行はれたもので，こゝに關係者の方々に厚く御禮を申し述べる。

---

5) 金井 淸，前出 4).
6) 金井 淸，前出 1).

18. *On the Damage to Japanese-style Buildings due to Earthquakes.*

By Kiyoshi Kanai,

Earthquake Research Institute.

In order to clear up the dynamical actions of the earthquakes causing damage to the Japanese-style wooden buildings we studied the relation among the totally-destructed, semi-destructed buildings and the ground conditions using the data of the past great earthquakes of 1891-1947.

In Figs. 1-5, marks ○ and ● indicate that the ratio of the number of the totally-destructed buildings to that of the semi-destructed buildings is larger and smaller than unity respectively. The blank area and the hatched area in these figures indicate alluvium and other geological formations respectively.

These figures show that Japanese-style wooden buildings are liable to be semi-destructed by earthquake on the alluvium, while they are liable to be totally-destructed on other geological formations.

From the above investigations, we found that there are two kinds of reasons for the damage done to Japanese-style wooden buildings by earthquakes from the dynamical point of view, one being the condition subjected to pure vibrational forces and the other the secondary condition caused by seismic vibrations, namely, the unequality in the settling of the foundation of buildings. The former conditions occur mainly on firm or rigid ground in the case of safe or else totally-destructed buildings, whereas the latter conditions take place mostly on soft gronnd with regard to large number of semi-destructed buildings.

昭和26年6月20日印刷
昭和26年6月25日發行

東京都文京區本富士町一番地
東京大學構内
編纂兼
發行者　東京大學地震研究所

東京都中央區新富町3丁目17番地
印刷者　笠井康頼

東京都中央區新富町3丁目17番地
印刷所　株式會社　國際文献印刷社

東京都千代田區神田一ツ橋通
賣捌所　岩波書店

東京都中央區日本橋二丁目六番地
丸善株式會社

Sold by
Iwanami Shoten,
Hitotsubashi dôri, Chiyoda, Tôkyô,
and
Maruzen Co., Ltd.,
Nihonbashi dôri, Chûô-ku, Tôkyô.
Price of this copy: 706 Yen. (Postage exclusive.) xclusive.)
昭和38年4月1日価格改訂

BULLETIN OF
THE EARTHQUAKE RESEARCH INSTITUTE
TOKYO UNIVERSITY

Vol. XXIX, Part 1. March, 1951.

Contents.

Papers and Reports.

Page

1. Y. SATÔ, Study on Surface Waves I. Velocity of Love-Waves. (in English) 1
2. Y. SATÔ, Seismic Focus without Rayleigh-Waves. (in English) 13
3. Y. SATÔ, Mathematical Study of the Propagation of Waves upon Stratified Medium. (2) (in English) 21
4. K. KANAI, On the M_2-waves (Sezawa-waves). (in English) 39
5. K. KANAI, On the Group Velocity of Dispersive Surface Waves. (in English) 49
6. T. RIKITAKE, Electromagnetic Induction within the Earth and Its Relation to the Electrical State of the Earth's Interior. Part III. (in English) ... 61
7. R. TAKAHASI, An Estimate of Future Tsunami Damage Along the Pacific Coast of Japan. (in English) 71
8. The Research Group for Explosion Seismology, Tokyo, Explosion-Seismic Observations in North-eastern Japan. (in English) 97
9. K. KANAI and T. TANAKA, Observations of the Earthquake-motion at the Different Depths of the Earth. I. (in English) 107
10. S. OMOTE, On the Coda Waves of Earthquake Motions. (Part 6) (in English) 115
11. E. INOUE, On the Vertical Displacements Accompanying Imaichi Earthquake in 1949. (in English) 143
12. T. RIKITAKE, A Miniature Earth-inductor. (in English) 147
13. T. RIKITAKE, Diffraction of Electromagnetic Waves around the Crater of Volcano Mihara. (in English) 153
14. T. RIKITAKE, The Distribution of Magnetic Dip in Ooshima (Oo-sima) Island and its Change that Accompanied the Eruption of Volcano Mihara, 1950. (in English) 161
15. S. OMOTE and S. MIYAMURA, Relations between the Earthquake Damage and the Structure of Ground in Nagoya City. (in English) 183
16. R. IKEGAMI, On Ground Vibrations Caused by Explosions. (in English) .. 197
17. K. KANAI and S. YOSHIZAWA. Relation between the Earthquake Damage of Non-wooden Buildings and the Nature of the Ground. II. (in English) .. 209
18. K. KANAI. On the Damage to Japanese-style Buildings due to Earthquakes. (in Japanese) 215

(For the papers written in Japanese or in occidental languages, the abstracts are given in occidental languages or in Japanese respectively.)

BULLETIN OF THE EARTHQUAKE RESEARCH INSTITUTE,
TOKYO UNIVERSITY. Vol. XXIX, Part 2. June, 1951.

東京大學
地震研究所彙報

第 29 號　第 2 册

昭和 26 年 6 月

目　次

論文及報告

頁
19. 表面波の研究 II　彈性板を傳はる表面波の速度（英文）…………… 佐藤泰夫 223
20. 地磁氣永年變化に對する遮蔽効果（英文）…………… 力武常次 263
21. 地電流變化と地下の電氣的性質（英文）…………… 力武常次 271
22. 灣水の運動と灣外に於ける津浪の波形（英文）…………… 力武常次 277
23. 地震斷層に沿う地塊運動 (2)（英文）…………… 那須信治 283
24. 地震の頻度とエネルギーについて（英文）…………… 淺田敏　鈴木次郎　友田好文 289
25. 今市地震の計測（第 2 報）（英文）…………… 越川善明 295
26. 1949 年今市地震の有感餘震の時間分布（英文）…………… 岸上冬彦 301
27. 土地の脈動の傳播性の研究（第 3 報）（英文）…………… 池上良平　岸上冬彦 305
28. 土地の脈動の傳播性の研究（第 4 報）（英文）…………… 池上良平 313
29. 藏王火山の地質學的研究（第 1 報）（英文）…………… 市村毅 327
30. 藏王火山産普通輝石及紫蘇輝石結晶（英文）…………… 市村毅　湊秀雄 341
31. 今市地震地域の地質 (2)（英文）…………… 森本良平 349
32. 最近の大島の噴火とその地震計測學的研究 (I)（英文）…………… 水上武　宮崎務　高橋智子 359
33. 1950 年 2 月の吾妻山の小活動（英文）…………… 水上武　平賀士郎 383
34. 地震による建物の破壞過程について（英文）…………… 金井清 393
35. 東京都江東區における土地の振動周期（英文）…………… 岸上冬彦 403
36. 東京都江東地區の地盤沈下（英文）…………… 岸上冬彦 407
37. 水槽鐵塔の振動について（英文）…………… 那須信治 413
38. 高周波域に於ける土の電氣的性質（邦文）…………… 力武常次　岸上冬彦 423
39. 1950 年 8 月 15 日アッサム・チベット地震觀測報告（英文）…………… 433

所報

(The titles in occidental languages are given on the back cover.)

本彙報ハ年4回 (但シ第1號ヨリ第6號マデハ不定期ニ，第7號ハ3冊トシテ發行セリ)，彙報別冊ハ不定期ニ發行ス．

本彙報掲載ノ論文及ビ報告ノ內容ニ關シテハ著者ノミニ其責任アルモノトス．

本彙報ニ關スル照會通信ハ東京大學地震研究所長ヘ宛テラレタシ．

The Bulletin is published quarterly. (Vols. I–VI were published at irregular intervals and Vol. VII consisted of three parts.)

Supplementary Volume is published at irregular interval.

The authors of the papers alone are responsible for the statements and opinions contained in their respective papers.

All communications relating to this Bulletin should be addressed to the Director of the Earthquake Research Institute, Tokyo University.

19. *Study on Surface Waves II.*
Velocity of Surface Waves Propagated upon Elastic Plates.

By Yasuo SATÔ,

Earthquake Research Institute.

(Read April 18, 1944.—Received March 31, 1951.)

1. introduction.

In this paper, we will discuss the nature of waves propagated upon infinite elastic plates. Of course it is impossible to find a plate with sides free from tractions and which extends infinitely in every direction. The largest plate we may find around us is probably the ice plate formed upon the surface of a lake. Moreover, observations of oscillations on lake ice have been often performed with excellent skill in many countries[1]. Hence it becomes necessary to perform calculations to analyse the seismograms obtained in such cases. Another reason why we take up this subject is as follows. In the famous book of A. E. H. Love[2], we can find simple calculations concerning Rayleigh-waves with superficial layer. Though K. Sezawa[3] and other prominent authors[4] have since been engaged in the task of explaining this problem, the problem is yet to be perfectly solved; for, although some branches of dispersion curves have been discovered and traced, satisfactory examinations of the equation have not been performed yet. Therefore, there is some reason to believe that our solution—which is simple but examined strictly —concerning the elastic plate lying upon liquid, gives some clue for our understanding of the nature of layered Rayleigh-waves.

Although we use the term "surface waves" in this paper, the waves in question do not necessarily satisfy the condition that the elastic energy is concentrated near the surface. However, other properties are in common with the ordinary surface waves, and the mathematical treatment is quite similar, therefore we may reasonably use this term for the present.

---

[1] F. KISHINOUYE, "Studies on Lake Ice." *Bull. Earthq. Res. Inst.*, **21** (1943), 298 (in Japanese); *Zisin*, **12** (1940), 156 (in Japanese). M. EWING, A. P. CRARY and A. M. THORN, Jr., "Propagation of Elastic Waves in Ice." Part I, *Journal of Applied Physics*, **5** (1934), 165; Part II, 181. Also see 17).

[2] A. E. H. LOVE, "Some Problems of Geodynamics," (1911). Chap. VII.

[3] K. SEZAWA and K. KANAI, *Proc. Imp. Acad.*, **11** (1935), 96; *Bull. Earthq. Res. Inst.*, **13** (1935), 471; **16** (1938), 1; **18** (1940) 1.

[4] K. KANAI, "On the Existence of the M_2 Waves in Actual Seismic Disturbance." *Bull. Earthq. Res. Inst.*, **26** (1948), 57, and so on.

2. Surface waves formed by SH waves in a plate.[5]

In the same way we employed for obtaining the velocity equation of Love-waves in the first paper, we can get an analogous equation in this case. Notations are the same with those in the former paper; i.e.

v	y-component of displacement vector.
β	$\begin{cases} \sqrt{(f^2-k^2)} \ldots\ldots\ldots\ldots\ldots\ldots f^2 \geq k^2 \\ i\sqrt{(k^2-f^2)} \equiv i\tilde{\beta} \ldots\ldots\ldots\ldots f^2 < k^2 . \end{cases}$

and the coordinate-axes are chosen so that the plane $z=0$ and $z=H$ coincide with the free surfaces.

Then the displacement v is expressed as

$$v=\{A\exp(\beta z)+B\exp(-\beta z)\}\exp(ifx+ipt) \qquad \ldots\ldots(2.1)$$

Conditions of free surfaces give

$$A=B$$

and

$$\exp\{i2\tilde{\beta}H\}=1 \quad \text{or} \quad \tilde{\beta}H=n\pi \qquad \ldots\ldots(2.2)$$

If we put

$$f=k\sin\theta,$$

we have

$$\tilde{\beta}H=kH\cos\theta\equiv\omega\cos\theta=n\pi \qquad \ldots\ldots(2.3)$$

$$\begin{aligned} v&=A\{\exp(ikz\cos\theta+ikx\sin\theta+ipt)+\exp(-ikz\cos\theta+ikx\sin\theta+ipt)\} \\ &=2A\cos(kz\cos\theta)\cdot\exp(ikx\sin\theta+ipt) \qquad \ldots\ldots(2.4) \end{aligned}$$

This is one of the simplest type of surface waves—so simple that one may hesitate to give them such a name. However, the process by which the above characteristic equation was obtained is strictly similar and the structure of waves are also equal to that of Love-waves in the part of layer; therefore we will treat them in our present study and denote the waves that satisfy (2.3) as Σ_n.

Since θ implies the angle between the direction of propagation and z-axis, the above waves are constructed by two kinds of component waves: one goes upwards and the other downwards (cf. upper expression of (2.4)). Thus they form standing waves with respect to the direction of z-axis, their wave front becomes perpendicular to the free surfaces, and their amplitude distribution is expressed by $\cos(kz\cos\theta)$ (cf. lower expression of (2.4)).

This explanation reminds us of that of Love-waves which we dealt with in the previous paper (cf. I, §3).[6] Phase velocity $\mathfrak{v}$ and group velocity $\mathfrak{V}$ (unit; V_s) are given by the formulae

---

[5] Three dimensional problem was treated by K. SEZAWA. cf. "Sindôgaku" 158, (in Japanese). He calls this type of waves as "second kind".

[6] "I" implies first paper of this study.

$$\mathfrak{v} = \operatorname{cosec}\theta, \quad \mathfrak{V} = \sin\theta \qquad \text{......(2.5)}$$

and the expression coincides with our above interpretation of Σ waves. For, upon the xy-plane the visual velocity of plane waves, which are propagated making the angle θ between wave line and z-axis, is $V_s \operatorname{cosec}\theta$, while the velocity of energy transportation to the x-direction is $V_s \sin\theta$.

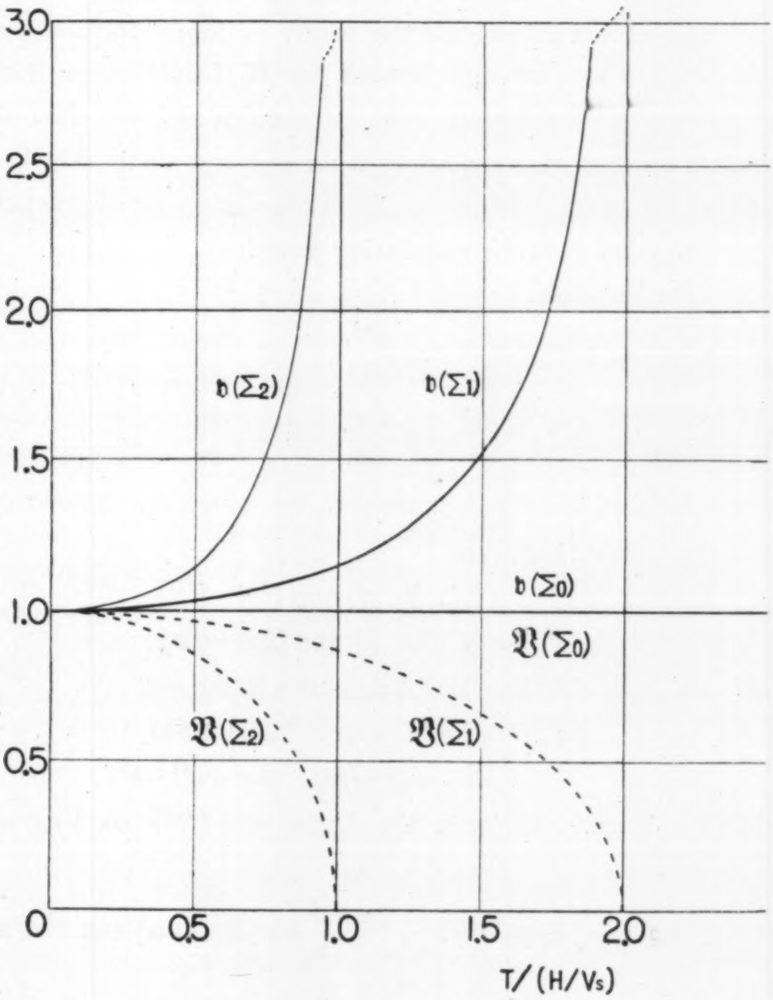

Fig. 1. Phase and group velocity of Σ.

Dispersion curve of Σ_n (n implies the number of node in the plate) is easily obtained from (2. 3) and (2. 5). The result is shown in Fig. 1. From (2. 3) the condition of existence of Σ_n is

$$kH \geq n\pi, \quad \text{or} \quad 2H/V_s \geq nT \quad (T \text{ means a period}) \qquad \text{......(2. 6)}$$

This condition requires that the time for waves to travel up and down the plate perpendicularly is not smaller than n-times of the period of them.

Surface waves formed by *P* and *SV* waves in a plate.[7]

3. Equation of motion and characteristic equation.

In the previous article we have assumed *SH* waves in elastic plates and using this simple model we have studied the generation and structure of surface waves. Now we will proceed and investigate the nature of those formed by *P* and *SV* waves. This problem was already treated by H. Lamb[8] some thirty years ago, but we will develop more comprehensive calculations and will find all branches of dispersion curves so that we may bring to an end our doubt whether there exist or not some other branches. Moreover, from the view-point of practical application, we think there is some value in calculating anew.

Using common notations

$$\left\{\begin{aligned} &\rho\frac{\partial^2 u}{\partial t^2}=(\lambda+2\mu)\frac{\partial \varDelta}{\partial x}+\mu\frac{\partial \varpi}{\partial z}, \qquad \varDelta=\frac{\partial u}{\partial x}+\frac{\partial w}{\partial z} \\ &\rho\frac{\partial^2 w}{\partial t^2}=(\lambda+2\mu)\frac{\partial \varDelta}{\partial z}-\mu\frac{\partial \varpi}{\partial x}, \qquad \varpi=\frac{\partial u}{\partial z}-\frac{\partial w}{\partial x} \end{aligned}\right. \qquad \ldots\ldots(3.\ 1),\ (3.\ 2)$$

Of the solutions of the above equations, we adopt the following type of expressions for our present purpose.

$$\left\{\begin{aligned} &\varDelta=\{A,\ B;\ \alpha\}\exp\{ipt-ifx\} \\ &\varpi=\{C,\ D;\ \beta\}\exp\{ipt-ifx\} \end{aligned}\right. \qquad \ldots\ldots(3.\ 3)$$

where

$$\begin{aligned} &\{A, B;\ \alpha\}=\{A\cosh\alpha z+B\sinh\alpha z\} \\ &\{C, D;\ \beta\}=\{C\cosh\beta z+D\sinh\beta z\} \\ &\alpha=\sqrt{(f^2-h^2)}, \quad \beta=\sqrt{(f^2-k^2)}\ . \end{aligned} \qquad \ldots\ldots(3.\ 4)$$

For simplicity's sake, we omit the factor $\exp\{ipt\}$ so long as no confusion occurs.

$$\left\{\begin{aligned} &\frac{\partial \varDelta}{\partial x}=-if\{A, B;\ \alpha\}\exp(-ifx), \qquad \frac{\partial \varDelta}{\partial z}=\alpha\{B, A;\ \alpha\}\exp(-ifx) \\ &\frac{\partial \varpi}{\partial x}=-if\{C, D;\ \beta\}\exp(-ifx), \qquad \frac{\partial \varpi}{\partial z}=\beta\{D, C;\ \beta\}\exp(-ifx) \end{aligned}\right. \qquad \ldots\ldots(3.\ 5)$$

From the above equation the following expression of u and w are obtained

$$\left\{\begin{aligned} &u=[(if/h^2)\{A, B;\ \alpha\}-(\beta/k^2)\{D, C;\ \beta\}]\exp(-ifx)+u_0+u_0't \\ &w=[-(\alpha/h^2)\{B, A;\ \alpha\}-(if/k^2)\{C, D;\ \beta\}]\exp(-ifx)+w_0+w_0't \end{aligned}\right. \qquad \ldots\ldots(3.\ 6)$$

While we are dealing with periodic solutions, we may put

---

7) *loc. cit.* 5). He calls this type as "first kind."

8) H. LAMB, "On Waves in a Elastic Plate." *Proc. Roy. Soc. Lond.*, **93** (1917), 114.

$$u_0 = u_0' = w_0 = w_0' = 0$$

On the other hand, the stress components are

$$\left\{\begin{aligned} \widehat{xx} &= \lambda\Delta + 2\mu\frac{\partial u}{\partial x} = [P\cdot\{A, B;\ \alpha\} + S\cdot\{D, C;\ \beta\}]\exp(-ifx) \\ \widehat{zz} &= \lambda\Delta + 2\mu\frac{\partial w}{\partial z} = [P_z\cdot\{A, B;\ \alpha\} + S_z\cdot\{D, C;\ \beta\}]\exp(-ifx) \\ \widehat{xz} &= \mu\left(\frac{\partial u}{\partial z} + \frac{\partial w}{\partial x}\right) = [P_x\cdot\{B, A;\ \alpha\} + S_x\cdot\{C, D;\ \beta\}]\exp(-ifx) \end{aligned}\right. \qquad \cdots\cdots(3.\ 7)$$

where

$$\left\{\begin{aligned} P &= \lambda + 2\mu f^2/h^2, & S &= i2\mu\beta f/k^2 \\ P_z &= \lambda - 2\mu\alpha^2/h^2, & S_z &= -i2\mu\beta f/k^2 \\ P_x &= i2\mu\alpha f/h^2, & S_x &= -\mu(f^2+\beta^2)/k^2 \end{aligned}\right.$$

Substituting boundary conditions ($z=0$; $\widehat{xz}=0$, $\widehat{zz}=0$: $z=H$; $\widehat{xz}=0$, $\widehat{zz}=0$) into the above expressions we have

$$\left\{\begin{aligned} P_xB + S_xC &= 0 \\ P_zA + S_zD &= 0 \\ P_xA\mathfrak{S} + P_xB\mathfrak{C} + S_xC\mathfrak{C}' + S_xD\mathfrak{S}' &= 0 \\ P_zA\mathfrak{C} + P_zB\mathfrak{S} + S_zC\mathfrak{S}' + S_zD\mathfrak{C}' &= 0 \end{aligned}\right. \qquad \cdots\cdots(3.\ 8)$$

in which

$$\mathfrak{C} = \cosh\alpha H, \quad \mathfrak{S} = \sinh\alpha H$$
$$\mathfrak{C}' = \cosh\beta H, \quad \mathfrak{S}' = \sinh\beta H$$

Elliminating A, B, C and D we obtain the characteristic equation.

$$2(1-\mathfrak{C}\mathfrak{C}') + \left(\frac{P_z}{P_x}\cdot\frac{S_x}{S_z} + \frac{P_x}{P_z}\cdot\frac{S_z}{S_x}\right)\mathfrak{S}\mathfrak{S}' = 0 \qquad \cdots\cdots(3.9)$$

So long as the above relation holds, A, B, C and D are expressed by using a constant G

$$\left\{\begin{aligned} A &= GS_xZ(\mathfrak{C}-\mathfrak{C}') \\ B &= -GS_x(Z\mathfrak{S}-\mathfrak{S}') \\ C &= GP_x(Z\mathfrak{S}-\mathfrak{S}') \\ D &= -GP_x(\mathfrak{C}-\mathfrak{C}') \end{aligned}\right. \qquad \cdots\cdots(3.10)$$

in which a new notation $Z = \dfrac{P_x}{P_z}\cdot\dfrac{S_z}{S_x}$ is introduced. ......(3.11)

Using this notation (3.10) becomes

$$2(1-\mathfrak{C}\mathfrak{C}') + (Z+1/Z)\mathfrak{S}\mathfrak{S}' = 0 \qquad \cdots\cdots(3.10)'$$

Solving this equation with respect to Z, we have

$$\left(Z - \frac{\mathfrak{C}-1}{\mathfrak{C}'-1}\frac{\mathfrak{S}'}{\mathfrak{S}}\right)\left(Z - \frac{\mathfrak{C}'-1}{\mathfrak{C}-1}\frac{\mathfrak{S}}{\mathfrak{S}'}\right) = 0 \qquad \cdots\cdots(3.12)$$

(3.12) is a very interesting result, for it shows that dispersion curves are perfectly separated into two groups which are represented by the two factors in the left hand side of (3.12). Simplifying the above equation further, we have

$$Z=\mathfrak{T}/\mathfrak{T}' \quad \text{or} \quad Z=\mathfrak{T}'/\mathfrak{T}$$

where

$$\mathfrak{T}=\tanh(\alpha H/2), \quad \mathfrak{T}'=\tanh(\beta H/2) \qquad \text{......(3.13)}$$

Here we will denote the dispersion curves gained from the former equation as Π^- and the latter as Π^+. These notations correspond to the branches named as "asymmetrical" and "symmetrical" by H. Lamb[9]. Later, it will be shown that the former involves a branch of anomalous dispersion, and the latter consists of branches of normal dispersion only. We will denote the Π^+ branch that satisfies the condition $\lim_{\mathfrak{v}^2\to 2}\xi=(2n+1)\pi$ as $\Pi_n{}^+$ and the Π^- branch of $\lim_{\mathfrak{v}^2\to 2}\xi=2n\pi$ as $\Pi_n{}^-(n\neq 0)$.

The branch of anomalous dispersion is $\Pi_0{}^-$, and the ordinary Rayleigh-waves corresponds to $\Pi_0{}^+$. M_2-wave of K. Sezawa and K. Kanai[7] seems to correspond to $\Pi_1{}^-$. $\Pi_n{}^-$ and $\Pi_n{}^+$ $(n=0,1,2......)$ represents all the branches of dispersion curves in elastic plates and no other branch can exist.

4. Numerical culculations.

We write again the expression (3.13) using original notations

$$\Pi^-;\ \frac{P_x}{P_z}\frac{S_z}{S_x}=\frac{\tanh(\alpha H/2)}{\tanh(\beta H/2)}, \quad \Pi^+;\ \frac{P_x}{P_z}\frac{S_z}{S_x}=\frac{\tanh(\beta H/2)}{\tanh(\alpha H/2)} \qquad \text{......(4.1)}$$

or

$$\left\{\begin{array}{l} \Pi^-;\dfrac{\surd(1-\mathfrak{v}^2/\gamma^2)\cdot\surd(1-\mathfrak{v}^2)}{(1-\mathfrak{v}^2/2)^2}=\dfrac{\tanh\left\{\frac{1}{2}\xi\surd(1-\mathfrak{v}^2/\gamma^2)\right\}}{\tanh\left\{\frac{1}{2}\xi\surd(1-\mathfrak{v}^2)\right\}} \\[2ex] \Pi^+;\dfrac{\surd(1-\mathfrak{v}^2/\gamma^2)\cdot\surd(1-\mathfrak{v}^2)}{(1-\mathfrak{v}^2/2)^2}=\dfrac{\tanh\left\{\frac{1}{2}\xi\surd(1-\mathfrak{v}^2)\right\}}{\tanh\left\{\frac{1}{2}\xi\surd(1-\mathfrak{v}^2/\gamma^2)\right\}} \end{array}\right. \qquad \text{......(4.1)}$$

in which

$$\left\{\begin{array}{ll} \mathfrak{v}=k/fV_s & \text{...phase velocity of surface waves (unit; } V_s) \\ \gamma=V_p/V_s & \text{...ratio of the velocity of } P \text{ and } S \text{ waves.} \\ \xi=fH & \text{.........wave number } (2\pi H/\text{wave length}) \\ \omega=pbH & \text{......circular frequency (time unit; } H/V_s) \\ \Lambda & \text{..............wave length (unit; } H) \end{array}\right. \qquad \text{......(4.2)}$$

Our subject in this article is to solve the equation (4.1) perfectly. Of course it is desirable to get an explicit analytical solution, which however is difficult judging from the form of the equation, so that we solved numerically.

---

[9] *loc. cit.* 8)

[10] *cf.* 3) and 4).

Our calculation covers the cases shown by the notation † in Tab. I. In this table we find notations * which indicate the existence of H. Lamb's calculations. His result, however, does not contain the points dense enough to trace the dispersion curve precisely, so we added new points to his results.

Table I.

$\gamma^2=V_P^2/V_S^2$	Π_0^-	Π_0^+	Π_1^-	Π_1^+	Π_2^-
3	†	† *	†	†	†
4	†	†	†	†	
∞	*	*	†	†	

The assumption $\gamma^2=3$ is the case of so-called Poisson's hypothesis ($\lambda=\mu$, or $\sigma=1/4$) and much of the substances around us satisfy this condition approximately, so we calculated this case precisely. Next, $\gamma^2=4$ is the case $\lambda=2\mu$, which is rarely found in ordinary investigations. However, one of the principal aims of the paper is to get theoretical foundations for the observations upon lake ice, so that we adopted this assumption since the physical constants of ice satisfy this relation

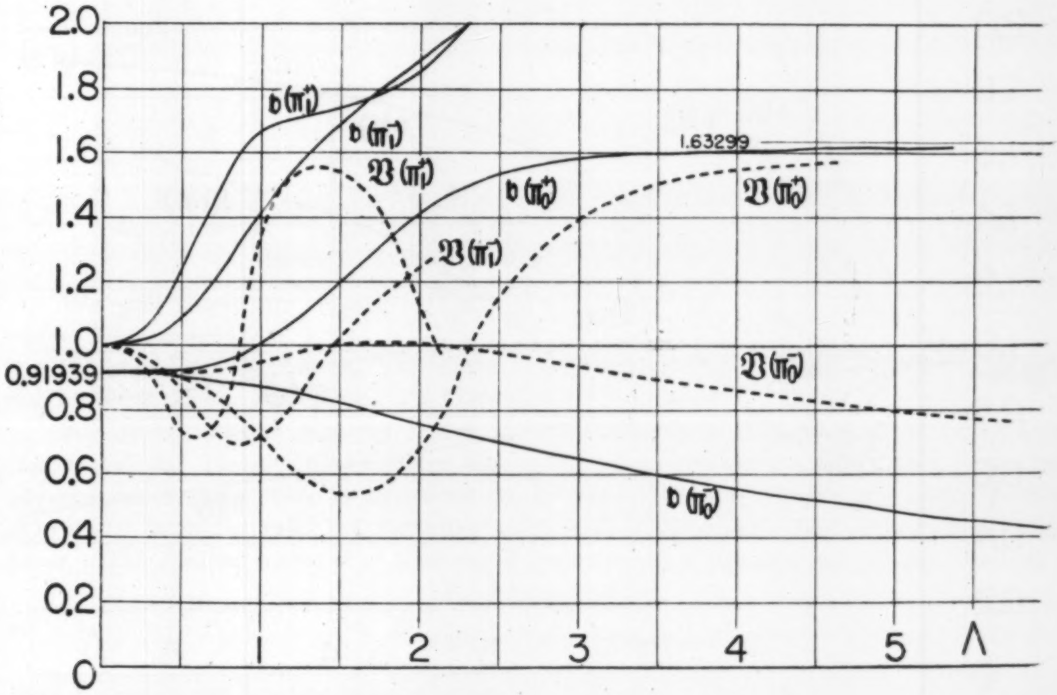

Fig. 2. Phase and group velocity of Π. ($\gamma^2=3$)

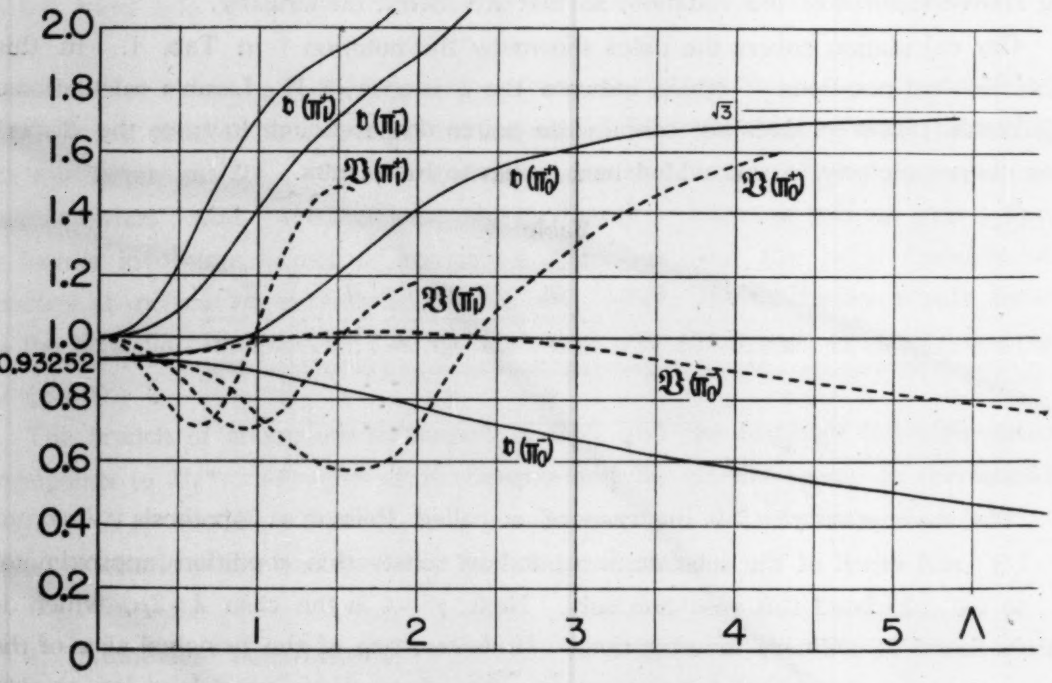

Fig. 3. Phase and group velocity of Π. ($\gamma^2=4$)

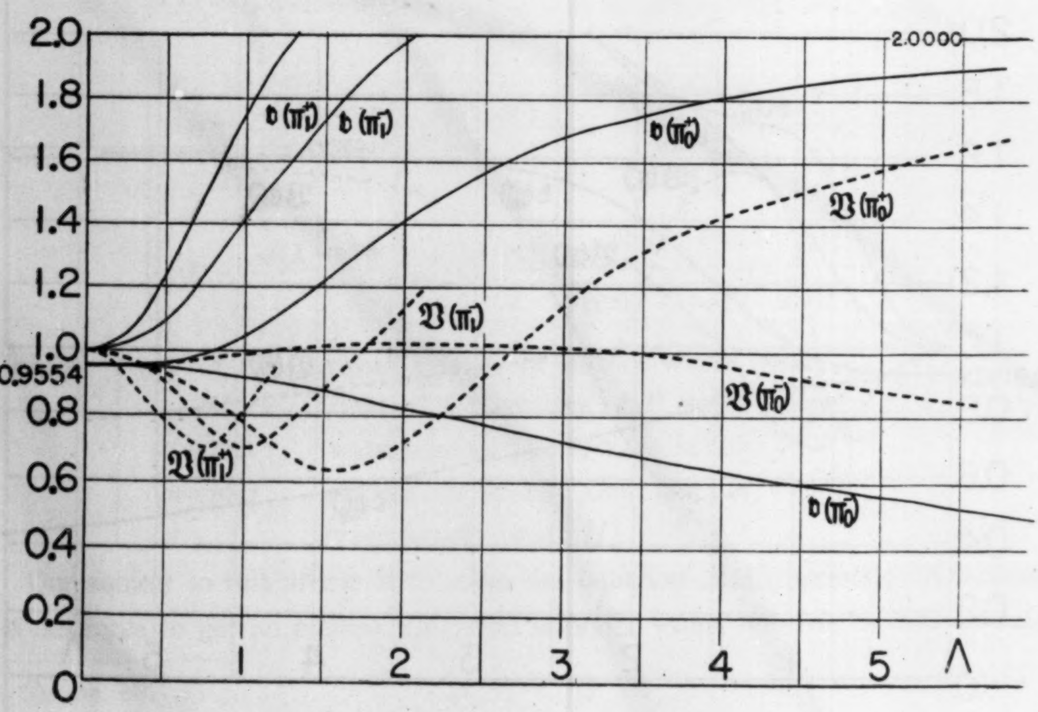

Fig. 4. Phase and group velocity of Π. ($\gamma^2=\infty$)

farely well. $\gamma^2=\infty$ implies imcompsessibility and the characteristic equation becomes very simple; for putting $1/\gamma=0$ and $\alpha=f$ into (4,1) we have

$$\left\{\begin{array}{l} \Pi^-;\ \sqrt{(1-\mathfrak{v}^2)}/(1-\mathfrak{v}^2/2)^2=\tanh(\xi/2)\Big/\tanh\left\{\dfrac{1}{2}\xi\sqrt{(1-\mathfrak{v}^2)}\right\} \\ \Pi^+;\ \sqrt{(1-\mathfrak{v}^2)}/(1-\mathfrak{v}^2/2)^2=\tanh\left\{\dfrac{1}{2}\xi\sqrt{(1-\mathfrak{v}^2)}\right\}\Big/\tanh(\xi/2) \end{array}\right. \quad \ldots\ldots(4.3)$$

Although we have little interest in this assumption, we calculated also this case to compare with the results obtained by H. Lamb and other authors.[11]

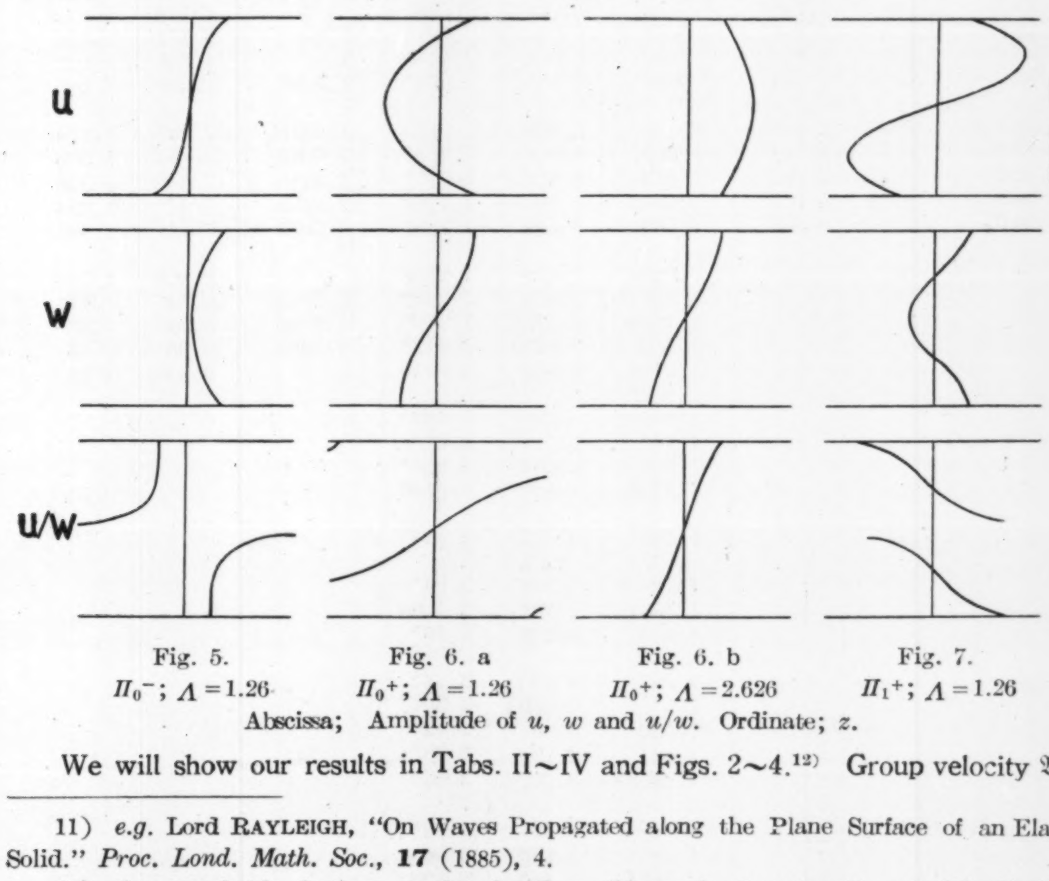

Fig. 5. Π_0^-; $\Lambda=1.26$ Fig. 6. a Π_0^+; $\Lambda=1.26$ Fig. 6. b Π_0^+; $\Lambda=2.626$ Fig. 7. Π_1^+; $\Lambda=1.26$

Abscissa; Amplitude of u, w and u/w. Ordinate; z.

We will show our results in Tabs. II~IV and Figs. 2~4.[12] Group velocity $\mathfrak{V}$ is

---

[11] *e.g.* Lord **Rayleigh**, "On Waves Propagated along the Plane Surface of an Elastic Solid." *Proc. Lond. Math. Soc.*, **17** (1885), 4.

[12] A remarkable fact we notice in these figures is that in Fig. 2 ($\gamma^2=3$), Π_n^- branch and Π_n^+ branch ($n\geqq1$) crosses each other, while in Figs. 3 and 4 ($\gamma^2=4$, ∞) no such phenomenon occurs. This is explained as follows. When $\gamma^2=3$, $Z=\sqrt{(1-\mathfrak{v}^2)}\sqrt{(1-\mathfrak{v}^2/\gamma^2)}/(1-\mathfrak{v}^2/2)^2$ takes the value -1 for some value of $\mathfrak{v}^2$, while when $\gamma^2=4$ or ∞, $Z=-1$ never holds. The limiting value of γ^2 whereby Z becomes -1 is obtained solving the equation

$$\text{Maximum of } Z^2=1$$

or

$$\frac{d}{d(\mathfrak{v}_1^2)}(Z^2(\mathfrak{v}_1^2))=0, \quad Z^2(\mathfrak{v}_1^2)=1\,.$$

Thus we obtain the limiting value of γ^2 as

$$\gamma^2=3.110\,.$$

Table II. Phase velocity of surface waves in elastic

Π_0^-			Π_0^+			Π_1^-		
$\mathfrak{v}$	ω	Λ	$\mathfrak{v}$	ω	Λ	$\mathfrak{v}$	ω	Λ
.91939	∞	0	.91939	∞	0	1	∞	0
.9165	7.66	.3758	.925	11.41	.509*	1.00995	51.3	.123
.8832	5.894	.4707	.942	8.552	.692*	1.0392	17.5	.370
.8485	4.206	.6338	.9487	7.553	.7314	1.0954	13.2	.519
.8124	3.236	.7888	.956	7.661	.784*	1.2247	10.46	.735
.7746	2.592	.9389	.969	7.215	.844*	1.3416	9.372	.8991
.7348	2.068	1.1160	.978	6.919	.888*	$\sqrt{2}$	$\pi 2\sqrt{2}$	1
.6928	1.672	1.301	.986	6.728	.921*	1.4491	8.671	1.050
.6403	1.330	1.512	.992	6.601	.944*	1.5	8.361	1.127
.6	1.0704	1.761	.997	6.533	.959*	1.5492	8.066	1.206
.5477	.8331	2.065	1	6.468	.9715	1.5875	7.825	1.274
.4899	.6271	2.454	1.003	6.411	.983*	1.6062	7.682	1.308
.4243	.4455	2.992	1.013	6.258	1.017*	1.6248	7.576	1.348
.3464	.2709	4.017	1.0392	5.929	1.1014	1.6432	7.47	1.384
.2449	.1205	6.385	1.049	5.838	1.129*	1.6882	7.14	1.486
0	0	∞	1.0954	5.499	1.2516	$\sqrt{3}$	6.868	1.584
			1.102	5.460	1.268*	1.7833	6.54	1.711
			1.1619	5.1751	1.4106	1.8166	6.34	1.800
			1.163	5.1754	1.412*	1.8974	5.88	2.03
			1.225	4.959	1.5520	2	5.44	2.31
			1.284	4.793	1.683*			
			1.285	4.789	1.6858			
			1.338	4.658	1.805*			
			1.3416	4.646	1.8146			
			1.386	4.527	1.924*			
			$\sqrt{2}$	$\pi\sqrt{2}$	2			
			1.428	4.398	2.04*			
			1.4491	4.321	2.1068			
			1.464	4.259	2.16*			
			1.495	4.13	2.28*			
			1.5	4.0894	2.3047			
			1.522	3.96	2.42*			
			1.544	3.77	2.58*			
			1.5492	3.707	2.626			
			1.564	3.53	2.78*			
			1.581	3.268	3.04			
			1.5874	3.143	3.173			
			1.596	2.949	3.40*			
			1.6062	2.633	3.833			
			1.609	2.534	3.99*			
			1.620	1.977	5.15*			
			1.6248	1.6201	6.302			
			1.630	1.045	9.8*			
			1.6296	0.9781	10.47			
			1.6323	0.4899	20.94			

plates. ($\gamma^2=3$)

Π_1^+			Π_2^-		
v	ω	Λ	v	ω	Λ
1	∞	0	1	∞	0
1.0198	38.27	.1674	1.00995	73.9	0.0861
1.0392	29.103	.2244	1.0392	29.5	.221
1.0954	20.956	.3284	1.0954	24.5	.280
1.2247	15.892	.4842	1.2247	22.2	.363
1.3416	14.083	.5984	1.3416	18.9	.445
$\sqrt{2}$	$\pi 3\sqrt{2}$	2/3	$\sqrt{2}$	$\pi 4\sqrt{2}$	1/2
1.4491	13.010	.6998	1.4491	17.4	.523
1.5492	12.130	.8024	1.5492	16.1	.604
1.6432	10.967	.9414	1.6432	15.2	.6792
1.6793	10.029	1.0521	$\sqrt{3}$	14.2	.7647
1.7146	8.446	1.275			
$\sqrt{3}$	7.696	1.414			
1.7833	6.477	1.730			
1.8166	6.113	1.867			
1.8974	5.6922	2.094			
2	5.44	2.31			

Table III. Phase velocity of surface waves in

Π_0^-			Π_0^+		
$\mathfrak{v}$	ω	Λ	$\mathfrak{v}$	ω	Λ
.93252	∞	0	.93252	∞	0
.9	6.206	.9113	.9798	7.482	.8228
.8832	5.087	1.0908	1.0677	5.900	1.1370
.8485	3.752	1.4209	1.1446	5.322	1.3512
.8124	2.929	1.743	1.2247	5.024	1.5323
.7746	2.343	2.027	1.2728	4.854	1.6474
.7348	1.901	2.429	1.3416	4.659	1.8086
.6481	1.248	3.264	$\sqrt{2}$	$\pi\sqrt{2}$	2
.5477	0.7777	4.425	1.4491	4.330	2.103
.4583	.4986	5.775	1.4900	4.178	2.241
.3464	.2635	8.267	1.5492	3.902	2.494
.2258	.1130	12.566	1.5875	3.664	2.726
.12288	.0369	20.943	1.6248	3.344	3.053
0	0	∞	1.6613	2.912	3.585
			1.6971	2.211	4.822
			1.7205	1.3768	7.854
			1.7292	0.69168	15.708
			$\sqrt{3}$	0	∞

Table IV. Phase velocity of surface waves in

Π_0^-			Π_0^+		
$\mathfrak{v}$	ω	Λ	$\mathfrak{v}$	ω	Λ
.9554	∞	0 *	.9554	∞	0 *
.954	16.83	.356*	.957	16.60	.362*
.934	7.847	.748*	.960	13.64	.442*
.917	5.551	1.038*	.963	11.82	.492*
.893	3.990	1.321*	.966	11.46	.530*
.866	3.371	1.614*	.968	10.86	.560*
.835	2.742	1.913*	.979	9.292	.662*
.800	2.202	2.282*	.989	8.606	.722*
.760	1.780	2.683*	.995	8.231	.759*
.714	1.422	3.157*	.999	8.058	.779*
.661	1.112	3.736*	1.0	8.004	.785*
.600	0.847	4.45 *	1.005	7.786	.811*
.527	.819	5.58 *	1.020	7.283	.880*
.436	.379	7.22 *	1.044	6.721	.976*
.312	.187	10.5 *	1.077	6.649	1.090*
0	0	∞ *	1.118	5.786	1.214*
			1.166	5.435	1.348*
			1.221	5.149	1.490*
			1.281	4.899	1.643*
			1.345	4.659	1.814*
			$\sqrt{2}$	$\pi\sqrt{2}$	2 *
			1.487	4.214	2.217*
			1.562	3.964	2.476*
			1.640	3.677	2.803*
			1.721	3.327	3.25 *
			1.803	2.876	3.94 *
			1.887	2.242	5.29 *
			1.972	1.146	10.8 *
			1.981	0.957	13.0 *
			1.989	.694	18.0 *
			1.998	.324	38.8 *
			2	0	∞ *

elastic plates. ($\gamma^2=4$)

Π_1^-			Π_1^+		
$\mathfrak{v}$	ω	Λ	$\mathfrak{v}$	ω	Λ
1	∞	0	1	∞	0
1.0954	13.408	.5133	1.0954	21.108	.3261
1.2247	10.514	.7342	1.2247	15.933	.4829
1.3416	9.379	.8987	1.3416	14.087	.5984
$\sqrt{2}$	$\pi 2\sqrt{2}$	1	$\sqrt{2}$	$\pi 3\sqrt{2}$	2/3
1.4491	8.671	1.0500	1.4491	13.011	.6998
1.5492	8.099	1.2018	1.5492	12.198	.7980
1.6432	7.562	1.3653	1.6432	11.451	.9016
$\sqrt{3}$	7.046	1.5455	$\sqrt{3}$	10.635	1.0233
1.8166	6.563	1.7391	1.8166	9.632	1.1851
1.8974	6.024	1.979	1.8974	8.451	1.4107
1.9748	5.776	2.148	1.9748	7.486	1.6574
2	5.672	2.215	2	7.256	1.7318
2.0493	5.521	2.332	2.0493	6.927	1.8586

elastic plates. ($\gamma^2=\infty$)

Π_1^-			Π_1^+		
$\mathfrak{v}$	ω	Λ	$\mathfrak{v}$	ω	Λ
1	∞	0	1	∞	0
1.0954	13.70	.5023	1.0954	21.40	.3216
1.2247	10.577	.7275	1.2247	16.02	.4762
1.3416	9.391	.8976	1.3416	14.100	.5972
$\sqrt{2}$	$\pi 2\sqrt{2}$	1	$\sqrt{2}$	$\pi 3\sqrt{2}$	2/3
1.4491	8.674	1.0497	1.4491	12.956	.7027
1.5492	8.138	1.1961	1.5492	12.251	.7945
1.6432	7.687	1.343	1.6432	11.642	.8868
$\sqrt{3}$	7.280	1.495	$\sqrt{3}$	11.115	.9792
1.8166	6.903	1.654	1.8166	10.634	1.0733
1.8974	6.556	1.818	1.8974	10.193	1.1696
1.9748	6.234	1.990	1.9748	9.785	1.2681
2	6.136	2.048	2	9.658	1.3011

obtained by the graphical differentiation of phase velocity. Using these data we calculated the amplitude distribution corresponding to some values of period in the case of $\gamma^2=3$. For this purpose, equations (3. 6) and (3. 11) are used. The results are shown in Figs. 5~7.[13]

5. **When some liquid exists on one side of a plate.**

In order to explain the observations upon lake ice theoretically, we must treat the model as if some liquid exists on one side of an elastic plate, and we must somewhat change the form of equations which we have solved in the previous articles.

The equation of motion in elastic part is the same with the former one, and that in the liquid part is

$$\begin{cases} \rho^* \dfrac{\partial^2 u^*}{\partial t^2} = \lambda^* \dfrac{\partial \Delta^*}{\partial x} \\ \rho^* \dfrac{\partial^2 w^*}{\partial t^2} = \lambda^* \dfrac{\partial \Delta^*}{\partial z} \end{cases} \qquad \text{......(5. 1)}$$

where * means the quantities in the liquid.[14]

We use the following notations, which will need no explanation.

$$\begin{aligned} &\Delta^* = \{M, N;\ *\} \exp\{ipt - ifx\} \\ &\{M, N;\ *\} = \{M \cosh \alpha^* z + N \sinh \alpha^* z\} \\ &\alpha^{*2} = f^2 - h^{*2} \\ &h^{*2} = a^{*2}p^2 = p^2/V^{*2} = p^2 \cdot \rho^*/\lambda^* \end{aligned} \qquad \text{......(5. 2)}$$

We take the depth of the water as D. If we may assume the bottom to be rigid, the vertical displacement w^* must vanish at $z=-D$. And the boundary conditions at the contact plane of water and ice $(z=0)$ are the continuity of normal stress $\widehat{zz}$, and vertical displacement w, and vanishing of tangential stress $\widehat{xz}$; therefore we have

1) $z=H;\quad \widehat{xz}=0;\quad P_x\mathfrak{S}A+P_x\mathfrak{C}B+S_x\mathfrak{C}'C+S_x\mathfrak{S}'D=0$

2) $z=H;\quad \widehat{zz}=0;\quad P_x\mathfrak{C}A+P_z\mathfrak{S}B+S_z\mathfrak{S}'C+S_z\mathfrak{C}'D=0$

3) $z=0;\quad \widehat{xz}=0;\quad P_x\ B+S_x\ C\qquad =0$

4) $z=0;\quad \widehat{zz}=\widehat{zz}^*;\quad P_zA\qquad +S_z\ D=\lambda^*M$

5) $z=0;\quad w=w^*;\quad -\dfrac{\alpha}{h^2}B-\dfrac{if}{k^2}C\qquad = \quad -\dfrac{\alpha^*}{h^{*2}}N$

6) $z=-D; u^*=0;\qquad 0\quad =-\mathfrak{S}^*=M+\mathfrak{C}^*N$

where $\mathfrak{C}^*=\cosh\alpha^*D,\ \mathfrak{S}^*=\sinh\alpha^*D$ ......(5. 3)

---

13) This calculation owes to Mr. T. Rikitake. The author is very much obliged to him.

14) λ^* is the modulus of compression usually denoted as k.

Here the condition 1), 2) and 3) are the same with three equations in (3. 9). If the water[15] is bottomless, we ought to put

$$\mathfrak{C}^* = \mathfrak{S}^*$$

into the last equation of (5. 3).[16]

From the six equations in (5. 3), we eliminate A, B, C, D and M, N,

$$-\Delta_{\text{III}}' = P_x P_z S_x S_z \left(-\frac{\alpha^*}{h^{*2}}\right)\left[-\Delta_{\text{I}} + \frac{1}{Z^*}\frac{1}{\mathfrak{T}^*}(\mathfrak{C}\mathfrak{S}' - Z\mathfrak{S}\mathfrak{C}')\right] \quad \ldots\ldots(5.\ 10)$$

in which

$$\frac{1}{Z^*} = \frac{h^{*2}}{\alpha^*}\frac{\lambda^*}{S_z}\left(\frac{\alpha}{h^2}\frac{S_x}{P_x} - i\frac{f}{k^2}\right) = \frac{\lambda^* h^{*2} k^2}{4\mu\alpha^*\beta f^2}$$

---

[15] Simply we write as "water" instead of "liquid".

[16] Equation of motion in the liquid part is not the same with the ordinary one which uses velocity potential. However, as is easily expected from the consideration of the constitution of equation, the two equations are identically equal when there is no general flow in the liquid. We will show the proof of it analytically.

Denoting velocity potential as ϕ^* we have

$$\begin{cases} u^* = -\partial\phi^*/\partial x \\ w^* = -\partial\phi^*/\partial z \end{cases} \quad \ldots\ldots(5.\ 4)$$

$$\partial^2\phi^*/\partial t^2 = (1/a^*)^2 \Delta^2 \phi^* \quad \ldots\ldots(5.\ 5)$$

where $1/a^*$ is the sound velocity in water.

ϕ^* satisfying (5. 5) is expressed as

$$\phi^* = \{M' \cosh \alpha^* z + N' \sinh \alpha^* z\} \exp(-ifx + ipt) \quad \ldots\ldots(5.\ 6)$$

$$\alpha^{*2} = f^2 - a^{*2} p^2$$

From this

$$\begin{cases} \dot{u}^* = if\{M' \cosh \alpha^* z + N' \sinh \alpha^* z\} \exp(-ifx + ipt) \\ \dot{w}^* = -\alpha^* \{M' \sinh \alpha^* z + N' \cosh \alpha^* z\} \exp(-ifx + ipt) \end{cases}$$

Deviation of pressure from the mean value is

$$\begin{aligned} \delta\pi &= -\rho^* \partial\phi/\partial t \\ &= i\rho^* p\{M' \cosh \alpha^* z + N' \sinh \alpha^* z\} \exp(-ifx + ipt) \end{aligned} \quad \ldots\ldots(5.\ 7)$$

The boundary conditions 1), 2), 3) in (5. 3) are not altered, while the remaining three are altered as follows.

$$\begin{array}{llll} \text{Instead of 4)} & \widehat{zz} = -\delta\pi; & P_z A & + S_z D = -i\rho^* p M' \quad \ldots\ldots\ldots 4)' \\ \quad 5) & \dot{w} = \dot{w}^*; & \frac{\alpha}{h^2} B + p\frac{f}{k^2} C & = \quad -\alpha^* N' \ \ldots\ldots 5)' \\ \quad 6) & w = 0; & & 0 = -M'\mathfrak{S}^* + N'\mathfrak{C}^* \ \ldots\ldots 6)' \ldots (5.8) \end{array}$$

Now, if we assume

$$\begin{cases} M' = (ip/h^{*2})M \\ N' = (ip/h^{*2})N \end{cases}$$

and put this relation into 4)′, 5)′ and 6)′ then we have

$$\begin{array}{lll} 4)'; & P_z A & + S_z D = (-i\rho^* p)(ip/h^{*2})M = \lambda^* M \\ 5)'; & (ip)\left[-\frac{\alpha}{h^2}B - i\frac{f}{k^2}C\right] & = \quad (ip)\left(-\frac{\alpha^*}{h^{*2}}N\right) \ldots (5.\ 9) \\ 6)'; & & 0 = \left(\frac{ip}{h^{*2}}\right)[-M\mathfrak{S}^* + N\mathfrak{C}^*] \end{array}$$

These three equations are identical with the three in (5. 3).

$$-\Delta_{\mathrm{I}}\equiv 2(1-\mathfrak{C}\mathfrak{C}')+(Z+1/Z)\mathfrak{S}\mathfrak{S}', \quad \mathfrak{T}^*=\tanh\{D\sqrt{(f^2-h^{*2})}\}$$

The last expression is the same with the left side of (5. 10). When the water is infinitely deep, putting $\mathfrak{T}^*=1$ we have

$$-\Delta_{\mathrm{II}}'\equiv P_xP_zS_xS_z\left(-\frac{\alpha^*}{h^{*2}}\right)\left[-\Delta_{\mathrm{I}}+\frac{1}{Z^*}(\mathfrak{C}\mathfrak{S}'-Z\mathfrak{S}\mathfrak{C}')\right]=0, \qquad \ldots\ldots(5.\,11)$$

when there is no water and both sides are free, putting $1/Z^*=0$

$$-\Delta_{\mathrm{I}}'\equiv P_xP_zS_xS_z\left(\frac{\alpha^*}{h^{*2}}\right)\Delta_{\mathrm{I}}=0 \qquad \ldots\ldots(5.\,12)$$

which is, of course, identical with the equation (3. 10).

We solved the equation (5. 11) numerically giving the physical constants as follows:

$$\left\{\begin{array}{l}\Gamma\equiv\rho^*/\rho=1.09\\ \gamma^2\equiv(\lambda+2\mu)/\mu=(V_p/V_s)^2=4\\ \gamma^{*2}\equiv(V^*/V_s)^2=1/1.44\end{array}\right. \qquad \ldots\ldots(5.\,13)$$

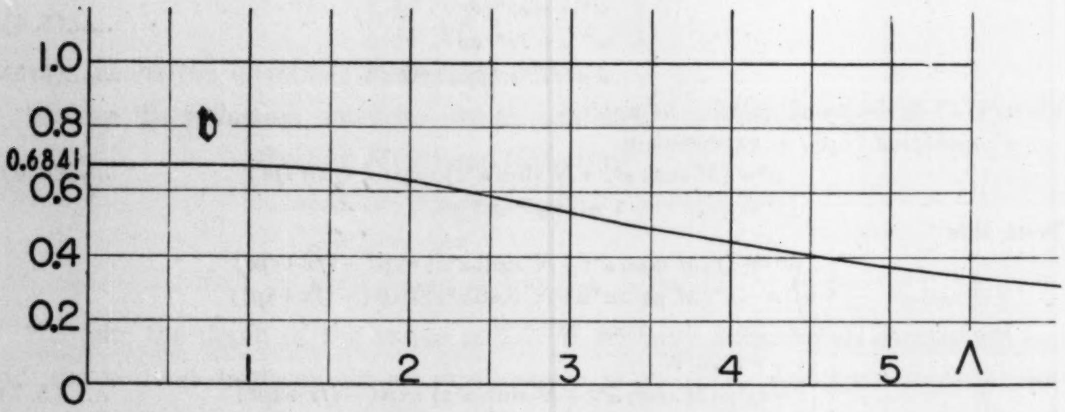

Fig. 8. Phase velocity of *II* when ice plate is in contact with water.

Table V. Phase velocity of surface waves when ice plate is in contact with bottomless water.
($\gamma^2=4$, $\gamma^{*2}=1/1.44$, $\rho^*/\rho=1.09$)

$\mathfrak{v}$	ω	Λ	$\mathfrak{v}$	ω	Λ
.68410	∞	0	.4243	.6220	4.286
.6708	2.938	1.4345	.4	.5472	4.593
.6326	2.010	1.977	.3162	.3336	5.956
.5657	1.3271	2.678	.2	.1390	9.041
.5477	1.2028	2.861	0	0	∞
.4899	.8867	3.471			

This assumption is not so unsuitable, for if we assume

$$V^* = 1450\ \text{m/sec}\,,$$

then $$V_s = 1740\ \text{m/sec}\,, \qquad \ldots\ldots(5.\,14)$$

and $$V_p = 3480\ \text{m/sec}\,.$$

These values are nearly equal to those which are presented by observations and experiments.[17] The result is shown in Fig. 8 and Table V.

In this calculation we notice a remarkable fact that there is no other branch than Π_0^- which shows the property of abnormal dispersion. Of course, this is not so astonishing if the combination of matters is of ice and water. However, even if the combination is of steel and water or steel and air, the above fact holds. We will consider this problem in § 6. 4 and § 8. 22.

6. **Solution by means of power series.**

In the previous articles we have solved the equation numerically. However as it is quite complicated and we cannot perform very comprehensive calculations, we cannot hope to obtain a wide view of the whole nature of the waves. To make up this defect, we will choose the case when the solution may be reduced to a simple form. For this purpose it is convenient to discuss long waves with wave-length much larger than the thickness of the plate. In this case we can expand the characteristic equation as a power series of ξ.

---

17) Hans Mothes gives; $V_p = 3400$ m/sec, $V_s = 1600$ m/sec. ("Seismische Dickenmessungen von Gletschereis." *Zeits. f. Geophys*, **3** (1927), 121.) Also he gives in another case; $V_p = 3600$ m/sec, $V_s = 1690$ m/sec and $V_p = 3140$ m/sec, $V_s = 1350$ m/sec. ("Neue Ergebnisse der Eisseismik." *Zeits. f. Geophys.*, **5** (1929), 120.) Results of Köhler's observations are; $V_p = 3200$ cm/sec, $V_s =$ 1700 m/sec. ("Beobachtungen an Profilen auf See-eis." *Zeits. f. Geophys.*, **5** (1929), 314.) E. Sorge gives from the observations in Greenland; $V_p = 3490$ m/sec, $V_s = 1690$ m/sec; $V_p = 3410$ m/sec, $V_s = 1605$ m/sec; $V_p = 3695$ m/sec, $V_s = 1820$ m/sec. ("Die erste Dickenmessungen des grönländischen Inlandeises." *Zeits. f. Geophys.*, **6** (1930), 22.) M. Ewing and others give; $E = 9.17 \pm 0.05 \times 10^{10}$ c.g.s., $\mu = 3.36 \pm 0.02 \times 10^{10}$, $K = 11.3 \pm 0.6 \times 10^{10}$, $\sigma = 0.365 \pm 0.007$, $a = 9.1 \pm 0.6 \times 10^{10}$, $\rho = 0.917$ from which we have $V_p = 3410$ m/sec. (cf. 1)) F. Gerecke gives the value $V_p = 3600$ m/sec, $V_s = 1700$ m/sec. ("Seismische Untersuchungen des Geophys. Institute in Göttingen." *Zeits. f. Geophys.*, **8** (1932), 65) And K. Wegener gives the value in various temperature. $V_p = 3600$ m/sec (0°C) 3720 m/sec (−6°C), 4000 m/sec (−16°C) ("Laufgeschwindigkeit c der Longitudinalwellen als Funktion der Temperatur." *Zeits. f. Geophys.*, **15** (1939), 390.) In Japan, F. Kishinouye gives at Lake Suwa; $V_p = 3.5 \pm 0.1$ km/sec and $V_s = 1600$ m/sec, and at Lake Haruna; $V_p = 2.82 \pm 0.06$ km/sec, and $V_s = 1.51 \pm 0.02$ km/sec, which is fairly small compared with the results of other observations. (cf. 1)

In "LANDOLDT, *Physikalische-chemische Tabellen* (p. 82)"

$$\text{Young's modulus} = \begin{cases} 1120\ \text{kgr. weight/cm perpendicular to freezing surface.} \\ 950 \quad ,, \quad \text{parallel} \quad ,, \end{cases}$$

This gives extremely small velocity.

The most general form of equation is (5. 10).

$$-\Delta_{\mathrm{III}}=-\Delta_{\mathrm{I}}+\frac{1}{Z^*}\frac{1}{\mathfrak{T}^*}(\mathfrak{C}\mathfrak{S}'-Z\mathfrak{S}\mathfrak{C}') \qquad \text{......(6. 1)}$$

Here, we will explain the notations used in the above equation.

$$\left\{\begin{array}{ll}
\Delta_{\mathrm{I}}\equiv 2(1-\mathfrak{C}\mathfrak{C}')-(Z-1/Z)\mathfrak{S}\mathfrak{S}', & \\
Z\equiv\alpha_1\beta_1/(1-\mathfrak{v}^2/2)^2, & \\
1/Z^*\equiv\Gamma\mathfrak{v}^4/4\beta_1\alpha_1^*, & (\Gamma\equiv\rho^*/\rho), \\
\mathfrak{C}\equiv\cosh\xi\alpha_1, & \mathfrak{S}\equiv\sinh\xi\alpha_1 \\
\mathfrak{C}'\equiv\cosh\xi\beta_1, & \mathfrak{S}'\equiv\sinh\xi\beta_1 \\
\mathfrak{T}^*\equiv\tanh\delta\xi\alpha_1^*, & (\delta\equiv D/H) \\
\alpha_1\equiv\sqrt{(1-\mathfrak{v}^2/\gamma^2)}, & (\gamma^2\equiv V_p^2/V_s^2) \\
\beta_1\equiv\sqrt{(1-\mathfrak{v}^2)}, & \\
\alpha_1^*\equiv\sqrt{(1-\mathfrak{v}^2/\gamma^{*2})}, & (\gamma^{*2}\equiv V^{*2}/V_s^2)
\end{array}\right. \qquad \text{......(6. 2)}$$

For simplicity's sake we will adopt the following notations:

$$\left\{\begin{array}{ll}
L_{ik}\equiv\frac{1}{i\,!}(1-\mathfrak{v}^2/\gamma^2)+\frac{1}{k\,!}(1-\mathfrak{v}^2) & \text{especially } L\equiv L_{11} \\
S_{ik}\equiv\frac{1}{i\,!}(1-\mathfrak{v}^2/\gamma^2)^2+\frac{1}{k\,!}(1-\mathfrak{v}^2)^2 & \text{especially } S\equiv S_{11} \\
C_{ik}\equiv\frac{1}{i\,!}(1-\mathfrak{v}^2/\gamma^2)^3+\frac{1}{k\,!}(1-\mathfrak{v}^2)^3 & \text{especially } C\equiv C_{11} \\
P\equiv(1-\mathfrak{v}^2/\gamma^2)(1-\mathfrak{v}^2) &
\end{array}\right. \qquad \text{......(6. 3)}$$

and

$$\left\{\begin{array}{l}
K\equiv\sqrt{(1-\mathfrak{v}^2/\gamma^2)}\cdot(1-\mathfrak{v}^2)(Z+1/Z) \\
\quad=(\mathfrak{v}^2-2)^{-2}\{8+(-12-4/\gamma^2)\mathfrak{v}^2+(6+4/\gamma^2)\mathfrak{v}^4-2\mathfrak{v}^6+\mathfrak{v}^8/4\} \\
K_1\equiv\sqrt{(1-\mathfrak{v}^2)}/Z^*=\Gamma\mathfrak{v}^4/4\sqrt{(1-\mathfrak{v}^2/\gamma^{*2})} \\
K_2\equiv\{\sqrt{(1-\mathfrak{v}^2/\gamma^2)}/\sqrt{(1-\mathfrak{v}^2)}\}Z \\
\quad=(1-\mathfrak{v}^2/\gamma^2)/(1-\mathfrak{v}^2)^2
\end{array}\right. \qquad \text{......(6. 4)}$$

Quantities in the expression (6. 1) are expressed by means of (6. 3) and (6. 4).

$$\mathfrak{C}\mathfrak{C}'=1+\xi^2\cdot\frac{1}{2}L+\xi^4\left(\frac{1}{24}S+\frac{1}{4}P\right)+\xi^6\left(\frac{1}{720}C+\frac{1}{48}PL\right)+\ldots\ldots$$

$$\mathfrak{S}\mathfrak{S}'=\xi^2\alpha_1\beta_1\left\{1+\xi^2L_{33}+\xi^4\left(S_{55}+\frac{1}{3!3!}P\right)+\ldots\ldots\right\}$$

$$\mathfrak{C}\mathfrak{S}'=\xi\beta_1\left[1+\xi^2L_{23}+\xi^4\left(S_{45}+\frac{1}{12}P\right)+\xi^6\left\{S_{67}+P\left(\frac{1-\mathfrak{v}^2/\gamma^2}{3!4!}+\frac{1-\mathfrak{v}^2}{2!5!}\right)\right\}+\ldots\ldots\right]$$

$$\mathfrak{S}\mathfrak{C}'=\xi\alpha_1\left[1+\xi^2L_{32}+\xi^4\left(S_{54}+\frac{1}{12}P\right)+\xi^6\left\{S_{76}+P\left(\frac{1-\mathfrak{v}^2/\gamma^2}{2!5!}+\frac{1-\mathfrak{v}^2}{3!4!}\right)\right\}+\ldots\ldots\right]$$

$$\begin{aligned}\therefore\quad &\frac{1}{Z^*}(\mathfrak{C}\mathfrak{S}'-Z\mathfrak{S}\mathfrak{C}')\\ &=K_1\Big[\xi(1-K_2)+\xi^3(L_{23}-K_2L_{32})+\xi^5\Big\{(S_{45}-K_2S_{54})+\frac{1}{12}P(1-K_2)\Big\}\\ &\quad+\xi^7\Big\{(S_{67}-K_2S_{76})+P\Big(\frac{1}{3!4!}-K_2\frac{1}{2!5!}\Big)(1-\mathfrak{v}^2/\gamma^2)\\ &\qquad+P\Big(\frac{1}{2!5!}-K_2\frac{1}{3!4!}\Big)(1-\mathfrak{v}^2)\Big\}+\ldots\ldots \qquad \ldots\ldots(6.5)\end{aligned}$$

Introducing these equations into (6.1) we can get the power-series of characteristic equation.

When both sides are free, we ought to put $1/\mathfrak{T}^*=0$.

When one side is in contact with bottomless water we ought to put $1/\mathfrak{T}^*=1$ in the equation (6.1).

Introducing (6.5) into (6.1) we have

$$\begin{aligned}-\varDelta_{\text{III}}\equiv\,&\xi\frac{1}{\mathfrak{T}^*}K_1(1-K_2)+\xi^2(-L+K)+\xi^3\frac{1}{\mathfrak{T}^*}K_1(L_{23}-K_2L_{32})\\ &+\xi^4\Big\{\Big(-\frac{1}{12}S-\frac{1}{2}P\Big)+\frac{1}{6}KL\Big\}+\xi^5\frac{1}{\mathfrak{T}^*}K_1\Big\{(S_{45}-K_2S_{54})+\frac{1}{12}P(1-K_2)\Big\}\\ &+\xi^6\Big\{\Big(-\frac{1}{360}C-\frac{1}{24}PL\Big)+K\Big(\frac{1}{120}S+\frac{1}{36}P\Big)\Big\}\\ &+\xi^7\frac{1}{\mathfrak{T}^*}K_1\Big\{(S_{67}-K_2S_{76})+P\Big(\frac{1}{3!4!}-K_2\frac{1}{2!5!}\Big)(1-\mathfrak{v}^2/\gamma^2)\\ &\qquad+P\Big(\frac{1}{2!5!}-K_2\frac{1}{3!4!}\Big)(1-\mathfrak{v}^2)\Big\}+\ldots\ldots=0\end{aligned}$$

$$\ldots\ldots(6.6)$$

$K_1, K_2, L_{ik}, S_{ik}, C_{ik}$ and so on are already defined in (6.4); therefore we have easily—although the procedure is complicated—the next expression.

$$\begin{aligned}D\equiv\,&\xi G\frac{1}{\mathfrak{T}^*}\Big\{-4(-1+\gamma^2)\mathfrak{v}^2+\gamma^2\mathfrak{v}^4\Big\}+\xi^2\frac{\gamma^2}{4}\Big\{-4(-1+\gamma^2)\mathfrak{v}^2+\gamma^2\mathfrak{v}^4\Big\}\\ &+\xi^3G\frac{1}{\mathfrak{T}^*}\frac{1}{6}\Big\{-8(-1+\gamma^2)\mathfrak{v}^2+(-4+8\gamma^4)\gamma^{-2}\mathfrak{v}^4+(-3-\gamma^2)\mathfrak{v}^6\Big\}\\ &+\xi^4\frac{1}{12}\Big\{4(-1+\gamma^2)^2+4(-1+\gamma^2)(1-2\gamma^2)\mathfrak{v}^2+(-1-2\gamma^2+4\gamma^4)\mathfrak{v}^4-\frac{1}{2}\gamma^2(1+\gamma^2)\mathfrak{v}^6\Big\}\\ &+\xi^5G\frac{1}{\mathfrak{T}^*}\frac{1}{30}\Big\{-8(-1+\gamma^2)\mathfrak{v}^2+(-8+12\gamma^4)\gamma^{-2}\mathfrak{v}^4+(1+5\gamma^2-10\gamma^4-4\gamma^6)\gamma^{-4}\mathfrak{v}^6\\ &\qquad+\frac{1}{4}(5+10\gamma^2+\gamma^2+\gamma^4)\gamma^{-2}\mathfrak{v}^8\Big\}\\ &+\xi^6\frac{2}{45}\Big\{(-1+\gamma^2)^2+0(\mathfrak{v}^2)\Big\}+\xi^7G\frac{1}{\mathfrak{T}^*}\Big\{0(\mathfrak{v}^2)\Big\}=0\end{aligned}$$

in which $D\equiv-\{\gamma^4(-2+\mathfrak{v}^2)^2/\mathfrak{v}^4\}\varDelta_{\text{III}},\ G\equiv\gamma^2\Gamma/4\sqrt{(1-\mathfrak{v}^2/\gamma^{*2})}$ ……(6.7)

We will discuss this equation in various cases separately.

6.1 When both sides are free.

Putting $1/\mathfrak{T}^*=0$ into (6.7) we have

$$D_{\text{I}}\equiv\xi^2\frac{\gamma^2}{4}\left\{-4(-1+\gamma^2)\mathfrak{v}^2+\gamma^2\mathfrak{v}^4\right\}$$
$$+\xi^4\frac{1}{12}\left\{4(-1+\gamma^2)^2+4(-1+\gamma^2)(1-2\gamma^2)\mathfrak{v}^2+(-1-2\gamma^2+4\gamma^4)\mathfrak{v}^4-\frac{1}{2}\gamma^2(1+\gamma^2)\mathfrak{v}^6\right\}$$
$$+\xi^6\frac{1}{45}\left\{(-1+\gamma^2)^2+0(\mathfrak{v}^2)\right\}=0 \qquad \text{......(6.8)}$$

6.11 Π_0^-. (the branch of $\lim\limits_{\xi\to0}\mathfrak{v}=0$.)

When a branch exists such as $\lim\limits_{\xi\to0}\mathfrak{v}=0$, we can get the following approximation formula;

1st approximation; $\xi^2\frac{1}{4}\gamma^2\{-4(-1+\gamma^2)\mathfrak{v}^2\}+\xi^4\frac{1}{12}\{4(-1+\gamma^2)^2\}=0$

$$\mathfrak{v}_{1\text{st}}^2=\xi^2(-1+\gamma^2)/3\gamma^2 \qquad \text{......(6.9)}$$

By successive approximation we have the 2nd approximation.

$$\mathfrak{v}_{2\text{nd}}^2=\xi^2\frac{-1+\gamma^2}{3\gamma^2}-\xi^4\frac{-1+\gamma^2}{3\gamma^2}\,\frac{-20+27\gamma^2}{60\gamma^2} \qquad \text{......(6.10)}$$

6.12 Π_0^+. (the branch of $\lim\limits_{\xi\to0}\mathfrak{v}\neq0$)

1st approximation is given by $\mathfrak{v}_{1\text{st}}^2=4(-1+\gamma^2)/\gamma^2\equiv\mathfrak{v}_0^2$. ......(6.11)

To compair with the values of other cases we must take 2nd approximation.

$$\mathfrak{v}_{2\text{nd}}^2=\mathfrak{v}_0^2-\xi^2\frac{1}{3}\mathfrak{v}_0^2\frac{1}{\gamma^4}\left(-1+\frac{1}{2}\gamma^2\right)^2 \qquad \text{......(6.12)}$$

6.2 When one side is in contact with infinitely deep water.

Putting $\mathfrak{T}^*=1$ into (6.7) we have the characteristic equation of this case easily.

6.21 Π_0^-. (the branch of $\lim\limits_{\xi\to0}\mathfrak{v}=0$).

1st approximation $\mathfrak{v}_{1\text{st}}^2=\xi^3(-1+\gamma^2)/3\gamma^2\Gamma$ ......(6.13)

This is quite different from the case without water; $\mathfrak{v}^2$ is proportional to ξ^3, not to ξ^2.

Taking the terms up to the order of ξ^7 we obtain the further approximation.

$$\mathfrak{v}_{3\text{rd}}^2=\xi^3\frac{1}{3\Gamma}\,\frac{-1+\gamma^2}{\gamma^2}-\xi^4\frac{1}{3\Gamma}\,\frac{-1+\gamma^2}{\gamma^2}\,\frac{1}{\Gamma}$$
$$+\xi^5\frac{1}{3\Gamma}\,\frac{-1+\gamma^2}{\gamma^2}\left(\frac{1}{\Gamma^2}-\frac{1}{5}\right) \qquad \text{......(6.14)}$$

6.22 Π_0^+ (the branch of $\lim\limits_{\xi\to0}\mathfrak{v}\neq0$).

1st approximation;

$$\mathfrak{v}_{1st}^2=\mathfrak{v}_0^2 \qquad \text{......(6.15)}$$

This formula gives the same value with the case without water. In order to make clear the difference from former case, we must take further approximation. Taking the terms of $0(\xi^3)$ and calculating the correction term by means of $\mathfrak{v}_{1st}^2$,

$$\mathfrak{v}_{2nd}^2=\mathfrak{v}_0^2-\xi^2\frac{4}{3}\mathfrak{v}_0^2\frac{1}{\gamma^4}\left(-1+\frac{1}{2}\gamma^2\right)^2 \qquad \text{......(6.16)}$$

In the same way, the third approximation is obtained, which is necessary to show the difference between the present case and that of finite depth.

$$\mathfrak{v}_{3rd}^2=\mathfrak{v}_0^2-\xi^2\frac{4}{3}\mathfrak{v}_0^2\frac{1}{\gamma^4}(-1+\frac{1}{2}\gamma^2)^2+\xi^3\frac{1}{\Gamma}\mathfrak{v}_0^2\frac{1}{\gamma^4}(-1+\frac{1}{2}\gamma^2)^2\sqrt{(1-\mathfrak{v}_0^2/\gamma^{*2})} \qquad \text{......(6.17)}$$

6.3 When one side is in contact with water of finite depth.

6.31 Π_0^- (the branch of $\lim\limits_{\xi\to0}\mathfrak{v}=0$).

In this case the expression (6.7) becomes the characteristic equation.

$$\mathfrak{v}_{1st}^2=\xi^4\frac{\delta}{3\Gamma}\frac{-1+\gamma^2}{\gamma^2}, \qquad \delta=D/H \qquad \text{......(6.18)}$$

This is an interesting result, for neither of the former two cases is the same with the above formula.

$$\mathfrak{v}_{2nd}^2=\xi^4\frac{\delta}{3\Gamma}\frac{-1+\gamma^2}{\gamma^2}-\xi^6\frac{\delta}{3\Gamma}\frac{-1+\gamma^2}{\gamma^2}\left(\frac{1}{3}\delta^2+\frac{\delta}{\Gamma}+\frac{1}{5}\right) \qquad \text{......(6.19)}$$

6.32 Π_0^+ (the branch of $\lim\limits_{\xi\to0}\mathfrak{v}\neq0$).

The first approximation is not different from the former formulae of first approximation (6.15). The second approximation is also the same with the case of infinite depth (6.16). We can show the difference only by the third approximation.

$$\begin{aligned}\mathfrak{v}_{3rd}^2=&\mathfrak{v}_0^2-\xi^2\frac{4}{3}\mathfrak{v}_0^2\frac{1}{\gamma^4}\left(-1+\frac{1}{2}\gamma^2\right)^2\\&+\xi^4\mathfrak{v}_0^2\frac{4}{\gamma^4}\left(-1+\frac{1}{2}\gamma^2\right)^2\left\{\frac{\delta}{4\Gamma}(1-\mathfrak{v}_0^2/\gamma^2)+\frac{1}{45}\frac{1}{\gamma^4}(44-40\gamma^2+3\gamma^4)\right\}\end{aligned} \qquad \text{......(6.20)}$$

6.4 Comparison of the three cases.

If we cast a glance at the equations (6.10), (6.14) and (6.19), we shall soon notice that the first term is already different. This is somewhat curious, for even if we rarefy the liquid that lies on one side of a plate until it vanishes, we cannot arrive at the case without liquid. This apparent paradox should be explained as follows. Recall the process by which we obtained the approximation formulae, then it becomes clear that we at first assumed that ξ is extremely small compared with other quantities. Therefore we are not allowed to assume the density, elastic constants and other physical quantities to take smaller values than ξ. So that we must perform another way of calculation in order to see the effect of rare substances to the nature of elastic waves.

Another curious fact which we notice in the above expressions is that we cannot get the formula corresponding to the case of bottomless water by making the depth D infinitely large. This is because of the assumption $\xi\delta \leqslant 1$, or that the wave length is far larger than the depth. Therefore, even if we make the depth of water large, the wave length can never be smaller than it.

In § 5 we have proved that the branch $\Pi_0{}^+$ cannot exist in the combination of water and ice. And yet, to our surprise, we have obtained the expression (6.17), which gives the relation between velocity and wave-length of the branch $\Pi_0{}^+$. It is also paradoxical that the velocity given by the formula (6.17) is complex number though in § 5 we searched only real roots. When the velocity takes complex value, such waves dissipate exponentially as they propagate. We will have a detailed discussion of this nature in § 8.22.

7. Relation between phase velocity, group velocity, wave length and period.

Using the formulae in the previous article, we can easily obtain the relations between phase velocity, group velocity, wave-length and period, which will prove more convenient for our practical purposes.

In the following expressions, (I), (II) and (III) imply the next meanings.

(I) When there is no liquid and both sides of plate are free.

(II) When there is bottomless liquid on one side of the plate.

(III) When there is liquid whose depth is $D \equiv \delta \cdot H$.

7.1 Relation between phase velocity and wave-number or wave length.

Calculating the square root of the expressions of $\mathfrak{v}^2$ we have the following formulae.

7.11 $\Pi_0{}^-$.

$$\text{(I)} \quad \mathfrak{v} = \xi\left(\frac{1}{12}\right)^{\frac{1}{2}}\mathfrak{v}_0\left\{1-\xi^2\frac{1}{120}\frac{1}{\gamma^2}(-20+27\gamma^2)\right\}$$

$$\text{(II)} \quad \mathfrak{v} = \xi^{\frac{3}{2}}\left(\frac{1}{12\Gamma}\right)^{\frac{1}{2}}\mathfrak{v}_0\left\{1-\xi\frac{1}{2\Gamma}+\xi^2\left(\frac{3}{8}\frac{1}{\Gamma^2}-\frac{1}{10}\right)\right\} \qquad \text{......(7.1)}$$

$$\text{(III)} \quad \mathfrak{v} = \xi^2\left(\frac{\delta}{12\Gamma}\right)^{\frac{1}{2}}\mathfrak{v}_0\left\{1-\xi^2\frac{1}{2}\left(\frac{1}{3}\delta^2+\frac{\delta}{\Gamma}+\frac{1}{5}\right)\right\}$$

7.12 $\Pi_0{}^+$.

$$\text{(I)}\quad \mathfrak{v}=\mathfrak{v}_0\{1-\xi^2\frac{1}{2}c_2{}^2\}$$

$$\text{(II)}\quad \mathfrak{v}=\mathfrak{v}_0\{1-\xi^2 2c_2{}^2+\xi^3\frac{3}{2\Gamma}\surd(1-\mathfrak{v}_0{}^2/\gamma^{*2})\cdot c_2{}^2\}$$

$$\text{(III)}\quad \mathfrak{v}=\mathfrak{v}_0\left\{1-\xi^2 2c_2{}^2+\xi^4\left[-2c_2{}^4+\frac{1}{2}c_2{}^2\left(3\frac{\delta}{\Gamma}(1-\mathfrak{v}_0{}^2/\gamma^{*2})\right.\right.\right.$$
$$\left.\left.\left.+\frac{4}{15}\frac{1}{\gamma^4}(44-40\gamma^2+3\gamma^4)\right)\right]\right\}$$

in which
$$c_2{}^2=\frac{1}{12}\frac{(-2+\gamma^2)^2}{\gamma^4} \qquad \text{......(7.2)}$$

When γ^* is smaller than $\mathfrak{v}_0$, $\mathfrak{v}$ becomes imaginary in (II). In this case the energy of waves in the plate should more or less propagate into the part of liquid and the amplitude becomes smaller because of this effect. This circumstances are already stated in § 6.4 and will be discussed in § 8.22.

7.2 Relation between phase velocity and frequency or period.

Since the relation between $\mathfrak{v}$ and ξ is obtained, we can transform and get the relation between phase velocity and circular frequency $\omega=\xi\mathfrak{v}$.

7.21 $\Pi_0{}^-$.

$$\text{(I)}\quad \mathfrak{v}=\omega^{\frac{1}{2}}\left\{\frac{1}{12}\mathfrak{v}_0{}^2\right\}^{\frac{1}{4}}\left\{1+\omega\frac{-1}{240}\frac{1}{\gamma^2}(-20+27\gamma^2)\left(\frac{1}{12}\mathfrak{v}_0{}^2\right)^{-\frac{1}{2}}+0(\omega^2)\right\}$$

$$\text{(II)}\quad \mathfrak{v}=\omega^{\frac{3}{5}}\left\{\frac{1}{12\Gamma}\mathfrak{v}_0{}^2\right\}^{\frac{1}{5}}\left\{1+\omega^{\frac{2}{5}}\frac{-1}{5}\frac{1}{\Gamma}\left(\frac{1}{12\Gamma}\mathfrak{v}_0{}^2\right)^{-\frac{1}{5}}\right.$$
$$\left.+\omega^{\frac{4}{5}}\frac{1}{25}\left(-\frac{2}{\Gamma^2}-1\right)\left(\frac{1}{12\Gamma}\mathfrak{v}_0{}^2\right)^{-\frac{2}{5}}+0(\omega^{\frac{6}{5}})\right\}$$

$$\text{(III)}\quad \mathfrak{v}=\omega^{\frac{2}{3}}\left\{\frac{\delta}{12\Gamma}\mathfrak{v}_1{}^2\right\}^{\frac{1}{6}}\left\{1+\omega^{\frac{2}{3}}\frac{-1}{6}\left(\frac{1}{3}\delta^2+\frac{1}{\Gamma}\delta+\frac{1}{5}\right)\left(\frac{\delta}{12\Gamma}\mathfrak{v}_0{}^2\right)^{-\frac{1}{3}}\right.$$
$$\left.+0(\omega^{\frac{4}{3}})\right\}$$

7.22 $\Pi_0{}^+$. ......(7.3)

$$\text{(I)}\quad \mathfrak{v}=\mathfrak{v}_0\left\{1+\omega^2(-\frac{1}{2}c_2{}^2)\mathfrak{v}_0^{-2}+0(\omega^4)\right\}$$

$$\text{(II)}\quad \mathfrak{v}=\mathfrak{v}_0\left\{1+\omega^2(-2c_2{}^2)\mathfrak{v}_0^{-2}+\omega^3\frac{1}{\Gamma}\surd(1-\mathfrak{v}_0{}^2/\gamma^{*2})\cdot\frac{3}{2}c_2{}^2\mathfrak{v}_0^{-3}+0(\omega^4)\right\}$$

$$\text{(III)}\quad \mathfrak{v}=\mathfrak{v}_0\left\{1+\omega^2(-2c_2{}^2)\mathfrak{v}_0^{-2}+\omega^4\left[-\frac{5}{2}c_2{}^4+c_2{}^2\left(\frac{3\delta}{2\Gamma}(1-\mathfrak{v}_0{}^2/\gamma^{*2})\right.\right.\right. \qquad \text{......(7.4)}$$
$$\left.\left.\left.+\frac{2}{15}\frac{1}{\gamma^4}(44-40\gamma^2+3\gamma^4)\right)\right]\mathfrak{v}_0^{-4}+0(\omega^6)\right\}$$

7.3 Group velocity and wave-number.

The velocity with which the change of amplitude is propagated is, as has been made clear by many authors, group velocity.[18] Therefore it will not be useless to introduce the formula connecting group velocity $\mathfrak{V}$ and wave-number ξ or frequency ω.

$\mathfrak{V}$ is expressed by the formula $\mathfrak{V}=d(\xi\mathfrak{v})/d\xi$.

Therefore, using (7.1) and (7.2), we have the following expressions.

7.31 Π_0^-.

$$\text{(I)}\quad \mathfrak{V}=\xi\cdot 2\left(\frac{1}{12}\right)^{\frac{1}{2}}\mathfrak{v}_0\left\{1-\xi^2\frac{1}{60}\frac{1}{\gamma^2}(-20+27\gamma^2)\right\}$$

$$\text{(II)}\quad \mathfrak{V}=\xi^{\frac{3}{2}}\frac{5}{2}\left(\frac{1}{12\Gamma}\right)^{\frac{1}{2}}\mathfrak{v}_0\left\{1-\xi\frac{7}{10}\frac{1}{\Gamma}+\xi^2\left(\frac{27}{40}\frac{1}{\Gamma^2}-\frac{9}{50}\right)\right\} \qquad \text{......(7.5)}$$

$$\text{(III)}\quad \mathfrak{V}=\xi^2\cdot 3\left(\frac{\delta}{12\Gamma}\right)^{\frac{1}{2}}\mathfrak{v}_0\left\{1-\xi^2\frac{5}{6}\left(\frac{1}{3}\delta^2+\frac{\delta}{\Gamma}+\frac{1}{5}\right)\right\}$$

7.32 Π_0^+.

$$\text{(I)}\quad \mathfrak{V}=\mathfrak{v}_0\{1-\xi^2\frac{3}{2}c_2^2\}$$

$$\text{(II)}\quad \mathfrak{V}=\mathfrak{v}_0\{1-\xi^2 6c_2^2+\xi^3 6\frac{1}{\Gamma}\sqrt{(1-\mathfrak{v}_0^2/\gamma^{*2})}\cdot c_2^2\}$$

$$\text{(III)}\quad \mathfrak{V}=\mathfrak{v}_0\left\{1-\xi^2 6c_2^2+\xi^4\left(-10c_2^4+\frac{5}{2}c_2^2\left[\frac{3\delta}{\Gamma}(1-\mathfrak{v}_0^2/\gamma^{*2})\right.\right.\right.$$
$$\left.\left.\left.+\frac{4}{15}\frac{1}{\gamma^4}(44-40\gamma^2+3\gamma^4)\right]\right)\right\} \qquad \text{......(7.6)}$$

7.4 Group velocity and frequency.

Using the expressions (7.3) and (7.4), and applying the formula

$$\mathfrak{V}=\mathfrak{v}/\left(1-\frac{\omega}{\mathfrak{v}}\frac{d\mathfrak{v}}{d\omega}\right) \qquad \text{......(7.7)}$$

we have the relation between $\mathfrak{V}$ and ω.

7.41 Π_0^-.

$$\text{(I)}\quad \mathfrak{V}=\omega^{\frac{1}{2}}\cdot 2\left(\frac{1}{12}\mathfrak{v}_0^2\right)^{\frac{1}{4}}\left\{1-\omega\frac{1}{80}\frac{1}{\gamma^2}(-20+27\gamma^2)\left(\frac{1}{12}\mathfrak{v}_0^2\right)^{-\frac{1}{2}}\right\}$$

---

18) *e.g.* HAVELOCK, "Propagation of Waves in Dipersive Media." (Cambridge, 1914). C. ECKART, "The Approximate Solution of One Dimensional Wave Equations." *Rev. Mod. Phys*, **20** (1948), 399.

$$\text{(II)}\quad \mathfrak{B}=\omega^{\frac{3}{5}}\cdot\frac{5}{2}\left(\frac{1}{12\Gamma}\mathfrak{v}_0{}^2\right)^{\frac{1}{5}}\left\{1+\omega^{\frac{2}{5}}\left(-\frac{2}{5}\frac{1}{\Gamma}\right)\left(\frac{1}{12\Gamma}\mathfrak{v}_0{}^2\right)^{-\frac{1}{5}}\right.$$

$$\left.+\omega^{\frac{4}{5}}\left(-\frac{5}{\Gamma^2}-3\right)\frac{1}{25}\left(\frac{1}{12\Gamma}\mathfrak{v}_0{}^2\right)^{-\frac{2}{5}}\right\}$$

$$\text{(III)}\quad \mathfrak{B}=\omega^{\frac{2}{3}}\cdot 3\left(\frac{\delta}{12\Gamma}\mathfrak{v}_0{}^2\right)^{\frac{1}{6}}\left\{1+\omega^{\frac{2}{3}}\left(-\frac{1}{2}\right)\left(\frac{1}{3}\delta^2+\frac{\delta}{\Gamma}+\frac{1}{5}\right)\left(\frac{1}{12\Gamma}\delta\mathfrak{v}_0{}^2\right)^{-\frac{1}{3}}\right\}$$

……(7.8)19)

7.42 $\Pi_0{}^+$.

$$\text{(I)}\quad \mathfrak{B}=\mathfrak{v}_0\left\{1+\omega^2\left(-\frac{3}{2}\right)c_2{}^2\mathfrak{v}_0{}^{-2}\right\}$$

$$\text{(II)}\quad \mathfrak{B}=\mathfrak{v}_0\left\{1+\omega^2(-6)c_2{}^2\mathfrak{v}_0{}^{-2}+\omega^3 6\frac{1}{\Gamma}\sqrt{(1-\mathfrak{v}_0{}^2/\gamma^{*2})}\cdot c_2{}^2\mathfrak{v}_0^{-3}\right\}$$

$$\text{(III)}\quad \mathfrak{B}=\mathfrak{v}_0\left\{1+\omega^2(-6)c_2{}^2\mathfrak{v}_0{}^{-2}+\omega^4\left[16c_2{}^2\mathfrak{v}_0{}^{-4}\right.\right.$$

$$\left.\left.+5\left\{-\frac{5}{2}c_2{}^4+c_2{}^2\left(\frac{3\delta}{2\Gamma}(1-\mathfrak{v}_0{}^2/\gamma^{*2})+\frac{2}{15}\frac{1}{\gamma^4}(44-40\gamma^2+3\gamma^4)\right)\right\}\mathfrak{v}_0^{-4}\right]\right\}$$

……(7.9)

Table VI.

$\Pi_0{}^-$

Expression	(I) Without liquid	(II) One side liquid, infinite depth.	(III) One side liquid, finite depth.
(6.9) (6.13) $\mathfrak{v}^2-\xi$ (6.19)	$\xi^2\frac{-1+\gamma^2}{3\gamma^2}=\xi^2\frac{1}{12}\mathfrak{v}_0{}^2$	$\xi^3\cdot\frac{1}{\Gamma}\frac{-1+\gamma^2}{3\gamma^2}$	$\xi^4\frac{\delta}{\Gamma}\frac{-1+\gamma^2}{3\gamma^2}$
(7.1) $\mathfrak{v}-\xi$	$\xi\left(\frac{1}{12}\mathfrak{v}_0{}^2\right)^{\frac{1}{2}}$	$\xi^{\frac{3}{2}}\left\{\frac{1}{12\Gamma}\mathfrak{v}_0{}^2\right\}^{\frac{1}{2}}$	$\xi^2\left\{\frac{\delta}{12\Gamma}\mathfrak{v}_0{}^2\right\}^{\frac{1}{2}}$
(7.3) $\mathfrak{v}-\omega$	$\omega^{\frac{1}{2}}\left(\frac{1}{12}\mathfrak{v}_0{}^2\right)^{\frac{1}{4}}$	$\omega^{\frac{3}{5}}\left\{\frac{1}{12\Gamma}\mathfrak{v}_0{}^2\right\}^{\frac{1}{5}}$	$\omega^{\frac{2}{3}}\left\{\frac{\delta}{12\Gamma}\mathfrak{v}_0{}^2\right\}^{\frac{1}{6}}$
(7.5) $\mathfrak{B}-\xi$	$\xi 2\left(\frac{1}{12}\mathfrak{v}_0{}^2\right)^{\frac{1}{2}}$	$\xi^{\frac{3}{2}}\frac{5}{2}\left\{\frac{1}{12\Gamma}\mathfrak{v}_0{}^2\right\}^{\frac{1}{2}}$	$\xi^2\cdot 3\left\{\frac{\delta}{12\Gamma}\mathfrak{v}_0{}^2\right\}^{\frac{1}{2}}$
(7.8) $\mathfrak{B}-\omega$	$\omega^{\frac{1}{2}}2\left(\frac{1}{12}\mathfrak{v}_0{}^2\right)^{\frac{1}{4}}$	$\omega^{\frac{2}{3}}\cdot\frac{5}{2}\left\{\frac{1}{12\Gamma}\mathfrak{v}_0{}^2\right\}^{\frac{1}{5}}$	$\omega^{\frac{2}{3}}\cdot 3\left\{\frac{\delta}{12\Gamma}\mathfrak{v}_0{}^2\right\}^{\frac{1}{6}}$

---

19) From the observation of Kishinouye (cf. 1)

$$\text{Velocity}=29.6\times T^{-0.74}\ \text{m/sec},$$

while from (II) we have

$$\text{Velocity}=54.4\times T^{-0.6}\ \text{m/sec}.$$

(We cannot apply (III), for the wave length and the depth of water is of the same order.)

$\Pi_0{}^+$

Expression	(I) Without liquid.	(II) One side liquid, infinite depth.	(III) One side liquid, finite depth.
(6.12) (6.16) $\mathfrak{v}^2-\xi$ (6.20)	$\mathfrak{v}_0{}^2\{1+\xi^2(-c_2{}^2)\}$	$\mathfrak{v}_0{}^2\{1+\xi^2(-4)c_2{}^2\}$	$\mathfrak{v}_0{}^2\{1+\xi^2(-4)c_2{}^2\}$
(7.2) $\mathfrak{v}-\xi$	$\mathfrak{v}_0\left\{1+\xi^2\left(-\frac{1}{2}c_2{}^2\right)\right\}$	$\mathfrak{v}_0\{1+\xi^2(-2)c_2{}^2\}$	$\mathfrak{v}_0\{1+\xi^2(-2)c_2{}^2\}$
(7.4) $\mathfrak{v}-\omega$	$\mathfrak{v}_0\{1+\omega^2(-\frac{1}{2}c_2{}^2)/\mathfrak{v}_0{}^2\}$	$\mathfrak{v}_0\{1+\omega^2(-2)c_2{}^2/\mathfrak{v}_0{}^2\}$	$\mathfrak{v}_0\{1+\omega^2(-2)c_2{}^2/\mathfrak{v}_0{}^2\}$
(7.6) $\mathfrak{V}-\xi$	$\mathfrak{v}_0\left\{1+\xi^2\left(-\frac{3}{2}c_2{}^2\right)\right\}$	$\mathfrak{v}_0\{1+\xi^2(-6)c_2{}^2\}$	$\mathfrak{v}_0\{1+\xi^2(-6)c_2{}^2\}$
(7.9) $\mathfrak{V}-\omega$	$\mathfrak{v}_0\left\{1+\omega^2\left(-\frac{3}{2}c_2{}^2\right)/\mathfrak{v}_0{}^2\right\}$	$\mathfrak{v}_0\{1+\omega^2(-6)c_2{}^2/\mathfrak{v}_0{}^2\}$	$\mathfrak{v}_0\{1+\omega^2(-6)c_2{}^2/\mathfrak{v}_0{}^2\}$

$$\mathfrak{v}_0{}^2=4(-1+\gamma^2)/\gamma^2,$$
$$c_2{}^2=\frac{1}{12}\,\frac{(-2+\gamma^2)^2}{\gamma^4}$$

We will summarize the results and show the approximation formula in Tab. VI.

8. Amplitude and particle orbit.

Since we have clarified the relation between velocity and wave-number, we can easily obtain the amplitude, and the particle orbit in plate and liquid. As calculation is complicated in spite of the simple principle, we will show only the results in this paper.

Displacement components u and w in the plate are given by (3.6), and u^* and w^* in the liquid are

$$\left\{\begin{aligned} u^*&=(if/h^{*2})\{M, N; *\}\exp\{ipt-ifx\} \\ w^*&=(-\alpha^*/h^{*2})\{N, M; *\}\exp\{ipt-ifx\} \end{aligned}\right. \qquad \text{......(8.1)}$$

The meaning of notations has been stated already in (5.3).

Since p and f satisfy the velocity equation (5.10), the coefficients A, B, C, D and M, N in (3.6) and (8.1) are given by the following expressions:

$$\left\{ A=\left(\frac{1}{Z}\mathfrak{S}-\mathfrak{S}'\right)+\frac{1}{Z^*\mathfrak{T}^*}\mathfrak{C}' \qquad M=-\frac{P_z}{\lambda^*}\,\frac{1}{Z^*\mathfrak{T}^*}(\mathfrak{C}-\mathfrak{C}') \right.$$

$$\left\{\begin{aligned} B&=-\frac{1}{Z}(\mathfrak{C}-\mathfrak{C}') \qquad\qquad N=-\frac{P_z}{\lambda^*}\frac{1}{Z^*}(\mathfrak{C}-\mathfrak{C}') \\ C&=\frac{P_z}{S_z}(\mathfrak{C}-\mathfrak{C}') \\ D&=-\frac{P_z}{S_z}\left\{\left(\frac{1}{Z}\mathfrak{S}-\mathfrak{S}'\right)+\frac{1}{Z^*\mathfrak{T}^*}\mathfrak{C}\right\} \end{aligned}\right. \qquad \text{......(8.2)}$$

$A, B, \ldots\ldots M, N$ in the above expressions are functions of ξ and $\mathfrak{v}$, while $\mathfrak{v}$ is represented as the power series of ξ by the formulae in § 7, therefore, using $A, B \ldots\ldots M, N$ the ampliudes of displacements u, w and u^*, w^* are also expressed as power series of ξ. This is the course of our calculation in this article.

At first we will introduce the relation (8.2) into (3.6) and (8.1), then we have (omitting $\exp\{ipt-ifx\}$)

$$\left\{\begin{aligned} u=\frac{if}{h^2}\Bigg[&\left\{(\cosh\alpha z-\cosh\beta z)+\frac{k^2}{2f^2}\cosh\beta z\right\}\left(\frac{1}{Z}\mathfrak{S}-\mathfrak{S}'\right) \\ &-\left\{\left(\frac{1}{Z}\sinh\alpha z-\sinh\beta z\right)+\frac{k^2}{2f^2}\sinh\beta z\right\}(\mathfrak{C}-\mathfrak{C}') \\ &+\left\{(\cosh\alpha z\cosh\beta H-\cosh\beta z\cosh\alpha H)+\frac{k^2}{2f^2}\cosh\beta z\cosh\alpha H\right\}\frac{1}{Z^*\mathfrak{T}^*}\Bigg] \\ w=\Bigg[&\left\{-\frac{\alpha}{h^2}\sinh\alpha z+\frac{if}{k^2}\frac{P_z}{S_z}\sinh\beta z\right\}\left(\frac{1}{Z}\mathfrak{S}-\mathfrak{S}'\right) \\ &+\left\{\frac{\alpha}{h^2}\frac{1}{Z}\cosh\alpha z-\frac{if}{k^2}\frac{P_z}{S_z}\cosh\beta z\right\}(\mathfrak{C}-\mathfrak{C}') \\ &+\left\{-\frac{\alpha}{h^2}\sinh\alpha z\cosh\beta H+\frac{if}{h^2}\frac{P_z}{S_z}\sinh\beta z\cosh\alpha H\right\}\frac{1}{Z^*\mathfrak{T}^*}\Bigg] \end{aligned}\right. \qquad \text{......(8.3)}$$

$$\left\{\begin{aligned} u&=-\frac{if}{h^{*2}}\frac{P_z}{\lambda^*}\frac{1}{Z^*}\left\{\frac{1}{\mathfrak{T}^*}\cosh\alpha^*z+\sinh\alpha^*z\right\}(\mathfrak{C}-\mathfrak{C}') \\ w^*&=\frac{\alpha^*}{h^{*2}}\frac{P_z}{\lambda^*}\frac{1}{Z^*}\left\{\frac{1}{\mathfrak{T}^*}\sinh\alpha^*Z+\cosh\alpha^*z\right\}(\mathfrak{C}-\mathfrak{C}') \end{aligned}\right. \qquad \text{......(8.4)}$$

To expand the functions in the above expressions is not difficult though somewhat troublesome. Introducing new notation

$$\zeta\equiv z/H \qquad \text{......(8.5)}$$

$$\begin{aligned} u=iH&\frac{1}{\xi}\frac{\mathfrak{v}^2/\gamma^2}{\sqrt{(1-\mathfrak{v}^2)}} \\ &\cdot\left[\xi\left\{\frac{1}{2}\gamma^2+\xi^2\zeta^2\frac{1}{4}(-2+3\gamma^2-\gamma^2\mathfrak{v}^2)\right\}\right. \\ &\qquad\times\left\{\frac{1}{4}\gamma^2\mathfrak{v}^2+\xi^2\frac{1}{6}\left[(-1+\gamma^2)-(-1+\frac{3}{4}\gamma^2)\mathfrak{v}^2-\frac{1}{4}\mathfrak{v}^4\right]\right. \end{aligned}$$

$$+\xi^4\frac{1}{120}\Big[2(-1+\gamma^2)+0(\mathfrak{v}^2)\Big]\Big\}$$

$$-\xi^3\zeta\frac{1}{2}(-1+\gamma^2)\Big\{\frac{1}{2}\gamma^2(1-\frac{1}{2}\mathfrak{v}^2)$$

$$+\xi^2\zeta^2\frac{1}{6}\Big[(-1+\frac{3}{2}\gamma^2)-(-1+\frac{7}{4}\gamma^2)\mathfrak{v}^2+(-\frac{1}{4}+\frac{1}{2}\gamma^2)\mathfrak{v}^4\Big]\Big\}$$

$$\times\{1+\xi^2\frac{1}{12}(2-(1+\gamma^2)\mathfrak{v}^2/\gamma^2)\}$$

$$+\frac{1}{8}\Gamma\gamma^2\mathfrak{v}^2\frac{1}{\sqrt{(1-\mathfrak{v}^2/\gamma^{*2})}}\{\gamma^2+\xi^2[-(-1+\gamma^2/2)+(-1+\frac{3}{2}\gamma^2)\zeta^2-\frac{1}{2}\mathfrak{v}^2(1+\gamma^2\zeta^2)]\}$$

$$\times\Big\{\frac{1}{\xi\delta\sqrt{(1-\mathfrak{v}^2/\gamma^{*2})}}[1+\frac{1}{3}\xi^2\delta^2(1-\mathfrak{v}^2/\gamma^{*2})]\Big\}\Big]$$

$$w=H\frac{\mathfrak{v}^2/\gamma^2}{\sqrt{(1-\mathfrak{v}^2)}}$$

$$\cdot\Big[\{-\xi\zeta(-1+\frac{1}{2}\gamma^2)+\xi^2\zeta^2\frac{1}{6}[(-2+\frac{3}{2}\gamma^2)+(1-\frac{1}{2}\gamma^4)\mathfrak{v}^2/\gamma^2]\}$$

$$\times\Big\{\frac{1}{4}\gamma^2\mathfrak{v}^2+\xi^2\frac{1}{6}[(-1+\gamma^2)-(-1+\frac{3}{4}\gamma^2)\mathfrak{v}^2-\frac{1}{4}\mathfrak{v}^4]\Big\}$$

$$+\xi\frac{1}{2}(-1+\gamma^2)(-1+\frac{1}{2}\mathfrak{v}^2)\Big\{\frac{1}{2}\gamma^2+\xi^2\zeta^2\frac{1}{2}[-(-1+\frac{1}{2}\gamma^2)-\frac{1}{2}\mathfrak{v}^2]\Big\}$$

$$\times\{1+\xi^2\frac{1}{12}(2-(1+\gamma^2)\mathfrak{v}^2/\gamma^2)\}$$

$$-\zeta\,\Gamma\gamma^2\mathfrak{v}^2\frac{1}{4\sqrt{(1-\mathfrak{v}^2/\gamma^{*2})}}\Big\{(-1+\frac{1}{2}\gamma^2)+\xi^2\Big[(-\frac{1}{4}\gamma^2+\zeta^2\frac{1}{6}(-1+\frac{3}{2}\gamma^2))$$

$$+\mathfrak{v}^2\Big(\frac{1}{4}-\frac{1}{6}\zeta^2(-1+\frac{1}{2}\gamma^4)/\gamma^2\Big)\Big]\Big\}$$

$$\times\frac{1}{\xi\delta\sqrt{(1-\mathfrak{v}^2/\gamma^{*2})}}(1+\frac{1}{3}\xi^2\delta^2(1-\mathfrak{v}^2/\gamma^2))\Big] \qquad \text{......(8.6)}$$

$$u^*=-iH\xi\mathfrak{v}^2\frac{1}{4}(-1+\gamma^2)(-1+\frac{1}{2}\mathfrak{v}^2)\frac{1}{\sqrt{(1-\mathfrak{v}^2)}\sqrt{(1-\mathfrak{v}^2/\gamma^{*2})}}$$

$$\cdot\{1+\xi^2\frac{1}{12}(2-(1+\gamma^2)\mathfrak{v}^2/\gamma^2)\}$$

$$\times\Big\{\Big[\frac{1}{\xi\delta\sqrt{(1-\mathfrak{v}^2/\gamma^{*2})}}(1+\frac{1}{3}\xi^2\delta^2(1-\mathfrak{v}^2/\gamma^{*2}))\Big]\cosh\{\xi\zeta\sqrt{(1-\mathfrak{v}^2/\gamma^{*2})}\}$$

$$+\sinh\{\xi\zeta\sqrt{(1-\mathfrak{v}^2/\gamma^{*2})}\}\Big\}$$

$$w^*=H\xi\mathfrak{v}^2\frac{1}{4}(-1+\gamma^2)(-1+\frac{1}{2}\mathfrak{v}^2)\frac{1}{\sqrt{(1-\mathfrak{v}^2)}}\{1+\xi^2\frac{1}{12}(2-(1+\gamma^2)\mathfrak{v}^2/\gamma^2)\}$$

$$\times\Big\{\cosh\{\xi\zeta\sqrt{(1-\mathfrak{v}^2/\gamma^{*2})}\}$$

$$+\left[\frac{1}{\xi\delta\sqrt{(1-\mathfrak{v}^2/\gamma^{*2})}}\left(1+\frac{1}{3}\xi^2\delta^2(1-\mathfrak{v}^2/\gamma^{*2})\right)\right]\sinh\{\xi\zeta\sqrt{(1-\mathfrak{v}^2/\gamma^{*2})}\}\Big\} \quad \ldots\ldots(8.7)$$

Just as we have treated the calculation in the previous article separating the cases corresponding to the two branches Π^- and Π^+, and the three cases (I), (II), and (III), we will follow the same way of calculation in this article. (Of course, in (I) terms involving Γ should be omitted, and in (II) $\frac{1}{\xi\delta\sqrt{(1-\mathfrak{v}^2/\gamma^{*2})}}$ should be replaced by an unity.)

8.11 $\Pi_0{}^-$. Without liquid.

Introducing the expression (6.10) into (8.6),

$$\left\{\begin{aligned} u&=iH\xi^4\frac{1}{24}\frac{1}{\gamma^2}(-1+\gamma^2)^2\Big[\{1+\xi^2\frac{1}{60}\frac{1}{\gamma^2}[30-32\gamma^2+\zeta^2(-60+90\gamma^2)]\}\\ &\qquad -2\zeta\{1+\xi^2\frac{1}{60}\frac{1}{\gamma^2}(20-17\gamma^2+\zeta^2(-20+30\gamma^2))\}\Big]\\ w&=-H\xi^3\frac{1}{12}\frac{1}{\gamma^2}(-1+\gamma^2)^2\\ &\qquad\cdot\Big[1+\xi^2\frac{1}{60}\frac{1}{\gamma^2}[20-17\gamma^2+\zeta(-60+30\gamma^2)+\zeta^2(60-30\gamma^2)]\Big]\end{aligned}\right. \quad \ldots\ldots(8.8)$$

This is not a convenient form of expression, so we will translate the coordinate axes so that the xy-plane passes the centre of the plate.

Putting $$\zeta=\zeta'+\frac{1}{2} \quad \ldots\ldots(8.9)$$

$$\left\{\begin{aligned} u&=iH\xi^4\frac{1}{24}\frac{1}{\gamma^2}(-1+\gamma^2)^2\zeta'\Big[-2+\xi^2\frac{1}{60}\frac{1}{\gamma^2}\{(-70+79\gamma^2)+\zeta'^2(40-60\gamma^2)\}\Big]\\ w&=-H\xi^3\frac{1}{12}\frac{1}{\gamma^2}(-1+\gamma^2)^2\Big[1+\xi^2\frac{1}{60}\frac{1}{\gamma^2}\{(5-19\gamma^2/2)+\zeta'^2(60-30\gamma^2)\}\Big]\end{aligned}\right. \quad \ldots\ldots(8.10)$$

By this expression, the amplitude of displacement and particle orbit becomes clear.

1) Ratio of amplitude is $|u/w|=\xi\zeta'+0(\xi^3)$, therefore w is far larger than u.

2) From 1) we may conclude that $\Pi_0{}^-$ is the bending motion of elastic plates.

3) Sense of rotation of particle orbit is the reverse of that of Rayleigh-waves.

4) Distribution of amplitude and the aspect of orbital motion is briefly shown in Fig. 9.

8.12 Π_0^-. Liquid of infinite depth.

Introducing (6.14) into (8.6) we have

$$\begin{cases} u=iH\xi^5\dfrac{1}{24\Gamma}\dfrac{1}{\gamma^2}(-1+\gamma^2)\left[1-2\zeta+\xi\dfrac{4}{\Gamma}\left(\dfrac{5}{12}-\dfrac{1}{2}\zeta\right)\right] \\ w=-H\xi^4\dfrac{1}{12\Gamma}\dfrac{1}{\gamma^2}(-1+\gamma^2)^2\left[1+\xi\dfrac{1}{\Gamma}+\xi^2\left\{\dfrac{1}{6}+\zeta\dfrac{1}{\gamma^2}\left(-1+\dfrac{1}{2}\gamma^2\right)\right.\right. \\ \qquad\qquad\qquad\qquad\left.\left.-\zeta^2\dfrac{1}{\gamma^2}\left(-1+\dfrac{1}{\gamma^2}\right)\right\}\right] \end{cases} \quad \text{......(8.11)}$$

Using the transformation (8.9)

$$\begin{cases} u=iH\xi^5\dfrac{1}{24\Gamma}\dfrac{1}{\gamma^2}(-1+\gamma^2)\left[-2\zeta'+\xi\dfrac{4}{\Gamma}\left(\dfrac{1}{6}-\dfrac{1}{2}\zeta\right)\right] \\ w=-H\xi^4\dfrac{1}{12\Gamma}\dfrac{1}{\gamma^2}(-1+\gamma^2)^2\left[1+\xi\dfrac{1}{\Gamma}+\xi^2\left\{\dfrac{1}{6}+\left(\dfrac{1}{4}-\zeta'^2\right)\dfrac{1}{\gamma^2}\left(-1+\dfrac{1}{2}\gamma^2\right)\right\}\right] \end{cases} \quad \text{......(8.12)}$$

These expressions are still symmetric with regard to ζ' so long as we are dealing only with first approximations. However, on account of the second term in [ ] of u, the said symmetry collapses if the wave-number is not so small.

The general feature of distribution of amplitude, ratio of them and the particle orbit is not different from the results obtaind in § 8.11. In this case, however, we must consider the motion in liquid.

Introducing the same relation into (8.7) we have

$$\begin{cases} u^*=iH\xi^4\dfrac{1}{12\Gamma}\dfrac{1}{\gamma^2}(-1+\gamma^2)^2\left[1-\xi\dfrac{1}{\Gamma}\right]\exp\{\xi\zeta\} \\ w^*=-H\xi^4\dfrac{1}{12\Gamma}\dfrac{1}{\gamma^2}(-1+\gamma^2)^2\left[1-\xi\dfrac{1}{\Gamma}\right]\exp\{\xi\zeta\} \end{cases} \quad \text{......(8.13)}$$

Since w and w^* are continuous at the boundary surface we find no peculiar phenomenon, while u and u^* are not necessarily continuous.

Indeed, at the boundary surface

$$w=w^* \quad \text{and} \quad |u^*|=|w^*| \qquad \text{......(8.14)}$$

Therefore from (8.12) u and u^* are discontinuous, and the orbit in liquid part is circular. The direction of rotation is reverse to that of elastic part on contact surface, and u^* and w^* diminishes exponentially with respect to $-z$, which is clear from the expression (8.13). (cf. Fig. 8)

8.13 Π^-. Liquid with finite depth.

Introducing (6.17) into (8.6)

$$\left\{\begin{aligned} u&=iH\xi^6\frac{\delta}{24\Gamma}\frac{1}{\gamma^2}(-1+\gamma^2)^2\Big[(1-2\zeta) \\ &\quad+\xi^2\frac{1}{180}\frac{1}{\gamma^2}\{(60-54\gamma^2-120\frac{\delta}{\Gamma}\gamma^2-40\gamma^2\delta^2)+\zeta\gamma^2(12+360\frac{\delta}{\Gamma}+120\delta^2) \\ &\qquad+\zeta^2(-180+270\gamma^2)-\zeta^3(-120+180\gamma^2)\}\Big] \\ w&=-H\xi^5\frac{\delta}{12\Gamma}\frac{1}{\gamma^2}(-1+\gamma^2)^2 \qquad \ldots\ldots(8.15) \\ &\quad\cdot\Big[1+\xi^2\frac{1}{60}\frac{1}{\gamma^2}\{-2\gamma^2-60\frac{\delta}{\Gamma}\gamma^2-20\gamma^2\delta^2+\zeta(-60+30\gamma^2)-\zeta^2(-60+30\gamma^2)\}\Big] \end{aligned}\right.$$

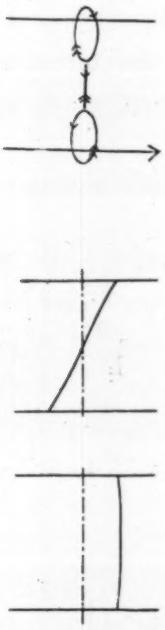

Fig. 9.
Orbit and amplitude distribution of Π_0^-.
When there is no liquid.

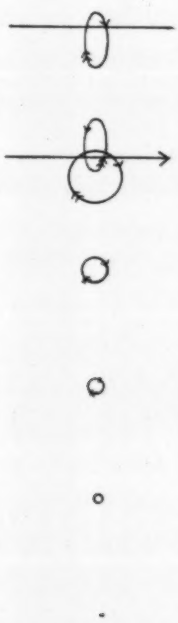

Fig. 10.
Orbit of Π_0^-.
When there is liquid with infinite depth.

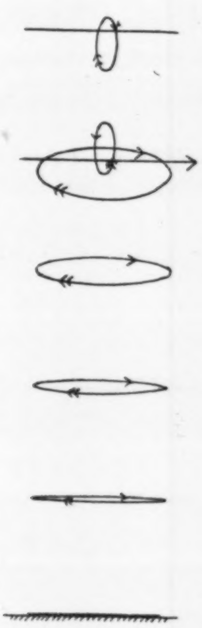

Fig. 11.
Orbit of Π_0^-.
When there is liquid with finite depth.

The nature of displacement in the plate are qualitatively same with the former case. Displacements in liquid part are, using (8.7)

$$\left\{\begin{aligned} u^*&=iH\xi^4\frac{1}{12\Gamma}\frac{1}{\gamma^2}(-1+\gamma^2)^2\Big[1+\xi^2\Big\{-\frac{1}{30}-\frac{\delta}{\Gamma}+\delta\zeta+\frac{1}{2}\zeta^2\Big\}\Big] \\ w^*&=-H\xi^5(\delta+\zeta)\frac{1}{12\Gamma}\frac{1}{\gamma^2}(-1+\gamma^2)^2 \qquad \ldots\ldots(8.16) \end{aligned}\right.$$

$$\cdot\Big[1+\xi^2\Big\{-\frac{1}{30}-\frac{\delta}{\Gamma}-\frac{1}{3}\delta^2+\frac{1}{3}\delta\zeta+\frac{1}{6}\zeta^2\Big\}\Big]$$

in which the factor $(\delta+\zeta)$ secures the vanishing of w^* at the bottom.

In this case w^* is a small quantity of higher order than u^*, therefore the orbit in the liquid part is a flat ellipse until it becomes a horizontal segment at the bottom of the liquid. The amplitude of u is nearly equal from the bottom to the boundary surface. The general feature is shown in Fig. 10, and amplitude ratio is

$$|u^*/u^*|=1\Big/\Big[\xi(\delta+\zeta)\Big\{1+\xi^2\Big(-\frac{1}{3}\delta^2-\frac{2}{3}\zeta\delta-\frac{1}{3}\zeta^2\Big)\Big\}\Big] \quad \text{......(8. 17)}$$

We will finish the calculations of Π^- by far.

8. 21 Π^+ Without liquid.

Introducing the equation (6. 12) into (8. 6) and neglecting the terms of $0(\xi^4)$ in u and $0(\xi^5)$ in w, we have

$$\left\{\begin{aligned}
u&=H2\frac{1}{\gamma}(-1+\gamma^2)^2/\surd(-4+3\gamma^2)\\
&\quad\cdot\Big[1+\xi^2\frac{1}{6}\frac{1}{\gamma^4}\Big\{[-4-8\gamma^2+19\gamma^4-8\gamma^6]/(-4+3\gamma^2)\\
&\qquad\qquad -\zeta 6\gamma^2(1-\frac{1}{2}\gamma^2)+\zeta^2 6\gamma^2(1-\frac{1}{2}\gamma^2)\Big\}\Big]\\
w&=-iH\xi 2\frac{1}{\gamma^3}(-1+\gamma^2)^2(-1+\frac{1}{2}\gamma^2)/\surd(-4+3\gamma^2)\\
&\quad\cdot\Big[-2\zeta\{1+\xi^2\frac{1}{6}\frac{1}{\gamma^4}[(-4-8\gamma^2+19\gamma^4-8\gamma^6)/(-4+3\gamma^2)+\zeta^2(4-2\gamma^2-\gamma^4)]\Big\}\\
&\qquad +\{1+\xi^2\frac{1}{6}\frac{1}{\gamma^4}[(4-18\gamma^2+20\gamma^4-13\gamma^6/2)/(-4+3\gamma^2)\\
&\qquad\qquad +\zeta^2(12-6\gamma^2-3\gamma^4)\}\Big]
\end{aligned}\right. \quad \text{......(8. 18)}$$

Introducing (8. 9)

$$\left\{\begin{aligned}
u&=H2\frac{1}{\gamma}(-1+\gamma^2)^2/\surd(-4+3\gamma^2)\\
&\quad\cdot\Big[1+\xi^2\frac{1}{6}\frac{1}{\gamma^4}\Big\{[-4-8\gamma^2+19\gamma^4-8\delta^6]/(-4+3\gamma^2)\\
&\qquad\qquad -\Big(\frac{1}{4}-\zeta'^2\Big)6\gamma^2\Big(1-\frac{1}{2}\gamma^2\Big)\Big\}\Big]\\
w&=-iH\xi^2\frac{1}{2\gamma^3}(-1+\gamma^2)^2(-1+\frac{1}{2}\gamma^2)/\surd(-4+3\gamma^2)
\end{aligned}\right.$$

$$\cdot(-2\zeta')\left[1+\xi^2\frac{1}{12}\frac{1}{\gamma^4}\{(-16-14\gamma^2+49\gamma^4-45\gamma^6/2)/(-4+3\gamma^2)\right.$$
$$\left.+\zeta'^2(8-4\gamma^2-2\gamma^4)\}\right]\quad\ldots\ldots(8.19)$$

Calculations to obtain the above expressions are extremely complicated, although the result is concise and it is clear that u is an even function of ζ' and w an odd function.

This is contrary to the property which we explained in § 8.11. Since the ratio of amplitude is

$$|u/w|=\frac{1}{\xi}\frac{\gamma^2}{-1+\gamma^2/2}\left[1+\xi^2\frac{1}{6}\frac{1}{\gamma^4}(2-\gamma^2-\gamma^4/2)\right]\quad\ldots\ldots(8.20)$$

horizontal component is far larger than the vertical one. Therefore this branch of dispersion curves is the longitudinal oscillation of elastic plates, and the particle orbit is a flat ellipse and the direction of rotation is the same with that of Rayleigh-waves.

The general feature of amplitude distribution and orbit is shown in Fig. 12.

8.22 Π^+. Liquid of infinite depth.

Adopting the expression (6.17) and introducing it into (8.6)

$$\left\{\begin{aligned}u&=H\frac{1}{\xi}\frac{1}{2}\gamma\mathfrak{v}_0^2/(-4+3\gamma^2)\cdot\Big[\xi(-1+\gamma^2)\\&\quad+\frac{\Gamma}{4}\mathfrak{v}_0^2\frac{1}{\sqrt{(1-\mathfrak{v}_0^2/\gamma^{*2})}}\Big(\gamma^2+\xi^2\frac{1}{6}\frac{1}{\gamma^2}\Big\{\gamma^2(-20+38\gamma^2-17\gamma^4)/(-4+3\gamma^2)\\&\quad-4\Big(-1+\frac{1}{2}\gamma^2\Big)^2\frac{\mathfrak{v}_0^2}{\gamma^{*2}}/(1-\mathfrak{v}_0^2/\gamma^{*2})-\zeta^2 6\gamma^2\Big(-1+\frac{1}{2}\gamma^2\Big)\Big\}\Big)\Big]\\w&=-iH\frac{1}{8}\gamma\Big(-1+\frac{1}{2}\gamma^2\Big)\mathfrak{v}_0^4/\sqrt{(-4+3\gamma^2)}\\&\quad\cdot[\xi(1-2\zeta)-\zeta\cdot 2\Gamma/\sqrt{(1-\mathfrak{v}_0^2/\gamma^{*2})}]\end{aligned}\right.\quad\ldots\ldots(8.21)$$

The amplitude distribution is not similar to that of the former case, for at the boundary surface w is a small quantity of the order of $H\xi$, while at the free surface it becomes the order of H.

Thus the distribution of ratio of amplitude $|u/w|$ takes the value

$$|u/w|=\frac{1}{\xi}\frac{\gamma^2\Gamma}{-1+\gamma^2/2}\frac{1}{+2\zeta\Gamma-\xi\sqrt{(1-\mathfrak{v}^2/\gamma^{*2})}}\quad\ldots\ldots(8.22)$$

The reason why at the free surface w is far more larger than at the boundary surface is that at the free surface there is no reaction while at the boundary there is the resistance due to liquid. The direction of rotation is, if $\sqrt{(1-\mathfrak{v}_0^2/\gamma^{*2})}$ is real, the same with the former case and the orbit is a flat ellipse. A brief sketch is shown in Fig. 13a.

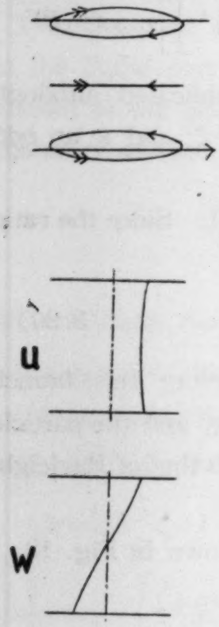

Orbit and amplitude distribution of Π_0^+. When there is no liquid.

Fig. 12.

Orbit of Π_0^+. When there is liquid with infinite depth.

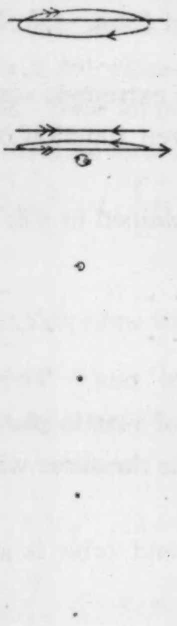

$(\mathfrak{v}_0<\gamma^*)$
Fig. 13 a.

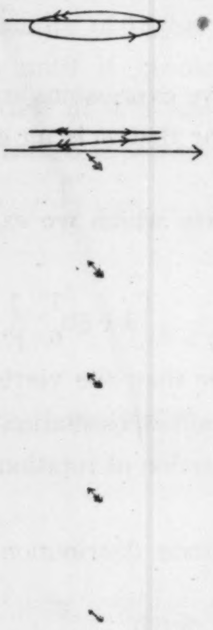

$(\mathfrak{v}_0>\gamma^*)$
Fig. 13 b.

Orbit of Π_0^+. When there is liquid with finite depth.

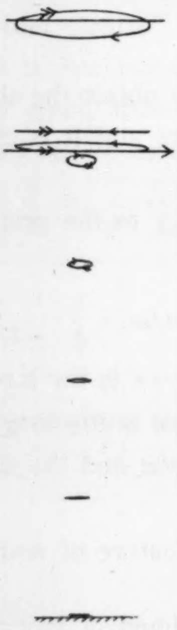

$(\mathfrak{v}_0<\gamma^*)$
Fig. 14 a.

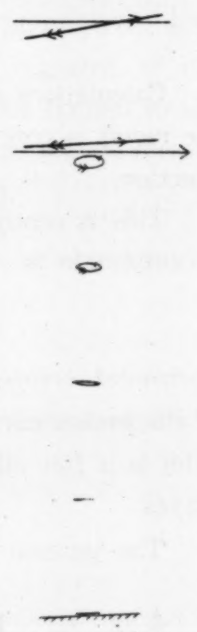

$(\mathfrak{v}_0>\gamma^*)$
Fig. 14 b.

At a point very near the boundary surface, the orbit becomes a horizontal segment.

If $\sqrt{(1-\mathfrak{v}_0^2/\gamma^{*2})}$ is imaginary, or if the limiting velocity of Π_0^+ is larger than that of sound waves in water, (cf. § 6.4 and § 7.12) the energy of waves propagate into the liquid part and the amplitude decreases exponentially with respect to x. (cf. Fig. 13b) Therefore these waves may not be received at fairly distant places from the origin. In such a case the velocity takes complex value; so as long as we are dealing with only real roots (such as the numerical calculations in § 5), we will not be able to find waves of surface type, even though the imaginary part is very small. However, in this section, we will aim at a more precise estimation of the magnitude of these waves, to understand the observations performed on lake ice.

We have noticed in § 7.12, that the velocity of Π_0^+ branch of three cases are nearly equal in spite of the existence of liquid or its bottom. This phenomenon may be interprected from the fact that Π^+ branch is the elongation and contraction, and thus the amplitude in liquid part is very small compared with that in elastic plate. (cf. Figs. 13 a and 13 b) So that it is easily inferred that the energy which dissipated into the liquid can by no means be large.

For example, if we assume

$$\left\{\begin{array}{l} V_s\mathfrak{v}_0=3000\text{ m/sec} \\ H=20\text{ cm} \\ \rho^*/\rho=1.09 \\ V_p^2/V_s^2=4 \\ V^{*2}/V_s^2=1/1.44 \end{array}\right.$$

$$\left\{\begin{array}{l} \text{period of the waves of } \Pi_0^+ \text{ branch}=0.01\text{ sec.} \\ \text{epicentral distance}=1000\text{ m} \end{array}\right.$$

then

$$\mathfrak{v}\doteqdot\sqrt{3}\left\{1-\frac{1}{24}\xi^2+i\,0.0528\,\xi^3\right\},$$

and $$\xi\doteqdot1/25\,,$$

thus the dissipation is only an order of

$$\exp\{-10^{-7}\}\,,$$

therefore its effect is negligibly small.

The motion in the liquid part is, introducing (6.17) into (8.7)

$$\left\{\begin{array}{l} u^*=-H\xi\frac{1}{8}\gamma\mathfrak{v}_0^4\left(-1+\frac{1}{2}\gamma^2\right)\frac{1}{\sqrt{(-4+3\gamma^2)}\sqrt{(1-\mathfrak{v}_0^2/\gamma^2)}}\exp\{\xi\zeta\sqrt{(1-\mathfrak{v}_0^2/\gamma^{*2})}\} \\ w^*=-iH\xi\frac{1}{8}\gamma\mathfrak{v}_0^4\left(-1+\frac{1}{2}\gamma^2\right)\frac{1}{\sqrt{(-4+3\gamma^2)}}\exp\{\xi\zeta\sqrt{(1-\mathfrak{v}_0^2/\gamma^{*2})}\} \end{array}\right. \quad\ldots\ldots(8.23)$$

The order of u^* and w^* is same and their ratio is

$$|u^*/w^*|=|1/\sqrt{(1-\mathfrak{v}_0^2/\gamma^{*2})}| \quad\ldots\ldots(8.24)$$

In this case also, if $\mathfrak{v}_0<\gamma^*$, the orbit becomes an ellipse and the direction of rotation is the same with the former case, while if $\mathfrak{v}_0>\gamma^*$ it becomes a straight line.

8.23 Π_0^+. Liquid with finite depth.

Introducing the relation of $\mathfrak{v}^2$ and ξ ((6.20)) into (8.6) we have

$$\left\{\begin{array}{l} u=H\frac{1}{\xi^2\delta}\frac{1}{8}\frac{\gamma^3\mathfrak{v}_0^4\Gamma}{\sqrt{(-4+3\gamma^2)}}\frac{1}{1-\mathfrak{v}_0^2/\gamma^{*2}} \\ \quad\cdot\left[1+\xi^2\frac{1}{6}\frac{1}{\gamma^4}\left\{\gamma^2(-20+38\gamma^2-17\gamma^4)/(-4+3\gamma^2)\right.\right. \\ \qquad\qquad -8\left(-1+\frac{1}{2}\gamma^2\right)^2\frac{\mathfrak{v}_0^2}{\gamma^{*2}}/(1-\mathfrak{v}_0^2/\gamma^{*2})+\delta^2 2\gamma^4(1-\mathfrak{v}_0^2/\gamma^{*2}) \end{array}\right.$$

$$
\left\{
\begin{aligned}
&\qquad\qquad +\delta 6\gamma^4\frac{1}{\Gamma}(1-\mathfrak{v}_0{}^2/\gamma^{*2})-\zeta^2 6\gamma^2\left(-1+\frac{1}{2}\gamma^2\right)\Big\}\Big]\\
&w=iH\frac{1}{\xi\delta}\left(-1+\frac{1}{2}\gamma^2\right)\frac{\gamma\mathfrak{v}_0{}^4\Gamma}{4\sqrt{(-4+3\gamma^2)}}\,\frac{1}{1-\mathfrak{v}_0{}^2/\gamma^{*2}}\\
&\qquad\cdot\Bigg[\zeta\Big\{1+\xi^2\frac{1}{6}\,\frac{1}{\gamma^4}\Big[(48-104\gamma^2+74\gamma^4-17\gamma^6)/(-4+3\gamma^2)\\
&\qquad\qquad -8\left(-1+\frac{1}{2}\gamma^2\right)^2\frac{\mathfrak{v}_0{}^2}{\gamma^{*2}}/(1-\mathfrak{v}_0{}^2/\gamma^{*2})+\zeta^2(4-2\gamma^2-\gamma^4)\\
&\qquad\qquad +\delta^2 2\gamma^4(1-\mathfrak{v}_0{}^2/\gamma^{*2})\Big]\Big\}\\
&\qquad\qquad +\xi^2\delta\left(\zeta-\frac{1}{2}\right)\frac{1}{\Gamma}(1-\mathfrak{v}_0{}^2/\gamma^{*2})\Bigg]
\end{aligned}
\right. \qquad \text{......(8.25)}
$$

At $\qquad \zeta=0, \quad |u/w|=0(\xi^{-3})$ ......(8.26)

while at $\qquad \zeta>\xi, \quad |u/w|=0(\xi^{-1})$ ......(8.27)

A brief sketch of the orbit of motion is given in Figs. 14a and 14b. If $\mathfrak{v}_0<\gamma^*$, the direction of the rotation of orbit, the proparty that the horizontal component is far larger than the vertical one, and that w is much larger at the free surface than at the boundary, are all the same with the former case, therefore Fig. 13a will also do in this case.

Displacements in the liquid part are from (8.7)

$$
\left\{
\begin{aligned}
&u^*=-H\frac{1}{\delta}\,\frac{1}{8}\gamma\mathfrak{v}_0{}^4\left(-1+\frac{1}{2}\gamma^2\right)\frac{1}{\sqrt{(-4+3\gamma^2)}}\,\frac{1}{1-\mathfrak{v}_0{}^2/\gamma^{*2}}\\
&\qquad\cdot\Big[1+\xi^2\Big\{\frac{1}{6}\,\frac{1}{\gamma^4}(40-90\gamma^2+68\gamma^4-17\gamma^6)/(-4+3\gamma^2)\\
&\qquad\qquad\qquad -\frac{4}{3}\,\frac{1}{\gamma^4}\left(-1+\frac{1}{2}\gamma^2\right)^2\frac{\mathfrak{v}_0{}^2}{\gamma^{*2}}/(1-\mathfrak{v}_0{}^2/\gamma^{*2})\\
&\qquad\qquad\qquad +(1-\mathfrak{v}_0{}^2/\gamma^{*2})\left(\frac{1}{3}\delta^2+\delta\zeta+\frac{1}{2}\zeta^2\right)\Big\}\Big]\\
&w^*=-iH\xi\frac{1}{\delta}(\delta+\zeta)\frac{1}{8}\gamma\mathfrak{v}_0{}^4\frac{-1+\gamma^2/2}{\sqrt{(-4+3\gamma^2)}}\\
&\qquad\cdot\Big[1+\xi^2\Big\{\frac{1}{6}\,\frac{1}{\gamma^4}(40-90\gamma^2+68\gamma^4-17\gamma^6)/(-4+3\gamma^2)\\
&\qquad\qquad\qquad +\zeta(2\delta+\zeta)\frac{1}{6}(1-\mathfrak{v}_0{}^2/\gamma^{*2})\Big\}\Big]
\end{aligned}
\right. \qquad \text{......(8.28)}
$$

The explanation of these expressions is not different from that in the previous article, therefore we will omit it and show only the general feature of the orbit. The horizontal component is nearly equal throughout the liquid, while the vertical component becomes smaller as it goes near the bottom. In this case the reflected waves come from the bottom and interference occurs between them and the direct waves. This phenomenon is somewhat analogous to the case of Love-waves. (cf. Fig. 14)

Thus we have finished the calculations by means of the power series of ξ.

The dispersion curves in elastic plates are represented by Π^- and Π^+, and no other branch can exist. Although the combination of ice and water permits only the Π_0^- branch under the condition that the velocity takes real value, we must take into consideration also the complex roots. Such knowledge will give some clue to the discussion of stratified Rayleigh-waves.

Résumé

In this paper we have discussed the theory of surface waves propagated upon elastic plates.

In §2, SH waves are considered as the simplest model of surface waves, and the dispersion curves and formation of them are discussed.

In §3, the characteristic equation of surface waves formed by P and SV waves is obtained. And in §4, the numerical calculation of the above equation was performed.

In §5, the characteristic equation, when there exists some liquid on one side of the plate, is obtained, and some numerical calculations are done.

In §6, the above equation was expanded as a power series of ξ and its solution of the form $\mathfrak{v}^2=\sum A_n\xi^n$ was obtained. There are two branches, of which one (Π_0^+) shows the nature of normal dispersion, while the other (Π_0^-) disperses abnormally.

In §7, we obtained the relation between phase velocity, group velocity, wave length and period using the results obtained in a previous article.

In §8, we discussed the distribution of amplitudes, their ratio and the particle orbit by means of the calculation of §6 and §7. It became clear by the above discussion that Π^- branch is the bending motion of plates, while Π^+ branch is the elongation and contraction of them. Hitherto, we have only discussed the real roots of velocity equations, however when the sound velocity in the liquid part is small compared with that of the elastic part ($\mathfrak{v}_0>\gamma^*$), we must pay some attention to the existence of the branch Π^+, and consider also the complex roots so long as we are dealing with seismograms recorded near the origin.

Appendix—Notations

Notations accompanying *, when not specially defined, mean corresponding quantities in liquid.

a, b	$=1/V_p,\ \ 1/V_s$
c_2^2	$=(-2+\gamma^2)^2/(12\gamma^4)$
$C_{ik},$	$=\frac{1}{i\,!}(1-\mathfrak{v}^2/\gamma^2)^3+\frac{1}{k\,!}(1-\mathfrak{v}^2)^3,\quad C=C_{11}.$ Cf. (6.3).
D	Depth of the liquid.
f	$=(2\pi/\text{wave length})$
H	thickness of the plate.
h, k	$=ap,\ \ bp$
$L_{ik},\ L$	$=\frac{1}{i\,!}(1-\mathfrak{v}^2/\gamma^2)+\frac{1}{k\,!}(1-\mathfrak{v}^2),\quad L=L_{11}.$ Cf. (6.3).
P	$=(1-\mathfrak{v}^2/\gamma^2)\cdot(1-\mathfrak{v}^2)$ Cf. (6.3)
$P,\ P_z,\ P_x$	$=\lambda+2\mu f^2/\mu^2,\quad \lambda-2\mu\alpha^2/h^2,\quad i2\mu\alpha f/h^2.$ Cf. (3.7).
p	circular frequency
$S,\ S_z,\ S_x$	$=i2\mu\beta f/k^2,\quad -i2\mu\beta f/k^2,\quad -\mu(f^2+\beta^2)/k^2.$ Cf. (3.7).
$S_{ik},\ S$	$=\frac{1}{i\,!}(1-\mathfrak{v}^2/\gamma^2)^2+\frac{1}{k\,!}(1-\mathfrak{v}^2)^2,\quad S=S_{11}.$ Cf. (6.3).
T	period
$u,\ v,\ w$	$x,\ y,\ z$-component of displacement vector.
$x,\ y,\ z$	rectangular coordinates. z-axis is taken vertically upward.
$V_p,\ V_s$	velocity of longitudinal and transverse waves.
V^*	sound velocity in liquid.
Z	$=\frac{P_x}{P_z}\frac{S_z}{S_x}=\frac{\sqrt{(1-\mathfrak{v}^2/\gamma^2)}\sqrt{(1-\mathfrak{v}^2)}}{(1-\mathfrak{v}^2/2)^2}.$ Cf. (3.11) and (4.11)′.
$1/Z^*$	$=(\lambda^* h^{*2}k^2)/(4\mu\alpha^*\beta f^2)$ Cf. (5.10).
$\alpha,\ \beta$	$=\sqrt{(f^2-h^2)},\ \ \sqrt{(f^2-k^2)}$
$\alpha_1,\ \beta_1$	$=\alpha/f(=\sqrt{(1-\mathfrak{v}^2/\gamma^2)}),\quad \beta/f(=\sqrt{(1-\mathfrak{v}^2)})$
Γ	$=\rho^*/\rho$
$\gamma,\ \gamma^*$	$=V_p/V_s,\ \ V^*/V_s$
$\Delta,\ \varpi$	dilatation and rotation of displacement vector.
$\Delta_{\text{I}},\ \Delta_{\text{II}},\ \Delta_{\text{III}}$ $\Delta_{\text{I}}',\ \Delta_{\text{II}}',\ \Delta_{\text{III}}'$	Cf. (5.10), (5.11) and (5.12).
δ	$=D/H$
$\zeta,\ \zeta'$	$=\frac{z}{H},\ \ \frac{z}{H}-\frac{1}{2}$

λ, μ	Lamé's constants.
Λ	$2\pi/\xi=2\pi\mathfrak{v}/\omega$ (=wave length (unit: H))
ρ	density.
ξ	$=fH$
ω	$=pb_H$ (=circular frequency (time unit: H/V_s))
Σ	surface waves formed by SH waves in elastic plates.
Π^-, Π^+	surface waves formed by P and SV waves in elastic plates.
$\mathfrak{C}, \mathfrak{C}'$	$=\cosh\alpha H, \quad \cosh\beta H$
$\mathfrak{S}, \mathfrak{S}'$	$=\sinh\alpha H, \quad \sinh\beta H$
$\mathfrak{T}, \mathfrak{T}'$	$=\tanh(\alpha H/2), \quad \tanh(\beta H/2)$
$\mathfrak{T}^*$	$=\tanh\{D\surd(f^2-h^{*2})\}$
$\mathfrak{v}, \mathfrak{V}$	phase and group velocity of surface waves (unit: V_s)
$\mathfrak{v}_0$	limiting value of the velocity of $\Pi_0{}^+$-branch when $\xi\to 0$ $(=2\surd(-1+\gamma^2)/\gamma$, unit: $V_s)$

---

19. 表面波の研究 II 弾性板を傳はる表面波の速度

地震研究所　　佐藤泰夫

弾性板を傳はる表面波の速度をしらべた．

最初に SH 波の作る表面波をラブ波にならつて求めたが，これは表面で反射をくりかへしつつ傳はる SH 波のよせ集めにすぎず，或は表面波と呼ぶ事がちうちよされるかもしれないが，筆者は表面波のもつとも基本的な型とみたい．

次に P 波と SV 波からなるものについて計算を行つた．これは先にラムも行つた事があるが，我我は數値計算を廣い範圍にわたつて行ひ，存在しうるすべての分散曲線について考察を行ふと共に二三の場合については變位の振幅の分布を求めた．

しかし兩面が自由で大きな彈性板といふものはめつたに存在しない．我我は湖氷の上での實驗に對する理論的な根據を與へる目的で板の一面に流體が在る場合について計算を行つた．板が氷で流體が水の場合については特に數値解法を試みた．

以上の計算は相當にこみ入つてゐる爲に，一般的な性質を見通すことが困難である．そこで，波長が十分に長い場合について，速度方程式をべき級數に展開し，これから $\mathfrak{v}^2-\xi$ の關係を求め，さらに之をもとにして，$\mathfrak{v}-\xi$, $\mathfrak{v}-\omega$, $\mathfrak{V}-\xi$, $\mathfrak{V}-\omega$ 等の關係式をもとめた．

主要な結果をあげれば，波長が十分に長い時 ($\xi\to 0$) 位相速度が 0 に近づく $\Pi_0{}^-$ 分枝と，有限値 $\mathfrak{v}_0$ に近づく $\Pi_0{}^+$ 分枝とがある．前者は彈性波に接する流體の有無，流體に底のあるなしによつて全く異つた關係式を與へるが．後者の第一近似には相違が表はれて來ない．この事は振幅の分布と軌道とを求めてみればすぐに了解される．

Π^- は板の屈曲の波であり，流體内の振幅は一般に板の中よりも大きい，從つて流體の存在が大きな影響を與へるが，之に反して Π^+ は板の伸縮の波であり，流體内の振幅は非常に小さいのでその存在は大した影響を與へないのである．

なほ注意すべき事は，特性方程式の實根のみを求めてゐたのでは十分でないといふ事である．例へば氷と水の組合せでは Π^+ の波はないかのやうに見えるが，複素數の解を求めるならばたしかに存在しうる．このやうな解は震央距離がますにつれて．指數函數的に減衰する波をあらはすが，その減衰は必ずしも大きなものではなく，ある場合には殆ど無視しうる程度である．上下動地震計によつて觀測する時，P の直接波は理論上この方向の成分をもたないから，板がうすい場合には Π^+ を初動と見誤るおそれがあると思ふ．

以上の計算は一方において氷上實驗に對する理論を與へると共に，他方層がある場合のレーリーの性質についての類推の材料を呈供すると考へる．

20. *Electromagnetic Shielding within the Earth and Geomagnetic Secular Variation.*

By Tsuneji RIKITAKE,

Earthquake Research Institute.

(Read Mar. 20, 1951.—Received Mar. 20, 1951.)

1. Introduction

One of the most striking features of the earth's magnetic field is the secular variation. According to the extensive investigation carried out by E. H. Vestine and his collaborators[1],[2], we find a number of foci of the secular variation distributed irregularly on the earth's surface, the foci having likely some tendencies of drift motion towards the west as appears in Vestine's map for four epochs at a distance of ten years during the period from 1905 to 1945. It was also found out that some of the foci disappeared and others newly appeared during the period. More than fifty years ago L. A. Bauer[3] and V. Carlheim-Gyllensköld[4] already pointed out the westerly drift of the secular variation. As a result of spherical harmonic analysis, Carlheim-Gyllensköld obtained 3147, 1381 and 454 *years* as the apparent periods of complete revolution respectively for the harmonics P_1^1, P_2^1 and P_2^2.

Though these old investigations were not always accurate as commented by S. Chapman and J. Bartels[5], it seems that the secular variation of world-wide scale has an apparent period or duration-time of order of 1000 *years*, while the regional one of 100 *years* as recently reconsidered by W. M. Elsasser[6] and E. C. Bullard.[7]

Elsasser[6] and Bullard[7] studied the electromagnetic induction in the earth's core with special relation to the origin of the earth's magnetic field and its secular change. According to them, the secular variation was recognized as a perturbation of the main field caused by fluid motion near the surface of the core. However, we have not yet gained sufficient knowledge about the electric properties and the fluid motion in the core, so these theories may be regarded as hypothetical notwithstanding their interesting and suggestive characters.

---

[1] E. H. VESTINE, L. LAPORTE, C. COOPER, I. LANGE and W. C. HENDRIX, "Description of the Earth's Magnetic Field and its Secular Change, 1905-1945." *Cairnegie Inst. of Washington, Publication No.* **578** (1947).

[2] E. H. VESTINE, L. LAPORTE, I. LANGE and W. E. SCOTT, "The Geomagnetic Field, Its Description and Analysis," *Carnegie Inst. of Washington, Publication No.* **580** (1947).

[3] L. A. BAUER, *Amer. Journ. Sci.*, **50** (1895), 109, 189 and 314.

[4] V. CARLHEIM-GYLLENSKÖLD, *Astron. Jaktagelser och Undersökm, Stockholms Observat.*, **5**, Nr 5 (1896), 36. *Astron. och Fysik.*, **3**, No. 7 Uppsala (1906), 5.

[5] S. CHAPMAN and J. BARTELS, *Geomagnetism* (1940), p. 667.

[6] W. M. ELSASSER, *Phys. Rev.*, **69** (1946), 106, **70** (1946), 202. *Rev. Mod. Phys.*, **22** (1950), 1.

[7] E. C. BULLARD, *M. N. R. A. S. Geophys. Suppl.* **5** (1948), 248. *Proc. Roy. Soc. London* A **197** (1949), 433, **199** (1949), 413.

Meanwhile, the earth's mantle has a finite electrical conductivity as clarified from the studies of geomagnetic variation of short period or duration-time which were developed by S. Chapman[8),9)], A. T. Price[9),10)], B. N. Lahiri[10)], K. Terada[11)] and the writer[12)]. Among the investigations, the writer approximately determined the conductivity-distribution down to a depth of about 1500 *km* by studying various variations such as **Sq** (solar daily variation on quiet days), **S$_D$** (solar daily disturbance variation), **Dst** (main phase of magnetic storm), bay-type disturbance, S. F. variation (magnetic effect associated with solar eruption or Dellinger effect), sudden commencement of magnetic storm, and 27-day period variation, the period or duration-time of these variations ranging from a few minutes to scores of days. It was found out that the electrical conductivity increases discontinuously at a depth of nearly 400 *km* from 10^{-15} *emu* to 10^{-12} *emu* and then increases gradually with the increase in depth, the most probable distribution being expressed by

$$\begin{aligned} \sigma &= \sigma' & q_1 < \rho < 1 \\ &= \sigma_0 \rho^{-l} & \rho < q_1 , \end{aligned}$$

where σ', σ_0, l, and q_1 is determined to be 10^{-15} *emu*, 1.0×10^{-12} *emu*, 11, and 0.94 respectively. ρ denotes the ratio of the radial distance r to the radius of the earth a.

Since the earth's mantle has some electrical conductivity as mentioned above, it should be borne in mind that the varying magnetic field which is hypothetically considered by Elsasser and Bullard will be shielded to some extent by the existence of the mantle. In his latest memoir, Elsasser[6)] has taken into account a rough estimate of the above mentioned effect. On the basis of the conductivity-distribution obtained by the writer, the writer will calculate here the electromagnetic

---

8) S. CHAPMAN, *Phil. Trans. Roy. Soc. London* A, **218** (1919), 1.

9) S. CHAPMAN and A.T. PRICE, *Phil, Trans. Roy. Soc. London* A, **229** (1930), 427.

10) B. N. LAHIRI and A. T. PRICE, *Phil. Trans. Roy. Soc. London* A, **237** (1939), 509.

11) K. TERADA, *Geophys. Mag.*, **13** (1939) 63, **16** (1948), 5.

12) T. RIKITAKE, *Trans. Oslo. Meeting I. U. G. G. A. T. M. E.* (1950), 435. *Bull. Earthq. Res. Inst.*, **28** (1950) 45, **29** (1951) 219 and 263.

shielding within the earth, which will be useful in checking the possibility of Elsasser and Bullards' interesting theories concerning the geomagnetic secular variation.

2. Theory.

We have not yet a concrete knowledge of the electrical properties in the core, whose upper boundary is situated, as determined from seismology, at a depth of 2900 *km* which is too deep for the electric currents induced by geomagnetic variation of external origin to reach as has been shown by the writer12). Though it is difficult to attack the problem by geophysical means, a number of investigators believes from the physical standpoint that the electrical conductivity should be appreciably high in the core, amounting to the order of 10^{-6} *emu* as estimated by Elsasser and Bullard. If it is supposed that the core is composed of iron, the conductivity would attain to such order through the effect of high temperature and pressure. Even if we take the view that the substance in the core assumes a state of high energy due to a phase transition of the silicates under enormous compression as suggested by W. H. Ramsey13), a high conductivity is expected in the core. Taking into consideration again the fact that the conductivity increases with the increase in depth as shown by geophysical studies, it may be allowable to assume that the conductivity takes a high value in the core though the precise order is still unknown.

In that case, the varying magnetic field that appears outside the core should be due to the currents flowing in a thin layer just below the boundary of the core as has been pointed out by Elsasser6). He estimated for the variation with a period of 100 *years* that the currents flowing at a depth much larger than 50 *km* from the boundary do not practically produce a magnetic field outside the core wheareas it would be allowed to assume the current-sheet approximation. The writer, for the sake of mathematical simplicity, also considered here a current-sheet that corresponds to the source of geomagnetic secular variation.

As may be seen in Fig. 1, we will take an earth-model in which the electrical conductivity σ is equal to σ'14), $\sigma_0\rho^{-l}$ 15) and σ_c 16) respectively for the regions 1, 2

---

13) W. H. Ramsey, *M. N. R. A. S.*, **108** (1948), 406. *M. N. R. A. S. Geophys. Suppl.*, **5** (1949), 409.

14) As already stated in Introduction, σ' amounts to only 10^{-15} *emu* down to a depth of 400 *km*, the value being so small that we can regard the substance to be non-conducting for very slow variation such as secular one.

15) Though the expression fits for the distribution up to a depth of about 1500 *km*, we tentatively assume that the expression is applicable throughout the mantle.

16) The conductivity is assumed to be constant in the core for the sake of simplicity.

and 3. The magnetic permeability is assumed as unity everywhere. In the non-conducting region, we have magnetic potential of which the typical term may be written as

$$W_n^m = a i_n(t)\rho^{-n-1}S_n^m, \tag{1}$$

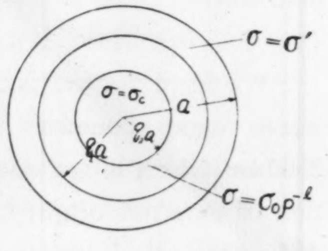

Fig. 1

where the external origin part is not taken into account since the secular variation originates in the earth. S_n^m denotes spherical surface harmonic having degree *n* and order *m*. In that case, the components of the magnetic field become

$$\left.\begin{aligned} H_r &= (n+1)\rho^{-n-2}i_n S_n^m, \\ H_\theta &= -\rho^{-n-2}i_n\partial S_n^m/\partial\theta, \\ H_\phi &= -\rho^{-n-2}i_n\partial S_n^m/(\sin\theta\partial\phi). \end{aligned}\right\} \tag{2}$$

On the other hand, we have in the conducting medium vector potential $\vec{A}$ which satisfies the relation

$$\nabla^2\vec{A} = 4\pi\sigma(\rho)\partial\vec{A}/\partial t \tag{3}$$

for the phenomenon is assumed to be quasi-stationary. The typical term of the solutions of (3) becomes

$$\vec{A}_n^m = af_n(t,\rho)[r\,\mathrm{grad}\,S_n^m], \tag{4}$$

where f_n satisfies the differential equation

$$\partial(\rho^2\partial f_n/\partial\rho)/\partial\rho = \{n(n+1)+4\pi a^2\sigma(\rho)\rho^2\partial/\partial t\}f_n. \tag{5}$$

Thus the components of the magnetic field are given by

$$\left.\begin{aligned} H_r &= -n(n+1)\rho^{-1}f_n S_n^m, \\ H_\theta &= -\rho^{-1}\frac{\partial}{\partial\rho}(\rho f_n)\partial S_n^m/\partial\theta, \\ H_\phi &= -\rho^{-1}\frac{\partial}{\partial\rho}(\rho f_n)\partial S_n^m/(\sin\theta\partial\phi). \end{aligned}\right\} \tag{6}$$

The function f_n becomes respectively for the regions 2 and 3 as follows;

$$f_{n,2} = \rho^{-1/2}\{C_2K_\nu(z)+D_2I_\nu(z)\} \qquad \text{for region 2,} \tag{7}$$

where C_2 and D_2 are both functions of time, K_ν and I_ν denote modified Bessel functions while

$$\rho^{1-l/2} = (l-2)z/(2\zeta),\ \nu = (2n+1)/(l-2),\ \zeta^2 = 4\pi a^2\sigma_0 p \tag{8}$$

and

$$f_{n,2} = C_3\rho^n F_n(\rho) \qquad \text{for region 3,} \tag{9}$$

where C_3 also denotes a function of time. F_n was fully studied in the studies of electromagnetic induction within the earth as given in the well-known book " *G-oe* *magnetism* "[17]. In the above treatment, $\partial/\partial t$ is replaced by p as is usual in operational calculus.

Now, on assuming a current-sheet at $\rho=q_2$, ($q_2=0.545$), the typical term of the current-function being given by

$$J_n^m=K_n^m S_n^m, \tag{10}$$

we get the next conditions from the continuity of magnetic field at the boundary of the core or $\rho=q_2$

$$\{\partial(\rho f_{n,2})/\partial\rho\}_{\rho=q_2}-\{\partial(\rho f_{n,3})/\partial\rho\}_{\rho=q_2}=(4\pi/a)K_n^m, \tag{11}$$

$$(f_{n,2})_{\rho=q_2}=(f_{n,3})_{\rho=q_2}. \tag{12}$$

We have also

$$n(f_{n,2})_{\rho=q_1}=-i_n q_1^{-n-1} \tag{13}$$

$$\{\partial(\rho f_{n,2})/\partial\rho\}_{\rho=q_1}=i_n q_1^{-n-1}, \tag{14}$$

from the boundary conditions at $\rho=q_1$.

Then, solving the simultaneous equations (11), (12), (13) and (14), we get with the aid of recurrence formulae, the relation

$$(4\pi/a)K_n^m=q_1^{-n-1}\frac{2n+1}{n}z_1\left\{\frac{z_2}{2\nu}\Big(I_{\nu+1}(z_2)K_{\nu+1}(z_1)-K_{\nu+1}(z_2)I_{\nu+1}(z_1)\Big)\right.$$
$$\left.+\frac{F_{n-1}(q_2)}{F_n(q_2)}\Big(I_\nu(z_2)K_{\nu+1}(z_1)+K_\nu(z_2)I_{\nu+1}(z_1)\Big)\right\}i_n,$$

where z_1 and z_2 respectively denote $z_{\rho=q_1}$ and $z_{\rho=q_2}$.

In case of periodic variation having a period $2\pi/\alpha$, the operator p is replaced by $i\alpha$ in the above expressions. When the period is larger than about 10 *years*, I_ν and K_ν are numerically calculated by use of ascending power series such as

$$\left.\begin{aligned} I_\nu(z)&=(\Phi_\nu+i\Psi_\nu)e^{i\nu\pi/4},\\ K_\nu(z)&=(\pi/2)\operatorname{cosec}\nu\pi\{(\Phi_{-\nu}+i\Psi_{-\nu})e^{-i\nu\pi/4}-(\Phi_\nu+i\Psi_\nu)e^{i\nu\pi/4}\}, \end{aligned}\right\} \tag{16}$$

where

$$\Phi_\nu=\sum_{s=0}^{\infty}\frac{(-1)^s(x/2)^{\nu+4s}}{(2s)!\,\Gamma(\nu+2s+1)} \qquad \Psi_\nu=\sum_{s=0}^{\infty}\frac{(-1)^s(x/2)^{\nu+4s+2}}{(2s+1)!\,\Gamma(\nu+2s+2)} \tag{17}$$

and

$$z=x\sqrt{i}.$$

When $x\ll 1$, (16) becomes

$$(4\pi/a)K_n^m=q_2^{-n-1}\frac{2n+1}{n}\left[\frac{F_{n-1}(q_2)}{F_n(q_2)}\right.$$
$$\left.+\frac{i}{\nu(\nu+1)}\left\{(x_2/2)^2+(q_2/q_1)^{2n+1}\left(\frac{F_{n-1}(q_2)}{F_n(q_2)}-1\right)(x_1/2)^2\right\}\right]i_n. \tag{19}$$

---

17) S. CHAPMAN and J. BARTELS, *loc. cit.*, p. 738.

Further, if σ_c is supposed to be zero, (19) becomes for $\sigma_c=0$.

$$(4\pi/a)K_n^m = q_2^{-n-1}\frac{2n+1}{n}\, i_n. \tag{20}$$

because F_{n-1}/F_n tends to 1 as σ_c approaches zero. As easily seen, (20) is just the same with the relation between the current and the magnetic potential when the conductivity is considered everywhere null. If we denote the coefficient of magnetic potential in that special case by $i_{n,0}$, the quantity $i_n/i_{n,0}$ is convenient for studying the shielding effect.

On the other hand, I_ν and K_ν are obtaind for smaller period by asymptotic expansions such as

$$\left.\begin{aligned} I_\nu(z) &= (2\pi z)^{-1/2} e^{z}\left\{1-\frac{4\nu^2-1^2}{1!8z}+\frac{(4\nu^2-1^2)(4\nu^2-3^2)}{2!(8z)^2}-\dots\dots\right\},\\ K_\nu(z) &= (\pi/2z)^{-1/2} e^{-z}\left\{1+\frac{4\nu^2-1^2}{1!8z}+\frac{(4\nu^2-1^2)(4\nu^2-3^2)}{2!(8z)^2}+\dots\dots\right\},\end{aligned}\right\} \tag{20}$$

while F_{n-1}/F_n is calculated by

$$\frac{F_{n-1}(x)}{F_n(x)}=\frac{2n+1}{x}\left\{1+\frac{n}{x}+\frac{n(n+1)}{2x^2}+\frac{n(n+1)}{2x^3}+\dots\dots\right\}, \tag{21}$$

and

$$F_n(x)=1+\frac{x^2}{2(2n+3)}+\frac{x^4}{2\cdot4(2n+3)(2n+5)}+\dots\dots \tag{22}$$

respectively for $|x|=\sqrt{2\pi\sigma_c\alpha}\,q\,a>1$ and $|x|<1$. By use of these expressions, *mod.* $i_n/i_{n,0}$ are calculated for various σ_c as shown in Fig. 2 where n is taken to be 1.

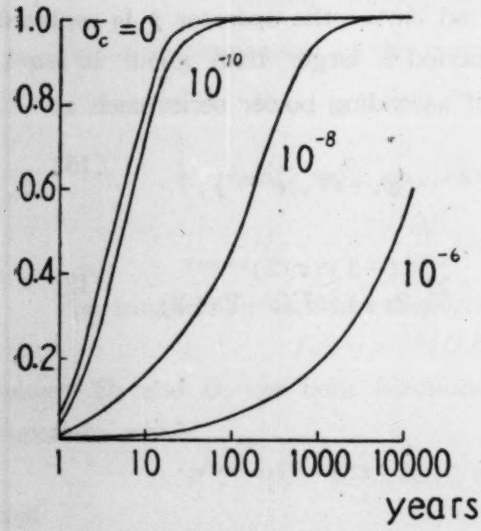

Fig. 2. The shielding effect for secular variation with various period.

3. Discussions

As seen in the figure, periodic variations having smaller period than 1 *year* seem to be almost shielded by the conducting mantle, only 5 *per cent* of its amplitude of 1 *year* period variation being expected at the earth's surface even in the case of non-conducting core. The larger the period is, the smaller becomes the shielding effect. Though the variation whose period is larger than sevral hundred *years* is partly shielded, it may be observed on the earth's surface if the conductivity amounts to the order of 10^{-6} *emu* or less in the core. Hence the geomagnetic secular change having period of several hundred *years* or more may not be shielded perfectly and will penetrate up to the earth's surface provided the action which is considered by Elsasser and Bullard is really occurring in the core. At least, it may be said that the existence of rapid geomagnetic variation having a period of 1 *year* or less is by no means likely.

4. Conclusion.

In order to estimate the shielding effect in the earth's interior to the hypothetical secular change, the writer has executed a calculation on the basis of the conductivity-distribution in the mantle which was previously obtained by the writer himself.

Since, however, the electrical property in the earth's core is ambiguous, no definite conclusion could be obtained except the fact that variation with period smaller than about 1 *year* should be almost shielded. But, it is likely that a part of secular variation with a period larger than several hundred *years* appears on the earth's surface even in case of appreciably high conducting core. Thus, if we assume the action in the core which is taken into account by Elsasser and Bullard, a part of the varying field would be observed on the earth's surface. Taking into consideration the actually observed variation, the result obtained here seems favourable to the hypothetical theories ventured by Elsasser and Bullard.

In conclusion, the writer wishes to express his hearty thanks to Dr. Hans G. Macht for his encouragement in this study.

---

20. 地磁氣永年變化に對する遮蔽効果

地震研究所　　力武常次

近年 Elsasser や Bullard によつて，地球内核中の流體運動と磁場との相互作用として，地磁氣永年變化の發生を説明しようという試みが行なわれている．一方筆者は地磁氣變化の解析より，1500 *km* 程度の深さまでの電氣傳導度分布を決定したが，その結果を利用して上述のような機構で永年變化が起るとしたときのシールディングを計算した　その結果は周期 1 年程度より短い變化はほとんど完全に遮蔽されて地表では觀測出來ないことになる．また數百年より長周期のものは大體に於いて遮蔽の程度が少なく，實際に觀測される永年變化を考えるとき，Elsasser や Bullard の云うような機構で永年變化が起つてもよいという結果を得た．

21. *Changes in Earth Current and their Relation to the Electrical State of the Earth's Crust.*

By Tsuneji RIKITAKE,

Earthquake Research Institute.

(Read Oct. 18, 1949.—Received Mar. 20, 1951.)

1. In the previous papers[1), 2)], the writer has studied electromagnetic induction in semi-infinite earth. It was shown in those papers that the horizontal components of the electric and magnetic forces at the earth's surface, perpendicular to each other, are connected by the next operational equation

$$E=\sqrt{\frac{\mu p}{\pi\sigma}}H \tag{1}$$

where μ and σ denote respectively magnetic permeability and electrical conductivity. Interpreting the operational equation, we find out that, in the case of periodic variation, (1) the amplitude ratio E/H is proportional to the inverse square root of the period, the so-called Terada's law[3)] being substantiated, and (2) the phase difference is always kept to be $\pi/4$.

According to H. Hatakeyama and M. Hirayamas' study[4)] on the observed results at Toyohara, however, the phase difference between the changes in the EW-component of the earth potential and in the horizontal one of the earth's magnetic field does not follow the above-mentioned simple relation. The phase difference becomes as small as 20°-30° for the changes of comparatively long period, though the difference seems to amount to about 45° for small period as shown in the writer's previous studies. In order to explain the results, Hatakeyama assumed a suitable distribution of the variation over the earth's surface. In this paper, an interpretation will be attempted from another stand-point.

As a matter of fact, the influence of the electrical property of the deep region of the earth's crust on the earth current which is observed at the earth's surface has never been quantitativery discussed. Studying the electromagnetic induction within the earth covered by a superficial layer, the present paper will deal with that

---

1) T. RIKITAKE, *Bull. Earthq. Res. Inst.*, **24** (1946), 1.
2) T. RIKITAKE, *Bull. Earthq. Res. Inst.*, **25** (1947), 9.
3) T. TERADA, *Journ. Col. Sci. Tokyo Imp. Univ.*, **37** (1917), Art. 9,56.
4) H. HATAKEYAMA and M. HIRAYAMA, *Journ. Meteorol. Soc. Japan* **12**, (1934), 449.

problem. Recently, K. Hirao[5] studied the above-mentioned influence, though not generally, in connexion with the anisotropy of the electrical conductivity of the earth's crust. As will be shown later, the writer's study includes Hirao's result as an extreme case.

2. According to the theory[6] of electromagnetic induction in a sphere which has an inner core covered by an outside layer of different conductivity, the typical term of the north component of the magnetic field at the earth's surface and the west component of the electric field in the outside layer are respectively given by the next expression in spherical coordinate,

$$H=\{1+I(p)\}\mathrm{e}_n^m\partial S_n^m/\partial\theta, \tag{2}$$

$$E=ap\{\overline{C}_2(p)\rho^n F_n(k_2\rho a)+\overline{D}_2(p)\rho^{-n-1}G_n(k_2\rho a)\}\mathrm{e}_n^m\partial S_n^m/\partial\theta, \tag{3}$$

where e_n^m, S_n^m, a and ρ denote respectively the coefficient of the external part of the magnetic potential, surface spherical harmonic of degree n and order m, the earth's radius and the ratio of the radial distance to the earth's radius. The conductivity and the boundaries are shown in Fig. 1. In the expressions, I, $\overline{C}_2$ and $\overline{D}_2$ are determined by the boundary conditions being given by

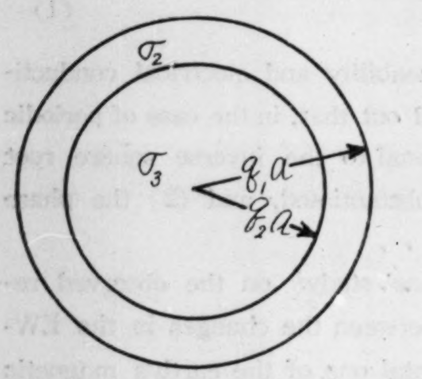

Fig. 1.

$$\left.\begin{aligned}
I(p)&=-q_1^{2n+1}\frac{n}{n+1}\frac{\left\{1-\dfrac{F_{n-1}(2,1)}{F_n(2,1)}\right\}\left\{1-\dfrac{F_{n-1}(3,2)}{F_n(3,2)}-\dfrac{G_{n+1}(2,2)}{G_n(2,2)}\right\}+\tau^{2n+1}\left\{\dfrac{F_{n-1}(3,2)}{F_n(3,2)}-\dfrac{F_{n-1}(2,2)}{F_n(2,2)}\right\}\dfrac{F_n(2,2)}{F_n(2,1)}\dfrac{G_n(2,1)}{G_n(2,2)}}{\dfrac{F_{n-1}(2,1)}{F_n(2,1)}\left\{1-\dfrac{F_{n-1}(3,2)}{F_n(3,2)}-\dfrac{G_{n+1}(2,2)}{G_n(2,2)}\right\}+\tau^{2n+1}\left\{1-\dfrac{G_{n+1}(2,1)}{G_n(2,1)}\right\}\left\{\dfrac{F_{n-1}(3,2)}{F_n(3,2)}-\dfrac{F_{n-1}(2,2)}{F_n(2,2)}\right\}\dfrac{F_n(2,2)}{F_n(2,1)}\dfrac{G_n(2,1)}{G_n(2,2)}}\\
\overline{C}_2(p)&=\frac{1}{n+1}\frac{1}{F_n(2,1)}\frac{1-\dfrac{F_{n-1}(3,2)}{F_n(3,2)}-\dfrac{G_{n+1}(2,2)}{G_n(2,2)}}{''}\\
\overline{D}_2(p)&=q_2^{2n+1}\frac{1}{n+1}\frac{F_n(2,2)}{F_n(2,1)}\frac{\dfrac{F_{n-1}(3,2)}{F_n(3,2)}-\dfrac{F_{n-1}(2,2)}{F_n(2,2)}}{''}
\end{aligned}\right\} \tag{4}$$

---

5) K. HIRAO, *Zisin* 2nd ser. **1** (1948), 12.

6) T. RIKITAKE, *Trans. Oslo Meeting, I.U.G.G. A.T.M.E.*, (1948), 435.
Kagaku **18** (1948), 469.
Bull. Earthq. Res. Inst., **28** (1950), 45 and **29** (1951), 219 and 263.

where

$$k_\nu^2 = 4\pi\sigma_\nu p$$

and μ is assumed to be unity. For the sake of simplicity, $F_n(k_\nu q_\mu a)$ and $G_n(k_\nu q_\mu a)$ are written respectively as $F_n(\nu,\mu)$ and $G_n(\nu,\mu)$ in the above expressions. We also wrote τ in place of q_2/q_1. F_n and G_n are modified Bessel functions whose nature has been fully investigated in the well-known book "*Geomagnetism*"7).

With these expressions, the relations between E and H can be obtained for given σ's and q's. If a is supposed to be large, the asymptotic expansions for F_n and G_n are available. After some calculations, we get

$$E = \frac{p}{\rho k_2} e^{-k_2(1-\rho)a} \frac{k_2 + k_3 + (k_2 - k_3)e^{-2k_2(\rho - q_2)a}}{k_2 + k_3 - \dfrac{n+1}{2n+1}(k_2 - k_3)e^{-k_2(1-q_2)a}} H, \qquad (5)$$

where the relation $q_1 = 1$ is taken into account.

Putting $\rho = 1$, then, the relation between E and H at the surface is written as

$$E = \frac{p}{k_2} \frac{k_2 + k_3 + (k_2 - k_3)e^{-2k_2D}}{k_2 + k_3 - \dfrac{n+1}{2n+1}(k_2 - k_3)e^{-2k_2D}} H \quad ^{8)} \qquad (6)$$

where D denotes the thickness of the outside layer. Making $n \rightarrow o$, (6) becomes the same with that obtained by Hirao.

In the case of a periodic variation of period T, the amplitude ratio and phase difference become respectively as follows:

$$\left.\begin{aligned}
A &= \frac{1}{\sqrt{2\sigma_2 T}} \\
&\times \left\{ \frac{1 + 2Ke^{-4\pi D\sqrt{\sigma_2/T}}\cos(4\pi D\sqrt{\sigma_2/T}) + K^2 e^{-8\pi D\sqrt{\sigma_2/T}}}{1 - \dfrac{2\sqrt{2}(n+1)}{2n+1} Ke^{-4\pi D\sqrt{\sigma_2/T}}\sin(\pi/4 - 4\pi D\sqrt{\sigma_3/T}) + \left(\dfrac{n+1}{2n+1}\right)^2 K^2 e^{-8\pi D\sqrt{\sigma_2/T}}} \right\}^{1/2}, \\
\psi &= \tan^{-1} \frac{1 + \sqrt{2}Ke^{-4\pi D\sqrt{\sigma_2/T}} \sin(\pi/4 - 4\pi D\sqrt{\sigma_2/T})}{1 + \sqrt{2}Ke^{-4\pi D\sqrt{\sigma_2/T}} \sin(\pi/4 + 4\pi D\sqrt{\sigma_2/T})}, \\
&\quad - \tan^{-1} \frac{\dfrac{n+1}{2n+1} Ke^{-4\pi D\sqrt{\sigma_2/T}} \sin(4\pi D\sqrt{\sigma_2/T})}{1 - \dfrac{n+1}{2n+1} Ke^{-4\pi D\sqrt{\sigma_2/T}} \cos(4\pi D\sqrt{\sigma_2/T})},
\end{aligned}\right\} \qquad (7)$$

---

7) S. CHAPMAN and J. BARTELS, *Geomagnetism* Vol. II, p. 738.

8) In the case of a sphere of uniform conductivity, the relation can be written as follows:

$$E = \frac{p}{k} e^{-ka(1-\rho)} H$$

which is the same with that obtained by the writer in the studies of the electromagnetic induction within semi-infinite earth.

where

$$K=(\sqrt{\sigma_2}-\sqrt{\sigma_3})/(\sqrt{\sigma_2}+\sqrt{\sigma_3})$$

Thus we can obtain the amplitude ratio and phase difference for given n, σ_2, σ_3, D and T.

3. In the first place, n is assumed to be unity. Then, A and ψ are calculated for certain combinations of σ_2 and σ_3. Their changes with increase of the period are shown in Figs. 2, 3 and 4 where D is taken to be 1, 10 and 100 km. As seen

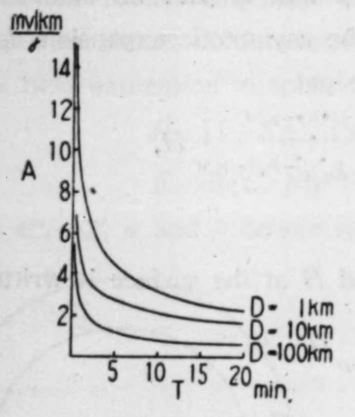

Fig. 2a. Amplitude ratio for $\sigma_2=10^{-13}emu$ and $\sigma_3=10^{-15}emu$.

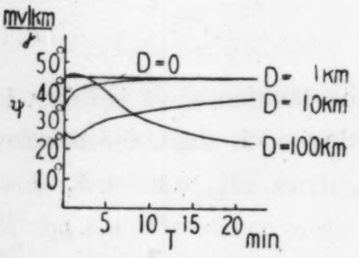

Fig. 2b. Phase difference for $\sigma_2=10^{-13}$ emu and $\sigma_3=10^{-15}emu$.

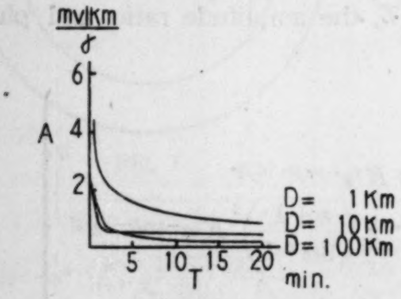

Fig. 3a. Amplitude ratio for $\sigma_2=10^{-12}$ emu and $\sigma_3=10^{-15}$ emu.

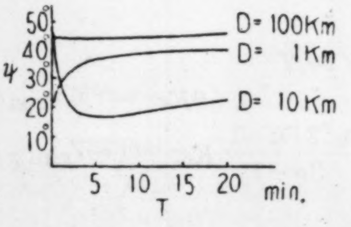

Fig. 3b. Phase difference for $\sigma_2=10^{-12}$ emu and $\sigma_3=10^{-15}$ emu.

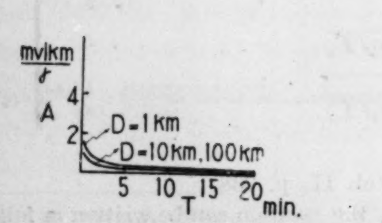

Fig. 4a. Amplitude ratio for $\sigma_2=10^{-11}$ emu and $\sigma_3=10^{-15}$ emu.

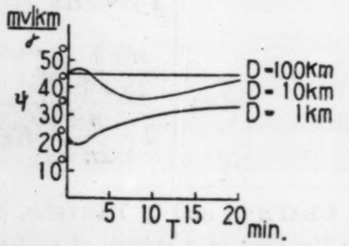

Fig. 4b. Phase difference for $\sigma_2=10^{-11}$ emu and $\sigma_3=10^{-15}$ emu.

in the figures, the phase difference varies remarkably with the period in some cases though the amplitude ratio is always roughly proportional to $1/\sqrt{T}$. Hence, the best combination of σ_2, σ_3 and D by which we can explain the actually observed $A-T$ and $\psi-T$ curves may be determined. From this point of view, Hatakeyama and Hirayamas' results can be interpreted as the electromagnetic induction within the earth covered by a layer having the conductivity amounting to the order of 10^{-12} ***emu*** while the thickness of it seems to amount to a few ***kilometers***. Since we have made few observations, however, detailed studies in regard to the actual earth will be postponed.

It must be studied, in the next place, how far A and ψ change with n. In Fig. 5, assuming $\sigma_2=10^{-12}emu$, $\sigma_3=10^{-15}emu$ and $D=5\ km$, A and ψ are calculated for different n. As seen in the figures, the effect of n is rather small. Physically saying, the influence of the wave-length of the variation is not so large as far as we treat the problems as quasi-stationary phenomena.

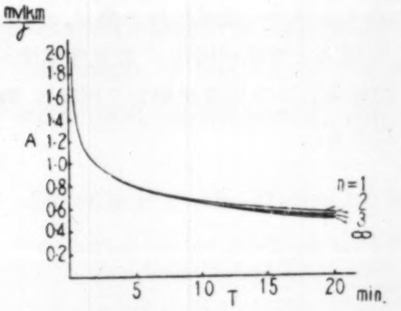

Fig. 5a. Amplitude ratio for various n.

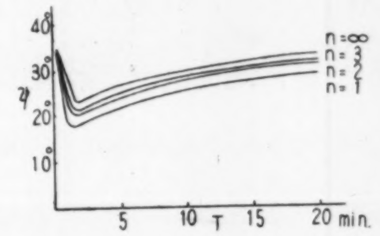

Fig. 5b. Phase difference for various n.

4. Studying the electromagnetic induction within the earth covered by an outside layer of different conductivity, we found out that the phase difference between magnetic and electric forces was seriously affected by the electrical state of the earth's crust. To sum up, it will be possible to determine approximately the electrical state near the earth's surface by analysing the changes in earth current and geomagnetic field.

21. 地電流變化と地下の電氣的性質

地震研究所　力武常次

前論文において，半無限大地中の電磁感應をしらべたが，その際互に直角な地磁氣 H および地電位差 E の成分間には

$$E=\sqrt{\frac{\mu p}{4\pi\sigma}}\ H$$

の如き關係が成立し，周期的變化の場合には振幅比 E/H は周期の自乘根に逆比例し，位相差は常に 45° となることがわかつた．

一方實際に觀測された結果をみると，位相差は周期によつて變化するようにみえる．この事實を說明するために，異なつた電氣傳導度をもつ層に被われた地球内の電磁感應を論じ，半徑を無限大とした極限において，前論文と比較した．その結果，位相差と周期の關係は電氣傳導度のとりかたによつて著しく變化することがわかつた．したがつて地磁氣および地電流變化を同時に觀測することにより，地下の電氣的構造が或程度推測出來ることになる．

22. *The Form of Tsunami-waves outside a Bay as Inferred from the Motion of Bay-water.*

By Tsuneji RIKITAKE,

Earthquake Research Institute.

(Read Sept. 20, 1949.—Received Mar. 31,1951.)

1. The motion of bay-water caused by tsunami-waves had been studied in detail by the members of the Institute[1],[2],[3],[4]. Among these studies, R. Takahasi investigated the motion of sea-water in a rectangular bay of uniform depth. He showed that the motion outside a bay could be inferred from the motion within the bay.

In this paper, a method of obtaining the motion outside a bay from the motion of bay-water will be described, the method being applicable to a bay of variable section.

2. According to the theory of long wave in a rectangular canal of uniform depth, the elevation of surface satisfies the differential eqation of the type

$$\frac{d^2\eta}{dx^2}-\frac{p^2\eta}{gh}=0 \tag{1}$$

where p denotes the operator $\partial/\partial t$. g and h denote respectively the acceleration of gravity and depth.

The solution by which $\partial\eta/\partial x$ becomes 0 at the head of the bay $(x=0)$ and $\eta=u(t)$ at the mouth $(x=a)$ is given by

$$\eta=\frac{\cosh(px/\sqrt{gh})}{\cosh(pa/\sqrt{gh})}\psi(p), \tag{2}$$

where $\psi(p)$ denotes the operational form of $u(t)$, that is the original form of tsunami-waves outside the bay. If the operational form of $\eta(t)$ is supposed to be $N(p)$, we have the operational equation

$$u(t)=\frac{\cosh(pa/\sqrt{gh})}{\cosh(px/\sqrt{gh})}N(p). \tag{3}$$

By solving (3), we can infer the tsunami-waves out of the bay.

Generally speaking, the method just mentioned is equivalent to the method

---

1) G. NISHIMURA and K. KANAI, *Bull. Earthq. Res. Inst. Suppl. Vol.* **1**, Part I (1934), 182.

2) G. NISHIMURA, K. KANAI and T. TAKAYAMA, *Bull. Earthq. Res. Inst.*, **31**(1935), 46

3) R. TAKAHASI, *Bull. Earthq. Res. Inst.*, **25** (1947), 1.

4) T. RIKITAKE and S. MURAUCHI, *Bull. Earthq. Res. Inst.*, **25** (1947), 21.

of the case wherein $u(t)$ is given as a solution of an integral equation, the equation being obtained by the well-known Stokes' method.

In practice, it is convenient to expand the righthand-side of (3) into the form

$$u(t)=\{exp[-p(x-a)/\sqrt{gh}]-exp[-p(3x-a)/\sqrt{gh}]+exp[-p(5x-a)/\sqrt{gh}]-\cdots +exp[-p(x+a)/\sqrt{gh}]-exp[-p(3x+a)/\sqrt{gh}]+exp[-p(5x+a)/\sqrt{gh}]-\cdots\}N(p). \tag{4}$$

Then interpreting term by term, we get

$$u(t)=\sum_{n=0}^{\infty}(-1)^n\Phi\{t-(2n+1)x/\sqrt{gh}+a/\sqrt{gh}\}, \tag{5}$$

where

$$\Phi(t)=\eta(t-2a/\sqrt{gh}). \tag{6}$$

The result agrees with R. Takahasi's. But he got a more general expression that is applicable to imperfect reflections at the head and mouth of the bay.

In the special case where $x=0$, it becomes

$$u(t)=(1/2)\{exp(-pa/\sqrt{gh})+exp(pa/\sqrt{gh})\}N(p) \tag{7}$$

or

$$u(t)=(1/2)\{\eta_0(t-a/\sqrt{gh})+\eta_0(t+a/\sqrt{gh})\}. \tag{8}$$

3. In the next place, we shall study a bay whose breadth and depth vary respectively as

$$b=b_0x/a \text{ and } h=h_0x/a. \tag{9}$$

In many cases, this approximation seems to be the most appropriate one for actual bays.

In that case, the differential equation becomes

$$\frac{d^2\eta}{dx^2}+\frac{2}{x}\frac{d\eta}{dx}-\frac{ap^2}{gh^2}\frac{\eta}{x^2}=0 \tag{10}$$

the solution of which is given by

$$\eta=\sqrt{a/x}\frac{I_1(2p\sqrt{ax/gh_0})}{I_1(2p\sqrt{a^2/gh_0})}\psi(p). \tag{11}$$

provided $\partial\eta/\partial x=0$ at $x=0$ and $\eta=u(t)$ at $x=a$. Hence, we have

$$u(t)=\sqrt{x/a}\frac{I_1(2p\sqrt{a^2/gh_0})}{I_1(2p\sqrt{ax/gh_0})}N(p). \tag{12}$$

We shall assume, for the sake of simplicity, that $\eta(t)$ or $N(p)$ is given at the head of the bay. In that case (12) becomes

$$u(t)=I_1(2p\sqrt{a^2/gh_0})N(p)/(p\sqrt{a^2/gh_0}). \tag{13}$$

As proved in the footnote[5], we get

$$I_1(pA)=\begin{cases}0 & \text{for } t<-A\,, \\ (1/\pi A)\sqrt{A^2-t^2} & \text{for } -A<t<A\,, \\ 0 & \text{for } A<t\,, \end{cases} \tag{14}$$

where

$$A=2\sqrt{a^2/gh_0}.$$

Consequently, adopting Borel's theorem, $u(t+A)$ becomes zero for $t<0$ and

$$u(t+A)=\begin{cases}(2/\pi A^2)\displaystyle\int_A^{t+A}\sqrt{A^2-(t-\tau)^2}\eta_0(\tau)d\tau & \text{for } 0<t<2A, \\ (2/\pi A^2)\displaystyle\int_{t-A}^{t+A}\sqrt{A^2-(t-\tau)^2}\eta_0(\tau)d\tau & \text{for } 2A<t. \end{cases} \tag{15}$$

Thus the motion of sea-water outside the bay can be obtained from that at the head of bay.

4. As examples of the application of the method to an actual bay, the tsunamis of Aug. 5, 1897 and Sept. 8, 1918 in Ayukawa Bay, Miyagi Prefecture are studied as follows.

As shown in Fig. 1, the approximate values of a and h_0 is respectively given by $a=1.3\,km$ and $h_0=16\,m$. The tide-gauge was installed at the head of the bay.

The mareograms[6] are reproduced in Figs. 2 and 3. The disturbances by the tsunami-waves are also shown in the figures, where the tide is eliminated by mean

---

[5] Let us consider a function

$$f(t)=\begin{cases}\sqrt{A^2-(t-A)^2} & \text{for } t<2A, \\ 0 & \text{for } 2A<t. \end{cases}$$

Then, Carson's integral of $f(t)$ becomes

$$\begin{aligned} p\int_0^\infty e^{-pt}f(t)dt &= p\int_0^{2A} e^{-pt}\sqrt{A^2-(t-A)^2}dt \\ &= pe^{-pA}\int_{-A}^{A} e^{-pt}\sqrt{A^2-t^2}dt \\ &= 2A^2pe^{-pA}\int_0^{\pi/2}\cosh(pA\cos\theta)\sin^2\theta d\theta \\ &= 2A^2pe^{-pA}\times\frac{\pi I_1(pA)}{2pA} \\ &= \pi Ae^{-pA}I_1(pA), \end{aligned}$$

whence we have

$$I_1(pA)=\begin{cases}0 & \text{for } t<-A, \\ (1/\pi A)\sqrt{A^2-t^2} & \text{for } -A<t<A, \\ 0 & \text{for } A<t. \end{cases}$$

[6] A. IMAMURA and M. MORIYA, *Jap. Journ. Astr. Geophys.*, **17** (1939), 119.

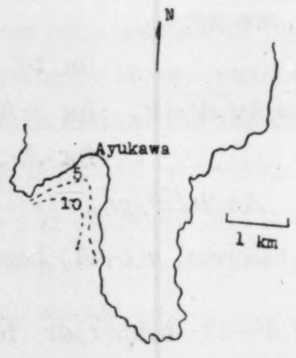

Fig. 1. Topography of Ayukawa Bay.

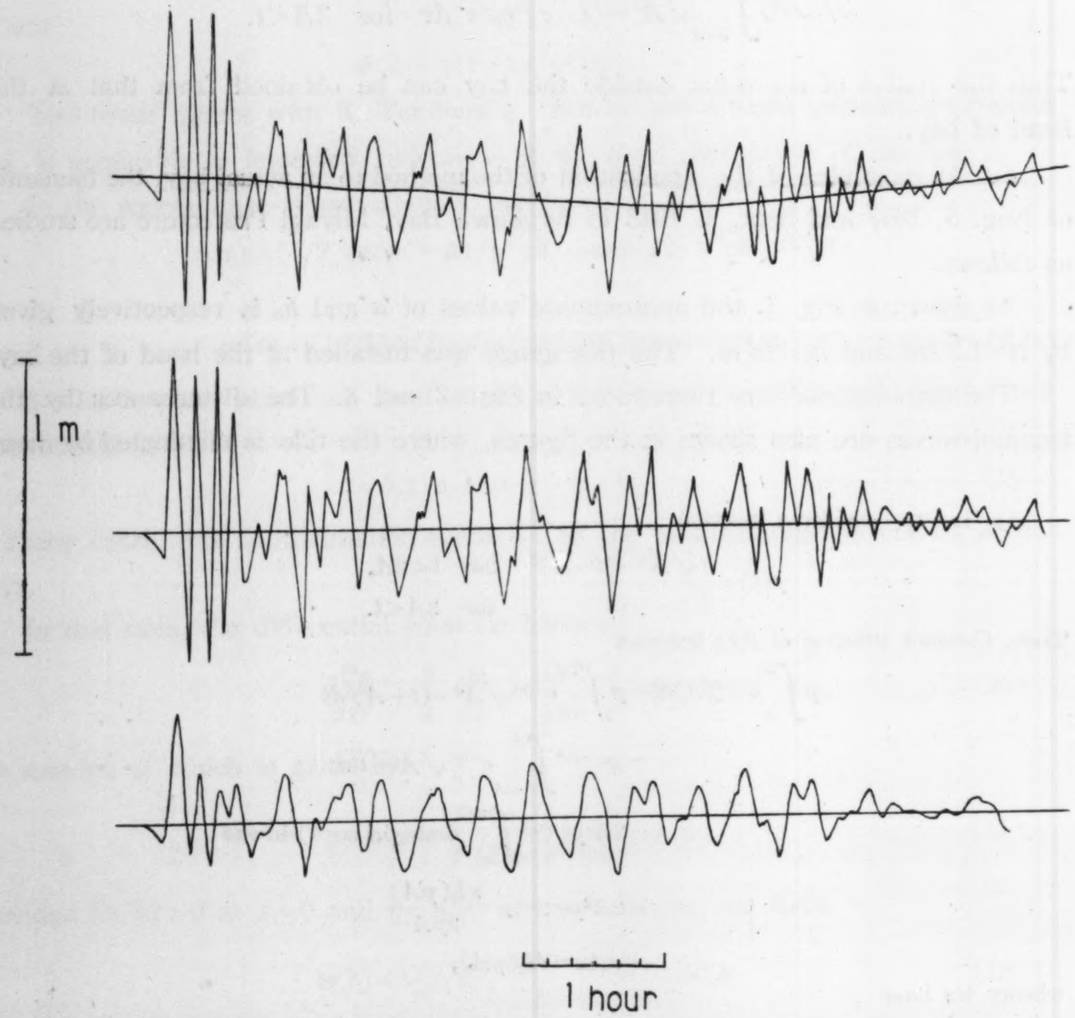

Fig. 2. The tsunami of Aug. 5, 1897 in Ayukawa Bay. Upper: Original record of tide gauge. Middle: Disturbance of bay-water from which the tide is eliminated. Lower: The elevation of sea-water at the mouth of the bay which is calculated by the present method.

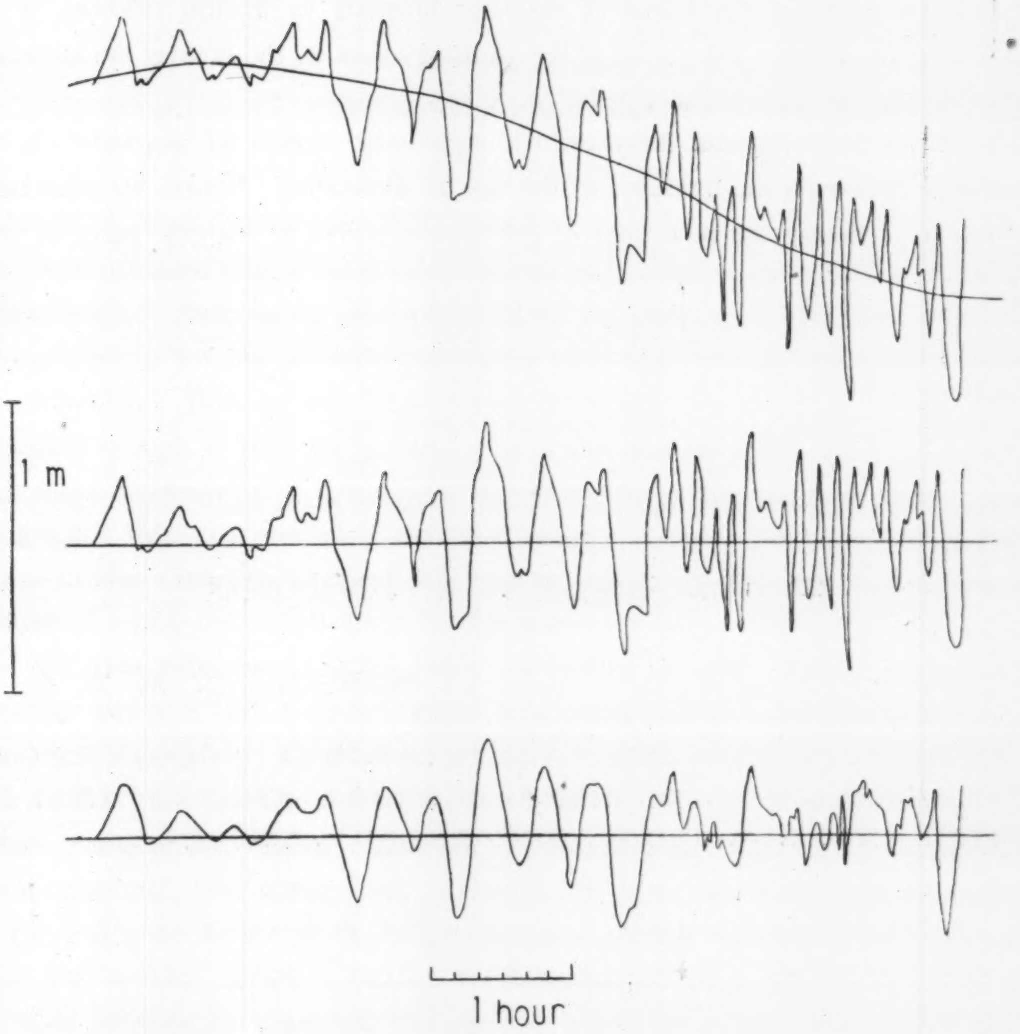

Fig. 3. The tsunami of Sept. 8, 1918 in Ayukawa Bay. Upper: Original record of tide gauge. Middle: Disturbance of bay-water from which the tide is eliminated. Lower: The elevation of sea-water at the mouth of the bay] which is calculated by the present method.

of running-average. Then, applying (15), the elevations at the mouth of the bay are calculated by means of numerical integration, the results being shown in the figures.

The decrease of the amplitudes at the mouth is clearly shown in the figures, especially in the case of the tsunami of Aug. 5, 1897 which was caused by an earthquake about 100 *km* away. On the contrary, the influence of the bay is not so remarkable in the case of the tsunami of Sept. 8, 1913 which came from Uruppu Island situated at a distance of more than 1000 *km*. Taking into consideration the fact that the period of the seiche of the bay amounts to several minutes, it is natural that the shorter the period of the tsunami-waves is, the greater the influence of the bay on the wave-forms will be.

As shown in the figures, however, the oscillatory motion of sea-water is so remarkable that even the influence of the bay is eliminated. Hence, we must take into account seriously the reflections of the tsunani-waves at various parts of the sea.

---

22. 灣水の運動と灣外に於ける津浪の波形

地震研究所　　力　武　常　次

演算子法を用いて，灣内の水の運動より灣外に於ける津浪の波形をしらべる方法を考案した．一様な深さをもつ矩形の灣については，高橋教授の得られた結果に一致する．ここでは深さおよび幅が直線的に變化する灣についても考察し，鮎川灣の檢潮記錄について解析を行つた．

23. *Block Movement along the Seismic Fault (2).*

By Nobuji NASU,
Earthquake Research Institute.

(Read March 20, 1951.—Received March 20, 1951.)

Change in Land-level in the Nōbi Plain.

It is probable that a remarkable change in the land-level occurred in the Nōbi (Mino-Owari) Plain as an accompaniment of the great earthquake of 1891. The changes along the regular routes of survey have been already discussed by several investigators.[1] But, as only three routes traversed this plain, the data are not sufficient enough to give the general idea of the changes which the whole area of this plain underwent. It is desirable to extend the survey so as to cover a wide area apart from the previously surveyed routes. For this purposes, a survey was made by the writer in October, 1950 in the middle part of the same plain, the results of which form the subject of this paper.

We have experienced in the Fukui earthquake of 1948[2] that by means of the leveling survey a fault may be located even when hidden from view by a thick unconsolidated sediment, provided the survey covers the whole area wherein the seismic fault is considered to exist. In such a survey, the elevations not only of the bench marks on the regular routes but of the triangulation points distributed in the area concerned were determined. Although the latter geodetic points are inferior to the first order bench mark in the accuracy of the determined value of elevation, the leveling survey extended to the triangulation points so far furnishes a valuable information regarding the general aspect of a large change which occurred in the great earthquake.

The triangulation survey in the Nōbi Plain was carried out in 1888, that is, three years before the great earthquake. Hence, on comparing the elevations of the triangulation points established by this survey with the elevations determined by the present survey, we can get an estimates of the changes which occurred mostly in the 1891 earthquake. We must ackowledge, however, that the change thus determined is only relative, because the recent survey does not extend beyond the plain.

---

[1] F. OMORI, *Report Earthq. Inv. Comm.*, No. 32.
A. IMAMURA, *Japanese Journ. Astro. Geophys.*, 6 (2), 1928.
C. TSUBOI, same Journal 10 (2), 1932–1933.

[2] *Report Special Comm. Fukui Earthquake*, 1950.

In the survey of 1950,[3] bench mark No. 179 of GSB which lay on the regular route was taken as a starting point (Fig. 1). Refering to this point, the elevations of twelve triangulation points[4] were determined along the routes as shown by thick broken line in this figure. In this case, the elevation of B.M. No. 179 was assumed to be 5.3624m., which was determined in 1944. The elevations of the points thus determined and the former values of 1888 are given in the next table.

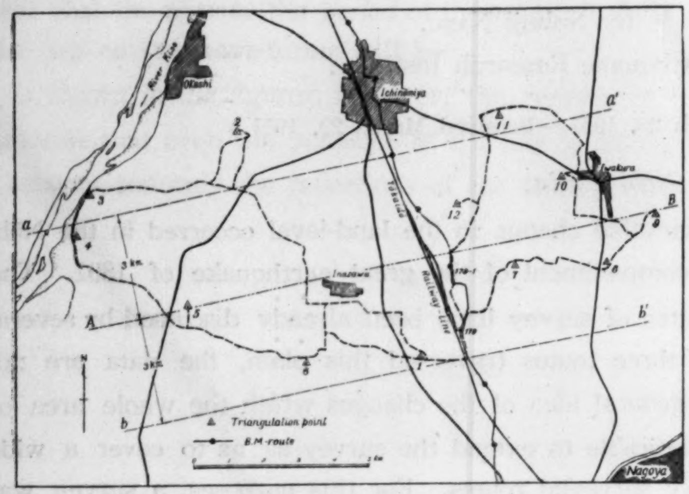
River Kiso
Okoshi
Ichinomiya
Iwakura
Inazawa
Nagoya
Tokaido
Railway Line
a
a'
A
B
b
b'
1
2
3
4
5
6
7
8
9
10
11
12
179
179-1
3 km
3 km
N
Triangulation point
B.M-route
0
1
2
3
4
5 km

Fig. 1.

Table I. Elevation of triangulation point.

No.	Place	Longitude	Latitude	Elevation (1888)	Elevation (1950)
1	Okuda	136° 49′ 9.1″	35° 14′ 1.3″	4.26 m.	4.181 m.
2	Kitaima	17 25.7	17 25.5	7.03	6.963
3	Nishinakano	42 46.6	16 30.0	11.81	11.570
4	Sanjuccho	42 32.7	15 50.9	16.46	16.244
5	Katahara-isshiki	44 43.2	14 46.5	2.70	2.641
6	Umesuga	46 56.3	13 54.9	4.76	4.839
7	Kajigaisshiki	50 55.5	15 22.9	8.44	8.385
8	Yakushiji	52 44.3	15 23.8	9.05	8.838
9	Ogi	53 36.1	16 9.4	12.89	13.038
10	Iwakura	51 53.6	16 43.3	9.63	9.634
11	Minamikobuchi	50 39.6	17 38.7	9.45	9.524
12	Mitsui	49 48.0	16 18.0	7.55	7.403

After deducing the relative changes, they are illustrated in the following manner.

Let us draw a line in a map passing through the approximate centre of the surveyed area in such a direction that it becomes nearly normal to the postulated fault having a trend of NNW-SSE. (The fault will be described later.) The line thus drawn is AB in Fig. 1. Then the triangulation points lying near this line are projected on AB to determine the abscissae of these points. In this case, however, it will be preferable to take the points lying on both sides of AB and within a distance of 3 km. from the same line, if the size of the network of triangulation is taken into account; a side of the triangle forming the network is about 4 km. The changes at the points thus taken may be represented as the change which occurred along line-AB, while the changes at the points at longer distances may differ, though slightly in the present case, from those along the same line.

---

[3] A 15-inch Wye-level and wooden staffs of 5 mm. division were used. The allowable error of closure was 4 $\sqrt{L}$ mm., L is the length of the surveyed route. The actual error along the western large roop of survey was 6mm. and along the eastern large roop it was 15mm.

[4] In the map of scale 1/50,000, there are fourteen triangulation points in the surveyed area, but two were lost.

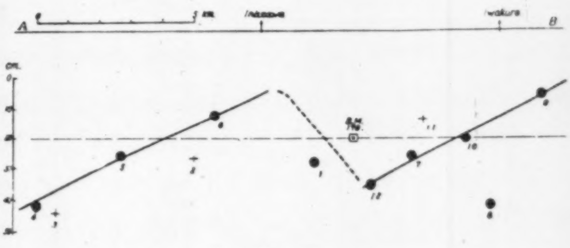

Fig. 2.

Now, in Fig. 2, line-AB is taken as the horizontal axis. Below this, a line is drawn parallel with AB at any distance from it as shown by a broken line. Taking this line as the datum level, the relative vertical changes are plotted on the vertical lines, each of which passes through the points corresponding to the abscissae on AB previously determined. In this figure, beside B.M. No. 179, the points which lie within 3 km. from AB are shown by dots, and those lying at farther distances by crosses. Although point No. 8 shows a departure from the general tendency, we can see a general upheaval of the eastern part of the surveyed area relatively to the western part. Point No. 8 just mentioned was situated on the river bank along which a considerable damage may have been caused in the 1891 earthquake.[5] Probably, the change was due to some local causes.

Further, an uplift of the ground can be seen also in the middle part of the surveyed area, thus exhibiting a N-shaped change which has been commonly revealed in the case of the seismic fault.

The upheaval in the eastern part just mentioned will surely continue towards the east, though gradually increasing in the amount, up to the point where F. Omori[6] drew the line of the maximum upheaval (Fig. 3), while the subsidence will continue to the line of the maximum depression also drawn by him. Regarding this line of depression, A. Imamura[7] stated that this line formed the western

---

5) *Report Earthq. Inv. Comm.*, 2 (1894).

6) F. OMORI, *Lecture of Seismology*, p. 341, 1907.

7) A. IMAMURA, *Theoretical and Applied Seismology*, p. 52, 1937.

boundary of the land block which subsided at the time of the 1891 earthquake.

Although there was no direct evidence of the seismic fault which appeared in Nōbi Plain, we must remember that there existed a line passing through the centre of this plain in the direction NNW-SSE and along which a fault is considered to have occurred in the underground. The line was pointed out by Omori[8] with the name "line-C" (see Fig. 3) being distinguished from "line-A" and "line-B"; line-A was assigned to the Neo-Valley fault and line-B to the Kurotsu-Nukumi fault. The direction of line-C when produced northward agrees with the main fault of Neo-Valley, while the southern part of the same line just passes through the middle part of the surveyed area. It is noteworthy that the position of line-C quite agrees with the point where a stepwise change has been actually revealed by the present survey. This gives a strong evidence in support of Omori's idea.

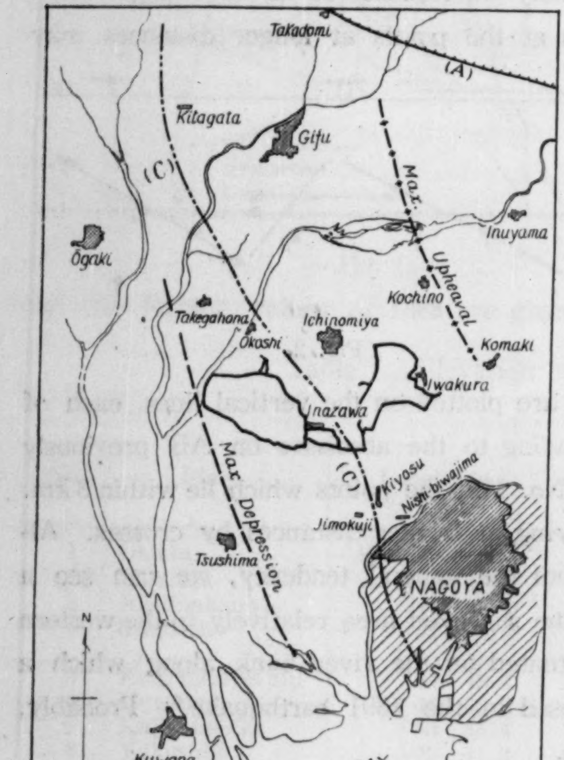
Takadomi
(A)
Kitagata
Gifu
(C)
Max. Upheaval
Inuyama
Ōgaki
Kochino
Takegahana
Ichinomiya
Okoshi
Komaki
Iwakura
Inazawa
(C)
Kiyosu
Nishi-biwajima
Jimokuji
Max. Depression
Tsushima
NAGOYA
N
Kuwana
ISE BAY
0 5 10 km.

Fig. 3

It has been known that in the alluvial plains such as Nōbi and Fukui Plains, there occurred a remarkable subsidence at the time of great earthquakes. At first thought, such a depression may be attributed to the compaction of the alluvial layers caused by violent shocks. Actually there were many places where the ground was disrupted or subsided by the shocks, but a close examination revealed that such disturbances were limited to comparatively small areas and the changes were due merely to local causes. Further, the compaction cannot account for the upheaval of the ground where no much difference in the geological formation can be found between the place of subsidence. Of course, there should be a certain amount of depression due to compaction of the soil layer, but it will be negligible when compared with the large changes as revealed by the survey. Further, so far as the relative movement of the land-blocks is concerned, we may put aside the question as to the effect of compaction, because the compaction occurs equally likely on both sides of the fault, at least near it.

---

[8] F. OMORI, *Report Earthq. Inv. Comm.*, 88 (II), 1919.

C. Tsuboi[9] stated that if the changes in the heights of bench marks as were revealed by the leveling survey were due to the accidental settling of the superficial soft soil, the change must have been more irregular than could be represented by the curves. According to his estimation, if the thickness of the soft layer be of the order of 100 m. and the amount of the observed depression be 10 cm., then, the rate of deformation must be of the order of 10^{-3}, which is far larger than the rate of 10^{-5} determined for the general earth's crust.

From the view-point of the physical property of soil, it seems that the vibration may not be the principal cause of the subsidence of the ground which took place generally in a wide area, at least one-half of the plain, if we think of the cohesion existing in the soil layer, even in the case of small cohesion of a few grams per square centimetre. Therefore, the large amount of the changes as determined by the present survey must be attributed to causes seated in more deeper place than in the superficial soil.

It should be kept in mind that as about 60 years have passed since the great earthquake, certain amount of secular change may be naturally involved in the change determined here, but this must be small as compared with the large change at the time of the 1891 earthquake.

The foregoing study was made with the financial assistance from the Grant in Aid for Fundamental Scientific Research of the Ministry of Education for the year 1950.

23. 地震斷層に沿う地塊運動 (2)

地震研究所　那須信治

明治 24 年の濃尾大地震に伴つて濃尾平野にはかなり大きい地形變動があつたと思われる. 正規の水準測量線以外に三角點の標高の再測によつてこの變動の大要を知ることができた. 即ち平野の東部と西部に於て數十 cm に達する變動があり, 同平野の中央部に於ては N 型の地形變動が認められることから根尾谷斷層の延長がこの平野を横切つているのではなかろうかという結論を得た.

---

9) C. TSUBOI, *loc. cit.*

24. *Notes on the Energy and Frequency of Earthquakes.*[*]

By Toshi Asada, Ziro Suzuki and Yoshibumi Tomoda,

Geophysical Institute, Tokyo University.

(Read July 18, 1950.—Received March 20, 1951.)

1) B. Gutenberg and C. F. Richter[1] made statistical studies of the energy and frequency of earthquakes. They arranged a great many shocks according to the "Instrumental Magnitude Scale" (hereafter expressed as M_I) introduced by the junior author[2]. They obtained the following relation

$$\log N = a + b(8 - M_I) \qquad (1)$$

where N is the annual number of earthquakes, of which the magnitude is between $M_I + 0.05M_I$ and $M_I - 0.05M_I$, and a and b the numerical constants. The values of the constants determined by them are

$$a = -0.48 \pm 0.02, \ b = 0.90 \pm 0.02$$

for the shallow schocks, where M_I is greater than 6, and

$$a = -2.04 \pm 0.09, \ b = 0.88 \pm 0.03$$

for the shocks occurring in South California, where M_I is between 4 and 6. Hereafter we shall discuss the value of "b" only.

Combining (1) with the relation according to Gutenberg and Richter[1]

$$\log E = 12 + 1.8M_I \qquad (2)$$

where E is the energy released in an earthquake having the magnitude of M_I, we get

$$\log NE = k + 0.9M_I \qquad (3)$$

for the shocks with the magnitude greater than 6, where "k" is a constant. For the shocks in South California we have the same relation as (3) excepting the value of "k". Since NE is the total energy annually released in shallow shocks within the range from $M_I\ (1+0.05)$ to $M_I\ (1-0.05)$, one can say from the relation (3) that the annual energy increases with M_I, if the earthquakes are classified at equal intervals of the M_I scale. Thus, Gutenberg and Richter wrote; "the results support in detail the previous conclusion that the smaller shocks almost never are sufficiently frequent to approximate the energy released in larger shocks. This means that great shocks are essentially independent events, uninfluenced by the occurrence of smaller earthquakes, which are at most symptons of the regional strains released in the major shocks." But according to the opinion of the present writers, the expression quoted above is liable to be misunderstood.

---

[*] communicated by T. Matsuzawa..

1) B. Gutenberg *and* C. F. Richter. *Seismicity of the Earth* (1949).

2) C. F. Richter. *Bull. Seis. Soc. Am.*, **25** (1935), 1.

The relation between the earthquake-magnitude and the frequency of earthquakes with such magnitude depends entirely on the nature of the magnitude-scale by which the shocks are classified. In order to avoid misunderstanding the following sentence is to be added to the above-quoted description, "if the earthquakes are classified according to Richter's magnitude scale". If the classification is done by other scales, the relation will be apparently quite different,

For instance, the energy E itself which is released in a shock may be taken as a magnitude-scale.

As the relation between M_I and E is known, we can transform the relation (3) into the expression with the new variable E in the same way as the usual distribution functions in statistics are transformed. The process is as follows. The formula (1) is rewritten as

$$N(M_I)\ dM_I = const \times 10^{-0 \cdot 9 M_I} dM_I \tag{4 a}$$

where $N(M_I)$ is the annual number of earthquakes of which the magnitude ranges between M_I and $M_I + dM_I$. When $N(M_I)$ and E are expressed as

$$N(M_I) dM_I = const \times 10^{-b M_I} dM_I \tag{4 b}$$

$$E = const \times 10^{c M_I} \tag{2 b}$$

put (2) b into (4) and get

$$N(M_I) dM_I = const \times E^{-\frac{b}{c}} dM_I$$

or
$$N(E) dE = const \times E^{-\frac{b}{c}} \frac{dM_I}{dE} dE$$

thus we have

$$N(E) dE = const \times E^{-\frac{b}{c}-1} dE$$

From the numerical values of b and c in (4) a and (2), we obtain the new formula

$$N(E) dE = const \times E^{-1 \cdot 5} dE \tag{5}$$

and

$$N(E) E\ dE = const \times E^{-0 \cdot 5} dE \tag{6}$$

This result shows that the total energy annually released in shocks having the energy between E and $E+dE$ becomes smaller with the increase in E. The apparent difference between the above-mentioned result and the one obtained by Gutenberg and Richter is due solely to the difference in the two magnitude scales by which the earthquakes are classified. It must be remarked that the formula (1) is wholly dependent on the nature of Richter's scale.

2) On the other hand, H. Kawasumi defined another magnitude-scale (hereafter called M_K). The intensity "I" of an earthquake in Japanese C.M.O. scale at the epicentral distance of 100 km is taken by him to be the M_K of that shock. According to Kawasumi's statistical investigations[3], the frequency of earthquake occurrences is expressed by

$$N(M_K)dM_K=const\times10^{-0.5\,M_K}\,dM_K \tag{7 a}$$

where $N(M_K)$ is the frequency of earthquakes occurring during a certain period, of which M_K ranges between M_K and M_K+dM_K. Kawasumi's result shows further that the relation between E and M_K is

$$E=const\times10^{\,M_K} \tag{8}$$

Combining (8) and (2), we get the relation between M_K and M_I

$$M_K=const+1.8M_I$$

Using this relation we can transform (7) into the expression with the parameter M_I. As

$$10^{\,M_K}=const\times10^{1.8M_I}$$

we obtain

$$N(M_K)dM_K=const\times10^{-0.9M_I}\,dM_K$$

or

$$N(M_I)dM_I=const\times10^{-0.9M_I}\,\frac{dM_K}{dM_I}dM_I$$

$$N(M_I)dM_I=const\times10^{-0.9M_I}dM_I \tag{7 b}$$

This relation is quite the same as that obtained by Gutenberg and Richter.

It is noteworthy that Kawasumi's result agrees with the result obtained by Gutenberg and Richter, although they dealt with different data, i. e. shocks occurring in different places and in different periods.

From the relation (7) and (8), we have

$$N\ M_K)EdM_K=const\times10^{0.5\,M_K}\,dM_K \tag{10}$$

In this relation, NE becomes larger as was the case by Richter's scale. This result is to be expected from the definitions of both magnitude-scales.

3) An experimental formula

$$N(a)da=ka^{-m}da \tag{11}$$

for the trace amplitude and frequency of earthquakes occuring in Kanto District was obtained by M. Ishimoto and K. Iida[4]. In this formula "a" is the trace amplitude, and $N(a)$ is the number of the earthquakes with trace amplitude between a and $a+da$, and "m" and "k" are numerical constants.

---

[3] H. KAWASUMI, Read at the meeting of Earthquake Research Institute (1943), No. 197.

The present authors found that the relation (11) holds also in some cases of aftershocks of great earthquakes.[5][6] Moreover, it was found that the same relation holds in "micro-earthquakes",[7][8] which could be recorded only by high sensitive seismometers with the magnification of scores of thousand or more. In many cases the value of the exponent "m" was 1.8 or 1.9.

On the other hand, it was mathematically deduced[6] that if Ishimoto-Iida's formula holds between the trace amplitude and the frequency of shocks, a similar formula

$$N(A_0)dA_0 = const \times A_0^{-m} dA_0$$

holds in the area where the shocks occur (A_0 is the amplitude of a shock at its focus). Then,

$$N(A)dA = const \times A^{-m} dA$$

must hold between the amplitude A at the place having an epicentral distance of 100 km and the frequency of the shocks with the amplitude between A and $A+dA$, when the formula (11) holds.

As "M_I" is defined as

$$M_I = const + \log A \tag{12}$$

we can compare Ishimoto-Iida's formula with the result (1) obtained by Gutenberg and Richter.

Transforming A in (11) into M_I, we have

$$\begin{aligned} N(A)dA &= const \times A^{-m} dA \\ &= const \times 10^{-mM_I} dA \end{aligned}$$

and,

$$N(M_I)dM_I = const \times 10^{-mM_I} \frac{dA}{dM_I} dM_I$$

or,

$$N(M_I)dM_I = const \times 10^{-(m-1)M_I} dM_I \tag{13}$$

Since the value of m is 1.8 or 1.9, this formula may be written as follows;

$$N(M_I)dM_I = const \times 10^{-0.8M_I} dM_I \qquad (14)\ a$$

$$N(M_I)dM_I = const \times 10^{-0.9M_I} dM_I \qquad (14\ \ b$$

---

4) M. ISHIMOTO and K. IIDA, *Bull. Earthq. Res. Inst.*, **17** (1939) 443.

5) Z. SUZUKI and T. ASADA, Geophysical Notes Vol. 1. No. 32 (1947).

6) Z. SUZUKI, Read at the meeting of Seismological Society of Japan, Oct. 1948.

7) T. ASADA and Z. SUZUKI, Geophysical Notes, Vol. 2, No. 16 (1949).

8) T. ASADA and Z. SUZUKI, *Bull. Earthq. Res. Inst.*, **28** (1951) 415.

This is quite the same as the formula (1). It is remarkable that the relation (14) coincides well with the relation (1) although the earthquakes treated in both cases are quite different in their magnitude, place and time of occurrence.

4 The summarized conclusion of this investigation will be as follows:

a) The relation between the energy and frequency of earthquakes obtained by B. Gutenberg and C. F. Richter

$$\log NE = k + 0.9\,M_I$$

is wholly dependent on the nature of the "Instrumental Magnitude Scale". If the earthquakes are classified by another scale, the relation will be apparently quite different from the above formula.

b) The result of Gutenberg and Richter coincides well with that of Kawasumi, although the latter treated only earthquakes which occurred near Japan. The relation coincides also with Ishimoto-Iida's formula for the smaller earthquakes such as aftershocks or micro-earthquakes.

In the end the authors wish to express their best thanks to Prof. T. Matuzawa and H. Kawasumi for their helpful suggestions and discussions. The authors' thanks are also due to Prof. C. Tsuboi for his kind encouragements.

---

24. 地震の頻度とエネルギーについて

東京大學地球物理學教室
浅田　敏
鈴木次郎
友田好文

B. Gutenberg 及 C. F. Richter は地震の頻度とエネルギーとの關係について

$$\log NE = \text{const} + 0.9\,M_I$$

とゆう式を求めて居り，これから「小地震の出すエネルギーは大地震のものに比して數の多さを考慮しても尙遙かに小さく從つて大地震は小地震に影響されない」と述べている．然し上の式は地震を粗分けする尺度によつて當然變るもので，例えばエネルギー E の等間隔にとれば

$$\log NE = \text{const} - 0.5 \log E$$

となり見かけ上逆の樣な印象を與える．從つて Gutenberg 及 Richter の式については Instrumental Magnitude Scale によつたものである事を注意せねばならない．

河角博士の統計結果は Magnitude Scale を變換すれば Gutenberg, Richter の結果と同じものである事が分る，又餘震や微小地震について成立する石本飯田の式もやはり同じ結果を與える．この樣に地震の頻度とエネルギーの關係は場所や時の如何を問わず又世界的な大地震から微小地震に至る迄の廣い範圍に亙つて同じものである事は面白い．

25. *Seismometrical Study of the Imaichi Earthquake on Dec. 26, 1949.*

(The second paper)

By Yoshiaki KOSHIKAWA,
Earthquake Research Institute.

(Read Jan. 16, 1951.—Received March 20, 1951.)

1. Introduction.

In the previous paper,[1] the writer made a report on the results of the location of epicentres of the Imaichi Earthquake. The epicentre of the first shock was determined independently by the arrival times of P^* and $\overline{S}$ at the stations near by, and the results were quite in concord with each other. But the epicentre of the second shock was determined by the arrival times of $\overline{P}$ only.

In this paper, the epicentre located by the arrival times of P^* of the second shock will be described as the complement of the previous paper.

2. Location of epicentre of the second shock.

At first, the place of 39° 41′ N lat. and 139° 40′ E long. was tentatively assumed as the epicentre. The data perceived as the arrival times of P^* were tested by the rejection limit of errors. They are shown in Table (I).

The rejection limit δ is as follows[2];

$$\delta=\pm u\sqrt{\frac{\Sigma+1}{\mathrm{N}}F}=\pm 2.56\ (\mathrm{sec.})\quad \text{for}\quad P_r\{F\geqq F_0\}=0.05\,,$$

where
$$u^2=\frac{\Sigma\varepsilon_1{}^2}{N-1}=1.206\,,$$

$$F=4.96 \text{ for the degree of freedom } n_1=1,\ n_2=10,$$

$$\mathrm{N}=11\,.$$

$\delta\varphi$, $\delta\lambda$, δV and δT (the deviations of latitude φ, longitude λ, propagation velocity V and the intercept time T_0) were determined by the method of least squares. The results are as follows;

$$\delta\varphi=+2'.66\pm 0'.63\,,$$

---

1) KOSHIKAWA, *Bull. Earthq. Res. Inst.*, **28** (1950).

2) W. R. THOMPSON, *Ann. Math. Stat.*, **6** (1935), 14. Afterwards extended by M. MASUYAMA.

Table I.

Station	Arrival time of P^* T	Epicentral distance Δ_1	Intercept time T_0	Residue $\varepsilon_1 = T_0 - (T_0)_m$	Epicentral distance Δ_2	Residue ε_2
1. Kofu	$8^h 25^m 20.4^s$	152.0 km	$8^h 24^m 55.07^s$	0.92^s	155.6 km	0.48^s
2. Funatsu	20.7	154.7	54.92	0.77	158.8	0.25
3. Matsumoto	21.1	159.8	54.47	0.32	161.2	0.25
4. Sendai	27.4	206.8	52.93	−1.22	202.7	−0.41
5. Shizuoka	30.0	221.5	53.08	−1.07	225.6	−1.65
6. Toyama	31.7	221.1	54.85	0.70	220.4	0.92
7. Kanazawa	38.0	269.7	53.05	−1.10	269.3	−0.97
8. Omaezaki	40.6	266.3	56.22	2.07	270.5	1.43
9. Mizusawa	43.0	301.1	52.82	−1.33	296.7	−0.57
10. Kameyama	52.8	353.6	53.87	−0.28	356.2	−0.75
11. Morioka	54.4	360.1	54.38	0.23	355.6	0.96

Mean of T_0: $(T_0)_m = 8^h\,24^m\,54.15^s$, $\sum\varepsilon_1^2 = 12.06$, $\sum\varepsilon_2^2 = 8.887$.

(Suffixes 1 and 2 denote the quantities concerning the tentative and the decided epicentre respectively.)

$$\delta\lambda = -0'.15 \pm 0'.99\,,$$

$$\delta T = +0.32 \pm 1.22 \text{ (sec.)}\,,$$

$$\delta V = -0.035 \pm 0.044 \text{ (km/s)}.$$

Then

$$\varphi = 36^\circ\ 43'.7 \pm 0'.6 \text{ N}\,,$$

$$\lambda = 139^\circ\ 39'.9 \pm 1'.0 \text{ E}\,,$$

$$T_0 = 8^h\,24^m\,53.8^s \pm 1.2^s \text{ (J. S. T.)}\,,$$

$$V = 5.97 \pm 0.04 \text{ (km/s)}.$$

The coordinates of epicentre calculated from $\overline{P}$ were [3]

$$\varphi = 36^\circ\ 43'.6 \pm 0'.4 \text{ N}\,,$$

$$\lambda = 139^\circ\ 38'.8 \pm 0'.6 \text{ E}.$$

Both pairs of the coordinates coincide surprisingly well. The most probable coordinates of the second shock's epicentre may be $\varphi = 36^\circ\,43'.7$ N, $\lambda = 139^\circ\,39'.4$ E.

The propagation velocity of P^* was previously obtained as

$$V = 6.00 \pm 0.24 \text{ (km/s)}$$

from the first shock. This value shows also a very good concordance with the velocity here obtained, and is nearly equal to the value obtained by Prof. T.

---

[3] Y. KOSHIKAWA, *loc. cit.* 1).

Matuzawa[4]. Thus the propagation velocity may probably be 6.0 km/s in the Kwanto District.

3. Estimation of the focal depth.

To estimate the focal depth, it is necessary to know the data of the near by stations whose epicentral distances are less than 50 km. Whereas, in this case, there is only one datum of the arrival time of P of the first shock at Utsunomiya; $8^{h}\,17^{m}\,35.2^{s}$. If it is reliable, we shall be able to calculate h by the equations[5]

$$\overline{T}=\frac{\sqrt{\varDelta_1^2+h^2}}{V}+\frac{\sqrt{\varDelta_1^2+h^2}}{\sqrt{\varDelta_1^2+h^2-r^2\varDelta_1^2}}\cdot\frac{d}{U}$$

$$=\frac{1}{V}\left\{\varDelta\sqrt{1+\xi^2}+\frac{1-r^2}{r}\cdot\frac{\sqrt{1+\xi^2}}{\sqrt{1+\xi^2-r^2}}\cdot d\right\}, \tag{1}$$

and the intercept time $$\overline{T}_0=\frac{1}{V}\cdot\frac{2-r^2}{2r}d, \tag{2}$$

where $r=U/V$, $\xi=h/\varDelta_1$ and $\Delta_1=\Delta-\Delta_2=\Delta-\dfrac{rd}{\sqrt{1+\xi^2-r^2}}$.

$$\therefore\quad \overline{T}-\overline{T}_0=\frac{1}{V}\left[\Delta\sqrt{1+\xi^2}-\left\{(2-r^2)-\frac{2(1-r^2)\sqrt{1+\xi^2}}{\sqrt{1+\xi^2-r^2}}\right\}\frac{d}{2r}\right]. \tag{3}$$

Then, $$\Delta\sqrt{1+\xi^2}-V\left(\overline{T}-\overline{T}_0\right)=\left\{(2-r^2)-\frac{2(1-r^2)\sqrt{1+\xi^2}}{\sqrt{1+\xi^2-r^2}}\right\}\frac{d}{2r}. \tag{4}$$

Put $$x=(2-r^2)-\frac{2(1-r^2)\sqrt{1+\xi^2}}{\sqrt{1+\xi^2-r^2}}, \tag{5}$$

$$\frac{dx}{dr}=\frac{2r}{(1+\xi^2-r^2)^{\frac{3}{2}}}\left\{(1-r^2)\left(\sqrt{1+\xi^2}-\sqrt{1+\xi^2-r^2}\right)+\xi^2\left(2\sqrt{1+\xi^2}-\sqrt{1+\xi^2-r^2}\right)\right\}.$$

In the domain of $1\geqq r>0$, $\dfrac{dx}{dr}>0$.

When $r=0$ and $r=1$, $x=0$ and $x=1$ respectively.

$$\therefore\quad x>0 \quad \text{in the domain of} \quad 1\geqq r>0.$$

So that, in the present case, where $\Delta=24.1$ km, $V=5.05$ km/s and $\overline{T}-\overline{T}_0=5.89$ (sec.), ξ must be greater than 0.723 from the condition

$$\Delta\sqrt{1+\xi^2}-V(\overline{T}-\overline{T}_0)>0.$$

Giving $\xi=0.73$, 0.75 and 0.80, d and h were calculated for the values of r (0.37, 0.38 and 0.40). The results are shown in Table (II). When $\xi=0.73$ and

---

4) T. MATUZAWA, *Bull. Earthq. Res. Inst.*, **6** (1929), 117.

5) Y. KOSHIKAWA, *loc. cit.* 1).

Table II.

	r	d	h
$\xi=0.73$	0.37	1.48$^{\text{km}}$	17.1$^{\text{km}}$
	0.38	1.48	17.2
	0.40	1.35	17.3
$\xi=0.75$	0.37	5.35	16.8
	0.38	5.05	16.9
	0.40	4.72	16.9
$\xi=0.80$	0.37	14.0	15.9
	0.38	13.5	15.9
	0.40	12.6	16.0

0.75, $d=1.4$ km and 5.0 km respectively. It is difficult to consider that the value of d (thickness of the superficial low-velocity layer) is greater than 5 km. Therefore, the values of ξ larger than 0.75 are unreasonable. So far as the arrival time of $\overline{P}$ at Utsunomiya is concerned, the value of h may be about 17 km.

As reported in the previous paper, $h-h'=4.4$ km, then h' may probably be 12.6 km. Thus, the focal depths of the first shock and of the second may probably be within the ranges of 18∼22 (km) and of 14∼18 (km) respectively.

4. Summary.

The epicentre of second shock was located by the arrival times of P^*, and compared with the epicentre obtained from $\overline{P}$. They showed a fairly good concordance. The most probable values of coordinate of the epicentre are

$$\varphi=36^\circ\ 43'.7\,\text{N} \text{ and } \lambda=139^\circ\ 39'.4\,\text{E}.$$

The propagation velocity of P^* obtained from the arrival times of the first shock and of the second shock turned out to be of nearly equal value, i.e. 6.0 km/s.

h, the part of focal depth in the granitic layer of the first shock will be about 17 km, so far as the arrival time of $\overline{P}$ at Utsunomiya is concerned. The thickness of the superficial layer ranges from 1.4 km to 5 km. Thus the focal depth of the first shock is estimated as 18 km∼22 km. Accordingly, the focal depth of the second shock may probably be within the range from 14 km to 18 km.

25. 今市地震の計測（第 2 報）

地震研究所　　越川善明

P^* 波の發震時を用いて第二震の震央を求め，これを前報告に於て $\overline{P}$ から求めたものと比較して非常によく一致することを確めた．兩者を平均した震央位置は北緯 36°43′.7, 東經 139°39.′4となる．今回求めた P^* 波の傳播速度は 5.97 km/s となり，前に第一震の P^* から求めた値 6.00 km/s とも極めてよく一致する．

震央距離 50 km 以内の觀測値は宇都宮に於ける第一震の發震時が唯一つあるのみで，これを用いて第一震の震源の深さを求めた．それによると表面低速度層の厚さ 1.4 km 乃至 5 km に對して震源の深さの所謂花崗岩層中の部分は 17 km となる．從つて第一震の震源の深さは 18 km 乃至 22 km となる．第 2 震は第一震より 4.4 km 程淺いということを前報告に記してあるが，從つて第二震の深さは 14 km 乃至 18 km となる．

26. Time Distribution of Felt Aftershocks of the Imaichi Earthquake of December 26, 1949.

By Fuyuhiko Kishinouye,
Earthquake Research Institute.

(Read Sept. 10, 1950 and Feb. 20, 1951.—Received Mar. 20, 1951.)

When the writer was at Kanuma, Tochigi Prefecture, to observe the aftershocks of the Imaichi earthquake in January 1950, Mr. Moichirō Fukuda visited him to tell some earthquake phenomena which had occurred nearby at Tajiri, Nagahata section, Ochiai Village, Tochigi Prefecture (Fig. 1). The writer at that time requested Mr. Fukuda to record the times of the aftershocks felt. So Mr. Fukuda since Jan. 3, 1950 has been recording the aftershocks faithfully. The records during the period between Jan. 3 and Dec. 31, 1950 will be described in this paper. The daily numbers of the aftershocks are shown in Table I, and the frequency distribution of the daily numbers of aftershocks in Table II. The frequency distribution does not agree with Poisson's distribution as is usually the case with earthquakes.

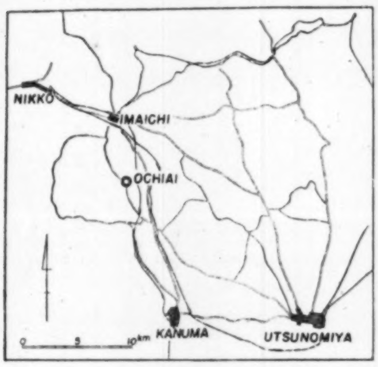

Fig. 1. Map showing position of Ochiai

The daily variation of the earthquake numbers is shown in Fig. 2. Assuming that the numbers of earthquakes recorded with seismographs at Utsunomiya re-

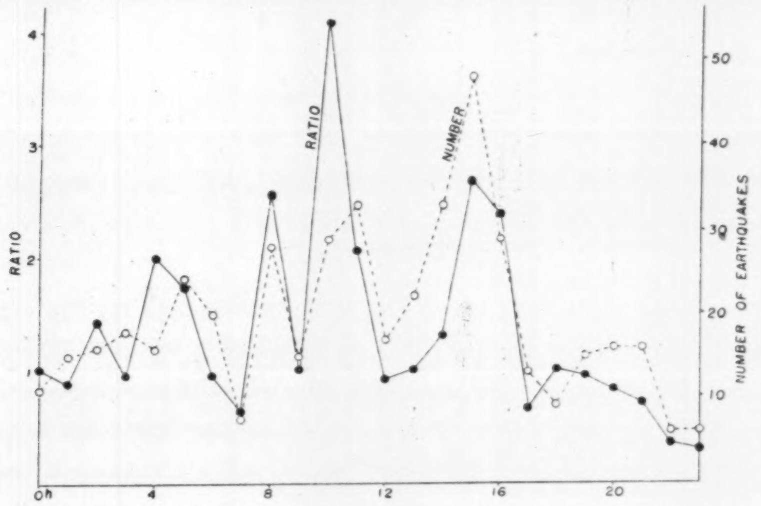

Fig. 2.

Table I. Daily numbers of earthquakes felt at Ochiai Village near Imaichi, Tochigi Prefecture, by Mr. M. Fukuda.

	Jan.	Feb.	Mar.	Apr.	May	June	July	Aug.	Sep.	Oct.	Nov.	Dec.	
1		7	2		2			2(2)				1	
2		2	5(4)	1									
3	12	19	2					3(1)					
4	13	4	3(1)		3	1(1)							
5	13	8(2)	4	8(3)		1(1)			1(1)		1		
6	20	12(3)	0	0		1							
7	14	9(5)	1	5(3)	1					1			
8	8	7(2)	1(1)	3(1)								2	
9	9	1(1)	2	2(1)					1				
10	11	5(2)	1	3(2)			2(2)		1			1	
												1	
11	12	5(5)	0	2(1)	4							1	
22	12	8(6)	2	1(1)	1	1(1)	2(2)						
13	9	1(1)		0	3	2(2)							
14	6	2(2)	13	0		2(1)		2					
15	12	1(1)	2	0	1	3(3)		1					
16	6	18(17)	1(1)	0	2								
17	11	2(2)	3(1)	0	2						2		
18	10	1		0	1						2		
19	19	5(4)	13	3	1						1		
20	7	36(34)	0	4(1)	2							1	
21	11	11(7)	2(1)										
22	4	0	4(4)										
23	8	1(1)	3	3(2)					1			1	
24	3	3(2)	1		1(1)	2(2)		2					
25	15	1	1	1(1)									
26	12	2	12(7)		1(1)	1(1)		1			2		
27	5	1	0	1(1)				2					
28	15	10(9)	1	3	1								
29	3	—		1									
30	1	—	1					1					
31	2	—	0	—		—			—				
		(111)	(20)	(17)	(2)	(12)	(4)	(3)	(1)				
Total	283	182	80	41	26	16	4	14	4	1	8	8	667

Number in parenthesis show that of earthquakes accompanied earthquake sound.

Table II.

No. of Eqkes	0	1	2	3	4	5	6	7	8	9	10	11	12	13	14	15	····	18	19	20	····	36
Freq. of daily No. of eqkes	218	50	30	15	6	6	2	3	5	3	2	4	7	4	1	2		1	2	1		1

present the seismic activity, the daily numbers at Ochiai were compared with those of the total numbers of earthquakes recorded at Utsunomiya, about 25 km distant from the epicentre of the main shock. As shown in Fig. 2, the ratios of earthquake numbers at Ochiai and Utsunomiya were large in day time. Although the proportion of felt earthquake is usually great at night, in this case earthquakes at night might not have been felt because the intensity of those earthquakes were too slight to wake up men asleep.

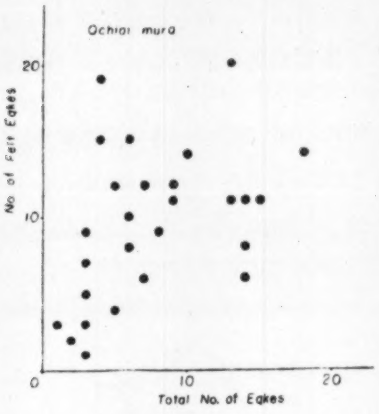

Fig. 3.

Correlation between the daily numbers of felt earthquakes at Ochiai or Utsunomiya and daily numbers of earthquakes recorded at the latter place are shown in Figs. 3 and 4. The correlation coefficient between numbers of earthquakes felt at Ochiai and those of total numbers at Utsunomiya was obtained as 0.35±0.12 (p. e.). But the correlation between felt earthquakes and total earthquakes at Utsunomiya was not close as seen in Fig. 4.

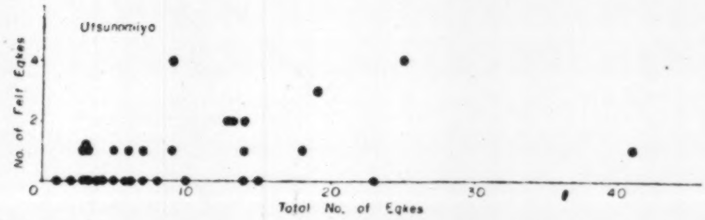

Fig. 4.

Earthquake sounds were heard accompanying most aftershocks of the Imaichi earthquake. The number or earthquake with sound are also shown in Table I. The recording of the numbers of sound might not be perfect, for almost all earthquakes occurred soon after the main shock was accompained by sound but the sound was not recorded till Feb. 5. So proportions of daily numbers of earthquake sound to total daily numbers were calculated from the data of the period between Feb. 5 and Sept. 30. The proportion was obtained as 52.4% in the average.

The above results may be regarded as a reference to study seismic activity recorded by human feeling without seismographs. And the writer considers that the human feeling may be a measure of the seismic activity near the epicentre. The result may be also useful for the study of the seismicity in old times when no seismographs were equipped.

The writer expresses thanks to mr. Moichirō Fukuda who recorded the aftershocks, and also to Miss Mieko Kotaka for her help in this study.

26. 1949年今市地震の有感餘震の時間分布

地震研究所　岸 上 冬 彦

栃木縣上都賀郡落合村大字長畑，田尻の福田茂一郎氏が1950年1月3日からその年末までに記録した有感餘震の時間分布について述べた．宇都宮の地震計によつて記録された地震の總數と落合村の有感地震の回數と比べると相關は比較的よい．それ故，地震計のない地方の地震活動は有感地震等の回數で知ることができると考へられる．このことは古い地震史料を調べることが無意味でないことを示すと思う．

27. *A Study on the Propagation of Microseismic Waves.*
Part III.

Ryôhei IKEGAMI and Fuyuhiko KISHINOUYE,
Earthquake Research Institute.

(Read Feb. 20, 1951.—Received March 20, 1951.)

1. Introduction.

We are studying microseisms in Tokyo, and some results have been already published[1]. But many problems about microseisms remain to be solved.

We set up four temporary stations at the compound of the Tokyo Astronomical Observatory in order to form two pairs of tripartite stations at the same time, but the stations were put farther apart than in the last case. The positions of the four stations, C, E, F, and G, are shown in Fig. 1. In Fig. 1 the tripartite stations in the

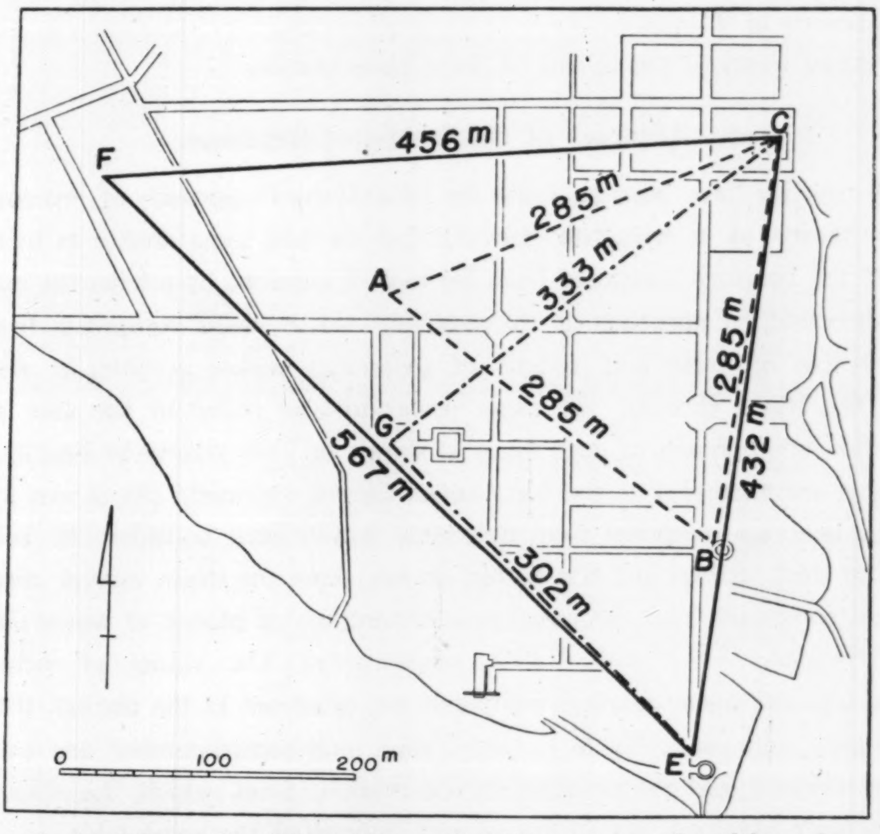

Fig. 1. Map of the Tokyo Astronomical Observatory and positions of temporary stations.

---

[1] R. IKEGAMI and F. KISHINOUYE, *Bull. Earthq. Res. Inst.*, **27** (1949), 75-80, **28** (1950), 115-119.

last case are indicated by A, B, and C. We used in this research five Kishinouye's horizontal tromometers which were adjusted to the same condition as in the last case, (namely $T=10$ sec., $v=\infty$). The magnification of records was two thousand on an ordinary day, but it was reduced to one thousand when the amplitude of microseismic waves was especially large. A tromometer was set up in NS-component at the stations, C, E, and G, respectively, and two tromometers were set up in NS- and EW-components at F-station.

For the purpose of examining the accuracy of arrival direction which are computed from the records observed at a tripartite network, we used two pairs of tripartite network CEF and CEG, and computed two values of the direction of approach of a microseismic wave simultaneously. Moreover, we were able to examine the relation between the direction of approach of mircoseisms and the motion of an earth particle in horizontal plane by using two records of NS- and EW-components at F-station.

This paper treats of the results of these observations.

2. Accuracy of the Computed Bearings.

Up to now we have been studying the directions of approach of microseismic waves by means of a tripartite network, but we had some doubts as to the reliability of the bearings computed from the records obtained by a tripartite network.

The directions of approach of microseismic waves were computed from the time differences of crests and troughs of individual waves arriving at E-, F-, C-, and G-stations through the same procedures as stated in the last papers. The direction of approach of each wave is shown by thin arrows in Fig. 2. These eight figures are examples of the forty seven figures obtained. As shown in these figures, the bearings computed from individual waves were considerably scattered about. The thick arrows and the dotted arrows show the mean arrival directions which were computed from the mean time differences of phases of waves observed with the triangles, CEF and CEG, respectively. The values of mean time differences and the mean bearings computed are tabulated in the second, the sixth, and the eighth columns of Table I. Date, time, and record-number are tabulated in the first column, and the numbers of observation, from which the mean time differences were obtained, are in the seventh column of the same table.

The difference between the two mean bearings computed from two observation-nets CEF and CEG was 11° at the maximum as tabulated in the ninth column of Table I, and the mean value of the differences 4.4°. This result sug-

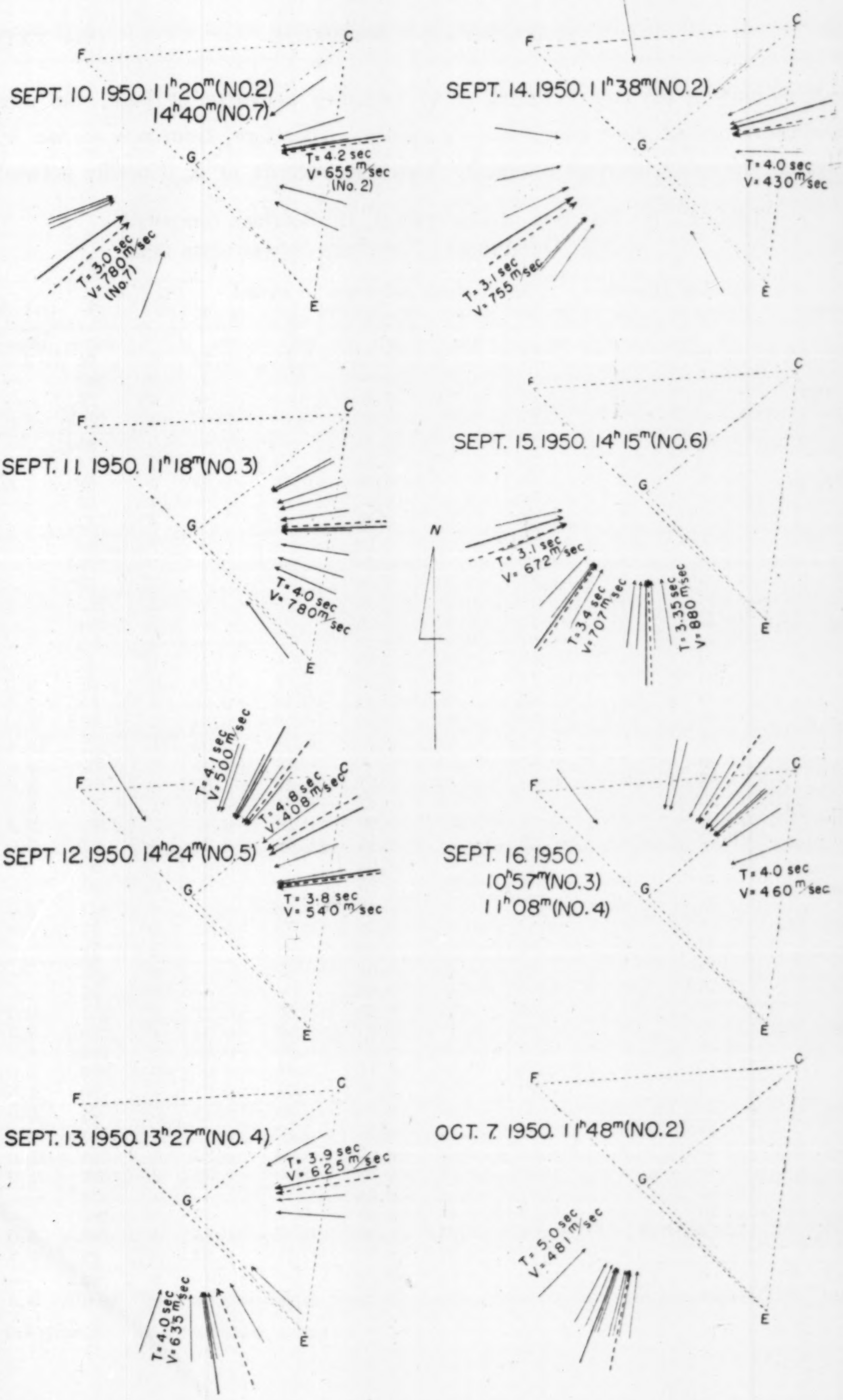
SEPT. 10. 1950. 11h20m(NO.2)
14h40m(NO.7)
F
C
G
E
T=4.2 sec V=655 m/sec (No. 2)
T=3.0 sec V=780 m/sec (No.7)
SEPT. 14. 1950. 11h38m(NO.2)
T=4.0 sec V=430 m/sec
T=3.1 sec V=755 m/sec
SEPT. 11. 1950. 11h18m(NO.3)
T=4.0 sec V=780 m/sec
SEPT. 15. 1950. 14h15m(NO.6)
N
T=3.1 sec V=672 m/sec
T=3.4 sec V=707 m/sec
T=3.35 sec V=880 m/sec
SEPT. 12. 1950. 14h24m(NO.5)
T=4.1 sec V=500 m/sec
T=4.8 sec V=408 m/sec
T=3.8 sec V=540 m/sec
SEPT. 16. 1950.
10h57m(NO.3)
11h08m(NO.4)
T=4.0 sec V=460 m/sec
SEPT. 13. 1950. 13h27m(NO.4)
T=3.9 sec V=625 m/sec
T=4.0 sec V=635 m/sec
OCT. 7. 1950. 11h48m(NO.2)
T=5.0 sec V=481 m/sec

Fig. 2. Directions of approach of microseismic waves. Thin arrows show the directions of approach of individual waves, thick arrows and dotted arrows show the mean arrival directions observed with triangles, ***CEF*** and ***CEG***, respectively.

gests us that, at the area including these tripartite networks at least, the mean bearings computed show considerable accuracy. Therefore, from now on we will use only the mean bearings computed from the records at a tripartite network,

Table I. N: Numbers of observation, B: Bearings computed,
D.B: Differences of bearings between two nets.

Date,	Starting time	Record-No.	Mean phase difference in second					N.	B.	D.B.
			E—C	F—C	E—F	G—C	G—E			
	h m		sec.	sec.	sec.	sec.	see.		degree	degree
Sep. 10, 1950.	11 20	2	−0.17	−0.64	0.47	−0.45	−0.28	6	81	2.0
	13 15	4	0.27	0.77	−0.61	—	—	6	265	—
	13 15	4	−0.29	−0.78	0.49	—	—	4	75	—
	14 40	7	0.37	0.51	−0.16	0.40	0.06	4	236	5.0
Sep. 11.	10 55	1	−0.13	−0.75	0.61	—	—	5	85	—
	11 05	2	−0.20	−0.57	0.34	—	—	6	74	—
	11 18	3	−0.10	−0.58	0.49	−0.31	−0.22	9	88	1.5
	14 12	7	−0.87	−0.01	−0.62	—	—	4	12	—
	14 12	7	0.28	−0.18	0.46	—	—	4	149	—
Sep. 12.	11 00	1	−0.45	−0.87	0.38	—	—	7	68	—
	14 04	3	0.30	0.91	−0.61	—	—	4	258	—
	14 04	3	−0.63	−0.30	−0.64	—	—	3	12	—
	14 14	4	0.19	0.61	−0.42	—	—	2	257	—
	14 14	4	−0.16	0.49	−0.65	—	—	3	294	—
	14 14	4	−0.67	−0.06	−0.57	—	—	4	2	—
	14 14	4	−0.99	−0.99	−0.01	—	—	1	43	—
	14 24	5	−0.78	−0.46	−0.26	−0.68	0.10	6	27	9.0
	14 24	5	−0.63	−1.06	0.43	−0.78	−0.08	2	58	3.5
	14 24	5	−0.21	−0.82	0.60	−0.54	−0.34	2	81	1.0
Sep. 13.	11 33	3	0.44	0.40	0.15	0.35	−0.09	1	222	10.0
	11 33	3	0.42	−0.09	0.56	0.13	−0.34	2	160	8.0
	11 33	3	0.09	−0.48	0.57	−0.41	−0.50	4	105	3.0
	11 33	3	−0.37	0.85	0.47	−0.71	−0.34	1	71	4.0
	13 27	4	0.63	−0.07	0.69	0.16	−0.47	7	170	3.5
	13 27	4	−0.25	−0.72	0.46	−0.50	−0.24	3	77	3.0
	13 40	5	0.45	0.47	−0.02	—	—	3	230	—
	13 40	5	−0.06	−0.91	0.85	—	—	5	93	—
Sep. 14.	11 38	2	0.36	0.55	−0.18	0.43	0.04	6	241	3.0
	11 38	2	−0.33	−0.96	0.59	−0.75	−0.42	5	77	4.0
	13 43	5	−0.19	−0.61	0.43	—	—	5	79	—
Sep. 15.	11 25	1	0.42	0.49	−0.07	—	—	4	231	—
	11 25	1	0.13	−0.49	0.60	—	—	5	111	—
	13 50	4	0.33	0.67	0.36	0.57	−0.22	4	251	0.0
	13 50	4	0.48	0.27	0.20	0.43	−0.04	4	208	8.5
	14 15	6	0.26	0.66	−0.40	0.42	−0.16	2	255	4.5
	14 15	6	0.53	0.42	−0.11	0.44	−0.01	3	218	2.0
	14 15	6	0.49	0.04	0.45	0.21	−0.25	4	180	1.5
Sep. 16.	10 57&11 08	3&4	−0.80	−0.71	−0.09	−0.67	0.13	9	42	6.0
Sep. 20.	13 47	2	−0.61	−0.79	0.19	−0.67	−0.07	4	55	0.5
	15 40	5	−0.11	0.46	−0.56	0.23	0.23	5	290	11.0
	15 40	5	0.39	0.87	−0.49	0.80	0.35	3	252	1.0
Oct. 5.	12 10	1	−0.57	0.08	−0.64	—	—	4	348	—
	12 10	1	−0.13	0.46	−0.59	—	—	3	298	—
	12 22	2	−0.04	−0.64	−0.69	0.13	0.18	4	282	5.0
	12 22	2	−0.67	−0.32	−0.36	−0.51	0.23	4	22	5.5
Oct. 6.	12 04	1	−0.09	0.64	−0.73	—	—	5	285	—
Oct. 7.	11 48	2	0.88	0.32	0.48	0.58	−0.38	8	201	9.5

Mean; 4.4

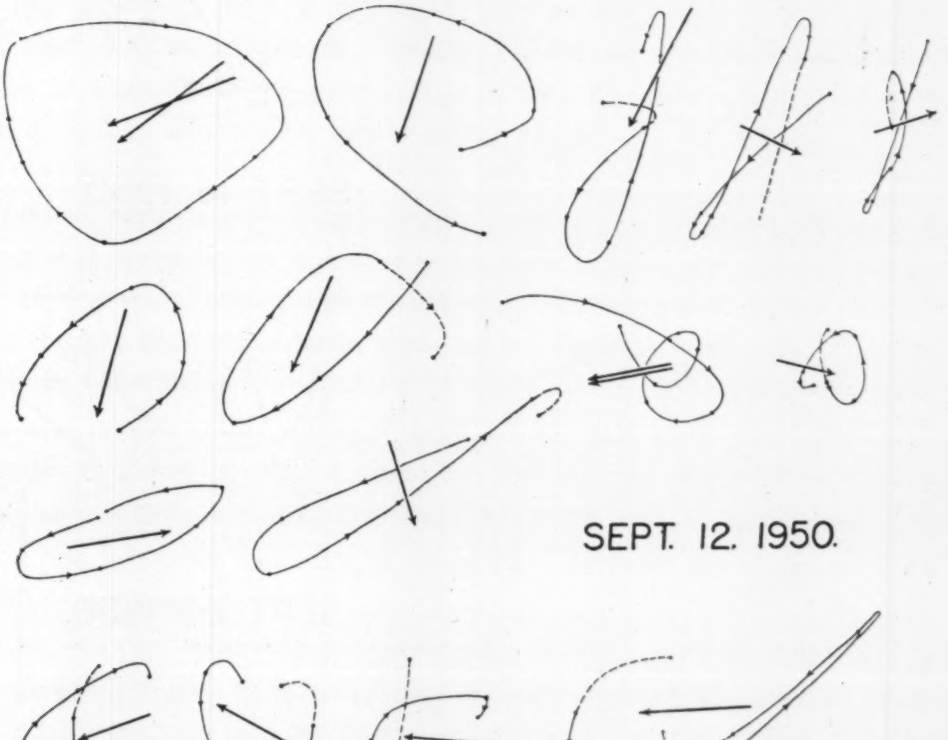
SEPT. 12. 1950.
N
SEPT. 13. 1950.
SEPT. 14. 1950.

Fig. 3. Horizontal orbits of an earth particle and directions of approach of microseismic waves.

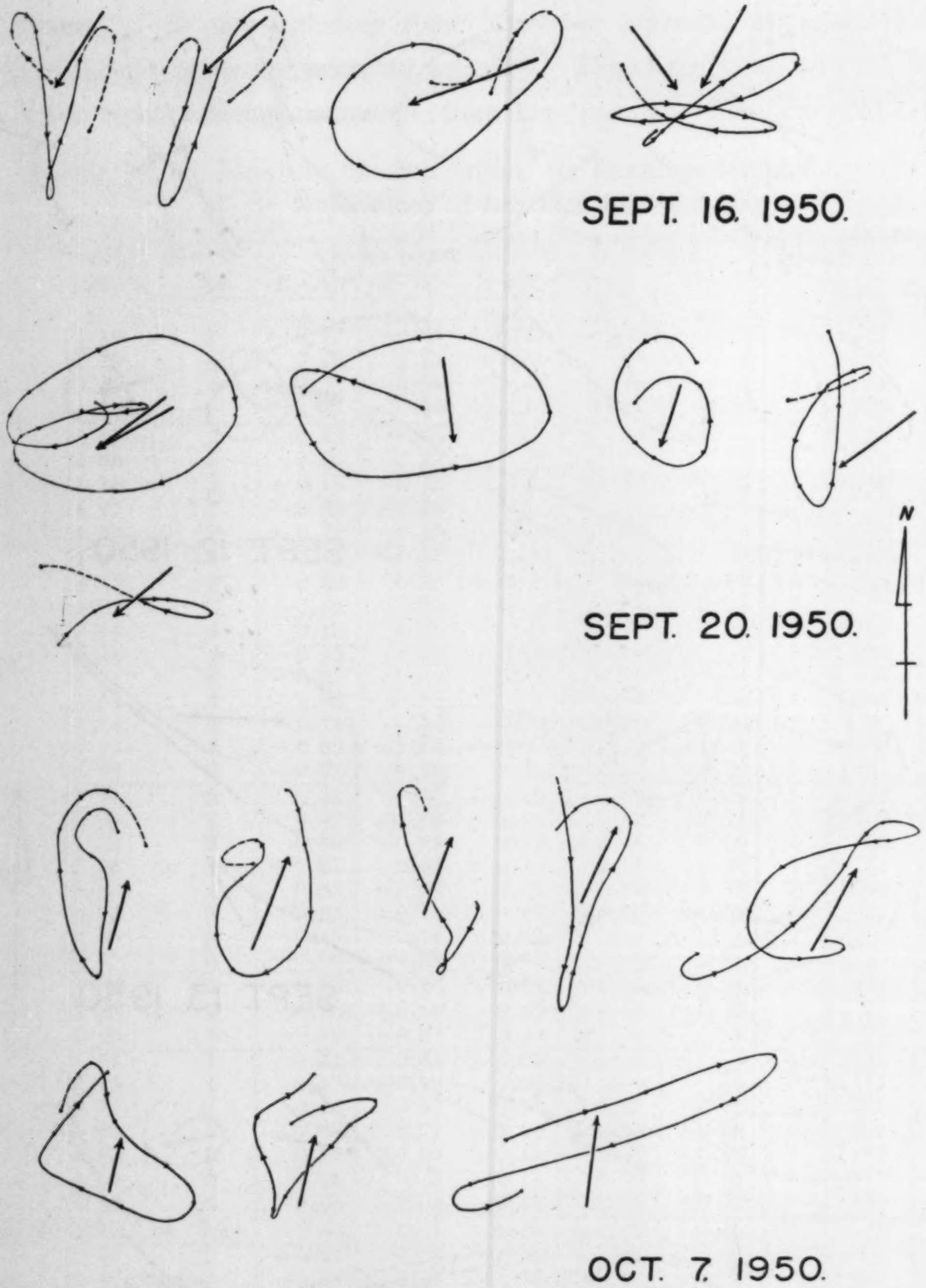
SEPT. 16. 1950.
SEPT. 20. 1950.
N
OCT. 7. 1950.

Fig. 3. Continued from the last page.

when the directions of approach of microseismic waves are dealt with.

3. Horizontal Orbits of Microseismic Motions.

The relation between the direction of approach of microseismic wave and the orbit of an earth particle of that wave has not been investigated, so, in order to draw the horizontal orbit of an earth particle, we set up two tromometers in ***EW***-, and ***NS***-components at ***F***-station. Some of the orbits obtained and the direction of approach of the wave computed from tripartite observations are shown in Fig. 3, and all others show also a similar trend.

If microseismic waves are of the Rayleigh-wave type, horizontal orbit of an earth particle must become longer longitudinally to the direction of approach of waves, and if these waves are of the Love-wave type, the orbit must become longer in transverse direction to the direction of approach.

We thought that microseismic waves of the Rayleigh-wave type alone may be propagated; nevertheless the orbits of an earth particle obtained by us show that microseisms consist of the waves of both the Rayleigh-wave type and the Love-wave type as shown in Fig. 3, and we see that the directions of approach of microseisms are independent of the direction of the axis of orbit, and that the waves of the two types came not so much from different directions as from the same direction mixed up.

As we are now observing microseisms by adding a vertical-component tromometer, we shall be able to investigate wave forms more clearly than up to now.

In conclusion, we express thanks to the staff of the Tôkyô Astronomical Observatory who permitted us to use some buildings in the compound of the Observatory to set our instruments. We also thank Miss M. Kotaka, Mr. J. Moroga and Mr. H. Yoshioka of our institute for their assistance in this investigation.

The cost of this investigation was defrayed from the Scientific Research Expenditure of the Department of Education.

27. 土地の脈動の傳播性の研究（第 3 報）

地震研究所 { 池上良平
岸上冬彦

所謂三點觀測法によつて求められた脈動の傳播方向がどの程度に信頼出來るものかその精度を檢する目的で，4點同時觀測を實施し，2組の三點觀測網 CEF 及び CEG を構成して，同一の脈動波についての傳播方向の2つの値を算出する事を試みた。その結果兩者の差は最大 11°，平均 4.4° と云ふ結果を得た。即ちこの觀測網を含む範圍內では，算出された脈動の傳播方向はこの程度の精度がある事が確められた。次に算出された傳播方向と，その時の地面の實際の動き方とを比較した。その結果傳播性の脈動の中には見かけ上レーリー波型のものとラブ波型のものとがあつて，この兩者が混り合つて同一方向から傳播して來る事が判つた。

28. *A Study on the Propagation of Microseismic Waves. Part IV.*

By Ryôhei IKEGAMI,

Earthquake Research Institute.

(Read Feb. 20, 1951.—Received March 21, 1951.)

1. Introduction.

We are studying microseisms by means of a tripartite network, and treated of the relation between the directions of approach of microseismic waves and the weather patterns at the time of observation, and some results were already published[1]. But we had some doubts about the reliability of the bearings computed from the records obtained by a tripartite network.

Therefore, we examined the accuracy of the arrival direction computed from the records of microseisms by using two pairs of tripartite stations CEF and CEG (See Part III of our paper), and could ascertain that, at the area including these stations at least, the mean bearings computed have considerable accuracy, and so we investigated microseisms by using only the mean bearings which were computed from the records observed at C-, E-, and F-stations shown in Fig. 1 of Part III.[2]

In this paper we will report the results of our observations from September 10 to 16 and September 20, and from October 5 to 7, 1950.

2. Relation between the Directions of Approach of Microseismic Waves and the Weather Patterns at the Time of Observation.

To begin with, we will state the results obtained from September 10 to 16, 1950, when a typhoon (named KEZIA) slowly travelled over the southern sea of Japan to Kyûshû and then passed northwards over the Japan Sea and over Hokkaidô. When the typhoon KEZIA passed through Kyûshû, another tropical storm had appeared over the southern sea. On the other hand, many cold-fronts or warm-fronts passed over the Pacific Ocean off the coast of Tôhoku District, throughout this period.

---

[1] R. IKEGAMI and F. KISHINOUYE, *Bull. Earthq. Rest. Inst.*, **27** (1949), 75-80, **28** (1950), 115-119.

[2] R. IKEGAMI and F. KISHINOUYE, *ditto*, **29** (1951), 305-312.

Microseisms observed during this period were more or less irregular, and microseisms which had periods of more than 4 seconds and moderate amplitude interposed those with periods of less than 3 seconds and small amplitude. (See Figs. 1(a) and (b), and Fig. 10(a).)

The individual microseismic waves were classified according to their periods, and the mean bearings were computed from the mean time differences arriving at *E*-, *F*-, and *C*-stations. These mean bearings are tabulated in the second column of Table I and shown by arrows in weather-maps (Figs. 2 to 8), which indicate the weather patterns at 9 o'clock (Japanese Civil Time) on those days, respectively. We think that these weather patterns did not differ much from those at the time of our observations, because we observed the microseisms from 11 to 15 o'clock

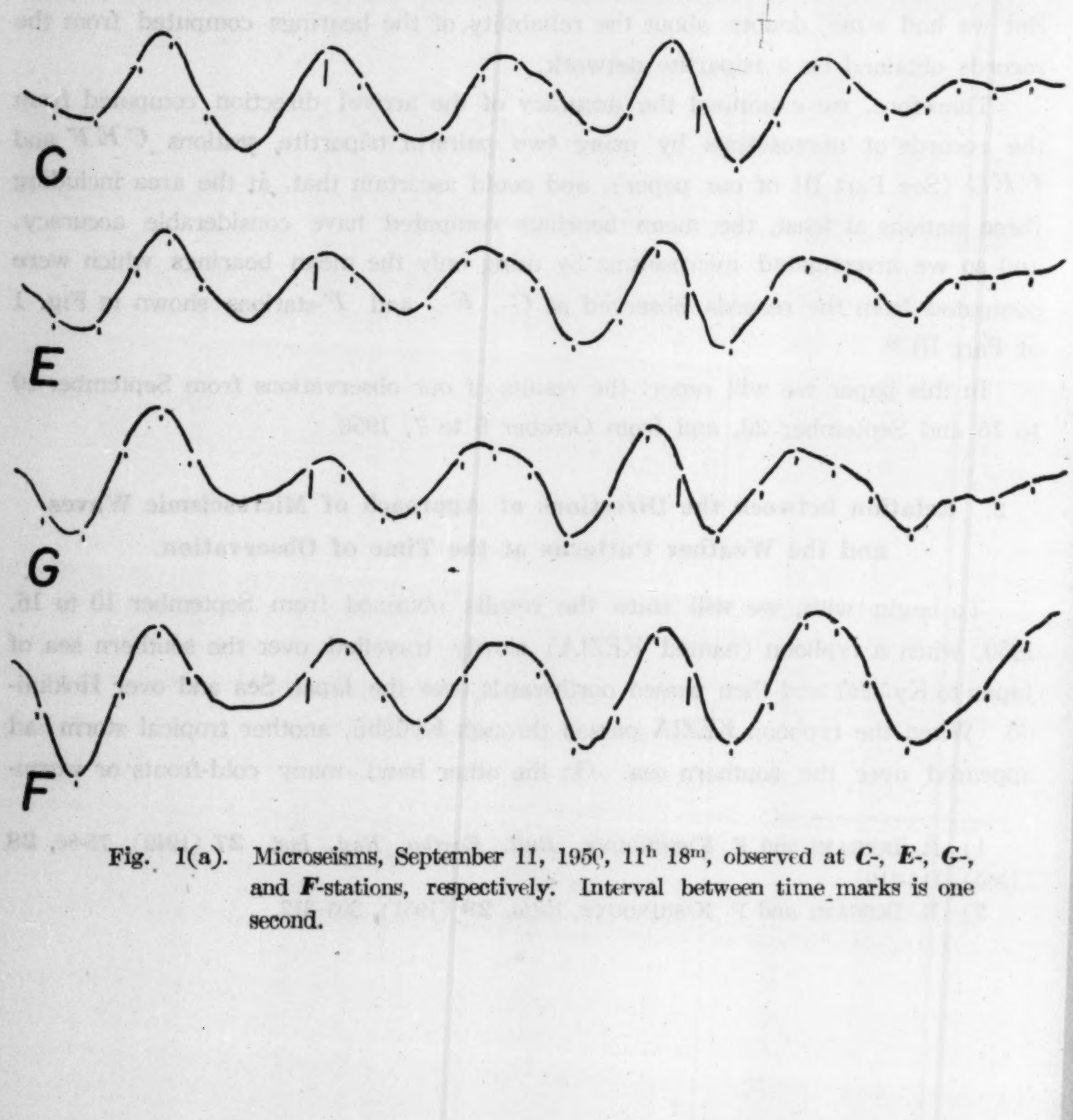

Fig. 1(a). Microseisms, September 11, 1950, $11^h\ 18^m$, observed at *C*-, *E*-, *G*-, and *F*-stations, respectively. Interval between time marks is one second.

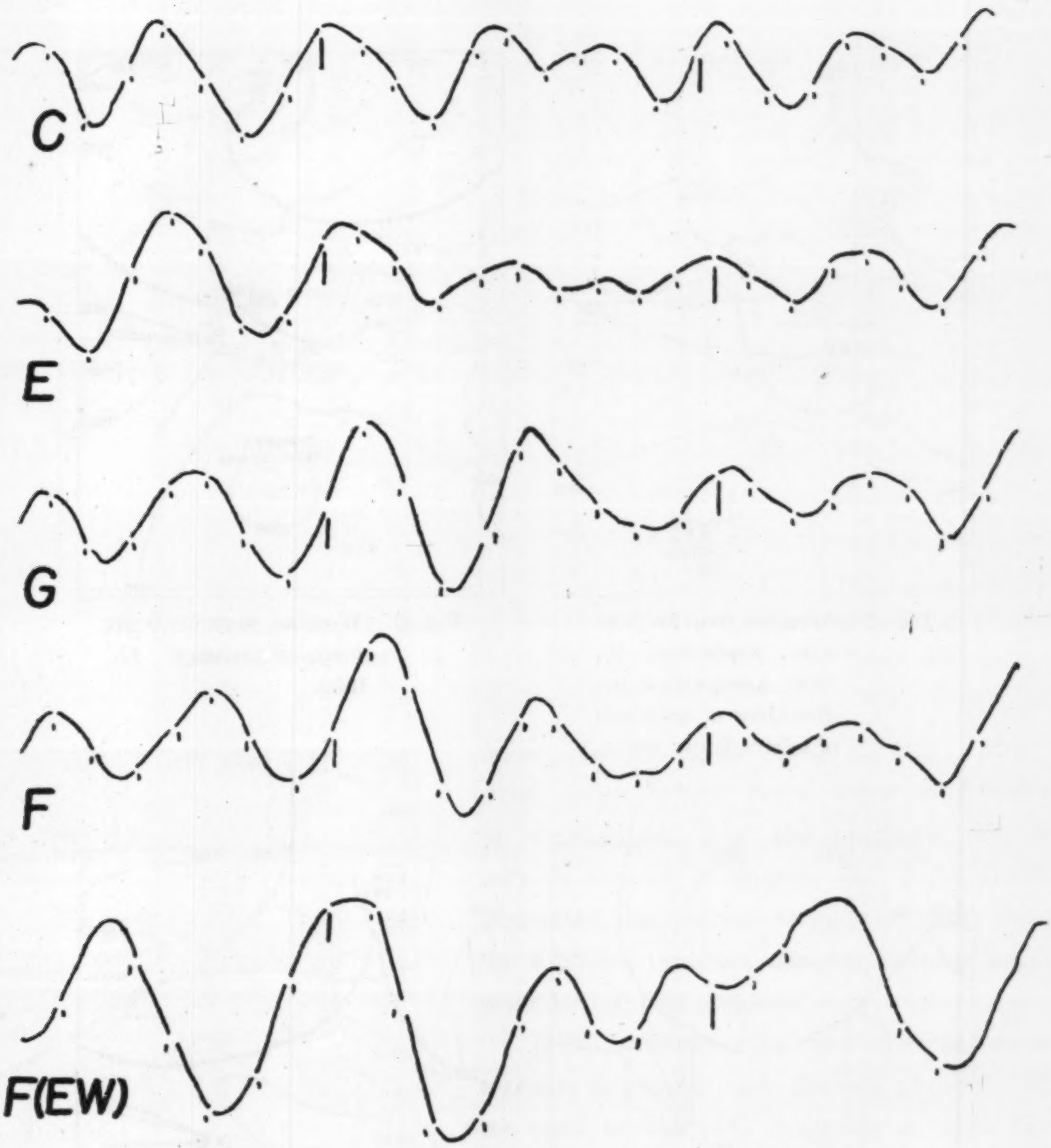

Fig. 1(b). Microseisms, September 13, 1950, 13^{h} 40^{m}.

every day.

We see from these figures that the microseisms which came from east or northeast remarkably predominated, nevertheless there was a fairly severe typhoon or tropical storms over the southern sea of Japan. There was no deep depression which generates microseisms over the eastern or the northeastern sea, according to the weather-maps of those days, and swells and sea waves of the northern sea were not higher than those of the southern sea, according to the reports of the observation ships belonging to the Central Meteorological Observatory and of the

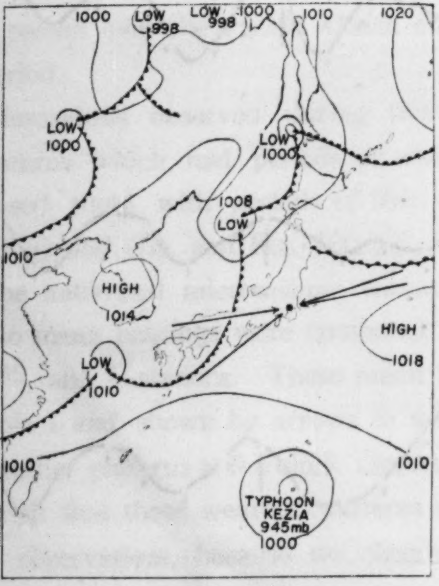
1000
LOW 998
LOW 998
1000
1010
1020
LOW 1000
LOW 1000
1008
LOW
1010
HIGH
1014
HIGH
1018
LOW
1010
1010
1010
TYPHOON
KEZIA
945mb
1000

Fig. 2. Weather map for 9:00 a.m., September 10, 1950. Arrows show the directions of approach of microseismic waves.

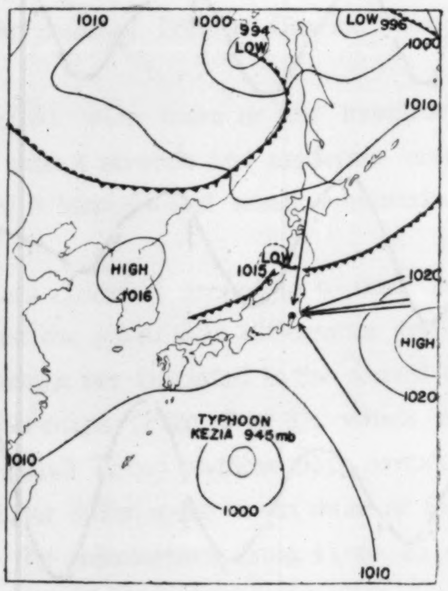
1010
1000
994
LOW
LOW 996
1000
1010
HIGH
1016
LOW
1015
1020
HIGH
1020
TYPHOON
KEZIA 945mb
1010
1000
1010

Fig. 3. Weather map for 9:00 a.m., September 11, 1950.

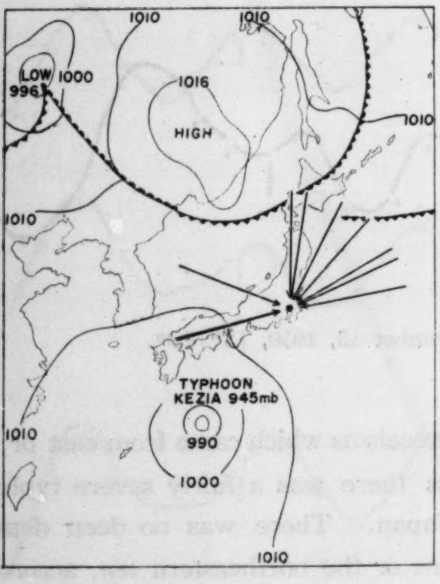
1010
1010
LOW
996
1000
1016
HIGH
1010
1010
TYPHOON
KEZIA 945mb
990
1000
1010
1010

Fig. 4. Weather map for 9:00 a.m., September 12, 1950.

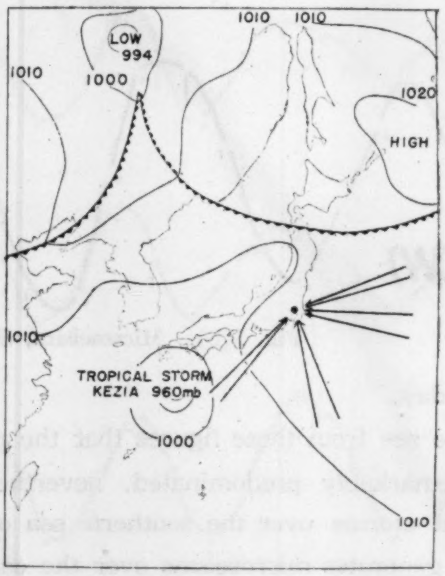
LOW
994
1010
1010
1010
1000
1020
HIGH
1010
TROPICAL STORM
KEZIA 960mb
1000
1010

Fig. 5. Weather map for 9:00 a.m., September 13, 1950.

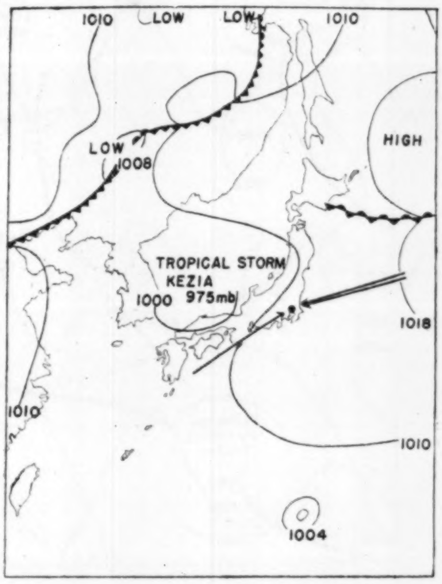
1010
LOW
LOW
1010
LOW
1008
HIGH
TROPICAL STORM
KEZIA
1000 975mb
1018
1010
1010
1004

Fig. 6. Weather map for 9:00 a.m., September 14, 1950.

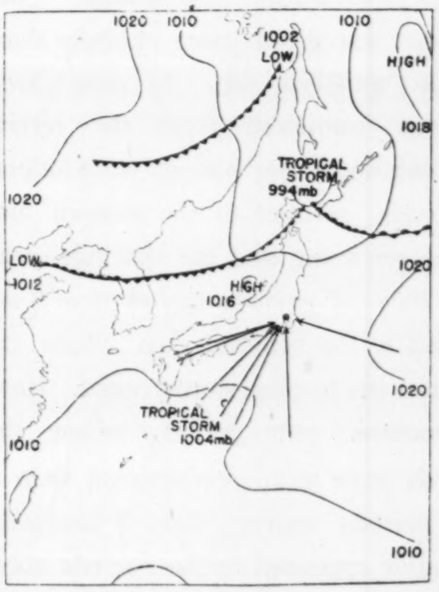
1020 1010
1002
LOW
1010
HIGH
1018
TROPICAL
STORM
994mb
1020
LOW
1012
HIGH
1016
1020
1020
TROPICAL
STORM
1004mb
1010
1010

Fig. 7. Weather map for 9:00 a.m., September 15, 1950.

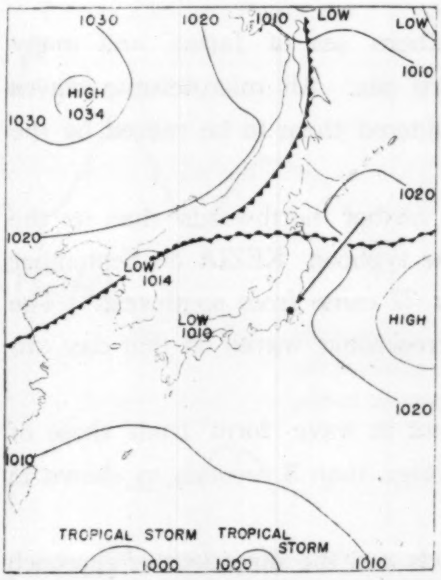
1030
1020
1010
LOW
LOW
1010
HIGH
1034
1030
1020
1020
LOW
1014
LOW
1010
HIGH
1020
1010
TROPICAL STORM
TROPICAL
STORM
1000
1000
1010

Fig. 8, Weather map for 9:00 a.m., September 16, 1950.

other Meteorological Observatories. Moreover, even when there were cold-fronts or warm-fronts over the northern sea, it may be difficult to suppose that those fronts generated microseisms more powerfully than the southern typhoon. But we have an interpretation of this problem.

It is a well-known fact that when a typhoon is passing over the sea of north off the coast of the Bôsô Peninsula or when the sea of the same area is rough, microseisms with large amplitude and long period always predominate remarkably in Tôkyô. The reason for this fact is not found yet, but we cannot neglect the fact that the northern sea is apt to generate microseisms more easily than the southern sea.

In this case it is true that the southern sea was much more rough than the northern sea throughout the period, but we can not refrain from thinking that "a force generating microseisms" of the northern sea acted more strongly than that of the southern sea. In most cases the bearings computed from the records of microseisms, whose periods were longer than 4 seconds, pointed to the eastern and the northeastern sea, and the bearings computed from those of periods shorter than 3 seconds pointed to the southern sea where the typhoon or the tropical storms raged. However, microseisms with periods longer than 4 seconds were more predominant than those with periods shorter than 3 seconds, and the latter appeared on the records only here and there when the former took a pause. It now becomes necessary to reconsider the bearings in case of the typhoon PATRICIA on October 26 and 27, 1949[3]. On October 26 the typhoon was situated far off in the southern sea of Japan, and many conspicuous cold-fronts passed over the northeastern sea. All microseismic waves that day came from the northeast, and we considered them to be caused by the northeastern cold-fronts.

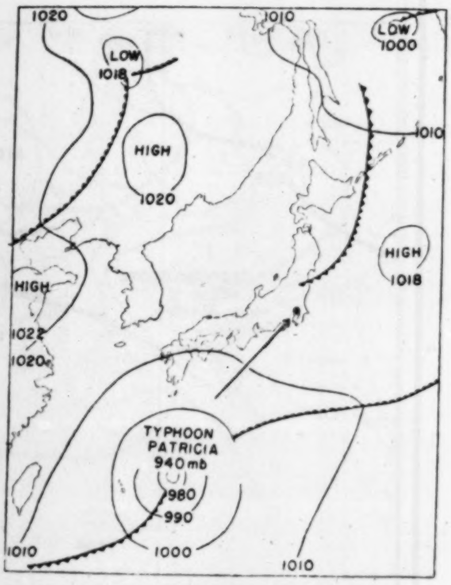

Fig. 9. Weather map for 9:00 a.m., October 27, 1949. Arrow shows the direction of approach of microseismic waves.

On October 27, 1949, the typhoon proceeded farther northwards than on the previous day, and its situation was near that of the typhoon KEZIA on September 12, 1950. All the microseismic waves on October 27 came from southwest. The weather-map and the direction of approach of microseismic waves on that day are shown in Fig. 9.

Microseisms of October 27 were quite different in wave form from those of September 12, 1950 and their periods were all shorter than 3 seconds as shown in Figs. 10(a) and (b), respectively.

We will refer to the relation between the periods and the directions of approach of microseismic waves later.

Next, we will state the results obtained on September 20 and from October 5 to 7, 1950. The weather patterns and the mean bearings computed from microseismic waves on those days are shown in Figs. 11—14.

---

3) R. IKEGAMI and F. KISHINOUYE, *loc. cit.*, **28** (1950), 115-119.

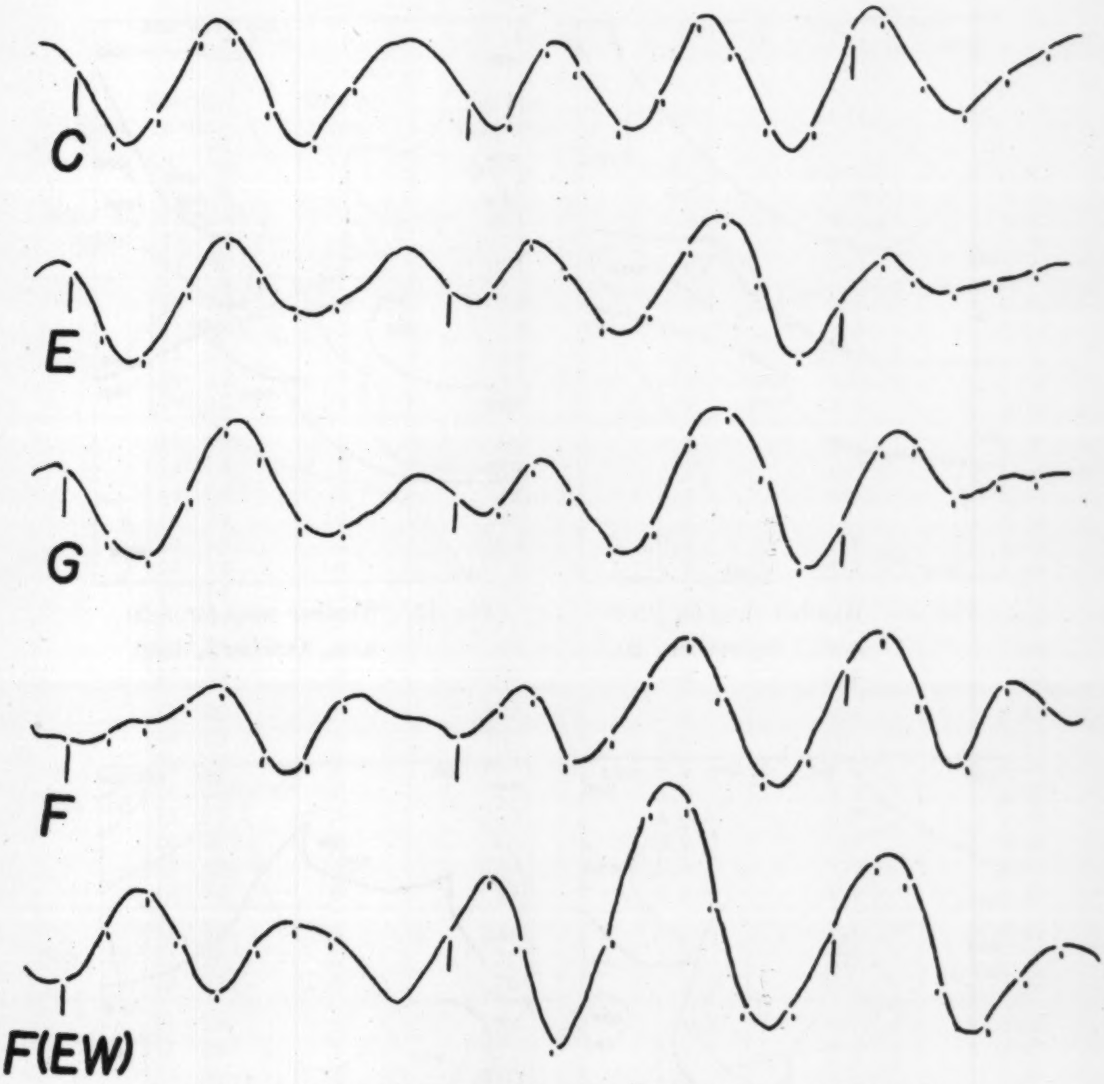

Fig. 10 (a). Microseisms, September 12, 1950, 14^h 14^m. Short-period microseisms appeared only here and there when long-period microseisms took a pause.

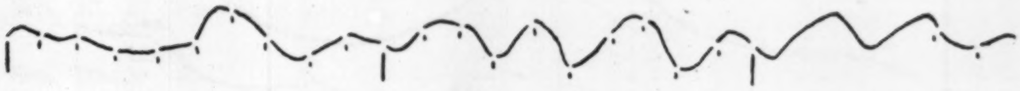

Fig. 10 (b). Microseisms, October 27, 1949, 12^h 25^m. All the periods of microseisms were shorter than 3 seconds. (observed at A-station.)

According to the weather-maps, on September 20 and October 5 and 6, there were fairly deep depressions and cold-fronts over the Pacific Ocean near the Japan Islands, but there were also low depressions or cold-fronts over the Japan Sea side, and the sea was rough during those days. The bearings computed indicated that

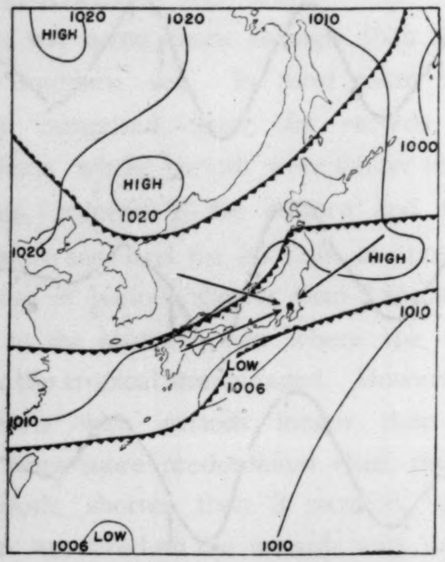
HIGH
1020
1020
1010
1000
HIGH
1020
1020
HIGH
1010
LOW
1006
1010
LOW
1006
1010

Fig. 11. Weather map for 9:00 a.m., September 20, 1950.

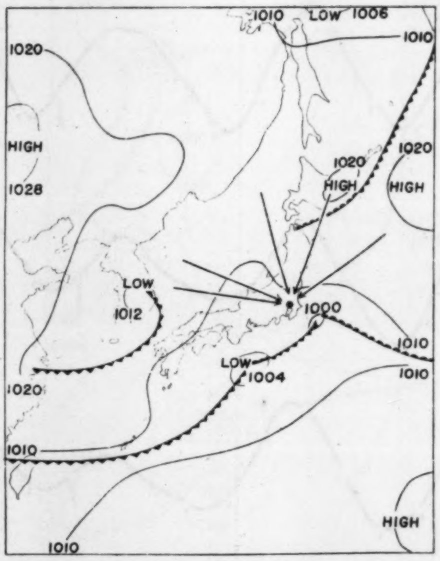
1010
LOW
1006
1010
1020
HIGH
1028
1020
HIGH
1020
HIGH
LOW
1012
1000
1010
LOW
1004
1010
1020
1010
HIGH
1010

Fig. 12. Weather map for 9:00 a.m., October 5, 1950.

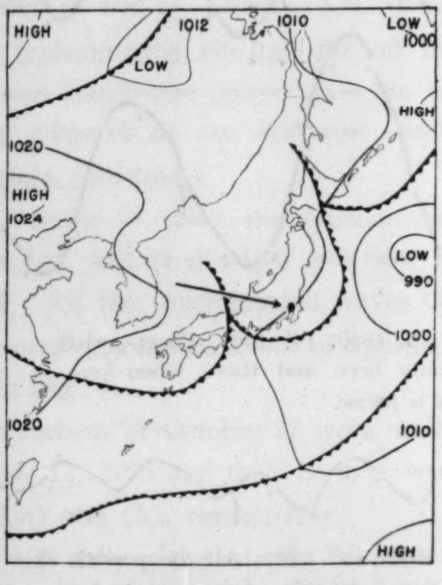
HIGH
1012
LOW
1010
LOW
1000
HIGH
1020
HIGH
1024
LOW
990
1000
1020
1010
HIGH

Fig. 13. Weather map for 9:00 a.m., October 6, 1950.

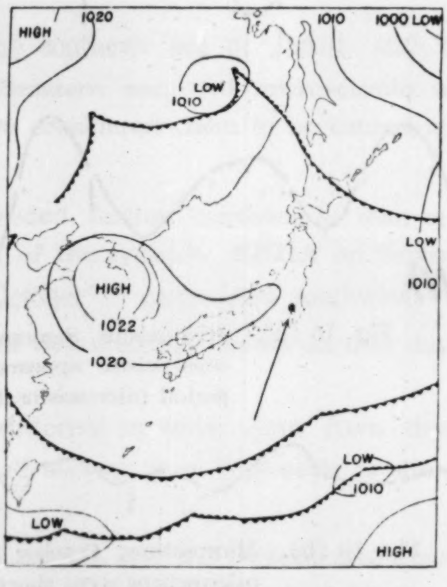
HIGH
1020
1010
1000
LOW
LOW
1010
LOW
1010
HIGH
1022
1020
LOW
1010
LOW
HIGH

Fig. 14. Weather map for 9:00 a.m., October 7, 1950.

on September 20 and October 5 and 6 the microseismic waves came from the direction of the Japan Sea. We insist that these conditions of the Japan Sea may cause microseisms, but we cannot explain satisfactorily the reason why we could entirely

Table I.

Date	Starting time	Record-No.	Bearings computed	Period	Velocity	Wave-length
	h m		degree	sec.	m/sec.	km.
Sep. 10, 1950.	11 20	2	81	4.2	655	2.75
	13 15	4	265	4.5	590	2.65
	13 15	4	75	4.4	565	2.48
	14 40	7	236	3.0	780	2.34
Sep. 11.	10 55	1	85	4.3	605	2.60
	11 05	2	74	3.9	780	3.04
	11 18	3	88	4.0	780	3.12
	14 12	7	12	5.7	495	2.82
	14 12	7	149	2.7	1200	3.24
Sep. 12.	11 00	1	68	4.4	500	2.20
	14 04	3	258	4.0	490	1.96
	14 04	3	12	4.5	670	3.01
	14 14	4	257	3.3	740	2.44
	14 14	4	294	3.8	815	3.09
	14 14	4	2	4.1	645	2.64
	14 14	4	43	5.2	343	1.78
	14 24	5	27	4.1	500	2.05
	14 24	5	58	4.8	408	1.95
	14 24	5	81	3.8	540	2.05
Sep. 13.	11 33	3	222	3.1	846	2.62
	11 33	3	160	3.0	885	2.65
	11 33	3	105	3.6	670	2.41
	11 33	3	71	5.0	473	2.36
	13 27	4	170	4.0	635	2.54
	13 27	4	77	3.9	625	2.43
	13 40	5	230	3.5	736	2.57
	13 40	5	93	4.2	553	2.32
Sep. 14.	11 38	2	241	3.1	755	2.34
	11 38	2	77	4.0	430	1.72
	13 43	5	79	3.6	730	2.62
Sep. 15.	11 25	1	231	3.5	752	2.63
	11 25	1	111	3.5	850	2.97
	13 50	4	251	4.0	600	2.40
	13 50	4	208	3.4	788	2.67
	14 15	6	255	3.1	672	2.08
	14 15	6	218	3.4	707	2.40
	14 15	6	180	3.4	880	2.99
Sep. 16.	10 57 and 11 08	3 and 4	42	4.0	460	1.84
Sep. 20.	13 47	2	55	4.5	490	2.20
	15 40	5	290	4.1	916	3.75
	15 40	5	252	5.2	504	2.62
Oct. 5.	12 10	1	348	4.7	729	3.42
	12 10	1	298	3.9	892	3.47
	12 22	2	282	4.0	693	2.77
	12 22	2	22	4.0	600	2.40
Oct. 6.	12 04	1	285	4.7	679	3.19
Oct. 7.	11 48	2	201	5.0	481	2.40
					Mean,	2.57 ±0.30

observe no microseismic waves coming from the Pacific Ocean side in the present situation of our study.

On October 27, 1950, according to the weather-map, the predominant high pressure area made a considerable advance from the Continent of Asia to east, and most part of the Japan Islands was covered with this high pressure. The low depressions and the cold-fronts over the Japan Sea moved away and the Japan Sea became calm, but there were as always low depressions and cold-fronts over the sea south of the Japan Islands. On this day the bearings computed indicated that all the microseismic waves came from south.

Judging from the results mentioned above, we consider that the cause of the microseisms generated is more complicated than many seismologists think. Recently, forecasting of typhoon or hurricane by utilizing the directions of approach of microseismic waves was advocated by American Seismologists and many valuable treatises on this problem were published. But, judging from our results, we doubt whether this problem can be similarly solved in Japan.

3. Velocity, Period, and Bearings of Microseismic Waves.

We have stated that, according to our results, the velocities of microseismic waves are connected with their periods, and that the products of both values, (viz. wave-length), maintained almost a constant value[4]. This relation between velocity and period was always maintained, though new data were added to the previous ones, but the mean wave-length varied from 2.2 km. to 2.57±0.30 km. as shown in Fig. 15.

It has been already stated that this relation can not yet be explained theoretically, if the velocities observed are phase-velocities.

On the other hand, we re-examined the relation between periods and bearings, and we obtained the relation shown in Fig. 16. The values of period, velocity, and wave-length are tabulated in the third, the fourth, and the fifth columns of Table I, respectively. In Fig. 16. except the two values on October 28, 1949 and October 7, 1950, (shown by white triangle and circle, respectively), we see that the periods of microseismic waves arriving at the stations from azimuths ranging between 0° and 150° (clockwise from north=0°), and between 240° and 360°, were from 3.5 to 5 seconds, and that the periods between 150° and 240° were

---

[4] R. IKEGAMI and F. KISHINOUYE, *loc. cit.*, **28** (1950), 118.

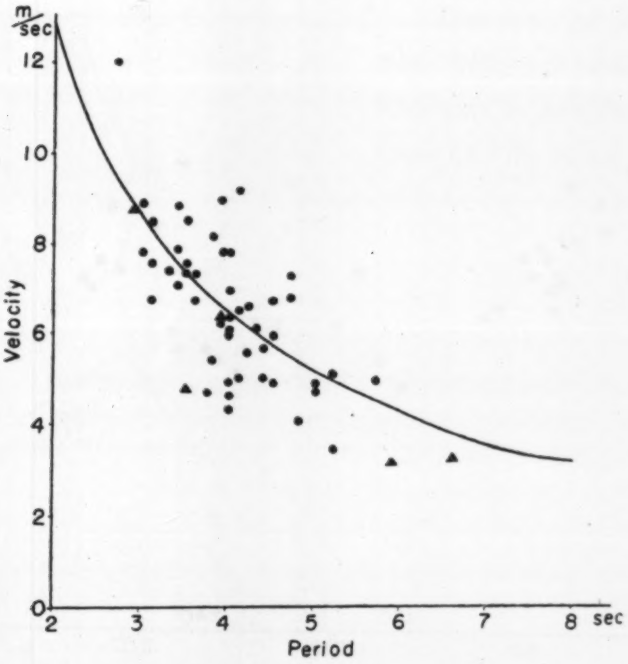

Fig. 15. Relation between mean velocity and period. Circles show the values observed this time, and triangles show the values observed last time, (viz. in case of typhoon PATRICIA).

from 2.5 to 3.5 seconds. The fact that the area between 150° and 240° coincided with the area of sea shallower than 6000 meters as shown in Fig. 17 aroused much interest in us. Judging from these results, the depth of sea in a certain place may be related with the periods of microseismic waves caused in that place, and it seems that microseismic waves caused in the area between 150° and 240° have shorter periods than those caused in other areas. This deduction will be consistent with the fact that microseisms caused in the sea of north of the Bôsô Peninsula have longer periods and larger amplitudes than those caused in the southern sea.

If the velocity of the short-period microseisms is larger than that of the long-period microseisms for some reasons, and if the former is different in kind from the latter, we need not hold fast to the view that the products of velocity and period have always a constant value. That is to say, we may take the view that the periods plotted in Fig. 15 may be all divided into two groups in accordance with their periods. But we can not determine which of the two views is to be adopted in the present situation. Microseisms having especially long-periods, as those on October 28, 1949 and October 7, 1950, are possibly exceptional, and they

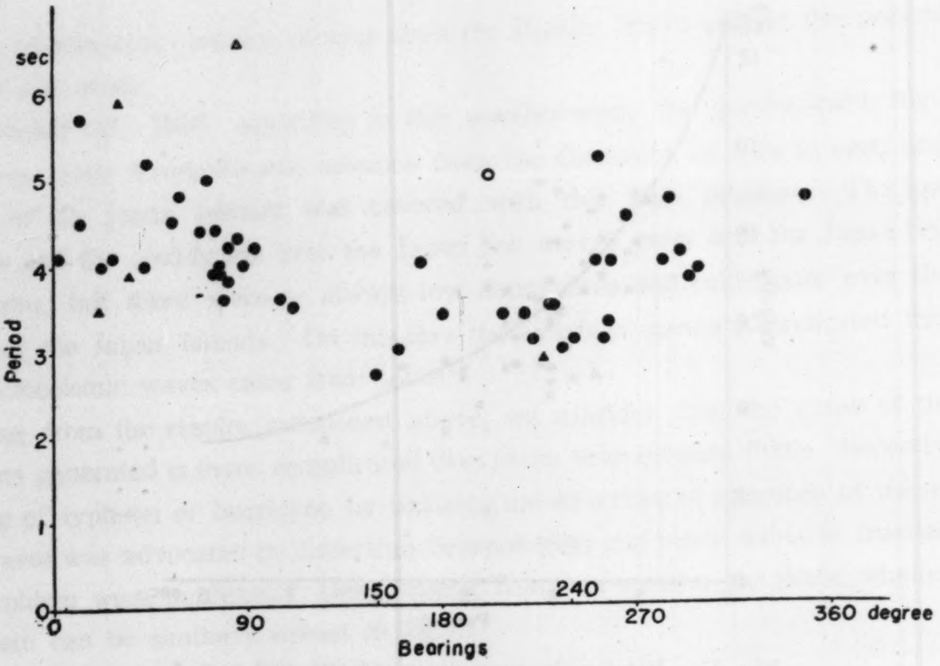

Fig. 16. Relation between period and direction (bearings) of approach of microseismic wave.
Circles show the values observed this time, and triangles the values observed last time, (viz. in case of typhoon PATRICIA). White triangle and circle show microseisms having especially long-periods, which seem to be different in kind from the other.

are different in kind from the others. F. Omori[5] formerly classified microseisms in Tôkyô into three types, i.e. the *q*-, Q_1-, and Q_2-types according to their period and amplitude, and the range of the period of *q*-type was from 2 to 3 seconds, that of Q_1-type about 4 seconds, and that of Q_2-type, from 6 to 9 seconds. We consider that this classification of microseisms has a new signification in the light of the results mentioned above.

4. Acknowledgement.

I wish to express my appreciation to Dr. F. Kishinouye for his guidance and advice, and to the other members of his seminary-room for their aids in the observations, and to the staffs of the Tokyo Astronomical Observatory for all the kindness they have shown us in our observations.

---

[5] F. OMORI, *Bull. Imp. Earthq. Invest. Commit.*, **3** (1909), 1-35.

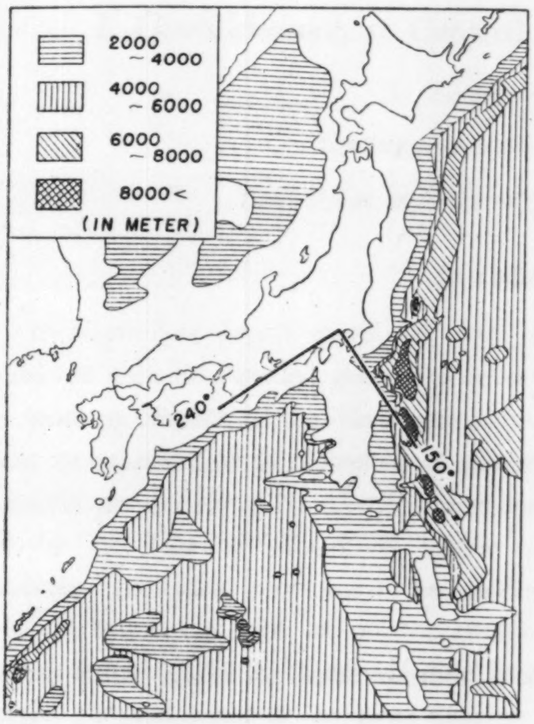

Fig. 17. Relation between depth of the Pacific Ocean and period of microseisms. Microseismic waves caused in the area between 150° and 240°, (depth of this area is shallower than 6000 meters), have shorter periods than those caused in the other area of Pacific Ocean.

The cost of this investigation was defrayed from the Scientific Research Expenditure of the Department of Education.

---

28. 土地の脈動の傳播性の研究

（第 4 報）

地震研究所　　池上良平

昭和 25 年 9 月 11 日乃至 16 日，及び 20 日，10 月 5 日乃至 7 日の脈動の傳播方向とその際の天氣圖の示す氣象狀態とを比較した．その結果東京の脈動發生に對しては房總半島以北の海が特に脈動を發生させ易い性質をもつてゐて，ここでは他の場所に於けるより一層弱い低氣壓とか寒冷前線等の通過によつても容易に大きな脈動を發生させる事が確められた．又脈動の傳播速度週期，傳播方向の關係を調べた結果傳播速度と週期の積が常に略々一定の値を保つような性質のある事は既に報告した所であるが，更に傳播方向と週期の間にも顯著な關係がある事が判つた．即ち太平洋岸で房總半島沖より以北の深い海（6000 米以上）に原因があると考へられる場合は週期 4 秒以上の脈動が多く發生し以南の淺い海では 3 秒以下の短週期脈動が多い．云ひかへれば海の深さと脈動の週期との間には密接な關係があるようである。

29. *Geological Investigations on the Zaō Volcanoes*
I. Goshiki-dake, a Central Cone of the Zaō Proper.

By Takeshi ICHIMURA,

Earthquake Research Institute.

(Read March 20, 1951.—Received March 20, 1951)

Introduction

In North-East Japan there are still many volcanoes which have long been neglected with no detailed geological investigation. On such volcanoes as explored by some geologists of the Earthquake Investigation Committee many years ago, some re-examination is requested at present. The same may be said of the Zaō volcanic group where no further investigation has been made since that carried out by A. Takada[1] about 30 years ago. There remains, however, various important geological problems to be confirmed, particularly on its structure and volcanic history as well as on the relationship between it and the Funagata or Azuma volcanoes of the same volcanic zone. For this purpose, the writer recently started his field work in the same district, which is yet to be completed. In the beginning, he studied the geological features of the area including Katta-dake and Goshiki-dake, because the area was the chief active center of the Zaō volcanic group in historic time. Of these, Goshiki-dake is a central cone which was formed within the destroyed crater of this area, being characterized by the repeated explosion which has taken place up to the recent. Since the central cone is deeply dissected along the Osawa as well as around a small crater lake generally called "Okama" it would be very fovorable to learn its internal structure and history of the activity which happened here. It is, therefore, desirable to the writer that the result of the geological investigation on Goshiki-dake is first summarized in this paper.

Location

The Zaō volcanic group rises up in the highly mountainous area between the Prefecture of Yamagata and Miyagi. It is situated approximately at the central part of the area enclosed by the parallels 38°0′ and 38°20′ N, and the meridians 140°15′ and 140°45′ E. Goshiki-dake is found in the explosion crater immediately to the east of Umanose which adjoins Kumano-dake in the north and Katta-dake

---

[1] A. TAKADA, *The Zao Volcanoes, M. S.* 1922.

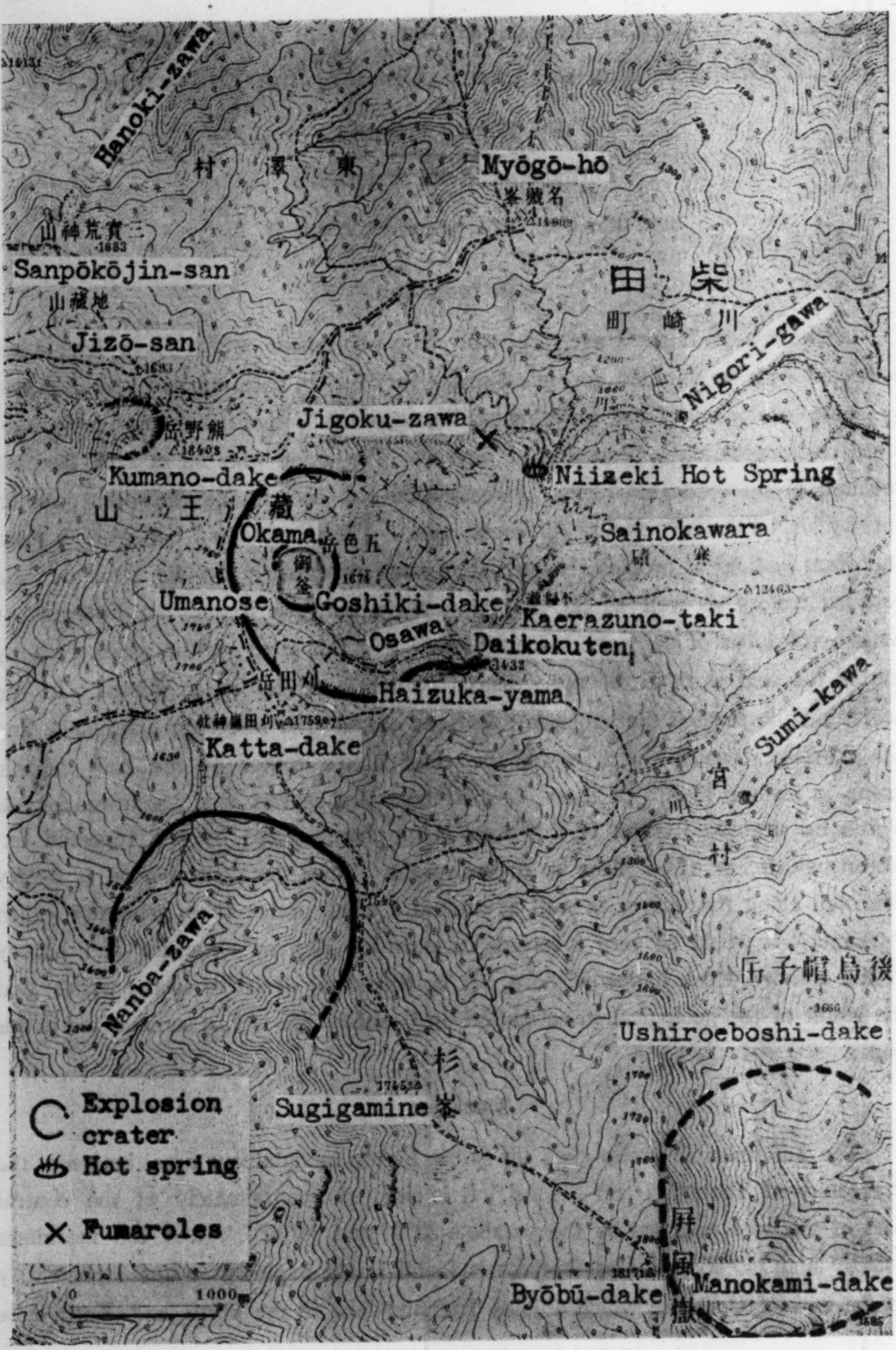
Hanoki-zawa
東澤村
Myōgō-hō
名號峯
Sanpōkōjin-san
Jizō-san
柴田
川崎町
Nigori-gawa
Jigoku-zawa
Niizeki Hot Spring
Kumano-dake
藏王山
Okama
五色岳
御釜
Sainokawara
Umanose
Goshiki-dake
Kaerazuno-taki
Osawa
Daikokuten
Haizuka-yama
刈田岳
Katta-dake
Sumi-kawa
宮川村
Nanba-zawa
後烏帽子岳
Ushiroeboshi-dake
Sugigamine
杉峯
屏風岳
Explosion crater
Hot spring
Fumaroles
0
1000m
Byōbū-dake
Manokami-dake

Fig. 1. Map showing the distribution of explosion craters.

in the south. It is easily accessible from Shiroishi or Ōgawara along the Tōhoku Railway Line and Kaminoyama or Yamagata of the Ōu Railway Line, the former passing through Tōgatta, Aone and Gaga and the latter Ozuzu or Takayu.

General Features of Geology in the Adjacent Area

In the beginning, it is necessary to give a short description of the general features of the surrounding area before the writer proceeds to the geological problems of Goshiki-dake.

The Zaō volcanic group is underlain by the Tertiary formation and granite cut by plagioliparite, basalt, etc. In this case, the Tertiary formation covers the eroded surface of biotite granite or hornblende biotite granite, being mostly composed of green tuff, conglomerate and shale. Of these, conglomerate is found at the bottom of this formation and contains many pebbles of granite, aplite and propylite.

The volcanoes here are topographically divided into two subgroups, north and south, along the Sumi-kawa and Nanba-zawa running respectively northeastwards and southwestwards through the central part of this area. The former includes Kumano-dake (1840.8 m.), Katta-dake (1795 m.), Goshiki-dake (1674 m.), Jizō-san (1694 m.), Sanpōkōjin-san (1683 m.), Torikabuto-yama (1401 m.), Yokokura-yama (1151.9 m.), Nakamaru-yama (1557 m.), Sarukura-yama (873 m.), Ryū-zan (1363.5 m.), etc., whereas the latter consists of Sugigamine (1745.3 m.), Byōbu-dake (1817.3 m.), Ushiroeboshi-dake (1656 m.), Maeeboshi-dake (1402.1 m.), Fubū-zan (1705.3 m.), Nyūdō-san (1600 m.), Manokami-dake (1585 m.), Nonomori-yama (733.3 m.), as well as Aoso-yama or Ōkatta-dake (799.9 m.). They are built up of various kinds of ejecta and lava flows represented mainly by two pyroxene andesite, olivine-bearing two pyroxene andesite, and olivine two pyroxene andesite, forming konides or homates with several explosion craters, large or small. Such explosion craters were sometimes the sources of big mud flows, as can be seen at Takayu and Numa.

The ejecta and lavas are very complicatedly distributed and overlapped, because they erupted repeatedly from many centers. They are also subjected to faulting, a remarkable example being traceable from northeast to southwest along the Hanoki-zawa and the northern scarp of Sanpōkōjin-san.

Some of these rest upon such base rocks as the Tertiary sediments and granites exposed along the Nigori-gawa, Sumi-kawa, Yoko-kawa and Zaō-gawa as well as near Takayu where the latter is not so thickly covered by the former as has hitherto been supposed. Moreover, the writer noticed that some of the lavas and ejecta from Aoso-yama are likely to be underlain by some horizontal beds composed of gravel, sand and clay assigned to the Quarternary.

So far as is known at present the Zaō group seems to have erupted repeatedly even in historic time. Its area is, however, restricted to the Zaō proper[1] which includes Katta-dake, Kumano-dake, Goshiki-dake, Jizō-san and Sanpōkōjin-san, etc. In this case, Goshiki-dake was its active center, and the most recent eruption here took place in 1939.

Large Explosion Crater at the Southern End of North Zaō

There is a large explosion crater at the southern end of North Zaō surrounded by Kumano-dake and Haizuka-yama. (Figs. 4.) The crater is a semicircular hollow with a diameter of about 2 kilometers from northwest to southeast and is opened northeastwards. It was formed by the destruction of a pre-existing crater. Most of its wall is highly cliffed down to the bottom where Goshiki-dake rises up as a central cone characterized by the presence of a small crater lake at its western foot. The Osawa, a branch of the Nigori-gawa, takes its origin here and runs down from east to north, deeply dissecting the eastern or southern foot of the crater wall which is about 200 meters at the highest part.

It is built up of the lavas and ejecta erupted from this pre-existing crater (Fig. 2). Whether younger or older, these volcanic rocks are mainly composed of olivine two pyroxene andesite, agglomerate and lapilli. Of these, the Osawa lava begins to expose itself on the cliff close to Umanose and is traceable down to Daikokuten along the Osawa. The best exposure is seen on the cliff between Haizuka-yama and Daikokuten, where it was intensely subjected to the solfataric action and almost altered into a grey or white rock mottled by a pink or dark grey color. The sulphur-rich part of this rock has once been mined on the steep slope near Daikokuten and also at the bottom of the Osawa.

Younger volcanics rest upon the eroded surface of this older lava, and they erupted mostly from the pre-existing crater as well as from Goshiki-dake. Of these, some of the Kumano-dake lavas and ejecta extend eastwards beyond Goshiki-dake. Exclusive of new ejecta supplied from Goshiki-dake, they are quite free of such alterations as mentioned above. It is, therefore, very easy to distinguish them from the Osawa lava.

The pre-existing crater here seems to have largely been destroyed by explo-

---

1) The term of "Zaō proper" was first used by B. Kotō (B. Kotō, *Jour. Geol. Soc. Japan*, **23** (1926), 34-35).

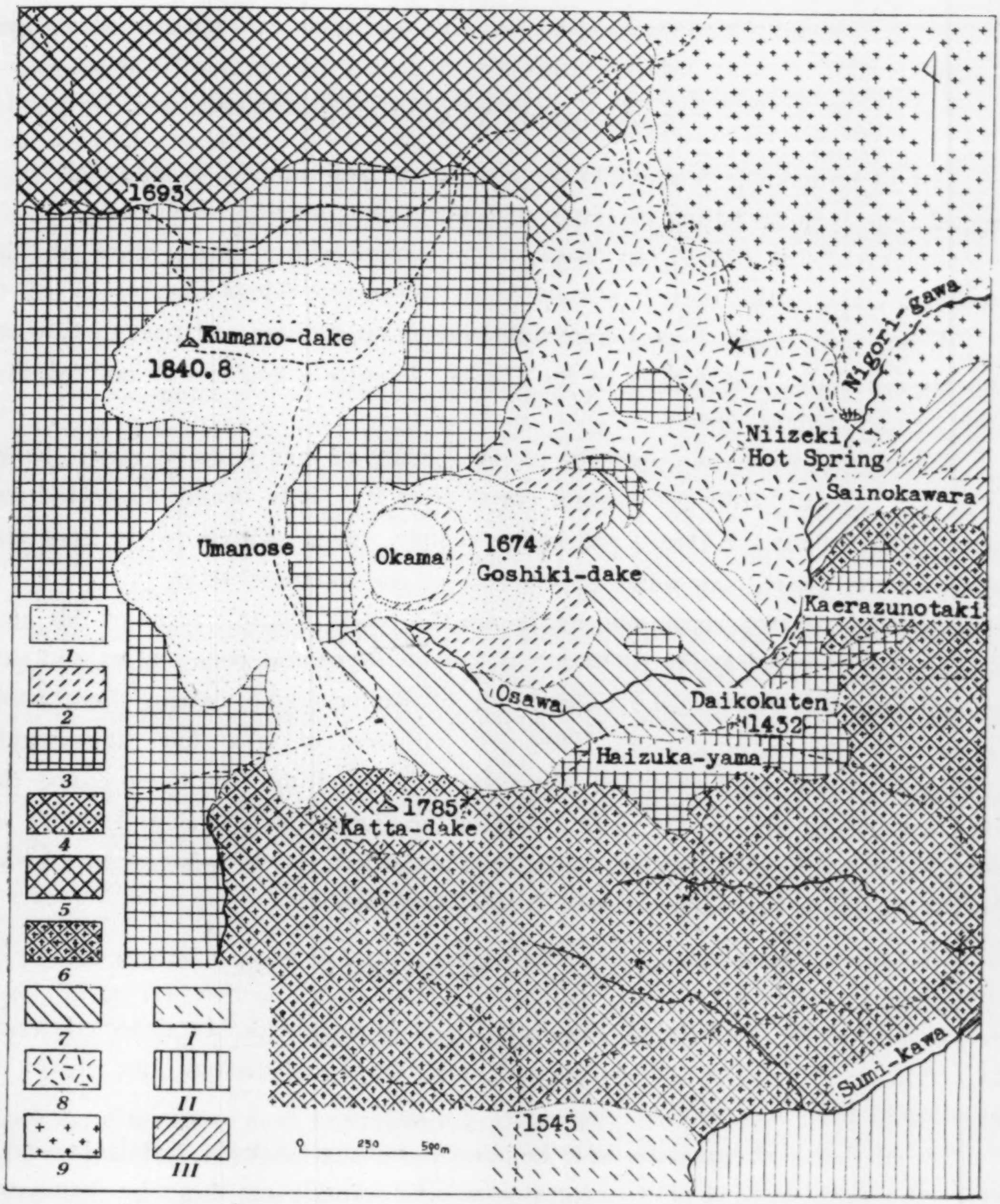
1693
Kumano-dake
1840.8
Umanose
Okama
1674
Goshiki-dake
Niizeki
Hot Spring
Nigori-gawa
Sainokawara
Kaerazunotaki
Osawa
Daikokuten
1432
Haizuka-yama
1785
Katta-dake
Sumi-kawa
1545
1
2
3
4
5
6
7
8
9
I
II
III
0 250 500m

Fig. 2. Geological map of Goshiki-dake and its surrounding area

1. Lapilli and ash (Goshiki-dake), 2. Ash and vol. sand (Goshiki-dake), 3, Kumano-dake lavas (ol. two pyrox. andesite and two pyrox. andesite) and ejecta, 4. Katta-dake lava (ol. two pyrox. andesite), 5. Jizō-san lava (ol. two pyrox. andesite), 6. Nanba-zawa lava (ol. bearing two pyrox. andesite) and ejecta, 7. Osawa lava (two pyrox. andesite), 8. Jigoku-zawa lavas and ejecta, 9. Biotite granite and hornblende biotite granite.

I. Sugigamine lava (ol. two pyrox. andesite), II. Byōbu-dake lava (ol. two pyrox. andesite), III. Sumi-kawa lava (ol. bearing two pyrox. andesite).

tion of the Kumano-dake lavas and ejecta, but the date can not be determined exactly.

Formation of Goshiki-dake

One of remarkable features in the area of the Zaō proper is indicated by a central cone built up within the large explosion crater already mentioned.

Goshiki-dake is a small but characteristic homate with a gentle slope and an explosion crater which opened westwards at the opposite side of Umanose (Figs. 4-7). It has a diameter of more than 1,000 meters at its base and rises up to about 200 meters above the bottom of the Osawa, forming a double volcano together with its surrounding somma.

This central cone rests upon the eroded surface of lava flows or ejecta which have their sources in the pre-existing crater (Fig. 2). It is deeply disseceted and highly cliffed along the Osawa and in the vicinity, being skirted by a large exposure of the Osama lava subjected intensely to the solfataric action.

The Jigoku-zawa lavas and ejecta are the oldest volcanic rocks of this area and are well exposed at the northeastern foot of the central cone and extend east or northeastwards down to the eastern foot of Kumano-dake, where these rocks are underlain by biotite granite. They are composed of lava flow, agglomerate and lapilli as well as of sand and ash alternately piled up. In these cases, the the Osawa lava rests directly upon a part of the Jigoku-zawa lavas and ejecta as can be seen on the cliff between Daikokuten and Kaerazuno-taki, but is capped with the Kumano-dake lava at the eastern foot of Goshiki-dake.

Structure of Goshiki-dake

As has already been stated, the central cone is so remarkably dissected along the Osawa as well as around Okama that its structure and geology can easily be investigated here and there.

One of the good exposures is to be seen at the opposite side of Haizuka-yama, where the southern flank of the central cone was abruptly cut down by the Osawa and formed a cliff about 70 meters in height. The beds of ash, sand and lapilli exposed on this cliff are well stratified and incline to the west at an angle of 10°-15° (Fig. 4). They are alternately accumulated with no intercalation of lava flows, showing various colors such as grey, brown, dark brown, dark reddish brown, etc. A similar bed is also exposed widely on the crater wall surrounding Okama. The crater wall here is about 50 meters high at its eastern side and gradually diminishes its height westwards. It is intricately colored from brown to dark reddish brown in good contrast with the beautiful color of lake water. Besides ash and sand beds distorted from place to place, there are agglomerate and scoria layers, 1 meter or thereabouts in thickness, at the top of the wall.

The surface of the cental cone is largely veiled with recent ejecta. Most of these are lapilli and are thinly accumulated, excluding the western periphery of Okama, where they are five meters in the thickest part.

Explosion Crater, "Okama"

An explosion crater, which is now filled up with water, is found at the western side of Goshiki-dake (Figs. 6, 7). It is called "Okama" or "Goshiki-numa" or "Zaō-numa" and has a nearly circular from with a diameter of about 300 meters. This small lake is surrounded by a highly cliffed wall at its eastern half, where thickly accumulated ejecta are well exposed showing various colors differing from place to place.

So far as is known at present, its bottom is deep at the east but shallow at the west. The picture taken by H. Minato in June of 1944 shows that there was still a bar near the western wall, stretching from north to south across the lake. The lake seems to be getting buried year by year by rock fragments crumbling down from the crater wall. It was once, however, 63 meters in depth, when a small explosion took place in 1939.

Volcanic Ejecta of Goshiki-dake

The central cone is built up of such ejecta as agglomerate, lapilli, sand and ash which are well stratified and have varying colors. Of these. agglomerate is exposed on the northern cliff as well as at its opposite side. It is only 1 meter or thereabouts in thickness and contains angular or subangular fragments of two pyroxene andesite, 1-15 centimeters in diameter.

There are two kinds of these fragments. One is black and compact andesite, whereas the other is a scoriaceous variety with the same color. They have a porphyritic texture. The mineral ingredients of the compact specimens are labradorite, bytownite, augite, hypersthene, magnetite and brown glass.

Under the microscope, such phenocrystic minerals as labradorite, bytownite, augite and hypersthene are abundantly found in the groundmass with a hyalopilitic or pilotaxitic texture. In this case, labradorite or bytownite has a fresh appearance and is well zoned. It is often characterized by the presence of turbid zone, including minute crystals of augite, hypersthene, magnetite and patches of brown glass. These turbid zones and inclosures generally indicate a regular arrangement parallel to the outline of crystals. The crystal mostly takes an anhedral or subhedral form, 2.97 mm.×1.36 mm. in the maximum size.

The phenocrysts of augite and hypersthene are present in almost same amount. They are usually anhedral or subhedral and include magnetite, labradorite, bytownite and brown glass. These minerals are respectively 1.65mm.×1.61mm. (augite) and 2.47 mm.×1.02 mm. (hypersthene) in the maximum size.

The optical characters of phenocrystic minerals are summarized in the following table.

	No. 1 (T. I., 48092201)	No. 2 (T. I., 48092204)
Plagioclase	An_{64-78}	An_{66-77}
Augite	$\beta_D = 1.692 \pm 0.002$ $2V = 50°$ $c \wedge Z = 40°$ $Ca_{41}Mg_{41}Fe_{18}$ (atom.%)	$\beta_D = 1.693 \pm 0.002$ $2V = 48°$ $Ca_{40}Mg_{41}Fe_{19}$ (atom.%)
Hypersthene	$\alpha_D = 1.688 \pm 0.002$ $\beta_D = 1.699 \pm 0.002$ $\gamma_D = 1.703 \pm 0.002$ $\gamma - \alpha = 0.015$ $(-)\ 2V = 58°$ $\rho > \upsilon$ about X $Mg_{73}Fe_{27}$ (atom. %)	$\alpha_D = 1.988 \pm 0.002$ $\beta_D = 1.700 \pm 0.002$ $\gamma_D = 1.703 \pm 0.002$ $\gamma - \alpha = 0.015$ $(-)\ 2V = 56°$ $\rho > \upsilon$ about X $Mg_{72}Fe_{28}$ (atom. %)

The optical properties of augite and hypersthene in this table were mainly investigated by R. Morimoto and F. Hori. Of these, indices of refraction were determined by Hori. To confirm 2V and the composition of augite and hypersthene the charts devised by H. H. Hess[1)] and G. C. Kennedy[2)] were respectively used.

The groundmass is composed of bytownite, augite, hypersthene, magnetite and glass.

Such mineral components as mentioned above are also to be seen in the scoriaceous variety.

---

1) H. H. HESS, *Amer. Min.*, **34** (1949), 634.

2) G. C. KENNEDY, *Amer. Min.*, **32** (1947), 564.

Sand and ash are the most important ejecta of this area, being well exposed on the cliff and the summit. They consist of plagioclase, augite, hypersthene, magnetite as well as of tuffaceous substance and minute fragments of two pyroxene andesite.

Recent ejecta are widely accumulated on the surface of the central cone and its surrounding area. The occurrence of such ejecta can easily be recognized at a distance, because the area has a white or grey color similar to that of the intensely altered Osawa lava. They are composed of ash and lapilli. The latter is represented by angular fragments of two pyroxene andesite, commonly 0.5 cm.—5 cm. in diameter. Most of these fragments have a light grey color, but there are frequently porous or compact andesites with a dark grey or grey color. Light grey or grey colored fragments are intensely subjected to the solfataric action and are reprensented by opalized andesites. This fact suggests that some of these have undoubtedly been teared off from the altered Osawa lava in the explosion of this central cone.

Fumaroles Formed in Association with the Recent Eruption of the Central Cone

Several small fumaroles are found on the slope near the entrance of the Jigoku-zawa tending eastwards from Kumano-dake, being situated about 2 kilometers northeast from the summit of Goshiki-dake and are accessible from the junction of trails for Kumano-dake and Hōzawa as well as from the Niizeki hot spring resort which is now desolate.

They are opened in the granite near the high cliff of volcanic rocks exposed on the slope about 100 meters above the valley bottom, emitting superheated steam with a minor amount of SO_2 (Fig. 3). The activity of these fumaroles started in the middle of April, 1940 after a small eruption took place within the crater of Goshiki-dake. In the beginning, it is said that they have

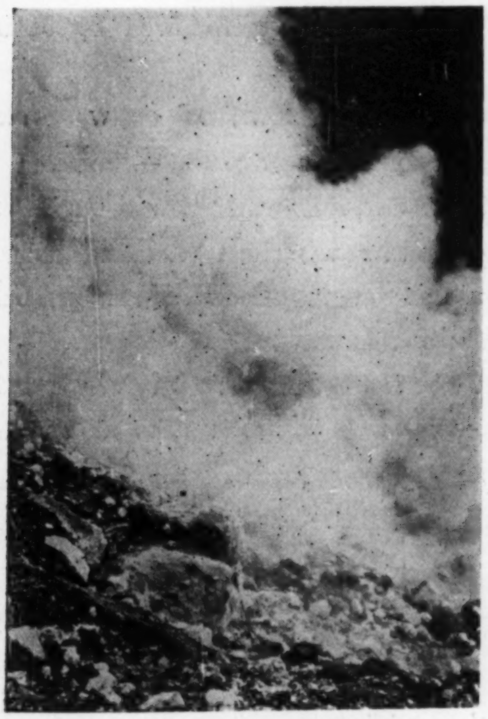

Fig. 3. Fumaroles on the slope about 1500 meters northeast from Goshiki-dake.

intensely exhaled poisonous gases here and there. The fumaroles show, even at present, a temperature of about 90°C at their mouth, where they are beautifully adorned with sulphur incrustation. The ground near the fumaroles is remarkably altered by solfataric action and is traversed by small fissures out of which hot sulphur spring is abundantly flowing out. The surface of the ground is thinly veiled with sulphur and halotrichite.

Volcanic Activities in Historic Time

It is unknown how many times volcanic activity took place in the area of Goshiki-dake since its first eruption. This may be also said of the volcanic activities in historic time, because it is partly obscured by insufficient data.

So far as is shown by the historic records compiled by F. Ōmori¹⁾ T. Kochibe²⁾ and T. Anzai³⁾, it took place in 884, 1230, 1331–1333, 1623 (May), 1624, 1669, 1821 (January 27). 1867 (October 21), 1873 (August—September), 1894 (July 3), 1895 (February 15, August 22 and September 27), 1897 (January 14), 1906 (?), 1918 (January—August), 1927 and 1939. They are mostly of little importance, but several of them requires a short description here.

(i) The activity in 1624, according to a local tradition, seems to have started with a rumbling noise which continued day and night, being followed by some minor explosions.

(ii) In 1669, a large amount of volcanic ashes was blown off eastwards to Shibata-gun and Katta-gun, where it caused a serious damage to the farming.

(iii) When the explosion took place in 1821, a muddy water flowed out from Okama down to the Nigori-gawa. It was preceded by a sudden rumbling noise. The lower course including the Shiroishi-gawa was thus visited by inundation, but fortunately no harm was done to men or beasts at that time.

(iv) A similar accident was repeated on October 21, 1867. An unexpected inundation due to the overflow of muddy water from Okama took place along the Nigori-gawa and killed three men who had stayed to take bath in the hot spring near the eastern foot of Goshiki-dake, In this case, the river rose more than 6 meters.

The exhalation of steam and occasional emission of black smoke lasted to rise

---

1) F. OMORI, *Rep. Earthq. Inv. Comm.*, **86** (1918), 150–153.
   〃 , *Tōyōgakugeizasshi*, **35** (1918), 565–574.

2) T. KOCHIBE, *Geol. Mem. Geol. Surv.*, **1** (1896), 23–32.

3) Personal communication by T. ANZAI.

up from Okama for several months even after the explosion ceased.

(v) On February 15, 1895, Okama broke out in a remarkable explosion soon after a rumbling noise took place. It was 9.30 in the morning, when the weather was exceedingly fine. In this volcanic activity, ash, lapilli and scoria were abundantly blown off northeastwards. As has repeatedly been indicated in previous explosions, the muddy water overflowed from Okama rushed down along the Matsukawa and Shiroishi-gawa, where many fishes were killed by the poisonous water.

An inundation due to the explosion of Okama also happened on September 27 of the same year and caused considerable damage to the district mentioned above. As a result of the explosion in 1895, the volcanic products thrown out from Okama accumulated extensively on the slope of the central cone and its surrounding area.

(vi) The most recent activity is represented by that which took place in 1939. Anzai[1] states that the water of Okama presented an extraordinary sight in July. According to his observation, the green colored water here was first mottled with many white spots due to the presence of innumerable sulphur grains which came up from the bottom. These grains had a hollow structure and are 1 millimeter or thereabouts in diameter.

When the lake changed its color, the temperature of water was 25°C on the surface, but 128°C at the bottom. Moreover, Okama increased its depth to 63 meters in October.

In connection with this volcanic activity, several fumaroles opened on the slope situated about 1.5 kilometers northeast from Okama. They were formed in the middle of April, 1940 and exhaled some poisonous gases which once rised to 100 meters in height. Simultaneously, the activity of some fumaroles started near the high cliff called "Keisei-iwa" at the bottom of the Zaō-gawa. Poisonous gases emitted here were SO_2 or H_2S and killed animals, birds and insects. The exhalation of these gases, however, has almost ceased at present.

Summary

(i) Goshiki-dake is a central cone of the Zaō proper and rises up to 1674 meter above the sea level. It is formed within the semi-circular explosion crater surrounded by Kumano-dake, Umanose, Katta-dake and Haizuka-yama.

(ii) This central cone rests upon the eroded surface of lava flows and ejecta which have their sources in the pre-existing crater destroyed largely by later ex-

---

1) Personal Communication by T. ANZAI.

plosions, being deeply dissected and highly cliffed along the Osawa and at the eastern side of Okama. It has a diameter of more than 1000 meters at its base and is about 200 meters high above the bottom of the Osawa.

(iii) The central cone is chracterized by the presence of explosion crater-called generally "Okama" which is found at its western side. It is a nearly circular depression about 300 meters in diameter, being now filled with beautifully-colored water.

(iv) The internal structure is well shown along the crater wall and high cliff dissected deeply by the Osawa. The cone is built up of ash, sand, lapilli and agglomerate which are distinctly stratified and incline to the west at an angle of 10°—15°. They have accumulated alternately with no intercalation of lava flows. The surface of the central cone and its surrounding area are largely veiled with recent ejecta thrown out from Okama. They are composed of ash and lapilli, the prevailing color being light grey or grey.

(v) Volcanic sand and ash here consist of plagioclase, augite, hypersthene and magnetite as well as of tuffaceous substances and minute fragments of two pyroxene andesite. The recent lapilli is, however, represented by two pyroxene andesite subjected mostly to solfataric action. Agglomerate contains angular or subangular fragments of two pyroxene andesite with such component minerals as labradorite, bytownite, augite, hypersthene, magnetite and brown glass.

(vi) The volcanic activities of the central cone are recorded since 884. The most recent one took place in 1939. So far as is shown by historic records, these activities always took place in Okama, and the explosion was frequently followed by the inundation of lake water which caused a serious damage to the district along the Nigori-gawa, Matsu-kawa, Shiroishi-gawa, etc. The fumaroles newly opened in 1940 are still active at present, their exhalation being composed mainly of superheated steam with a small amount of SO_2.

In conclusion, the writer's thanks are due to Dr. H. Tsuya who allowed him to continue his work in the Earthquake Research Institute of Tokyo University. The writer is also deeply indebted to Mr. R. Morimoto and Mr. F. Hori for their co-operation in his laboratory work.

The expense of this research was defrayed from the fund for the Scientific Research of the Educational Ministry.

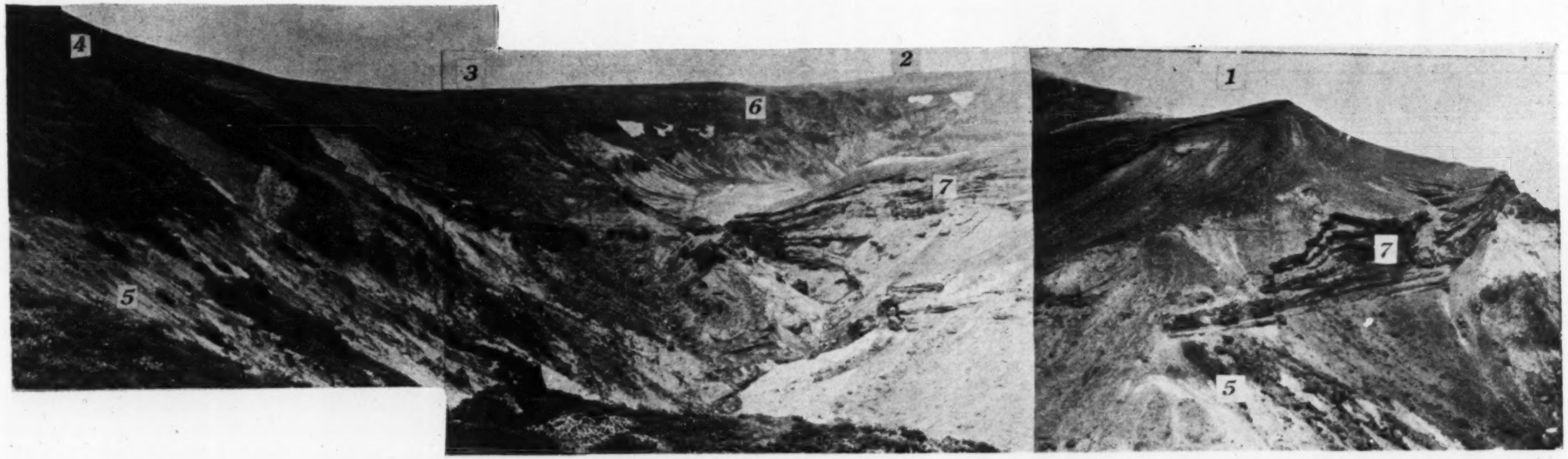

Fig. 4. Goshiki-dake viewed from the cliff between Katta-dake and Haizuka-yama. It is highly cliffed along the Osawa, being surrounded by a large explosion crater which extends to Kumano-dake in the north and Haizuka-yama in the south.

1 = Goshiki-dake, *2* = Kumano-dake, *3* = Umanose, *4* = Katta-dake,
5 = Osawa lava, *6* = Kumano-dake lavas and ejecta, *7* = Ash and volcanic sand.

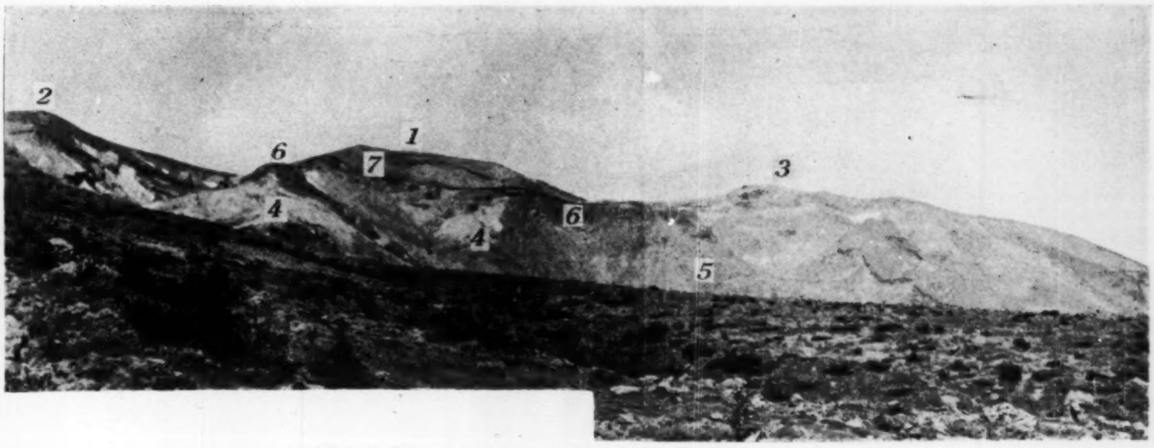

Fig. 5. Goshiki-dake viewed from the hill between Atomizaka and Daikokuten.
1 = Goshiki-dake, *2* = Katta-dake, *3* = Kumano-dake, *4* = Osawa lava,
5 = Jigoku-zawa lavas and ejecta, *6* = Kumano-dake lava,
7 = Ash and volcanic sand from Goshiki-dake.

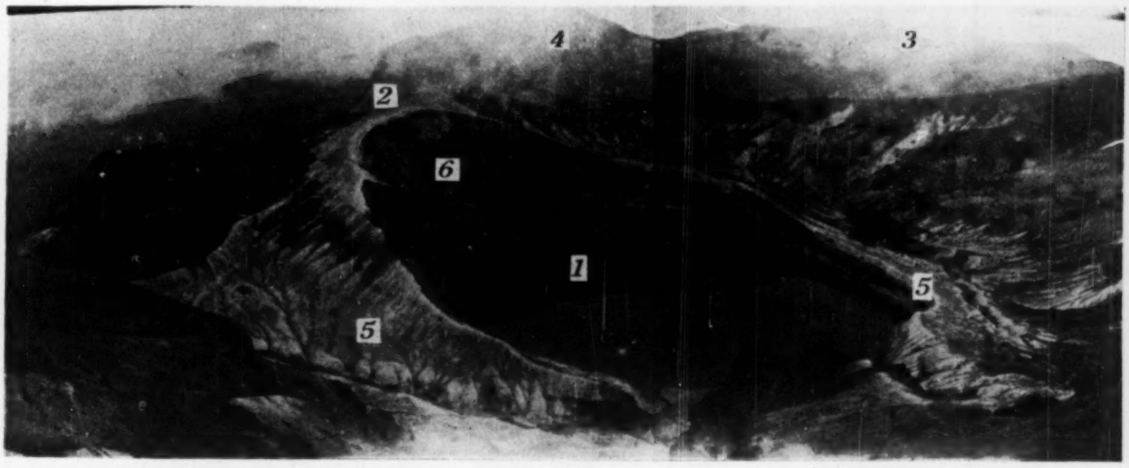

Fig. 6. Goshiki-dake and its explosion crater called generally "Okama" viewed from Kumano-dake.
1 = Okama, *2* = Goshiki-dake, *3* = Byōbu-dake, *4* = Ushiroeboshi-dake,
5 = Recent lapilli and ash, *6* = Ash and volcanic sand.

（震研彙報 第二十九號 圖版 市村）

[illegible]

[illegible] the hill between [illegible] and [illegible]
[illegible]
[illegible]
[illegible]

[illegible]
[illegible]
[illegible]
[illegible]

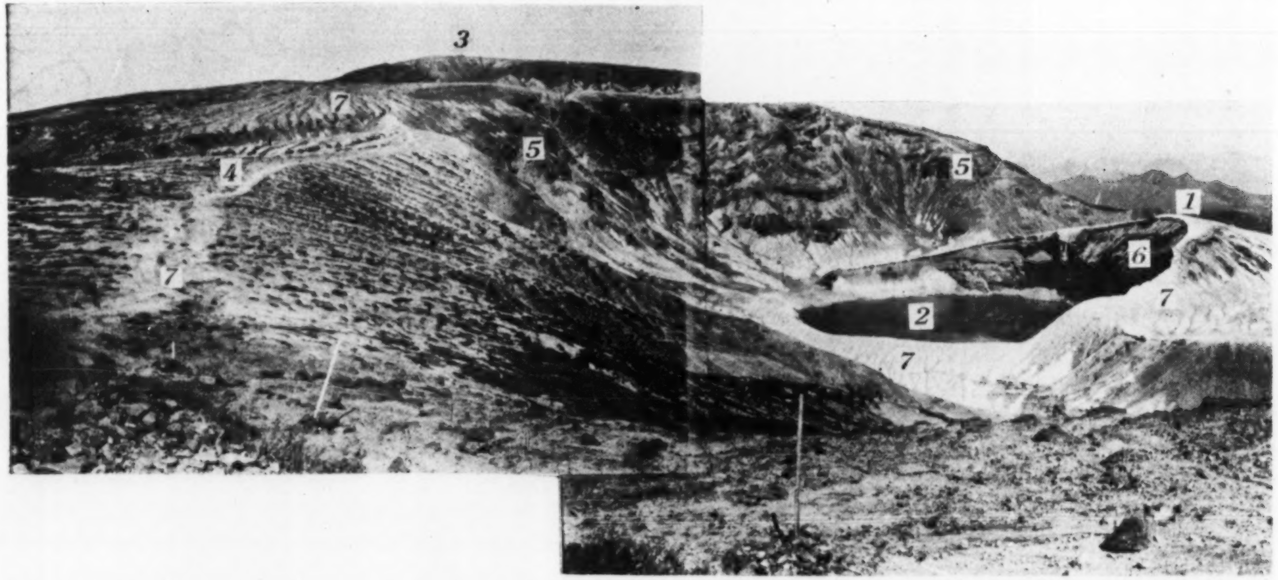

Fig. 7. Goshiki-dake and its explosion crater, "Okama", viewed from the summit of Katta-dake.

1 = Goshiki-dake, *2* = Okama, *3* = Kumano-dake, *4* = Umanose,
5 = Kumano-dake lava, *6* = Ash and volcanic sand, *7* = Recent lapilli and ash.

The surface of Goshiki-dake, Umanose and Kumano-dake is thinly covered with recent lapilli and ash from Goshiki-dake.

29. 藏王火山の地質學的研究（第 1 報）

地震研究所　市村毅

藏王火山に關する地質學的研究の結果を報告するに當り，先づその中心に位する五色岳から始めて逐次他の部分に及ぶことにした．

五色岳は藏王火山群の中でも最も新しい火山であり，所謂馬ノ脊大爆裂火口の内部に生じた中央火口丘である．少くとも有史以後の活動は皆此火口丘を中心として行われ，その活動は最近にまで及んでいる．新しい火山なのにも拘らず，開析の程度が著しいために，火山の構造が御澤と御釜の緣に沿うて明かに認められる．從つて藏王火山に登る人々にとつては御釜爆裂火口の存在と共に此場所が最も興味を覺える處である．本文には此五色岳を取卷く馬ノ脊大爆裂火口，五色岳の生成及其地質構造，御釜爆裂火口，五色岳を構成する火山噴出物，最近の活動に際して生じた噴氣孔，五色岳の活動等に關する事項が纏められている．

30. *Augite and Hypersthene Crystals from the Zaō Volcanoes.*

By Takeshi ICHIMURA, Earthquake Research Institute
and
Hideo MINATO, Institute of Earth Science, Tokyo University.

(Read March 20, 1951.—Received March 20, 1951)

Introduction

The augite crystals from Sainokawara of the Zaō volcanoes are generally characterized by their elongated prismatic habits like hornblende or hypersthene. This unusual crystal habit has already been noticed by one of the writers (Ichimura) since 1914, when he first obtained some specimens from one of his colleagues who had collected them at the locality mentioned above. The mineral, however, has long been neglected without any detailed investigation made into it up to the present.

In the summer of 1950, the writers were given an opportunity to carry out their field work together on this volcanic area. At that time, they collected many specimens from several places between the Gaga hot spring and Katta-dake, where two pyroxene andesite, olivine-bearing two pyroxene andesite and olivine two pyroxene andesite as well as agglomerate are extensively exposed. Moreover, it is very noteworthy that some small but very beautiful specimens of hypersthene were obtained together with specimens of augite at Sainokawara. They were mineralogically investigated by the writers, and many new faces were found by Minato.

The results of these investigations are summarized in this paper.

Occurrence.

Augite crystals are abundantly found together with those of hypersthene in the extensive area of Sainokawara and also on the summit of Haizuka-yama. These localities are situated nearly at the central part of the Zaō volcanoes and are easily accessible from the Shiroishi or Ōgawara station of the Tōhoku Railway Line, passing through the Gaga hot spring resort and Tōgatta as well as through Aone (Fig. 1).

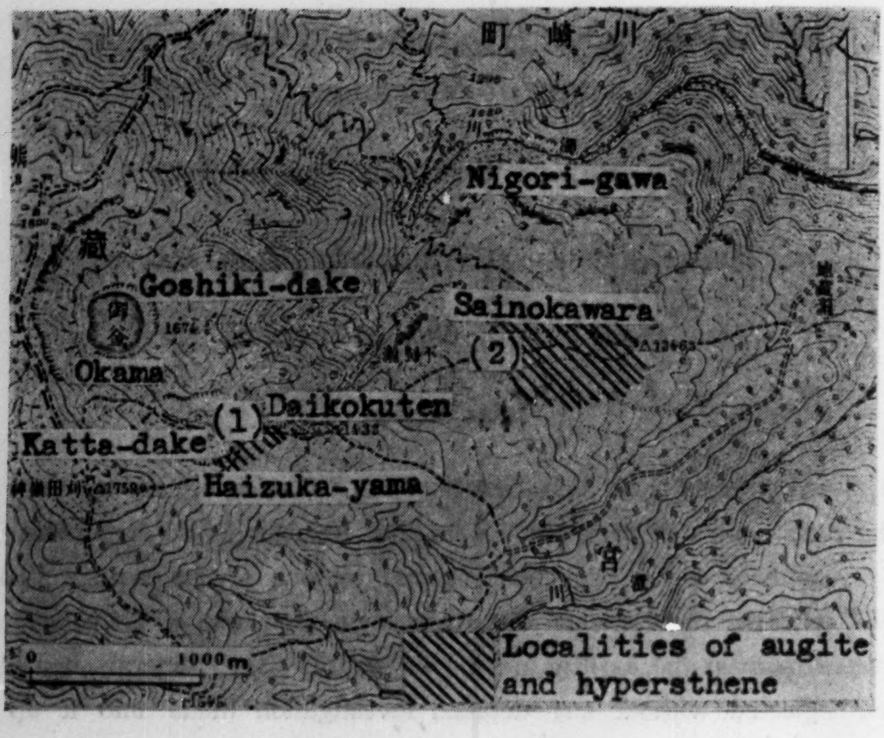
川崎町
Nigori-gawa
蔵
Goshiki-dake
Sainokawara
Okama
1674
(2)
(1)
Daikokuten
1432
Katta-dake
1759
Haizuka-yama
0
1000m
▨ Localities of augite and hypersthene

Fig. 1. Map showing the localities of augite and hypersthene on the Zaō volcanoes.
(1) Locality of Augite. (2) Locality of augite and hypersthene.

The mother rocks of augite and hypersthene under consideration are two pyroxene andesite and agglomerate. When these rocks are intensely subjected to weathering, they usually disintegrate into loose sandy or pebbly substances, isolating their component minerals on the surface. Augite or hypersthene crystals detached from their mother rorks in this way are often washed out and sorted by the rain water to be gathered into the depressions of the ground or its gently sloping surface. Under a favorable condition, many well-formed crystals can easily be picked up in a little while.

(1) Of the two localities mentioned above, Sainokawara is a monotonous and barren table land which slopes very gently eastwards or northeastwards, and it is abruptly cut down by the Nigori-gawa. It is almost built up of the Sumi-kawa lava (olivine-bearing two pyroxene andesite), being partly or thinly covered with erosion remnants of agglomerate corresponding to the basal part of the Nanba-zawa lava (olivine-bearing two pyroxene andesite). Augit and hypersthene crystals here are thus obtained from the disintegrated products (sands and gravels) of this agglomerate.

(2) A similar condition is also seen on Haizuka-yama which adjoins the Katta-dake northwestwards and forms the northern wall of the Umanose explosion crater along the Osawa. The volcanics of this place are two pyroxene andesite and agglomerate as well as sand and ash. These rocks may belong to the Kumano-dake lavas and ejecta.

Two pyroxene andesite is a compact or porous rock with a black color in fresh specimens, but assumes a dark brown or reddish brown color in weathering and gradually disintegrates into loose sands. This rock is characterized by an abundance of large phenocrystic augite which occasionally project out on the weathered surface.

Agglomerate, sand and ash accumulated on the andesite lava show a distinct stratification. In this case, agglomerate contains augite crystals smaller than those of andesite lava. Isolated good specimen of this mineral are abundantly found on the ground where the disintegration changed mother rocks into sandy materials.

Crystal Forms

Augite crystals collected from Sainokawara and Haizuka-yama are generally characterized by an elongated crystal habit like that of hypersthene. It is, therefore, difficult to distinguished the minerals from one another without examining their thin sections, when they are found together as small crystals. Moreover, large augite crystals subjected to weathering are so spoiled that their angles are mostly unmeasurable. This can also be said of hypersthene crystals. Hence, the writers had to select small but well-formed specimens with a fresh appearance for this purpose. The morphological investigation of these crystals were chiefly carried out by one of the writers (Minato).

(1) Augite: Augite crystals obtained from two localities mentioned above are usually 5-15 mm. long and 1-7 mm. across, indicating that small specimens have a tendency to be nice crystals bounded by well arranged faces. Accordingly, the crystals, 5-7mm. long, were mostly subjected to the goniometric experiment. It was also confirmed that there is no morphological difference between smaller or larger crystals. The measurement of angles are carried out by using the B-type of V. Goldschmidt's two-circle goniometer. In this case, six well-formed crystals were measured, and the occurrence of the following faces was confirmed.

E (520), g (210), D (320), m (110), Y̊ (350), a (100), b (010), e (011), z (021), u (111), μ (121), C (352), X (432), V (332), s $(\bar{1}11)$, x $(\bar{2}21)$, j $(\bar{5}22)$, 𝔥 $(\bar{4}32)$, Z $(\bar{4}11)$, B $(\bar{5}52)$, 𝔈 $(\bar{3}52)$, ℭ (102), c (001).

Of these, faces as E (520), D (320), C (352), X (452), V (332), j $(\bar{5}22)$, 𝔥$(\bar{4}32)$, Z $(\bar{4}11)$, B $(\bar{5}52)$, 𝔈 $(\bar{3}52)$ and ℭ (102) were newly found in the specimens from this area. The results of goniometric experiments for four faces indicated by (352), $(\bar{4}11)$, $(\bar{5}52)$ and $(\bar{3}52)$, however, may be not so accurate. Of the six speccimens measured, two are differently twinned, whereas the remaining four are represented by single crystals.

The angles measured for augite are shown in the following table.

Table I. Angle table for augite from the Zaō volcanoes.

Form	Measured		Calculated*		Number of faces measured
	ρ	φ	ρ	φ	
E (520)	90°00′	67°15′	90°00′	67°11	1
g (210)	″	62 59	″	62 55	2
D (320)	″	54 10	″	54 58	1
m (110)	90 02	43 41	″	43 33	20
Y (350)	90 00	28 05	″	29 42	1
a (100)	″	90 02	″	90 00	12
b (010)	89 59	0 02	″	0 00	10
e (011)	33 07	25 11	33 11	25 43	4
z (021)	50 10	13 29	50 29	13 32	7
μ (121)	54 52	35 15	55 19	35 15	6
X (432)	56 31	56 13	58 56	57 49	2
s $(\bar{1}11)$	33 15	-25 00	33 04	-25 07	16
x $(\bar{2}21)$	55 22	-35 12	55 19	-35 22	8

*Calculated angles were obtained from V. Goldschmidt's "Winkeltabelen."

(520), (320) and (432) were calculated from the axial ratio and β. ($a:b:c = 1.0934:1:0.5894$; $\beta = 105°51'$)

(1) Single crystals:—Most of the single crystals are long or short prismatic in habit, being bounded by such faces as a(100), b(010), m(110) and s$(\bar{1}11)$ (Figs. 2-5). One of their characteristic features is the presence of several pyramids which are well grown at the terminals of these crystals.

(2) Twin crystals:—Two kinds of twin crystals are known in these specimens. One of them is the crystal with a(100) as the twinning plane (Figs. 6-7). It is the commonest type of twinning in augite crystals.

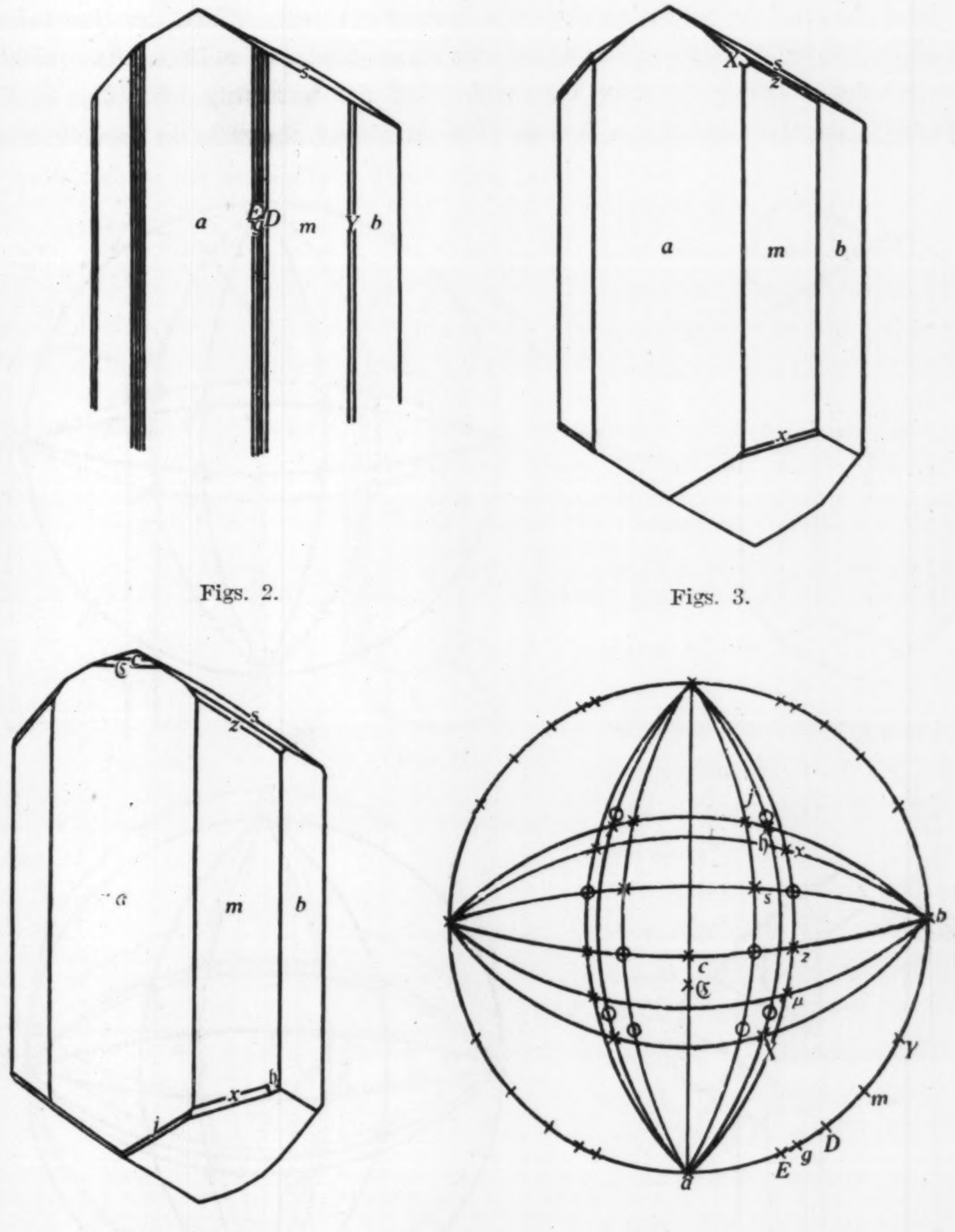
s
a
D
m
Y
b
X
s
z
a
m
b
x
c
ℭ
z
s
a
m
b
x
h
i
j
h
x
s
b
z
c
ℭ
μ
Y
m
D
g
E
a

Figs. 2.

Figs. 3.

Figs. 4.

Figs. 5.

Figs. 2–5. Augite crystals from the Zaō volcanoes.

The twinning plane of another type is supposed as w$(\bar{1}22)$. In this twinning, two individuals cross each other at an angle of nearly 60° (Figs. 6–9). It is proved by an angle of ρ (59°29′) that the twinning plane is $(\bar{1}22)$. This condition, however can be understood by supposing that two individuals with a(100) as the twinning plane rotate 60° about the twinning axis perpendicular to a(100). As a method of expression, this may be more reasonable than the possibility of $(\bar{1}22)$ as the twinning plane, because such a face as $(\bar{1}22)$ is almost absent in the common types

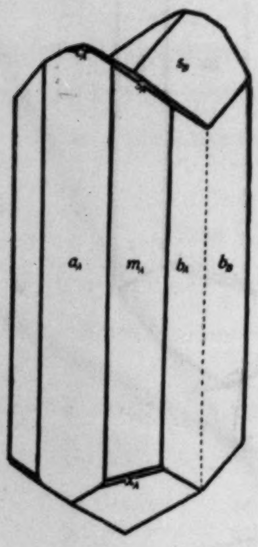
s_B
a_A
m_A
b_A
b_B

Fig. 6.

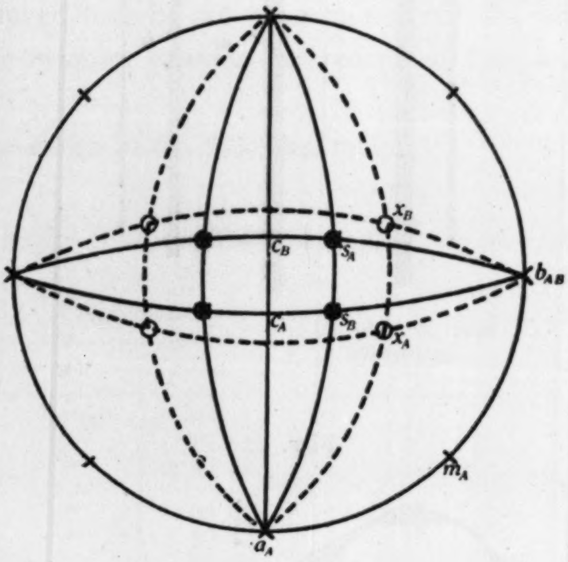
x_B
c_B
s_A
b_AB
c_A
s_B
x_A
m_A
a_A

Fig. 7.

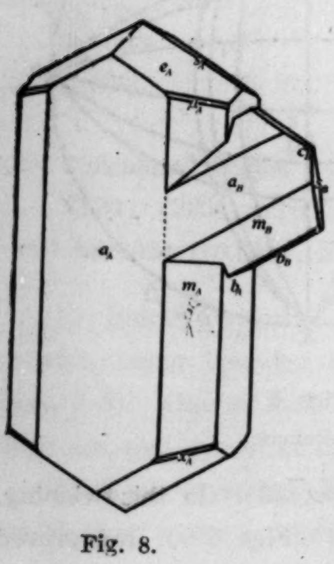
e_A
a_B
m_B
b_B
a_A
m_A
b_A
x_A

Fig. 8.

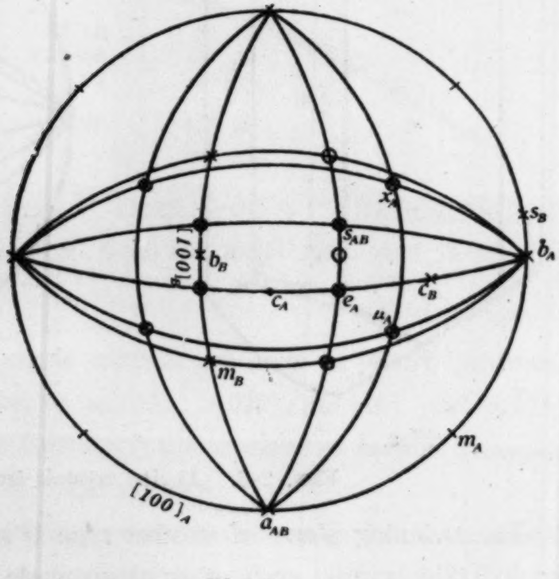
x_A
s_B
S_AB
b_A
[001]
b_B
c_A
e_A
c_B
u_A
m_B
m_A
[100]_A
a_AB

Fig. 9.

Figs. 6–9. Twin crystals of augite from the Zaō volcanoes.

of augite crystals. This opinion has already been proposed by N. Katayama.¹⁾

(2) Hypersthene:—Small hypersthene crystals were collected from Sainokawara, where they are largely distributed together with augite crystals in loose sands derived from weathered agglomerates. They are sometimes found as beautiful crystals, which are generally 2-3 mm. long and 0,5-1 mm. across. Most of these crystals have a fresh appearance and their angles are, therefore, quite measurable. Hence, they were easily and accurately measured as compared with the augite crystals, and ten faces were found as follow (Figs. 10-12).

λ(250), n(120), Y(530), m(110), β(320), z(210), a(100), b(010), e (212), i (211). Of these, Y(530) is a new face determined on the crystals from Sainokawara. Crystallographically speaking, b(010) is the largest face of all, and the next is followed by a(100). They have a long prismatic habit and are somewhat flattened along the b-axis. Both terminals of prismatic crystals are cut by eight pyramids corresponding to e(212). Besides this, the occurrence of some small subordinate faces are known in most of specimens. The angles measured for hypersthene are indicated in the following table.

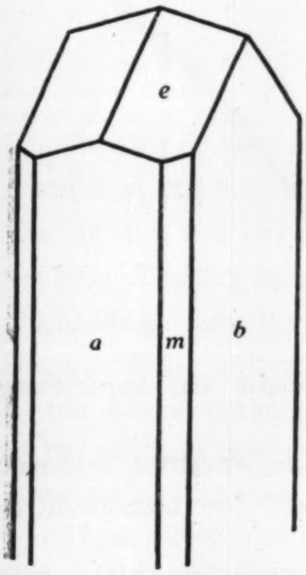

Fig. 10.

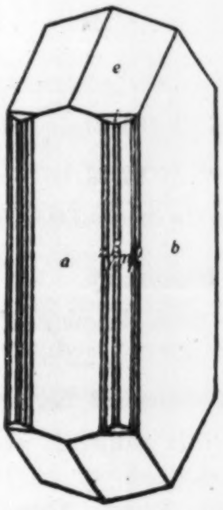

Fig. 11.

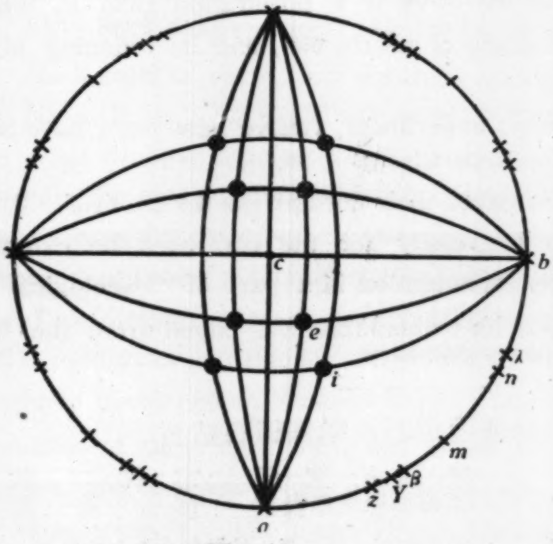

Fig. 12.

Fig. 10-12. Hypersthene crystals from the Zaō volcanoes.

---

(1) T. Itō, *Beitrage zur Mineralogie von Japan, Neue Folge* I (1935), 133-140.

Table II. Angle table for hypersthene from the Zaō volcanoes.

From	Measured		Calculated*		Number of faces measured
	ρ	φ	ρ	φ	
λ (250)	90°00′	21°17′	90°00′	22°23′	2
n (120)	〃	26 56	〃	27 14	1
m(110)	〃	45 42	〃	45 50	8
β (320)	〃	57 54	〃	57 05	1
Y (530)	〃	60 54	〃	60 20	2
z (210)	〃	66 09	〃	64 07	1
a (100)	〃	−0 01	〃	0 00	4
b (010)	〃	90 01	〃	90 00	4
e (212)	33 14	64 46	33 09	64 07	12
i (211)	51 55	63 52	52 33	〃	8

* Culculated from the axial ratio (a:b:c=0.97133:1:0.57037).

Summary

(1) No description has hitherto been known of the augite and hypersthene crystals from Zaō volcanoes.

(2) Most of the augite crystals collected here have an elongated prismatic habit. It is an unusual form for this mineral which looks like hornblende or hypersthene at a glance.

(3) Two types of twinning are found. One of these is the crystal with a(100) as the twinning plane, whereas the other is a penetration twin in which two individuals cross each other at an angle of nearly 60°, and its twinning plane is supposed to be $W(\bar{1}22)$.

(4) As the result of the goniometric experiment, twelve new faces have been found for augite, and one new face for hypersthene.

In conclusion, the writers wish to express their cordial thanks to Prof. T. Itō of the Mineralogical Institute, Tokyo University for the courtesies he extended throughout the laboratory work, This investigation is a part of "Geological Investigations on the Zaō Volcanoes," and its expenditure was payed from the fund for the Scientific Research of Educationary Ministry.

---

30. 藏王火山產普通輝石及紫蘇輝石結晶

地震研究所　市村　毅
東京大學地學教室　湊　秀雄

藏王山に產する普通輝石の多くは，角閃石とか紫蘇輝石の様に長い柱狀結晶をなす點に，特徵が認められる．然し此結晶の形態に就いては從來その研究されたものが一つも發表されていない．

筆者達は昭和 25 年夏，藏王火山の地質學的研究を行うた際に，數多の普通輝石結晶と共に紫蘇輝石の結晶をも採集し，それ以來これ等の結晶の形態を研究して來た．

本文にはその結果が述べられている．

31. *Geology of Imaichi District with Special Reference to the Earthquake of Dec. 26, 1949. (II)*

By Ryōhei Morimoto,

Earthquake Research Institute.

(Read Jan. 16, Apr. 18, 1950—Received Dec. 20, 1950.)

III. Change of the surface.

Changes of the surface caused by the earthquake which the writer intends to mention in this chapter, include the land slips or rock falls that took place at the time of the two principal shocks in this meizoseismic area. Changes occurred not only of natural surfaces of the ground but also of artificial structures of civil engineering. Damages to the artificial structures are not described here. Of these changes of the surface, there are some that were brought about or were amplified by the earthquake motion of the most severe aftershock of 5:54 p.m., Dec. 27. Most of the damages done to living creatures, roads, forests, and farms are ascribed to these surface changes.

These changes of the surface are described below by grouping them according to the geological and topographical conditions of the lands attacked.

(1) Rock falls or earth falls along steep slopes or cliffs.

Rock falls or earth falls occurred at many points along the upper stream of the Name River. Of them, conspicuous rock falls took place at the rocky cliff of the ridge running through the 527 m peak. As was mentioned in the foregoing chapter, the ridge is formed of the highly silicified hard Palaeozoic slate or shale and of compact biotite-quartz-porphyry intruding the former. The earth falls were observed at many points along the marginal cliff of the fan of Diluvial age, composed almost uniformly of the stratified succession of yellowish pumice (Kanuma-soil), reddish brown pumice (Imaichi-soil), brownish clayey bed called "loam" extensively developed in Kwanto Region, and thick gravel. One of the most typical examples of these earth falls was shown in Fig. 5. These earth falls, all of similar feature, are commonly found along the left side of the Name River from Itagabata to Matsunokiuchi. The underlying rocks exposed along the cliff are thickly bedded Diluvial gravel at the east of Murose-namegawa, and auto-brecciated andesite at the west of Murose-namegawa. Remarkable earth falls are seen near the junction of two tributaries, to the Name River on its upper course (Fig. 14*A*). Falling of rock fragments or blocks of smaller scale were reported to have taken place at some places, e.g. at the road-side near Shinkyo, Nikko, near Funyu, etc.

(2) Destructive land slips of comparatively large scale near Murose-namegawa, Town Imaichi.

Land slips occurred near Murose-namegawa, about 2 km southeast of the town of Imaichi. One of the most destructive land slips of a large scale occurred at the steep slope, on the northern side of the 527 m peak. A land slip of about the same scale was simultaneously brought about at the southern slope of the same peak, and a smaller one took place along the adjacent gully on the northern side of the ridge. Localities of these land slips are shown in the annexed map (Fig. 9) on an exaggerated scale. All of these slips occurred at the time of the second principal shock of 8:26 a.m., Dec. 26. Two rural houses standing in the valley at the opposite side of the slope were badly wrecked; one was burried *in situ* and the other (*A* in Fig. 15) was pushed down and was carried away by a muddy flow towards the lower stream along the valley. By this accident, four persons were killed (burried alive) and a horse wounded to death. According to the personal account by a survived inhabitant of one of the wrecked houses, a crack was formed on the mountain-side and rock fragments fell at the time of the first principal shock of 8:18 a.m., and the collapse took place about a minute later than he had felt the second shock of 8:26 a.m., and the catastrophe came to the end within about 10 seconds. The mass of rock and earth, being roughly estimated as $3\times10^4\,m^3$ in volume, rushed down along the slope for about 150 m and slipped further on to the opposite side of the valley about 25 m beyond the river (*B* in Fig. 15). The collapsed mass consists of fragments or blocks of compact biotite-quartz-porphyry intermingled with pumiceous earth. A photographic survey of this area was performed by H. Kawasumi and his associates.

On the southern side of the same ridge, along dendritically developed gullys, a land slip of about the same scale was brought about simultaneously with the above-mentioned one; slipped rock mass from each head of these gullys rushed down the slope, (about 20°-30° in inclination), and combined together into a larger mass, and this larger mass moved down along the lower ravine and increased its volume more and more combining with collapsed reddish brown pumice deposited on the porphyry. At the foot of the southern slope of the ridge, where the pumice deposits increase in thickness, the mode of occurence of the land slips is some what different from that of the above-mentioned one. It resembles to some extent that of those described in the succeeding section. The occurrence of the above-mentioned rock or earth falls and land slips, can not be explained to certain geologic structures of the spots where they occurred. One of the favourable conditions in bringing about these surface changes may be that the relief of the surface in these spots was comparatively high as a result of differential erosion, though such topographic features are not peculiar to these spots, but are common in the mountainland of this seismic area. The surface changes along the valley, the upper stream of the Name River, are more remarkable and of larger scale, compared with those in the other parts of this seismic area. It may be considered that the shock of the earthquake was felt more violent there than at the adjacent area.

(3) Slipping of surface soil in the region where granite or Palaeozoic strata are exposed.

In the southwestern mountainland of the present meizoseismic area composed geologically of biotite-granite and compact Palaeozoic rocks, slipping of surface soil took place. The area most severely attacked by the slipping is a granite terrain between Okurugawa and Kusagyu, the upper stream of the Kuro River and the Ooashi River. There, porphyritic crystals of microperthite are predominant in the biotite-granite. The potash-felspar contained in the granite promoted the rock decompostion and the coarse arkose sand came to coat the surface. The slipping

Fig. 7. Slipping of the soil along the weathered layer at the surface of the porphyritic granite, near Kusagyu.

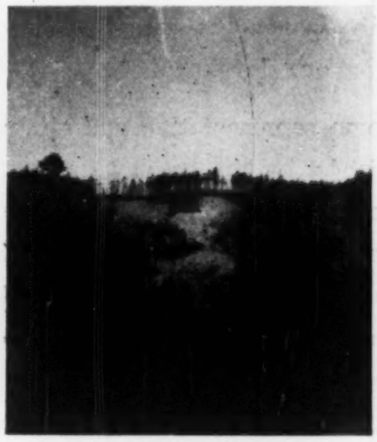

Fig. 8. Slipping of the thin soil on the slope of Palaeozoic mountain near Yamaguchi, on the right side of the Kuro River.

took place along the bottom of the layer of the surface soil. The thickness of the slipping layer is less than 1 m in most places in this granite region (Fig. 7). At Nakayama, a granite terrain, land slips are not so conspicuous as at the above-mentioned granite terrain. The granite of Nakayama is different in its rock facies from the granite near Kusagyu or Okurugawa; it contains no porphyritic perthite. The occurrence of the remarkable surface changes in the granite terrain near Kusagyu and Okurugawa may be attributed chiefly to the petrographic cause. Slippings of the comparatively thin deposits of surface soil with similar appearance are frequently met with on the slopes of the mountainland in the southwetern part of this meizoseismic area where the compact Palaeozoic rocks are exposed (Fig. 8). The Palaeozoic rocks in this district are shale, slate, sandstone, conglomerate, and hornfels derived from them, and in many cases they are highly silicified into hard compact rocks. In these rocks as well as in the granite, there is no geological discontinuity. The distribution of these land slips which are exclusively of small scale is greatly influenced by the local topography. Some of them were destructive and took place along road cuttings, e.g. those along the Ooashi River.

(4) Land slips characteristic of the region where Diluvial pumice deposits are developed.

Some representative and characteristic changes of the surface brought about in this district by the present earthquakes are a number of land slips found in the region where pumice and clay are uniformly and thickly deposited. The land slips of this type are marked with solid circles in the annexed map (Fig. 9). In spite of the slight difference in the mode of their occurrence owing to the local topography of each place, they always show the same feature in general. This feature is due mainly to the same geological conditions of the Diluvial formation in this district. Before describing representative landslips of this type, a supplementary note of the geology of these Diluvial beds will be given.

As was already mentioned in the foregoing chapter, the Diluvium of this district consists almost uniformly of yellowish pumice bed (the uppermost Kanumazuchi), reddish brown pumice bed (Imaichizuchi) and loam (Kwanto loam), underlaid with gravel beds or a lava flow of augite-hypersthene-andesite. On the comparatively gentle slopes of the mountainland, these beds of pumice or loam are deposited directly on the basal rocks such as granite, porphyry, and Palaeozoic strata. Geologic succession and thickness of these Diluvial beds at many localities in this district are shown

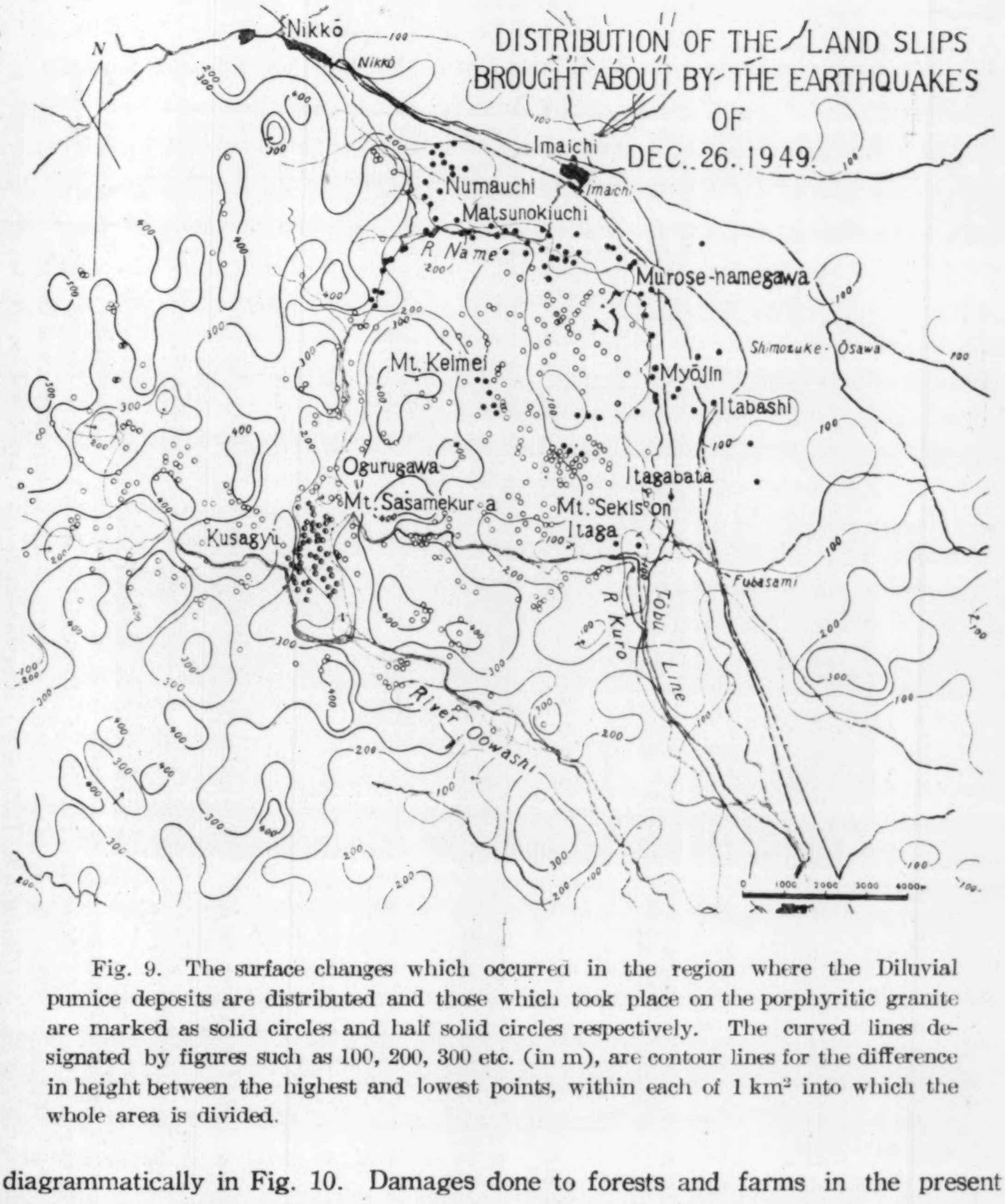
DISTRIBUTION OF THE LAND SLIPS
BROUGHT ABOUT BY THE EARTHQUAKES
OF
DEC. 26. 1949
N
Nikkō
Nikkō
Imaichi
Imaichi
Numauchi
Matsunokiuchi
R. Name
Murose-hamegawa
Shimozuke-Ōsawa
Mt. Keimei
Myōjin
Itabashi
Ogurugawa
Itagabata
Mt. Sasamekura
Mt. Sekison
Itaga
Kusagyū
R. Kuro
Tobu Line
Fubasami
River Oowashi
100
200
300
400
0 1000 2000 3000 4000m

Fig. 9. The surface changes which occurred in the region where the Diluvial pumice deposits are distributed and those which took place on the porphyritic granite are marked as solid circles and half solid circles respectively. The curved lines designated by figures such as 100, 200, 300 etc. (in m), are contour lines for the difference in height between the highest and lowest points, within each of 1 km² into which the whole area is divided.

diagrammatically in Fig. 10. Damages done to forests and farms in the present seismic area are mainly due to the collapse of these pumiceous beds. Earth falls or land slips are remarkedly found in the northeastern part of the macroseismic area where these deposits are developed; especially conspicuous in the area between the Namegawa valley and the Daiya River (Fig. 14 *C*). These changes in the area where such pumiceous beds are distributed, occurred not only on the steep slope or on the cliff, but also on the quite gently sloped surface. Of these changes, the

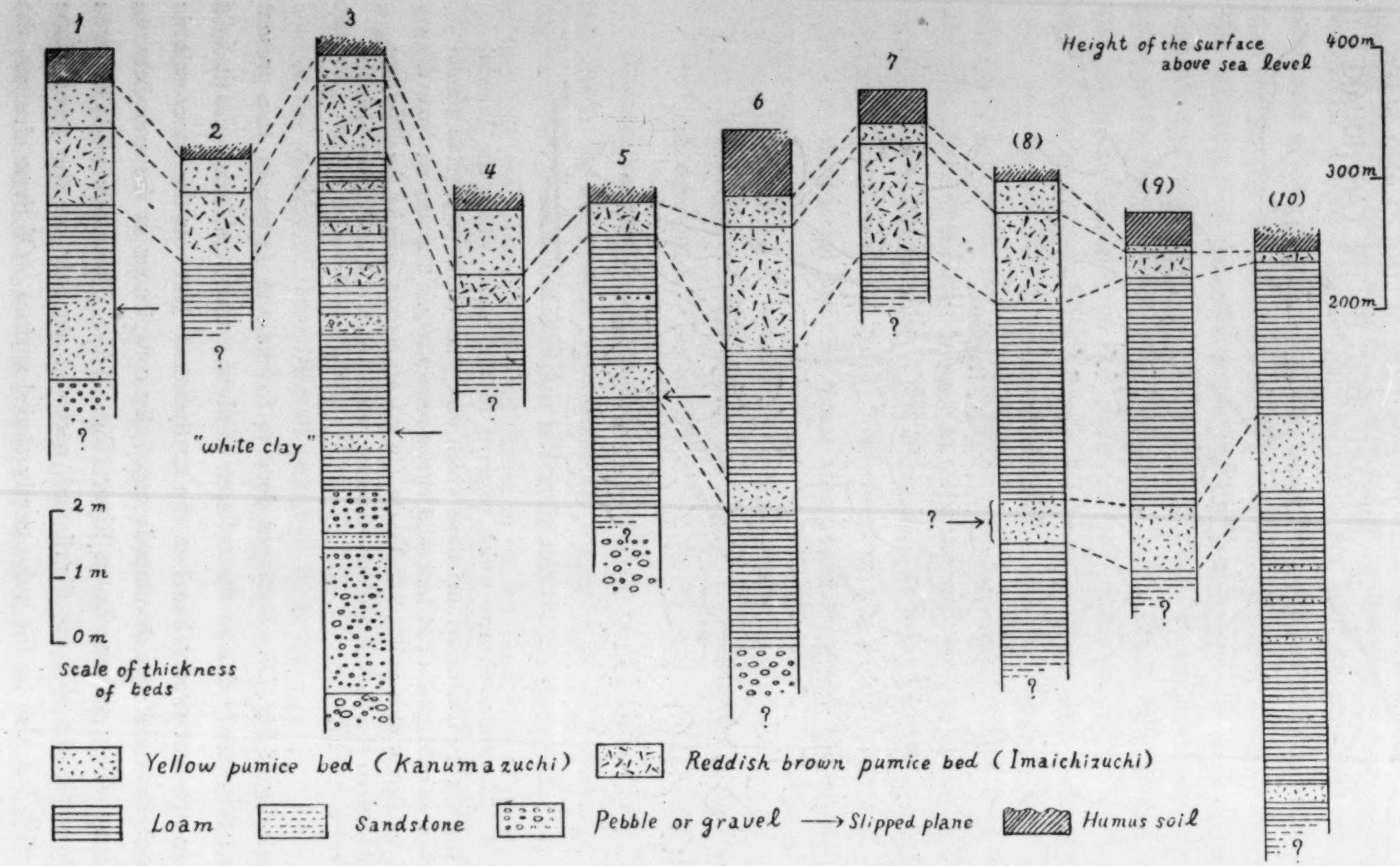
1
2
3
4
5
6
7
(8)
(9)
(10)
Height of the surface above sea level
400m
300m
200m
"white clay"
2 m
1 m
0 m
Scale of thickness of beds
?
Yellow pumice bed (Kanumazuchi)
Reddish brown pumice bed (Imaichizuchi)
Loam
Sandstone
Pebble or gravel
→ Slipped plane
Humus soil

Fig. 10. The main geological columns of the Diluvial beds in this district. 1: Yamakubo, 2: Takachiya-Ochata, 3: Imaichi, 4: Shimagane, Itaga, 5: Ushiroyama, Myojin, 6: Itabashi, 7: Jukkokuzaka in Oosawa village, (8): Oosawa, (9): Shimokojiro, (10): Fubasami. The columns (8), (9), and (10) are quoted from Kawamura and Harada (K. KAWAMURA & M. HARADA, *Jour. of Sci. of Soil and Manure* **6** (1932) 414.); all others 1, 2, ..., 7 are based on the writer's observations.

two land slips which took place at Numauchi near Yamakubo and at Oosawa, 1 km north of Itabashi, respectively are representative.

Chasms were formed on the wheat corn field at Numauchi, 3 km west of Imaichi, and 3 km southeast of the town of Nikko, at the time of the earthquake of 8:18 a.m., December 26. The gently sloped surface of the corn field changed into an amphitheatre-like topography, about 100 m long in EW-direction and about 5 m deep (Fig. 11) at the time of the succeeding earthquake of 8:26 a.m. The original dips of the surface and of the strata were gentle, not attaining to 10 degrees southwards. Displacement of the slipped land mass was not uniform; larger in the central portion of the collapsed area, smaller in the marginal portion, attaining to 30 m or more in the remarkedly slipped portion. The area of the corn field damaged is roughly estimated as 4×10^3 m^2. The mass which slipped or collapsed into mosaic aggregate of blocks consists mainly of reddish brown pumice. The slipped plane was not recognized here.

Fig. 11. A northward view of the amphitheatre-like land slip at Numauchi, about 100 m across in the E-W direction.

The surface changes, which are similar in form and comparable in scale to the just-mentioned land slip, were conspicuously observed side by side on the hill between the Akahori River and the valley of the upper stream of the Name River. Nowhere the slipping attained to the depth of 5 km from the surface. From this, it appears that the slipping was caused in the loamy bed. For, in this neighbourhood, pumice beds (the uppermost Kanumazuchi and Imaichizuchi) of 2–3 m in thickness uniformly and conformably cover the so-called loam. The latter, consisting mainly of volcanic glass stained with iron, intercalates thin beds or laminae of other material such as fine pebble, sand, lappili, pumice etc., somewhere.

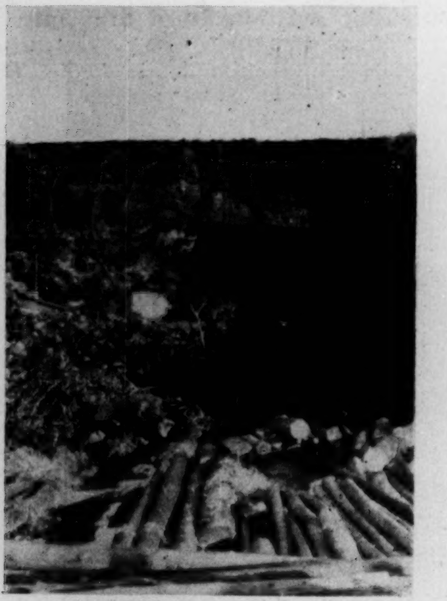

Fig. 12. The geologic succession of the strata near Itabashi. (Cf. Figs. 9 and 10. Photo. by H. Kawasumi.)

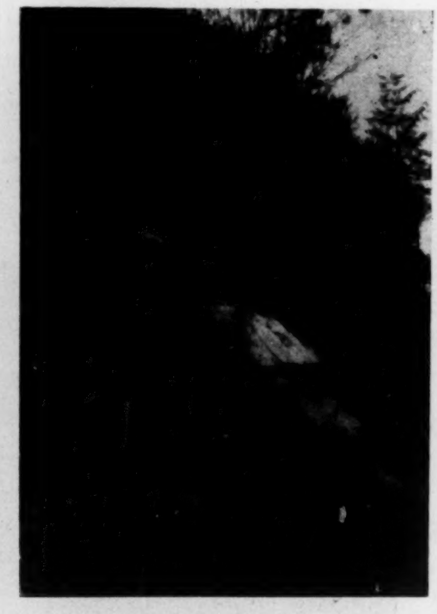

Fig. 13. An exposure along the road-cutting through Ushiroyama. Notice the slipping along the lower boundary of a white clay bed intercalated in the loam beds. (Cf. Figs. 9 and 10, Photo. by H. Kawasumi.)

Slipping is apt to be brought about along the boundary plane with these intercalated beds. Near Numauchi, a compact clayey loam bed, overlaid conformably with the above-mentioned aeolian pumice beds, such as the uppermost "Kanumazuchi" and "Imaichizuchi", suddenly grades into a coarse undecomposed pumice bed at the depth of 3.7 m from the surface, and further into a coarse sandy bed at 5 m. There is no evidence to show that any displacement of the strata under this compact loam took place.

At Oosawa, 1 km north of Itabashi, corn fields and forests of about 25,000 m^2 in area were attacked by land slips; a portion of the upper beds of the strata occupying a semicircular area of about 18,000 m^2, and another portion of about

7,000 m^2 slipped to southwest and to northeast respectively, toward a common line, resulting in heaving up of the surface. The strata of this area are as a whole nearly horizontal. Locally, however, they are slightly dipping in parallel with the surface. Dip of the strata is about 7 degrees here. The plane along which the overlying strata slipped down could not be directly observed at this place. A white pumice bed, so-called "white clay",[8] intercalated in the compact loam, is exposed at Itabashi and at Myojin (Figs. 12 and 13). It must have played an important rôle in causing such low-angled land slips, the strata overlying this greasy bed being easily movable along it by the earthquake shock. In fact, the slipping of the strata along the lower boundary of the "white clay" was observed at the road-cutting through the hill between Myojin and Ushiroyama (Fig. 13). T. Honda and his pupils of the Imaichi Middle School[9] found the regional slipping of the strata along this "white clay" from observing dislocations on the walls of water wells in the town of Imaichi and its adjacent area. The dislocations observed at Oosawa coincide in the direction of their slip with the movement of the strata on the surface.

The so-called "white clay" consists mainly of natural glass of volcanic origin. Porphyritic crystals of plagioclase, hypersthene, magnetite etc., are contained. The glass is altered mostly into hydrated halloysite;[10] montmorillonite is also found, and the latter is remarkable in some parts. As compared with the natural glass in the loam bed in which the bed of this white clay is intercalated, the volcanic glass in this "white clay" is more advanced in alteration (kaolinization). The white bed which contains much water forms a kind of impermeable bed. It may mainly be due to this mineralogical composition of the bed that the land slips were brought about remarkably in this seismic area, in spite of low-angled inclinations of the strata and of rather unsevere shocks of the present earthquakes[11]. In short, of the changes of the surfaces in the region covered with these Diluvial deposits, it

---

8) Correlated to the "1st Kanumazuchi" of Kawamura. K. KAWAMURA and M. HARADA, *Jour. of Science of Soil and Manure*, **6** (1932), 411–434. (in Japanese)

9) T. HONDA, *Bull. Earthq. Res. Inst.*, **28** (1950), 449–455.

10) Identified by X-ray powder photgraph as follows:

$2L$ (cm)	I	d (A)
17.4	10	10.3
39.6	8	4.54
53.0	7	3.33
69.0	4	2.57
106.8	2	1.70
123.8	5	1.48
146.5	2	1.28
152.5	2	1.24

[Cu $K\alpha$ $\lambda = 1.5374$ Å
3.2 kV, 15 mA, 3.5 hr.
Radius of camera: 5.68 cm]

may be said as follows: The loose aeolian deposits of pumice such as the uppermost "Kanumazuchi" and "Imaichizuchi" were easily collapsed by the earthquake shocks and the strata easily slipped along the greasy intercalated beds, especially of "white clay" in the "loam".[12]

31. 今市地震地域の地質(2)

地震研究所　森本良平

昭和 24 年 12 月 26 日の，栃木縣今市町附近に起つた地震の震域の地質の概要と，地變について述べた。この地方の基盤岩石は，少しくホルンフェルス化され，著しく珪化された古生層の砂岩，頁岩，礫岩，それを貫く黑雲母花崗岩，花崗斑岩，石英斑岩などの酸性岩類からなり，石英斑岩は所によつて噴出岩的岩相(石英粗面岩)を伴ふ。これらの基盤岩石は差別浸蝕によつて，珪化された古生層は山稜を，花崗岩類，特に加里長石に富む斑狀花崗岩は低地を形成した。以上の先第三紀乃至第三紀岩石を削つて，大治川の扇狀地が形成され，その上に日光火山群の比較的古期の熔岩(おそらくは女峯――赤薙の)が，ほゞ，いまの行川上流の谷に沿ひ室瀨近くまで流れた。この熔岩噴出の時代をも含めて，引續いて，ロームをつくつた火山物質が堆積し，更に今市土，鹿沼土をつくつた浮石が，比較的緩やかな山地斜面やこの扇狀地一帶に堆積した。現在の大治川その他の河川及び行川は，更に，これらの洪積層を削つて流れてゐる。今回の地震で，烈しい地變が集中した行川上流の谷は少くとも洪積紀の扇狀地の形成及び上記安山岩噴出以前からあつた地形に基いてゐる。地變は，地震の規模が小さかつた割合に著しく起きた。これは，この地域に廣く厚く分布してゐる洪積紀の火山性堆積物の性質に歸因するものである。なかでも，地辷りの絕好な辷り面になつたものはロームに夾まれた，一部粘土化した浮石層であつた。この地變に關與した，火山性堆積物については，また稿を改めて述べたい。

---

11) H. KAWASUMI, *Bull. Earthq. Res. Inst.*, **28** (1950), 364.

12) The writer's sincere thanks are due to Prof. Seitaro Tsuboi of this institute for his reviewing this chapter of the present paper in manuscript, to Prof. Hiroshi KAWASUMI for his kind instruction during investigation of the surface changes, and to Mr. A. Zitukawa for the loan of his photographs.

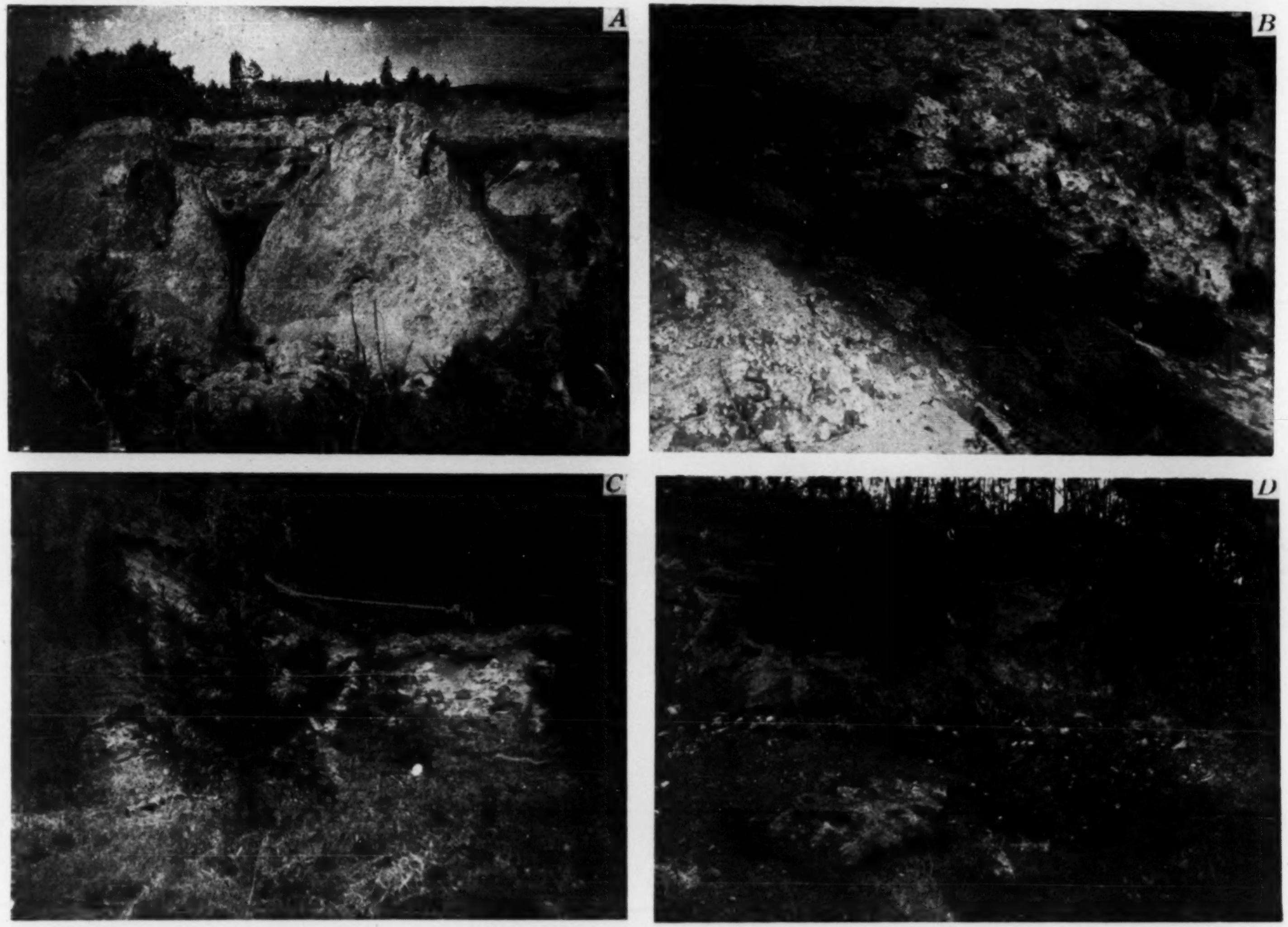

Fig. 14. (*A*) A large-scale collapse of the cliff, on the left side of the upper stream of the Name River, near the joint of two tributaries, at Matsunokiuchi, Nikko-machi. (*B*) The base of an auto-brecciated lava flow of augite-hypersthene-andesite underlaid with hornblende-bearing vitric tuff deposited on an erroded surface of the Palaeozoic sandstone and granite-porphyry. (*C*) A small-scale landslip which occurred on the hill-side covered by aeolian pumice deposits, 500 m northwest of Shimagane, Ochiai-mura. Loose pumice deposits collapsed. (*D*) Terminal front of the auto-brecciated lava flow of augite-hypersthene-andesite, overlaid with gravel, loam, and pumice beds, at Murose-namegawa, Imaichi-machi.

（震研彙報　第二十九號　圖版　森本）

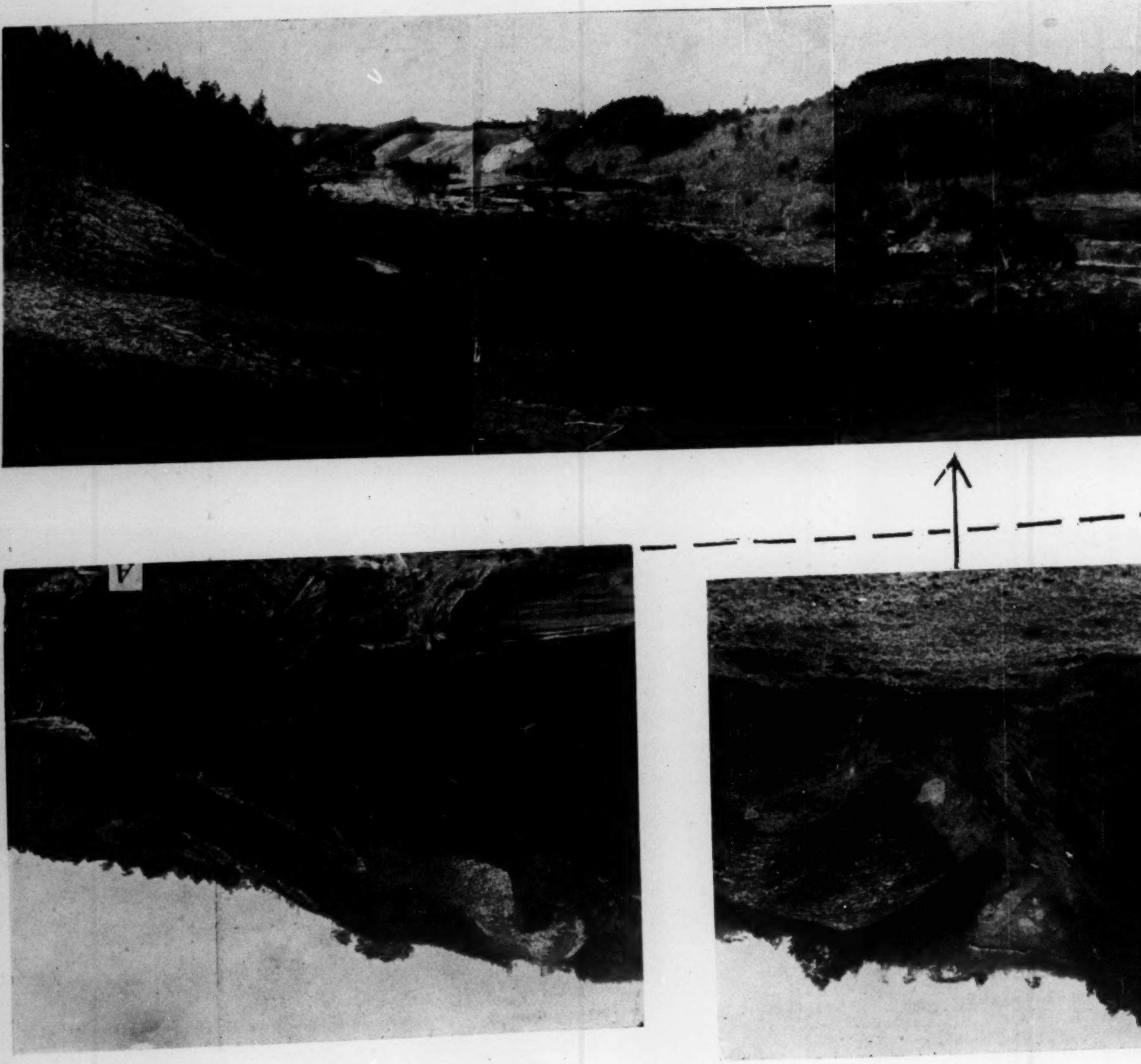

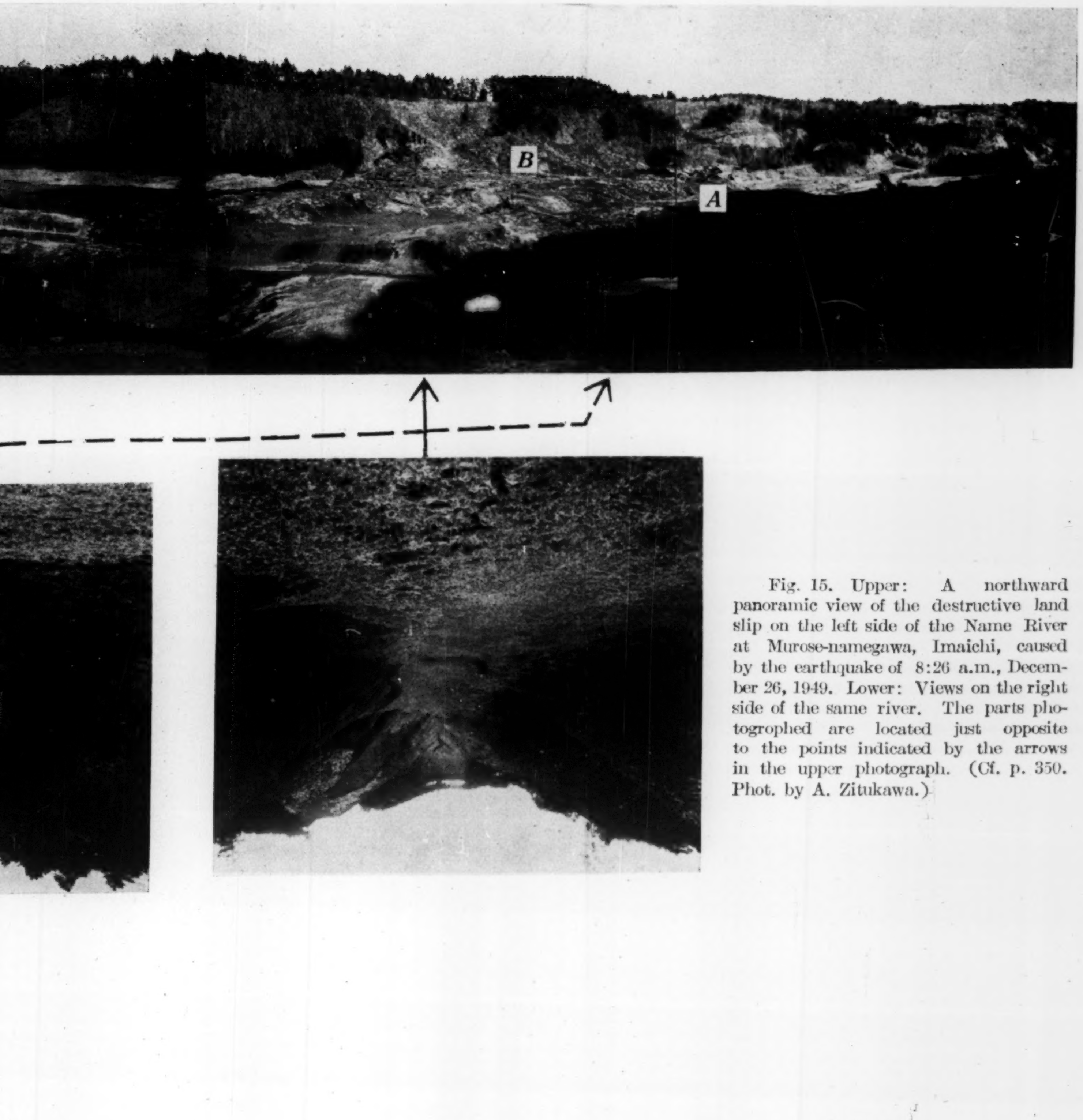

Fig. 15. Upper: A northward panoramic view of the destructive land slip on the left side of the Name River at Murose-namegawa, Imaichi, caused by the earthquake of 8:26 a.m., December 26, 1949. Lower: Views on the right side of the same river. The parts photogrophed are located just opposite to the points indicated by the arrows in the upper photograph. (Cf. p. 350. Phot. by A. Zitukawa.)

32. *The 1950–1951 Eruption of Oo-sima and Its Seismometrical Investigations.* (*I*).

By Takeshi MINAKAMI, Tsutomu MIYAZAKI
and Tomoko TAKAHASHI,

Earthquake Research Institute.

(Read Dec. 19, 1950.—Received Mar. 20, 1951.)

1. **Introduction**.

Oo-sima, an insular volcano which is the largest of the Seven Izu Islands belonging to the Huzi (Fuji) volcanic zone and easy of access, lying about 110 km SSW of Tokyo city, is well known for its frequent eruptions of the Strombolian type in historical time.

Therefore, since the end of the 19th century, investigations and observations concerning the Oo-sima volcano have been conducted from various standpoints including geology, geophysics and geochemistry. At the occasion of the 1912-1914 eruption of this volcano, F. Omori(1) investigated its developments and its nature together with those of its historical activities. During the fairly long period from 1900 up to date, S. Nakamura(2) frequently visited the place to carry out various observations with his associates.

On the other hand, S. Tsuboi(3) reported in 1920 on the general geology and petrography of the Oo-sima Island, and after that H. Tsuya(4) studied the same problem in connection with other volcanoes belonging to the Huzi volcanic zone.

As concerns the geophysical study of this volcano, investigations were mainly conducted by R. Takahasi, T. Nagata and their associates(5) in the period from 1936 to 1941 including the minor activity of 1940. Their researches include not only the geomagnetic, gravimetric and geodetic surveys but also continuous observa-

---

1) F. OMORI, *Rep. Earthq. Inv. Comm.*, **81** (1951), 1 *etc.*

2) S. NAKAMURA, and others, *Jour. Geogr. Soc. Tokyo*, **20** (1908), 682 *and* 786, *etc.*.

3) S. TSUBOI, *Jour. Coll. Sc. Imp. Univ. Tokyo*, **43** (1920), 139.

4) H. TSUYA, *Bull. Earthq. Res. Inst.*, **15** (1937), 215, *etc.* .

5) R. TAKAHASI and T. NAGATA, *Bull. Earthq. Res. Inst.*, **15** (1937), 441 and 1047, *etc.*.
R. TAKAHASI, T. NAGATA and K. HIRANO, *Bull. Earthq. Res. Inst.*, **16** (1938), 16
T. NAGATA, *Bull. Earthq. Res. Inst.*, **16** (1938), 288 and 714; **17** (1939), 93; **18** (1940), 102 and 281; **19** (1941), 402, *etc.* .

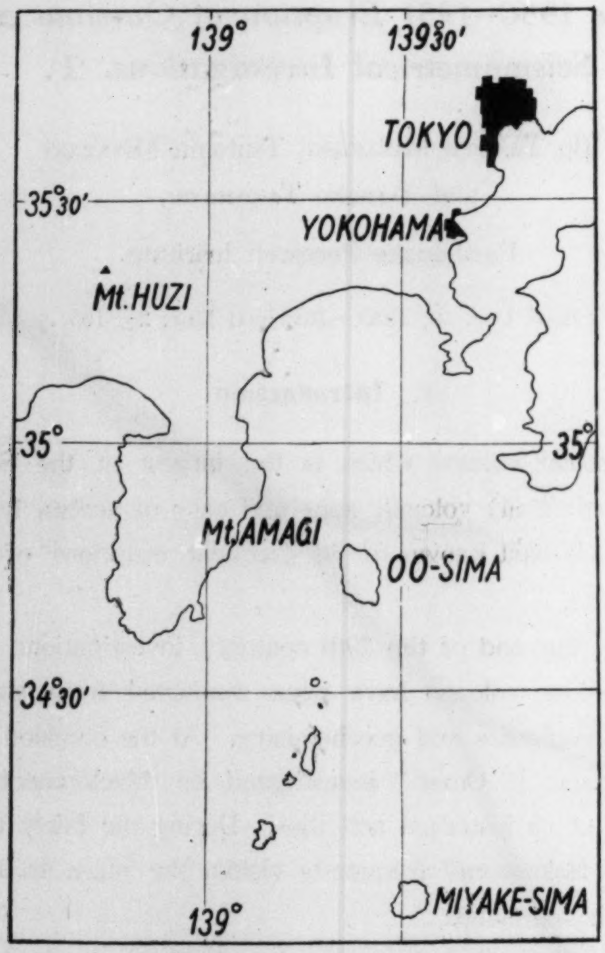

Fig. 1. Geographical position of Volcano Oo-sima.

tions of earthquakes and other volcanic phenomena originating from Oo-sima.

Unfortunately, various difficulties during and after the recent war prevented us from visiting the volcano, which resulted in an interruption of our observations.

However, the present eruption which began on July 16,1950, gave us an opportunity to restart the study of this volcano. In fact, as soon as the Oo-sima resumed its explosive activity, seismometric, geomagnetic and petrological investigations as well as general observations with respect to the developments of effusive phenomena were carried out precisely by a number of geophysicists, geologists and geochemists of the Tokyo University and other Institutes.

In the present eruption of Oo-sima, the writers devoted themselves mainly to the seismometric investigation of earthquakes originating below this volcano and micro-tremors of continuous train accompanying the incessant explosions of the Strombolian type. Although this paper deals with this latter phenomenon, it is necessary to give an outline of the development of the 1950 eruption which is closely related with the occurrence of the micro-tremors.

2. Brief Description of the Development of the 1950 Eruption.

As will be seen to some extent in the topographical map of the Oo-sima volcano in Fig. 3, the summit crater or pit crater which was 250 m deep and about 300 m in its diametre before the present activity, is surrounded by two sommas, the inner somma is of quite circular form with a diametre of 700 m and the outer wanting in its northern part is located at a distance of 1-1.5 km in an elliptic form. Rocks forming this volcano and the recent ejecta are generally characterized by the saturated basalt or andesitic basalt.

After a period of quiescence of just ten years since the minor activity of August 19, 1940, Volcano Oo-sima resumed explosive activity toward 10 h on July 16, 1950, ejecting ash and lava fragments from a lower part of the southern wall of the pit crater. For 70 days from that day to September 23, remarkable eruption of the Strombolian type continued without interruption, belching out molten lava in fountain fashion from several sources on the floor of the pit crater, and on the other hand, ejecting volcanic bombs of incandescent state and scoriae of various sizes every few seconds with detonations which were audible on the flank of the outer somma and sometimes at the sea side, 6 km distant from the active crater. As the result of incessant eruption, a cinder cone (A) grew rapidly around center of paroxysmal eruption through the accumulation of ejecta, and molten lava welling up buried by degree the pit crater. However, it may be said that the general features of eruption suffered little change throughout the present eruption, though afterwards the center of eruption moved about 100 m southeastwards and was newly formed there, and the volume of out-pouring lava as well as the intensity of explosion should undergo some change according as the eruption developed.

After the fluidal lava originating from the jet-like sources filled the pit crater on August 15, it began to overflow its crater wall and invaded the flat area inside the inner somma. On the other hand, the cinder cone (A) grew markedly up to that date, 50 m high as measured from its base.

As soon as the explosive eruption in the craterlet of the cinder cone (A) came to an end on August 23, another craterlet newly opened near the southern base of the former cinder cone and volcanic bombs together with smaller ejecta were thrown up incessantly 100 m high and sometimes 200 m high in the air. Since the paroxysmal eruption at the newly formed craterlet (B) lasted in such state for

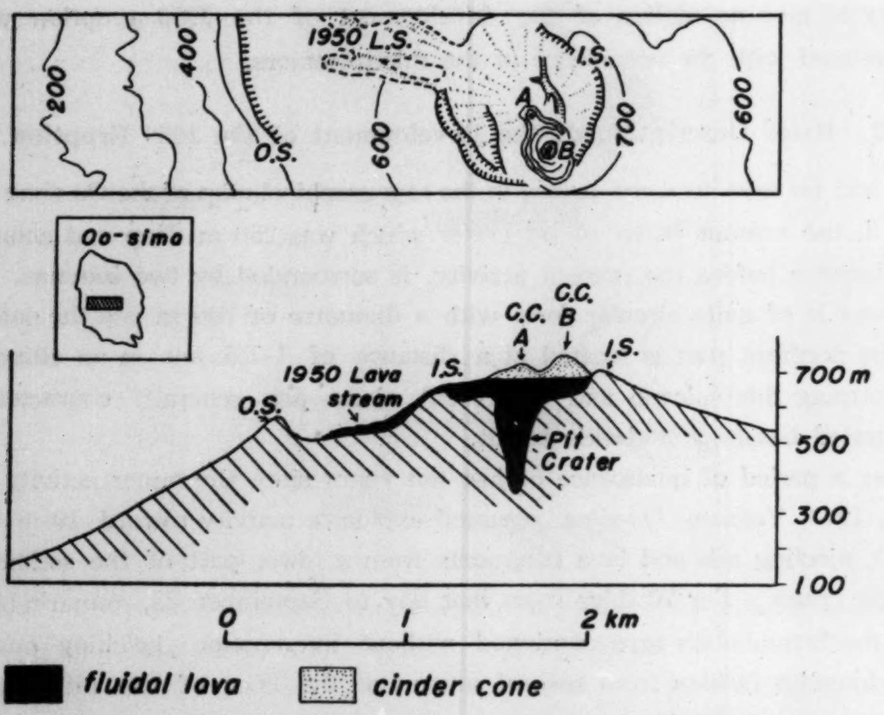

Fig. 2. Topographical sketch in the vicinity of the summit crater.
C.C.A.; cinder cone A, C.C.B.; cinder cone B,
I.S.; inner somma, O.S.; outer somma.

a month without marked change in the intensity of eruption as well as in the position of the center of ejection, a cinder cone (B) was rapidly built there in the same way as in the former case. Therefore, the latter cinder cone (B) on September 20 reached a height of 100 m from its base, or 760 m above the sea-level which is only few metres lower than the highest point of the Oo-sima volcano or the north part of the inner somma. In Figs. 25 and 26, the night views of the eruption at the cinder cone (B) are represented.

At the earlier stage of activity at the cinder cone (B), or in other words, during the period from August 23 to September 5, the craterlet lacking the northeastern part of its crater-wall, formed a horseshoe shape, as may be seen clearly in Fig. 27, and fresh lava welling up from its vent flowed down through this opening towards the north part of atrio of the inner somma. Since the fluidal lava from various sources was collected within the inner somma, a lava pool was formed there, as may be seen in Fig. 25, usually elevating its surface. It will be, however, needless to say that the inner part of the lava pool was in a fluidal and incandescent state according to observations at fissures, though its surface was cooled and solidified, forming lava blocks of various sizes soon after the outpouring. Towards September 10, the horseshoe craterlet closed its opened part with the accumulation of ejecta and after several days a regular form of cinder cone was completely built.

On September 12, the incandescent lava collected in the lava pool began to flow out from two places of the inner somma and went down along its steep flank. This overflowing of lava from the lava-pool lasted for 11 days, forming ten several narrow streams, each being 2–5 m wide and 0.5–1.5 m thick at its upper part, and enlarging at the base of the inner somma both in width and thickness. Judging from the nature of these lava streams, it may be said that they are of block type or aa type, though they formed in spots ropy structure.

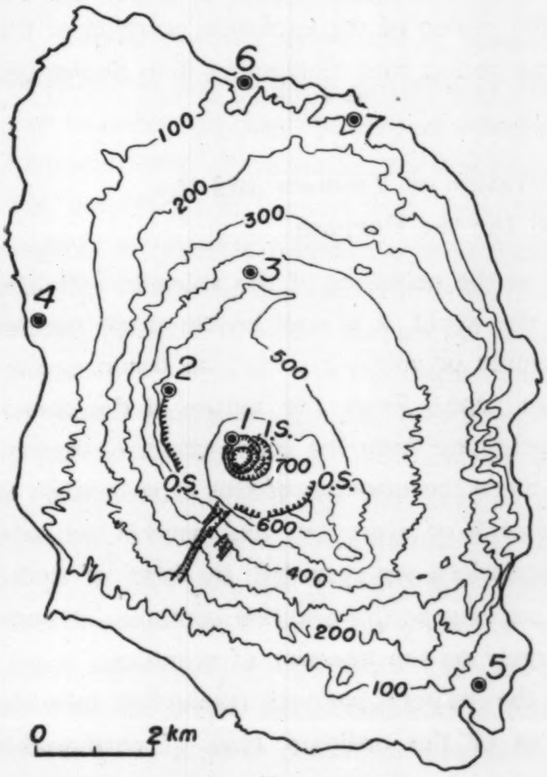

Fig. 3. Topographical map of Oo-sima.
I.S.; inner somma,
O.S.; outer somma.
1~7, temporary seismometric stations.

According to the temperature measurements of fresh lava made by S. Murauchi[6] and others[7], maximum temperatures in the lava pool and at the upper part of the lava streams ranged from 1000°C to 1100°C.

After the 1950 eruption of Oo-sima developed in the manner as just mentioned, it ceased suddenly on September 23.

However, the volcano recovered its activity towards the beginning of February 1951 and the eruption of the same type as described above still continues up to date at the craterlets which were newly opened on the flank of the 1950 cinder cone (B). With respect to the 1951 eruption, the writers will report in detail in the forthcoming Bulletin.

---

6) S. Murauchi, *Natural Science and Museum*, **17** (1950), 1.

7) R. Morimoto, I. Murai, N. Nasu and A. Sugimura, Read at the monthly meeting of E.R.I. on October 17, 1950.

At any case, the present seismometric investigation of tremors with which the present paper deals, was carried out in the course of the explosive eruption at the cinder cone (B), or in other words, in the period from September 5 to September 22, 1950.

3. The Seismometric Observation of Tremors and the Seismographs used for the Purpose.

From the seismometric studies made at the occasions of the volcanic activities in Japan as well as in the other part of the world, it is well known that[8] besides the earthquakes of the ordinary type, tremors or volcanic pulsations occur accompanying the eruption of the Strombolian type. From the nature of the phenomena, it is supposed that these tremors originate from the active crater or directly below it, and not from the deep place. Since the eruption of this type consists of minor explosive eruption of every few seconds or every ten and several seconds, earthquakes caused by those numerous explosions are recorded in form of continuous train on the seismograms and last as long as the eruption continues, though the amplitude of the tremors depends largely on the intensity of eruption.

In the present activity of Oo-sima, the writers planned researches into the nature of this type of tremors, as well as of the ordinary type of earthquakes which occurred under this volcano. However, it will be needless to say that, so long as the eruption lasted as mentioned above, tremors of continuous train disturbed seriously the recording of the earthquakes of the other type. Since the explosive eruption stopped on September 23, 1950, the writers planned out the observation of the earthquakes of the other type, with which the forthcoming paper will deal.

The seismographs used for these purposes were of the inverted pendulum type for recording the horizontal motion of vibration, of which the instrumental constants were 1.0 second for the period of proper vibration and were variable with respect to the geometrical magnification according to our purposes. In other words, the magnification is 200 in recording on the smoked paper, and 4000, 2000' or 1200 in the case of the optical record, which is easily adjustable with the aid of the length of optical lever.

---

[8] F. OMORI, *Bull. Earthq. Inv. Comm.*, **5**, **6**, **7**, **8** and **9** (1911–1921), *etc.*.
K. SASSA, *Mem. Coll. Sc. Kyoto Imp. Univ., Ser.* A, **18** (1935), 255: **19** (1936) 11, 171.
T. MINAKAMI, *Bull. vol.*, **10** (1950), 59; *Bull. Earthq. Res. Inst.*, **19** (1941), 171.
R. H. FINCH, *Bull. Seism. Soc. Am.*, **39** (1949), 39 *etc.*.
G. C. OMER, *Bull. Seism. Soc. Am.*, **40** (1950), 175.

Seeing that the amplitudes of tremors differed greatly according to the distances from the origin of vibration or from the active crater, it was necessary to put in order the magnification of seismographs without changing their instrumental characteristics. In addition, for the observation at the distant stations in which the amplitudes of tremors were remarkably attenuated, the optical recorder was applied in order to reduce the solid frictions of the instruments.

To determine the acceleration of tremors, the plate springs of the pendulum were replaced by other springs by which the proper period of vibration was adjusted to 0.1 second. As the result of the procedure, the seismographs were used as acceleration-seismographs, with a sensibility of 2.0 gal per 1 mm on the smoked paper and 0.025, 0.05 or 0.083 gal per 1mm on the optical recorder.

It must be added that the speed of the recording paper was adjusted to the range from 2 mm/sec to 5 mm/sec according as the purposes of observation.

It is believed that the volcanic tremors would show several times of ebb and flow in accordance with variations in the intensity of the eruptive phenomena which lasted for 70 days from July 16. However, our seismometric observation covered the period from September 3 to 23, when the Strombolian eruption in the crater B, as already described, was in a quite constant state. According to the observations of the eruptive phenomena made near the active crater, the explosive eruption after 16 h on September 23 lost by degree its intensity and tending towards a dormant state came to a standstill at the noon of the following day. On the other hand, the phenomena were confirmed also by continuous seismometric observations at Station No. 4 located at Moto-mura, where the volcanic tremors of a constant state lasting up to nearly 14h of September 23, began to decrease in amplitude and completely disappeared on the seismogram after 16h of the following day. Fig. 4 shows the developments of the tremors observed at Moto-mura, by taking the mean value of the largest-five amplitudes for every four hours.

At Station No. 1 on the inner somma lying only 600 m distant from the active craterlet B, tremors or shocks were so intense as to be felt every several seconds, and at the nearer place on the northeastern part on the same somma, 400m apart, tremors were always felt but not so sharply as at the base of the cinder cone B, only 200 m apart from the active craterlet. On the basis of these facts, it may be reasonable to infer that the tremors originated inside the active craterlet B or directly under its floor not exceeding 200-300 m in depth. This assumption con-

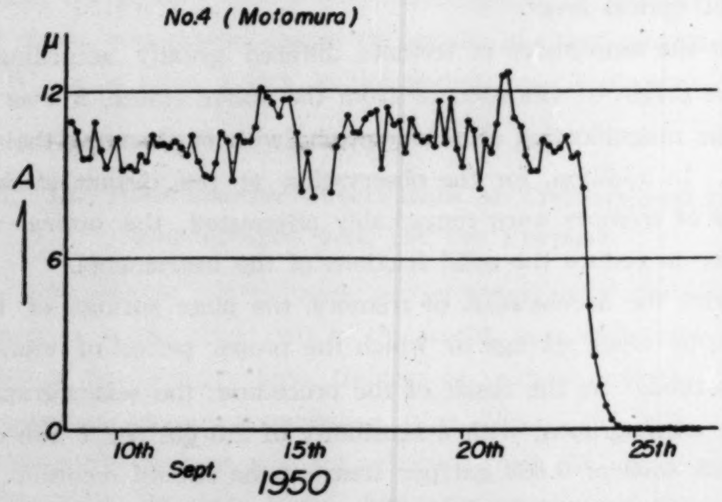

Fig. 4. Development of volcanic tremors at the standard station.
A: Mean amplitude of the five largest tremors for every four hours.

cerning the origin of the vibration is supported from the features of propagation of the tremors, especially from the relation between their amplitude at each seismometric station and the distance from the craterlet B, with which we will deal in the following paragraphs.

A seismometric station was established as the standard station at Moto-mura (No. 4) and observations have been continued without interruption during the period from September 3 to the present (March 1951). Seismographs of the same type as those of the standard station were removed from one temporary station to another in the period from September 3 to 23, in order to record the tremors at various places including the base, flank and summit of the Oo-sima volcano. The positions of these stations are indicated on the map of Fig. 3, and in Table I the distance between each station and the craterlet B or the origin of tremors, together with the height above the sea-level at each station are given.

The present seismometric observations were made mainly with respect to the two components of horizontal motion with the aid of the same type of seismographs, one being set in the direction towards the active crater and the other in the rectangular direction to the former.

However, observation at Station No. 7 which commenced on September 23, was excluded from the present research, for the reason that the eruption stopped in the course of the seismometric observation at this station.

Table I. The locality of the temporary seismometric station.

Station No.	Locality	Epic. dist.
1	Inner somma (Kako-Tyaya)	0.6 Km
2	Outer somma (Gozinka-Tyaya)	2.0 〃
3	Yuba	3.6 〃
4	Moto-mura	4.6 〃
5	Habuko-mura	5.8 〃
6	Okata-mura	6.7 〃
7	Senzu-mura	

4. The Nature of Volcanic Tremors Recorded by the Displacement Seismographs.

1) Analyses of Seismograms.

In order to throw a light on the nature of the volcanic tremors and the mode of their propagation, the writers made the analyses with respect to their amplitudes and vibration periods, on the basis of the seismograms recorded by means of the displacement-seismographs at each station. Figs. 21 and 22 show the seismograms recorded on the smoked papers and Fig. 23 those obtained optically.

Firstly, the amplitudes and vibration periods of the tremors were read carefully on these seismograms and then the amplitude-period diagrams were made, by taking the double amplitude in ordinate and its vibration period in abcissa, as shown in Figs. 5∼11. Of these figures, Figs. 5 and 6 are those at Station No. 1 and both stand for the radial component of the active crater, of which Fig. 5 is based on the seismogram recorded in an interval from 16h 55m on September 16 to 16h 57m of the same day, and Fig. 6 from 17h 35m to 36m. As these two figures indicate clearly, the character concerning the amplitude and the vibration-period of the tremors, especially the maximum amplitude of each vibration-period is in a fixed relation, or in other words is independent of the time of observation. Seeing that the phenomena just mentioned are in the same manner at the other five stations including the standard station No. 4, it may be said that the nature and magnitudes of the tremors did not change with respect to the time throughout the present survey, excepting the observation at Station No. 7.

Figs. 5∼11 show the diagrams for six stations of various epicentral distances, in which the components I and II represent those for the two horizontal components of the tremors as already mentioned. By comparing these diagrams, it is

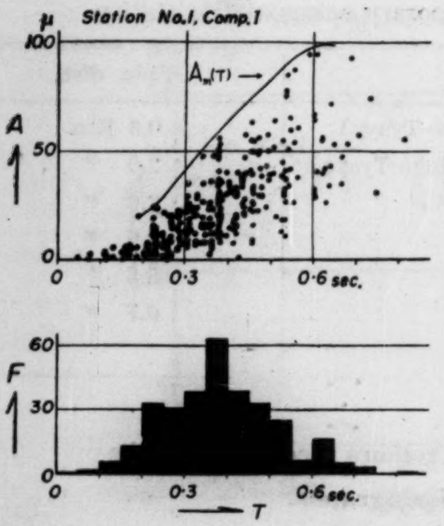

Fig. 5. Amplitudes and vibration-periods of the tremors during 2 minutes from 16h 55m on September 16, at the station No. 1.

(Comp. I. Component towards the origin.)

(Comp. II. Component rectangular to the former.)

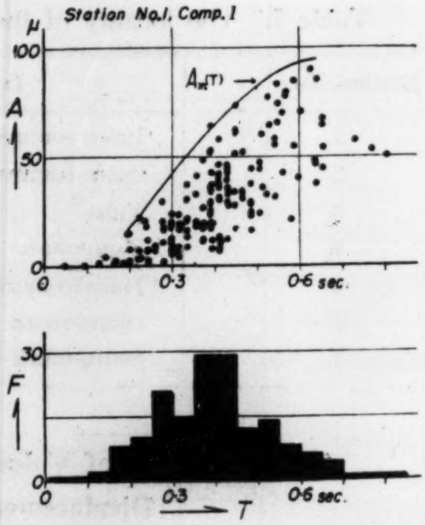

Fig. 6. Amplitudes and vibration-periods of the tremors during 1 minute from 17h 35m on September 16.

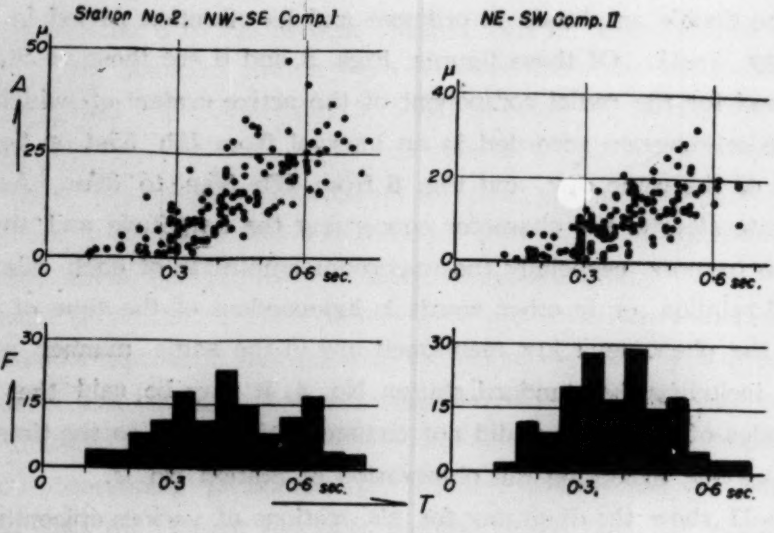

Fig. 7. Amplitudes and vibration-periods of the tremors at the Station No. 2.

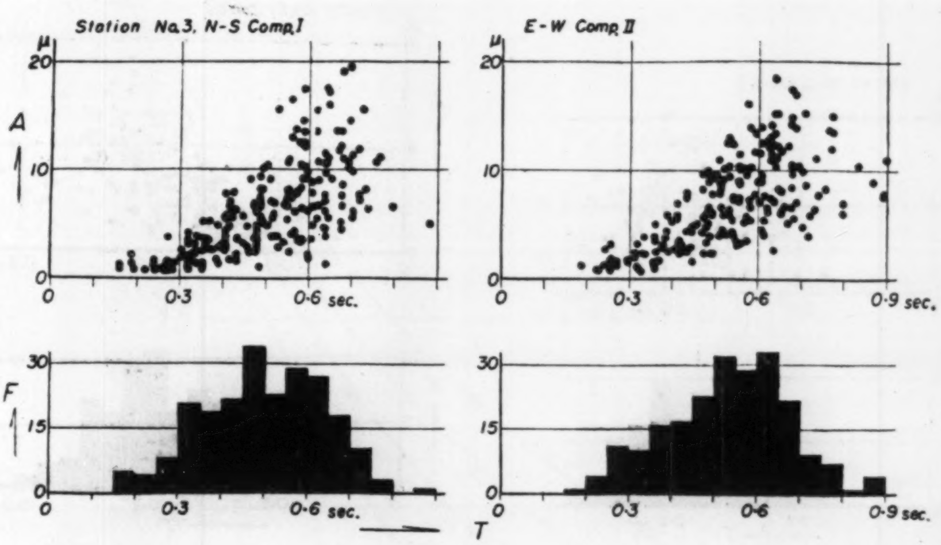

Fig. 8. Amplitudes and vibration-periods of the tremors at the Station No. 3.
F; frequency

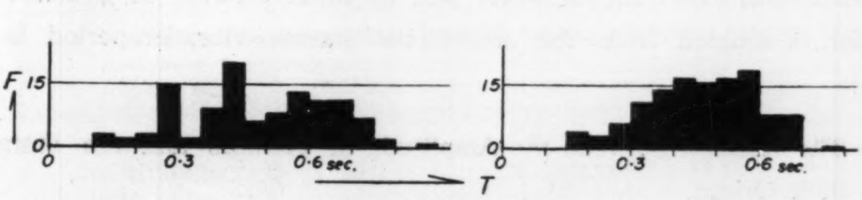

Fig. 9. Amplitudes and vibration-periods of the tremors at the Station No. 4.
F; frequency of tremors for respective vibration-periods.
T; vibration-period.

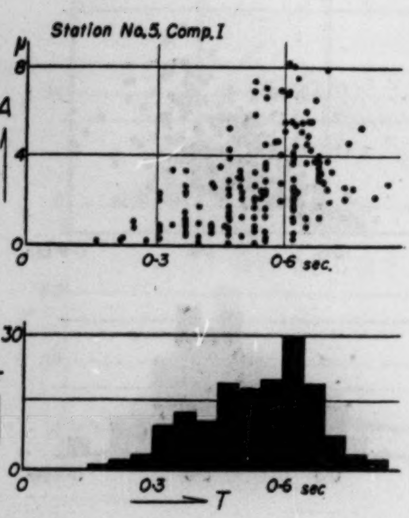

Fig. 10. Amplitudes and vibration-periods of the tremors at the Station No. 5.

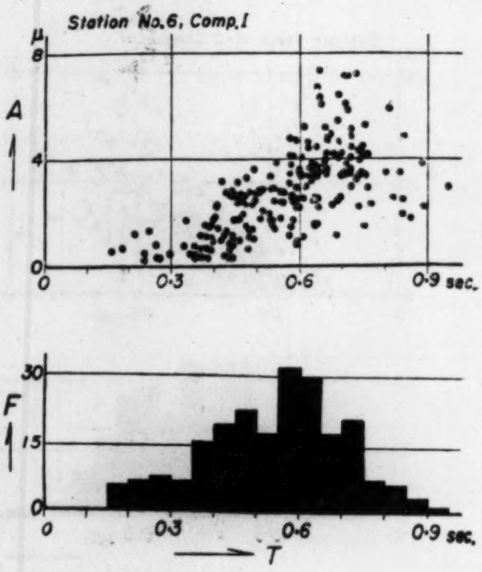

Fig. 11. Amplitudes and vibration-periods at the Station No. 6.

evident that the forms of the diagrams, or to be more exact, the maximum amplitude and the vibration period resemble each other in their general feature, notwithstanding the fact that the magnitude of amplitude varies greatly according to the epicentral distance. However, if these diagrams are precisely examined, the above relations concerning the maximum amplitudes and their vibration-periods are found to depend more or less on the epicentral distance. For instance, the vibration period of the largest amplitude at each station becomes longer by degree according to the distance from the origin, namely 0.6 second at the stations No. 1 and No. 2, and 0.7 second for the stations more distant than the formers. The phenomena are evident also from the frequency diagrams with respect to the vibration periods shown on the lower part of these figures, in which the nearer the station is situated from the origin, the shorter vibration-period is predominant.

2) The Relation between the Amplitude of Tremors and the Distance from their Origin.

The maximum amplitudes for various vibration-periods at the six stations are given in Table II, in which the double amplitudes are taken in micron unit. In addition, the relation between the maximum amplitudes of the tremors with respect to the five vibration periods, namely 0.2, 0.3, 0.4, 0.5 and 0.6 second, and the epicentral distances of these six stations is illustrated in Fig. 12, in taking the logarithmic amplitude in ordinate.

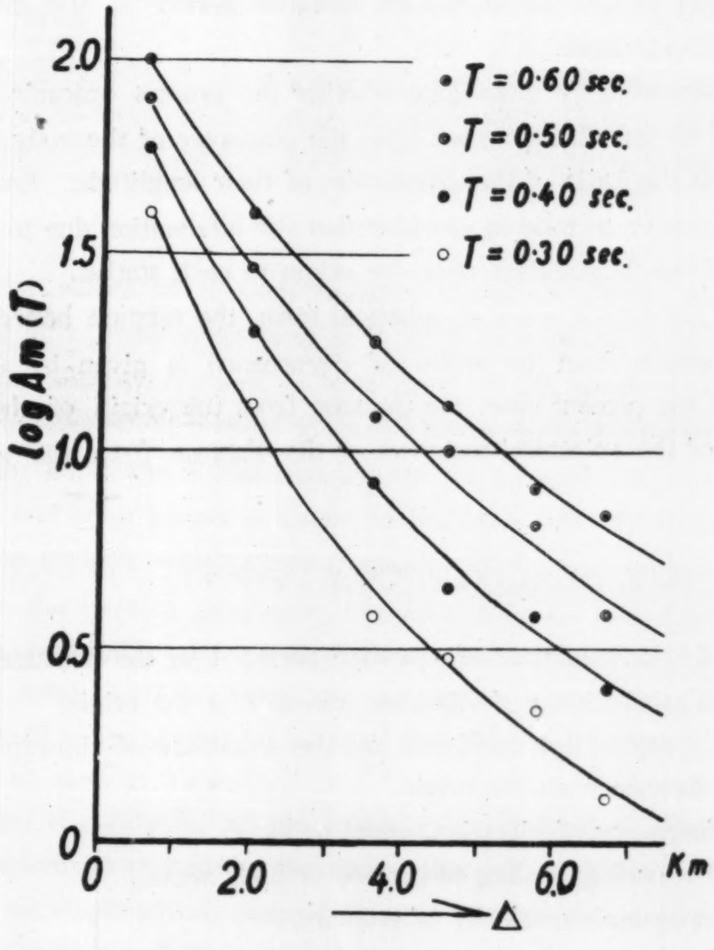

Fig. 12. Relation between the maximum amplitude at each station and its distance from the origin.

Table II. Maximum amplitudes of various vibration periods.

Station No.	Maximum amplitudes of various vibration periods				
	0.6 sec.	0.5 sec.	0.4 sec.	0.3 sec.	0.2 sec.
1	100.0μ	80.0μ	58.0μ	40.0μ	18.0μ
2	40.0	29.0	20.0	13.0	8.0
3	19.0	12.0	8.5	5.0	3.5
4	13.0	10.0	4.5	3.0	2.3
5	8.2	6.5	3.8	2.2	1.5
6	7.0	3.9	2.5	1.5	1.2

As will be seen clearly in this figure, the attenuation of amplitude with respect to the epicentral distance is remarkable and is evidently related with the vibration period, or in other words, the shorter the vibration period is, the more seriously the amplitude is attenuated.

It will be interesting to investigate whether the present volcanic tremors accompanying the Strombolian eruption have the character of the body wave or the surface wave, on the basis of the attenuation of their amplitude. For this examination, it is necessary to take in consideration the attenuation due to the damping in the course of the propagation from the origin to each station.

Concerning the elastic wave of spherical form, the relation between its amplitude and the distance from the centre of disturbance is given by the following formula, and in the present case, the distance from the origin of the tremors is similar to that of the epicentral distance, or the distance from the active craterlet (B).

$$A(T, \varDelta) = A_0(T) \cdot e^{-k(T)\Delta} \cdot \varDelta^{-n} \cdot e^{ip(t-\frac{\Delta}{V})},$$

where $A(T, \varDelta)$, amplitude of vibration period T at the distance $\varDelta$,

$A_0(T)$, amplitude of vibration period T at the origin,

$k(T)$, attenuation coefficient for the amplitude of vibration period T,

$\varDelta$, distance from the origin,

p, frequency of vibration, equal to $2\pi/T$,

n, 1/2 or 1 according to surface or body wave,

V, propagating velocity of tremors,

Since, the above relation in the present case, is applied to the maximum amplitudes of the respective vibration periods, the quantities relating to the time are constant as described already and therefore, the above formula may be written in the following form;

$$\frac{A_m(T, \varDelta_m)}{A_1(T, \varDelta_1)} = \frac{e^{-k(T)\cdot\Delta m} \cdot \varDelta_m^{-n}}{e^{-k(T)\cdot\Delta 1} \cdot \varDelta_1^{-n}}, \quad (m=2, 3, 4, 5, 6).$$

With the aid of the relation obtained from the observation (Fig. 12) and the above relation, the attenuation coefficient (k) and the value of n are determined by the method of the least square, the result of which is given in the following table;

Table III. Values of n and k for the respective vibration periods.

Vibration period	n	k
0.6 sec.	0.47	2.7×10^{-6} C.G.S.
0.5 〃	0.45	3.2 〃
0.4 〃	0.55	3.1 〃
0.3 〃	0.62	3.3 〃

Although the values of n vary to some extent according to the vibration periods, almost all of them come near to 1/2. Consequently, it is reasonable to conclude that the volcanic tremors, at least those of the present Oo-sima, propagate in the two-dimensional manner or in the mode of the surface wave.

On the other hand, the attenuation due to the internal friction in the course of propagation and other causes is shown in the same table by its coefficients for various vibration periods, which range from 2.7×10^{-6} C.G.S. to 3.3×10^{-6} C.G.S.. However, since the tremors propagate two-dimensionally, the attenuation coefficient k may be reasonably redetermined from the the calculation in which the value of n is taken as 1/2. From the calculation made by the above assumption, the values of k are given in a range from 2.5×10^{-6} C.G.S. to 3.9×10^{-6} C.G.S., as will be seen in Table IV.

Judging from the relation of the attenuation coefficients with the vibration periods, the phenomena concerning the attenuation are consistently interpreted if the attenuation of amplitude are caused by the viscous damping proportional to the inverse square of its vibration period, though another alternative interpretation is possible, for instance, an interpretation from the complex structures of the volcano formation.

From the assumption9) that the attenuation of amplitude is caused entirely by the viscosity of the surface formation of this volcano, its coefficients for the respective vibration periods are given in a range from 2.7×10^{9} C.G.S. to 1.0×10^{9} C.G.S..

As is shown in Table IV, the viscosity coefficient based on the attenuation of longer periods is larger than those given from the shorter vibration periods. However the phenomena are consistently explained if the vibrations of longer period affect the deeper parts of the volcano formation than in the case of the rapid

---

9) K. **Sezawa** and K. **Kanai**, *Bull. Earthq. Res. Inst.*, **18** (1940), 169, *etc.*
A. **Kubotera**, *Zisin*, *Ser.* 2, **3** (1950), 16.

Table IV. Attenuation coefficients and viscosity coefficients for various vibration periods.

Vib. period	Atten. Coef.	Vis. Coef.
0.60 sec.	$2.5\pm0.1 \times 10^{-6}$/cm	2.7×10^{9} C.G.S.
0.50 〃	3.0 ± 0.2	2.2 〃
0.40 〃	3.4 ± 0.3	1.6 〃
0.30 〃	3.9 ± 0.5	1.0 〃

vibrations, and, in addition, the extremely upper parts of the volcano formation have smaller viscosity than the deeper parts.

The mean vibration period of the tremors at each station is represented in Fig. 13 and Table V in relation to the epicentral distance, which show the period near the origin to be shorter than that at the distant stations. The phenomena

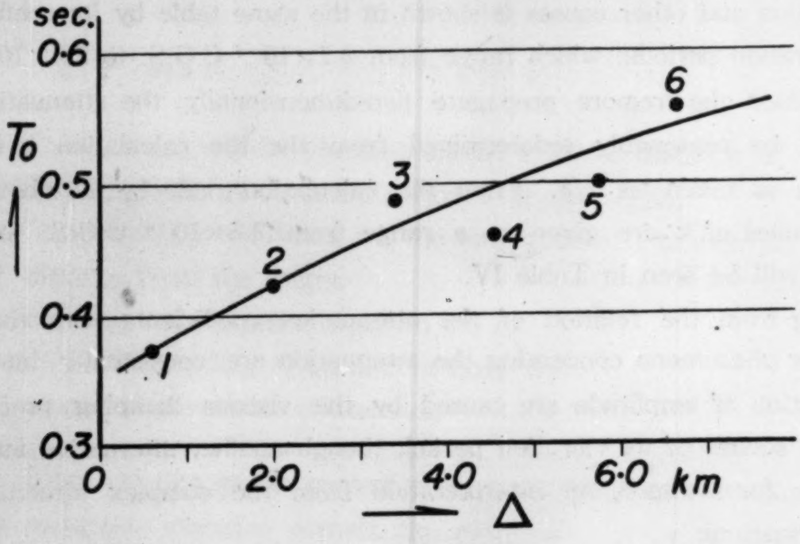

Fig. 13. Mean vibration-period of tremors and distance from their origin.

Table V.

Station No.	Epic. Dis.	Mean vib. period
1	0.6 km	0.37 sec.
2	2.0	0.42
3	3.6	0.49
4	4.6	0.46
5	5.8	0.50
6	6.7	0.56

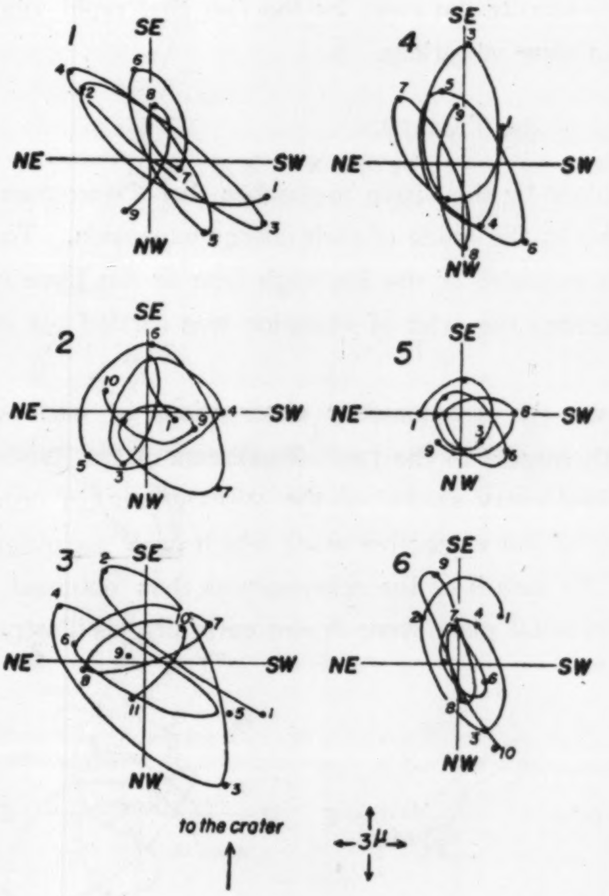

Fig. 16. Horizontal motions of the tremors at Station No. 4.

directly the type of the surface wave from the present investigations. However, the problem must be reexamined with the aid of the complete observations of the three components of the tremors including their vertical motions.

5. The Nature of Volcanic Tremors Recorded by the Acceleration Seismographs.

Besides the observations by use of the displacement seismographs with which the previous paragraph deals, the writers made the measurements of acceleration of the tremors with the aid of the acceleration seismographs.

Examples of these seismograms are shown in Fig. 24. The analyses based on the acceleration seismograms were made with respect to the vibration period and amplitude, as in the former seismograms, and the results of the analyses are indicated in the form of amplitude-period diagrams together with the frequency of vibration periods. As these diagrams of Figs. 17∼19 show clearly, the vibration are explained, as is usually the case, by the fact that rapid vibrations are damped more seriously than slow vibrations.

3) The Orbits of the Tremors.

It was made clear by the above researches that the tremors have the character of the surface wave in the mode of their energy expansion. To determine whether the tremors have the nature of the Rayleigh type or the Love type, the following investigation concerning the orbit of vibration was carried out on the basis of the seismograms.

For this purpose, the seismometric observations at each station were made simultaneously with respect to the two components of the horizontal motion, and the time was marked every second on the seismograms, in order to make exact the correspondence of the respective wave which was separately recorded by its two components. By means of the seismograms thus obtained the orbits of the tremors on the horizontal plane were drawn carefully, as illustrated in Figs. 14—16.

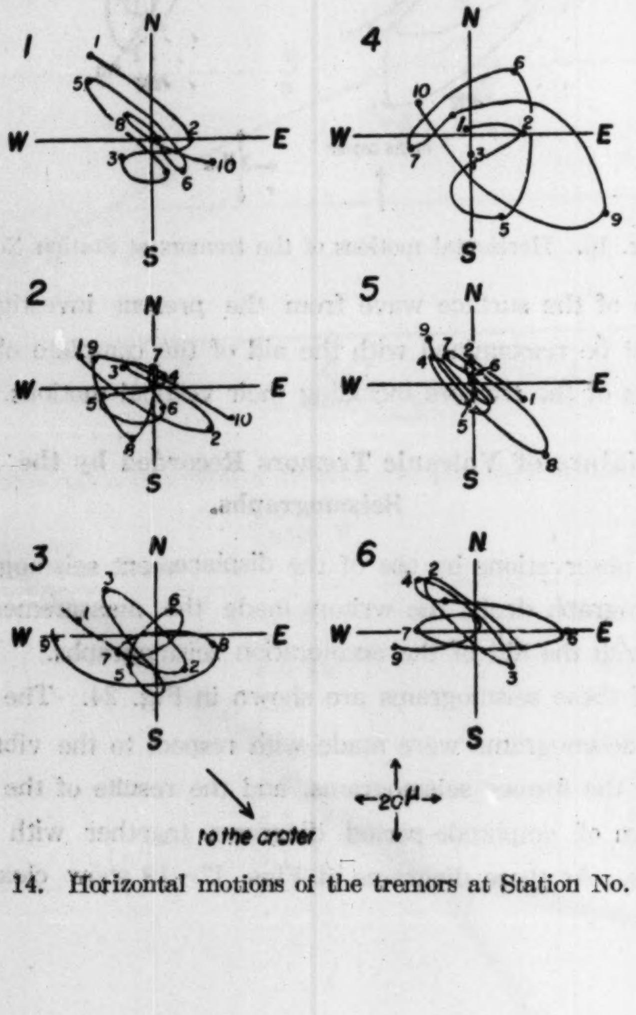

Fig. 14. Horizontal motions of the tremors at Station No. 2.

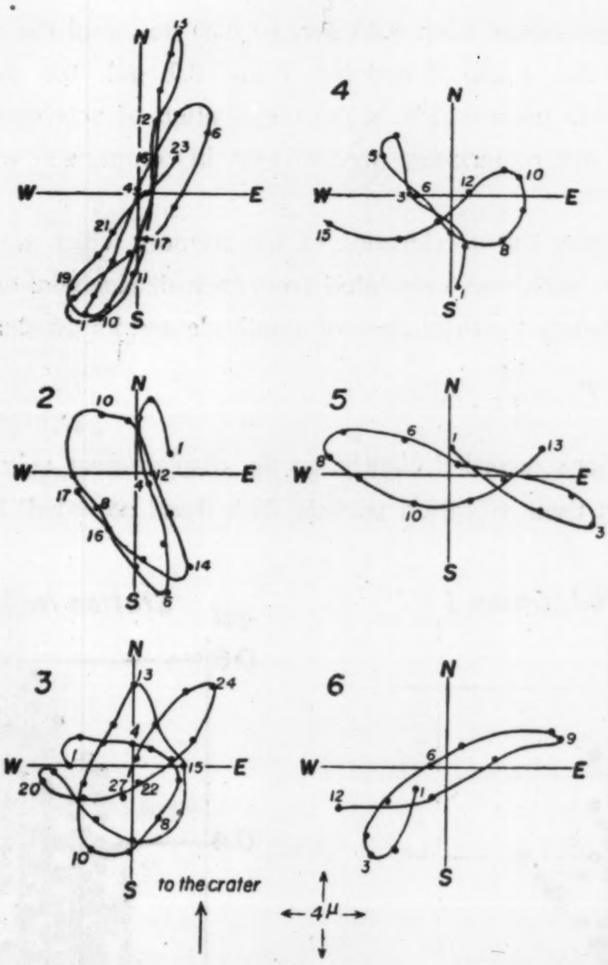

Fig. 15. Horizontal motions of the tremors at Station No. 3.

As will be seen in these figures, the orbits are mostly of elliptic form, but the prevailing direction of vibration, or in other words, the direction of the longer radius of these elliptic orbits does not keep one direction and changes every few seconds. Therefore, the volcanic tremors show by no means a simple mode of vibration, in which vibrations predominate in the direction connecting the station to the origin of the tremors or in the rectangular direction to the former.

On the other hand, K. Sassa10) studied the same problem concerning volcanic tremors accompanying the 1932 eruption of Mt. Aso, on the basis of comparison of three components of the tremors. As the result, he determined the type of the tremors and classified them into four kinds.

Since the phenomena are unexpectedly complex, it is impossible to determine

---

10) K. SASSA, *loc. cit.*

periods at each station range from 0.05 sec. to 0.35 sec. and the maximum amplitudes at the stations No. 1, No. 2 and No. 4 are 2.1 gal, 0.8 gal and 0.11 gal respectively. It is only natural that in the observation of acceleration, the tremors of the short periods are remarkably predominant in comparison with the displacement observation.

In order to compare the acceleration of the tremors which was observed in the above-described way, with that calculated from their displacment amplitude, the following relation concerning the displacement amplitude and its acceleration was used;

$$\ddot{A}(T)=\frac{4\pi^2}{T^2}A(T).$$

Since the vibrations recorded clearly by the displacement seismograph do not always harmonize in their vibration periods with those recorded by the accelera-

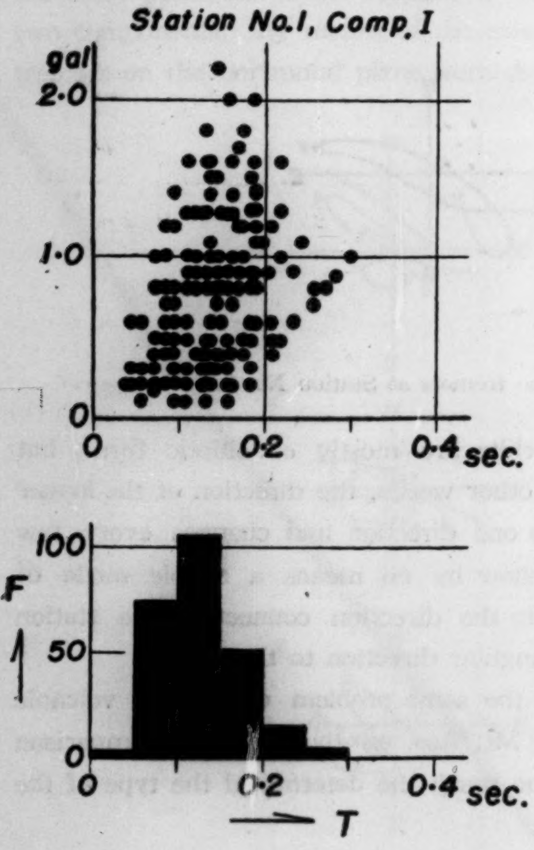

Fig. 17. Acceleration of tremors and their vibration-periods observed at the Station No. 1.

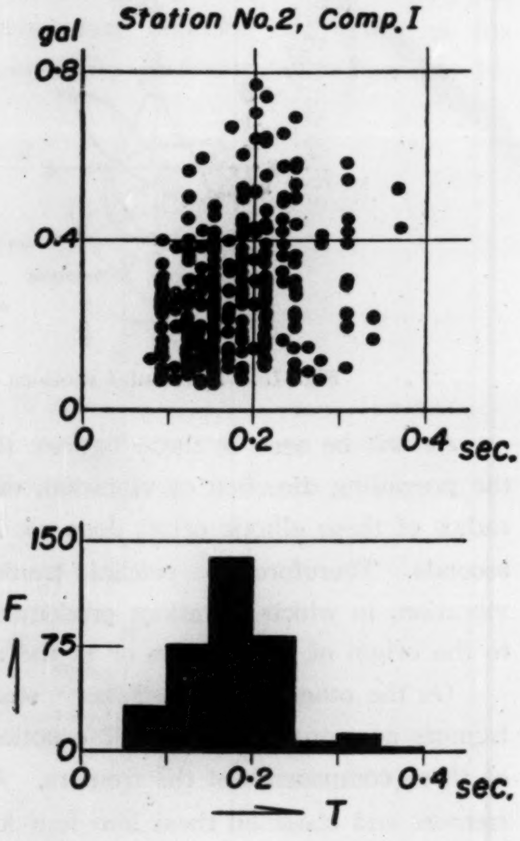

Fig. 18. Acceleration of the tremors and their vibration-periods observed at the Station No. 2.

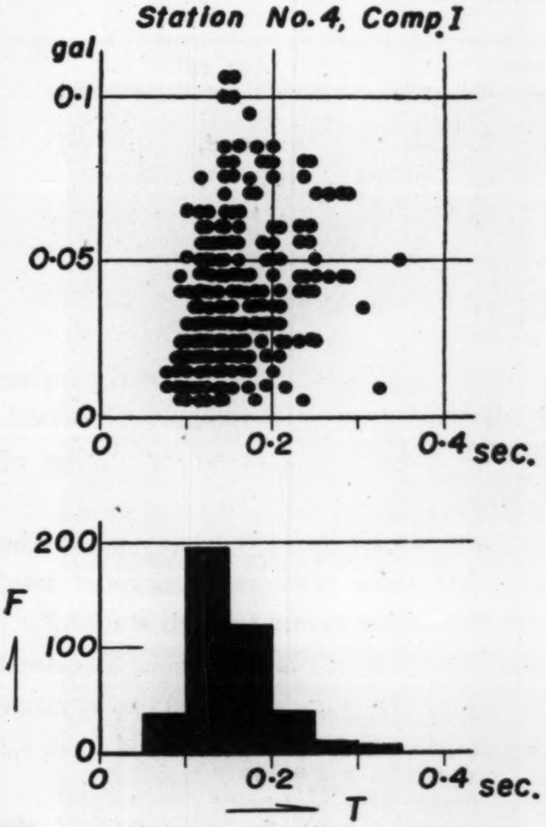

Fig. 19. Acceleration of the tremors and their vibration-periods observed at the Station No. 4.

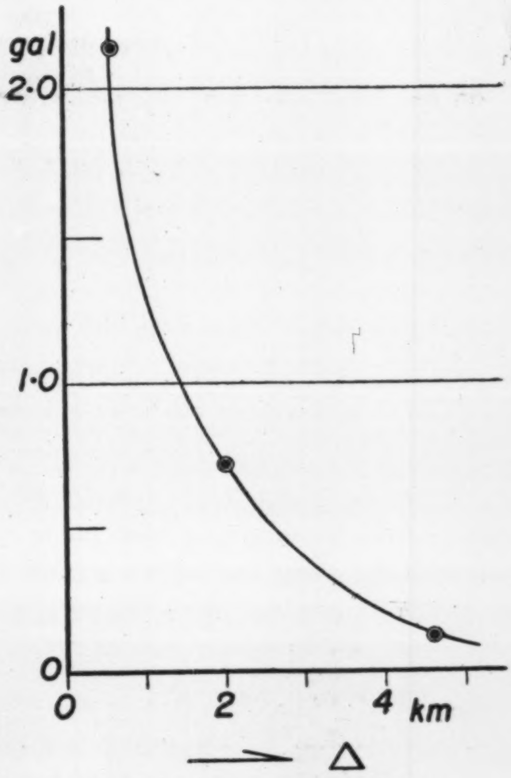

Fig. 20. The maximum acceleration of the tremors(vibration-period, 0.15 sec.) and the distance from their origin.

tion seismograph, the comparison of these two kinds of acceleration, the observed and the calculated, are made only for the tremors of 0.2 sec. and 0.3 sec. in their vibration periods and for their maximum amplitude.

As will be seen in Table VI, the accelerations calculated at the Station No. 2 are only 50 per cent of those directly observed. It seems that this discrepancy comes from the difficulty in reading the rapid and small vibrations in question on the displacement seismograms which are seriously masked by large vibrations of 0.5 and 0.6 second in their periods.

Fig. 20 shows the attenuation of the acceleration amplitude with respect to the epicentral distance.

Table VI.

Locality	Epic. Dis.	Acc. obs.		Acc. cal.	
		0.2 sec.,	0.3 sec.	0.2 sec.,	0.3 sec.
St. No. 1	0.6 km	1.7 gal,	1.0 gal	0.89 gal,	0.88 gal
St. No. 2	2.0 〃	0.8 〃,	0.6 〃	0.40 〃,	0.31 〃
St. No. 4	4.6 〃	0.09 〃,	0.06 〃	0.11 〃,	0.07 〃

6. Résumé.

1. This report deals with the nature of the volcanic tremors accompanying the 1950 eruption of Oo-sima, with a brief description of its development included. The present research of the tremor is based on observations made by means of the displacement and acceleration seismographs.

2. On the basis of the relation between the amplitude of the tremor and the distance from its origin, it was made clear that these tremors propagated two-dimensionally along the earth's surface from the active crater to each station.

3. From the assumption that the attenuation of amplitude is entirely caused by the viscosity of the mountain-formation, its coefficients are estimated to the range from 1.0×10^9 to 1.6×10^9 C.G.S. for the upper part of the formation and from 2.2 to 2.7×10^9 C.G.S. for the deeper part.

4. In order to make clear whether the tremors have the character of the Rayleigh type or the Love type, the problem was investigated with respect to the orbit of vibration. But the research failed to arrive at a final conclusion for the reason that the mode of vibrations was remarkably complex.

5. The acceleration of tremor observed directly by the acceleration-seismograph was compared with that calculated from the seismograms recorded by the displacement-seismograph.

6. The seismometric investigations of Oo-sima are still under way and this report deals only with vibrations of continuous train accompanying the Strombolian eruption. The research concerning the earthquakes of the ordinary type which occurred in the course of the present activity, will be reported in the forthcoming Bulletin.

In conclusion, the writers wish to express their sincere thanks to Mr. S. Hiraga for the valuable assistance be afforded them in the seismometric observations at Oo-sima.

[T. MINAKAMI, T. MIYAZAKI and T. TAKAHASHI.]

[Bull. Earthq. Res. Inst., Vol. XXIX, Pl. XIV.]

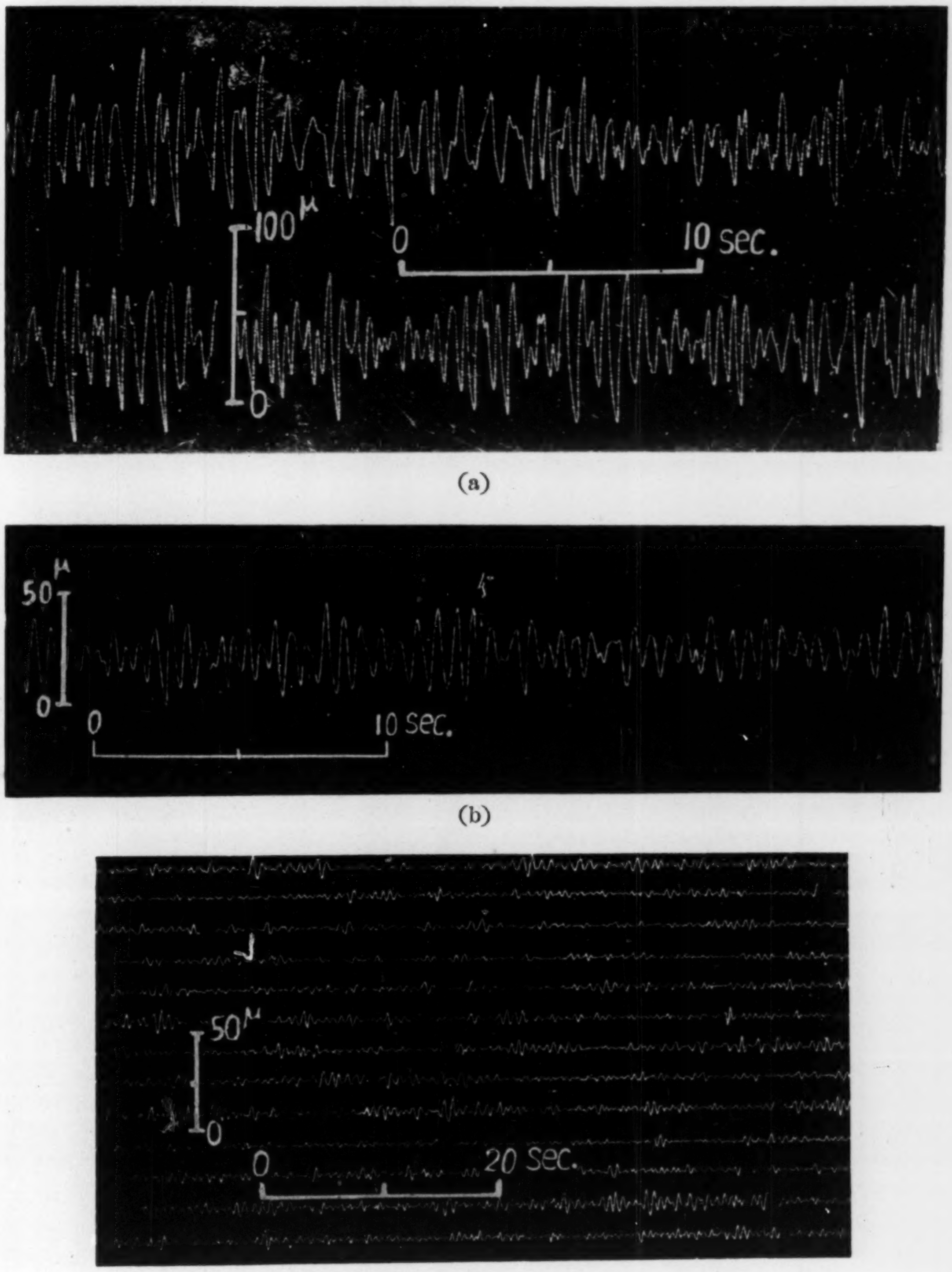

(a)

(b)

(c)

Fig. 21. Seismograms recorded at Stations Nos. 1, 2, and 3.

（震研彙報 第二十九號 圖版 水上・宮崎・高橋）

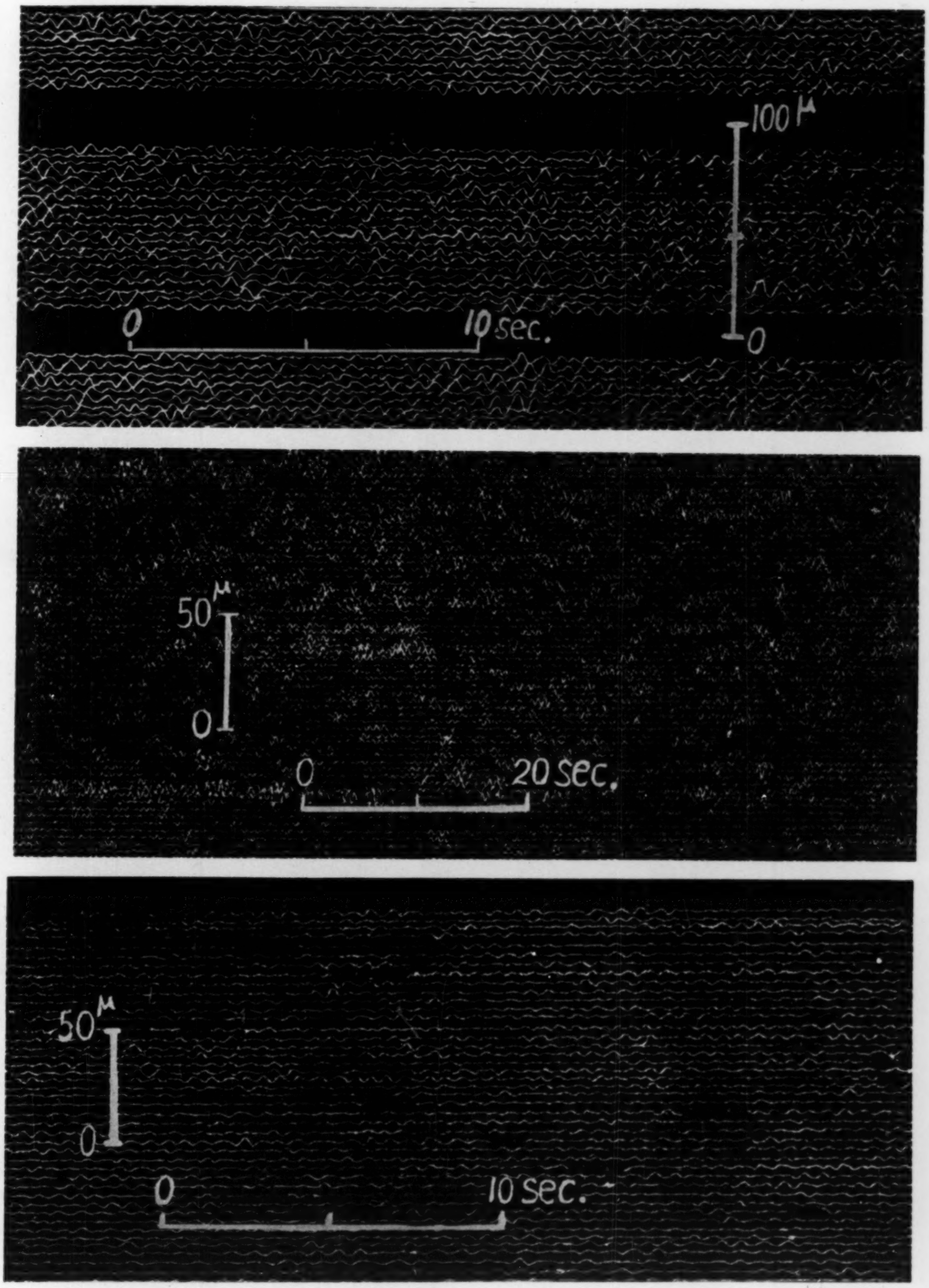

Fig. 22. Seismograms recorded at Stations Nos. 4, 5 and 6.

（震研彙報 第二十九號 圖版 水上・宮崎・高橋）

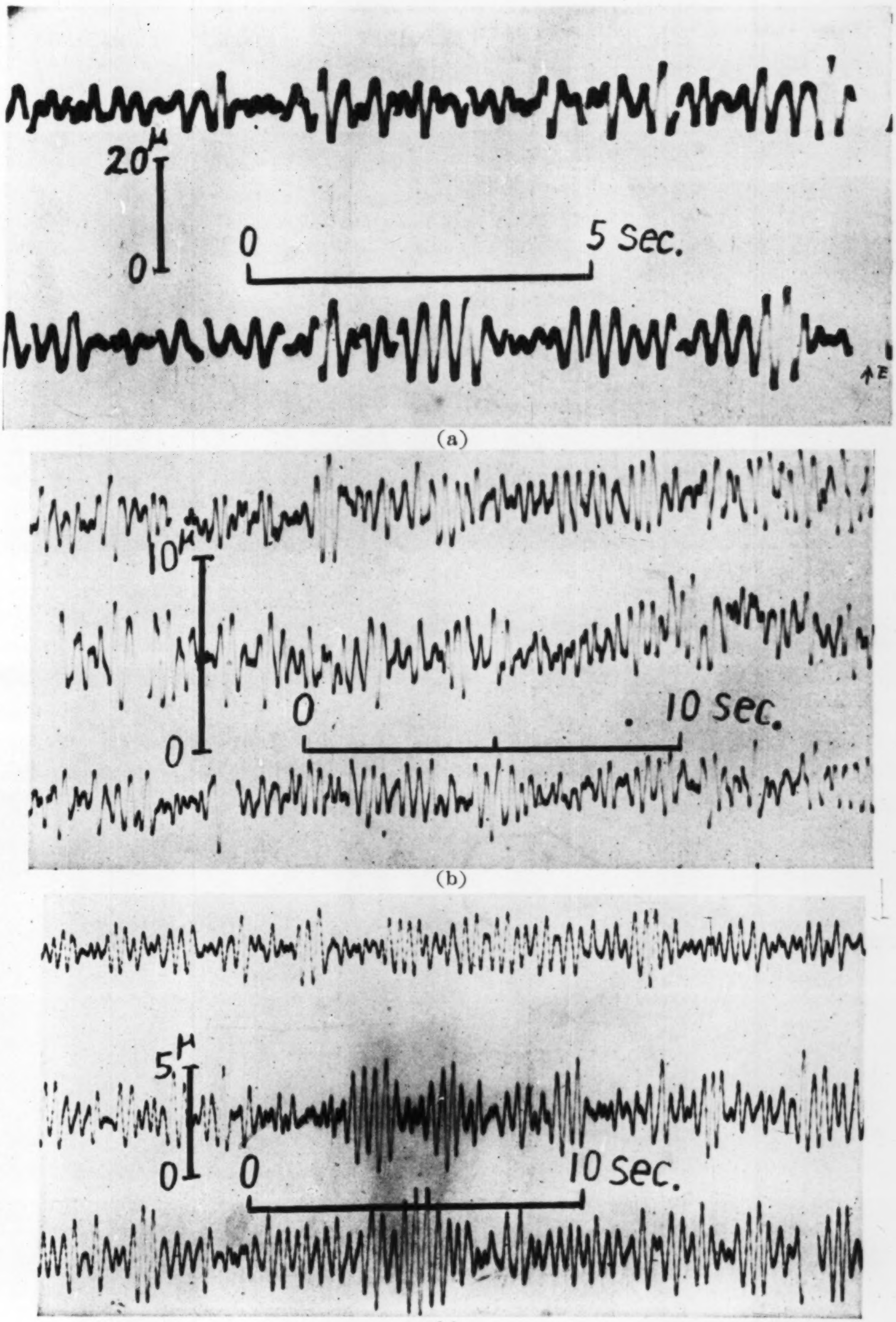

(a)

(b)

(c)

Fig. 23. Seismograms recorded optically at Stations Nos. 3, 4 and 5.

[T. MINAKAMI, T. MIYAZAKI and T. TAKAHASHI.]

[Bull. Earthq. Res. Inst., Vol. XXIX, Pl. XVII.]

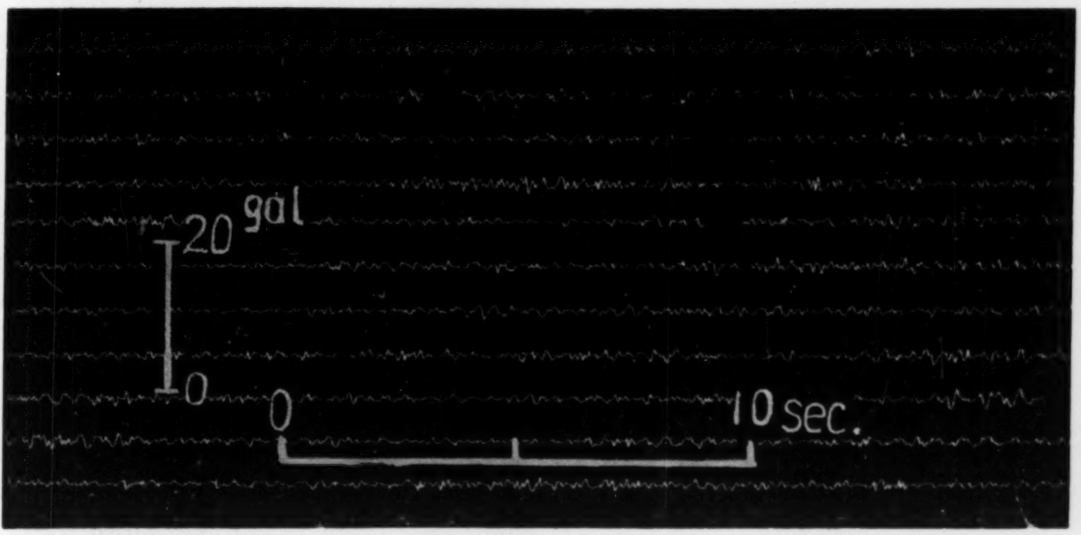

(a)

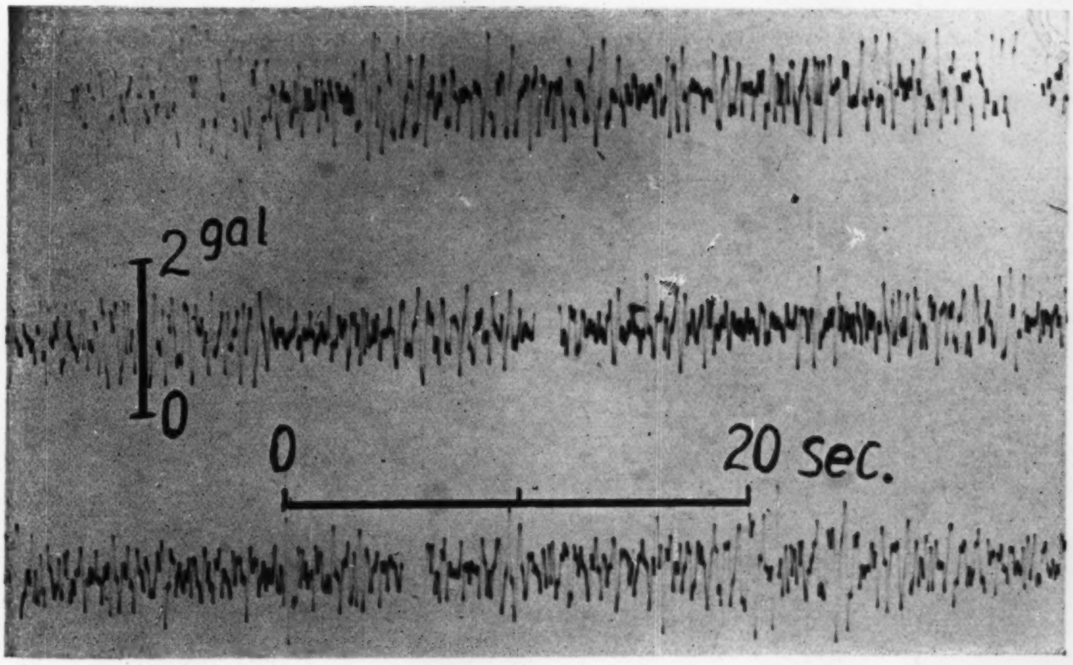

(b)

Fig. 24. Acceleration seismograms recorded at Stations Nos. 1 and 2.

(震研彙報 第二十九號 圖版 水上・宮崎・高橋)

[T. MINAKAMI, T. MIYAZAKI and T. TAKAHASHI.]

[Bull. Earthq. Res. Inst., Vol. XXIX, Pl. XVIII.]

（震研彙報 第二十九號 圖版 水上・宮崎・高橋）

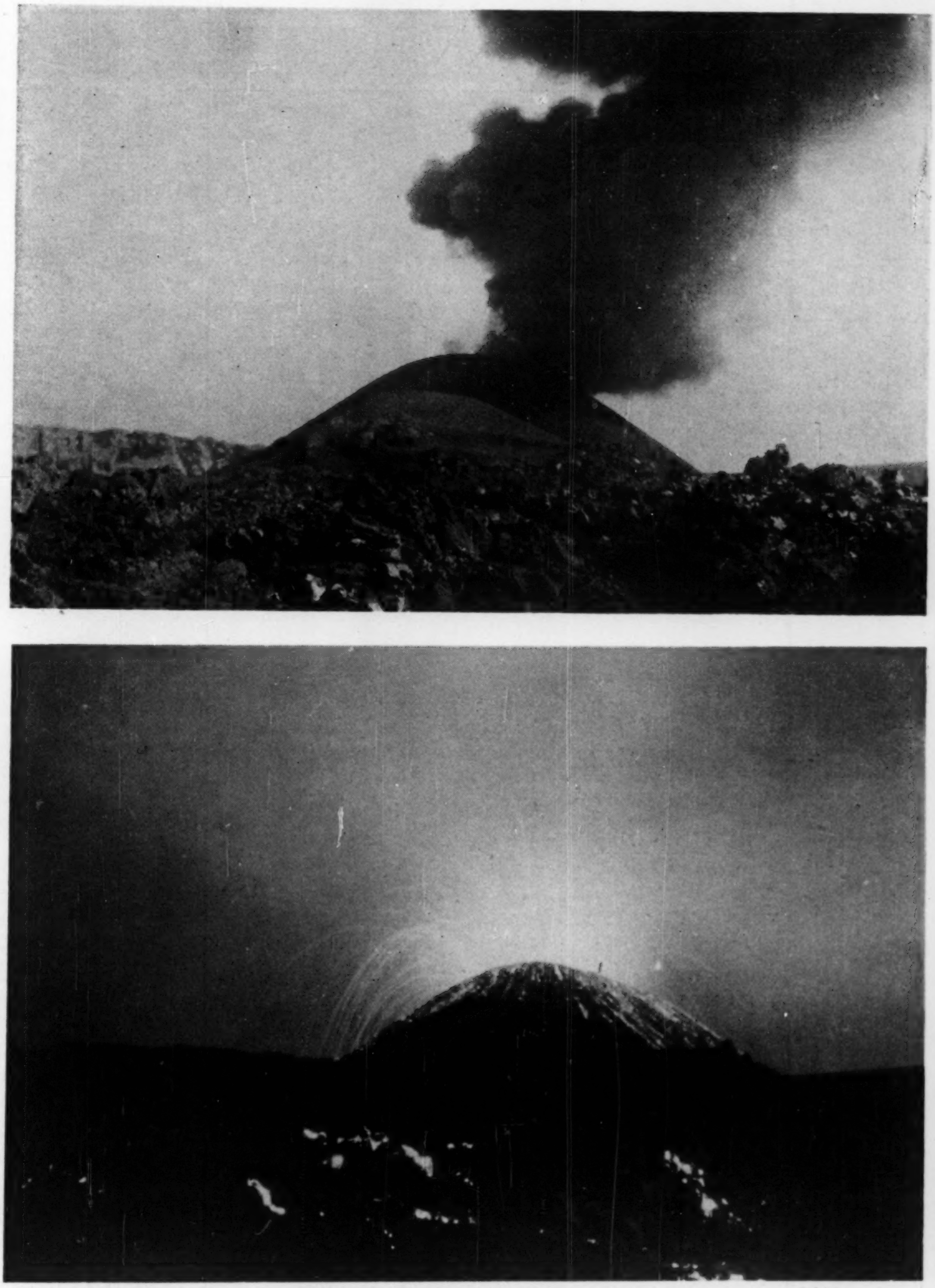

Fig. 25. The cinder cone (B) viewed from Station No. 1 on the inner somma. (September 16, 1950)

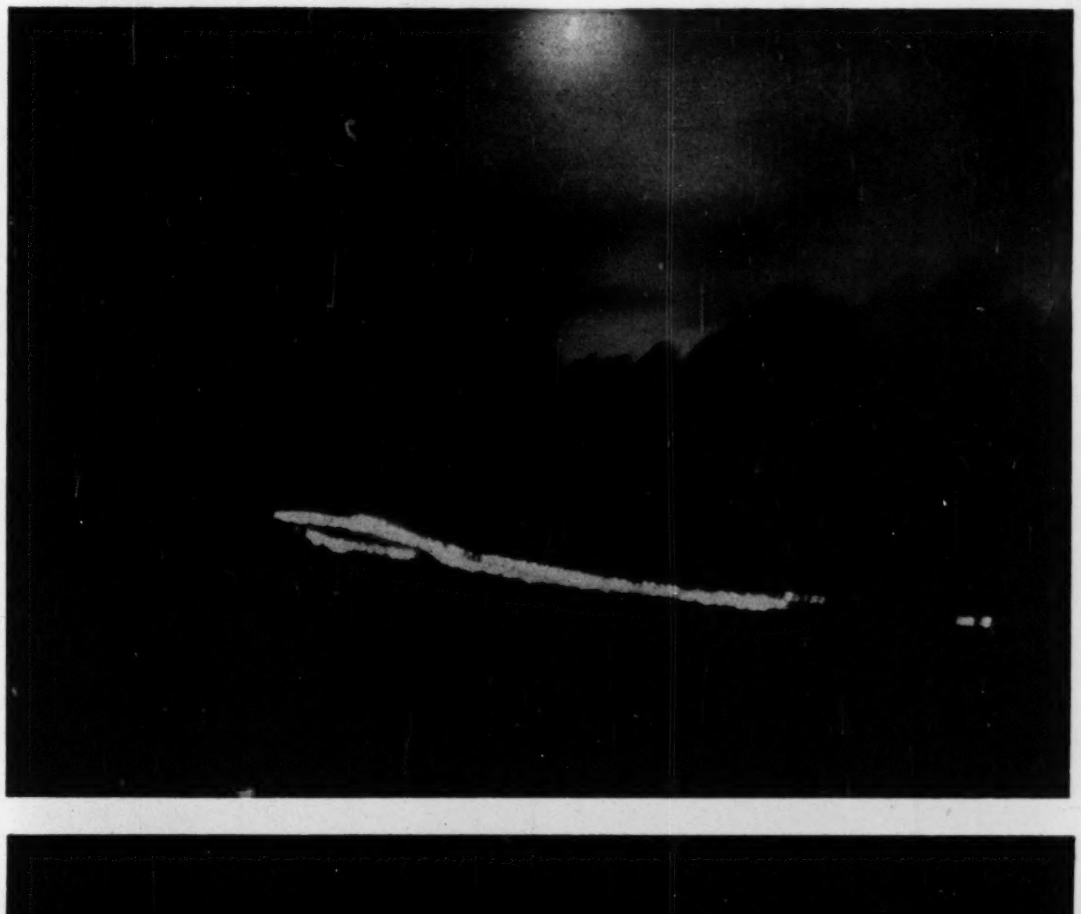

Fig. 26. Lava streams flowing down on the flank of the inner somma. (September 16, 1950)

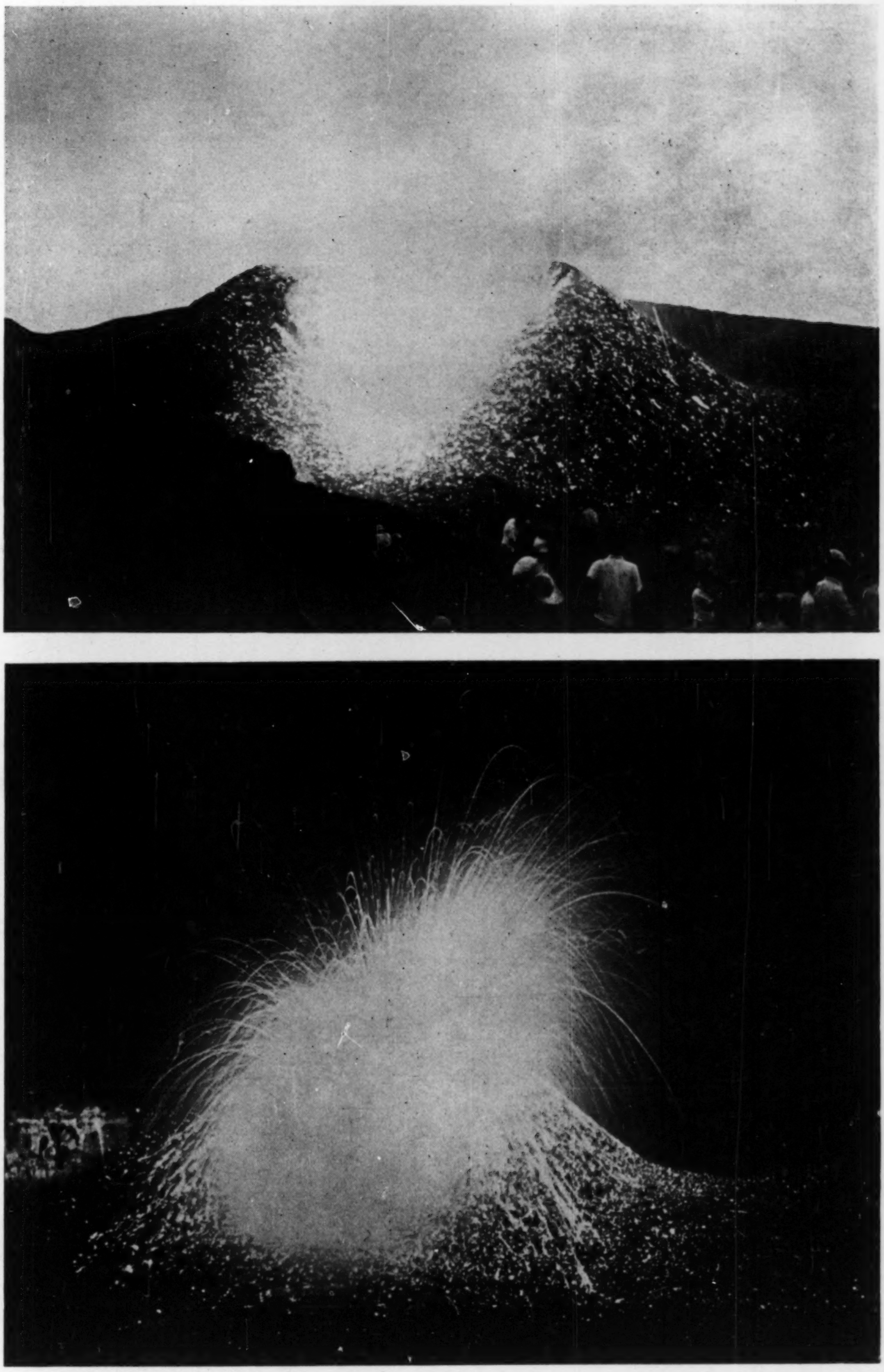

Fig. 27. The newly formed cinder cone (B) and its craterlet of a horseshoe shape.
(September. 1, 1950) (After S. Murauchi)

（震研彙報 第二十九號 圖版 水上・宮崎・高橋）

32. 最近の大島の噴火とその地震計測學的研究 (I)

水上　武
地震研究所　宮崎　務
高橋智子

大島火山は 1940 年の小噴火以來約 10 年ぶりで, 1950 年 7 月 16 日より約 70 日に亙つて著しい活動を示した. その後約 4 ヶ月間は平穩な狀態を續けたが 1951 年 2 月以來再び噴火を開始し熔岩を流出し, 現在 (1951 年 3 月 31 日) 尙活動中である. 本文は 1950 年の第 1 期活動のストロンボリ式噴火に伴つた火山脈動の計測學的研究についての報告である.

火山脈動はストロンボリ式噴火と密接な關係があるので 7 月 16 日より 9 月 23 日に至る今回の大島の噴火現象についても, 簡單に記述してある.

今回の調査に使用した地震計は周期 1.0 秒, 幾何倍率は 200 倍, 及び光學的記錄を用いて, 脈動の振幅に應じて, 4,000, 2,000 並に 1,200 倍にして使用した. 更に脈動の加速度を觀測するために, 振子の板ばねを取りかえて周期を 0.1 秒の加速度地震計として使用した.

活動中の火口から種々の距離に於いて觀測した結果並にその火口附近に於ける有感脈動の強度分布等から判斷して脈動の震動源は火口の下 200〜300 米より淺い所にあるらしい.

脈動の振幅と震動源との距離の關係から脈動は地表に沿うて二次元的な擴りを以つて傳播している事を確めた.

振幅の減衰が傳播中に於いて火山體を構成する物質內部の粘性に由るものとしてその係數を求めた. その結果, 周期 0.5〜0.6 秒の脈動の減衰よりは粘性係數の値として $2.2\sim2.7\times10^9$ C.G.S., 0.3〜0.4 秒の脈動からは $1.0\sim1.6\times10^9$ C.G.S. を得た. 長周期脈動の方が地表下深部まで影響を持つ事を考えれば, 大島火山は地表面よりやや深い部分を構成する火山堆積物の方が極めて地表近くを構成するものに較べてやや粘性が大きい事を示すものである.

水平二成分の觀測より地表面に於ける脈動の orbit の模樣を調べたが, 振動の方位は極めて複雜に變化して特定の方向に卓越する事實は認められなかつた. 從つてこれから直ちに表面波の type を定めることは困難であつた. しかしこの問題は上下動を加えた完全なる觀測によつて再び檢討する必要がある.

加速度地震計による觀測結果について上記と略同樣に脈動の傳播についてその性質を考究した. また變位地震計による觀測から算出された加速度と加速度地震計によつて直接觀測された結果とを比較し, 略滿足する結果を得た.

本研究は目下尙進行中であるが, 1951 年 3 月中の同火山の活動の際にも同樣の測定を行い, 第一期噴火中の脈動の性質と相異するか否かについて目下檢討を行つている.

33. *The Minor Activity of Volcano Azuma in February 1950.*

By Takeshi MINAKAMI and Shiro HIRAGA.

Earthquake Research Institute.

(Read Dec. 19,1950.—Received Mar. 20,1951.)

1. Introduction.

Mt. Azuma is located at the north-eastern part of the mainland of Japan and is 1948.3 m above the sea-level at its main cone, Issaikyo, of which the geographical latitude and longitude are 37°43′.0 N and 140°15′.0 E respectively. In the vicinity of Volcano Azuma, there are two other volcanoes, Mt. Bandai and Mt. Adatara, the first lying 21 km distant to the south-west of Azuma and the other 13 km to the south-east.

These three volcanoes[1] went into violent eruption one after another within a period of 11 years from 1888 to 1899, notwithstanding the fact that they had been in a perfect dormant state for several centuries. Of these volcanic activities, the 1888 eruption of Mt. Bandai was in fact catastrophic in its nature as well as in its magnitude, and resulted in the lost of Ko-Bandai, one of the two main cones, of which the volume of destroyed formation was estimated at 1.2 km³ by S. Sekiya and Y. Kikuchi.[2] Since the 1888 eruption of Bandai, the volcanologists in Japan have payed special attention to the volcanic or seismic activity of these three volcanoes including Azuma.

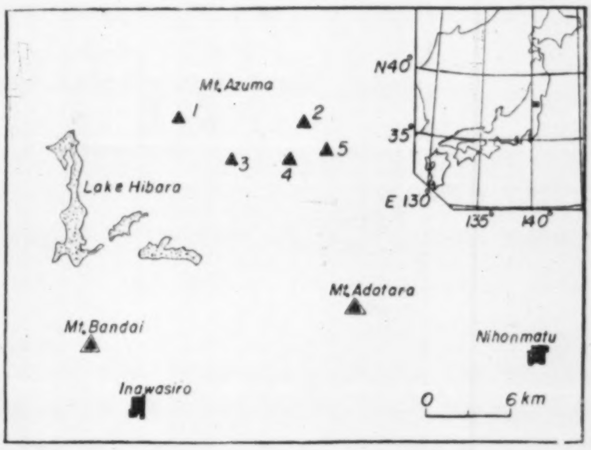

Fig. 1. Localities of Mt. Azuma and its main cones.
1. Nisi-Azuma, 2. Issaikyo,
3. Naka-Azuma, 4. Higasi-Azuma,
5. Azuma-Kohuzi.

At first, it will be necessary to introduce briefly the morphology and an outline of the previous eruption of Mt. Azuma. Besides the main cone, Issaikyo, this volcano has four cones on the circular platform, namely Higasi-Azuma, Nisi-Azuma, Naka-Azuma and Ko-Huzi, and in addition several crater-lakes of various sizes including Gosiki-numa and Kama-numa etc. which are located on the flank or at the base of these cones. Therefore, it may be said that Volcano Azuma is not formed in a simple 'conide' and has rather a complex structure from the morphological view-point. Judging from the fact that hot spring and fumaroles issue from numerous spots at the skirts, flanks and summits of these cones, the

---

[1] F. OMORI, *Rep. Earthq. Inv. Comm.*, **86** (1918), 135.

[2] S. SEKIYA and Y. KIKUCHI, *Jour. Sc. Coll.*, **3** (1890), 91.

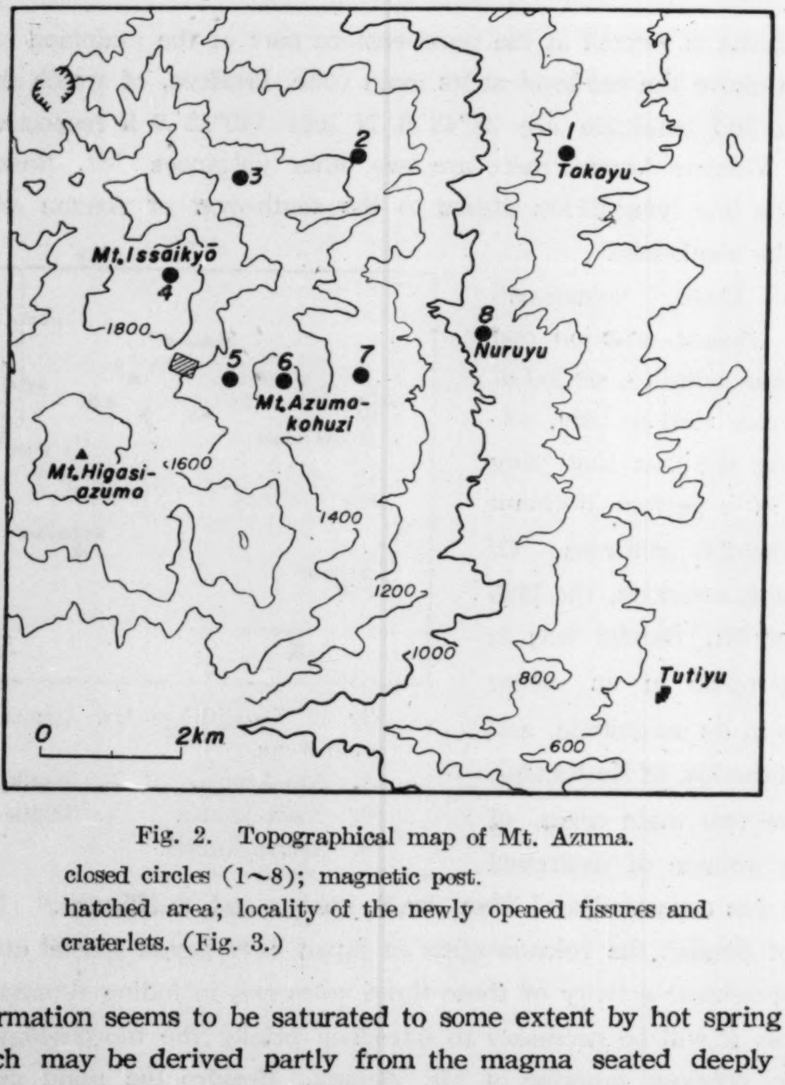

Fig. 2. Topographical map of Mt. Azuma.
closed circles (1~8); magnetic post.
hatched area; locality of the newly opened fissures and craterlets. (Fig. 3.)

mountain formation seems to be saturated to some extent by hot spring water and vapour which may be derived partly from the magma seated deeply and partly from the circulating water. The phenomena just mentioned are frequently observed in the volcanoes showing fumarolic activity such as Kusatu-sirane, Kurikoma-dake etc.

On May 19, 1893[3] Mt. Azuma erupted from an ancient crater and from the newly formed craterlets in its vicinity, which were all located at the south-eastern flank of Issaikyo, and ejected volcanic detritus with vapour to the top of Issaikyo, of which the total volume of ejecta on the first day of the eruption was estimated at 10^6 tons. After eruptions of similar feature occurred at the same craters on 4,5 and 7 June of the same year, the volcano remained in calm state up to February 1894. However, Mt. Azuma resumed again several minor eruptions during the periods from March to April 1894, from March to September 1895 and September 1896. The ejecta from these outbursts were composed of only detritus and fine mud-like ash which both had formed a part of the mountain formation at the craters newly into action, and no juvenile material from the magma was found.

Since the 1893-1896 activities, we have had no information available for the subsequent 57 years concerning the volcanic or seismic activity of this volcano.

2. The Minor Fumarolic Activity in February 1950.

Towards 19h 30m on February 10, 1950, Mt. Azuma outburst, with no noticeable forerunning phenomenon, in the neighbourhood of the craters newly opened in the previous eruption. Another explosion followed in the same location accompanied with rumblings at about 18h 30m on the 19th of the same month, nine days after the first explosion.

In order to study the nature of the present eruption of Azuma, the writers with their associates carried out two series of investigations, the first being devoted to seismometric observations for two months soon after the first outburst and the other including the topographical survey of the craterlets newly formed in the present eruption and the geomagnetic survey of this volcano.

Several craterlets and numerous fumaroles were newly formed in the present explosions on the south-eastern flank of Issaikyo, as in the case of the 1893 eruption. The locality of these craterlets and fumaroles is shown on the map of Fig. 3, which was made with the aid of the plain-table method during the period from June to July 1950. As shown clearly on this map, these craterlets and fumaroles are arranged on three fissure lines (A_1A_1', A_2A_2', and A_3A_3'), the first of which runs in the east-west direction passing through an ancient crater partly buried and the other two in parallel are located at the western side of the 1893 crater.

---

[3] F. OMORI, *loc. cit.*

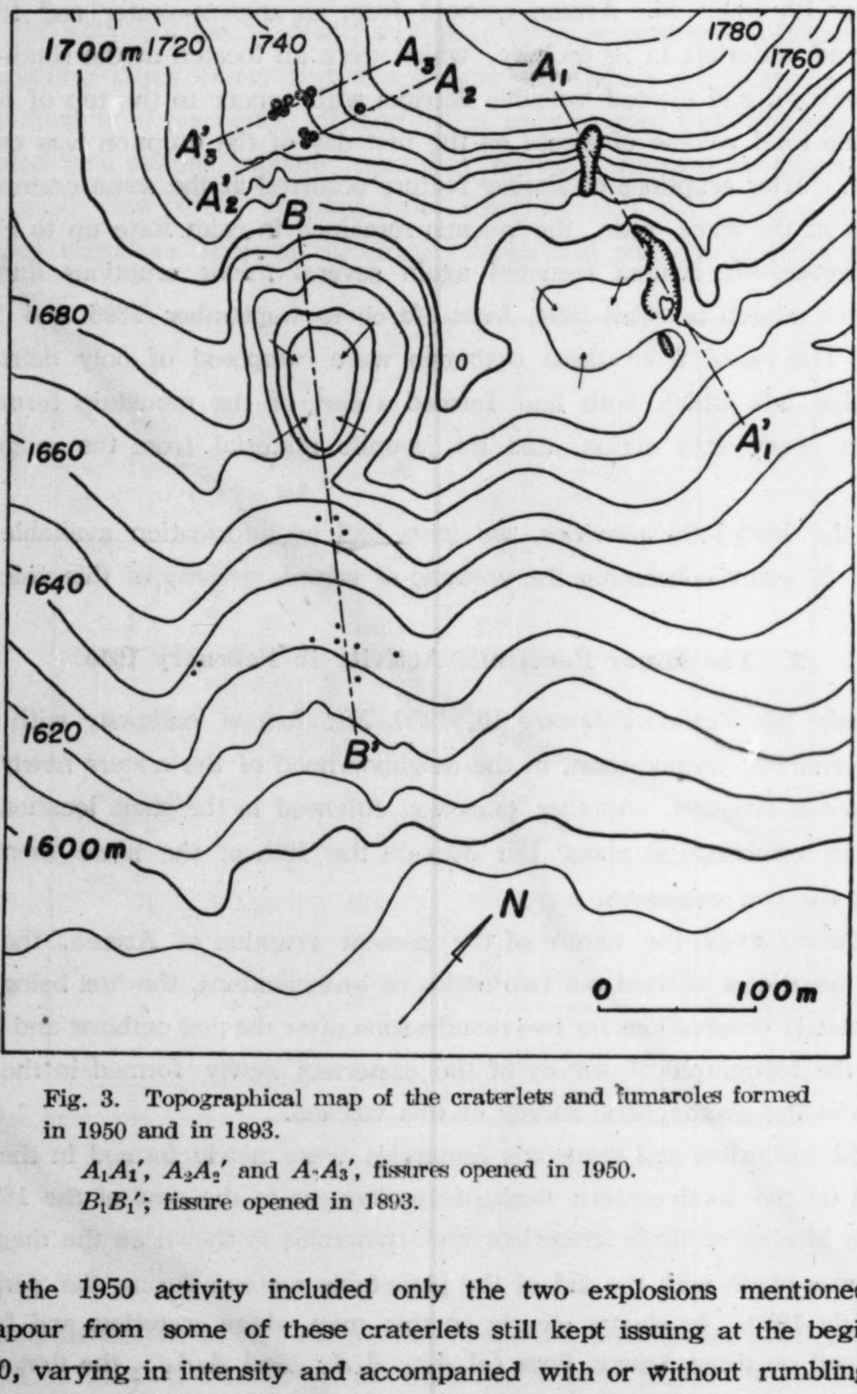
1700m
1720
1740
1780
1760
A_3
A_2
A_1
A_3'
A_2'
B
1680
0
1660
A_1'
1640
1620
B'
1600m
N
0
100m

Fig. 3. Topographical map of the craterlets and fumaroles formed in 1950 and in 1893.

A_1A_1', A_2A_2' and A_3A_3', fissures opened in 1950.
B_1B_1'; fissure opened in 1893.

Although the 1950 activity included only the two explosions mentioned above, steam vapour from some of these craterlets still kept issuing at the beginning of June 1950, varying in intensity and accompanied with or without rumblings. Fig. 7 shows a portion of the crater and fumaroles on the fissure line A_1A_1' on June 28, 1950.

It must be added that the crater and fumaroles along the BB' line on the map of Fig. 3 were formed in the 1893 activity, and from these fumaroles, vapours with evaporated sulphur have issued incessantly for 57 years from the previous eruption up to the present. As the result, sublimates rich in condensed sulphur were observed at the margin of the orifice of each fumarole. Besides the activity of these fumaroles, hot springs, about 95°C in their orifice temperature, have welled up from several spots on this fissure line and flowed down to the eastern base in a narrow stream, though not so abundant in volume.

As described above, the activity of both the fumarole and hot spring which formed in 1893, did not change so remarkably as to be noticed by several observations throughout the present eruption, notwithstanding the fact that they are situated near the active fissures newly opened.

The orifice temperatures of mineral water issuing from the fumaroles formed in 1893 and in 1950, were measured on June 29, 1950, the result of which is given in the following table:

Table I. Orifice temperature of mineral water.

(a) The 1893 fumaroles.

No.	(1)	(2)	(3)	(4)	(5)	(6)
Orif. Temp.	94°C	95°C	88°C	94°C	94°C	56°C

(b) The 1950 fumaroles.

No.	(7)	(8)
Orif. Temp.	95°C	94°C

The present ejecta including volcanic detritus and fine fragmental rocks, which are petrologically characterized by pyroxyne-andesite, were not originated from the fresh magma as was the case in the previous and historical activities of this volcano.

According to the field investigation carried out in the summer of 1950, the present volcanic detritus of larger sizes, 20-50 cm in their diametre, were mostly distributed within a distance of 500 m and towards the eastern side of the newly opened craterlets, or in other words, towards the base of Issaikyo. It is quite natural that the distribution of detritus of large diametre, as mentioned above, should have been affected greatly by the topography of the area in which the present craterlets were opened. On the other hand, the fine ejecta such as ash and fine fragmental rocks fell on the south-eastern flank and foot of the mountain, blown there by the wind prevailing at the time of the present two explosions.

Judging from the size of the newly formed craterlets and the distribution of ejecta, we may conclude reasonably that the 1950 eruption was of a smaller scale than the 1893 eruption in the volume of ejecta as well as in the intensity of outburst.

3. Seismometric Investigation.

On the basis of the seismometric investigations[4] and the ancient records[5] both concerning numerous volcanoes in Japan as well as in the other parts of the world, it will be remarked that earthquakes at a depth of several kilometres under the volcanoes take place predominantly prior to and in the course of remarkable eruptions, in which fresh lava, especially that of acidic character such as andesite or dacite is extruded to the earth's surface. Thus it may be interesting to investigate whether such phenomenon appears or not in the eruption of the fumarolic type extruding no fresh material from the magma as was the case in the present activity of Azuma.

In the fumarolic activities of Volcano Kusatu-sirane[6] during 1937–1942, earthquakes of this type did not appear, notwithstanding the fact that the seismometric observation near the active crater was made by means of a highly sensible seismograph throughout the active period, though only microtremors caused by incessant steam explosions throwing mud-like ash were recorded as in the cases of the Strombolian eruption. However, in the 1949 activity of Mt. Yake-yama[7] which was apparently similar to those of Kusatu-sirane and Azuma in the nature of eruption, earthquakes of various depth ranging from several kilometres to the earth's surface took place in the course of the 1949 activity, and especially predominated for two or three days before the main explosions. Therefore, one of the writers[8] concluded in the previous Bulletin that the 1949 activity of Mt. Yake-yama or its effusive force at least must have originated directly from the depth of several kilometres under the volcano, or in other words, from the intrusive force of the fresh magma, which was not extruded to the earth's surface.

In contrast to that, it may be said that the eruptive force of Kusatu-sirane

---

4), 5) F. OMORI, *Bull. Earthq. Inv. Comm.*, **5**, **6**, **7**, **8** and **9** (1911—1921).
T. MINAKAMI, *Bull. Volcanol.* (*I.U.G.G*), *Sér*, II, **10** (1950), 59.

6) T. MINAKAMI, *Bull. Earthq. Res. Inst.*, **17** (1939), 590: **20** (1942), 505.

7) S. SAKUMA, and T. MINAKAMI, *Bull. Earthq. Res. Inst.*, **27** (1949), 117.

8) *loc. cit.*

just mentioned was derived through a mechanism similar to the geyser near the earth's surface and not from the fresh magma deeply seated.

Which is actually the case for the present fumarolic activity of Azuma? To throw a light on this problem, a seismometric observation was carried out for two months soon after the first explosion on February 10, at Tutiyu at the south-eastern skirt of the volcano, 8.5 km distant from the active craterlets. Notwithstanding the fact that a highly sensible seismograph (or to be more exact, the instrumental constants were always 1.0 second in its proper period of vibration and 200 on the smoked paper and 4,000 on the bromide paper both in its geometrical magnification) was used for this purpose, no earthquake from Azuma was recorded through the period of observation.

On the basis of the facts discussed above together with the feature of the present activity, it seems that the 1950 outburst of Mt. Azuma was not caused directly by the activity of fresh magma inferred to exist under the volcano. But this conclusion does not deny the idea that the heat energy necessary for the present fumarolic activity of Azuma and of Kusatu-sirane may have been supplied slowly or rapidly in the form of vapour and other gases of high temperature derived from the fresh magma.

4. Geomagnetic Survey of Mt. Azuma.

One of the writers has devoted himself to the geomagnetic surveys of the active and dormant volcanoes in Japan such as Asama, Huzi (Fuji), Miyake-Sima, Sakura-zima and Kusatu-sirane[9] etc. and also from now on intends to continue this investigation in order to elucidate the magnetic feature of volcanoes relating to the characteristics of each volcanic zone.

In the present investigation of Azuma, the writers spent several days on the magnetic survey, in which only the inclination of the geomagnetic field was measured at eight localities, which, as is shown on the map of Fig. 2, are distributed on the summit, flank and foot of the mountain. The results of measurement are given in Table II together with the heights above sea-level of the eight spots, and in addition, the relationship between these two kinds of value is illustrated in Fig. 4. As the figure shows clearly, the value of the magnetic dip increases in accordance with the height of the localities on which the measurement was made, though this relation is to some extent affected by the irregularities in topography.

---

[9] T. MINAKAMI, *Bull. Earthq. Res. Inst.*, **16** (1938), 100: **18** (1940), 178: **19** (1941), 356: **18** (1940), 318: **16** (1938), 117.

Table. II. Magnetic inclinations and the heights above the sea-level of the eight spots at Mt. Azuma.

No.	Date	Mag. incl.	Height (a.s.l.)
1	June 27 (1950)	50° 3.′4	700 m
2	〃	51 56.9	1370
3	〃	51 15.9	1550
4	〃	53 6.0	1949
5	June 28	50 31.7	1560
6	June 29	51 47.8	1700
7	〃	51 7.0	1330
8	〃	49 8.3	900

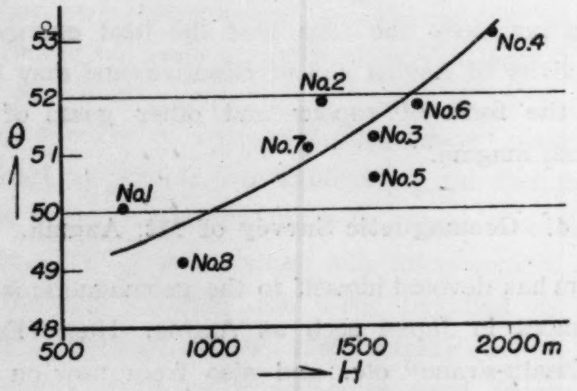

Fig. 4. The magnetic dip of eight points at Mt. Azuma and their heights above sea-level.

So far as the mode of magnetization[10] of the volcano is concerned, the phenomena are common with those of the volcanoes mentioned above. However, it must be remarked that the intensity of magnetization of Azuma is similar to that of the andesite volcanoes such as Asama, Sakura-zima and Kusatu-sirane etc., or in other words, with a third or a fifth of that of the saturated basalt volcanoes such as Huzi, Oo-sima and Miyake-sima. Seeing that the rocks forming Mt. Azuma are mainly characterized by pyroxyne-andesite as in the former andesit group of volcanoes, it will be only natural that the feature concerning the magnetic property of Azuma also coincides with the former.

---

[10] T. NAGATA, *Bull. Earthq. Res. Inst.*, **21** (1943), T. MINAKAMI, *loc. cit.*

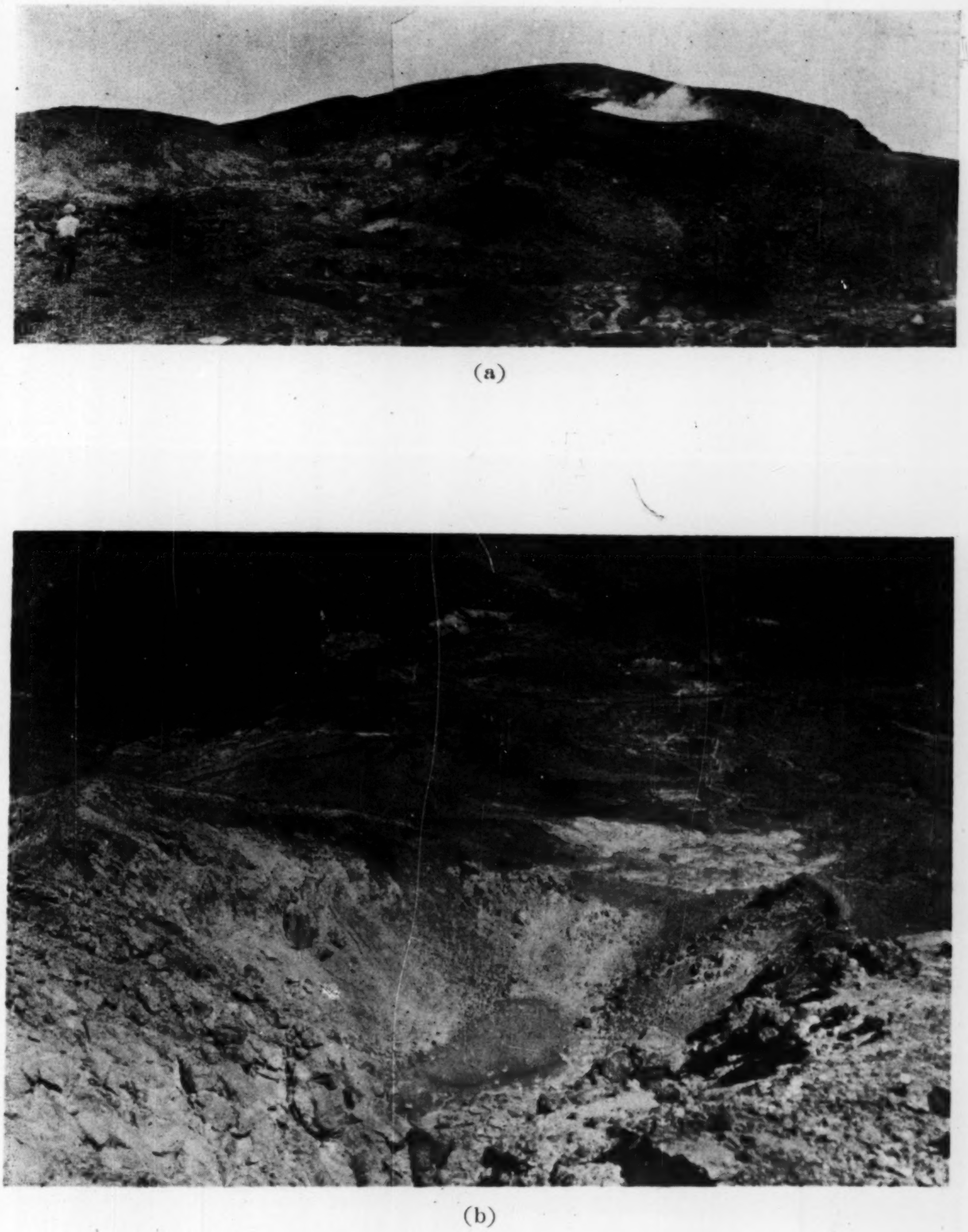

Fig. 5. (a) Mt. Issaikyo, main cone of Azuma, viewed from its south-eastern base.
(b) The crater formed in 1893.

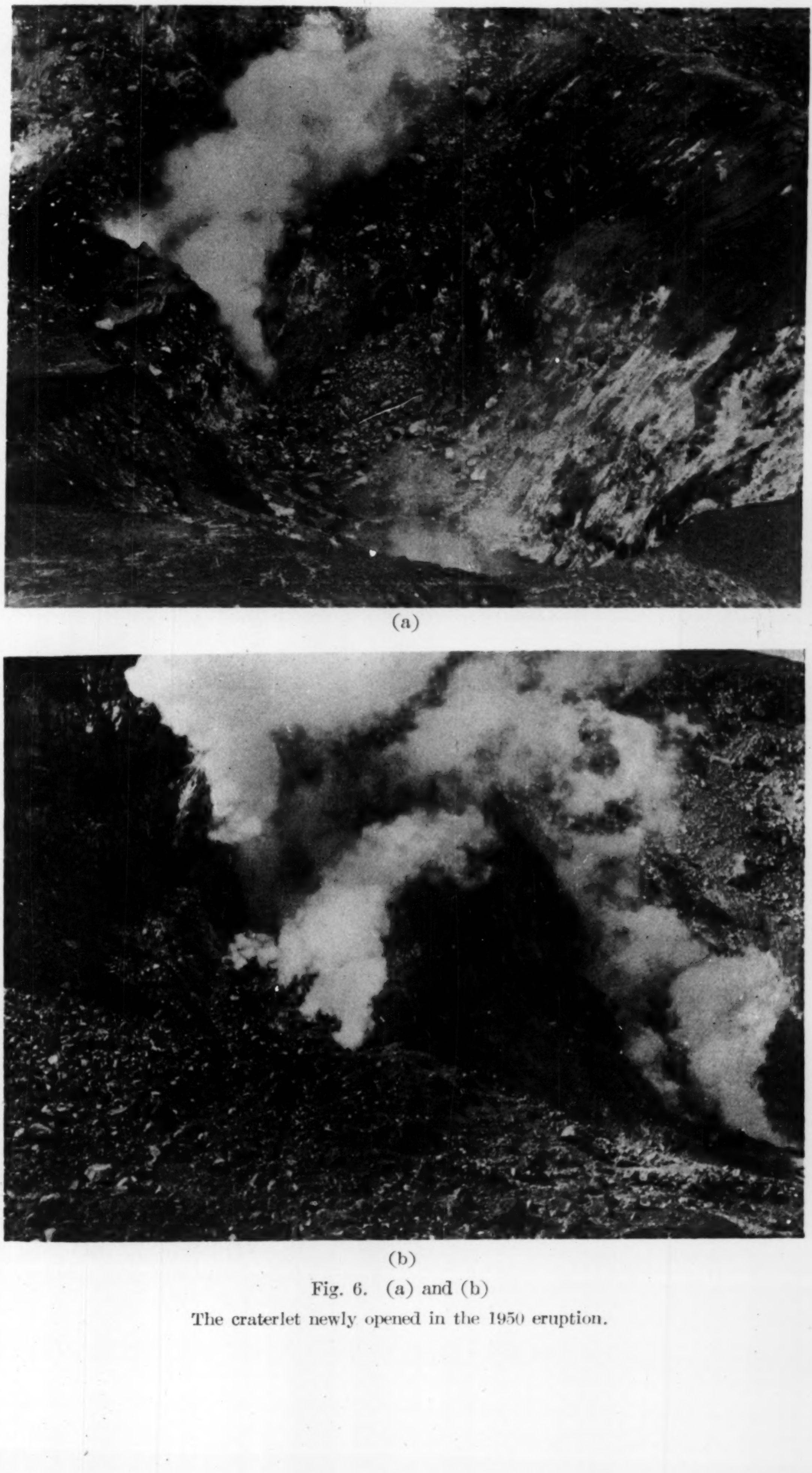

(a)

(b)

Fig. 6. (a) and (b)
The craterlet newly opened in the 1950 eruption.

（震研彙報 第二十九號 圖版 水上・平賀）

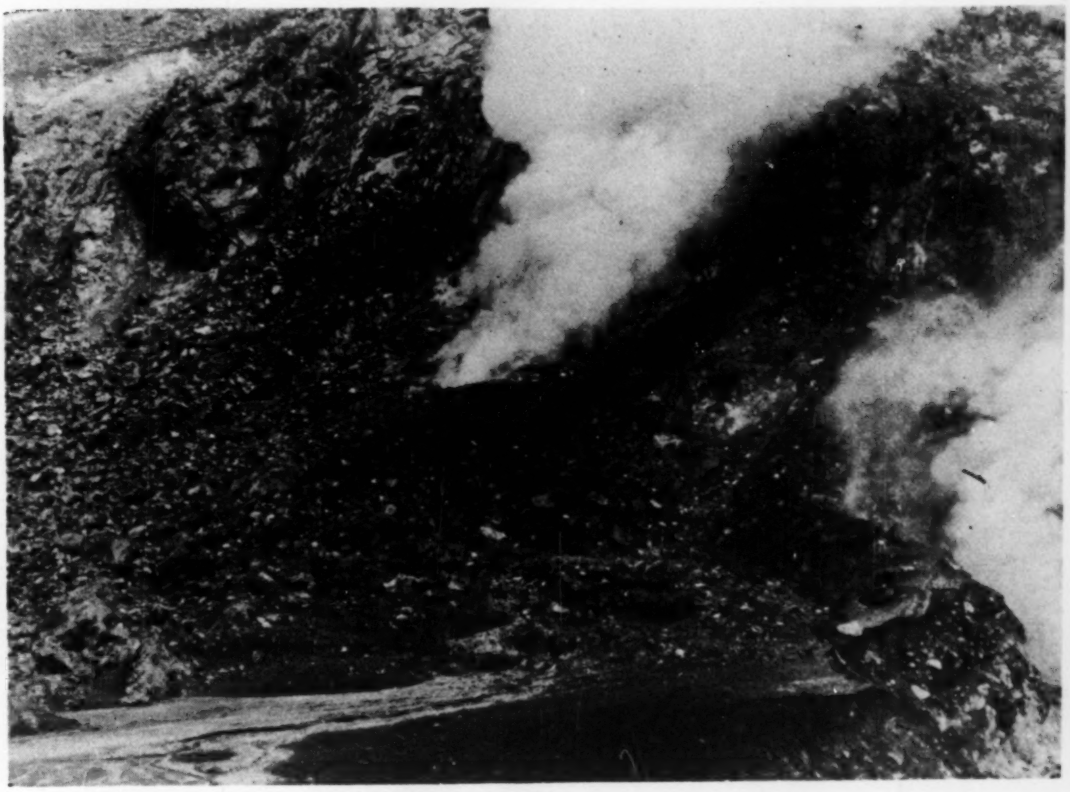

(a)

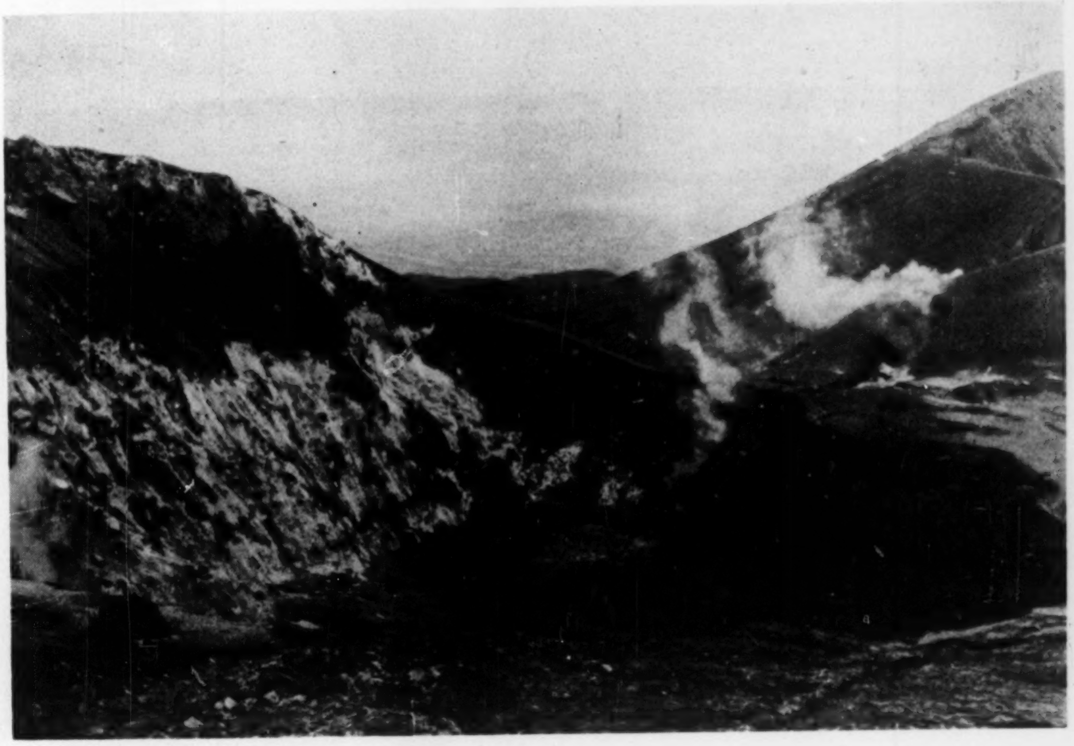

(b)

Figs. 7. (a) and (b)
The craterlet and fumaroles on the the fissure line (A_1A_1') opened in February, 1950.

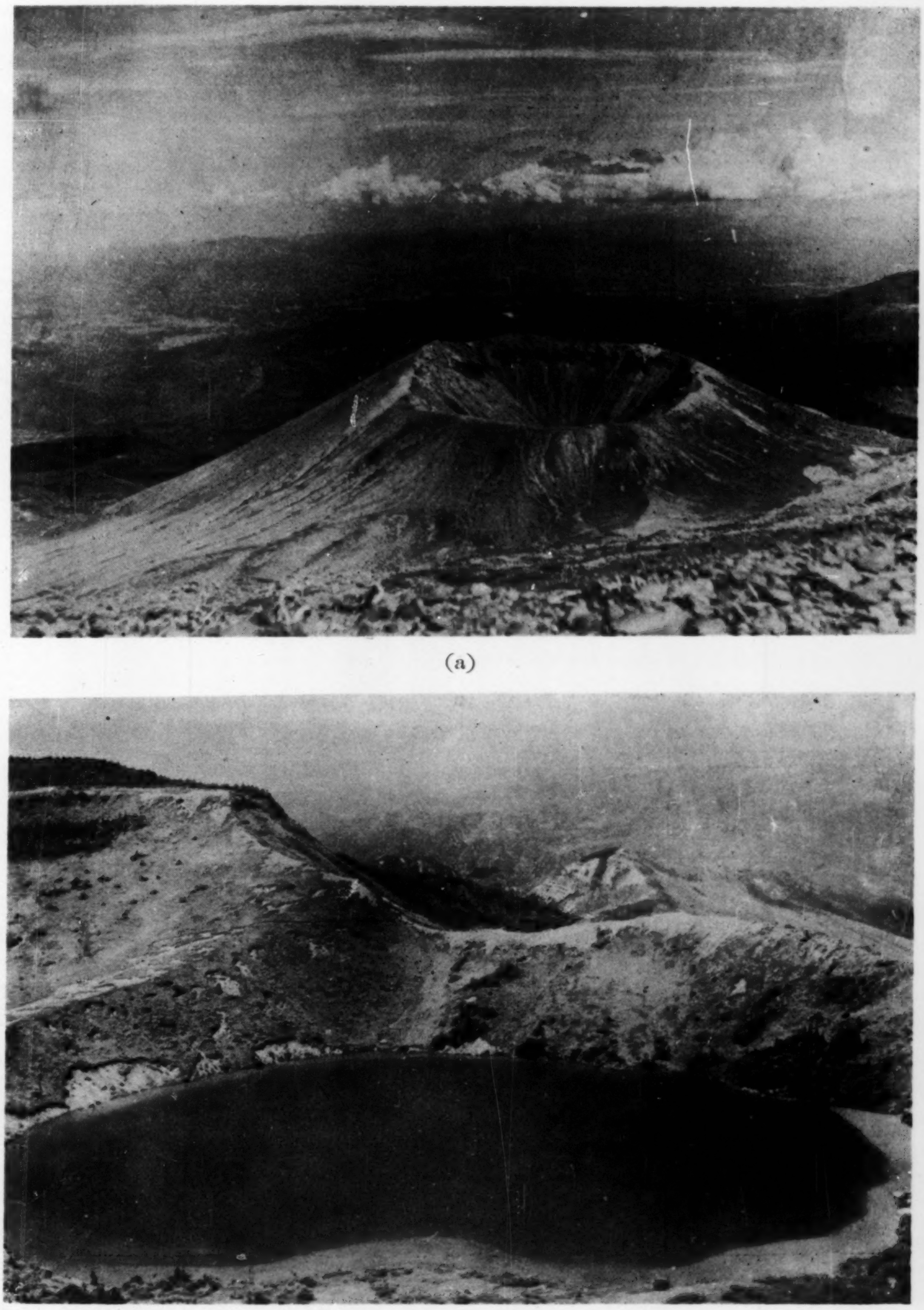

(a)

(b)

Fig. 8, (a) Azuma-Kohuzi viewed from the top of Mt. Issaikyo.
(b) Gosiki-numa, a crater lake, viewed from the top of Mt. Issaikyo.

（震研彙報 第二十九號 圖版 水上・平賀）

In conclusion, the writers wish to express their cordial thanks to Mr. M. Izeki, Chief of Civil Engineering Section of the Hukusima Prefecture for the facilities given them in the present investigation, and to Mr. T. Miyazaki for his valuable assistance in the field investigation.

The expense necessary for this research was defrayed from the Funds for Scientific Research of the Department of Education.

---

33. 1950年2月の吾妻山の小活動

地震研究所 水上　武
地震研究所 平賀士郎

吾妻山は1893年の噴火以來57年ぶりで1950年2月に活動した．前回の噴火は磐梯山の大爆發及び安達太郎山の噴火と共に1888年より1899年の間にこれ等の互に近接する3火山が相次いで活動を示した．從つて今回の吾妻山の噴火が他の隣接する諸火山に波及するか否かについて大いに注目された．しかし一年後の今日迄は他火山に異常は認められない．

今回の吾妻山の噴火後直ちにその山麓の土湯に高倍率の地震計を設置して約2ヶ月間觀測したが火山に源を持つ地震は全く發生しなかつた．

1950年7月に，2月の噴火で生じた小火口群及び噴氣孔の位置を定めるためにその附近の地形測量を行つたが，同時に火山の帶磁の狀態を知るために磁氣伏角の測定を行つた．

地震觀測の結果並に噴火の性質から判斷して，今回の吾妻山の噴火は地表近くの温泉現象に類似する活動であつて，同火山の下或る深さに存在すると推定される岩漿の噴出作用に直接關連する活動とは考えられない．

またその活動の規模は，1893年の噴火に較べて，その噴出岩屑の量においても，その噴出力においても著しく小さいものであつた．

34. *Destruction System of Building by Earthquake.*

By Kiyoshi KANAI,
Earthquake Research Institute.

(Read Sept. 20, 1949; Jan. 16, 1951.–Recieved Mar. 20, 1951.)

1. Introduction.

Buildings are destroyed most easily when the period of earthquake motion approximates to the natural period of the buildings, in other words when the vibration state of buildings comes near the resonance condition.

At the time of earthquake, if a building is at the resonance condition and destruction occurs anywhere in it, its proper period becomes longer. Therefore, when the period of earthquake motion remains constant, the building will be out of the resonance condition. As to the phenomena following, we may consider two cases.

(1) Since the building comes out of resonance condition, the vibration amplitude or the strain of the building will diminish so that the destruction will advance no further, or

(2) though the building comes out of resonance condition, the stiffness of building diminishes. Therefore the vibration amplitude or the strain becomes rather larger and the destruction will advance.

The influence of the building damping is the cause of these two different cases. In the present study, the condition which causes these phenomena practically is pursued through theoretical investigation, and applying the results of this investigation to practical cases, the earthquake damage of building is examined.

2. The influence of the inner-damping of building.

First, in the case of the single-storeyed Rahmen structure with the assumption that the beam is of infinite rigidity and the mass of column is concentrated on the floor, we studied, taking the various coefficients of solid viscosity of column, how the maximum of bending moment varies in accordance with the decrease of the column stiffness or the change of its connection to the beam. In this case the equation of column motion is

$$\frac{\partial^4 y}{\partial x^4}=0, \quad \text{......................}(1)$$

and its solution is

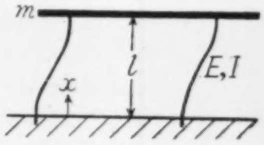

Fig. 1.

$$y=(A+Bx+Cx^2+Dx^3)e^{ipt}, \quad \text{.........................} \quad 2)$$

where A, B, C, and D are the arbitrary constants to be determined by boundary conditions, and $p=2\pi/T$, T=period.

As the boundary conditions

$$x=0; \qquad y=\begin{cases}\mathfrak{A}e^{ipt}, \\ 0,\end{cases} \qquad \frac{\partial y}{\partial x}=0, \quad \text{....................} \quad (3),\ (4)$$

$$x=l; \qquad \left(EI+\xi I\frac{\partial}{\partial t}\right)\frac{\partial^2 y}{\partial x^2}=-K\frac{\partial y}{\partial x}, \quad \text{..........................}(5)$$

$$m\frac{\partial^2 y}{\partial t^2}-\left(EI+\xi I\frac{\partial}{\partial t}\right)\frac{\partial^3 y}{\partial x^3}=\begin{cases}0, \\ Fe^{ipt},\end{cases} \quad \text{........................}(6)$$

where l, E, I and ξ denote the height, Young's modulus, moment of inertia and coefficient of solid viscosity of column respectively, while m is the concentrated mass and K the constant determined by the fixing condition of the column to the beam.

Putting equation (2) into (3)~(6), we get

$$y=\mathfrak{A}e^{ipt}+\frac{p^2m\mathfrak{A}e^{ipt}}{E_0I_0\Phi}[-2\{(\eta+\kappa)+i\tau\eta\sqrt{\gamma}\}x^2+3\{(2\eta+\kappa)+2i\tau\eta\sqrt{\gamma}\}x^3], \quad (7a)$$

$$y=\frac{Fe^{ipt}}{E_0I_0\Phi}[\quad '' \quad], \quad \text{..}(7b)$$

where

$$\left.\begin{aligned}\Phi &=\{12\eta(\eta+\kappa)-\gamma(4\eta+\kappa+12\tau^2\eta^2)\}+4i\tau\eta\sqrt{\gamma}\{3(2\eta+\kappa)-\gamma\}, \\ \gamma &=\frac{mp^2l^3}{E_0I_0}, \quad \eta=\frac{EI}{E_0I_0}, \quad \kappa=\frac{Kl}{E_0I_0}, \quad \tau=\frac{\xi}{E}\sqrt{\frac{E_0I_0}{ml^3}}.\end{aligned}\right\} \quad \text{.........}(8)$$

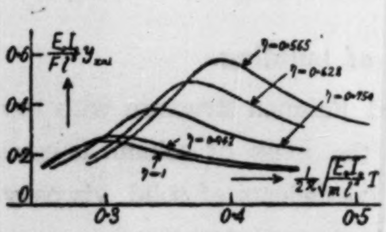

Fig. 2. The resonance curves for the various cases of stiffness of columns, under the condition of the clamped fixing between beam and column, that is to say, $\kappa(=Kl/E_0I_0)=\infty$, and $\tau(=\xi/E\sqrt{E_0I_0/ml^3})=0.1$

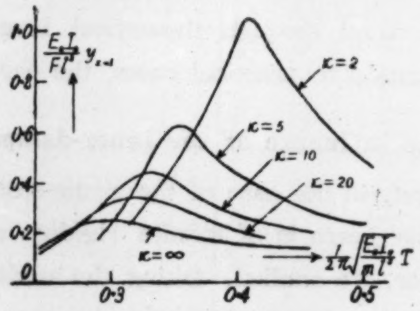

Fig. 3. The resonance curves for the various types of the fixing between beam and column, under the condition $\eta(=EI/E_0I_0)=1$ and $\tau(=\xi/E\sqrt{E_0I_0/ml^3})=0.1$

Using equation (7b), we plot in Fig. 2 the resonance curve, keeping the fixing of beam to column in the state of clamp and varying the stiffness of column. Fig. 3 illustrates the resonance curve at varying condition of fixing between the beam and the column of which the stiffness is kept constant. It is already known that the natural period of building becomes longer and the resonance amplitude larger as the stiffness of column diminishes or when the fixing of the column to the beam is not in good state. In Figs. 2 and 3, if the resonance curve of non-damaged building $\eta=1$ and $\kappa=\infty$, the abscissa 0.3 corresponds to the proper period. When the ordinate represents the ratio of the amplitude of the other curve corresponding to abscissa 0.3 in Figs. 2 and 3 to the resonance amplitude of non-damaged building and the abscissa represents the ratio of the natural period of damaged building (T) to that of the non-damaged one (T_0), the function between them are shown in Fig. 4. These figures show that when the earthquake motion is of constant period and the building is destroyed at the resonance condition, its natural period becomes longer and the building comes out of resonance condition, nevertheless that destruction advances further is a possible phenomenon within a certain range ($T/T_0<1.17$ in case of $K=$constant, and $T/T_0<1.23$ in case of $EI=$constant) without the vibration amplitude being diminished.

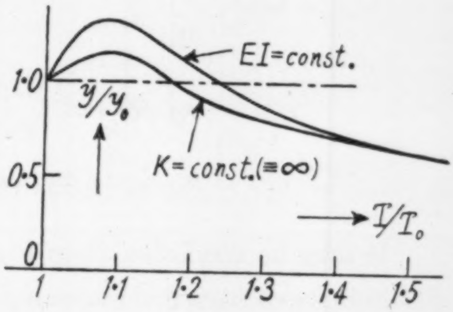

Fig. 4.

Next, the case where the fixing of column to the beam forms a perfect clamp ($K\to\infty$) was studied. Fig. 5 represents the relation of the following two ratios at varying coefficients of solid viscosity: the ratio of the bending moment in the case where the external force of the same period is given in the state of diminished stiffness to that under resonance condition, and the ratio of the natural period of the building with diminished stiffness to that of yet undamaged building.

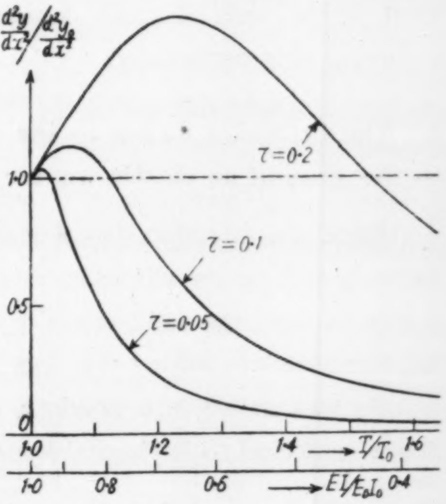

Fig. 5.

From Fig. 5, we have to clarify the relation between the coefficient of solid viscosity and the range within which the ratio of the value of bending moment of damaged building to that at the resonance condition of undamaged building, in case the period of external force is constant, is more than 1. This is shown in Fig. 6.

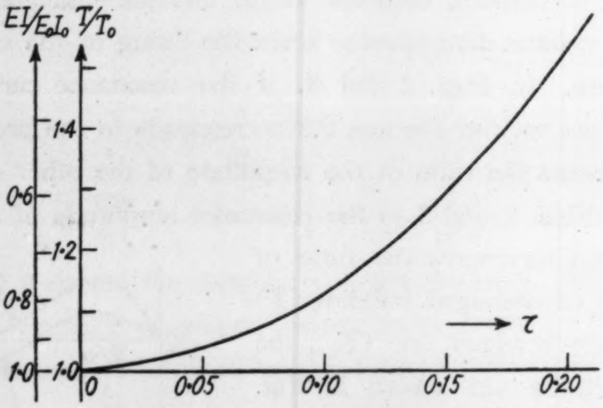

Fig. 6. Range within which destruction will advance.

It may be concluded from Fig. 6 that if a building with small damping diminishes in its stiffness and comes out of the resonance condition even slightly, the bending moment of column becomes smaller than in the resonance condition, but in case of large damping, such a phenomenon does not occur unless the stiffness diminishes considerably and the state of building is far from the resonance condition of original building. In other words, in case the damping of a building is large, although the building may not be destroyed so easily due to its small resonance amplitude, once begun, the destruction advances rapidly. On the other hand, in the case of small damping, there is much possibility of the destruction occurring only sectionally.

3. The influence owing to the vibration energy of building which dissipates to the ground as elastic waves.

Since the vibration damping of a comparatively heavy building is more likely to be caused by its vibration energy which dissipates to the ground as elastic waves than by the solid viscosity of the material, we made the following theoretical investigation, taking this fact into consideration.

As was shown in a previous paper1), the motion of a tall building with rigid floors subjected to horizontal oscillation of the ground is analogous to the case of

---

1) K. SEZAWA and K. KANAI, "Some New Problems of Free Vibrations of Structure", *Bull. Earthq. Res.Inst.*, **12** (1934), 819.

shearing vibrations of a simple structure, so we shall deal with the vibration problem of a tall structure with rigid floors subjected to incident transverse waves under the dissipation of vibrational energy in the form of elastic waves into the ground.

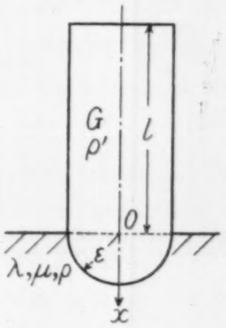

Fig. 7.

Let the incident transverse waves with their displacements orientated vertically be

$$u_0=\cos(pt+kx). \quad \ldots\ldots\ldots\ldots\ldots\ldots\ldots(9)$$

The final solution of the stress in a structure is expressed by[2)]

$$S=4\pi\varepsilon^2 Gk'\sqrt{\frac{\Gamma_1^2+\Gamma_2^2}{P^2+Q^2}}\sin k'(x+l)$$

$$\cdot\cos\left(pt+\tan^{-1}\frac{\Gamma_2}{\Gamma_1}-\tan^{-1}\frac{Q}{P}\right), \quad (10)$$

where

$$\left.\begin{aligned}
&P=2\Gamma_1\cos k'l+\frac{3G\varepsilon}{\mu l}\Lambda_1 k'l\sin k'l,\\
&Q=2\Gamma_2\cos k'l+\frac{3G\varepsilon}{\mu l}\Lambda_2 k'l\sin k'l,\\
&\Gamma_1=3\left(\frac{\lambda}{\mu}+2\right)+\nu(k'l)^2\left(\frac{\lambda}{\mu}-3\sqrt{\frac{\lambda}{\mu}+2}\right),\\
&\Gamma_2=\sqrt{\nu}\,k'l\left\{3\left(\frac{\lambda}{\mu}+2+\sqrt{\frac{\lambda}{\mu}+2}\right)+\nu(k'l)^2\left(\sqrt{\frac{\lambda}{\mu}+2}-2\right)\right\},\\
&\Lambda_1=\left(\frac{2\lambda}{\mu}+5\right)-\nu(k'l)^2, \qquad \Lambda_2=\sqrt{\nu}\,k'l\left(2\sqrt{\frac{\lambda}{\mu}+2}+1\right),\\
&\nu=\frac{\rho G\varepsilon^2}{\rho'\mu l^2}, \qquad k'^2=\frac{\rho' p^2}{G},
\end{aligned}\right\} \quad \ldots\ldots\ldots(11)$$

in which ρ, λ, μ; $\rho'(=m/a_1l_1)$, $G(=12.4\,Ej/l_1^2)$ stand for the density and the elastic constants of the earth, and the effective density and the effective rigidity of the structure, and E, j, l_1, l, a_1 and ε for Young's modulus, radius of gyration of section, length of the column between two adjacent floors, height of the structure, sectional area of the column and radius of the column respectively.

Using equation (10), we studied the change of stress when the building decreases in stiffness and is to be out of resonance condition assuming that the period and the amplitude of the earthquake motion are constant as in the previous chapter. In Fig. 8, the abscissa represents the ratio of rigidity and the ordinate the ratio

---

2) K. SEZAWA and K. KANAI, "Some Improved Theory of Energy Dissipation in Seismic Vibrations of a Structure", *Bull. Earthq. Res. Inst.*, **14** (1936), 168.

between the stress at resonance condition and that out of it. In this case the ratio between the radius and the height of the building, (ε/l), is 1/2. We see that when the rigidity ratio of the building to the ground is small, the stress becomes smaller than at the resonance condition with a slight decrease in the rigidity of the building, but if the rigidity ratio is comparatively large, the stress be it ever so slightly, becomes larger than at the resonance condition till the building decreases in its rigidity to a considerable degree.

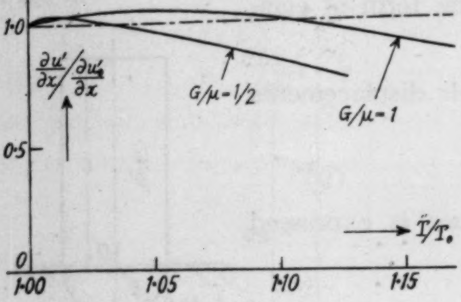

Fig. 8. $\varepsilon/l=1/2$.

Let the abscissa be the rigidity ratio of the ground to the building, and the ordinate the range of the ratio between the stress at the resonance condition and the stress in the state of decreased stiffness (out of the resonance condition), keeping the period and amplitude of the earthquake motion constant, less than 1, the function between them is shown by the full line in Fig. 9.

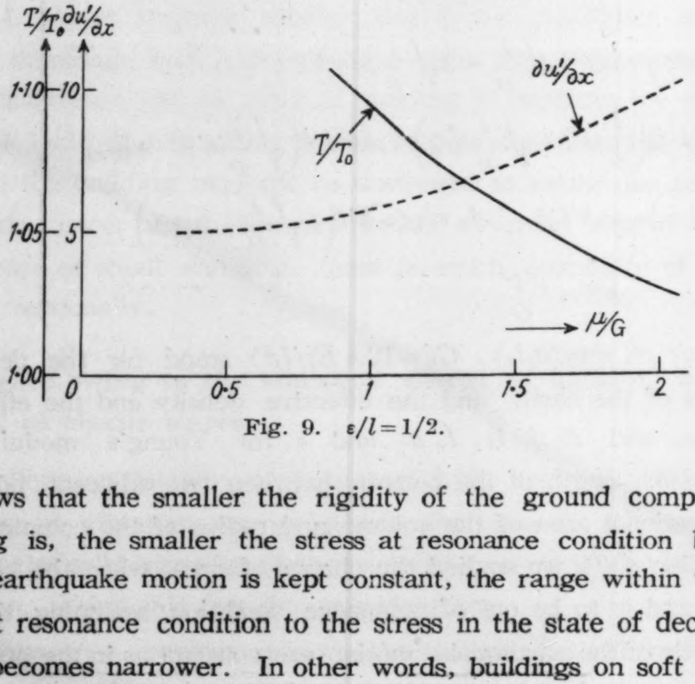

Fig. 9. $\varepsilon/l=1/2$.

Fig. 9 shows that the smaller the rigidity of the ground compared with that of the building is, the smaller the stress at resonance condition becomes, but if the period of earthquake motion is kept constant, the range within which the ratio of the stress at resonance condition to the stress in the state of decreased stiffness is less than 1, becomes narrower. In other words, buildings on soft ground, having larger vibration damping, are more unlikely to collapse than those on hard ground, but once the destruction begins, it advances rapidly.

Keeping the rigidity ratio of building to ground constant and varying the ratio between the building radius and height, we will calculate as we did previously. The result is shown in Figs. 10 and 11.

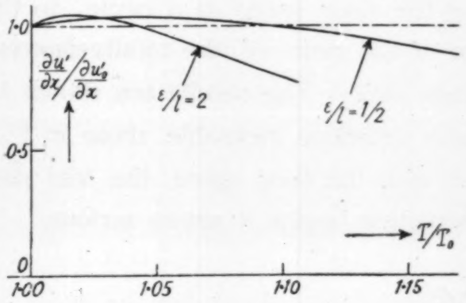

Fig. 10. $G/\mu=1$.

We know from Fig. 11 that as the ratio of ε/l decreases, the stress at resonance condition becomes smaller, nevertheless the range within which the ratio of the stress at resonance condition to the stress in the state of decreased rigidity is less than 1 becomes narrower, when the period of earthquake motion is kept constant. This means that the larger the height-to-area-ratio of the building is, the larger the vibration damping will be, so that destruction is not easily caused, but once begun, it advances very rapidly.

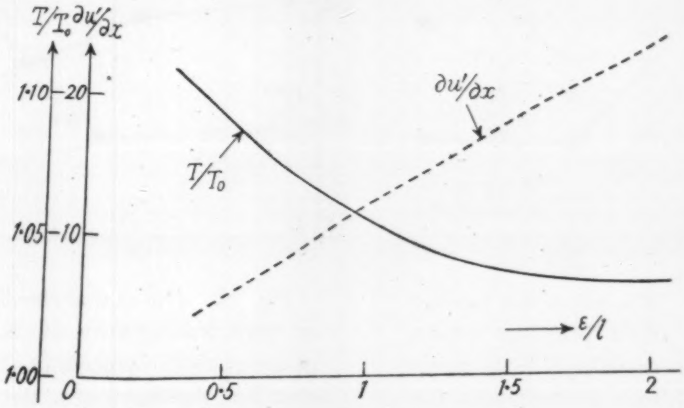

Fig. 11. $G/\mu=1$. Full line; range within which destruction will advance.

4. The practical examination of earthqugke-damage of building.

The broken line in Fig. 12 shows the damage ratio of brick buildings in old Tokyo-shi at the time of the Kwanto Earthquake of 1923. The ratio is divided into three according to the thickness of alluvium. When the ordinate represents the quotient of the ratio between the totally-destroyed and the semi-destroyed buildings divided by the damage ratio, a full line is drawn. The relation shown in Fig. 12 is quite similar to the relation shown in Fig. 9. Thus it has been found that the brick houses on soft ground are not destroyed as easily as those on hard ground, but once the destruction begins, it will not stop till a much damage has been done. From this fact we find that the theoretical investigations coincide at least quantitatively with the practical facts in the study of quake-damage.

In the next place, using the same data, we inquired into the relations among the ratio of the building radius ε' (considering the floor space as a circle) to the height (l), the damage ratio and the quotient of the ratio of the totally-destroyed to the semi-destroyed divided by the damage ratio. The results are shown by the broken line and full line in Fig. 13. These relations resemble those in Fig. 11. The higher the building is in comparison with the floor space, the less destructible it is by earthquake, but once the destruction begins it grows serious.

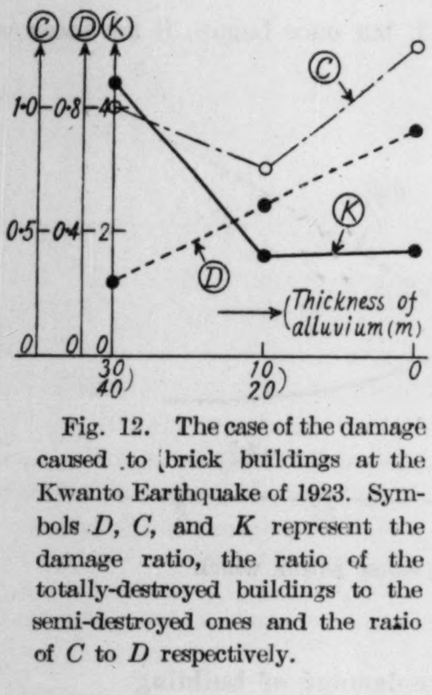

Fig. 12. The case of the damage caused to brick buildings at the Kwanto Earthquake of 1923. Symbols D, C, and K represent the damage ratio, the ratio of the totally-destroyed buildings to the semi-destroyed ones and the ratio of C to D respectively.

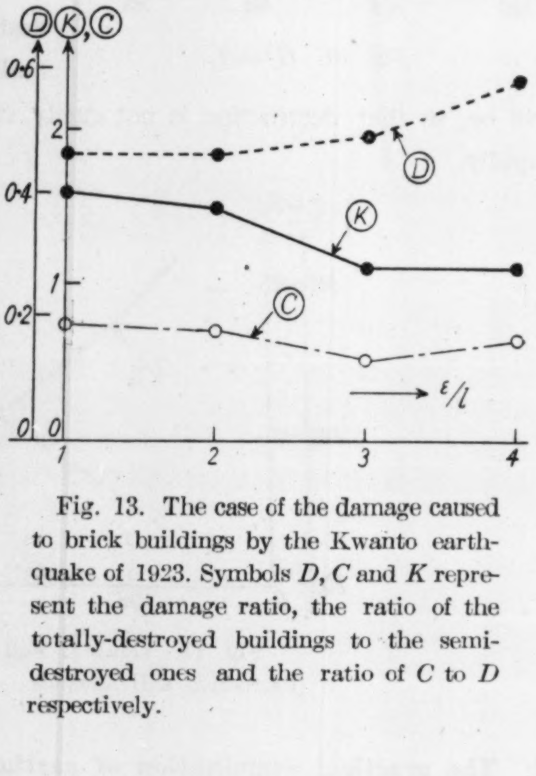

Fig. 13. The case of the damage caused to brick buildings by the Kwanto earthquake of 1923. Symbols D, C and K represent the damage ratio, the ratio of the totally-destroyed buildings to the semi-destroyed ones and the ratio of C to D respectively.

5. Conclusion

From theoretical studies as well as from statistical studies dealing practically with the earthquake-damage, the following facts have been made clear.

The larger the building damping is, the less destructive the building is, but once the destruction begins, it advances rapidly.

The result of theoretical study which has been developed from the idea that the vibration energy dissipates into the ground as elastic waves at the time of earthquake is ascertained quantitatively by the coincidence with results obtained by the practical study of earthquake damage concerning five points: i.e. the relation between the nature of ground and damage ratio[3], ground and the degree of damage, the height of building and damage ratio[4], the height and the degree of damage, and finally the ground and the height of the place which suffered most damage[5]. Therefore by developing this problem qualitatively, it may become possible to construct the most reasonable earthquake-proof building according to the property of the ground.

In conclusion, I wish to express my thanks to Miss S. Yoshizawa for the valuable assistance she offered in the present investigation.

---

34. 地震による建物の破壊過程について

地震研究所　金　井　清

建物の振動減衰性が大きい程，地震による破壊は起り難いが，一旦どこかに破壊が起つた場合には，小破壊に止らないで，大破壊に進んで行く傾向があることが數理的研究で明かになつた．又この數理的研究結果は實際の震害に關する統計的研究結果とよく合うことが確められた．

地震の際に，建物の震動勢力が彈性波として地中に逸散するという思想から出發した數理的研究結果は實際の震害の統計的研究結果と少くとも定性的には一致することが次の5つの關係で確められた．卽ち，地盤と被害率，被害程度及び建物の最大被害を受ける場所の高さとの關係；建物の高さと被害率，被害程度との關係がそれである．

從つて，この研究を定量的な方向に進めることができれば，地盤の性質を考慮に入れた經濟的で合理的な耐震構造を作ることができる筈である．

---

3) K. Kanai and S. Yoshizawa, "Relation between the Earthquake Damage of Non-wooden Buildings and the Nature of the Ground. II", *Bull. Earthq. Res. Inst.*, **29** (1951), 219.

4) *loc. cit.*, 3).

5) K. Kanai, "*ditto.*", *Bull. Earthq. Res. Inst.*, **27** (1949), 97.

[illegible] Bull. Seism. Soc. Am., 29 (1939).

[illegible] Bull. Seism. Soc. Am., 27 (1937).

35. *Periods of Earth Vibrations at Kōtō-ku, Tokyo.*

By Fuyuhiko KISHINOUYE,

Earthquake Research Institute.

(Read Dec. 19, 1950—Received March 20, 1951)

Introduction.

Periods of earth vibrations at Tokyo were studied by K. Suyehiro¹⁾, M. Ishimoto²⁾ and others about 20 years ago. K. Suyehiro stated his views as follows: The only thing that I wish to emphasize is that every locality has its own natural motion during an earthquake, and we must pay careful attention to it.

They found out the "prevailing period" of earthquake motions, and found that it varies with place, namely 0.3 sec on the high ground of Tokyo and 0.6 sec on the low ground. And the distribution of damage caused by the great earthquake of 1923 was considered to be closely connected with the prevailing periods.

The writer observed microseismic disturbances at the Seismological Institute of the Tokyo University, and found two periods of earth vibrations: about 0.5 sec and 0.1 sec. The short period vibrations were caused when motor-cars passed near the seismograph³⁾.

In May and June 1950, the writer carried out some experiments of elastic waves with other members of our institute at Sunamachi, Kōtō-ku, Tokyo. We used two horizontal seismographs designed by the writer⁴⁾ adjusted in the following conditions: free vibration period $T_0 = 5.0$ sec., geometrical magnification $V = 480$, and damping critical.

With these instruments longitudinal and transverse compoents of the vibrations were recorded at several places, and the records were studied.

Periods of vibrations due to underground explosion of dynamite.

Earth vibrations caused by explosion of dynamite at about 4 metres deep under the groud were recorded. An example of the records is shown in Fig. 1. In this

---

1) K. SUYEHIRO, *Collected Papers*, Tokyo, 1934, 418.

2) M. ISHIMOTO, *Bull. Earthq. Res. Inst.*, **12** (1934), 234–248; **13** (1935), 438–441; **15** (1937), 526–543.

3) F. KISHINOUYE, *Disin (Earthquake)*, **9** (1937), 452–459.

4) F. KISHINOUYE, *Bull. Earthq. Res. Inst.*, **20** (1942), 216–219.

case the amount of explosive was 45 grams with an electric detonating cap, and the recording distance was 48 m. The short period observed was 0.035–0.038 sec, and the long period was 0.22–0.25 sec in large amplitudes.

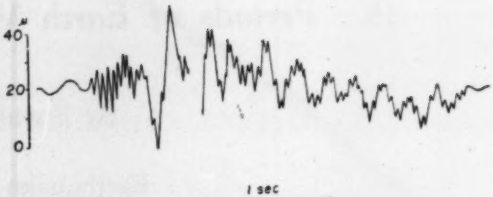

Fig. 1. Transverse vibrations due to underground explosion.

Earth vibrations caused by the Vibrator A.

Simple harmonic motions of earth were generated by two vibrators, which were distinguished arbitrary with letter *A* and B. The Vibrator *A* consisted of three unbalanced rotating wheels (total weight of unbalance 60 kg and the eccentric distance of the masses 21 cm) and was driven by human power. At the experiments the wheels were at first rotated as fast as possible, and then slowed down. The amplitude variation of the earth motions according to the rate of rotations of the wheels were observed as shown in Fig. 2. The increase of amplitude is found at frequencies 4–5, in other words, the earth resonated at the periods about 0.25 sec and 0.2 sec. It may be noticeable that these periods are nearly equal to those obtained in the case of the explosion.

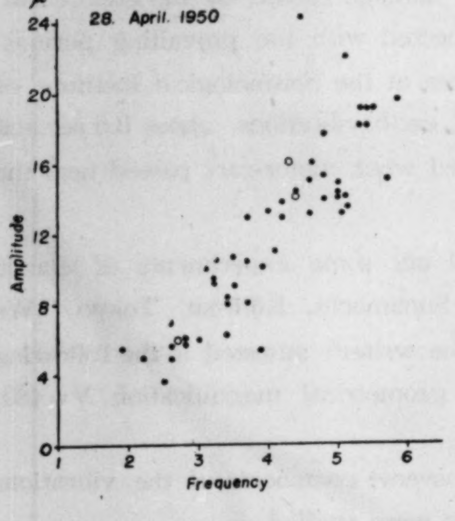

Fig. 2.

Earth vibrations caused by the Vibrator B.

The Vibrator *B* was smaller than the Vibror *A*, and consisted of two unbalanced wheels (unbalance weight 1.2 kg, and eccentric distance 3.8 cm) driven by a single phase A. C. motor. Amplitude-period relation obtained is shown in Figs. 3 and 4. The maximum amplitudes were found at frequencies about 9, 16, 28, and 38 or in the period 0.1, 0.06, 0.036 and 0.026 sec. These periods may be harmonics of 0.2 sec period obtained before.

Period of microseisms.

When the wind blew strong, microseisms with the period about 0.2 sec. the double amplitude about 4μ were observed. And small vibrations, their double am

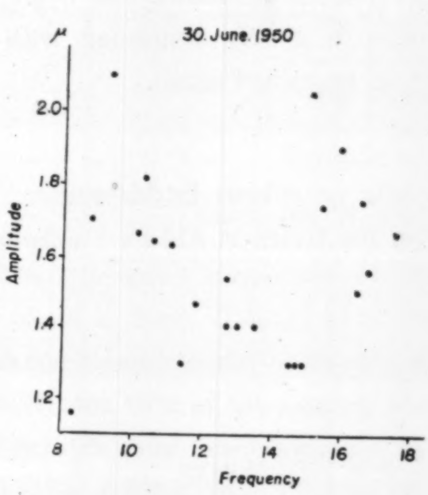

Fig. 3.

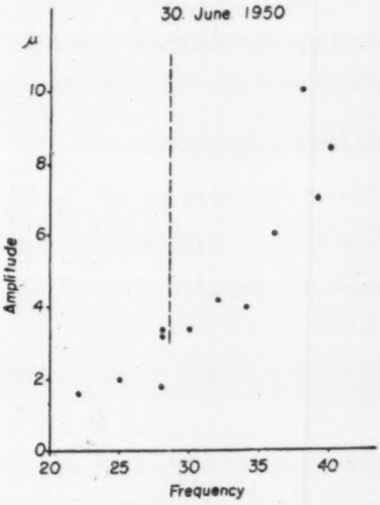

Fig. 4.

plitude about 1μ in period 0.035 sec were superposed on 0.2 sec period vibrations.

Period of earth vibrations due to electric cars passed by.

Traffic of electric cars was about 30 metres distant from the seismographs. When cars passed by, earth vibrations of about 0.035 sec period were caused. The amplitude of this vibration varied and its range is shown in Fig. 4 as a broken line.

Period of earthquake motions.

M. Ishimoto as mentioned above observed earthquake motions with his acceleration seismographs at many places in the neighbourhood of Tokyo and Yokohama. His result obtained at Kōtō-ku is reproduced in Fig. 5. As seen in the diagram, periods of 0.2–0.3 sec are noticeable, and on the contrary period of 0.6 sec which is common in the low ground of Tokyo is not clear.

Conclusion.

As the proper periods of the earth vibrations at Kōtō-ku, 0.2 sec and 0.035 sec may be considered. These may correspond to the periods 0.3–0.5 sec and 0.1 sec which are usualy observ-

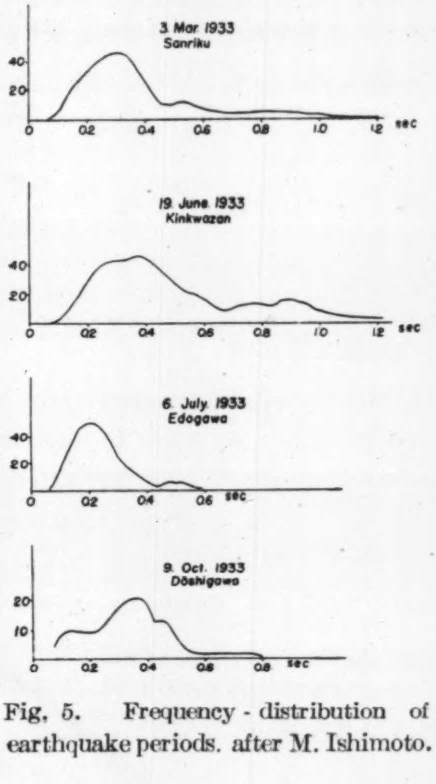

Fig. 5. Frequency - distribution of earthquake periods. after M. Ishimoto.

ed in the high ground of Tokyo respectively. From these results the hypothesis that earthquake damage done to houses in Tokyo is closely connected with the prevailing periods 0.3 and 0.6 sec may have to be examined again.

Acknowledgement.

The author thanks Mr. J. Moroga for the help he offered in this study.

The cost of this research was defrayed from the Grant in Aid for Fundamental Scientific Research.

---

35. 東京都江東區における土地の振動周期

地震研究所　岸上冬彦

東京都江東區南砂町で，火薬爆發による土地の振動周期，起振機の振動に共鳴する周期，土地の脈動の周期，電車による振動周期などを測つた所，何れの場合にも約 0.2 秒と約 0.035 秒の周期が見られた．又以前石本博士が測定した深川の振動周期の記錄を見るとやはり 0.2 秒が認められる．東京の山手では 0.3 秒，下町では 0.6 秒の周期といはれて，それによつて 1923 年の地震の際の家屋の損害も共振現象によると考へられてゐたが，江東區では 0.6 でなく 0.2 秒であるとすると，以前の震害分布說も考へ直さなくてはならないであらう．

---

36. *Sinking of the Kōtō Region, Tokyo.*

By Fuyuhiko KISHINOUYE,

Earthquake Research Institute.

(Read Jan. 16, 1951.—Received March 20, 1951.)

After the great earthquake of 1923, all bench marks in the Kōtō region, Tokyo, were found to have subsided according to results of precise levellings. And the subsidence was cosidered to be due to the earthquake. But in the following years till 1938, the rate of the sinking became greater than before. It was so remarkable that its cause was discussed by many men.[1] In 1929 for the purpose of studying the sinking, the city office of Tokyo increased the number of bench marks in the city to as many as 364 sets, and levelling of these bench marks were repeated at intervals of a few years.

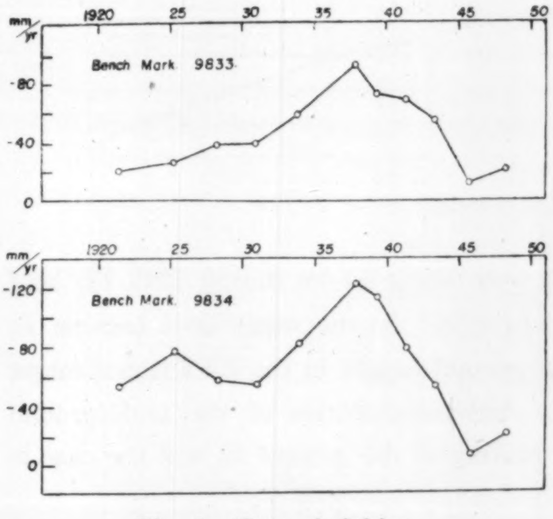

Fig. 1. Rote of sinking

During the years 1938 and 1944–45, the rate decreased rapidly, and some bench marks even upheaved. But since 1945 the bench marks began sinking again (see Fig. 1). To show the amount of sinking exactly, the changes of height at two places, as typical examples, are shown in Fig. 2. The rate of sinking later became small during the recent War. The decrease of the rate was considered to be due to the restoring of the pressure of the underground water which might be an effect of the decrease of the amount of water pumped up at factories because of the burning of them by the air-raids. Recently as the factories restored their activities, the underground water-level became lower and lower, and the sinking also became noticeable again.

The water-level of a deep well in the compound of the Tokyo University, Bunkyō-ku, Tokyo, has been measured continuously since 1932. The height of the

---

[1] N. MIYABE, *Bull. Earthq. Res. Inst.*, **10** (1932), 844–857; **13** (1935), 587–591 and 763–771; **15** (1939), 102–108.:

G. KITAZAWA, *Trans. Inst. Jap. Archit.*, **13** (1939), 275–282.: and others.

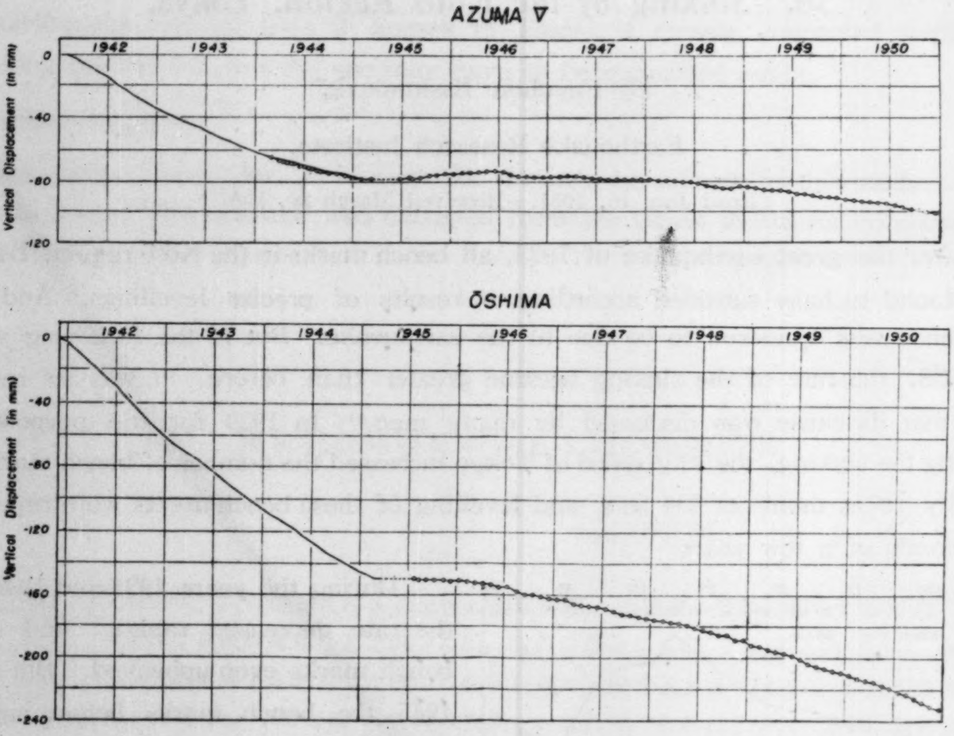

Fig. 2. Change of height.

level lowered about 90 cm during 1932–43, rose about 50 cm during 1943–48, and in 1950 sank about 40 cm under the level of 1948. So the water level became as low as in 1943.[2] Then the change of the ground height in the Kōtō region might be closely connected with the water-level. And the condition of the underground water may be an important factor in the sinking of the ground as was the case in Osaka city.[3]

Although the sinking is noticeable in Kōtō region, the amount of pumped-up water is now great at other parts of the city; Adachi-ku, Edogawa-ku and Sumida-ku. Then the underground water of a wide area must be investigated.

From the above data, the relation between recent subsidence since 1938 and the subsidence before 1938 was studied. The correlation diagram of the amounts of subsidence in two time intervals is shown in Fig. 3. The correlation is posi-

---

[2] Y. SATO read a paper on the water level of a deep well at Bunkyo-ku, Tokyo, at the monthly Meeting of our institute on Dec. 19, 1950.

[3] K. WADATI, *Rep, Disast. Res. Inst. Osaka*, **2** (1939), **3** (1940).
K. WADATI, and T. HIRONO, *do.* **5** (1942).

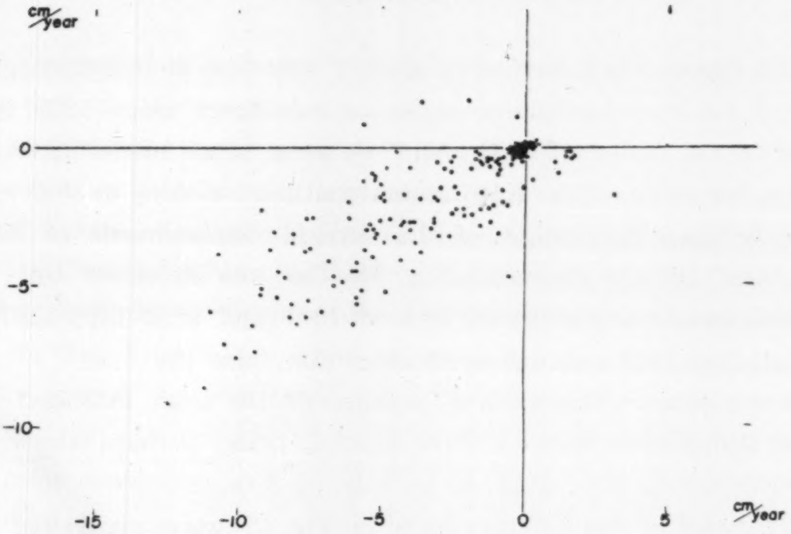

Fig. 3. Correlation between amount of subsidence of bench marks before 1938 (abscissa) and that after 1938 (ordinate).

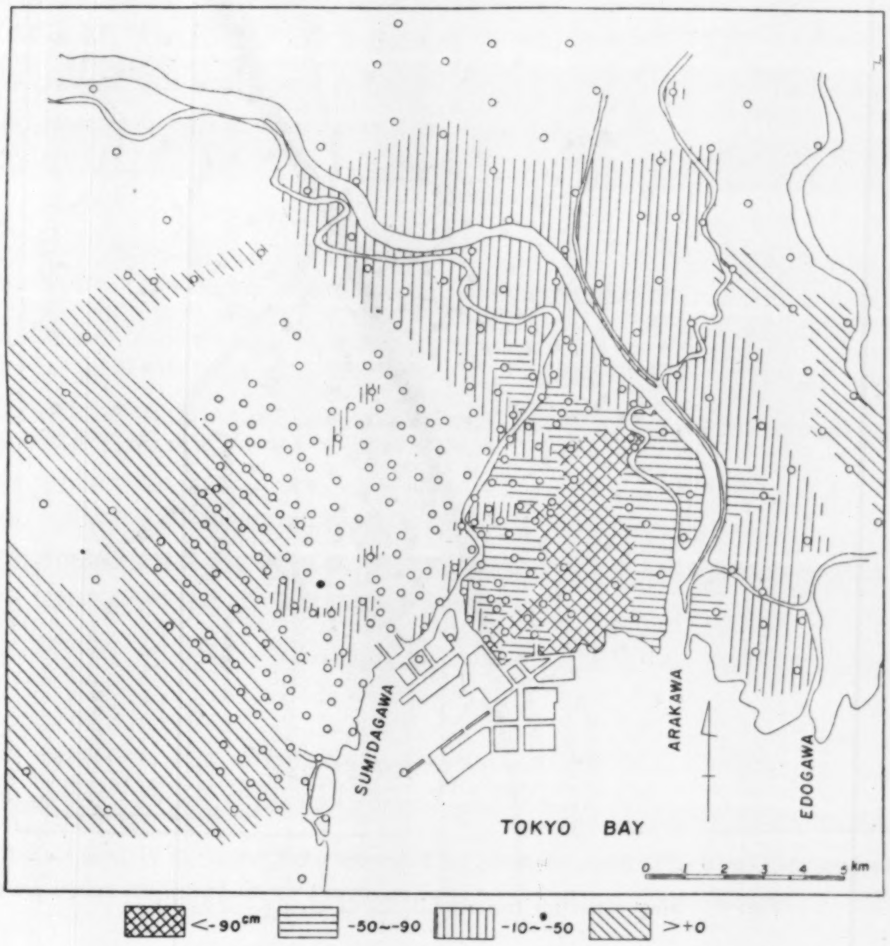
SUMIDAGAWA
ARAKAWA
EDOGAWA
TOKYO BAY
0 1 2 3 4 5 km
<-90cm
-50~-90
-10~-50
>+0

Fig. 4, Map showing change of height. Black circle is the position of the standard bench mark.

tive, so bench marks which have sunk greatly may sink in like manner hereafter.

The areal distribution of the amounts of subsidence since 1929 is shown in Fig. 4. During the period of 1938 and 1944, some bench marks upheaved as mentioned above, but those at the Kōto region continued sinking through all the years. The relation between the changes of the vertical displacements of bench marks before and after 1944 is shown in Fig. 5. The area indicated by (+) always upheaved, the area (+ −) upheaved before 1944 and sank afterward, the area (− +) subsided till 1944 and upheaved after that, and the area (−) kept sinking through the years. The surface geology of the area indicated by (+) is tertiary, and that of the area (−) is alluvial, being perhaps the delta of the Arakawa (river).

The boundaries of the different signs in Fig. 5 were considered by several

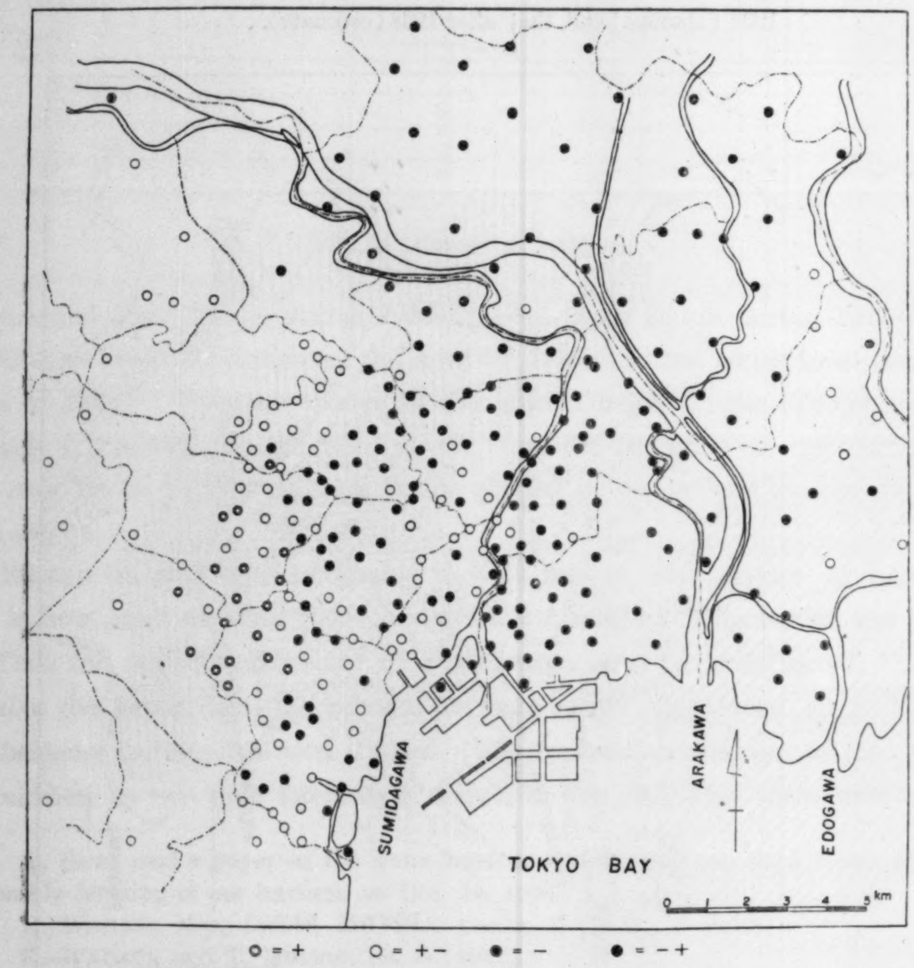

Fig. 5. Map showing the variations of change of height.

investigators to be geological faults.[4] But the boundary of subsidence of different rate may be that of different thickness of layer of silt clay which contracts though decrease of underground water pressure.

On the other hand the sinking is regarded as an effect of earthquakes which occurred near Tokyo. For example, A. Imamura[5] considered that the Kōtō block sank by the earthquake of May 21, 1928 in the northern part of Tokyo Bay. On Jan. 9, 1951 a moderate earthquake occurred in the same place as the above mentioned. In these two cases other small earthquakes accompanied, and the sinking of the ground was also noticeable. The sinking then seems to have some relation with the seismic activity at the Edogawa (river). Whether these earthquakes had some connection with the sinking of the ground or not may be an interesting problem.[6]

The writer expresses thanks to Mr. G. Oka, the director, and Mr. Y. Inaba of the Civil Engineering Research Bureau, Tokyo Metropolis Government for their kind help in giving him their data concerning the present problem. He also thanks Miss M. Kotaka for her assistance in this study.

The cost of this study was defrayed from the Grant in Aid for Developmental Scientific Research of the Department of Education.

---

36. 東京都江東地區の地盤沈下

地震研究所　岸　上　冬　彦

1930 年頃沈下速度が著しかつた江東地區も 1938 年頃から次第に少くなつて，1945 年頃には沈下が止まつたようであつたが，最近又さがり始めた．この沈下と前回の場合とを合せて調べてみた．各地點の前回と最近の變動量の相關圖をかくと，その間に相關が認められた．

最近江戸川流域に地震が時々あるが，前に沈下の激しかつた頃も東京灣北部に地震が多かつた．このことも江東地區の地盤沈下と關係があるかも知れない．

---

[4] A. IMAMURA, *Jap. Journ. Astro. Geophys.*, **8** (1930-31), 177-186.
K. NISHIO, *Journ. Geogr.*, (Japan), **41** (1929), 766-776.

[5] A. IMAMURA, *loc. cit.*

[6] Some parts of the area were surveyed by precise levelling in Dec. 1950 and Feb. 1951, The result will be published in this journal.

37. *Vibration of a Tank Tower.*

By Nobuji Nasu,

Earthquake Research Institute.

(Read March 20,1951.—Received March 20,1951.)

For the purpose of determining the vibrational characteristics, vibration tests were made on a steel tower with a 100,000 gallons tank at its top. The tower was an independent structure isolated from the neighbouring houses. The tank was supported by six columns and the platform around the tank was of a height of 34.75 m. above the ground (Fig. 1). It has been designed so as to resist the horizontal earthquake motion of an intensity of 0.3 g.

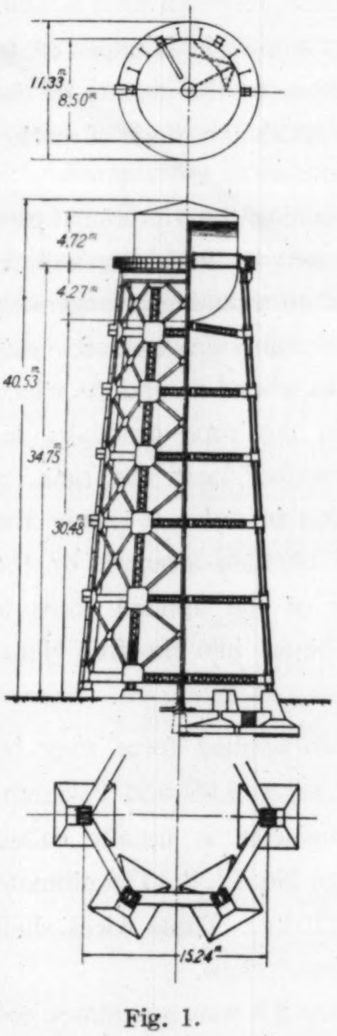

Fig. 1.

Instruments. The instruments mostly used in the tests were the horizontal component seismographs having a period of 1.0 second, magnification of 200 and a damping ratio of about 10 which was secured by an air-damper. The instruments were usually placed on the platform of the tank between two consecutive columns. When the records of two component-motions were required, two sets of instruments were installed at right angles to each other.

For the measurement of small vibrations such as of the foundation, instruments of optical registration were used. These instruments were a set of Wood-Anderson torsion seismometer and a vertical motion seismometer. The magnification of these instruments was 2,000 when the optical distance was kept at 1.0m.

The recording drum of every instument was driven by a small synchronous moter which was motivated by the 50-cycle and 100-volt alternating current.

Vibration by wind. A considerable effect upon the tower is expected, if wind is strong. During the tests, there was one windy day. According to the observation made at 10 m. above the ground, the wind-velocity was between 7.6 and 8.9 m. per second and the wind-direction was mostly from the north. The tower actually oscillated the whole day with its own period. Fig. 2 shows a portion of the records of vibration of the

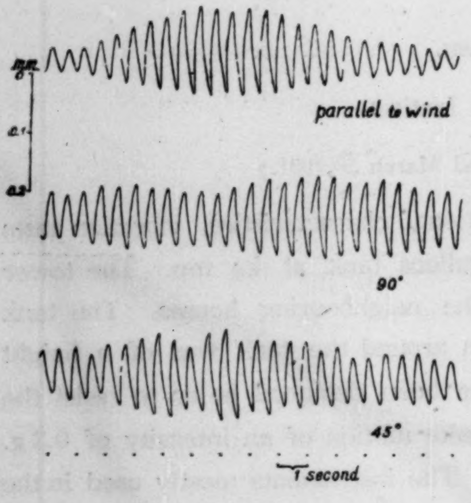

Fig. 2

tower taken on that day. These records were made with a single component seismograph placed first in the direction of wind, and then at 90° and 45° against the wind direction. In all records, the waves represent the fundamental translatory vibration of the tower whose period is nearly constant and 0.57 second. There is no wave with a period differing from this value, When the records were being taken, the tank was kept full of water.

The maximum amplitude is expected to increase in proportion to the square of the wind velocity, so if the velocity reaches 40 m./sec., the maximum range of motion near the top of this tower will become 0.55 cm.

Pull-test. The pull-test is the best method of determining the vibrational property of such tall structure as a tank-tower. It is conducted by attaching a rope to a member near the tank and connecting the other end to a pulling arrangement which is anchored on the ground. In this test, a truck (cargo) was used for this pulling machine and the rope was slowly pulled as it was wound around the winch attached at the head of the truck. Thus, the tension in the rope gradually increases. Instead of attaching the rope directly to the member near the tank, a wire is used between this member and the end of the rope in order to apply the force through this wire. When the tension reaches the ultimate strength of the wire, the wire will naturally break. Thus, the release of the applied force is effected in this moment, and thenceforth the tower will be set into the free vibration which usually lasts for several minutes.

By changing the thickness of the wire, the maximum applied force may be rendered to any desired value. In our tests, galvanized wires 4.05 and 2.75 mm. in diameters were used; the wire having the former diameter is usually called "wire No. 8" and the wire of the latter diameter "wire No. 12." The ultimate tension in the former wire is 440 kg. and in the latter 110 kg. These wires shall be denoted by wire ♯8 and wire ♯12 in the following descriptions.

In the actual test, the maximum force applied by wire ♯8 was sometimes too large and that applied by wire ♯12 was too small to cause the vibration recorded by the seismometer of a convenient scale. It was found then that double wires of

♯12 were the most convenient for the present test, and wire ♯8 should be specially used for applying such strong force as to cause the torsional vibration of the tower.

It is desirable to make this pull test in various directions of the tower. Usually the tower is pulled in the directions radial and tangential to the tank (Fig. 3). The radial pull, however, may be given in two ways; first, the pull is in a direction parallel to one of the diagonals of a hexagon which is formed by joining the six columns; secondly, the pull is in a direction normal to one of the sides of this hexagon. In these two cases, the translatory vibration of the tower will be caused. The another pull which is applied to one of the columns and directed tangentially to the tank will cause the torsional vibration.

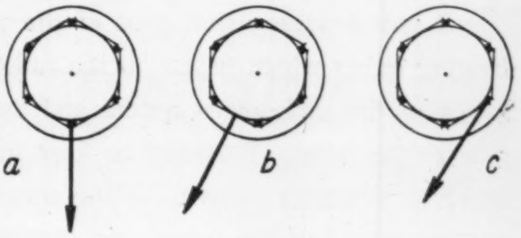

Fig. 3.

Translatory vibration. The tower was pulled in the two directions mentioned above. The tests were made for the various heights of the water in the tank. Initially the tank was full, when the water-level was set at a height of 7.7 m. from the hemispherical bottom of the tank. Thereafter, the water-level was lowered stepwise to various heights and finally to zero (empty).

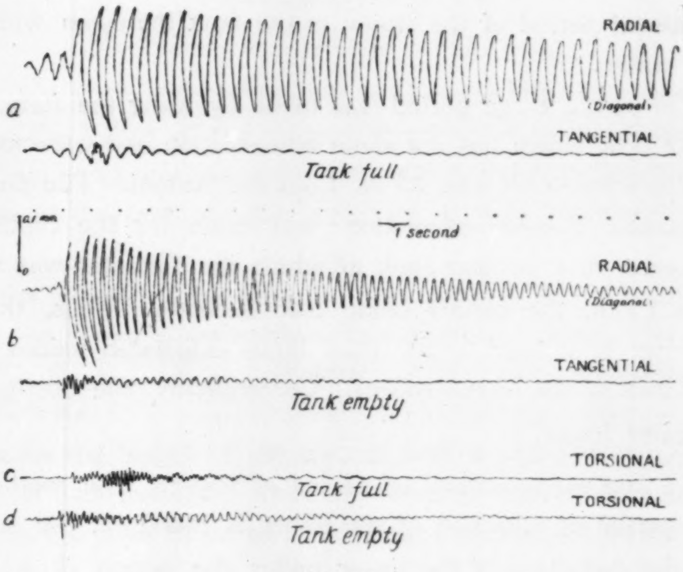

Fig. 4.

Fig. 4. shows specimen records of the pull tests. The sudden departure from the rest position represents the release of the applied force and succeeding to this, the free vibration of the tower can be seen which gradually decreases in amplitude. Of course, the motion on the tangential component is far smaller than that in the direction of the pull.

It is noteworthy that none of the vibrograms so far made of this tower shows beating effect which is due to the union of two vibrations, that is the natural vibration of the tank-tower system and the vibration of the water surging from one side to the other. It should be kept in mind that the body of water constitutes a separate vibrating system. If the surge period of the water is nearly equal to the natural period of the tower, the beating effect will be enormously displayed.

For the purpose of estimating the surge period, let us take a simple case of a rectangular tank. The period in this case, T_w will be given by equation,

$$T_w=\frac{2L}{v}=\frac{2L}{\sqrt{gh}} \tag{1}$$

where L is the length of the tank, h the average depth of water and g the acceleration due to gravity. In other words, T_w is the time which the gravitational wave takes to reach the opposite side of the tank and come back again with velocity v. In a tank of circular or any other section, the evalution of T_w will not be as simple as in this case, and if h varies, as is the case when the bottom is hemispherical, the relationship becomes more complicated. However, the fact remains that the gravitational period of the water in the tank increases with the decrease in the depth of water.

An estimation of the surge period was made by using the formula given above for a rectangular tank which has the same cross-section and capacity as the actual tank in which the water-level was 7.7 m. from the bottom. The period in this case became 1.92 seconds. Further calculation[1] was made for the fundamental period of the surging water in a circular tank of which the diameter was 8.5 m. and the water-level was 7.7 m, the results being 3.05 seconds. Thus, the gravitational period of the water is at least longer than these calculated values and of course far longer than that of the tower system. Consequently, the beating effect is quite small in the present tower.

Computation and measurement of period of tower. The method for computing the natural period of vibration of the tower is based on the relation between the period and the deflection of the tower under the action of a horizontal load equal to its own weight. The period of vibration is then given by the equation

---

[1] Takuji SUZUKI calculated.

$$T=2\pi\sqrt{\frac{\delta_{st}}{g}}\doteqdot 0.200\sqrt{\delta_{st}}, \qquad (2)$$

where T is the period in second, δ_{st} the deflection in cm. of the top of thet ower under a static horizontal load equal to its own weight and load.

Let us assume that the deflection of the tower during vibration is equivalent to that of a heavy mass (W) supported on a weightless spring having one degree of freedom. In this case, the deflection may be calculated simply for a horizontal beam which is loaded as shown in Fig. 5.

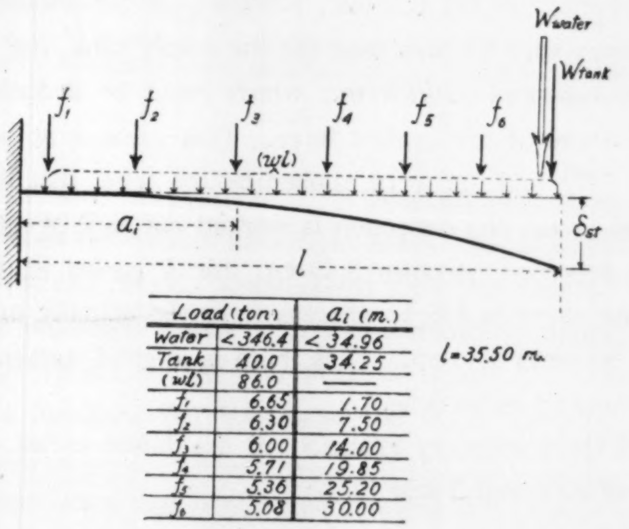

Load (ton)		a_i (m.)
Water	< 346.4	< 34.96
Tank	40.0	34.25
(wl)	86.0	——
f_1	6.65	1.70
f_2	6.30	7.50
f_3	6.00	14.00
f_4	5.71	19.85
f_5	5.36	25.20
f_6	5.08	30.00

Fig. 5.

Supposing that the weight of the six columns and the bracings be distributed uniformly along the length of the column, this load is shown by wl in this figure. The weights of the horizontal beams and tie rods act as loads designated as $f_1, f_2 \ldots\ldots f_6$ and the weights of the tank and the water act at their respective points as shown in the figure.

Let E be the Young's modulus and I the moment of inertia of the section of a beam to which the tower is assumed to be equivalent. Then, the total deflection,

$$\delta_{st}=\frac{(wl)l^3}{8\,EI}+\sum\frac{f_i}{6\,EI}(3a_i^2l-a_i^3)+\frac{Wwater}{6\,EI}(3a_w^2l-a_w^3)+\frac{Wtank}{6EI}(3a_t^2l-a_t^3), \quad (3)$$

in which l denotes the length of the column and a the distance of the point of application of the load measured from the foundation in general.

According to the assumption of a weightless spring, the deflection, δ_{st}, becomes as

$$\delta_{st}=\frac{[w]}{3EI}l^3. \qquad (4)$$

By the calculation using the values as shown in the figure, the equivalent mass, when the tank is empty, was found to be

$$[W]=91.68 \text{ tons.}$$

From this value and the measured period of the tower with empty tank (period = 0.30 second), EI can be deduced as follows:

$$EI=6.05\cdot 10^{17} \text{ gram. cm}^2.$$

As previously mentioned, δ_{st} may be calculated by equation (2), if the period is known. Then, the deflection of the empty tank tower becomes as 2.25 cm.

The actual deflection in the pull-test, however, is far smaller than this calculated value. When wire #8 was used for the empty tank, the deflection at the top of the column measured 0.01075 cm., which could be deduced from the first motion after the release of the applied force. This value must be proportional to the ratio between $[W]$ and the force applied by the wire, that is, 208:1. Hence, from the measured value, the deflection is worked out as 2.24 cm. In the case of the full tank, the deflection becomes 8.45 cm. for a period of 0.578 second and the ratio mentioned above is 815:1, whereas from the actually measured amplitude of 0.0104 cm., δ_{st} becomes 8.48 cm. Thus there is a good agreement between the calculated and measured deflections.

The period of the translatory vibration of the tower varies considerably with the water-height (Fig. 6 and Table I).

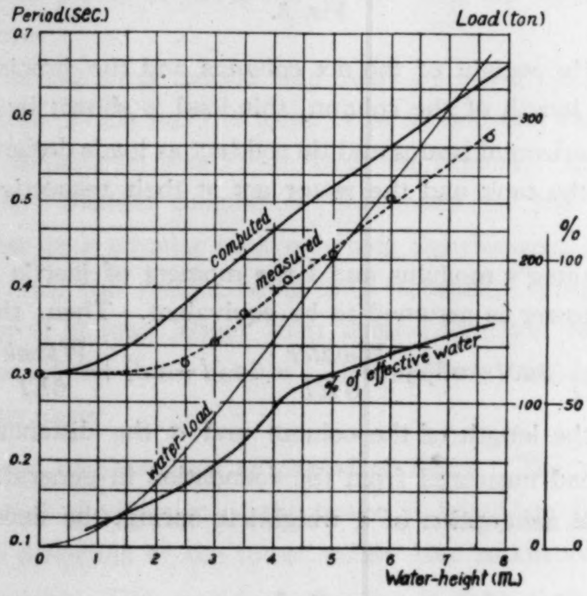

Fig. 6.

Table I. Period and damping of tower vibration,

Water-level in tank	Direction of pull	Period		Damping ratio (v)		ξ/E
		normal to side	diagonal			
7.7 m	b	0.580 sec.	0.575 sec.	1.026		
	a	0.580	0.570		1.026	7.66.10^{-3}
6.0	b	0.507	0.500	1.030		7.47
5.0	a	0.440	0.440		1.035	7.77
4.3	b	0.420	0.400	1.039		7.89
3.5	a	0.370	0.370		1.043	7.76
3.0	a	0.334	0.340	1.050		7.82
2.5	b	0.310	0.325		1.047	7.84
0	b	0.305	0.295	1.053		7.86
	a	0.300	0.300		1.053	

(Direction of pull; see Fig 3.)

As the water does not all act as a rigid mass, the computed period becomes longer than the measured period. Calculations show that the equivalent translational mass of the water increases rapidly with the increase in depth, When the tank is nearly full, about 78 per cent of the mass is apparently effective. But, when the water is in the hemispherical bottom of the tank, the rate of the effective water is considerably small, probably due to greater movement of the water relative to the tank than when the tank is more nearly full.

A close examination of the period revealed that excepting the case of the empty tank, one or two waves after the release of the pull had usually slightly longer periods than the subsequent waves. For example, when the tank was full, the period of the first wave was 0.590 second, the period of the second wave 0.585 second and that of the third wave 0.582 second, whereas the periods of the waves elsewhere were 0.578 second in the mean. This suggests that at the instant of the release of the applied force, more mass of the water was effective than in the subsequent vibrations. Contrariwise when the tower was continuously set into vibration, such as by the wind, the period was slightly shorter than any period mentioned above. The period determined in the wind records was 0.570 second. Perhaps in this case, the effective mass of water became smaller than in the case of any pull-test made on the full tank.

Damping of tower vibration. According to K. Suyehiro[2], the decay of the free vibration of a beam is given by $e^{-\frac{kt}{2}}$

---

[2] K. SUEHIRO, *Bull. Earthq. Res. Inst.*, **6**(1929), 63.

in which k stands for $\frac{\xi}{\mathrm{E}}\left(\frac{2\pi}{Tr}\right)^2$, ξ the coefficient of normal viscosity of the material composing the beam (in actual structures, the dissipation of vibrational energy through the foundation and that due to other causes is to be included in this), E Young's modulus, Tr the undamped natural period of the beam, e the base of the Napilian logarithm. Thus, the decay constant $\frac{k}{2}$ is inversely proportional to the square of the natural frequency, n, if the material of the beam is known. Therefore, from the logarithmic decrement of the amplitude and the natural period of a vibration, we can deduce the value of $\frac{\xi}{E}$ as shown in the last column of Table I. These values of $\frac{\xi}{E}$ are comparativery larger than those which Suyehiro calculated for the brick chimneys and reinforced concrete frame, that is,

$$\text{for brick chimneys, } \frac{\xi}{E}=4.78\sim 1.95\times 10^{-3},$$

$$\text{for reinforced concrete frame, } \frac{\xi}{E}=1.85\times 10^{-3}.$$

This may be due to the greater dissipation of the vibrational energy through the large number of joints existing in the tower than in the case of the brick chimneys or concrete frame for which the above values were calculated.

The effect of the water in the tank upon the tower vibration, like the effect of the water in the Schlingertank[3] for stabilizing ship cannot be considered in this case, because the damping is stronger for the empty tank than for the tank partially empty or full.

Torsional vibration. When the tower is pulled in such a direction as shown in Fig. 3–c, torsional vibration will be caused in the tower after the release of the pull. The records of such vibrations are shown in Fig. 4–c and–d. It was found that the period of the torsional vibration did not vary according to the waterload as in the case of the translatory vibration and was nearly constant throughout the tests. The period was 0.14 second. Thus, in the torsional vibration, the effective mass of water was quite small. By the way, waves of smaller periods of 0.04∼0.08 second which are seen in the earlier stage of vibration, are due to the vibration of the steel members struck by the end of the rope cut down at the release of the applied force.

Movement of foundation. As the movement of the foundation was very small, the optical instruments were set on the concrete foundation. For recording a horizontal component motion, one set of Wood-Anderson torsion seismometer was used. For the vertical motion, a vertical component seismograph specially designed for the field work was used. The period of the former seismometer was 1.0 second and that of the latter 0.7 second. In both instruments, the static magnification was 2,000 when the optical distance was set at 1.0 m.

---

[3] S. TIMOSHENKO, *Vibration Problems in Engineering.*

A comparative observation was made on the platform of the tower and the foundation with the result that the maximum range of motion of the platform was 0.230 mm., and against this value, the maximum range of motion on the foundation was 0.001 mm. Further, the motions of the top of the tower and the foundation were found to be in the same phase. A slight rotatory yielding of the tower's foundation was suggested by a vertical motion which was observed to be 0.001 mm. at its maximum.

The ratio of the displacements of the platform and the foundation stated above is 230:1. This exceeds the value of 200:1 reported[4] to be the value determined for towers standing on firm grounds and of course it is greater than the value of 150:1 determined for towers on yielding grounds where piling was required.

The ground on which the present tower is standing is of a hard loam whose bearing power is estimated to be greater than 50 tons per square meter. Thus, the ground may be classed as "good" or "firm" and the yielding effect of the foundation upon the vibration will be very slight.

In conclusion it must be added that the most probable cause of the seismic damage of the tank tower is the beating effect between the tower and the water in the tank, so the tower should be designed so as to make its natural period of vibration quite different from that of the surging water. From this point of view, the present tower may be said to be faultless.

37.　水槽鐵塔の振動について

那 須 信 治

100,000 ガロンの水槽を有する鐵塔の振動試驗を行つた.（1）風に對する振動は規則正しい波動の連續であつて，弛緩部分による不規則な振動は認められなかつた.（2）引張り試驗により，水の容量と塔の振動週期との關係を調査した．水槽内の水の動搖週期は塔の週期より遙に大であつて共鳴の現象は實際上認められなかつた．水の固體として振動に寄與する有效率を求めた。又捩れ振動に對して水の影響は殆んどないものと思われる．塔の振動減衰は比較的早いようである．これは多數の接合點に於て振動エネルギーが逸散される結果であろう．基礎の yielding は少なく，振動週期其他に及ぼす影響もこの場合少い.

---

4) *Special Publication, Coast and Geodetic Survey*, No. 201 (1934-1935). 95.

38.　高周波域に於ける土の電氣的性質

地震研究所　力武常次・岸上冬彥

（昭和21年7月16日發表――昭和22年9月18日受理）

1. 緒　　言

筆者の一人[1]はさきに電磁波の偏波狀態から土地の電氣抵抗を所謂双極子法に依つて測定した結果を發表したが，このような方法を用いて地下探査を企てる場合に土の電氣的性質が如何なるものであるかを具體的に知る必要があり更に土中の緩和現象を研究する豫備的實驗として，今回は土の試料を用いて含水率および周波數を種々變化した場合に電媒常數および比抵抗が如何に變化するかを實驗室內で測定した.

高周波に依る土の電氣的性質の測定は種々の文獻[2][3][4]があり，今回採用した測定方法も概ねこれ等の方法と同じであるが，測定の結果得られる見掛け上の値から眞の値を求める爲に考慮を拂つた.

また測定の結果の解釋に際して，土の電氣的モデルを考えることによつて，二三の理論的考察を行い，水分の影響を論じた.

今回の電氣的方法に依る測定が從來本研究所に於て行われて來た土の物理的性質の研究に對して若干寄與するところがあれば幸いである.

2. 測定方法および裝置

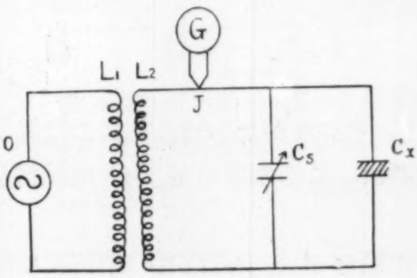

第1圖　測定裝置結線圖

測定方法は絕緣物の電媒常數及び損失角測定に用いられる方法と同一であつて，回路は第1圖に示してある．圖に於て 0 は三極眞空管を使用した Hartley 型發振器であつて，2.5～7.5 *MC* の發振範圍をもつている．發振出力は L_1 に極めて疎に結合した L_2 を經て二次回路に供給される．この結合が密に過ぎると，共振時に發振器の發振電壓が變化し二次回路に誘導する起電力を一定に保つことが不可能になる．C_s は較正した可變空氣蓄電器であつて，今回の測定には 25～85 $\mu\mu F$ および 10～300 $\mu\mu F$ のものを併用した．C_x は眞鍮製平行圓板蓄電器であつて，兩板の間に試料を挿入する，J は眞空熱電對で，二次回路の電流は J につないだ檢流計に依つて測定

---

1) 力武常次　地震研究所談話會（昭和21年3月）

2) J. A. RATCLIFFE and F. W. G. WHITE, *Phil. Mag.*, **10** (1930), 667.

3) R. L. SMITH-ROSE, *Proc. Roy. Soc.*, **140** (1933), 359.

4) BIMALENDU SEN-GUPTA and S. R. KHASTIGIR, *Phil. Mag.*, **22** (1936), 265.

される.

被測定蓄電器に試料を挿入した時，電氣傳導度が有限であれば，容量と抵抗を併列につないだものと考えることが出來るから，測定回路は第 2 圖のように考えてもよい. かゝる結合回路の電氣振動はよく知られたように次の微分方程式の解として表わされる.

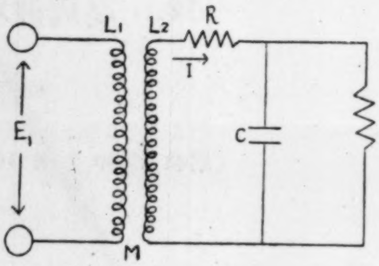

第 2 圖 測定裝置等價回路

$$\frac{d^2I}{dt^2}+\frac{1}{L}(R+R_e)\frac{dI}{dt}+\frac{1}{LC_e}I=-\frac{1}{L_1L}\frac{dE_1}{dt} \tag{1}$$

但し $E_1=e_1\cos\omega t$ の時

$$L=L_2\left(1-\frac{M}{L_1L_2}\right), \tag{2}$$

$$R_e=\frac{R_x}{1+\omega^2C^2R_x{}^2}, \tag{3}$$

$$C_e=C\left(1+\frac{R_x}{\omega^2C^2R_x{}^2}\right). \tag{4}$$

吾々の取扱う場合に於ては，R_x は $K\Omega$ 程度以上であつて

$$C_e=C \tag{5}$$

としてよいから (1) より振幅は

$$A=\frac{1}{L_1L}\frac{e_1}{\omega}\frac{1}{\sqrt{\left(\frac{1}{CL\omega^2}\right)^2+\left(\frac{R+R_e}{\omega L}\right)}} \tag{6}$$

となる.

i) 電媒常數の測定

第 1 圖の C_s を調節することに依つて，はじめ C_x をつながない時の共振の位置を求め，次に試料を挿入した場合の共振の位置を測定すれば，この兩者の差 $\varDelta C$ は試料を挿入した爲の容量の增加である.

一方 C_x の圓板の半徑を r, 厚さを b, 兩圓板の距離を d とすればこの平行圓板蓄電器の容量は Kirchhoff[5] に依つて求められたように

$$\left.\begin{aligned} C_0&=C_{01}+C_{02}, \\ C_{01}&=\frac{r^2}{4d}, \\ C_{02}&=\frac{r}{4\pi}\left\{\log\frac{14\pi r(d+b)}{d^2}+\frac{b}{d}\log\frac{d+b}{b}-1\right\} \end{aligned}\right\} \tag{7}$$

となる. 但し兩電極とも絶縁されているものとする.

---

5) G. Kirchhoff, *Gesamm. Abhandl.*, p. 112.

今全空間を電媒常數 ε なる電媒質でみたしたとすれば

$$\Delta C=\varepsilon C_0$$

となる筈であるが，實際は兩電極の間にのみ電媒質をみたしたのであるからこの關係は成立しない．

今見掛けの電媒常數として

$$\varepsilon_{app.}=\frac{\Delta C}{C_{01}} \tag{8}$$

を定義する．$\varepsilon_{app.}$ を眞の ε に引直す爲に次の如き考察を爲す．先ず漏電場による補正項 C_{02} に依る部分は小いと考えて

$$\Delta C=\varepsilon C_{01}+k\varepsilon C_{02} \tag{9}$$

と假定する，電極の距離 d を種々に變化して，夫々の場合に對する C_{01}，C_{02} を計算に依つて求め，ΔC を測定すれば，最小自乘法に依り ε 及び k を同時に決定することが出來る．實際は k は d によつて少しく異るが，d の小さい値に對しては不變として取扱つた．

今回の測定に使用した平行圓板蓄電器は $r=2.90cm$, $b=0.40cm$ であつて，ワセリンを使用して種々の d に對する見掛けの電媒常數を測定した結果は第3圖の通りであつて，$d\to0$ の極限として得られる ε の値は最小自乘法に依つて求めた値($\varepsilon=1.88$ $k=0.233$）に一致する．かくして決定した k の値を用いて，任意の電媒質の ε を同じ蓄電器を用いて得られた $\varepsilon_{app.}$ より求めることが出來る．

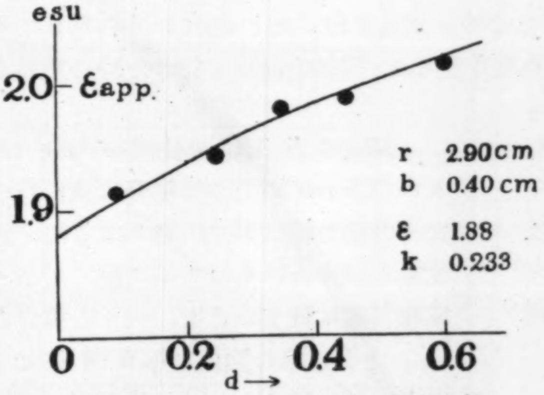

第 3 圖　ワセリンの見かけの電媒常數

ii）比抵抗の測定

C_s を變化せしめて，電流の共振曲線を測定し，振幅が最大振幅の $\dfrac{1}{\sqrt{2}}$ になつた時の容量を C とすれば，(6) より

$$\frac{1}{2\left(\dfrac{R+R_e}{L\omega}\right)^2}=\frac{1}{\left(\dfrac{1}{CL\omega^2}-1\right)^2+\left(\dfrac{R+R_e}{\omega L}\right)^2}$$

從つて C の値は二つ存在して，C_a 及び C_b は夫々

$$\frac{1}{C_aL\omega^2}-1=\frac{R+R_e}{\omega L},$$

$$\frac{1}{C_bL\omega^2}-1=-\frac{R+R_e}{\omega L}$$

を滿足するわけである．故に

$$R+R_e=\frac{1}{2\omega}\left(\frac{1}{C_a}-\frac{1}{C_b}\right) \tag{10}$$

R は C_x を接續しない狀態で測定して置くことが出來るから，(10) より R_e を求め，從つて (3) より R_x を求めることが出來る．一方比抵抗 ρ は

$$\rho=\frac{\pi r^2}{d}R_x \tag{11}$$

なる關係を有するから，結局共振振幅の $\frac{1}{\sqrt{2}}$ になる時の容量を求めて，ρ を決定することが出來る．この場合檢流計のふれは，熱電對を用いているので，電流の自乘に比例し結局檢流計のふれが最大値の $\frac{1}{2}$ になる時の容量を求めればよいことになる．

3. 測定結果（含水量との關係）

東京大學理學部構內より赤土を採取して測定試料とした．採取時期は降雨直後であつて，水分は比較的大であつた．試料を蓄電器にみたし，測定をなすとともに重量を測定し，50°～60°C の溫度で熱して水分を蒸發させ時々測定を行つた．遂にいくら熱しても重量が減少しなくなる時の試料の重さを土の重さと考え，電氣的測定を行つた時の重量から水分の量を求め，含水率 w を決定した．

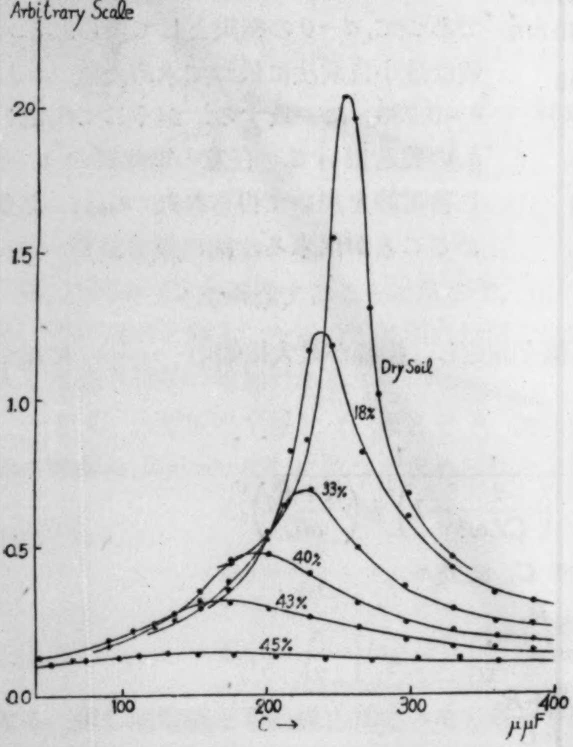

第 4 圖 東大構內に於いて採取した赤土の含水率と共振曲線

測定は 5 MC に於て $d=0.6$ cm 及び 1.5 cm の二つの場合に就て行つた．共振曲線は第 4 圖のように，含水率の減少とともに次第に銳くなる．電媒常數に就て云えば，夫々の場合の ε_{app} と含水率の關係は第 5 圖の如くなり，前に述べた k の値を用いて補正を行うと第 6 圖の如くなる．ε は含水率が小さい間は二つの場合ともよく一致するが，含水率が大になると喰違いが顯著になつてくる．ε の大きな値に對しては，(9) の如き簡單な假定が成立たないのであろう．

電媒常數は含水率の增大に伴い急激に增大して，20～30 というような大きな値に達することは，水分の量が土の電氣的性質に極めて大なる影響をおよぼすことを示す．

次に比抵抗であるが，第 7 圖に

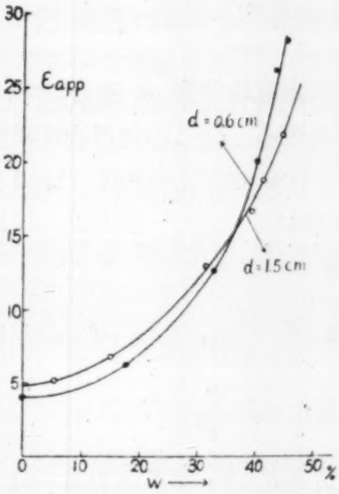

第 5 圖　赤土の見かけの電媒常數と含水率(5MC)

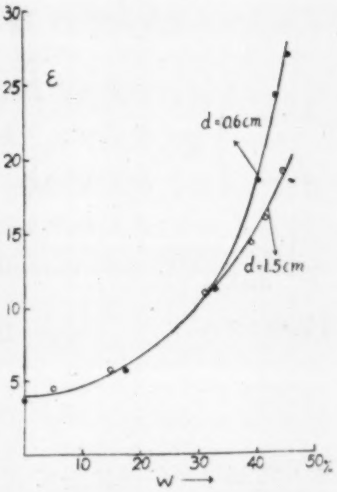

第 6 圖　赤土の電媒常數と含水率 (5MC)

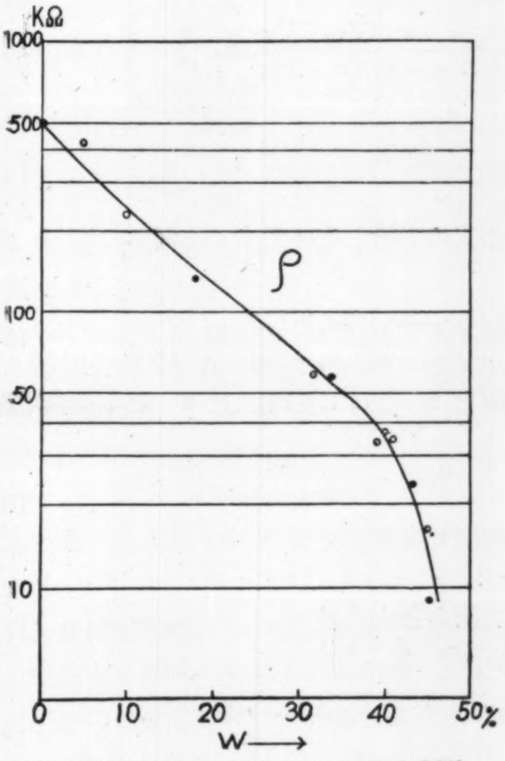

第 7 圖　赤土の比抵抗と含水率 (5MC)

示す如く含水率の增大に伴い急激に減少している．圖中黑點は $d=0.6\ cm$ の場合の測定値，白點は $d=1.5\ cm$ の場合の測定値である．減少の模様は大略指數函數的であるが含水率 40 %のあたりで減少の程度が更に急激になるように見える．大略の模様は，筆者の一人[6]に依つて，直流によつて測定された結果と大體一致している．

4. 含水率と電氣的性質との關係に就ての理論的考察

土の粒子の間隙にしみこんでいる水分が如何なる狀態にあるか，種々議論のあるところであるが，此處では簡單なモデルを考えて大體のことを議論してみよう．

第 8 圖に示すように，土の粒子は半徑 a なる小球であるとし，水はこれと同心になつていると考え，その半徑を b とする．このような土の粒子と水とからなる小球が多數存在する場合に見掛け上如何なる電氣的性質を示すかを調べるわけであるが，角周波數 ω なる交番電場に於ては

---

6) 岸上冬彦　地震　**13** (1941), 113.

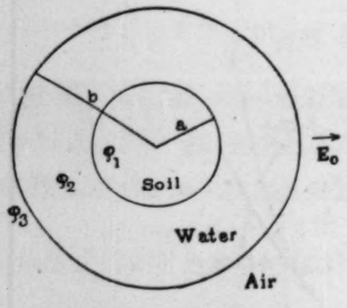

第 8 圖 土の電氣的モデル

$$\kappa=\varepsilon+\frac{\sigma}{i\omega} \tag{11}$$

で與えられる複素電媒常數 κ をとつて，靜電場的取扱いを爲すことが出來る．今このような小球が一箇あつて，他は空氣であるとすれば，土の粒子，水及び空氣中の靜電ポテンシヤルは夫々

$$\left.\begin{aligned}\varphi_1&=Ax\ ,\\ \varphi_2&=Bx+C\frac{x}{r^3}\ ,\\ \varphi_3&=-E_0x+D\frac{x}{r^3}\end{aligned}\right\} \tag{12}$$

で與えられる．但し電場は無限遠に於て x 方向に E_0 なる値をもつとする．土の粒子，水および空氣の複素電媒常數を夫々 κ_1, κ_2 および 1 とすれば，$r=\mathrm{a}$ および $r=\mathrm{b}$ に於ける境界條件により，A, B, C および D 等の常數を決定することが出來て，空氣中のポテンシヤルは

$$\varphi_3=-E_0x+\frac{\mathrm{b}^3}{3}\frac{(\kappa_1+2\kappa_2)(\kappa_2-1)+(\kappa_1-\kappa_2)(2\kappa_2+1)q}{(\kappa_1+2\kappa_2)(\kappa_2+2)+2(\kappa_1-\kappa_2)(\kappa_2-1)q}E_0\frac{x}{r^3} \tag{13}$$

で與えられる．但し

$$q=\frac{\mathrm{a}^3}{\mathrm{b}^3} \tag{14}$$

である．この樣な小球が n 箇あつたとして，相互の影響を省略出來ると考えれば r が大きいところでは

$$\varphi_3=-E_0x+n\frac{\mathrm{b}^3}{3}\frac{(\kappa_1+2\kappa_2)(\kappa_2-1)+(\kappa_1-\kappa_2)(2\kappa_2+1)q}{(\kappa_1+2\kappa_2)(\kappa_2+2)+2(\kappa_1-\kappa_2)(\kappa_2-1)q}E_0\frac{x}{r^3} \tag{15}$$

となるが，一方この小球 n 箇を含んだ球の半徑を b′ として見掛け上 κ' なる複素電媒常數を示すものとすれば，ポテンシヤルは

$$\varphi'_3=-E_0x+\frac{\mathrm{b}^3}{3}\frac{\kappa'-1}{\kappa'+2}E_0\frac{x}{r^3} \tag{16}$$

從つて (15) と (16) を比較することによりより

$$\frac{\kappa'-1}{\kappa'+2}=s\frac{(\kappa_1+2\kappa_2)(\kappa_2-1)+(\kappa_1-x_2)(2\kappa_2+1)q}{(\kappa_1+2\kappa_2)(\kappa_2+2)+2(\kappa_1-\kappa_2)(\kappa_2-1)q} \tag{17}$$

但し

$$s=n\frac{\mathrm{b}^3}{\mathrm{b}'^3} \tag{18}$$

である．

(17) より κ' を求めて

$$\kappa'=\frac{(\kappa_1+2\kappa_2)\{\kappa_2+2+2s(\kappa_2-1)\}+2q(\kappa_1-\kappa_2)\{\kappa_2-1+s(2\kappa_2+1)\}}{(\kappa_1+2\kappa_2)\{\kappa_2+2-s(\kappa_2-1)\}+q(\kappa_1-\kappa_2)\{2(\kappa_2-1)-s(2\kappa_2+1)\}} \tag{19}$$

を得るが，水分は土の粒子に比して，電媒常數，電氣傳導度とも充分大きいと考えられるから κ_1 を κ_2 にくらべて省略すると，(19) は

$$\kappa_1=\frac{2(1+2s)(1-q)\kappa_2+2(1-s)(2+q)}{2(1-s)(1-q)\kappa_2+(2+s)(2+q)} \tag{20}$$

となる．従つて (20) の實數部，虚數部より見掛けの電媒常數及び電氣傳導度を求めると

$$\varepsilon'=\frac{2\{(1+2s)(1-q)\varepsilon_2+(1-s)(2+q)\}\{2(1-s)(1-q)\varepsilon_2+(2+s)(2+q)\}+4\dfrac{\sigma_2^2}{\omega^2}(1+2s)(1-s)(1-q)^2}{\{2(1-s)(1-q)\varepsilon_2+(2+s)(2+q)\}^2+4\dfrac{\sigma_2^2}{\omega^2}(1-s)^2(1-q)^2} \tag{21}$$

$$\sigma'=2\sigma_2\frac{(2+s)(1+2s)-2(1-s)^2}{\{2(1-s)(1-q)\varepsilon_2+(2+s)(2+q)\}^2+4\dfrac{\sigma_2^2}{\omega^2}(1-s)^2(1-q)^2}(1-q)(2+q) \tag{22}$$

となるが，今回の測定を行つた $f=10^6$ *c.p.s.* 程度の周波數では，水の ε, σ 等の値を考慮すると，(21) 及び (22) の分母の第一項は第二項に比して小さくなるので，$q=1$ 卽ち後に述べるように含水率が極めて小い附近をのぞいて

$$\varepsilon'\simeq\frac{1+2s}{1-s}\,, \tag{23}$$

$$\sigma'\simeq\frac{\omega^2}{2\sigma_2}\;\frac{(2+s)(1+2s)-2(1-s)^2}{(1-s)^2(1-q)}(2+q) \tag{24}$$

となる．これ等の式中の q, s 等はその定義より，土，水および空氣の體積を V_s, V_w 及び V_a とすれば

$$q=\frac{V_s}{V_s+V_w}\,,\qquad s=\frac{V_s+V_w}{V_s+V_w+V_a}$$

であるから

$$q=\frac{1-w}{1+(\rho_s-1)w}\,,\qquad s=\frac{1-P}{1-w}\{1+(\rho_s-1)w\} \tag{25}$$

となる，こゝに w, P は含水率及び間隙率の 1/100 の値であり，ρ_s は土の眞の密度である，

故に間隙率，土の眞の密度を與えれば，(23) により見掛けの電媒常數の含水率による變化を一義的に知ることが出來，更に水の比傳導度及び周波數を與えれば，(24) から見掛けの比傳導度従つて比抵抗の含水率による變化を求めることが出來る．一例として，$P=0.7$，$\rho_s=2.7$，$\sigma_2=10^{-4}\,ohm^{-1}cm^{-1}$，$f=5\times10^6$ *c.p.s.* とした場合に (23)，(24) に従つて計算した結果を示せば 第 9 圖 及び第 10 圖のようになる．含水率小のところでは，土の粒子の ε, σ 等が省略出來なくなると同時に (22) 式中の分母の第一項の影響がきいてくるから，計算が複雜になるので省略するが，大體の様子は實驗の結果を比較的よく説明することが出來る．含水率 40% あたりで，ρ が急に小さくなることは近時

生化學で問題となつているように土中の水分の一部が結合水となるのではあるまいか？この點については將來研究したい．

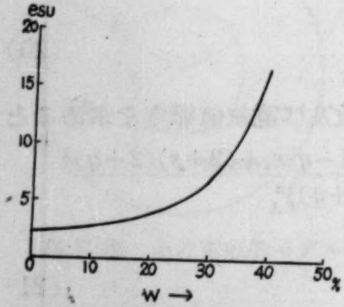

第 9 圖 電媒常數と含水率の理論的關係

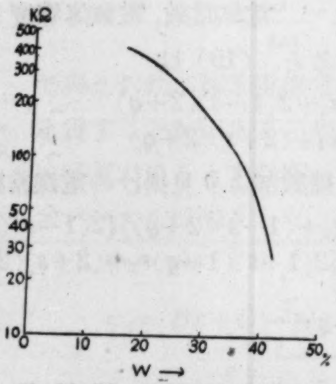

第 10 圖 比抵抗と含水率の理論的關係

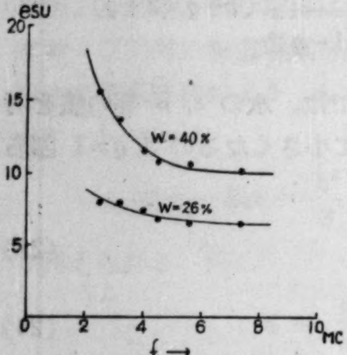

第 11 圖 赤土の電媒常數の周波數による變化

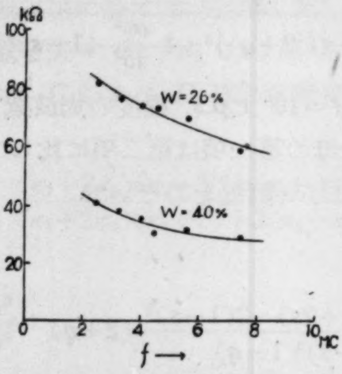

第 12 圖 赤土の比抵抗の周波數による變化

5. 測定結果

（周波數による變化）

次に測定周抵數を變化せしめて，電氣的性質が如何に變化するかを調べた．測定は含水率 40% 及び 26% の二つの場合に就て行つたが，結果は第 11 圖及び第 12 圖に示してある．

電媒常數，比抵抗ともに周波數の減少とともに增大の傾向を示す．このことは前述の諸文獻に記されている傾向と一致し，電波の傳播を論ずる場合には留意すべきことがらであろう．しかしながら土中の電氣的緩和現象を研究しさらに力學的緩和現象との關係を論じるにはもつと廣い周波數範圍にわたつて測定を行う必要があるので詳細は次の機會に讓る．

6. 結 語

本報文に於ては，高周波を使用した土の電氣的性質の測定方法を述べ，一つの試料に就いて含水率および測定周波數の變化に伴つて，電媒常數および比抵抗が如何なる變化をなすかを調べ，更に簡單なモデルからこれ等の變化がほゞ豫期出來ることを述べた．

含水率に依る變化は極めて著しいものがあり，土中の水分が極めて重要な役割をしていることが明らかになつた．自然狀態に於て，土中の水分の量がどの程度變化し得るものか明らかでないが，例えば電磁波に依る地下探査を企てるような場合には，含水量に關して正確な知識をもつていなければならないわけである．

この水分の影響は，上述の簡單なモデルを考えた理論的考察に依つて，定性的および定量的にほゞ說明可能であつて，電氣的性質を問題とする限りこの程度の土のモデルが大略適當しているものと思われる．

周波數變化に伴う電氣的性質の變化は，周波數の可變範圍が現在の装置では比較的せまい範圍に限られているので，充分な議論が出來ない．しかし前述のモデルに依る見掛けの電氣的量が周波數の函數となつていて，その函數型は定性的に實驗結果と一致している．土の電氣的性質が周波數に依ることは，電磁波の傳播特に所謂双極子法によつて土地の有效電氣抵抗を測定する場合に注意しなければならないことである．

いずれにしても，今回の測定に依つて測定された電氣的量は，含水率が零の場合に於ても種々の粒子が適當な間隙をもつて或る配列をなした場合に於ける全體としての有效量であつて，土を構成する各種鑛物の粒子自身或いはそれらの平均としての電氣的性質そのものではないから，鑛物成分或いは化學成分との關係を論ずるに至らない．また今回の測定は本郷に於ける赤土のみに就て行はれたのであつて，例へば砂や粘土の量が著しくちがう場合に如何様な結果を示すかは明かでない．これ等の事項は，今後の機會に吟味する心算であり，更に地層に依る電氣的性質の相異，地下水位との關係等應用上の問題に就ても今後適當な機會に研究してみたい．また土の可塑性による土中の力學的および電氣的緩和現象との關連，さらに近頃生物學等で問題となつている結合水の問題等の種々興味深い研究も今後の問題として殘されている．

---

38. *Electrical Properties of Soil at Radio Frequencies.*

By Tsuneji RIKITAKE and Fuyuhiko KISHINOUYE,
Earthquake Research Institute.

In order to get some data for radio-geology, the writers measured the dielectric constant and electrical resistivity of soil at radio-frequencies. Soil specimens, taken from the ground of Tokyo University, were inserted between two plates of a condenser which was connected with a resonance-circuit composed of a coil, a variable condenser and a thermo-junction. The circuit is loosely coupled with a high frequency oscillator. By means of a galvanometer connected with the thermo-junction, we measured the changes in the electric current induced in the resonance-circuit whence we could determine the electrical properties of soil after some reduction.

It was found that the electrical properties of soil were seriously affected by water contained in it. Dielectric constant changes from 4 to more than 30 and resistivity from 500 to 10 ***kiloohms*** as the water-content changes from 0 to 50%. The changes in the electrical properties with frequency were also measured. In order to interpret these phenomena, the writers took a model, an aggregate of spherical soil-particles concentrically surrounded by water, by which we could approximately explain the observed facts.

In short, the electrical properties of soil seem to be almost determined by its water-content as well as its mechanical properties. We wish to study in the future the nature of the water contained in soil in relation to the so-called "bound water" which has often been studied in colloidal chemistry. As to the relaxation phenomena which is closely connected with the plastic properties of soil, the electrical researches may also contribute in relation to the measurement of relaxation-time.

39. *Seismological Report for the Assam-Tibet Earthquake on Aug. 15, 1950.*

Location of station

Station	Latitude (N)	Longitude (E)	Height
Tokyo (Hongo)	35° 43′	139° 46′	18m
Tukuba	36 13	140 07	280

Instrumental constants

Station	Instrument	Component	Natural period	Magnification	Damping constant($h=\varepsilon/n$)
Tokyo (Hongo)	No. 1, Omori	E. W.	45.0 sec	15	0.13
	No. 2, Omori	N. S.	57.7	20	0.005
	No. 3, Omori	N. S.	120.0	1.5	1.13
	No. 4, Gray-Ewing	Vert.	8.5	20	0.02
Tukuba	Hagiwara Inverted Pendulm	E. W.	6.5	42	0.71
		N. S.	5.8	44	0.63

Station	Phase	Arrival time (G.M.T.)	Maximum amplitude (2 A) (Period)	Remarks
Tokyo (Hongo)	P (E N Z	14^h 16^m 41.5^s		$\Delta=37.°1$ B.C.I.S. Epicentre:* 28.°6N, 96.°5 E
	PP (E N Z	18 11.5		
	S (E N Z	22 31.3		
	L_Q (N	26 09.8	22.8^{mm}(N) (60^{sec})	
	L_R (N Z	28 52.3	22.6 (N) (36)	

---

* Union Geodesique et Geophysique Internationale, Bureau Central Séismologique de Strasbourg.

March, 1951.

The Earthquake Research Institute.

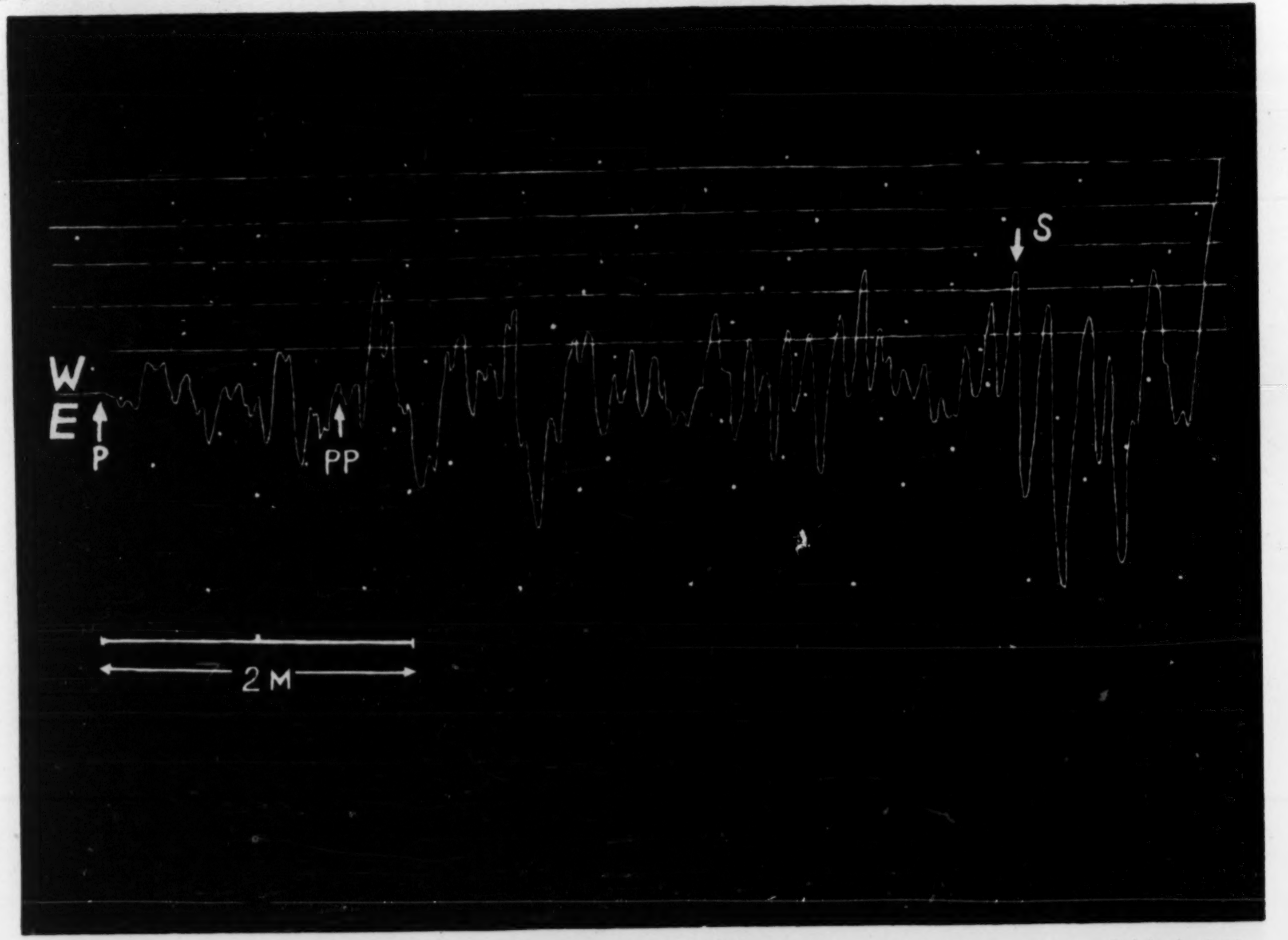

Instrument No. 1. (Tokyo)

Original × 1.08

（震研彙報 第二十九號 圖版 地震研究所）

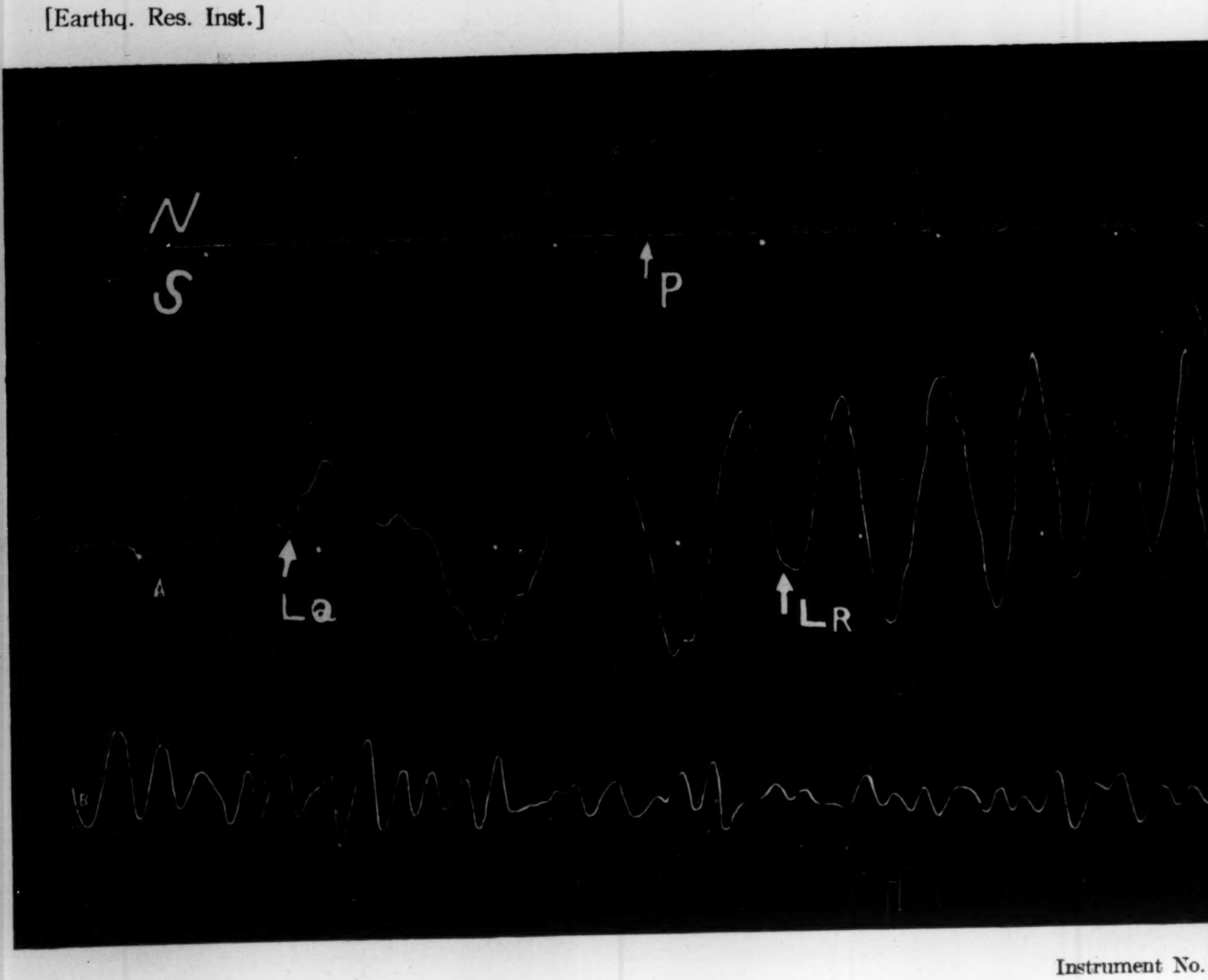

Instrument No.

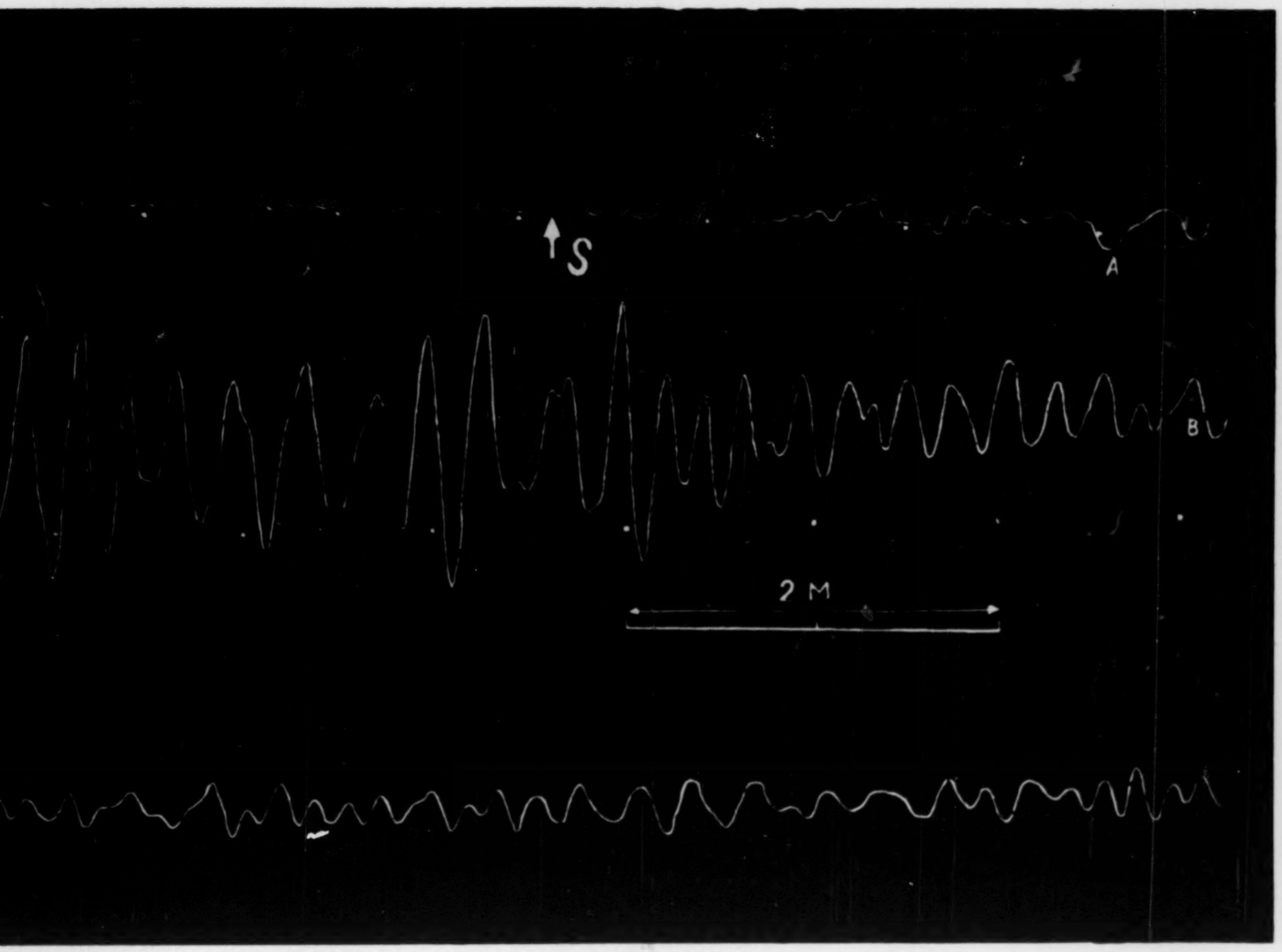

No. 3. (Tokyo)

Original × 0.94

[Earthq. Res. Inst.]

（震研彙報　第二十九號　圖版　地震研究所）

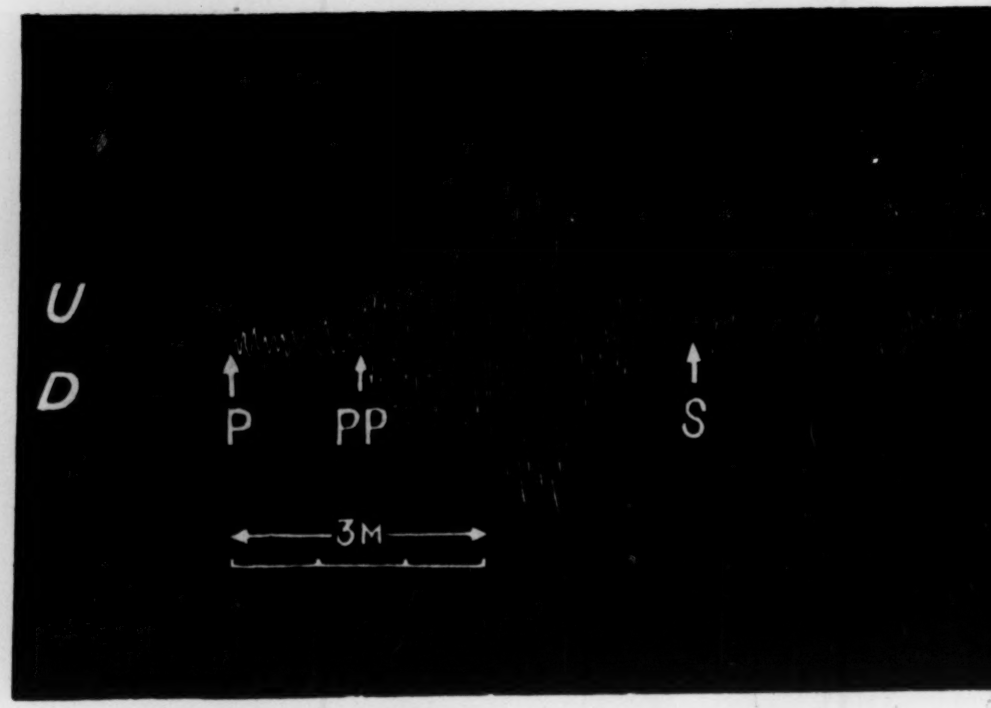

Instrun

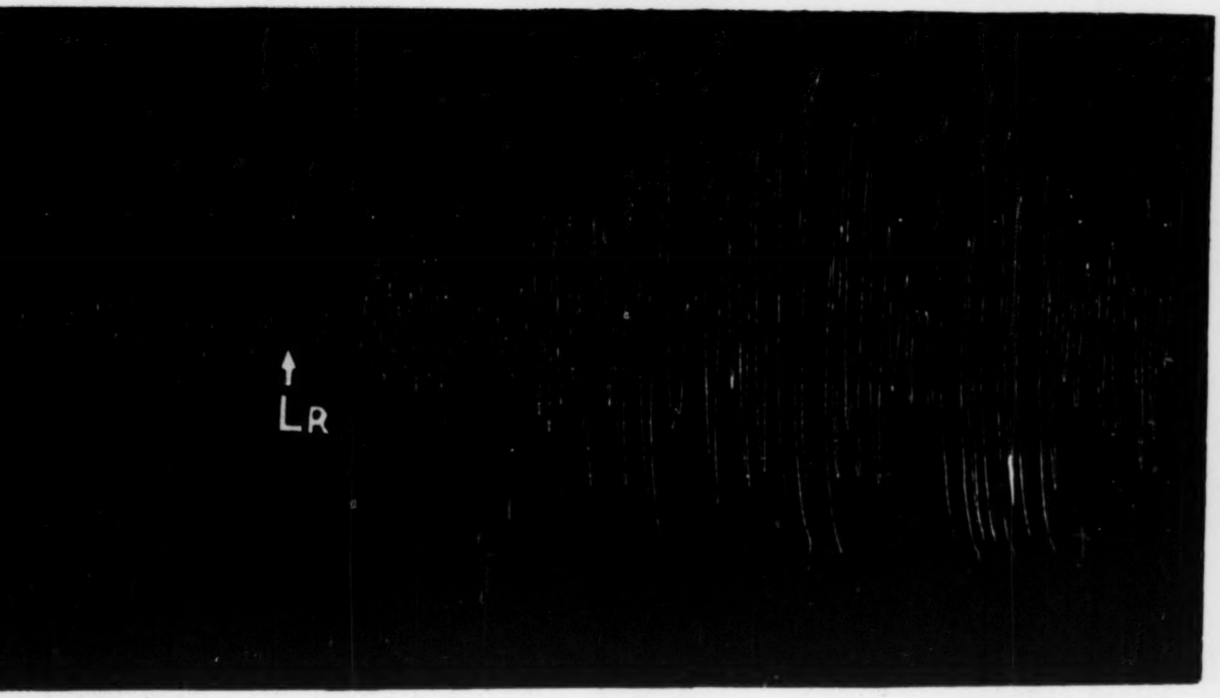

strument No. 4. (Tokyo)

Original × 0.49

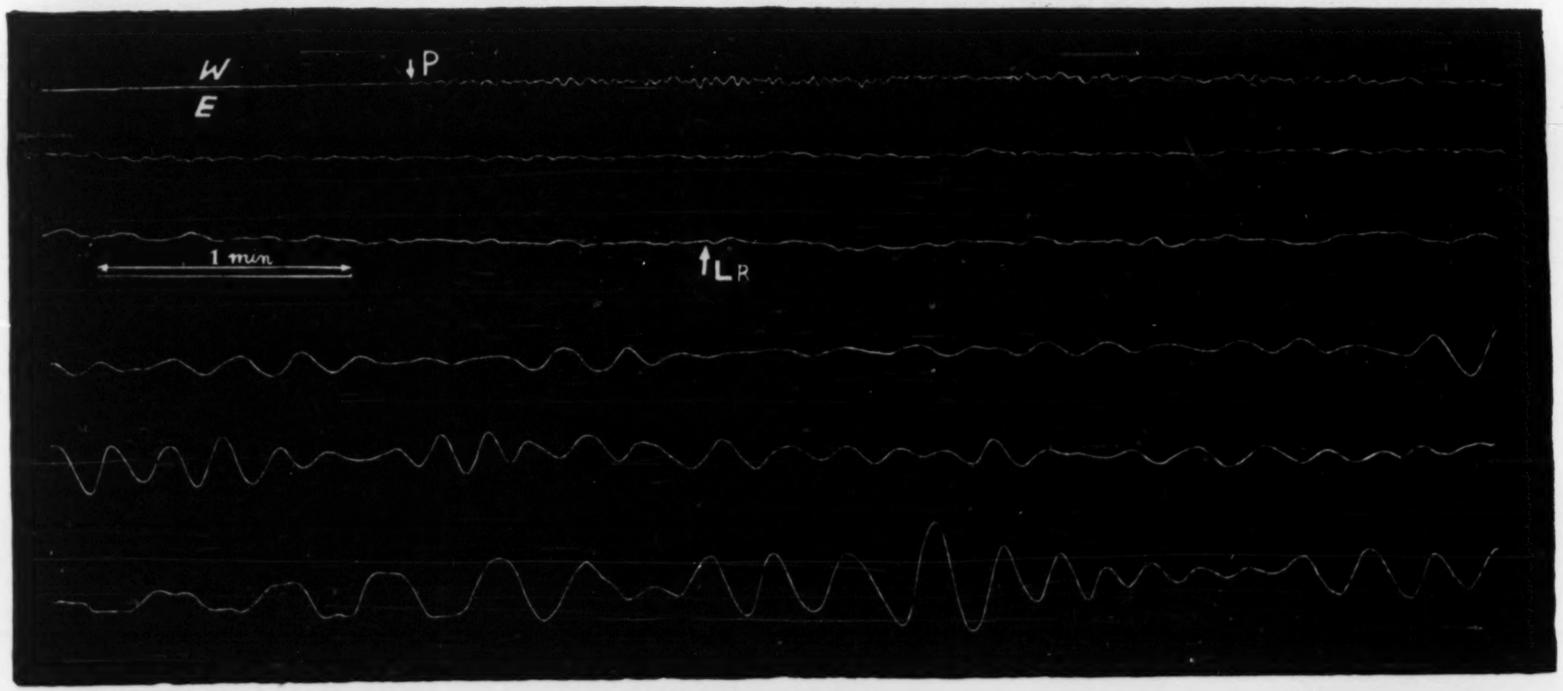

Tukuba observation. Original × 0.52

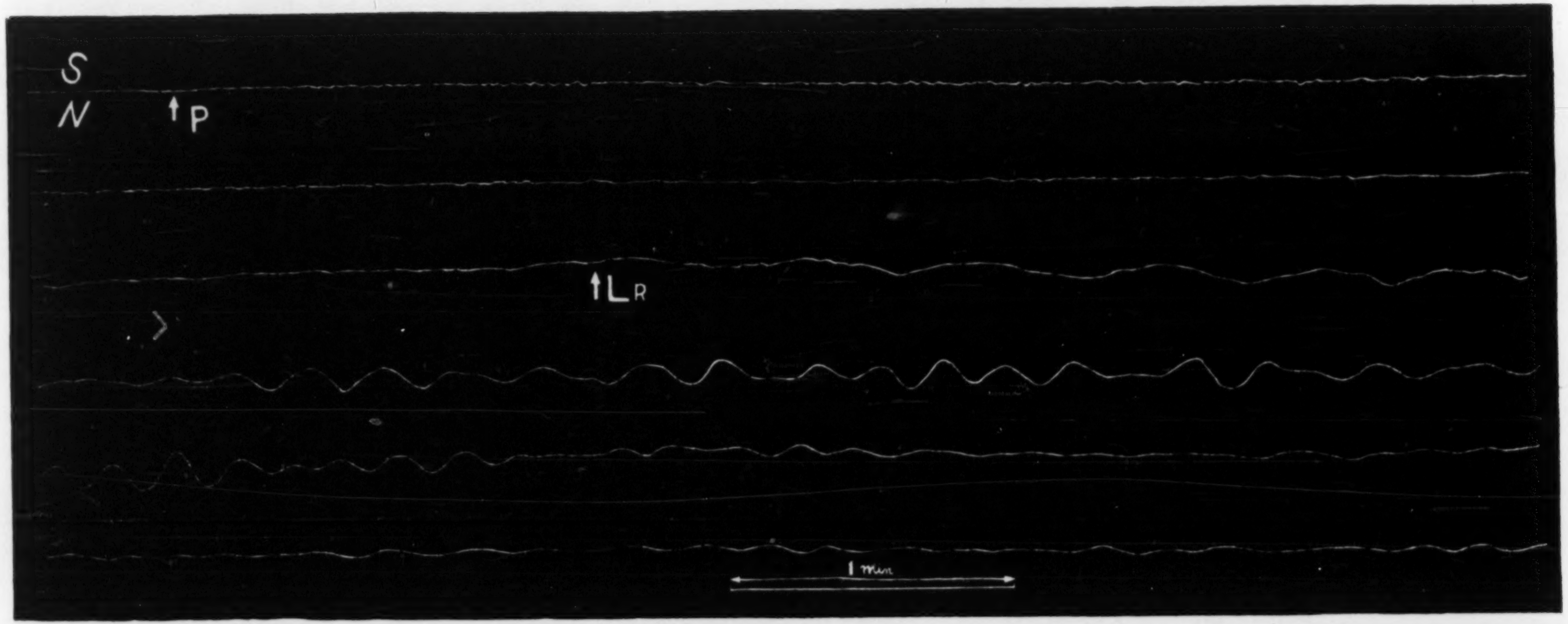

Tukuba observation.　　Original × 0.56

——所　報——

◎ 談話會記事

第 274 回談話會（昭和 26 年 1 月 16 日）

1. 建築物の大振動實驗結果 第一報 （東建式組立鋼筋コンクリート造の場合）	鈴木正治 鈴木富三郎 （金井技官紹介）
2. 地震による建物破壞の機構（續報）	金井清 吉澤靜代
3. 大島三原山噴火調査報告 昇華物その他	津屋弘逵 森本良平 小坂丈予
4. 震源の決定について	越川善明
5. 物體の落下による地表面の振動に關する實驗	秋間哲夫
6. 東京下町の地盤沈下について	岸上冬彦

第 275 回談話會（昭和 26 年 2 月 20 日）

1. 土地の振動の傳播性の研究（第三報）	池上良平 岸上冬彦
2. 今市地震の有感餘震	岸上冬彦
3. 震研本館及び二號館の振動實驗	那須信治
4. 地震の大きさの研究（續報） 「附」 最大振幅と震央距離との關係	河角廣

第 276 回談話會（昭和 26 年 3 月 20 日）

1. 旣設電話線を利用する搬送電話による地震觀測用刻時傳送と保守通話の實驗	宮村攝三 辻浦賢
2. 捩り振子低域濾波器による地震波の研究（其の三） —— 電磁制振式新濾波器に就て ——	秋間哲夫
3. 湖氷の中に發生する震動の研究（序報）	表俊一郎 山崎良雄 村内必典
4. 日立鑛山における地震記象に見られる一二の事項について	金井清
5. レーリー波を發生しない表面應力の分布	佐藤泰夫
6. 藏王火山の地質學的研究（第一報）	市村毅
7. 藏王火山產普通輝石	市村毅 湊秀雄
8. ウオルドン重力計による重力測定に就て	坪井忠二 實川顯 岡田惇 田島廣一

9.	地磁氣永年變化に對する遮蔽効果	力武常次
10.	東京都江東地區地盤沈下の測量	那須信治 岸上冬彦 岡田惇
11.	水槽鐵塔の振動測定結果	那須信治
12.	濃尾平野の地盤變動の測定	那須信治

第 277 回談話會（昭和 26 年 4 月 17 日）

1.	丸の内地盤沈下の終熄と粘土層含水率の減少	北澤五郎
2.	土地の脈動について	岸上冬彦 諸我丈吉
3.	一九五〇年八月十五日のインド地震記象の濾波記録について	秋間哲夫
4.	大島新熔岩の温度と粘性	水上武

第 278 回談話會（昭和 26 年 5 月 15 日）

1.	レーリー波を發生しない表面應力の分布（續）	佐藤泰夫
2.	日立鑛山における地震記象に見られる一二の事項について 補遺	金井清
3.	日立鑛山における電氣探鑛（第六報）	岸上冬彦
4.	伊豆大島地磁氣伏角測量（第三報） その後の地磁氣伏角變化について	力武常次 齋藤貞夫 菱山よね子
5.	油壺における地殼變動の研究（其の四） 土地傾斜 伸縮の經年變化について	萩原尊禮 笠原慶一 山田重平 齋藤貞夫

第 279 回談話會（昭和 26 年 6 月 19 日）

1.	提案の三次元應力函數の一般性の説明について	谷本勉之助 （西村所員紹介）
2.	一九五〇年九月二十三日の淺間山爆發による ガラス窓被害について	佐久間修三
3.	昭和二十六年六月九日十日の三原山噴火活動の觀測	村内必典 （津屋所員紹介）
4.	三原山內輪山内部の地形變化と噴火活動開始との關係（その一）	村内必典
5.	三原山一九五〇年噴出熔岩その他	津屋弘逵 森本良平 小坂丈予
6.	三原山の高さに就いて	高橋龍太郎 平能金太郎 下鶴大輔
7.	鹿沼市で觀測された今市地震餘震の解析	池上良平
8.	脈動の傳播性の研究（第四報）	池上良平 岸上冬彦

9. 物の倒れた方向から震央を求める事　佐藤泰夫
10. 日立鑛山における深さと彈性波速度との關係　金井清
11. 四國地方の重力測定　坪井忠二　實川顯　岡田惇　田島廣一
12. 油壺における地殼變動の研究（その五）　萩原尊禮　笠原慶一　齋藤貞夫　岡田惇
  (イ) 今月行つた油壺附近の精密水準測量と傾斜觀測との比較
  (ロ) 潮汐荷重による土地變形の模樣は經年變化をするか
13. 川崎市附近の地盤沈下について　那須信治　岸上冬彦

昭和26年8月25日印刷
昭和26年8月30日發行

東京都文京區本富士町一番地
東京大學構內
編纂兼 發行者　東京大學地震研究所

東京都中央區日本橋茅場町二丁目十番地
印刷者　笠井康賴

東京都中央區日本橋茅場町二丁目十番地
印刷所　株式會社　國際文献印刷社

東京都千代田區神田一ツ橋通
賣捌所　岩波書店

東京都中央區日本橋二丁目六番地
丸善株式會社

Sold by
Iwanami Shoten,
Hitotsubashi dôri, Chiyoda, Tôkyô,
and
Maruzen Co., Ltd.,
Nihonbashi dôri, Chûô-ku, Tôkyô.
Price of this copy: 870 Yen. (Postage exclusive.)

BULLETIN OF

THE EARTHQUAKE RESEARCH INSTITUTE

TOKYO UNIVERSITY

Vol. XXIX, Part 2. June, 1951.

Contents.

Papers and Reports.

Page

19. Y. **SATÔ**, Study on Surface Waves II. Velocity of Surface Waves Propagated upon Elastic Plates. (in English) 223
20. T. **RIKITAKE**, Electromagnetic Shielding within the Earth and Geomagnetic Secular Variation. (in English) 263
21. T. **RIKITAKE**, Changes in Earth Current and their Relation to the Electrical State of the Earth's Crust. (in English) 271
22. T. **RIKITAKE**, The Form of Tsunami-waves outside a Bay as Inferred from the Motion of Bay-water. (in English) 277
23. N. **NASU**, Block Movement along the Seismic Fault (2). (in English) 283
24. T. **ASADA**, Z. **SUZUKI** and Y. **TOMODA**, Notes on the Energy and Frequency of Earthquakes. (in English) 289
25. Y. **KOSHIKAWA**, Seismometrical Study of the Imaichi Earthquake on Dec. 26, 1949. (The second paper) (in English) 295
26. F. **KISHINOUYE**, Time Distribution of Felt Aftershocks of the Imaichi Earthquake of December 26, 1949. (in English) 301
27. R. **IKEGAMI** and F. **KISHINOUYE**, A Study on the Propagation of Microseismic Waves. Part III. (in English) 305
28. R. **IKEGAMI**, A Study on the Propagation of Microseismic Waves. Part IV. (in English) 313
29. T. **ICHIMURA**, Geological Investigations on the Zaō Volcanoes I. Goshiki-dake, a Central Cone of the Zaō Proper. (in English) 327
30. T. **ICHIMURA** and H. **MINATO**, Augite and Hypersthene Crystals from the Zao Volcanoes. (in English) 341
31. R. **MORIMOTO**, Geology of Imaichi District with Special Reference to the Earthquake of Dec. 26, 1949. (II) (in English) 349
32. T. **MINAKAMI**, T. **MIYAZAKI** and T. **TAKAHASHI**, The 1950-1951 Eruption of Oo-sima and Its Seismometrical Investigations. (I). (in English) 359
33. T. **MINAKAMI** and S. **HIRAGA**, The Minor Activity of Volcano Azuma in February 1950. (in English) 383
34. K. **KANAI**, Destruction System of Building by Earthquake. (in English) 393
35. F. **KISHINOUYE**, Periods of Earth Vibrations at Kotō-ku, Tokyo. (in English)... 403
36. F. **KISHINOUYE**, Sinking of the Kōtō Region, Tokyo. (in English) 407
37. N. **NASU**, Vibration of a Tank Tower. (in Fnglish) 413
38. T. **RIKITAKE** and F. **KISHINOUYE**, Electrical Properties of Soil at Radio Frequencies. (in Japanese) 423
39. Seismological Report for the Assam-Tibet Earthquake on Aug. 15, 1950. (in English) 433

Institute Notes.

(For the papers written in Japanese or in occidental languages, the abstracts are given in occidental languages or in Japanese respectively.)

BULLETIN OF THE EARTHQUAKE RESEARCH INSTITUTE,
TOKYO UNIVERSITY. Vol. XXIX, Part 3. September, 1951.

東京大學
地震研究所彙報

第29號　第3册

昭和26年9月

目　次

論文及報告

頁
40. 表面波の研究 III 二つの表面層をもつラブ波（英文）………… 佐藤泰夫 435
41. レーリー波を發生しない表面應力の分布（英文）………… 佐藤泰夫 445
42. 油壺における地殼變動の觀測（第4報）（英文）………… 萩原尊禮・笠原慶一・山田重平・齋藤貞夫 455
43. 有史以來の地震活動より見たる我國各地の地震危險度及び最高震度の期待値（英文）………… 河角廣 469
44. 土地の脈動の周期と振幅について（英文）………… 岸上冬彦 483
45. 1951年に噴出した大島熔岩の溫度と粘性について（英文）………… 水上武 487
46. 三原火山の活動に伴う地磁氣變化（第2報）（英文）………… 力武常次 499
47. 地下における彈性波速度の測定結果（英文）………… 金井清 503
48. 建物振動に伴う土地の震動の測定結果（英文）………… 金井清・長田甲斐男 511

(The titles in occidental languages are given on the back cover.)

本彙報ハ年4回（但シ第1號ヨリ第6號マデハ不定期ニ，第7號ハ3冊トシテ發行セリ），彙報別冊ハ不定期ニ發行ス．

本彙報掲載ノ論文及ビ報告ノ內容ニ關シテハ著者ノミニ其責任アルモノトス．

本彙報ニ關スル照會通信ハ東京大學地震研究所長ヘ宛テラレタシ．

The Bulletin is published quarterly. (Vols. I–VI were published at irregular intervals and Vol. VII consisted of three parts.)

Supplementary Volume is published at irregular interval.

The authors of the papers alone are responsible for the statements and opinions contained in their respective papers.

All communications relating to this Bulletin should be addressed to the Director of the Earthquake Research Institute, Tokyo University.

ERRATUM.

Bulletin of the Earthquake Research Institute, Volume 29, Part 2.

Instead of in the order of p. 375, p. 376, p. 377, please read in the order of p. 376, p. 377, p. 375.

正　誤

地震研究所彙報 第29號 第2冊 に於て

375, 376, 377 の三頁を 376, 377, 375 頁の順序に讀まれたし．

Errata of Bull. Earthq. Res. Inst., 29 (1951), 2,

A Study on the Propagation of Microseismic Waves. Part IV.

By Ryôhei IKEGAMI.

Page 323, Ordinate of Fig. 15: 2, 4, ... 12

Read 200, 400, ... 1200 m/sec.

($\times 10^2$ m/sec.)

40. *Study on Surface Waves III.*
Love-Waves with Double Superficial Layer.

By Yasuo Satô,

Earthquake Research Institute.

(Read Jan. 18, 1949.—Received June 20, 1951.)

1. Introduction.

In the previous paper⁽¹⁾ we have calculated the velocity of Love-waves with a single layer. However, from the observational facts our earth seems to have double superficial layer, and calculations for such cases have already been performed by some authors[2]. But the general theory of the waves in such cases has not been fully discussed, and still there even remain doubts about the condition of existence and on the nature of dispersion, so we have good reason to believe that our new calculation has some value.

2. Characteristic equation.

First we will obtain the characteristic equation.

Density ρ_k, rigidity μ_k, velocity of *S*-waves V_k and the thickness of layers H_k are taken as are illustrated in Fig. 1.

We will further assume the following notations which are not the same with those adopted in the other works of us in accordance with those used by H. Menzel[3].

$$s_k \equiv f\sqrt{\{(V^2/V_k^2)-1\}} \quad \text{when} \quad V>V_k \qquad (k=1,2,3)$$
$$\equiv i\sigma_k \qquad\qquad V<V_k \qquad \ldots\ldots(2.1)$$

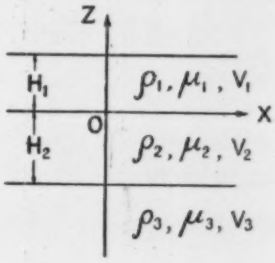

Fig. 1.

in which V is the velocity of Love-waves.

---

[1] Y. Satô, "Study on Surface Waves I." *Bull. Earthq. Res. Inst.*, **29** (1951), 1.

[2] T. Matuzawa, "Propagation of Love-Waves along a Doubly Stratified Layer." *Proc. Phys.-Math. Soc. Jap.* **[iii]** **10** (1928), 25. R. Stoneley and E. Tilotson, *M.N.R.A.S. Geo. Sup.*, **1** (1927), 521. H. Menzel, "Dispersion von seismischen Oberflächenwellen nach Registrierungen in Kopenhagen und Groß-Raum." *Beitr. z. Geophys.*, **54** (1939), 348.

[3] *loc. cit.* 2)

Displacements in three media are assumed to be

$$\begin{cases} V_1=\{A_1\exp(is_1z)+B_1\exp(-is_1z)\}\exp(ifx-ipt) \\ V_2=\{A_2\exp(is_2z)+B_2\exp(-is_2z)\}\exp(ifx-ipt) \\ V_3=\{\qquad\qquad\qquad +B_3\exp(-is_3z)\}\exp(ifx-ipt) \end{cases} \quad \ldots\ldots(2.2)$$

Boundary conditions are

$$\begin{array}{llll} \text{at}\quad z=H_1; & \widehat{xz}_1=0\ , & \widehat{yz}_1=0 & \\ z=0\ ; & \widehat{xz}_1=\widehat{xz}_2\ , & \widehat{yz}_1=\widehat{yz}_2\ , & v_1=v_2 \\ z=-H_2; & \widehat{xz}_2=\widehat{xz}_3\ , & \widehat{yz}_2=\widehat{yz}_3\ ; & v_2=v_3 \end{array} \quad \ldots\ldots(2.3)$$

From (2.3), we have

$$D\equiv\begin{vmatrix} \exp(is_1H_1) & -\exp(-is_1H_1) & 0 & 0 & 0 \\ 1 & 1 & -1 & -1 & 0 \\ \mu_1s_1 & -\mu_1s_1 & -\mu_2s_2 & \mu_2s_2 & 0 \\ 0 & 0 & \exp(is_2H_2) & \exp(is_2H_2) & -\exp(is_3H_2) \\ 0 & 0 & \begin{matrix} i\mu_2s_2 \\ \cdot\exp(is_2H_2)\end{matrix} & \begin{matrix} -i\mu_2s_2 \\ \cdot\exp(is_2H_2)\end{matrix} & \begin{matrix} \mu_3s_3 \\ \cdot\exp(is_3H_2)\end{matrix} \end{vmatrix}=0 \quad .(2.4)$$

which may be reduced to

$$D\equiv D^c+D^s=0$$

$$\begin{cases} D^c=\mu_2s_2\cos s_1H_1\,(+\mu_3's_3\cos s_2H_2+\mu_2s_2\sin s_2H_2) \\ D^s=\mu_1s_1\sin s_1H_1\,(-\mu_3's_3\sin s_2H_2+\mu_2s_2\cos s_2H_2) \end{cases} \quad \ldots\ldots(2.4a)$$

$$\mu_3'\equiv i\mu_3$$

Further, modifying the above expressions, we have

$$\begin{cases} D^c=C_{21}\,(C_{32}+S_{22}) \\ D^s=S_{11}\,(-S_{32}+C_{22}) \end{cases}$$

in which

$$\begin{cases} C_{jk}\equiv\mu_js_j\cos s_kH_k \\ S_{jk}\equiv\mu_js_j\sin s_kH_k \qquad (j,\ k=1,\ 2,\ 3) \end{cases} \quad \ldots\ldots\ldots\ldots\ldots\ldots(2.4b)$$

(when $j=3$, μ_j implies μ_3')

3. Condition of existence.

Now we will discuss the condition of existence[4].

Since we assume double superficial layer and the lower semi-infinite body, we have three kinds of media, which we call *A*, *B*, *C* according to the ascending order of velocity of S-waves in respective media. Let us further show, for example, by the notation $\begin{pmatrix} B \\ A \\ C \end{pmatrix}$ that the intermediate layer is the medium of lowest velocity, the upper is that of middle value, while, the semi-infinite part gives the highest velocity. Of the 27 possible permutations of the three notations A, B and C we exclude trivial (on physically identical) cases and have the following 13 ones; viz.

---

[4] This problem was already discussed by T. Matuzawa. *loc. cit.* 2)

$$[1]\begin{pmatrix} A \\ A \\ A \end{pmatrix},\ [2]\begin{pmatrix} A \\ A \\ B \end{pmatrix},\ [3]\begin{pmatrix} A \\ B \\ A \end{pmatrix},\ [4]\begin{pmatrix} A \\ B \\ B \end{pmatrix},\ [5]\begin{pmatrix} A \\ B \\ C \end{pmatrix},\ [6]\begin{pmatrix} A \\ C \\ B \end{pmatrix}$$

$$[7]\begin{pmatrix} B \\ A \\ A \end{pmatrix},\ [8]\begin{pmatrix} B \\ A \\ B \end{pmatrix},\ [9]\begin{pmatrix} B \\ A \\ C \end{pmatrix},\ [10]\begin{pmatrix} B \\ B \\ A \end{pmatrix},\ [11]\begin{pmatrix} B \\ C \\ A \end{pmatrix} \qquad \dots\dots\dots\dots(3.1)$$

$$[12]\begin{pmatrix} C \\ A \\ B \end{pmatrix},\ [13]\begin{pmatrix} C \\ B \\ A \end{pmatrix}.$$

Since v_3 must vanish at $z=-\infty$, s_3 must have positive imaginary part Remembering that

$$s_3/i=\sigma_3=f\sqrt{\{1-(V^2/V_3^2)\}},$$

the above condition is replaced by

$$V<V_3. \qquad \dots\dots\dots\dots\dots\dots\dots\dots(3.2)$$

If V_3 takes the smallest or one of the smallest value among V_k $(k=1, 2, 3)$, s_1 and s_2 also become imaginary from the relation (3.2). Therefore, putting $s_k=i\sigma_k$ into (2.4a), we have

$$\begin{aligned} iD=&\mu_2\sigma_2\cosh\sigma_2H_2\,(\mu_3\sigma_3\cosh\sigma_2H_2+\mu_2\sigma_2\sinh\sigma_2H_2) \\ &+\mu_1\sigma_1\sinh\sigma_1H_1\,(\mu_3\sigma_3\sinh\sigma_2H_2+\sigma_2\sigma_2\cosh\sigma_2H_2)=0 \qquad \dots\dots(3.3) \end{aligned}$$

Since all the terms involved in this equation are positive, this cannot be satisfied by the real value of V.

Thus of the thirteen cases in (3.1), [1], [3], [7], [10], [11] and [13] must be omitted. The remaining cases are

$$[2]\begin{pmatrix} A \\ A \\ B \end{pmatrix},\ [4]\begin{pmatrix} A \\ B \\ B \end{pmatrix},\ [5]\begin{pmatrix} A \\ B \\ C \end{pmatrix},\ [6]\begin{pmatrix} A \\ C \\ B \end{pmatrix},\ [8]\begin{pmatrix} B \\ A \\ B \end{pmatrix},\ [6]\begin{pmatrix} B \\ A \\ C \end{pmatrix},\ [12]\begin{pmatrix} C \\ A \\ B \end{pmatrix}\dots(3.4)$$

Of these seven cases, the existence of the solution of first two cases ([2] and [4]) is self-evident, and the third one ([5]) has been already treated by T.

Matuzawa and R. Stoneley⁵⁾. So we will here discuss the four remaining cases separately.

3.1 Examples.

In order to prove the existence of Love-waves it is sufficient for us to show a single example of solutions satisfying the conditions (2.3) for a given succession of the media. And indeed, we can easily give an example in each case.

I. Example of case [8].... $\begin{pmatrix} B \\ A \\ B \end{pmatrix}$.

We assume:

$$\left.\begin{aligned} & H_1=H_2\equiv H_0 \\ & \rho_1=\rho_2=\rho_3\equiv\rho \\ & \mu_1=10\mu_2=\mu_3\equiv\mu \end{aligned}\right\} \qquad\qquad (3.5)$$

then we can get the solution of (2.4), which we will give in Fig. 2 and Tab. I. For comparison we also give the dispersion curve of simple Love-waves. (Thickness of the layer; 2H₀. Density; ρ. Rigidity of upper layer is one tenth of that of lowest medium.) A remarkable point which we notice in the figure is that the phase velocity of simple Love-waves is larger than that of the above case when the wave-length is fairly large.

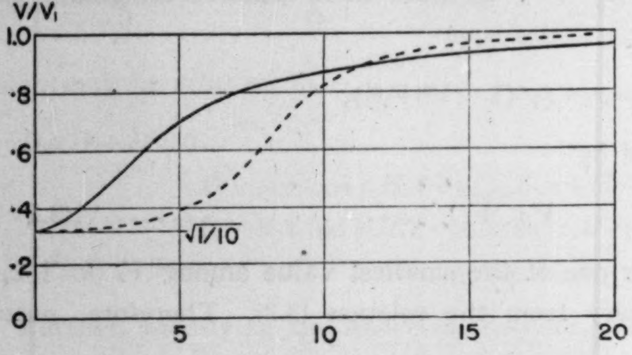

Fig. 2. Dispersion curve of example I (Case [8]).
Abscissa: Wave length (unit: H_0)
Broken line shows the dispersion curve of simple Love-waves. (Unit of wave length is same with above.)

Table I.

$(V/V_1)^2$	fH_0
0	0
0.99	0.10965
0.96	0.21405
0.9039	0.3322
0.84	0.4525
0.75	0.6471
0.64	0.9078
0.51	1.2169
0.4375	1.4149
0.36	1.6844
0.2775	2.1182
0.19	3.089
0.1536	4.08
0.10	∞

II. Example of case [6].... $\begin{pmatrix} A \\ C \\ B \end{pmatrix}$

We assume:

---

5) *loc. cit.,* 2)

$$\begin{aligned} &H_1=H_2\equiv H_0 \\ &\rho_1=\rho_2=\rho_3\equiv\rho \qquad \ldots\ldots\ldots\ldots\ldots\ldots\ldots\ldots(3.6) \\ &10\mu_1=\mu_2=3\mu_3\equiv\mu \end{aligned}$$

The results of calculations are given in Fig. 3 and Tab. II. In this case the upper limit of wave-length of period exists, and we will call this value as the "cut-off period", which gives a phase velocity equal to that of S-wave in the lowest medium[6]. The proof is as follows.

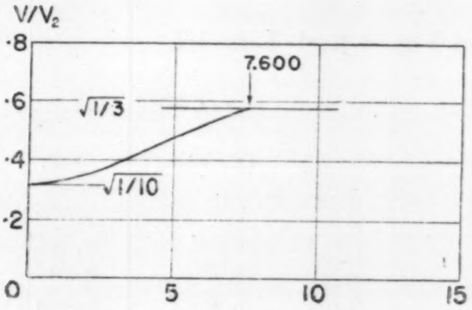

Fig. 3. Dispersion curve of example II (Case [6])

Table II.

$(V/V_2)^2$	fH_0
1/3	0.8268
0.325	0.8645
0.319375	0.8840
0.3111	0.9120
0.2775	1.0295
0.2256	1.272
0.19	1.536
0.1536	2.034
0.1351	2.5429
0.125775	2.986
0.1	∞

When $V^2=V_3^2(1-\varepsilon^2), \qquad (\varepsilon\ll 1)$

$$\begin{aligned} &s_1=f\sqrt{(r_1^2-1)}+0(\varepsilon^2), \quad s_2=f\sqrt{(r_2^2-1)}+0(\varepsilon^2), \quad (r_j=V_3/V_j) \quad \ldots.(3.7) \\ &s_3=i\varepsilon f \end{aligned}$$

Therefore, on neglecting small quantities, velocity equation takes the following form,

$$\begin{aligned} D=&\mu_2\sqrt{(r_2^2-1)}\cdot f^2\cos\{\sqrt{(r_1^2-1)}\cdot\xi\}\cdot\mu_2\sqrt{(r_2^2-1)}\cdot\sin\{\sqrt{(r_2^2-1)}\cdot\xi\} \\ &+\mu_1\sqrt{(r_1^2-1)}\cdot f^2\sin\{\sqrt{(r_1^2-1)}\cdot\xi\}\cdot\mu_2\sqrt{(r_2^2-1)}\cdot\cos\{\sqrt{(r_2^2-1)}\cdot\xi\} \quad ..(3.8) \\ &=0 \qquad\qquad (\xi\equiv fH_0) \end{aligned}$$

Since r_2 is smaller than unity in this case, the above expression is reduced to

$$\begin{aligned} &-\mu_2\sqrt{(1-r_2^2)}\cdot\tanh\{\sqrt{(1-r_2^2)}\cdot\xi\} \\ &+\mu_1\sqrt{(r_1^2-1)}\cdot\tan\{\sqrt{(r_1^2-1)}\cdot\xi\}=0 \qquad \ldots\ldots\ldots\ldots.(3.9) \end{aligned}$$

which is satisfied by some finite value of ξ. ($\xi=0$ is an isolated point.)

---

6) If we judge from the Fig. 3a. of the paper of T. Matuzawa, $V=b_3$ (b_3 corresponds to our V_3) seems to be an asymptote, which however, does not apply to this case. (cf. Fig. 3)

III. Example of case [9]....$\begin{pmatrix} B \\ A \\ C \end{pmatrix}$.

This case is fully discussed by T. Matuzawa, so we will only give the example of calculations in this paper.

The assumption of this case is

$$\begin{aligned} &3\mu_1=10\mu_2=\mu_3\equiv\mu \\ &H_1=H_2\equiv H_0 \\ &\rho_1=\rho_2=\rho_3\equiv\rho \qquad \dots\dots\dots\dots\dots\dots\dots\dots (3.10) \end{aligned}$$

Numerical results will be found in Fig. 4 and Tab. III.

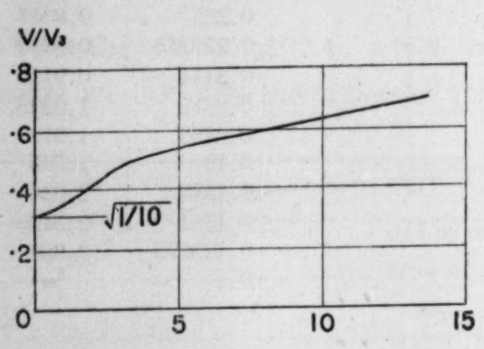

Fig. 4. Dispersion curve of example III (Case [9]).

Table III

$(V/V_3)^2$	fH_0
1	0
0.941	0.1443
0.725	0.2802
0.584	0.375
0.500	0.459
0.389	0.668
0.325	0.962
0.244	1.881
0.200	2.556
0.149	3.984
0.125	6.556
0.1	∞

IV. Example of case [12]....$\begin{pmatrix} C \\ A \\ B \end{pmatrix}$.

Existence of solution can be easily supposed by the former three cases. We will only give an example, of which no explanation will be necessary.

The assumption of this case is:

$$\begin{aligned} &H_1=H_2\equiv H_0 \\ &\rho_1=\rho_2=\rho_3\equiv\rho \qquad \dots\dots\dots\dots\dots\dots\dots\dots (3.11) \\ &\mu_1=10\mu_2=3\mu_3\equiv\mu \end{aligned}$$

The results of calculations are given in Fig. 5 and Tab. IV. In this case, too, there exists the cut-off period. For, putting $\sqrt{(r_1^2-1)}=i\sqrt{(1-r_1^2)}$ into (3.8), we have

$$\begin{aligned} &\mu_2\sqrt{(r_2^2-1)}\cdot\tan\{\sqrt{(r_2^2-1)}\cdot\xi\} \\ &-\mu_1\sqrt{(1-r_1^2)}\cdot\tanh\{\sqrt{(1-r_1^2)}\cdot\xi\}=0\,, \qquad \dots\dots\dots\dots (3.12) \end{aligned}$$

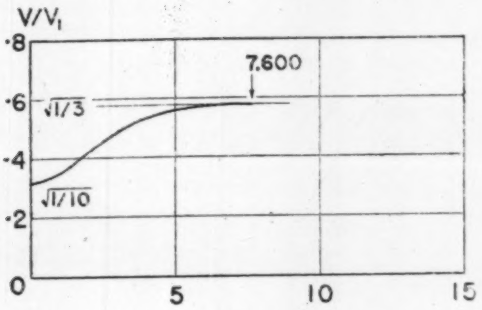

Fig. 5. Dispersion curve of example IV (Case [12]).

Table IV.

$(V/V_1)^2$	fH_0
0/3	0.8268
0.325	1.1120
0.319375	1.1940
0.311	102997
0.2775	1.6459
0.2256	2.209
0.19	2.267
0.1536	3.785
0.1351	4.808
0.125775	5.706
0.1	∞

from which we can easily obtain the above conclusion[7].

Summing up the discussion of this article we may assert that the condition of existence of Love-waves in double superficial layer is:

"The velocity of lowest medium is not the smallest of three values corresponding to three media."

4. Discussion of the paper of H. Menzel.[8]

H. Menzel discusses in his paper published some ten years ago that the group velocity of Love-waves propagated on double superficial layer has a discontinuity at the point where the phase velocity of Love-waves takes equal value with that of S-waves in the intermediate layer. He asserts that the above inference is to be confirmed theoretically as well as by observation[9]. Our doubt on this statement resulted in the following discussion.

His theoretical evidence resides in his calculation that the denominator of the expression for group velocity vanishes when the phase velocity takes the value $\sqrt{(\mu_2/\rho_2)}$. However, he does not examine whether the numerator does not vanish at the same time, so that his evidence is not sufficient.

In this article we will show that the said numerator vanishes at the same time with the denominator and the limiting value of ratio, after all, becomes finite.

---

[7] See also the foot-note of p. 439.

[8] *loc. cit.*, 2)

[9] It is quite easy to percieve that apparent discontinuity in the velocity may result if the identification of a wave at two stations is mistaken by one wave length.

Denoting the group velocity as U, we have

$$U=\frac{dp}{df}$$

$$=V+\frac{p}{V}\frac{dV}{dp}U$$

$$\therefore\quad \frac{1}{U}=\frac{1}{V}\left(1-\frac{p}{V}\frac{dV}{dp}\right) \quad\ldots\ldots\ldots\ldots\ldots\ldots\ldots(4.1)$$

Putting

$$e\equiv 1/V^2 \quad\ldots\ldots\ldots\ldots\ldots\ldots\ldots\ldots\ldots(4\cdot 2)$$

in (4.1), we have

$$\frac{1}{U}=\frac{1}{V}\left(1+\frac{p}{2/V^2}\frac{de}{dp}\right),$$

while e is an implicit function of p defined by (2.4), therefore

$$\frac{1}{U}=\frac{1}{V}\left(1+\frac{pD_p}{-2eD_e}\right) \quad\ldots\ldots\ldots\ldots\ldots\ldots\ldots(4.3)$$

where the suffixes p and e mean partial differentiation.

We employ a new notation

$$e_k=1/V_k^2 \quad\ldots\ldots\ldots\ldots\ldots\ldots\ldots\ldots\ldots(4.4)$$

then

$$\left\{\begin{aligned} &s_k=p\sqrt{(e_k-e)}\\ &\frac{\partial}{\partial p}C_{jk}=\frac{1}{p}(C_{jk}-s_kH_kS_{jk})\\ &\frac{\partial}{\partial p}S_{jk}=\frac{1}{p}(S_{jk}+s_kH_kC_{jk})\end{aligned}\right. \quad\ldots\ldots\ldots\ldots\ldots\ldots(4.5)$$

After a little calculation

$$\begin{aligned}(D^C)_p&=(C_{21})_p(C_{32}+S_{22})+C_{21}\{(C_{32})_p+(S_{22})_p\}\\ &=\frac{1}{p}\{(2C_{21}-s_1H_1S_{21}-s_2H_2S_{11})C_{32}+(-S_{32}+C_{22})(2S_{11}+s_1H_1C_{11})\}\end{aligned}$$

$$\ldots.(4.6a)$$

Similarly

$$(D^S)_p=\frac{1}{p}\{(2C_{21}-s_1H_1S_{21}-s_2H_2S_{11})S_{22}+(-S_{22}+C_{22})s_2H_2C_{21}\} \ldots\ldots(4.6b)$$

From (4.6a) and (4.6b) we can get pD_p.

Next we will consider eD_e.

Introducing a new notation

$$e/(e_k-e)\equiv\eta_k \quad\ldots\ldots\ldots\ldots\ldots\ldots\ldots\ldots(4.7)$$

We have

$$\begin{aligned}\frac{\partial}{\partial e}C_{jk}&=-\frac{1}{2e}\{\eta_jC_{jk}-\eta_ks_kH_kS_{jk}\}\\ \frac{\partial}{\partial e}S_{jk}&=-\frac{1}{2e}\{\eta_jS_{jk}+\eta_ks_kH_kC_{jk}\}\end{aligned}\qquad\cdots\cdots(4.8)$$

Therefore

$$\begin{aligned}(D^C)_e&=-\frac{1}{2e}[C_{21}\{(\eta_2+\eta_3)C_{32}+2\eta_2S_{22}\}\\ &\qquad-\{\eta_1s_1H_1S_{21}(C_{32}+S_{22})+\eta_2s_2H_2C_{21}(S_{32}-C_{22})\}]\\ (D^S)_e&=-\frac{1}{2e}[S_{11}\{-(\eta_1+\eta_3)S_{32}+(\eta_1+\eta_2)C_{22}\}\\ &\qquad+\{\eta_1s_1H_1C_{11}(-S_{32}+C_{22})-\eta_2s_2H_2S_{11}(C_{32}+S_{22})\}]\end{aligned}\qquad\cdots\cdots(4.9)$$

Introducing (2.4b)

$$\begin{aligned}-2eD_e=&\,\eta_2\{(-s_2H_2C_{32}+S_{32})S_{11}+C_{21}S_{22}+s_2H_2(C_{21}(S_{32}-C_{22})-S_{11}S_{22})\}\\ &+\{\eta_3C_{21}C_{32}+(-(\eta_1+\eta_3)S_{32}+\eta_1S_{22})S_{11}+\eta_1s_1H_1(-S_{21}C_{32}+(-S_{32}+C_{22})C_{11})\}\end{aligned}\qquad\cdots\cdots(4.10)$$

Near the point $V=V_2$, neglecting the terms of $0\{s_2^3\}$, we have

$$\left\{\begin{aligned}p(D^C)_p&=(2\mu_2s_2\cdot\cos s_1H_1-s_1H_1\cdot\mu_2s_2\cdot\sin s_1H_1-s_2H_2\cdot S_{11})\mu_3's_3\\ &\qquad+(-\mu_3's_3\cdot s_2H_2+\mu_2s_2)\cdot(2S_{11}+s_1H_1\cdot C_{11})+0\{s_2^3\}\\ p(D^S)_p&=0\{s_2^3\}\end{aligned}\right.\qquad\cdots\cdots(4.11)$$

or, simplifying further,

$$\begin{aligned}p(D_p)=\mu_2s_2C_{11}\Big\{&2\frac{\mu_3'}{\mu_1}\cdot\frac{s_3}{s_1}+\Big(-\frac{\mu_3'}{\mu_1}\cdot s_3H_1-3\frac{\mu_3'}{\mu_2}s_3H_2+2\Big)\tan s_1H_1\\ &+\Big(-\frac{\mu_3'}{\mu_2}s_3H_2+1\Big)s_1H_1\Big\}\end{aligned}\qquad\cdots\cdots(4.12)$$

and similarly

$$\begin{aligned}-2e(D_e)=\mu_2s_2C_{11}\Big\{&f_2^2H_2^2\Big[\Big(\frac{1}{3}\frac{\mu_3'}{\mu_2}s_3H_2-1\Big)\tan s_1H_1-\frac{\mu_3'}{\mu_1}\frac{s_3}{s_1}+2\frac{\mu_2}{\mu_1}\frac{1}{s_1H_2}\Big]\\ &+\Big[-\eta_1s_1H_1\cdot\frac{\mu_3'}{\mu_1}\frac{s_3}{s_1}\cdot\tan s_1H_1+\eta_3\frac{\mu_3'}{\mu_1}\frac{s_3}{s_1}\\ &+\eta_1(\tan s_1H_1+s_1H_1)\Big(-\frac{\mu_3'}{\mu_1}s_3H_2+1\Big)\\ &-\eta_3\frac{\mu_3'}{\mu_2}s_3H_2\tan s_1H_1\Big]\Big\}\end{aligned}\qquad\cdots\cdots(4.13)$$

in which $f_2=[f]_{V=V_2}$

Using the above two expressions, we can obtain the value of U.

$$\left[\frac{1}{U}\right]_{V=V_2}=\frac{1}{V_2}\{1+(pD_p)/(-2eD_e)\}_{V=V_2} \qquad \text{...........}(4.14)$$

Employing the numerical constants of T. Matuzawa[10]

k	1	2	3	
ρ_k	2.7	3.0	3.4	gr. cm^{-3}
V_k	3.3	4.0	4.5	km. sec^{-1}
μ_k	29.4	48.0	68.9	km. gr. sec.
H_k	20	30		km

we have

$$f_2H_2=1.47$$

$$s_1H_1=0.67\,, \qquad s_3H_2=i0.46$$

$$(pD_p)/(-2eD_e)=0.156\,,$$

and if we adopt the values due to R. Stoneley[11], $H_1=H_2\equiv H_0$ and

k	1	2	3	
ρ_k	2.7	3.0	3.4	gr. cm^{-3}
V_k	3.15	3.90	4.40	km. sec^{-1}

we have

$$f_2H_2=1.02$$

$$s_1H_0=0.75\,, \qquad s_3H_0=i0.48$$

$$(pD_e)/(-2eD_e)=0.220\,.$$

If we introduce these numerical values, it will be soon noticed that the value of U in every case, takes finite value ($U/V_2=0.865$ (Matuzawa), 0.820 (Stoneley)). Thus we may conclude that group velocity does never become infinite at the point.

40. 表面波の研究 III

二つの表面層をもつラブ波

地震研究所 佐藤泰夫

表面に二層ある場合のラブ波の存在條件は，三つの媒質内のS波速度を比べた時，最下部のものが，最小の値をとらないことである。但し，二層のいづれか一方が，下部よりも大きな値を持つ時には，ラブ波の周期には上限が存在し，これより長周期の波は存在しえない。

H. Menzel は，かつてラブ波の位相速度が中間層の速度と等しくなる所では，群速度が無限に大きくなると主張したが，これはあやまりである。

---

10) *loc. cit.*, 2)

11) *loc. cit.*, 2)

41. *Distribution of Surface Stress Generating No Rayleigh-Waves.*

By Yasuo Satô,

Earthquake Research Institute.

(Read May. 15, 1951.—Received June 20, 1951.)

1. Introduction.

In a previous paper entitled "Seismic Focus without Rayleigh-waves,"[1] we have investigated the nature of origin situated in the semi-infinite elastic body. We have found examples of focus which radiate no Rayleigh-waves in spite of the generation of bodily waves. We began this study mainly from theoretical interest, however in this paper, we will treat a similar problem such as the distribution of surface stress which generates no Rayleigh-waves rather from the practical point of view.

Recently Don Leet[2] published a paper concerning "delay blasting" which seems to us an effort to find a technique of blasting which generates no surface waves. This is of practical importance in seismic prospecting, because the surface waves often obliterate later useful phases of P group.

In the following, we will show the way of applying surface stress without generating Rayleigh-waves.

2. Fundamental solution.

First we will start from the results obtained by Lamb[3] in his famous work "On the Propagation of Tremors over the Surface of Elastic Solid".

In three-dimensional semi-infinite elastic solid, displacement components u, v, and w which have axial symmetry around the vertical axis are expressed by using the potentials ϕ and χ as follows

$$u=\frac{\partial\phi}{\partial x}+u', \qquad v=\frac{\partial\phi}{\partial y}+v', \qquad w=\frac{\partial\phi}{\partial z}+w' \quad \ldots\ldots\ldots(2.1)^{4)}$$

---

[1] Y. Satô, *Bull. Earthq. Res. Inst.*, **29** (1951), 13.

[2] Don Leet, "Vibration from Delay Blasting." *Bull. Seism. Soc. Amer.*, **39** (1949), 9.

[3] H. Lamb, *Phil. Trans.*, **A 203** (1904), 1–42.

[4] *ibid.*

in which

$$\begin{cases} (\nabla^2+h^2)\phi=0\,, \qquad \nabla^2=\dfrac{\partial^2}{\partial x^2}+\dfrac{\partial^2}{\partial y^2}+\dfrac{\partial^2}{\partial z^2} \\ h^2=p^2/V_p^2 \\ V_p{}^2=(\lambda+2\mu)/\rho \end{cases} \qquad \ldots\ldots\ldots\ldots(2.2)$$

and p means circular frequency, while λ, μ and ρ are Lamé's constants and density respectively.

On the other hand u', v' and w' are

$$u'=\frac{\partial^2\chi}{\partial x\partial z}\,, \qquad v'=\frac{\partial^2\chi}{\partial y\partial z}\,, \qquad w'=\frac{\partial^2\chi}{\partial z^2}+k^2\chi \quad \ldots\ldots\ldots(2.3)$$

in which

$$\begin{cases} (\nabla^2+k^2)\chi=0 \\ k^2=p^2/V_s^2\,, \qquad V_s^2=\mu/\rho \end{cases} \qquad \ldots\ldots\ldots\ldots\ldots\ldots\ldots(2.4)$$

From the assumption of axial symmetry

$$\nabla^2=\frac{\partial^2}{\partial\varpi^2}+\frac{1}{\varpi}\frac{\partial}{\partial\varpi}+\frac{\partial^2}{\partial z^2}$$

where ϖ is the distance from z-axis.

(2.1) and (2.3) are identical with the following expression.

$$q=\frac{\partial\phi}{\partial\varpi}+\frac{\partial^2\chi}{\partial\varpi\partial z}\,, \qquad w=\frac{\partial\phi}{\partial z}+\frac{\partial^2\chi}{\partial z^2}+k^2\chi \quad \ldots\ldots\ldots\ldots(2.5)$$

here q implies the displacement component in ϖ-direction.

Adopting the fundamental solution of the type

$$\phi=A\exp(-\alpha z)\,J_0(\xi\varpi), \qquad \chi=B\exp(-\beta z)\,J_0(\xi\varpi) \quad \ldots\ldots(2.6)$$

where

$$\alpha=\sqrt{(\xi^2-h^2)}, \qquad \beta=\sqrt{(\xi^2-k^2)}$$

$$\begin{cases} q=\{-\xi A\exp(-\alpha z)+\xi\beta B\exp(-\beta z)\}\,J_1(\xi\varpi) \\ w=\{-\alpha A\exp(-\alpha z)+\xi^2 B\exp(-\beta z)\}\,J_0(\xi\varpi) \end{cases} \qquad \ldots\ldots\ldots(2.7)$$

and the surface stress $[\widehat{\varpi z}]_0$ and $[\widehat{zz}]_0$ are, at $z=0$

$$\begin{cases} [\widehat{\varpi z}]_0=\mu\left[\dfrac{\partial q}{\partial z}+\dfrac{\partial w}{\partial\varpi}\right]_0=\mu\{2\xi\alpha A-(2\xi^2-k^2)\xi B\}\,J_1(\xi\varpi) \\ [\widehat{zz}]_0=\mu\left[\lambda\Delta+2\mu\dfrac{\partial w}{\partial z}\right]_0=\mu\{(2\xi^2-k^2\}A-2\xi^2\beta B\}\,J_0(\xi\varpi) \end{cases} \qquad \ldots\ldots\ldots(2.8)$$

3. Surface stress generating no Rayleigh-waves.

Solutions shown in the equations (2.6), (2.7) and (2.8) satisfy fundamental equation of motion regardless of ξ. Therefore we may take any functional form for A and B.

If the surface stress such as

$$\widehat{\tilde{\omega}z}=\mu X(\xi)\,J_1(\xi\tilde{\omega})\exp(ipt),\qquad \widehat{zz}=\mu Z(\xi)\,J_0(\xi\tilde{\omega})\exp(ipt)\quad\ldots.(3.1)$$

are applied on $z=0$, we must take A and B, so that they may satisfy

$$\left\{\begin{aligned}&2\xi\alpha A-(2\xi^2-k^2)\xi B=X(\xi)\\&(2\xi^2-k^2)A-2\xi^2\beta B=Z(\xi)\end{aligned}\right.\quad\ldots\ldots\ldots\ldots\ldots\ldots(3.2)$$

From this

$$\left\{\begin{aligned}&A=\{-2\xi\beta X(\xi)+(2\xi^2-k^2)Z(\xi)\}\,/\,F(\xi)\\&B=\{-(2\xi^2-k^2)X(\xi)+2\xi\alpha Z(\xi)\}\,/\,\xi F(\xi)\end{aligned}\right.\quad\ldots\ldots\ldots\ldots(3.3)$$

$$F(\xi)=(2\xi^2-k^2)^2-4\xi^2\alpha\beta$$

Surface displacement q_0 and w_0 are, putting $z=0$ in (2.7), and introducing the above relations

$$\left\{\begin{aligned}&q_0=[k^2\beta X(\xi)+\xi\{2\alpha\beta-(2\xi^2-k^2\}Z(\xi)]\,J_1(\xi\tilde{\omega})\,/\,F(\xi)\\&w_0=[\xi\{2\alpha\beta-(2\xi^2-k^2)\}X(\xi)+k^2\alpha Z(\xi)]\,J_0(\xi\tilde{\omega})\,/\,F(\xi)\end{aligned}\right.\quad\ldots\ldots(3.4)$$

Even if we integrate the above expressions, with respect to ξ new functions $\int q_0 d\xi$ and $\int w_0 d\xi$ also represent displacement components upon the free surface of the same medium. Denoting them by Q and W,

$$\left\{\begin{aligned}&Q=\int_0^\infty[k^2\beta X+\xi\{2\alpha\beta-(2\xi^2-k^2)Z]\,J_1(\xi\tilde{\omega})\,/\,F(\xi)\cdot d\xi\\&W=\int_0^\infty[\xi\{2\alpha\beta-(2\xi^2-k^2)\}X+k^2\alpha Z]\,J_0(\xi\tilde{\omega})\,/\,F(\xi)\cdot d\xi\end{aligned}\right.\quad\ldots\ldots.(3.5)$$

If $$X(-\xi)=X(\xi)\text{ and }Z(-\xi)=-Z(\xi)\quad\ldots\ldots\ldots\ldots.(3.6)$$

$$\begin{aligned}Q&=\int_0^\infty[\qquad\qquad]\,\tfrac{1}{2}\,\{H_1^{(1)}(\xi\tilde{\omega})+H_1^{(2)}(\xi\tilde{\omega})\}\,/\,F(\xi)\cdot d\xi\\&=\tfrac{1}{2}\int_{-\infty}^\infty[\qquad\qquad]\,H_1^{(1)}(\xi\tilde{\omega})\,/\,F(\xi)\cdot d\xi\quad\ldots\ldots\ldots\ldots\ldots\ldots(3.8)\end{aligned}$$

Similarly

$$W=\tfrac{1}{2}\int_{-\infty}^\infty[\qquad\qquad]\,H_0^{(1)}(\xi\tilde{\omega})\,/\,F(\xi)\cdot d\xi\quad\ldots\ldots\ldots\ldots\ldots\ldots(3.8)$$

Displacement due to Rayleigh phase is

$$\left\{\begin{aligned}&Q[R]=i\pi[k^2\beta X(\xi)+\xi\{2\alpha\beta-(2\xi^2-k^2)\}Z(\xi)]\cdot H_1^{(1)}(\xi\tilde{\omega})\,/\,F'(\xi)_{\xi=-K}\\&W[R]=i\pi[\xi\{2\alpha\beta-(2\xi^2-k^2)\}X(\xi)+k^2\alpha Z(\xi)]\cdot H_0^{(1)}(\xi\tilde{\omega})\,/\,F'(\xi)_{\xi=-K}\end{aligned}\right.\quad..(3.9)$$

in which

$$F'(\xi)=\frac{d}{d\xi}F(\xi) \text{ and } F(K)=0$$

If the two factors in [ ] vanish; i.e. if

$$\begin{cases}[k^2\beta X(\xi)+\xi\{2\alpha\beta-(2\xi^2-k^2)\}Z(\xi)]_{\xi=-K}=0\\ [\xi\{2\alpha\beta-(2\xi^2-k^2)\}X(\xi)+k^2\alpha Z(\xi)]_{\xi=-K}=0\end{cases} \quad \ldots\ldots\ldots(3.10)$$

hold, $Q[R]$ and $W[R]$ both vanish at any point of epicentral distance. Although (3.9) are simultaneous equations, the determinant of coefficients fortunately vanishes: i.e.,

$$\begin{vmatrix} k^2\beta & \xi\{2\alpha\beta-(2\xi^2-k^2)\} \\ \xi\{2\alpha\beta-(2\xi^2-k^2)\} & k^2\alpha \end{vmatrix}_{\xi=-K}=0$$

Therefore, the ratio of $X(-K)$ and $Z(-K)$ is uniquely determined.

$$X(-K)/Z(-K)=-X(K)/Z(K)=[-\xi\{2\alpha\beta-(2\xi^2-k^2)\}/k^2\beta]_{\xi=-K} \quad \ldots(3.12)$$

which is a constant depending neither on ξ nor p. Since it is the function of Poisson's ratio, we will denote it as $-C(\sigma)$. Then (3.12) becomes as

$$X(K)/Z(K)=C(\sigma) \quad \ldots\ldots\ldots\ldots\ldots\ldots\ldots(3.13)$$

4. Numerical calculations.

4.1 $C(\sigma)$.

When $\lambda:\mu=1$, or $\sigma=1/4$; $C(1/4)=1.4679$
$\lambda:\mu=2$, or $\sigma=1/3$; $C(1/3)=1.5652$ …………(4.1)
$\lambda:\mu=\infty$, or $\sigma=1/2$; $C(1/2)=1.8413$

4.2 Surface stress.

Assume the distribution of surface stress as

$$[\widehat{\tilde{\omega}z}]_{z=0}=\Psi(\tilde{\omega}), \qquad [\widehat{zz}]_{z=0}=\Phi(\tilde{\omega}) \quad \ldots\ldots\ldots\ldots\ldots(4.2)$$

then

$\xi\Psi^*(\xi)\equiv\xi\int_0^\infty \Psi(\tilde{\omega})\,J_1(\xi\tilde{\omega})\tilde{\omega}d\tilde{\omega}$ is an even function of ξ

and $\xi\Phi^*(\xi)\equiv\xi\int_0^\infty \Phi(\tilde{\omega})\,J_0(\xi\tilde{\omega})\tilde{\omega}d\tilde{\omega}$,, odd ,, .

Therefore we may adopt the above two functions as our $X(\xi)$ and $Z(\xi)$. (cf. (3.6))

If we choose the magnitude of both functions appropriately so that $X(K)$ and $Z(K)$ may satisfy the condition (3.13), then we shall have no Rayleigh phase from such an origin.

5. Examples.

5.1 Simple harmonic origin.

We will show an example of simple harmonic origin in the following calculations.

First we assume the functional form of $\Psi(\tilde{\omega})$ and $\Phi(\tilde{\omega})$ as follows (cf. Fig. 1);

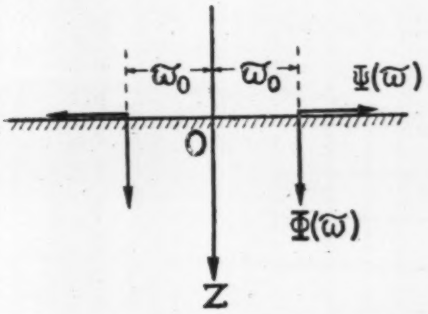

Fig. 1.

$$\Psi(\tilde{\omega})=\begin{cases}-\dfrac{\Psi_0}{\varepsilon}\ , \\ 0\ ,\end{cases}\qquad \Phi(\tilde{\omega})=\begin{cases}-\dfrac{\Phi_0}{\varepsilon} & \ldots.\tilde{\omega}_0<\tilde{\omega}<\tilde{\omega}_0+\varepsilon \\ 0 & \ldots.\tilde{\omega}<\tilde{\omega}_0 \text{ or } \tilde{\omega}_0+\varepsilon<\tilde{\omega}\end{cases}\qquad \ldots(5.1)$$

in which ε is very small.

Then $X(\xi)$ and $Z(\xi)$ are

$$\begin{cases}X(\xi)\equiv\xi\displaystyle\int_0^\infty\Psi(\tilde{\omega})\,J_1(\xi\tilde{\omega})\tilde{\omega}d\tilde{\omega} \\ \qquad\fallingdotseq-\xi\Psi_0J_1(\xi\tilde{\omega}_0)\tilde{\omega}_0 \\ Z(\xi)=\xi\displaystyle\int_0^\infty\Phi(\tilde{\omega})\,J_0(\xi\tilde{\omega})d\tilde{\omega} \\ \qquad\fallingdotseq-\xi\Phi_0J_0(\xi\tilde{\omega}_0)\tilde{\omega}_0\end{cases}\qquad\ldots\ldots\ldots\ldots\ldots\ldots(5.2)$$

Therefore the condition (3.13) becomes

$$[-K\Psi_0J_1(K\tilde{\omega}_0)\tilde{\omega}_0\,/\,-K\Phi_0J_0(K\tilde{\omega}_0)\tilde{\omega}_0]=C(\sigma)$$

or

$$\frac{J_1(K\tilde{\omega}_0)}{J_0(K\tilde{\omega}_0)}=C(\sigma)\frac{\Phi_0}{\Psi_0}\qquad\ldots\ldots\ldots\ldots\ldots\ldots\ldots(5.3)$$

This equation has an infinite number of roots, of which we will show the smallest two values of $K\tilde{\omega}_0$ as the functions of Φ_0/Ψ_0 in Fig. 2 and Tab. I.

$$\left(K\tilde{\omega}_0=\frac{2\pi}{T}\frac{\tilde{\omega}_0}{V\,(\text{Rayleigh})}=2\pi\frac{\tilde{\omega}_0}{\lambda\,(\text{Rayleigh})}\right)$$

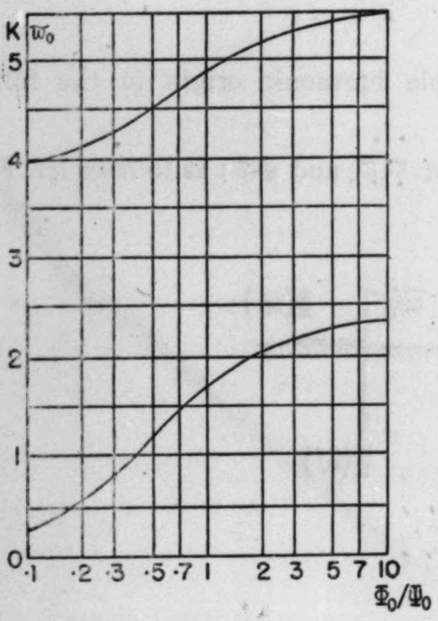

Fig. 2.

Table I.

Φ_0/Ψ_0	$K\tilde{\omega}_0$	
0.10	0.2905	3.9802
0.15	0.4302	4.0545
0.2	0.5640	4.1277
0.3	0.8070	4.2679
0.5	1.1908	4.5092
0.7	1.4552	4.6952
1.0	1.7072	4.8886
1.5	1.9315	5.0765
2	2.0499	5.1814
3	2.1698	5.2920
5	2.2650	5.3727
7	2.3053	5.4222
10	2.3356	5.4546

5.2 Aperiodic type of origin.

Usually, in prospecting or explosion a simple harmonic origin is not employed, and that of the aperiodic type is commonly met with. Therefore, in this article, we will discuss such problems.

The condition (3.13) involves the frequency p, so that even if this relation holds for some value of p, it does not hold for the other values. Thus we are not allowed simply to integrate the solution of (3.9) and get a seismic origin without Rayleigh-waves.

However, there is a way to get rid of this inconvenience. If we assume the two functions $X(\xi)$ and $Z(\xi)$ to be identical (excluding the constant factor) and make the ratio $X(\xi)/Z(\xi)$ equal to $C(\sigma)$, then the condition (3.13) holds regardless of p. Of course we cannot choose such functions strictly satisfying the above relation, for $X(\xi)$ is an even function of ξ and $Z(\xi)$ is an odd function. So we choose two functions, of which one is even and the other is odd, nearly equal on the positive half of real axis. Then the condition (3.13) can be approximately satisfied throughout the range of p, and we can make the Rayleigh-waves extremely small compared with the ordinary seismic origins.

Pairs of two functions having the said property are not few, but we will here show an example most simple and common.

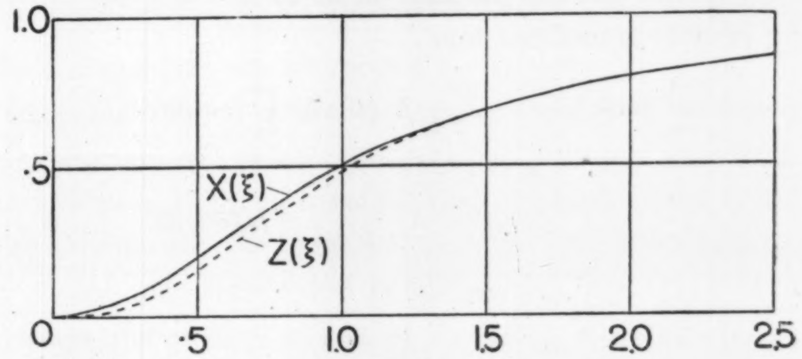

Fig. 3.

We take

$$X(\xi)=\frac{\xi^2}{\xi^2+1}$$

and

$$Z(\xi)=\frac{\xi^2}{\xi^2+1}\cdot\tanh 2\xi \qquad \text{.....................(5.4)}$$

then the stress distribution at the surface is

$$\begin{cases} [\widehat{\varpi z}]_{z=0}=\Psi(\varpi)=\displaystyle\int_0^\infty X(\xi)\,J_1(\xi\varpi)d\xi \\ [\widehat{zz}]_{z=0}=\Phi(\varpi)=\displaystyle\int_0^\infty Z(\xi)\,J_0(\xi\varpi)d\xi \end{cases} \qquad \text{..............(5.5)}$$

Introducing (5.4), we have[5]

$$\begin{cases} \Psi(\varpi)=\displaystyle\int_0^\infty \frac{\xi^2}{\xi^2+1}\,J_1(\xi\varpi)d\xi=K_1(\varpi) \\ \Phi(\varpi)=\displaystyle\int_0^\infty \frac{\xi^2}{\xi^2+1}\cdot\tanh 2\xi\cdot J_0(\xi\varpi)d\xi \\ \qquad =\displaystyle\int_0^\infty J_0(\xi\varpi)d\xi-\int_0^\infty\frac{1}{\xi^2+1}J_0(\xi\varpi)\,d\xi+\int_0^\infty(\tanh 2\xi-1)\frac{\xi^2}{\xi^2+1}\,J_0(\xi\varpi)d\xi \\ \qquad =\dfrac{1}{\varpi}-\dfrac{\pi}{2}\{I_0(\varpi)-\boldsymbol{L}_0(\varpi)\}+\displaystyle\int_0^\infty(\tanh 2\xi-1)\frac{\xi^2}{\xi^2+1}J_0(\xi\varpi)d\xi\,. \end{cases}$$

........(5.6)

The evaluation of the above expressions are performed in the following way.

Table of $e^x K_1(x)$ is found in Watson's famous book[6].

---

[5] WATSON, *Theory of Bessel Functions.* p. 425.

Table of $\boldsymbol{L}_0(x)$ cannot be found in any book, so we calculated the value of $I_0(x)-\boldsymbol{L}_0(x)$ by the formula[7]

$$I_0(x)-\boldsymbol{L}_0(x)=\frac{2}{\pi}\int_0^{\pi/2}\exp(-x\cos\theta)\,d\theta \quad \ldots\ldots\ldots\ldots(5.7)$$

using Simpson's $\frac{3}{8}$-rule (taking the interval as 10°).
The last term of $\Phi(\tilde{\omega})$ is modified into

$$\int_0^a(\tanh 2\xi-1)\frac{\xi^2}{\xi^2+1}J_0(\xi\tilde{\omega})\,d\xi+\int_a^\infty\cdots d\xi \quad \ldots\ldots\ldots\ldots(5.8)$$

and

$$\begin{aligned}\left|\int_a^\infty\right| &< \int_a^\infty|\tanh 2\xi-1|\cdot\frac{\xi^2}{\xi^2+1}\cdot|J_0(\xi\tilde{\omega})|\,d\xi\\ &< \int_a^\infty(1-\tanh 2\xi)\,d\xi\\ &< 2\int_a^\infty\exp(-4\xi)\,d\xi\\ &= \exp(-4a)/2 \qquad \ldots\ldots\ldots\ldots(5.9)\end{aligned}$$

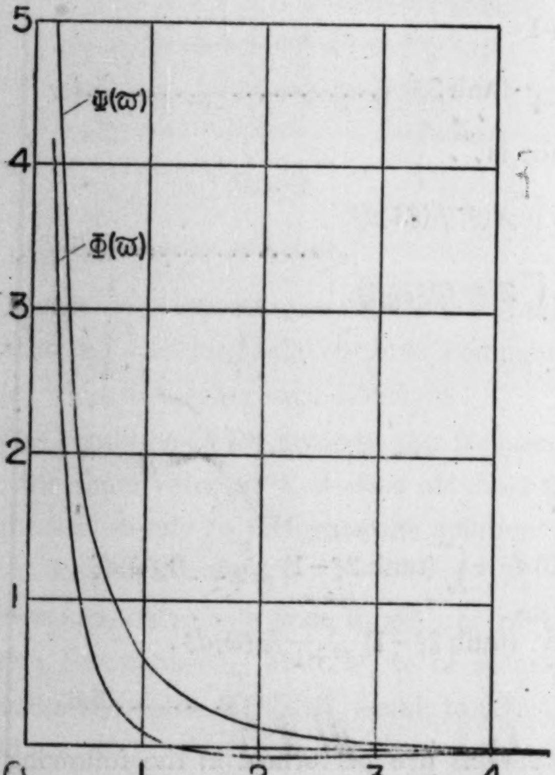

Fig. 4.

Table II.

$\tilde{\omega}$	$\Psi(\tilde{\omega})$	$I_0(\tilde{\omega})-\boldsymbol{L}_0(\tilde{\omega})$	$\int_0^\infty$	$\Phi(\tilde{\omega})$
0	∞	1	.036	∞
0.2	4.776	.882	.036	3.578
0.4	2.184	.781	.035	1.238
0.6	1.303	.695	.035	.541
0.8	.862	.620	.033	.243
1.0	.602	.559	.032	.090
1.2	.435	.501	.030	.017
1.4	.321	.452	.028	−.024
1.6	.241	.410	.026	−.046
1.8	.183	.374	.024	−.056
2.0	.140	.342	.022	−.059
2.5	.074	.279	.016	−.054
3.0	.040	.232	.011	−.043
3.5	.022	.198	.008	−.032
4.0	.012	.171	.005	−.024
4.5	.007	.151	.003	−.017

---

6) *loc. cit.*, 5) p. 698.

7) *do.*, p. 425.

Therefore if we assume a to be 1.8, the error due to the integral $\int_a^\infty$ is smaller than 0.0004. The first term of was integrated numerically.

The results of computations are given in Tab. 2 and illustrated in Fig. 4.

6. Conclutions.

The above discussions are interpreted as follows.

If the stress distribution of simple harmonic type are applied on the free surface of the elastic body and their functional form are appropriately chosen so that the condition (3.13) is satisfied, then Rayleigh-waves is not generated from such an origin. Of course, we can find any number of examples, of which we have given only one simple case in § 5.1.

If the stress distribution varies its intensity according to an arbitrary function with respect to time, the above circumstances become more complicated, and we cannot find the distribution that strictly satisfies the condition of no Rayleigh-waves. However we can find examples which nearly satisfy the conditions, and the calculation given in § 5.2 is a simple case of such cases[8]. If we put $X(\xi)$ and $Z(\xi)$ given in (5.4) into (3.7) and (3.8), we must calculate the terms which appear from the poles of these two functions. However these terms decrease rapidly with $\bar{\omega}$, so that we have no need to take them into consideration.

We hope the above theory will be used effectively for practical purposes.

---

41. レーリー波を發生しない表面應力の分布

地震研究所　　佐　藤　泰　夫

半無限彈性體の表面に應力を加へる時，レーリー波を發生することは，ラムの論文以來よくしられてゐる事であるが，加へる應力の分布如何によつては，レーリー波を發生しないこともあり得るのではないか。もしこのやうな場合が存在すれば，理論的にも，地震探鑛等の實用にも，興味ある事と思ふ。

本論文においては，まづ應力の時間的な變りかたが $\exp(ipt)$ に比例するものについて，上の問題の肯定的な解を示し，次に數値を代入して，周期的な場合及び非周期的場合について，それぞれ簡單な例題をといた。

---

[8] We chose these functions not because they agree well with our theory, but because they are simple and the calculation may be performed easily; so that if we do not mind the trouble of complicated numerical calculations, we can give sets of functions which satisfy (3.13) more strictly.

42. *Observation of the Deformation of the Earth's Surface at Aburatsubo, Miura Peninsula. Part IV.*

By Takahiro Hagiwara, Keichi Kasahara, Juhei Yamada
and Sadao Saito,

Earthquake Research Institute.

(Read May 15, June 19, 1951.—Received June 20, 1951.)

Contents.

Introduction.

1. Secular variation of the inclination of the earth's surface observed with the water-tube tiltmeter.
   a) The water-tube tiltmeter and its observational results.
   b) Eliminating the effect of the tidal load.
   c) Eliminating the effect of the temperature.
   d) Secular variation of the inclination of the earth's surface.
   e) Some considerations on the results.
2. Secular variation of the linear strain of the earth's surface observed with the silica-tube extensometer.
   a) The silica-tube extensometer and its observational results.
   b) Eliminating the effect of the temperature on the silica-tube.
   c) Eliminating the effect of the tidal load.
   d) Eliminating the annual variation.
   e) Secular variation of the linear strain in the earth's surface.

Introduction.

The writers, in the previous paper[1], have reported the outline of the observations of the deformation of the earth's surface at Aburatsubo (35°09′N, 139°37′E), near the southern extremity of the Miura Peninsula, which commenced in 1948. The main instruments used were two components of the water-tube tiltmeter, and three components of the silica-tube extensometer, the construction of which was already described in Part I of this paper. Those instruments were installed in the gallery that was bored horizontally through the sandstone of the hill side near the sea-shore in the Bay of Aburatsubo. As the first step of study, the periodic deformation of the earth's surface caused by the variation of the tidal load was investigated and discussions concerning it have been reported in Part II[2] and III[3] of this paper. The main object of the observation was to obtain continuously the deformation of the earth's crust, but the accumulation of observational data was requisite for this purpose. Hence, the investigation of the secular variation was postponed to the present day.

---

[1] T. Hagiwara, T. Rikitake, J. Yamada, *Bull. Earthq. Res. Inst.*, **26** (1948), 23.

The deformation of the earth's crust that is occurring gradually in this country in the ordinary time has been revealed by revising the precise leveling, the triangulation, and the measurement of the length of the base line. Among them, the precise leveling proved to be the most effective because of its simplicity in the field work and of its precision in the result. The analysis of the results of the precise levelings that were carried out in various regions in this country made an important contribution to geophysics by clarifying the characters of the deformation of the earth's crust. At present we can say that the precise leveling is an indispensable method for detecting the crustal deformation. The best thing would be to repeat the precise leveling constantly throughout the country but, in practice, it is impossible to do so by economical reason. For this reason, any kind of instrumental observation which would detect the crustal deformation was required. However, the observations made hitherto with the tiltmeter of horizontal pendulum type showed a too large secular change in inclination, amounting to several or several tens degrees in arc during a year. Such large amount of inclination was not seen in the results of the precise leveling except in the case where the levelings were carried out before and after the destructive earthquake. According to the revision of the precise leveling, the peninsulas on the Pacific coast of this country, such as Miura Peninsula, Izu Peninsula, Kii Peninsula, and Muroto Peninsula, were found to be inclining gradually towards south, the respective inclining speed being as follows:

Miura Pen.	Izu Pen.	Kii Pen.	Muroto Pen.
0.05″/year	0.11″/year	0.025″/year	0.051″/year

These speeds of inclination belong to the largest of the crustal deformation occuring in this country in ordinary time. Therefore, we can not believe the result that was obtained by the tiltmeter of horizontal pendulum type. The changes that were recorded by this small instrument are considered to

---

2) T. HAGIWARA, T. RIKITAKE, K. KASAHARA, J. YAMADA, *Bull. Earthq. Res. Inst.*, **27** (1948), 35.

3) T. HAGIWARA, T. RIKITAKE, K. KASAHARA, J. YAMADA, *Bull. Earthq. Res. Inst.*, **27** (1948), 39.

indicate the locally limited deformations of the ground surface and not the deformation of the "earth's crust".

The success of the precise leveling must be due to the long distance put between the bench marks. Hence, if we use the water-tube tiltmeter with considerable distance between two water-reservoirs, installed at certain depth under the ground to avoid surface disturbances, such local disturbance as occurred in the case of the tiltmeter of horizontal pendulum type will be eliminated. By the same reason, the silica-tube extensometer that has sufficient length will serve as an instrument to record the crustal deformation.

In the present paper, some discussions will be made whether the secular variations that were observed with the water-tube tiltmeter and the silica-tube extensometer installed at Aburatsubo are reliable enough as an indicator of the deformation of the earth's crust or not.

1. Secular Variation of the Inclination of the Earth's Surface Observed with the Water-tube Tiltmeter.

1-a. The water-tube tiltmeter and its observational result.

The apparatus that measures the changes in inclination of the earth's surface by reading the difference of height of the water surface at both ends of a horizontal water-tube has been devised by A. A. Michelson. The same apparatus was installed in the Earthquake Research Institute about twenty years ago, but it has been out of use. Since the all-silica tiltmeter of horizontal pendulum type was invented, the water-tube tiltmeter has been regarded by the geophysicists of this country to be unuseful. However, as already stated, the experience of observation for ten years showed the tiltmeter of horizontal pendulum type to be unsuitable for observing the secular changes in inclination of the earth's surface and the water-tube tiltmeter came into use again[4].

The construction of the water-tube tiltmeter that was installed at Aburatsubo, as already reported in Part I of this paper, consists of two water-reservoirs connected by a glass-tube with 10 mm diameter. The change in inclination is obtained from the difference between the readings of both ends. The length of the water-tube is respectively 25m for S 22°E* component and 10m for E 9°S** component. As to the reading device, a micrometer with a sharp platinum point was used and the moment at which the point touches the water-surface

---

4) T. HAGIWARA, *Bull. Earthq. Res. Inst.*, **25** (1947), 27.

* For the brevity, we call it N′S′-component.

** For the brevity, we call it E′W′-component.

was detected electrically with a glim-lamp. Remote controlling system was also employed by means of the self-synchronous motors. However, after several months since the beginning of the observation, the platinum point of the micrometer was found to be spoiled remarkably notwithstanding the previous test done in the laboratory. Therefore, the reading device was entirely converted as shown in Fig. 1., in which R is the reservoir made of gun metal (the inside is lacquered), M the micrometer made of stainless steel, and T the water-tube. The contact of the sharp point of the micrometer-spindle to the water surface is discriminated by an ordinary microscope. The observation with this new reading device was commenced from October in 1949. The observation with the old one was abandoned because the reading was considered to be unreliable. The reading of the instrument was done twice a day, namely, at 8h and 16h. To investigate the secular change, the monthly mean was made with respect to the reading of 8h and 16h respectively and they were plotted on the upper part of Fig. 2. In the Figure, the full line and the broken line represent the monthly mean for observation at 8h and 16h respectively. (Since N′S′-component is not affected by the tidal load, both readings of 8h and 16h of that component in the same day are almost equal. So that monthly means for N′S′-component are entirely equal with respect to both observations at 8h and 16h.) For the sake of comparison, the ordinary monthly mean of the sea level[5], the monthly mean of the sea level at 8h on successive days, and the same for 16h, the monthly mean of air temperature in the gallery, and the monthly sum of the precipitation were plotted.

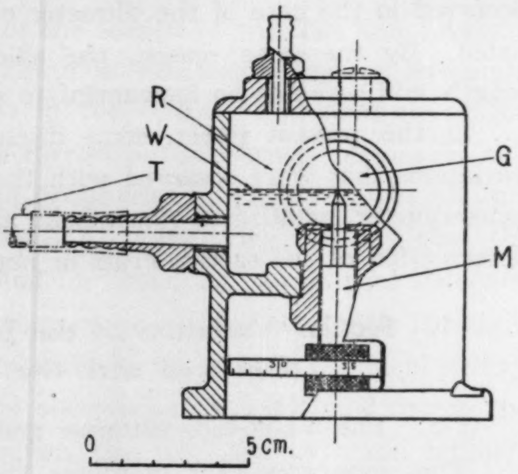

Fig. 1. R: Water reservoir, W: Water surface, G: Glass window, T: Glass-tube, M: Micrometer.

The observation in the present case is not affected by the precipitation as was seen in the tilt observation at Mt. Tsukuba[6] and other places. Underground water does not ooze out into the gallery even in the case of heavy

---

[5] Data of the level are due to the mareographic observation at Aburatsubo equipped by the Geographycal Survey Bureau.

[6] T. HAGIWARA, *loc. cit.*.

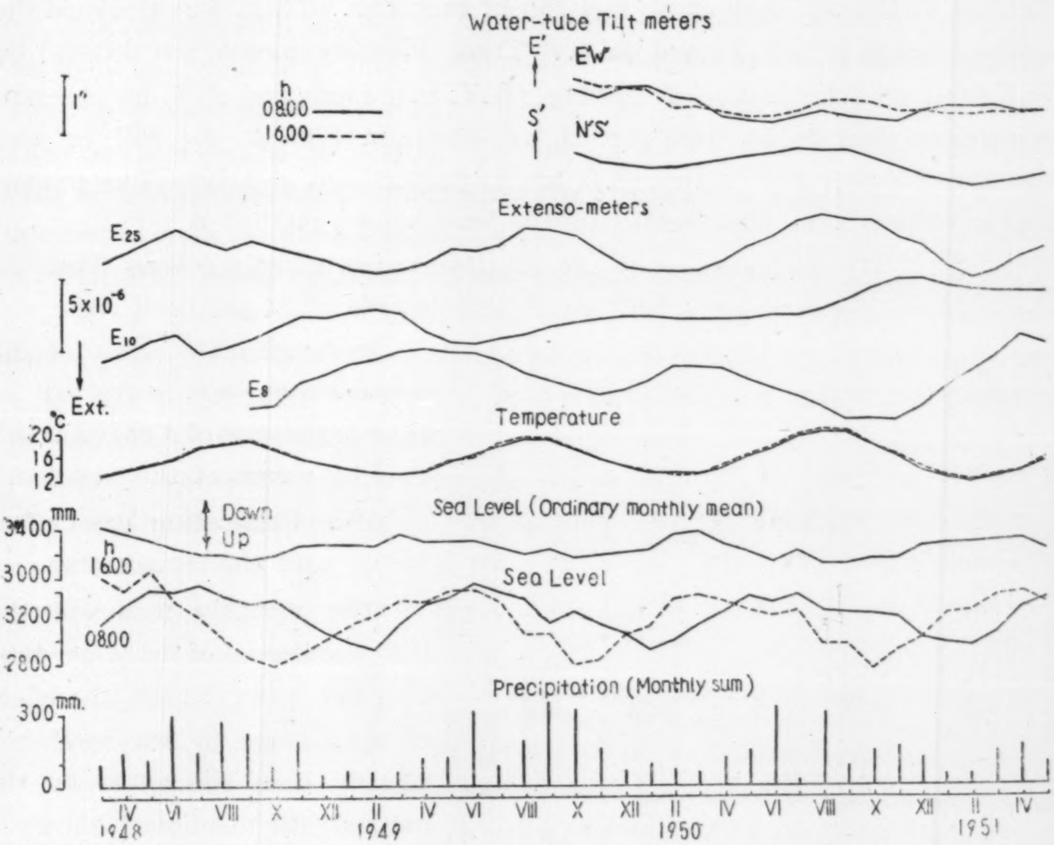

Fig. 2. From upside: E′W′ component of tilt, N′S′ component of tilt, E_{25}=N22°E component of linear strain (25 m length), E_{10}=E9°S component of linear strain (10 m length), E_8=N25°W component of linear strain (8m length), Air temperature in the gallery, Ordinary monthly mean sea level (measured from the fixed B.M. on the land: Ascending curve means subsidence of sea level), Sea level at 8h and 16h, monthly sum of precipitation.

rain. This seems to be the main reason why the effect of the precipitation does not appear.

1–b. Eliminating the effect of the tidal load.

When we investigate the secular variation of the observational result of the water-tube tiltmeter, it is necessary to eliminate the changes due to the variation in the sea level, because the tilting of the ground is caused by the load of sea water near the observation point. In the present case, the E′W′-component of the tiltmeters is greatly affected by the change in sea level, while it is not so with the N′S′-component.

To determine the amount of change in inclination caused by the change in sea level, we obtained $\delta W.T.$ and $\delta S.L.$; where $\delta W.T.$ is the difference of the inclination measured with the water-tube tiltmeter at 8h and 16h, and $\delta S.L.$ is the difference of the sea level at 8h and 16h of each day. Then, we calculated the monthly means of $\delta W.T.$ and $\delta S.L.$. These monthly means are denoted by $\Delta W.T.$ and $\Delta S.L.$ respectively. Taking $\Delta W.T.$ as ordinate and $\Delta S.L.$ for abscissa, the corresponding points were plotted, as shown in Fig. 3. As will be seen from the Figure, $\Delta W.T.$ and $\Delta S.L.$ are in proportional relation. The proportional coefficient that was decided by the least square method is

for E′W′-component 0.54″/m (E′ downwards when sea level rises),
for N′S′-component 0.04″/m (S′ downwards when sea level rises).

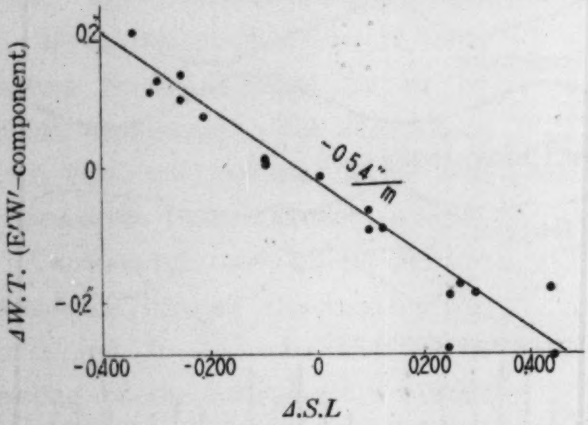

Fig. 3.

Each monthly mean of the measurement was corrected so as to fit the case of a constant sea level by means of this relation.

1–c. Eliminating the effect of the temperature.

The monthly mean of the N′S′-component of the water-tube tiltmeter from which the effect of the change in sea level has already been eliminated by the method just mentioned shows a remarkable annual variation. This variation is entirely parallel to the variation of the air temperature in the gallery. Hence, if we plot the values taking the monthly mean of the tilting as ordinate and the monthly mean of the temperature for abscissa, we obtain a straight line that is shown in Fig. 4. The proportional coefficient between the tilting and the temperature that was determined by the least square method is as follows.

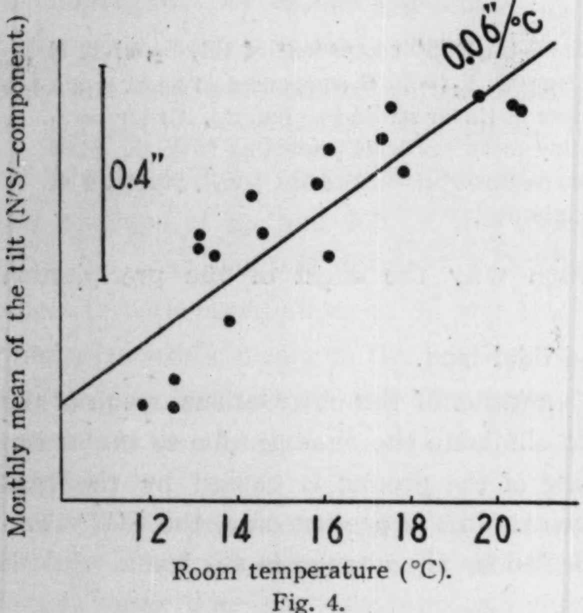

Fig. 4.

N′S′-component 0.06″/°C (S′ downwards when the temperature increases)
E′W′-component 0

The reason why the N′S′-component alone is affected by the air temperature seems to be traceable to the thermal expansion of the concrete block on which the water reservoir of the water-tube tiltmeter is settled. The height of the two concrete blocks on which the reservoirs are set are entirely equal in the case of E′W′-component, while, there is a difference amounting to 35 cm in the height from the ground surface in the case of N′S′-component. If the thermal coefficient of linear expansion of the concrete were taken to be 1.4×10^{-5}/°C, the value written in ordinary handbooks, the apparent change in inclination due to the expansion of the concrete block corresponds to 0.04″/°C (S′ down when the temperature increases). Both values, the actual and the calculated, are considered to coincide well.

Next, we will examine how the temperature of the concrete follows the air temperature surrounding it. To simplify the mathematical calculation, we consider an endless long cylinder with radius a. When the temperature of the outside of the cylinder varies as $b \cos nt$, the temperature T of the inside of the cylinder is given by

$$T(r)=\frac{\mathrm{ber}\sqrt{\frac{n}{k^2}}r\,\mathrm{ber}\sqrt{\frac{n}{k^2}}a+\mathrm{bei}\sqrt{\frac{n}{k^2}}r\,\mathrm{bei}\sqrt{\frac{n}{k^2}}a}{\left(\mathrm{ber}\sqrt{\frac{n}{k^2}}a\right)^2+\left(\mathrm{bei}\sqrt{\frac{n}{k^2}}a\right)^2}\,b\cos nt$$

$$+\frac{\mathrm{ber}\sqrt{\frac{n}{k^2}}r\,\mathrm{bei}\sqrt{\frac{n}{k^2}}a-\mathrm{bei}\sqrt{\frac{n}{k^2}}r\,\mathrm{ber}\sqrt{\frac{n}{k^2}}a}{\left(\mathrm{ber}\sqrt{\frac{n}{k^2}}a\right)^2+\left(\mathrm{bei}\sqrt{\frac{n}{k^2}}a\right)^2}\,b\sin nt\,,$$

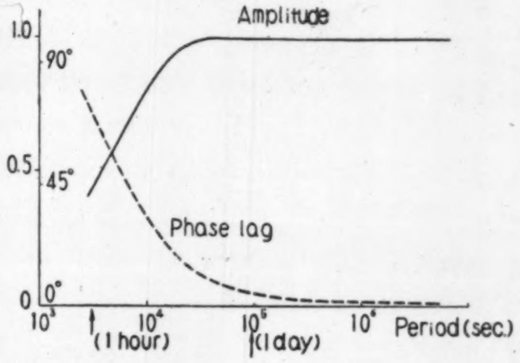

Fig. 5. Ordinate: the ratio and the phase difference of the temperature at the center of cylinder and that at the outside of cylinder.
Abscissa: period of the changes in temperature.

where r is the distance from the central axis of the cylinder, a the radius of the cylinder, and k^2 the thermometric conductivity.

In the present case, the concrete block is a square column with a side of 20 cm. If we replace it by a cylinder with diameter of approximately 20 cm, the temperature and its phase-lag at the center of the cylinder are calculated by the above formula, as shown in Fig. 5. As seen in the Figure, when the air temperature varies slowly with a period longer than one day, the temperature of the concrete block falls in with the air temperature surrounding it. Hence, we may be able to correct exactly the effect of the expansion of the concrete by using the air temperature in the gallery itself when we deal with the slow changes.

By the above-mentioned reason, each monthly mean of N′S′-component was corrected by subtracting the corresponding monthly mean value of the air temperature in the gallery producted by the coefficient 0.06″/°C.

1–d. Secular variation of the inclination of the earth's surface.

Each monthly mean in which the effect of the variation in tidal load and of the variation in air temperature were eliminated is shown graphically in Fig. 10.

1–e. Some considerations on the results.

The leveling route is running along the west coast of the Miura Peninsula, branching off from the Tokaido highway to the fixed bench mark at the mareographic station at Aburatsubo equipped by the Geographical Survey Bureau (Fig. 6). The revisions of the leveling on this route were frequently made after the Kanto Great Earthquake, 1923, in order to check the height of the geodetic origin placed in Tokyo. The changes in height of the bench marks

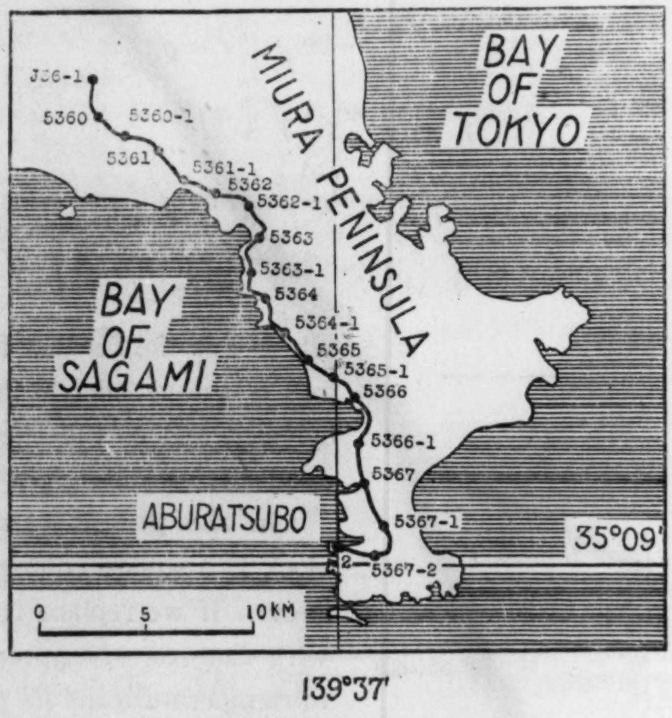
J36-1
5360
5360-1
5361
5361-1
5362
5362-1
5363
5363-1
5364
5364-1
5365
5365-1
5366
5366-1
5367
5367-1
2
5367-2
MIURA PENINSULA
BAY OF TOKYO
BAY OF SAGAMI
ABURATSUBO
35°09′
0
5
10KM
139°37′

Fig. 6. Leveling route in Miura Peninsula.

in the peninsula that were made clear by the revisions of the precise leveling are shown in Fig. 7, in which the changes in height of the bench marks with respect to B.M. J-36-1 (Fujisawa) were plotted, assuming the change of each bench mark to be zero in 1925. As already pointed out by Y. Harada[7], the peninsula is inclining constantly as one block, having undulatory motions with smaller wave length on it.

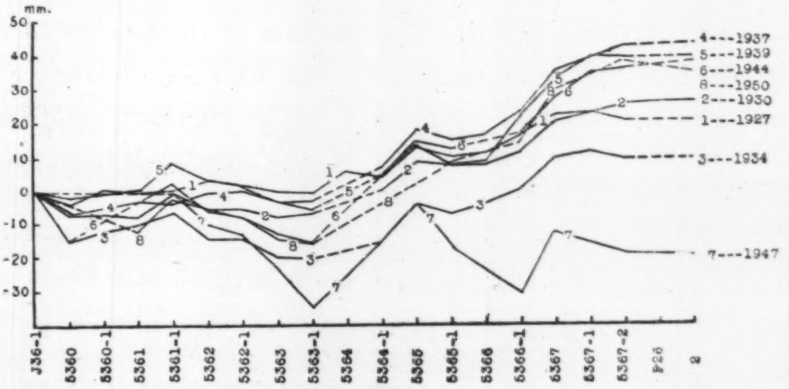

Fig. 7. Changes in height of B.M. in Miura Pen. with respect to B.M. J36-1 (Changes in 1925 were taken to be zero).

Since our observational station is placed in the neighbourhood of the southern extremity of this leveling route, the results of the tilt observation shall be compared with the changes in height of the bench marks such as B.M. 5367, 5367-1, 5367-2 and 2. As will be seen in Fig. 7, the difference in height between 2 and 5367-2, which is on a line of E.W. direction, remains constant always, so that this region seems to make an inclinational motion approximately towards north and south direction. The changes of the difference of height between B.M. J-36-1 and 2 and the changes of the same kind between B.M. 5367 and B.M. 5367-2 were plotted in Fig. 8. The scale drawn in the right-hand side of the Figure is the corresponding value of inclination angle between two bench marks. As will be seen in

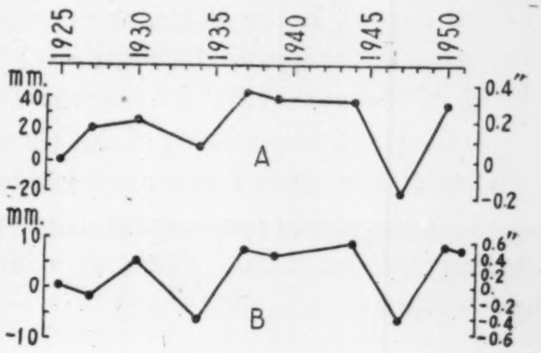

Fig. 8. A: Change in height of B.M. 2 with respect to B.M. J36-1,
B: Change in height of B.M. 5367-2 with respect to B.M. 5367.

---

[7] Y. HARADA, *Journ. Seism. Soc. Japan* (in Japanese), II Ser., **1** (1948), 52, and **2** (1948), 17.

the Figure, the two curves, the upper and the lower, are very similar to each other except the period just after the Kanto Great Earthquake. Therefore, it can be said that the local movement of the region on which B.M. 5367 and B.M. 5367-2 are placed is related intimately to the movement of the peninsula as one body.

We are to compare the observational results of the water-tube tiltmeter with the changes in inclination between B.M. 5367 and 5367-2 determined by the revision of the precise leveling. The revision of the precise leveling along the route in the peninsula was made only once on Feb., 1950 after our observation of tilt was commenced. Hence, in order to check our observational result, we carried out newly the revision of the precise leveling against B.M. 5367, 5367-1, 5367-2, F-26, and 2 on May, 1951. The result of the leveling is shown in the following Table.

Table I.

B.M.	1950 (Feb.)	1951 (June)	h	h
5367				mm 0.0
	m +74.5438	m +74.5432	mm −0.6	
5367-1				−0.6
	− 6.3382	− 6.3391	−0.9	
5367-2				−1.5
	−53.9948	−53.9942	+0.6	
F-26				−0.9
	−11.9591	−11.9595	−0.4	
2				−1.3
	− 1.6178	− 1.6141	+3.7	
Mareograph				+2.4

As will be seen in the Table, the changes in height of the bench marks are very small in the interval between Feb., 1950 and June, 1951. The observational results of the water-tube tiltmeter show very small inclination in this interval too.

A thorough examination of the observational results, needless to say, can be conducted only after further observation and more numbers of the revision of precise leveling has been made. The writers are planning to revise the precise leveling on that region whenever a large inclination is detected by the water-tube tiltmeter.

2. Secular Variation of the Linear Strain of the Earth's Surface Observed with the Silica-tube Extensometer.

2-a. The silica-tube extensometer and its observational results.

The observation of the silica-tube extensometers in three directions was carried on in parallel with the measurement of the water-tube tiltmeters. The construction of the instruments has been already reported in Part I of this paper. Elements of each component are shown in Table II.

Table II.

Name of component	Length	Direction	Extension corresponding to 1 cm on the record.	Commencement of observation
E_{25}	25m	N22°E	1.3×10^{-6}	III, 1948
E_{10}	10m	N81°W	3.3×10^{-6}	III, 1948
E_8	8m	N25°W	3.5×10^{-6}	IX, 1948

The hourly values were read off from the record of the extensometer, and adding together these values, the daily mean values were obtained. And from these the monthly mean values were obtained. These monthly means are shown graphically in Fig. 2.

2–b. Eliminating the effect of the temperature on the silica-tube.

Since the silica-tube has the thermal expansion coefficient of 0.42×10^{-6}/°C, the values of observation were reduced to the state of same temperature (10°C).

2–c. Eliminating the effect of the tidal load.

As reported in Part II and III, the earth's surface extends and contracts owing to the variation of the load of sea water. Hence, this effect shall be eliminated when the secular variations of extension of the earth's surface are investigated. As to the extension of the earth's surface due to the load of M_2-tide has been reported in Part II of this paper. According to it, the extension caused by the rise of sea level was

$$E_{25}: 0.7\times10^{-7}/\text{m},\quad E_{10}: 14.4\times10^{-7}/\text{m},\quad E_8: 9.4\times10^{-7}/\text{m}.$$

Assuming these proportional coefficients to be available for the variation of a long period, the effect of sea level were eliminated from the monthly means of the observation.

The monthly means of the variation of extension of the ground in which the correction of the thermal expansion of the silica-tube and the variation of

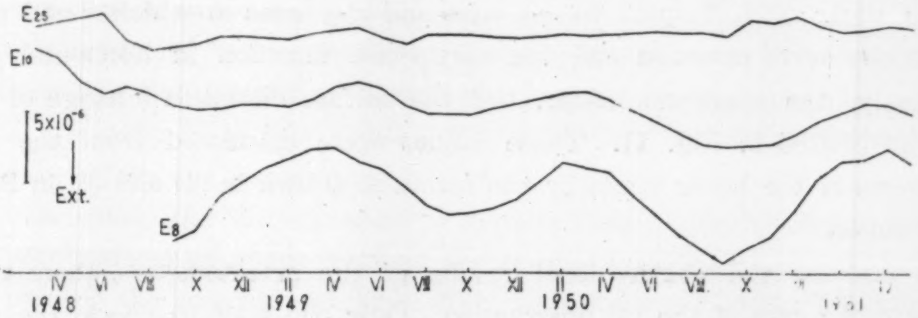

Fig. 9, Monthly mean of linear strains (Thermal expansion of silica-tube and effect of tidal load eliminated).

sea level were made are plotted in Fig. 9.

2-d. Eliminating the annual variation.

The curves shown in Fig. 9 show the remarkable change with annual period. The periodic term was taken out from the two curves, of the strain and of the temperature, by the least square method, assuming the variation to be composed of three terms, that is, the term varying linearly with time, the pure periodic term with the period of one year, and the irregular ones. The result is as follows.

$$\begin{array}{lll} E_{25} & E_{10} & E_{8} \\ 0 & 11.1\times10^{-7}\cos\left(360^\circ\times\frac{n}{12}-240^\circ\right) & 24.3\times10^{-7}\cos\left(360^\circ\times\frac{n}{12}-240^\circ\right) \end{array}$$

Temperature

$$3.7^\circ\times\cos\left(360^\circ\times\frac{n}{12}-210^\circ\right)$$

in which n is the number of month, taking $n=0$ for January. The phase angle of the periodic term of the strain does not coincide with that of the air temperature in the gallery but differs by 30°. Since the phase of annual variation of the air temperature in the gallery is equal to that of the air temperature outside of the gallery, we can not decide which temperature causes the annual variation of linear strain of the ground.

Although the mechanism in which the air temperature affects the linear strain of the ground is not evident from the present data, we are able to obtain the desired secular variation by subtracting the pure periodic term from the curves shown in Fig. 9.

2-e. Secular variation of the linear strain in the earth's surface.

The final results in which the term of annual variation was eliminated by the method just mentioned are shown Fig. 10.

The shear with respect to x-y axes and x'-y' axes in which x and x' are taken in the north direction and the north-west direction in horizontal plane respectively, the maximum shear, and the surface dilatation (change of area) were also plotted in Fig. 11. These values were calculated from the three components of the linear strain by the formulae shown in (4) and (5) in Part II of this paper.

To examine the observational results of the extensometers, there are no data as in the case of the tilt observation. Only one way to check the order of variation is to compare our results with the measurements of the base lines

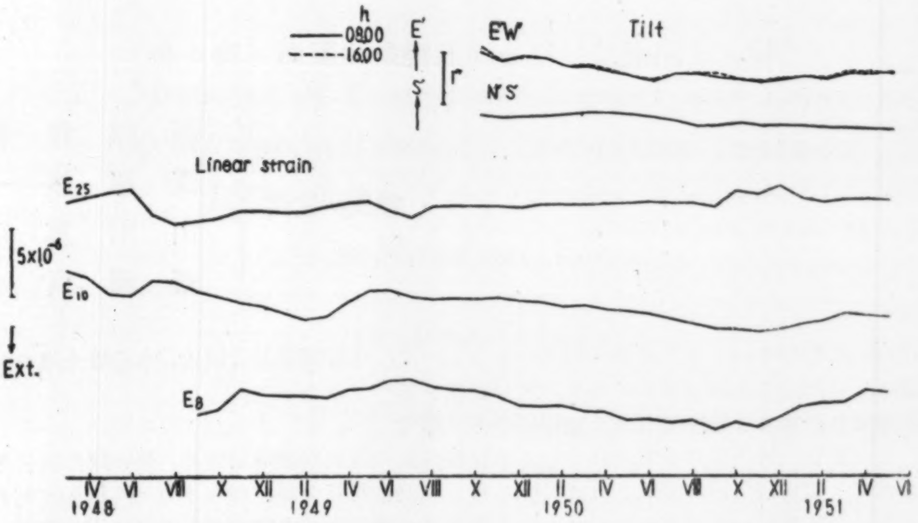

Fig. 10. Corrected monthly mean values of change in inclination and linear strains of the earth's surface.

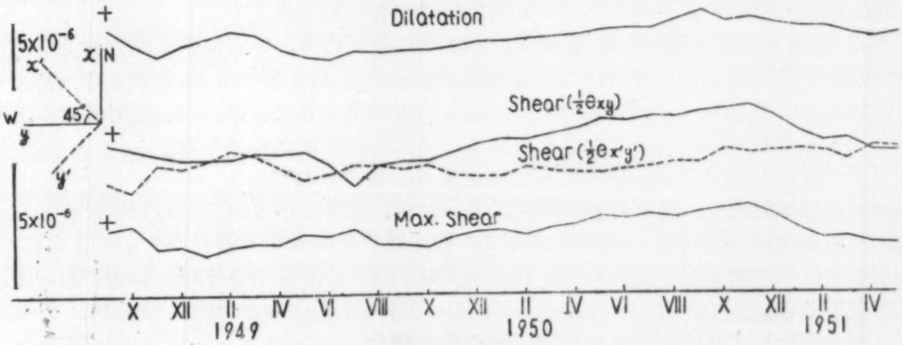

Fig. 11. Dilatation and shears calculated from linear strains of the earth's surface.

at Mitaka, in the west of Tokyo. There are base lines of rhombus shape in the compound of the Tokyo Astronomical Observatory at Mitaka. The length of these base lines have been occasionally measured by experts of the Geographical Servey Bureau since 1916, but unfortunately the revision of the measurement has not yet been carried out since our observation began. However, the results of the measurements in the past shows that the length of the base lines did not remain constant but underwent certain changes, the amount of which is ordinarily in the order of 10^{-6} in a year. This value is of the order of the linear strain observed by our instruments.

In conclusion, the writers wish to express their cordial thanks to Mr. A. Okada who assisted us in the work of the precise leveling.

A part of the expenses of this study was defrayed from the Scientific Research Expenditure of the Department of Education.

42. 油壺における地殼變動の觀測（第4報）

地震研究所
萩原尊禮
笠原慶一
山田重平
齋藤貞夫

油壺において行つている地殼變動の觀測の主なものは，水管傾斜計2成分，水晶管土地伸縮計3成分であるが，今回はその觀測結果につき，經年變化を調べてみた。

1. 水管傾斜計により觀測された土地傾斜の永久變化

1-a この報告の第1報に記載されている水管傾斜計の電氣式讀取裝置は，長い間に白金先端が侵蝕されるので，顯微鏡で直接讀取る方式に改めた。觀測は每日2回，即ち 8h と 16h に行われている。その各の讀取値につき月平均を求めた。月平均値の變化は第2圖に示してある（實線は 8h 讀取値の月平均，破線は 16h の讀取値の月平均）。

1-b 觀測點附近の海水の荷重變化により傾斜變化が起るので，驗潮儀から知られた海水位の値を使つて，傾斜變化の月平均値を補正し，一定海水位の場合に直した。

1-c 傾斜 N′-S′ 成分の年變化は，觀測壕內の溫度の年變化と，非常に良く似た變化をしている。これは水管傾斜計の兩端のコンクリート柱の地表面からの高さに 35cm の差があるため，コンクリート柱の熱膨脹により見かけの傾斜變化が現れるものと解釋された。從つて，壕內溫度の月平均値を用いて，N′-S′ 成分の傾斜變化月平均値を補正し，一定溫度の場合に直した。

1-d 以上の補正を施した傾斜變化月平均値は第 10 圖に示してある。

1-e 傾斜の經年變化は，現在の觀測期間においては，非常に小さい。この期間に行われた2回の水準測量結果から附近の水準點の變動を求めてみると同じく變動が非常に小さいことが確められた。將來もし土地傾斜に大きな經年變化が示された場合は，直ちに附近の水準點の改測を行い觀測結果と比較する計畫である。

2. 水晶管伸縮計により觀測された土地伸縮の經年變化

2-a 水晶管伸縮計は，感光紙を使つた連續觀測であるので，記錄紙より每時の變化を讀取り，先づ日平均値を求め，さらにこれを加えて月平均値を作つた。月平均の生の値は第2圖に示してある。

2-b 水晶管は $0.42\times10^{-7}/^{\circ}\mathrm{C}$ の線膨脹係數を持つているので，伸縮月平均に補正を加えて壕內氣溫が一定の場合の値に直した。

2-c 傾斜變化と同じく，土地伸縮も海水荷重に影響されるので，これに關する補正を行い，伸縮月平均値を一定海水位の場合の値に直した。この補正には，前報告において M_2 潮につき求めた海水位變化と土地伸縮との比例關係が長周期變動にも適用できると假定した。

2-d 以上の補正を施した伸縮變化は第9圖に示す通りであるが，これには著しい年周變化が見られるのである。伸縮變化及び壕內氣溫の年變化から，それぞれ最小自乘法によつて年周期の項を取出して見ると，兩者の位相に相當の差が見られる。現在のところ如何なる機構で氣溫變化が土地伸縮を起しているか分からない。そこで差當つて，三年間の材料の解析によつて定められた伸縮の年周變化の項を差引いて經年變化を求めることとした。

以上の三種の補正を加えた伸縮經年變化は第 10 圖に示す通りである。

2-e 伸縮3成分の經年變化から土地の shear, maximum shear, dilatation 等の經年變化も計算した。Dilatation（面積變化）の經年變化のオーダーは三鷹ロンバスの測量から求められた値に一致している。

43. *Measures of Earthquake Danger and Expectancy of Maximum Intensity Throughout Japan as Inferred from the Seismic Activity in Historical Times.*

By Hirosi KAWASUMI,

Earthquake Research Institute.

(Read Nov. 21, 1950.—Received June 20, 1951.)

One of the urgent problems of the practical seismology in earthquake country is to determine the degree of danger threatening human lives at any locality. It has been demanded from the engineering circle to furnish these informations, and recently we are also requested from the Ministry of Construction to determine the maximum earthquake intensity to which we may possibly encounter at any locality for the reference in determining the standard strength of the earthquake proof constructions, the standard being to be designated in the building code in preparation. The following is the result of our study on the above problems.

Our feeling of danger depends not only to the magnitude and frequency of liable danger but also to the imminence and certainty of the coming danger. We must therefore determine these aspects to fulfil the request. However, notwithstanding Omori, Imamura and others have predicted some earthquakes from the knowledge of the time and space distributions of earthquakes and some precursory phenomena, yet our knowledge is still too meagre to guarantee the prediction of the earthquake occurrence determinately. Moreover evidences of stochastic nature of the earthquake occurrence have been accumulated so much that we are by no means able to discuss especially the imminence and certainty of the coming earthpuake danger from the deterministic point of view.

We must therefore discuss only the side of the magnitude and frequency of the future danger on the statistical point of view from the data of past seismic activity. In Japan seismic records remain since more than one thousand years in most part of her territories, so that we may obtain a reliable mean probability from the mean activity in these historical times, even if we consider the long cycle of reccurrence of large earthquakes at a locality, which according to Imamura, is from 800 to 1000 years. The resemblance of seismic activities in recent 80 years and in historical times may be another testimony in favour of this point.

Thus we may derive the probability spectrum $P(I)$ from the frequency spectrum $n(I)$ of seismic intensity I as experienced at a point by the following formula

$$NP(I)\,dt=\frac{n(I)}{T}\,dt \quad\ldots\ldots\ldots\ldots\ldots\ldots\ldots\ldots\ldots\ldots\ldots (1)$$

where N is the total number of observed intensity at all the localities throughout historical times of length T. The right hand side of the eq. (1), which denotes the mean frequency of earthquakes of intensity I, serves as a direct measure of earthquake danger at a point, and if we want to know, for example, expectancies of total number of subversion of houses or total amount of damage in current price or number of casualties etc., they may be determined from this mean frequency, since these damages are respectively functions of the intensity of an earthquake. These expectancies themselves also serve as the practical indices of earthquake danger. It is also to be noted that we can also derive a physical index of earthquake danger from the parameter of the function denoting the mean frequency spectrum $n(I/T$. Indeed we know that the functional form of $n(I)$ is $C\times 10^{-\varepsilon I}$ so that $n(I_0)/T$ or its sum $S(I_0)/T=\sum_{I_0}^{\infty} n(I)/T$ may be used as a physical index of earthquake danger.

Let us now consider the determination of the standerd intensity for designing earthquake proof constructions. It is most ideal to build a building so strong as to resist the strongest earthquake intensity which may be encountered in the life-time or the duration of endurence of the structure. But, as we have stated, the future earthquake cannot be predicted determinately, so that we have only to use the expectancy of the maximum intensity as the standard. Such expectancy in the interval t is determined from the condition that stronger earthquake than the critical intensity can never be expected in the interval, or in other words the expectancy of the number of stronger earthquake than I_0 just reaches unity in t, i. e.

$$S(I_0)t/T=1 \quad\ldots\ldots\ldots\ldots\ldots\ldots\ldots\ldots\ldots\ldots\ldots\ldots (2)$$

Physically considered, the condition

$$n(I_0)t/T=1 \quad\ldots\ldots\ldots\ldots\ldots\ldots\ldots\ldots\ldots\ldots\ldots\ldots (3)$$

may be more appropriate, but from the practical point of view the former is adopted here for safety.

Let us now enter the practical calculation. Earthquake records in Japan were collected by Sekiya and Omori and later enlarged by Imamura and Musya in the latest "Materials for the Earthquake History of Japan".

Imamura has determined the epicentres and magnitudes of the historical earthquakes from the perusal of these materials based on his knowledge and experience of his life-long seismological study. Recently Musya compiled a catalogue of large earthquakes in Japan and the writer revised the manuscript and supplemented it with all the data concerning the earthquake intensity at any locality. Based on this catalogue the writer redetermined

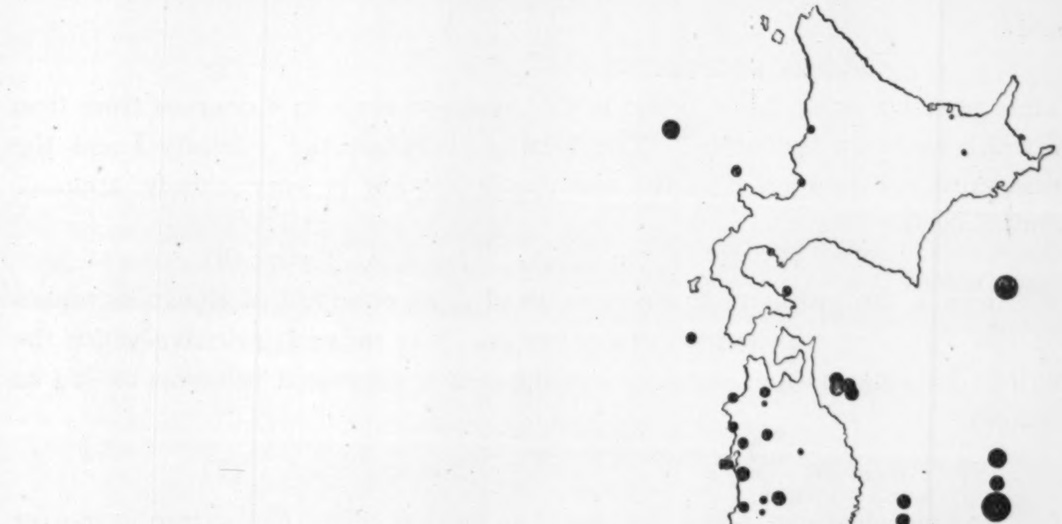

Fig. 1. Distribution of epicentres of major historical earthquakes in Japan. Radius of the spot denotes the magnitude.

the epicentres and magnitudes of these earthquakes. The results are tabulated in the annexed table 1 and shown in Fig. 1.

M_k in the table 1 denotes the magnitude in the writer's scale and represents the intensity at the epicentral distance of 100 km. According to the recent study the magnitude M_k is also related to the maximum ground amplitude A_{100} at the same distance and Richter magnitude M by the following formulas:

$$A_{100}=10^{1.5+0.5M_k} \quad \cdots\cdots\cdots\cdots (4)$$

and

$$M=4.85+0.5M_k \quad \cdots\cdots\cdots\cdots (5)$$

The intensity scale here in use is the Japanese scale in 8 degrees from 0 to 7 which is shown in Table 2. The relation between the intensity I and the maximum acceleration α of the earthquake motion is very closely approximated by the relation

$$\overline{\alpha}=0.45\times 10^{0.5\,I} \quad \text{(in gals)}, \quad \cdots\cdots\cdots\cdots (6)$$

where $\overline{\alpha}$ is the geometrical mean value of α as observed at Hongo by means of the Ishimoto acceleration seismographs. The mean $I(\Delta)$ curve which the writer determined from some 80 earthquakes is expressed in terms of M_k as follows:

$$e^I=\left(\frac{100}{\Delta}\right)^2 e^{M_k-0.00183(\Delta-100)} \quad (\Delta \text{ in km}) \cdots\cdots\cdots (7)$$

for the epicentral distance Δ greater than 100 km. The $I(\Delta)$ curve in shorter distance was calculated for the case of an earthquake having a hypocentral depth of 18 km, taking the extinction coefficient as determined from the discussion of observed frequency spectrum $n(I,r)\,dr$ in the interval r and $r+dr$ of hypocentral distance. Thus using the relation

$$A=\frac{r_0A_0}{r}e^{-k(r-r_0)} \quad \cdots\cdots\cdots\cdots (8)$$

(where A_0 and r_0 denote the values at $\Delta=100$ km) and the equations (6) and (7), we have

$$I=M_k+2\log_{10}(r_0/r)+2k(\log_{10}e)(r-r_0) \cdots\cdots\cdots (9)$$

whose k being 0.0192 per km for S waves.

By means of these formulas (7) and (9) the seismic intensity at any locality is found for any earthquake of known epicentre and magnitude, the focal depth being assumed at 18 km with Gutenberg and Richter.

In this way we determined the intensity at 350 mesh points of 1/2 degree intervals of longitude and latitude arronud the land area of our country in case of 342 historical earthquakes already mentioned. The frequency spectrum for I greater than 5 and the sum $S(I)$ are determined. The latter are shown at the mesh points on Fig. 2 A, B and C. The lengths of historical times T are different at respective districts. For simplicity's sake our country is devided into three parts: middle and west, north east and Hokkaido

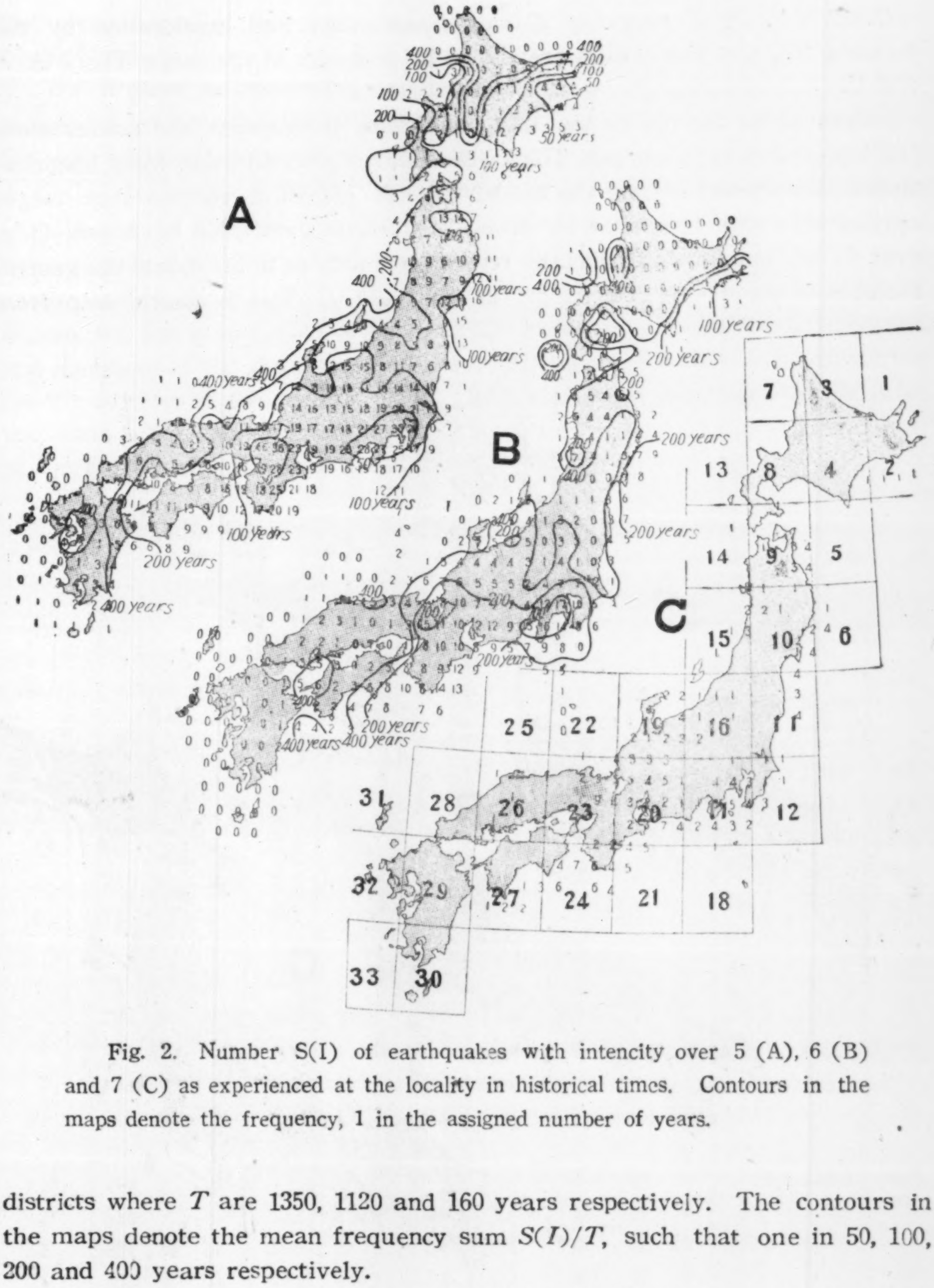
A
400 years
200 years
100 years
50 years
B
C
1
2
3
4
5
6
7
8
9
10
11
12
13
14
15
16
18
19
20
21
22
23
24
25
26
27
28
29
30
31
32
33

Fig. 2. Number S(I) of earthquakes with intencity over 5 (A), 6 (B) and 7 (C) as experienced at the locality in historical times. Contours in the maps denote the frequency, 1 in the assigned number of years.

districts where T are 1350, 1120 and 160 years respectively. The contours in the maps denote the mean frequency sum $S(I)/T$, such that one in 50, 100, 200 and 400 years respectively.

The expectancies of the maximum intensity I_0 for the interval t of 75, 100 and 200 years were determined by the relation (2). In the calculation $n(I)$ for I less than 4 was extrapolated where necessary by the relation $n(I)$

$=C\times 10^{-0.5\,I}$. The resulting I_0 was transformed into acceleration by the formula (6), and the results are shown by contours in the maps Fig. 3 A, B and C.

From these figures we see that maximum frequencies and accelerations are found around Kyoto and Tokyo, the centres of civilization from historical times. But it seems from the nature of our historical records that larger earthquakes with intensities as strong as to cause demolition of houses (i. e. over 6) are not missing from the records so much as to invalidate the general features of the earthquake danger in our country. This is clearly seen from

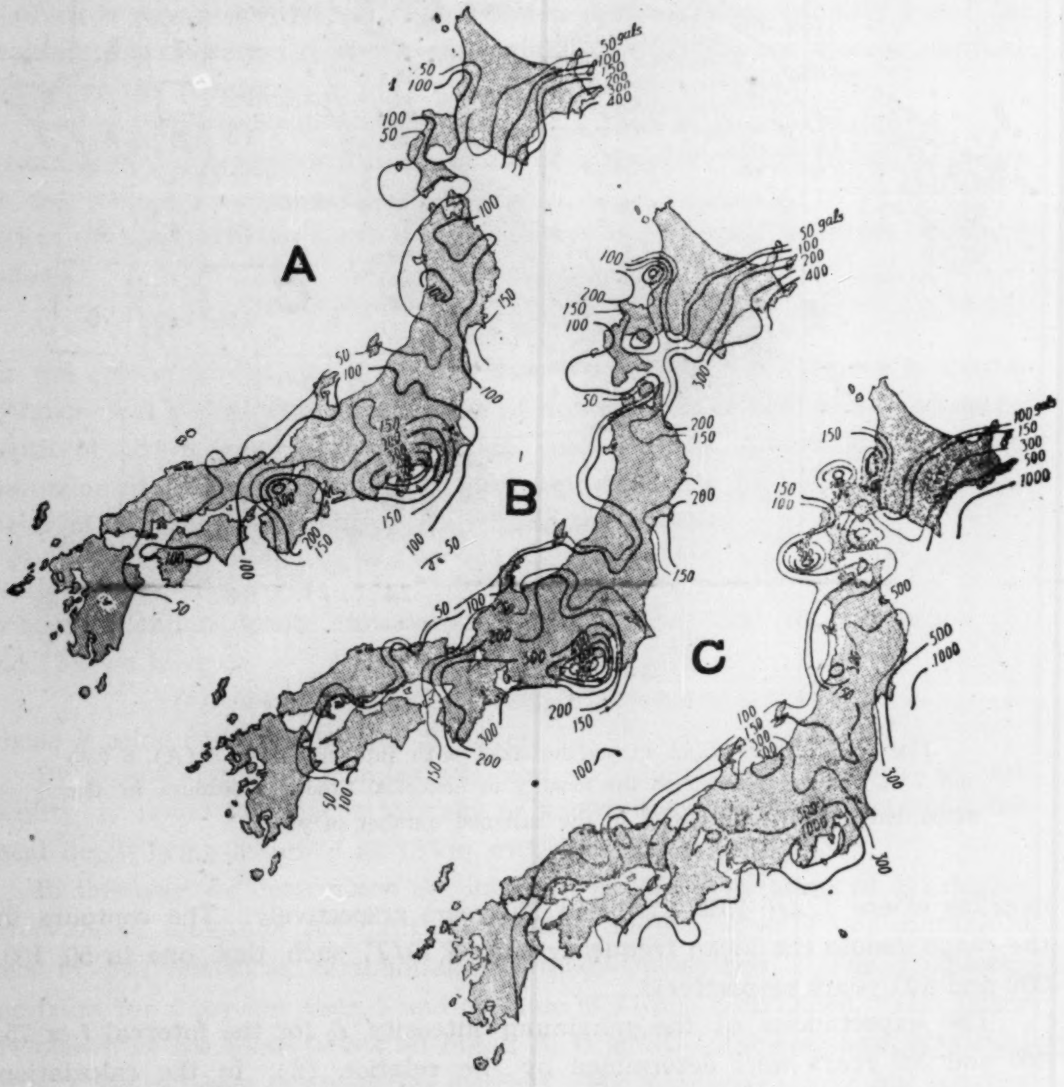
A
50 gals
100
150
200
300
400
50
100
100
50
100
150
50
100
100
150
300
300
200
150
100
100
150
100
50
50
B
50 gals
100
200
400
100
200
150
100
300
50
200
150
200
150
50
100
200
300
200
150
300
200
150
50
100
100
C
100 gals
150
300
500
1000
150
150
100
500
500
1000
150
100
150
300
500
300
500
1000
300

Fig. 3. Expectancy of maximum acceleration of earthqakes in 75 (A), 100 (B) and 200 (C) years.

the resemblance of the present result to that of recent 80 years as obtained by K. Kanai.

But it must be mentioned that the intensity of an earthquake is se much influenced by the condition of the underground, that the underground factor for each building cite must be multiplied to the accelerations shown in Fig. 3 A, B, C in determining the standard strength of earthquake proof constructions. Distributions of the underground factor in major cities as Tokyo, Osaka etc. have already been determined. and will be reported in future.

In conclusion the writer wishes to express his sincere thanks to Mr. K. Musya, for the preparation of the earthquake catalogue, and to the director and members of the Architecture Research Institute, Ministry of Construction for the support of the present study. It is also to be mentioned with thanks that kind suggestions were given to the writer by Drs. Takahasi and Kanai of the Earthquake Research Institute.

Table Ⅰ. Catalogue of Large Earthquakes in Japan.

(Earthquakes marked by * were accompanied by tsunami)

No.	Date.			Epicentre.		M_k	No.	Date.			Epicentre.		M_k
				φ degree N	λ degree E						φ degree N	λ degree E	
1	599	Ⅴ	28			4.3	16	841			35.1	138.9	4.3
2	679			32.7	130.4	3.6	17	850			39.1	140.	4.3
3*	684	Ⅺ	29	32.5	134.	7.	18	856					3.1
4	701	Ⅴ	12	35.6	135.4	4.3	19	857	Ⅳ	4	40.3	140.6	4.3
5	715	Ⅶ	4	35.1	137.9	3.1	20*	863	Ⅶ	10	37.1	138.1	4.3
6	715	Ⅶ	5	34.7	135.4	3.6	21	868	Ⅷ	3	34.8	134.8	4.5
7	734	Ⅴ	18	34.3	136.1	4.3	22*	869	Ⅶ	13	38.5	143.8	7.5
8	744	Ⅵ	30			3.	23	878	Ⅺ	1	35.5	139.3	5.0
9	745	Ⅵ	5	35.5	136.6	6.	24	880	Ⅺ	23	35.4	132.8	5.
10	762	Ⅵ	9	35.6	137.3	5.1	25	881	Ⅰ	13			3.1
11*	799	Ⅸ	18				26*	887	Ⅷ	2	37.5	138.1	4.3
12*	818			35.2	139.3	6.	27*	887	Ⅶ	26	33.	135.3	7.5
13	827	Ⅷ	11	34.9	135.6	3.6	28	887	Ⅷ	26	36.6	138.1	5.1
14	830	Ⅱ	3	39.8	140.1	5.1	29	890	Ⅶ	10			2.6
15	841			36.6	137.8	3.6	30*	922			33.8	136.7	4.3

(to be continued.)

(continued.)

No.	Date.			Epicentre.		M_k	No.	Date.			Epicentre.		M_k
				φ degree N	λ degree E						φ degree N	λ degree E	
31	934	VII	16			2.6	61	1423	XI	23	39.2	140.1	3.6
32	938	V	22	34.8	135.8	4.0	62*	1433	XI	7	34.9	139.5	4.5
33	976	VII	22	34.9	135.8	3.6	63	1433	XI	7	37.7	139.8	3.6
34	1038	I	30	34.3	135.6	3.6	64	1449	V	13	35.	135.6	3.1
35	1041	VIII	25			3.1	65	1456	II	14			3.1
36	1070	XII	1	34.8	135.8	(3)	66	1466	V	29			2.6
37	1091	IX	28	34.3	135.8	2.6	67	1494	VI	19	34.6	135.7	3.
38	1093	III	19			3.1	68	1498	VII	9			
39*	1096	XII	17	34.2	137.3	7.0	69*	1498	IX	20	34.1	138.2	7.5
40	1099	II	22	34.7	135.7	3.	70	1502	I	28	37.2	138.2	4.
41	1099	IX	20			3.1	71	1510	IX	21	34.6	135.7	3.6
42	1137	VIII	10			2.6	72	1517	VII	18			3.1
43	1177	XI	26	34.7	135.8	2.6	73*	1520	IV	4	33.6	136.3	4.3
44	1185	VIII	13	35.9	136.1	5.	74	1525	IX	20			2.5
45	1213	VI	13			3.1	75	1555	IX	14			3.1
46	1227	IV	1			2.6	76	1579	II	25	34.7	135.5	2.6
47	1240	III	24			3.1	77	1586	I	18	36.	136.8	6.
48*	1241	V	22	35.25	137.25	4.3	78	1589	III	21	34.8	138.2	3.6
49	1245	VIII	27			2.6	79	1592	X	18			3.6
50*	1257	X	9	35.2	140.9	4.3	80*	1596	IX	4	33.3	131.7	4.
51	1293	V	28			4.5	81	1596	IX	5	34.8	135.7	4.3
52	1317	II	24	35.1	135.8	3.6	82	1597	IX	10	33.7	131.6	3.
53	1325	XII	5	35.6	136.1	3.6	83*	1605	I	31	A. 34.3 B. 33.	140.4 134.9	6. 6.
54	1331	VIII	15	33.7	135.2	4.3	84	1611	IX	27	37.5	139.7	4.
55	1350	VII	6			2.6	85*	1611	XII	2	37.7	144.3	6.5
56*	1360	XI	22	33.4	136.2	4.3	86*	1614	XI	26	37.5	138.	5.7
57*	1361	VIII	3	33.	135.	7.0	87	1615	VI	26	35.7	139.7	3.1
58	1369	IX	7			2.5	88*	1616	IX	9	38.1	142.	4.3
59*	1403			33.7	136.5	4.3	89	1619	V	1			2.6
60*	1408	I	21	33.8	136.9	4.3	90	1628	VIII	20			2.5

(to be continued.)

(continued.)

No.	Date.			Epicentre.		M_k	No.	Date.			Epicentre.		M_k
				φ degree N	λ degree E						φ degree N	λ degree E	
91	1630	VIII	2			3.7	121	1674	IV	15			2.
92*	1633	III	1	35.6	139.2	4.5	122	1675	IV	4			2.
93	1635	III	12			2.5	123	1676	VII	12	34.4	131.7	3.5
94	1639	XII		35.9	136.2	2.5	124*	1676					
95	1640	XI	23	36.2	136.2	3.6	125*	1677	IV	13	38.7	144	6.5
96	1643	XII	6			2.6	126*	1677	XI	4	36.6	141.5	5.1
97	1644	IV				2.	127	1678	X	2	38.6	142.3	5.
98	1644	X	18	39.4	140.1	4.	128	1683	VI	17	36.7	139.6	3.
99	1646	VI	9	37.7	141.7	5.5	129	1683	VI	18	36.8	139.7	4.8
100	1647	VI	16			3.	130	1683	X	20			3.8
101	1648	VI	12	35.1	139.3	4.5	131	1685					3.1
102	1649	III	17	33.7	132.4	4.5	132	1685	XII	29			2.
103	1649	VII	29	36.1	139.7	4.5	133	1686	I	4	34.	132.3	4.3
104	1649	IX	1	35.5	139.6	3.	134	1686	X	3	34.6	137.4	4.3
105	1650	IV	24			3.5	135*	1687	X	22			
106	1658	V	5			2.6	136	1691			36.3	136.3	2.6
107	1659	IV	21	37.2	139.8	3.7	137	1694	VI	19	40.2	140.2	4.3
108	1661	XII	10			2.5	138	1694	XII	12			2.5
109	1662	VI	16	35.3	136.	5.5	139	1696	VI	1			
110*	1662	X	31	31.7	132.	5.5	140*	1696	II	25			
111	1664	I	4			2.	141	1697	XI	25	35.8	139.5	4.
112	1664	VIII	3			3.5	142*	1703	XII	31	34.7	139.8	6.6
113	1665	VI	25			2.5	143	1704	V	27	40.4	140.	4.
114	1666	II	1	37.1	138.2	3.	144	1706					
115*	1666	V	31				145*	1707	X	28	33.2	135.9	7.
116	1667						146	1710	IX	13			3.0
117	1667	VIII	22			3.	147	1710	X	3	35.5	133.8	3.5
118	1668	VIII	28			2.	148	1711	III	19	35.4	133.8	3.5
119	1669	VI	29			2.	149*	1711	XII	20	34.3	134.	3.7
120	1670	VII	21	35.4	139.2	3.	150	1714	IV	28	36.7	137.8	3.

(to be continued.)

(continued.)

No.	Date.			Epicentre.		M_k	No.	Date.			Epicentre.		M_k
				φ degree N	λ degree E						φ degree N	λ degree E	
151	1715	II	1	35.4	136.6	2.7	181	1766	III	8	40.8	140 6	4.0
152	1717	V	13	39.	142.7	5.5	182	1767	V	4			
153	1718	II	26			2.6	183*	1768	VII	22			
154	1718	VIII	22			3.1	184	1768	IX	8			2.
155	1718	X	5			2.6	185	1769	VII	22			2.
156	1723	XII	18	33 2	130.4	2.6	186	1769	VIII	29	32.3	132.	5.
157	1725	V	29			3.5	187	1770	V	27	38.6	142.	5.
158	1725	VI	17	36.4	136.4	2.	188*	1771	IV	24			5.1
159	1725	VIII	14	35.8	138.1	2.5	189	1772	VI	3	39 3	142.7	5.
160	1725	XI	8.9	32.7	129.8	2.6	190	1778	II	14	34.6	132.7	3.5
161	1729	VIII	1	37.6	137.6	4.	191*	1780					4.3
162	1731	X	7	37.9	140.6	3.5	192	1782	VIII	23	35.1	139.7	4.8
163	1732	XII	21			2.6	193	1782	IX	21			2.5
164	1733	IX	18			3.5	194	1784	VIII	29			2.5
165	1735	IV	6			2.	195	1789	V	10	32.9	134.5	5.
166	1736	IV	30	38.3	140.8	2.6	196*	1791	V	13			
167	1739	VIII	16			4.	197*	1792	V	21	32.8	130.3	3.
168*	1741	VIII	28	41.5	139.4	4.	198*	1792	VI	13	43.6	140.3	4.
169	1746	V	14			4.	199*	1793	II	8	40.7	140.	4.
170	1749	V	25	33.4	132.2	4.3	200*	1793	II	17	38 3	142.4	5.5
171	1751	III	26			3.	201	1799	VI	29	36.6	136.6	3.0
172	1751	V	20	37.2	138.	3.5	202	1801	V	26	35.3	140.	
173	1755	III	29			2.6	203	1802	XII	9	37.8	138.4	3.5
174	1755	IV	21			2.6	204*	1804	VII	10	39.	140.	4.5
175	1760	V	15				205	1810	II	4			
176	1762	III	29			2.	206*	1810	IX	25	39.9	139.9	3.5
177*	1762	X	31	38.1	138.7	3.5	207	1812	IV	21	33.8	132.5	4.
178*	1763	I	29	40.8	142.	5.	208	1812	XII	7	35.4	139.6	3.5
179	1763	III	11	40.7	142.	5.3	209	1814	XI	22			2.6
180*	1763	III	15			4.5	210	1815	III	1	36.4	136.5	2.7

(to be continued.)

(continued.)

No.	Date.	Epicentre.		M_k	No.	Date.	Epicentre.		M_k
		φ degree N	λ degree E				φ degree N	λ degree E	
211	1819 VIII 2	35.2	136.3	5.	241	1857 X 12	33.8	132.8	3.
212	1820			2.	242	1858 IV 9	36.1	137.2	4.
213	1821 IX 12			2	243		36.2	136.3	3.
214	1821 XII 13	37.4	139.5	2.5	244	1858 IV 23	36.6	138.2	2.
215	1823 X 23	40.	141.1	2.	245	1859 I 5	34.7	131.8	2.
216	1826 VIII 23	36.2	137.3	2.6	246	1859 III 9 ?	35.9	139.6	2.
217	1828 V 26	32.8	129.9	2.	247	1859 X 4	34.7	131.9	2.
218	1828 XII 18	37.6	138.9	4.	248*	1861 X 21	37.7	141.6	3.
219	1830 VIII 19	35.	135.7	3.	249*	1863 IX 20			2.
220	1831 XI 13	33.2	130.3	2.5	250	1864 III 6	35.	134.8	3.
221	1833 V 27	35.5	136.6	3.	251	1872 III 14	34.8	132.	4.5
222*	1833 XII 7	38.7	139.2	5.	252	1874 II 28	43.9	141.6	3.
223	1834 II 9	43.3	141.4	3.	253	1880 II 22			2.
224	1835 VII 20	37.9	141.9	5.5	254	1881 X			
225	1836 IX 5			2.	255	1886 VII 23	37.1	138.4	2.4
226	1841	35.	138.5	3.	256	1887 VII 22	37.7	139.	2.6
227	1843 III 9	35.7	139.1	3.5	257	1889 VII 28	32.8	130.7	2.8
228*	1843 IV 25	41.8	144.8	7.	258	1890 IV 16	34.3	139.3	2.6
229	1847 V 8	36.7	138.2	5.	259	1891 X 28	35.6	136.6	7.0
230	1848 I 11	33.2	130.3	2.	260	1892 XII 9	36.9	136.6	1.9
231	1848 I 13	40.7	140.6	2.	261*	1893 VI 4			3.5
232	1853 I 26	36.5	138.1	2.	262	1893 IX 7	31.3	130.5	3.0
233	1853 III 11	35.8	139.1	3.3	263	1894 I 4			2.
234	1854 VII 9	34.8	136.2	4.	264*	1894 III 22			6.
235*	1854 XII 23	34.1	137.8	7.	265	1894 VI 20			5.2
236*	1854 XII 24	33.2	135.6	7.	266	1894 X 22	39	140.1	4.8
237	1854 XII 26	33.4	132.1	4.3	267	1895 I 18	35.9	140.4	4.8
238	1855 XI 11	35.8	139.8	4.	268	1896 IV 2	37.5	137.3	3.5
239*	1856 VIII 23	42.	141.1	4.	269*	1896 VI 15	39.4	144.4	5.4
240	1857 VII 14	34.8	138.2	3.	270	1896 VIII 31	39.5	140.7	5.2

(to be continued.)

(continued.)

No.	Date.	Epicentre.		M_k	No.	Date.	Epicentre.		M_k
		φ degree N	λ degree E				φ degree N	λ degree E	
271	1897 I 17	36.6	138.2	2.9	301*	1915 XI 1	38.8	143.2	5.2
272	1897 II 20	37.8	141.6	5.9	302	1916 II 22	36.4	138.4	2.3
273*	1897 VIII 5	38.2	143.7	5.6	303	1916 XI 26	34.6	135.	2.8
274	1898 IV 23	38.8	142.3	5.8	304	1917 V 18	35.2	138.1	2.8
275	1898 V 26			3.7	305*	1918 IX 8			6.1
276	1898 VIII 10	33.5	130.2	3.3	306*	1918 XI 8	44.5	151.5	5.1
277	1898 IX 1				307	1918 XI 11	36.5	137.8	2.4
278	1899 III 7	34.	136.2	5.4	308	1921 XII 8			4.5
279	1900 III 22	36.	136.2	3.6	309	1922 IV 26	35.7	139.7	4.0
280	1900 V 12			4.8	310	1922 XII 8	32.8	130.1	3.2
281	1900 XI 5	34.	139.5	3.8	311	1923 I 14			2.9
282	1901 VI 24			6.0	312*	1923 IX 1	35.	139.8	6.0
283*	1901 VIII 9	40.3	141.8	5.7	313	1924 I 15	35.5	139.2	4.6
284	1902 I 30	40.3	141.8	5.1	314	1925 V 23	35.7	134.8	4.3
285	1903 VIII 10			1.7	315	1927 III 7	35.6	135.	5.1
286	1905 VI 2	34.2	132.3	5.4	316	1927 X 27			1.
287	1905 VI 7	34.8	139.2	4.2	317	1929 XI 20			2.7
288	1908 V 13	33.4	138.3	5.6	318	1930 XI 26	35.	138.9	4.3
289	1908 VII 11			3.3	319	1931 IX 21	36.	139.2	3.7
290	1909 III 13	35.3	140.9	6.7	320*	1933 III 3	39.1	144.2	8.3
291	1909 VIII 14	35.4	136.3	4.1	321	1935 VII 11	35.	138.3	3.4
292	1909 VIII 29				322	1936 II 21	34.6	135.7	3.6
293	1909 XI 10	32.1	133.1	6.0	323	1936 XII 27	34.3	139.2	3.1
294	1910 VII 24	42.5	140.8	3.2	324	1938 I 12	33.6	135.2	4.3
295	1910 IX 8			2.	325	1938 V 23	36.7	141.5	5.3
296	1911 VI 15	29.	129.	8.0	326	1938 V 29	43.5	144.3	2.
297	1913 VI 29	31,6	130.5	3.0	327*	1938 XI 5	37.1	141.3	3.2
298	1914 I 12	31.6	130.7	2.6	328*	1939 III 20	32.4	131.8	3.7
299	1914 III 15	39.5	140.4	3.1	329*	1939 V 1	40.	139.8	3.5
300	1914 III 28	39.8	140.9	1.9	330*	1940 VIII 2	44.1	139.2	2.

(to be continued.)

(continued.)

No.	Date.	Epicentre.		M_k	No.	Date.	Epicentre.		M_k
		φ degree N	λ degree E				φ degree N	λ degree E	
331	1941 VII 15	36.7	138.3	3.0	336	1943 IX 10	35.4	134.1	4.8
332*	1941 XI 19	32.2	132.3	4.3	337	1943 X 13	36.8	138.2	2.2
333	1943 III 4	35.6	134.2	3.	338*	1944 XII 7	34.	137.1	6.8
334	1943 III 5	35.6	134.1	3.	339	1945 I 13	34.8	137.2	4.
335	1943 VIII 12	37.2	139.8	2.2	340*	1946 XII 21	33.	134.8	6.5
					341	1948 VI 28	36.1	136.2	4.7
					342	1949 XII 26	36.7	139.7	3.2

Table II. Japanese Seismic Intensity Scale.

0; No feeling: too weak to cause human feeling, to be registered only by seismographs.

I; Slight: to be felt only feebly by persons at rest or by those who are observant to an earthquake.

II; Weak: to be felt by most persons, causing slight shaking of windows and Japanese latticed sliding doors (Shōji).

III; Rather strong: to cause shaking of houses and buildings, heavy rattling of windows and Japanese latticed sliding doors, swinging of hanging objects stopping sometimes pendulum clocks and moving of liquids in vessels. Some persons are so frightened as to run out of doors.

IV; Strong: to cause strong shaking of houses and buildings, overturning of unstable objects, spilling of liquids out of vessels.

V; Very strong: to cause cracks in the brick and plaster walls, overturing of stone lanterns and grave stones etc. and damaging of chimneys and mud-and-plaster warehouses. Landslides in steep mountains are to be observed.

VI; Disastrous: to cause demolition of Japanese wooden houses of more than 1%; intense landslides, fissures on the flat ground accompanied sometimes by spouting of mud and water in low fields.

VII; Ruinous: to cause demolition of almost all the houses, large fissures and fault are to be observed.

43. 有史以來の地震活動より見たる我國各地の地震危險度及び最高震度の期待値

地震研究所　河　角　　廣

地震國の國民にとつて最大の關心事は地震の危險度であり，それに應じての對策が第一に要望されるわけである。さりながら地震豫知不可能な現狀に於ては絕對的な危險度を知る事は出來ないが，故きを溫ねて過去の地震活動の趨勢から，統計學的に將來を豫測する事は不可能ではない。最近建築基準法制定に伴ふこの要請に應へて，有史以來の破壞的地震の活動を調査し，我國各地の古來の震度別地震回數を求め，その平均頻度に基づき最高震度の期待値を計算した。

この調査は筆者年來の研究に基づく，地震の大きさと震度分布との關係((7)及び(9)式)を用ひて出來たもので，それにより先づ第一表に示す古來の破壞的地震の記錄よりその地の震度を定め，その分布により，震央及び地震の大きさを決定した。次にそれによつて逆にすべての點の震度が決定出來るので，之等342箇の地震による全國各地(經度緯度各半度每の網目點350點)の震度を定め，各點について，震度5（强震）以上の震度別地震回數を統計した。その結果は第2圖に圖示してある。之を各地の記錄期間の長さで割つて平均頻度を求め，それらの震度別頻度の關係から，その割合では一定期間にそれ以上の强さの地震の起る確率が1に達しないと云ふ條件を充す最高震度の期待値を求めた。この結果を震度の等値線で第3圖に示した。但しその一定期間の長さ(t)としては75年(A)，100年（B）及び200年（C）をとつた。耐震構造物の壽命に應じて適當な（t）を選び基準震度をとることが出來るであらう。

但し實際の震度はその地の地盤の良否に關係するから震度の地盤係數を忘れてはならない。

尙筆者の用ひた地震の大きさ Mk と Richter, Gutenberg の M との關係(5)も最近の研究により記してある。

44. *On the Period and the Amplitude of Microseismic Movement.*

By Fuyuhiko KISHINOUYE,

Earthquake Research Institute.

(Read April 17, 1951.—Received June 20, 1951.)

The word 'microseisms' includes many kinds of continuous earth oscillations, but in this paper microsisms of period between 3 and 10 sec are discussed. F. Omori1) divided the microseisms at Hongō, Tokyo, in three classes with the periods of oscillations; q : 2.9 sec., Q_1 : 4.5 sec., Q_2 : 7.5 sec. And many investigators classified the osciliations by weather or other conditions at the time when the miscroseisms occurred2). But as the relation between the conditions and miscroseisms might not be clear, the writer studied the period and amplitude of microseisms in order to classify them.

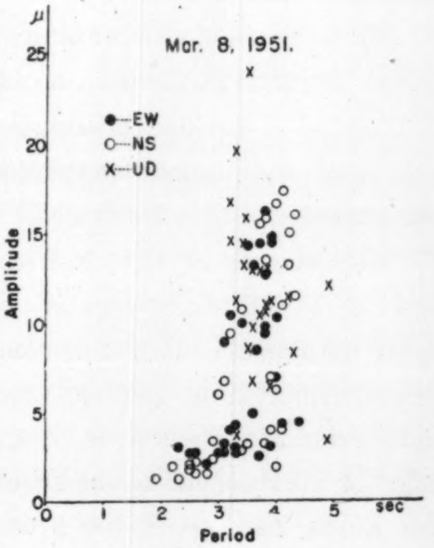

Fig. 1.

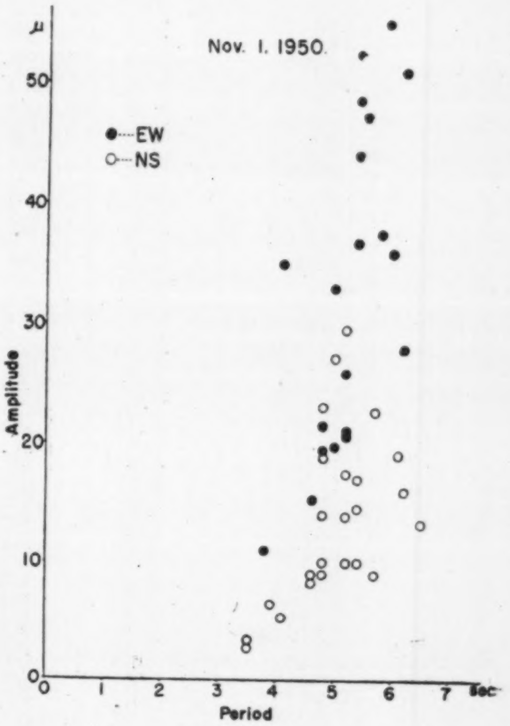

Fig. 2.

---

1) F. OMORI, *Bull. Earthq. Inv. Comm.*, **3** (1909), 1–35.

2) B. GUTENBERG, *Die seismische Bodenunruhe*, Berlin, 1924.
M. H. GILMORE, *Trans. Amer. Geophys. Un.*, **27** (1946), 466–473.

The records of microseisms used in this study were obtained with the portable tromometers designed by the writer[3] for the recording of microseisms set at the Tokyo University, Hongō, at the Koishikawa Botanical Garden, and at the Tokyo Astronomical Observatory, Mitaka, for the investigation on the propagation of microseismic waves[4].

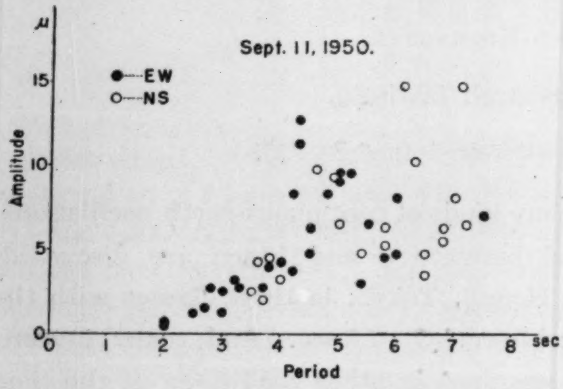

Fig. 3.

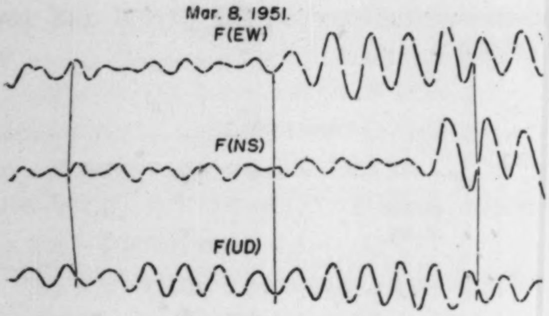

Fig. 4. ($\frac{1}{3}$ the actual)

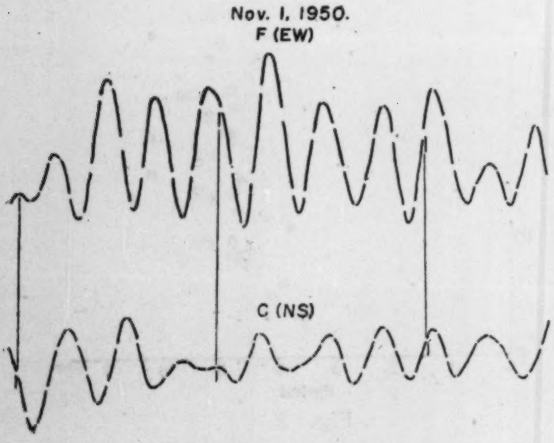

Fig. 5. ($\frac{1}{3}$ the actual)

From these records, correlation diagrams of period and amplitude were made. The diagrams were classified into three kinds, example of which are shown in Figs. 1, 2, and 3. The portions of seismograms which correspond to Figs. 1, 2 and 3 are inserted as Figs. 4, 5 and 6. The frequency-distributions of periods of microseisms can also be classified (Figs. 7, 8 and 9) as above. The characteristics of the classes are as follows:

Microseisms of the 1st kind are almost regular in form of oscillation, period of oscillation being 3-4 sec., and the double amplitudes less than 20μ.

Microseisms of the 2nd kind Figs. 2, 5 and 8 are regular and large oscillations with the frequency-distribution of periods sharp and maximum at about 6 sec. Amplitudes of microseisms of the 1st and 2nd kinds vary as if the ground resonated at the period of 4 sec. or 6 sec..

---

3) F. KISHINOUYE, *Bull. Earthq. Res. Inst.*, **20** (1942), 215-219.

4) R. IKEGAMI and F. KISHINOUYE, *ditto*, **27** (1949), 75-80.

Microseisms of the 3rd kind (Figs. 3, 6 and 9) are irregular in form and the frequency-distribution of periods is not sharp. Microseisms of this kind may be mixed oscillations of those of the 1st and 2nd kinds. The amplitudes may have a somewhat linear relation with the periods.

In all cases the prevailing periods varied in a small amount. For instance, the period of the 2nd kind changed between 5 and 6 sec. in the data used in this study. The cause of the variation is yet unknown.

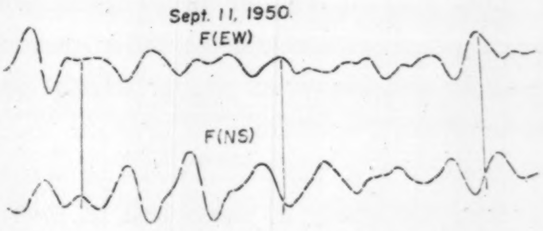

Fig. 6. ($\frac{1}{3}$ the actual)

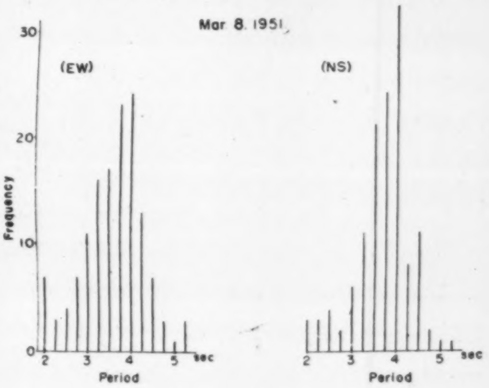

Fig. 7.

Looking at the frequency-distribution of periods, two periods, 4 sec. and 6 sec, can be found at any rate, and for the 1st kind only the 4 sec period and for the 2nd kind the 6 sec period were prevailing. For the 3rd kind both periods occurred simultaneously.

Concerning the change of periods of microseisms, R. Ikegami and the writer[5] have obtained the following results: Microseisms of 4 sec period were observed when the centre of cyclones were on the sea to the south of Tokyo. When the sea to the northeast of Tokyo was very rough, the period and amplitude of microseisms became large at

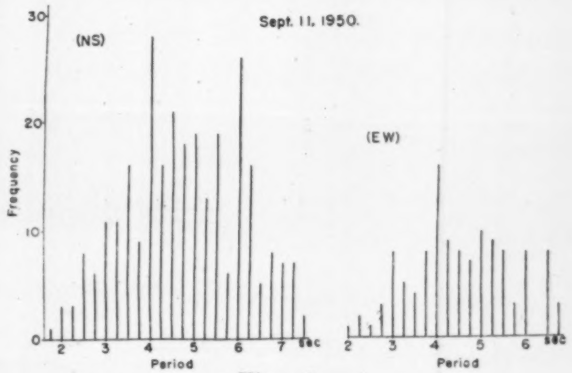

Fig. 8.

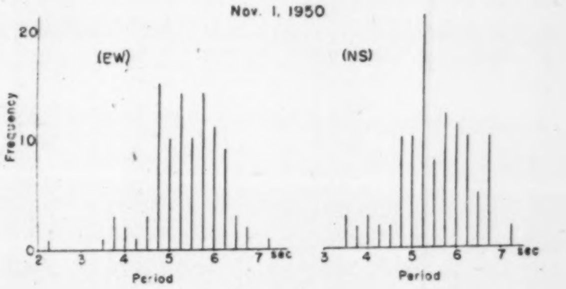

Fig. 9.

---

[5] R. Ikegami and F. Kishinouye, *Bull. Earthq. Res. Inst.*, **29** (1951), 305–312. R. Ikegami, *ditto*, 313–325.

Tokyo. And the variation of their periods was found to be in some relation with the velocity of propagation[6].

From the above results, microseisms seem to be combined with two kinds of oscillations of periods 4 sec and 6 sec. It is remarkable that the periods of microseisms are almost always definite everywhere in the world. Recently the periods came to be considered as one half of the periods of sea waves[7]. The theory may be favourable, for winds and waves can be regarded as uniform everywhere and sea waves caused by winds may be similar in periods. But the writer has been informed that at some place microseisms of other periods occurs[8]. If it is true, microseisms may be considered as proper oscillations of the ground excited by meteorological or oceanic conditions, otherwise oscillation of the ground due to proper oscillations of sea waves. Then the writer must attend to such conditions concerning the study of the origin of microseisms.

Acknowledgement. The writer expresses his thanks to Mr. J. Moroga for his assistance in this study.

The cost of this study was defrayed from the Grant in Aid for Fundamental Scientific Research.

---

44. 土地の脈動の周期と振幅について

地震研究所　岸上冬彦

東京附近の観測について土地の脈動を調べ，周期と振幅との關係や周期の頻度分布を見ると，4秒周期のもの，6秒周期のものと，4秒と6秒と同時に含むものとに分けられた。其等を第一種，第二種，第三種の脈動と名付けた。第一種と第二種は夫々4秒又は6秒に於て振幅が大きく，土地の自己振動が此等の周期に，共振したように見える規則正しい振動である。第三種は振幅が周期に凡そ比例し，振動記象の形も周期の頻度分布も他の種と明らかにちがう。

---

[6] R. IKEGAMI and F. KISHINOUYE, *Bull. Earthq. Res. Inst.*, **28** (1950), 118.

[7] M. S. LONGUET-HIGGINS *Phil. Trans. Roy. Soc. London*, **243** (1950), 1–35.

[8] At the symposium on microseisms at the general meeting of the Seism. Soc., Japan, on May 24, 1951, Dr. T. Hirono of the Central Met. Obs. of Japan, reported that the periods of microseisms at Onahama, Fukushima, are always only 2 sec.

45. *On the Temperature and Viscosity of the Fresh Lava Extruded in the 1951 Oo-sima Eruption.*

By Takeshi MINAKAMI,

Earthquake Research Institute.

(Read April 17, 1951.—Received June 15, 1951.)

1. Introduction.

It is well known that the nature of volcanic eruption depends closely on the chemical and petrological characters of extruded lavas, or in other words, on whether they are basalt, andesite or dacite etc.. In fact, the eruptions of the Hawaiian volcanoes, Oo-sima and Miyake-sima, Asama and Sakura-zima, and Usu show respective characteristics in the manner of extrusion of lava and in their subsequent phenomena, and on the other hand, their extruded lavas in recent years are respectively characterized by the olivine basalt, the oversaturated basalt (or tholeitic basalt), pyroxyne andesite and dacite. However, what seems to be an important clue for determining the nature of eruption is the viscosity of intruded and extruded lavas which vary greatly according to their chemical compositions including gas content and their temperature.

Although several experiments on this problem have been conducted up to the present, our knowledge concerning the fluidity of molten lava at the instant of extrusion is yet quite unsatisfactory, the experiment based on actual phenomena being not always simple in its method.

We can, however, obtain some information from laboratory experiments, though the nature of rocks dealt with in the laboratory does not always represent that of fresh lava at the moment of ejection, specially in respect to the volatile gas content.

In order to obtain data on this problem, the writer conducted measurements of the temperature and viscosity of molten lava which spurted out in the 1951 eruption of Oo-sima, which shall be the main subject of the present report.

2. The Nature of the 1951 Lava-Flows of Oo-sima.

In the 1950 eruption of Oo-sima which lasted for 70 days from July 16 to September 23, the molten lava which first buried the pit crater, 200 m in its depth, and then filled the atrio of the inner somma, overflowed at last from the two lower places of this somma forming several narrow streams. After a period of quiescence for four months, the Oo-sima volcano resumed its activity at the beginning of February 1951, when the molten lava spouted abundantly in the manner of fountain as was the case in the 1950 eruption and, forming several lava streams, descended the flank of the inner somma towards the sand sea or the caldera surrounded by the outer somma.

Since the sources of extruding lava and these lava flows were easy of approach, the writer, on March 19, 1951, carried out measurements of the temperature of fresh lava and obtained data necessary for determining its viscosity, including the flowing velocity of the lava flow. It will be needless to say that, for the determination of the relation between the two quantities, it is necessary to measure the temperature as precisely as possible, because the viscosity of lava depends remarkably on its temperature. For this purpose, the temperature measurements were carried out with the aid of two kinds of thermo-junctions, one being platinum—platinum-rhodium and the other copper—constantan.

Since the lava streams were in a molten and incandescent state, and we could easily poke a wooden stick into them, we were able to measure not only the temperature of the surface but also that of the interior part.

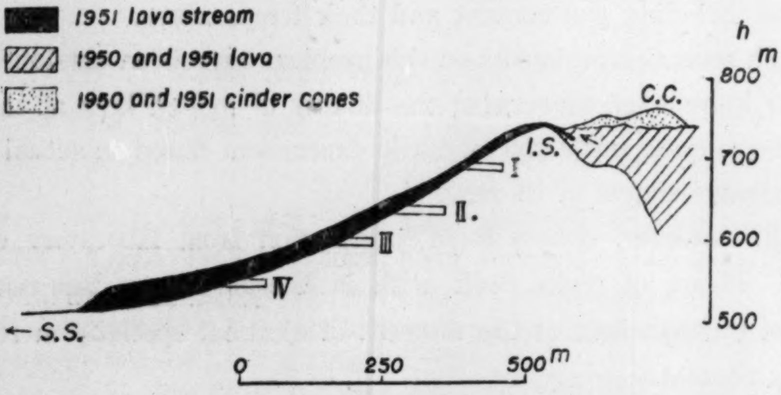

Fig. 1. The 1951 lava stream along the flank of the inner somma and the four positions for the present observation.

Since both ends of the junction used for the present investigation were protected by an unglazed porcelain tube, of which the end was closed, it took at least ten minutes to obtain the equilibrium temperature between the molten lava and the hot junction. However, we had to carry out the measurement within several seconds for the temperature of the lava which was flowing at a speed of over 50 cm per second. For this purpose, 5 cm of the closed end of the tube was cut off and the hot junction was put in direct contact with the molten lava. As the result of that, it was possible to reduce the time required for measurement to five seconds.

During the present investigation, four lava flows, each of which formed a narrow stream, were descending the western flank of the inner somma, of which the inclination is measured as 35° at the upper part and gradually decreases in steepness towards its base. Of these lava streams, the writer chose a stream flowing on the southern most side as the main object of the present investigation, and measured various elements at four positions of this flow including the upper stream near the source.

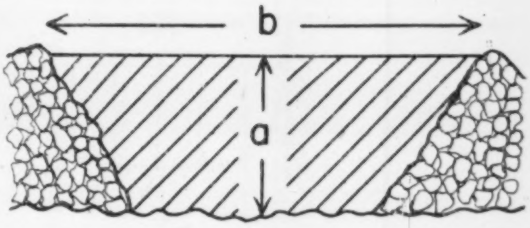

Fig. 2. The section of the flowing lava stream.

The thickness of various parts of this stream was measured by a wooden stick which we could easily poke into it. On the basis of the investigation just mentioned, the profile or the section of the stream was made as is shown in Fig. 2. In this figure, the banks at both sides of the stream were formed by accumulation of lava blocks of rather small sizes which fell off from the lava flow in its downward course.

The lava stream from its source to a distance of 300 m, including the upper three positions (I, II and III) was in a molten and jelly-like state. However, in the vicinity of position IV, its surface which is 5° or 7°C cooler than its interior, was covered by a thin layer, 2–3 cm in thickness, of gum-like character, and at the distance of more than 500 m from its origin, its surface came to be markedly cooled and covered by solidified lava blocks of small size, forming the aa-type flow, though the inner part was still fluidal and incandescent, being 1000°C–1030°C in its temperature. Therefore, the flowing velocity at the surface of the middle stream between 300 m and 500 m from its source was to some extent, reduced as compared with the flowing velocity at a slightly deeper part, and as is illustrated in Fig. 3, the velocity distribution of a section of the stream shows features varying in accordance to the distance from its source.

The elements necessary for determining the viscosity of lava, namely, the thickness, width, maximum flowing velocity and inclination of the slope, each of which was measured at the four positions mentioned above, are given in Table I.

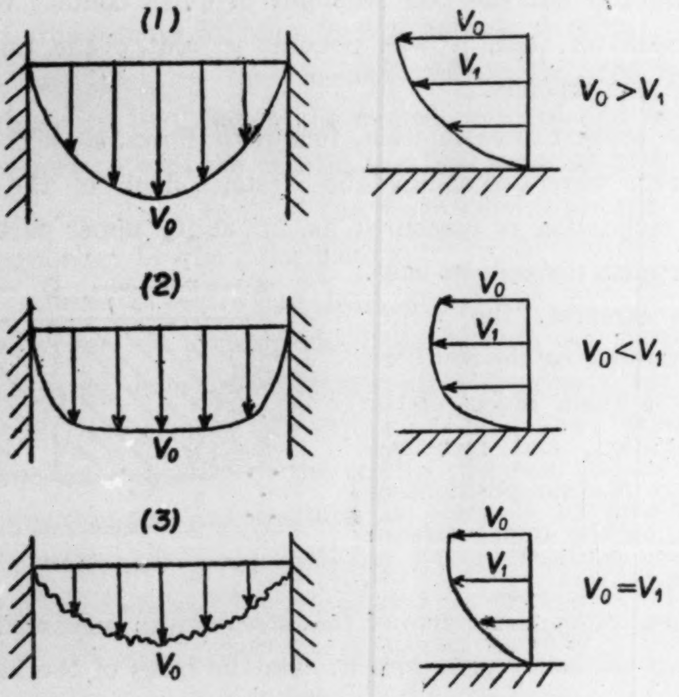

Fig. 3. Distribution of the flowing velocity of the lava stream.

V_0, surface velocity. V_1, inner velocity.
(1) upper stream. (2) middle stream.
(3) lower stream.

Table I. Elements for determining the viscosity of flowing lava.

Position	Thickness (a)	Width	Inclination (φ)	Max. flowing vel. (v)
I	31 cm	110 cm	35°	102±8 cm sec.
II	50	160	27	35±4
III	77	210	16	15±3
VI	130	250	11	8±2

3. The Viscosity and Temperature of the Fresh Lava Extruded in the 1951 Eruption of Oo-sima.

To simplify the calculation of the viscosity of lava, the problem is here dealed with as a two-dimensional flow, and with respect to the form of the section of the stream, the following two cases are considered. In the first case, in which the stream is remarkably wide and of a constant thickness, and therefore hardly affected by the internal friction given from both sides, the viscosity coefficient (η') is given by the following relation with the elements in Table I;

$$\eta' = \frac{\rho g \sin \varphi}{2v} a^2 .$$

In the other case, in which the form of the section is replaced by a semi-circle and its radius is taken similar to the thickness of the stream, the relation between the viscosity coefficient and the other elements is expressed by the following formula,

$$\eta = \frac{\rho g \sin \varphi}{4v} a^2 .$$

The values of the viscosity coefficient based on the above extreme cases are connected in the following relation,

$$\eta' = 2\eta .$$

Therefore, seeing that the present research is to examine the number of the figure of the viscosity coefficient, it will be sufficient for this purpose to apply either the former assumption or the other. Although, strictly speaking, the actual case assumes an intermediate character between the above two extreme cases, the latter assumption is naturally more adaptable to the 1951 lava stream dealt with in this paper than the former. Thus the values of the viscosity coefficient given in Table II are calculated by the latter formula.

Table II. The viscosity coefficient and temperature of the molten lava measured at a lava stream of the 1951 Oo-sima eruption.

Position	Vis. coef. (η)	Temperature (θ)
I	5.6×10^3 poises (C.G.S.)	1125°C
II	1.8×10^4 〃	1108 〃
III	7.1×10^4 〃	1083 〃
IV	2.3×10^5 〃	1038 〃

It must be added that each element concerning the lava flow given in Table I includes an observation error of about ten per cent, so the true value of the viscosity is estimated to range from twice to half of the obtained value.

As mentioned already, the temperature of the flowing lava was precisely measured at the four positions (I–IV), the result of which is shown in Table

II, together with the viscosity coefficient at the respective temperature. As will be seen clearly in Table II, the fresh lava at the position I, 10 m distant from its outpouring source shows 1125°C in its temperature and 5.6×10^5 poises in its viscosity, and that at the lower position IV, 400 m distant from the origin, 1038°C and 2.3×10^5 poises respectively.

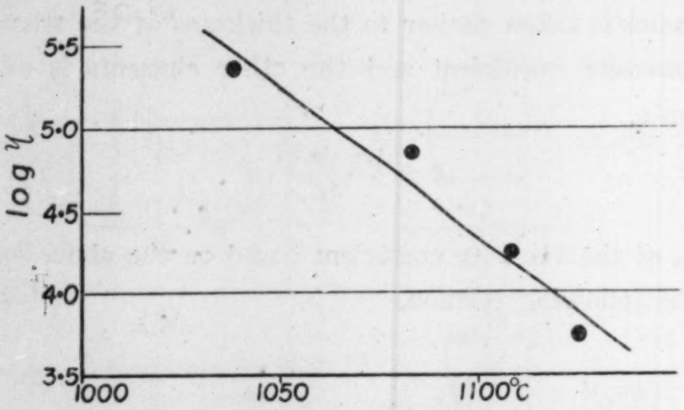

Fig. 4. Temperature and viscosity coefficient of the Oo-sima lava measured in the present investigation.

The relation between the two kinds of quantity, temperature and viscosity, based on the present investigation, is expressed by the following formula at the range of temperature (θ) from 1000°C to 1150°C;

$$\log \eta = 6.155 - 0.0181\ (\theta - 1000),$$
$$1150°\mathrm{C} \geq \theta \geq 1000°\mathrm{C}.$$

From the above relation, it becomes clear that the viscosity of the present Oo-sima lava is doubled when the temperature at 1100°C or 1000°C falls by 11°C or 16°C respectively.

On the basis of the present investigation, it may be concluded that the 1951 lava of Oo-sima was 1200°–1150°C in its temperature and nearly 10^3 poises in its viscosity in the course of intrusion into the vent and at the instant of extrusion.

Regarding the 1950 lava of this volcano, S. Murauchi[1] and I. Murai with their associates[2] measured its temperature with the aid of an optical pyrometer and its viscosity from its flowing velocity, the result of which is as follows;

Table III.

Temp.	Vis. coef.
1060°	1.7×10^5 C.G.S.
1050	3.3×10^7 〃
1040	1.3×10^5 〃

---

[1] S. MURAUCHI, *Natural Science and Museum*, **12** (1950), No. 3 and 4.

[2] I. MURAI, N. NASU and A. SUGIMURA, *Read at the Meeting of E.R.I.* (Oct., 1950).

Since an optical pyrometer was used for their temperature measurement, and the result thus includes an observation error of 30°C or 50°C at least, it is impossible to compare the 1951 lava with the 1950 lava with respect to their temperature and viscosity. However, the 1950 lava, at least in form of its flow, which overflowed after it had filled the atrio of the inner somma, seems to have been of lower temperature and of larger viscosity than those of the 1951 flow.

It must be added that R. Takahasi and T. Nagata[3] in 1937, gave 5×10^4 poises at 1060°C for the molten lava in the Oo-sima pit creater, from the observation of standing gravity wave on its surface and from the temperature measurement by means of an optical pyrometer.

It will be necessary to refer to the chemical and petrological properties of the present Oo-sima lava. According to H. Tsuya, R. Morimoto and J. Osaka[4] the 1951 lava is chemically and petrologically almost similar to those which flowed out in our historical age including the 1950 lava, being all characterized by the oversaturated basalt (or tholeitic basalt) of 52-53% in silica content, bearing no olivine.

4. The Pressure which acted under the Oo-sima Volcano in its 1951 Eruption.

To what degree did the pressure act under the Oo-sima volcano or on the lower end of the vent in the present eruption?

During the period from March 10 to 31, 1951, the molten lava was outpouring incessantly in a fountain fashion from four sources located near the western summit of the inner somma, of which the diameter was estimated at 70 cm-120 cm respectively. From the present field investigation, it may be assumed that these jet-like sources were connected one another under the ground at the depth not exceeding 300 m, and the main conduit had an estimated diameter of 2-3 m. Moreover, the elevating velocity of molten lava passing through the main conduit is also estimated at 2-3 m per second from the outpouring velocity at the four sources.

Moreover, on April 6, 1951, a fountain-like eruption as may be seen in Fig. 8, occurred in the central part of the inner-somma and the height of the lava fountain and the diameter of its jet were estimated at about 10 m and 3-4 m respectively.

---

[3] R. Takahasi and T. Nagata, *Bull. Earthq. Res. Inst.*, **15** (1837), 1047.

[4] H. Tsuya, R. Morimoto and J. Osaka, *Personal Communication.*

However, the pressure exerted at the part slightly deeper than the lower end of the conduit and necessary in ejecting the molten lava in the manner just mentioned, may be approximately expressed as follows;

$$P = P_1 + P_2 ,$$

$$P_1 = \rho g l , \qquad P_2 = \frac{4\eta v l}{a^2} + \frac{1}{2}\rho v'^2 ,$$

$$\text{where} \quad v' \doteqdot \frac{2}{3} v \ .$$

In the above expression, the first term (P_1) represents the normal ground pressure at the depth l and second (P_2) the pressure necessary for driving the lava with a velocity v at the central axis of the circular conduit.

The ratio of the second term to the first ranges from 1/10 to 1/100 for the present two cases according to the above relation. In other words, if the subterranean pressure increases by one tenth of the normal ground pressure, it will be possible enough to cause such an eruption as in the present Oo-sima.

On the other hand, noticeable forerunning phenomena including earthquakes originating from the Oo-sima volcano did not appear in the 1950 eruption as well as in the 1951 one, notwithstanding the fact that those eruptions were the most remarkable ones on record of this volcano. This fact may be reasonably interpreted by the marked fluidity of the intruded and extruded lava and accordingly by the moderate pressure acting under this volcano even at its eruption.

In addition, as regards eruptions caused by such moderate pressure, it also depends on whether a conduit through which the fresh lava may extrude, exists or not, namely, on the structure of the volcano.

However, we do not lack facts supporting the assumption mentioned above, which were made clear from observations of volcanic activities of various types in Japan as well as in the other parts of the world.

For examples, the 1944 eruption of Volcano Usu[5], in Hokkaido, was preceded not only by severe earthquakes localized near the active crater, but also by marked rise of the ground, which resulted in the birth of a new mountain. The extruded lava in this eruption is characterized by the dacite of 70% silica content and of extraordinary high viscosity, forming a lava dome 100 m high without flowing. Moreover, since this volcano had no opened crater through which the fresh lava could extrude, the 1944 as well as the 1910 eruption[6] both occurred from the newly opened craters at the base of this volcano. Judging from these phenomena, it is quite natural to assume that a remarkable pressure was at work under this volcano not only in the midst of eruption, but also in the course of intrusion or at the pre-volcanic stage.

---

[5] T. MINAKAMI, *Bull. Earthq. Res. Inst.*, **25** (1947), 65, 71; **27** (1949), 123, 129; **8** (1950), 145.
T. MINAKAMI, T. ISHIKAWA and K. YAGI, *Bull. Volcanol.*, **11** (1951), 45.

According to the eminent work of A. Lacroix[7], local earthquakes lasting for about two weeks preceded the 1902 eruption of Volcano Pelée, which resulted in the total lost of 26000 habitants of Saint-Pierre. Seeing that the extruded lava forming a 'Spine' and the dome at this eruption were in an exceedingly viscous state and not in a fluidal state, it will be reasonable to infer that an enormous pressure brought forth the extrusion.

Mt. Asama is noted for its severe paroxysmal eruption of the Vulcanian type which is characterized by rapid ejection of a large amount of incandescent lava for a moment in form of lava-block and volcanic bomb including fine ejecta. Recent eruptions of Asama always occurred in the summit crater, at the bottom of which the fresh lava usually appeared. The Asama lava[8] extruded in our historical time, is characterized by the two pyroxyne andesite with 60–62% silica, and its viscosity at the moment of extrusion, has an intermediate character between the Usu and Oo-sima lavas. However, the forerunning phenomena of the Asama eruption[9] including earthquakes and topographical deformations both of volcanic origin were not so remarkable as in the case of Usu, but they have been observed manifestly through instrumental investigations.

Finally, we must touch on the Hawaiian volcanoes, of which the eruptions are characterized by abundant outflow of fluidal lava from their summit craters and sometimes from their flank fissures. According to chemical and petrological researches, the extruded lavas are mainly of the olivine basalt containing 48–50% silica.

T. A. Jaggar, R. H. Finch and G. A. Macdonald[10] of the Hawaiian Volcano Observatory have studied strenuously the volcanic phenomena of these volcanoes for about 70 years. By their researches, it may be said that the eruptions of Kilauea and Mauna-Loa are not always preceded by numerous earthquakes and marked land deformations so evidently as in the cases of Usu and Asama etc., though T. A. Jagger and R. H. Finch[11] succeeded in predicting several eruptions of Mauna-Loa including the 1935, 1940 and 1942 eruptions on the basis of the periodic cycle of its volcanic activity and sometimes of predominant earthquakes.

---

[6] F. OMORI, *Bull. Imp. Earthq. Inv. Comm.*, **5** (1911), 1 and **9** (1920), 41.

[7] A. LACROIX, *La Montagne Pelée et ses Eruption*, (1904).

[8] H. TSUYA, *Bull. Earthq. Res. Inst.*, **11** (1935), 575.

[9] T. MINAKAMI, *Bull. Earthq. Res. Inst.*, **20** (1942), 431 ; *Bull. Volcanol.*, **10** (1950), 59.

[10] T. A. JAGGAR, R. H. FINCH and G. A. MACDONALD, *Vol. Let. etc.*,

On the other hand, R. L. Nichols[12] obtained the viscosity of the Alika and 1887 flows of Hawaii by means of their flowing velocities with the result of 4.3×10^{4} poises for the former and 4.8×10^{4} poises for the latter, though their exact temperature could not be made clear. However, it must be added that these values of viscosity given by Nicholas does not represent those just after the outflow from the crater or at the instant of eruption. Moreover, H. S. Palmer[13] gave the viscosity coefficient of 1.5×10^{-1} poises for the same lava flow, which differs too much from that given by the former investigator. For this problem, R. H. Finch[14] concluded from his steady observations concerning the features of the molten lava at Kilauea and Mauna-Loa, that its viscosity must range from 10^{3} to 10^{4} poises. Judging from the nature of their eruption and the chemical character of extruded lava, his estimation may be reasonable and harmonizes with our expectation.

If the erupting lava is so fluidal as to be less than 10^{2} poises in its viscosity, the Hawaiian eruption may have been caused by a pressure only slightly larger than the normal ground pressure, and as the result, without any marked forerunning phenomena, as in the present case of Oo-sima.

Although we are lacking in the exact and abundant knowledge of the physical properties of intruding lava it would be safe to say that the richer the silica content is, the less fluidal the fresh lava at the moment of eruption and in the course of intrusion is.

In any case, it may be said that the fluidity of fresh lava is closely related not only with the nature of eruption but also with its forerunning and subsequent phenomena.

5. Comparison of the Present Result with the Laboratory Experiment.

Since we have not much opportunity available for investigating the character of the molten lava in field, several investigators have made the experiments of

---

11) G. A. MACDONALD, *Am. Jour. Sc.*, **241** (1943), 241; P. E. SCHULZ, *Bull. Geol. Soc. Am.*, **54** (1943), No. 6.

12) R. L. NICHOLS, *Jour. Geol.*, **67** (1939), 290.

13) H. S. PALMER, *Bull. Hawaiian Vol. Obs.*, **15** (1927), 1.

14) R. H. FINCH, *Vol. Let.*, **480** (1943), 2.

viscosity and temperature of lava remolten in laboratory. Of these laboratory works, K. Kani[15] carried out one concerning various basaltic rocks including the Oo-sima lava forming the outer somma of this volcano, of which the chemical composition is almost similar to that of the 1951 lava.

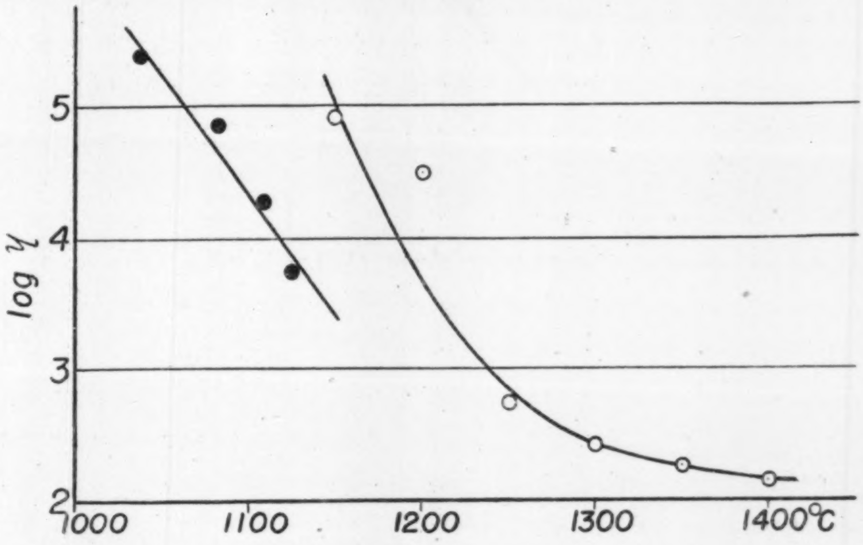

Fig. 5. Comparison of the present result with the Kani experiment: closed circle, the present result, opened circle, K. Kani's result.

In Fig. 5, the result of his experiment is compared with that of the 1951 lava in the natural state, with which the foregoing paragraphs dealt. A glance of this figure shows that the remolten lava is exceedingly viscous as compared with the lava in field as the same temperature, or to be more exact, the former is nearly 5×10^4 poises and the latter 4×10^3 poises both at the temperature of 1150°C.

It is, however, believed that the discrepancy between the above two cases, the one in the natural state and the other in laboratory, is mainly caused by the richer content of gas in the former. Although a more suitable interpretation is necessary for the result obtained in laboratory, valuable informations concerning the characters of the fresh lava will be surely supplied from experiments on remolten rocks.

In addition, the relation concerning the mobility or viscosity of various lavas and their chemical composition, specially their silica content as mentioned in the previous paragraph, is supported, at least in its qualitative character, by the

---

[15] K. Kani, *Proc. Imp. Acad.*, **10** (1934), 79.

laboratory experiment made by M. Volarovic[16]. According to his research, the viscosity of basalt (49% silica), Techenite (51% silica) and andesite (64% silica) is 1.1×10^3, 1.3×10^4 and 4.0×10^4 poises respectively at the temperature of 1150°C.

The writer proposed in this report an hypothesis concerning the relation of the mobility of fresh lava with the nature of eruptions of respective volcanoes and their forerunning phenomena, but there must be many faults in this research. It is, however, his desire that this difficult but interesting problem be developed with the aid of precise and newly planned observations of the active volcanoes throughout the world.

45.　1951年に噴出した大島熔岩の温度と粘性について

地震研究所　水　上　武

火山の噴火は各々の火山によつて夫れ夫れ著しい特性を示すことはよく知られている事實である。これを決定する重要な要素として噴出時の熔岩の粘性が著しく相異することを擧げることができる。1951年の大島の噴火に際して，噴出直後の熔岩流について，白金及び白金ロヂウムの熱電對を用いて熔岩流の表面及びその内部の溫度を測定し，同時に斜面を流れる速度から粘性係數を求め，兩者の關係を明かにした。その結果今回の大島熔岩の噴出時の或は噴出直前の溫度は 1150°C，その粘性係數は 10^3 poises (C. G. S.) 程度であつたことが明かになつた。これ位の小さい粘性の熔岩を地下から押し上げるために必要な壓力は安山岩質熔岩の場合に較べて桁外れに小さい事を示すものである。

一方ハワイ火山の噴出時の熔岩の溫度は 1200°C 位で大島のそれとは餘り相違しないが，その粘性は 1 poises 程度と推定されているから大島の約1千分の1に相當する。淺間山，櫻島等の安山岩質熔岩の噴出時の粘性は餘りよく測定されていないが，10^7 poises 以上，その溫度は 1100°～1050° 位と推定されている。最近の有珠山の活動に於いて熔岩丘を形成した熔岩や，プレ火山の1902年のドームの熔岩は 10^{10} poises 程度と考えられる。

今迄に測定された結果によれば，玄武岩質の熔岩は酸性熔岩に較べてやや高い溫度で噴出している事を示してをり，從つてこの溫度の相異からその粘性が必然的に相異するわけではあるが，それだけでは以上に示した粘性が著しく相異する事實は量的には到底說明されない。從つて瓦斯含有量の多少を考慮に入れた噴出熔岩の物質的相異に基づくものと考えざるを得ない。この事はヴオラロヴイッチ氏の行つた熔融火山岩の溫度と粘性に關する實驗に於いても，同一溫度に於いてシリカ成分の少ないもの程粘性が小さい結果を得ている。

また可兒氏の大島元村熔岩についての實驗結果は，今回の熔岩の化學成分と殆んど同じであるにかかわらず 1150° の溫度に於いて今回の測定結果の數十倍の大きい粘性を示している。これは實驗室內に於ける再熔融岩石と新鮮な熔岩とでは瓦斯含有量が著しく異なることによるものであろう。

---

[16] M. Volarovic, *Comp. Rend. Acad. Sc. U.R.S.S.*, I (1932), 564.

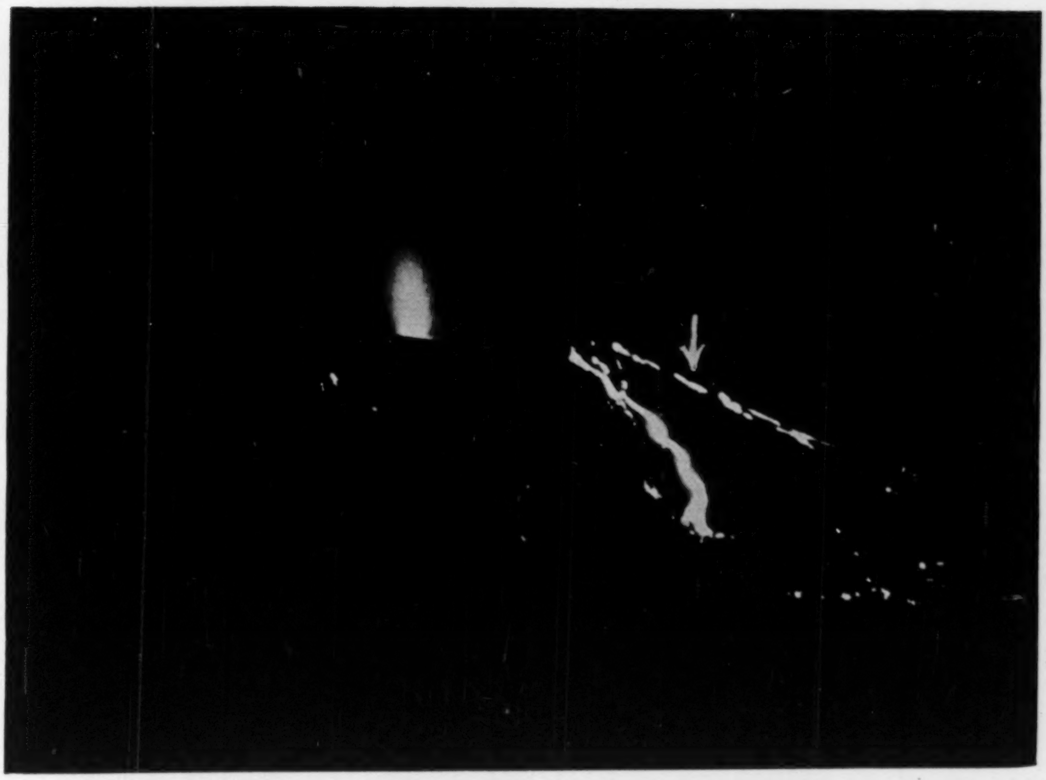

Fig. 6. The lava streams flowing on the flank of the inner somma on March 19, 1951.
I, The lava stream dealt with in the present investigation.

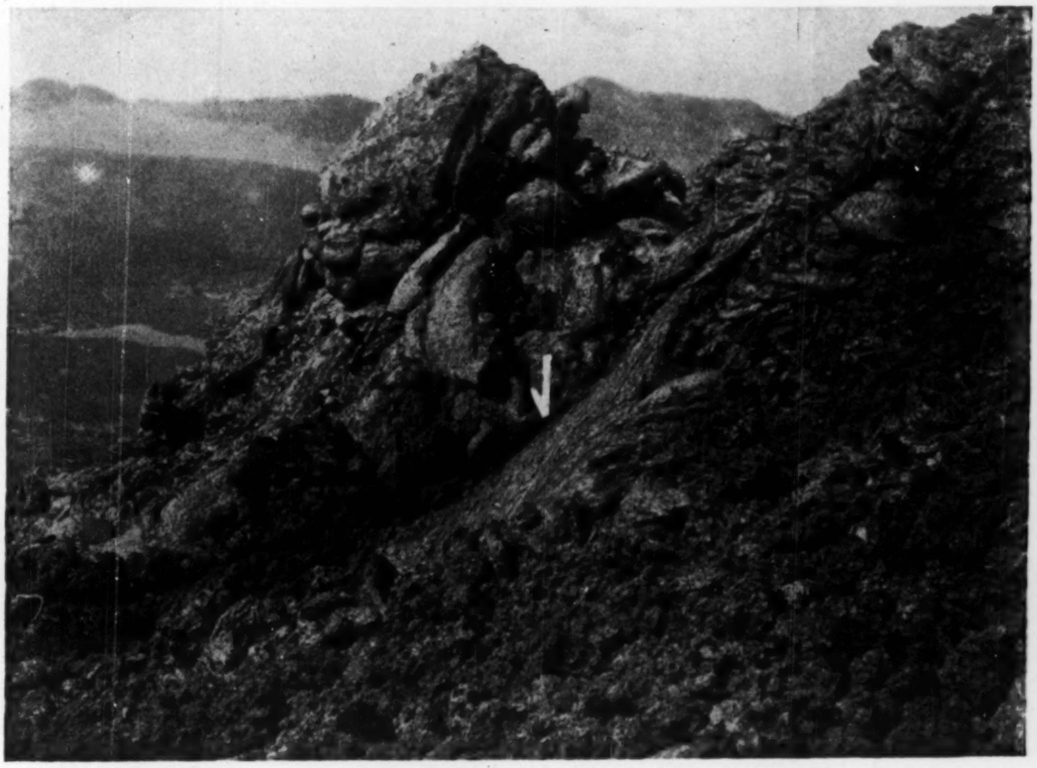

Fig. 7. The lava river near its source on March 18, 1951.
(arrow mark indicates the flowing lava.)

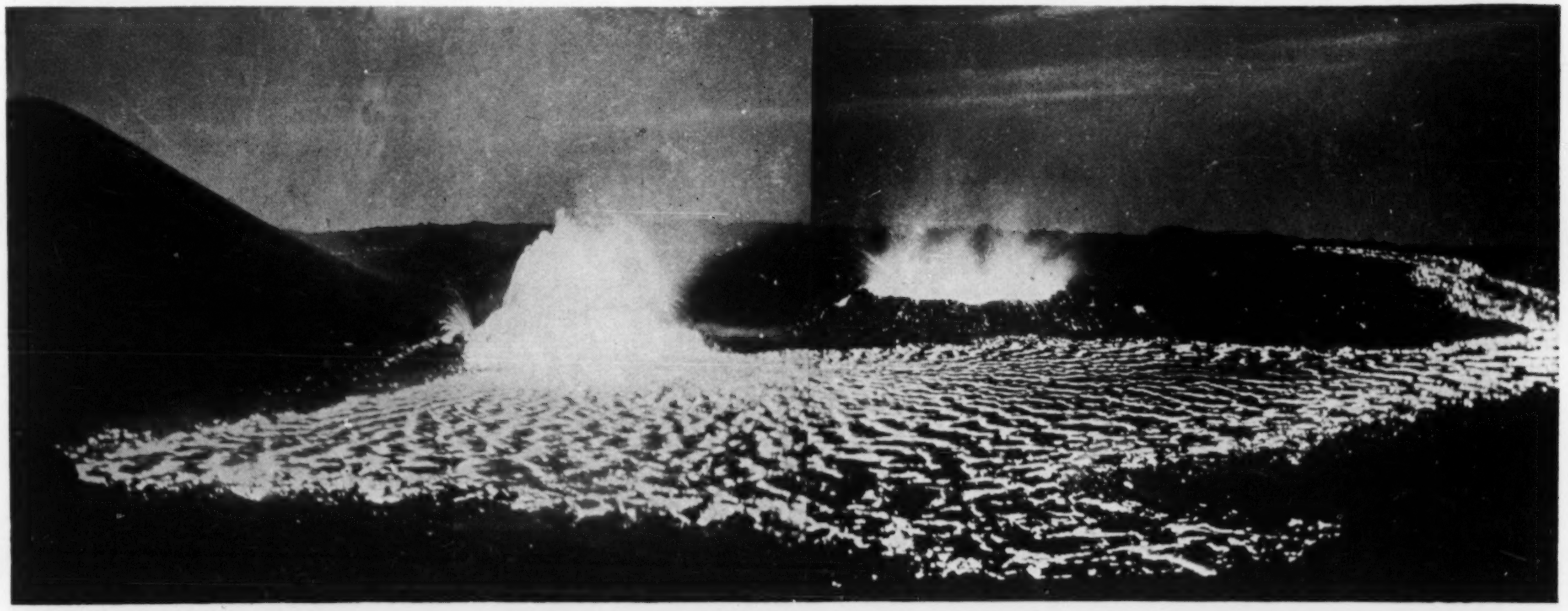

Fig. 8. The lava fountain and lava pool in the inner somma on May 7, 1951. (Photo. Y. Takagi.)

46. *Changes in Magnetic Dip that Accompanied the Activities of Volcano Mihara.*

(The second report)

By Tsuneji RIKITAKE,

Earthquake Research Institute.

(Read May 15, 1951.—Received June 20, 1951.)

As has been reported in his previous paper[1], the writer conducted a series of geomagnetic dip survey over Ooshima (Oo-sima) Island in connexion with last year's eruption of Volcano Mihara and found out remarkable changes in the earth's magnetic field. Though Volcano Mihara has been quiet for several months after the sudden stop of its eruption on Sept. 23, 1950, a new activity took place in the beginning of February this year. The activity continued up to the beginning of May, though the eruption tended to become intermittent towards the end of the activity. Of course, a considerable amount of new lava welled up during the period, the lava overflowing the central cone as before and filling up the interior of the first and second somma.

In order to investigate the geomagnetic state of the volcano, the writer and his associates executed the third survey during the period from March 28 to April 1 with the same instrument which was used in previous surveys.

The results are shown in Table I. Diurnal variation and general changes in the earth's magnetic field are eliminated by means of the same method as used in the previous paper where Kakioka Magnetic Observatory is taken as the standard point. Thus $\delta\theta$ in Table I may be regarded as the local anomalous changes in Ooshima Island during the period from surveys II to III. Unfortunately, however, many stations in the vicinity of the crater has been covered by the new lava-flow, making it impossible for the writer to reoccupy them. As shown in the Table, changes in dip-angle are generally small except at the station No. 12 where the change amounts to -52.7 *minutes* of arc. The station, however, was surrounded by a new lava-flow which already cooled down to some extent. Since the point nearest the new lava was only $2\,m$, the change should be attributed to the intense magnetization of the lava and be excluded from the discussion of general aspects.

---

[1] T. RIKITAKE, *Bull. Earthq. Res. Inst.*, **29** (1951), 161.

Table I.

No. of Station	Survey III		$\theta_{III}-\theta_{II}$	$\theta_{k,\,III}-\theta_{k,\,II}$	$\delta\theta$
	Date	Dip			
1	1951 Mar. 31st 09h 59m	48°40′.9	−2′.0	−1′.7	−0′.3
2	09 18	49 32 .1	−1 .1	−1 .8	+0 .7
3	08 33	48 18 .4	−3 .7	−1 .4	−2 .3
4	29th 17 48	51 16 .4	−2 .2	+0 .4	−2 .6
5	—	—	—	—	—
6	—	—	—	—	—
7	30th 14 23	53 30 .4	−3 .8	−1 .6	−2 .2
8	—	—	—		—
9	—	—	—	—	—
10	29th 18 31	52 37 .1	−3 .0	+1 .0	−4 .0
11	—	—		—	—
12	30th 15 05	48 56 .0	−54 .3	−1 .6	−52 .7
13	16 04	48 40 .3	−0 .5	−1 .4	+0 .9
14	31st 13 19	48 23 .8	−0 .6	−1 .5	+0 .9
14′	13 40	50 16 .1	−2 .3	−1 .5	−0 .8
15	14 50	51 05 .1	−2 .8	−1 .5	−1 .3
16	15 43	48 36 0	−1 .1	−1 .5	+0 .4
17	11 15	46 42 .9	+0 .1	−1 .7	+1 .8
18	—	—	—	—	—
19	29th 15 49	48 08 .8	−1 .9	−2 .5	+0 .6
20	14 29	49 45 .6	−0 .9	−3 .4	+2 .5
21	13 19	48 40 .5	−4 .4	−4 .2	−0 .2
22	11 13	47 40 .5	−1 .8	−3 .9	+2 .1
23	11 59	49 57 .1	−3 .2	−4 .7	+1 .5
24	28th 10 09	47 25 .4	−3 .2	−3 .1	−0 .1
25	Apr. 1st 11 11	47 27 .6	−2 .7	−1 .1	−1 .6
26	12 14	46 57 .5	−2 .0	−0 .9	−1 .1
27	13 20	47 59 .0	+1 .7	−1 .3	+3 .0
28	15 24	48 18 .9	−3 .6	−1 .4	−2 .2
29	—	—		—	—
30	Mar. 30th 13 18	52 47 .5	−1 .5	−2 .1	+0 .6
31	—	—	—	—	—
32	—	—	—	—	—
33	11 17	51 23 .9	−3 .3	−1 .9	−2 .4
34	10 15	50 37 .5	−6 .1	−1 .5	−4 .6
35	29th 10 30	46 41 .8	−1 .8	−3 .2	+1 .4
36	—	—	—	—	—

Though the changes at the station along the coast are small and scattered, we see a systematic decrease in dip-angle near the central part of the island as shown in Fig. 1, the maximum decrease amounting to 4.6 *minutes* of arc. Taking into account the accuracy of measurement, we may say that a slight decrease in magnetic dip occurred in the central part of the island during the period from September, 1950 to April, 1951. On the other hand, we found out remarkable decreases in dip-angle during the period from July to September of 1950, the maximum decrease amounting to as much as 30 *minutes* of arc. Since the changes of III-II resemble those of II-I in their modes, we presume that some changes that occurred in the volcano at the early period of the activity have been maintained up to now and slightly enlarged. If we are allowed to ascribe the decreases in the dip-angle to the loss of rock-magnetism due to temperature-rise in the volcano, we may say that such a high temperature is still kept up in the interior of Volcano Mihara.

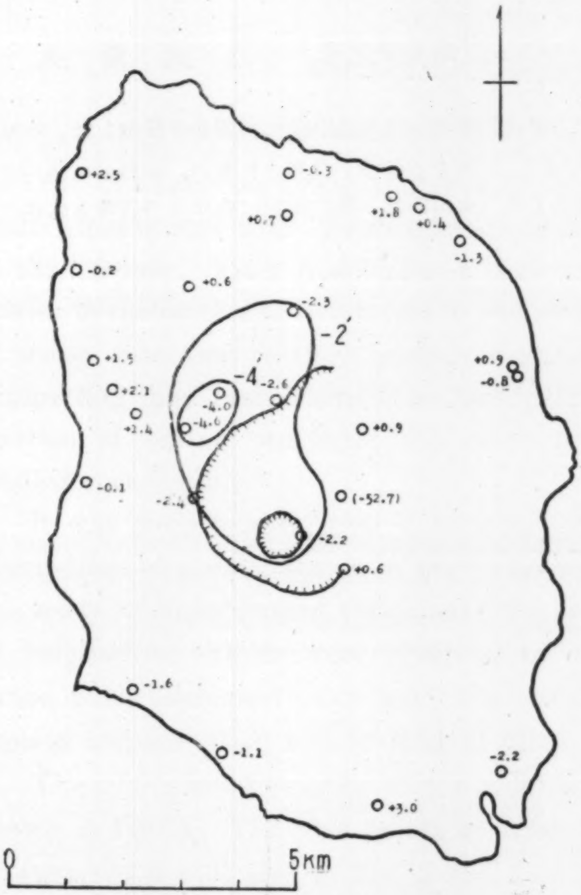

Fig. 1. Changes in dip-angle during the surveys II and III.

In conclusion, the writer wishes to express his hearty thanks to Professor H. Tsuya and Dr. T. Nagata for their encouragement in the course of this study. To Dr. S. Imamiti and Mr. M. Hirayama of the Kakioka Magnetic Observatory who placed magnetic data at the writer's disposal, the writer's cordial thanks are also due. The writer also wishes to express his appreciations to Mr. S. Saito and Miss Y. Hishiyama who assisted the writer in the field-measurement.

46. 三原火山の活動に伴う地磁氣變化（第2報）

地震研究所　　力　武　常　次

1951年3月28日より4月1日の期間に，伊豆大島の第三回地磁氣伏角測量を實施した。昨年9月の測量と比較して島の中央部に於て，最大4.′6に達する減少が見出されたが，前報告に述べた變化にくらべればいちじるしく小さい。この結果より，火山内部の熱的狀態は昨年9月當時と大差ないと推定される。

---

47. *The Result of Observation of Wave-velocity in the Ground.*

By Kiyoshi Kanai,

Earthquake Research Institute.

(Read Mar. 20, May 15, June 19, 1951.—Received June 20, 1951.)

The problem concerning the velocity distribution of seismic waves in the earth already was paid attention to by many seismologist from the early part of this century. They had believed that as there are two or three discontinuities in the earth and two layers in the earth crust, in each layer the velocity of waves increases as they advance further into the interior. Since seismic prospecting has been carried on very actively recently, the velocity-depth relation of seismic waves at the part very near the earth surface has been studied considerably[1].

It was quite recently that it became necessary for us to know the velocity distribution of seismic waves in the interior of the earth in order to promote the study of underground earthquake motions[2]. For this purpose, the velocity of longitudinal waves were observed by causing artifical earthquake. The range of measurement was from the earth-surface to 450 meter under the ground and the place was at Hitachi Mine, Ibaraki Prefecture in Japan.

The geological formation of the neighbouring part of observing station is shown in Fig. 1. The shot points and observing points in the first and second experiments is indicated in Fig. 2 and 3 as well as in Table I and II. Owing to the circumstance of the place, the observing point could not be taken on a line veritcal to the shot point, thus making the analysis of the observation very complicated.

In the first observation the Yokogawa-type 3-elements oscillograph was used and in the second a 6-elements oscillograph of the same type. The speed

---

[1] N. Nasu, "Studies on the Propagation of an Artificial Earthquake Wave....", *Bull. Earthq. Res. Inst.*, **18** (1940), 289, (in Japanese).

N. Haskell, "The Relation Between Depth, Lithology and Seismic Wave Velocity in Tertiary Sandstones and Shales", *Geophysics*, **6** (1941), 318.

L. Faust, "Seismic Velocity as a Function of Depth and Geologic Time," *Geophysics*, **16** (1951), 192.

[2] K. Kanai, T. Tanaka, "Observations of the Earthquake-motion at the different Depths of the Earth. I", *Bull. Earthq. Res. Inst.*, **29** (1951), 107.

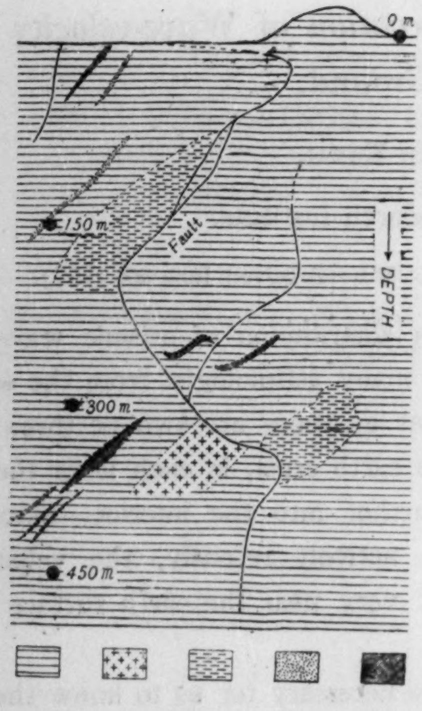
0 m
150 m
300 m
450 m
Fault
DEPTH
Amphi-bolite
Biotite schist
Chlorite schist
Sericite schist
Epidia-base.

Fig. 1. Geological formations of the neighbouring part of observing stations at Hitachi Mine, Ibaraki Prefecture in Japan.

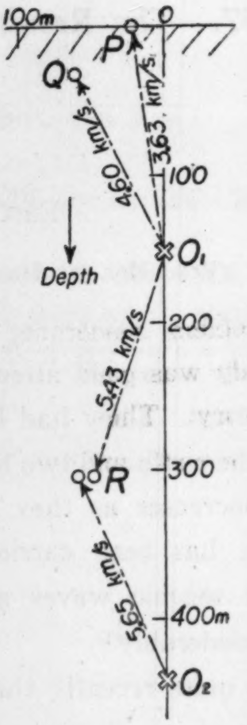
100m
0
P
Q
3.63 km/s
4.60 km/s
100
O₁
Depth
200
5.43 km/s
300
R
5.65 km/s
400m
O₂

Fig: 2. Vertical section view of the positions of shot points (O_1, O_2) and observing points (P, Q, R) in the first experiment.

of recording paper was 4 m/sec—2 m/sec, with 1/1,000 sec time marking. As an explosive, 1 kg of dynamite was used.

The result of the first observation is shown in Fig. 2 and denoted in Table I. From Fig. 2 and Table I it is found that, within the depth of about 250 m, seismic wave increases its velocity according as it goes further. Beyond that

Table I. The relation between shot points and observing points, and the result of the first experiment.

Shot points		Observing points					Travel-time (sec)	Mean velocity (km/sec)
	Depth (m)		Depth (m)	Distance from the shot point (m)				
				Horiz.	Vert.	Direct		
O_1	152.5	P	0	22	152.5	154	0.0424	3.63
〃	〃	Q	31.0	61	121.5	136	0.0296	4.60
〃	〃	R	303.7	49	151.2	159	0.0293	5.43
O_2	439.2	〃	〃	60	135.5	148	0.0262	5.65

depth velocity seems to remain constant. Its value may be estimated at about 5.5 km/sec.

Table II shows the result of the second observation which was carried out for the purpose of studying the velocity distribution within the depth of 150 m precisely. Seeking the velocity distribution in the ground from Table II, we analysed under the conditions that the velocity in one horizontal plane is

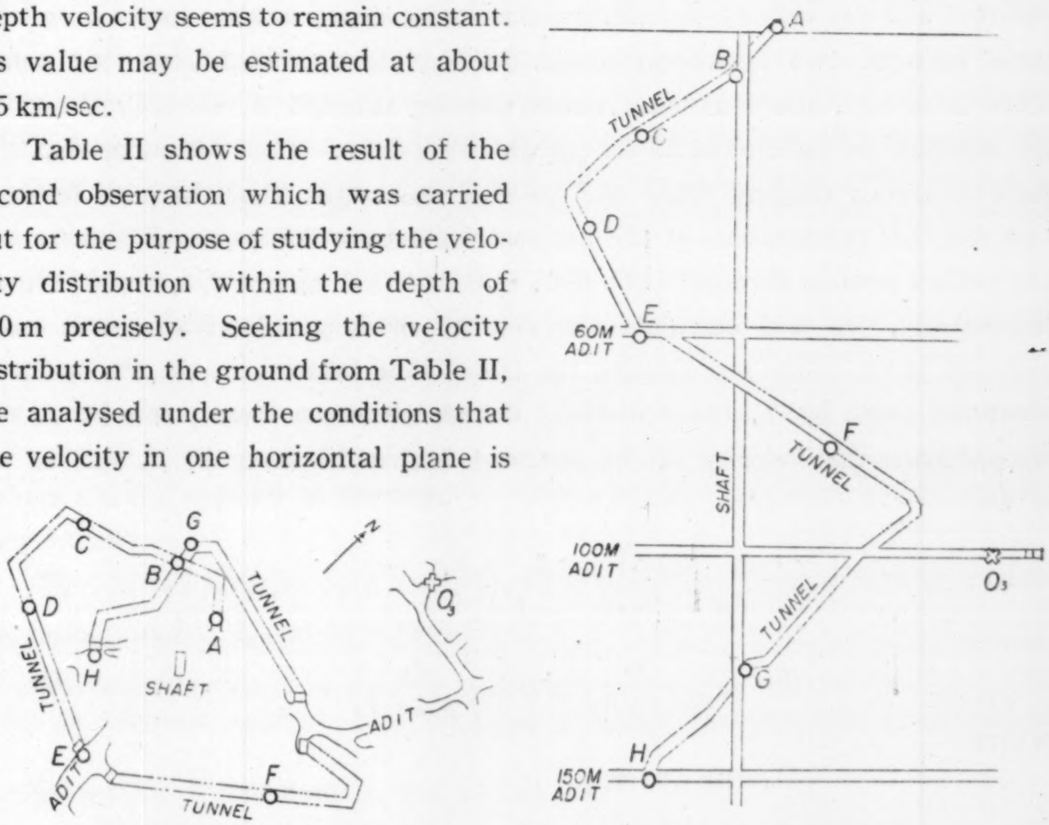

a. Horizontal section view. b. Vertical section view.

Fig. 3. The positions of shot point (O_3) and observing points (A, B,....G, H) in the second experiment.

Table II. The relation between shot point and observing points, and the result of the second experiment.

Shot point		Observing points					Travel-time (sec)		
	Depth (m)		Depth (m)	Distance from the shot point (m)			Observ.		Calcul.
				Horiz.	Vert.	Direct	1 st	2 nd	
O_3	108.0	A	0	46.0	108.0	117.4	0.0368	0.0366	0.0357
〃	〃	B	9.8	53.9	98.2	112.0	0.0309	0.0299	0.0298
〃	〃	C	22.8	75.0	85.2	113.5	0.0298	—	0.0294
〃	〃	D	41.7	85.0	66.3	107.8	0.0267	0.0259	0.0271
〃	〃	E	63.7	81.0	44.3	92.3	0.0232	0.0229	0.0230
〃	〃	F	86.1	54.0	21.9	58.3	0.0148	0.0140	0.0143
〃	〃	G	130.6	51.5	22.6	56.2	0.0135	0.0133	0.0134
〃	〃	H	153.1	73.0	45.0	85.8	0.0200	0.0196	0.0204

constant and the velocity distribution concerning depth is also constant in the layer between two horizontal planes passing through each observing point. That is to say, the horizontal planes passing through A, $B\ldots G$, H and O_3 are assumed to be discontinuous planes of velocity. Then assuming that the path of waves ranging from O_3F to O_3G is straight, that the path between O_3E and O_3H refracts once at the horizontal planes which passes F and G, and the pathes passing through O_3D, O_3C, O_3B and O_3A refract 2, 3, 4 and 5 times respectively, we will calculate the velocity of longitudinal waves in each assumed layer. Now representing the travel time taken from the shot point to observing point by T, the horizontal distance between those points by x, and the thickness and velocity of the assumed horizontal layer by z_s and v_s we obtain

$$x=\sum_1^n \frac{z_s(cv_s)}{\sqrt{1-(cv_s)^2}}=\sum_1^n \frac{z_s V_s}{\sqrt{1-V_s^2}}\,, \quad \ldots\ldots\ldots\ldots\ldots\ldots\ldots (1)$$

$$T=\sum_1^n \frac{z_s}{v_s\sqrt{1-(cv_s)^2}}=c\sum_1^n \frac{z_s}{V_s\sqrt{1-V_s^2}}\,, \quad \ldots\ldots\ldots\ldots\ldots\ldots (2)$$

where

$$V_s(\equiv \sin i_s)=cv_s\,, \quad \ldots\ldots\ldots\ldots\ldots\ldots\ldots\ldots\ldots\ldots\ldots\ldots (3)$$

c is a constant determined by the path of waves which implies $(\sin i_s)/v_s$, i_s the normal angle, and n the number of assumed horizontal layers between the shot point and the observing point.

By means of the successive approximation which we adopted, the velocity of O_3—F layer is calculated using the equation $v_1=\overline{O_1F}/T$. Next the velocity

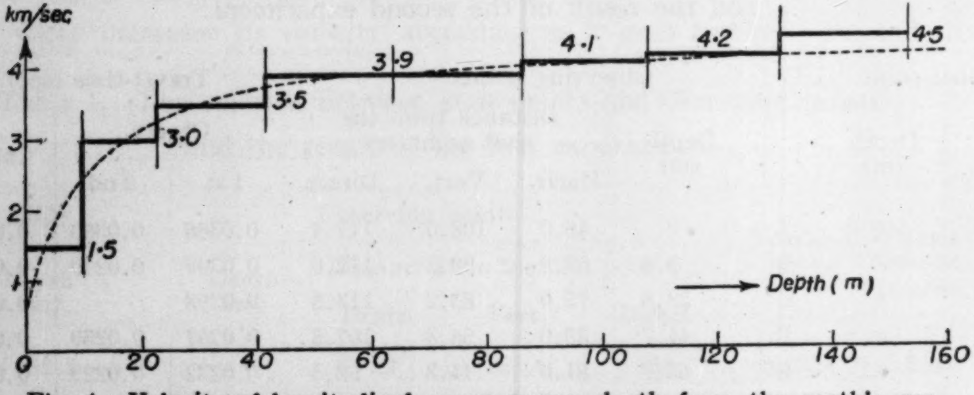

Fig. 4. Velocity of longitudinal waves versus depth from the earth's surface obtained mathematically using the values of experimental result. Broken line represents the calculated result using the empirical formula of v (km/sec) $=0.6\ \{1+718z\,(\mathrm{km})\}/\{(1+96z\,(\mathrm{km})\}$

of $F—E$ layer is obtained from equation (1) applying the trial-and-error method on V_1 and V_2. By placing those values into equation (2), c can be determined. Then after placing c and V_1 into equation (3), we repeat the trial-and-error method till v_1 which was calculated before can be satisfied. By repeating this method the velocity of each layer is given one after another. The results of the calculation are shown in Fig. 4.

When the stepped velocity-depth distribution shown in Fig. 4 is replaced by a curve denoted by broken line in the same figure, its empirical formula becomes

$$v=0.6\times\frac{1+718z}{1+96z} \quad \dots\dots\dots\dots\dots\dots\dots\dots(4)$$

where v is the velocity at the depth z. The units of v and z are km/sec and km respectively.

Next let us examine to what degree the empirical formula satisfies the observation values. Equation (4) results in

$$V=k\,\frac{1+az}{1+bz} \quad \dots\dots\dots\dots\dots\dots\dots\dots\dots(5)$$

where $a=718$, $b=96$, $k=0.6c$, and $c=(\sin i)/v$.
Now, putting the relation of equation (5) into x (the horizontal distance between the shot point and observing point) and T (its travel-time) we get

$$x=\int_{z_1}^{z_2}\frac{Vdz}{\sqrt{1-V^2}}=k\int_{z_1}^{z_2}\frac{(1+az)dz}{\sqrt{\pm z^2(\pm b^2\mp a^2k^2)+2z(b-ak^2)+(1-k^2)}}$$

$$=\frac{k}{\sqrt{\pm b^2\mp a^2k^2}}\left[(1\mp a\alpha)\left\{\begin{matrix}\log\{(z+\alpha)+\sqrt{(z+\alpha)^2-\beta^2}\}\\ \sin^{-1}\left(\frac{z-\alpha}{\beta}\right)\end{matrix}\right.\pm a\sqrt{\pm(z\pm\alpha)^2\mp\beta^2}\right]_{z_1}^{z_2}$$

$$\dots\dots\dots(6)$$

$$T=\int_{z_1}^{z_2}\frac{cdz}{V\sqrt{1-V^2}}=\frac{c}{k}\int_{z_1}^{z_2}\frac{(1+bz)^2dz}{(1+az)\sqrt{\pm z^2(\pm b^2\mp a^2k^2)+2z(b-ak^2)+(1-k^2)}}$$

$$=K\left[\pm b^2\sqrt{\pm(z\pm\alpha)^2\mp\beta^2}+\left(2b-\frac{b^2}{a}-b^2\alpha\right)\left\{\begin{matrix}\log\{(z+\alpha)+\sqrt{(z+\alpha)^2-\beta^2}\}\\ \sin^{-1}\left(\frac{z-\alpha}{\beta}\right)\end{matrix}\right.\right.$$

$$+\frac{\pm\left(\frac{2b}{a}-\frac{b^2}{a^2}-1\right)}{\sqrt{\pm\left(\alpha\mp\frac{1}{a}\right)^2\mp\beta^2}}\log\left\{\frac{2}{z+1/a}\left\{\pm\left(\alpha\mp\frac{1}{a}\right)^2\mp\beta^2\right\}\right.$$

$$+2\left(\alpha\mp\frac{1}{a}\right)+2\sqrt{\pm\left(\alpha\mp\frac{1}{a}\right)^2\mp\beta^2}$$

$$\times\sqrt{\left\{\pm\left(\alpha\mp\frac{1}{a}\right)^2\mp\beta^2\right\}\frac{1}{(z+1/a)^2}+\frac{2(\alpha\mp 1/a)}{z+1/a}\pm 1\Bigg\}\Bigg]_{z_1}^{z_2} \quad \dots\dots\dots(7)$$

where

$$K=\frac{c}{ka\sqrt{\pm b^2\mp a^2k^2}},\quad \alpha=\frac{b-ak^2}{\pm b^2\mp a^2k^2},\quad \beta^2=\alpha^2-\frac{1-k^2}{b^2-a^2k^2} \quad \dots\dots(8)$$

in (6)~(8) the upper and the lower notation represent the case of $(b^2-a^2k^2)>0$ and $(b^2-a^2k^2)<0$ respectively.

And in the case of $(b^2-a^2k^2)=0$, we get

$$x=\frac{k}{b-ak^2}\left[\left\{1-\frac{a(\{1-k^2)-z(b-ak^2)\}}{3(b-ak^2)}\right\}\sqrt{2z(b-ak^2)+(1-k^2)}\right]_{z_1}^{z_2}, \quad \dots(6')$$

$$T=\frac{1}{a(b-ak)}\left[\left\{\left(2b-\frac{b^2}{a}\right)-\frac{b^2\{(1-k^2)-z(b-ak)\}}{3(b-ak)}\right\}\sqrt{2z(b-ak)+(1-k^2)}\right]_{z_1}^{z_2}$$

$$+\frac{\frac{1}{a}\left(1-\frac{2b}{a}+\frac{b^2}{a}\right)}{\sqrt{(1-k^2)-\frac{2}{a}(b-ak)}}\left[\log\frac{\sqrt{P}+\sqrt{Q}}{\sqrt{P}-\sqrt{Q}}\right]_{z_1}^{z_2}, \quad ..(7')$$

where

$$\left.\begin{aligned} P&=\frac{2(b-ak)}{z+1/a}+\left\{(1-k^2)-\frac{2}{a}(b-ak)\right\}, \\ Q&=\left\{(1-k^2)-\frac{2}{a}(b-ak)\right\} \qquad [Q>0] \end{aligned}\right\} \quad \dots\dots\dots\dots(9)$$

From equation (6) we will calculate, using the trial-and-error method, the value of k that can satisfy x, and which is put into equation (7) in order to get T. In other words, the path ranging from the shot point to the observing point, and the travel time taken in this path are given from (6) and (7) respectively. The travel time thus obtained is denoted in the right column of Table II. In this table it is found that the observed value agrees very well with the calculated one within the depth of about 130 m. Therefore it may be said that the empirical formula (4) represents approximately the natural state.

We presume that a discontinuity surface of velocity lies near the depth of 130 m, but the lack of data prevents us from making more complicated discussion on the distribution beyond that depth.

As the result of this investigations is inexplicable by the velocity versus pressure relation for rock[3], we will discuss in the near future the causes of such distribution by examining the property of elastic constants and other properties referring to the samples found there.

In conclusion the author wishes to express his hearty thanks to the personnel of the Motoyama Office, Hitachi Mine, for their kind assistance, and also to Messrs. T. Tanaka, T. Suzuki, K. Osada and Miss S. Yoshizawa without whose help this work could not be done.

47. 地下における彈性波速度の測定結果

地震研究所　金井　清

日立鑛山における地下 130 m 位までの縱波の速度分布は次式の關係で表し得ることがわかつた。

$$v=0.6\times\frac{1+718z}{1+96z} \qquad (1)$$

ここに v は縱波の速度で單位は km/sec, z は地表面よりの深さで單位は km である。

250m 位以下の平均速度は 5.4 km/sec ぐらいとなり，130m 附近に速度の不連續面があるようにも見えるが，データが不足で，これ以上のことは現在のところ言えない。

(1)式の關係は壓力のみでは說明が困難なことがらであるから，そのうちに試驗片について種々の物理的常數を調べてみる豫定である。

なお，日立鑛山一帶の地質構造は，秩父古生層で，御荷鉾層に對比される所謂赤澤層より秩父古生層上部に屬する鮎川層上部に至る一般走向 N 45°E, 西又は東に 70° 內外の傾斜を存する累層より成り，これを東北及び西北の三方より屛擁する火成岩とから構成される。岩石は成層岩の角閃片岩及び角閃岩を主とし絹雲母片岩，綠泥片岩，黑雲母片岩，硅質片岩，結晶質石灰岩等種々の變成岩より成り，火成岩は花崗閃綠岩を主として閃綠岩，變輝綠岩，石英斑岩等の岩脈又は岩床を伴ひ又西方には橄欖岩の大岩脈を見る。

---

[3] D. S. HUGHES and H. J. JONES "Elastic Wave Velocities in Sedimentary Rocks", *Trans. Amer. Geophs. Union,* **32** (1951), 173.

48. *The Result of Observation concerning the Waves caused in the Ground by Building Vibration.*

By Kiyoshi KANAI and Kaio OSADA,

Earthquake Research Institute.

(Read Jan. 17, July 18, 1950.—Received June 20, 1951.)

1. Introduction.

It had been believed that the damping resistance of buildings implies the damping in the material used in structure, the air-resistance and the plasticity of the foundation. But recently we came to have the idea that the dissipation of vibrational energy in the form of seismic waves transmitted into the ground is also a contributory cause,[1] and the theoretical result obtained from this concept was found to agree very well with the various statistics concerning earthquake damage[2]. Naturally the relation of the building to the ground became an important factor in the aseismatic property of buildings.

The present paper treats the experiments conducted in order to ascertain the above-mentioned property. We observed the motion of the ground caused by the vibration of a full-size 3-storied building made for experiments and a small one-storied house of masonry of reinforced concrete blocks. They were located on the Loam Layer in the compound of Architectural Research Institute, Hyakunin-chō, Shinjuku-ku, Tokyo.

2. The case of small one-storied house.

Fig. 1 is the schematic view showing the buildings for vibration experiments and the observing points of the ground. The left part of the figure represents those in the case of the one-storied small house, while the right part those in the case of the full-size 3-storied building.

In the former case vibration was caused by the vertical-type vibrator consisting of 4 wheels set on 2 counter rotating shafts (unbalanced mass = 50 kg, eccentricity = 11 cm) which was installed on the roof floor. Table I indicates the constants of seismographs used in the vibration observation of the ground.

---

[1] K. SEZAWA and K. KANAI, "Improved Theory of Energy Dissipation in Seismic Vibrations of a Structure", *Bull. Earthq. Res. Inst.*, **14** (1936), 164.

[2] K. KANAI and S. YOSHIZAWA, "Relation between the Earthquake Damage of Non-wooden Buildings and the Nature of the Ground. II", *Bull. Earthq. Res. Inst.*, **29** (1951), 209.

Table I. The constants of the seismographs.

	Number	Period (sec)	Geometr. Magnif.
Horizont.	2	3	14
	3	1	180
Vertical	1	0.09	4.5 gal./mm

Observation was made on the points of 0.2, 6.3, 14.3 and 27.8 m off the side of the building.

The ground vibration was examined by observing three components. Neglecting the vertical component and horizontal one normal to the vibration direction of the building, as they are very small, we have treated in this paper the observed ground vibration concerning only the horizontal component in the direction of building vibration. The result of observation is shown Fig. 2.

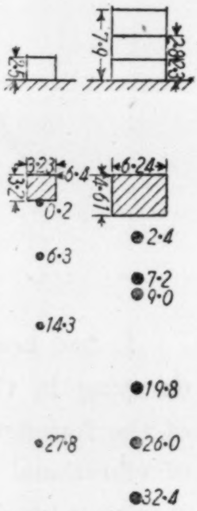

Fig. 1. Schematic view showing the buildings for vibration experiments and the observing points of the ground.

The record of observation shows that the displacement at the ground close to the building is almost equal to the amplitude at the

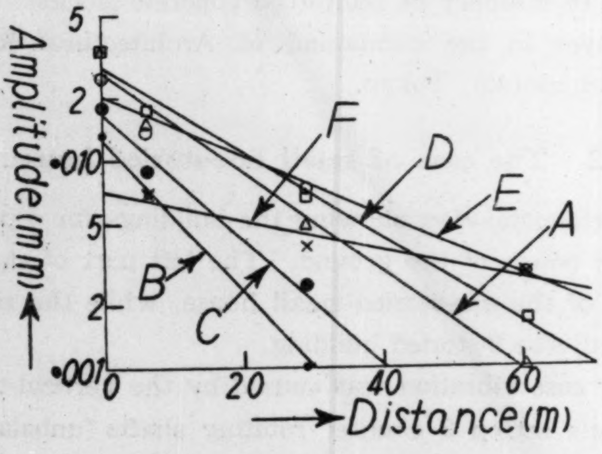

Fig. 2. Relation between the amplitude of ground oscillations and the distance from the building.

A; $T=0.134$ sec, $k=0.055\ \mathrm{m}^{-1}$, B; $T=0.140$, $k=0.0090$,
C; $T=0.156$, $k=0.068$, D; $T=0.184$, $k=0.0433$,
E; $T=0.201$, $k=0.0341$, F; $T=0.260$, $k=0.0216$.

building base, and the wave form is always sinusoidal even at the point nearest to the building.

In the vibration experiments we saw at the boundary of the ground and the building opening and shutting motion done or the ground crumble. This seemed to indicate the elastical discontinuity of building and ground, but as the result of observation we concluded that it is natural to think that these phenomena appear only on the surface and under the ground the building vibration propagates as elastic waves into the ground.

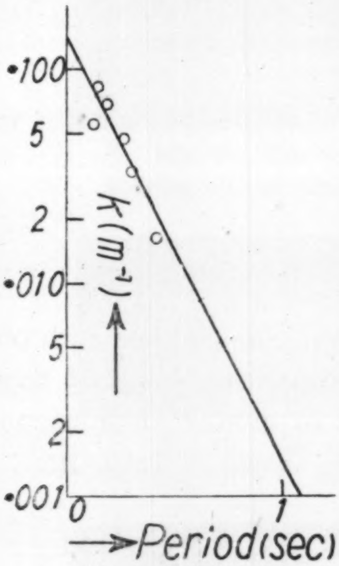

Fig. 3. Relation between the damping coefficient and the period of ground oscillations.

From Fig. 2 it is found that the relation of the amplitude at observing point (a) to the distance between the building and observing point (x) can be expressed as follows:

$$a \propto e^{-kx} \quad \text{...........(1)}$$

where k denotes the damping coefficient concerning the distance of which the value is a constant at each vibration period. Fig. 3 represents the relation between the damping coefficent (k) and the period (T) of ground oscillations. Then we have

$$k \propto T^{-2}. \quad \text{...........(2)}$$

From equation (1) and (2), we get

$$a = Ae^{-\frac{kx}{T^2}}. \quad \text{.........................(3)}$$

Equation (3) shows that the property of the vibration in the ground in this case corresponds to that of the plane waves propagating in elastic body of solid viscosity. Namely the propagation of visco-elastic wave is denoted by[3]

$$a = Ae^{ip\left(t-\frac{x}{v}\right)-\frac{\xi}{2\rho}\frac{p^2}{v^3}x} \quad \text{..................(4)}$$

where $p = 2\pi/T$, T = period, ξ = damping coefficient, ρ = density and v = velocity. Calculated from the result of the experiment, ξ becomes 7.6×10^5 C.G.S. Comparing it with other experimental values[4] we obtain Table II, which shows

---

[3] K. SEZAWA, "On the Decay of Waves in Visco-Elastic Solid Bodies", *Bull. Earthq. Res. Inst.*, **3** (1927), 43.

[4] T. SUZUKI, *Zisin*, **16** (1944), 170, (in Japanese).

Table II.

Ground	v (m/sec)	$\xi/2\rho$ (C.G.S.)	$\xi/2\rho v^3$ (C.G.S.)	Operator
Sandstone	3,300	1.8×10^9	5×10^{-3}	Suzuki
Tuff-shale	2,000	1.4×10^9	18 〃	〃
Loam	700	1.2×10^8	35 〃	〃
	80	1.9×10^5	37 〃	authors

that the difference due to the physical property of ground becomes small if we take $\xi/2\rho v^3$ into consideration.

3. The case of the full-size 3-storied building.

In this case vibration was forced by a horizontal-type vibrator with one wheel (unbalanced mass = 130 kg, eccentricity = 100 cm) set on the roof floor. The constants of seismographs used in observation of ground vibration, the observing points and the direction of measurement are shown in Table III.

Table III. Constants of the seismographs, the observing points and the direction of measurement.

No. of exper.	Seismographs									
	No. 1		No. 2		No. 3		No. 4		No. 5	
	Period = 1.0 sec						4.0 sec			
	Geometr. Magnif. = 210						10			
	dist. (m)	direct.	dist. (m)	direct.	dist. (m)	direct.	dist. (m)	direct.	dist. (m)	direct.
I	—	—	0	EW	—	—	2.4	NS	2.4	EW
II	0	EW	2.4	EW	2.4	NS	—	—	—	—
III	—	—	2.4	EW	—	—	2.4	NS	0	NS
IV	7.2	EW	2.4	EW	7.2	NS	—	—	—	—
V	9.0	EW	19.8	EW	9.0	NS	—	—	—	—
VI	26.0	EW	19.8	EW	26.0	NS	—	—	—	—
VII	—	—	32.4	EW	46.5	NS	—	—	—	—

The observed records of ground oscillations are shown in Fig. 4.

The maximum acceleration at the roof floor of the building in NS direction

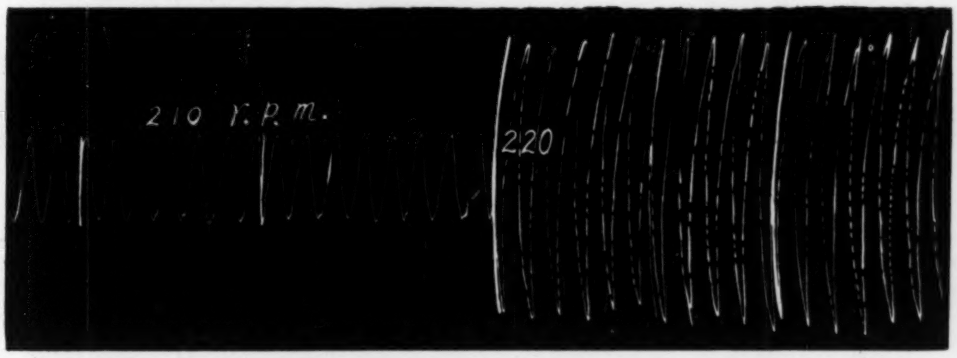

Fig. 4a. The record (Original) of transversal waves. Distance from the building ; 9.0 m, Magnif. of seismograph ; 210, No. of exper. ; V.

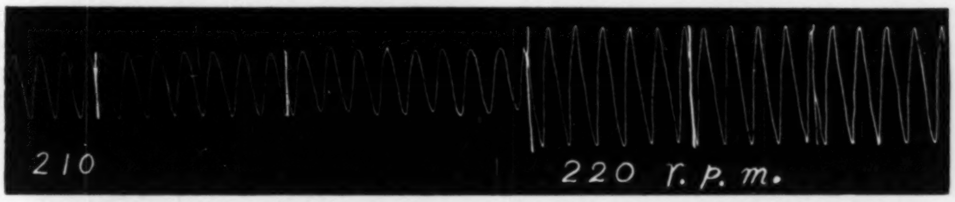

Fig. 4b. The record (Original) of longitudinal waves. Distance from the building ; 19.8 m, Magnif. of seismograph ; 210, No. of exper. ; V.

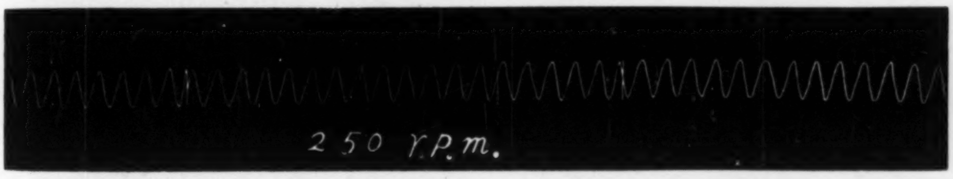

Fig. 4c. The record (Original) of longitudinal waves. Distance from the building ; 32.4 m, Magnif. of seismograph ; 210, No. of exper. ; VII.

is about 600 gal and in EW direction 400 gal⁵⁾. The record of the waves in the travelling direction (EW direction) and normal direction (NS-direction) shows sinusoidal form even in a point considerably near the building. The waves of travelling and normal direction come to have the properties of longitudinal and transversal waves respectively according to the phase relation. Thus we found that the vibration of the base of the building which was vibrated by the horizontal-type vibrator is transmitted into the ground in the form of longitudinal and transversal waves.

The relation between the amplitude at the observing point (a) and the distance from the observing point to the building (x) is denoted in Table IV and Figs. 5, 6. These figures show that there exists the relation approximate to

---

5) *Report of the Committee for Seismic Tests of Structures*, **1** (1948–1950), 104, (in Japanese).

Table IV. The values of amplitudes of dissipated waves in mm unit.

Direct.	Period (sec)	Distance (m)							
		0	2.4	7.2	9.0	19.8	26.0	32.4	46.5
NS (Trans. Waves)	0.35	.086	—	.024	.0205	—	.0048	—	—
	0.40	.082	.053 .051	.013	.014	—	.0029	—	.0009
	0.45	.076	.044 .042	.0093	.0105	—	.0024	—	.0007
EW (Longi. Waves)	0.35	.160	.044	.026	.022	.0125	.0093	.0083	—
	0.40	.116	.020	.0094	.0087	.0048	.0040	.0037	—
	0.45	.081	.014	.0074	.0058	.0034	.0026	.0024	—

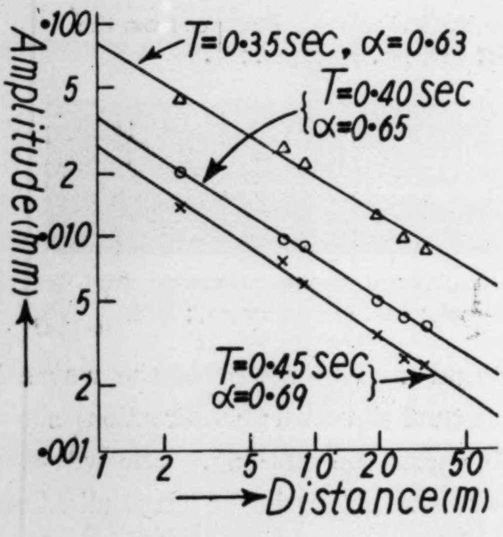

Fig. 5. Relation between the amplitude of longitudinal waves and the distance from the building.

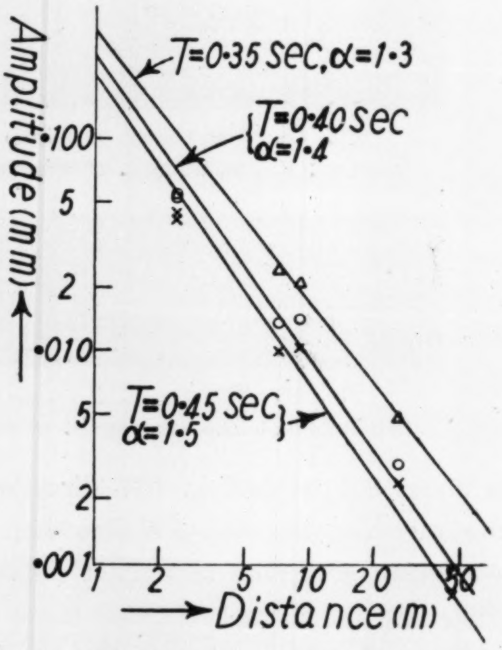

Fig. 6. Relation between the amplitude of transversal waves and the distance from the building.

$$a \propto x^{-\alpha} \quad \dots\dots\dots\dots\dots\dots\dots\dots (5)$$

α in equation (5) is a constant, and each figure in the diagram represents α concerning correspondent curve. When the waves propagate in two dimensions, $\alpha=0.5$, and in three dimensions, α will be 1. According to the value of α shown here, it can be seen that the damping of waves of large amplitude in travelling and normal directions tends to be a little larger than the damping of vibration amplitude concerning the distance when the wave propagates in two and three dimensions.

Then, assuming the damping of vibration concerning distance to be

$$a \propto x^{-\alpha} \cdot e^{-kx} \quad \ldots\ldots\ldots\ldots\ldots\ldots\ldots\ldots (6)$$

and k to be the value obtained in the previous chapter, we can replace Fig. 5 and 6 by Fig. 7 and 8. Fig. 7 and 8 indicate that the longitudinal and transversal waves propagate in the form of

$$a \propto \frac{e^{-kx}}{\sqrt{x}}, \quad a \propto \frac{e^{-kx}}{x}. \quad \ldots\ldots\ldots\ldots\ldots\ldots (7)$$

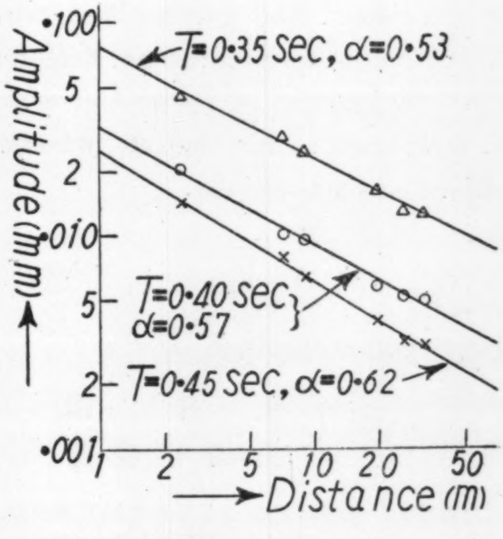

Fig. 7. Relation between the amplitude of longitudinal waves excluding the influence of solid viscosity of ground and the distance from the building.

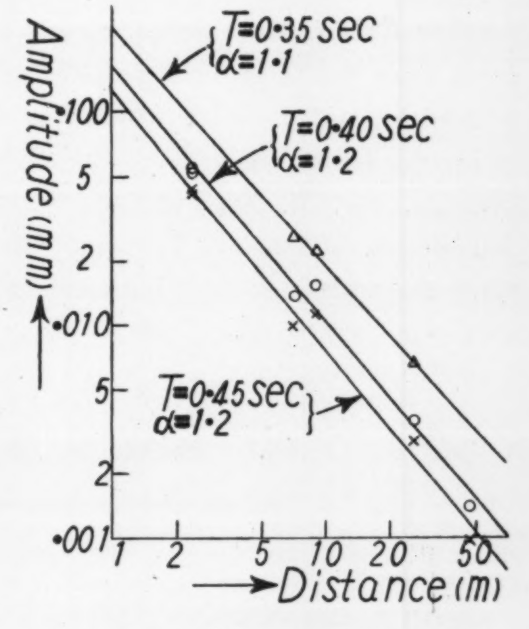

Fig. 8. Relation between the amplitude of transversal waves excluding the influence of solid viscosity of ground and the distance from the building.

4. Conclusion.

The result of the observation stated in previous chapters made us understand that the displacement at the building base is transmitted into the ground in the form of seismic waves. Since this property is considered to determine the damping resistance of building, it becomes very important to take into consideration the relation between the construction of building and the ground property, in order to design aseismatic buildings economically and rationally.

As to the damping resistance of dissipated waves concerning distance, there are two kinds of property. When the direction of forced vibration is single, the damping has a property of plane waves in longitudinal waves: when the direction is rotated, it has the property of longitudinal waves transmitted in two dimensions and transversal ones transmitted in three dimensions. In each case there is the damping due to solid viscosity of which the value is $\xi/2\rho v^3 \fallingdotseq 3.7\times10^{-7}$ C.G.S., where ξ = viscosity coefficient, ρ = density, and v = velocity. It was found that even when the physical property of ground differs somewhat the value will always assume the same order if the form $\xi/\rho v^3$ is used.

In conclusion it must be added that the above is a research work as a member of the Committee for Seismic Tests of Structures, undertaken under the grant from the Scientific Research Expenditure of Department of Education to whom the authors wish to express their gratitude. The authors also wish to express their hearty thanks to Mr. K. Nakagawa of the Architectual Research Institute, Mr. M. Suzuki of the Faculty of Engineering of Tokyo University and Messrs. T. Tanaka, T. Suzuki, Miss S. Yoshizawa of our Institute, who has aided the authors in carrying out the investigations successfully.

---

48. 建物振動に伴う土地の震動の測定結果

地震研究所
金井 清
長田甲斐男

起振機使用の建物の振動に伴う，土地の震動を測定した結果，建物の基礎のところの振動變位は，そのまま土地に彈性波として傳播して行くことが明かになつた。この性質は，建物の振動減衰性を支配するものと考えられるから，耐震建築を經濟的でしかも合理的に行うには，建物の構造と地盤の性質との關係を考慮に入れることが極めて大切なことになる。

なお，建物からの逸散波の距離についての減衰性は起振方向が1方向の場合には縱波の平面波の性質を示し，起振方向を回轉させた場合には2次元的に傳播する縱波と3次元的に傳播する橫波の性質を示す2種類がある。いづれの場合にも土地の固體粘性による減衰の性質があらわれ，その値はξを粘性係數，ρを密度，vを速度とすると，$\xi/2\rho v^3 \fallingdotseq 3.7\times10^{-7}$ C.G.S. となる。縱波，橫波のいづれについても，$\xi/\rho v^3$の形にすると，大體同じ値となり，土地の物理的性質が少しぐらいかわつても$\xi/\rho v^3$の形にすると大體同じぐらいの數になることもわかつた。

昭和26年9月30日印刷
昭和26年10月5日發行

東京都文京區本富士町一番地
東京大學構內
編纂兼發行者　東京大學地震研究所

東京都中央區日本橋茅場町二丁目十番地
印刷者　笠井康頼

東京都中央區日本橋茅場町二丁目十番地
印刷所　株式會社　國際文献印刷社

東京都千代田區神田一ツ橋通
賣捌所　岩波書店

東京都中央區日本橋二丁目六番地
丸善株式會社

Sold by
Iwanami Shoten,
Hitotsubashi dôri, Chiyoda, Tôkyô,
and
Maruzen Co., Ltd.,
Nihonbashi dôri, Chûô-ku, Tôkyô.
Price of this copy: 310 Yen. (Postage exclusive.)

BULLETIN OF
THE EARTHQUAKE RESEARCH INSTITUTE
TOKYO UNIVERSITY
Vol. XXIX, Part 3. September, 1951.

Contents.

Papers and Reports.

Page
40. Y. SATÔ, Study on Surface Waves III. Love-Waves with Double Superficial Layer. (in English) 435
41. Y. SATÔ, Distribution of Surface Stress Generating No Rayleigh-Waves. (in English) 445
42. T. HAGIWARA, K. KASAHARA, J. YAMADA and S. SAITO, Observation of the Deformation of the Earth's Surface at Aburatsubo, Miura Peninsula. Part IV. (in English) 455
43. H. KAWASUMI, Measures of Earthquake Danger and Expectancy of Maximum Intensity Throughout Japan as Inferred from the Seismic Activity in Historical Times. (in English) 469
44. F. KISHINOUYE, On the Period and the Amplitude of Microseismic Movement. (in English) 483
45. T. MINAKAMI, On the Temperature and Viscosity of the Fresh Lava Extruded in the 1951 Oo-sima Eruption. (in English) 487
46. T. RIKITAKE, Changes in Magnetic Dip that Accompanied the Activities of Volcano Mihara. (The second report) (in English) 493
47. K. KANAI, The Result of Observation of Wave-velocity in the Ground. (in English) 509
48. K. KANAI and K. OSADA, The Result of Observation concerning the Waves caused in the Ground by Building Vibration. (in English) 511

(For the papers written in Japanese or in occidental languages, the abstracts are given in occidental languages or in Japanese respectively.)

BULLETIN OF THE EARTHQUAKE RESEARCH INSTITUTE,
TOKYO UNIVERSITY. Vol. XXIX, Part 4. December, 1951.

東京大學

地震研究所彙報

第29號　第4册

昭和26年12月

目　次

論文及報告

頁
49. 表面波の研究 IV　二重の表面層と同等な單一層 (英文)………… 佐藤泰夫 519
50. P波の周期がS波の周期よりも短くなる可能度 (英文)………… 金井清 529
51. 地球内の電磁感應およびその地球内部の電氣的性質との關係 第4報 (英文)………… 力武常次 539
52. 迷走地電流について (英文)………… 岸上冬彦 549
53. 油壺における地殼變動の觀測 (第5報) (英文)………… 萩原尊禮 笠原慶一 557
54. 伊豆大島三原山1950年熔岩の化學成分 (英文)………… 津屋弘逵 森本良平 563
55. 土地の脈動の傳播性の研究 (第5報) (英文)………… 池上良平 岸上冬彦 571
56. 土地の脈動と海の波 (英文)………… 岸上冬彦 577
57. 三原山の地球磁氣學的研究　第3報　地磁氣三成分測量および偏角變化の連續觀測 (英文)………… 力武常次 横山泉 岡田惇子 菱山よね子 583
58. 1950年9月23日の淺間火山爆發の空氣波による窓ガラス被害 (英文) 佐久間修三 605
59. 實在鐵筋コンクリート建物の振動實驗結果 (英文)………… 金井清 田中貞二 617

所　報

索　引

(The titles in occidental languages are given on the back cover.)

本彙報ハ年4回 (但シ第1號ヨリ第6號マデハ不定期ニ，第7號ハ3冊トシテ發行セリ)，彙報別冊ハ不定期ニ發行ス．

本彙報掲載ノ論文及ビ報告ノ內容ニ關シテハ著者ノミニ其責任アルモノトス．

本彙報ニ關スル照會通信ハ東京大學地震研究所長ヘ宛テラレタシ．

The Bulletin is published quarterly. (Vols. I–VI were published at irregular intervals and Vol. VII consisted of three parts.)

Supplementary Volume is published at irregular interval.

The authors of the papers alone are responsible for the statements and opinions contained in their respective papers.

All communications relating to this Bulletin should be addressed to the Director of the Earthquake Research Institute, Tokyo University.

49. *Study on Surface Waves IV.*
Equivalent Single Layer to Double Superficial Layer.

By Yasuo SATÔ,

Earthquake Research Institute.

(Read Sept. 18, 1951.—Received Sept. 19, 1951.)

1. Introduction.

Evidences hitherto revealed by the perusal of seismograms have lead us to believe that the surface crust of our earth has at least a doubly stratified structure in most places. But notwithstanding this almost universal fact, we often treat the problems of seismic surface waves theoretically under the assumption of semi-infinite elastic body with a single superficial layer[1]. It is certain that this is mainly due to the difficulties of problems in case of multiply stratified medium, but it may be partly due to our vague confidence that the nature of waves and their propagation will not suffer much change by such simplified assumption, since a single layer, if chosen suitably, might be equivalent to the double layer. Indeed this confidence does not seem unreasonable in view of the close resemblance of the shape of dispersion curves for Love-waves propagated on doubly stratified medium and on single layered medium. Thus it seems possible for us to find an equivalent structure of single layer, so long as the velocity of the waves is concerned. In this paper, we will call such a layer as "equivalent single layer", and the structure as "simple structure". But, has this equivalent layer an appropriate value of thickness? Do not the values of density and rigidity of the layer differ markedly from those of two layers? Can we regard them as representing truly the original structure of the medium?

Recently it has been repeatedly suggested that the dispersion curves of surface waves may be used in determining the surface structure supplementally to the data of bodily waves[2]. But such doubts as mentioned above must be cleared up before the dispersion curves can be safely used in underground prospecting.

---

[1] The number of the investigation of surface waves with doubly stratified medium is extremely small compared with the papers treating the media with one or without layer.

With this aim in mind, the following calculations are made taking some typical examples to clarify the difference of the estimated thickness, density and rigidity of equivalent single layer from those of the original doubly stratified structure.

2. Fundamental equations.

It is well known that we can observe two kinds of surface waves in seismograms: the Rayleigh- and the Love-waves. Although we have as much interest in the former kind of waves as in the latter, we can hardly discuss the dispersion curves of Rayleigh-waves propagated on doubly stratified medium on account of the enormous labour involved in the calculation[3]. Consequently, in this paper, we will confine ourselves to the discussion of Love-waves only.

Characteristic equation of Love-waves assumed to be proportional to $\exp\{ipt-ifx\}$ in doubly stratified medium is as follows;[4]

---

[2] B. GUTENBERG, "Dispersion und Extinktion von seismischen Oberflächenwellen und der Aufbau der obersten Erdschichten." *Physikalische Zeits.*, **25** (1924), 377.

P. BYERLY, "Seismic Waves and the Surface Layer of the Earth." *Bull. Nat. Res. Council*, **61** (1927), 88.

R. STONELEY, "The Thickness of the Continental Layers of Europe." *M.N.R.A.S. Geo. Sup.*, **2** (1929), 429.

P. BYERLY, "The Dispersion of Seismic Waves of the Love Type and the Thickness of the Surface Layer of the Earth under the Pacific." *Beitr. z. Geophys.*, **26** (1930), 27.

P. BYERLY, "The California Earthquake of Nov. 28, 1929, and the Surface Layer of the Earth in California." *Proc. Nat. Acad. Sci.*, **17** (1931), 91.

W. MÜHLEN, "Über seismische Oberflächenwellen und ihre Beziehung zum geologischen Aufbau des eurasiatischen Kontinents." *Zeits. f. Geophys.*, **8** (1932).

D. S. CARDAR, "Seismic Surface Waves and the Crustal Structure of the Pacific Region." *Bull. Seism. Soc. Amer.*, **24** (1934), 231.

J. F. DE LISLE, "On Dispersion of Rayleigh Waves from the North Pacific." *Bull. Seism. Soc. Amer.*, **31** (1941), 303.

J. T. WILSON and ORHAM BAYKAL, "Crustal Structure of the North Atlantic Basin as Determined from Rayleigh Wave Dispersion." *Bull. Seism. Soc. Amer.*, **38** (1948), 41.

[3] Rayleigh-waves in double layer was once studied by H. Kawasumi and I. Yamasita. Monthly meeting of the Earthq. Res. Inst. March 1940. Although there are a few investigations concerning the same problem, not even a single paper has been published.

[4] Y. SATÔ, "Study on Surface Waves III. Love-waves with Double Superficial Layer." *Bull. Earthq. Res. Inst.*, **29** (1951), 435.

$$D \equiv D^c + D^s = 0$$

where

$$D^c/\mu_2^2 f^2 \equiv \quad \mathfrak{A}_2 \cos\{\xi h_1 \mathfrak{A}_1\}\,[-\chi_{32}\mathfrak{A}\cos\{\xi h_2\mathfrak{A}_2\} + \mathfrak{A}_2 \sin\{\xi h_2 \mathfrak{A}_2\}]$$

$$D_s/\mu_2^2 f^2 \equiv \chi_{12}\mathfrak{A}_1 \sin\{\xi h_1 \mathfrak{A}_1\}\,[\quad \chi_{32}\mathfrak{A}\sin\{\xi h_2\mathfrak{A}_2\} + \mathfrak{A}_2 \cos\{\xi h_2 \mathfrak{A}_2\}] \quad \ldots\ldots.(2.1)$$

in which

$$\begin{aligned} \mathfrak{A}_k &\equiv \sqrt{(r_k^2\mathfrak{v}^2-1)} \quad , & k&=1,\ 2,\ 3 \\ \mathfrak{A} &\equiv \sqrt{(1-\mathfrak{v}^2)} \quad , & & \\ \mathfrak{v}_k &\equiv V/V_k \quad , & k&=1,\ 2,\ 3 \\ \mathfrak{v} &\equiv \mathfrak{v}_3 \quad , & & \\ r_k &\equiv V_3/V_k \quad , & k&=1,\ 2. \\ \xi &\equiv fH \quad , & & \\ \chi_{jk} &\equiv \mu_j/\mu_k \quad , & & \end{aligned}$$

where V is the velocity of Love-waves while the other notations are illustrated in Fig. 1.

On the other hand, the characteristic equation in the simple structure is[5)]

$$\omega = \sec\theta\,[\mathrm{Tan}^{-1}\{\chi\sec\theta\cdot\sqrt{(\sin^2\theta-\sin^2\theta_0)}\}] \ldots\ldots\ldots(2.2)$$

in which

$$\begin{aligned} \sin\theta_0 &\equiv V_e/V_e' \quad , \\ \sin\theta_0/\sin\theta &\equiv \mathfrak{v}_e \quad , \\ \omega &\equiv pH_e/V_e \quad , \\ \chi &\equiv \mu_e'/\mu_e \quad , \end{aligned}$$

where suffix e denote the value in equivalent simple structure, and $\mathfrak{v}_e V_e'$ the phase velocity of Love-waves in simple structure, while the other notations are illustrated in Fig. 2.

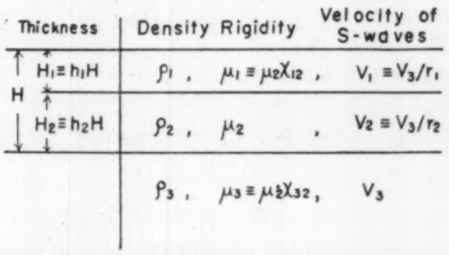
Thickness
Density
Rigidity
Velocity of S-waves
H
$H_1 \equiv h_1 H$
$H_2 \equiv h_2 H$
ρ_1 , $\mu_1 \equiv \mu_2\chi_{12}$, $V_1 \equiv V_3/r_1$
ρ_2 , μ_2 , $V_2 \equiv V_3/r_2$
ρ_3 , $\mu_3 \equiv \mu_2\chi_{32}$, V_3

Fig. 1.

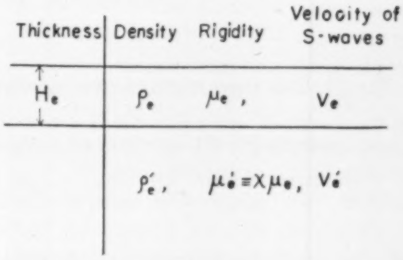
Thickness
Density
Rigidity
Velocity of S-waves
H_e
ρ_e μ_e , V_e
ρ_e' , $\mu_e' \equiv \chi\mu_e$, V_e'

Fig. 2.

---

5) Y. Satô, "Study on Surface Waves I. Velocity of Love-Waves." *Bull. Earthq. Res. Inst.*, **29** (1951), 1. Expression (4.6).

3. Examples.

It seems so difficult to slove the problem described in § 1 generally that we will discuss this subject by taking some typical examples in this section.

Example 1.

As is given in the upper rows of Table II the velocity of S-waves in the upper two layers are assumed to be equal, although the density and rigidity vary discontinuously at the depth H from the free surface.

The relation between the velocity and period of Love-waves are calculated by the expression (2.1) and is given in Table I and also by the full line in Fig. 3.

Table I.

Relation between $\mathfrak{v}^2$ and ξ in the example 1.

$3\mathfrak{v}^2$	ξ
3	0
2.96	.1572
2.8225	.3316
2.69	.4312
2.44	.6116
2.21	.7562
2	.918
1.81	1.086
1.64	1.286
1.49	1.531
1.36	1.848
1.25	2.282
1.16	2.926
1.1229	3.382
1.09	3.989
1.0625	4.836
1.04	6.105
1	∞

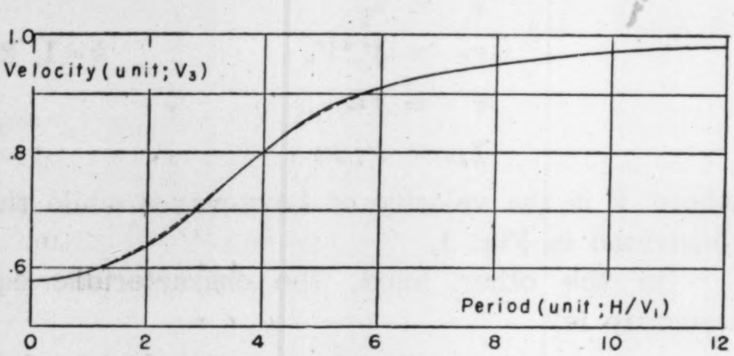

Fig. 3.

On the other hand we searched for a dispersion curve of simple Love-waves which fits well with the above curve. The broken line in Fig. 3 gives the result, showing extremely good coincidence with the full line. Material constants and the thickness of the layer employed for writing this curve is

$$\chi \equiv \mu_e'/\mu_e = 3, \qquad H_e/H = 1. \ldots\ldots(3.1)$$

Namely the estimated structure by the idea of equivalent single layer is as follows[6]:

---

[6] To fit the two curves we always assume as

$$V_e = V_1 \quad \text{and} \quad V_e' = V_3, \qquad \ldots\ldots(3.2)$$

which are necessary to secure the equality of the velocities of extremely short and long waves in two structures.

Further, we adopt the assumptions

$$\mu_e = \mu_1 \ , \qquad \rho_e = \rho_1 \ , \qquad \ldots\ldots(3.3)$$

because the surface values are directly determined by other observations and measurements.

Under such conditions we search for a most appropriate values of μ_e'/μ_e and H_e/H. In this study, however, the word "most appropriate" is not used in the sense of "least squares" principle, but just in the macroscopic sense.

Table II.

		Thickness	Density	Rigidity	Velocity of S-Waves
Real struture with double layer	Upper layer	$\left.\begin{matrix}\frac{1}{2}H\\ \frac{1}{2}H\end{matrix}\right\}H$	$\frac{3}{10}\rho$	$\frac{1}{10}\mu$	$\sqrt{\left(\frac{1}{3}\frac{\mu}{\rho}\right)}$
	Middle layer		ρ	$\frac{1}{3}\mu$	$\sqrt{\left(\frac{1}{3}\frac{\mu}{\rho}\right)}$
	Semi-infinite part	—	ρ	μ	$\sqrt{\left(\frac{\mu}{\rho}\right)}$
Simple structure with equivalent single layer	Layer	H	$\frac{3}{10}\rho$	$\frac{1}{10}\mu$	$\sqrt{\left(\frac{1}{3}\frac{\mu}{\rho}\right)}$
	Semi-infinite part	—	$\frac{3}{10}\rho$	$\frac{3}{10}\mu$	$\sqrt{\left(\frac{\mu}{\rho}\right)}$

As is clear from the above table, the estimation of the thickness is quite good, and is equal to the sum of thickness of two layers of real structure. The coincidence however of the physical constants is not so good as that of the thickness. If we estimate the value of density and rigidity by the above method we shall make a grave mistake.

Example 2.

We will next take another example which we gave in the previous paper[7]. The distribution of matters in this case is a very peculiar one, which is to be rarely found in natural state. (cf. Table III, upper rows.)

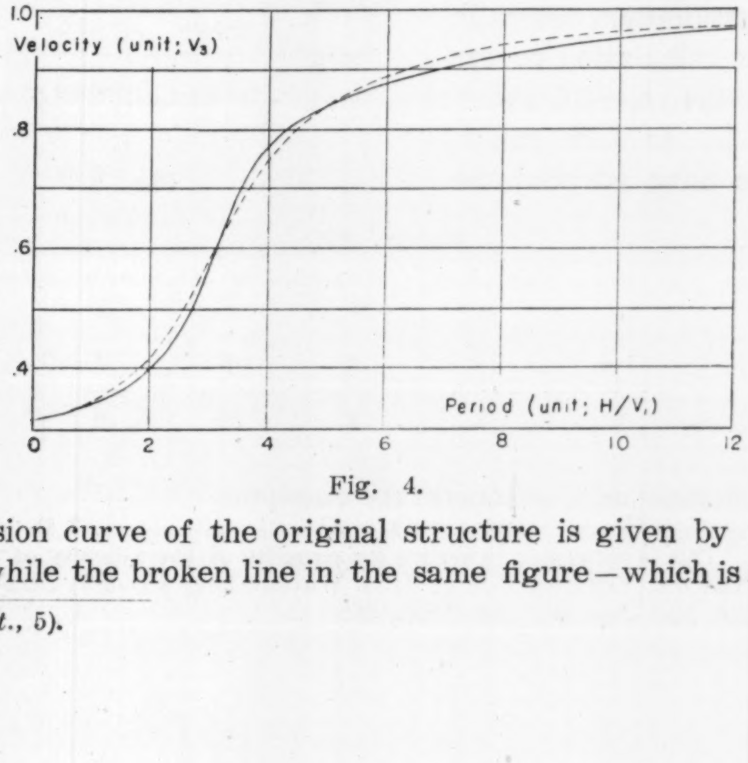

Fig. 4.

Dispersion curve of the original structure is given by a full line in Fig. 4, while the broken line in the same figure—which is constructed by the constants $\mu_e'/\mu_e=4.5$ and $H_e/H=2/3$—shows that of simple structure[8]. We will give the estimated constants of simple structure in the following table as before, although we could not find a curve which fits so well as in the former case. In this case also, the discrepancy of the values of physical constants is not small as will be seen from Table III.

---

[7] *loc. cit.*, 5).

Table III.

		Thickness	Density	Rigidity	Velocity of S-waves
Real structure with double layer	Upper layer	$\left.\begin{array}{l}\frac{1}{2}H\\[4pt] \frac{1}{2}H\end{array}\right\}H$	ρ	μ	$\sqrt{\left(\frac{\mu}{\rho}\right)}$
	Middle layer		ρ	$\frac{1}{10}\mu$	$\sqrt{\left(\frac{1}{10}\frac{\mu}{\rho}\right)}$
	Semi-infinite part	—	ρ	μ	$\sqrt{\left(\frac{\mu}{\rho}\right)}$
Simple structure with equivalent single layer.	Layer	$\frac{2}{3}H$	ρ	$\frac{1}{10}\mu$	$\sqrt{\left(\frac{1}{10}\frac{\mu}{\rho}\right)}$
	Semi-infinite part	—	$\frac{9}{20}\rho$	$\frac{9}{20}\mu$	$\sqrt{\left(\frac{\mu}{\rho}\right)}$

Example 3.

Study on the propagation of Love-waves along a doubly stratified earth was performed by T. Matuzawa[9], in which he employed the assumption shown in Fig. 5. His calculation covers the cases $h_1=0.4$, $h_2=0.6$ and $h_1=0.9$, $h_2=0.1$. In this paper, however, we have adopted the

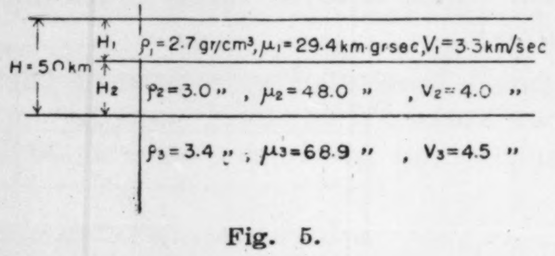
H = 50 km
H_1
H_2
$\rho_1=2.7$ gr/cm³, $\mu_1=29.4$ km·gr·sec, $V_1=3.3$ km/sec
$\rho_2=3.0$ " , $\mu_2=48.0$ " , $V_2=4.0$ "
$\rho_3=3.4$ " ; $\mu_3=68.9$ " , $V_3=4.5$ "

Fig. 5.

Table IV.

Case		a	b	c	d	e
h_1	1.0	.9	.8	.6	.4	.2
h_2	0	.1	.2	.4	.6	.8

---

[8] In this example only, we adopted the assumption

$$V_e=V_2\,,\qquad\text{and}\qquad \rho_e=\rho_2 \qquad\ldots\ldots\ldots\ldots(3.4)$$

instead of (3.3). This is necessary to secure the equality of the velocity of short waves.

[9] T. MATUZAWA, "Propagation of Love Waves along a Doubly Stratified Layer". *Proc. Phys.-Math. Soc. Jap.* [iii], **10** (1928), 25.

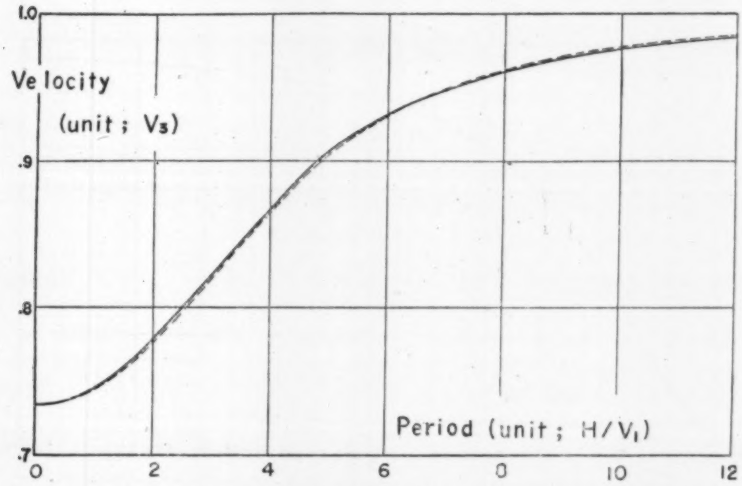

Fig. 6 a.

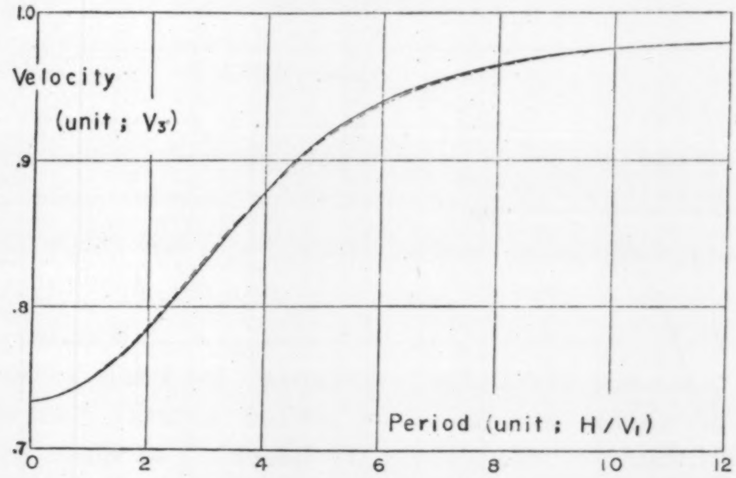

Fig. 6 b.

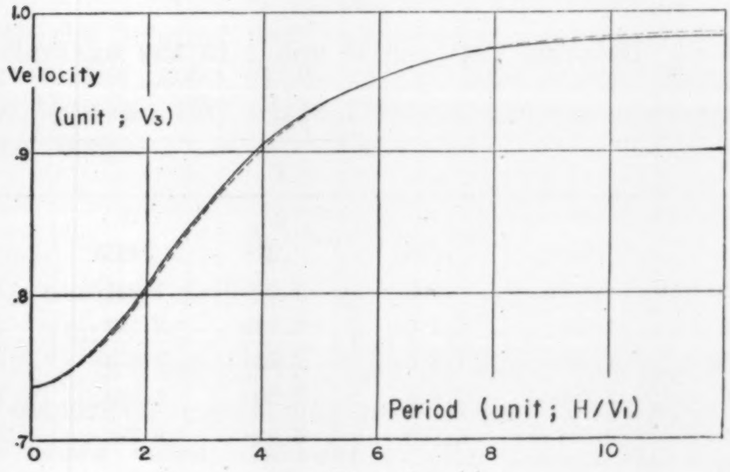

Fig. 6 c.

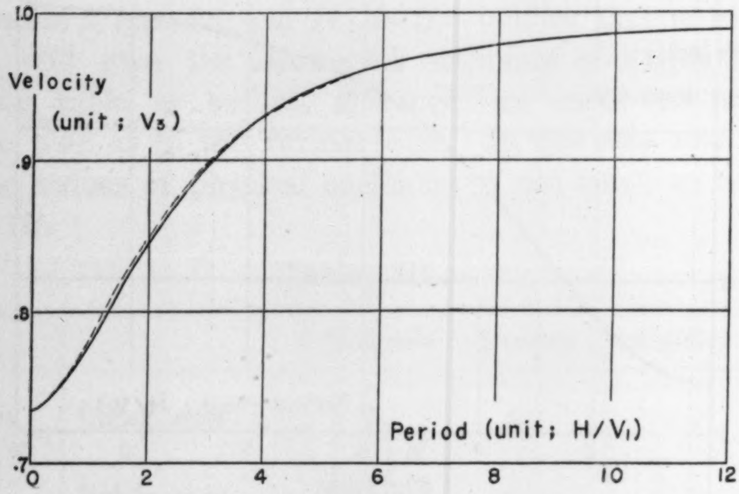

Fig. 6 d.

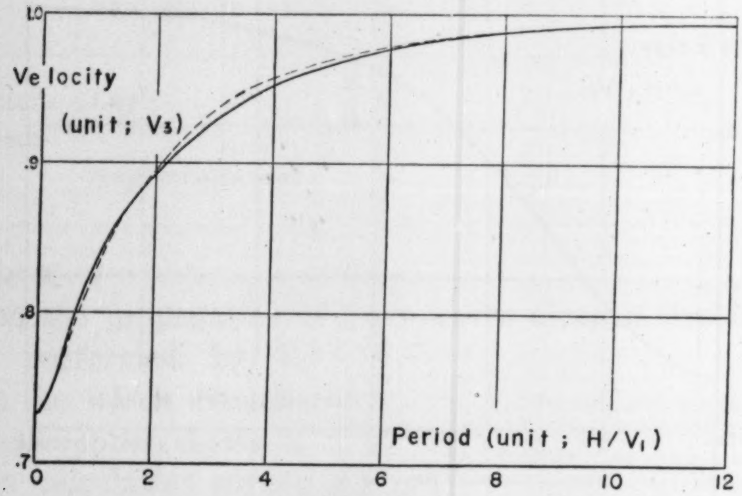

Fig. 6 e.

Table V. Relation between v^2 and ξ in the example 3.

Case	a	b	c	d	e
v^2	ξ				
1	0	0	0	0	0
.987654	.3187	.3365	.378	.4355	.5115
.916543	.8550	.906	1.040	1.221	1.507
.8217285	1.386	1.476	1.722	2.122	2.935
.7585186	1.762	1.875	2.236	2.873	4.560
.679506	2.496	2.692	3.300	4.582	8.823
.592593	4.554	4.960	6.338	9.388	18.793
.537778	∞	∞	∞	∞	∞

Table VI.

Case		a	b	c	d	e
$h_1 \equiv H_1/H$	1	.9	.8	.6	.4	.2
$h_2 \equiv H_2/H$	0	.1	.2	.4	.6	.8
H_e/H (estimated)	1	4/3	10/9	1/1.05	1/2.1	1/5
H_e (,,) km	50	66.7	55.6	47.6	23.8	10.0
H (original)	50 km					
μ_e'/μ_e (estimated)	2.344	2.5	2.0	2.0	1.05	0.6
μ_e' (,,) km. gr. sec.	68.9	73.5	58.8	58.8	30.9	17.6
μ_3 (original)	68.9 km. gr. sec.					
ρ_e'/ρ_e (estimated)	1.2592	1.344	1.076	1.076	.5647	.3227
ρ_e' (,,) gr/cm^3	3.40	3.63	2.90	2.90	1.52	.871
ρ_3 (original)	3.40 gr./cm^3					

five ceases in Table IV, and calculated the dispersion curve in every case respectively. The results are given in Fig. 6 a, b, c, d, e (full line) and in Table V.

On the other hand we calculated tentatively the velocity in simple structure, giving various values of μ_e'/μ_e and H_e/H. The obtained results, which seem to fit fairly well with the original curves are the broken lines in the same figures.

The adopted values of μ_e'/μ_e and H_e/H are tabulated in Table VI together with the original real values of the medium.

In spite of the good fitting of full and broken lines, the discrepancies lying between the original values and the estimated ones are generally very large.

4. Conclusions.

In the preceding articles we have examined the possiblity of finding the "simple structure" with an "equivalent single layer." The answer is in the affirmative, and we could find the simple structure whose dispersion curve fits pretty well with that of original structure in every case. However, with regard to the estimated values of the thickness of the layer, the results are not always so satisfactory as in the case of fitting the curve. Moreover, between the density and rigidity calculated by the above method and the original values there is a marked discrepancy. Consequently, judging from the above results, crude and scanty as they are, we are obliged to give a pessimistic conclusion to the questions raised in the introduction of this paper. Namely, the equivalent single layer with regard to dispersion curve does not always give an appropriate value of thickness of the crustal layers; and the estimated density and rigidity are often considerably different from those of two layers; hence we can not regard it as a good representation of the original structure of the medium. So long as we are ignorant of the correct structure, which is quite difficult to grasp, the knowledge of the dispersion curve of the surface waves will be of little use for our practical purpose of prospecting the underground structure.

The above discussion is limited only to the theory of Love-waves; however, we cannot expect to obtain a greatly differing conclusion even if we extend our study to the case of Rayleigh-waves.

---

49. 表面波の研究 IV

二重の表面層と同等な單一層

地震研究所　佐藤泰夫

我我の地球が，表面に二つの層をもつた構造をなす事は，今日多くの人の承認する所である。しかしながら，理論的な研究は主として單一層のものについて行われている狀態である。これは一つには計算の簡單ということもあるが，又一方には，適當な厚さの層を一つ考へれば，二重の層の場合とほぼ同等の效果のある事が，暗に豫期されてゐるからでもあろう。

そこで以上の考への當否を調べるために，まづ二重の表面層を持つた構造をいくつか假定し，この中を傳はるラブ波の分散曲線を正確に求める。次に，單一の表面層を持つた構造で，その中のラブ波が上に求められた分散曲線となるべく似た形の分散曲線をもつように，表面層のあつさや，密度，剛性率などを色色加減する。このようにすると，いづれの場合にも，二つの曲線はかなりよく——我我が地震記象から分散を求める場合の精度よりはるかによい程度に——重なり合ふ。

しからば，このようにして求められた構造は，もとのものに比べてどんな關係を示して居るであろうか。層の厚さについて言ふならば，極めてよくあふ場合もあるけれども，全然ことなつた値を示すこともある。又，兩方の構造において，表面での密度，剛性率をひとしく置くと，半無限體內での値は，多くの場合において非常なへだたりを示して居り，到底單一層の構造をもつて，もとのものの代表と考へる事は困難である。

從つて我我は，上のやうな考へを以てしては，表面波の分散から地球表面の構造を推定しようといふくわだてに，悲觀的な結論を下さざるを得ない。

以上の議論はラブ波に關するものであるが，レーリー波についても，さほど異つた結果は出ないであろう。

50. *Possibility of the Period of P-waves becoming smaller than those of S-waves.*

By Kiyoshi KANAI,

Earthquake Research Institute.

(Read Sept. 18, 1951—Received Sept. 20, 1951.)

1. Introduction.

It is a well-known fact that the amplitudes of P-waves are smaller than those of S-waves and the periods of P-waves shorter than those of S-waves in general. The smallness of the amplitudes of the P-waves has been explained by the shortness of the periods of them. This comes out directly from the theory of propagation of waves in visco-elastic bodies.[1] But, the reason of the shortness of the periods of the actually generated P-waves has been left untouched by us.

In the previous paper[2], using operational calculus, the problem of transmission of arbitrary elastic waves generated from a spherical source, oscillating spheroidally, was solved. However, the features discussed in that paper was restricted to separating the distortional waves and the dilatational waves respectively into free waves and forced waves, both generated from the spherical source.

As a matter of fact, the features of the vibrational period and damping of P-waves as well as S-waves have not yet been precisely discussed. In the present paper, we will discuss the feature of the three modes of free waves at a relatively large focal distance.

We will deal with two cases, namely, of the waves resulting from pressure change and of those arising from the change in shearing force at the spherical origin. As to the type of exciting force at the origin, only the rectangular type beginning from a quiescent state will be treated.

---

[1] K. SEZAWA and K. KANAI, "Amplitudes of P- and S-waves at Different Focal Distances", *Bull. Earthq. Res. Inst.*, **10** (1932), 299.

[2] K. SEZAWA and K. KANAI, "Transmission of Arbitrary Elastic Waves from a Spherical Source, Solved with Operational Calculus", *Bull. Earthq. Res. Inst.*, **19** (1941), 151, 417, **20** (1942), 1.

2. The case of pressure change at the origin.

The integral expressions of displacements of the waves for any n were given in the previous paper. Rewriting these expressions, we get

$$\left.\begin{aligned}\Delta &= \frac{1}{2\pi i}\int_{c-i\infty}^{c+i\infty}\frac{e^{zt}dz}{z}\,\frac{A_n H^{(1)}_{n+1/2}\,(izrc_1)}{\sqrt{r}}\,P_n(\cos\theta)\,,\\ 2\varpi &= \frac{1}{2\pi i}\int_{c-i\infty}^{c+i\infty}\frac{e^{zt}dz}{z}\,\frac{B_n H^{(1)}_{n+1/2}\,(izrc_2)}{\sqrt{r}}\,\frac{dP_n(\cos\theta)}{d\theta}\,,\end{aligned}\right\}\quad\ldots\ldots\ldots(1)$$

$$\left.\begin{aligned}u_1 &= \frac{1}{2\pi i}\int_{c-i\infty}^{c+i\infty}\frac{e^{zt}dz}{z}\,\frac{A_n}{z^2c_1^2}\,\frac{d}{dr}\left\{\frac{H^{(1)}_{n+1/2}(izrc_1)}{\sqrt{r}}\right\}P_n(\cos\theta),\\ v_1 &= \frac{1}{2\pi i}\int_{c-i\infty}^{c+i\infty}\frac{e^{zt}dz}{z}\,\frac{A_n}{z^2c_1^2}\,\frac{H^{(1)}_{n+1/2}(izrc_1)}{r^{3/2}}\,\frac{dP_n(\cos\theta)}{d\theta}\,,\\ u_2 &= \frac{1}{2\pi i}\int_{c-i\infty}^{c+i\infty}\frac{e^{zt}dz}{z}\,\frac{n(n+1)B_n}{z^2c_2^2}\,\frac{H^{(1)}_{n+1/2}(izrc_2)}{r^{3/2}}\,P_n(\cos\theta)\,,\\ v_2 &= \frac{1}{2\pi i}\int_{c-i\infty}^{c+i\infty}\frac{e^{zt}\,dz}{z}\,\frac{B_n}{z^2\,c_2^2}\,\frac{1}{r}\,\frac{d}{dr}\{\sqrt{r}\,H^{(1)}_{n+1/2}(izrc_2)\}\,\frac{dP_n(\cos\theta)}{d\theta}\,.\end{aligned}\right\}$$

$$\ldots\ldots\ldots\ldots\ldots\ldots\ldots\ldots(2)$$

Using the same conditions at the spherical boundary, $r=a$, as in the previous paper, we get

$$\widehat{rr}=\lambda\Delta+2\mu\frac{\partial\,(u_1+u_2)}{\partial r}=\frac{P_n(\cos\theta)}{2\pi i}\int_{c-i\infty}^{c+i\infty}\frac{e^{zt}}{z}\,g(z)\,dz,\ \ldots(3)$$

$$\widehat{r\theta}=\mu\left\{\frac{\partial\,(v_1+v_2)}{\partial r}-\frac{(v_1+v_2)}{r}+\frac{1}{r}\,\frac{\partial(u_1+u_2)}{\partial\theta}\right\}=0.\ \ldots\ldots(4)$$

when

$$g(z)=z\int_0^\infty e^{-zt}f(t)\,dt\ \ldots\ldots\ldots\ldots\ldots\ldots\ldots\ldots(5)$$

Replacing the form of $g(z)$, corresponding to a given exciting force, $f(t)$, it is possible to evaluate the integrals in (2)

The expressions for displacements[3] at a relatively large focal distance, that is, $r\to\infty$, for the case $f(t)=p_0$ for $t>0$ and $f(t)=0$ for $t<0$, in the state of $n=2$, $\lambda=\mu$ show that the radial component of the displacement of the free waves of dilatational waves and the transversal one of distortional waves are inversely proportional to the radial distance from the origin, while the displacement of forced waves of P-waves as well as S-waves the transversal component of the displacement of the free waves of P-waves and the radial one of S-waves are inversely proportional to the square of the radial distance.

---

[3] Page 427 and 428 in the second paper in foot note 2).

The expressions for the radial component of the displacement of the free waves of P-waves and the transversal one of S-waves is reduced to

$$\left.\begin{aligned} u_{f1}\Big/\frac{a^2p_0}{\mu r}P_2(\cos\theta) & \\ =0.06486\,e^{-0.8033\frac{t-c_1(r-a)}{ac_2}} & \sin\left\{1.0406\frac{t-c_1(r-a)}{ac_2}-2.639\right\} \\ -0.06929\,e^{-1.8015\frac{t-c_1(r-a)}{ac_2}} & \sin\left\{4.1852\frac{t-c_1(r-a)}{ac_2}+1.4875\right\} \\ +0.217\,e^{-3.648\frac{t-c_1(r-a)}{ac_2}} & \sin\left\{1.4410\frac{t-c_1(r-a)}{ac_2}+2.661\right\}, \end{aligned}\right\} \quad (6)$$

$$\left.\begin{aligned} v_{f2}\Big/\frac{a^2p_0}{\mu r}\,\frac{dP_2(\cos\theta)}{d\theta} & \\ =-0.2315\,e^{-0.8033\frac{t-c_2(r-a)}{ac_2}} & \sin\left\{1.0406\frac{t-c_2(r-a)}{ac_2}-0.051\right\} \\ +0.03156\,e^{-1.8015\frac{t-c_2(r-a)}{ac_2}} & \sin\left\{4.1852\frac{t-c_2(r-a)}{ac_2}+0.7361\right\} \\ -0.05867\,e^{-3.468\frac{t-c_2(r-a)}{ac_2}} & \sin\left\{1.4410\frac{t-c_2(r-a)}{ac_2}+2.542\right\}. \end{aligned}\right\} \quad (7)$$

The three terms of each equation mean the three kinds of mode of free oscillation at spherical origin, when $n=2$.

The results of numerical calculation for each term of equations (6) and (7) are shown in Figs. 1 and 2.

It will be seen from equation (7) and Fig. 2 that the first term is the largest in amplitude, the smallest in logarithmic decrement and the longest in period. Then, the resultant of the three terms, as shown in Fig. 3, takes a relatively simple form.

While, equation (6) and Fig. 1 show that the term of the largest amplitude, that is, the third term, has the largest logarithmic decrement. Then the resultant of the three terms, as shown in Fig. 4, has a somewhat complicated form. The above results tell us that the period as well as the amplitude of *P*-waves would be small compared with those of S-waves.

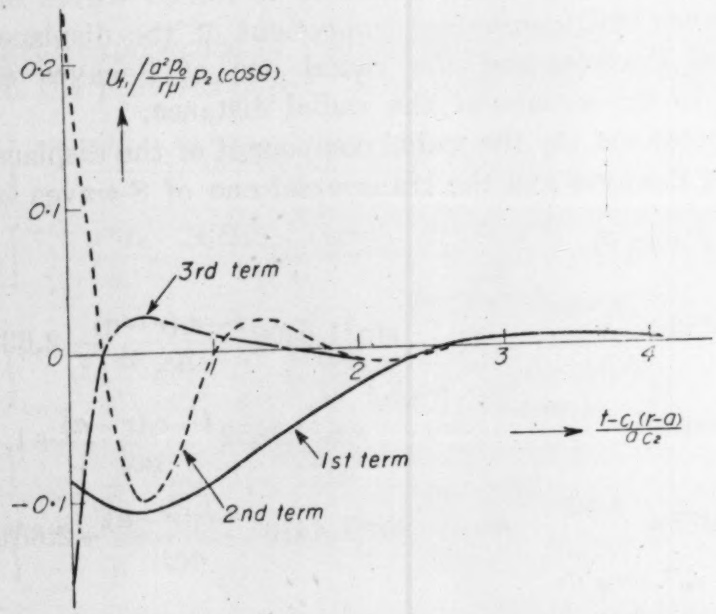

Fig. 1. Every term of free waves of radial displacement of P-waves in the case of pressure change at the origin.

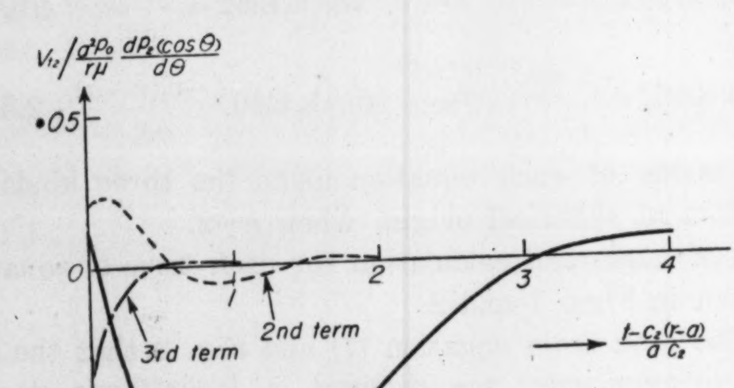

Fig. 2. Every term of free waves of transversal displacement of S-waves in the case of pressure change at the origin.

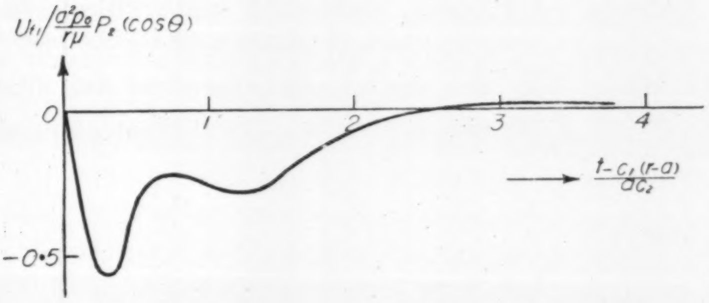

Fig. 3. Radial displacement of P-waves in the case of pressure change at the origin.

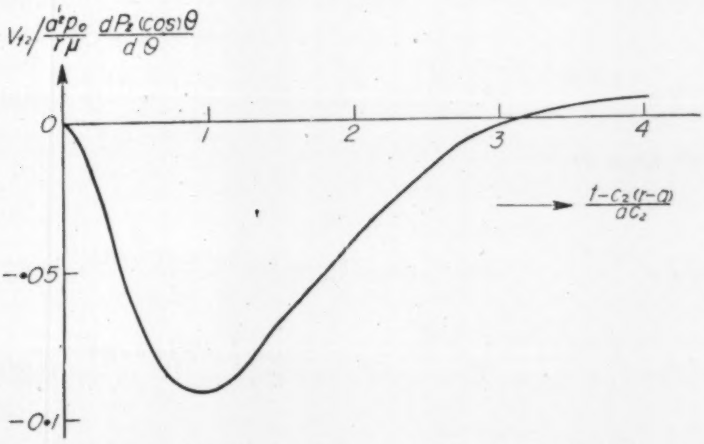

Fig. 4. Transversal displacement of S-waves in the case of pressure change at the origin.

3. The case of change in shearing force at the origin.

In this case, the conditions at the spherical boundary, $r=a$, as in the previous paper, are

$$\left.\begin{aligned}\widehat{r\theta}&=\mu\left\{\frac{\partial(v_1+v_2)}{\partial r}-\frac{(v_1+v_2)}{r}+\frac{1}{r}\frac{\partial(u_1+u_2)}{\partial\theta}\right\}\\&=\frac{dP_n(\cos\theta)}{d\theta}\frac{1}{2\pi i}\int_{c-i\infty}^{c+i\infty}\frac{e^{zt}}{z}g(z)dz,\end{aligned}\right\}\quad\dots\dots\dots(8)$$

$$\widehat{rr}=\lambda\Delta+2\mu\frac{\partial(u_1+u_2)}{\partial r}=0.\quad\dots\dots\dots\dots\dots\dots\dots\dots\dots(9)$$

The final expressions for displacements[4] at a relatively large focal distance, that is, $r\to\infty$, for the case $f(t)=p_0$ for $t>0$ and $f(t)=0$ for

---

[4] Page 8 in the third paper in foot note 2).

$t<0$, in the state of $n=2$, $\lambda=\mu$, show the same rule as in the previous section.

The expressions for the radial component of the displacement of the free waves of P-waves and the transversal one of S-waves is reduced to

$$
\left. u_{f_1} \middle/ \frac{a^2 p_0}{\mu r} P_2(\cos\theta) \right.
$$

$$
\left.\begin{aligned}
&= -0.1931\, e^{-0.8033\frac{t-c_1(r-a)}{ac_2}} \cos\left\{1.0406\frac{t-c_1(r-a)}{ac_2}-1.120\right\} \\
&\quad -0.2808\, e^{-1.8015\frac{t-c_1(r-a)}{ac_2}} \cos\left\{4.1852\frac{t-c_1(r-a)}{ac_2}-2.593\right\} \\
&\quad -0.4378\, e^{-3.648\frac{t-c_1(r-a)}{ac_2}} \cos\left\{1.4410\frac{t-c_1(r-a)}{ac_2}+1.209\right\},
\end{aligned}\right\} \quad (10)
$$

$$
\left. v_{f_2} \middle/ \frac{a^2 p_0}{\mu r} \frac{dP_2(\cos\theta)}{d\theta} \right.
$$

$$
\left.\begin{aligned}
&= -0.6874\, e^{-0.8033\frac{t-c_2(r-a)}{ac_2}} \cos\left\{1.0406\frac{t-c_2(r-a)}{ac_2}-1.674\right\} \\
&\quad -0.1278\, e^{-1.8015\frac{t-c_2(r-a)}{ac_2}} \cos\left\{4.1852\frac{t-c_2(r-a)}{ac_2}-0.202\right\} \\
&\quad -0.1179\, e^{-3.648\frac{t-c_2(r-a)}{ac_2}} \cos\left\{1.4410\frac{t-c_2(r-a)}{ac_2}+4.227\right\}.
\end{aligned}\right\} \quad (11)
$$

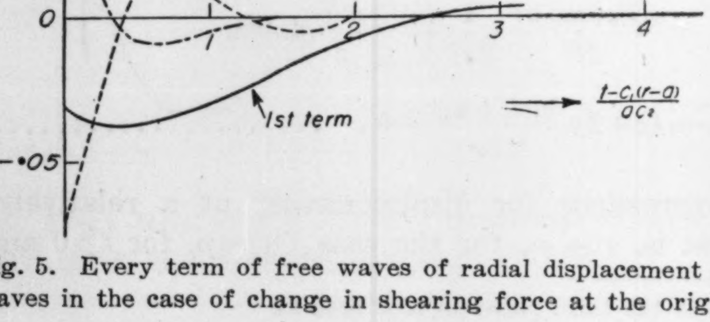

Fig. 5. Every term of free waves of radial displacement of P-waves in the case of change in shearing force at the origin.

The results of numerical calculation for each term and resultant of equation (10) and (11) are shown in Figs. 5-8.

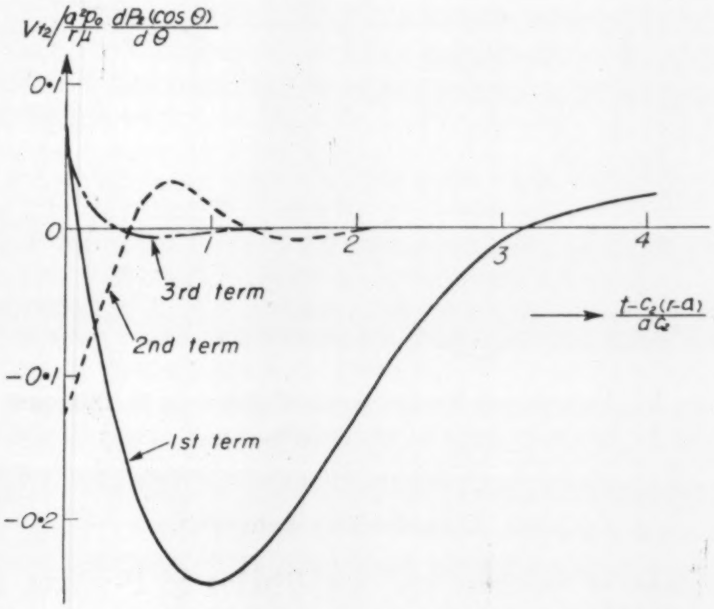

Fig. 6. Every term of free waves of transversal displacement of S-waves in the case of change in shearing force at the origin.

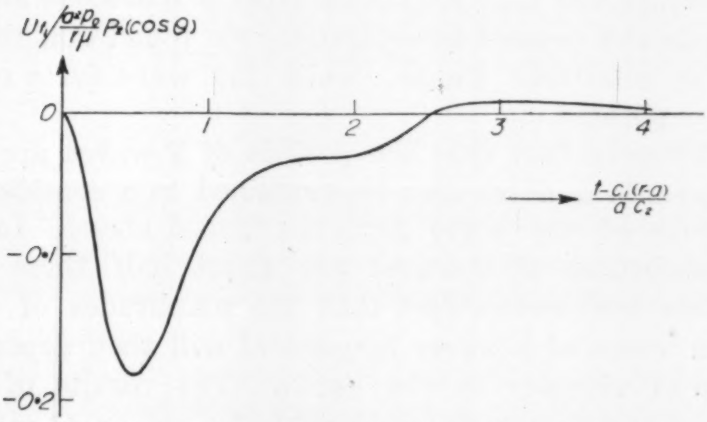

Fig. 7. Radial displacement of P-waves in the case of change in shearing force at the origin.

It has been found that the difference of wave form between P-waves and S-waves is similar to that in the case of pressure change at the spherical origin.

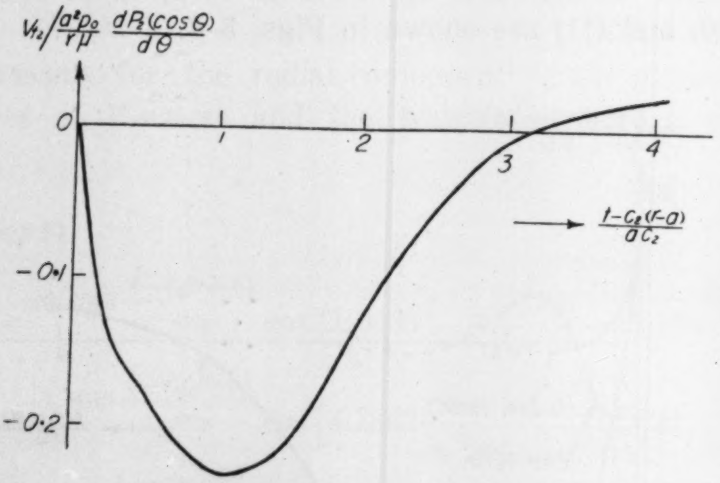

Fig. 8. Transversal displacement of S-waves in the case of change in shearing force at the origin.

4. Concluding remarks.

The problem of periods and amplitudes of P-waves as well as S-waves has been discussed somewhat precisely.

We have here dealt with two cases, that is, of the waves resulting from pressure change and of those arising from change in shearing force at the spherical origin. As to the type of exciting force at the origin, the rectangular type beginning from a quiescent state has been treated. From the present investigation, we found that the wave form of S-waves is relatively simple, while the wave form of P-waves is somewhat complicated.

The well-known fact that the periods of P-waves are shorter than those of S-waves in general may be explained to a considerable degree by the feature of the wave form mentioned above. In the present case, the amplitudes of P-waves are about half those of S-waves. Then the other well-known fact that the amplitudes of P-waves are smaller than those of S-waves in general will then depend mainly on the influence of viscosity in the earth. The results of the present investigation are ascertained considerably by means of seismographical study[5], which will be shown in the second paper in a forthcoming Bulletin.

---

[5] Meeting of Earthq. Res. Inst., Sept. 18, 1951.

50. P波の周期がS波の周期よりも短くなる可能度

地震研究所　金井　清

彈性體中の球窩面に急激に壓力又は剪斷力が働いた場合の數理的研究を一層解析的に行つた。

その結果として，$n=2$ の場合の自由振動には 3 つの型があり，震源から遠く離れたところでは，S 波は，3 つの型のうち，減衰係數が一番小さく，振動周期が一番長い型の振幅が一番大きく，P 波は減衰係數の一番大きい型の振動振幅が一番大きいことがわかつた。

從つて，S 波と P 波について夫々 3 つの型を加え合せた波形をくらべると，S 波は周期が長くて波形が單純であるが，P 波は見掛上の周期が短くて波形が複雜である。

このような機構で發生した P 波 S 波が複雜な地殼の中を通過してくると，2 つの波の間の波形の複雜さの差違は益々大きくなり，實際の地震記象に見られる，P 波の周期が S 波の周期にくらべて，はつきりと短いような現象が起りうることになる。

又，P 波と S 波の振幅の關係は，振動方向やそのほか特別な事項に支配されるが，絕對振幅は，この場合には，S 波は P 波の約 2 倍である。從つて，P 波は S 波に比べて周期が短いために減衰作用を多く受けるという性質を合せると，實際の地震記象に現れる，P 波と S 波の振幅の差違も一應の說明がつく。

なお，この研究で假定した震源機構から發生した P 波 S 波の性質をもつた地震波が，實際にあるらしいことについての研究については，次號で報告する豫定である。

51. Electromagnetic Induction within the Earth and Its Relation to the Electrical State of the Earth's Interior. Part IV.

By Tsuneji RIKITAKE,

Earthquake Research Institute.

(Read July 17, 1951.—Received Sept. 5, 1951.)

1. Introduction.

In Part I, II and III of this paper[1], the writer studied electromagnetic induction within the earth by various variations in the earth's magnetic field, the slowest of them being the apparent 27-day period variation. Even in case of such slow variation, the induced electric currents decay completely at a depth of about 1500 *km* and consequently the electric property at the depth of about 1200 *km* is the most effective for the determined electrical conductivity. Hence the distribution of the electrical conductivity, which, as determined in the previous papers, is expressed by

$$\left.\begin{aligned} \sigma &= \sigma' && \text{for} \quad q<\rho<1 \\ &= \sigma_0\rho^{-l} && \text{for} \quad \rho<q \end{aligned}\right\} \quad \dots\dots\dots\dots\dots(1)$$

(where $\sigma'=10^{-15} emu$, $\sigma_0=1.0\times10^{-12} emu$, $l=11$, $q=0.94$ and ρ denotes the radial distance from the earth's centre divided by the earth's radius), is only valid for the upper part of the earth, that is, down to the depth of about 1200 *km*. As to the deeper part, we must study slower variations.

In order to estimate the period of variations by which we can infer the electrical state of the earth's deep interior, the writer will calculate here electromagnetic induction within an earth-model having the previously obtained conductivity-distribution in its upper part or mantle, while the conductivity in the core is tentatively assumed to take a constant value σ_c. Since we have no detailed knowledge about the electrical property in the core, the calculation will be made for various values of σ_c.

---

[1] T. RIKITAKE, *Trans. Oslo Meeting, I.U.G.G.A.T.M.E.*, (1950), 435. *Bull. Earthq. Res. Inst.*, **28** (1950), 45, 219 and 263, **29** (1951), 61.

2. Theory.

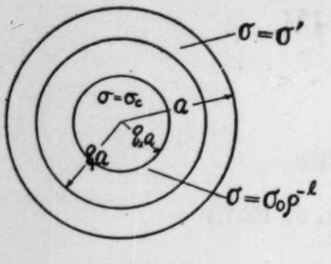

Fig. 1.

As may be seen in Fig. 1, we take an earth-model in which the electrical conductivity is equal to σ' (σ' is so small that we can regard the substance to be non-conducting for such slow variations as treated in this article), and $\sigma_0\rho^{-l}$ and σ_c stand respectively for the regions 1, 2 and 3, while the magnetic permeability is assumed to be unity everywhere.

In the non-conducting region, we have magnetic potential whose typical term is written as

$$W_n^m = a\{\boldsymbol{e}_n(t)\rho^n + \boldsymbol{i}_n(t)\rho^{-n-1}\}S_n^m \quad \dots\dots\dots\dots\dots\dots\dots\dots(2)$$

where $\boldsymbol{e}_n$ and $\boldsymbol{i}_n$ denote respectively the coefficients of the magnetic potential of external and internal origins. S_n^m denotes spherical surface harmonic having degree n and order m. In that case, the components of the magnetic field become

$$\left.\begin{aligned} &H_r = -\{n\boldsymbol{e}_n\rho^{n-1} - (n+1)\boldsymbol{i}_n\rho^{-n-2}\}S_n^m, \\ &\left.\begin{matrix} H_\theta \\ H_\phi \end{matrix}\right\} = -(\boldsymbol{e}_n\rho^{n-1} + \boldsymbol{i}_n\rho^{-n-2})\partial S_n^m \Big/ {}^{\partial\theta}_{(\sin\theta\partial\phi)} . \end{aligned}\right\} \quad \dots\dots\dots\dots\dots(3)$$

On the other hand, in the conducting medium, we have vector potential $\overrightarrow{A}$ which satisfies the relation

$$\nabla^2\overrightarrow{A} = 4\pi\sigma(\rho)\partial\overrightarrow{A}/\partial t \quad \dots\dots\dots\dots\dots\dots\dots\dots\dots\dots(4)$$

for the phenomenon is assumed to be quasi-stationary. The typical term of the solution of (3) becomes

$$\overrightarrow{A}_n^m = a\, f_n(t,\rho)\,[\,\overrightarrow{r}\ grad\ S_n^m], \quad \dots\dots\dots\dots\dots\dots\dots\dots(5)$$

where f_n satisfies the differential equation

$$\partial(\rho^2\partial f_n/\partial\rho)/\partial\rho = \{n(n+1) + 4\pi a^2\sigma\rho^2\partial/\partial t\}f_n. \quad \dots\dots\dots\dots(6)$$

Thus the components of the magnetic field are given by

$$\left.\begin{aligned} &H_r = -\rho^{-1}n(n+1)f_n S_n^m, \\ &\left.\begin{matrix} H_\theta \\ H_\phi \end{matrix}\right\} = -\rho^{-1}\partial(\rho f_n)/\partial\rho\ \partial S_n^m \Big/ {}^{\partial\theta}_{(\sin\theta\partial\phi)} . \end{aligned}\right\} \quad \dots\dots\dots\dots\dots\dots(7)$$

The function f_n becomes for the regions 2 and 3 respectively as follows;

$$f_{n,2}=\rho^{-1/2}\{C_2K_\nu(z)+D_2I_\nu(z)\} \qquad \text{for region 2} \quad (8)$$

where C_2 and D_2 are both functions of time, K_ν and I_ν denote modified Bessel functions, while

$$\rho^{1-l/2}=(l-2)z/(2\zeta), \quad \nu=(2n+1)/(l-2), \quad \zeta^2=4\pi a^2\sigma_0 p, \qquad (9)$$

and

$$f_{n,3}=C_3\rho^nF_n(\rho) \qquad \text{for region 3} \quad (10)$$

where C_3 also denotes a function of time, F_n being fully studied in the well known book "*Geomagnetism*"[2]. In the above treatment, $\partial/\partial t$ is replaced by p as often used in operational calculus.

From the continuity of magnetic field at $\rho=q_1$ and q_2 ($q_2=0.545$), we have four simultaneous equations. On solving the equations, we get

$$\left.\begin{aligned}
C_2&=q_1^{n+1/2}(n+1)^{-1}(2\nu/z_1)\Psi(p)\{(z_2/2\nu)I_{\nu+1}(z_2)\\
&\quad+(F_{n-1}(q_2)/F_n(q_2))I_\nu(z_2)\}e_n\,,\\
D_2&=q_1^{n+1/2}(n+1)^{-1}(2\nu/z_1)\Psi(p)\{(z_2/2\nu)K_{\nu+1}(z_2)\\
&\quad-(F_{n-1}(q_2)/F_n(q_2))K_\nu(z_2)\}e_n\,,\\
C_3&=(q_1/q_2)^{n+1/2}(n+1)^{-1}\Psi(p)(z_1F_n(q_2))^{-1}e_n\,,
\end{aligned}\right\}\quad\ldots\ldots\ldots\ldots\ldots(11)$$

where

$$\begin{aligned}
1/\Psi(p)&=K_{\nu+1}(z_1)\{(z_2/2\nu)I_{\nu+1}(z_2)+(F_{n-1}(q_2)/F_n(q_2))I_\nu(z_2)\}\\
&\quad-I_{\nu+1}(z_1)\{(z_2/2\nu)K_{\nu+1}(z_2)-(F_{n-1}(q_2)/F_n(q_2))K_\nu(z_2)\}\,,\quad\ldots\ldots(12)
\end{aligned}$$

and where z_1 and z_2 denote respectively $z_{\rho=q_1}$ and $z_{\rho=q_2}$.

Since the intensity of the induced current is given by

$$\vec{c}=-\rho\,\partial\vec{A}/\partial t\,,$$

we can obtain the current intensity from (11), (12) and

$$\left.\begin{aligned}
\vec{c}^{\,m}_{n,2}&=-\sigma_0ap\rho^{-(l+1/2)}\{C_2K_\nu(z)+D_2I_\nu(z)\}[\vec{r}\;grad\;S^m_n]\,,\\
\vec{c}^{\,m}_{n,3}&=-\sigma_c ap\rho^nC_3F_n(\rho)\,[\vec{r}\;grad\;S^m_n]\,.
\end{aligned}\right\}\quad\ldots\ldots(13)$$

In case of periodic variation having period $2\pi/\alpha$, the operator p and e_n are replaced by $i\alpha$ and $Ee^{i\alpha t}$ in the above expressions. When the period is larger than about ten years, I_ν^1 and K_ν^1 are calculated with the aid of ascending power expansion, whence (13) become

---

[2] S. CHAPMAN and J. BARTELS, *Geomagnetism* p. 738.

$$\left.\begin{aligned}\vec{c}^{\,m}_{n,2}&=-a\sigma_9\rho^{-l+n}i\alpha(n+1)^{-1}(q_2/q_1)^{1/2}Ee^{i\varkappa t}[\vec{r}\ grad\ S_n^m]\\&\quad\times\frac{F_{n-1}(q_2)+i\nu^{-1}(\nu+1)^{-1}(x_2/2)^2F_n(q_2)+(q_2/\rho)^{2n+1}(F_n(q_2)-F_{n-1}(q_2))}{F_{n-1}(q_2)+i\nu^{-1}(\nu+1)^{-1}\{(x_2/2)^2F_n(q_2)-(q_2/q_1)^{2n+1}(x_1/2)^2(F_n(q_2)-F_{n-1}(q_2))\}},\\\vec{c}^{\,m}_{n,3}&=-a\sigma_c\rho^n i\alpha(n+1)^{-1}(q_2/q_1)^{1/2}Ee^{i\varkappa t}[\vec{r}\ grad\ S_n^m]\\&\quad\times\frac{F_n(\rho)}{\nu},\end{aligned}\right\}\quad(14)$$

where x denotes $z\sqrt{i}$, higher order terms of $x/2$ being neglected.

On the contrary, asymptotic expansions for modified Bessel functions are available for variations having short period. In that case, we have

$$\left.\begin{aligned}&C_2\simeq q_1^{n+1/2}(n+1)^{-1}(2\nu/z_1)(1/K_{\nu+1}(z_1))e_n\,,\\&D_2\simeq 0\,,\\&D_3\simeq 0\,.\end{aligned}\right\}\quad\ldots\ldots\ldots\ldots(15)$$

Hence, the current intensity for short period variation becomes just the same with the cases discussed by Price, Lahiri [3] and the writer. Physically speaking, since the induced currents do not penetrate into great depth in case of short period variation, the electrical property of the deep interior, as of the core, does not contribute to the calculation.

3. The distribution of the induced currents and their contribution to the magnetic field at the earth's surface.

From (13), (14) and (15), the distribution of the amplitude of the induced currents in the earth is calculated for various periods and σ_c. The degree is taken to be 1. As shown in the left side of Fig. 2 in an arbitary scale, the currents do not practically penetrate into the core in case of periods shorter than 10 *days*. On the right side of the figure, the contribution of the currents flowing at any depth to the magnetic field at the earth's surface is also shown in an arbitary scale, the contribution being proportional to $|\vec{c}|\,\rho^{n+2}$ as is well known.

---

[3] A. T. PRICE and B. N. LAHIRI, *Trans. Roy. Soc. London A*, **237** (1939), 509.

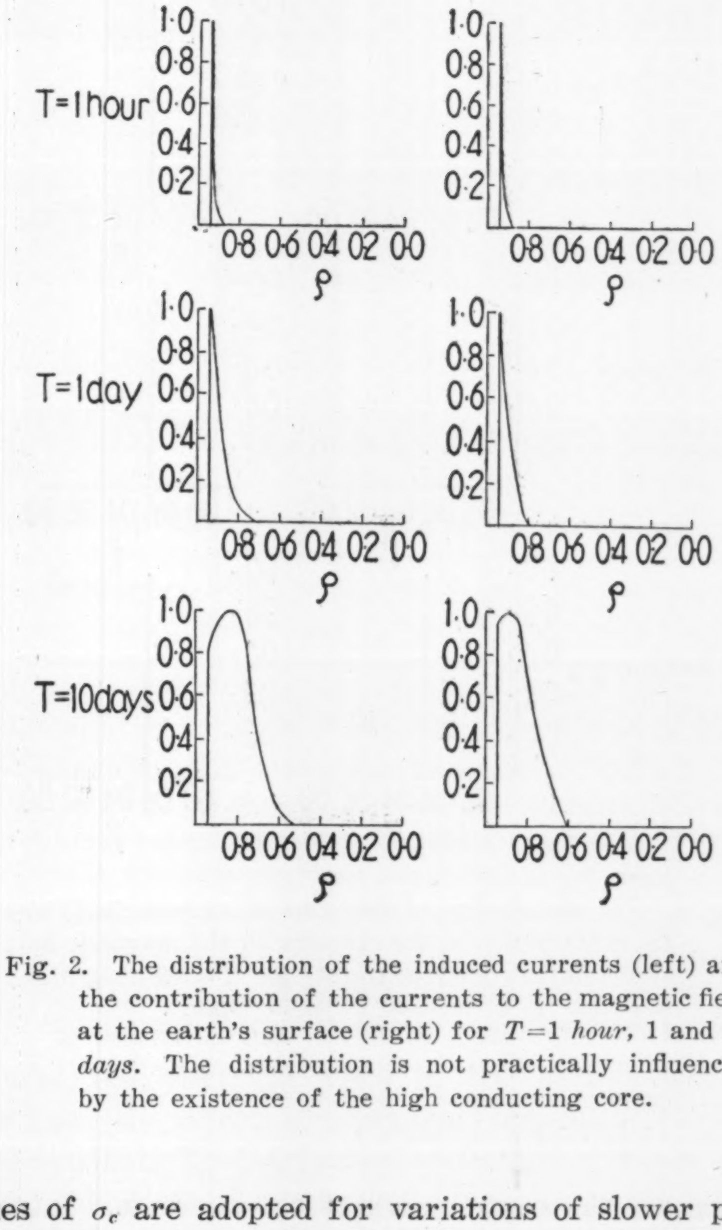

Fig. 2. The distribution of the induced currents (left) and the contribution of the currents to the magnetic field at the earth's surface (right) for $T=1$ *hour,* 1 and 10 *days.* The distribution is not practically influenced by the existence of the high conducting core.

Three values of σ_c are adopted for variations of slower period such as 100 *days,* 1 and 10 *years.* The distribution of the induced currents and the contribution to the magnetic field at the earth's surface are both calculated for $\sigma_c=10^{-6}$, 10^{-8} and 10^{-10} *emu* as respectively shown in Figs. 3, 4 and 5. As seen in the figures, it is clearly shown that the longer the period is, and the higher the conductivity in the core is, the deeper penetrate the currents into the earth.

As often done in the writer's previous paper, we define the "effective radius" of the electrical conductivity by

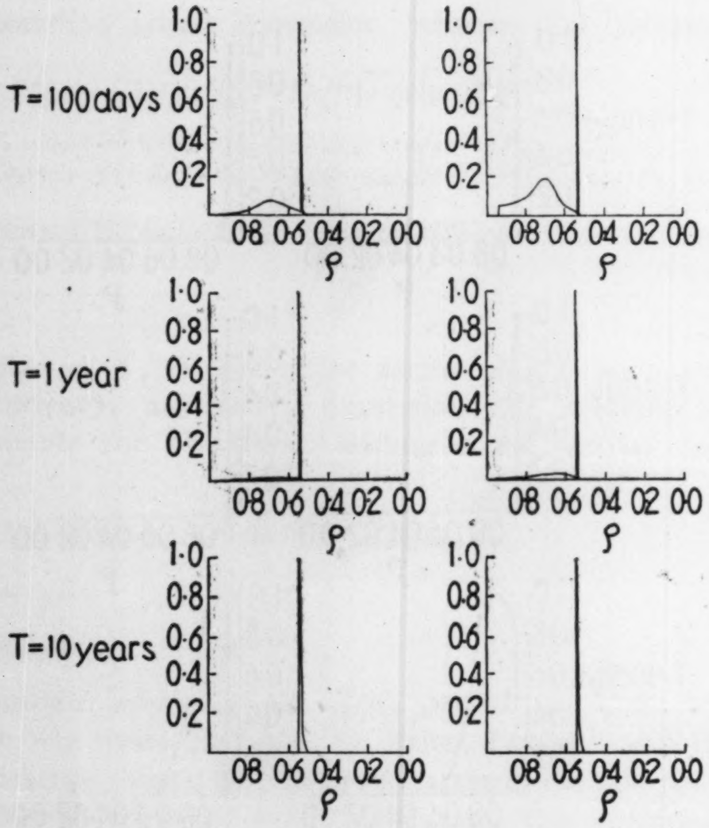

Fig. 3. The distribution of the induced current (left) and the contribution of the currents to the magnetic field at the earth's surface (right) for $T=100$ *days*, 1 and 10 *years*. σ_c is sssumed to be 10^{-6} *emu*.

$$\int_0^1 \rho\varphi(\rho)d\rho \Big/ \int_0^1 \varphi(\rho)d\rho \,,$$

where $\varphi(\rho)$ denotes the contribution of the currents. Introducing this convenient concept, the most effective depth of the electrical conductivity may be tentatively obtained for variations of various periods. The "effective depth" thus determined is shown in Fig. 6 where the influence of high conductivity in the core is not so remakable for variations of shorter period than 1 *year*. But the influence becomes considerable for longer periods. Anyhow, we see that variations having periods longer than 10 *years* or more should be studied in order to infer the electric property in the core.

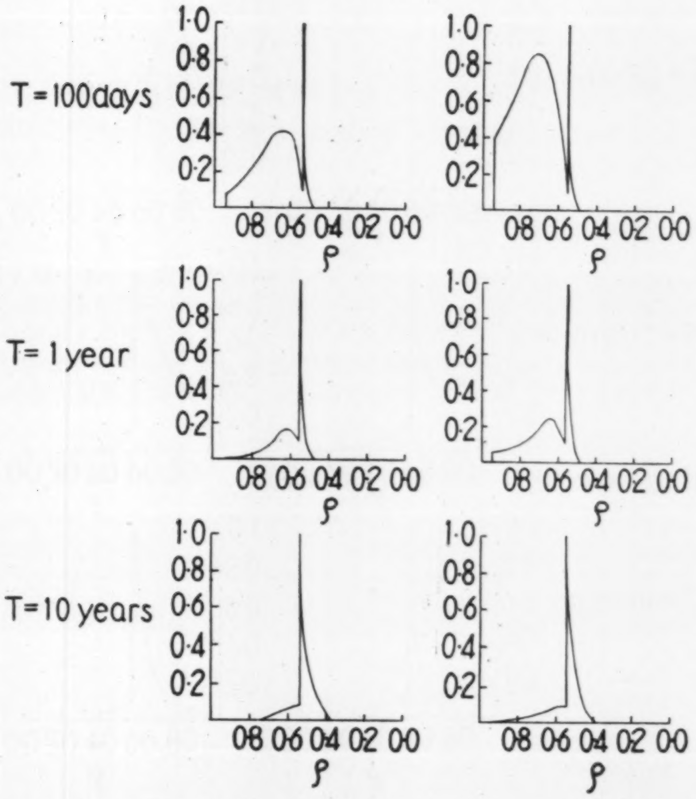

Fig. 4. The distribution of the induced currents (left) and the contribution of the currents to the magnetic field at the earth's surface (right) for $T=100$ *days*, 1 and 10 *years*. σ_c is assumed to be 10^{-8} *emu*.

4. Conclusion.

In order to estimate the period of geomagnetic variation by which we may infer the electrical state in the earth's deep interior, the relation between the effective depth and the period is obtained on the basis of the conductivity-distribution previously obtained by the writer. It has been made clear that we should analyse geomagnetic variations having periods longer than 10 *years* to determine the conductivity in the core. If we could analyse geomagnetic condition varying with sun-spot cycle, it might be possible to discuss the electric property in the earth's core.

In conclusion, the writer wishes to express his hearty thanks to Professor M. Hasegawa by whose suggestion this study was made. To Dr. T. Nagata who always encouraged the writer, the writer's cordial thanks are also due.

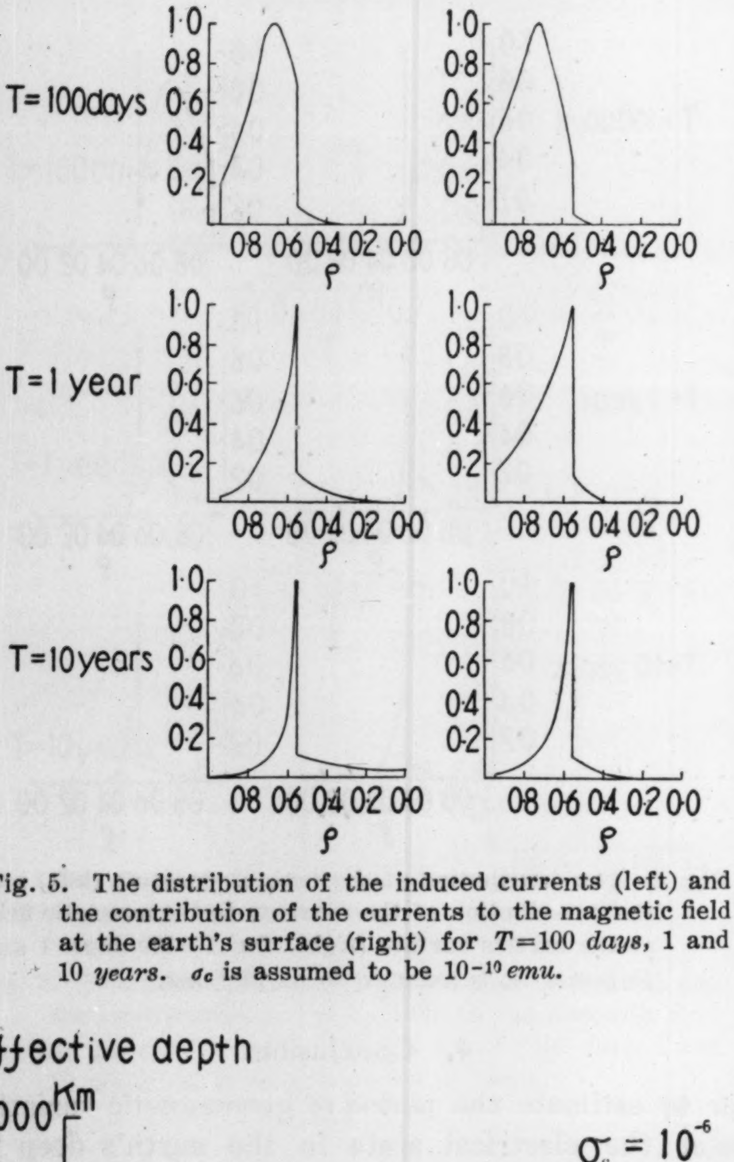

Fig. 5. The distribution of the induced currents (left) and the contribution of the currents to the magnetic field at the earth's surface (right) for $T=100$ *days*, 1 and 10 *years*. σ_c is assumed to be 10^{-10} *emu*.

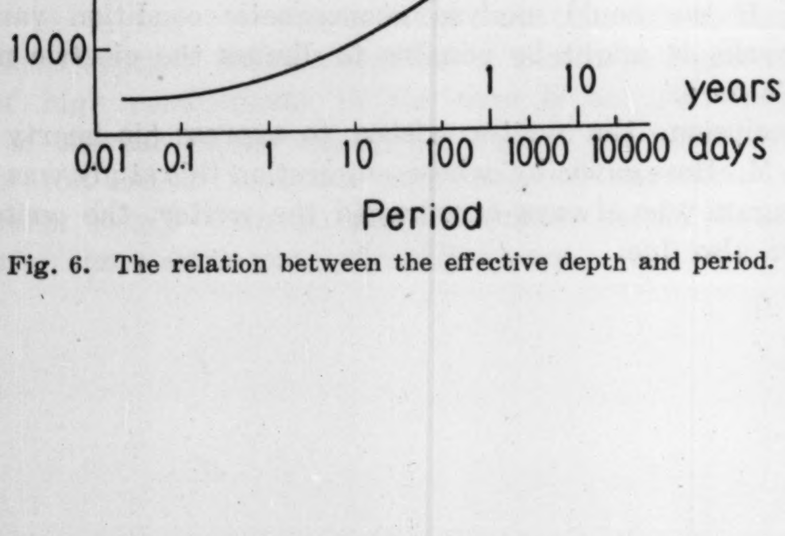

Fig. 6. The relation between the effective depth and period.

51. 地球内の電磁感應およびその地球内部の電氣的性質との關係 第4報

地震研究所 力武常次

第1,2および3報に於いて求めた地球のモデルについて，地球核の電氣的性質を決定出来るためには，どのぐらいの周期の變化を取扱うべきかを計算した。核の電氣傳導度として 10^{-10}, 10^{-8} および 10^{-6} *emu* の値をとる時，10年以上の長周期地磁氣變化を解析しなければならないことになる。現在の觀測の精度ではこのような長周期變化を議論することは，かなり困難のように思われる。この研究は京大長谷川萬吉教授の示唆により行われたものであることを記して，同教授に感謝の意を表する。

52. *Notes on Stray Earth Currents.*

By Fuyuhiko KISHINOUYE,

Earthquake Research Institute.

(Read Oct. 17, 1950 and May 15, 1951.—Received Sept. 20, 1951.)

During the years 1946-47, the writer carried out electrical prospecting by the method of spontaneous polarization at the Hidachi Mine, Ibaragi Prefecture. The measurements of electrical potential was so much disturbed by stray earth currents that the reading of potentiometer changed from time to time and would not give a definite value of potential differences. The distribution of potential differences is as shown in Fig. 1. The potential decreased to the NE direction in the surveyed area as much as 500 mV, and there seemed to be no limit to the deceasing of the potential.

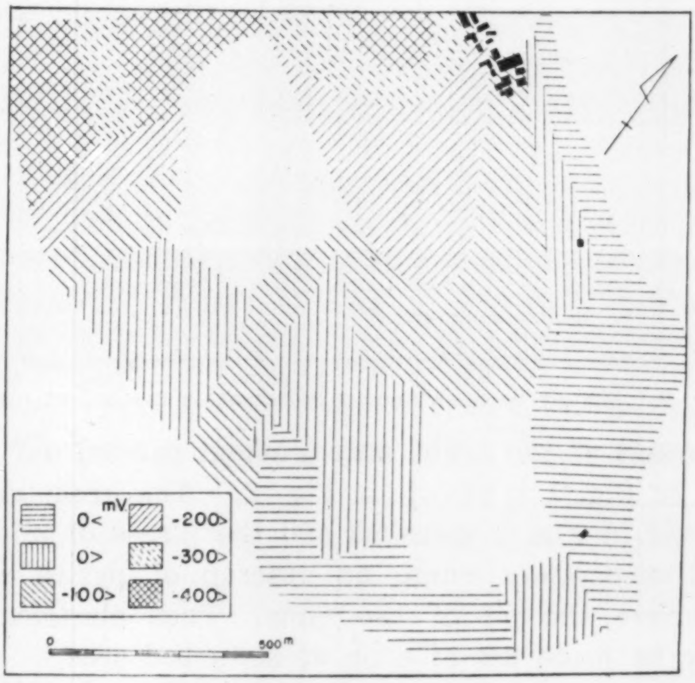

Fig. 1. Survey by spontaneous polarization method in day time.

The disturbance or the fluctuation of the potential was ascribed to electric currents which returned to the earth from electric cars at the mine. And the apparent endless decrease of the potential was considered as a consequence of the return currents from electric cars or leakage currents of the electrical refinary about 4 km ESE from the observed area.

Then the writer recorded the currents on photographic papers with galvanometers for several days.1) As a result of the observations, the daily variation of the current was made clear. The currents are strong in day time, and weak during midnight or between 23 h and 5 h in the next day. Since the daily variation was found out, the prospecting by the method of spontaneous polarization was carried out at night to avoid the disturbances by the stray currents at the Hidachi Mine. The result of the night measurement carried out in the same area as that of Fig. 1 is shown in Fig. 2. The great negative value of the potential in Fig. 1 vanished and the places of minimum potential coincided with places where an outcrop of pyrite was found or are nearly above the pit of the mine. Thus electrical prospecting at night may be made use of even at disturbed area.

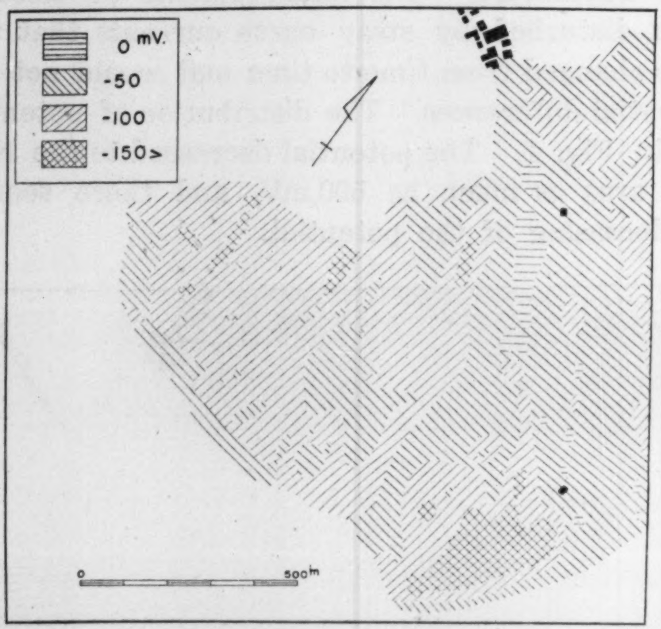

Fig. 2. Survey by spontaneous polarization method at night.

For the above measurements, non-polarizing electrodes were used and the two electrodes were set at a distance of 10 m apart.

---

1) THE SPEC. COMM. EXPLORATION OF MINERAL DEPOSITS, GEOLOGY, *Ore Deposit and Geophysical Prospecting. II.* Tokyo, 1951, 119–131.

The Direction of Stray Currents

Comparing the distribution of the potential with the geological map, the writer considered that the distribution of the potential is connected to some measure with the electrical property of rocks. For example, the boundary of -100 mV and -200 mV in Fig. 1 nearly coincides with that of granodiorite and schist. As such boundary the variation of stray currents may be found out by observing the amount and bearings of the currents. But for the sake of simplicity, the writer measured only the direction of the stray currents at many places near the Hidachi mine to test the new method of prospecting. The result may prove not satisfactory, but it will be described here.

The method of determining the bearings of the currents was simple; two pairs of non-polarizing electrodes were set 10 m apart in two directions, E-W and N-S or NE-SW and NW-SE, and the bearings were obtained from the ratio of potentials in the two directions

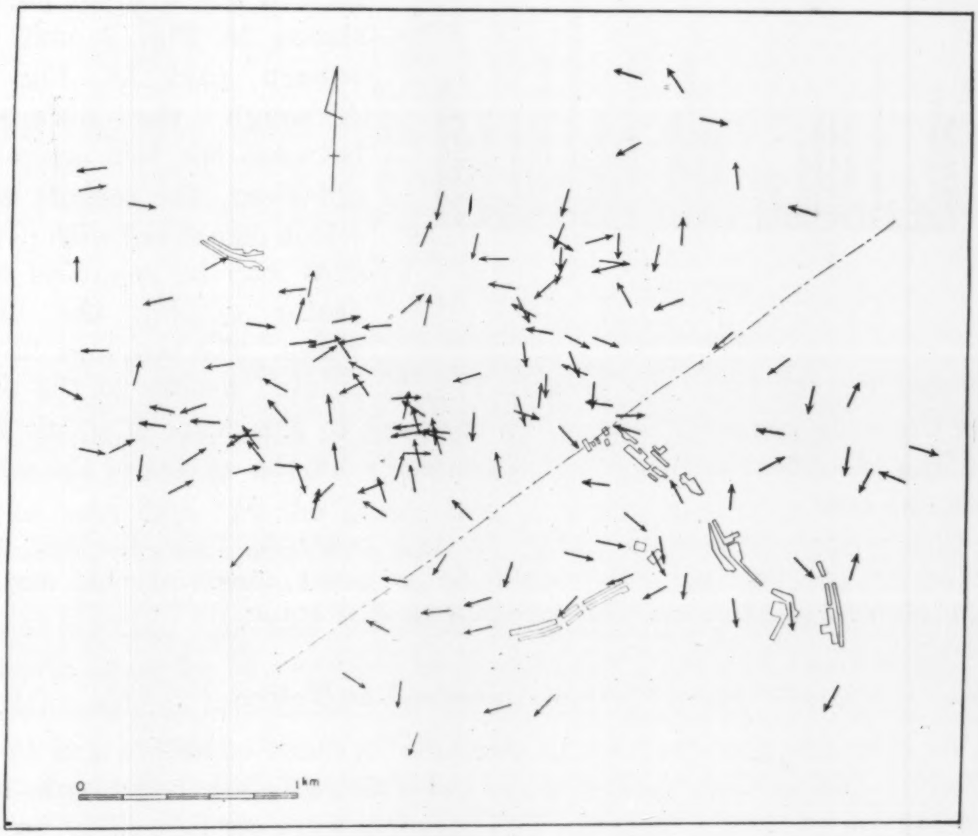

Fig. 3. Direction of stray currents.

measured by a bridge circuit. The sensitivity of the galvanometer used for the circuit was 2.2×10^{-7}A. The bearings at the neighbourhood of the Hidachi mine were partly shown in Fig. 3. Of course, the directions are nearly perpendicular to the equipotential lines in Fig. 1. During the measurement the writer thought most of the directions pointed to the west in the western area of the measurement. Dividing the area of the measurement into two by the narrow zone of sericite, frequency-distributions of the bearings were obtained: the bearings in the eastern part is shown in Fig. 4 and the wesern part in Fig. 5. Although the difference between the two areas are not clear, the sericite zone which associated with pyrite ores may be regarded as a factor causing the difference. The bearings in the area east far off from the area in Fig. 3, pointed mostly to the east. Then the stray currents were then ascribed to the current which flew from the electrical refinary which is nearly at the centre of the whole measured area.

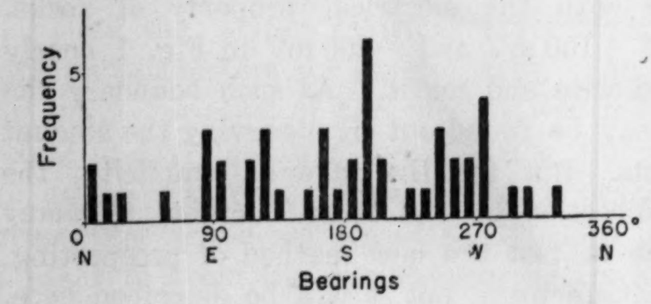

Fig. 4.

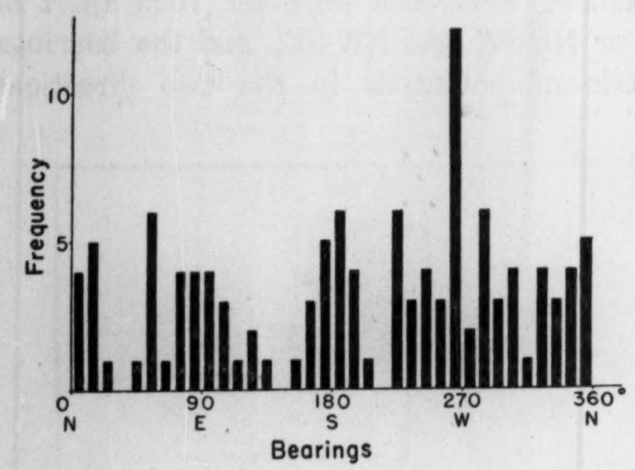

Fig. 5.

The writer wishes to carry on the present study further as a method of prospecting. It would be a great merit of this method for it may be made easy and possible in day time.

Stray Currents observed at Tokyo

To compare the stray earth currents in quiet condition and in disturbed condition, the writer observed changable earth currents near our Institute at Hongo, Tokyo. The currents were considered to be due to the return currents of electric street cars which are driven by D.C.

In this case carbon electrodes were used and the electrode distance was 2.3 m at the depth of 10 cm under the surface of the ground. The currents were strong that high resistance was put in series into the galvanometer circuit, and the so sensitivity of the galvanometer was sometimes decreased with a shunt.

The variation was different from that at Hidachi in that it was greater than those observed at Hidachi, and was irregular as shown in Figs. 6 (1) and 6 (2). Periods of the variation were in confusion, and amplitudes were from 1/3 to 1/10 of the mean currents.

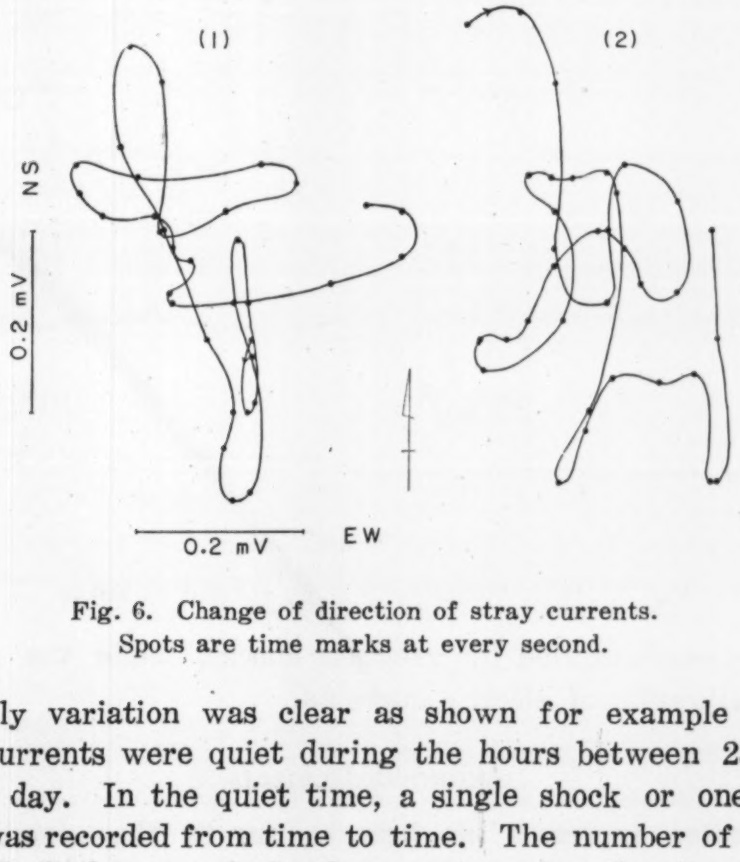

Fig. 6. Change of direction of stray currents.
Spots are time marks at every second.

The daily variation was clear as shown for example in Fig. 7. The stray currents were quiet during the hours between 23 *h* and 5 *h* of the next day. In the quiet time, a single shock or one-sided displacement was recorded from time to time. The number of the shocks became suddenly large early in the morning when the city electric cars began moving. As the numbers of moving cars increased the stray currents came to be recorded as continuous irregular oscillations.

Microseisms are sometimes considered as earth vibrations caused by many irregular shocks. The cause may be similar to that of the stray currents. But microseisms are rather regular, and the stray currents are always irregular. The difference may be due to the property of the ground: That is to say, microseism are proper vibra-

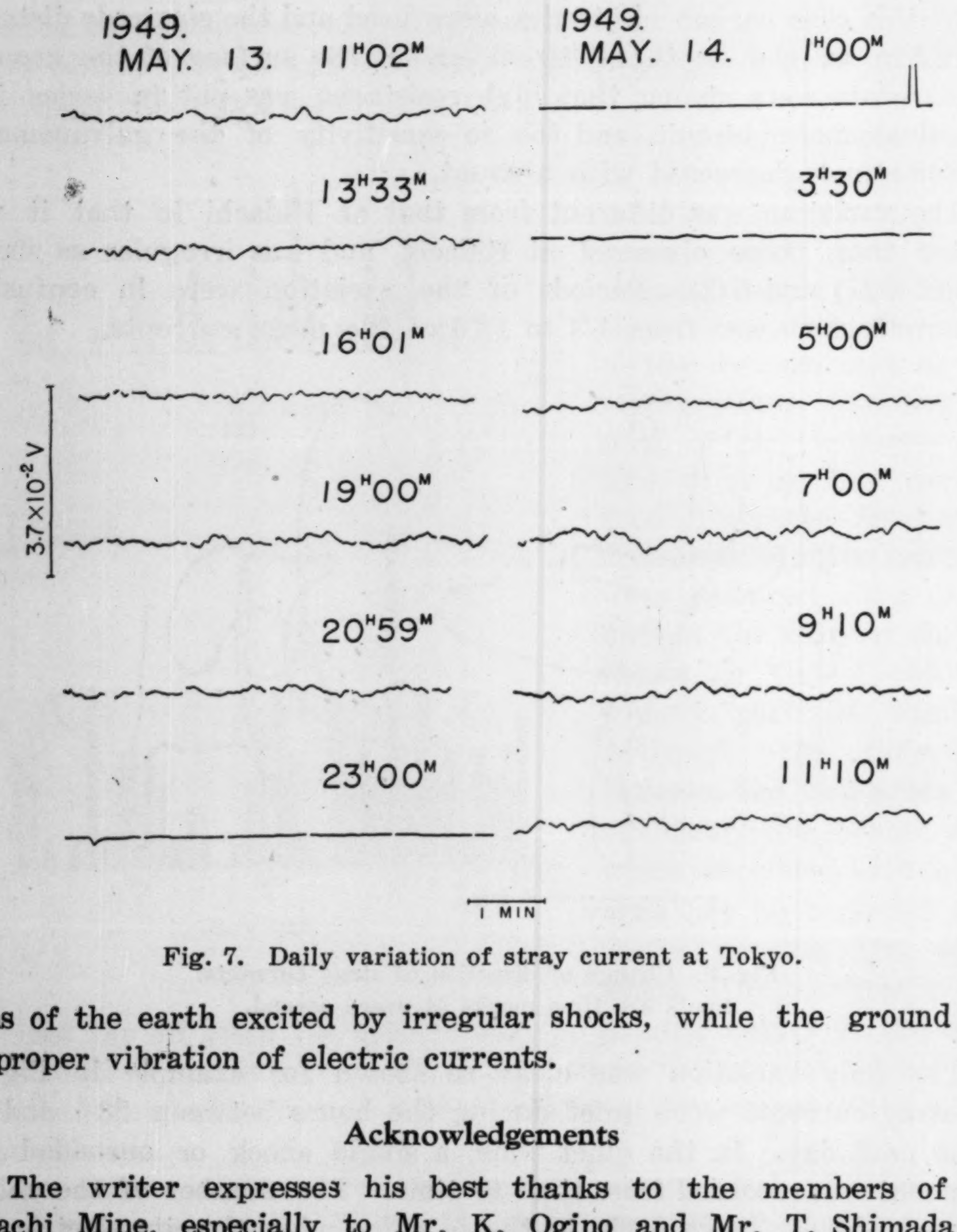

Fig. 7. Daily variation of stray current at Tokyo.

tions of the earth excited by irregular shocks, while the ground has no proper vibration of electric currents.

Acknowledgements

The writer expresses his best thanks to the members of the Hidachi Mine, especially to Mr. K. Ogino and Mr. T. Shimada for their kind help offered to his investigations there. Also he thanks Miss M. Kotaka for her assistance in the study of stry currents at Tokyo.

The cost of this investigation was defrayed from the Scientific Research Expenditure of the Department of Education.

52. 迷走地電流について

岸上冬彦

茨城縣日立鑛山附近で自然電位法による電氣探鑛を行つた時，迷走電流の爲測定が妨害された。又，測定地域の北に 500 mV 以上の負電位が現われ正電位に向う所が見つからなかつた。これは鑛山の電車などの接地線のため，迷走電流が一方に向けて流れるものと考へた。これについての研究は既に「地質鑛床と物理探鑛下卷」に記した。その後この電流の方向の分布を測定したので，その結果を圖示した。次に日立と比べるために東京において記錄した結果をのべた。日立では凡そ方向が求められたが東京では不規則である。

53. *Observations of the Deformation of the Earth's Surface at Aburatsubo, Miura Peninsula. Part V.*

By Takahiro HAGIWARA and Keichi KASAHARA,

Earthquake Research Institute.

(Read June 19, 1951—Received Sept. 20, 1951.)

E. Nishimura[1], Kyoto University, has reported that the amplitude of earth-tide observed with the fused silica tiltmeter at Makimine, Kyushu Province, showed a wide variation with the lapse of time. He stated that this curious phenomenon may be considered to be caused by the change in the elasticity of the earth crust near the observation point and seems to have some relations with the occurrence of earthquakes. The present writers felt a keen interest in his report and investigated their own data obtained at Aburatsubo in order to examine whether such a phenomenon existed or not.

As reported in the writers' previous papers[2], the observations of the deformation of the earth's surface have been continued at Aburatsubo since 1948 to the present. In the present paper, the following problems were examined.

1. Is the ratio of the tilt observed with the water-tube tiltmeter to the change in sea level constant with respect to time?
2. Is the ratio of the linear strain observed with the silica-tube extensometer to the change in sea level constant with respect to time?
3. Is the M_2-component of the linear strain recorded by the extensometer constant with respect to time?

The investigation was restricted only to the E′W′-component of the tilt and to the E_{10}-component of the linear strain, because these components were mostly affected by the oceanic tide.

1. Ratio of the tilt observed with the water-tube tiltmeter to the change in sea level.

Since the reading of the water-tube tiltmeter was made twice a day, namely, at 8h and 16h, we obtained $\delta W.T.$ and $\delta S.L.$ for determining the amount of tilt caused by the oceanic tide; where $\delta W.T.$ is the difference of the tilt measured by the water-tube tiltmeter at 8h and 16h, and $\delta S.L.$ the difference of the sea level at 8h and 16h of each day. We then assumed that $\delta W.T.$ and $\delta S.L.$ were in the linear relation expressed by the following equation

---

[1] E. NISHIMURA, *Trans. Am. Geophys. Union*, **31** (1950), 357.

[2] T. HAGIWARA and collaborators, *Bull. Earthq. Res. Inst.*, **26** (1948), 23; **27** (1949), 35; **27** (1949), 39; **29** (1951), 455.

$$(\delta W.T.) = \alpha(\delta S.L.),$$

where α is a numerical constant. By using this equation, we determined the value of α by the least square method for a particular month. As an example, the relation between $\delta W.T.$ and $\delta S.L.$ in January, 1951 is shown in Fig. 1. The values of α of each month thus determined are shown in Table I and Fig. 3.

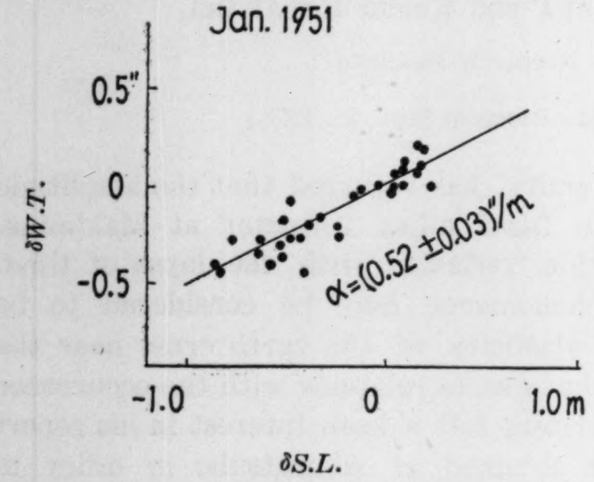

Fig. 1.

2. Ratio of the linear strain observed with the extensometer to the change in sea level.

We applied the method just mentioned to the linear strain. We thus obtained δE and $\delta S.L.$; where δE is the difference of linear strain in E_{10}-component at 8h and 16th and $\delta S.L.$ the difference of sea level at 8h and 16h. The values of δE were obtained from the record of the extensometer. Then, we determined the value of α for a particular month by the use of the following equation

$$\delta E = \alpha(\delta S.L.),$$

where α is a numerical constant. As an example, the

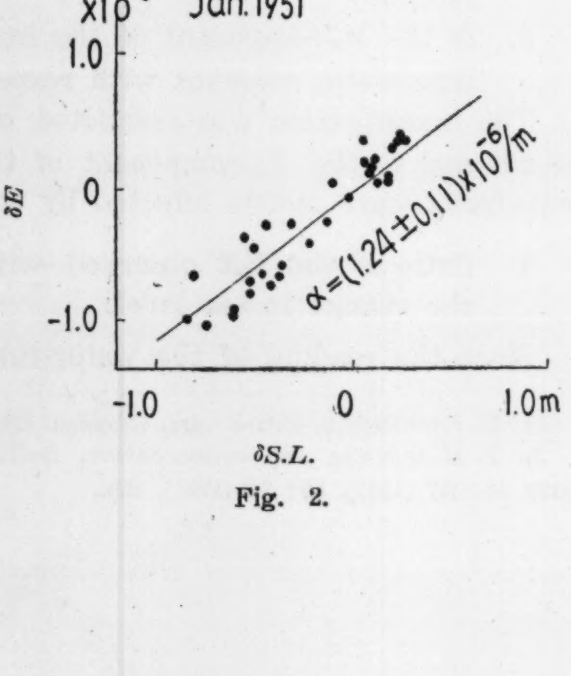

Fig. 2.

determination of a of January 1951 is shown in Fig. 2. The values of a determined by the least square method with respect to each month are shown in Table I and Fig. 3.

3. M_2-component of the linear strain recorded by the extensometer.

In the next place, we computed the M_2-component of the linear strain from the record of the extensometer by using the ordinary method of tidal analysis. The analysis was made with respect to each month by using data of 29 days for the corresponding month. The amplitudes and phase lags of the M_2-component of the linear strain thus determined are shown in Table I and Fig. 3.

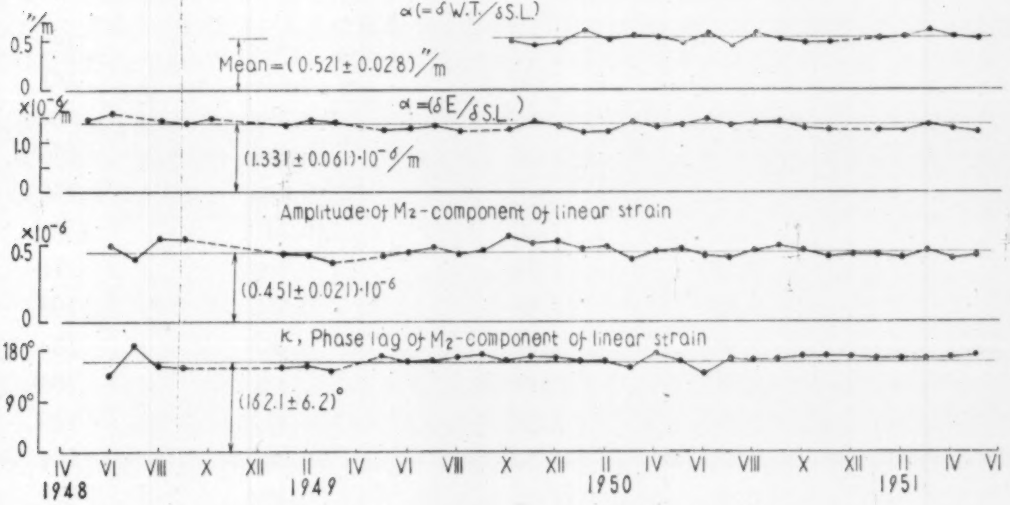

Fig. 3.

Conclusion.

As will be seen in Table I and Fig. 3, the ratio of the tilt or of the liner strain to the change in sea level does not show any large secular variation. Considering the errors in observation, we can say that it remained constant throughout the interval of observation. The same conclusion may be given in regard to the M_2-component of the linear strain. At all events, we could not find such a phenomenon as was observed in Makimine.

Table I.

Month		$\alpha(=\delta W.T./\delta S.L.)$	$\alpha(=\delta E/\delta S.L.)$	Amplitude of M_2 (E_{10})	Phase lag of M_2 (E_{10})
1948	5		1.43×10^{-6}/m	— $\times10^{-6}$	— °
	6		1.55	0.496	132
	7		—	(0.407)	(185)
	8		1.41	(0.538)	(156)
	9		1.38	(0.536)	(149)
	10		1.46	—	—
	11		—	—	—
	12		—	—	—
1949	1		1.31	(0.434)	(147)
	2		1.43	0.430	149
	3		1.40	(0.383)	(141)
	4		—	—	—
	5		1.26	0.429	168
	6		1.26	0.449	161
	7		1.33	0.478	164
	8		1.23	0.453	170
	9		—	0.462	176
	10	0.50″/m	1.26	(0.547)	(162)
	11	0.46	1.41	0.508	171
	12	0.48	1.34	0.515	168
1950	1	0.60	1.21	0.467	160
	2	0.51	1.21	0.481	166
	3	0.55	1.38	0.417	149
	4	0.53	1.30	0.464	171
	5	0.49	1.34	0.468	158
	6	0.57	1.43	0.430	132
	7	0.45	1.32	0.413	162
	8	0.57	1.36	0.463	163
	9	0.51	1.41	0.487	169
	10	0.49	1.28	0.460	167
	11	0.48	1.25	0.422	166
	12	—	—	0.428	168
1951	1	0.52	1.24	0.435	163
	2	0.53	1.24	0.409	163
	3	0.60	1.35	0.454	164
	4	0.54	1.26	0.406	166
	5	0.52	1.20	0.421	169
Mean value		0.521±0.028	1.331±0.061	0.451±0.021	162.1±6.2

The values put in parentheses are unreliable by lack of continuous observation and were not used in figuring the mean value given at the bottom.

The amplitude and phase lag of the M_2-component of the oceanic tide in Aburatsubo Bay are respectively 35.2 cm and 152.6°.

53. 油壺における地殼變動の觀測 (第5報)

地震研究所 { 萩原尊禮
笠原慶一

京大の西村英一氏は，九州槇峰においてシリカ傾斜計による地殼潮汐の觀測を行つた結果，地殼潮汐の分潮の振幅が時と共に非常に大きな變動を示すことを報告している。氏はこの現象を觀測點近傍の地殼の彈性の大きな變化によるものと考え，地震發生とも關連が見られると言つている。このような現象——相當廣い範圍の地殼の彈性率が數ケ月の中に數十％も變わる現象——は物理的には考えにくいことであるが，實際そのような事柄が觀測されたとすれば重大なことであるので，このような現象が著者等が數年來行つている油壺における土地の傾斜や伸縮の觀測結果にも見られるかどうかを調べて見た。

その結果，海洋潮汐の荷重によつて起される土地變形の量は，油壺においては時と共に變わらないことが確められた。

Errata.

Part II of the present study (Bull. Earthq. Res. Inst., **27** (1949)).
For page 37, equation (2), read as follows:

$$\left.\begin{aligned} e_{xx} &= 0.586\,e_1 - 0.196\,e_2 + 0.611\,e_3 \\ e_{yy} &= 0.198\,e_1 + 1.040\,e_2 - 0.238\,e_3 \\ e_{xy} &= -1.348\,e_1 - 0.064\,e_2 + 1.412\,e_3 \end{aligned}\right\}$$

〃 〃, symbols e_1, e_2, and e_3 in Fig. 2
read e_2, e_3, and e_1, respectively.
〃 〃, 22nd line, axes, read strains.
For page 37, between the 24th and 25th line, following letters should be interposed:
$\theta = 66°$ (Direction of maximum principal strain).

Part IV of the present study (Bull. Earthq. Res. Inst., **29** (1951)).
For page 456, 19th line, degrees, read seconds.

54. *Petrography of the 1950-lavas of Oshima volcano, Seven Izu Islands, Japan.*

By Hiromichi TSUYA and Ryōhei MORIMOTO,

Earthquake Research Institute.

(Read June 19, 1951—Received Sept. 20, 1951.)

After 10 years' quiescence, Mt. Mihara, the central cone of the volcano Oshima, one of the Seven Izu Islands, suddenly began her recent eruption at 9 : 15 (Japan standard time) on the morning of July 16, 1950. The activity continued for 10 weeks till it stopped on September 23 at midnight. During the 70 days, about 50,000,000 tons[1] of new lava filled up successively the central pit (August 15) and the

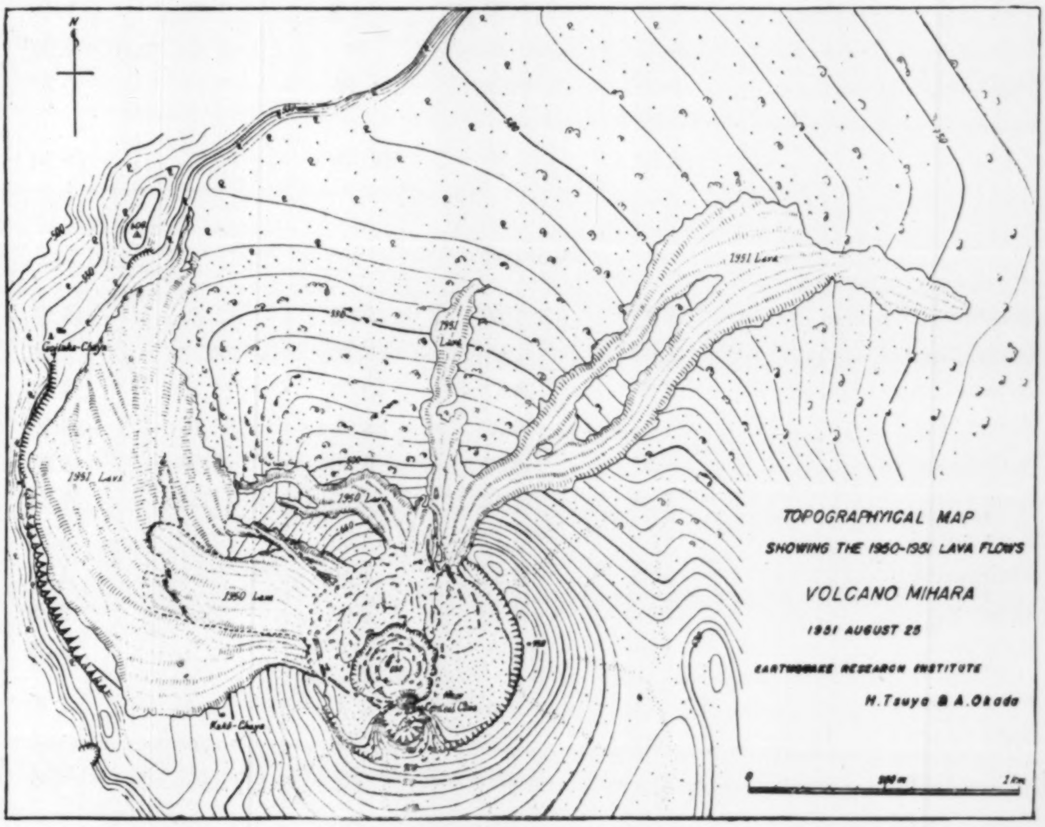
N
TOPOGRAPHYICAL MAP
SHOWING THE 1950-1951 LAVA FLOWS
VOLCANO MIHARA
1951 AUGUST 25
EARTHQUAKE RESEARCH INSTITUTE
H. Tsuya & A. Okada
1951 Lava
1951 Lava
1951 Lava
1950 Lava
1950 Lava
Gojinka-Chaya
Kakō-Chaya
Central Cone
0
500m
1km

Fig. 1.

---

[1] An estimate based on the topographic survey of the new lava field by R. Takahashi and D. Shimozuru. The bulk specific gravity was weighed in our laboratory as 1.7 for the cinder, 2.2 for the lavas which flowed down from the crater, and 2.7 for the lava on the crater floor.

Table I. Chemical Composition of the 1950-lavas.
(Analyst J. Ossaka)

Constitutents	1	2	3	4	5
SiO_2	52.68	52.02	52.25	52.25	52.30
Al_2O_3	15.28	15.83	15.55	15.33	15.50
Fe_2O_3	2.78	2.28	2.92	3.84	2.96
FeO	10.56	10.80	10.22	9.46	10.26
MgO	4.59	4.47	4.86	4.65	4.64
CaO	9.78	9.48	9.92	9.41	9.65
Na_2O	1.47	1.58	1.72	1.65	1.61
K_2O	0.26	0.29	0.39	0.37	0.33
H_2O+	0.20	0.99	0.71	0.91	0.70
H_2O-	0.11	0.24	0.21	0.28	0.21
TiO_2	1.67	1.52	1.57	1.21	1.49
P_2O_5	0.17	n. d.	tr.	n. d.	0.09*
MnO	0.09	0.09	0.06	0.15	0.10
	99.64	99.59	100.38	99.51	99.84

Norms

Quartz		11.83	10.39	9.25	11.23	10.75
Orthoclase		1.67	1.67	2.23	2.23	2.23
Albite		12.58	13.11	14.68	14.16	13.63
Anorthite		34.21	35.32	33.65	33.10	33.93
Wollastonite		5.57	4.88	6.50	5.69	5.46
Enstatite		11.44	11.14	12.15	11.54	11.54
Ferrosilite		14.51	15.57	13.85	12.53	13.98
Magnetite		3.94	3.24	4.17	5.56	4.40
Ilmenite		3.19	2.88	3.04	2.28	2.88
Apatite		0.33	n. d.	tr.	n. d.	0.33
NF	or	3	3	4	4	5
	ab	26	26	29	29	27
	an	71	71	67	67	68
NPl	An	73	73	70	70	71
NPy	Wo	18	16	20	19	18
	En	36	35	37	39	37
	Fs	46	49	43	42	45

(to be continued)

Modes**

Constitutents	1	2	3	4	5
Plagioclase	4.6	5.1	9.8	7.4	6.7
Hypersthene.........	0.5	tr.	0.3	0.9	0.4
Augite	0.2	tr.	tr.	0.7	0.2
Groundmass	94.5	94.9	89.9	91.0	92.6

1. Bomb ejected on July 22 (cf. Fig. 4). The groundmass consists of brown glass with microlites of plagioclase and pigeonite and iron ore dust.
2. Lava filled up the crater on August 23. The groundmass consists mainly of pigeonite, about half percent in volume, bytownite (An 75) and dark brown glass. The hypersthene phenocrysts are replaced by pigeonite grains.
3. Lava flowing out from the crater to the direction of Nomashi on September 18 (cf. Fig. 5). The groundmass consists of pigeonite, bytownite (An 75), skeletal crystals of magnetite and brown glass.
4. Bomb ejected on September 23. The groundmass is composed of light coloured porous glass. Thin film of iron ores is found on the surface of the bomb.
5. Mean chemical composition of 1–4.

* Mean of 1 and 3. ** Percentage in volume.

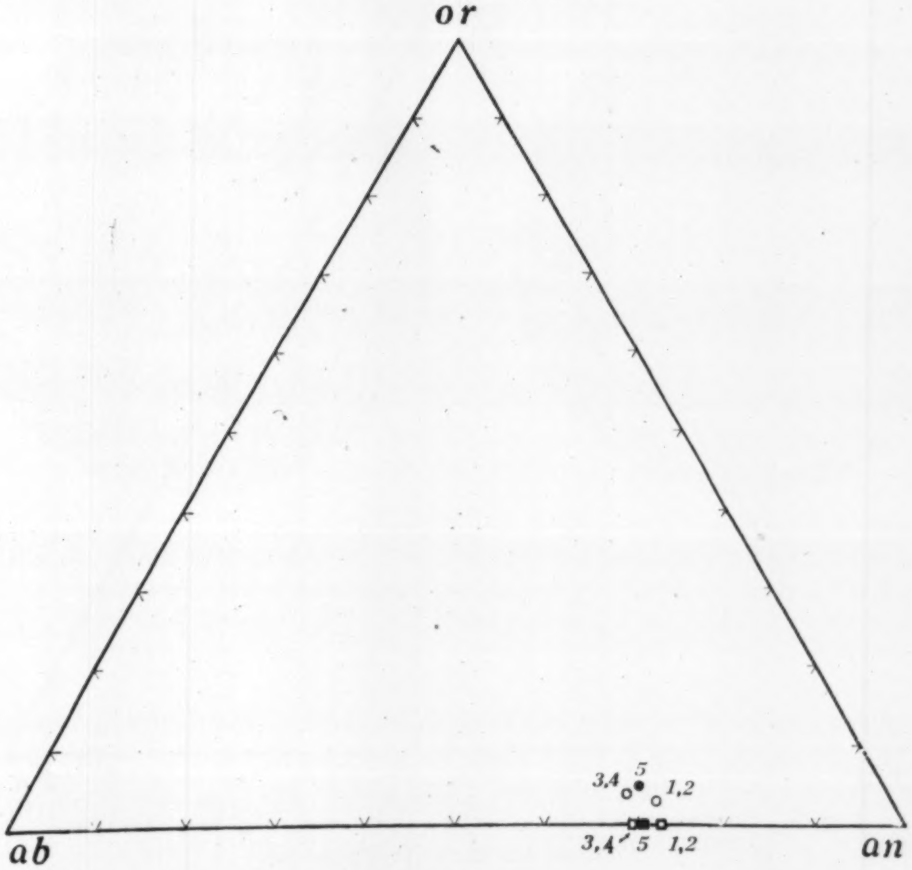

Fig. 2. Compositions of normative feldspars of the 1950-lavas. Figures are same in Table I. Normative plagioclases are shown by squares.

surrounding crater-floor (September 13), then flowed out from the crater to the atrio (Fig. 1). In February, 1951, the activity of the volcano revived in eruption of larger scale, with more extensive lava outflow. In this paper, the writers present a preliminary note on the petrography of the 1950-lavas.

Both the lavas and fragmental ejecta (scoriaceous cinder and bombs) of 1950 are petrographically identified as an uniform augite-hypersthene-bytownite-basalt. Their chemical and mineralogical compositions are shown in the following tables (Table I, II). The peculiarity in the chemical composition of historic lavas of the volcano[2] is revealed as usual in the petrochemical features of the present lavas. The high excess of silica in the norm is reflected in the presence of cristobalite in the higher crystalline groundmass, although it is entirely occult in

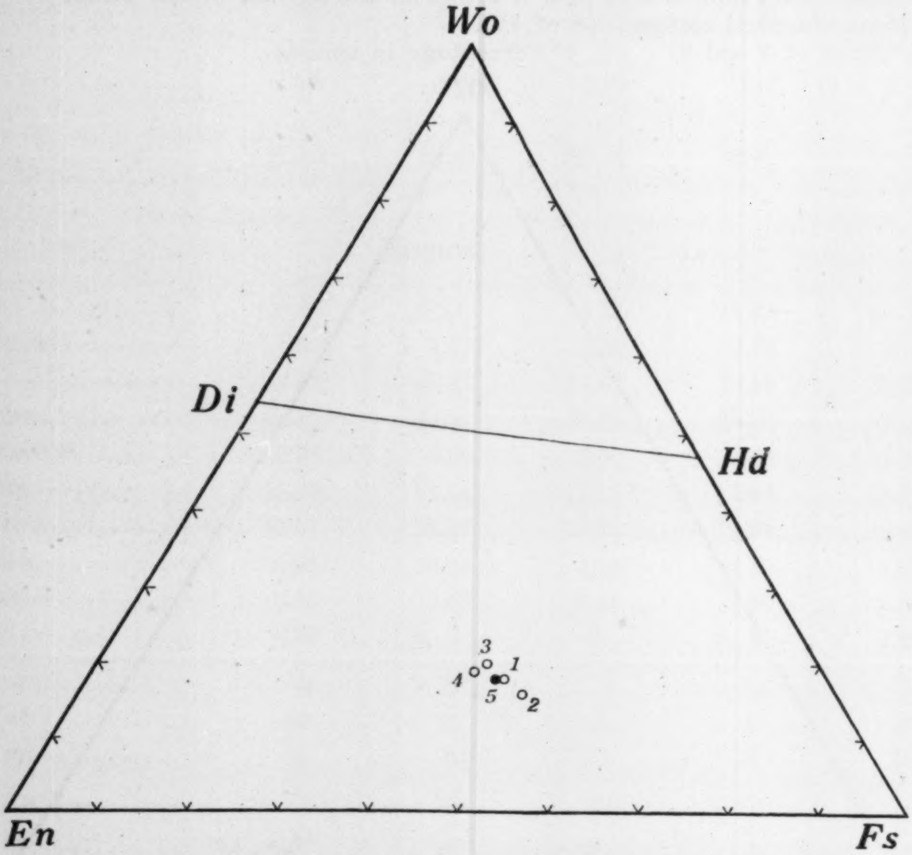

Fig. 3. Compositions of normative pyroxenes of the 1950-lavas. Figures are same in Table I.

---

[2] S. TSUBOI, *Jour. Col. Sci. Imp. Univ. Tokyo, Art 6,* **43** (1920), 86–7.

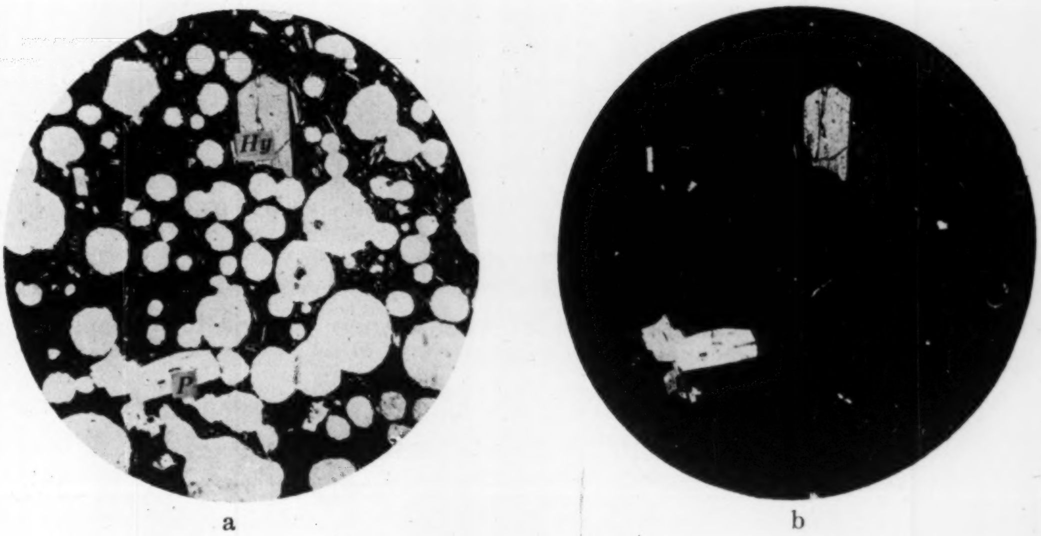

Fig. 4. Photomicrographs of 1950-bomb. a...Polarizer only, b...Analyser being inserted. Hy: hypersthene, P: plagioclase (× ca. 14).

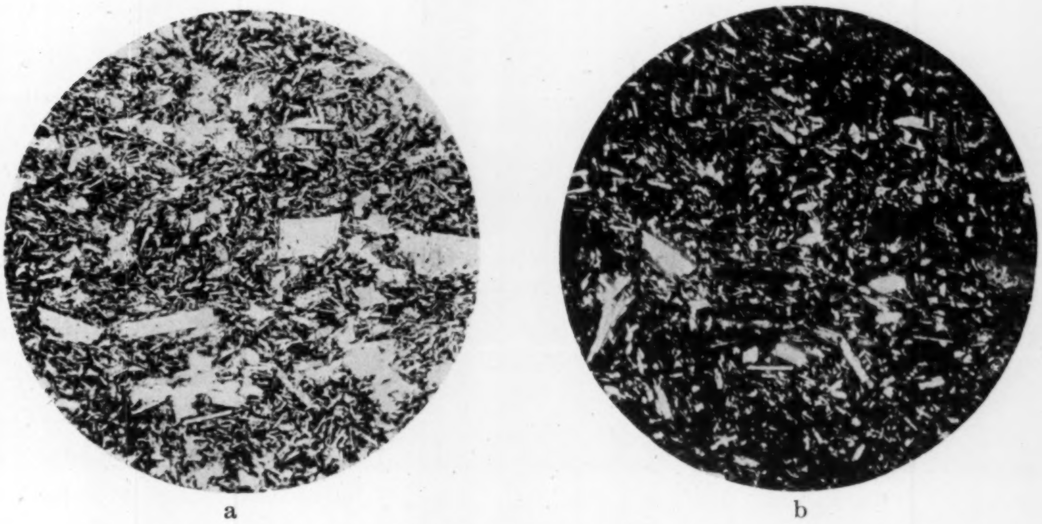

Fig. 5. Photomicrographs of 1950-lava. Microphenocrysts of bytownite are embedded in the groundmass composed of pigeonite, sodic bytownite and dark brown glass. a...Polarizer only, b...Analyser being inserted (× ca. 14).

the glassy groundmass. Compositions of normative feldspars are markedly calcic (Fig. 2). High content of iron oxides and large ratio of total iron to magnesia are also noticeable.

This oversaturated basalt contains anorthite-bytownite, hypersthene and augite as porphyritic minerals scattered in the groundmass composed of bytownite, pigeonite, iron ores and glass. Cristobalite is found in the higher crystalline portion of the lava. Porphyritic structure is not so remarkable: phenocrysts occupy 5–10 percents of the rock in volume; they scarcely attain to 3 mm or more in length; they are seriate to the groundmass minerals in size in the higher crystalline portion of the rock. In spite of its various contents of phenocrysts, especially of plagioclase, the rock is quite uniform in bulk composition, as shown in Table I.

The main constituent minerals of the rock have optical properties as shown in Table II. Their mode of occurrence is briefly described as follows:

Plagioclase: The mineral occurs as the most essential constituent both of the phenocrysts and the groundmass. In composition, it varies from anorthite and calcic bytownite in phenocrysts to sodic bytownite in groundmass.

Hypersthene: Phenocrysts of hypersthene are always found in the rock either as single-crystals or grouped ones associated with or without plagioclase and augite. In the glassy bombs, the mineral occurs as clear euhedral prisms, attaining to 0.5–1.0 mm in length, while in the higher crystalline lavas, it is always fringed with minute grains of quasi-uniaxial pigeonite. It is almost entirely replaced by the latter in the portion of the lava showing a more advanced crystallization.

Augite: Augite is nearly always found as microphenocrysts, but in quite a subordinate amount. Twinnings on 100 are common. There is no microscopic feature showing any discontinuity of crystallization between the augite microphenocrysts and the groundmass pigeonite.

Pigeonite: Pigeonite is the main constituent mineral, occurring as minute grains in the higher crystalline groundmass, either as spindle-formed microphenocrysts or swallow-tailed acicular crystals in the glassy groundmass. Twinnings on 100 are common. Aggregates of pigeonite grains as a pseudomorph of the hypersthene phenocryst are commonly found in the more crystalline portion of the lavas.

Cristobalite: In the highly crystalline groundmass of the present lavas, silica mineral occurs as cristobalite in cavities. Besides, transparent glass of low refractive index occurs in the interstices of the same groundmass.

Iron ores: Magnetite is found in the groundmass only, occurring as euhedral octahedrons in the more crystalline portion of the mass and dendritic or skeletal crystals in the less crystalline part. In the glassy parts of the lavas and bombs, magnetite or hematite is also found as a thin film covering the rock surface. The glass coated with such films of iron-oxides is comparatively high in transparency, while the glass in the more crystalline portion of the lavas is subtransparent in thin slices. Interstitial glass of the rock in which magnetite occurs as euhedral octahedrons is quite transparent and colourless in thin section.

Table II. Optical properties of the main constituent minerals.

Phenocrysts	Groundmass
Plagioclase: An 96–83* An 85–82 (microphenocryst)	Plagioclase: An 75–70
Hypersthene: $(-)\ 2V=63°—60°$ $\rho > v$ about X $En_{63}Fs_{37}$—$En_{60}Fs_{40}$**	—
Augite: (microphenocrysts) $2V=51°$, $51°$ in (010)	Pigeonite: $2V \doteqdot 0°$ in (010) $\beta=1.700$—1.704 $Wo_{11}En_{41}Fs_{48}$***

* Inferred from n_1' on cleavage frakes by means of Tsuboi's diagram. S. TSUBOI, *Jap. Jour. Geol. Geogr.* **11** (1934), 326–7.

** Inferred from 2V and type of dispersion by means of the diagram by Kuno. H. KUNO, *Proc. Imp. Acad. Tokyo,* **17** (1941), 205.

*** Inferred from 2V and β by means of the diagram by Kuno. H. KUNO, *Jap. Jour. Geol. Geogr.* **13** (1936), 110.

This study was carried out with the aid of the Fund for Scientific Rerearch of the Department of Education. The writers' thanks are due to Messers. A. Okada and J. Ossaka for their kind assistance in the field and in the laboratory.

54. 伊豆大島三原山1950年熔岩の化學成分

地震研究所　津屋弘逵
森本良平

伊豆大島三原山の1950年の活動中に噴出した，代表的な熔岩，火山彈を選んで，その岩石化學的性質を記載した。

55. *A Study on the Propagation of Microseismic Waves. Part V.*

By Ryôhei IKEGAMI and Fuyuhiko KISHINOUYE,

Earthquake Research Institute.

(Read June 19, 1951.—Received Sept. 10, 1951.)

Introduction.

In 1929, L. Don Leet[1] proposed a method of determining the direction of approach of microseisms at a station equipped with three-component seismometer assuming microseisms as Rayleigh waves.

In 1935, A. W. Lee[2] proposed a statistical method to determine the direction of approach of microseisms by examining the most probable phase differences between the horizontal- and the vertical-components on assumption that microseisms are Rayleigh waves. He applied this method to the records of microseisms observed at Kew-Observatory to determine the direction of approach of microseisms, and emphasized that Love-waves were not to be found in microseismic waves.

We[3] also applied his method to the records of microseisms observed at Tokyo University, but we could not get such clear results as those obtained by Lee.

In 1938, J. B. Ramirez[4] described the orbits of an earth particle in accordance with the records of microseisms observed with the three components of Galitzin-Wilip seismographs at Florissant station, and he concluded that microseismic waves were of the Rayleigh-wave type. On the other hand he observed microseisms by means of the tripartite method at St. Louis and determined the mean directions of approach of microseisms, and he emphasized that all the determined directions of incoming microseisms at St. Louis point to a deep barometric low over the ocean.

---

1) L. DON LEET, *Publ. Dominion Obs., Ottawa*, **7** (1931).
2) A. W. LEE, *Proc. Roy. Soc., London*, **149** (1935), 183–199.
3) F. KISHINOUYE and R. IKEGAMI, *Bull. Earthq. Res. Inst.*, **25** (1947), 43–48.
4) J. E. RAMIREZ, *Bull. Seism. Soc. Amr.*, **30** (1940), 28–35, 128–139.

L. Don Leet[5] applied further his above-mentioned method to the study of a microseismic storm in New England, and he obtained the results that microseisms do not radiate exclusively from the center of a well-developed low-pressure storm area, and that their directions of approach are correlated with the position of a cold front associated with the generation of the storm when passing over the ocean. In 1948, he[6] asserted again his results. Thereafter he[7] argued with S. Katz[8] about this hard problem.

As stated above, many studies concerning the type of microseismic wave-motion have been published, but we think that these studies have some weak points, respectively. Namely, Lee's method is unfit for studying the directions of approach of individual microseismic waves, because his is a statistical method. Ramirez obtained his results by simply contrasting the mean directions of approach of microseismic waves at St. Louis with the paths of an earth particle at Florissant about 21.8 km. apart from St. Louis. It seems to be improper to treat the results observed at two points standing apart from each other with equal weight, in studying microseismic waves.

Leet's method has also some weak points because he made use of only the three-component records observed at one station, Harvard, and did not obtain the direction of approach of microseismic waves which ought to have been compared with the orbits.

Thereby in addition to the tripartite observations, we intended to get the records of three-component tromometer at one of tripartite stations so as to clarify the relation between the orbits of an earth particle and the determined direction of approach of these waves.

We were able to set up our three-component tromometer at the end of February, 1951, but could record microseisms for only one day i. e. March 8, 1951, when the amplitudes of microseismic waves were fairly large and regular. In this paper we will report the results obtained by the records.

Microseisms of March 8, 1951.

We used in this research four horizontal tromometers[9] which were adjusted to $T_n=10$ sec., $v=\infty$, $V=2000$, and one vertical tromometer[10] which was adjusted to $T_n=6.5$ sec., $v=6.33$, and $V=840$ as shown in Table I. One horizontal tromometer was set up in NS-component at the two stations, C and E of Fig. 1 of our last paper, Part III[11], respectively, and two horizontal- and one vertical-tromometers were set up in NS-, EW- and UD-components at F-station.

---

[5] L. DON LEET, *Geophysics*, **12** (1947), 639–650.

[6] L. DON LEET, *Bull. Seism. Soc. Amr.*, **38** (1948), 173–178.

[7] L. DON LEET, *ditto*, **39** (1949), 249–255, **40** (1950), 229–304.

[8] S. KATZ, *ditto*, **39** (1949), 181–186.

[9] F. KISHINOUYE, *Bull. Earthq. Res. Inst.*, **20** (1942), 215–219.

We could obtain simultaneously the orbits of an earth particle at F-station and the directions of approach of microseismic waves at the tripartite stations, C, E and F.

There is a certain amount of difference between the constants of horizontal component and those of vertical component mentioned above, but the difference in the phase lag caused by the differences of constants of tromometer is only 1°24′ to the forced vibration of 4 sec. period as shown in Table I. This difference is only about 0.016 sec., converted into time, and it may have scarcely no effect upon the orbits of an earth particle.

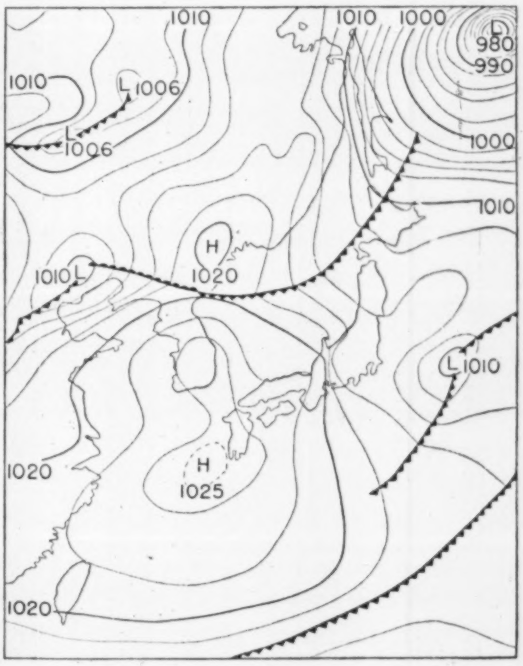

Fig. 1. Weather map for 9^h00^m a. m., March 8, 1951.

Table I. Constants of the tromometers.

	Period of free vibration	Damping ratio	Geometrical magnification	Period of forced vibration=4 sec.	
				Phase lag	Magnification coeff.
NS- and EW-components	sec. 10	∞	2000	136°24′	0.86
UD-component	6.5	6.33	840	135°	1.14

On March 8, 1951, there were two barometric lows over the

---

[10] This vertical tromometer was also designed by F. KISHINOUYE, and the paper about this was read at the monthly meeting of the Institute on July 6, 1943.

[11] R. IKEGAMI and F. KISHINOUYE, *Bull. Earthq. Res. Inst.*, **29** (1951), 305–312.

Pacific Ocean on the east of Kwantô-District and Kamchatka Peninsula, respectively, and the cold fronts stretched southeastwards from the respective lows as shown in Fig. 1. It was blowing 20∼25 m./sec. from the previous day and the Pacific Ocean near Kwantô-District was very rough.

Fig. 2 shows a part of the records of microseisms obtained under the weather condition mentioned above.

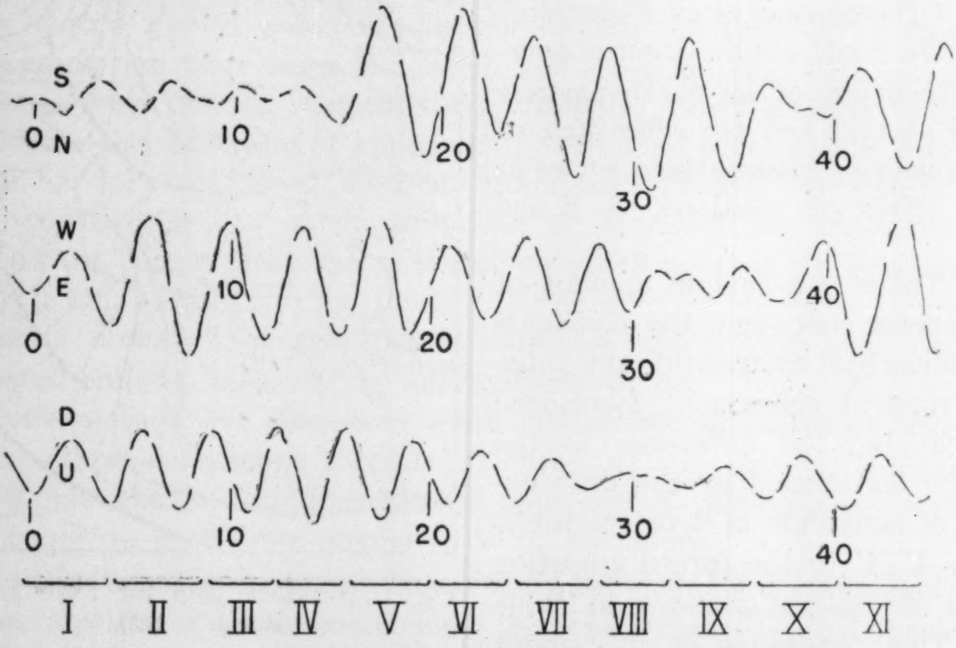

Fig. 2. A part of the three-component seismogram at F-station.
(This figure is one half of the actual size.)

The projections of the path of an earth particle on horizontal, meridional and prime vertical planes, which were illustrated in accordance with the three-component records observed at F-station, are shown in Fig. 3. We have given the orbits of five wave-portions, V, VI, VII, VIII and IX, illustrated in Fig. 2, because the orbits of the other wave-portions show also, on the whole, the same tendency. In Fig. 3, the direction of approach of a microseismic wave judged from the orbit is shown by an arrow, and the direction determined by tripartite method on the same wave is shown by a dotted arrow. The tendencies will be made clear by a glance at these figures. Namely, the waves, V, VI and VII express the well-developed forms in three components, and an earth particle is revolved on the vertical plane nearly elliptically. The directions of approach judged from the

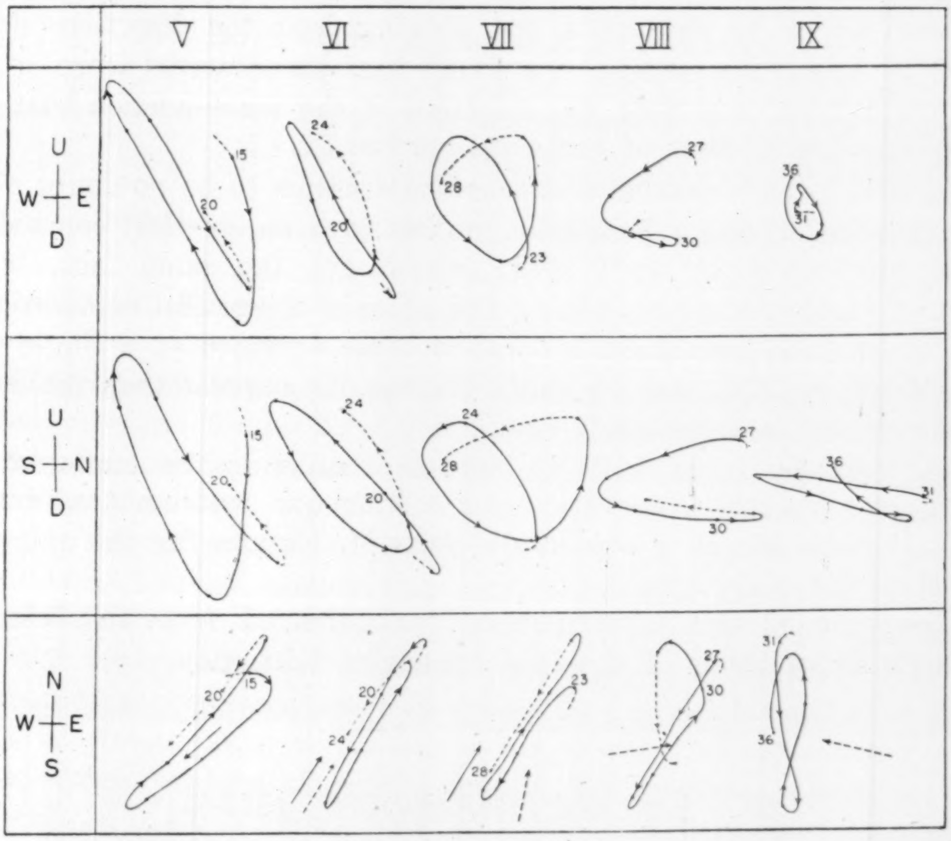

Fig. 3. Projection of the path of an earth particle. Orbits, V, VI, VII, VIII and IX, correspond to the wave-portions, V to IX, of Fig. 2, respectively. The arrow shows the direction of approach of a microseismic wave judged from the direction of rotation of orbit, and the dotted arrow shows the direction of the same wave determined by the tripartite method.

orbits are quite in agreement with the directions determined by tripartite method. But it is very suggestive that the direction of the wave-portion V is quite opposite to the direction of the wave-portion VI though no irregularity is to be seen on the records of these waves, and in all probability this fact seems to afford a key for the solution of the nature of microseismic waves.

We found also that the directions of approach of the individual microseismic waves are fairly scattered about, and that they are radiated from a fairly wide area rather than from a restricted source.

In the wave-portions VIII and IX the amplitudes of vertical motion become remarkably small, and only the motions of horizontal component are developed. We could not decide the direction of approach of these waves by the orbits, but judging from the directions determined by tripartite method, we found that these waves were of the Love-wave type, and that the direction of the wave-portion VIII was nearly opposite to that of the wave-portion IX.

In 1947 Leet[12] pointed out that there seems to be no doubt about the existence of also a horizontal motion with no vertical component. In our previous paper we[13] again pointed out the same fact, which can now made clearer by adding the records of vertical component.

The results mentioned above are those obtained at a single day, i. e., March 8, 1951, but we think the results suggest that the origin of microseisms is exceedingly complex.

In conclusion, we wish to express thanks to the staffs of the Tokyo Astronomical Observatory for setting our instruments, and to Mr. J. Moroga, Mr. H. Yoshioka and Miss M. Kotaka for the aids they offered in the observations.

The cost of this investigation was defrayed from the Scientific Research Expenditure of the Department of Education.

---

55. 土地の脈動の傳播性の研究 （第5報）

地震研究所 池上良平
地震研究所 岸上冬彦

3 點觀測法によつて脈動波の到來方向を調べると同時に，3 觀測點の內少くとも1點に3成分の地震計を据えて到來方向の判つたその同じ脈動波が如何なる型の表面波であるかを調べた。即ち3觀測點 C, E, F の內 F 觀測點に上下成分を加へた3成分を設置して目的を達する事が出來た。

今回報告するものは1951年3月8日の唯1日の記錄に基くものであるが，それでも可成り興味ある結果が得られた。

i) 連續した脈動波について地面の動き方から判斷して，レーリー型と思はれるものとラブ型と思はれるものとの兩型の脈動波が見られた。

ii) レーリー型の部分については，上下成分と水平成分を組合せた地動の向きから判斷した脈動波の到來方向と，その同じ脈動波について3點觀測法によつて決定した到來方向とは殆ど一致してゐた。

iii) 上下成分の振幅が極端に少さくなつた部分では，レーリー型に於けるように地動の向きからは到來方向を決める事は出來ないが，3點觀測法から決めた到來方向から考へて，この部分は明らかにラブ型の表面波の性質を示してゐた。

iv) 兩型の脈動波共一見連續してゐる如く見える相隣つた波に於ても，その到來方向が全く逆向きになる場合がある。

---

[12] L. Don Leet, *Geophysics*, **12** (1947), 639–650.

[13] R. Ikegami and F. Kishinouye, *Bull. Earthq. Res. Inst.*, **29** (1951), 305–312.

56. *Microseisms and Sea Waves.*

By Fuyuhiko KISHINOUYE,

Earthquake Research Institute.

(Read July 18, 1951.—Received Sept. 20, 1951.)

In 1903 E. Wiechert[1] published a hypothesis on the origin of microseisms. He considered that microseisms are generated by sea waves breaking against a steep coast. This hypothesis was developed by B. Gutenberg[2] and followed by many seismologists. The sea waves are thought to be raised by winds of cyclone, so correlations between microseisms and sea conditions or winds were investigated at various places. Gherzi[3] considered that microseisms are generated by pressure variation at the sea bottom, the variation being due to 'pumping' of the atmosphere at the centre of cyclones. S. K. Banerji[4] also held to a similar view, only the variation is assumed to be made by sea waves generated by the monsoon. In Japan F. Omori[5] noticed that microseisms at Tokyo occur when the centre of cyclones are about 1000 km. SW of Tokyo, and he classified them by their periods into three: 2.9, 4.5, and 7.5, in sec. T. Matuzawa[6] described that periods of microseisms at Tokyo change from 4 sec to 6 sec when cyclones passed east off Bōsō Peninsula. The writer[7] stated that microseisms are earth oscillations excited by oceanic waves in some unknown manner.

Recently the writer was given the chance to read Longuet-Higgins's paper 'A Theory of the Origin of Microseisms'[8] by his kindness, and was informed about recent developments of the theory in Europe. According to the recent theory, microseisms are generated by sea waves, and periods of microseisms are to be twice those of sea waves. Thus with available data the writer proceeded to investigate the relation between waves and microseisms.

---

[1] E. WIECHERT, *Verh. Zweit. Internat. Seism. Konf.*, 1903.
[2] B. GUTENBERG, *Bull. Seism. Soc. Amer.*, **21** (1931), 1-24.
[3] E. GHERZI, *Note de Sism. Obs, Zika-wai.*, **5** (1923), 1-16.
[4] S. K. BANERJI, *Phil. Trans. Roy. Soc. London*, A **229** (1930), 287-328.
[5] F. OMORI, *Bull. Imp. Earthq. Inv. Comm.*, **3** (1905), 1-35.
[6] T. MATUZAWA, *Journ. Fac. Sci. 2, Tokyo Univ. Sec.* 2, **2** (1927), 295-263.
[7] F. KISHINOUYE, *Bull. Earthq. Res. Inst.*, **18** (1940), 418.
[8] M. S. LONGUET-HIGGINS, *Phil. Trans. Roy. Soc. London*, A **243** (1950), 1-35.

Records of microseisms were obtained at Tokyo, and those of waves were observed by two weather observation ships of the Central Meteorological Observatory of Japan. The positions of the ships were about 39.°5 N, 152° E for the North Station and 28.°5 N, 135° E for the South Station (The stations are abbreviated N and S in the following diagrams). The relation between periods and heights of waves is shown in Fig. 1. The values of periods ranged from 6 sec. to 13 sec. regardless of height. The frequency distribution of periods of waves are shown in Fig. 2. The distribution at the South Station is wide and that at the North Station is narrow. Such difference is also to be

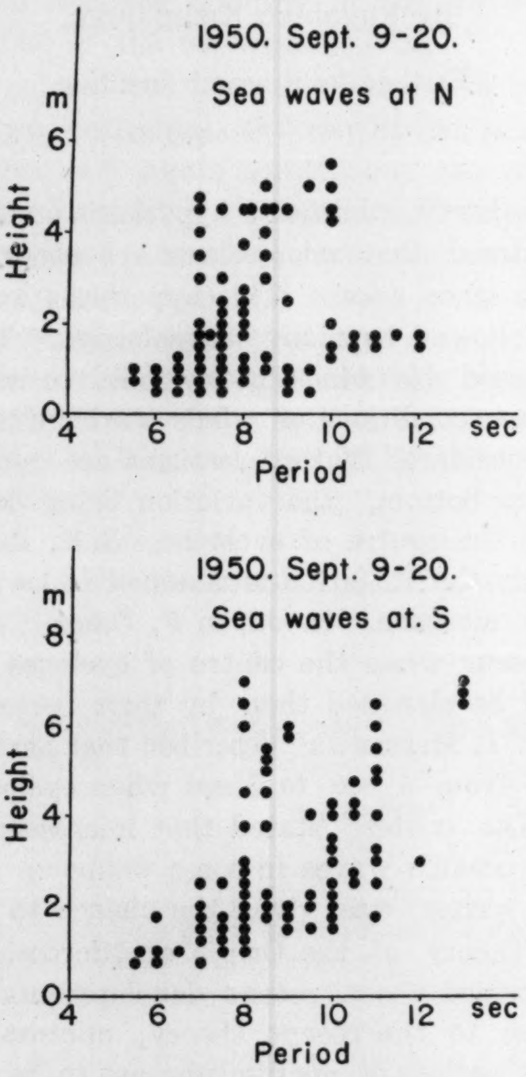

Fig. 1. Period and height of sea waves.

seen between periods of microseisms propagated from south to Tokyo and from north east. In other words, the kinds of microseisms classified by the writer in the previous paper[9] may be closely connected with the difference of periods of swells at the two stations on the Pacific Ocean (Compare Fig. 2 with Figs. 7-9 in the above-mentioned paper).

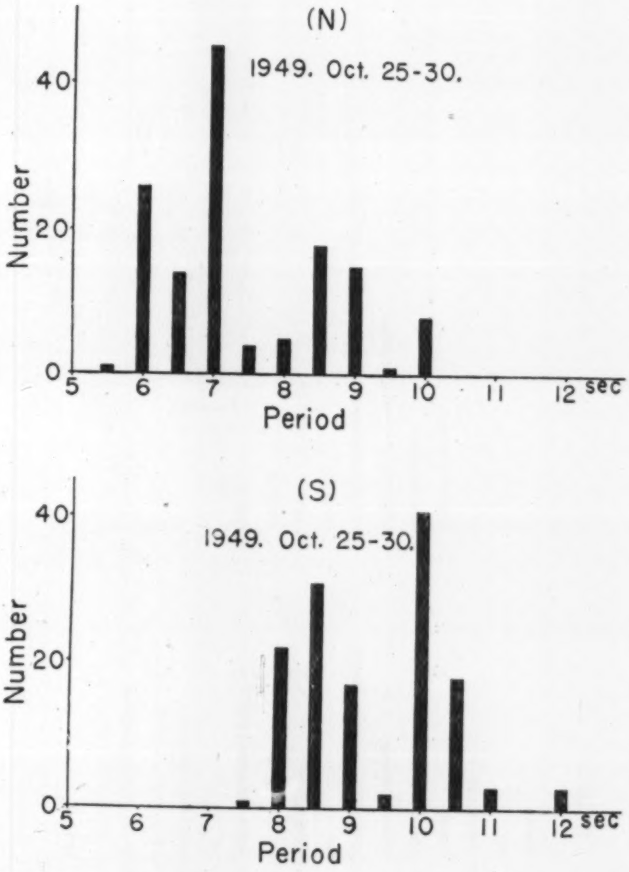

Fig. 2-a. Frequency distribution of periods of sea waves.

The timely change of microseisms or the change of microseisms with regard to the position of the centre of cyclones were studied in connection with the conditions of sea waves. The time variation of double amplitudes and the periods of microseisms at Tokyo were compared with the variations of wave heights and periods of waves respectively (Figs. 3 and 4). The amplitudes of microseisms became maximum when the centre of cyclone passed east of Tokyo. It may be assumed that the wave height is high near the centre of cyclone, and microseisms are generated there. The periods of swells were not always twice the periods of microseisms as stated in the recent theory. The frequency distribution of periods of microseisms at Tokyo during similar interval of the data in Fig. 4 are shown in Fig. 5. for comparison with the frequency distribution of swells.

---

[9] F. KISHINOUYE, *Bull. Earthq. Res. Inst.*, **29** (1951), 485.

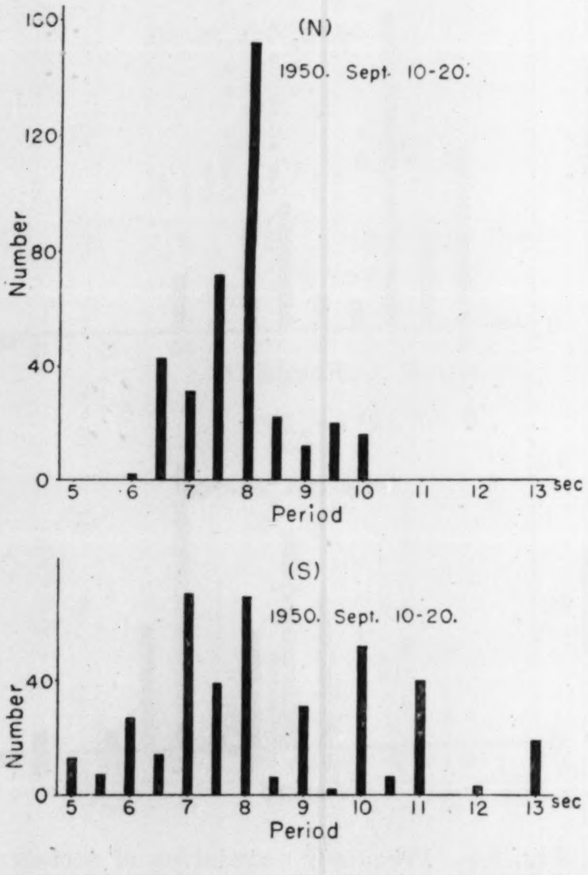

Fig. 2-b. Frequency distribution of periods of sea waves.

The above investigation was carried out with data at hand and the results obtained will perhaps not stand comparison with those obtained in foreign countries. Therefore the witer wishes further studies on microseisms and waves to be carried on in Japan as foreign countries.

Acknowledgements.

The writer wish to express his thanks to the members of the Central Meteorological Observatory for the data of sea waves made

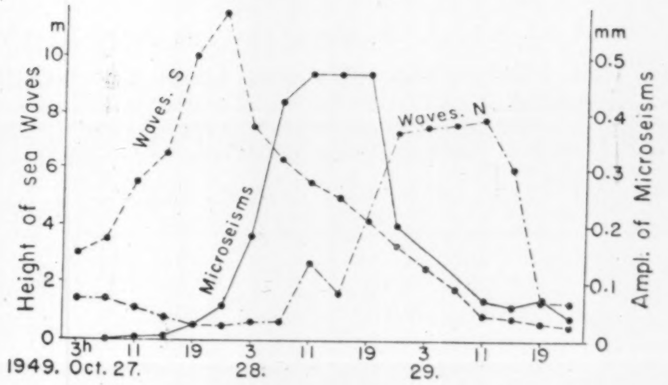

Fig. 3.

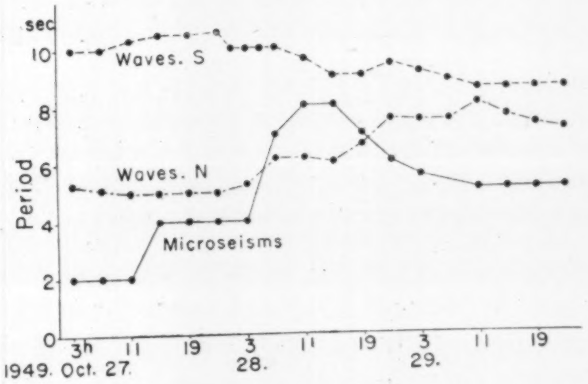

Fig. 4.

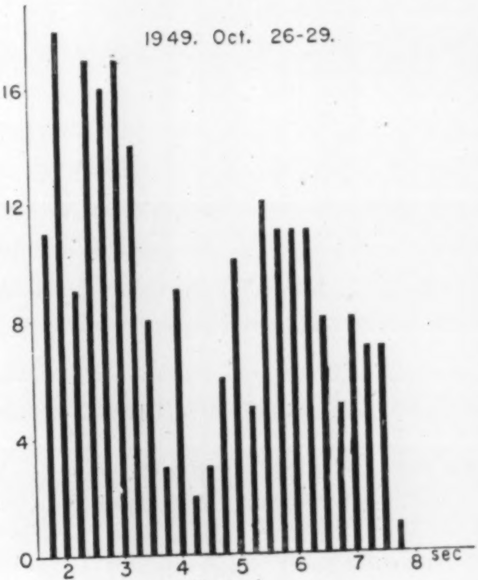

Fig. 5. Frequency distribution of periods of microseisms in Figs. 3 and 4.

available to him, and to Mr. J. Moroga for his help in this study.

The cost of this study was defrayed from the Grant in Aid for Fundamental Scientific Research.

---

56. 土地の脈動と海の波

岸上冬彦

近頃ヨーロッパで脈動は風によつて起された海の波が海底に及ぼす壓力變化によつて生ずると考へる說が盛んである。この說によると脈動の周期は海の波の周期の 2 分の 1 になる筈である。筆者は中央氣象臺の觀測船の海の波の觀測結果をかりて脈動との關係を調べた。周期の關係は明らかではないが，東京に北又は南から傳はつてきたと思はれる脈動の周期の頻度分布と，北點又は南點で觀測船の觀測した波浪の周期の分布と似ていることに注意をひいた。

57. *Geomagnetic Studies of Volcano Mihara. The 3rd paper. (Magnetic Survey and Continuous Observation of Changes in Geomagnetic Declination.)*

By Tsuneji RIKITAKE, Izumi YOKOYAMA, Atsushi OKADA,
and Yoneko HISHIYAMA,

Earthquake Research Institute.

(Read July 17, 1951.—Received Sept. 5. 1951.)

1. Introduction.

After the outbreak of the 1950 eruption of Volcano Mihara in Ooshima Island, the writers conducted magnetic dip surveys over the island in July and September of 1950 and March of 1951, and found out marked changes in geomagnetic dip that accompanied the volcanic activity as has already been reported by one of the writers[1]. On analyzing the results of the surveys, we made some interesting interpretations concerning the changes in thermal condition within the volcano. As was also detected in the case of the 1940 eruption of Miyake-sima Island[2,3,4,5], marked changes in the earth's magnetic field usually occur in connexion with severe activities of volcanoes composed of basaltic rocks, thus the changes may be made use of in forming conjectures respecting the interior of volcanoes.

In order to study in detail the character of geomagnetic changes just mentioned, the writers executed a survey of three geomagnetic components over Ooshima Island in May, 1951. The stations occupied by the writers amounted to ten in number, while they reoccupied the three stations on which the measurements were made by R. Takahasi and T. Nagata[6] in 1936.

At the same time, a continuous recording of changes in geomagnetic declination was commenced from April at Nomashi Village, about 4 *km* distant from the crater in the west direction. Meanwhile, Volcano Mihara was still active during the period from February to June of this year, eruptions of Strombolian type occurring intermittently in April, May and June. Although the writers have obtained no conclusive result concerning the relation between changes in geomanetism and volcanic activity, an outline of the geomagnetic studies in Ooshima Island will be briefly described in this paper.

---

[1] T. RIKITAKE, *Bull. Earthq. Res. Inst.*, **29** (1951), 161 and 499.

[2] R. TAKAHASI and K. HIRANO, *Bull. Earthq. Res. Inst.*, **19** (1941), 82 and 373.

[3] T. NAGATA, *Bull. Earthq. Res. Inst.*, **19** (1941), 335.

[4] T. MINAKAMI, *Bull. Earthq. Res. Inst.*, **19** (1941), 356.

[5] Y. KATO, *Proc. Imp. Acad. Japan*, **16** (1940), 440.

[6] R. TAKAHASI and T. NAGATA, *Bull. Earthq. Res. Inst.*, **15** (1937), 441.

2. The magnetic survey.

The writers carried out a magnetic survey with a G. S. I. type magnetometer⁽⁷⁾ lent by the Geographical Survey Institute, Ministry of Construction. As the magnetometer is of electromagnetic type, it is appropriate for use in the vicinity of an active volcano where, owing to short period microtremors of volcanic origin, occassional vibrations of the suspended magnet makes it almost impossible to carry out an

Fig. 1-1. Station No. 37. Mr. Masaka's garden.

Fig. 1-2. Station No. 38. Yuba.

Fig. 1-3. Station No. 39. Gojinka-chaya.

Fig. 1-4. Station No. 14. Zoo (Dobutsuyen).

---

7) I. TSUBOKAWA, *Journ. Geomagn. Geoelectr.*, **1** (1949), 10.

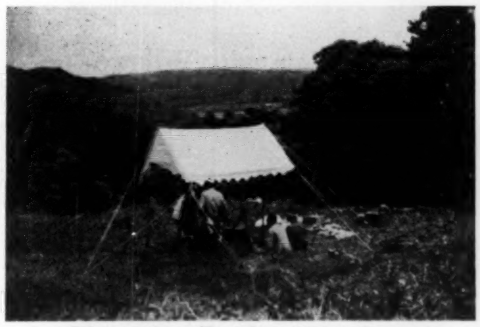

Fig. 1–5. Station No. 41.
Sashikiji, Yokawa.

Fig. 1–6. Station No. 26.
Mabushi.

accurate measurement with a usual magnetometer. The accuracy of measurement with the magnetometer is 0.1 *minutes* of arc in declination and inclination and 1 γ in horizontal intensity, while about ten *minutes* are needed for a set of observations of three components. Some scenes of measurement are shown in Figs. 1.

The measurements were carried out in the main on the stations of the previous dip surveys, including three stations which were occupied by Takahasi and Nagata in 1936. A few stations were added newly. Sketch maps of these stations are given in Figs. 2. The results of the observations are also given in Tables I∼X.

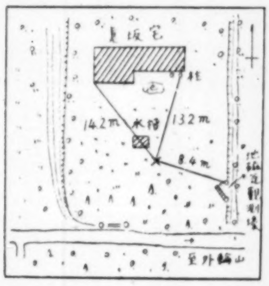

Fig. 2–1. Station No. 37.
Mr. Masaka's garden.

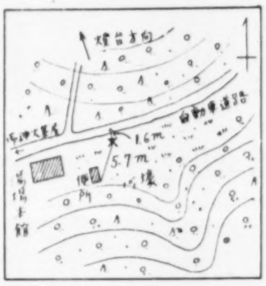

Fig. 2–2. Station No. 38.
Yuba.

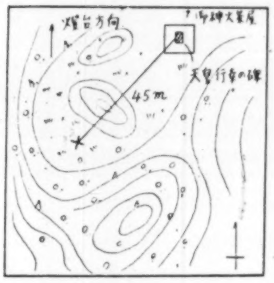

Fig. 2–3. Station No.
39. Gojinka-chaya.

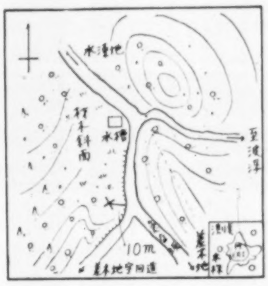

Fig. 2–4. Station No.
41. Sashikiji-Yokawa.

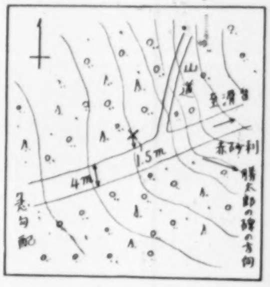

Fig. 2–5. Station No.
40. Suberidai.

Table I.

Station, No. 37 Mr. Masaka's garden, Nomashi Village
Lat. = 34°43′.6 Long. = 139°21′.5 May, 1951

Declination and Dip

Date	Time	*D*	*I*
9	13*h*02*m*	6°17′.4	47°21′.1
9	14 19	6 15 .9	47 21 .9
9	15 28	6 14 .8	47 21 .1
9	16 41	6 13 .4	47 22 .1
9	17 41	6 14 .5	47 23 .6
	Mean	6 15 .2	47 22 .0

Horizontal Intensity

Date	Time	*H*
9	13*h*15*m*	30043 γ
9	14 30	30052
9	15 39	30044
9	16 50	30015
9	17 50	29995
	Mean	30030

Table II.

Station, No. 24 Nomashi Village
Lat. = 34°43′.8 Long. = 139°21′.5 May, 1951

Declination and Dip

Date	Time	*D*	*I*
10	11*h*48*m*	5°10′.1	47°18′.3
10	13 08	5 10 .3	47 19 .0
	Mean	5 10 .2	47 18 .6

Horizontal Intensity

Date	Time	*H*
10	12*h*02*m*	30724 γ
10	13 15	30724
	Mean	30724

Table III.

Station, No. 19 Ooshima meteorol. station
Lat. = 34°45′.8 Long. = 139°22′.6 May, 1951

Declination and Dip

Date	Time	*D*	*I*
10	22*h*43*m*	6°18′.8	48°13′.3
10	23 41	6 15 .7	48 14 .1
	Mean	6 17 .2	48 13 .7

Horizontal Intensity

Date	Time	*H*
10	22*h*56*m*	29965 γ
10	23 50	29938
	Mean	29952

Table IV.

Station, No. 38 Yuba
Lat. = 34°45′.2 Long. = 139°23′.9 May, 1951

Declination and Dip

Date	Time	*D*	*I*
11	14*h*58*m*	5°04′.0	49°27′.2
11	15 55	5 02 .4	49 27 .5
11	16 51	5 01 ·9	49 29 .3
11	17 50	4 59 .8	49 29 .4
	Mean	5 02 .0	49 28 .4

Horizontal Intensity

Date	Time	*H*
11	15*h*08*m*	28945 γ
11	16 03	28943
11	17 01	48922
11	17 01	28916
	Mean	28932

Table V.

Station, No. 39 Gojinka-chaya

Lat. = 34°44′.2 Long. = 139°22′.9 May, 1951

Declination and Dip

Date	Time	*D*	*I*
12	14*h*56*m*	3°51′.2	52°16′.3
12	16 02	3 51 .3	52 15 .7
12	17 08	3 51 .2	52 15 .9
12	18 43	3 51 .8	52 16 .9
	Mean	3 51 .4	52 16 .2

Horizontal Intensity

Date	Time	*H*
12	15*h*09*m*	28529 γ
12	16 10	28537
12	17 15	28515
12	18 52	28514
	Mean	28524

Table VI.

Station, No. 14 Zoo

Lat. = 34°45′.2 Long. = 139°26′.5 May, 1951

Declination and Dip

Date	Time		*I*
13	18*h*35*m*	6°22′.0	48°23′.1
13	19 32	6 21 .3	48 21 .9
	Mean	6 21 .6	48 22 .5

Horizontal Intensity

Date	Time	*H*
13	18*h*46*m*	30113 γ
13	19 42	30105
	Mean	30109

Table VII.

Station, No. 16 Senzu primary school

Lat.=34°46′.6 Long.=139°25′.3 May, 1951

Declination and Dip

Date	Time	*D*	*I*
13	23*h*46*m*	5°23′.6	48°36′.8
14	00 36	5 24 .7	48 37 .4
	Mean	5 24 .2	48 37 .1

Horizontal Intensity

Date	Time	*H*
13	23*h*54*m*	30176 γ
14	00 42	30181
	Mean	30178

Table VIII.

Station, No. 40 Suberidai

Lat.=34°42′.9 Long.=139°22′.5 May, 1951

Declination and Dip

Date	Time	*D*	*I*
17	13*h*58*m*	4°06′.0	50°41′.7
17	15 30	4 04 .1	50 40 .6
17	17 10	4 03 .3	50 40 .4
17	18 22	4 04 .7	50 40 .3
	Mean	4 04 .5	50 40 .8

Horizontal Intensity

Date	Time	*H*
17	14*h*18*m*	28955 γ
17	15 58	28974
17	17 23	28975
17	18 41	28959
	Mean	28965

Table IX.

Station, No. 41 Sashikiji Yokawa

Lat. = 34°41′.5 Long. = 139°25′.6 May, 1951

Declination and Dip

Date	Time	*D*	*I*
18	13*h*25*m*	8°02′.0	48°23′.9
18	14 50	8 00 .7	48 23 .9
18	15 56	7 59 .8	48 23 .2
	Mean	8 00 .8	48 23 .7

Horizontal Intensity

Date	Time	*H*
18	13*h*38*m*	31658 γ
18	15 01	31666
18	16 14	31651
	Mean	31658

Table X.

Station, No. 26 Mabushi

Lat. = 34°41′.3 Long. = 139°23′.3 May, 1951

Declination and Dip

Date	Time	*D*	*I*
19	12*h*48*m*	5°16′.3	46°56′.7
19	13 54	5 15 .7	46 57 .5
19	14 24	5 14 .9	46 56 .9
	Mean	5 15 .6	46 57 .0

Horizontal Intensity

Date	Time	*H*
19	13*h*02*m*	31555 γ
19	14 04	31558
	Mean	31557

3. The distribution of three components in Ooshima Island.

From the results of the surveys in 1936, 1950 and 1951, the writers newly constructed magnetic charts for 1951.4 in Ooshima Island as follows. The distribution of the geomagnetic field is so complicated as is the case in other volcanoes that we can only express the general tendency of the distribution unless we make observations at many more stations than ours. In expressing the general tendency, we have neglected the corrections for diurnal variation and geomagnetic storms, adopting only the arithmetical means at each station. As to the 1936 survey, corrections for secular change are added where the Kakioka Magnetic Observatory is taken as the standard point.

In Figs. 3, 4, and 5, the distribution of the horizontal intensity, declination and dip are respectively shown. The general tendency of the distribution agrees well with those of other volcanoes which were surveyed by a number of investigators, for example Mt. Asama(8), Mt. Mayu(9), Mt. Fuji (Huzi)(10), Mt. Omuro(11) and so on. As already pointed out by the investigators, the anomaly in the earth's magnetic field near volcanoes may be fairly ascribed to the magnetization of the volcanoes, the direction of magnetization nearly agreeing with the general geomagnetic field there. Of course, the anomaly in Ooshima Island is interpreted from the same standpoint as has been also clarified by the writers' estimate of the magnetic field on a magnetized circular cone(1).

4. The changes in the geomagnetic field in Ooshima Island during these twenty years.

On four stations in Ooshima Island, measurements of three geomagnetic components were made by the Hydrographic Department in the years 1913, 1933 and 1943. Of these stations, the station Mabushi is in the same place where the measurements of the 1936 survey and the 1951 survey were made respectively by Takahasi and Nagata and by the writers. Meanwhile, the stations Nomashi and Zoo (Dobutsuyen) were occupied by the writers as well as Takahasi and Nagata. As to the dip-angle on these stations, some observations were added by Nagata in 1937 and by one of the writers in 1950 and 1951. Col-

---

8) T. MINAKAMI, *Bull. Earthq. Res. Inst.*, **18** (1940), 178.

9) W. YODA, *Chikyu-Butsuri*, **3** (1939), 26. (in Japanese).

10) T. MINAKAMI, Not yet published.

11) T. NAGATA, *Trans. Oslo Meeting I.U.G.G.A.T.M.E.*, (1950).

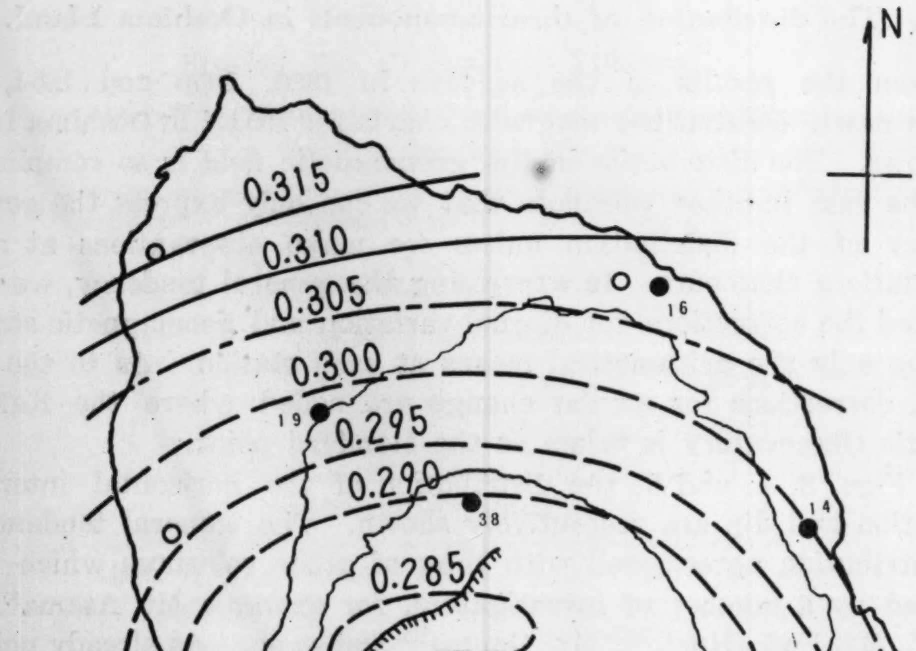
N
0.315
0.310
0.305
0.300
0.295
0.290
0.285
600m
400m
200m
0.310
0.315
0.310
16
19
14
38
39
24
37
40
26
41
0
5Km

Fig. 3. The distribution of the horizontal intensity in Ooshima Island for 1951.4. The stations occupied by the writers are shown with black circles, the number of them are also shown with small numerals. The stations in the 1936 survey are indicated with hollow circles.

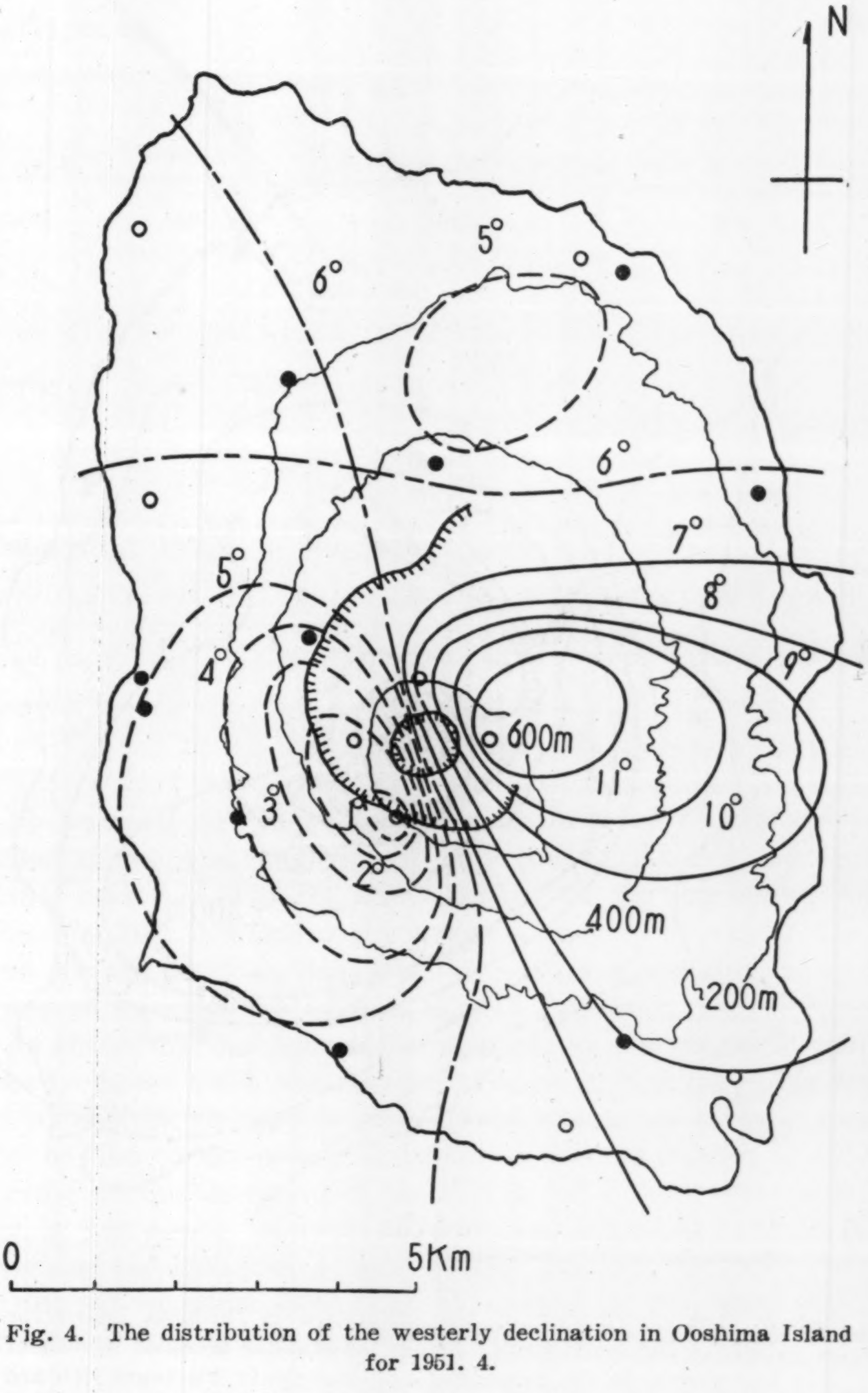
N
5°
6°
6°
7°
8°
9°
5°
4°
600m
11°
10°
3°
2°
400m
200m
0
5Km

Fig. 4. The distribution of the westerly declination in Ooshima Island for 1951. 4.

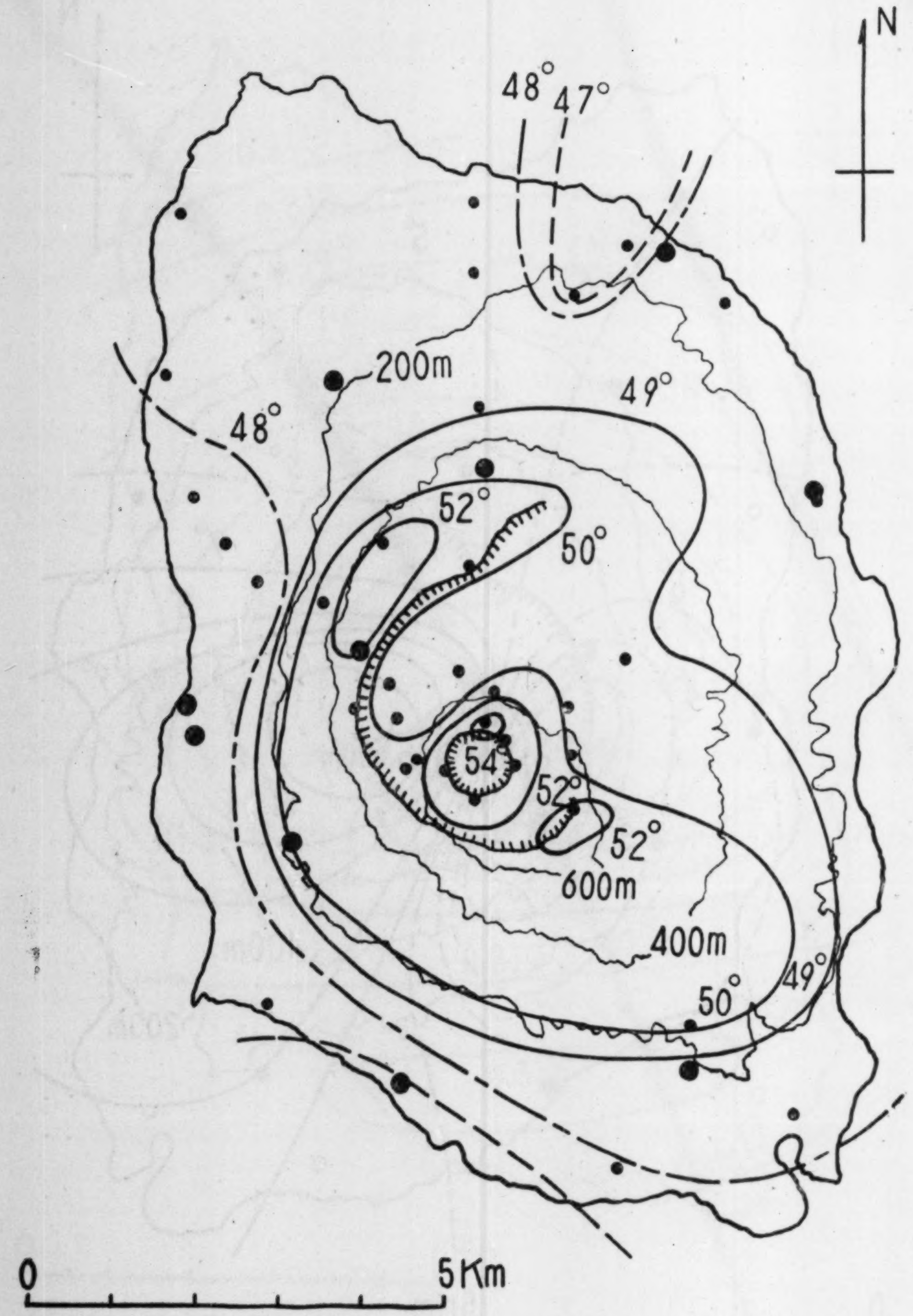
N
48°
47°
200m
49°
48°
52°
50°
54
52°
52°
600m
400m
49°
50°
0
5Km

Figs. 5. The distribution of the inclination in Ooshima Island for 1951.4. The small circles denote the stations occupied by one of the writers in the geomagnetic dip surveys in the years 1950 and 1951.

lecting the available data mentioned above, the writers will attempt here to investigate the changes in the geomagnetic field during these twenty years.

The observed values thus collected are tabulated in Table XI.

Table XI. The observed values of the geomagnetic elements.

Date / Station	1913. 1			1933. 1			1930. 7			1913. 1
	H	***D***	***I***	***H***	***D***	***I***	***H***	***D***	***I***	***I***
Mabushi	31117γ	4°6′.9W	47°11′.4	31171γ	4°42′.7W	47°8′.5	31176γ	4°44′.5W	47° 5′.0	47° 5′.4
Nomashi	—	—	—	—	—	—	30179	4 27 .0	47 44 .6	47 44 .5
Zoo	—	—	—	—	—	—	29787	5 59 .0	48 37 .2	—

Table XI. (Continued)

Date / Station	1943. 1			1950. 6	1950. 7	1951. 2	1951. 4		
	H	***D***	***I***	***I***	***I***	***I***	***H***	***D***	***I***
Mabushi	31416γ	4°56′.7W	46°51′.0	47° 2′.3	46°59′.5	46°57′.5	31557γ	5°15′.5W	46°57′.0
Nomashi	—	—	—	47 40 .3	47 28 .6	47 25 .4	30716	5 9 .7	47 19 .1
Zoo	—	—	—	48 34 .6	48 24 .4	48 23 .8	30109	6 21 .6	48 22 .5

No corrections for geomagnetic disturbance or diurnal variation is added to the observed values, only the arithmetrical means being adopted here. In Fig. 6, the changes in the horizontal intensity, declination and inclination are graphically shown, where the annual means at the Kakioka Magnetic Observatory are also shown for the purpose of showing the general secular change in central Japan.

As shown by the figures, the changes in the magnetic components generally agree with the secular change at Kakioka. We see, however, anomalous changes in dip in 1950 which, as already reported[1], might be due to the severe eruption of Volcano Mihara in 1950, while the cause of the deviation of the dip in 1943 from the general tendency is not clear. In order to get the difference between the 1951 survey and the 1936 one, general secular changes, magnetic disturbance and diurnal variation have been eliminated by the same method used by Nagata[12] and one of the writers[1]. For example, ***D*** denotes the

---

[12] T. NAGATA, *Bull. Earthq. Res. Inst.*, **15** (1937), 497.

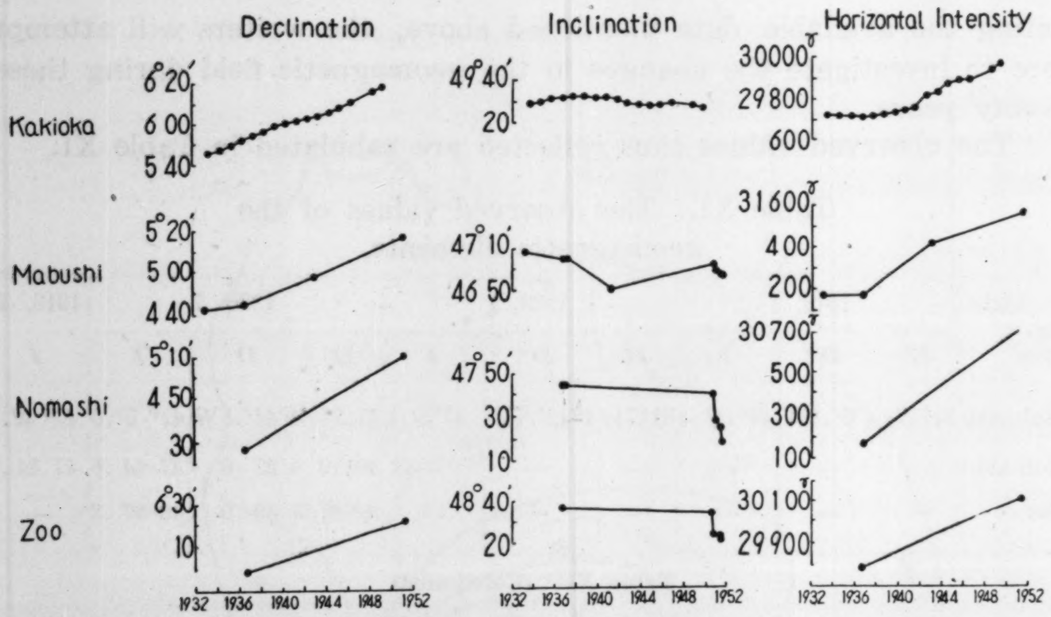

Fig. 6. The secular changes in the components of the earth's magnetic fiield at the three stations in Ooshima Island and the Kakioka Magnetic Observatory.

observed declination at a station in Ooshima Island and D_k that at Kakioka Observatory at exactly the same time. Then from $D_{1951}-D_{1936}$ and $D_{k,1951}-D_{k,1936}$, we obtain

$$\delta D=(D_{1951}-D_{1936})-(D_{k,1951}-D_{k,1936}).$$

Table XII. Changes in the magnetic field during the period from 1936 to 1951.

Station	$H_{1951}-H_{1936}$	$H_{k,1951}-H_{k,1936}$	δH	$D_{1951}-D_{1936}$	$D_{k,1951}-D_{k,1936}$
Mabushi	381γ	344γ	+ 37γ	31′.0	32′.7
Nomashi	518	359	+159	43 .2	36 .2
Zoo	322	307	+ 15	22 .6	29 .1

Table XII. (Continued)

Station	δD	$I_{1951}-I_{1936}$	$I_{k,1951}-I_{k,1936}$	δI
Mabushi	−1′.7	− 8′.0	−8′.3	+ 0′.3
Nomashi	+7 .0	−26 .0	−9 .1	−16 .9
Zoo	−6 .5	−14 .1	−6 .4	− 7 .7

δD thus obtained may be regarded as the local anomalous change in geomagnetic declination from which the influences of general magnetic disturbance were eliminated. Similar procedures are also applied to horizontal intensity H and dip I as shown in Table XII where arithmetical means of the several measurements are taken for H, D, and I.

5. Some considerations on the changes during the period from 1936 to 1951.

From the changes in H, D, and I thus obtained, those in the northward (X), westward (Y), and downward (Z) components are calculated as shown in Table XIII. Combining δX and δY, the disturbing vectors in the horizontol plane are shown in Fig. 7 where δZ is also shown with numerals.

Table XIII. The local anomalous changes in the geomagnetic components during the period 1936–1951.

Station	δX	δY	δZ
Mabushi	+ 38	− 13	+ 83
Nomashi	+154	+ 74	−150
Zoo	+ 21	− 54	−135

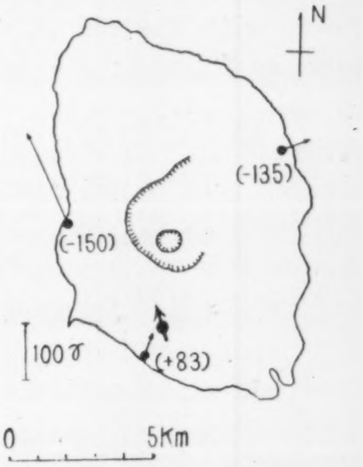

Fig. 7. The disturbing vectors of the local anomalous change in the geomagnetic field during the period from 1936 to 1951.

δZ are shown with numerals in the brakets(Unit: γ). The position and direction of the magnetic dipole that corresponds to the origin of the change is also shown in the figure.

Since only three stations are available, we cannot study the nature of the anomalous change in great detail. Looking at the figure, however, we may see that the distribution is approximately expressed by the field of a magnetic dipole, the direction of the north-seeking end of it being approximately to the north. Here, the writers will determine the position, direction and intensity of the dipole by the distribution obtained above may be best expressed.

In the first place, let us consider a sphere with all the three stations situated on its surface. Since the three stations are on a horizontal plane, the centre of the sphere should be situated on the vertical line across the centre of the circle that passes the three stations. Denoting the radius of the sphere by a, the magnetic potential of the local anomalous change δW is given by

$$\delta W = a\sum_{n=1}^{\infty}\sum_{m=0}^{n}(a/r)^{n+1}P_n^m(a_n^m\cos m\phi+b_n^m\sin m\phi)\ldots\ldots\ldots\ldots\ldots\ldots(1)$$

provided the magnetic matter is all included in the sphere, and we have

$$\left.\begin{aligned}
\delta X&=-\left(\sin\theta\cos\phi\frac{\partial}{\partial r}+\cos\theta\cos\phi\frac{\partial}{r\partial\theta}-\sin\phi\frac{\partial}{r\sin\theta\partial\phi}\right)\delta W,\\
\delta Y&=-\left(\sin\theta\sin\phi\frac{\partial}{\partial r}+\cos\theta\sin\phi\frac{\partial}{r\partial\theta}+\cos\phi\frac{\partial}{r\sin\theta\partial\phi}\right)\delta W,\\
\delta Z&=\left(\cos\frac{\partial}{\partial r}-\sin\theta\frac{\partial}{r\partial\theta}\right)\delta W,
\end{aligned}\right\}\quad(2)$$

where x, y, and z axes are taken to be positive northward, westward, and upward respectively. In case of n, $m\leqq 2$, (12) are written at $r=a$, with the aid of recurrence formulae of spherical surface harmonics, as follows;

$$\left.\begin{aligned}
\delta X&=\sqrt{3}\,a_1{}^0P_2{}^1\cos\phi-a_1{}^1P_2{}^0+\sqrt{3}\,P_2{}^2(a_1{}^1\cos 2\phi+b_1{}^1\sin 2\phi)\\
&\quad+\sqrt{6}\,aP_2{}^0{}_3{}^1\cos\phi-\sqrt{3}\,a_2{}^1P_3{}^0+\sqrt{5}\,P_2{}^2(a_2{}^1\cos 2\phi\\
&\quad+b_2{}^1\sin 2\phi)-\frac{1}{\sqrt{2}}P_3{}^1(a_2{}^2\cos\phi+b_2{}^2\sin\phi)\\
&\quad+\frac{\sqrt{30}}{2}P_3{}^3(a_2{}^2\cos 3\phi+b_2{}^2\sin 3\phi),\\
\delta Y&=\sqrt{3}\,a_1{}^0P_2{}^1\sin\phi-b_1{}^1P_2{}^0+\sqrt{3}\,P_2{}^2(-b_1{}^1\cos 2\phi+a_1{}^1\sin 2\phi)\\
&\quad+\sqrt{6}\,a_2{}^0P_3{}^1\sin\phi-\sqrt{3}\,b_2{}^1P_3{}^0+\sqrt{5}\,P_3{}^2(-b_2{}^1\cos 2\phi\\
&\quad+a_2{}^1\sin 2\phi)-\frac{1}{\sqrt{2}}P_3{}^1(\mathrm{b}_2{}^2\cos\phi-a_2{}^2\sin\phi)\\
&\quad+\frac{\sqrt{30}}{2}P_3{}^3(-b_2{}^2\cos 3\phi+a_2{}^2\sin 3\phi),\\
-\delta Z&=2a_1{}^0P_2{}^0+\sqrt{3}\,P_2{}^1(a_1{}^1\cos\phi+b_1{}^1\sin\phi)+3a_2{}^0P_3{}^0\\
&\quad+2\sqrt{2}\,P_3{}^1(a_2{}^1\cos\phi+b_2{}^1\sin\phi)+\sqrt{5}\,P_3{}^2(a_2{}^2\cos 2\phi\\
&\quad+b_2{}^2\sin 2\phi).
\end{aligned}\right\}\quad(3)$$

By assuming a value for the radius of the sphere that is large enough to contain all the magnetic matter to which the anomalous field is due, we obtain a set of nine simultaneous equations from the observed values at the three stations. On solving the equations by the least square method, the coefficients a_1^0, a_1^1, b_1^1,...are determined. Assuming $\theta=30°$, they are obtained as shown in Table XIV.

Table XIV.
The determind coefficients.

Coef.	Value
a_1^0	-131γ
a_1^1	-391
a_2^0	100
a_2^1	283
a_2^2	-80
b_1^1	-123
b_2^1	138
b_2^2	-190

In the next place, the magnetic centre is determined by the method devised by Ad. Schmidt[13] and J. Bartels[14] in connexion with the eccentric dipole of the earth's main field, the centre being chosen so as to minimize the square sum of the second degree coefficients. Thus the dipole should be located at the position which is also shown in Fig. 7, the depth, magnetic moment, direction of the north-seeking end and dip of the dipole being respectively determined as $6.1\,km$, $2.8\times10^{15} emu$, $-17°$ and N18°W. The direction of the dipole is also shown in the figure with thick arrows in the horizontal plane.

Since, however, the instruments used in the two surveys are not the same, there will exist some systematic errors of the order of several *gammas*. The accuracy of the identification of the stations, which are mainly identified with the aid of sketch maps, also amount to a few *meters*. As the gradient of the magnetic field near the volcanoes is appreciably large, some errors will occur from this source. And we must expect some errors in the procedure of eliminating the general secular change and transient geomagnetic disturbance. To sum up, errors of the order of 10 *gammas* are contained in the local anomalous change during the period 1936~1951, thus the determination of the magnetic centre or the dipole has no decisive meaning because some of the values tabulated in Table XIII are not much larger than the presumed order of the errors. However, the writers will make a second survey in the near future expecting to get results for more accurate discussion on local anomalous change.

In conclusion, it may be said, at some places near the volcano, some marked changes in the geomagnetic field of the order of 100 *gammas* occurred during these fifteen years though their detailed distribution is not clear.

---

[13] Ad. SCHMIDT, *Gerl. Beitr. z. Geophys.*, **41** (1934), 346.

[14] J. BARTELS, *Terr. Magn.*, **41** (1936), 225.

6. Continuous recording of changes in geomagnetic declination.

As already investigated by the writers, it is an established fact that some anomalous changes in the earth's magnetic field occur in connexion with the activity of Volcano Mihara as also confirmed in the case of the 1940 eruption of Volcano Miyake-sima, both volcanoes being composed of basaltic rocks. In order to infer the day-to-day changes more clearly, the writers set up a temporary station at Nomashi Village situated at the foot of the volcano, the distance from the crater being about 4 *km*. The position of the station is shown in Fig. 8. At the station, changes in geomagnetic declination are continuously recorded with a magnetometer which is installed in a cave of which the depth is about 5*m*. A *MK* magnet whose magnetic moment amounts to about 100 *emu* is suspended with a fine phosphor-bronze ribbon, the effect of the torsional force of the ribbon being neglected as pointed out by T. Minakami[15]. Adopting an optical lever of 220 *cm*, the change in the direction of a mirror attached to the magnet is recorded on a photographic paper with a sensitivity of 0.78 *minutes* of arc per *mm*. the paper is wound on a drum which rotates once a week. An example of the record is to be seen in Fig. 9. The observation began from the beginning of April, 1951. The day-to-day change in daily mean of the declination is shown

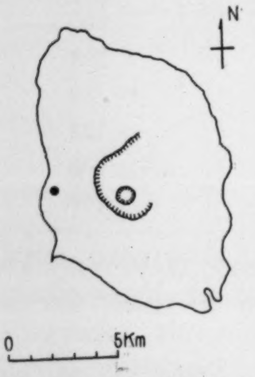

Fig. 8. The position of the station where the variometer was set up.

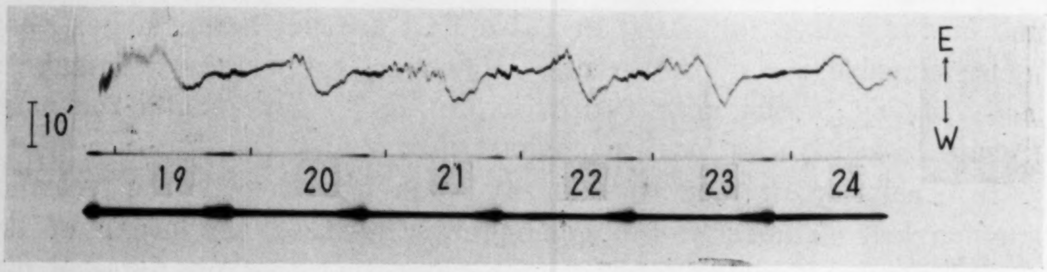

Fig. 9 An example of the record. At the beginning of the declination curve, the vibration of the suspended magnet caused by the microtremors of volcanic origin is to be seen clearly. (From Apr. 18 to 24, 1951).

---

[15] T. MINAKAMI, *Bull. Earthq. Res. Inst.*, **22** (1944), 110.

in Fig. 10 where the daily mean at Kakioka Observatory is also shown. On the other hand, absolute measurements of declination were carried out just before the cave on Apr. 2[16], May 9[17] and July 10[18]. The

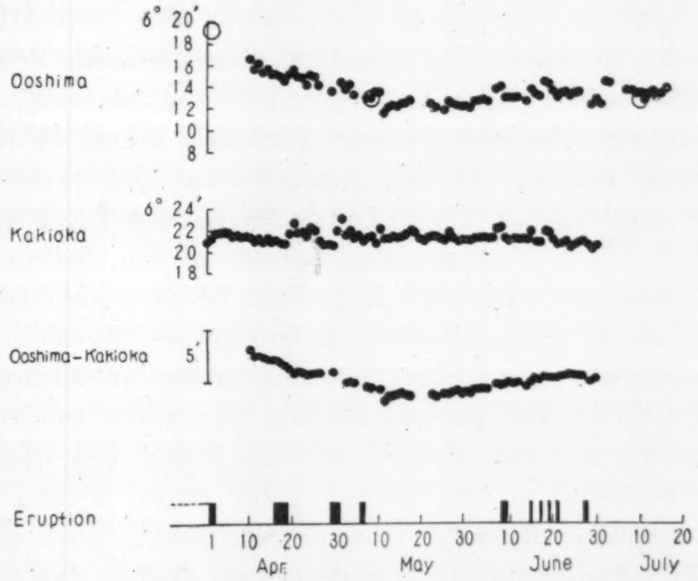

Fig. 10. The day to day change in daily mean of the westerly declination at Ooshima and Kakioka. The results of the absolute measurements are also shown with large hollow circles. The difference curve is also shown. At the lowest part of the figure, the periods during which the eruption of Volcano Mihara continued are illustrated.

---

[16] The results are as follows, where only the declination was observed with a magnetic theodolite.

Time	D
Apr. 2nd	
14*h*00*m*	6°24'.5W
15 00	22 .5
16 00	21 .5

Mean=6°22'.8W

The reduced value to the daily mean on Apr. 2: 6°19'.3W.

[17] See Table I.

[18] The three components were measured with the G. S. I. magnetometer. The results are as follows;

Declination and Dip

Time	D	I
July 10th		
18*h*02*m*	6°12'.5W	47°25'.3
20 22	12 .8	25 .2
21 10	12 .9	24 .1
22 36	12 .5	24 .9
23 42	12 .5	24 .8
July 11st		
0 29	12 .7	24 .9
Mean	6°12'.6W	47°24'.9

Horizontal intensity

Time	H
July 10th	
18*h*20*m*	29993γ
20 31	29999
21 21	30011
22 45	30006
23 52	29999
July 11th	
0 40	29993
Mean	30001

The reduced value of the declination to the daily mean on July 10: 6°12'.9W.

base-line value referred to the measurement on May 9 is adopted here. As may be seen in the figure, the day-to-day change at the station shows marked decrease in its westerly declination from the beginning of April to the end of May, when the declination turns to increase. As the results of the absolute measurements reduced to the daily mean agree well with the record of the variometer as is also shown in the figure, the change thus recorded seems to be plausible. During the same period, on the contrary, the day-to-day change at Kakioka is not appreciable. In order to bring out these results more clearly, the differences between the values of the declination at Ooshima and Kakioka are also plotted in Fig. 10 by which procedure the irregularities due to geomagnetic storms are elimenated and we see clearly the anomalous change in the declination at Ooshima. At the lowest part of Fig. 10, the periods during which the microtremors due to the eruption of Volcano Mihara are occurring are illustrated, the tremors being recorded on the photographic paper through the vibration of the suspended magnet. It is of interest to note that a marked decrease in the declination was observed during the period when the volcanic activity that had continued from Feb. 4 became weak while an increase in the declination was observed just before the active period in June. Judging from the chart of the declination in Fig. 4, the decrease in the westerly declination may correspond to the increase of the magnetization of the volcano, and the increase in the declination to the decrease of the magnetization. Thus we may presume that the change observed here is caused by the change in magnetization of the volcano which may be probably ascribed to the changes in thermal condition within the volcano. However, we must accumulate much more data to establish the relation between anomalous change in geomagnetic field and volcanic activity. The result considered here is only a preliminary study of the said relation.

7. Summary and conclusion.

Conducting surveys over Ooshima Island with a G. S. I. type magnetometer, the writers constructed magnetic charts of three components more complete than those ever obtained, the anomaly in the earth's magnetic field thus made clear being ascribed to the magnetization of Volcano Mihara as is the case in other volcanoes. A comparison of the observed values to those of the 1936 survey was made at the three stations and a local anomalous change of order of 100 *gammas* was found out though its distribution was not clear.

Meanwhile, the writers set up a temporary station at the western skirt of the volcano, about 4 *km* distant from the crater, where changes in geomagnetic declination has been continuously recorded with a variometer since April this year. An anomalous eastward change in the declination of an order of 5 *minutes* of arc occurred during the period from the beginning of April to the end of May, while the activity of the volcano which continued from February became weaker during the period. And the westerly declination turned to increase slightly before the activity in June. These changes were also confirmed by the absolute measurements made just before the cave in which the changes were recorded. Although we have not yet obtained sufficient data to discuss the relation between anomalous change in geomagnetism and volcanic activity, it will be possible to get a more comprehensive relation by repeating the magnetic survey and continuing the observation with the variometer.

In summary, the writers wishes to express their appreciations to Professor H. Tsuyâ, Professor T. Hagiwara and Dr. T. Nagata for their helpful advices. The G.S.I. type magnetometer became available through the courtesy of the Geographical Survey Institute, and the writers' hearty thanks are especially due to Mr. I. Tsubokawa of the Institute. Dr. S. Imamiti of the Kakioka Magnetic Observatory and Mr. S. Imai of the Hydrographic Department placed magnetic data at the writers' disposal, to whom the writers' cordial thanks are also due. In the course of the field-observation, Mr. T. Masaka of the Nomashi Village and Mr. T. Yanai of the Nomashi primary school assisted the writers kindly. The writers wish to express their sincere thanks to them. A part of this study was done with the financial aid of the research grant given to one of the writers from the Department of Education, and the writers wish to express many thanks for the grant received.

57. 三原山の地球磁氣學的研究 第3報

地磁氣三成分測量および偏角變化の連續觀測

地震研究所 力武常次
横山泉
岡田惇
菱山よね子

火山活動と地磁氣變動との關係を更に詳細に調べる目的で，伊豆大島全島にわたり地理調査所型磁氣儀による第1回三成分測量を1951年5月に實施した。1936年の測量結果と比較して1936―1951の期間の局地的地磁氣異常變化について若干の議論を行うとともに，1951.4に對する地磁氣分布圖を作製した。

また地磁氣の時間的變化を知るために野增村に於いて，偏角の連續記錄が4月以降實施されつゝある。その日平均値の變化をみると，柿岡の値を不變としたときに，約5分に達する東偏およびその回復が4～6月の期間に起つたことがわかる。このことは，さらに隨時行われた絕對觀測の結果によりたしかめられ，火山活動の消長と關係あるように思われるが詳細はさらに資料の集積をまって吟味する豫定である。

58. *Damage on Window-panes by the Air-waves of Explosion of Volcano Asama on Sept. 23, 1950.*

By Shūzō SAKUMA,

Earthquake Research Institute.

(Read June 19, 1951.—Received Sept. 19, 1951.)

1. Introduction.

The activities of Asama have been typically Vulcanian in recent years. A large amount of bombs and other volcanic materials is hurled out in an instantaneous explosion with the velocity of 150–200 m/s, accompanied by strong detonations which are often audible as far as 200 km from the volcano. In addition, such violent explosions sometimes cause damage to windows, doors and walls of wooden houses at the foot of the volcano by their strong air-shocks.

As to the propagation of audible air-waves, detailed descriptions of the sound-areas of the detonations of the volcano were given by the late F. Omori[1], and the phenomenon was treated by S. Fujiwara[2] from the meteorological standpoint. The air-waves of longer period, however, have hitherto scarcely been recorded or studied, with the exception of barographic observations by F. Omori[1], on the basis of which T. Matuzawa[3] discussed the pressure at the instant of explosion.

The explosion of Asama on 4 h 37.5 m of Sept. 23, 1950 was one of the most violent in recent years[4]. A number of large incandescent lava blocks were thrown out in an instant together with gases, vapour, ash and other volcanic materials, and some of the bombs fell to the ground even at a distance of 3 km from the crater. The initial velocity of the bombs was estimated at about 200 m/s on the basis of the distance of their flight[5]. The total kinetic energy for the ejection of volcanic bombs was estimated at about 10^{20} ergs. The volcanic smoke was blown off eastward by the west wind which prevailed in the upper atmosphere at that time, and ash fell to the east of the volcano. Detonations were heard as far as 200 km skipping over a non-audible region from about 100 km to 150 km. The damage done to window-panes by the present explosion was the most remarkable in these thirty years since glass-windows came into common use in the district around Volcano Asama. As no instrumental observation was carried out at that time except those by barographs for meteorological purposes, the writer planned to study the character of the air-shock from the damage.

---

[1] F. OMORI, *Bull. Earthq. Inv. Comm.*, **6**; **7** (1914).

[2] S. FUJIWARA, *Bull. Centr. Meteor. Obs.*, **2** (1912), 1.

[3] T. MATUZAWA, *Zisin*, **6** (1934), 588; **7** (1935), 47. (In Japanese).

[4] T. MINAKAMI, Reported to International Association of Vulcanology, I.U.G.G., Brussells Assembly, August, 1951.

[5] T. MINAKAMI, *Bull. Earthq. Res. Inst.*, **20** (1942), 65,

2. Collected Data and Method of Investigation.

As 29 primary, junior high and senior high schools kindly accepted the writer's request to ask their pupils to report on the numbers of both broken and total window-panes in the respective directions of their own houses, several results could be obtained about the nature of the air-shock according to the reports. Reports were sent from 2,582 families around the volcano, with the exception of the northwestern quadrant and close neighbours of the volcano. The total of the broken panes reported amounted to 5,520. In dealing with them, the following points were noticed and taken into consideration.

(1) Since some of the reports include the number of panes inside their houses while some do not, the "total number" of window-panes cannot hold one definite meaning and a kind of error is introduced here. Fortunately, pupils belonging to the same family gave their reports independently, and 327 such cases could be examined. As the result, we could infer that the errors in the total number might probably be about 10% including the errors due to miscounting. It must also be added that the "broken number" of window-panes reported independently by those of the same family showed satisfactory coincidence.

(2) The number of window-panes was given for the four directions in most of the reports. Some were given in N, E, S and W, and others in NE, SE, SW and NW, according to the aspect of each house. In dealing with these data statistically, the writer rearranged the directions in the four directions of "craterward", "anticraterward" and "lateral" (left and right seen from the crater) in the following way. At first, the nearest direction towards the crater among the eight directions is adopted as the "craterward" direction. When

none of the reported directions of a house coincides with the above defined craterward direction and differs 45° in arc, the average value of both broken and total number of the two neighbouring directions is supposed, for convenience sake, to represent the state of matters in case the directions of the house should coincide with the above defined ones. Functional relations between the angle of impact of the air-waves and breaking of panes are not yet made clear, so the error which might be introduced into the results through the above procedure cannot be estimated quantitatively. Qualitatively, however, it may be said that the damage obtained thus is slightly increased in the anticraterward direction and slightly diminished in the craterward direction in comparison with the houses facing exactly to the crater.

When we consider the characters of the collected materials, it is to be noticed that the situation we face is quite similar to that when we attempt to infer the nature of earthquake-motions quantitatively from the damage caused by the earthquake. Though not impossible the work is quite difficult.

As the first step for studying the intensity of air-waves, the percentage of damage in every house and every village is adopted as a measure and is discussed in this paper.

Even in one village where azimuth and distance from the crater

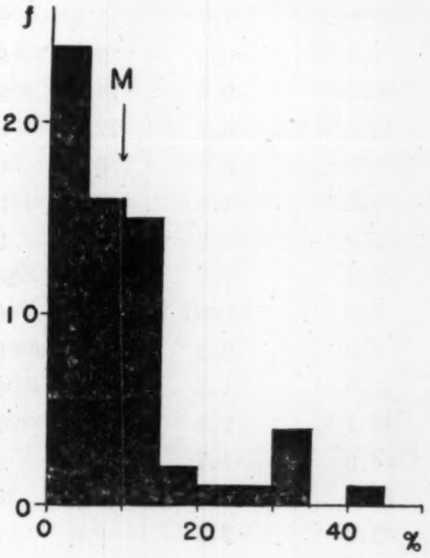

Fig. 1. Frequency of occurrence of damage-percentage M for every house at Komoro. (craterward)
M: average broken percentage

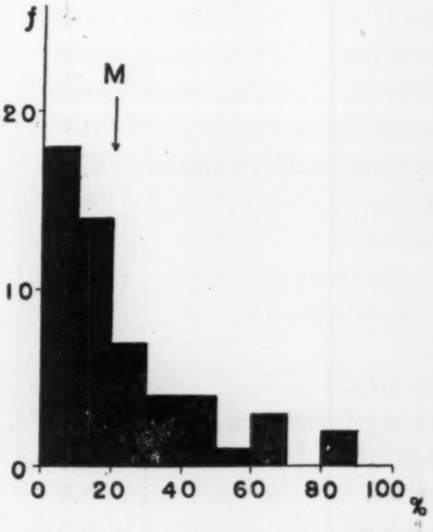

Fig. 2. Frequency of occurrence of damage-percentage M for every house at Kutukake. (craterward)
M: average broken percentage

are nearly the same, the damage percentage differs very much from one another. Examples are given in Figs. 1 & 2 for two villages in order to show how much the percentages for windows of every house differ from one another, by taking the damage-percentage in abscissa and its frequency of occurrence in the village in ordinate. This disparity was caused more by the existence of obstacles in the path of air-waves such as trees, houses and sometimes outer wooden sliding doors than by differences in the strength of window-glasses. For this reason, those houses whose windows were not damaged were omitted from the following calculation of percentages. The writer adopted an average percentage (M) in the four directions as representing the damage as follows:

$$\mathrm{M}=\frac{\text{sum of the number of broken window-panes in one direction}}{\text{sum of the number of total window-panes in the same direction.}}$$

The value of M are tabulated in Table I and illustrated in Figs. 3 & 4.

Table I. Average broken percentage M for villages.

Location	From the crater		Damage in M (%)			
	Distance (km)	Azimuth	Craterward	Anticrater-ward	Lateral	
					Left	Right
Sengataki	7.2	E34°S	9.0	0.2	4.4	2.1
Oiwake	7.6	E72°S	9.9	1.2	3.5	2.9
Kariyado	8.2	E59°S	12.2	1.7	11.9	0.9
Kose	8.8	E14°S	1.4	0.0	2.4	0.0
Kutukake	9.0	E44°S	20.3	2.6	16.1	5.8
Toriibara	10.0	E51°S	15.0	0.3	17.7	3.7
Mikasa	10.0	E20°S	0.0	0.0	0.0	0.0
Hanareyama, Minamihara	10.4	E39°S	7.6	1.6	9.9	5.0
Yui	10.6	E56°S	12.9	4.2	9.9	3.8
Siozawa	11.3	E47°S	10.1	9.7	12.8	10.1
Kyū-Karuizawa	11.6	E26°S	5.9	0.3	2.2	0.9
Sin-Karuizawa	12.2	E32°S	3.3	2.2	1.1	2.6
Hotti	12.2	E58°S	12.3	1.8	14.5	1.1
Kami-Hotti	14.0	E57°S	12.1	2.3	3.3	3.4
Minami-Karuizawa	14.1	E46°S	4.3	1.7	6.1	0.9
Siono	8.4	S18°W	36.0	3.3	19.4	10.9
Norise	9.6	S24°W	41.0	3.8	9.8	1.6
Maseguti	9.8	S13°W	11.9	2.6	7.2	0.8
Miyota	11.0	S 8°W	9.0	2.8	4.8	3.2
Hatiman	11.0	S28°W	20.4	2.7	3.0	16.6

(to be continued)

(continued)

Location	From the crater		Damage in M (%)			
	Distance (km)	Azimuth	Craterward	Anticrater-ward	Lateral	
					Left	Right
Kasiwagi	11.4	S31°W	22.5	0.9	5.1	16.7
Hirahara	11.6	S24°W	13.7	1.6	3.7	2.5
Ōsato	11	S55°W	12.0	0.0	0.0	5.7
Komoro	12.3	S43°W	8.8	0.7	2.0	3.9
Mikage	12.4	S20°W	8.4	0.0	0.0	0.0
Yotuya, Otome	12.8	S35°W	9.7	1.5	0.7	7.2
Obara	13.8	S38°W	10.0	1.1	0.7	17.6
Sibauda	14.4	S61°W	7.2	0.0	0.0	0.0
Moriyama, Mimitori	14.6	S32°W	4.5	0.0	0.5	7.5
Kawabe	14	S41°W	2.8	2.1	1.8	3.3
Mitui	16	S 5°W	very slight			
Nakatu	18	S31°W	1.1	0.2	0.6	1.3
Minamiomaki	19	S41°W	no damage			
Kitaomaki	19	S60°W	no damage			
Gorobeesinden	19	S33°W	no damage			
Motomaki	21	S42°W	no damage			
Mituwa	21	S54°W	no damage			
Yokodori	24	S51°W	no damage			
Kyōwa	24	S43°W	very slight			
Agata	18	S70°W	no damage			
Kanou	18	S80°W	no damage			
Hosimata	14.2	N 6°W	5.7	0.6	—	—
Kita-Karuizawa	9.0	E43°N	11.5	1.6	5.5	7.3
Ōmae, Kambara, Ōzasa	12.0	E83°N	14.6	13.0	3.9	0.0
Ōkuwa	13.0	E59°N	13.3	2.5	4.0	14.1
Mihara	14.4	E80°N	3.1	0·0	0.9	0.6
Naganohara	19	E55°N	no damage			

3. Discussion.

A glance at the geographical distribution of M will show that the value of M is remarkably diminished here and there even within a short distance from the crater as at Oiwake and Sengataki. These anomalies can be explained mostly by obstacles in the course of the

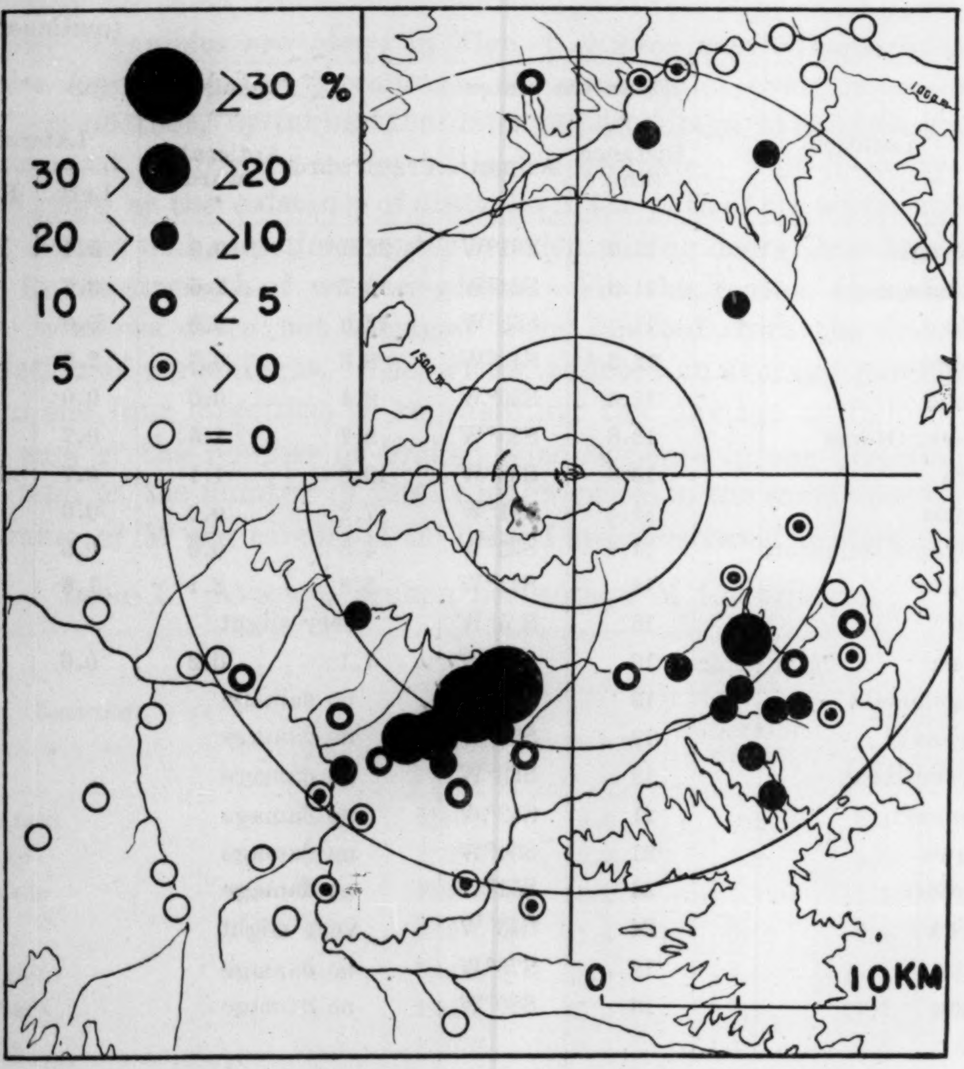

Fig. 3. Geographical distribution of average damage-percentage M for every village. (magnitude in craterward direction)

air-waves from Asama. Almost all the villas in Sengataki, for example, are surrounded by trees and were protected from air-shocks at that time. In contrast to that, percentages were high at those villages where the houses faced directly to the volcano. It is also remarkable that the breaking of window-panes was not restricted to the craterward direction but occurred, to some extent, also in the lateral and anticraterward sides. This phenomenon may be ascribed to the reflection and refraction by the neighbouring obstacles of high reflective power such as houses. Neither the errors due to the procedures in arranging the original data nor the effect of topographies of large scale can explain this phenomenon which was experienced in almost all villages.

The effects of those obstacles which existed near the villages were so great that problems concerning azimuthal distribution of intensity of air-waves at the instant of burst, and those of reflection and refraction due to such large topographies as sommas cannot be treated with ease. In this connection, though tentatively and qualitatively, it may be pointed out that the main direction of damage was not exactly craterwards in most of the villages in the SE and SW quadrants of Fig. 4, but the damage seemed to be caused by air-waves coming from a somewhat northern direction.

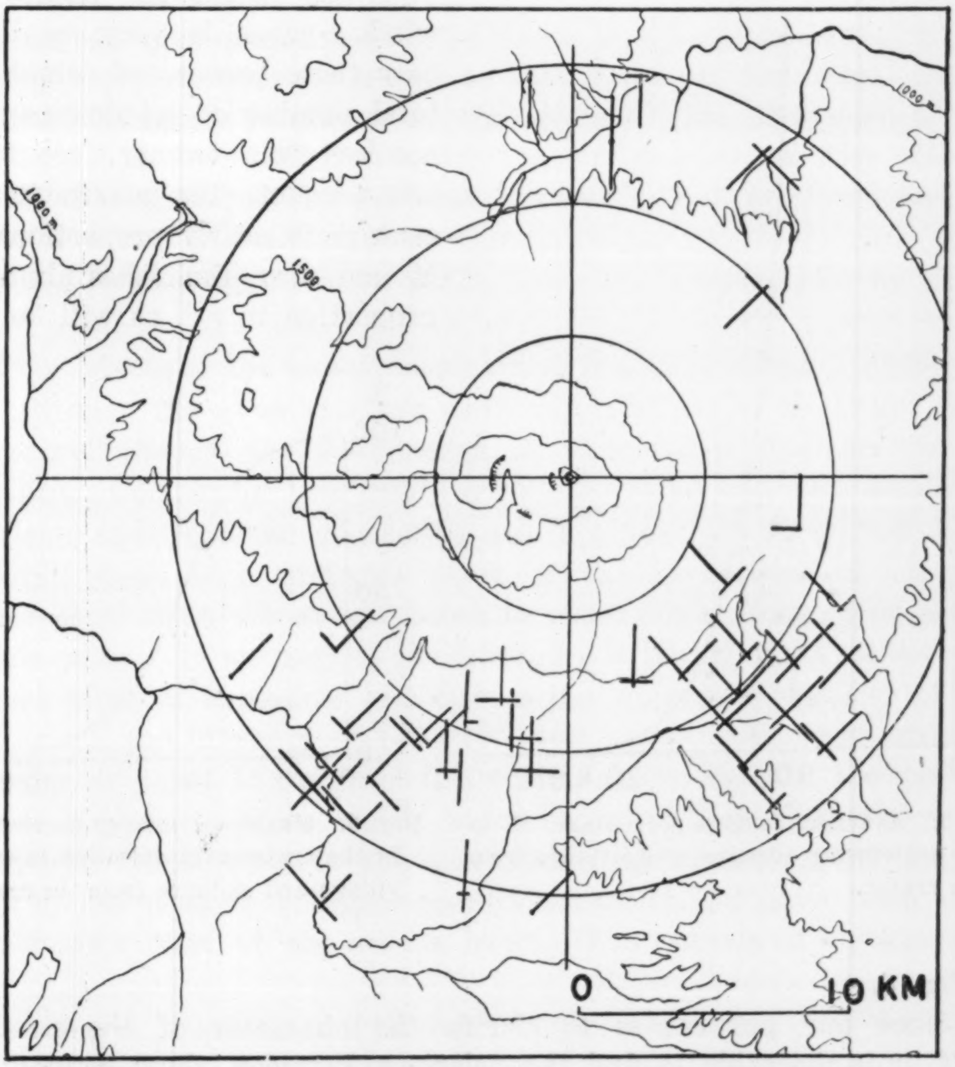

Fig. 4. Geographical distribution of average damage-percentage M for every village. (Ratio of magnitude in four directions, taking the largest M as unity)

In order to study the relations between the intensity of air-waves and distance, such local effects should be excluded by adopting maximum values of M for respective distances. The curve with full line in Fig. 5 was thus drawn and it became clear that the average percentage for the craterward direction decreased in proportion to r^{-4} from 8 to 20 km. The value, of course, should draw close to 100% nearer the crater.

Maximum percentages in respective villages were also studied in place of the average percentage M. It would rather be going too far to adopt maximum percentages, especially when the number of window-panes is very small. If only those houses, of which the total number of window-panes is not less than twenty, are taken into account, the maximum percentage is nearly proportional to M and also diminishes almost in proportion to r^{-4} as will be seen in Fig. 6.

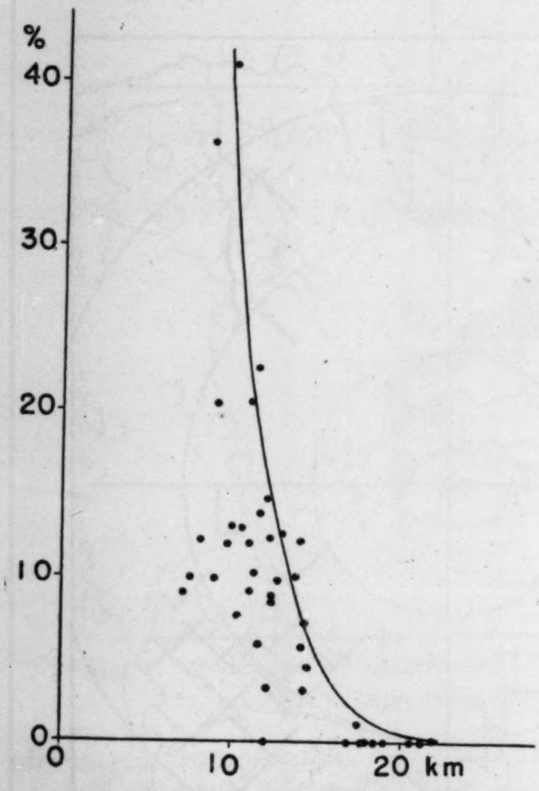

Fig. 5. Average damage-percentage M in the craterward direction and distance from the crater.

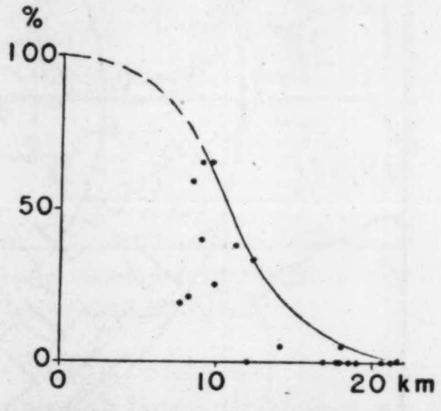

Fig. 6. Maximum damage-percentage in the craterward direction in every village and distance from the crater.

Since our purpose is to clarify the character of the air-shock itself, it is desirable to find the relations between those percentages and the intensity or period of the air-shock. The breaking strength of glass-plate has been treated both mathematically and experimentally by many authors[6]. Changes undergone by glass-plates under various kind of loads are known in detail. Experiments on breaking glass-plates by impact of impulsive air-waves were also carried out[7]. Most of them, however, are concerned with a plate clamped or supported by a sufficiently rigid frame. The mode of causation of strains in the actual window-panes is not so simple as that in perfectly clamped or perfectly supported plate but differs from one another in boundary conditions. The wooden frames and besels of windows which could be deformed easily by the air-waves might have caused localization and concentration of stress in the glass plate in a haphazard manner, in addition to heterogeneities in the glass-plate itself. The size and thickness of glass-plate also differ from one another. In addition, some of the panes were reported to have come off the weak frames and been smashed to pieces on the ground. The phenomenon is so complicated as described above that the writer gave up the attempt to find the exact relation between the intensity of air-shock and the percentages on the basis of those experiments.

Damage on actual window-panes, however, is caused also by explosions of powders and bombs. The writer compares here the present results with the effects of the atomic bomb which fell on Hirosima. According to K. Muto[8], the glass-windows were damaged as far as 16 km from the centre, though the distribution of this kind of damage was not described. Comparing this result with theoretical and field studies by American and Japanese physicists and engineers[8][9] we obtain $1\text{–}2\times 10^{-2}$ atm. press. as a probable value of the lower limit of intensity for air-blast from the atomic bomb to cause slight damage on actual window-panes. If we neglect the difference in period of waves between the two kinds of explosions and discuss the apparent intensity of the shock-wave, the intensity of $1\text{–}2\times 10^{-2}$ atm. press. may be regarded as the value at about 18 km from the crater at the time of the present volcanic explosion. More words must be spent here lest the result should lead immediately to the conclusion that the energy of the air-waves of the present volcanic manifestations should have been comparable with that of the atomic bomb. The periods of air-waves of

---

6) "Glass in Architecture and Decoration" (1937), London.

7) G. SHINKAI and others, *Trans. Inst. Japan Arch.*, **5** (1937), 45.

8) Japan Science Council, "Report on the Damage Caused by Atomic Bombs" (1951), (in Japanese).

9) "The Effects of Atomic Weapons" (1950).

explosion of Volcano Asama and its difference from that of the atomic bomb is known to some extent. The initial positive phase of air-waves of explosions of Asama which were observed in 1913 and 1914 by F. Omori [10] was nearly 2–3 sec. at the distance of 3 km from the crater, and the greater the eruption was, the longer the duration became. The duration of the initial positive phase of the atomic bomb can be estimated by calculation at 1.8 sec. at the distance of 16 km from the centre [11]. As the volcanic explosion in 1950 was on a greater scale than those in 1913 and 1914, the air-waves might have contained waves of much longer periods. Besides the above-mentioned differences in the character of waves, the differences in the mechanism and mode of both explosion and propagation must be taken into consideration. Consequently, our comparison of the two phenomena should be limited to the intensity of air-waves that could cause damage to window-panes.

Trace-amplitudes on barograms at the weather stations are tabulated in Table II for reference. It must be remembered that these records have been obtained through Stevenson screens and thus the air-waves may have been much reduced.

Table II. Amplitude of barographic disturbance.

(After weather stations).

Station	From the crater	Amplitude in mm Hg	
		Increase	Decrease
Kutukake	9 km SW	3.1	2.2
Nagano	43 km NW	0.4	—
Maebasi	50 km E	1.6	1.0
Matumoto	54 km SWW	—	—
Kumagaya	87 km SE	—	—

4. Resumé.

The damage caused to window-panes by the air-shock in the 1950 explosion of Asama was confined to the region within nearly 18 km distant from the crater.

Air-waves were reflected and refracted by various obstacles in their path of propagation, and consequently, the resultant effect became complex.

---

[10] F. OMORI, *loc. cit.*, 1).

[11] *loc. cit.*, 9).

The degree of damage was expressed by percentages. Though this expression is still imperfect, several problems concerning the air-wave could be discussed to some degree, as may be seen in Figs. 3 & 4.

It is also interesting and useful to compare the present result with effects of explosion of the atomic bomb.

In concluding, the writer wishes to express his cordial thanks to Dr. T. Minakami by virtue of whose guidance and encouragement the present research was made possible, and to those schools which supplied the writer with the reports on damage. The expense for this study was defrayed from the Funds for Scientific Research of the Ministry of Education.

---

58. 1950年9月23日の淺間火山爆發の空氣波による窓ガラス被害

地震研究所　佐久間修三

表記の爆發は，最近の淺間火山の爆發の中で最大級に屬し，山麓の窓ガラスに生じた被害は甚しかつた。火山周邊の各學校の協力により，各學童の家についての方位別の窓ガラス總數及び破壞數の報告を得，これを整理して次の結果を得た。

1) 被害は火口からの距離が大きくなるにつれて急にへり，火口から大約 18 粁が有被害の限界であつた。
2) 被害は家屋や部落の立地條件に著しく左右され，火口に直面する位置では被害が大きい一方，樹木其他の小地物の遮蔽效果が著しいらしく，火口から 10 粁以内でも被害の輕かつた部落もある。
3) 被害は家屋の方向の中では火口に直面する方向は著しいが，それ以外の方向にも被害のある例が多い。これは家屋附近の地物による空氣波の反射や回折を考へれば大體說明出來る。又，もつと大きい地形又は噴出時の條件によるとも思われる樣な，廣い範圍にわたつての被害方位の偏りがある。
4) 被害から直ちに空氣波の性質を量的に論ずることは難かしいが，原子爆彈被害の類推から有被害の限界地附近では大約 $1\sim2\times10^{-2}$ 氣壓程度の壓力振幅であつたと推定される。

59. *Vibration Test of Actual Reinforced Concrete Building.*

By Kiyoshi KANAI and Teiji TANAKA,

Earthquake Research Institute.

(Read Feb. 18, 1947.—Received Sept. 20, 1951.)

1. Introduction.

Since the strength test of actual reinforced concrete building necessarily becomes large in scale, not so many buildings have been submitted to the test of this kind. The number of satisfactory seismic tests of applied to concrete buildings is still smaller. For in the test of strength against earthquake, the ordinary method of measuring the strength by applying to the building statical force does not satisfy the purpose fully, so a vibration test becomes necessary.

Generally in the vibration measurement of actual reinforced concrete buildings, the vibrations caused by the wind or small earthquake are observed and the natural period and oscillation type of the building are obtained. On rare occasions the free oscillation of building is measured by pulling the building and letting it go to get its natural period and damping coefficient.

However, it is quite difficult to learn the aseismatic property of building fully from such experiments only. This time, we applied for the first time the method, by which the vibration of wooden-house may be measured[1], to concrete buildings. The method is to apply forced vibration to the building.

The experiment showed that this method is considerably effective for the seismic test of reinforced concrete building, for we could get the exact value of the proper period and damping coefficient of the building as well as the quite approximate oscillation type and the data concerning the state of the base under the ground.

---

[1] T. SAITA, "Study of Vibrations of Wooden House", (in Japanese), *Report Invest. Comm. Earthq.-proof Const. Japan Soc. Prom. Scien. Res.*, No. **1** (1937), 60, No. **2** (1942), 32.

K. KANAI, "Vibration Experiments with an Actual Wooden Building", (in Japanese), *Bull. Earthq. Res. Inst.*, **20** (1942), 538, **21** (1943), 206.

2. The building submitted to the experiment.

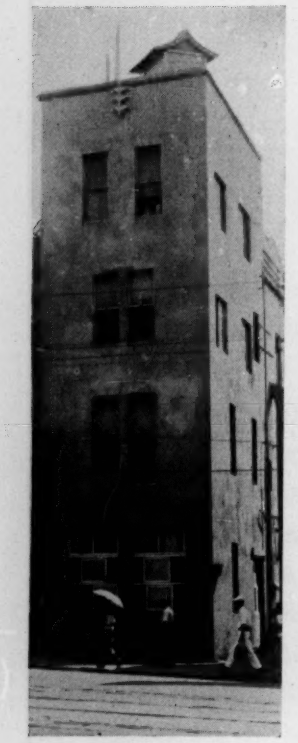

Fig. 1.

The building submitted to this experiment is four-storied reinforced concrete one, located at Kobiki-cho, Chuo-ku, Tokyo, and was once burnt during the late war. Figs. 1 and 2 show the photograph and plan view of the building respectively. As shown in this photograph and the plan view, the building, being small and simply constructed with a width of 4.4 m in beam direction and 11.6 m in girder direction, is suitable for analysing the experimental result.

Table I shows the floor height and the weight of each part of the building which is calculated from the plan.

In Table I the height of foundation was calculated inversely from the experimental result. The weight of the roof includes the parapet and the vertical members of the foundation, and the floor weight is a roughly estimated value.

From data obtained by boring the neighbouring ground we found that the building stands on ground having piled soil and reclaimed soil of 4 m thickness and diluvium of 14 m under them.

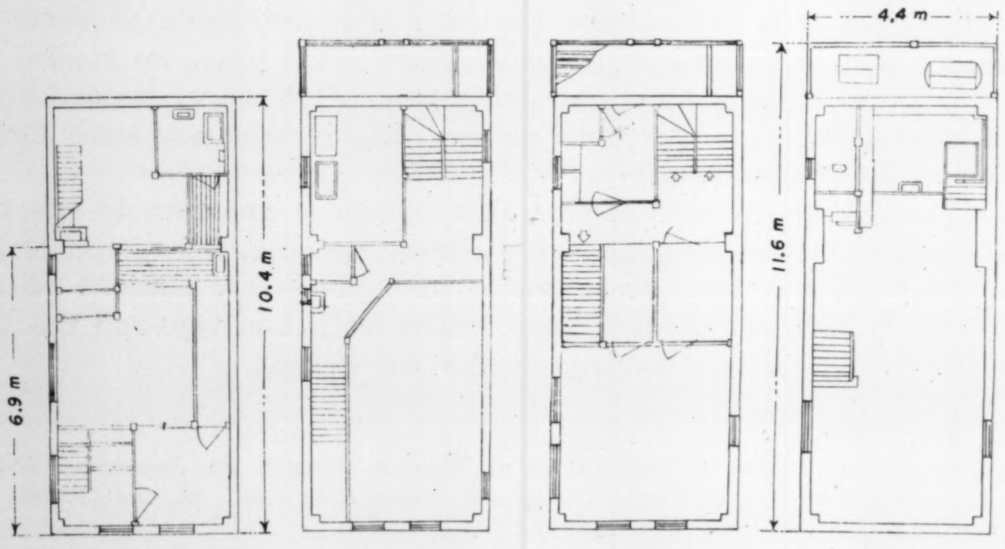

Fig. 2. The plan view of the building subjected to the experiment.

Table I.

Number of stories			Base	1	2	3	4	Roof
Height of column (m)			2.0	3.7	3.2	3.1	3.2	—
Weight (ton)	Floor+Beam	Dead load	—	16.8	16.8	16.8	16.8	11.0
		Live load	—	14.4	14.4	14.4	14.4	12.8
		Total	—	31	31	31	31	24
	Column+Wall+Staircase		66	76	71	66	64	—

3. Method of experiment.

As for the experiment, the vibration was caused on the building by a vibrator installed on the roof floor, driven by an electric motor and producing centrifugal force, and amplitudes of vibration corresponding to various r.p.m. were measured by two kinds of portable seismograph. One of them is of inverted pendulum type with air-damper, smoked paper for recording, period of 6 sec and magnification of 20. Another has an oscillograph for recording equipped with induction type transducer, of which the magnification is about 200 at critical damping.

Vibrational force was given to beam direction and girder direction individually, and vibrational displacement of each floor was observed by carrying the transducer to every floor. The observed displacement was compared with the one measured by seismograph installed on the floor of forth story.

4. Results of Observation.

The vibrational force produced by the vibrator is represented by $F=M(4\pi^2/T^2)r(\sin\theta/\theta)$, where $M=5.5\,\mathrm{kg}$, $r=20\,\mathrm{cm}$, $\theta=44°$. Therefore, the observed values represent the amplitudes corresponding to the applied force which changes according to frequency. This makes theoretical consideration rather complicated. So the values are converted into the amplitudes supposing that the constant force acts regardless of frequency. Next, as the transducer is of the induction type which records the values proportional to velocity, the values were also converted into vibrational displacement. Making these two conversions we made clear the relations of amplitude and frequency concerning every floor of the building, which are shown by mark ● in Figs. 3$\sim$7. The

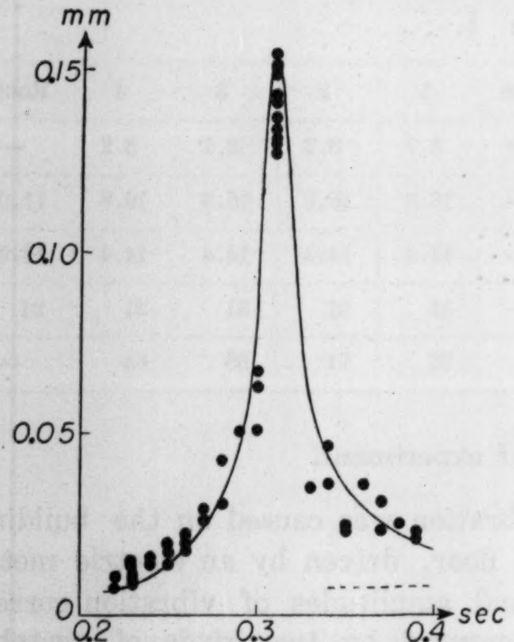

Fig. 3. Relation of amplitude at roof floor and vibration period. Mark ● ; experimental result, curved line ; theoretical result.

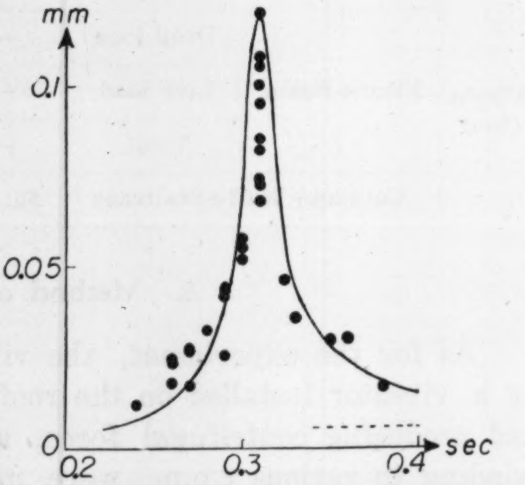

Fig. 4. Relation of amplitude at third floor and vibration period. Mark ● ; experimental result, curved line ; theoretical result.

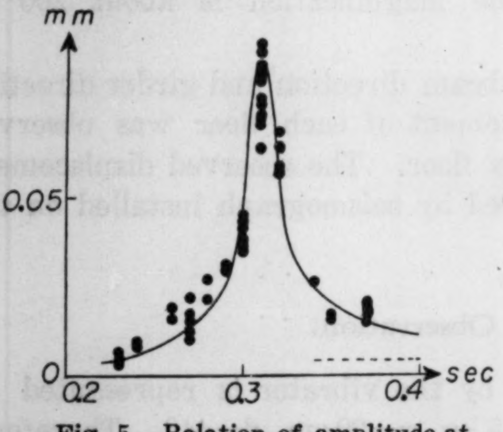

Fig. 5. Relation of amplitude at second floor and vibration period. Mark ● ; experimental result, curved line ; theoretical result.

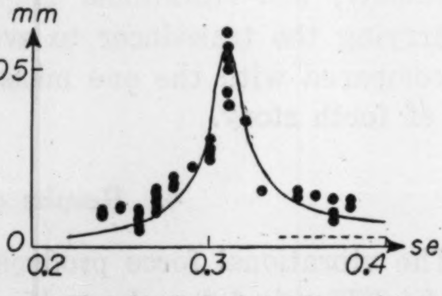

Fig. 6. Relation of amplitude at first floor and vibration period. Mark ● ; experimental result, curved line ; theoretical result.

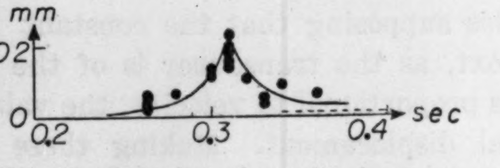

Fig. 7. Relation of amplitude at ground floor and vibration period. Mark ● ; experimental result, curved line ; theoretical result.

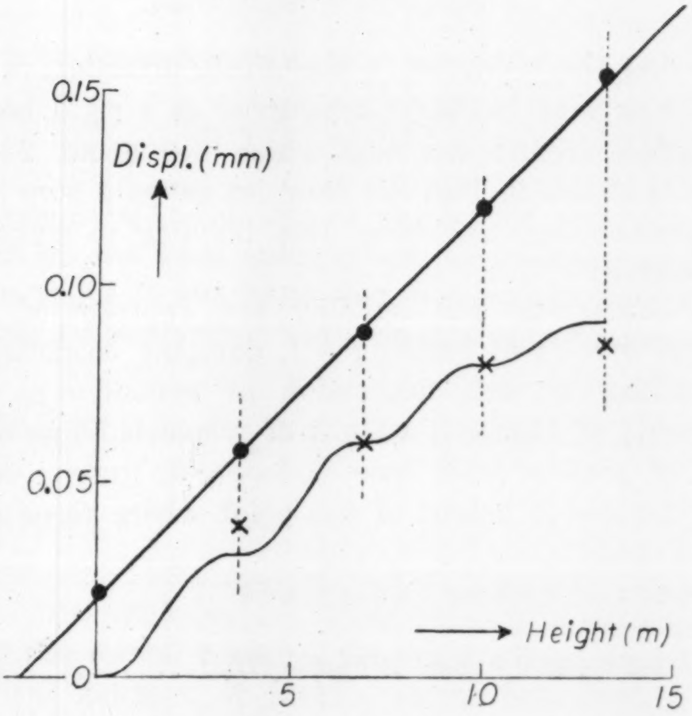

Fig. 8. Distribution of resonance amplitude of each floor. Mark ●; beam direction, × ; girder direction. Two lines represent the theoretical results of rocking vibration and bending vibration respectively.

constant force applied here is $F=5\times 10^7$ dyne which means actual force in case of $T=0.31$ sec.

The maximum amplitudes (resonance amplitudes) of each floor in both the beam and girder direction are represented respectively by ● and × in Fig. 8. At the present it is difficult to speed up the rotation of vibrator over 300 r. p. m. For this reason, the relation between frequency and amplitude in the girder direction, where the resonance frequency is very high, cannot be made so clear as in the beam direction.

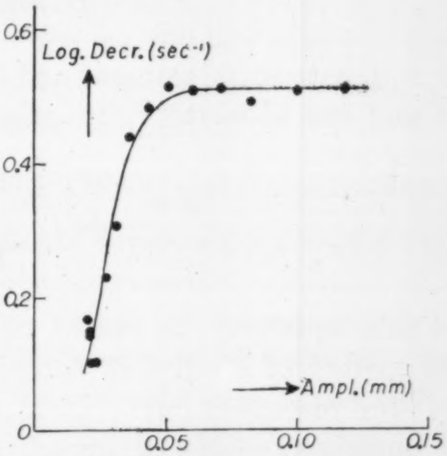

Fig. 9. Relation of damping coefficient and vibration amplitude of the beam direction.

Producing free oscillation, we got damping coefficient as shown in Fig. 9,

5. Theoretical consideration.

In considering the vibration in the girder direction, we found that the whole building may be fairly considered as a rigid body making a rocking oscillation around the axis which lies about 2 m under the ground. This is shown in Fig. 8. Now let us go a step further with theoretical consideration, assuming this building to make a complete rocking oscillation.

Constants concerning the building are represented as follows: mass moment of inertia of building $= I$, damping coefficient $= \varepsilon$, pressure corresponding to unit depression of ground $= p_0$, geometrical moment of inertia of base $= i$, weight of whole building $= W$, height of the center of gravity from base surface $= h$, gravity acceleration $= g$, vibrational force $= f$, height of the point where force acts from the base $= H$.
Then the equation of rocking oscillation is

$$I\ddot{\theta} + 2\varepsilon\dot{\theta} + (p_0 i - Wh)g\theta = fH. \ldots\ldots\ldots\ldots\ldots\ldots\ldots (1)$$

if we represent the vibrational force $f = F \sin pt$ and write $\varepsilon/I = \lambda$, $(p_0 i - Wh)g/I = n^2$, θ becomes

$$\theta = \frac{FH}{I} \frac{\sin(pt-\delta)}{\sqrt{(n^2-p^2)^2 + 4\lambda^2 p^2}} \qquad \left[\delta = \tan^{-1}\left(\frac{2\lambda p}{n^2-p^2}\right)\right] \ldots\ldots (2)$$

If x denotes displacement and L the height from the base surface, $x = \theta l$ and the absolute value of equation (2) becomes

$$|x| = \frac{FHT^2L}{4\pi^2 I} \frac{1}{\sqrt{\left\{\left(\frac{T}{T_0}\right)^2 - 1\right\}^2 + \frac{\lambda^2 T^2}{\pi^2}}} \ldots\ldots\ldots\ldots\ldots (3)$$

In this equation, T_0 means the natural period of the building, and T the period of oscillation force. As F, H, l, I, T_0 and λ are known, we get the resonance curve from equation (3). I is calculated from Table I, namely, $I = 3.8 \times 10^{14}$ grcm², $F = 5 \times 10^7$ dyne, $H = 1520$ cm, T and λ are found to be $T_0 = 0.31$ sec, and $\lambda = 0.5$ sec^{-1} according to the experiment.

Putting these value in equation (3), the resonance curve of every floor is got, which is shown in Fig. 3~7. Every curve agrees well with the values of which show the experimental results.

The period of rocking oscillation T_0 is

$$T_0=2\pi\sqrt{\frac{I}{(p_0i-Wh)g}}\,, \quad \text{.................} (4)$$

and p_0 results in from equation (4)

$$p_0=\frac{I}{ig}\left(\frac{2\pi}{T_0}\right)^2+\frac{Wh}{i}. \quad \text{..................} (5)$$

Now let us assume that the side of the buried part (l) of the building and the half of the base surface act as resisting surface. t and b represent the width in the beam direction and in the girder direction of the building respectively. Then the geometrical moment of inertia i becomes

$$i=\frac{bt^3}{24}+\frac{bt^3}{8}\left\{\frac{\sin\varphi}{2\cos^2\varphi}+\frac{1}{4}\log\left(\frac{1+\sin\varphi}{1-\sin\varphi}\right)\right\} \quad \text{................} (6)$$

where

$$\varphi=\tan^{-1}\left(\frac{l}{t/2}\right). \quad \text{........................} (7)$$

The first and the second term on the right side of equations (6) denote the geometrical moment of inertia at the base surface and the side surface respectively. Putting $b=1040$, $t=440$, $l=200$ into equations (6) and (7), we have

$$i=16.4\times10^9\text{cm}^4. \quad \text{......................} (8)$$

Next, we put this value of i and the values calculated from Table. I, that is, $I=3.8\times10^{14}\,\text{grcm}^2$, $W=4.9\times10^8\,\text{gr}$ and $h=750\,\text{cm}$, and $T_0=0.31$ sec which was obtained from experiment, into equation (5). Then p_0, the pressure corresponding to unit depression of ground is

$$p_0=9.5\times10^3\,\text{gr/cm}^3. \quad \text{..................} (5')$$

This value is almost equal to p_0 of Loam layer, $4.8\times10^3\sim9.6\times10^3$ gr/cm³.[2]

From these two examinations into the values of resonance curve and the pressure corresponding to the unit depression of ground, the vibration in the beam direction in this experiment was found to be an almost perfect rocking oscillation.

The experiment concerning the oscillation in the girder direction has not produced satisfactory results due to imperfection in the instal-

---

2) K. SUYEHIRO, "The Vibration of Structures and a Method of Measuring It", *Journ. Archit. Inst. Japan,* **40** (1926), 531, (in Japanese), *Tech. Papers A. Inokuty* (1928), *Memor. Lect.*, 138,

lation of the vibrator, but we shall at present make a brief examination taking into consideration the amplitude only.

Assuming that the columns are clamped completely to the base and the beam, that the masses of vertical members are concentrated at each floor and that the columns of each story have equal stiffness, height and concentrated mass, we made the calculation regarding the four storied building. Then the displacement distribution becomes as is shown by the lower curve in Fig. 8 which fairly coincides with the experimental results denoted by × marks.

If it is taken into consideration that the floor height of the first story is larger and the mass of roof floor smaller than those of the other stories, the result concerning the first floor have a tendency to be more and the result concerning the roof floor to be less. Therefore the results almost coincide with bending oscillation form of concentrated mass under clamped condition.

Thus, from the result of theoretical analysis of the vibration in both the beam and the girder directions, we found that if the effective resistance in the contact surface of building and ground is small as in case of the beam direction, it produces rocking oscillation, and if the effective resistance is as large as in the case of the girder direction, it is near to a bending oscillation with fixed base.

The condition to overturn a rigid structure with basement by vibration is complicated. For the simplest case, we take the worst condition for a building, that is the state of resonance, to seek the condition under which the vertical line through the centre of gravity of the building comes off the base surface.

If a represents the horizontal acceleration of earthquake, θ becomes

$$\theta = \tan^{-1}\frac{t}{H} = \frac{ahT_0M}{4\pi I\lambda} \quad \dots\dots\dots\dots\dots\dots (9)$$

and putting the constants of building and measured value into this equation, we have

$$a = 5.9\times10^3\ \mathrm{cm/sec^2}\,. \quad \dots\dots\dots\dots\dots\dots (10)$$

Namely, even in the case of resonance condition where the basement is of no use in preventing the building from overturning, an acceleration more than ten times larger than that of actual great earthquake is neccessary for the overturning of this building. Therefore, we can induce from the experiments that there is no possibility of an earthquake large enough to overturn this building.

5. Conclusion.

From the experiments above stated, it was made clear that rigid structures on soft ground is very capable of rocking oscillation. As the damping at basement in case of rocking oscillation is larger than damping due to solid viscosity etc., in case of elastic oscillation, if there is even a little rocking property in vibration, it is proof of so much aseismaticity of the building.

Considering the character of oscillation induced from these experiments as well as the improvement of the tendency that the vibration energy of building dissipates to the ground again transforming itself into the elastic waves as the rigidity of the building becomes larger in comparison with that of the ground, we find that the softer the ground on which rigid structure stands is, the less serious its damage by earthquake is. This coincides with the data obtained from the exploration of damaged districts.[3]

However, there are pretty many cases of earthquake damage due to inequal sinking of building base on soft ground, against which caution must be taken in designing and executing.

In conclusion, the writers wish to express their hearty thanks to Mr. M. Tachikawa and Prof. H. Tsuya for the greatest help to this experiment and they are also indebted to Messrs. T. Suzuki and S. Kaneko for their kind assistance throughout the progress of this experiment.

---

[3] K. KANAI, "Relation between the Earthquake Damage of Non-wooden Buildings and the Nature of the Ground", *Bull. Earthq. Res. Inst.*, **27** (1949), 97, **29** (1951), 209.

59. 實在鐵筋コンクリート建物の振動實驗結果

地震研究所 { 金井 清
田中貞二

建物の耐震性を調べる方法として，近年，遠心力を利用する起振機が盛に使われ，起振機の改良や測定方法の研究が次々に行われてきた。

本報告の實驗は，起振機を使つて，實在の鐵筋コンクリート建物の振動實驗を行つた，おそらく最初のものであるから，今日からみると，いろいろ不備なところが，めだつようである。

實驗建物は，東京都中央區木挽町にある 4.4×11.6 m の 4 階建の焼ビルで，構造が簡單なので，實驗結果を數理的に吟味するのに適している。

實驗結果から，軟弱地盤上の剛構造物は地震のときに動搖振動をする可能性が多いことが，一層明かになつた。この性質は，地震のときに建物の振動勢力が逸散波として地中に再び出てゆく性質とあいまつて，構造物の振動減衰性を増すことに役にたつ。従つて，構造物は軟弱地盤上の方が耐震的に有利なことになり，關東地震のときの非木造建物の震災調査の結果と合うことになる。

たゞし，軟弱地盤上では，地震中に，基礎の不同沈下をおこす可能性が相當にあり，そのため思はぬ災害を受けた實例も少くない。この點は設計ならびに施工上で十分に注意を要するところであろう。なお，土の單位壓下に要する壓力として，9.5×10^3 gr/cm²/cm という値が得られたが，この値は，かつて，末廣博士が推定した値に一致する。

所　報

◎談話会記事

第280回談話會（昭和26年7月17日）

1.	改良した煤書用電磁記錄器の試驗結果	田中貞二
2.	三原山の地球磁氣學的研究（其の 4） 地磁氣三成分測量および偏角連續觀測	力武常次 横山泉 岡田惇 菱山よね子
3.	地球内部の電氣的性質（其の 9） 地球核の電氣的性質を推定することの可能性	力武常次
4.	土地の脈動と海の波との關係	岸上冬彦

第281回談話會（昭和26年9月18日）

1.	表面波の研究（6） 二重の表面層と同等な單一層	佐藤泰夫
2.	霞ケ浦軟弱地盤の彈性波速度	表俊一郎 山崎良雄
3.	物體の落下による地動の觀測	岸上冬彦
4.	P波の周期がS波の周期よりも短くなる可能度	金井淸
5.	任意形地動による振子の運働 （地震計記象による震源機構の假定の吟味）	金井清 吉沢静代
6.	潮位觀測より見たる四國地方の地盤變動（續報）	河角広
7.	四國松山における地殼變動の觀測（第2報） 經年變化について	萩原尊禮 山田重平
8.	標準强震計試作　第1報	標準强震計試作試驗研究班
1.	計畫及び設計	高橋龍太郎
2.	理論	河角廣

第282回談話會（昭和26年10月16日）

1.	精密階差法の境界條件について	谷本勉之介 （西村所員紹介）
2.	内揷法によるアングル型及び十字型斷面柱の捩り剛さの計算について	谷本勉之介 （西村所員紹介）
3.	鹿沼市で觀測された今市地震餘震について（補遺）	池上良平
4.	南海大地震後に於ける室戸岬近傍の傾斜變動（續報）	永田武 岡田惇
5.	火山の帶磁	力武常次
6.	地球内部の電氣的性質（其の10）温度との關係	力武常次

第283回談話會（昭和26年11月20日）

1. 筑波山斑糲岩の帶磁と地磁氣異常　第1報	横山泉
2. 地球內部の電氣的性質（其の 11） 再び溫度との關係について	力武常次
3. 彈性波の發生機構に關する實驗（序報）	笠原慶一
4. 低域濾波器に依る表面波の研究（其の 4） ——1950年のインド地震に關して——	秋間哲夫
5. 日立鑛山における地震動の觀測結果 （地震波の反射屈折の問題）	金井清 吉澤清代

Index to Vol. XXIX.

Page

ASADA, T., SUZUKI, Z. and TOMODA, Y., (24) Notes on the Energy and Frequency of Earthquakes. (in English).................. 289

HAGIWARA, T., KASAHARA, K., YAMADA, J. and SAITO, S., (42) Observation of the Deformation of the Earth's Surface at Aburatsubo, Miura Peninsula. Part IV. (in English)......... 455

HAGIWARA, T. and KASAHARA, K., (53) Observations of the Deformation of the Earth's Surface at Aburatsubo, Miura Peninsula. Part V. (in English).. 577

HIRAGA, S. and MINAKAMI, T., (33) The Minor Activity of Volcano Azuma in February 1950. (in English)...................... 383

HISHIYAMA, Y., RIKITAKE, T., YOKOYAMA, I. and OKADA, A., (57) Geomagnetic Studies of Volcano Mihara. The 3rd paper. (Magnetic Survey and Continuous Observations of Changes in Geomagnetic Declination.) (in English)...................... 583

ICHIMURA, T., (29) Geological Investigations on the Zaō Volcanoes I. Goshiki-dake, a Central Cone of the Zaō Proper. (in English). 327

ICHIMURA, T. and MINATO, H., (30) Augite and Hypersthene Crystals from the Zaō Volcanoes. (in English)........................ 341

IKEGAMI, R., (16) On Ground Vibrations Caused by Explosions. (in English).. 197

IKEGAMI, R., (28) A Study on the Propagation of Microseismic Waves. Part IV. (in English).............................. 313

IKEGAMI, R. and KISHINOUYE, F., (27) A Study on the Propagation of Microseismic Waves. Part III. (in English)................ 305

IKEGAMI, R. and KISHINOUYE, F., (55) A Study on the Propagation of Microseismic Waves. Part V. (in English)................. 571

INOUE, E., (11) On the Vertical Displacements Accompanying Imaichi Earthquake in 1949. (in English)........................... 143

KANAI, K., (4) On the M_2-waves (Sezawa-waves). (in English)..... 39

KANAI, K., (5) On the Group Velocity of Dispersive Surface Waves. (in English).. 49

KANAI, K., (18) On the Damage to Japanese-style Buildings due to Earthquakes. (in Japanese)................................. 215

KANAI, K., (34) Destruction System of Building by Earthquake. (in English).. 393

Kanai, K., (47) The Result of Observation of Wave-velocity in the Ground. (in English) 503

Kanai, K., (50) Possibility of the Period of P-waves becoming smaller than those of S-waves. (in English) 529

Kanai, K. and Osada, K., (48) The Result of Observation concerning the Waves caused in the Ground by Building Vibration. (in English) 511

Kanai, K. and Tanaka, T., (9) Observations of the Earthquake-motion at the Different Depths of the Earth. I. (in English). 107

Kanai, K. and Tanaka, T., (59) Vibration Test of Actual Reinforced Concrete Building. (in English) 617

Kanai, K. and Yoshizawa, S., (17) Relation between the Earthquake Damage of Non-wooden Buildings and the Nature of the Ground. II. (in English) 209

Kasahara, K. and Hagiwara, T., (53) Observations of the Deformation of the Earth's Surface at Aburatsubo, Miura Peninsula. Part V. (in English) 577

Kasahara, K., Yamada, J., Saito, S. and Hagiwara, T., (42) Observation of the Deformation of the Earth's Surface at Aburatsubo, Miura Peninsula. Part IV. (in English) 455

Kawasumi, H., (43) Measures of Earthquake Danger and Expectancy of Maximum Intensity Throughout Japan as Inferred from the Seismic Activity in Historical Times. (in English) ... 469

Kishinouye, F., (26) Time Distribution of Felt Aftershocks of the Imaichi Earthquake of December 26, 1949. (in English) 301

Kishinouye, F., (35) Periods of Earth Vibrations at Kōtō-ku, Tokyo. (in English) 403

Kishinouye, F., (36) Sinking of the Kōtō Region, Tokyo. (in English) 407

Kishinouye, F., (44) On the Period and the Amplitude of Microseismic Movement. (in English) 483

Kishinouye, F., (52) Notes on Stray Earth Currents. (in English). 549

Kishinouye, F., (56) Microseisms and Sea Waves. (in English) 577

Kishinouye, F. and Ikegami, R., (27) A Study on the Propagation of Microseismic Waves. Part III. (in English) 305

KISHINOUYE, F. and Ikegami, R., (55) A Study on the Propagation of Microseismic Waves. Part V. (in English) 571

KISHINOUYE, F. and RIKITAKE, T., (38) Electrical Properties of Soil at Radio Frequencies. (in Japanese) 423

KOSHIKAWA, Y., (25) Seismometrical Study of the Imaichi Earthquake on Dec. 26, 1949. (The second paper) (in English)...... 295

MINAKAMI, T., (45) On the Temperature and Viscosity of the Fresh Lava Extruded in the 1951 Oo-sima Eruption. (in English).... 487

MINAKAMI, T. and HIRAGA, S., (33) The Minor Activity of Volcano Azuma in February 1950. (in English) 383

MINAKAMI, T., MIYAZAKI, T. and TAKAHASHI, T., (32) The 1950–1951 Eruption of Oo-sima and Its Seismometrical Investigations. (I). (in English)... 359

MINATO, H. and ICHIMURA, T., (30) Augite and Hypersthene Crystals from the Zaō Volcanoes. (in English) 341

MIYAMURA, S. and OMOTE, S., (15) Relations between the Earthquake Damage and the Structure of Ground in Nagoya City (in English)... 183

MIYAZAKI, T., TAKAHASHI, T. and MINAKAMI, T., (32) The 1950–1951 Eruption of Oo-sima and Its Seismometrical Investigations. (I). (in English)... 359

MORIMOTO, R., (31) Geology of Imaichi District with Speciol Reference to the Earthquake of Dec. 26, 1949. (II) (in English)......... 349

MORIMOTO, R. and TSUYA, H., (54) Petrography of the 1950-lavas of Oshima volcano, Seven Izu Islands, Japan. (in English)..... 563

NASU, N., (23) Block Movement along the Seismic Fault (2). (in English) 283

NASU, N., (37) Vibration of a Tank Tower. (in English)........... 413

OKADA, A., HISHIYAMA, Y., RIKITAKE, T. and YOKOYAMA, I., (57) Geomagnetic Studies of Volcano Mihara. The 3rd paper. (Magnetic Survey and Continuous Observation of Changes in Geomagnetic Declination.) (in English) 583

OMOTE, S., (10) On the Coda Waves of Earthquake Motions. (Part 6) (in English) 115

OMOTE, S. and MIYAMURA, S., (15) Relation between the Earthquake Damage and the Structure of Ground in Nagoya City. (in English) 183

OSADA, K. and KANAI, K., (48) The Result of Observation concerning the Waves caused in the Ground by Building Vibration. (in English) 511

RIKITAKE, T., (6) Electromagnetic Induction within the Earth and Its Relation to the Electrical State of the Earth's Interior. Part III. (in English) 61

RIKITAKE, T., (12) A Miniature Earth-inductor. (in English) 147

RIKITAKE, T., (13) Diffraction of Electromagnetic Waves around the Crater of Volcano Mihara. (in English) 153

RIKITAKE, T., (14) The Distribution of Magnetic Dip in Ooshima (Oo-sima) Island and its Change that Accompanied the Eruption of Volcano Mihara, 1950. (in English).................... 161

RIKITAKE, T., (20) Electromagnetic Shielding within the Earth and Geomagnetic Secular Variation. (in English).................. 263

RIKITAKE, T., (21) Changes in Earth Current and their Relation to the Electrical State of the Earth's Crust. (in English) 271

RIKITAKE, T., (22) The Form of Tsunami-waves outside a Bay as Inferred from the Motion of Bay-water. (in English)......... 277

RIKITAKE, T., (46) Changes in Magnetic Dip that Accompanied the Activities of Volcano Mihara. (The second report) (in English). 499

RIKITAKE T., (51) Electromagnetic Induction within the Earth and Its Relation to the Electrical State of the Earth's Interior. Part IV. (in English).................... 539

RIKITAKE, T. and KISHINOUYE, F., (38) Electrical Properties of Soil at Radio Frequencies. (in Japanese).................... 423

RIKITAKE, T., YOKOYAMA, I., OKADA, A. and Hishiyama, Y., (57) Geomagnetic Studies of Volcano Mihara. The 3rd paper. (Magnetic Survey and Continuous Observation of Changes in Geomagnetic Declination.) (in English) 583

SAITO, S., HAGIWARA, T., KASAHARA, K. and YAMADA, J., (42) Observation of the Deformation of the Earth's Surface at Aburatsubo, Miura Peninsula. Part IV. (in English) 455

SAKUMA, S., (58) Damage on Window-panes by the Air-waves of Explosion of Volcano Asama on Sept. 23, 1950. (in English)... 605

SATÔ, Y., (1) Study on Surface Waves I. Velocity of Love-Waves. (in Englise).................... 1

SATÔ, Y., (2) Seismic Focus without Rayleigh-Waves. (in English). 13

SATÔ, Y., (3) Mathematical Study of the Propagation of Waves upon Stratified Medium. (2) (in English) 21

SATÔ, Y., (19) Study on Surface Waves II. Velocity of Surface Waves Propagated upon Elastic Plates. (in English) 223

SATÔ, Y., (40) Study on Surface Waves III. Love-Waves with Double Superficial Layer. (in English) 435

SATÔ, Y., (41) Distribution of Surface Stress Generating No Rayleigh-Waves. (in English) 445

SATÔ, Y., (49) Study on Surface Waves IV. Equivalent Single Layer to Double Superficial Layer. (in English) 519

SUZUKI, Z., TOMODA, Y. and ASADA, T., (24) Notes on the Energy and Frequency of Earthquakes. (in English) 289

TAKAHASI, R., (7) An Estimate of Future Tsunami Damage Along the Pacific Coast of Japan. (in English) 71

TAKAHASHI, T., MINAKAMI, T. and MIYAZAKI, T., (32) The 1950–1951 Eruption of Oo-sima and Its Seismometrical Investigations. (I). (in English) 359

TANAKA, T. and KANAI, K., (9) Observations of the Earthquake-motion at the Different Depths of the Earth. I. (in English). 107

TANAKA, T. and KANAI, K. (59) Vibration Test of Actual Reinforced Concrete Building. (in English) 617

TOMODA, Y., ASADA, T. and SUZUKI, Z., (24) Notes on the Energy and Frequency of Earthquakes. (in English) 289

TSUYA, H. and MORIMOTO, R., (54) Petrography of the 1950-lavas of Oshima volcano, Seven Izu Islands, Japan. (in English) 563

YAMADA, J., SAITO, S., HAGIWARA, T. and KASAHARA, K., (42) Observation of the Deformation of the Earth's Surface at Aburatsubo, Miura Peninsula. Part IV. (in English) 455

YOKOYAMA, I., OKADA, A., HISHIYAMA, Y. and RIKITAKE, T., (57) Geomagnetic Studies of Volcano Mihara. The 3rd paper. (Magnetic Survey and Continuous Observation of Changes in Geomagnetic Declination.) (in English) 583

YOSHIZAWA, S. and KANAI, K., (17) Relation between the Earthquake Damage of Non-wooden Buildings and the Nature of the Ground. II. (in English) 209

(8) Explosion-Seismic Observations in Northeastern Japan. By the Research Group for Explorion Seismology, Tokyo. (in English) 97

(39) Seismological Report for the Assam-Tibet Earthquake on Aug. 15, 1950. (in English) 433

索引 第29號

頁

淺田　敏・鈴木次郎・友田好文　(24)　地震の頻度とエネルギーについて(英文) …… 289

萩原尊禮・笠原慶一・山田重平・齋藤貞夫　(42)　油壺における地殼變動の觀測 (第 4 報) (英文) …… 455

萩原尊禮・笠原慶一　(53)　油壺における地殼變動の觀測 (第5報) (英文)　577

平賀士郎・水上　武　(33)　1950年2月の吾妻山の小活動 (英文) …… 383

菱山よね子・力武常次・横山　泉・岡田　惇　(57)　三原山の地球磁氣學的研究　第 3 報　地磁氣三成分測量および偏角變化の連續觀測 (英文)　583

市村　毅　(29)　藏王火山の地質學的研究 (第1報) (英文) …… 327

市村　毅・湊　秀雄　(30)　藏王火山產普通輝石及紫蘇輝石結晶 (英文) …　341

池上良平　(16)　火藥の爆發によつて起される地動について (英文) …… 197

池上良平　(28)　土地の脈動の傳播性の研究 (第4報) (英文) …… 313

池上良平・岸上冬彥　(27)　土地の脈動の傳播性の研究 (第3報) (英文) …　305

池上良平・岸上冬彥　(55)　土地の脈動の傳播性の研究 (第5報) (英文) …　571

井上英二　(11)　今市地震 (1949) に伴う地殼の垂直變動について (英文)　143

金井　清　(4)　M_2波 (妹澤波)について (英文) …… 39

金井　清　(5)　分散性表面波の群速度について (英文) …… 49

金井　清　(18)　木造家屋の震害について (邦文) …… 215

金井　清　(34)　地震による建物の破壞過程について (英文) …… 393

金井　清　(47)　地下における彈性波速度の測定結果 (英文) …… 503

金井　清　(50)　P波の周期がS波の周期より短くなる可能度 (英文) …… 529

金井　清・長田甲斐男　(48)　建物振動に伴う土地の震動の測定結果 (英文)　511

金井　清・田中貞二　(9)　地下における地震動の觀測結果 (第1報) (英文)　107

金井　清・田中貞二　(59)　實在鐵筋コンクリート建物の振動實驗結果 (英文) …… 617

金井　清・吉澤靜代　(17)　非木造建物の震害と地盤の性質との關係　第2報 (英文) …… 209

笠原慶一・萩原尊禮　(53)　油壺における地殼變動の觀測 (第5報) (英文)　577

笠原慶一・山田重平・齋藤貞夫・萩原尊禮　(42)　油壺における地殼變動の觀測 (第4報) (英文) …… 455

河角　廣　(43)　有史以來の地震活動より見たる我國各地の地震危險度及び最高震度の期待値 (英文) …… 469

岸上冬彥　(26)　1949年今市地震の有感餘震の時間分布 (英文) …… 301

岸上冬彥　(35)　東京都江東區における土地の振動周期 (英文) …… 403

岸上冬彥　(36)　東京都江東地區の地盤沈下 (英文) …… 407

岸上冬彦 （44） 土地の脈動の周期と振幅について （英文） ………… 483
岸上冬彦 （52） 迷走地電流について （英文） ………… 549
岸上冬彦 （56） 土地の脈動と海の波 （英文） ………… 577
岸上冬彦・池上良平 （27） 土地の脈動の傳播性の研究 （第3報） （英文） … 305
岸上冬彦・池上良平 （55） 土地の脈動の傳播性の研究 （第5報） （英文） … 571
岸上冬彦・力武常次 （38） 高周波域における土の電氣的性質 （邦文） ……… 423
越川善明 （25） 今市地震の計測 （第2報） （英文） ………… 295
水上　武 （45） 1951年に噴出した大島熔岩の溫度と粘性について （英文） 487
水上　武・平賀士郎 （33） 1950年2月の吾妻山の小活動 （英文） ………… 383
水上　武・宮崎　務・高橋智子 （32） 最近の大島の噴火とその地震計測學的研究 （I） （英文） ………… 359
湊　秀雄・市村　毅 （30） 藏王火山產普通輝石及紫蘇輝石結晶 （英文） … 341
宮村攝三・表　俊一郎 （15） 名古屋市における地盤と震害の關係 （英文） … 183
宮崎　務・高橋智子・水上　武 （32） 最近の大島の噴火とその地震計測學的研究 （I） （英文） ………… 359
森本良平 （31） 今市地震地域の地質 （2） （英文） ………… 349
森本良平・津屋弘逵 （54） 伊豆大島三原山1950年熔岩の化學成分 （英文） 563
那須信治 （23） 地震斷層に沿う地塊運動 （2） （英文） ………… 283
那須信治 （37） 水槽鐵塔の振動について （英文） ………… 413
岡田　惇・菱山よね子・力武常次・横山　泉 （57） 三原山の地球磁氣學的研究 第3報 地磁氣三成分測量および偏角變化の連續觀測 （英文） … 583
表　俊一郎 （10） 地震動の尾部について （其の6） （英文） ………… 115
表　俊一郎・宮村攝三 （15） 名古屋市における地盤と震害の關係 （英文）… 183
長田甲斐男・金井　清 （48） 建物振動に伴う土地の震動の測定結果 （英文） ………… 511
力武常次 （6） 地球内の電磁感應及びその地球内部の電氣的性質との關係 第3報 （英文） ………… 61
力武常次 （12） 小型磁氣感應儀 （英文） ………… 147
力武常次 （13） 三原山火口附近における放送電波の廻折 （英文） ……… 153
力武常次 （14） 伊豆大島における地磁氣伏角分布と三原山噴火に伴うその變化 （英文） ………… 161
力武常次 （20） 地磁氣永年變化に對する遮蔽効果 （英文） ………… 263
力武常次 （21） 地電流變化と地下の電氣的性質 （英文） ………… 271
力武常次 （22） 灣水の運動と灣外に於ける津浪の波形 （英文） ………… 277
力武常次 （46） 三原火山の活動に伴う地磁氣變化 （第2報） （英文） ……… 499
力武常次 （51） 地球内の電磁感應およびその地球内部の電氣的性質との關係 第4報 （英文） ………… 539
力武常次・岸上冬彦 （38） 高周波域に於ける土の電氣的性質 （邦文） … 423

力武常次・横山　泉・岡田　惇・菱山よね子 (57) 三原山の地球磁氣學的研究 第3報 地磁氣三成分測量および偏角變化の連續觀測 (英文) …… 583

齋藤貞夫・萩原尊禮・笠原慶一・山田重平 (42) 油壺における地殼變動の觀測 (第4報) (英文) …… 455

佐久間修三 (58) 1950年9月23日の淺間火山爆發の空氣波による窓ガラス被害 (英文) …… 605

佐藤泰夫 (1) 表面波の研究 I ラブ波の速度 (英文) …… 1

佐藤泰夫 (2) レーリー波を發生しない震源 (英文) …… 13

佐藤泰夫 (3) 層のある媒質を傳はる表面波の研究 (2) (英文) …… 21

佐藤泰夫 (19) 表面波の研究 II 彈性板を傳はる表面波の速度 (英文) … 223

佐藤泰夫 (40) 表面波の研究 III 二つの表面層をもつラブ波 (英文) … 435

佐藤泰夫 (41) レーリー波を發生しない表面應力の分布 (英文) …… 445

佐藤泰夫 (49) 表面波の研究 IV 二重の表面層と同等な單一層 (英文) … 519

鈴木次郎・友田好文・淺田　敏 (24) 地震の頻度とエネルギーについて (英文) …… 289

高橋龍太郎 (7) 本邦太平洋沿岸各地に於ける津浪の危險度 (英文) …… 71

高橋智子・水上　武・宮崎　務 (32) 最近の大島の噴火とその地震計測學的研究 (I) (英文) …… 359

田中貞二・金井　清 (9) 地下における地震動の觀測結果 第1報 (英文) …… 107

田中貞二・金井　清 (59) 實在鐵筋コンクリート建物の振動實驗結果 (英文) …… 617

友田好文・淺田　敏・鈴木次郎 (24) 地震の頻度とエネルギーについて (英文) 289

津屋弘逵・森本良平 (54) 伊豆大島三原山1950年熔岩の化學成分 (英文) 563

山田重平・齋藤貞夫・萩原尊禮・笠原慶一 (42) 油壺における地殼變動の觀測 (第4報) (英文) …… 455

横山　泉・岡田　惇・菱山よね子・力武常次 (57) 三原山の地球磁氣學的研究 第3報 地磁氣三成分測量および偏角變化の連續觀測 (英文) …… 583

吉澤靜代・金井　清 (17) 非木造建物の震害と地盤の性質との關係 第2報 (英文) …… 209

(8) 東北日本における爆破地震動の觀測 (爆破地震動研究グループ——東大地震研究所・東大地球物理學教室・中央氣象臺地震課・地質調査所 第4部) (英文) …… 97

(39) 1950年8月15日 アツサム・チベツト地震觀測報告 (英文) …… 433

BULLETIN

OF THE

EARTHQUAKE RESEARCH INSTITUTE

TOKYO UNIVERSITY

VOL. XXIX

1951

東京大學

地震研究所彙報

第 29 号

昭和 26 年

CONTENTS.

Vol. XXIX.

Part 1. March, 1951.

Papers and Reports.

Page

1. Y. SATÔ, Study on Surface Waves I. Velocity of Love-Waves. (in English) 1
2. Y. SATÔ, Seismic Focus without Rayleigh-Waves. (in English).. 13
3. Y. SATÔ, Mathematical Study of the Propagation of Waves upon Statified Medium. (2) (in English) 21
4. K. KANAI, On the M_2-waves (Sezawa-waves). (in English).... 39
5. K. KANAI, On the Group Velocity of Dispersive Surface Waves. (in English) 49
6. T. RIKITAKE, Electromagnetic Induction within the Earth and Its Relation to the Electrical State of the Earth's Interior. Part III. (in English) 61
7. R. TAKAHASI, An Estimate of Future Tsunami Damage Along the Pacific Coast of Japan. (in English)............. 71
8. The Research Group for Explosion Seismology, Tokyo, Explosion-Seismic Observations in North-eastern Japan. (in English) 97
9. K. KANAI and T. TANAKA, Observations of the Earthquake-motion at the Different Depths of the Earth. I. (in English). 107
10. S. OMOTE, On the Coda Waves of Earthquake Motions. (Part 6) (in English) 115
11. E. INOUE, On the Vertical Displacements Accompanying Imaichi Earthquake in 1949. (in English) 143
12. T. RIKITAKE, A Miniature Earth-inductor. (in English)....... 147
13. T. RIKITAKE, Diffraction of Electromagnetic Waves around the Crater of Volcano Mihara. (in English) 153
14. T. RIKITAKE, The Distribution of Magnetic Dip in Ooshima (Oo-sima) Island and its Change that Accompanied the Eruption of Volcano Mihara, 1950. (in English)............ 161

15. S. OMOTE and S. MIYAMURA, Relations between the Earthquake Damage and the Structure of Ground in Nagoya City. (in English) 183

16. R. IKEGAMI, On Ground Vibrations Caused by Explosions. (in English) 197

17. K. KANAI and S. YOSHIZAWA, Relation between the Earthquake Damage of Non-wooden Buildings and the Nature of the Ground. II. (in English) 209

18. K. KANAI, On the Damage to Japanese-style Buildings due to Earthquakes. (in Japanese) 215

Part 2. June, 1951.

19. Y. SATÔ, Study on Surface Waves II. Velocity of Surface Waves Propagated upon Elastic Plates. (in English) 223

20. T. RIKITAKE, Electromagnetic Shielding within the Earth and Geomagnetic Secular Variation. (in English) 263

21. T. RIKITAKE, Changes in Earth Current and their Relation to the Electrical State of the Earth's Crust. (in English) 271

22. T. RIKITAKE, The Form of Tsunami-waves outside a Bay as Inferred from the Motion of Bay-water. (in English) 277

23. N. NASU, Block Movement along the Seismic Fault (2). (in English) 283

24. T. ASADA, Z. SUZUKI and Y. TOMODA, Notes on the Energy and Frequency of Earthquake. (in English) 289

25. Y. KOSHIKAWA, Seismometrical Study of the Imaichi Earthquake on Dec. 26, 1949. (The second paper) (in English) 295

26. F. KISHINOUYE, Time Distribution of Felt Aftershocks of the Imaichi Earthquake of December 26, 1949. (in English) 301

27. R. IKEGAMI and F. KISHINOUYE, A Study on the Propag tion of Microseismic Waves. Part III. (in English) 305

28. R. IKEGAMI, A Study on the Propagation of Microseismic Waves. Part IV. (in English) 313

29. T. ICHIMURA, Geological Investigations on the Zaō Volcanoes I. Goshiki-dake, a Central Cone of the Zaō Proper. (in English) 327

30. T. ICHIMURA and H. MINATO, Augite and Hypersthene Crystals from the Zaō Volcanoes. (in English) 341
31. R. MORIMOTO, Geology of Imaichi District with Special Reference to the Earthquake of Dec. 26, 1949. (II) (in English) 349
32. T. MINAKAMI, T. MIYAZAKI and T. TAKAHASHI, The 1950–1951 Eruption of Oo-shima and Its Seismometrical Investigations. (I). (in English)............ 359
33. T. MINAKAMI and S. HIRAGA, The Minor Activity of Volcano Azuma in February 1950. (in English) 383
34. K. KANAI, Destruction System of Building by Earthquake. (in Englisn)............ 393
35. F. KISHINOUYE, Periods of Earth Vibrations of Kōtō-ku, Tokyo. (in English)............ 403
36. F. KISHINOUYE, Sinking of the Kōtō Region, Tokyo. (in English). 407
37. N. NASU, Vibration of a Tank Tower. (in English) 413
38. T. RIKITAKE and F. KISHINOUYE, Electrical Properties of Soil at Radio Frequencies. (in Japanese)............ 423
39. Seismological Report for the Assam-Tibet Earthquake on Aug. 15, 1950. (in English) 433

Part 3. September, 1951.

40. Y. SATÔ, Study on Surfaces Waves III. Love-Waves with Double Superficial Layer. (in English) 435
41. Y. SATÔ, Distribution of Surface Stress Generating No Rayleigh-Waves. (in English) 445
42. T. HAGIWARA, K. KASAHARA, J. YAMADA and S. SAITO, Observation of the Deformation of the Earth's Surface at Aburatsubo, Miura Peninsula. Part IV. (in English) 455
43. H. KAWASUMI, Measures of Earthquake Danger and Expectancy of Maximum Intensity Throughout Japan as Inferred from the Seismic Activity in Historical Times. (in English).. 469
44. F. KISHINOUYE, On the Period and the Amplitude of Microseismic Movement. (in English)............ 483
45. T. MINAKAMI, On the Temperature and Viscosity of the Fresh Lava Extruded in the 1951 Oo-sima Eruption. (in English).. 487

46. T. RIKITAKE, Changes in Magnetic Dip that Accompanied the Activities of Volcano Mihara. (The second report) (in English) 499
47. K. KANAI, The Result of Observation of Wave-velocity in the Ground. (in English) 503
48. K. KANAI and K. OSADA, The Result of Observation concerning the Waves caused in the Ground by Building Vibration. (in English) 511

Part 4. December, 1951.

49. Y. SATÔ, Study on Surface Waves IV. Equivalent Single Layer to Double Superficial Layer. (in English) 519
50. K. KANAI, Possibility of the Period of P-waves becoming smaller than those of S-waves. (in English) 529
51. T. RIKITAKE, Electromagnetic Induction within the Earth and Its Relation to the Electrical State of the Earth's Interior. Part IV. (in English) 539
52. F. KISHINOUYE, Notes on Stray Earth Currents (in English) .. 549
53. T. HAGIWARA and K. KASAHARA, Observations of the Deformation of the Earth's Surface at Aburatsubo, Miura Peninsula. Part V. (in English) 557
54. H. TSUYA and R. MORIMOTO, Petrography of 1950-lavas of Oshima Volcano, Seven Izu Islands, Japan. (in English) 563
55. R. IKEGAMI and F. KISHINOUYE, A Study on the Propagation of Microseismic Waves. Part V. (in English) 571
56. F. KISHINOUYE, Microseisms and Sea Waves. (in English) 577
57. T. RIKITAKE, I. YOKOYAMA, A. OKADA and Y. HISHIYAMA, Geomagnetic Studies of Volcano Mihara. The 3rd paper. (Magnetic Survey and Continuous Observation of Changes in Geomagnetic Declination.) (in English) 583
58. S. SAKUMA, Damage on Window-panes by the Air-waves of Explosion of Volcano Asama on Sept. 23, 1950. (in English). 605
59. K. KANAI and T. TANAKA, Vibration Test of Actual Reinforced Concrete Building. (in English) 617

目次

第29號

第1冊　昭和26年3月

論文及報告

頁
1. 表面波の研究 I　ラブ波の速度（英文）……………… 佐藤泰夫 1
2. レーリー波を発生しない震源（英文）……………… 佐藤泰夫 13
3. 層のある媒質を伝はる表面の研究 (2)（英文）……………… 佐藤泰夫 21
4. M_2波（妹沢波）について（英文）……………… 金井清 39
5. 分散性表面波の群速度について（英文）……………… 金井清 49
6. 地球内の電磁感応およびその地球内部の電氣的性質との関係 第3報（英文）……………… 力武常次 61
7. 本邦太平洋沿岸各地に於ける津浪の危険度（英文）……………… 高橋龍太郎 71
8. 東北日本における爆破地震動の観測（英文）……………… 爆破地震動研究グループ
{東大地震研究所 東大地球物理学教室 中央氣象台地震課 地質調査所第4部} 97
9. 地下における地震動の観測結果　第1報（英文）……………… {金井清 田中貞二} 107
10. 地震動の尾部につい（其の6）（英文）……………… 表俊一郎 115
11. 今市地震（1949）に伴う地殼の垂直変動について（英文）… 井上英二 143
12. 小型磁氣感応儀（英文）……………… 力武常次 147
13. 三原山火口附近における放送電波の廻折（英文）……………… 力武常次 153
14. 伊豆大島における地磁氣伏角分布と三原山噴火に伴うその変化（英文）……………… 力武常次 161
15. 名古屋市における地盤と震害の関係（英文）……………… {表俊一郎 宮村攝三} 183
16. 火薬の爆発によつて起される地動について（英文）……………… 池上良平 197
17. 非木造建物の震害と地盤の性質との関係　第2報（英文）… {金井清 吉沢静代} 209
18. 木造家屋の震害について（邦文）……………… 金井清 215

第2冊　昭和26年6月

19. 表面波の研究 II 彈性板を伝はる表面波の速度（英文）…… 佐藤泰夫 223
20. 地磁氣永年変化に対する遮蔽効果（英文）……………… 力武常夫 263
21. 地電流変化と地下の電氣的性質（英文）……………… 力武常次 271

22. 灣水の運動と灣外に於ける津浪の波形（英文）……………… 力武常次 277
23. 地震断層に沿う地塊運動（2）（英文）……………… 那須信治 283
24. 地震の頻度とエネルギーについて（英文）……………… 淺田 敏 鈴木次郎 友田好文 289
25. 今市地震の計測（第2報）（英文）……………… 越川善明 295
26. 1949年今市地震の有感餘震の時間分布（英文）……………… 岸上冬彦 301
27. 土地の脈動の伝播性の研究（第3報）（英文）……………… 池上良平 岸上冬彦 305
28. 土地の脈動の伝播性の研究（第4報）（英文）……………… 池上良平 313
29. 蔵王火山の地質学的研究（第1報）（英文）……………… 市村 毅 327
30. 蔵王火山産普通輝石及紫蘇輝石結晶（英文）……………… 市村 毅 湊 秀雄 341
31. 今市地震地域の地質（2）（英文）……………… 森本良平 349
32. 最近の大島の噴火とその地震計測学的研究（I）（英文）……………… 水上 武 宮崎 務 高橋智子 359
33. 1950年2月の吾妻山の小活動（英文）……………… 水上 武 平賀士郎 383
34. 地震による建物の破壊過程について（英文）……………… 金井 清 393
35. 東京都江東区における土地の振動周期（英文）……………… 岸上冬彦 403
36. 東京都江東地区の地盤沈下（英文）……………… 岸上冬彦 407
37. 水槽鉄塔の振動について（英文）……………… 那須信治 413
38. 高周波域に於ける土の電氣的性質（邦文）……………… 力武常次 岸上冬彦 423
39. 1950年8月15日アッサム・チベット地震觀測報告（英文）……………… 433

第3冊　昭和26年9月

40. 表面波の研究 Ⅲ 二つの表面層をもつラブ波（英文）……………… 佐藤泰夫 435
41. レーリー波を発生しない表面応力の分布（英文）……………… 佐藤泰夫 445
42. 油壺における地殻変動の観測（第4報）（英文）……………… 萩原尊礼 笠原慶一 山田重平 齋藤貞夫 455
43. 有史以來の地震活動より見たる我国各地の地震危険度及び最高震度の期待値（英文）……………… 河角 広 469
44. 土地の脈動の周期と振幅について（英文）……………… 岸上冬彦 483
45. 1951年に噴出した大島熔岩の温度と粘性について（英文）…… 水上 武 487
46. 三原火山の活動に伴う地磁氣変化（第2報）（英文）……………… 力武常次 499
47. 地下における弾性波速度の測定結果（英文）……………… 金井 清 503

48. 建物振動に伴う土地の震動の測定結果（英文）……………… 金井清・長田甲斐男 511

第4冊 昭和26年12月

49. 表面波の研究 IV 二重の表面層と同等な単一層（英文）… 佐藤泰夫 519
50. P波の周期がS波の周期よりも短くなる可能度（英文）…… 金井清 529
51. 地球内の電磁感応およびその地球内部の電氣的性質との関係（第4報）（英文）…………………………………… 力武常次 539
52. 迷走地電流について（英文）…………………………………… 岸上冬彦 549
53. 油壺における地殼変動の観測（第5報）（英文）…………… 萩原尊礼・笠原慶一 557
54. 伊豆大島三原山 1950 年熔岩の化学成分（英文）…………… 津屋弘逵・森本良平 563
55. 土地の脈動の伝播性の研究（第5報）（英文）……………… 池上良平・岸上冬彦 571
56. 土地の脈動と海の波（英文）…………………………………… 岸上冬彦 577
57. 三原山の地球磁氣学的研究 第3報 地磁氣三成分測量および偏角変化の連續観測（英文）……………………… 力武常次・横山泉・岡田惇・菱山よね子 583
58. 1950 年 9 月 23 日の浅間火山爆発の空氣波による窓ガラス被害（英文）………………………………… 佐久間修三 605
59. 実在鉄筋コンクリート建物の振動実験結果（英文）………… 金井清・田中貞二 617

昭和26年12月10日印刷
昭和26年12月15日發行

東京都文京區本富士町一番地
東京大學構內
編纂兼發行者　東京大學地震研究所

東京都中央區日本橋茅場町二丁目十番地
印刷者　笠井康賴

東京都中央區日本橋茅場町二丁目十番地
印刷所　株式會社國際文献印刷社

東京都千代田區神田一ツ橋通
賣捌所　岩波書店

東京都中央區日本橋二丁目六番地
丸善株式會社

Sold by
Iwanami Shoten,
Hitotsubashi dôri, Chiyoda, Tôkyô,
and
Maruzen Co., Ltd.,
Nihonbashi dôri, Chûô-ku, Tôkyô.
Price of this copy: 460 Yen. (Postage exclusive.)

BULLETIN OF

THE EARTHQUAKE RESEARCH INSTITUTE

TOKYO UNIVERSITY

Vol. XXIX, Part 4. December, 1951.

Contents.

Papers and Reports.

Page

49. Y. SATÔ, Study on Surface Waves IV. Equivalent Single Layer to Double Superficial Layer. (in English) 519
50. K. KANAI, Possibility of the Period of P-waves becoming smaller than those of S-waves. (in English) 529
51. T. RIKITAKE, Electromagnetic Induction within the Earth and Its Relation to the Electrical State of the Earth's Interior. Part IV. (in English) ... 539
52. F. KISHINOUYE, Notes on Stray Earth Currents. (in English) 549
53. T. HAGIWARA and K. KASAHARA, Observations of the Deformation of the Earth's Surface at Aburatsubo, Miura Peninsula. Part V. (in English) .. 557
54. H. TSUYA and R. MORIMOTO, Petrography of the 1950-lavas of Oshima volcano, Seven Izu Islands, Japan. (in English) 563
55. R. IKEGAMI and F. KISHINOUYE, A Study on the Propagation of Microseismic Waves. Part V. (in English) 571
56. F. KISHINOUYE, Microseisms and Sea Waves. (in English) 577
57. T. RIKITAKE, I. YOKOYAMA, A. OKADA and Y. HISHIYAMA, Geomagnetic Studies of Volcano Mihara. The 3rd paper. (Magnetic Survey and Continuous Observation of Changes in Geomagnetic Declination.) (in English). 583
58. S. SAKUMA, Damage on Window-panes by the Air-waves of Explosion of Volcano Asama on Sept. 23, 1950. (in English) 605
59. K. KANAI and T. TANAKA, Vibration Test of Actual Reinforced Concrete Building. (in English) 617

Institute Notes.

Index.

(For the papers written in Japanese or in occidental languages, the abstracts are given in occidental languages or in Japanese respectively.)